

Cole - H02754 - 2 - P 024335

The American Journal of PATHOLOGY

APRIL 1972

THE AMERICAN ASSOCIATION OF
PATHOLOGISTS AND BACTERIOLOGISTS

OFFICIAL PUBLICATION OF



THE AMERICAN SOCIETY FOR
EXPERIMENTAL PATHOLOGY

In this issue:

Blood Coagulation Components in Inflammation: A review

BOARD OF EDITORS

Thomas D. Kinney, *Editor-in-Chief*

Donald B. Hackel, *Associate Editor*

Orville T. Bailey

Frederick M. Becker

Baruj Benacerraf

Kurt Benirschke

Kenneth M. Brinkhous

Joel G. Brunson

John R. Carter

Charles G. Cochrane

John M. Craig

Frank J. Dixon, Jr

John T. Ellis

Frank W. Fitch

Patrick J. Fitzgerald

David G. Freiman

Jack C. Geer

Gabriel Godman

John B. Hazard

Robert H. Heptinstall

Morris J. Karnovsky

Paul Kotin

Averill A. Liebow

Guido Majno

Donald G. McKay

Henry D. Moon

Councilman Morgan

Hans J. Müller-Eberhard

Goetz W. Richter

David T. Rowlands, Jr

Philippe Shubik

Edward A. Smuckler

Leon Sokoloff

Benjamin H. Spargo

Jacinto J. Vazquez

F. Stephen Vogel

Editorial Assistant: Virginia Hotelling

To protect her next baby..



Gamulin® Rh Rh_o(D) immune globulin (human)

...complete with a disposable syringe
in a compact, space-saving package.



As a major producer of blood fractions, Dow now brings you a new source for Rh_o(D) immune globulin to protect the Rh negative mother's next baby from probability of hemolytic disease.

Studies to demonstrate its safety and effectiveness show that Gamulin Rh is effective in suppressing the production of Rh_o(D) antibodies.

And it comes in a space-saving, compact package that includes a vial, disposable syringe, lay literature, patient laboratory form, ID card, package insert and a crossmatch vial.

DESCRIPTION: GAMULIN Rh, Rh_o(D) Immune Globulin (Human), is a sterile concentrated solution of gamma globulin derived from blood of human donors known to have antibodies to Rh_o(D). It is standardized to contain 10.0 to 18.0 percent globulins with a level of antibody to Rh_o(D) equal to or greater than that of the NIH Reference Rh_o(D) Immune Globulin (Human). The final product contains 0.2 to 0.3 molar glycine as a stabilizer and 1:10,000 thimerosal as a preservative.

INDICATIONS: GAMULIN Rh suppresses the immune response of nonsensitized Rh_o(D) negative mothers following Rh incompatible pregnancies. The criteria for an Rh incompatible pregnancy are: That the mother shall be Rh_o(D) negative, D^u negative; and the infant shall be Rh_o(D) positive or D^u positive.

CONTRAINDICATIONS: Gamulin Rh must not be given to the infant. Gamulin Rh also should not be administered to an Rh_o(D) positive or D^u positive individual, to a recipient of an Rh_o(D) positive blood transfusion, or to an Rh_o(D) negative mother previously sensitized by an Rh incompatible pregnancy. Do not give intravenously.

PRECAUTIONS AND REACTIONS: It is essential that certain diagnostic and laboratory criteria be met before administering this product. (See package literature.) An occasional patient has shown a systemic reaction manifested by a low grade fever. Allergic reactions, although not expected, could occur.

ADMINISTRATION: Consult package insert for detailed instructions.

This product must be administered within 72 hours post-partum.

Gamulin® Rh

Rh_o(D) immune globulin (human)



THE DOW CHEMICAL COMPANY
Rx Pharmaceuticals
Indianapolis

P 24,335

*A perfect balance of quality
and convenience*



Esco

microscope slides

GUARANTEED* PRE-CLEANED

*Satisfaction guaranteed or merchandise replaced.

- ☐ Made in U. S. A. from finest L•O•F glass
- ☐ Individually selected for uniform cleanliness
- ☐ Precision-ground edges on all four sides
- ☐ Annealed to minimize chipping and breakage
- ☐ Thin, flat, highly resistant to corrosion or fogging
- ☐ Dispensing package allows easy removal of slides

Esco

micro cover glasses

SUPERIOR QUALITY—MAXIMUM CLARITY

- ☐ Individually selected
- ☐ Superior resistance to corrosion and fogging
- ☐ Free from striae, oily film, fingerprints
- ☐ Precision uniformity in thickness, flatness and size
- ☐ Free from ragged edges
- ☐ Clear-vue crush-resistant plastic box



ERIE SCIENTIFIC
SYBRON CORPORATION

WRITE FOR BROCHURE NO. 9

BUFFALO, NEW YORK 14210

The American Journal of PATHOLOGY



APRIL 1972 • Volume 67, Number 1

CONTENTS

- 1 Spontaneous Atherosclerosis in Pigeons: A Model System for Studying Metabolic Parameters Associated with Atherogenesis
Robert F. Santerre, Thomas N. Wight, Samuel C. Smith and David Brannigan
- 23 Endotoxin-Induced Hepatic Damage in BCG-Infected Mice
J. W. Shands, Jr and V. C. Senterfitt
- 41 Experimental Concussion: Ultrastructural and Biochemical Correlates
W. Jann Brown, N. Yoshida, T. Canty and M. Anthony Verity
- 69 Peroxidase Arthritis. I. An Immunologically Mediated Inflammatory Response with Ultrastructural Cytochemical Localization of Antigen and Specific Antibody
Richard C. Graham, Jr and Sarajayne Lampert Shannon
- 95 Fetal Renal Structure and the Genesis of Amniotic Fluid Disorders
Richard L. Naege and William A. Blanc
- 109 Ultrastructural Changes in the Capillary Bed of Human Pituitary Tumors
Joel Schechter
- 127 Myonecrosis Induced by Rattlesnake Venom
John M. Stringer, Robert A. Kainer and Anthony T. Tu
- 141 Light and Electron Microscopic Studies of Rat Kidney After Administration of Inhibitors of the Citric Acid Cycle *In Vivo*. II. Effects of Sodium Malonate on Proximal Convoluted Tubule
Elizabeth M. McDowell
- 159 Macrophage Accumulation, Division, Maturation, and Digestive and Microbicidal Capacities in Tuberculous Lesions. I. Studies Involving their Incorporation of Tritiated Thymidine and their Content of Lysosomal Enzymes and Bacilli
Kiyoshi Shima, Arthur M. Dannenberg, Jr, Masayuki Ando, Saroj Chandrasekhar, Judith A. Seluzicki and Jacob I. Fabrikant
- 181 REVIEW ARTICLE: Participation of Components of the Blood Coagulation System in the Inflammatory Response
Donald G. McKay
- 211 **Animal Model for Human Disease:** Hydranencephaly, Porencephaly, Cerebral Cysts, CNS Malformations
B. I. Osburn and A. M. Silverstein

© 1972 by The American Association of Pathologists and Bacteriologists

The seal commemorates The Year of Pathology, being celebrated from October 1971 to October 1972 by the major national pathology societies. Special educational events will emphasize the expanding role of pathology and the medical laboratory in modern health care.

Medical Department

• HARPER & ROW, PUBLISHERS

The American Journal of PATHOLOGY

GENERAL INFORMATION

Editorial Communications: All correspondence concerning editorial matters should be addressed to the Editor-in-Chief, DR. THOMAS D. KINNEY, Department of Pathology, Duke University Medical Center, Durham, N.C. 27706.

Business Communications: All subscriptions and advertising inquiries should be addressed to: MEDICAL DEPARTMENT, HARPER & ROW, PUBLISHERS, 2350 Virginia Ave., Hagerstown, Md. 21740.

Rates: THE AMERICAN JOURNAL OF PATHOLOGY is issued monthly, four volumes per year. Regular (individual) subscriptions: \$27.50 per year in the U.S. and Possessions; \$30.00 per year in Canada and countries of the Pan-American Postal Union; and \$31.00 elsewhere. Special rate for Interns and Residents: \$16.00 per year (\$1.50 extra postage in Canada and countries of the Pan-American Postal Union; \$2.50 extra postage elsewhere). Regular (individual) subscriptions and Resident and Intern subscriptions must be in the names of, and billed to, individuals. Institutional subscriptions, available to all libraries, schools, clinics, and hospitals, to all government agencies, local or national, and to all private or public institutions and organizations: \$35.00 per year in the U.S. and Possessions; \$37.50 per year in Canada and countries of the Pan-American Postal Union; \$38.50 per year elsewhere. All subscriptions are payable in advance. Single copies, when available, \$4.00.

Back Issues: Single issues and complete volumes of THE JOURNAL published prior to 1961 may be purchased from Walter J. Johnson, Inc., 111 Fifth Ave., New York, N.Y. 10003.

INDEX TO ADVERTISERS

Dow Chemical Company ..	2nd Cover, 1
Erie Scientific Div. of Sybron Corp. . . .	2
Harper & Row, Publishers	8, 12, 13, 16, 17
E. Leitz, Inc.	4th Cover
Lipshaw Manufacturing Corporation ..	5
The C. V. Mosby Company	14
Ortho Diagnostics	9, 10, 18
Sigma Chemical Company	7
Unitron Instrument Company	15
John Wiley & Sons, Inc.	6
The Williams & Wilkins Company	11

MOVING?

To avoid interruption in your receipt of this Journal, we need to know your new address—six weeks in advance.

When writing us, be sure to type or print clearly your name and your new address—complete with zip code. It is *essential* that you also list your old address.

IMPORTANT: We publish a number of medical and scientific periodicals. Therefore, please be sure to give the name of THIS Journal when you write us.

Thank you for cooperating!

MEDICAL DEPARTMENT
Harper & Row, Publishers, Inc.
2350 Virginia Ave.,
Hagerstown, Md. 21740.

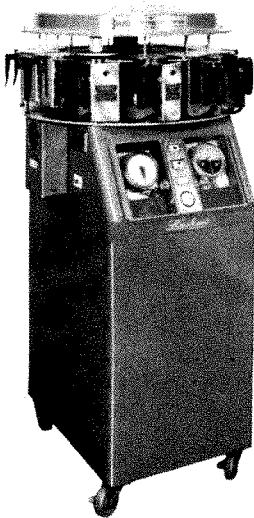
Lipshaw

No. 2500

TRI3MATIC

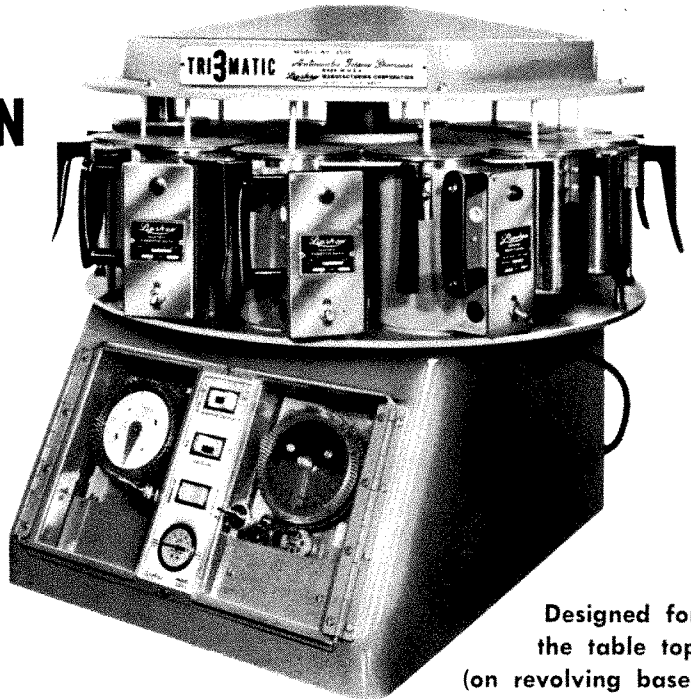
*Automatic
Tissue Processor*
(PATENTS APPLIED FOR)

**TRIPLE
AUTOMATION**
*three
operations
in one*



Mounted on
portable
floor cabinet

Please Request
Complete Literature



Designed for
the table top
(on revolving base)

TRI-MATIC, as the name implies, provides the tissue laboratory with a **MULTI-PURPOSE** instrument designed for continual use. With the flick of the selector switch, the following operations are at your service . . .

1. CONVENTIONAL FIXATION, DEHYDRATION AND IMPREGNATION
2. VACUUM AND HEAT FACILITIES FOR FAST TISSUE PROCEDURES
3. AUTOMATIC STAINING



**LOOK
TO
LIPSHAW**

for the world's most complete line of equipment for the Pathologist: Microtomes, Cryotomes, Tissue Processors, Embedding Appliances, Stainers, Slide Cabinets, Ovens, Autopsy Tables, Instruments and allied products.

Lipshaw

MANUFACTURING CORPORATION
7446 CENTRAL AVENUE • DETROIT, MICHIGAN 48210

WILEY-INTERSCIENCE

DEVELOPMENTAL PSYCHOBIOLOGY

An International Journal

Editor-in-Chief: **Gilbert W. Meier,**

University of Nebraska College of Medicine

Associate Editors: **Robert J. Ellingson,** *Nebraska Psychiatry Institute;*

Williamina A. Himwich, *Galesburg State Research Hospital;*

Austin H. Riesen, *University of California, Riverside*

**What are the pathological consequences of undernutrition
in the young rat?**

**How can inhibition of taurine levels affect organ development
in vertebrates?**

What are the effects of chronic prenatal irradiation in mice?

These are just a few of the issues explored and reported in past issues of this up-to-the-minute journal for every worker concerned with the relation of physiological, environmental, and genetic factors to an organism's development and function. Founded in 1968 to insure prompt publication of research investigations, DEVELOPMENTAL PSYCHOBIOLOGY continues to provide a forum for the rapid dissemination of human and animal studies of pre- and post-natal, and early adolescent organisms experimentally treated and assessed for neurological, endocrinological, enzymatic, and behavioral consequences.

Recent issues have included—

DEVELOPMENT OF A FATTED MALE PHENOMENON IN CALIFORNIA SEA LIONS—*Ronald J. Schusterman and Roger L. Gentry*

ONTOGENY OF VISION IN THE PEKING DUCK (*Anas platyrhynchos*): THE PUPILLARY LIGHT REFLEX AS A MEANS FOR INVESTIGATING

VISUAL ONSET AND DEVELOPMENT ON AVIAN EMBRYOS—*Marieta B. Heaton*

PROBLEMS IN RECORDING VISUAL EVOKED RESPONSES IN HUMAN INFANTS—*R. J. Ellingson*

Due to appear in future issues—

BEHAVIORAL EFFECTS OF NEONATAL IRRADIATION OF THE CEREBELLUM. III. QUALITATIVE OBSERVATIONS IN AGED RATS—*Robert B. Wallace, Craig E. Daniels, and Joseph Altman*

RESPONSIVENESS TO SIMPLE AND COMPLEX AUDITORY STIMULI IN THE HUMAN NEW-

BORN—*Gerald Turkewitz, Herbert G. Birch, and Kenneth K. Cooper*

THE TRANSITION FROM FILIAL TO REPRODUCTIVE FUNCTION OF "COITUS-RELATED" RESPONSES IN YOUNG GUINEA PIGS—*Lawrence V. Harper*

Volume 5—Four Issues Subscription Price: \$15.00 (Foreign Postage: \$2.00)

Available directly from the publisher—

WILEY-INTERSCIENCE, Dept. 093-A 2670-WI, 605 Third Avenue, New York, N.Y. 10016
In Canada: 22 Worcester Road, Rexdale, Ontario

WILEY-INTERSCIENCE, Dept. 093-A 2670-WI, 605 Third Avenue, New York, N.Y. 10016

Gentlemen: Please enter _____ subscription(s) to DEVELOPMENTAL PSYCHOBIOLOGY: An International Journal, beginning with Volume 5, No. 1

Subscription Price: \$15.00

Foreign Postage: \$ 2.00

(Back issues available on request.)

☐ My check (money order) for \$ _____ is enclosed.

☐ Please bill me.*

NAME _____

TITLE _____

COMPANY _____

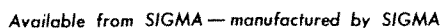
ADDRESS _____

CITY _____

STATE _____ ZIP _____

wiley

*Restricted to the
continental United States.



(NAD-Diaphorase)

Technicon Reference No. 0193

For the Colorimetric determination of LDH per AutoAnalyzer®, AA-II®, and SMA® Procedures. Reconstitute with water to prepare "working solution".

Order: Stock No. 940-3	25 ml lyophilized vial	\$ 7.75
	40 ml lyophilized vial	10.50

Larger quantities - Inquire - We guarantee the best prices.

CIF Destination Anywhere in the World via Air

For those laboratories that prefer to prepare their own blend, we offer the finest NAD and Diaphorase individually and at most competitive prices.

Also available from SIGMA — manufactured by SIGMA

(DPNH/MDH; NADH/MDH)

Technicon Reference No. 0444

For the Ultraviolet determination of SGOT per AA-II® and SMA® Procedures. Reconstitute with water to prepare "working solution".

Order: **Stock No. 936-3** 50 ml lyophilized vial 12 vials \$37.50

Larger quantities • Inquire

CIF Destination Anywhere in the World via Air

If you prepare your own blend, call Sigma for the highest purity NADH (DPNH) and MDH (Malic Dehydrogenase).

® - Registered Trade Marks of Technicon Corporation

DON'T YOU BELIEVE the false rumors being circulated by a misguided competitor who claims that he is the only basic manufacturer of Diaphorase and certain other reagents.

SIGMA is the World's Foremost manufacturer of most of the important Enzymes and Substrates used in Automated and Manual Procedures. All of the above DIAPHORASE, DPN, DPNH, and MDH are produced by SIGMA.

Our Quality is guaranteed to be TOPS; our Prices are guaranteed to be BOTTOM!

It's a pleasure doing business with Sigma

ORDER DIRECT — TELEPHONE COLLECT from ANYWHERE in the WORLD
Day, Station to Station, 314-771-5750 (Including Saturday and Sunday until 1 P.M.)

Night, **Person to Person**, Dan Broida, 314-993-6418

TWX [Teletype] Day or Night: COLLECT 910-761-0593

TELEGRAM: SIGMACHEM, Saint Louis, Missouri

The Research Laboratories of

P.O. BOX 14508 • SAINT LOUIS, MISSOURI 63178 U.S.A.

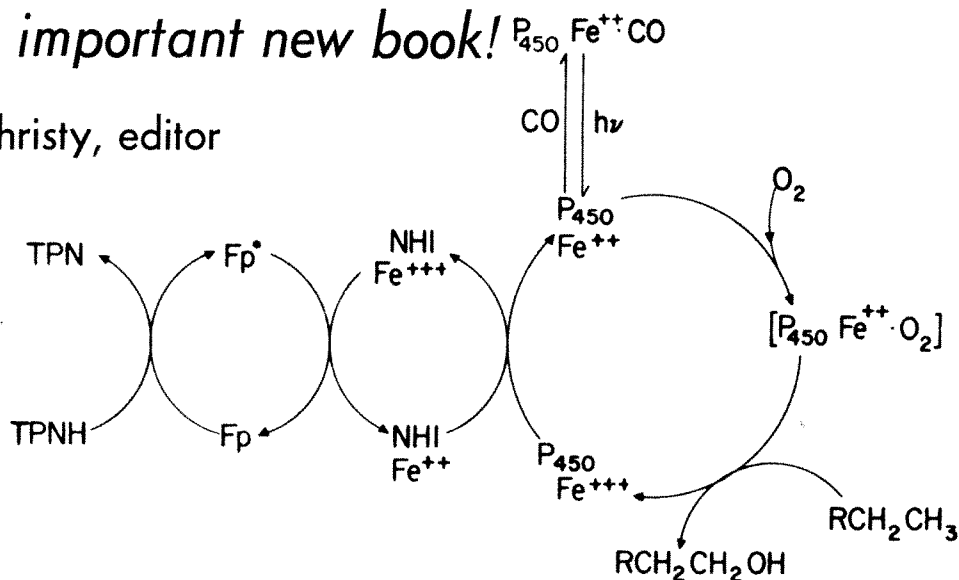
MANUFACTURERS OF THE FINEST BIOCHEMICALS AVAILABLE

Distributed through:

SIGMA LONDON Chem. Co. Ltd. • 12, Lettice St., London, S.W.6., England • Telephone: 01-736-5823 (Reverse Charges)
SIGMA ISRAEL Chem. Co. Ltd. • 28 Kel-Gimel St., Givataim, Israel • Telephone: 03 760654 (Reverse Charges)

An important new book!

Christy, editor



The Human Adrenal Cortex

NEW! Written by twenty-three leading authorities who have made outstanding contributions in their field, this new book examines the biochemistry, physiology, pathologic physiology, and clinical aspects of adrenocortical function and disease. It's extensive with new approaches in chapters concerning mode of action of adrenocortical steroids, control of secretion, iatrogenic Cushing's, naturally-occurring Cushing's syndrome (including excerpts from a Russian paper previously unpublished in English), aldosterone, and others. There is a unique discussion of fetal adrenal cortex as well as an exhaustive treatment of all forms of hyper- and hypofunction of the adrenal cortex. Special treatment of the physical state of adrenal hormones in the blood and an unusually comprehensive view of the metabolism of steroids are also included. Pathogenesis, clinical features, and the management of adrenal disease are all covered authoritatively.

By 23 Authors. Edited by **Nicholas P. Christy, M.D.**, Chairman, Department of Medicine, Roosevelt Hospital; Clinical Professor of Medicine, College of Physicians and Surgeons Columbia University; Visiting Physician, Francis Delafield Hospital; Associate Attending Physician, Vanderbilt Clinic—all in New York City.

552 Pages. 72 Illustrations. \$25.00

HARPER & ROW, Publishers, Inc.

Medical Department

Mail Order Dept. 2350 Virginia Avenue Hagerstown, Md. 21740

Please send me on approval:

☐ Christy: **THE HUMAN ADRENAL CORTEX**.....\$25.00

Name.....

Address.....

City.....State.....Zip.....

AJP-4.

A superior
guidance system
totally programmed
for blood
compatibility
control

the program...

a self-contained, complete and concise
procedural manual...designed to standardize
and control blood bank procedures.



ORTHO DIAGNOSTICS

Raritan, New Jersey 08869

the programmer...

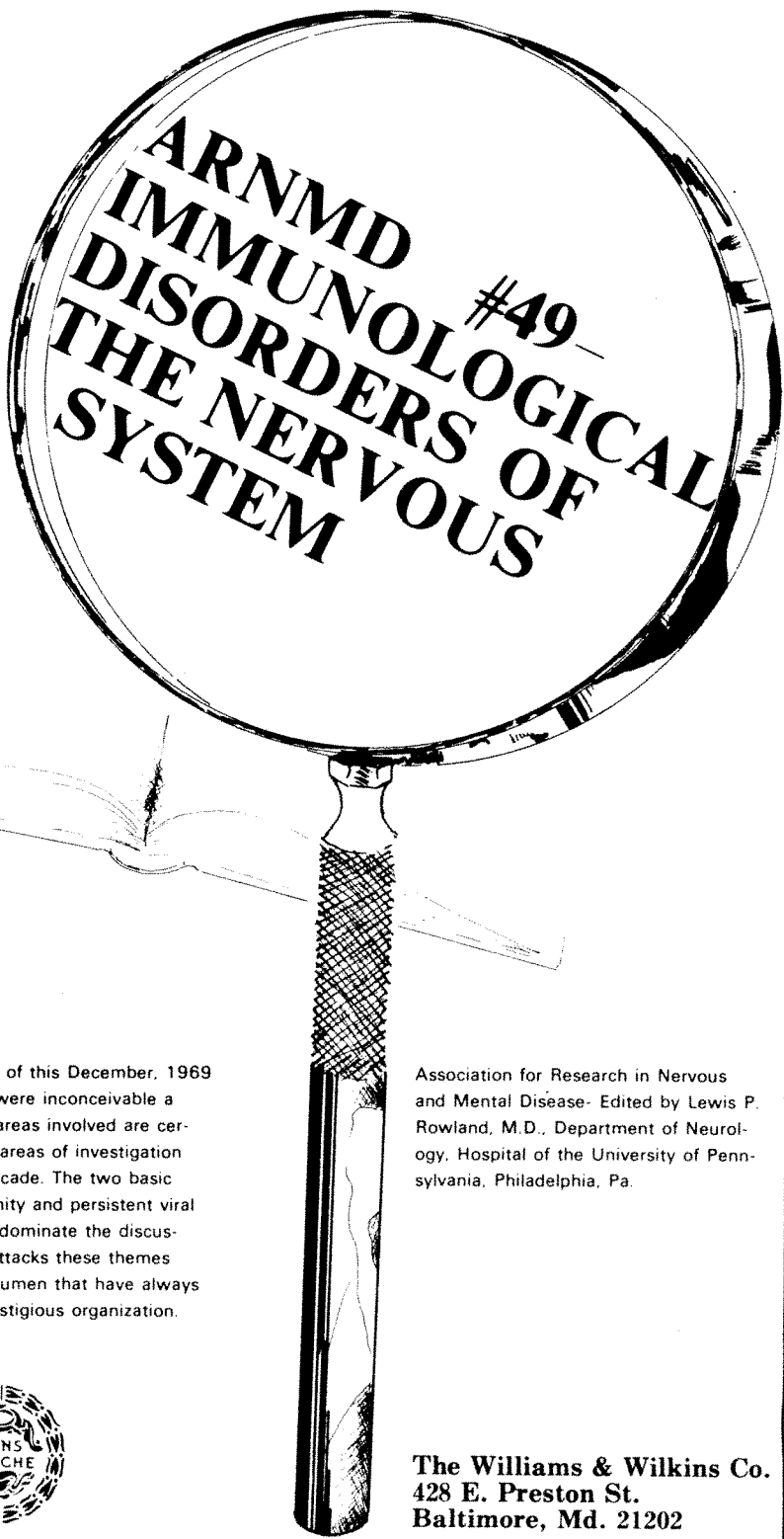
an integrated, complete system
for blood processing
with the built-in capability
for establishing
continuity and control
in grouping and typing,
antibody screening,
reverse grouping
and compatibility testing.

your ORTHO Representative
will show you how this
unique program can benefit
your laboratory.



ORTHO DIAGNOSTICS

Raritan, New Jersey 08869



ARNMD #49- IMMUNOLOGICAL DISORDERS OF THE NERVOUS SYSTEM

Some of the subjects of this December, 1969 meeting of ARNMD were inconceivable a decade ago, but the areas involved are certain to be prominent areas of investigation during the coming decade. The two basic themes of autoimmunity and persistent viral infection seem to predominate the discussions, and ARNMD attacks these themes with the vigor and acumen that have always characterized this prestigious organization.

1971/\$25.00



Association for Research in Nervous and Mental Disease- Edited by Lewis P. Rowland, M.D., Department of Neurology, Hospital of the University of Pennsylvania, Philadelphia, Pa.

The Williams & Wilkins Co.
428 E. Preston St.
Baltimore, Md. 21202

Professional Opportunities

INTERNSHIPS/RESIDENCIES

BERKSHIRE MEDICAL CENTER—PATHOLOGY residency; a 425 bed acute care teaching hospital affiliated with Albany Medical College; fully approved for American Boards in pathologic anatomy and clinical pathology; year round vacation area, skiing, sailing, tennis, etc; close to Tanglewood (Boston Symphony Orchestra) and other music festivals; 2½ hours to Boston, 3 hours to New York, 4½ hours to Montreal; salary, internship \$9000; residency \$9600-\$13,000; rooms are available for single house staff to rent at \$40 per month; hospital-owned apartments for married house officers are available for rental; opportunities for additional income; large well equipped highly automated air-conditioned laboratories with computer being installed; approved School of Cytotechnology with 2 students; approved School of Medical Technology with 16 students; five Board certified pathologists and a Ph.D. chemist; each principal section of the laboratory, i.e., anatomic pathology, microbiology, clinical chemistry, hematology and blood bank is in the charge of a pathologist with special interest, experience and qualifications in these fields who devotes 95% of his time to the work of his section; ECFMG certificate required. Apply Dr. W. Beautyman, Pathologist, Berkshire Medical Center, 725 North Street, Pittsfield, Mass. 01201.

PATHOLOGIST. CERTIFIED AP AND CP, Ph.D IN BIOCHEMISTRY, 6 years experience. Desires academic position. Reply: Box 58 c/o AJP.

CLASSIFIED ADVERTISING INFORMATION

RATES:

	1 Time	3 Times	6 Times or more
Non Display:			
20 words or less	\$19.00	\$16.00	\$14.00
Each additional word	.50	.50	.50
Box Service—\$2.00—First insertion only			

	1 Time	3 Times	6 Times or more
Classified Display:			
	\$35.00	\$30.00	\$25.00
	per inch	per inch	per inch

Minimum Space—One (1) column inch

SEND ALL COPY,
AND BOX NUMBER INQUIRIES TO:

**THE AMERICAN JOURNAL
OF PATHOLOGY**

Classified Dept.
131 Mineola Blvd.
Mineola, N. Y. 11501
(516) PI 6-0092

A book for every physician

THE DIAGNOSTIC INTERVIEW

by Ian Stevenson, M.D.

Formerly titled **MEDICAL HISTORY-TAKING**, this new edition describes in a systematic manner what is known about the *do's* and *don'ts* of medical history-taking. Part I discusses the important factors affecting the doctor-patient relationship and how this relationship influences the outcome of medical interviews. It also considers other general principles of importance for the interview. Part II describes what information is to be obtained during the interview. In Part III, the author considers the techniques to be employed. Numerous examples of actual interviews are given including examples of common errors that should be avoided. Throughout the book, the author emphasizes the importance of observing the patient's non-verbal communications as well as his verbal statements.

In the new second edition, more emphasis has been given to the influence of the interviewer-patient relationship in shaping the information given by the patient. Greater emphasis is also given to the current situation of the patient as an influence on how he sees and describes his earlier life.

The references have been completely updated. This book is written for the practitioners of all branches of medicine, at all levels, who wish to improve their skills in interviewing while avoiding specialized psychiatric jargon.

By **IAN STEVENSON, M.D.**, *Alumni Professor of Psychiatry, Department of Psychiatry, University of Virginia School of Medicine, Charlottesville.* 320 pp., 12 illus., \$6.00.

HARPER & ROW, Publishers

Medical Department
Mail Order Department
2350 Virginia Avenue, Hagerstown, Md. 21740

Please send me on approval.

☐ Stevenson:

THE DIAGNOSTIC INTERVIEW\$6.00

☐ Bill me ☐ Check enclosed (SAVE!
We pay postage and handling)

Name

Address

City State Zip.....

AJP-4.

Announcing for 1972!

infectious diseases

With over 80 contributors, edited by Dr. Paul D. Hoeprich, this major reference work considers diseases caused by viruses, chlamydia, rickettsia, mycoplasmas, bacteria, spirochetes, protozoa, helminths and some ectoparasites. Each disease is discussed as a discrete clinical entity and is presented from the point of view of the organ-system involved thus affording to its reader a clinical and practical approach to diagnosis and treatment. Epidemiology and pathogenesis are emphasized throughout as they are keys to understanding the interactions of host and parasite. With some 300 illustrations to complement the text, *this book offers a completeness previously unavailable in one volume!*

Advance orders now accepted!

HARPER & ROW, Publishers, Inc.

Medical Department

Mail Order Dept.

2350 Virginia Avenue

Hagerstown, Maryland 21740

☐ Please send me *on approval*, when it is published:

INFECTIOUS DISEASES

Name

Address

City State Zip AJP-4.

Widely accepted as THE classic reference. . . newly modified to reflect changing concepts and clinical practice!

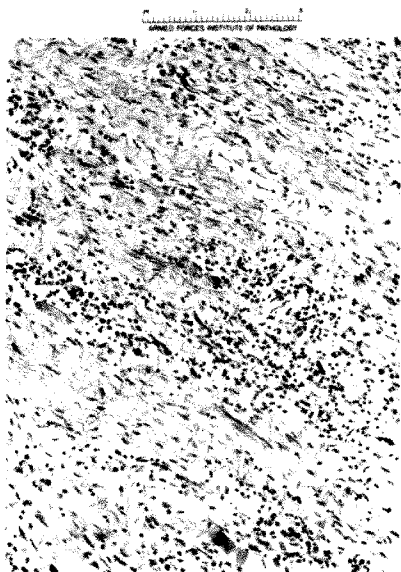


Fig. 24-22. Graves' disease with malignant exophthalmos. **A**, Severe periorbital edema and chemosis as well as protopsis. **B**, Massively enlarged extraocular muscles. **C**, Markedly degenerated extraocular muscles scarred and infiltrated by mononuclear inflammatory cells. (**A**, AFIP 55-3860; **B**, AFIP 55-10706; **C**, x145; AFIP 58-13128.)

New 6th Edition!

PATHOLOGY

Edited by W. A. D. Anderson,
M.D., M.A., F.A.C.P., F.C.A.P.

Widely recognized as the foremost authority on both general and specialized pathology, this newly revised two-volume reference has been modified to include significant advances in knowledge and understanding of disease processes. Updated and expanded discussions by 45 eminent contributors correlate pathologic concepts with clinical practice. In addition, this unmatched compendium reflects the growing interrelationship of the medical sciences and biology, recording progress in the fields of ultrastructure, cytology, genetics, immunopathology, and biochemistry.

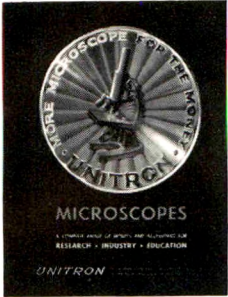
Completely rewritten chapters examine inflammation and healing, drug and chemical injury, ophthalmic pathology, upper respiratory tract and ear, lower urinary tract, prostate and male genitalia, hemopoietic system, thymus, pituitary gland, thyroid gland, parathyroid glands, adrenal glands, and nervous system and skeletal muscle. Major changes highlight the material on hypersensitivity diseases and immunopathology, mycotic infections, viral diseases, neoplasms, and diseases of kidney, lung, liver and pancreas.

Unsurpassed in scope and scientific accuracy, this new 6th edition maintains its place as the most widely accepted single reference on all aspects of clinical pathology. Evaluate its usefulness as a day-by-day source of practical information . . . order your copy today!

Edited by W. A. D. ANDERSON, M.A., M.D., F.A.C.P., F.C.A.P., Professor of Pathology and Chairman of the Department, University of Miami School of Medicine, Miami, Fla.; with 45 contributors. November, 1971. 6th edition, 2 volumes, 1,862 pages plus Fm I-XIV and duplicate indexes, 7 $\frac{1}{4}$ " \times 10 $\frac{1}{2}$ ", 1,566 illustrations and 6 color plates. Price, \$29.50.

MOSBY
TIMES MIRROR

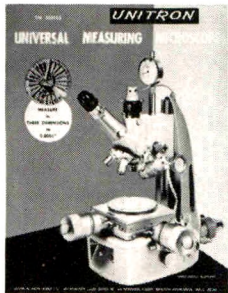
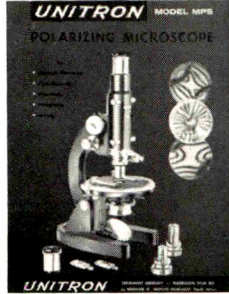
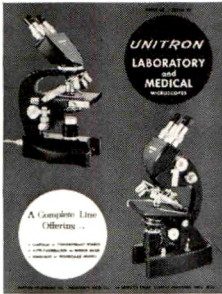
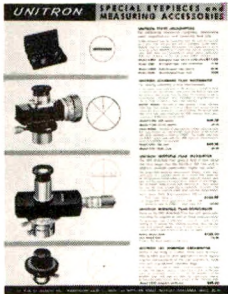
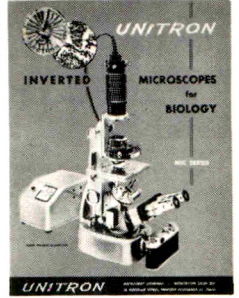
THE C. V. MOSBY COMPANY
11830 WESTLINE INDUSTRIAL DRIVE
ST. LOUIS, MISSOURI 63141



FREE MICROSCOPE BUYING GUIDE

Shown here in miniature are just some of the informative brochures which comprise the UNITRON Catalog . . . your buying guide to quality microscopes at prices within your budget. Whether your application is routine laboratory analysis, advanced biological research, or industrial quality control, you will find the instrument you need in UNITRON's complete line.

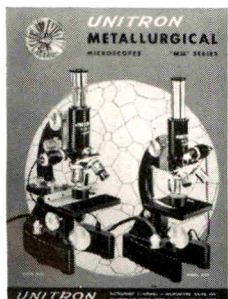
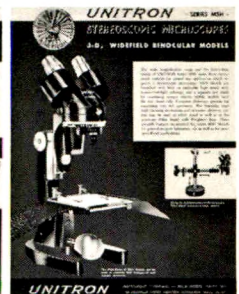
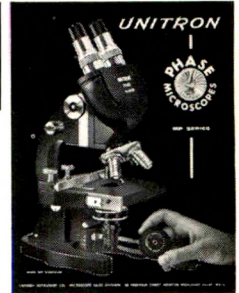
A UNITRON MICROSCOPE CATALOG is Yours for the Asking.



TRY ANY UNITRON MICROSCOPE FREE FOR 10 DAYS

A salesman's demonstration gives you only about 30 minutes to examine a microscope, hardly the best conditions for a critical appraisal. But UNITRON's Free 10 Day Trial gives you the opportunity to evaluate any model in your own laboratory and prove its value in your own application before you decide to purchase. See for yourself, as have thousands of other buyers, why . . .

UNITRON Means More Microscope for the Money.



Please send UNITRON's Microscope Catalog No. Q-16

Name _____

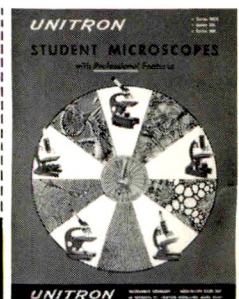
Company _____

Address _____

City _____ State _____ Zip _____

UNITRON
INSTRUMENT COMPANY

MICROSCOPE SALES DIVISION
66 NEEDHAM STREET
NEWTON HIGHLANDS
MASSACHUSETTS 02161



Laboratory

**it's brand new now...
and
for years to come,
it will stay that way...**

Medicine

Editor: George J. Race, M.D., M.S.P.H., Ph.D., Pathologist-in-Chief and Director of Laboratories, Baylor University Medical Center, Dallas, Texas.

Associate Editors: Clinical Pathology—Samih Y. Alami, M.D., Ph.D. Hematology—Eugene P. Frenkel, M.D. Chemistry—Robert J. Speer, Ph.D., Harold H. Varon, M.D., and Joel E. Young, Ph.D. Microbiology—Ralph Tompsett, M.D. With 100 Contributors.

In Three Volumes. Here is a new exhaustive coverage presented for the first time as a loose-leaf reference. The dynamic loose-leaf concept means that your three volumes will always be new and updated through the ANNUAL SERVICE. *Volume 1* is entirely devoted to Clinical Chemistry, including the most modern automated techniques in use. *Volume 2* concerns Hematology, Blood Banking, Medical Microbiology, Virology, Serology, and Immunology. *Volume 3* covers Body Fluids including Urine, Cytology and Cytogenetics, Special Techniques (with modern methods and approaches to forensic pathology), and Laboratory Management and Function. A separate annually revised index is included. *For all the future information coming out in the various fields covered in these volumes, it is a worthwhile investment for knowledge and practice.*

ANNUAL SERVICE includes:

"New pages for old." Partially or completely rewritten monographs, addenda and chapters on new subjects supplied annually along with a completely revised index.

HARPER & ROW, Publishers, Inc.
2350 Virginia Avenue

Medical Department
Hagerstown, Maryland 21740

☐ Please send more information on LABORATORY MEDICINE
LABORATORY MEDICINE (3 vols. & 1st yr. Annual Service):
About \$200.00.

About \$30.00 a year thereafter for Annual Service. (Terms Available)

☐ Bill me @ full price. ☐ Bill me @ \$_____ a month
(minimum \$10.00 a month)

Name

Address

City State Zip AJP-4.

never a case of masked identity



differentiate with
MONOSPOT
TRADEMARK
slide test for infectious mononucleosis



ORTHO DIAGNOSTICS

Raritan, New Jersey 08869

© O. D. 1988

Spontaneous Atherosclerosis in Pigeons

A Model System for Studying Metabolic Parameters Associated with Atherogenesis

Robert F. Santerre, PhD, Thomas N. Wight, MS, Samuel C. Smith,
PhD and David Brannigan, MS

The interpretation of metabolic studies related to early changes in spontaneous atherosclerosis has been hampered by the focal nature of the disease and by the lack of a well-defined model system of the disease process. Gross, histologic and ultrastructural observations of lesion development at the celiac bifurcation of the aorta in atherosclerosis-susceptible White Carneau and atherosclerosis-resistant Show Racer pigeons are compared and discussed in terms of hemodynamics, muscular aggregation and altered metabolism of smooth muscle cells. Detailed knowledge of the morphologic sequence of events in lesion localization makes the celiac bifurcation in White Carneau and Show Racer pigeons a useful model for genetic comparisons of arterial wall metabolism and for investigating metabolic alterations occurring with atherogenesis. (Am J Pathol 67:1-22, 1972)

CORRELATION OF THE MANY FACTORS reportedly influencing atherosclerosis has proven difficult in experiments with intact animals. Diet, blood lipids, environmental stress, hemodynamics, alterations in arterial structure, and metabolism are but a few of the factors implicated in initiating atheromatous changes. Moreover, interpretation of reports associating metabolic alterations in the intact aorta with atherosclerosis has been hampered by the focal nature of the disease and by an inability to follow these alterations through transition stages in lesion development.¹ In an effort to control these variables, much research has been done with experimental atherosclerosis as a model system.

From the Biomolecular Hygiene Laboratories, Department of Animal Sciences and Department of Zoology, University of New Hampshire, Durham, NH.

Supported in part by the New Hampshire Heart Association and by the New Hampshire Agricultural Experiment Station.

Accepted for publication September 16, 1971.

Address reprint requests to Dr. Samuel C. Smith, Department of Animal Sciences, Kendall Hall, University of New Hampshire, Durham, NH 03824.

However, spontaneous atherosclerosis has been shown to differ from the experimentally induced disease in many respects², and there are no well-defined model systems for study of the spontaneous process.

Clarkson, Lofland, Prichard and co-workers³⁻⁸ have described spontaneous aortic atherosclerosis in White Carneau pigeons and pointed out its close resemblance to the human disease. Cooke and Smith⁹ subsequently described ultrastructural aspects of normal and diseased pigeon aortas. Differences in susceptibility between inbred strains of pigeons have been utilized to study relationships between various metabolic patterns and atherosclerosis.¹⁰⁻¹²

This communication extends previous work by describing the sequential development of atheromatous lesions in the celiac bifurcation of aortas from atherosclerosis-susceptible White Carneau and atherosclerosis-resistant Show Racer pigeons. Lesion development is related to histology, topography, hemodynamics, and intimal thickening. Spontaneous atherogenesis in the celiac bifurcation is presented as a model system for the study of metabolic parameters in the arterial wall that may be associated with the disease.

Materials and Methods

Subjects

Forty-three White Carneau (WC) and 30 Show Racer (SR) pigeons were examined. The majority were between 1 and 6 years of age with a few embryos and post-hatch squabs included. Sexes were nearly equally represented. All birds were derived from inbred lines maintained by the Palmetto Pigeon Plant, Sumter, SC. Most of the birds older than 1 year were housed in fly-coops, and the 1-year-old birds were reared in battery cages with approximately 2 sq ft of floor space per bird. The pigeons were fed either a mixture of yellow corn, wheat, peas, kafir and health grit or Purina pigeon pellets and similar health grit.

Light Microscopy

All birds were sacrificed by exsanguination. The entire aorta from the arch down to, but usually not including the trifurcation, was removed, washed in warm (37 C) buffered saline, pH 7.4, cleaned of excess connective tissue, and fixed at room temperature for 30-90 minutes in 3% phosphate-buffered glutaraldehyde, pH 7.4. After fixation, aortas were rinsed briefly in saline, immersed in Tissue-Tek O.C.T. Compound (Ames Company, Miles Laboratories, Inc, Elkhart, Ind) and quick-frozen at -18 C. A serial survey of each aorta was made by cutting two or three 8- μ cross sections every 700-800 μ ; the sections were stained with hematoxylin-eosin, hematoxylin-oil red O (ORO), and sometimes Alcian blue-safranin O.

A severity index was obtained for each aorta by comparing hematoxylin-ORO stained sections with a series of 6 grades ranging from 0 to 5 (see Fig 7-11). The grading system was based on the following five criteria:

1. Amount of lipid present.
2. Extent of proliferation.
3. Amount of luminal circumference affected.

4. Degree of luminal occlusion.
5. Extent of necrosis, calcification and vascularization.

Although the entire aorta was surveyed, the celiac bifurcation demonstrated the most severe lesions and most important breed differences at 6 years. For this reason the detailed study of lesion development in this segment was undertaken.

Electron Microscopy

Advanced plaques were fixed in 3% glutaraldehyde—0.1 M cacodylate buffer, pH 7.3, washed in cacodylate-buffered 6% sucrose, postfixed in 2% osmium-Veronal, pH 7.3, dehydrated in a graded series of alcohols and embedded in Epon. Adjacent thick (1 μ) and thin sections were cut on a Porter-Blum MT-2 ultramicrotome. Thin sections were stained with saturated uranyl acetate solution and Reynolds lead citrate, and examined with a Philips EM200 electron microscope.

Results

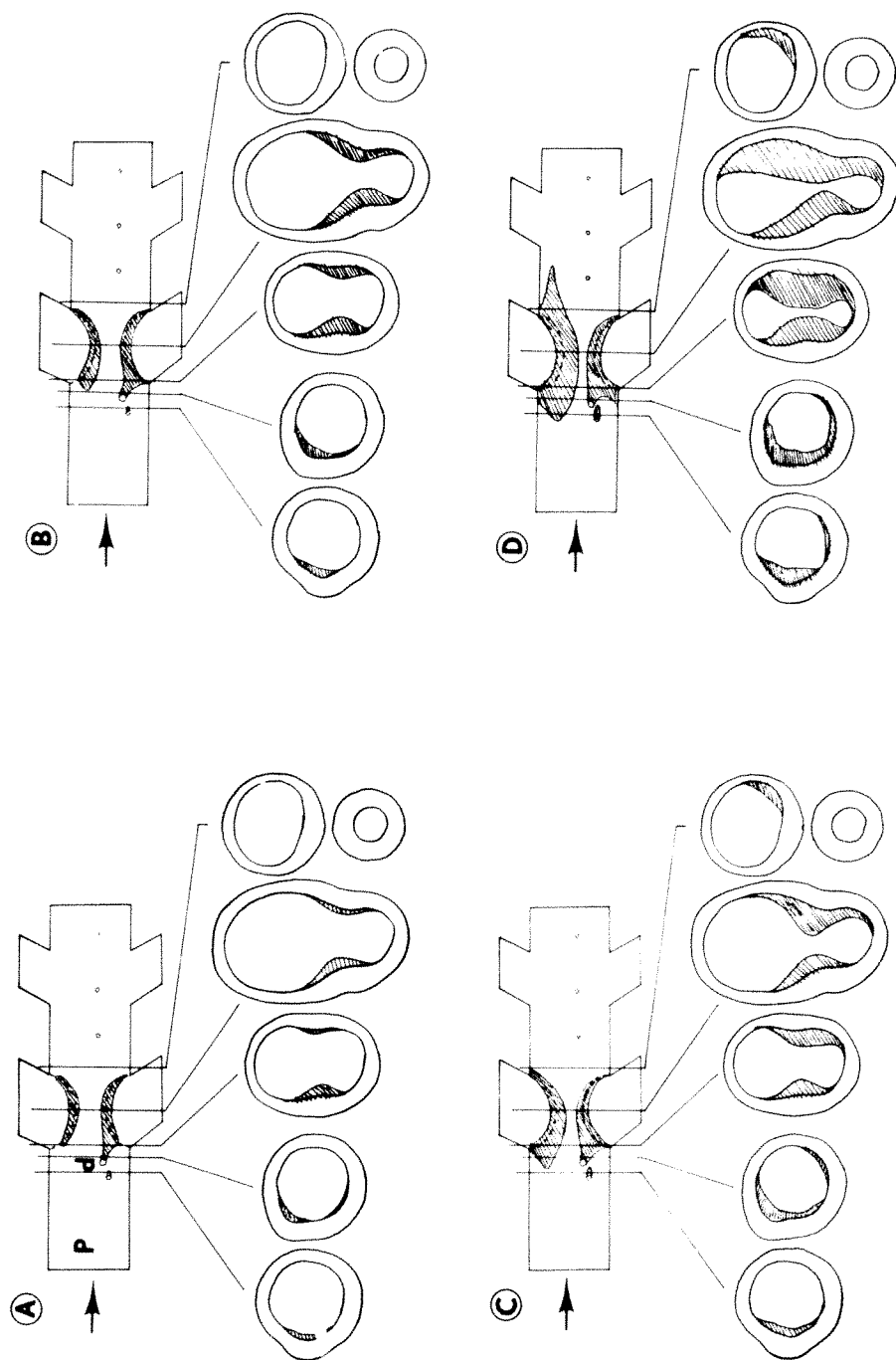
Gross Observations

In the aortas of squabs, prior to the appearance of lipid, ridge-like thickenings were seen arising from the lateral edges of the celiac orifice and extending diagonally in a proximal direction (Fig 1). At 4–6 months, the earliest visible lipid accumulation appeared as a fine white stippling on the surface of these cushions. As lesion development continued, the lipid became yellow and the surface of the area was raised and was either rough or smooth. At later stages, the main plaque, projecting well into the lumen, had a nodular, pearly appearance and was usually surrounded by a roughened, yellow skirt of involved tissue, sometimes fan-shaped and extensive in the proximal aspect (Fig 2). In advanced lesions, ulceration sometimes was evident, particularly in centrally depressed regions of the largest plaques.

The topography of lesion development in the celiac bifurcation was quite specific (Text-fig 1). In the young WC pigeon, lesions appeared earliest in the left lateral cushion lying below the ductus arteriosus. In older birds, lesion development in the right lateral cushion progressed more rapidly, and, by 6 years, involvement was greatest in this cushion. No consistent differences in lesion development between right and left cushions were seen in the SR. In both breeds, involvement of areas surrounding the cushions progressed mainly upstream and laterally.

Light Microscopy

A prominent feature of the celiac bifurcation in embryos and very young birds was the presence of paired muscular intimal thickenings corresponding to the ridge-like thickenings observed grossly (Fig 3). The smooth muscle cells in these cushions were oriented longitudinally and the laminar organization of elastica present in the media is



TEXT-FIG. 1—Diagrammatic representation of lesion progression in the cushions of the celiac orifice. In A and B, the left cushion (*lower*) beneath the ductus arteriosus (*d*) is the most highly involved. The more rapid progression of the right cushion (*upper*) is depicted in C and D. Lesions progress mainly in the lateral and proximal direction (*P*). The extent of luminal occlusion can be followed in the cross-sectional diagrams. Cross-hatching represents proliferative growth with lipid accumulation. Direction of blood flow is indicated by arrows.

interrupted here (Fig 4). The muscular nature of these cushions was emphasized because only in these smooth muscle cell aggregations did significant lipid accumulate leading to the production of advanced plaques.

The earliest evidence of atherosclerotic change in 4- to 6-month-old birds was the appearance of fine lipid droplets in the endothelium and subendothelium of the cushion (Fig 5). Later, fine lipid droplets became more prominent, appearing in the deeper regions of the cushion. Some proliferation of smooth muscle cells could also be seen at this time (Fig. 6). By 1 year, this proliferative response could be a distinctive feature (Fig 7A), and lipid involvement was frequently more extensive with some larger lipid pools (probably extracellular) accumulating (Fig 7B). Fragmentation of elastic laminae was also evident (Fig 7A).

With further development, luminal protrusion of the lesion was amplified, producing partial occlusion of the vessel. Large amorphous pools of lipid were found in necrotic centers of these plaques (Fig 8A and B). In this and later stages, lesions expanded not only luminally, but laterally and medially as well, by muscular transition of normal elastic areas.

Beyond this stage, most lesions developed a fibrous cap of modified smooth muscle cells. In regions underlying the fibrous cap, fatty degeneration and formation of cholesterol clefts were frequently seen. Luminal occlusion was a striking feature at this stage (Fig 9A and B). In the most advanced stages, a variety of features were commonly encountered: massive fibrosis (Fig 10A), sometimes nearly complete luminal occlusion, necrosis and further lipid accumulation, vascularization (Fig 10B), ossification (Fig 10C) and ulceration. No thrombi and very few lymphocytes or macrophages were seen. Accumulation of acid mucopolysaccharide was also commonly seen in advanced plaques.

Electron Microscopy

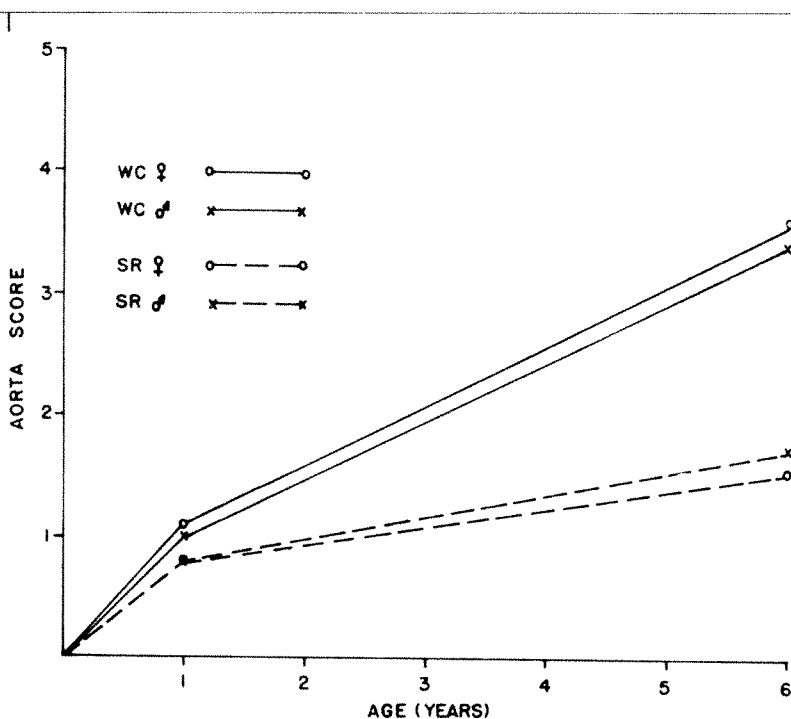
Ultrastructurally, the fibrous cap of advanced lesions contained long, spindle-shaped, modified smooth muscle cells, foam cells and prominent collagen bundles. Upper regions of the cap contained modified smooth muscle cells having few myofilaments with fusiform dense bodies, a patchy basement membrane envelope, typical pinocytotic vesicles along the cell membrane, numerous mitochondria, much granular endoplasmic reticulum and many polysomes and free ribosomes (Fig 11). Modified smooth muscle cells in deeper regions of the fibrous cap

contained a similar array of organelles, often including a prominent Golgi apparatus (Fig 12). However, these cells contained many more myofilaments with fusiform and marginal dense bodies, as well as a distinct basement membrane envelope. Many of the cells contained darkly stained inclusions. In both regions, the extracellular space contained little or no elastin, much collagen and a large amount of vesiculated material perhaps representing cell debris and extracted lipid.

Lesion Scores

Based on the severity index, there was little difference in atherosclerotic involvement between the two breeds up to 1 year of age. However, by 6 years, lesions in the celiac bifurcation averaged 2 grades higher in the WC than in the SR (Text-fig 2). Furthermore, 100% incidence of some degree of histologic lipoidal involvement was found in both breeds of pigeons at 1 and 6 years. The developmental history and histopathology of atherosclerotic plaques of a given grade were similar for both breeds.

While there were no significant differences in severity between sexes



TEXT-FIG 2—Atherosclerotic grade in the celiac bifurcation of male and female White Carneau and Show Racer pigeons as a function of age. Lines between 1 and 6 years are least-square regression plots.

in either breed, the sample size was too small to be conclusive. A trend toward higher grades in the WC female and the SR male was found at 6 years (Text-fig 2).

Discussion and Conclusions

As McGill *et al*¹ pointed out, the lack of data on site-specific lesion development in humans has made it difficult to follow transition stages in atherosclerotic involvement. Our observations in the celiac bifurcation of the pigeon aorta show that fatty streaks can develop into fibrous plaques in a manner similar to that suggested for humans.^{13,14}

Our findings are essentially similar to those in original reports on spontaneous atherosclerosis in pigeons by Clarkson, Lofland, Prichard, and co-workers.³⁻⁸ However, several important distinctions were noted. While they reported a difference in incidence of atherosclerosis between the two breeds^{4,7} our birds exhibited 100% incidence of some degree of involvement in the celiac bifurcation at both 1 and 6 years. We found the major difference between breeds to be a much lower severity index in the SR than in the WC at 6 years. No difference were found in incidence, location, developmental history or histopathology of WC and SR lesions, as has been reported.^{4,7} These similarities suggest that the resistance of the SR may result from subtle metabolic factors.

The pattern of lesion localization and development at the celiac bifurcation is quite predictable. Similar findings have been reported for atherosclerosis in human cerebral and coronary arteries^{15,16} and for arteriosclerosis of the lower extremities.¹⁷ Hemodynamics undoubtedly plays a role in this localization as suggested by numerous workers.¹⁸⁻²³ The work of Caro *et al*²⁴ is most consistent with our observations. As predicted by their model, we find atheroma localized lateral to the celiac orifice and progressing upstream, thus suggesting the presence of low shear rates and poor nutrition due to decreased exchange of materials in these regions. However, hemodynamics is probably not the sole factor causing localization since unique metabolic capabilities have been associated with susceptible regions of the aorta in other animals.^{25,26}

Another very important factor, apparently acting synergistically with hemodynamics to localize lesion development, is the presence of raised muscular cushions representing a normal feature of vascular architecture at the celiac bifurcation and elsewhere.²⁷⁻²⁹ Muscular aggregations exhibit the earliest enzymatic changes associated with atherogenesis³⁰ and proliferative reactions induced by cholesterol feeding are also prominent there.³¹ In our system, aggregations of smooth muscle cells seem to be a necessary prerequisite for lipid accumulation. Further

work on the development of cushions and the role of blood flow in vascular morphogenesis is needed.

The role of smooth muscle cells as the major cell type involved in the development of atherosclerotic lesions in a variety of animals, including cows,³² swine,³¹ rabbit,³³ baboons,³⁴ humans,³⁵ chickens³⁶ and pigeons,⁹ has been well documented. Lesions expand by a proliferative response of normal smooth muscle cells adjacent to regions of necrosis in a manner similar to that seen in the healing of arterial wounds.³⁷ This study and others^{9,31-36,38} suggest that modified smooth muscle cells found in early atheromatous lesions and even those found in fibrous caps of advanced lesions are very active metabolically. Such an interpretation is consistent with the presence of increased granular endoplasmic reticulum, many polysomal rosettes, a prominent Golgi apparatus, and numerous mitochondria in these cells. As Zemlenyi³⁰ has emphasized, the smooth muscle cell seems to dominate the metabolism of the normal arterial wall and of lesions at all stages of atherosclerotic involvement.

This study demonstrates that atherosclerosis in the celiac bifurcation is a predictable phenomenon in terms of histopathology, topography, age and breed differences. It should be possible to isolate metabolic changes associated with the spontaneous disease process in this model system. A better understanding of the role of energy production, altered enzyme patterns and acid mucopolysaccharide metabolism is needed. Unequivocal answers to these questions and others concerning the role of metabolism in atherogenesis will be obtained only through the use of such a defined model system.

References

1. McGill HC, Geer JC, Strong JP: Natural history of human atherosclerotic lesions, *Atherosclerosis and Its Origins*. Edited by M Sandler, GH Bourne. New York, Academic Press Inc, 1963, p 60
2. Comparative Atherosclerosis. Edited by JC Roberts, R Straus. New York, Harper and Row Publishers, 1965
3. Clarkson TB, Prichard RW, Netsky MG, Loffland HB: Atherosclerosis in pigeons: its spontaneous occurrence and resemblance to human atherosclerosis. *Arch Pathol* 68:143-147, 1959
4. Loffland HB, Clarkson TB: A biochemical study of spontaneous atherosclerosis in pigeons. *Circ Res* 7:234-237, 1959
5. Prichard RW, Clarkson TB, Loffland HB, Goodman HO, Herndon CN, Netsky MG: Studies on the atherosclerotic pigeon. *JAMA* 179:49-52, 1962
6. Prichard RW, Clarkson TB, Goodman HO, Loffland HB: Aortic atherosclerosis and its complications. *Arch Pathol* 77:224-257, 1964

7. Prichard RW, Clarkson TB, Loffland HB, Goodman HO: Pigeon atherosclerosis. *Am Heart J* 67:715-717, 1964
8. Prichard RW: Spontaneous atherosclerosis in pigeons,² pp 45-49
9. Cooke PH, Smith SC: Smooth muscle cells: the source of foam cells in atherosclerotic White Carneau pigeons. *Exp Mol Pathol* 8:171-189, 1968
10. Loffland HB, Clarkson TB, Artom C: Lipid synthesis in aorta preparations from atherosclerosis-susceptible or resistant pigeons. *Arch Biochem Biophys* 88:105-109, 1960
11. Loffland HB, Clarkson TB: Certain metabolic patterns of atheromatous pigeon aortas. *Arch Pathol* 80:291-296, 1965
12. St. Clair RW, Loffland HB: Composition and synthesis of fatty acid in atherosclerotic aortas of the pigeon. *J Lipid Res* 9:739-747, 1968
13. McGill HC: Fatty streaks in the coronary arteries and aorta. *Lab Invest* 18:560-564, 1968
14. Strong JP, McGill HC: The pediatric aspects of atherosclerosis. *J Atheroscler Res* 9:251-265, 1969
15. Resch JA, Okabe N, Loewenson RB, Kimoto K, Katsuki S, Baker AB: Pattern of vessel involvement in cerebral atherosclerosis: a comparative study between a Japanese and Minnesota population. *J Atheroscler Res* 9:239-250, 1969
16. Tjøtta E: The distribution of atheromatosis in the coronary arteries. *J Atheroscler Res* 3:253-261, 1963
17. Haimovici, H: Patterns of arteriosclerotic lesions of the lower extremity. *Ann NY Acad Sci* 149:997-1021, 1968
18. Fry DL: Certain chemorheologic considerations regarding the blood vascular interface with particular reference to coronary artery disease. *Circulation* 40:Suppl 4:IV38-IV56, 1969
19. Gutstein WH, Schneek DJ, Marks JO: In vitro studies of blood flow disturbance in the region of separation. *J Atheroscler Res* 8:381-388, 1968
20. Mitchell JRA, Schwartz CJ: *Arterial Disease*. Philadelphia, FA Davis Co, 1965, p 50
21. Mustard JF, Murphy EA, Roswell HC, Downe HG: Platelets and atherosclerosis. *J Atheroscler Res* 4:1-28, 1964
22. Packham MA, Roswell HC, Jorgensen L, Mustard JF: Localized protein accumulation in the wall of the aorta. *Exp Mol Pathol* 7:214-232, 1967
23. Texon M: The role of vascular dynamics in the development of atherosclerosis,¹ pp 167-198
24. Caro CG, Fitz-Gerald JM, Schroter, RC: Arterial wall shear and distribution of early atheroma in man. *Nature* 223:1159-1161, 1969
25. Haimovici H, Maier N: Experimental atherosclerosis in aortic grafts implanted into juglar veins. *Circulation* 38:VI8, 1968, abstr
26. Zemlenyi T, Mrhova O, Urbanova D, Hladovec J: Selective susceptibility of vascular segments and atherosclerosis. *Vitalst Zivlilisationskr* 13:184-186, 1968
27. Hassler O: Physiological intima cushions in the large cerebral arteries of young individuals. I. Morphological structure and possible significance for the circulation. *Acta Pathol Microbiol Scand* 55:19-34, 1962
28. Mark W: *Über Arterienwulste bei den Vogeln*. *Z Zellforsch Mikrosk Anat* 37:1-55, 1952

29. Menschik Z, Dovi SF: Normally occurring intraluminal projections in the arterial system of the mouse. *Anat Rec* 153:265-274, 1965
30. Zemplyni T: *Enzyme Biochemistry of the Arterial Wall*. London, Lloyd-Luke Ltd, 1968, p 197
31. Imai H, Lee KJ, Lee SK, Lee KT, O'Neal RM, Thomas WA: Ultrastructural features of aortic cells in mitosis in control and cholesterol fed swine. *Lab Invest* 23:401-415, 1970
32. Knieriem, HJ: Electron-mircoscopic study of bovine arteriosclerotic lesions. *Am J Pathol* 50:1035-1060, 1967
33. Imai H, Lee KT, Pastori S, Panlilio E, Florentin R, Thomas WA: Atherosclerosis in rabbits: architectural and subcellular alterations of smooth muscle cells of aortas in response to hyperlipemia. *Exp Mol Pathol* 5:273-310, 1966
34. Geer JC, Catsulis C, McGill HC, Strong JP: Fine structure of the baboon aortic fatty streak. *Am J Pathol* 52:265-288, 1968
35. Geer JC: Fine structure of human aortic intimal thickening and fatty streaks. *Lab Invest* 14:1764-1783, 1965
36. Moss NS, Benditt EP: The ultrastructure of spontaneous and experimentally induced arterial lesions. II. Spontaneous plaque in the chicken. *Lab Invest* 23:231-245, 1970
37. Murray M, Schodt GR, Berg HF: Role of smooth muscle cells in healing of injured arteries. *Arch Pathol* 82:138-146, 1966
38. Esterly JA, Glagov S, Ferguson DJ: Morphogenesis of intimal obliterative hyperplasia of small arteries in experimental pulmonary hypertension: an ultrastructural study of the role of smooth-muscle cells. *Am J Pathol* 52:325-347, 1968

Portion of thesis submitted by the senior author to the University of New Hampshire in partial fulfillment of the requirements for a PhD and completed during his tenure as a predoctoral fellow of the New Hampshire Heart Association. Published with the approval of the director of the New Hampshire Agricultural Experiment Station as Scientific Contribution No. 561. Technical assistance by Mrs. Helen Langley and Rose Thomas.

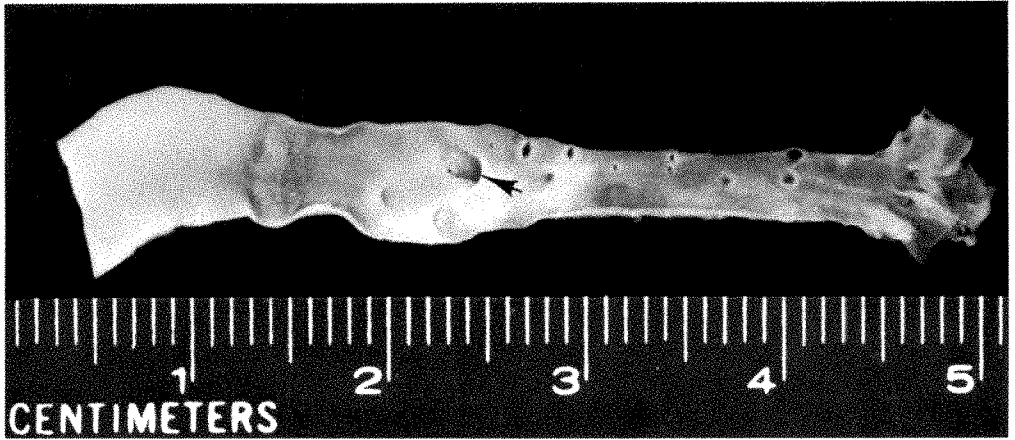


Fig 1—Noninvolved aorta with ridge-like thickenings extending diagonally proximal from the celiac orifice (arrow). White Carneau male, 3-weeks-old (unstained whole mount, $\times 2.6$).

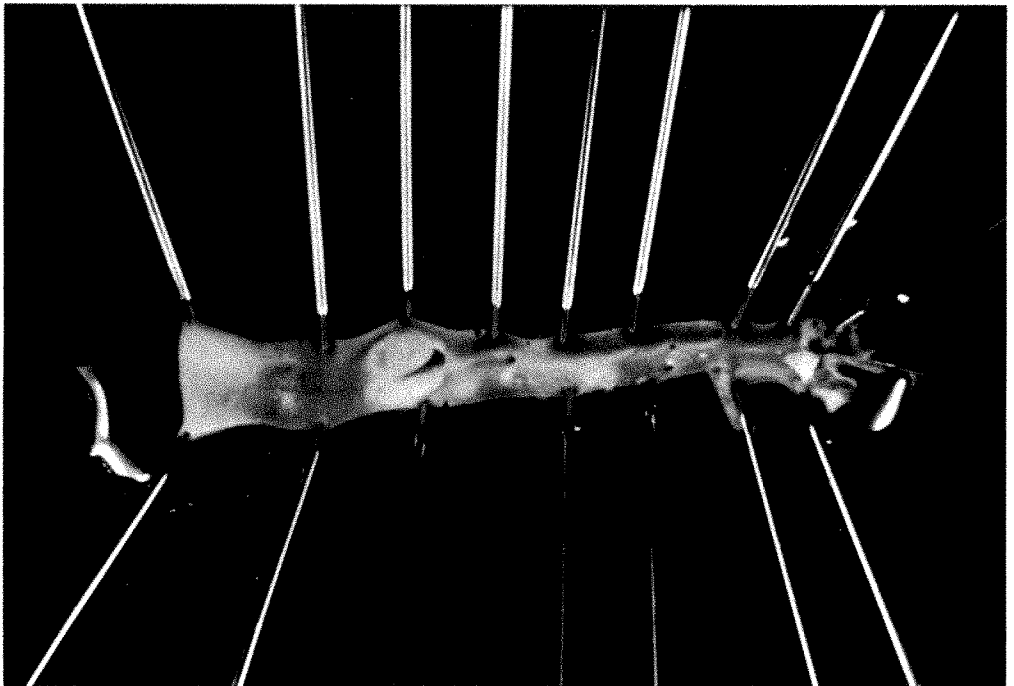
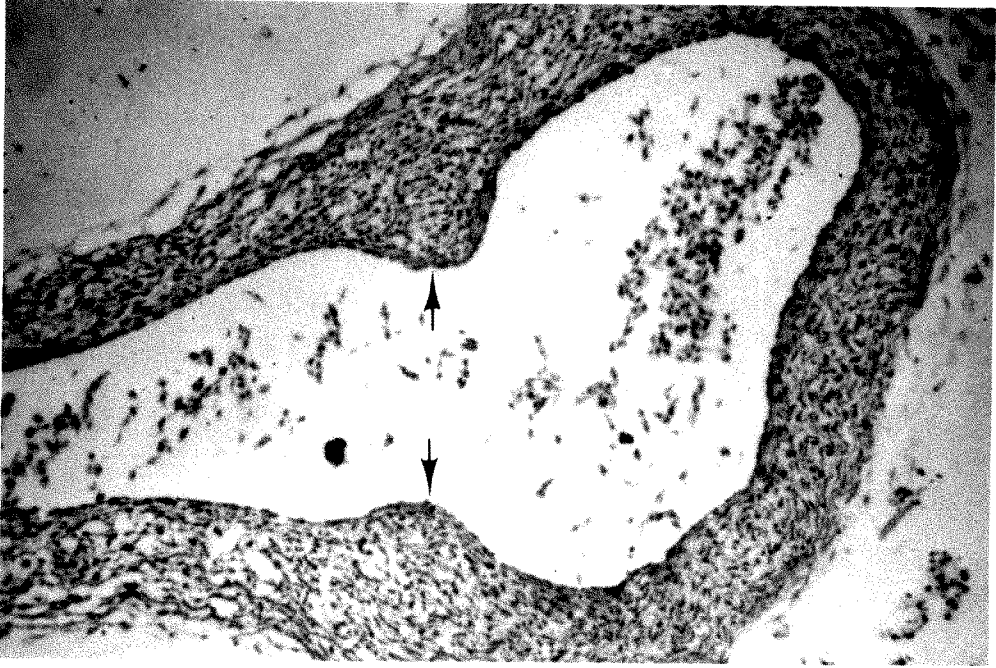


Fig 2—Two large plaques on either side of the celiac orifice. Smaller plaques are also present at the renal branches and in the trifurcation. White Carneau female, 5-years-old (unstained whole mount, $\times 2.1$).

3



4

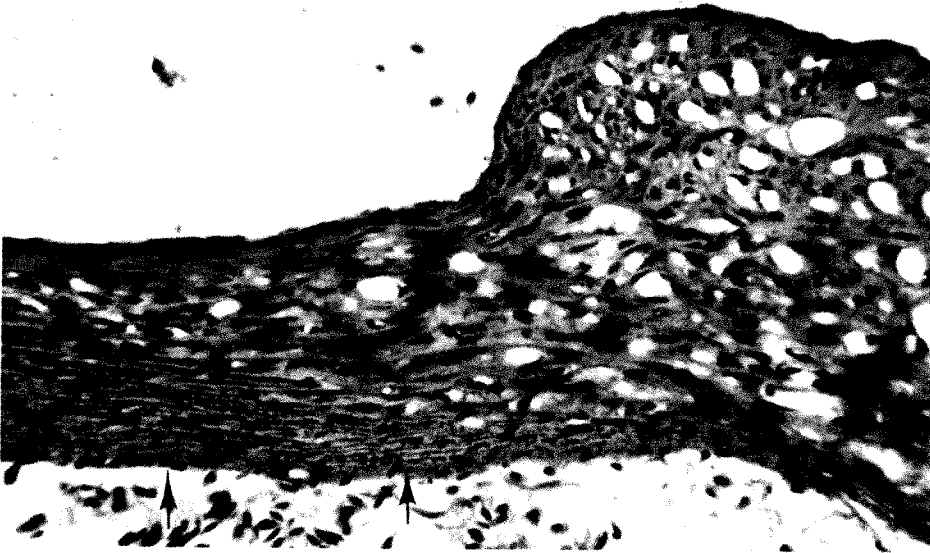
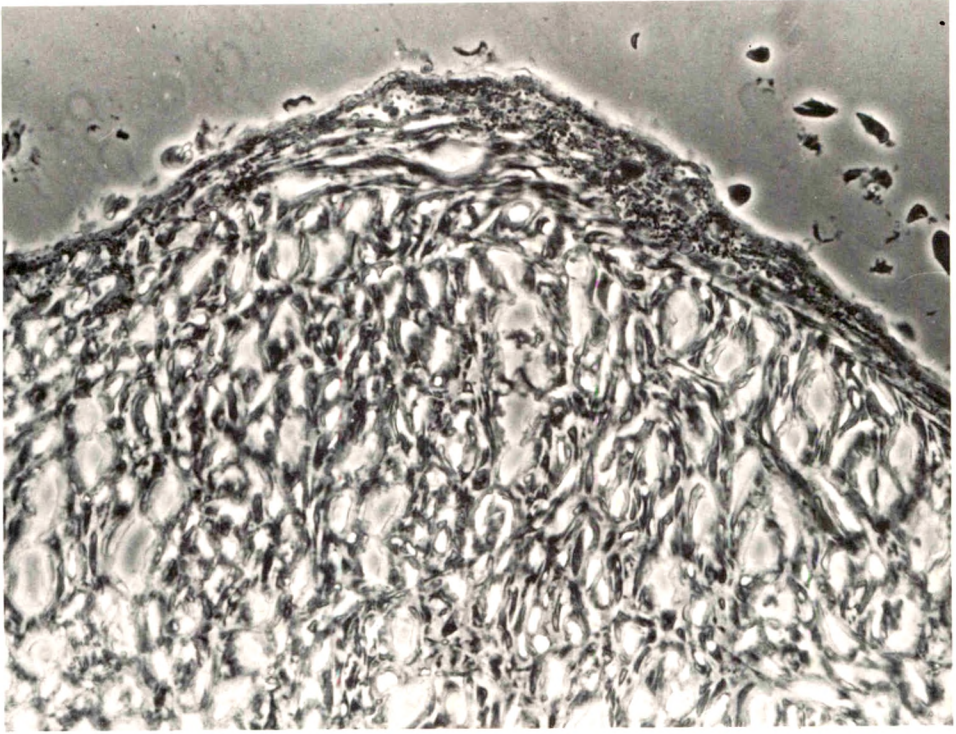
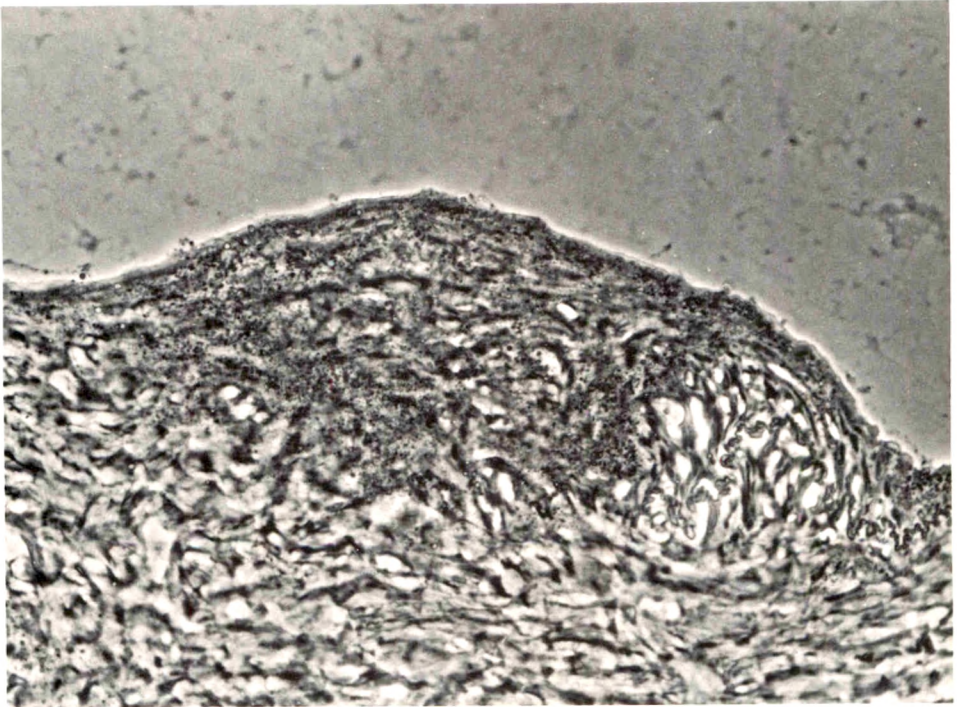


Fig 3—Cushions of smooth muscle cells protruding into the aortic lumen at the celiac bifurcation (arrows). White Carneau 10-day embryo (H&E, $\times 150$). **Fig 4**—Normal cushion with circumferentially oriented smooth muscle cells. Laminar organization of elastic laminae at left (arrows) of figure is disrupted in the region of the cushion. Show Racer female, 4-weeks-old (H&E, $\times 330$).



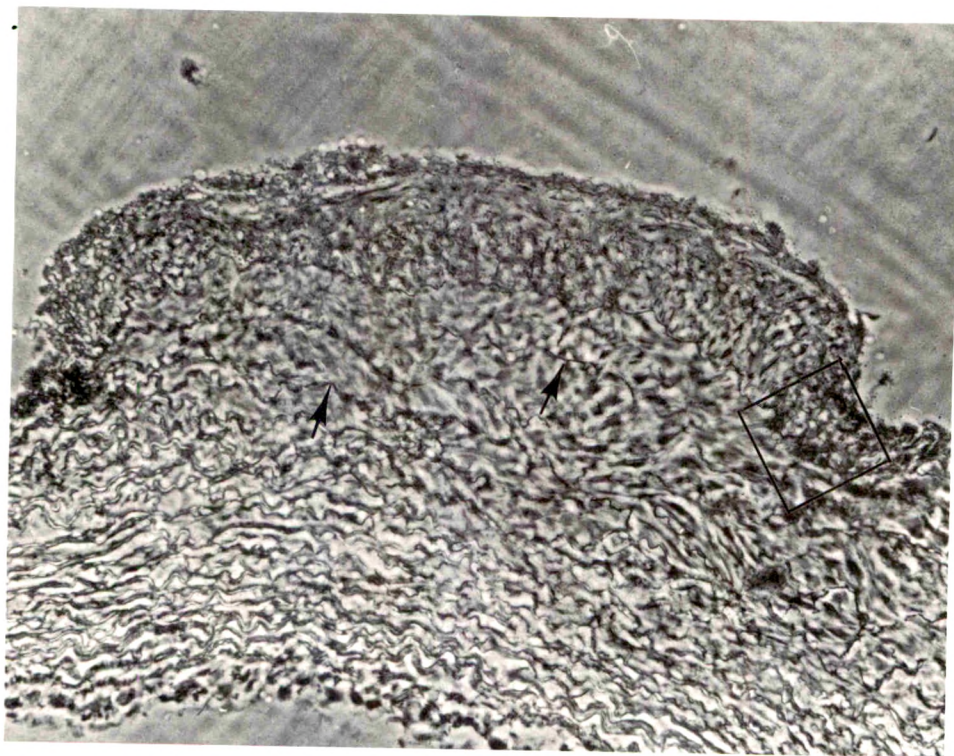
5



6

Fig 5—Endothelial and subendothelial lipid deposition in an otherwise normal celiac cushion. White Carneau female, 3-months-old (hematoxylin–oil red O, phase contrast, $\times 420$). **Fig 6**—Grade 1 lesion. Many fine lipid droplets are present, some in deeper regions. Slight proliferation is visible. Show Racer male, 6-years-old (hematoxylin–oil red O, phase contrast, $\times 420$).

A



B

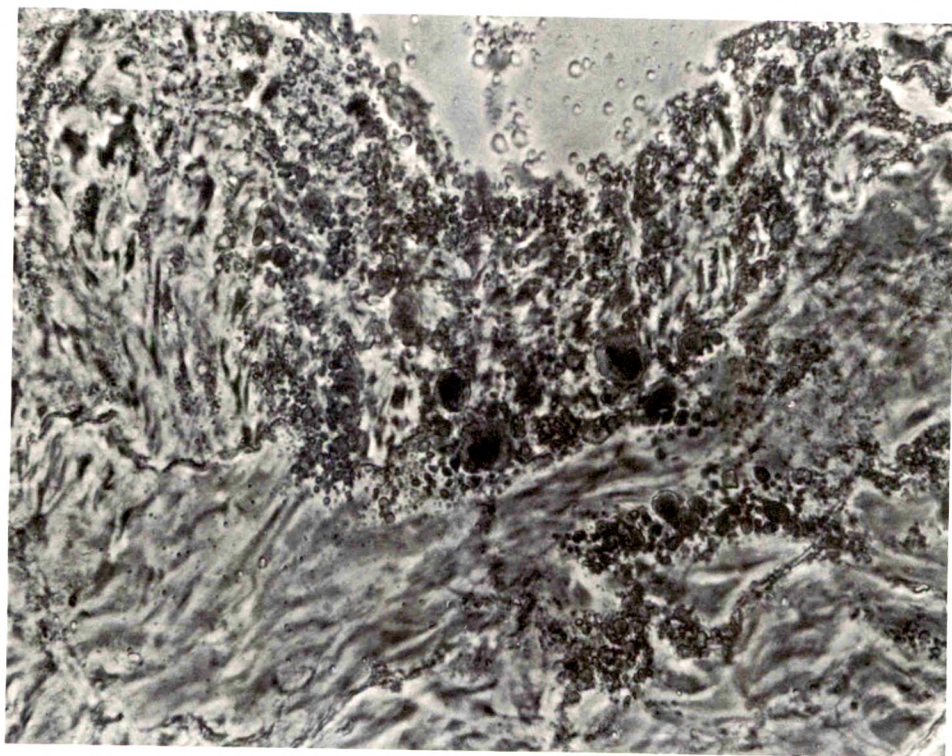
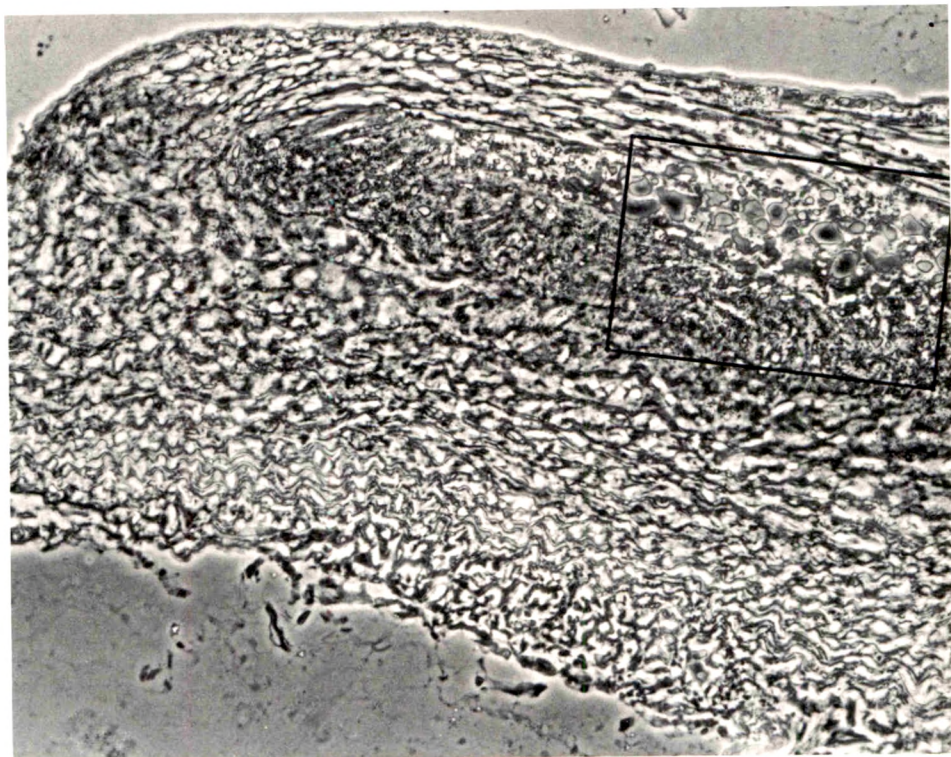
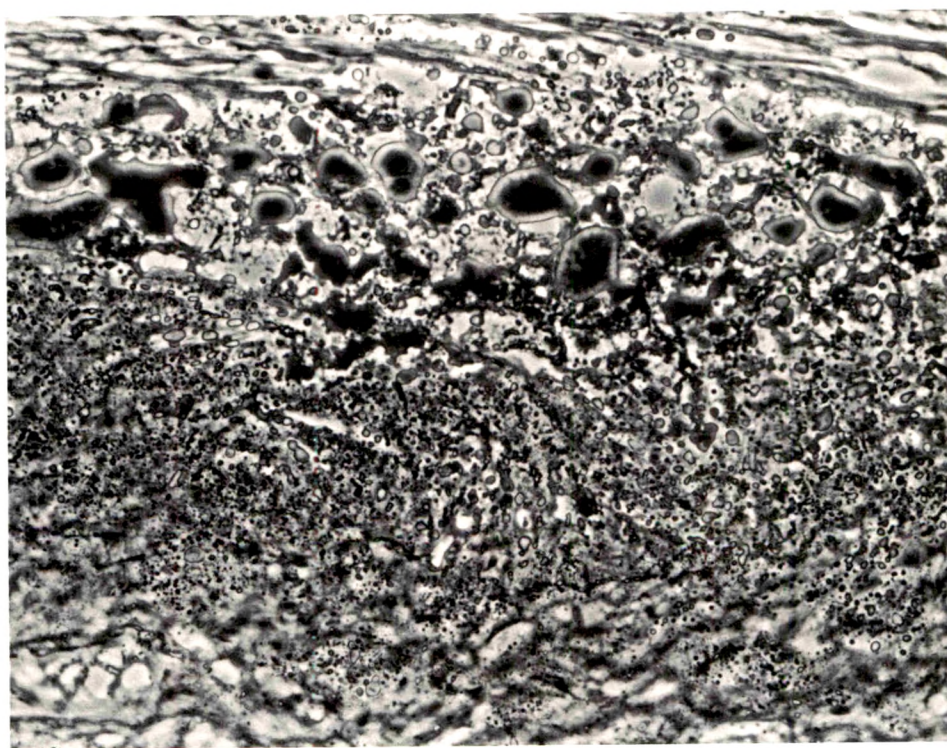


Fig 7—Grade 2 lesion. Show Racer female, 1-year-old. **A**—Marked proliferation has enlarged this cushion. Fragmented elastica is evident (arrows) (hematoxylin—oil red O, phase contrast, $\times 165$). **B**—Higher magnification of area outlined in 7A. Lipid in large pools as well as fine droplets can be seen ($\times 660$).



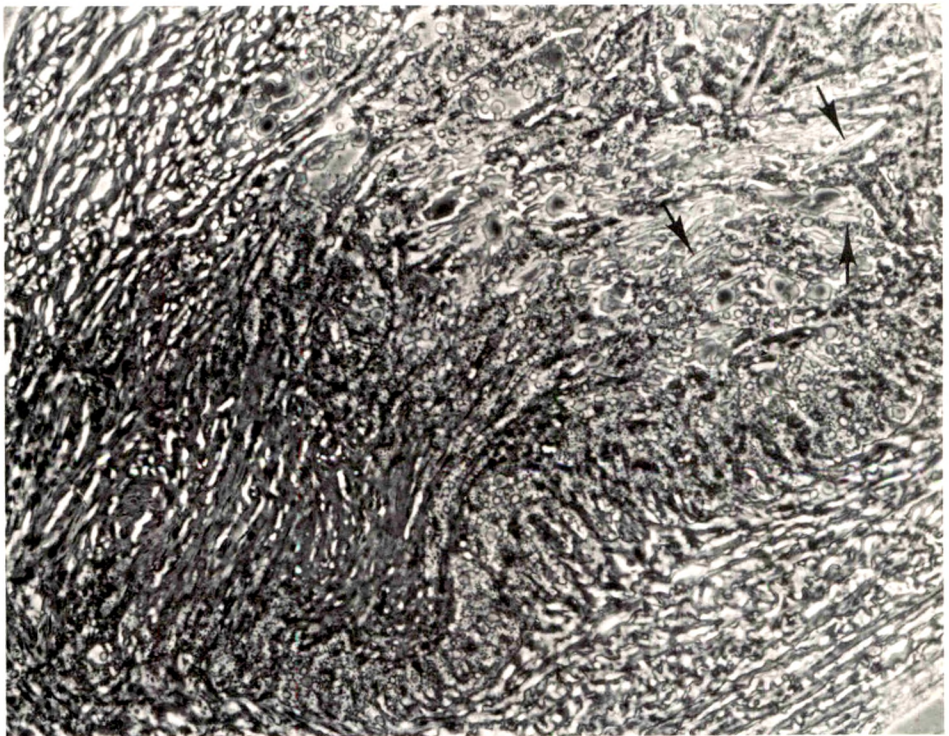
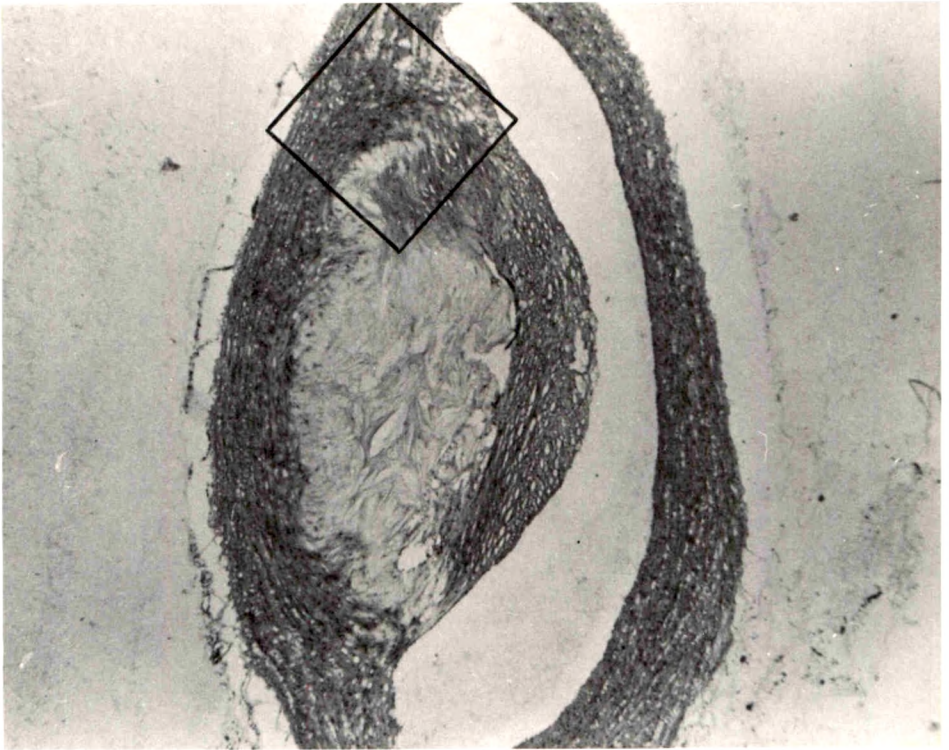
A



B

Fig 8—Grade 3 lesion. White Carneau female, 6-years-old. **A**—Lipid-filled plaque exhibiting considerable luminal protrusion, central necrosis, and involvement of surrounding media (hematoxylin–oil red O, phase contrast, $\times 165$). **B**—Higher magnification of area outlined in a. Necrosis and large amorphous lipid pools are evident. $\times 420$.

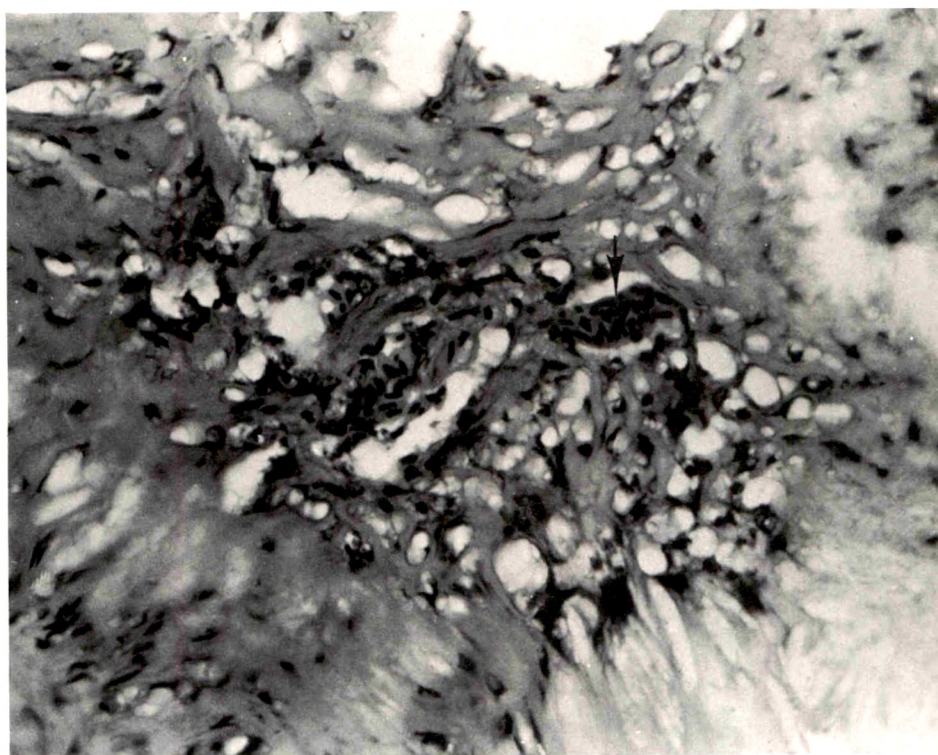
Fig 9—Grade 4 lesion. White Carneau male, 6-years-old. **A**—A large fatty lesion with prominent fibrous cap and extensive central necrosis (H&E, $\times 60$). **B**—Higher magnification of an adjacent serial section depicting cholesterol clefts (*arrows*) in the area outlined in 9A (hematoxylin–oil red O, phase contrast, $\times 165$).



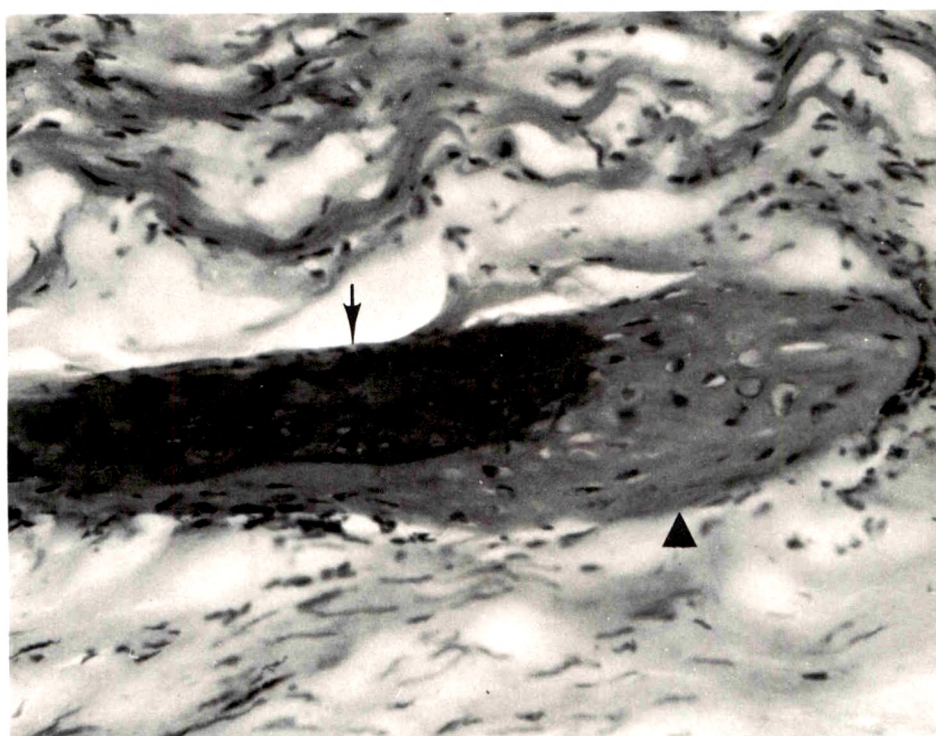
A



Fig 10—Grade 5 lesion. White Carneau male, 6-years-old. **A**—Massive fatty lesion occluding more than half the lumen, of this vessel (H&E, $\times 60$). **B**—Higher magnification of an adjacent serial section showing clusters of red blood cells (*arrow*) in the center of the plaque (H&E, $\times 420$). **C**—Higher magnification of an adjacent serial section showing bone formation (*arrow*) and what appears to be formation of cartilage (*dart*) (H&E, $\times 420$).



B



C



Fig 11—Modified smooth muscle cell in the upper region of the fibrous cap from an advanced lesion in a 7-year-old White Carneau female containing myofilaments (*mf*) with dense bodies (*darts*), much granular endoplasmic reticulum (*GER*), many mitochondria (*M*) and glycogen (*G*). Pinocytotic vesicles are prominent (*arrows*). The extracellular space contains fragmented basement membrane envelope (*bme*) and some collagen (*C*). Numerous vacuoles (*V*) containing material resembling that found in extracellular spaces are present ($\times 18,900$).

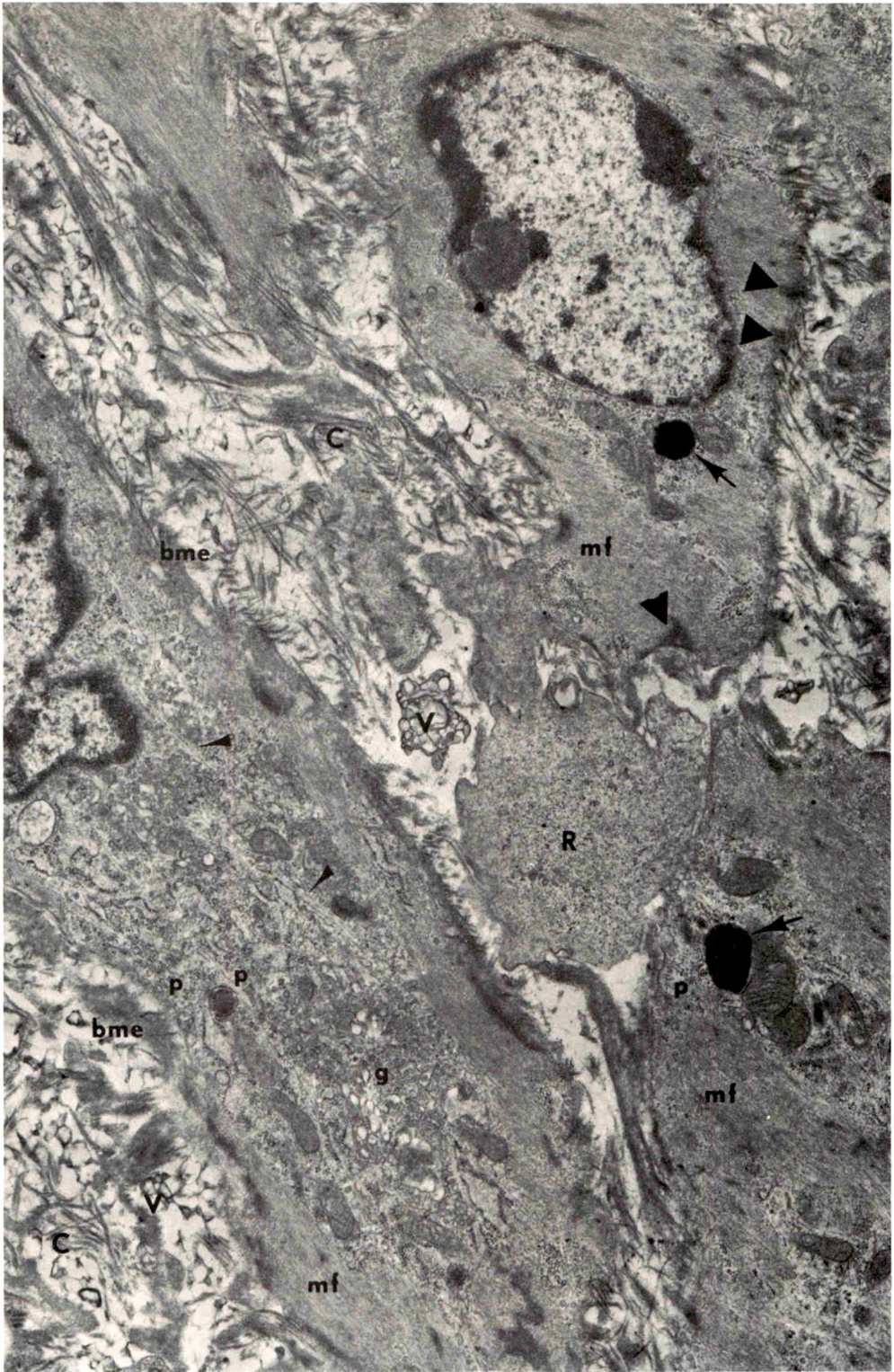


Fig 12—Deeper-lying region of the fibrous cap shown in Fig 11. Modified smooth muscle cells in this region contain a similar array of organelles including a prominent Golgi apparatus (*g*), many free ribosomes (*R*) and polysomes (*p*), and microtubules (*small darts*). These cells have many more myofilaments (*mf*) with dense bodies (*large darts*) and a distinct basement membrane envelope (*bme*). Darkly stained inclusions (*arrows*) are present, and extracellular vesiculated material (*V*) is abundant. Collagen (*C*) is more prominent here ($\times 16,500$).

[End of Article]

Endotoxin-Induced Hepatic Damage in BCG-Infected Mice

J. W. Shands, Jr, MD and V. C. Senterfitt, MS

Systemic infection of mice with *Mycobacterium* BCG leads to focal liver damage by producing many granulomas. By undefined mechanisms, this infection markedly enhances the animal's susceptibility to the lethal effect of endotoxin. Small doses of endotoxin given to BCG-infected mice were found to cause acute hepatic damage, as demonstrated by elevated activities of liver enzymes in serum and by morphologic alterations documented by light and electron microscopy and by histochemical technics. The morphologic alterations caused by endotoxin included glycogen depletion, mitochondrial swelling, disruption of the continuity of sinusoidal endothelium and focal injury characterized by marked vacuolization of hepatocytes and distension and fragmentation of rough endoplasmic reticulum. Histochemical studies revealed the apparent release of acid phosphatase from granules in the central portions of granulomas, and the release of β -glucuronidase from the cytoplasm of hepatocytes. (Am J Pathol 67:23-40, 1972)

INJECTING ENDOTOXIN into normal mice leads to complex, interacting, physiologic and metabolic derangements which may culminate in death of the animal. Of the many biochemical abnormalities observed, alterations in carbohydrate metabolism have received particular attention.¹⁻⁷ The injection of endotoxin has been reported to cause a transient hyperglycemia followed by hypoglycemia and depletion of carbohydrate stores.²⁻⁷ Results of *in vitro* studies of the livers of endotoxin-poisoned rats by LaNoue *et al*⁸ suggested that this hypoglycemia was a consequence of impaired gluconeogenesis. Since the major gluconeogenic activity occurs in the liver, dysfunction of this organ may play a role in the pathogenesis of endotoxin poisoning. Its implication in the process is strengthened further by the observation that hepatic necrosis induced by carbon tetrachloride leads to marked susceptibility to the lethal action of endotoxin.⁹

The metabolic consequences of injecting endotoxin are far more striking in mice rendered hyperreactive to endotoxin than in normal mice. In mice and rabbits made hyperreactive by infection with *Mycobacterium bovis* BCG, profound hypoglycemia was found to occur several hours after endotoxin was given, and the animals often died con-

From the Department of Immunology and Medical Microbiology, University of Florida, College of Medicine, Gainesville, Fla 32601.

Supported by Grants AI 07257 and 5TIAI 0128 from the National Institutes of Health.

Accepted for publication September 19, 1971.

Address reprint requests to Dr. Joseph W. Shands, Jr.

vulsively in less than 5 hours.⁶ This hypoglycemia, which could be caused by as little as 25–50 ng of endotoxin, was also found to be the result of impaired gluconeogenesis.⁷ This observation suggested the presence of hepatic dysfunction in the endotoxin-poisoned BCG-infected mice, probably of a much greater degree than that observed in normal mice, since the hypoglycemia occurred more rapidly and was more severe. In this paper, we report on the pathology of the liver of BCG-infected mice given a lethal dose of endotoxin (1.0 μg), as reflected by elevations in serum enzyme levels, light and electron microscopy, and histochemistry.

Materials and Methods

Animals

CD-1, pathogen-free, female mice were obtained from Charles River Breeding Laboratories, North Wilmington, Mass. The animals were housed 10 to a cage and were fed chow and water *ad libitum*.

Endotoxin

The endotoxin used was prepared in this laboratory using a smooth strain of *Salmonella typhimurium*. Formalin-fixed whole cells were extracted by the phenol-water procedure as described previously.¹⁰ A small amount of contaminating RNA was removed by RNase digestion followed by reextraction with phenol. The endotoxin was suspended in physiologic saline and injected intravenously in a 0.2 ml volume.

BCG Infection

Mice were made hyperreactive to endotoxin by intravenously injecting 0.2 ml of a 10–14 day culture of *M bovis* BCG in Dubos broth base (Difco). This was equivalent to approximately 10^8 *Mycobacteria* per mouse. Unless otherwise stated, the mice were used in experiments 14 days after infection with BCG, the time of maximal reactivity to endotoxin.¹¹ The endotoxin LD₅₀ in these mice was approximately 0.4 μg . In contrast, the endotoxin LD₅₀ for normal mice was approximately 200 μg .

Serum Enzymes

Serum glutamic oxaloacetic transaminase (SGOT) and serum glutamic pyruvic transaminase (SGPT) were determined by Determatube tests (Worthington Biochemical Corp, Freehold, NJ) using 0.02 ml of serum from each mouse. Serum acid phosphatase was assayed by the method of Lowry *et al*¹² and serum β -glucuronidase was assayed by the method of Talalay *et al*,¹³ using 0.05 ml of serum.

Histological Technics

Mouse livers were fixed in Bouin's fluid, embedded in paraffin, sectioned, and stained with hematoxylin and eosin (H&E) for light microscopy. Specimens of liver for electron microscopy were fixed either by immersing small pieces of tissue

in 2.5% glutaraldehyde in 0.1 M phosphate buffer (pH 7.4) for 2 hours at 0 C followed by postfixation in 1% OsO₄ in phosphate buffer for 2 hours, or by perfusing the portal vein *in situ* with 2.5% glutaraldehyde in phosphate buffer. After perfusion, the liver was cut into small pieces and postfixed in OsO₄. After the tissue was dehydrated in a graded series of alcohols (75–100%) and embedded in Epon,¹⁴ sections were made on a Porter-Blum LT-2 ultramicrotome. Thick sections were stained with toluidine blue, and thin sections with uranyl acetate followed by lead citrate. Observations and photographs were made in a Siemens I electron microscope. Two experiments were performed in which livers were examined from control animals and from animals given endotoxin 1 and 3 hours previously. In each experiment, 5 mice were included in each experimental group.

Histochemistry

Control 14-day BCG-infected mice and BCG-infected mice given 1.0 µg of endotoxin 2½ hours previously were killed by cervical fracture. The livers were removed quickly and 6-µ frozen sections were cut in a cryostat (International Harris). After adhesion to glass slides, unfixed sections were stained for acid phosphatase activity by a modified Burstone method.¹⁵ Five milligrams naphthol AS-MX phosphoric acid (Sigma Chemical Co) was dissolved in 0.25 ml *N, N*-dimethylformamide and added to 50 ml 0.1 M acetate buffer (pH 5). Thirty-five mg of diazonium salt (fast red violet LB, Verona Dyestuffs, Union, NJ) was added and the solution filtered into Coplin jars. The freshly cut sections were incubated at 25 C for 1 hour and fixed in neutral formalin. After counterstaining with Meyer's hematoxylin, the sections were mounted with coverslips using glycerin jelly. Similar sections on slides were placed in cold, neutral formalin immediately after cutting and were left in formalin overnight. After washing in distilled water for 2 hours, they were stained for β-glucuronidase activity using the substrate of Fishman and Baker.¹⁶ The sections were kept 18 hours at 6 C in a Coplin jar containing the substrate solution and then incubated for 1½ hours at 37 C. After rinsing briefly in distilled water, the sections were transferred to 0.5 M oxalate buffer (pH 4.5) for 15 minutes at 25 C, and rinsed again. The slides were transferred to freshly prepared 2% potassium ferrocyanide and after 10 seconds an equal volume of 1 N HCl was added for an additional 2 minutes. After rinsing, the potassium ferrocyanide was again added for 10 seconds followed by HCl again for 10 minutes. After rinsing in distilled water, the Prussian blue-stained sections were counterstained with 0.1% nuclear fast red (Matheson, Coleman and Bell, East Rutherford, NJ) in 5% aluminum sulfate. The sections were dehydrated in alcohol, cleared in xylene and mounted with Permount. Renal tissue was also stained for β-glucuronidase to check for the known distribution of the enzyme.¹⁷

Results

Table 1 shows (1) the effect of BCG infection alone on serum enzyme activities; (2) the effect of BCG infection plus endotoxin on the serum enzyme activities and (3) the responsiveness of the mice to endotoxin toxicity. BCG infection alone caused an elevation in the SGOT and SGPT and the elevation apparently was maximal at the time when the mice were maximally susceptible to endotoxin. On the fifteenth day after BCG infection, the mice had both their highest serum enzyme activities and the highest mortality after endotoxin. In a separate ex-

Table 1—Effect of Endotoxin on Serum Enzyme Levels at Intervals after BCG Infection*

Days after BCG	SGOT†		SGPT†		Acid phosphatase‡		β-Glucuronidase§		Lethality of LPS	
	Control	After 1 μg LPS	Control	After 1 μg LPS	Control	After 1 μg LPS	Control	After 1 μg LPS	Dose (μg)	Dead/total
0	125 ± 5 (7)	133 ± 21 (6)	165 ± 4 (7)	207 ± 8 (7)	1.53 ± .04 (7)	2.24 ± .16 (6)	—	—	—	—
5	140 ± 15 (7)	325 ± 162 (7)	206 ± 7 (7)	261 ± 66 (7)	2.69 ± .50 (7)	2.50 ± .20 (7)	<20 (7)	<20 (7)	0.1 1.0 10.0	0/5 0/5 0/5
10	205 ± 23 (7)	2365 ± 488 (6)	284 ± 35 (7)	923 ± 281 (7)	2.10 ± .18 (7)	12.00 ± .38 (6)	<20 (7)	406 ± 105 (6)	1.0 10.0	1/5 3/5
15	442 ± 83 (7)	2659 ± 506 (7)	444 ± 63 (7)	917 ± 171 (7)	2.57 ± .27 (7)	18.23 ± .38 (7)	<20 (7)	552 ± 87 (6)	0.1 1.0 10.0	2/5 5/5 4/5

* Blood samples were drawn via cardiac puncture 2 hours after endotoxin was injected.

† Glutamic oxalacetic and glutamic pyruvic transaminases are expressed as mean absorbancy units/ml of serum ± standard error (number of mice in parentheses).

‡ Expressed as μmoles of p-nitrophenol produced in 40 minutes/ml of serum.

§ Expressed as μg of phenolphthalein produced in 1 hour/ml of serum.

periment, we found that by day 29 the SGOT and SGPT had fallen to approximately one half their peak activities and that the mortality was also diminished. This suggested that serum enzyme elevations were correlated with hyperreactivity to endotoxin.

BCG infection alone also caused a modest elevation in serum acid phosphatase as was reported previously by Saito and Suter.¹⁸ β -Glucuronidase activity was undetected in BCG mice before endotoxin because accurate determinations were not possible with sera of individual mice. However, Saito and Suter, using pooled plasma, showed that BCG infection alone caused a 20-fold increase in plasma β -glucuronidase.¹⁸

When endotoxin was injected into the mice, and serum enzymes were measured 2 hours later, the following effects were noted (Table 1): In the normal mice (0 days after BCG), there were insignificant elevations in SGOT and SGPT and a modest elevation in acid phosphatase. On days 10 and 15 after BCG infection, when hyperreactivity was manifest, remarkable increases in SGOT, SGPT, acid phosphatase and β -glucuronidase occurred after endotoxin, approximately sixfold for acid phosphatase and >20-fold for β -glucuronidase. These data suggest considerable lysosomal release and hepatocellular damage. Of interest is the fact that when normal mice were given an LD₅₀ of endotoxin, elevations in enzyme activities were noted, but the levels obtained did not approach those observed with endotoxin-poisoned, BCG-infected mice (Table 2).

Histologic studies of BCG-infected mice revealed the following:

H & E-Stained Sections. Fig 1 shows mouse liver 14 days after BCG infection. While normal-appearing liver cords are present, it is obvious that the overall architecture of the liver is disturbed by the numerous granulomas studding the parenchyma. Two hours after 1.0 μ g of endotoxin, little change was noted by H&E stain except for a possible dilation of the sinusoids.

Table 2—Effect of Endotoxin on Serum Enzyme Levels of Normal Mice

	SGOT*	SGPT*	Acid Phosphatase†
Controls	125 \pm 5 (7)	165 \pm 4 (7)	1.53 \pm .04 (7)
2 hours after 200 μ g of LPS	143 \pm 4 (4)	285 \pm 56 (4)	2.75 \pm .11 (4)

* Glutamic oxalacetic and glutamic pyruvic transaminases are expressed as mean absorbancy units/ml of serum \pm standard error (number of mice in parentheses).

† Expressed as μ moles of p-nitrophenol produced in 40 minutes \pm standard error.

Toluidine Blue-Stained Sections. These were prepared from the Epon-embedded tissue sectioned at a $1\ \mu$ thickness. Fig 2 shows a portion of liver 14 days after BCG infection. The hepatocytes and sinusoids in the noninflamed portions of liver appear normal with only minor vacuolization of the hepatocytes. Dark-staining areas in the parenchymal cells probably represent glycogen deposits. One hour after injection of $1.0\ \mu\text{g}$ of endotoxin, several changes were noted. First, the sinusoidal spaces seemed to be dilated. Second, dark areas seen in the cytoplasm of hepatocytes, probably representing glycogen, disappeared. Third, in scattered areas of the liver, small, peripheral vacuoles appeared in the hepatocytes, some of which seemed to be open to Disse's space. Three hours after endotoxin, these changes were quite evident (Fig 3). Extensive vacuolization was occasionally observed, and in some areas this appeared to be of sufficient degree to suggest severe focal injury (Fig 4). In addition, stacking of erythrocytes in sinusoids occurred in scattered areas of the liver, suggesting circulatory stasis. In livers that were fixed by immersion, the stacking of erythrocytes was sometimes observed as early as 10 minutes after endotoxin. There was a loss of the staining properties of some hepatocytes, such that subcellular organelles (probably mitochondria) became quite distinct.

Electron Microscopy

Fig 5 and 6 depict mouse liver 14 days after intravenous infection with BCG. The architecture of the hepatocytes appeared to be normal, with good preservation of cytoplasmic organelles and abundant glycogen. Generally, small vacuoles were fairly prominent and some contained myelinic figures as in Fig 5. Fig 6 depicts an area adjacent to a granuloma, and shows an injured hepatocyte adjacent to cells of the granuloma. Such cells were commonly found in these areas and probably were the source of the elevated serum enzymes caused by BCG infection.

One hour after $1.0\ \mu\text{g}$ of endotoxin, at least two types of focal changes were noted. First, there was a disappearance of glycogen granules. Some cells were almost totally devoid of glycogen while others appeared to have a normal amount. Second, in some areas a dissolution of mitochondrial matrix could be observed, along with apparent mitochondrial swelling. In Fig 7, there is a large sinusoid mostly filled with processes of Kupffer cells. The mitochondria of the surrounding hepatocytes appear swollen, pale, and in some, the cristae have fragmented. This lesion was not observed in all animals, and when it was present, it was limited to focal involvement. Although the hepatocytes contained a

fair number of lipid droplets, they seemed no more numerous than in control hepatocytes.

Three hours after 1.0 μ g of endotoxin, ultrastructural changes were more apparent. There was a general depletion of glycogen granules. The vacuolization seen by light microscopy (Fig 3) was quite evident, and many of these vacuoles communicated with the space of Disse (Fig 8). In addition, the space of Disse appeared to be distended and processes of sinusoid lining cells appeared to be separated more widely than usual. Finally, at 3 hours extensive injury to hepatocytes was observed (Fig 9). This is a micrograph of a portion of the vacuolated cells seen in Fig 4 and shows portions of hepatocytes containing large vacuoles and dilated, fragmented ergastoplasm. The mitochondria, however, appear normal.

Histochemistry

Histochemical staining for acid phosphatase showed that in the livers of BCG-infected mice the enzyme appeared to be associated with granules (Fig 10), and it was particularly concentrated in the central portion of the granulomas, as has been reported by Grogg and Pearse.¹⁹ In contrast, β -glucuronidase did not appear to be associated with granules and was found diffusely throughout the cytoplasm of hepatocytes (Fig 11). A surprising finding was the absence of β -glucuronidase activity in the granulomas (G) which are especially rich in granules containing acid phosphatase.

Endotoxin in BCG-infected mice seemed to cause some redistribution of acid phosphatase in some of the cells of the granuloma. Fig 12 shows that the stain no longer appeared only in discrete granules but in some cells appeared to be distributed throughout the cytoplasm (*arrows*). However, redistribution of β -glucuronidase activity was much more apparent. In two of three separate experiments, injecting 1.0 μ g of endotoxin to BCG-infected mice resulted in a decreased intensity of the stain for β -glucuronidase. In one of the experiments, there was almost complete blanching of the hepatocytes, especially in the periportal areas, 2 hours after endotoxin. Fig 13 and 14 illustrate the loss of staining for β -glucuronidase caused by endotoxin. Fig 13 shows BCG-infected, control liver β -glucuronidase and Fig 14 shows the decreased stain intensity in the liver from an endotoxin-poisoned, BCG-infected mouse.

Discussion

BCG-infected mice are remarkably sensitive to endotoxin, and are killed by approximately one thousandth of the usual mouse lethal dose.

In molecular terms, assuming the average molecular weight of endotoxin to be in the range of 10^6 daltons, and LD_{50} represents approximately 5×10^{11} particles, almost as potent as some exotoxins. The endotoxin death of BCG-infected mice is more rapid than that of normal mice (4 hours versus 18 hours) and it is often preceded by convulsions.^{4,6} The blood glucose concentration falls precipitously between 3 and 4 hours after endotoxin in BCG-infected mice,^{4,6} and previous work showed that endotoxin caused a marked impairment in gluconeogenesis in BCG-infected mice. Since the liver is the chief organ for gluconeogenesis, liver damage was suggested.

The experiments reported in this paper showed that BCG infection alone produced elevations in the serum levels of GOT, GPT, and also in serum acid phosphatase. Saito and Suter showed previously that the plasma levels of acid phosphatase and β -glucuronidase were elevated in BCG-infected mice.¹⁸ The increased levels of SGOT and SGPT suggest hepatic parenchymal damage, whereas the increase in the acid phosphatase and β -glucuronidase might reflect lysosomal instability. Our morphologic data are consistent with hepatic parenchymal damage by BCG infection alone. Injured hepatocytes were found in areas adjacent to granulomas (Fig 6) and the histochemical data suggested that the reported elevation in plasma β -glucuronidase by BCG infection¹⁸ was actually due to hepatocyte damage, since the enzyme appeared to be concentrated largely throughout the cytoplasm of hepatocytes. This might also explain the observation by Saito and Suter that while BCG infection resulted in a twofold increase in plasma acid phosphatase, plasma β -glucuronidase was elevated 20-fold.¹⁸

In addition to the focal hepatic damage in mice resulting from BCG infection alone, this treatment, in some manner, conditioned the mice such that small doses of endotoxin caused acute hepatic injury. Large increases in SGOT, SGPT, and serum β -glucuronidase occurred after a dose of endotoxin that produced only minor changes in SGOT and SGPT in normal mice. In addition, a lethal dose of endotoxin in normal mice failed to produce such striking alterations in the serum levels of these enzymes.

The reality of endotoxin-induced hepatic damage in BCG-infected mice was confirmed by morphologic observations. Four morphologic features were found in the livers of BCG-infected mice after endotoxin. First, there was rapid focal depletion of glycogen which by 3 hours usually involved extensive depletion throughout the liver. Second, there were focal areas of mitochondrial pathology, usually occurring within the first hour after endotoxin. Third, there was distention of the sub-

sinusoidal space and vacuolization of hepatocytes, usually occurring between 1 and 3 hours after endotoxin. Fourth, 3 hours after endotoxin, foci of hepatocyte injury were detected.

A number of papers have described endotoxin-induced liver pathology in mice, dogs and hamsters²³⁻²⁸, and in these reports the pathologic changes observed were very similar to those reported in this paper, including depletion of glycogen, changes in sinusoidal endothelium, congestion of hepatic vessels, mitochondrial pathology and focal injury. The only differences between these reports and our observations are the minute amounts of endotoxin required to produce the hepatic damage in BCG-infected mice, and the acuteness of the damage as demonstrated by the precipitous release of hepatic enzymes into the circulation. Also, although some of our observations suggest circulatory stasis in the liver (Fig 4), we have not observed platelet thrombi in the livers of endotoxin-poisoned, BCG-infected mice, in spite of the fact that they appear to suffer from a consumption coagulopathy.²⁹ Such thrombi have been reported in endotoxin-poisoned mice by others.^{24,26}

To what extent the reported changes in the livers of normal animals are due to shock and/or altered hepatic circulation or a direct effect of endotoxin is far from clear, and the same uncertainty applies to our work with BCG-infected mice. In all probability, the various focal changes that were observed were due to a multiplicity of factors including altered circulation in the liver, perhaps a direct toxicity of endotoxin and even hypoglycemia.

Histochemical studies were performed because release of lysosomal enzymes might be a mechanism by which endotoxin effects tissue damage.²⁰ Saito and Suter reported^{18,21} that acid hydrolases were increased approximately twofold in the livers and in the peritoneal macrophages of BCG-infected mice and that endotoxin given to these animals caused striking elevations of β -glucuronidase and less striking elevations of acid phosphatase in plasma. Furthermore, they demonstrated a correlation between the release of these enzymes into plasma and the hyperreactive state of the BCG-infected mice. Our enzyme data are consistent with theirs. Endotoxin caused a six- to sevenfold increase in serum acid phosphatase after 2 hours, but a greater than 20-fold increase in β -glucuronidase. Our histochemical data showed that β -glucuronidase was present in greatest amount in the cytoplasm of hepatocytes and, surprisingly, essentially absent from the granulomas. Others have reported that some of the so-called lysosomal enzymes may have dual localizations,²² and in particular that β -glucuronidase in

liver not only is lysosomal in location but also is distributed throughout the endoplasmic reticulum of hepatocytes. Our data suggest that a major source of the endotoxin-induced elevation of serum β -glucuronidase is injured hepatocytes. The lesion shown in Fig 9 revealing dilation and fragmentation of the endoplasmic reticulum as a response to endotoxin could account for the dramatic increases of this enzyme in serum. A similar lesion adjacent to a granuloma (Fig 6) could account for the high levels of serum β -glucuronidase resulting from BCG infection alone.¹⁸ Certainly our data suggest that little of the serum β -glucuronidase comes from the cells making up the granulomas, since they seem to be virtually devoid of the enzyme. This, however, does not rule out the Kupffer cells as a source of the enzyme, since in the BCG-infected mice these cells are particularly rich in lysosomes (Fig 6 and 7).

Unlike the serum β -glucuronidase which appears to come from injured hepatocytes in BCG-infected mice given endotoxin, at least some of the serum acid phosphatase appears to come from lysosomal release in the granulomas, and, although we have no data on the point, some of the serum enzyme released by endotoxin may also come from Kupffer cells. Our data, therefore, suggest both lysosomal labilization in granulomas with enzyme release and hepatocyte damage with enzyme release, but they allow no conclusion as to the cause and effect. The concept that endotoxin effects its damage through lysosomal labilization, therefore, remains moot.

References

1. Evans CL, Zeckwer IT: On the nature of the hyperglycemic response to injections of certain killed bacteria. *Br J Exp Pathol* 8:280-288, 1927
2. Kun E, Miller CP: Effect of bacterial endotoxins on carbohydrate metabolism of rabbits. *Proc Soc Exp Biol Med* 67:221-225, 1948
3. Berry LJ, Smythe DS, Young LG: Effects of bacterial endotoxin on metabolism. I. Carbohydrate depletion and the protective role of cortisone. *J Exp Med* 110:389-405, 1959
4. Berry LJ, Smythe DS, Kolbye SM: Effects of bacterial endotoxins on metabolism. V. The hyperactivity of mice infected with *Mycobacterium tuberculosis*, strain BCG. *J Exp Med* 116:897-911, 1962
5. Fukuda T: On the mechanism of endotoxin intoxication in rabbits. *Japan J Physiol* 13:155-168, 1963
6. Shands JW Jr, Miller V, Martin H: The hypoglycemic activity of endotoxin. I. Occurrence in animals hyperreactive to endotoxin. *Proc Soc Exp Biol Med* 130:413-417, 1969
7. Shands JW Jr, Miller V, Martin H, Senterfitt V: Hypoglycemic activity of endotoxin. II. Mechanism of the phenomenon in BCG-infected mice. *J Bacteriol* 98:494-501, 1969
8. LaNoue KF, Mason AD Jr, Daniels JP: The impairment of glucogenesis by gram-negative infection. *Metabolism* 17:606-611, 1968

9. Farrar WE Jr, Watson JG: Hypoglycemia following endotoxin administration in animals with liver damage. *Proc Soc Exp Biol Med* 115:833-837, 1964
10. Ciznar I, Shands JW Jr: Effect of alkali on the immunological reactivity of lipopolysaccharide from *Salmonella typhimurium*. *Infection and Immunity* 2:549-555, 1970
11. Suter E, Kirsanow EM: Hyperreactivity to endotoxin in mice infected with *Mycobacteria*: induction and elicitation of the reactions. *Immunology* 4:354-365, 1961
12. Lowry OH, Roberts NR, Wu ML, Hixon WS, Crawford EJ: The quantitative histochemistry of brain. II. Enzyme measurements. *J Biol Chem* 207:19-37, 1954
13. Talalay P, Fishman WH, Huggins C. Chromogenic substrates. II. Phenolphthalein glucuronic acid as substrate for the assay of glucuronidase activity. *J Biol Chem* 166: 757-774, 1946
14. Luft JH: Improvements in epoxy resin embedding methods. *J Biophys Biochem Cytol* 9:409-414, 1961
15. Burstone MS: Histochemical comparison of naphthol AS-phosphates for the demonstration of phosphatases. *J Natl Cancer Inst* 20:601-615, 1958
16. Thompson SW: *Selected Histochemical and Histopathological Methods*. Springfield Ill, Charles C Thomas Publisher, 1966, pp 683-688
17. Fishman WH, Baker JR: Cellular localization of β -glucuronidase in rat tissues. *J Histochem Cytochem* 4:570-587, 1956
18. Saito K, Suter E: Lysosomal acid hydrolases in mice infected with BCG. *J Exp Med* 121:727-738, 1965
19. Grogg E, Pearse AGE: The enzymic and lipid histochemistry of experimental tuberculosis. *Br J Exp Pathol* 33:567-576, 1952
20. Janoff A, Weissman G, Zweifach BW, Thomas L: Pathogenesis of experimental shock. IV. Studies on lysosomes in normal and tolerant animals subjected to lethal trauma and endotoxemia. *J Exp Med* 116:451-466, 1962
21. Saito K, Suter E: Lysosomal acid hydrolases and hyperreactivity to endotoxin in mice infected with BCG. *J Exp Med* 121:739-749, 1965
22. Fishman WH, Goldman SS, DeLellis R: Dual localization of β -glucuronidase in endoplasmic reticulum and in lysosomes. *Nature* 213:457-460, 1967
23. Boler RK, Bibighaus AJ. Ultrastructural alterations of dog livers during endotoxin shock. *Lab Invest* 17:537-561, 1967
24. Levy E, Reubner BH: Hepatic changes produced by a single dose of endotoxin in the mouse: light microscopy and histochemistry. *Am J Pathol* 51:269-285, 1967
25. Levy E, Reubner B: Hepatic changes produced by single dose of endotoxin in the germfree mouse: histochemistry, light microscopy, fluorescence microscopy and electron microscopy. *Am J Pathol* 52:97-110, 1968
26. Levy E, Slusser RJ, Reubner BH: Hepatic changes produced by a single dose of endotoxin in the mouse. *Am J Pathol* 52:477-502, 1968
27. Rangel DM, Byfield JE, Adomian GE, Stevens GH, Fonkalsrud EW: Hepatic ultrastructural response to endotoxin shock. *Surgery* 68:503-511, 1970
28. Stewart GJ: Effect of endotoxin on the ultrastructure of liver and blood cells of hamsters. *Br J Exp Pathol* 51:114-117, 1970
29. Senterfitt VC, Shands JW Jr: Unpublished data

Fig 1—Liver from a 14-day BCG-infected mouse (H&E, $\times 320$).

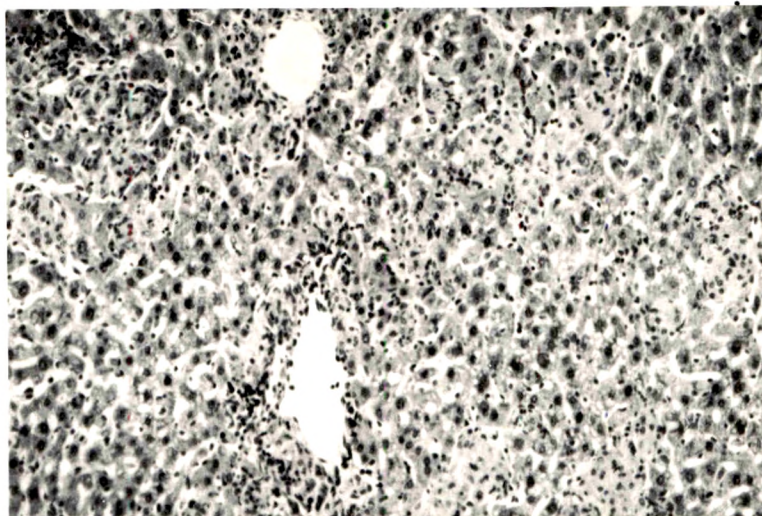


Fig 2—Perfusion-fixed liver from a 14-day BCG-infected mouse (toluidine blue, $\times 960$).

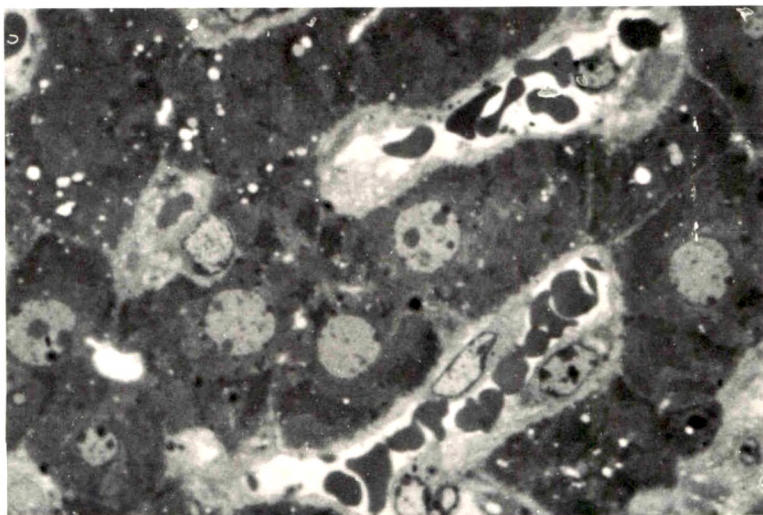
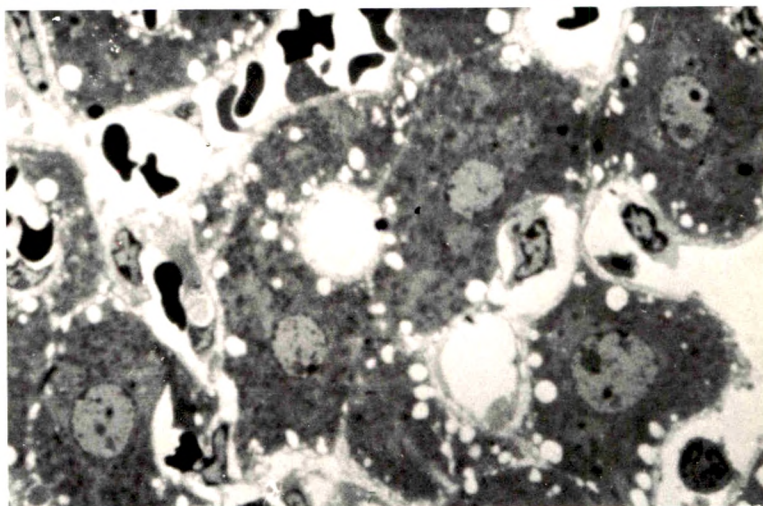


Fig 3—Perfusion-fixed liver from a 14-day BCG-infected mouse given 1.0 μg of endotoxin 3 hours previously (toluidine blue, $\times 960$).



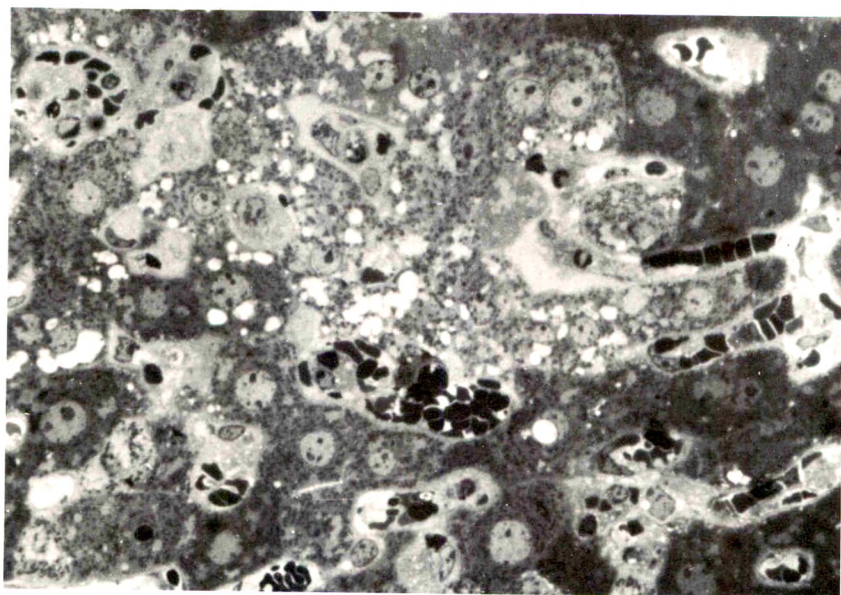


Fig 4—Immersion-fixed liver from a 14-day BCG-infected mouse given 1.0 μg of endotoxin 3 hours previously (toluidine blue, $\times 448$).

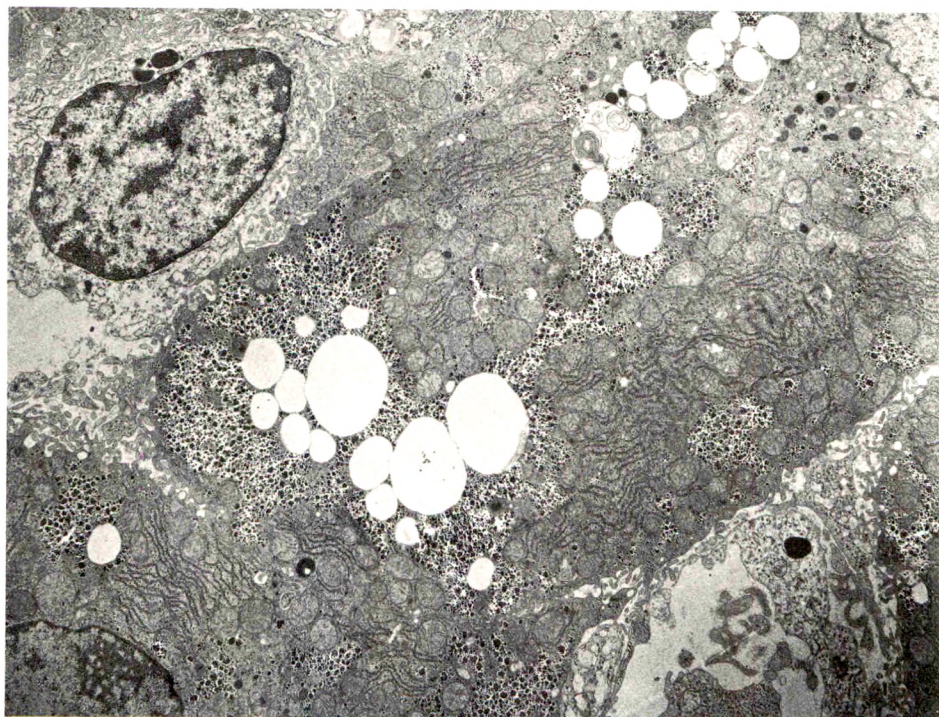


Fig 5—Liver from a 14-day BCG-infected mouse (uranyl acetate and lead citrate, $\times 3000$).

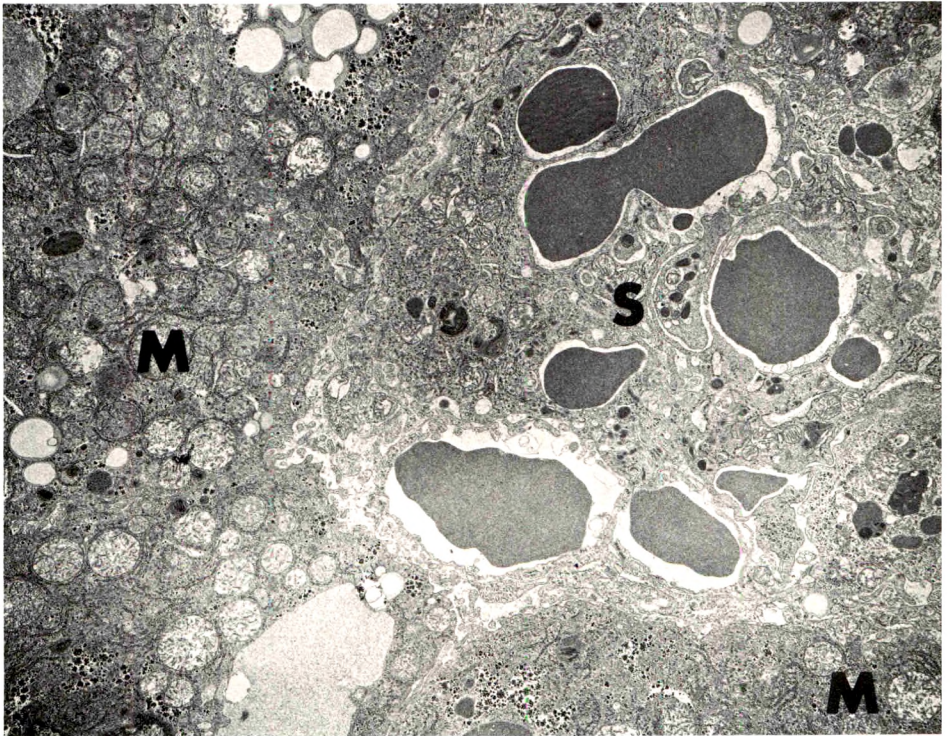
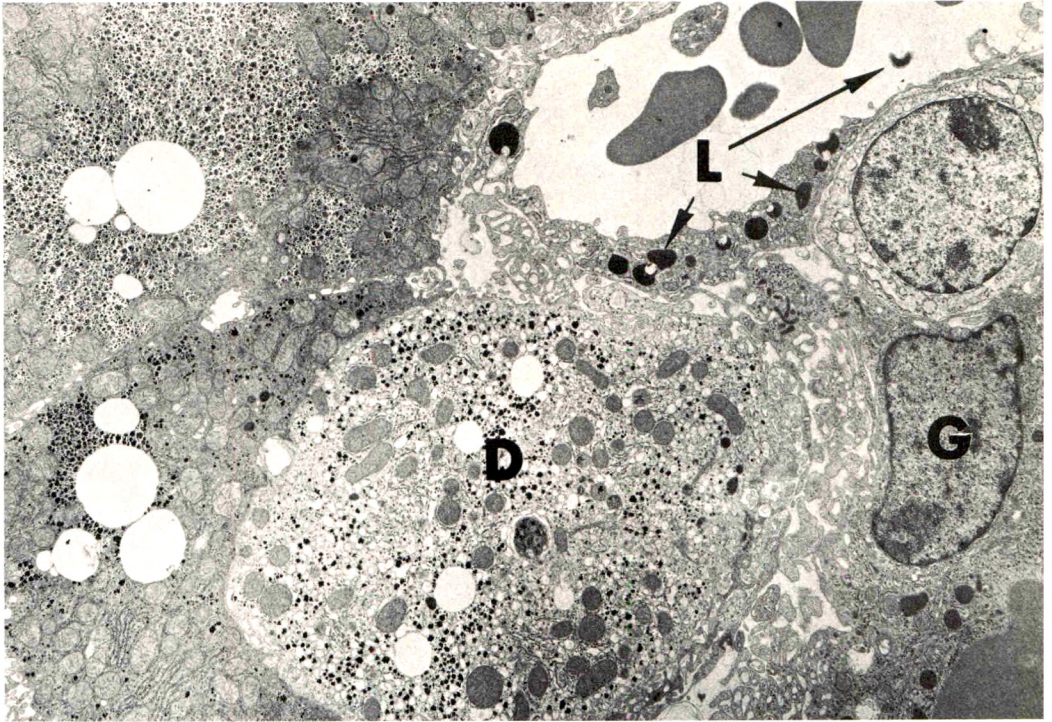


Fig 6—Same as Fig 5, showing the edge of a granuloma (G), an injured hepatocyte (D) and abundant lysosomes in a sinusoidal epithelial cell (L) ($\times 3000$). **Fig 7**—Liver from a 14-day BCG-infected mouse given $1.0 \mu\text{g}$ of endotoxin 1 hour previously, showing a sinusoid filled with Kupffer cells (S), and portions of two hepatocytes with swollen and occasionally fragmented mitochondria (M) ($\times 2800$).

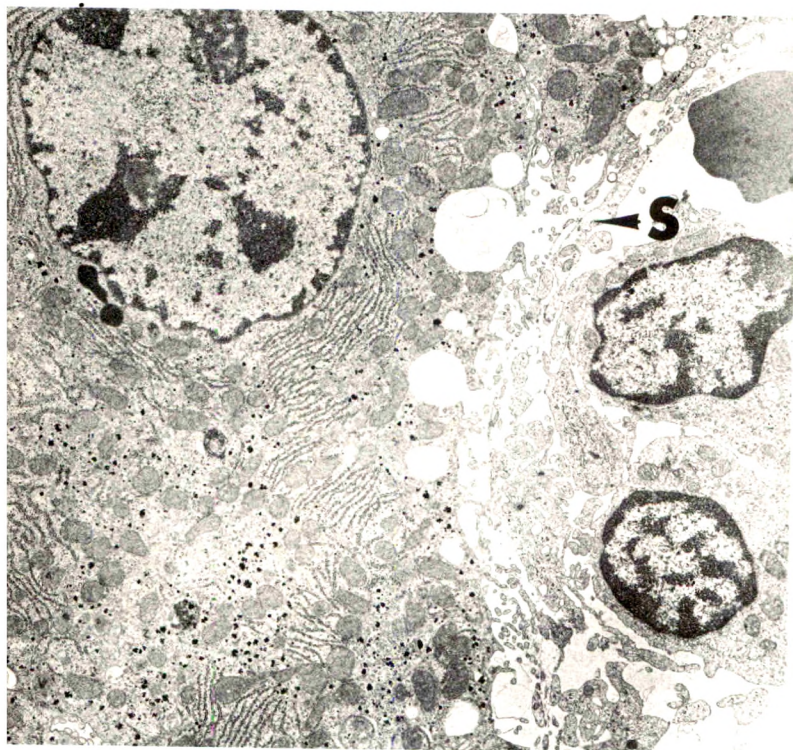
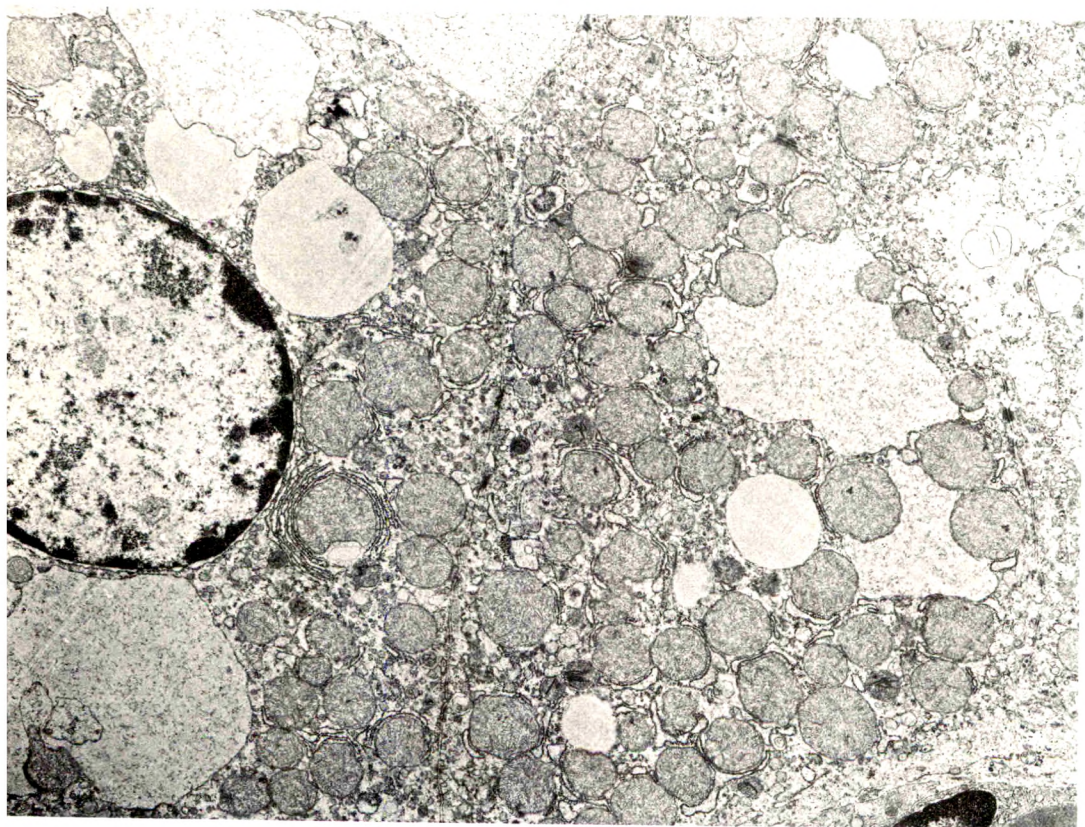


Fig 8—Liver from a 14-day BCG-infected mouse given 1.0 μg of endotoxin 3 hours previously, showing dilation of the subsinusoidal space (S) and vacuoles communicating with Disse's space ($\times 3000$). **Fig 9**—Same as in Fig 8, illustrating injured hepatocytes with relatively well-preserved mitochondria ($\times 3000$).



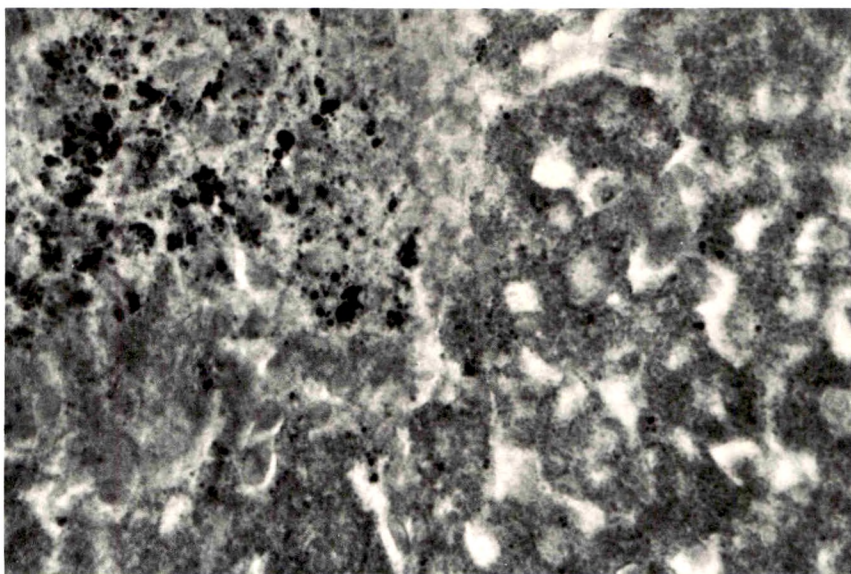


Fig 10—Acid phosphatase stain of control BCG-infected liver showing dense staining in discrete granules in a granuloma ($\times 514$).

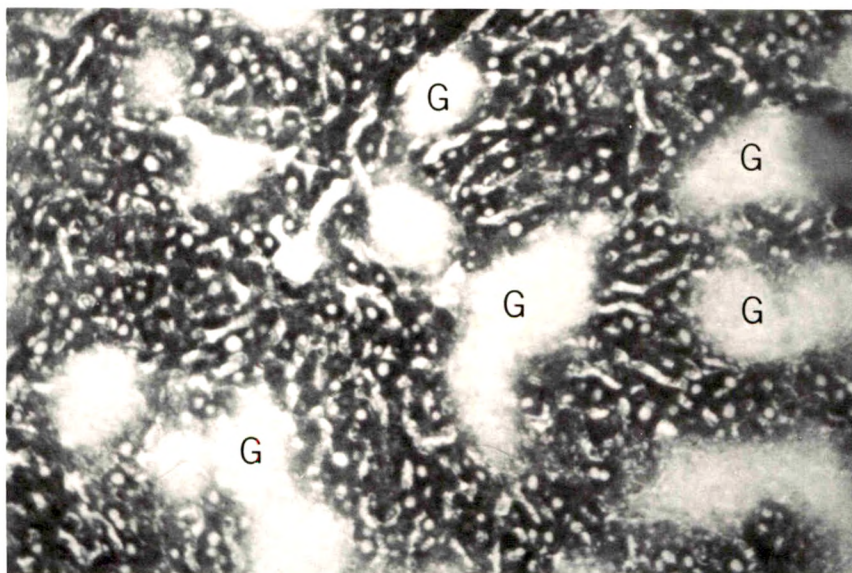


Fig 11— β -glucuronidase stain of control BCG-infected liver showing dense staining of hepatic cords and absence of stain in granulomas (G) ($\times 112$).

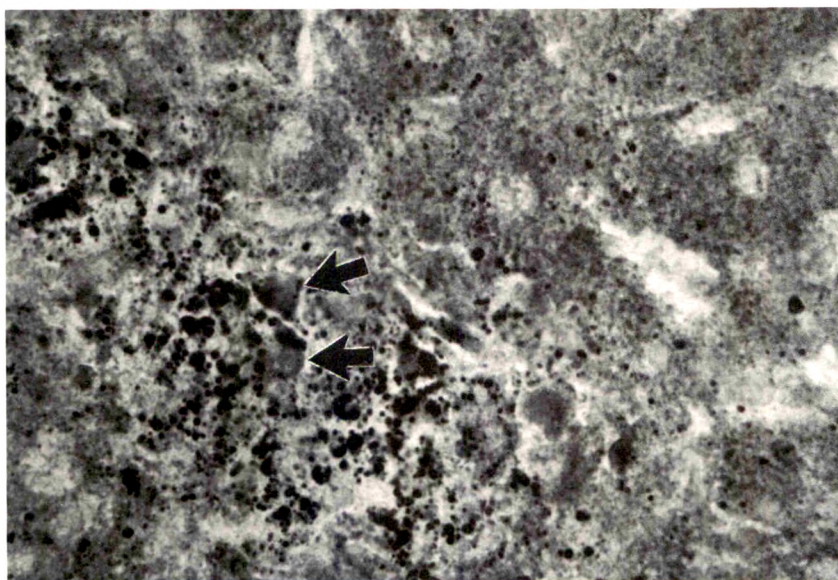


Fig 12—Acid phosphatase stain 2½ hours after endotoxin, showing diffuse staining of some cells (× 514).

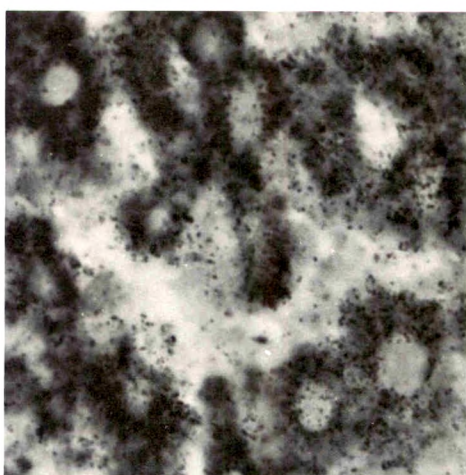
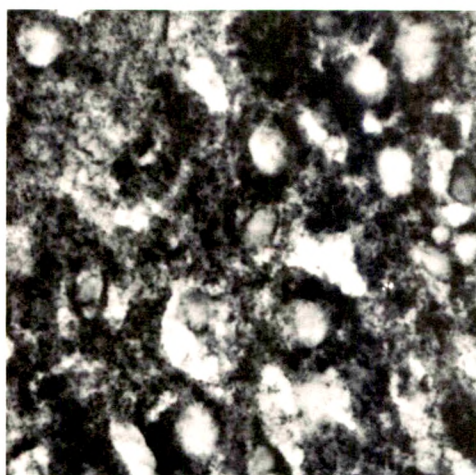


Fig 13— β -glucuronidase stain of control BCG-infected liver, showing dense stain in cytoplasm of hepatocytes (× 514). **Fig 14**— β -glucuronidase stain 2½ hours after endotoxin, showing decreased intensity of cytoplasmic staining (× 514).

Experimental Concussion

Ultrastructural and Biochemical Correlates

W. Jann Brown, MD, N. Yoshida, MD, T. Canty, MD and
M. Anthony Verity, MD

Ultrastructural and biochemical alterations were studied in the brainstem reticular formation of animals in which transient coma had been induced by controlled blows to the head. After a period of 7–10 days, animals that did not show obvious injury were artificially respired and sacrificed by perfusion with buffered formalin and glutaraldehyde. Histochemistry and light microscopy revealed chromatolysis of 10–15% of the neurons of pertinent segments of the nucleus gigante cellularis. There was much PAS-positive, diastase-sensitive material in the associated neuropil. Electron microscopy of the region confirmed the polysaccharide accumulation in dendrites, presynaptic boutons and preterminal axons. Similar material was found in some astrocytes. A longitudinal microchemical investigation with suitable controls of glycogen concentration in the brainstem demonstrated peak values at 5–7 days after concussion. No significant change in phosphorylase activity was demonstrated. The significance of glycogen accumulation in postconcussive injury and possible mechanisms for its accumulation in relation to changes in electrolyte balance and alterations in Krebs's cycle intermediates are discussed. (*Am J Pathol* 66:41–68, 1972)

THE BASIC MECHANISMS involved in the pathogenesis of concussion and the postconcussive state have not been elucidated despite long and intensive investigative efforts on the part of numerous investigators.^{1–5} Contributing to this problem are not only the unknown factors stemming from traumatic effects on the nervous system, but also difficulties in directly relating the syndrome in partially anesthetized experimental animals to that in man and the inability to standardize or measure the concussive effects of trauma in the human being. Ommaya⁶ recently defined concussion as a term implying traumatic disruption of the functional integrity of the nervous system, the most dramatic manifestation of which is sudden loss of consciousness. There are obvious limitations in the use of laboratory animals in this regard, and the degree of awareness and/or a memory deficit is not easily determined. A standard method for establishing an admittedly imperfect experimental model of the syndrome has been worked out by Denny-

From the Department of Pathology (Division of Neuropathology), Center for the Health Sciences, University of California, Los Angeles, Calif 90024.

Supported in part by Grants MH-06415 and EY-00361 from the US Public Health Service.

Accepted for publication September 21, 1971.

Address reprint requests to Dr. W. Jann Brown.

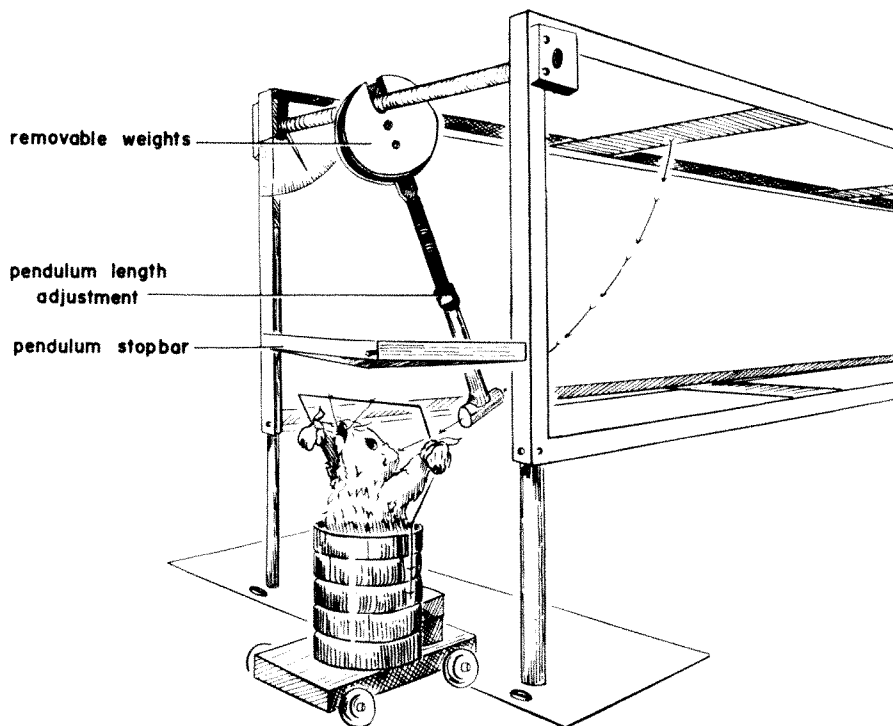
Brown and Russell.¹ The technic is based upon loss of certain critical brainstem reflexes which is transient in lightly anesthetized animals. The duration and intensity of the reflex change is related to the severity of the initial traumatic episode.

Electrophysiologic studies using superficial and deep recordings have shown that the period of unconsciousness correlates well with lessening cortical electric activity of variable duration.⁷⁻⁹ Rhines, Magoun and Windle¹⁰ demonstrated an inhibitory mechanism stemming from the brainstem reticular activating system. Though the structural-biochemical correlates involved in the underlying basis of concussion are not clear, it is evident that this segment of the brainstem is somehow affected.

Windle and colleagues¹¹⁻¹³ induced concussion in guinea pigs and found a characteristic distribution of chromatolysis in roughly 10-20% of the large neurons of the midline reticular nuclei, lateral vestibular nuclei and red nuclei. The chromatolytic changes followed a time course of development similar to that of retrograde chromatolysis secondary to axonal injury; however, some morphologic differences were claimed by the authors. Such chromatolysis has been induced by other investigators in dogs, monkeys and cats.¹⁴⁻¹⁷ We have confirmed the light microscopic findings of Windle and these other investigators but have looked, in addition, at the ultrastructural pathology of neurons and neuropil of the brainstem reticular formation. A parallel study of some aspects of glycogen metabolism related to ultrastructural findings of increased glycogen accumulations in this region were also explored.

Materials and Methods

Young 250 g female guinea pigs were lightly anesthetized with pentobarbital (60 mg/kg/body weight) intraperitoneally. The animal was prepared as demonstrated in Text-fig 1. This arrangement kept the head in a midline position but allowed movement in the direction of the concussive impulse. Animals were struck in the parieto-occipital region with a weighted pendulum similar to that used by Denny-Brown and Russell.¹ Criteria used to evaluate the clinical state after the blow were: unconsciousness as manifested by absence of corneal and pinna reflexes, loss of pain appreciation and an inspiratory gasp followed by a period of apnea and bradycardia. These changes were transient and their duration directly related to the severity of the blow. A model No. 1020 Endevco piezo-electric microaccelerometer with a sensitivity of 4.75 m/gravity with a range of 1-10,000 g was previously fixed to the animal's forehead with a stainless-steel screw and dental cement. Acceleration in the direction of the applied force was measured by feeding the accelerometer output into a model No. S65 Tektronix oscilloscope, then into a Tektronix recording camera. By proper calibration, direct measurement of the intensity and duration of acceleration of the head was obtained, but a varying number of blows often had to be applied using a consistently weighted pendulum swung through an arc until "concussion" could be demonstrated by the clinical criteria cited above. After



TEXT-FIG 1—Line drawing of concussion apparatus with weighted eccentric pendulum. Anesthetized guinea pig in freely moving position.

impact, the pendulum and the head were allowed to travel 2.5 cm before the pendulum came to rest against a fixed rubber stopper (Text-fig 1). The animal rolled clear of any secondary impact.

The electrocardiogram was recorded on a Gilson Medical Electronics polygraph and the electroencephalogram taken from two indwelling scalp needle electrodes in the parieto-occipital region on an Offner portable electroencephalograph (type 10). These physiologic data were taken both during the unconscious state and the short recovery period.

Successful light and electron microscopic observations were made on 4 animals 7–10 days after concussion. A total of 14 animals were submitted to the concussive regimen, but clinical, physiologic and/or perfusion of the brainstem for electron microscopy was not considered optimal in the remainder. Any animal that revealed evidence of injury to skull, meninges or brain was discarded. Animals were prepared for optical study as follows: light pentobarbital narcosis was induced, a glass cannula inserted into the ascending aorta and iso-osmotic 10% formalin–acacia mixture¹⁸ introduced at 60–70 mmHg pressure at room temperature. Cross sections of the medulla were made, embedded in paraffin, step sections cut at 10 μ and the sections stained with cresylviolet or buffered thionine.

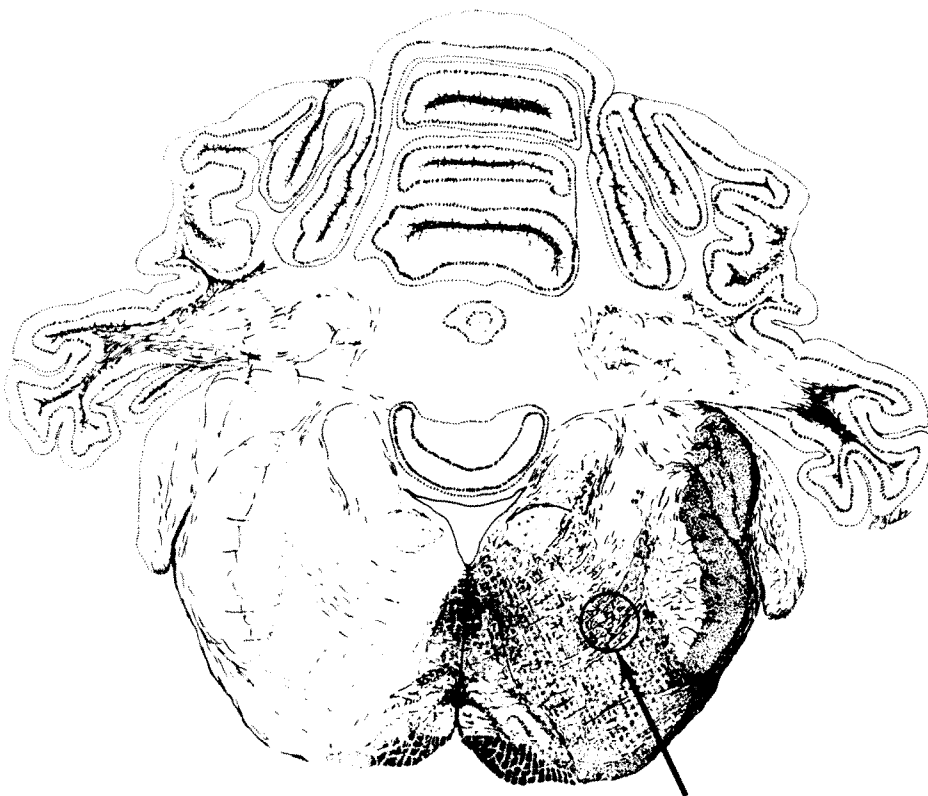
After a similar postconcussive period, comparable animals were selected for electron microscopy. Under light pentobarbital anesthesia, a tracheostomy was done and respiration artificially maintained by administering 95% O₂ and 5% CO₂. The chest was opened, a cannula quickly tied into the ascending aorta, the right

atrium opened and the brain perfused by 20 ml of 5% CO₂ and 95% O₂ saturated Ringer's solution followed by 450 ml of 1.0% paraformaldehyde and 1.0% redistilled, norite-purified glutaraldehyde in 0.135 M phosphate buffer (pH 7.2-7.4). The animals were allowed to stand undisturbed in the cold for about 1 hour. The firmly fixed brains were removed carefully, sectioned across at the midolive medullary level and above. Pertinent blocks were removed from the reticular formation just lateral to the medial lemniscus, to include the nucleus giganto cellularis (Text-fig 2).

The blocks were placed in fresh 1.0% glutaraldehyde in buffer for 4 hours, then finely sliced with acetone-cleaned razor blades. The small blocks were rinsed in buffer and placed in phosphate-buffered 2% osmium tetroxide solution. After 1 hour, blocks were rinsed twice with 2.4% NaCl solution, dehydrated in graded ethyl alcohols and embedded in Epon resin 812. One-micron-thick sections were stained with toluidine blue for orientation and cell selection. Thin sections of revised blocks were cut with glass and diamond knives, placed on copper grids previously coated with formvar, stained variously with lead monoxide¹⁹ or lead citrate²⁰ and aqueous uranyl acetate. Examinations were made with the Hitachi HU-11 and Siemens 1A microscopes.

Chemistry

Glycogen Determinations. Female Swiss mice weighing 25-27 g were decapi-



TEXT-FIG 2—Diagrammatic cross section of brain stem and cerebellum of guinea pig. Cells examined were from nucleus giganto cellularis of reticular formation (arrow).

tated directly into liquid nitrogen. The skull was exposed over the occipital region, the bone removed and the cerebellum dissected free. The brainstem was rapidly excised in the cold room and weighed before being placed in hot 30% KOH and heated to 95 C for 20 minutes. One milliliter of glass-distilled ethanol was added to the cooled digestate which was allowed to stand at 2 c for 3 hours. The ethanol-KOH mixture was centrifuged at 4000 rpm for 5 minutes and the supernatant decanted; 1.5 ml of methanol-chloroform (4:1 v/v) was added and the sediment stirred with a glass stirring rod into the extraction medium to remove cerebrosides. The methanol-chloroform mixture was warmed at 50 C for 15 minutes before centrifugation at 4000 rpm for 10 minutes. The resulting supernatant was carefully removed with a disposable Pasteur pipet and the sediment allowed to drain. The glycogen button was solubilized with 0.5 ml of 0.1 N HCl. Of this solution, 0.1 ml was assayed for glycogen, using the modified microanthrone procedure of Verity and Brown.²¹

Glycogen Phosphorylase. Phosphorylase was measured by the conversion of glucose-1-phosphate to glycogen with liberation of inorganic phosphate. Mice were decapitated in liquid nitrogen and the midbrain plus brainstem rapidly removed and placed in 1 ml of ice-cold 50 mM sodium fluoride and 5 mM EDTA. The tissue was homogenized in a small glass Potter-Elvehjem type of homogenizer. Aliquots of homogenate were placed in an assay system of 0.5 ml total volume containing 0.08 M citrate buffer, pH 6.7; 150 mM glucose-1-phosphate and 20 mg glycogen. A 0.1 ml aliquot was removed from the assay medium at zero time and protein precipitated in an equal volume of 0.5 N perchloric acid. At the end of 30 minutes of incubation, a further 0.1 ml aliquot was removed from the assay system and precipitated by 0.5 N perchloric acid. After the precipitated protein was centrifuged, the supernatant was neutralized by 25 ml of 2.5 N potassium carbonate and the potassium perchlorate formed removed by centrifugation. One-tenth milliliter aliquots of the supernatant were assayed for phosphate after the method of Verity and Bevan.²² Phosphorylase activities were determined in the absence and presence (total) of 1 mM adenosine monophosphate (AMP).

Protein was determined on homogenates by the method of Lowry *et al*²³ using bovine serum albumin as protein standard.

Results

Reticular Formation (Nucleus Giganto Cellularis) in Control Animals

Optical Microscopy

Cresylviolet- or thionine-stained preparations of these nuclei revealed three types of neurons, roughly classed as large, intermediate and small. The large cells had extensive masses of Nissl substance in their cytoplasm (Fig 1). The masses were smaller in the intermediate cells and the smallest cells had rather sparse clumps of Nissl substance. In 4 experimental animals, roughly 10-15% of the large neurons appeared to have undergone chromatolytic alteration. Chromatolysis was of the central type (Fig 2) and appeared to be similar to the neuron changes seen in axonal injury. There was no obvious proliferation or unusual collection of astrocytes, oligodendrogliaocytes or reactive cells in the region of the involved neurons. Weil and Gies stains revealed no other abnormalities of the neuropil. Periodic acid-Schiff preparations disclosed increased particulate masses of PAS-positive, diastase-sensitive

material throughout the reticular formation, which is indicative of polysaccharide accumulation.

Electron Microscopy

Neurons from control guinea pigs that contained within their cytoplasm normal-appearing Nissl substance and nuclear orientation, were selected from 1- μ toluidine blue-stained sections. A portion of a thin section of a control large neuron from the nucleus giganto cellularis is shown in Fig. 3. The arrays and plates of cisternae of the ribosome-studded rough endoplasmic reticulum are formed into large aggregates representing Nissl material. Some free polysomes may be noted between the cisternae and stacks of paranuclear-orientated Golgi membranes. A few dense bodies and condensed mitochondria are found with no particular arrangement. In this region of the brainstem, there is an extensive maze of myelinated axons and interweaving dendrites, synapses and glia. The heavy myelination of the reticular substance makes thin sectioning difficult. Glycogen rosettes were virtually absent from the neuronal perikaryon. Typical neurotubules were abundant throughout the cell soma.

Synaptic bulbs and preterminal axons contained mitochondria, numerous neurofilaments, neurotubules and abundant synaptic vesicles. The vesicles in some end bulbs were tubular or oval, whereas other presynaptic bulbs were filled with typical spherical vesicles (Fig 4).

Those endings containing spherical vesicles are additionally characterized by fewer mitochondria and less packing of spherical vesicular profiles. Moreover, a greater tendency for the spherical profiles to abut the region of the synapse was noted; in contrast, the preterminal endings characterized by tubular profiles were larger, contained more densely packed vesicles per unit area, and were evenly distributed through the presynaptic bouton. The average diameter of the spherical profiles varied from 400 to 530Å. The tubular profiles, on the other hand, were more heterogeneous with mean longitudinal diameters of 635Å and short axes of 250Å. The occasional larger dense cored vesicle (Type I) had a mean diameter of 1030Å.

Of possible neurophysiologic significance was the arrangement of fine neurofilaments in regions relatively clear of any organelles in many preterminal synaptic bulbs characterized by spherical vesicles. This finding in certain preterminal synaptic knobs has also been described by Gray and Guillery.^{24,25} Some preterminal axons while having no apparent neurofibrils did have many microtubules. It was our impression that such tubules were found in axons whose terminals contained ellip-

soid vesicles, but a critical assessment of much material and associated variations is necessary before such a singular feature as the differential distribution of neurofibrils and tubules in relation to types of vesicles could be a descriptive reality. Bowsher and Westman^{26,27} have also commented upon fine fibrils occurring both singly and in small fascicles along the sides of preterminal knobs in a position apposing collections of synaptic vesicles in the reticular formation of the cat. A further characteristic feature of this region in the guinea pig is that both Type I and Type II synapses²⁸ end on dendrites and somata of the reticular neurons (Fig 4 and 5).

Occasionally, small rosettes of darkly stained glycogen were noted, admixed with the various types of synaptic vesicles. The glycogen masses were similar to such rosettes found in hepatic cells²⁹ and in centrifuged preparations of pure glycogen.³⁰ The polysaccharide stained intensely with lead salts, but only vague ghosts were noted when staining primarily with aqueous uranyl acetate.

Postconcussion Animals

In the chromatolytic neuron cytoplasm of the injured guinea pig, there was a general picture of disarray. The rough-surfaced endoplasmic reticulum was no longer arranged in stacks of cisternae, but appeared dispersed to the periphery away from the nucleus, and the membranes consisted of short segments and strands (Fig 6). Ribonucleoprotein particles and polysomes were loose and scattered throughout the cytoplasm. Small orderly collections of neurofibrillae were seen in the cytoplasm, sometimes in seemingly linear array in relation to mitochondria (Fig 6).

In general, abnormalities in mitochondrial morphology were not seen except for rare instances of autophagic vacuole formation and lipid inclusions. Swelling and abnormalities of cristall morphology were not observed. Intramitochondrial densities were absent. The Golgi lamellae were normally distributed about the nucleus but occasional bizarre dilatation of cisternae was noted (Fig 7).

Bowsher and Westman^{26,27} have described, in this region of the brainstem of the cat, two main types of neurons: in one, the dendrite conformation is polydendritic and in the other, oligodendritic. The plasma membrane of the polydendritic neuron was characterized as having multiple short, blunt spines which projected into the surrounding neuropil. Such structures are the sites of synaptic specialization, with presynaptic knobs containing either spherical or ellipsoidal vesicles, synapsing on their surfaces. The presynaptic knobs appeared to

clasp the spine. No special apparatus was noted within the spinous process, but near the neck of the spines there were usually one to three coated vesicles. These vesicles, throughout all neurons examined, measured 500–1200Å. Such a relationship was still retained in the chromatolytic neuron (Fig 6 and inset). The spines, in this situation, are accentuated by greatly enlarged extracellular spaces, but such spaces were rare.

A number of chromatolytic neurons exhibited dilatation of the apposed Golgi cisternae and contained some amorphous dense material and numerous scattered small vesicles (Fig 7), some had a few multivesicular bodies. Further, some of the parallel arrangement of the Golgi lamellae in relation to the nuclear envelope was greatly altered by the dilatation of cisternae. Mitochondria remained numerous, but scattered, and their usual structure appeared unchanged by the alterations seen in the neuron cytoplasm (Fig 6 and 7). Chromatolysis, though of lesser degree, was noted in a number of scattered intermediate and small-size neurons of the reticular network.

Mitochondria of the presynaptic bulbs and preterminal axons of the neuropil of this region of the guinea pig brainstem exhibited no apparent modifications of contour or matrix (Fig 8 and 9). The numbers of these organelles in preterminal endings varied greatly, however. Synaptic vesicles were spherical or tubular, and in many presynaptic bulbs, dense-cored bodies with a thick nimbus-like bounding membrane were commonly found (Fig 8). These dense-cored particles measured 900–1500 Å in diameter and were analogous to type I granular vesicles.³¹

Significant early and late degenerative changes were easily identified in presynaptic bulbs. These alterations were seen in preterminal endings containing both tubular and spherical vesicular profiles. Moreover, many postsynaptic dendrites were contiguous with both abnormal- and normal-appearing presynaptic structures (Fig 10). Minimal morphologic evidence of presynaptic injury was observed in the increased accumulation of glycogen, normal-appearing and often increased numbers of synaptic mitochondria and, rarely, numerous Type I granular vesicles (Fig 8–10). Later evidence of presynaptic injury was characterized by fragmentation and dilatation of membranes that seem akin to smooth ER profiles and the incorporation of rosettes of glycogen within membranous multilamellar structures suggestive of autophagic vacuoles (Fig 10). In similar boutons, numbers of residual bodies were evident. (Fig 11).

Glycogen was not found within either chromatolytic or uninvolved

neuron somata. Associated astroglia did contain some polysaccharide within cytoplasm.

Physiologic Studies

These data were obtained primarily as a means to control the production of concussion. The blows to the head consistently produced changes in the electroencephalogram that varied from marked slowing to almost complete flattening of the record in the immediate post-concussive period. Gradual recovery occurred with the appearance of high-amplitude slow waves and then eventual reversion to "normal" preconcussion fast electrical activity. Electroencephalographic recovery closely followed clinical recovery of critical reflexes used in establishing criteria of concussion. The data obtained was similar to other more detailed investigations of postconcussive EEG activity.^{7-10,12}

We did not always see bradycardia with concussion, but in some animals we noted either no change, an increase in heart rate, occasional arrhythmia or actual heart block. Concussion did, however, consistently induce an immediate inspiratory gasp followed by a period of apnea, often lasting 1-2 minutes and requiring respiratory assistance in some instances. Respiration gradually recovered with irregular deep gasping, which steadily progressed to the respiratory rate and rhythm of the pre-concussive state.

Biochemical Studies

With cerebral ischemia, glycogenolysis of brain glycogen ensues rapidly.^{32,33} To obviate changes in cerebral glycogen due to ischemia, it was necessary to rapidly freeze the brain. Moreover, the deeply situated midbrain will take some seconds to reach a core temperature less than 0 C. For this reason and because previous control studies on cerebral glycogen phosphorylase and glycogen content had been performed in adult mice, correlative biochemical data are presented in this animal, a species in which more rapid freezing and preservation of *in situ* glycogen and phosphorylase activity after decapitation may be ensured.

A single concussive episode did not produce significant change in brainstem glycogen content during a period of 7 days after concussion. Four regular concussive episodes over a period of 6 hours provided a suitable model for studying postconcussive alterations in glycogen and phosphorylase. Mean brainstem wet weight was 37.6 mg (N = 20). Statistical data is presented in Table 1 on the change in brainstem

glycogen at 4, 7 and 11 days after experimental concussion. A significant increase above the control value of 40.6 ± 6.5 $\mu\text{g}/100$ mg frozen wet weight was seen at all three postconcussive periods, with a maximal value of 75.5 ± 3.8 $\mu\text{g}/100$ mg frozen wet weight at 7 days.

Glycogen phosphorylase in intact brain is predominantly in an inactive form but can be converted within seconds to an active form.³⁴ The process of activation is dependent upon the presence of adenosine-5-phosphate (AMP). Inactivation and reactivation of the phosphorylase moiety was prevented by fluoride and EDTA, hence homogenization of the frozen brain was performed in a mixture of sodium fluoride and EDTA, thereby preventing interconversion that might have occurred during the preparation of the homogenate prior to analysis. The change in phosphorylase activity during the postconcussive period is summarized in Table 2. As can be seen, no significant change in total, activated phosphorylase activity in the presence of AMP is evident. Additionally, no significant change in the active component of the enzyme in the absence of AMP is noted. It is conceivable that the methods of brain quenching and preparation used are such as to preclude any measure of activation or inactivation of the normal "active" component of the total enzyme complex. In fact, Breckenridge and Norman³⁴ have demonstrated the significance of freezing the brain *in situ* as compared with decapitation into liquid nitrogen. Their studies confirm that the phosphorylase in cerebral cortex frozen *in situ* is predominantly in the inactive form, whereas that from mice decapitated into liquid nitrogen contains a much higher proportion of the active enzyme. The data do demonstrate that no significant change in the potential activity of phosphorylase, expressed on a protein basis, is noted in the brainstem at any time after concussion, when increased amounts of glycogen have been documented (Table 1).

Table 1—Effect of Experimental Concussion on Brainstem Glycogen*

Control	Glycogen ($\mu\text{g}/100$ mg frozen wet weight)		
	Days postconcussion		
	4	7	11
40.6 ± 6.5 (N = 7)	$54.4 \pm 3.1^\dagger$ (N = 5)	$75.5 \pm 3.8^\dagger$ (N = 4)	56.7 ± 2.4 (N = 4)

* Mice were submitted to four concussive blows over a period of 6 hours. The brainstem was removed rapidly in the cold room after decapitation into liquid N_2 . Glycogen was determined in KOH digests by the anthrone procedure after washing in $\text{MeOH}-\text{CHCl}_3$. Values are means \pm SE.

† Means different from control at $P < 0.01$.

Table 2—Glycogen Phosphorylase of Brainstem After Concussion*

Fraction	Glycogen phosphorylase (μ moles/min/100 mg protein)			
	Days Postconcussion			
	Control (N = 8)	1 (N = 3)	4 (N = 4)	7 (N = 3)
"Active" fraction	11.2 \pm 0.7	10.7 \pm 1.8	11.5 \pm 1.1	10.5 \pm 1.6
plus 1mM AMP	14.0 \pm 0.6	12.6 \pm 1.3	13.6 \pm 2.1	12.5 \pm 1.3
% "Active" fraction	80	84.9	84.5	84.0

* Determined in mouse brainstem removed after rapid freezing of whole head in liquid nitrogen. Activities are expressed in presence and absence of 1 mM AMP.

Discussion

It has been proposed by many that concussion is the result of direct mechanical damage to the neurons of the brainstem and/or cerebral cortex, and the injury that occurs is secondary to a number of factors, including pressure gradients^{4,5} and resultant shear forces,³⁵ rotation of the brain within the calvarium,³⁶ cavitation,³⁷ and general breakdown of cell membranes or synaptic complexes. The real significance of all or any of these factors is not known at present.

Since the descriptions by Windle, Groat and Fox^{11-13,38,39} of alterations in neurons of the brainstem of the guinea pig seen after concussion, little has been added to the picture until recently when Friede and co-workers induced a variant of concussive injury in cats.^{3,17,40} They indicated that the chromatolysis of neurons of the brainstem seen in the cat was due to interruption of ascending fibers in the mediocentral regions of the cervical spinal cord. The lesions described resulted from blows that accelerated a freely moving head in such a way that maximum energy of the blow was felt at the craniocervical junction during acute flexion. They surmised that the axonal injury and attendant chromatolysis could be controlled by the use of a collar that would restrict the movement of the head at the time of the blow. Thus, the syndrome of acceleration-concussion with its concomitant abolition of reflexes was proposed as the result of axonal injury and retrograde chromatolysis.⁴⁰ One feature of Friede's experiments that is convincing and seems to support such a concept is the time course of development of the concussion chromatolysis which closely paralleled that of retrograde chromatolysis due to other injury. Our data neither confirms nor denies the role of the cervical component in the induction of the syndrome.

Reports concerning the electron microscopy of retrograde chromatolysis are few.^{41,42} An early feature is a dispersion of the rough-surfaced endoplasmic reticulum, an extensive detachment of ribonucleoprotein particles from the same membranes and dilatation of Golgi cisternae. Vesco and Giuditta⁴³ have quantitated such disaggregation of brain polysomes which they induced by multiple convulsive episodes. Our studies have revealed certain alterations of axon terminals and presynaptic bulbs of the reticular formation, the most striking feature of which is the accumulation of large amounts of glycogen which is seemingly associated with a decrease in synaptic vesicles from within the end bulb. Synaptic bars and other membranes nearby appeared undisturbed, although in several of these endings a series of loose encircling membranes enclose numerous small masses of glycogen.

Other changes suggestive of degenerative and increased catabolic activity include the formation of autophagic vacuoles, dilatation of membrane cisternae, and increased numbers of lysosome-like residual bodies. While no quantitative data on the type I granular vesicle population is available, our observations suggested the presence of increased numbers of these vesicles in synaptic end bulbs characterized by tubular or spherical agranular synaptic vesicles. Moreover, such type I vesicles were often associated with masses of intraterminal glycogen. Similar masses of glycogen and numerous mitochondria have been described by Sotelo and Palay⁴⁴ in distal segments of dendrites of the lateral vestibular nucleus. They have interpreted their findings as possibly indicating growing tips of dendrites in mature vestibular nucleus. While such profiles were not found in our control material, the possibility exists that such characteristic dendrites may extend to the reticular formation from the lateral vestibular nucleus.

The polysaccharide seen in our preparations was found in both dendrites and in axon terminals. The presence of clear spherical vesicles admixed with the glycogen helps to identify the axon terminal. The nature of the membranous structures enclosing particulate glycogen are compatible with cytolysosome and/or early autophagic vacuole formation, although similar formations revealed in the electron micrographs of the lateral vestibular nucleus suggest the possible transitional development from mitochondria.⁴⁴

The ultrastructural recognition of glycogen in the brain and its localization within neurons, dendrites, synaptic structures and glial cells is doubtlessly related to perfusion fixation.^{45,46} The polysaccharide is quickly degraded and commonly missed in many biologic preparations. We found no glycogen in the neuron soma in either control or injured

subjects. In presynapses of controls, a few rosettes of glycogen were found, although it was not too common. Similarly, glycogen was found in astrocytes but not in any profusion. The increased polysaccharide deposition observed electron microscopically was confirmed biochemically. Our staining procedure allows us to recognize the two basic types of glycogen particle, although the α particle,³⁰ a complex unit commonly referred to as a rosette, consisting of β particles, were abundant in the injured animals.

No microchemical studies were performed within a 24-hour period after the concussive episode. Our studies failed to define the mechanism of the postconcussive accumulation of glycogen, as the microchemical data was gathered primarily to confirm the change in fine structure. A variety of pathologic conditions results in the accumulation of glycogen in the mammalian brain.^{33,46-50} The fundamental lesion underlying the mechanism for such accumulation in these various studies has not been defined. Two aspects of this problem, however, may be considered. Firstly, what changes in metabolic pathways occur during the increased accumulation of glycogen and, secondly, why does glycogen preferentially accumulate in astroglia?

From studies of glycogen accumulation occurring after stab wounds, ionizing radiation or hypoxic injury, it was considered by Ibrahim *et al*⁴⁹ that in addition to an inhibition of anaerobic glycolysis, there may also occur an increase in glycogenesis. We would like to suggest a possible mechanism for the postconcussive accumulation of glycogen that is based upon this concept. The concussive episode is accompanied by a massive neuronal stimulation with diffuse generalized total membrane depolarization. This leads to electrical quiescence of the cortex and presumably deeper neuronal centers which we and others have found. Such a period is of variable length, depending upon the magnitude of the concussive insult. However, the phase of repolarization, characterized by rapid extrusion of Na^+ from dendrites depends upon the high-energy phosphate reserve, and because of the magnitude of the depolarization it is expected that dendrite energy reserve is rapidly depleted. After a variable period of time, the neuronal membrane returns to its state of polarization. However, during this period, abnormal amounts of sodium ions have been extruded into the interstitial clefts and are probably removed from the cleft space by the closely adjacent astroglial compartment. In this way, the astroglial potassium is diluted and astroglial swelling occurs. The astrocyte thus acts as a spatial buffer for cations present in the intercellular clefts, which in this case, because of the massive recovery from depolarization, will contain predominantly

sodium. Hence, the normal high potassium content of the astroglial cytoplasm⁵¹ is diluted by an increased concentration of Na^+ . Anaerobic and aerobic glycolysis is dependent upon an adequate concentration of K^+ ; increasing $[\text{K}^+]$ or omitting Ca^{2+} from media in which cerebral cortex slices are incubated, increases their rate of aerobic glycolysis.^{52,53} Takagaki⁵⁴ has concluded that pyruvate kinase (phosphoenolpyruvate kinase) is a rate-limiting step in aerobic lactate formation and that K^+ and Ca^{2+} change the overall rate of aerobic glycolysis directly through their effects upon pyruvate kinase activity. Moreover, Na^+ is inhibitory to pyruvate kinase.⁵⁴ Hence, in the presence of increased $[\text{Na}^+]$, decreased $[\text{K}^+]$ and increased $[\text{Ca}^{2+}]$, a significant inhibition of aerobic glycolysis will occur, with commensurately decreased pyruvate concentration and increased phosphoenolpyruvate levels and subsequent increase in Krebs' cycle intermediates. The decreased formation of pyruvate will limit the utilization of intermediates of the tricarboxylic acid cycle in oxidative phosphorylation as the primary energy source for ATP production.

The failure to demonstrate changes in phosphorylase does not preclude a possible variation in phosphorylase content *in situ*. Further studies utilizing more critical freezing technics of tissues to determine phosphorylase-b and phosphorylase-a activities are necessary to elucidate this apparent paradox. Additionally, increased glycogen content may result from increased synthetase activity in the absence of alterations in the action of the catabolic pathway. Biochemical data does not permit a choice between mechanisms at this point.

References

1. Denny-Brown D, Russell WR: Experimental cerebral concussion. *Brain* 64:93-164, 1941
2. Denny-Brown D: Cerebral concussion. *Physiol Rev* 25:296-325, 1945
3. Friede R, Hollister N, Jolley WP, Horne RG: Biophysics of Concussion, Part 2. Wright Air Development Center Technical Report pp 58-193. Dayton, Ohio. Armed Services Technical Information Agency, 1958 (Document No. AD 203385)
4. Gurdjian ES, Lissner HR, Latimer FR, Haddad BF, Webster JE: Quantitative determination of acceleration and intracranial pressure in experimental head injury. *Neurology* 3:417-423, 1953
5. Gurdjian ES, Lissner HR, Webster JE, Latimer FR, Haddad BF: Studies on experimental concussion: relation of physiologic effect to time duration of intracranial pressure increase at impact. *Neurology* 4:674-681, 1954
6. Ommaya AK, Rockoff SD, Baldwin M: Experimental concussion: a first report. *J Neurosurg* 21:249-265, 1964
7. Williams D, Denny-Brown D: Cerebral electrical changes in experimental concussion. *Brain* 64:223-238, 1941

8. Dow RS, Ulett G, Tunturi A: Electroencephalographic changes following head injuries in dogs. *J Neurophysiol* 8:161-172, 1945
9. Ward JW, Clark SL: Electroencephalogram in experimental concussion and related conditions. *J Neurophysiol* 11:59-74, 1948
10. Rhines R, Magoun HW, Windle WF: Bulbar inhibitory mechanism in concussion. *Am J Physiol* 146:344-347, 1946
11. Windle WF, Groat RA, Fox CA: Experimental structural alterations in brain during and after concussion. *Surg Gynecol Obstet* 79:561-572, 1944
12. Windle WF, Groat RA, Magoun HW: Functional and structural changes in central nervous system during and after experimental concussion. *Trans Am Neurol Assoc* 70:117-122, 1944
13. Groat RA, Windle WF, Magoun HW: Functional and structural changes in the monkey's brain during and after concussion. *J Neurosurg* 2:26-35, 1945
14. Evans JP, Scheinker IM: Histologic studies of the brain following head trauma: VI. Post-traumatic central nervous system changes interpreted in terms of circulatory disturbances. *Res Publ Assoc Nerv Ment Dis* 24:254-273, 1944
15. Chason JL, Haddad BF, Webster JE, Gurdjian ES: Alterations in cell structure following sudden increases in intracranial pressure. *J Neuropathol Exp Neurol* 16:102-107, 1957
16. Chason JL, Hardy WG, Webster JE, Gurdjian ES: Alterations in cell structure of the brain associated with experimental concussion. *J Neurosurg* 15:135-139, 1958
17. Friede RL: Experimental concussion acceleration: pathology and mechanics. *Arch Neurol* 4:449-462, 1961
18. Koenig H, Groat RA, Windle F: Physiological approach to perfusion-fixation of tissues with formalin. *Stain Technol* 20:13-22, 1945
19. Karnovsky MJ: Simple methods for "staining with lead" at high pH in electron microscopy. *J Biophys Biochem Cytol* 11:729-732, 1961
20. Venable JH, Coggeshall RA: A simplified lead citrate stain for use in electron microscopy. *J Cell Biol* 25:407-408, 1965
21. Verity MA, Brown WJ: Rapid micromethod for glycogen: application to hepatic needle biopsies. *J Lab Clin Med* 62:846-852, 1963
22. Verity MA, Bevan JA: Membrane adenosine triphosphatase activity of vascular smooth muscle. *Biochem Pharmacol* 18:327-338, 1969
23. Lowry OH, Rosebrough NJ, Farr AL, Randall RJ: Protein measurement with the Folin phenol reagent. *J Biol Chem* 193:265-275, 1951
24. Gray EG, Guillery RW: The basis for silver staining of synapses of the mammalian spinal cord: a light and electron microscope study. *J Physiol (Lond)* 157:581-588, 1961
25. Gray EG, Guillery RW: Synaptic morphology in the normal and degenerating nervous system. *Int Rev Cytol* 19:111-182, 1966
26. Bowsher D, Westman J: Gigantocellular reticular region and its spinal afferents: a light and electron microscope study in the cat. *J Anat* 106:23-36, 1970
27. Bowsher D, Westman J: Ultrastructural characteristics of the caudal and rostral brain stem reticular formation. *Brain Res* 28:443-457, 1971
28. Gray EG: Axosomatic and axodendritic synapses of the cerebral cortex (an electron microscope study). *J Anat* 93:420-433, 1959

29. Revel JP: Electron microscopy of glycogen. *J Histochem Cytochem* 12:104-114, 1964
30. Drochmans P: Morphologie du glycogene: etude au microscope electronique de colorations negatives du glycogene particulaire. *J Ultrastruct Res* 6:141-163, 1962
31. Grillo MA: Electron microscopy of sympathetic tissues. *Pharmacol Rev* 18:387-399, 1966
32. Kerr SE, Ghantus M: Carbohydrate metabolism of brain. *J. Biol Chem* 116:9-20, 1936
33. Wolfe LS, Klatzo I, Miguel J, Tobias C, Haymaker W: Effect of alpha-particle irradiation on brain glycogen in the rat. *J Neurochem* 9:213-218, 1962
34. Breckenridge BM, Norman JH: Glycogen phosphorylase in brain. *J Neurochem* 9:383-392, 1962
35. Strich SJ: Shearing of nerve fibres as a cause of brain damage due to head injury: a pathological study of twenty cases. *Lancet* 2:443-448, 1961
36. Pudenz RH, Schelden CH: The Lucite calvarium: a method for direct observation of the brain. II. Cranial trauma and brain movement. *J Neurosurg* 3:487-505, 1946
37. Gross AG: A new theory on the dynamics of brain concussion and brain injury. *J Neurosurg* 15: 548-561, 1958
38. Windle WF, Groat RA: Disappearance of nerve cells after concussion. *Anat Rec* 93:201-209, 1945
39. Groat RA, Magoun HW, Dey FL, Windle WF: Functional alterations in motor and supranuclear mechanisms in experimental concussion. *Am J Physiol* 141:117-127, 1944
40. Friede RL: Specific cord damage at the atlas level as a pathogenic mechanism in cerebral concussion. *J Neuropathol Exp Neurol* 19:266-279, 1960
41. Bodian D: An electron microscopic study of the monkey spinal cord. *Bull Johns Hopkins Hosp* 114:13-119, 1964
42. Kirkpatrick JB: Chromatolysis in the hypoglossal nucleus of the rat (an electron microscopic analysis). *J Comp Neurol* 132:189-211, 1968
43. Vesco C, Giuditta A: Disaggregation of brain polysomes induced by electroconvulsant treatment. *J Neurochem* 15:81-85, 1968
44. Sotelo C, Palay SL: Fine structure of the lateral vestibular nucleus in the rat. *J Cell Biol* 36:151-179, 1968
45. Yamamoto T: Some observations on the fine structure of the sympathetic ganglion of bullfrog. *J Cell Biol* 16:159-170, 1963
46. Maxwell DS, Kruger L: The fine structure of astrocytes in the cerebral cortex and their response to focal injury produced by heavy ionizing particles. *J Cell Biol* 25:141-157, 1965
47. Shimizu N, Hamuro Y: Deposition of glycogen and changes in some enzymes in brain wounds. *Nature* 181:781-782, 1958
48. Woolley DE, Timiras PA: Changes in brain glycogen concentration in rats during high altitude (12,470 ft.) exposure. *Proc Soc Exp Biol Med* 114:571-574, 1963
49. Ibrahim MZM, Pascoe E, Alam S, Miguel J: Glycogen and phosphorylase activity in rat brain during recovery from several forms of hypoxia. *Am J Pathol* 60:403-415, 1970

50. Klatzo I, Miguel J, Tobias C, Haymaker W: Effects of alpha particle radiation on the rat brain, including vascular permeability and glycogen studies. *J Neuropathol Exp Neurol* 20:459-483, 1961
51. Kuffler SW, Nicholls JG: The physiology of neuroglial cells. *Ergeb Physiol* 57:1-90, 1966
52. McIlwain H: Phosphates of brain during *in vitro* metabolism: effects of oxygen, glucose, glutamate, glutamine and calcium and potassium salts. *Biochem J* 52:289-295, 1952
53. Rolleston FS, Newsholme EA: Control of glycolysis in cerebral cortex slices. *Biochem J* 104:524-533, 1967
54. Takagaki G: Control of aerobic glycolysis and pyruvate kinase activity in cerebral cortex slices. *J Neurochem* 15:903-916, 1968

The present address of Dr. Yoshida is the Department of Neuropsychiatry, Kurume University, Kurume, Japan.

The present address of Dr. Canty is Children's Hospital, Boston, Mass.

[*Illustrations follow*]

Fig 1—Large-size neuron of nucleus giganto cellularis with adjacent astrocyte and oligodendrogliaocyte. Note maze of variably sized myelinated and nonmyelinated axons in the surround. Gray masses of Nissl substance are evident in perikaryon of the neuron (Epon, toluidine blue, $\times 1000$).

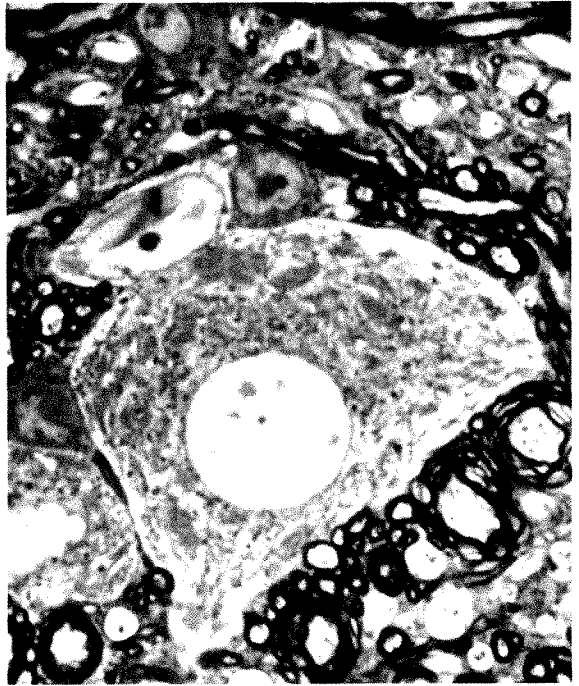


Fig 2—Large and intermediate-size neurons of nucleus giganto cellularis with Nissl substance partially dispersed from vicinity of the nucleus. Surrounding neuropil reveals myelinated axons and scattered dendrites or nonmyelinated axons (Epon, toluidine blue, $\times 1000$).

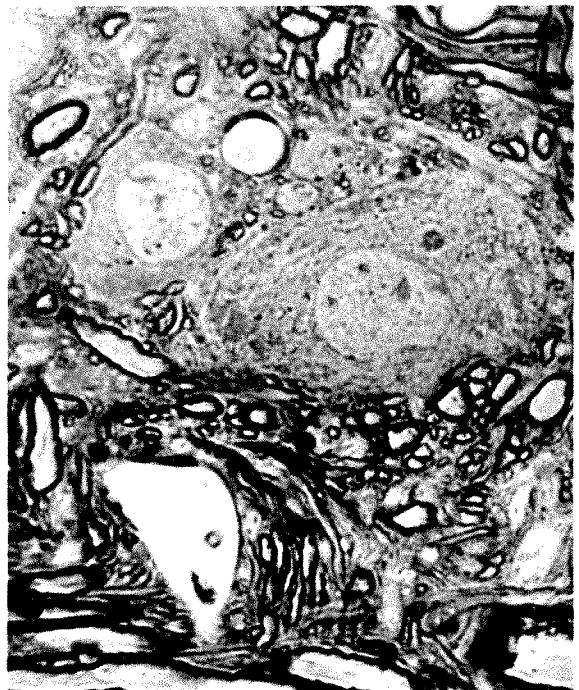




Fig 3—Cytoplasm and nucleus of large neuron from nucleus gigante cellularis of control guinea pig. Note distribution of Golgi membranes (g) in a rough arc in a paranuclear distribution, normal contour and density of mitochondria, several lysosomes and segments of rough endoplasmic reticulum at lower right of picture (uranium and lead stains, $\times 13,500$).



Fig 4—Two presynaptic bulbs and clefts on large dendrite (*d*) in control *n. giganteus*. Glycogen is not prominent. One of the two bulbs (*s*) contain spherical synaptic vesicles 400–530 Å in diameter. These knobs are Type I synapses. The unmarked bulb is filled with tubular, ellipsoidal synaptic vesicles. Two Type I granular vesicles are also seen (↓) (uranium and lead stains, $\times 54,000$).

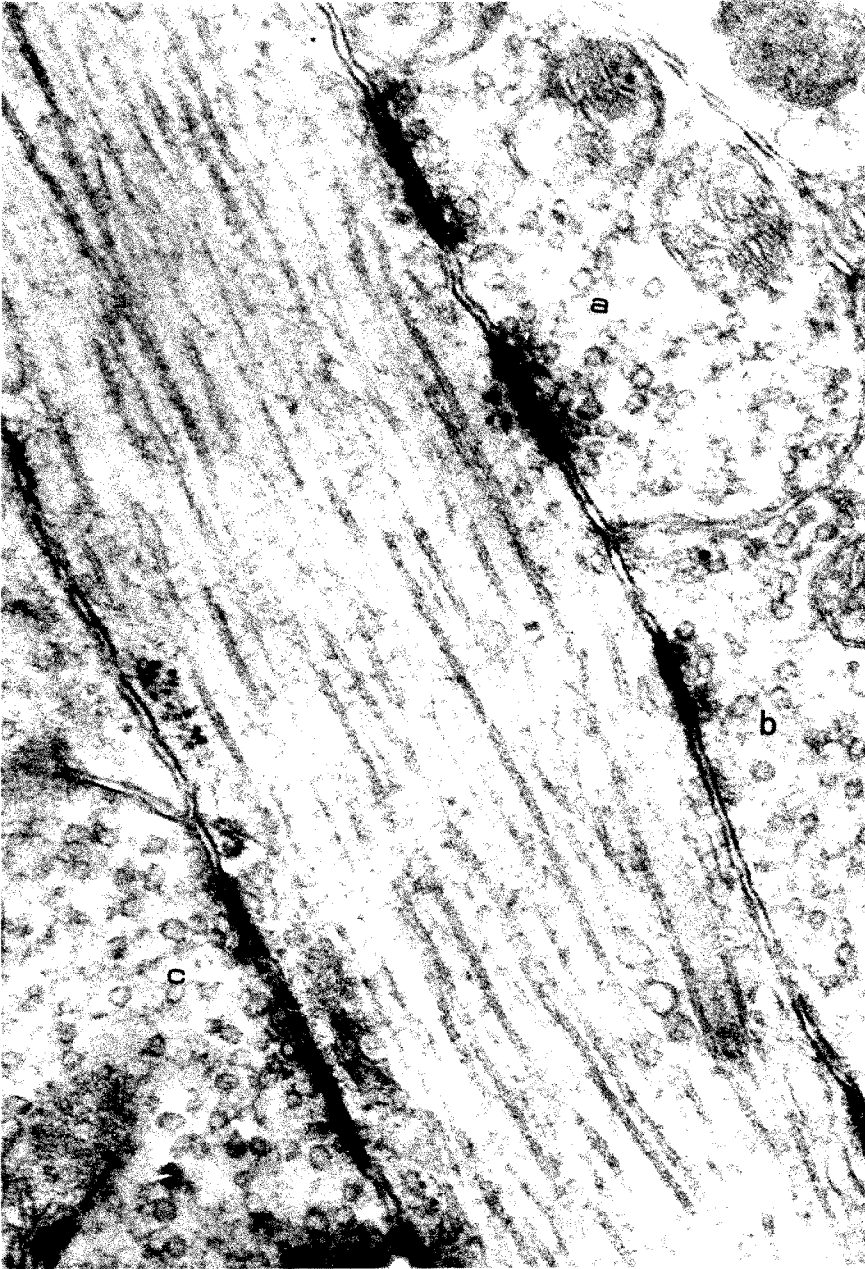


Fig 5—Longitudinal section of a large dendrite which contains numerous microtubules. Several Type II synapses are shown on the dendrite (a,b,c). Spherical vesicle profiles may be noted crowded against the synaptic bars (uranium and lead stains, $\times 65,900$).

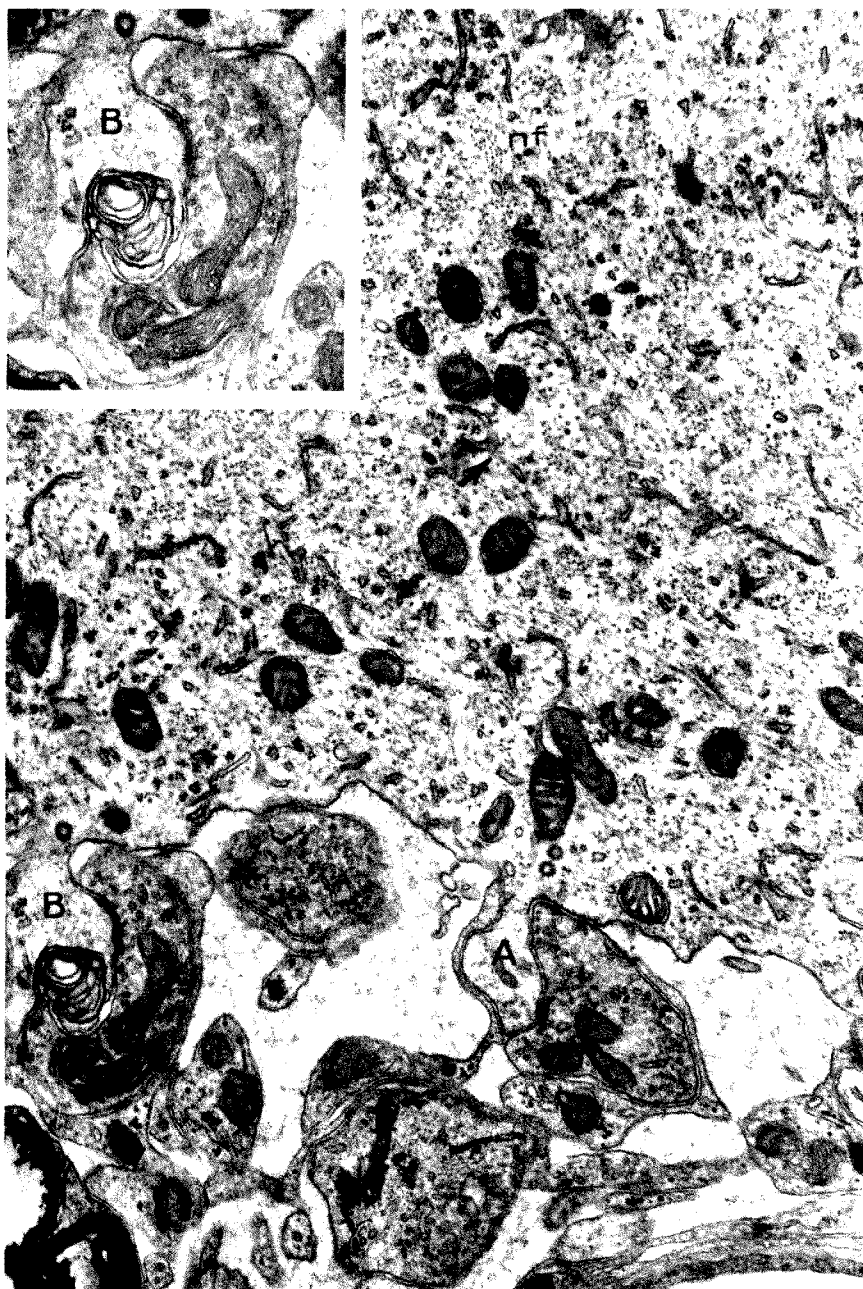


Fig 6—Segment of large neuron cytoplasm from reticular formation which has undergone chromotolysis. Note strands of endoplasmic reticulum (Ψ) and loose scattered RNP particles. There is no change in the mitochondria nor is glycogen seen. Fascicles of slender neurofibrillae (*nf*) are clearly apparent. Two blunt somatic spines are noted (*A,B*) partially encompassed by irregularly shaped pre-synaptic endings filled with ellipsoidal synaptic vesicles. An abnormal increase in the intercellular space is evident but no increase in width of the synaptic cleft. At the neck of each spine coated vesicles may be noted. These relationships are more easily studied in the inset (uranium and lead stains, $\times 40,000$; inset $\times 53,000$).

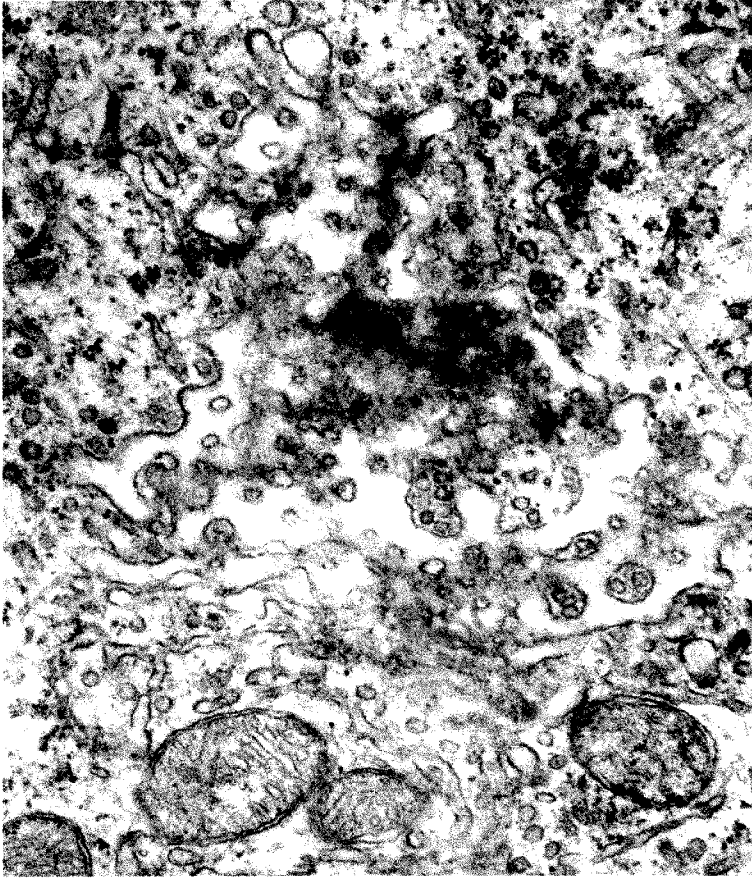


Fig 7—Distorted Golgi apparatus in chromatolytic neuron with greatly dilated cisternae. Small scattered segments of endoplasmic reticulum, some with attached RNP particles, are noted but other ribosomal particles are free (uranium and lead stains, $\times 40,000$).



Fig 8—Presynaptic bulb from reticular formation 8 days postconcussion. Note dense-cored Type I granular vesicles, (C) scattered glycogen masses (β particles) (gl) and spherical synaptic vesicles (SV). The synaptic bar (SB) in upper field abuts a segment of dendrite (uranium and lead stains, $\times 40,000$).

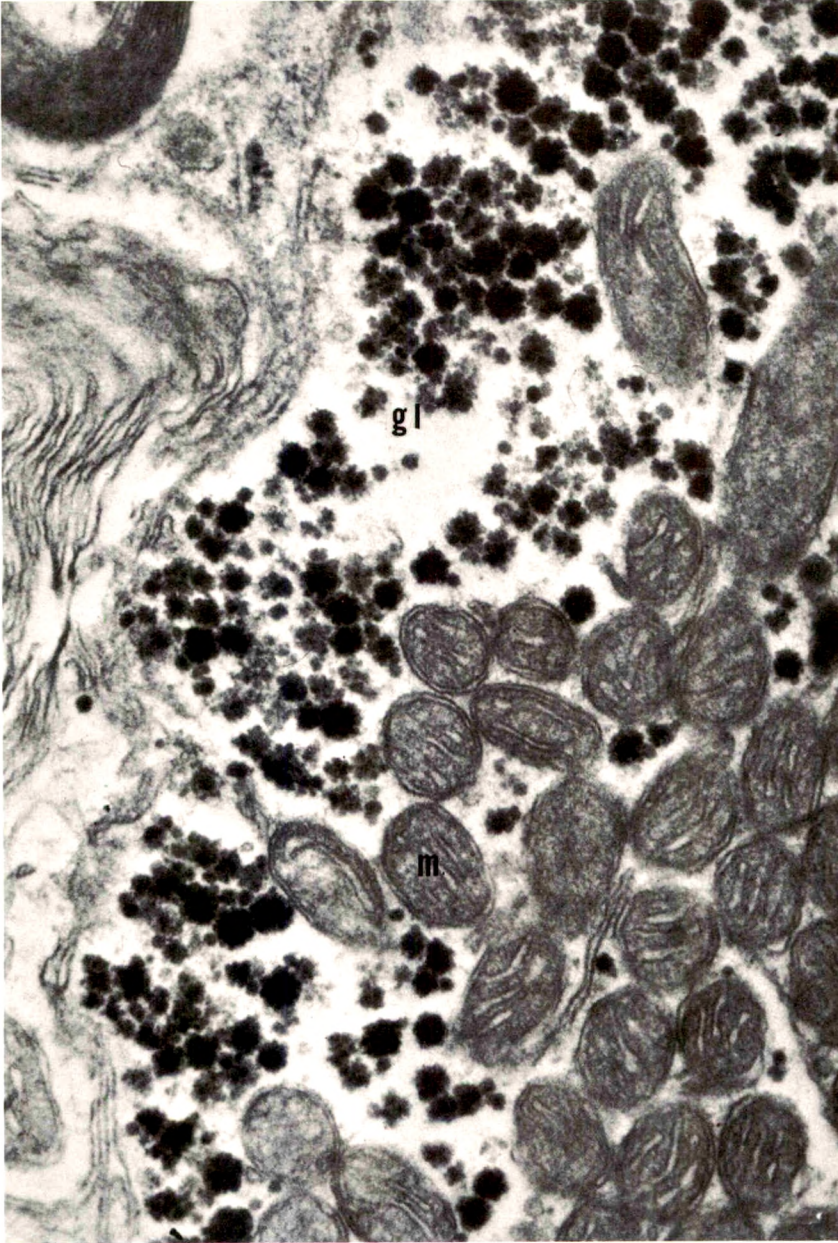


Fig 9—Axon terminal showing large rosette masses of glycogen (α particles) (gl) and numerous mitochondria. Very few synaptic vesicles are noted. Synaptic bars and membranes not seen in picture (uranium and lead stains, $\times 40,000$).

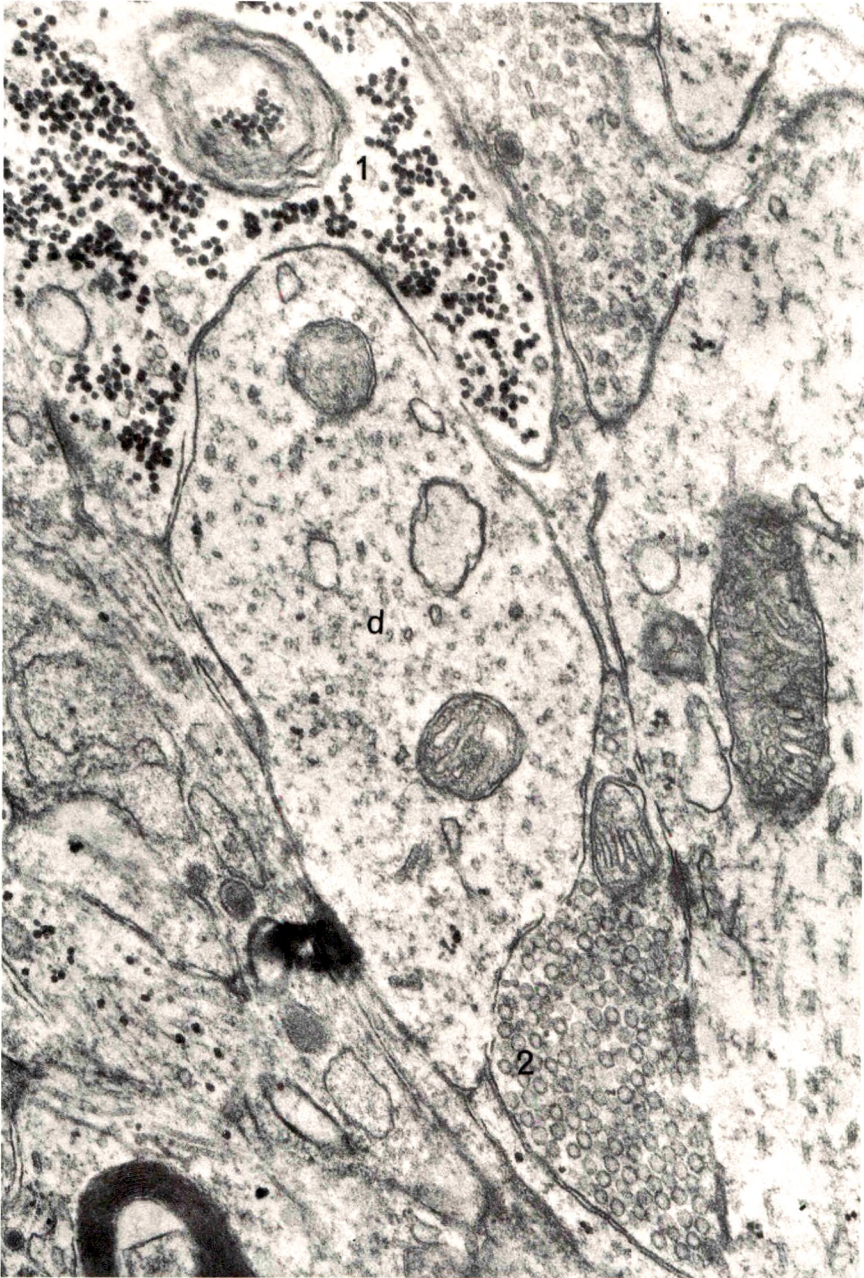


Fig 10—Cross section of dendrite (*d*). Adjacent presynaptic input reveals: (1) glycogen-filled presynaptic terminal with rare spherical vesicles. A conspicuous multilamellar autophagic vacuole containing glycogen β particles is noted. Opposite is a normal-appearing (2) spherical vesicle-laden presynaptic terminal (uranium and lead stains, $\times 43,000$).

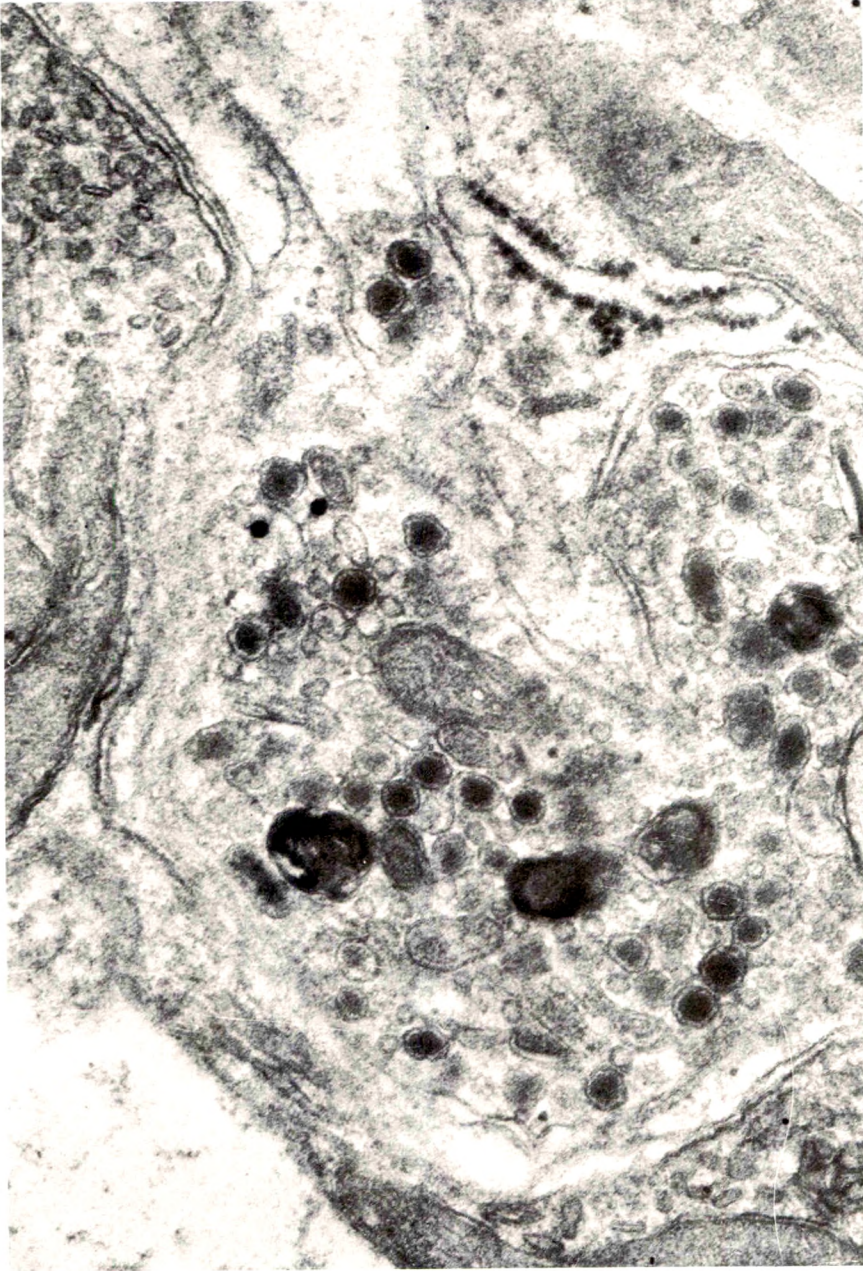


Fig 11—A large roughly spherical presynaptic bulb characterized by spherical agranular synaptic vesicles, large numbers of type I granular vesicles and densely staining residual lysosome-like bodies (uranium and lead stains, $\times 41,000$).

Peroxidase Arthritis

I. An Immunologically Mediated Inflammatory Response with Ultrastructural Cytochemical Localization of Antigen and Specific Antibody.

Richard C. Graham, Jr, MD and Sarajayne Limpert Shannon

Synovitis was produced in rabbits by daily intra-articular injections of the heterologous antigen horseradish peroxidase. The resulting "peroxidase arthritis" resembled rheumatoid arthritis histologically. Many of the subsynovial plasma cells, plasmablasts and immunoblasts contained specific antibody to horseradish peroxidase; the remainder appeared to contain immunoglobulins of other specificities. Peroxidase arthritis has unique advantages for the study of the cellular and sub-cellular events in the pathogenesis of the local immune inflammatory response to heterologous antigen. Antigen and specific antibody can be localized precisely by ultrastructural cytochemical technics. The reaction can be terminated at any stage, permitting observation of the early events in its pathogenesis. (Am J Pathol 67:69-94, 1972)

THERE IS MUCH EVIDENCE suggesting that immunologic mechanisms are involved in the pathogenesis of rheumatoid arthritis. Immunoglobulins,¹ complement² and extranuclear nucleoprotein³ have been identified by immunofluorescence in rheumatoid synovial membranes. Complement levels are reduced in rheumatoid synovial fluids⁴ and rheumatoid synovial fluid leukocytes contain characteristic cytoplasmic inclusions in which immunoglobulins, complement and nucleoprotein have been identified.^{3,5,6} Finally, rheumatoid arthritis frequently is accompanied by the presence of rheumatoid factor, a macroglobulin with antibody specificity toward IgG.⁷

The antigenic stimulus for the immunologic phenomena accompanying rheumatoid arthritis is unknown. Accumulating evidence suggests that an infectious agent may be involved.⁸⁻¹⁰ It has been suggested that the pathogenesis of rheumatoid inflammation might depend on the host immunologic response to such a microbial antigen. Chronicity could be explained either by persistence of the heterologous antigen⁸ or by an autoimmune reaction to antigens made available by the initial inflammatory response.¹¹

From the Department of Medicine, Case Western Reserve University, University Hospitals of Cleveland, Cleveland, Ohio 44106.

Supported by Research Grant AM-11308 from the National Institute of Arthritis and Metabolic Diseases, and by an award from National Institutes of Health General Research Support Grant FR 05410 to Case Western Reserve University.

Accepted for publication September 21, 1971.

Address reprint requests to Dr. Richard C. Graham, Jr.

In the studies described in this series of reports, repeated intra-articular injections of antigen were employed to study the synovial response to prolonged local antigenic stimulation. In the resulting synovitis, which resembles rheumatoid arthritis histologically, local antibody synthesis occurs within the synovial inflammatory infiltrate. When the antigen used is horseradish peroxidase (HRPO), both antigen¹² and specific antibody¹³ can be localized precisely by ultrastructural cytochemical techniques. In this report, the general morphologic and immunologic characteristics of "peroxidase arthritis" are described.

Materials and Methods

Procedure and Injection Schedules

Nineteen female albino rabbits were used in the following procedures. All animals were anesthetized by titration with sodium thiamylal (Parke-Davis, Detroit, Mich) and both knees were shaved and cleaned with 70% ethanol. In fourteen rabbits, the knees were injected intraarticularly with 2 mg horseradish peroxidase (HRPO) (Sigma Chemical Company, Type VI, RZ 3.0) in 0.5 ml 0.15 M NaCl. The left knees were injected with 0.5 ml of a 1:30 dilution of autologous serum in 0.15 M NaCl. In the remaining 5 rabbits, both right and left knees were injected with 2 mg HRPO in 0.5 ml 0.15 M NaCl. All solutions were sterilized by Millipore filtration prior to injection. In early experiments, a variety of dosages and intervals between injection were used. It was found that daily injections using 2 mg per knee produced the desired reaction most consistently (see Table 1).

Two rabbits were given 14 daily intra-articular injections of 2 mg bovine serum albumin (BSA) in 0.5 ml 0.15 M NaCl. Procedures were otherwise identical to those described for the HRPO-injected rabbits.

All rabbits were sacrificed by an overdose of sodium thiamylal 24 hours after the last injection of HRPO. Both of the knee joints, spleens, popliteal lymph nodes and kidneys were removed. All tissues were fixed for 4 hours in 2.5% glutaraldehyde and 2% formaldehyde in 0.05 M phosphate buffer, pH 7.4.¹⁴ The tissues were washed overnight in 0.05 M phosphate buffer, pH 7.4.

Localization of Antigen (HRPO) and Antibody (anti-HRPO)

The fixed synovial membrane and underlying tissue was carefully removed from the connective tissue medial and lateral to the patella and cut into strips approximately 1 mm in thickness. These tissues were divided into two portions.

One portion was incubated according to the method described by Graham and Karnovsky¹² for the detection of peroxidase activity. The tissues were preincubated in 5 mg of 3,3'-diaminobenzidine (Sigma Chemical Co, St Louis) in 10 ml of 0.05 M Tris-HCl buffer, pH 7.4, for 25 minutes prior to the addition of 0.1 ml 1% H₂O₂. The tissues were incubated in the complete medium for 10–15 minutes. They then were washed three times in distilled water.

The other portion of tissue was treated according to the method of Leduc *et al*¹³ for the detection of anti-HRPO activity. Both whole-tissue strips and 40- μ frozen sections were gently agitated in 5–10 ml of 0.05 M phosphate buffer, pH 7.4, containing 0.5 mg/ml HRPO (type VI) for 2 hours at 4 C. They then were washed and refixed in 2.5% glutaraldehyde in 0.05 M phosphate buffer,

Table I—Injection Schedules, Serum Antibody Titers and Intensity of Reaction in Rabbits Studied

Rabbit	Dose of HRPO (mg/injection)	Knee injected*	Interval†	Duration (days)	Serum PHA	Antibody‡ precipitin	Intensity of reaction§
I-A	1	R	2	18	320	2	+
I-B	1	R	2	18	320	0	+
II-A	1	R	4	18	320	0	+
II-B	1	R	4	18	40	0	+
III-A	1	R	6	18	160	0	+
III-B	1	R	6	18	40	0	+
V-A	2	R	1	19	1280	8	3+
V-B	2	R	1	19	640	2	
VI-B	1	R	1	15	320	Undil	2+
VI-C	1	R	1	15	320	4	2+
B-8	1	R	1	12	80	0	2+
VII-A	2	R	1	35	5120	8	4+
VII-B	2	R	1	35	1280	4	3+
VIII-A	2	B	1	15	1280	4	3+
IX-A	2	B	1	9	40	0	2+
IX-B	2	B	1	9	20	0	2+
12	2	B	1	15	320		3+
16	2	B	1	37	10240	8	4+
1-F					163840	16	

* R, right knee; B, both knees.

† 1, daily; 2, every other day; 4, every fourth day; 6, every sixth day.

‡ Reciprocal of titer. PHA, passive hemagglutination

§ Intensity of reaction is expressed in arbitrary units with 4+ representing maximal intensity.

|| Reference serum from animal immunized with HRPO in complete Freund's adjuvant in conventional manner.

pH 7.4, for 15 minutes. They were washed again in buffer before incubation for peroxidase activity, as described above, for 30 minutes. Incubation was followed by three washes in distilled water.

Both portions of tissue were additionally fixed in 1% OsO₄ in 0.05 M phosphate buffer, pH 7.4, for 1 hour, washed in 0.1 M sodium maleate buffer, pH 5.2, and stained with 2% uranyl acetate in 0.05 M sodium maleate buffer, pH 5.2, for 2 hours. After this, the tissues were dehydrated in ethanol and embedded in Araldite. Thick sections (0.5–1 μ) were cut, stained with toluidine blue and examined by light microscopy to determine appropriate areas for thin sectioning. Thin sections were cut with glass knives on Sorvall MT-1 or MT-2 ultramicrotomes, stained with uranyl acetate and lead citrate and examined in an AEI EM-6B electron microscope.

Light Microscopy

Articular cartilage and adjacent synovial tissue from the knee joints of rabbits receiving daily HRPO injections for 35 or 37 days were taken and fixed in 2.5% glutaraldehyde and 2% formaldehyde in 0.05 M phosphate buffer, pH 7.4, overnight. The tissues were washed for several hours, dehydrated and embedded in paraffin. Sections were cut and stained with hematoxylin and eosin (H&E).

Synovial fluids from the knee joints of all rabbits were aspirated into heparinized plastic syringes. Smears were made directly from the syringe to achieve maximum preservation of the cells. The smears were stained with tetrachrome.

Serologic Studies

Both the passive hemagglutination test and Ouchterlony precipitin test were used for the detection of circulating antibody. For use in the passive hemagglutination test, HRPO was coupled to fresh sheep erythrocytes with glutaraldehyde according to the method of Avrameas *et al.*¹⁶ Passive hemagglutination tests were carried out in 100 × 75 mm glass test tubes by a standard technic.

Serial dilutions of sera were assayed for precipitating antibodies by double diffusion in agar gel according to the standard Ouchterlony technic.

"Enzyme immunoelectrophoresis"¹⁷ was carried out on sera from 5 different animals. Standard immunoelectrophoretic patterns were developed in agarose gel with goat anti-rabbit whole serum (kindly supplied by Dr. Abram Stavitsky). Slides were then washed at room temperature for 3 days in 0.15 M phosphate-buffered saline, pH 7.2, before incubation overnight at room temperature in a solution of 0.1 mg HRPO/ml in phosphate-buffered saline. The slides were then washed for 5 days at 4 C in repeated changes of 0.15 M NaCl to remove unprecipitated HRPO. Finally, they were reacted by the Graham-Karnovsky technic (see above) to reveal sites of peroxidase activity.

Results

Controls

Joints receiving 12 to 35 daily injections of diluted autologous serum appeared entirely normal upon both gross and microscopic examination (Fig 1). No peroxidase activity was detectable in these tissues.

Peroxidase Arthritis

Gross Observations

After 12-16 Daily HRPO Injections. The external appearance of the joints was not striking. In most rabbits, external evidence of mild swelling of joints was evident. Upon opening the joints, the synovial tissue appeared markedly thickened and hyperemic. The articular cartilages showed no apparent abnormality. The synovial fluid, which was increased in amount, was turbid and quite viscous.

After 35 or 37 Daily Injections of HRPO. The joints were markedly swollen. The appearance of the synovial tissue was similar to that described above, except that synovial thickening was much more marked. Inflamed synovial tissue partially obscured the surface of the articular cartilages. The synovial fluid resembled that seen after the shorter series of injections, except that it was present in larger amounts.

Cellular Composition of Synovial Fluid

Examination of tetrachrome-stained smears of synovial fluid by light

microscopy revealed the cellular composition to be similar after 12–37 daily HRPO injections. Of the cells, 75% or more were polymorphonuclear leukocytes. The remainder included lymphocytes, macrophages and cells that appeared to be detached synovial cells.

Light and Electron Microscopic Histopathology

After 12–16 Daily HRPO Injections. The histologic appearance of the inflamed synovial tissue was qualitatively similar in all rabbits examined. The magnitude of the reaction varied somewhat from animal to animal, tending to be greater in those rabbits given 2 mg HRPO in each daily injection, and in those injected with HRPO in both knees (Table 1). Within a given joint, the magnitude of the reaction varied considerably in synovial tissues taken from different areas of the joint.

The synovial lining cells were increased in number, with the lining layer varying from two to five cells in thickness (Fig 2). Most of the synovial lining cells were highly irregular in shape. Their surfaces displayed an extensive and complex network of pseudopods, which was most prominent on the aspect of the cell facing the synovial cavity. Mitotic figures frequently were observed (Fig 3). When viewed by light microscopy, numerous brown granules of reaction product were seen in the cytoplasm of most of the synovial lining cells. A few of the synovial cells contained only scattered granules of reaction product. When examined by electron microscopy, the majority of the synovial cells were seen to contain numerous cytoplasmic vacuoles, many of which contained peroxidatic reaction product (Fig 3). Other vacuoles enclosed ferritin, cellular debris or entire dead and degenerating cells (Fig 4). In a small minority of synovial lining cells, there were few scattered small vacuoles containing reaction product, and the cell surface displayed fewer and less complex pseudopods. Rough-surfaced endoplasmic reticulum was abundant in these cells (Fig 5). Occasional lymphocytes, plasma cells and polymorphonuclear leukocytes were seen within the synovial lining layer. Fibrin frequently was present in the intercellular spaces between the synovial lining cells.

The subsynovial tissues were infiltrated with a variable number of inflammatory cells. In many areas, this infiltrate was quite extensive, with the involved tissue being 1 mm or more in thickness. The infiltrate was composed of numerous plasma cells, lymphoid cells and macrophages, moderate numbers of fibroblasts and polymorphonuclear leukocytes and occasional eosinophils (Fig 2).

Electron microscopy revealed the majority of the plasma cells to be typical mature plasma cells, with numerous, regularly spaced stacks of

rough-surfaced endoplasmic reticulum (Fig 6). The nuclei were round and eccentrically placed, with peripheral condensations of chromatin. Smaller numbers of plasmablasts, distinguished by their prominent nucleoli and the less regular orientation of their rough-surfaced endoplasmic reticulum, were observed. Plasmablasts in mitosis occasionally were seen.

A spectrum of lymphoid cells was present (Fig 7 and 8). Some were typical small lymphocytes, with condensed nuclear chromatin and scant cytoplasm containing few organelles. Others had more abundant cytoplasm containing variable numbers of free polyribosomes (Fig 8). Still others had less condensed nuclear chromatin and numerous free polyribosomes in their cytoplasm (Fig 8). Such cells have been referred to by others as "activated" lymphocytes.¹⁸ Moderate numbers of "immunoblasts" were observed. The nuclei of these cells had prominent nucleoli and highly dispersed chromatin, and the cytoplasm contained abundant free polyribosomes and a few profiles of rough-surfaced endoplasmic reticulum (Fig 8 and 9). Such cells frequently were seen in mitosis (Fig 10).

The plasma cells and lymphoid cells often were aggregated in clusters, and were more numerous in the deeper part of the infiltrate. The clusters, which frequently were found near venules, varied in their cellular composition. In some, lymphoid cells predominated (Fig 7). Others were composed mainly of plasma cells (Fig 6). In still others, a mixture of plasma cells and lymphoid cells was observed.

Plasma cells and lymphoid cells were closely associated with each other and with macrophages. These cellular interrelationships, which were quite varied and complex, will be described in detail in a subsequent paper.

Polymorphonuclear leukocytes most often were seen in the superficial part of the infiltrate, immediately beneath the synovial lining cells. Macrophages and fibroblasts were found throughout the infiltrate.

Striking alterations were seen in the larger venules situated in the deeper subsynovial tissue, and in some of the smaller superficial vessels as well. The endothelial cells, which were increased in number, bulged into the vascular lumen, giving the endothelium a pseudocolumnar appearance. Such vessels were the site of emigration of lymphoid cells, monocytes and polymorphonuclear leukocytes. Fenestrated capillaries rarely were observed in the fully developed arthritis. The development of these changes, as well as the mechanism of cellular emigration, will be described in detail in a subsequent communication.

After 35-37 Daily Injections of HRPO. The appearance of the syn-

ovial tissue was qualitatively similar to that observed after the shorter series of injections. The cellular infiltrate, however, was much more extensive. Examination of paraffin sections stained with hematoxylin and eosin revealed necrosis of cartilage at sites of contiguity with the inflammatory infiltrate (Fig 11).

Electron microscopy showed that the synovial cells, which were greatly increased in number, had numerous cytoplasmic vacuoles variously containing HRPO, cellular debris, ferritin or lipid (Fig 12). Lymphoid cells and occasional polymorphonuclear leukocytes were found among the synovial cells.

The subsynovial infiltrate contained more cells per unit area than was the case after shorter series of injections (Fig 13 and 14). The cellular composition of the infiltrate resembled that observed after fewer injections. Mature and immature plasma cells, lymphoblasts and the various types of lymphocytes all still were present. Fibroblasts were numerous among bundles of collagen which apparently were newly formed (Fig 15). Scattered throughout the infiltrate were many macrophages, the cytoplasmic vacuoles of which variously contained HRPO, ferritin, cellular debris or lipid (Fig 16). In some of the macrophages, lipid-containing vacuoles were strikingly numerous. Extensive fibrin deposition was observed both in the synovial lining layer and in the subsynovial tissue (Fig 12). The great majority of the small blood vessels were of the pseudocolumnar type described above. Fenestrated capillaries rarely were seen.

Cytochemical Demonstration of Specific Antiperoxidase Antibody

Study of synovial tissue from rabbits receiving 12-37 daily intra-articular injections of HRPO revealed similar findings, and these will be reported together. The method used was that of Leduc and her associates,¹⁴ in which aldehyde-fixed tissue is incubated with antigen (HRPO). The HRPO, which binds to anti-HRPO in antibody-synthesizing cells, serves as a cytochemical marker indicating the location of the antibody. In peroxidase arthritis, many but not all of the plasma cells and plasmablasts contained anti-HRPO in the rough-surfaced endoplasmic reticulum (Fig 17). In some of the plasma cells and all of the plasmablasts with anti-HRPO activity, this activity was localized in the perinuclear space as well (Fig 17 and 18). Some of the immunoblasts had anti-HRPO activity in the perinuclear space and in scattered profiles of rough-surfaced endoplasmic reticulum (Fig 19). Specific antibody was observed both in blasts undergoing mitosis and in those that were not (Fig 19). Both cells with (Fig 20) and without anti-HRPO

activity were observed in association with macrophages. Differentiation of plasma cells from lymphoplasmacytes, recently described by Avrameas and Leduc,¹⁷ was not possible since we did not study tissues fixed only in formaldehyde.

The presence of plasma cells without antiperoxidase antibody was unlikely to have been an artifact caused by poor penetration of HRPO during the Leduc procedure, or by poor penetration of the cytochemical reagents. Plasma cells without specific antibody frequently were seen at the very edge of the tissue strip. Such cells also were seen immediately adjacent to plasma cells that unequivocally had specific antibody. Finally, when frozen sections were used, penetration appeared essentially complete, and cells with and without antiperoxidase activity were found throughout the entire thickness of the tissue.

Detection of Antiperoxidase Antibody in Serum

Specific antibody was detectable both by double diffusion in agar and by passive hemagglutination as shown in Table I. Titers varied from animal to animal, and were higher in rabbits receiving larger doses of HRPO in each injection, and in those receiving the greatest number of injections (see Table I). The titers obtained were considerably lower than those obtained in rabbits immunized with HRPO in complete Freund's adjuvant by conventional techniques (Table I).

Immunoglobulin Classes of Serum Antiperoxidase Antibody

Sera were analyzed by the enzyme immunoelectrophoresis technic described by Avrameas and Leduc.¹⁷ This method depends upon the ability of specific antiperoxidase antibody in the immunoglobulin precipitin lines to bind HRPO. The bound HRPO is identified by the peroxidatic oxidation of 3,3'-diaminobenzidine, which stains the relevant precipitin lines brown.

In sera from rabbits given 16 daily intra-articular injections of HRPO, anti-HRPO activity was detectable in both IgG and IgM precipitin lines (Fig 21). Sera from rabbits given 35 or 37 daily HRPO injections had detectable anti-HRPO activity only in the IgG precipitin line (Fig 21).

Effect of Repeated Intra-Articular Injection of Bovine Serum Albumin (BSA)

Rabbits receiving 14 daily intra-articular injections of BSA developed an arthritis similar to that evoked by an equivalent number of HRPO injections. Study by both light and electron microscopy revealed no important morphologic differences between the reactions evoked by the two antigens, although that elicited by BSA was somewhat greater in

magnitude. No antiperoxidase antibody was found in plasma cells or lymphoid cells in BSA arthritis when studied by the Leduc technic. Sera from the rabbits with BSA arthritis contained precipitating antibody against BSA when assayed by double diffusion in agar.

Discussion

Peroxidase arthritis presents unique opportunities for the study of the synovial inflammatory response to repeated local antigenic stimulation. Its most important advantage is that antigen and specific antibody can be localized precisely by electron microscopy. In addition, with a given dose of antigen and number of injections, the changes produced are reproducible, so that the development of the reaction can be studied easily at any stage. Although giving repeated intra-articular injections to rabbits perhaps is somewhat inconvenient, with experience the injections can be done easily and quickly. Moreover, autologous serum controls have established that the trauma of repeated injection *per se* causes no significant change in the synovial tissues.

Despite the unique methodologic advantages of the peroxidase arthritis model, its ultimate value depends upon the relevance of observations made with it to the pathogenesis of human disease. In this regard, the morphologic and immunologic similarities between the synovitis of rheumatoid arthritis and that of peroxidase arthritis are of some interest. Whether these similarities reflect similar pathogenic mechanisms is, of course, as yet unknown. The histopathologic changes in the human rheumatoid synovial membrane have been well described at both the light ^{19,20} and electron ^{21,22} microscopic levels. There is proliferation of synovial lining cells, accompanied by subsynovial infiltration with lymphocytes, plasma cells, macrophages, fibroblasts and a few polymorphonuclear leukocytes. The cells of the subsynovial infiltrate frequently are found in focal aggregates resembling lymphoid follicles. As the disease progresses, inflammatory tissue frequently encroaches on adjacent cartilage and bone, resulting in necrosis of these tissues.

On purely morphologic grounds, the similarities between peroxidase arthritis and rheumatoid arthritis are striking. In both, the proliferation of synovial lining cells is accompanied by greatly augmented synovial endocytic activity. In peroxidase arthritis, synovial endocytosis of large quantities of specific antigen occurs; whether a similar phenomenon occurs in rheumatoid arthritis of course must await the identification of a specific etiologic agent.

The cellular populations of the subsynovial infiltrates in peroxidase arthritis and rheumatoid arthritis are quite similar. Although in peroxi-

dase arthritis there is a definite tendency for the cells to aggregate in follicle-like clusters, the process in general is more diffuse than usually is observed in rheumatoid arthritis. This difference perhaps reflects the greater duration of the usual rheumatoid process before histologic examination is carried out. Like rheumatoid arthritis, peroxidase arthritis is associated with necrosis of cartilage if the reaction is sufficiently prolonged.

In both peroxidase arthritis and rheumatoid arthritis, polymorphonuclear leukocytes make up but a small percentage of the inflammatory infiltrate. In contrast, they are abundant in the synovial fluid. The reason for this discrepancy is not entirely clear. Presumably, the polymorphonuclear leukocytes, after emigrating from subsynovial blood vessels, migrate quite rapidly through the synovial membrane into the synovial cavity. Rapid migration of these cells in the same direction could reflect the presence of a chemotactic stimulus. Possibly, chemotactic factors are released in the synovial fluid through the activation of complement by antigen-antibody complexes.²³

The endothelial changes and associated interactions of lymphocytes with endothelium that occur in peroxidase arthritis are quite complex and will be discussed in detail in a subsequent paper. Whether significant endothelial changes occur in rheumatoid arthritis is disputed.²⁴ However, rheumatoid synovial tissues must be studied when they have reached a relatively more advanced stage than the peroxidase arthritis lesions. In this respect, it is of interest that in peroxidase arthritis the endothelial changes reach their peak at 12–16 days and then recede, despite continued intensification of the inflammatory response.

Synthesis of immunoglobulins by cells in the synovial inflammatory infiltrate occurs in both rheumatoid arthritis and peroxidase arthritis. With the exception of rheumatoid factor, the antibody specificity of the immunoglobulins produced in the rheumatoid synovial membrane is unknown. In peroxidase arthritis, some of the synovial immunocytes have been shown to produce anti-HRPO. It is likely, however, that immunoglobulins of other specificities are produced as well, since many of the subsynovial plasma cells are without anti-HRPO activity when examined with the Leduc technic. The nature of the immunoglobulins produced by these cells is as yet unknown. The interesting possibility that at least some of them may produce autoantibodies is being investigated in our laboratory.

There has been much interest in the possibility that an infectious agent may provide the initial antigenic stimulus in rheumatoid arthritis.⁸ It has been shown that membranes of *Mycoplasma fermentans* inhibited

leukocyte migration in 67% of patients with rheumatoid arthritis, but had no effect in patients with osteoarthritis or normal controls.¹⁰ It is of interest that certain species of *Mycoplasma* cause an arthritis in swine that resembles rheumatoid arthritis both histologically and serologically.^{25,26} Further evidence in support of the presence of an infectious agent in rheumatoid arthritis has come from the demonstration that a slurry from rheumatoid synovial tissue causes swelling and reddening of extremities when injected into mice.⁹ These changes were transmissible to the second and third generations of mice without further injection.

The peroxidase arthritis reaction provides a model of a synovial immune inflammatory reaction in response to prolonged stimulation by a heterologous antigen. Comparison with a response to an infectious agent obviously is inexact; the response to a soluble protein antigen may differ from the response to a microbial antigen, which probably is membrane bound. Moreover, the intermittent introduction of antigen can only approximate the stimulus presented by a persistent microorganism, to which the host presumably is continuously exposed. Nevertheless, it seems quite possible that the approximation provided by the model is close enough that in the synovial tissue the mechanisms of response are similar.

Experimental arthritis in animals has been produced in numerous ways. The literature before 1960 has been reviewed well by Gardner.²⁷ Subsequent interesting models include adjuvant arthritis, produced by the intradermal injection of complete Freund's adjuvant in certain strains of rats.^{28,29} Histologically, the arthritis somewhat resembles rheumatoid arthritis and in some rats becomes chronic and is characterized by exacerbations and remissions. Its pathogenesis is uncertain, but may involve an immunologic response to mycobacterial antigens. Another interesting form of experimental arthritis has been produced by immunizing rabbits with heterologous fibrin in Freund's adjuvant, followed by injection of fibrin into a joint.³⁰ The resulting arthritis resembles rheumatoid arthritis histologically in some respects, and may persist for months without further injection of antigen. Other antigenic proteins can substitute for fibrin in this model.¹¹ It has been suggested that persistence of inflammation in this model depends upon an autoimmune reaction to products of the initial immune inflammatory response.¹¹

Peroxidase arthritis lacks the prominent systemic manifestations and the chronicity characteristic of rheumatoid arthritis, and for the study of these aspects, another of the models would seem more appropriate. Further, for quantitative studies in which a large sample is required,

such as evaluation of anti-inflammatory or immunosuppressive drugs, one of the other models would be more practical. On the other hand, peroxidase arthritis appears to have unique advantages for the study of the cellular and subcellular events in the pathogenesis of this type of immune inflammatory response. Antigen and antibody can be localized by both light and electron microscopy, and the reaction can be controlled so that any stage of its development can be readily studied. Morphologic information obtained can be correlated with the results of conventional immunologic technics.

References

1. Fish AJ, Michael AF, Gewurz H, Good RA: Immunopathologic changes in rheumatoid arthritis synovium. *Arthritis Rheum* 9:267-280, 1966
2. Rodman WS, Williams RC Jr, Bilka PJ, Müller-Eberhard HJ: Immunofluorescent localization of the third and the fourth component of complement in synovial tissue from patients with rheumatoid arthritis. *J Lab Clin Med* 69:141-150, 1967
3. Brandt KD, Cathcart ES, Cohen AS: Studies of immune deposits in synovial membranes and corresponding synovial fluids. *J Lab Clin Med* 72:631-647, 1968
4. Fostiropoulos G, Austen KF, Bloch KJ: Total hemolytic complement ($C'H_{50}$) and second component of complement ($C'2^{hu}$) activity in serum and synovial fluid. *Arthritis Rheum* 8:219-232, 1965
5. Rawson AJ, Abelson NM, Hollander JL: Studies on the pathogenesis of rheumatoid joint inflammation. II. Intracytoplasmic particulate complexes in rheumatoid synovial fluids. *Ann Intern Med* 62:281-284, 1965
6. Barnett EV, Bienenstock J, Bloch JJ: Possible participants in the rheumatoid inclusion body. *JAMA* 198:143-148, 1966
7. Lightfoot RW Jr, Christian CL: Rheumatoid arthritis, Textbook of Immunopathology. Edited by PA Miescher, HJ Müller-Eberhard. New York, Grune and Stratton, 1969, pp 733-744
8. Christian CL: Rheumatoid arthritis: etiologic consideration. *Arthritis Rheum* 7:455-466, 1964
9. Warren SL, Marmor L, Liebes DM, Hollins R: Active agent from human rheumatoid arthritis which is transmissible in mice: preliminary report. *Arch Intern Med* 124:629-634, 1969
10. Williams MH, Brostoff J, Roitt IM: Possible role of *Mycoplasma fermentans* in pathogenesis of rheumatoid arthritis. *Lancet* 2:277-280, 1970
11. Glynn LE: Heberden oration: the chronicity of inflammation and its significance in rheumatoid arthritis. *Ann Rheum Dis* 27:105-121, 1968
12. Graham RC, Karnovsky MJ: The early stages of absorption of injected horseradish peroxidase in the proximal tubules of mouse kidney: ultrastructural cytochemistry by a new technique. *J Histochem Cytochem* 14:291-302, 1966
13. Leduc EH, Avrameas S, Bouteille M: Ultrastructural localization of antibody in differentiating plasma cells. *J Exp Med* 127:109-118, 1968
14. Karnovsky MJ: A formaldehyde-glutaraldehyde fixative of high osmolality for use in electron microscopy. *J Cell Biol* 27:137A, 1965, abstr

15. Venable JH, Coggeshall RA: A simplified lead citrate stain for use in electron microscopy. *J Cell Biol* 25:407-408, 1965
16. Avrameas S, Tandow B, Chuilon S: Glutaraldehyde, cyanuric chloride and tetraazotized *o*-dianisidine as coupling reagents in the passive hemagglutination test. *Immunochemistry* 6:67-76, 1969
17. Avrameas S, Leduc EH: Detection of simultaneous antibody synthesis in plasma cells and specialized lymphocytes in rabbit lymph nodes. *J Exp Med* 131:1137-1168, 1970
18. Astrom KE, Webster HdeF, Arnason BG: The initial lesion in experimental allergic neuritis: a phase and electron microscopic study. *J Exp Med* 128:469-495, 1968
19. Parker F Jr, Keefer CS: Gross and histologic changes in the knee joint in rheumatoid arthritis. *Arch Pathol* 20:507-522, 1935
20. Kulka JP, Bocking D, Ropes MW, Bauer W: Early joint lesions of rheumatoid arthritis. *Arch Pathol* 59:129-150, 1955
21. Norton WL, Ziff M: Electron microscopic observations on the rheumatoid synovial membrane. *Arthritis Rheum* 9:589-610, 1966
22. Wyllie JC, Haust MD, More RH: The fine structure of synovial lining cells in rheumatoid arthritis. *Lab Invest* 15:519-529, 1966
23. Ward PA: Neutrophil chemotactic factors and related clinical disorders. *Arthritis Rheum* 13:181-186, 1970
24. Branemark PI, Ekholm R, Goldie I: To the question of angiopathy in rheumatoid arthritis: an electron microscopic study. *Acta Orthop Scand* 40:153-175, 1969
25. Barden JA, Decker JL: *Mycoplasma hyorhinis* swine arthritis. I. Clinical and serologic features. *Arthritis Rheum* 14:193-201, 1971
26. Ennis RS, Dalgard D, Willerson JT, Barden JA, Decker JL: *Mycoplasma hyorhinis* swine arthritis II. Morphologic features. *Arthritis Rheum* 14:202-211, 1971
27. Gardner DL: The experimental production of arthritis: a review. *Ann Rheum Dis* 19:297-317, 1960
28. Pearson CM, Wood FD: Studies of polyarthritis and other lesions induced in rats by injection of mycobacterial adjuvant. I. General clinical and pathologic characteristics and some modifying factors. *Arthritis Rheum* 2:440-459, 1959
29. Waksman BH, Pearson CM, Sharp JT: Studies of arthritis and other lesions induced in rats by injection of mycobacterial adjuvant. II. Evidence that the disease is a disseminated immunologic response to exogenous antigen. *J Immunol* 85:403-417, 1960
30. Dumonde DC, Glynn LE: The production of arthritis in rabbits by an immunological reaction to fibrin. *Br J Exp Pathol* 43:373-383, 1962
31. Graham RC, Shannon SL: Peroxidase arthritis: a model of immunologically mediated inflammation permitting ultrastructural cytochemical localization of antigen. *J Clin Invest* 48:31a, 1969, abstr

We thank Drs. George M. Bernier, Phillip J. Catanzaro and Oscar D. Ratnoff, who reviewed the manuscript and made many helpful suggestions.

A preliminary report of a portion of this work has been presented in abstract form.³¹

Dr. Graham is a recipient of Research Career Development Award AM 42,397 from the National Institute of Arthritis and Metabolic Diseases.

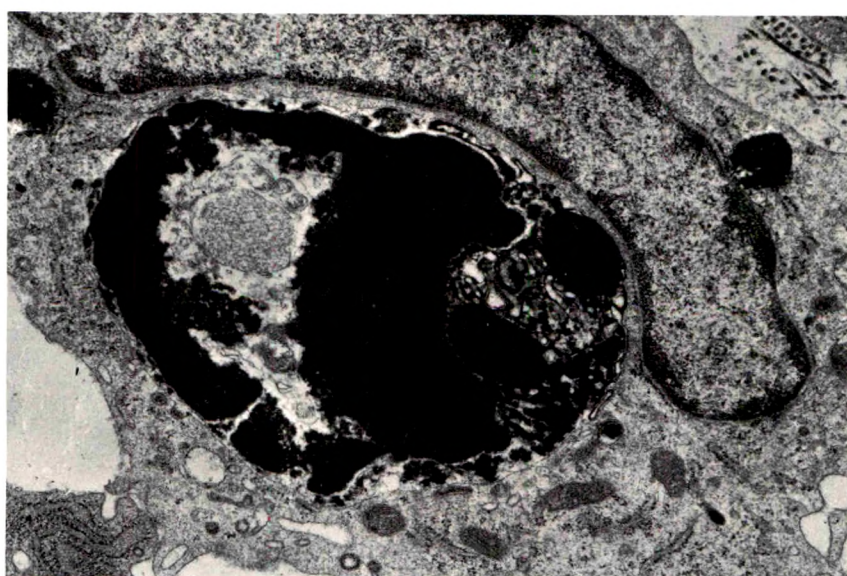
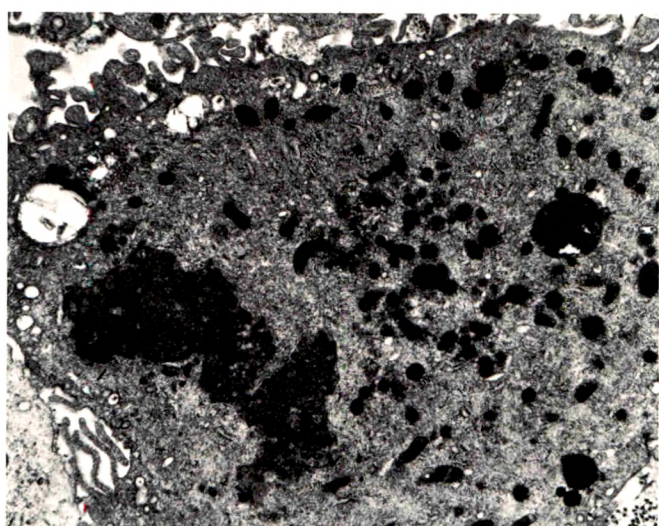
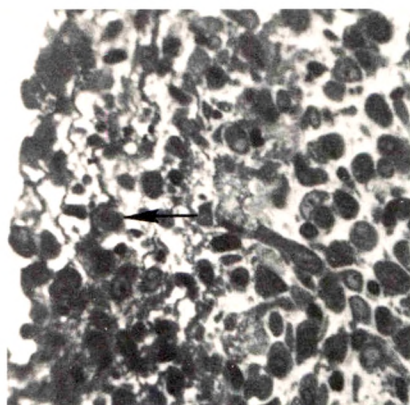
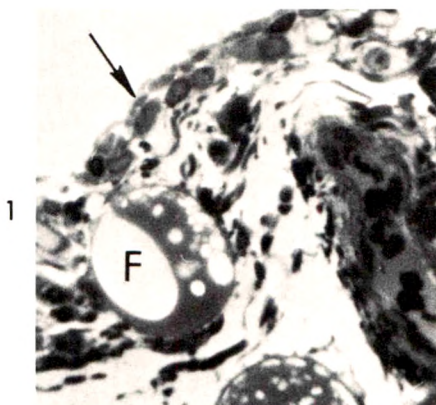
Legends for Figures

Fig 1—Synovial membrane from rabbit control knee joint given 35 daily injections of diluted autologous serum. The synovial lining cells (*arrow*) are normal in number and appearance. No inflammatory cells are seen around the small blood vessel or elsewhere in the subsynovial connective tissues. Two fat cells (*F*) are present (light micrograph, toluidine blue, $\times 300$).

Fig 2—Synovial membrane and subsynovial infiltrate from rabbit given 16 daily injections of HRPO. The number of synovial lining cells (*arrow*) is increased. The subsynovial connective tissue contains many macrophages, plasma cells, lymphocytes and fibroblasts (light micrograph, toluidine blue, $\times 440$).

Fig 3—Synovial cell from a rabbit receiving 15 daily injections of HRPO. Numerous cell processes and pseudopods are seen extending from the plasma membrane. Many vesicles and vacuoles containing reaction product are present in the cytoplasm. The clumped nuclear chromatin and incomplete nuclear membrane suggest the cell is in an early phase of mitosis (electron micrograph, $\times 9000$).

Fig 4—Synovial lining cell from rabbit receiving 12 daily HRPO injections. The large cytoplasmic vacuole contains the remains of a degenerating cell. Two smaller vacuoles contain electron-opaque peroxidatic reaction product (electron micrograph, $\times 16,000$).



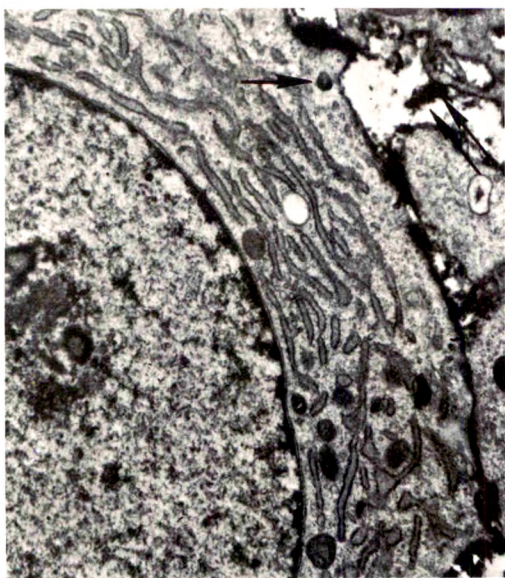


Fig 5—Synovial lining cell from rabbit receiving 16 daily HRPO injections. In contrast to the majority of synovial cells, this cell contains only a few cytoplasmic vesicles and vacuoles, and abundant rough-surfaced endoplasmic reticulum. Peroxidatic reaction product, which is abundant outside the cell (*double arrows*), is seen only in occasional small vesicles (*single arrow*) within the cell (electron micrograph, $\times 20,000$).

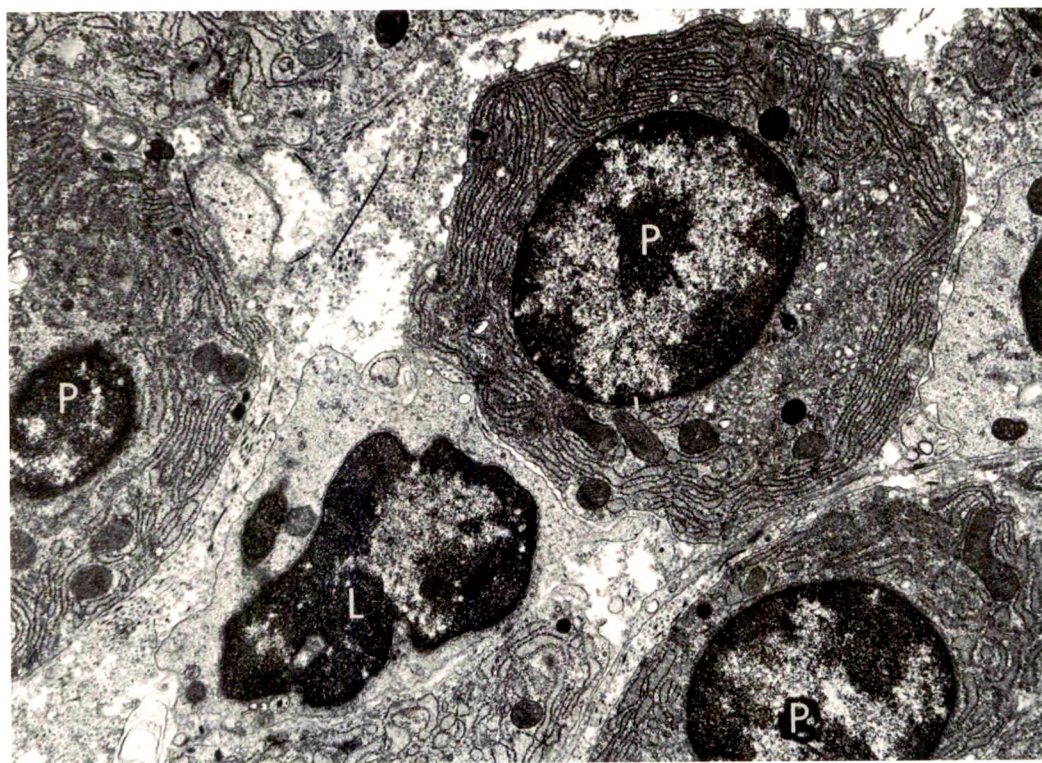


Fig 6—Portion of subsynovial infiltrate from rabbit given 16 daily HRPO injections. Mature plasma cells contained typical stacks of rough-surfaced endoplasmic reticulum and peripherally condensed nuclear chromatin. A medium lymphocyte (*L*), closely opposed to a plasma cell (*P*) contains scant cytoplasmic organelles and condensed nuclear chromatin. Collagen fibers of varying orientation lie between the cells (electron micrograph, $\times 10,000$).

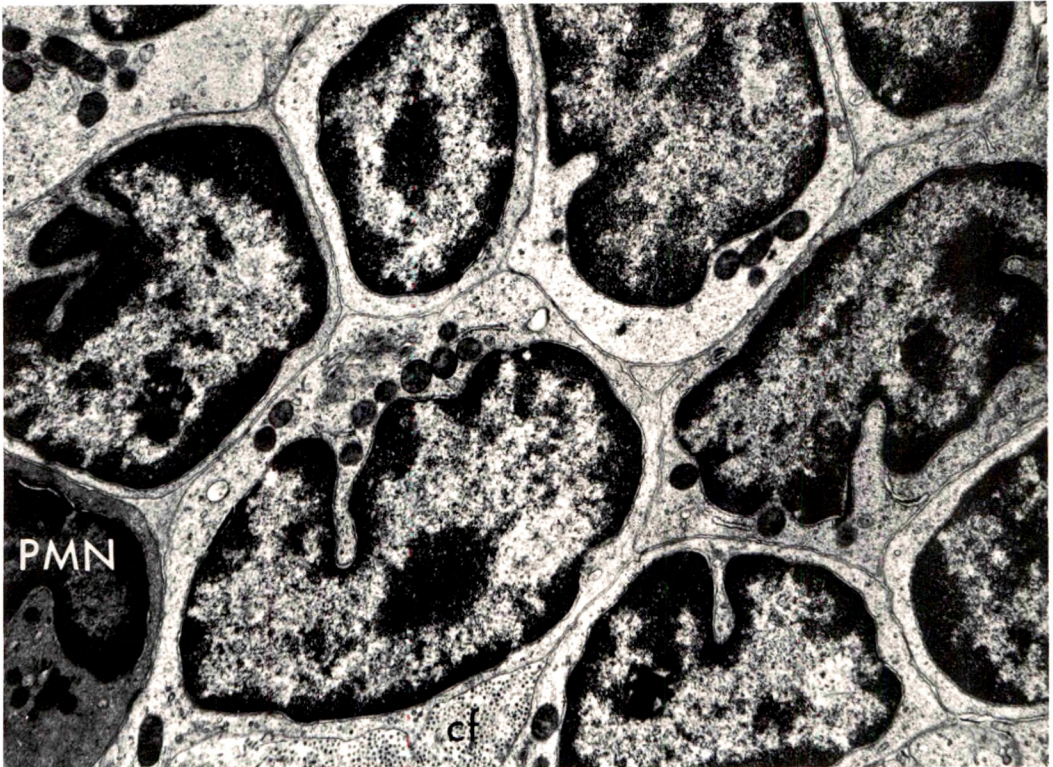


Fig 7—Cluster of lymphocytes in the subsynovial infiltrate from a rabbit receiving 16 daily HRPO injections. The cells are typical of small to medium lymphocytes, with condensed nuclear chromatin and scant cytoplasm containing few organelles. The lymphocytes are closely apposed with very little intercellular space intervening. A bundle of collagen fibers (*cf*) and a portion of a polymorphonuclear leukocyte (*PMN*) are at the lower left (electron micrograph, $\times 10,000$).

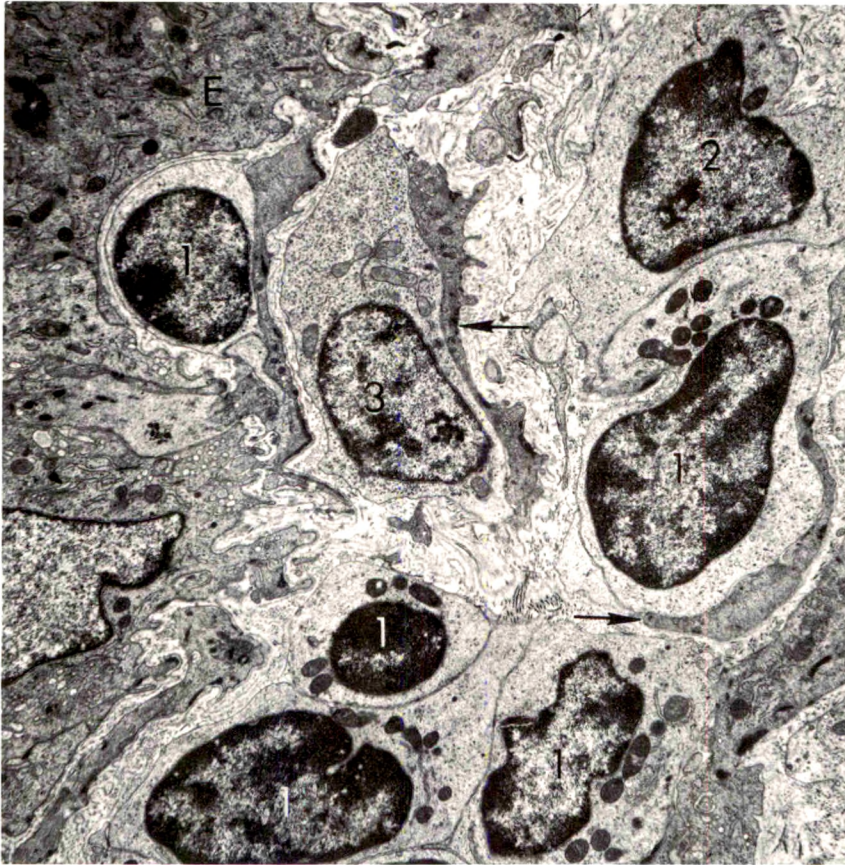
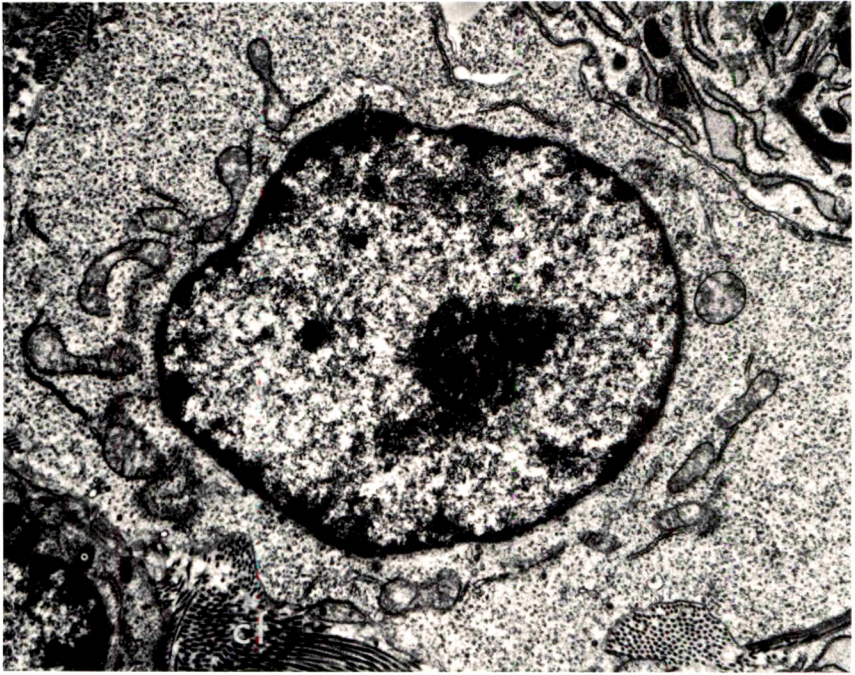


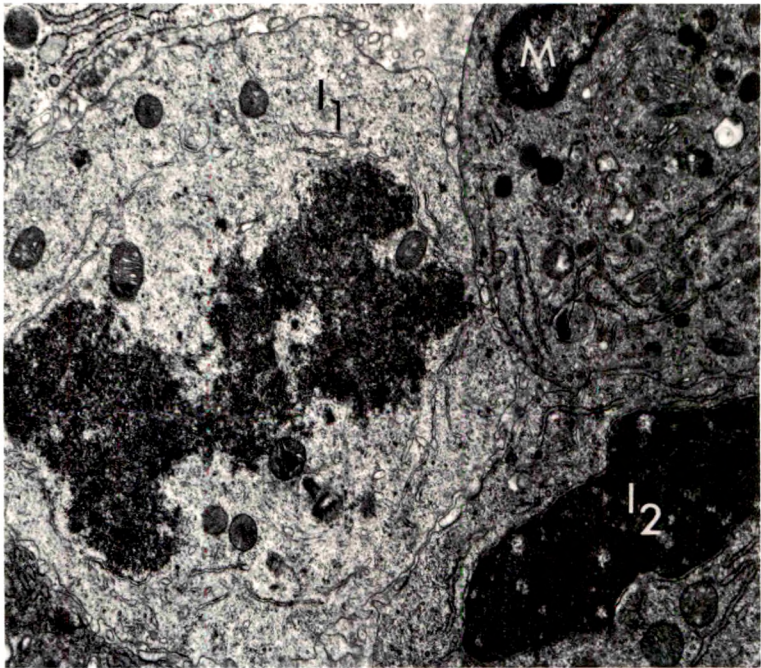
Fig 8—Perivascular lymphoid cells from subsynovial tissue of rabbit given 16 daily HRPO injections. The albuminal aspect of the endothelium (*E*) is at the left. Small to medium lymphocytes (*1*) have condensed nuclear chromatin and bland cytoplasm. A large lymphocyte (*2*) has a prominent nucleolus and moderate numbers of free polyribosomes in the cytoplasm. An immunoblast (*3*) has a prominent nucleolus, dispersed nuclear chromatin, and abundant free polyribosomes. A single profile of rough-surfaced endoplasmic reticulum is evident. Slender processes of pericytes (*arrows*) are interposed between the lymphoid cells (electron micrograph, $\times 6000$).

Fig 9—Subsynovial immunoblast from animal killed after 12 daily injections of HRPO. Note the prominent nucleolus, dispersed nuclear chromatin, abundant free polyribosomes and scant elements of rough-surfaced endoplasmic reticulum. Collagen fibers (*cf*) are seen in the interstitial space (electron micrograph, $\times 14,000$).

Fig 10—Subsynovial cells from rabbit given 16 daily HRPO injections. An immunoblast (*I*₁) is in mitosis. A similar cell (*I*₂) recently has divided. A macrophage (*M*) is closely associated with the two immunoblasts (electron micrograph, $\times 10,000$).

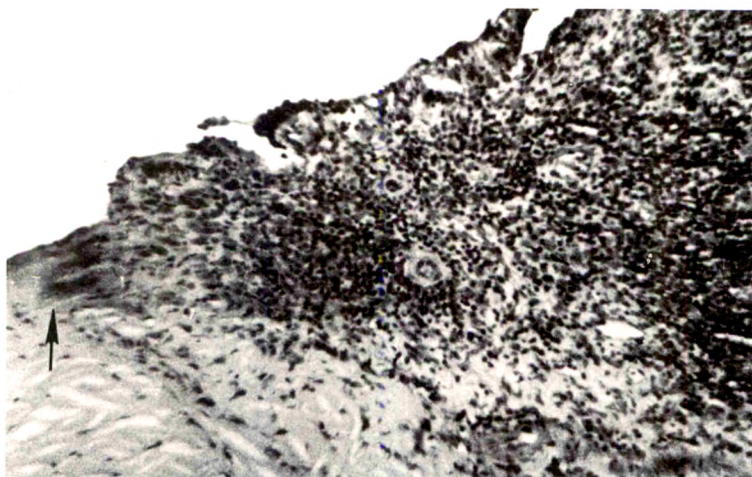


9



10

11



12

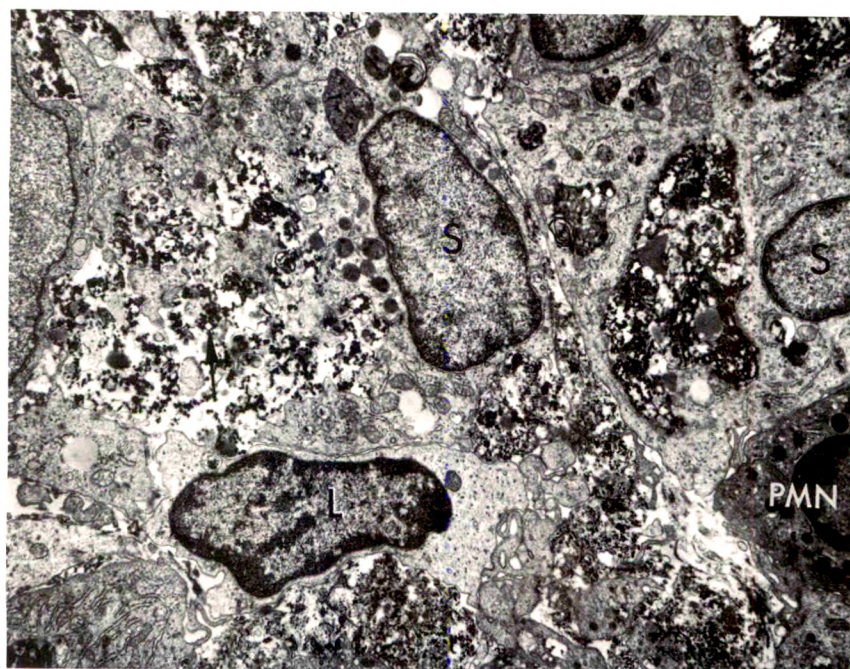
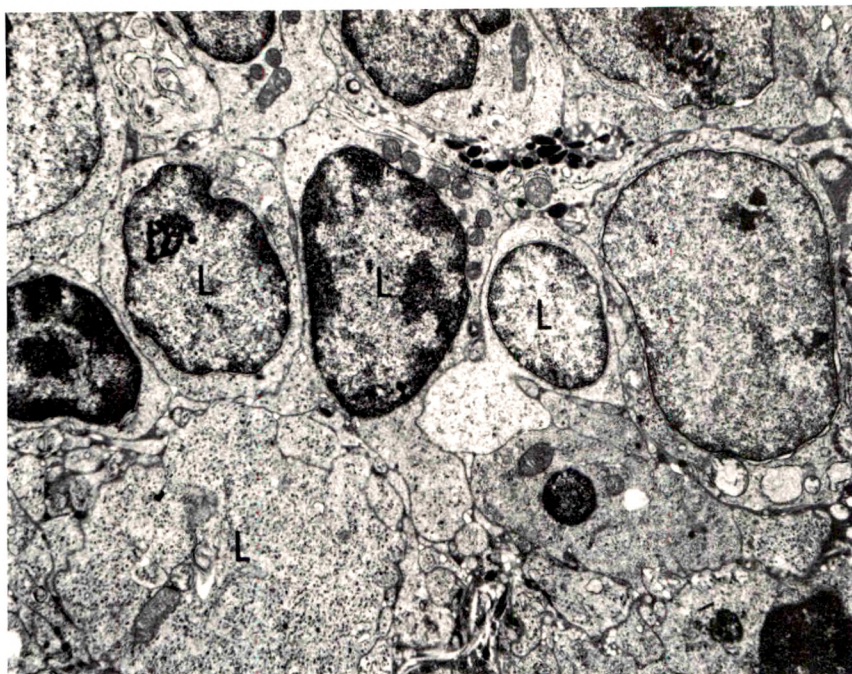
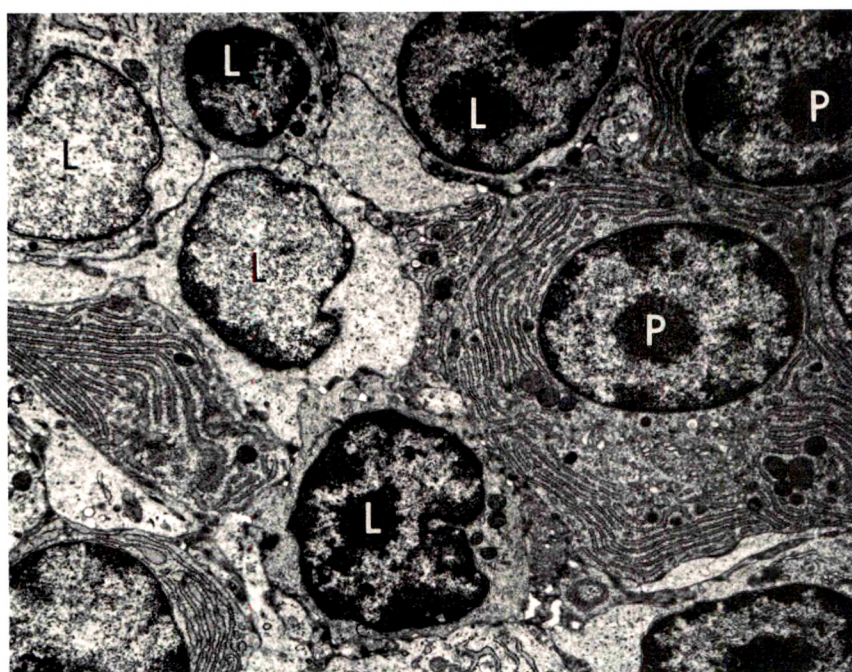


Fig 11—Inflammatory synovial tissue and cartilage from rabbit given 35 daily HRPO injections. The dense inflammatory infiltrate consists primarily of lymphocytes and macrophages. The altered staining characteristics of the cartilage adjacent to the inflammatory infiltrate (*arrow*) reflect necrosis of cartilage (light micrograph, H&E, $\times 120$). **Fig 12**—A portion of the synovial membrane from an animal sacrificed after 37 daily injections. The synovial cells (S) appear highly active with large vacuoles containing cellular debris and other dense material. Extracellular fibrin and precipitated protein are present in abundance between the cells (*arrow*). A lymphocyte (L) and polymorphonuclear leukocyte (PMN) are seen within the synovial lining layer (electron micrograph, $\times 5000$).



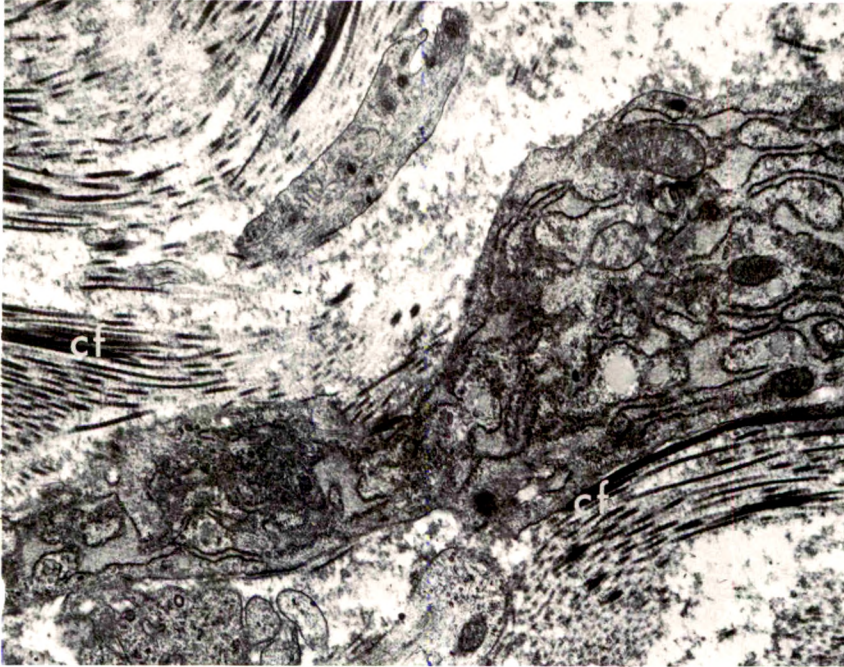
13



14

Fig 13—Subsynovial infiltrate from rabbit killed after 37 daily HRPO injections. A spectrum of lymphoid cells (L) is present. There are several small to medium lymphocytes, with condensed nuclear chromatin and scant cytoplasm containing few organelles. Other lymphoid cells have more dispersed nuclear chromatin and moderate numbers of cytoplasmic free polyribosomes. The cells are closely packed, with little intercellular space intervening ($\times 6000$). **Fig 14**—Subsynovial infiltrate from rabbit receiving 37 daily HRPO injections. Portions of several plasma cells (P) and a variety of lymphoid cells (L) are visible. As in Fig 13, very little intercellular space is present between adjacent cells ($\times 6000$).

15



16

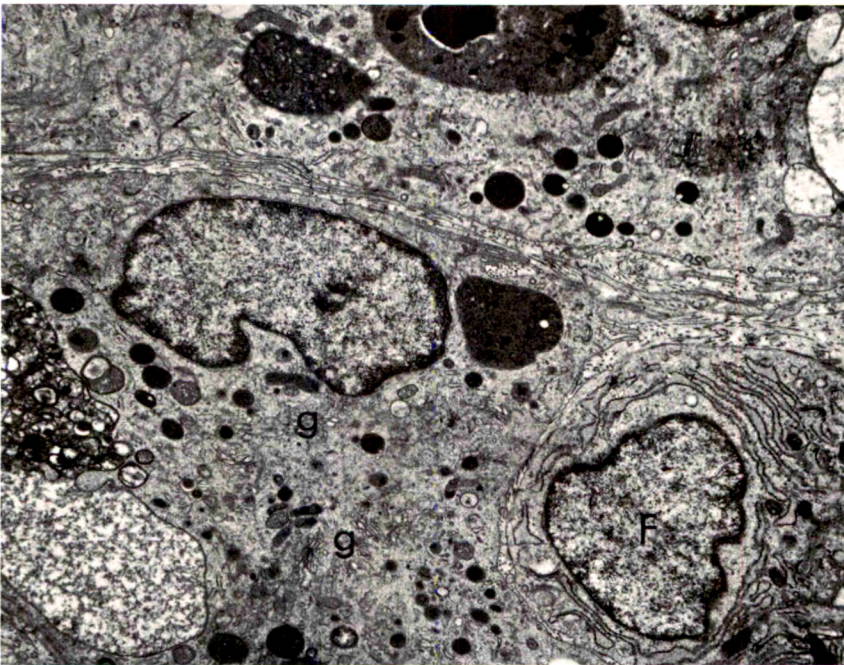
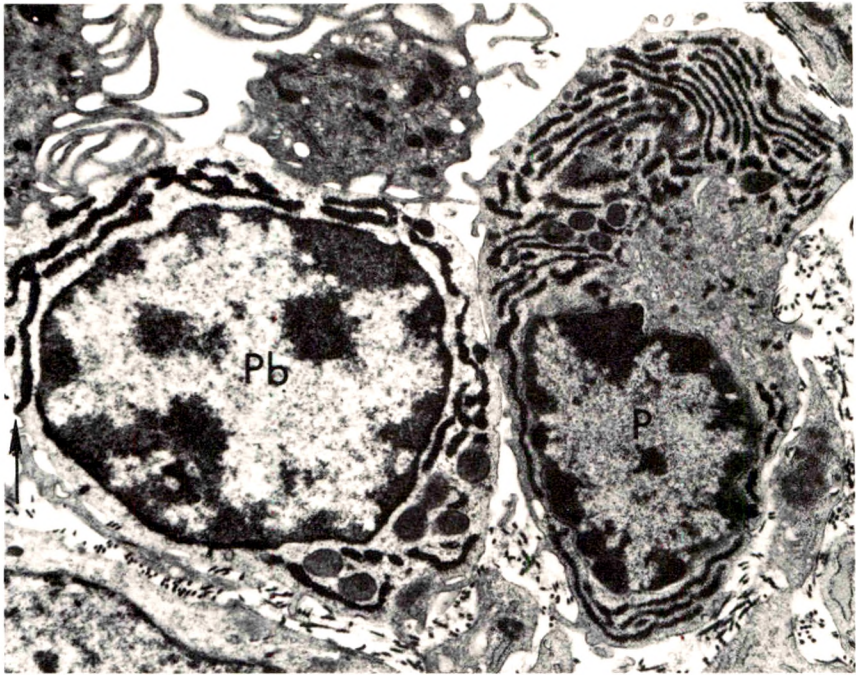
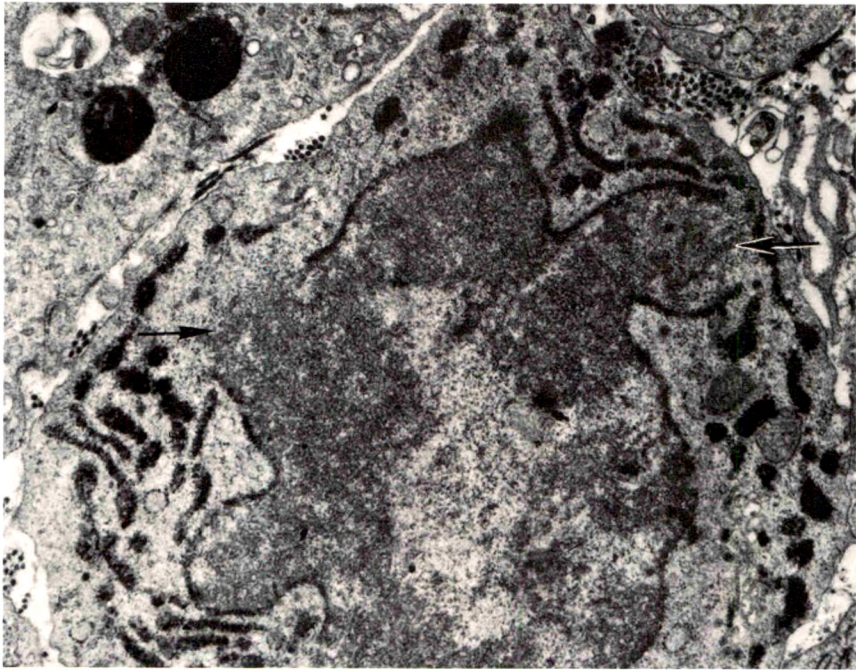


Fig 15—Fibroblast in subsynovial infiltrate of rabbit given 37 daily HRPO injections. The dilated rough-surfaced endoplasmic reticulum contains granular material which presumably is precipitated protein. Numerous collagen fibers (cf) surround the fibroblast ($\times 16,000$). **Fig 16**—Macrophages from subsynovial tissue of rabbit given 35 daily HRPO injections. Numerous cytoplasmic vesicles and vacuoles variously contain cellular debris or amorphous material of varying electron opaqueness. The Golgi complex (g) is well developed. The cell at the right (F) with the extensive rough-surfaced endoplasmic reticulum probably is a fibroblast (electron micrograph, $\times 10,000$).



17



18

Fig 17—Subsynovial plasma cell (*P*) and plasmablast (*Pb*) from rabbit receiving 15 daily HRPO injections. The procedure of Leduc and Avrameas was used to reveal sites of anti-HRPO activity. Such activity, revealed by peroxidatic reaction product, is present in the rough-surfaced endoplasmic reticulum of both cells. The perinuclear space of the plasmablast also contains anti-HRPO activity. The membrane of one of the profiles of rough-surfaced endoplasmic reticulum appears to be continuous with the plasma membrane of the plasmablast (arrow) (electron micrograph, $\times 12,000$). **Fig 18**—Subsynovial plasmablast from rabbit sacrificed after 15 daily HRPO injections. Tissue reacted by method of Leduc and Avrameas to reveal anti-HRPO activity. Such antibody activity is indicated by peroxidatic reaction product in the rough-surfaced endoplasmic reticulum and perinuclear space. The nuclear membrane is discontinuous at several points (arrows), suggesting beginning mitosis (electron micrograph, $\times 15,000$).

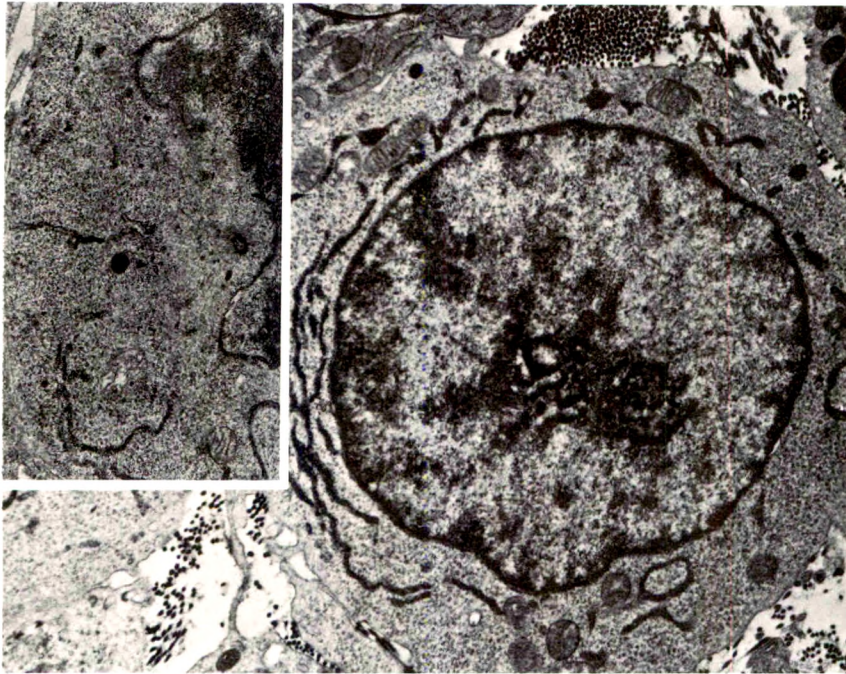
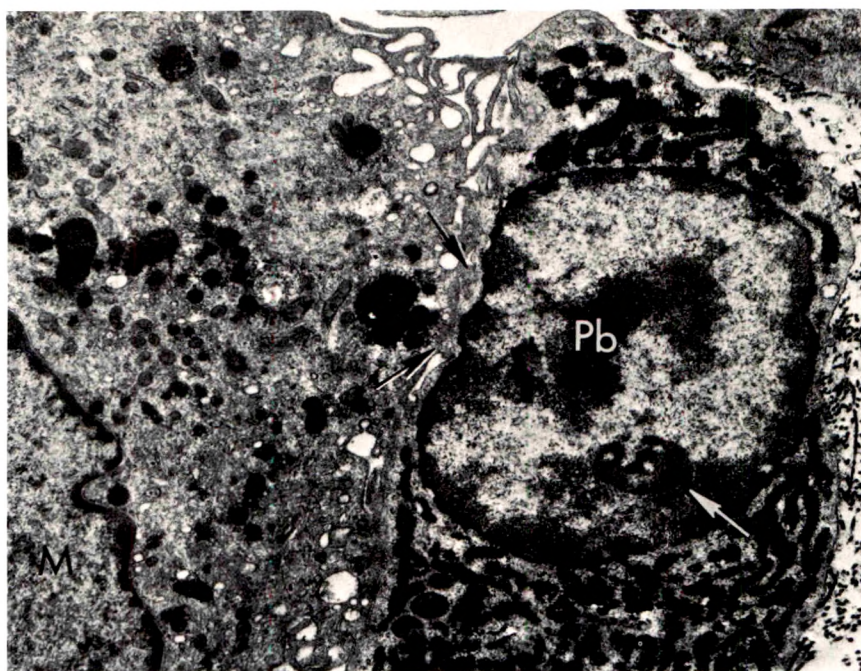
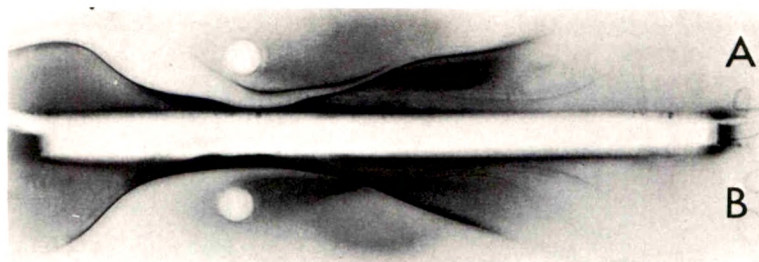


Fig 19—Subsynovial immunoblast from rabbit given 15 daily HRPO injections. Technic of Leduc and Avrameas was used to reveal anti-HRPO activity. The cell has a prominent nucleolus and dispersed nuclear chromatin. Several profiles of rough-surfaced endoplasmic reticulum show anti-HRPO activity (electron micrograph, $\times 10,000$). **Inset** shows a similar cell in mitosis (electron micrograph, $\times 7500$).

Fig 20—Subsynovial macrophage (*M*) and plasmablast (*Pb*) from rabbit given 15 daily HRPO injections. Anti-HRPO activity revealed by method of Leduc and Avrameas. The macrophage contains many HRPO-containing vesicles and vacuoles. The plasma membrane of the macrophage exhibits a complex network of pseudopods and is very closely associated with the plasma membrane of the plasmablast (*black arrows*). The nucleus of the plasmablast has peripheral condensations of chromatin and a prominent nucleolus (*white arrow*). Anti-HRPO activity is present in the rough-surfaced endoplasmic reticulum and perinuclear space of the plasmablast (electron micrograph, $\times 10,000$). **Fig 21**—Enzyme immunoelectrophoresis in Agarose gel of sera from rabbits receiving 16 (*A*) and 35 (*B*) daily HRPO injections. **Top**—Patterns photographed by reflected light reveal the precipitin lines in which peroxidatic reaction product reveals anti-HRPO activity. With the 16-day serum (*A*), specific antibody activity is present in both *IgG* and *IgM* lines, while with the 35-day serum (*B*), it is confined to the *IgG* line. **Bottom**—Same patterns are photographed by transmitted light to reveal the many precipitin lines without anti-HRPO activity.



20



21



[*End of Article*]

Fetal Renal Structure and the Genesis of Amniotic Fluid Disorders

Richard L. Naeye, MD and William A. Blanc, MD

Newborn recipient twins in the transplacental transfusion syndrome have dilated renal tubules, enlarged bladders and an increased urinary output in the early neonatal period, suggesting that increased fetal micturition is responsible for hydramnios in the syndrome. There is the possibility that such micturition contributes to hydramnios in other disorders as well. In the present study, renal tubules were found to be dilated in single-born infants with a diverse group of disorders having hydramnios as a common feature. Many of the neonates had hypoplastic lungs, an abnormality whose role in the hydramnios is undetermined. Renal tubular lumina were of normal size in neonates associated with oligohydramnios due to chronic leak of amniotic fluid. Donor members of parabioc transfusion pairs had contracted renal tubules which helps to explain their oligohydramnios. (Am J Pathol 67:95-108, 1972)

VARIOUS STUDIES OF PREGNANCY cite an incidence of hydramnios varying from 0.13 to 3.20%.¹ In almost half of such cases, the fetus or newborn infant dies.² Such deaths are sometimes caused by fetal malformations incompatible with life but many are due to prematurity, the hydramnios having induced early delivery. In some of the cases, there is no obvious maternal, fetal or placental abnormality to which the fluid disorder can be related.³ Even when a maternal, fetal or placental abnormality has been identified, the exact mechanism of the hydramnios is often uncertain.

The oldest and simplest explanation for the origin of amniotic fluid is attributed to Hippocrates who is reported to have held that such fluid is the product of the fetal kidneys.⁴ Many investigators have discounted such a role for the kidneys because the fluid disorder is occasionally found in cases where congenital closure of the lower genitourinary tract has made fetal micturition impossible.⁴⁻⁷ However, there is much other evidence that fetal urine significantly contributes to the volume of amniotic fluid.⁸⁻¹¹ Recent studies from our own laboratory have

From the Department of Pathology, Milton S. Hershey Medical Center, The Pennsylvania State University, Hershey, Pa and the Department of Pathology, Columbia University, College of Physicians & Surgeons, New York City, NY.

Supported by grants HE-11688-04 and NICHD 2-T01-HD 0018-04 from the US Public Health Service.

Accepted for publication September 29, 1971.

Address reprint requests to Dr. Richard Naeye, Milton S. Hershey Medical Center, Hershey, Pa 17033.

shown that anencephalic infants associated with hydramnios have patent renal collecting tubules, suggesting some fetal micturition while those without hydramnios have almost closed tubules.¹² Newborn donor twin members of a parabiologic pair in the transplacental twin transfusion syndrome have almost closed renal tubules and oligohydramnios while their recipient partners have dilated tubules and hydramnios.¹² These donor twins have small bladders and a small neonatal urinary output while their recipient partners have abnormally large bladders and an increased urinary output. The present study gives evidence that fetal micturition is active in a variety of other clinical situations in which hydramnios is found.

Case Material

A decade of clinical and autopsy charts were searched at Babies Hospital, New York City for cases of hydramnios and oligohydramnios in which well-preserved autopsy material was available. Cases with anencephaly or gross renal or gastrointestinal malformations which might explain the amniotic fluid disorder were excluded. Remaining were 26 cases of hydramnios and 13 cases of oligohydramnios (Tables 1 and 2). Hydramnios was defined as an amniotic volume over 2500 ml at birth, oligohydramnios as the absence of amniotic fluid. Gestational ages ranged from 25 to 40 weeks. Ten infants were stillborn; the remainder died within a few hours of birth.

Congenital Heart Disease

Four of the neonates associated with hydramnios had congenital heart disease (Table 1). One had an ostium secundum type of atrial septal defect and another a preductal coarctation of the aorta with absent ductus and hypoplasia of the aortic arch. Both of these infants were hydropic. A third infant had a large ventricular septal defect, a dilated patent ductus arteriosus and a persistent left superior vena cava entering the coronary sinus. The fourth infant had chromatin positive Turner's syndrome, a vascular ring anomaly involving the aorta and ductus arteriosus and a defect in the pericardium with herniation of the right auricle. Neither of these last 2 infants was hydropic. One of the 4 mothers had a previous gestation with hydramnios recorded.

Hydrops

Three of the infants associated with hydramnios had hydrops of unknown cause and 1 infant had the fluid disorder associated with erythroblastosis fetalis due to Rh incompatibility (Table 1). One of the infants with idiopathic hydrops had a large pleural and peritoneal effusion.

Possible Defects in Fetal Deglutition

Seven neonates had congenital malformations that might have interfered with swallowing before birth (Table 1). Three had large diaphragmatic defects with abdominal viscera in the thorax. Although never proven, such abnormally placed viscera might compress the esophagus. One of the neonates with a diaphragmatic defect and 2 other infants had severe hydrocephalus, a disorder that might interfere with swallowing through a central mechanism. The importance of this central

Table 1—Mean Body and Organ Values in Newborn Infants Whose Gestations Were Associated with Hydramnios*

	Recipient twins	Congenital heart	Idiopathic hydrops	RH hydrops	Swallowing defects	Diabetic mothers	Placental angiomatosis	Hepatitis and cirrhosis	Other
Body weight	100 ± 31	121 ± 23	129 ± 22	136	109 ± 27	126	101	139	115
Body length	101 ± 3	94 ± 7	101 ± 4	101	98 ± 3	106	98	101	101
Heart weight	115 ± 40	101 ± 18	117 ± 7	168	86 ± 28	103	100	—	109
Lungs weight	118 ± 40	38 ± 12†	83 ± 32	63	41 ± 25†	109	55	96	60
Spleen weight	123 ± 44	91 ± 36	77 ± 30	680	95 ± 45	94	34	448	68
Liver weight	113 ± 40	103 ± 25	112 ± 25	207	106 ± 37	125	112	92	98
Adrenals weight	80 ± 22	58 ± 21†	93 ± 25	143	80 ± 25	56	59	156	65
Kidneys weight	105 ± 37	85 ± 25	122 ± 63	93	110 ± 24	61	100	93	56
Thymus weight	102 ± 42	79 ± 29	136 ± 28	40	60 ± 32†	62	182	49	87
Brain weight	117 ± 22	115 ± 14	105 ± 3	94	99 ± 14	97	101	—	92
No. of cases	5	4	3	1	7	2	1	1	2

* All figures are in percent of control values as defined in the text.

† P value of 0.05 or less in comparison with controls.

Table 2—Mean Body and Organ Values in Newborn Infants Whose Gestations Were Associated With Oligohydramnios*

	Chronic amniotic fluid leak	Donor twins
Body weight	104 ± 14	81 ± 25
Body length	105 ± 5	98 ± 7
Heart weight	100 ± 11	89 ± 33
Lungs weight	68 ± 18†	86 ± 36
Spleen weight	93 ± 37	75 ± 24
Liver weight	106 ± 13	89 ± 35
Adrenals weight	122 ± 60	77 ± 44
Kidneys weight	108 ± 13	82 ± 33
Thymus Weight	123 ± 35	50 ± 12
Brain weight	99 ± 9	107 ± 18
No. of cases	8	5

* All figures are in percent of control values as defined in the text.

† P value of 0.05 or less in comparison with controls.

mechanism is suggested by the observation that anencephalic fetuses often do not swallow. Another infant had amyoplasia congenita, a muscular disorder which might alter deglutition while still another neonate had major deformities of the thoracic cage, possibly leading to esophageal compression. One of the infants with hydrocephalus had a small Y chromosome and arthrogryposis. One of the neonates with a large diaphragmatic defect was an iniencephalic monster and had a cleft palate.

Diabetic Mothers

Two neonates had mothers with overt diabetes mellitus who required insulin during gestation. Neither newborn had any gross congenital malformations.

Other Cases

One hydropic newborn infant had placental angiomatoses; his mother had taken isoniazid and para-aminosalicylic acid throughout pregnancy. Still another infant had congenital hepatitis with giant-cell transformation and early cirrhosis of the liver; the two previous pregnancies of his mother had been complicated by hydramnios. One of the final 2 neonates associated with hydramnios had a calcified thrombosis of the ductus venosus and the other was a fraternal twin with a separate placenta.

Recipient Twins

Five neonates were recipient members of twin pairs with the transplacental transfusion syndrome (Table 1). Clinical details have been published previously.¹⁵

Oligohydramnios

The study also included 13 infants of gestations with recorded oligohydramnios. Five were the donor members of the aforementioned parabiotic twin pairs. The other 8 had a chronic leak of amniotic fluid for 3 or more weeks prior to delivery; in 7 instances this led to the amniotic fluid infection syndrome. All 8 had abnormal facies and vernix granulomatosis of the amnion was observed in the 4 with available placentas.

The infants with amniotic fluid disorders were compared with 25 control infants, matched for gestational age, who had body weights within 10% of mean normal values for gestational age.¹⁶ None had recorded disorders of amniotic fluid volume. In the control infants, death was due to cerebral hemorrhage, pulmonary hemorrhage, fetal or intrapartum hypoxia.

Methods

Organ weights and body measurements were obtained from autopsy protocols. In each case, weights and measurements of body size and organs were calculated as percentages of mean values for "normal" infants of the same gestational age.¹⁶ The percentage of kidneys comprising of cortex and inner and outer zones of the medulla was determined for each case by using a planimeter on camera lucida drawings of cross sections of the organ. The method of line sampling was used to quantitate individual components in the kidneys.^{17,18} By this means, the percentage of various components comprising a tissue can be determined. In addition, the relative size and number of cells and cellular components can be calculated. In virtually every instance, more than 100 cells of an individual type were measured; sections were cut at 5 μ .

After determining the percentages of individual components of the kidney in individual cases, a mean percentage for each component was calculated for each grouping of cases.

Results

Body and most organ weights were within normal limits in the infants associated with hydramnios, a major exception being the lungs, which were subnormal in size in most of the subgroups (Table 1). The adrenals were also subnormal in weight in several groups, especially the one containing the infants with congenital cardiac malformations (Table 1).

Glomeruli were abnormally enlarged in the recipient twins and in the infants with possible abnormalities in fetal deglutition (Table 3). Tubular luminal area was abnormally large in all but 2 of the hydramnios groups (Table 3, Fig 1-3). Infants with congenital heart disease had a subnormal mass of cytoplasm in individual cells of both the proximal and distal convoluted tubules (Table 3).

Except for small lungs, body and organ measurements were normal in 8 infants with oligohydramnios due to chronic amniotic fluid leak (Table 2). Most such measurements were subnormal in the donor twins by comparison with their recipient partners (Table 2). Nephron measurements, including tubular luminal areas, were normal in the infants with chronic leak of amniotic fluid (Table 4, Fig 4).

Discussion

Previous studies from our laboratory showed that the relative size of renal tubular lumina can be correlated with the volume of amniotic

Table 3—Nephron Measurements in Newborn Infants Whose Gestations Were Associated with Hydramnios*

	Recipient twins	Congenital heart	Idiopathic hydrops	RH hydrops	Swallowing defects	Diabetic mothers	Placental angiomatosis	Hepatitis and cirrhosis	Other
Glomeruli									
Mean diameter	131 ± 28†	82 ± 16	82 ± 21	101	126 ± 10†	104	94	91	95
Proximal convoluted tubules									
Diameter nuclei	101 ± 9	100 ± 9	100 ± 13	104	101 ± 9	107	99	98	92
Cytoplasm/cell	113 ± 34	78 ± 31	87 ± 32	90	90 ± 16	109	97	87	91
Distal convoluted tubules									
Diameter nuclei	104 ± 10	96 ± 16	89 ± 17	99	100 ± 9	99	106	99	101
Cytoplasm/cell	104 ± 14	61 ± 22†	127 ± 45	92	115 ± 43	101	100	94	108
Collecting tubules outer zone medulla									
Diameter nuclei	100 ± 13	99 ± 12	110 ± 112	98	100 ± 12	102	92	99	103
Cytoplasm/cell	152 ± 42	72 ± 30	109 ± 29	68	133 ± 57	83	123	55	141
Luminal area	167 ± 54*	323 ± 138†	228 ± 69†	103	145 ± 49†	156	68	163	79
Thin Segment of Henle's Loop									
Luminal area	191 ± 78†	195 ± 58†	268 ± 124†	104	222 ± 101†	117	64	205	69

* All figures are in percent of control values as defined in the text.

† P value of 0.05 or less in comparison with controls.

Table 4—Nephron Measurements in Newborn Infants Whose Gestations Were Associated with Oligohydramnios*

	Chronic leak of amniotic fluid	Donor twins
Glomeruli		
Mean diameter	102 ± 16	70 ± 17†
Proximal convoluted tubules		
Diameter nuclei	102 ± 11	97 ± 7
Cytoplasm/cell	112 ± 19	81 ± 16†
Distal convoluted tubules		
Diameter nuclei	98 ± 17	99 ± 14
Cytoplasm/cell	108 ± 24	81 ± 22
Collecting tubules, outer zone medulla		
Diameter nuclei	102 ± 9	99 ± 11
Cytoplasm/cell	128 ± 42	101 ± 17
Luminal area	88 ± 31	49 ± 36†
Thin segment of Henle's loop		
Luminal area	89 ± 26	65 ± 20†

* All figures are in percent of control values as defined in the text.

† P value of 0.05 or less in comparison with controls.

fluid in both anencephaly and the twin transplacental transfusion syndrome.^{12,13} In the current study, such tubular lumina were found dilated in other groups of newborn infants whose gestations were complicated by hydramnios. None of these infants had gross pituitary or gastrointestinal malformations that might explain the hydramnios. If dilated tubules reflect increased micturition as an important contributor to hydramnios, oligohydramnios might be associated with normal or reduced-size lumina; such proved to be the case in the present study.

It has been established by many investigators that the fetal kidney normally adds to the amniotic volume but currently available physiologic methods are not sensitive enough to permit quantitation of its contribution to the genesis of hydramnios. Fetal urine is hypotonic late in gestation and its contribution to the amniotic fluid is a logical explanation for the decreasing concentration of solutes in the amniotic fluid near term.⁸⁻²¹ When the primate fetus is experimentally removed from the uterus late in gestation, the remaining amniotic fluid comes to resemble the amniotic fluid of early gestation, its high solute content resembling a transudate of maternal plasma.¹⁰ Other evidences of fetal urine contribution are the amniotic fluid's increased levels of urea and creatinine and decreased concentration of glucose late in gestation. Finally, radioactivity promptly appears in the amniotic fluid after diodrast-¹³¹I is injected into the fetal circulation of monkeys. Since

iodine is normally excreted by the renal tubules, Pitkin has suggested that fetal micturition constitutes an appreciable source of amniotic fluid.¹¹

There is normally a very rapid exchange of water between the mother, fetus and amniotic fluid; disappearance curves for water in the amniotic cavity show a normal half-life of only 95 minutes.^{4,19-21} With such rapid fluid exchanges, a daily amniotic volume increase of only 150 ml can induce hydramnios; this requires an amniotic inflow rate only 1-2% greater than the outflow rate.²² Such differences are too small to be measured by currently available methods especially when it is desired to individually quantitate the sources of the fluid.

Even if increased micturition contributed to the hydramnios in many of the current cases, it is far from certain that this renal activity was a primary phenomenon. Such an increase in fetal urine flow might be a compensatory response to an increased fetal blood volume, an increased water load or a deficiency of antidiuretic hormone (ADH). None of the current neonates (except for the recipient twins) and some of the infants with possible swallowing defects had enlarged glomeruli; glomerular enlargement is one evidence of an increased blood volume during fetal and neonatal life.^{15,23} There is little evidence of ADH deficiency since none of the current neonates had an abnormal pituitary gland or a deficiency of cellular cytoplasm in the medullary tubules; the latter is an abnormality previously shown to be characteristic of infants with an absent posterior pituitary.^{12,13} The small adrenal glands in infants with congenital heart disease might be important since there was a moderate deficiency of cytoplasm in epithelial cells of the proximal and distal convoluted tubules of this subgroup of neonates (Table 3). Deficiencies of the anterior pituitary and adrenals have been previously shown to lead to this tubular abnormality.^{12,13}

Other mechanisms aside from fetal micturition probably contributed to hydramnios in the current cases. A number of the neonates were hydropic and it has been postulated that hydramnios in such cases is due to circulatory failure from mechanical interference—*ie*, pressure on the great veins. This hypothesis is highly speculative at best.²⁴ Driscoll has raised the possibility that the hydramnios in such cases might be due to a primary immune mechanism.²⁵ A number of investigators have reported that placental vascular anomalies have a frequent association with hydramnios, perhaps indicating that the placenta might be the site of increased amniotic fluid formation.²⁶ The one such case in the current study had subnormal-size renal tubular lumina,

perhaps indicating that some mechanism other than increased micturition was responsible for the hydramnios (Table 3). Finally, Goodlin has suggested that perhaps any severely ill human fetus will swallow less (oligoposia) with resultant accumulation of amniotic fluid.²⁷ Data in the current study neither add to nor detract from this hypothesis.

The association of hypoplastic lungs with hydramnios is easily explained in only a few of the cases. Two of the neonates had large diaphragmatic defects with abdominal viscera in the thoracic cavities. This often leads to subnormal-size lungs, apparently through a restriction of the lungs' growth. A third newborn infant had a thoracic deformity which might have restricted lung growth. Two other infants with hydramnios had pleural effusions of 50 and 65 ml; volumes of this magnitude might also have restricted lung growth. No other neonate had a volume of pleural fluid exceeding 10 ml. In the other cases, the frequent association of pulmonary hypoplasia with hydramnios is a new finding. It is not easily attributed to compression of the thorax by the increased volume of amniotic fluid because in most cases of hydramnios, intrauterine amniotic fluid pressure is normal.

In most instances the pathogenesis of oligohydramnios is easier to understand than the genesis of hydramnios. Many cases of oligohydramnios are due to an underdeveloped or obstructed fetal urinary tract.²⁸ Other important causes are chronic leak of amniotic fluid and the twin transplacental transfusion syndrome, both included in the current study.^{14,15,28,29} The reduced amniotic volume associated with donor twins has been postulated to be due to subnormal blood volume, subnormal-size glomeruli with reduced glomerular filtration and a small volume of fetal micturition as evidenced by reduced luminal size of renal tubules, subnormal-size bladders and low neonatal urinary output.^{12,14,15} A chronic leak of amniotic fluid is probably the commonest cause of oligohydramnios.^{28,29} In the present study, such leaks did not appear to alter fetal renal structure, probably indicating that fetal micturition continues despite the fact that the fetus is deprived of body water usually gained by swallowing.

References

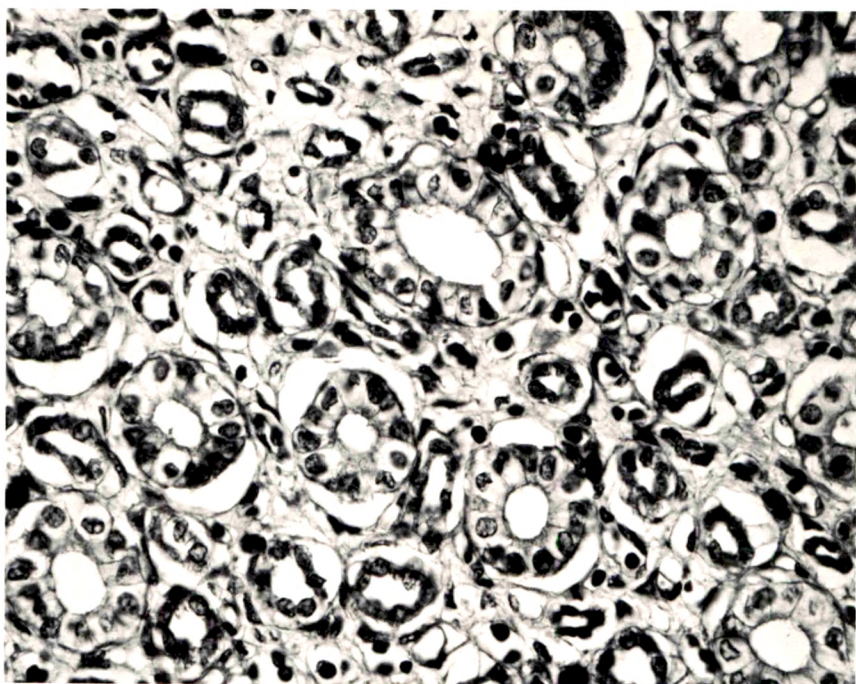
1. Kramer EE: Hydramnios, oligohydramnios and fetal malformations. *Clin Obstet Gynecol* 9:508-519, 1966
2. Eastman JJ, Hellman LM: *Williams Obstetrics*. New York, Appleton-Century-Crofts, 1961, p 603
3. Jacoby HE, Charles D: Clinical conditions associated with hydramnios. *Am J Obstet Gynecol* 7:910-919, 1966

4. Plentl AA: Formation and circulation of amniotic fluid. *Clin Obstet Gynecol* 9:427-439, 1966
5. McGaughey HS Jr, Corey EL, Scoggin WA, Bobbitt OB, Thorton WH Jr: Observations on the equilibrium of urea between mother and fetus. *Am J Obstet Gynecol* 78:844, 1959
6. Fink AZ: Ein Tierexperimenteller Beitrag zur Entstehung des Hydramnions. *Geburtshilfe Gynaekol* 140:18-21, 1954
7. McCance RA, Widdowson EM: Renal function before birth. *Proc R Soc Lond [Biol]* 141:489-497, 1953
8. Smith FG Jr, Adams FH, Borden M, Hilburn J: Studies of renal function in the intact fetal lamb. *Am J Obstet Gynecol* 96:240-245, 1966
9. Alexander DP, Nixon DA: The foetal kidney. *Brit Med Bull* 17:112, 1961
10. Behrman RE, Parer JT, de Lannoy DW Jr: Placental growth and the formation of amniotic fluid. *Nature* 214:678-680, 1967
11. Pitkin, RM, Reynolds WA, Burchell RC: Fetal contribution to amniotic fluid. *Am J Obstet Gynecol* 100:834-838, 1968
12. Naeye RL, Milic AMB, Blanc W: Fetal endocrine and renal disorders: clues to the origin of hydramnios. *Am J Obstet Gynecol* 108:1251-1256, 1970
13. Naeye RL, Blanc W, Milic AMB: Renal development in dysplasia of the fetal pituitary. *Pediatr Res* 4:257-261, 1970
14. Schatz RL: Eine besondere Art von einseitiger Polyhydramnie mit anderseitiger Oligohydramnie bei eineiigen Zwillingen. *Arch Gynakol* 19:329-333, 1882
15. Naeye RL: Human intrauterine parabiocytic syndrome and its complications. *N Engl J Med* 268:804-808, 1963
16. Schulz DM, Giordano DA, Schulz, DH: Weights of organs of fetuses and infants. *Arch Pathol* 74:244-250, 1962
17. Uotila W, Kannas O: Quantitative histological method of determining proportions of principal components of thyroid tissue. *Acta Endocrinol [Kbh]* 11:49, 1952
18. Naeye RL: Organ and cellular development in mice growing at simulated high altitude. *Lab Invest* 15:700-706, 1966
19. Friedman EA: The role of the monkey fetus in the exchange of the water and sodium of the amniotic fluid. *J Clin Invest* 38:961-970, 1959
20. Scoggin WA, Harbert GM, Anslow WO Jr, Van T Riet B, McGaughey HS Jr: Fetomaternal exchange of water at term. *Am J Obstet Gynecol* 90:7-16, 1964
21. Plentl AA: Dynamics of the amniotic fluid. *Ann NY Acad Sci* 75:746-761, 1959
22. Hutchinson DL, Hunter CB, Nelson ED, Plentl AA: Exchange of water and electrolytes in the mechanism of amniotic fluid formation and the relationship to hydramnios. *Surg Gynecol Obstet* 100:391-396, 1955
23. Naeye RL: Early glomerular changes with cardiac malformations. *Biol Neonat* 6:297-308, 1964
24. Kohler HG: Congenital cystic malformation of the lung; its relation to hydrops and hydramnios. *Arch Dis Child* 45:146, 1970
25. Driscoll SG: Hydrops fetalis. *N Engl J Med* 275:1432-34, 1966
26. Bhargava I, Raja PTK: Foetal blood vessels on the chorial surface of the

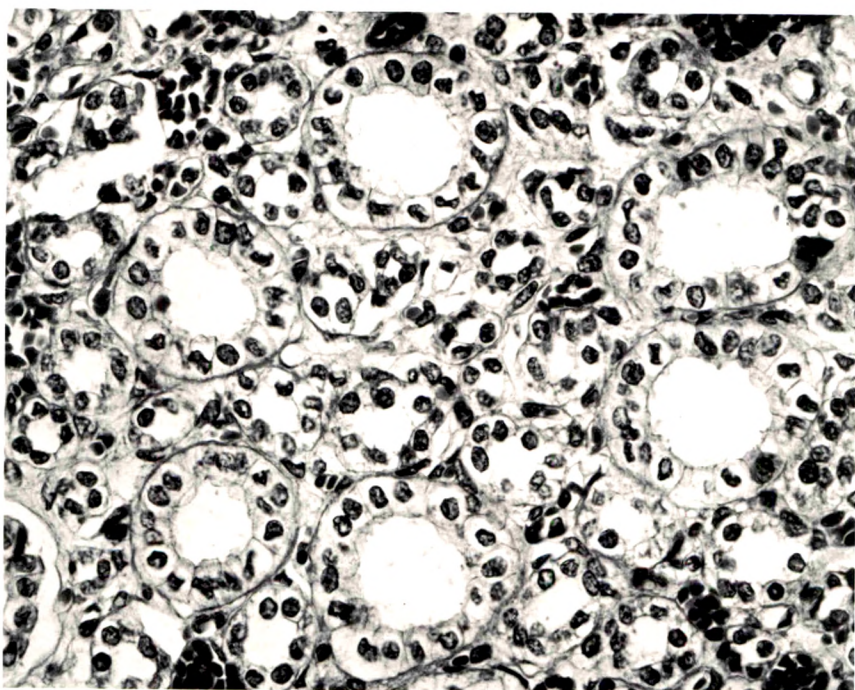
- human placenta in abnormal pregnancy and development. *Experimentia* 25:520-521, 1969
27. Goodlin, RC, Belsher LJ: Acute hydramnios, fetal oligoposia, and heart failure. *Lancet* 2:218, 1969
 28. Blanc WA, Apperson JW, McNally J: Pathology of the newborn placenta in oligohydramnios. *Bull Sloane Hosp Women* 8:51-64, 1962
 29. Bain AD, Smith II, Gauld IK: Newborn after prolonged leakage of liquor amnii. *Br Med J* 2:598-599, 1964

The authors are indebted to Mr. W. S. Dellinger for technical assistance and to Dr. Gilbert Mellin, Babies Hospital, New York City for the computer search of clinical records that made the study possible.

[Illustrations follow]



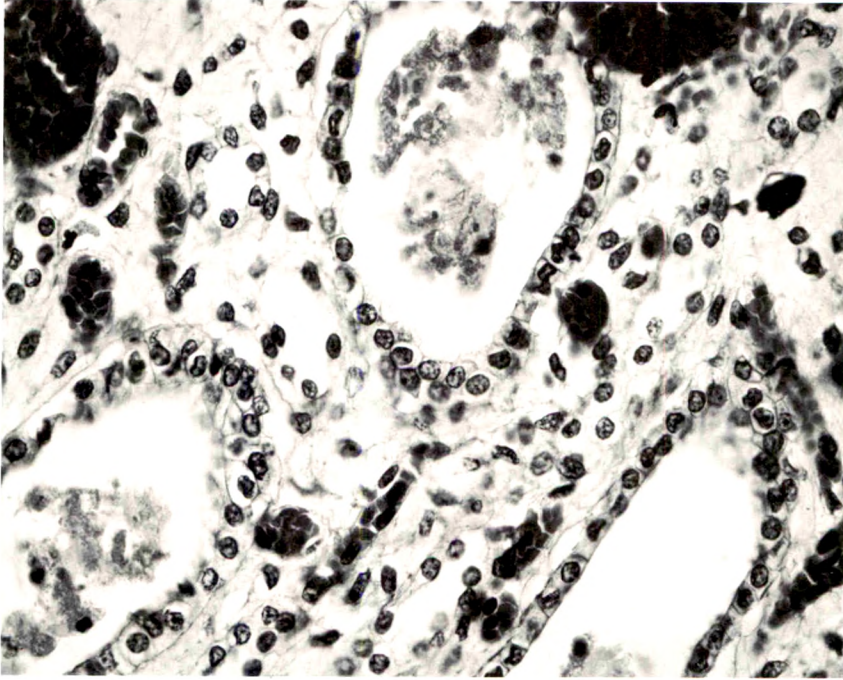
1



2

Fig 1—The lumina of collecting tubules and tubules in the loop of Henle are normally patent in this kidney of a control newborn infant (H&E, $\times 600$). Fig 2—The lumina of collecting tubules are abnormally enlarged in this kidney of a newborn infant who was associated with hydramnios (H&E, $\times 600$).

3



4

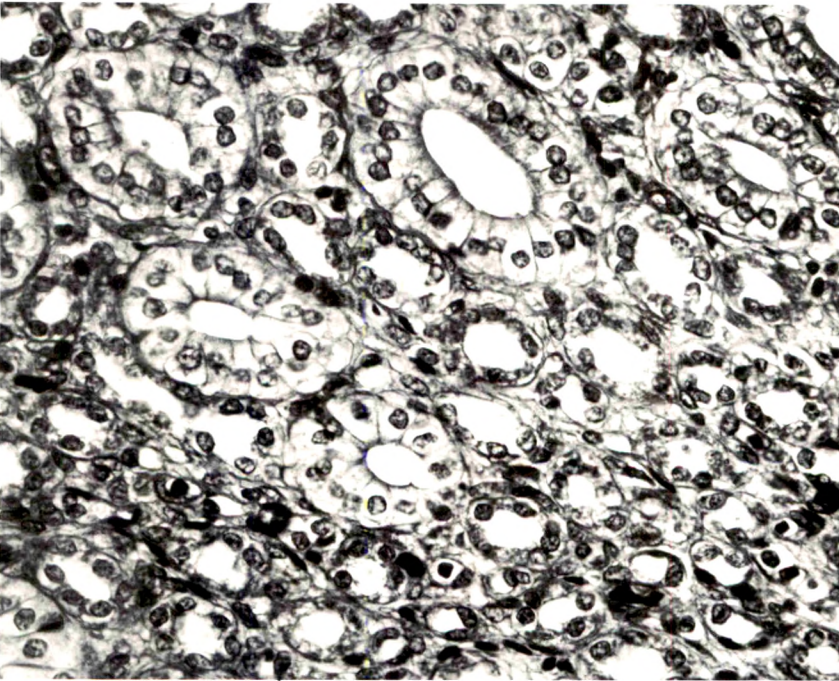


Fig 3—The lumina of collecting tubules and tubules in the loop of Henle are markedly dilated in this kidney of a newborn infant who was associated with hydramnios (H&E, $\times 600$). **Fig 4**—The lumina of collecting tubules and tubules in the loop of Henle are near normal size in this kidney from a newborn infant who was associated with oligohydramnios due to a chronic leak of amniotic fluid (H&E, $\times 600$).

Ultrastructural Changes in the Capillary Bed of Human Pituitary Tumors

Joel Schechter, PhD

The fine structure of the capillary bed of the anterior pituitary has been studied in 19 cases of pituitary tumor and 1 autopsy specimen. Tumor specimens were less well vascularized than the autopsy specimen. Endothelial cells within tumor specimens were often observed with swollen portions of cytoplasm, or cytoplasmic blebs, projecting into the capillary lumen. Blebbing, in many cases, nearly obstructed the capillary lumen and was most often associated with endothelial cells that had an electron-lucent cytoplasm, in contrast to endothelial cells that had an electron-dense cytoplasm, even within the same capillary profile. Compared with electron-lucent cells, electron-dense cells contained more endothelial filaments. Also observed were capillaries that had apparently broken apart releasing their contents into the pericapillary space and shrunken remnants of capillaries. A number of abnormal features were observed in the pericapillary spaces—*ie*, disruption of the parenchymal-pericapillary interface, disorganization of basal laminae, increased amounts of plasma proteins and cellular debris within the space and, ultimately, complete loss of the normal limits and characteristics of the space. Similar, though less pronounced, changes were observed in the autopsy specimen. The hypothesis is advanced that changes observed in the capillary bed are, in large part, a result of tumor growth, which increasingly disrupts tissue organization at the parenchymal-pericapillary interface and, because the tumor mass in the sella turcica can only enlarge upwards, compresses the pituitary stalk and portal veins. The result is ischemia and eventual necrosis. The observations are then in good agreement with recent reports on changes in capillary fine structure associated with ischemia. (Am J Pathol 67:109–126, 1972)

THE FINE STRUCTURAL FEATURES of capillaries of the “normal” anterior pituitary gland are now well established.^{1–5} However, the extent to which these capillaries are affected or structurally modified by their association with pituitary neoplasms has at present received very little attention. Electron microscopic studies of pituitary tumors either do not mention the capillary network^{6–10} or make only brief comment that the capillaries appear “rather normal.”^{11,12} Furthermore, a search of the literature has uncovered only preliminary reports¹³ on the broader topic—ultrastructural changes in capillaries associated with tumors. Recent physiologic studies¹⁴ demonstrated changes in pituitary hemodynamics in association with tumors, but provided no morphologic

From the Department of Anatomy, School of Medicine, University of Southern California, Los Angeles, Calif 90033.

Supported in part by Grant ACS-IDC 10, 1 N-21-K from the American Cancer Society, administered through the University of Southern California Interdepartmental Cancer Research Committee and in part by a Department of Health, Education and Welfare-National Institutes of Health Grant 5 S01-RR05356-10.

Accepted for publication September 29, 1971.

Address reprint requests to Dr. Schechter.

correlates. After inducing pituitary adenomas in rats, Tiboldi *et al*¹⁴ demonstrated that blood flow to the neoplastic pituitaries (blood flow/pituitary weight) was actually reduced in comparison to controls. These authors postulated that the changes which they observed in pituitary hemodynamics would likely be correlated with structural transformations of the pituitary capillaries. The present study pursues this point and reports the extent of the structural modifications taking place in capillaries of human pituitary tumors.

Materials and Methods

The material used in this study included samples of 20 different pituitary glands. The first of these was obtained at autopsy within 20 minutes of death. This individual was a 25-year-old female afflicted with lateral sclerosis. There were no clinical indications of any pituitary abnormality, and on removal at autopsy, the pituitary was within normal limits. The remaining 19 pituitary specimens were obtained as surgical biopsies; of these the clinical diagnosis of ten chromophobe adenomas and nine acidophil adenomas was later confirmed by histologic examination (employing hematoxylin and eosin and orange G-PAS stains) in surgical pathology. The particular interest of the neurosurgical staff in acidophil adenomas has resulted in numerous referrals and accounts for the atypical distribution of acidophil adenomas in this group of tumors.

Immediately after they were removed, samples of pituitary were immersed in a fixative solution composed of 2% glutaraldehyde, 2% paraformaldehyde converted to formaldehyde, 0.070 M cacodylate (dimethyl sodium arsenate), 0.02% CaCl_2 , pH 7.3. The samples were then diced into smaller pieces and allowed to remain in the fixative solution for 1 to 2 hours. Occasionally, some samples were refrigerated in fixative solution overnight. After this initial fixation, tissue samples were placed for 2 hours in 1% OsO_4 solution containing CaCl_2 and cacodylate buffer at the same concentration as in the aldehyde fixative and at the same pH. The tissue was then dehydrated in a graded series of alcohols, and after propylene oxide rinses, was embedded in Araldite 502. After curing, the blocks were cut on a Porter-Blum MT-1 ultramicrotome. Thin sections, giving silver interference colors, were collected on copper grids, stained with lead citrate, and examined either with a Hitachi HU-11A or AEI-6B electron microscope. After 2 or 3 grids were thus filled, 0.5–0.75 μ sections were cut and collected on separate glass slides. The Araldite was removed by the method of Berkowitz *et al*,¹⁵ and the sections were stained with toluidine blue (pH 8.0).

Results

Autopsy Specimen, Light Microscopy

Light microscopic examination of this specimen revealed pituitary parenchymal cell cords interwoven by a rich capillary network (Fig 1). The capillaries varied in diameter; some were quite dilated, others had a narrower diameter, though all appeared patent. Pericapillary spaces generally stained faintly with toluidine blue in contrast to the darker cell cords, and could, therefore, be distinguished rather easily around

most capillaries. However, around some or portions of capillaries, it was difficult to judge the limits of the pericapillary space, since staining properties of the space matched that of adjacent parenchymal cells (Fig 1).

Autopsy Specimen, Electron Microscopy

Pituitary capillaries were fenestrated, with the fenestrae measuring 500–1000 Å in diameter, and bridged by a continuous diaphragm (Fig 2). The endothelial cells comprising these capillaries varied in thickness and luminal surface contours. Some areas were thin-walled with smooth luminal contours, while in other areas, there were diffuse swellings or bleb-like expansions of endothelial cell cytoplasm (Fig 2). In some of the capillaries, the blebs protruded conspicuously into the lumen (Fig 3). The cytoplasm associated with the blebs was consistently electron-lucent, but otherwise contained a normal array of cytoplasmic organelles. Precipitated plasma proteins were observed within the capillary lumen as a flocculent material of intermediate electron density (Fig 2 and 3).

Pericapillary spaces around many capillaries were clearly defined as electron-lucent zones between the basal laminae of pituitary parenchymal cells and capillary endothelial cells (Fig 2). Fibrocytes were the most frequently encountered cell type within the pericapillary space. Collagen fibers were found in small bundles throughout pericapillary spaces, and in some areas were collected into larger fiber bundles. It was not always possible to assess the contents or limits of pericapillary spaces, for around some capillaries, or portions of capillaries, the entire space had a rather homogeneous electron density with indistinct limits (Fig 2 and 3). This appeared to be related to 3 factors: First, a flocculent material was often evident within the pericapillary space (Fig 2 and 3). This material was essentially identical to the precipitated plasma proteins, noted above, within the lumina of capillaries. Second, it was observed that there were discontinuities in parenchymal tissue—*ie*, interrupted cell membranes, particularly in the vicinity of the parenchymal basal lamina (Fig 2 and 3). At these points, the cytoplasmic density of the parenchymal cells appeared to blend gradually into that characteristic of the pericapillary space. Third, it was observed that the parenchymal and capillary basal laminae were frequently thrown into complex redundant patterns or were of increased thickness (Fig 4). Combinations of these factors thus contributed to obscuring the pericapillary space, which then appeared homogeneously electron-dense and with indistinct boundaries.

Biopsy Specimens

Changes in capillary fine structure observed in 19 pituitary tumors could not be correlated with any one particular type of tumor. Changes in the capillaries appear to represent a more generalized phenomenon, a response of the capillaries to the process of tumor growth, and these changes are, therefore, reported here as a single group.

Light Microscopy

Light microscopically, the parenchyma of pituitary tumors (Fig 5-7) appeared markedly less vascularized when compared with samples from the autopsy specimen. In addition, the capillaries which were present often appeared narrowed or compressed and pericapillary spaces could not be clearly defined (Fig 5). Also evident were red blood cells which did not appear to be within capillaries (Fig 7); they were either packed in tightly between parenchymal cells or within clefts between parenchymal cells.

Electron Microscopy

Capillaries within the tumors frequently were comprised of dark, electron-dense and light, electron-lucent, endothelial cells in sharp juxtaposition to one another within the same capillary profile (Fig 8-10). That portion of the capillary formed by an electron-lucent endothelial cell often appeared enlarged and thicker than its electron-dense counterpart. Portions of the endothelial cells, particularly the electron-lucent cells, protruded as large blebs (Fig 9) into the capillary lumen, at times almost totally obliterating the lumen (Fig 10). Where the blebbing was extensive, there were no fenestrae. The electron-dense endothelial cells did not generally appear to be enlarged, though smaller blebs were evident along their luminal surface. Fenestrations were more apparent in association with electron-dense cells (Fig 8). The cytoplasm of both types of endothelial cells contained mitochondria, small channels of endoplasmic reticulum, free ribosomes, coated and smooth vesicles and cytoplasmic filaments or tubules. The morphologic basis for the differences in electron density is the apparently greater quantities and concentrations of cytoplasmic filaments in electron-dense as compared with electron-lucent cells. Precipitated plasma proteins were evident within capillary lumina.

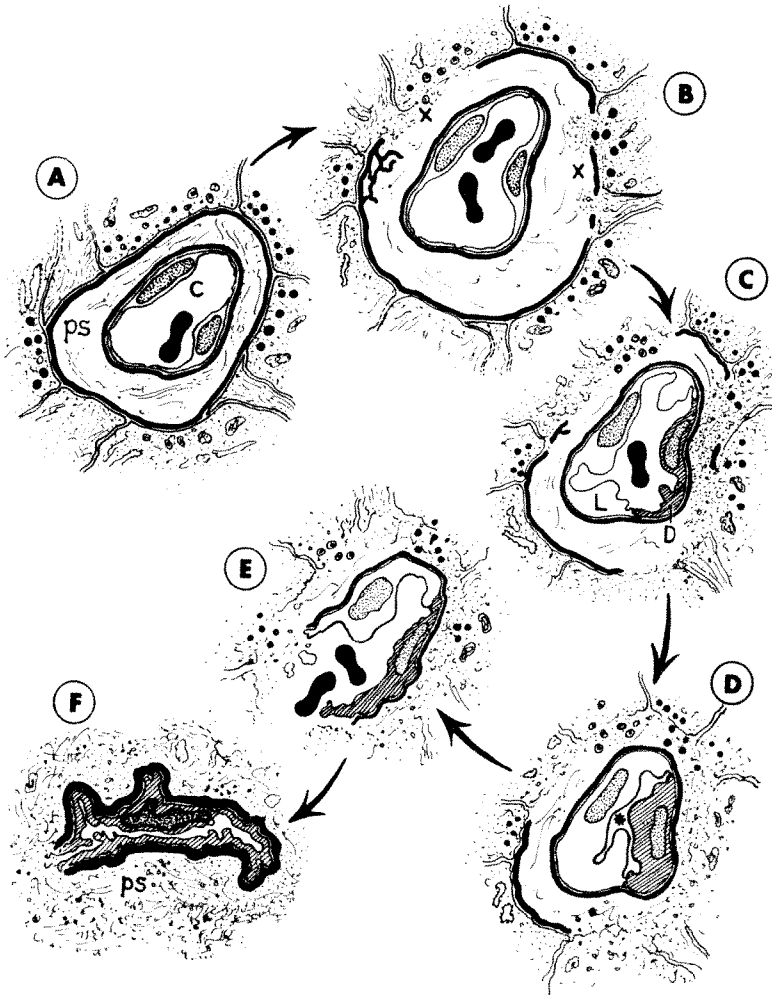
Pericapillary spaces in tumor specimens differed from those of the autopsy specimen in the following ways: In the tumor specimens, the pericapillary spaces were consistently more difficult to delineate because basal laminae of capillaries and pituitary parenchymal cells were typi-

cally fragmented or absent (Fig 8–10). These changes were particularly obvious with respect to the parenchymal basal lamina which was most frequently absent. Furthermore, pituitary parenchymal cells at the interface with the pericapillary space were often disrupted. The pericapillary spaces were thus converted into irregular spaces filled with cell debris, fragments of basal laminae, collagen and flocculent material identical to precipitated plasma proteins found within the capillary lumen. Red blood cells not confined to capillary channels were observed in open clefts or channels between parenchymal cells (Fig 10 and 11). In addition to red blood cells, clefts contained materials that appeared to be plasma proteins and an assortment of cellular debris, vesicles, secretory granules, fragments of cytoplasm, etc (Fig 11). Occasional sections revealed capillaries or portions of capillaries which appeared to have broken apart (Fig 12). The pericapillary spaces around these capillaries were consistently disorganized, with no parenchymal basal lamina and containing an assortment of cellular debris. In specimens revealing the most dramatic changes, capillaries appeared shrunken and collapsed, with irregular contours (Fig 13). The endothelial cells were electron-dense with dark, necrotic nuclei, and the capillary basal lamina appeared thickened and obscured due to the accumulation of a feltwork of electron-dense materials, and cellular debris. Parenchymal basal laminae could not be recognized at this stage.

Text-fig 1 proposes a possible step-by-step progression for the present observations.

Discussion

An interpretation of the fine structural changes in the capillaries of pituitary tumors must begin by considering the particular site at which these events are taking place at the macroscopic level. The pituitary rests in the rigid, bony sella turcica connected with the median eminence by a stalk which traverses the diaphragma sella. The diaphragma sella is composed of dense collagenous connective tissue. The pituitary stalk conveys the fragile portal veins, bringing the greater part of the blood supply to the anterior pituitary. In studies on swelling of the pituitary due to shock after automobile accidents, Kornblum and Fisher¹⁶ concluded that only the small circular opening in the diaphragma sella provided any room for the pituitary gland to expand. If and when the gland swelled, it expanded upward through the opening, the likely result being compression of the portal veins against the free edge of the diaphragma sella. It seems likely that neoplastic growth within the pituitary would also follow the same path of least resistance,



TEXT-FIG 1A—Profile of pituitary capillary in “normal” or “pretumor” state. The pericapillary space (ps) is limited by parenchymal and capillary basal lamina (*thick black lines*), and there are no disruptions of tissue components at the parenchymal-pericapillary interface. Capillary lumen (c) is wide and contains a red blood cell. B–F depict the postulated progression of changes within the vascular bed suggested by the morphologic observations of tumor specimens. B—Neoplastic growth has resulted in a breakdown of tissue components (x) at the parenchymal-pericapillary interface. C—Continued growth of the tumor further disrupts tissue integrity at the parenchymal-pericapillary interface and releases cellular fragments into the space. Increased materials within the pericapillary space, and compression of the pituitary stalk by the enlarging tumor mass, precipitate ischemic changes in the pituitary capillaries—*ie*, electron-lucent (L) and electron-dense (D) endothelial cells. D—Swelling and blebbing of endothelial cells now almost totally obstruct the capillary lumen (*asterisk*). The limits of the pericapillary space are difficult to distinguish, and cell debris and plasma proteins accumulate outside of the capillaries. E—The capillary has ruptured, releasing its contents into the surrounding tissue. The limits of the pericapillary space are now almost totally unrecognizable. F—The capillary has collapsed and appears necrotic. The pericapillary space (ps) contains a combination of materials and there is no discernible parenchymal interface.

similarly affecting the pituitary stalk and its portal veins. The result would induce a chronic ischemia compounded by the continued advancement of the tumor. The changes observed in the present study are therefore interpreted in large part as a manifestation of ischemic conditions. In this case, events at the macroscopic level—*ie*, compression of the stalk by the enlarging tumor mass—induce the changes in capillaries of the anterior pituitary observed at the fine structural level. Disruption of the tumor mass, noted at the interface with the pericapillary space, may also contribute an increasing amount of cellular debris to this space, such that the tumor mass could exert a direct compressive effect upon capillaries. In either case, the observations are in good agreement with recent reports on fine structural changes in capillaries during ischemia.

Endothelial cell blebbing and swelling have been described in capillaries of skin and cerebral cortex by Willms-Kretschmer and Majno,¹⁷ Chiang *et al*,¹⁸ and Hills,¹⁹ after experimentally induced ischemia. None of these studies was associated with the vascular bed within a tumor, though Willms-Kretschmer and Majno¹⁷ observed a progression of vascular injury almost identical to that reported here—*ie*, diffuse swelling and blebbing of individual endothelial cells which resulted in a narrowing and gradually increasing obstruction of the capillary lumen. These authors further noted that the swollen endothelial cells characteristically had an electron-lucent cytoplasm. Furthermore these events were accompanied by extravascular changes—*ie*, accumulation of plasma proteins and free red blood cells outside of the vessels.

In studies on the permeability characteristics of capillaries in virally induced brain tumors, Brightman¹³ reported changes in capillary permeability which, in some instances, could be correlated with the formation of fenestrations. In the present study, there were no increases of fenestrations, rather swelling of the endothelial cells appeared to decrease the number of fenestrations. However, capillaries which had broken open were observed, an event which would release the capillary contents into extravascular spaces. It is also possible, as Kent²⁰ and others have pointed out, that injury to endothelial cells may in itself alter the permeability properties of capillaries so that increased amounts of plasma proteins are lost to extravascular spaces in the absence of physical rupture of the vessels.

The functional implication of increased amounts of endothelial cell filaments is unknown. Increasing attention has been given to the possibility that endothelial filaments may represent contractile proteins²¹ which then could function to alter endothelial cell junctions, and thus affect capillary permeability. It is also possible that filaments are related

to supportive functions—*eg*, maintenance of capillary shape. Hills¹⁹ reported that endothelial filaments in capillaries of rat cerebral cortex were “perhaps” more abundant after ischemia. Endothelial filaments were decidedly more abundant in electron-dense cells described in the present study. Considering the breakdown and disruption of tissue components within the tumor mass, this suggests that the abundance of filaments may be related to supportive functions—*ie*, a cellular attempt to maintain normal tissue integrity in the presence of a changing environment. Hills described disorganization of basal laminae after ischemia, which could also account for changes in the basal laminae observed in the present study. An alternate explanation would be that the alterations in basal lamina morphology are secondary to the breakdown of tumor cells at the parenchymal-pericapillary interface.

The endothelial cell blebbing, modifications of the basal laminae and changes in capillary permeability all may be interpreted as being part of a series of changes in capillary structure related to vascular injury, and resulting from tumor growth in pituitary parenchymal cells. The sequence of events would seem to be as follows: Tumor growth in the anterior pituitary disrupts normal tissue patterns at the parenchymal-pericapillary interface. Continued enlargement of the tumor further disrupts tissue integrity at the parenchymal-pericapillary interface and also compresses the pituitary stalk and the blood supply to the anterior pituitary. The capillaries reflect these changes by endothelial swelling and blebbing, increased endothelial filaments, altered permeability properties with increased loss of materials to the pericapillary space. This process ultimately leads to obstructed capillaries, fragmentation, shrinkage and eventual death of endothelial cells, accompanied by complete loss of the normal characteristics of the pericapillary space.

That only a single pituitary suitable for electron microscopy was obtained from autopsy, necessitates cautious evaluation of this specimen. Two tentative interpretations of the observations would be the following: First, the apparent, though less pronounced, similarities between capillaries in this specimen and those within tumors suggest the possibility that the autopsy specimen was not, in fact, “normal,” even though it was described grossly at autopsy as being “normal.” Pathologists have known for some time that the pituitary is a common site of small subclinical tumors which are apparent on histologic examination. The autopsy specimen used here may have been a small subclinical tumor of this type. The observed features of these capillaries could, therefore, represent the initial response of the vascular bed to tumor growth. Second, it is possible that the observed alterations in capillary structure

are related to aging phenomena within the vascular bed itself. In this regard, Rosenquist and Bernick²² have recently described marked thickening of the basal laminae of glomerular capillaries with aging, and Buerger and Hevelke²³ reported that aging could be correlated with decreased luminal diameter and increased endothelial thickening in small vessels. Additional autopsy specimens will be required to clarify these possibilities.

References

1. Rinehart JF, Farquhar MG: The fine vascular organization of the anterior pituitary gland (rat). *Anat Rec* 121:207-240, 1955
2. Farquhar MG: Fine structure and function in capillaries of the anterior pituitary gland. *Angiology* 12:270-292, 1961
3. Cardell R: The cytophysiology of the anterior pituitary gland. *Henry Ford Hosp Bull* 11:409-430, 1963
4. Fujita H, Kataoka K: Capillary endothelial cells of the anterior pituitary should be excluded from the reticulo-endothelial system. *Z Anat Entwickl lungsgesch* 128:318-328, 1969
5. Bergland RM, Torack RM: An ultrastructural study of follicular cells in the human anterior pituitary. *Am J Pathol* 57:273-297, 1969
6. Gusek W: Vergleichende licht- und elektronenmikroskopische untersuchungen menschlicher hypophysenadenome bei akromegalie. *Endokrinologie* 42: 257-283, 1962
7. Fukumitsu T: Electron microscopic study of the human pituitary adenomas. *Arch Jap Chir* 33:329-349, 1964
8. Cardell RR, Knighton RS: The cytology of a human pituitary tumor: an electron microscopic study. *Trans Am Microsc Soc* 85:58-78, 1966
9. Porcile E, Racadot J: Ultrastructure of Crooke cells seen in the human hypophysis during Cushing's disease. *CR Acad Sci* 263:948-951, 1966
10. Paiz C, Hennigar GR: Electron microscopy and histochemical correlation of human anterior pituitary cells. *Am J Pathol* 59:43-72, 1970
11. Schelin U: Chromophobe and acidophil adenomas of the human pituitary gland: a light and electron microscopic study. *Acta Pathol Microbiol Scand: Suppl* 158:5-80, 1962
12. Kuromatsu C: The fine structure of the human pituitary chromophobe adenoma with special reference to the classification of this tumor. *Arch Histol Jap* 29:41-61, 1968
13. Brightman MW: Fenestrated capillaries as a route of protein leakage in virally-induced brain tumors. *Anat Rec* 169:283-284, 1971
14. Tiboldi T, Nemessanyi Z, Csernay I, Kovacs K: Effect of estrogen on pituitary blood flow in rats. *Endocrinol Exp* 1:73-77, 1967
15. Berkowitz LR, Fiorello O, Kruger L, Maxwell DS: Selective staining of nervous tissue for light microscopy following preparation for electron microscopy. *J Histochem Cytochem* 16:808-814, 1968
16. Kornblum RN, Fisher RS: Pituitary lesions in craniocerebral injuries. *Arch Pathol* 88:242-248, 1969
17. Willms-Kretschmer K, Majno G: Electron microscopic study of vascular injury. *Am J Pathol* 54:327-354, 1969

18. Chiang J, Kowada M, Ames A, Wright RL, Majno G: Cerebral ischemia. III. Vascular changes. *Am J Pathol* 52:455-476, 1968
19. Hills CP: Ultrastructural changes in the capillary bed of the rat cerebral cortex in anoxic-ischemic brain lesions. *Am J Pathol* 44:531-552, 1964
20. Kent S: Diffusion of plasma proteins into cells: a manifestation of cell injury in human myocardial ischemia. *Am J Pathol* 50:623-638, 1967
21. Becker CG, Murphy GE: Demonstration of contractile protein in endothelium and cells of the heart valves, endocardium, intima, arteriosclerotic plaques, and Aschoff bodies of rheumatic heart disease. *Am J Pathol* 55:1-37, 1969
22. Rosenquist TH, Bernick S: Histochemistry of renal basal laminae: adolescent compared with senescent rats. *J Gerontol* 26:176-185, 1971
23. Buerger M, Hevelke G: Do human beings have the age of their blood vessels? *Angiology* 7:137-151, 1956

The author gratefully acknowledges the fine technical assistance of Mrs. Olga Fiorello and Mrs. Sharon Sampogna, and wishes to thank Dr. David Maxwell, UCLA, Department of Anatomy, who graciously permitted access to the Hitachi electron microscope. The pituitary specimens were obtained through the cooperation and continued support of Dr. Robert Rand, Dr. Ulrich Batzdorf, and Mrs. Viven Gold, UCLA, Division of Neurosurgery.

[Illustrations follow]

Legends for Figures

Fig 1—Autopsy specimen stained with toluidine blue. This specimen contains an abundance of capillaries (c) which vary in diameter though all appear patent. Pale-staining pericapillary spaces (p) are evident around most of the capillaries. The arrow at lower right indicates a region in which the pericapillary space can not be clearly distinguished from adjacent parenchymal cells ($\times 700$).

Fig 2–4 are electron micrographs of the autopsy specimen stained with lead citrate. **Fig 2**—The wall of this capillary varies in thickness, being thin with fenestrations (arrows) in some areas, and with cytoplasmic blebbing (bb) in other areas. Plasma proteins (pr) are evident within the capillary lumen and within the pericapillary space. The limits of the pericapillary space (ps) in upper right can be distinguished, bounded by capillary and parenchymal basal laminae. The pericapillary space (ps) in left of figure is difficult to distinguish, owing to disruption of parenchymal cells and increased electron density of materials within the space. Portion of fibrocyte (F) ($\times 16,700$).

Fig 3—Blebbing (bb) of endothelial cell cytoplasm in this capillary is extensive and protrudes into the capillary lumen. Plasma proteins (pr) are evident within the capillary lumen and within the pericapillary space. Loss of cellular integrity and fragmentation of the parenchymal basal lamina (bl) at the parenchymal-pericapillary interface are evident, permitting portions of parenchymal cells (G) to mix with the contents of the pericapillary space and contributing to an increased electron density of the space ($\times 25,500$). **Fig 4**—Complex redundant configurations of the basal lamina (bl) contribute to an increased electron density of the pericapillary spaces. Also demonstrated is the loss of cellular integrity (arrows)—ie, absence of plasma membranes, in parenchymal cells at the parenchymal-pericapillary interface ($\times 14,100$).

Fig 5–7 are light micrographs of 3 tumor specimens stained with toluidine blue.

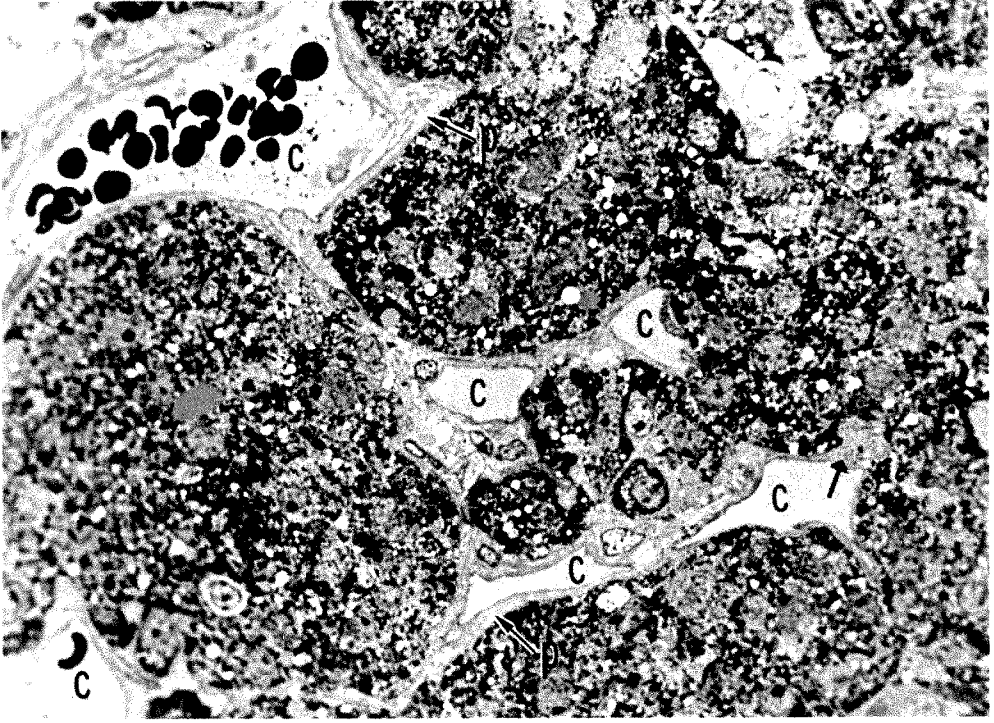
Fig 5—Tumor specimen. Capillaries (c) are few and widely separated in this specimen, and pericapillary spaces can not be distinguished from the parenchymal cells ($\times 700$). **Fig 6**—Tumor specimen. The mass of parenchymal tumor cells that fills this field appears totally avascular. The large dark shapes (arrows) may be remnants of red blood cells compressed between the tumor cells ($\times 700$). **Fig 7**—Tumor specimen. A number of red blood cells (arrows) are evident compressed between tumor cells or in cleft-like channels (x) between the tumor cells ($\times 700$).

Fig 8–13 are electron micrographs of tumor specimens stained with lead citrate.

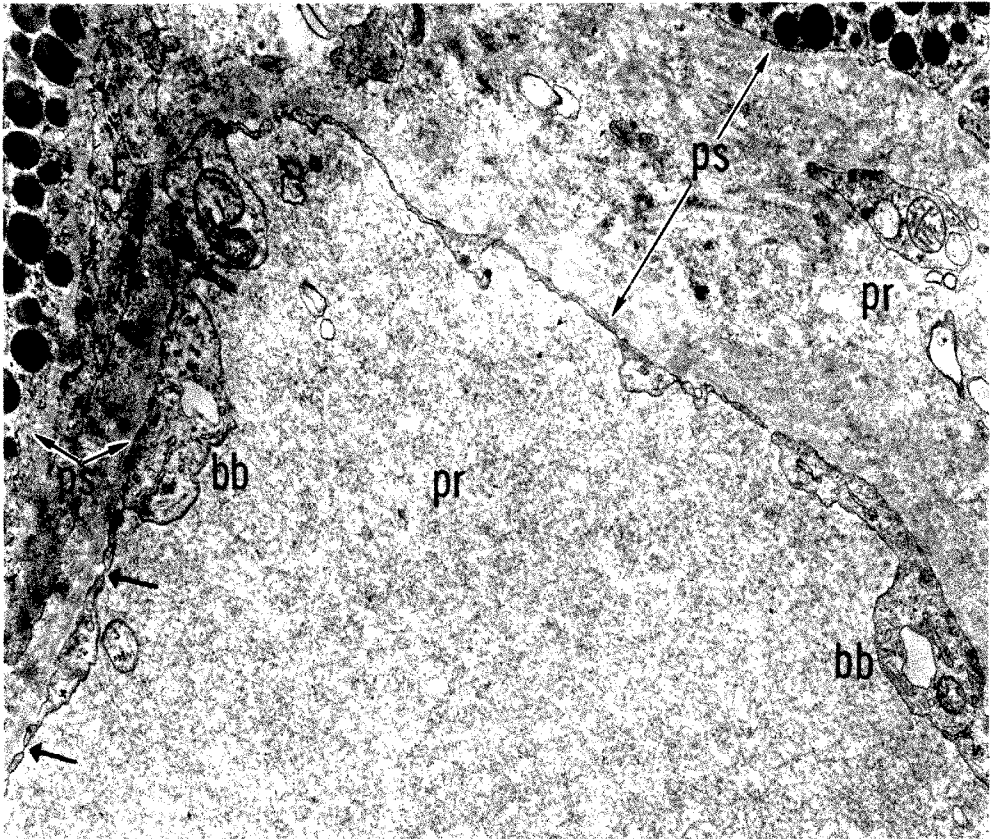
Fig 8—Tumor specimen. Electron-lucent (L) and electron-dense (D) endothelial cells are demonstrated within a single capillary profile. Fenestrations (arrows) were most often associated with electron-dense cells which generally did not exhibit as pronounced swelling or blebbing as their electron-lucent counterparts. Endothelial cell filaments (f) were most abundant within the electron-dense cells. Limits of the pericapillary space (ps) are not clear because parenchymal basal lamina is absent and tissue components are disrupted at parenchymal-pericapillary interface. Cellular debris (Cd) is spilling into pericapillary space ($\times 19,000$). **Fig 9**—Tumor specimen. Electron-lucent (L) endothelial cells typically exhibit more pronounced swelling and blebbing than those that are electron-dense (D). Plasma proteins (pr) are found within the capillary lumen and in considerable amounts within pericapillary spaces. Parenchymal basal lamina (bl) delimits a pericapillary space in some locations but is absent at other sites (lower left) where tissue components are disrupted ($\times 16,000$).

Fig 10—Tumor specimen. Swelling and blebbing of endothelial cells can attain such proportions as to almost totally obstruct the capillary lumen (asterisk). Pericapillary spaces are increasingly difficult to define and contain considerable amounts of cellular debris (Cd) and a red blood cell (lower right) which is not within a capillary. L indicates electron-lucent endothelial cells; D, electron-dense endothelial cell ($\times 16,000$). **Fig 11**—Tumor specimen. Channels (X) which are not lined by endothelium are found between the parenchymal tumor cells (A, B and C). These channels contain red blood cells (R), plasma protein (pr), and cellular debris (Cd) ($\times 9600$).

Fig 12—Tumor specimen. This capillary, comprised of electron-lucent (L) and electron-dense (D) endothelial cells, has apparently broken apart (B) releasing its contents into the pericapillary space. The pericapillary space reveals considerable disorganization and disruption of parenchymal tissue components, and is accumulating cellular debris (Cd) and plasma proteins (pr). Red blood cell (R) ($\times 10,250$). **Fig 13**—Tumor specimen. Ultimately the capillaries appear collapsed and shrunken with irregular contours. Endothelial cell nuclei (N) are dense and necrotic in appearance, and pericapillary spaces (ps) are filled with a combination of materials. A parenchymal-pericapillary interface cannot be identified. Capillary basal lamina indicated by bl; capillary lumen by C ($\times 12,800$).

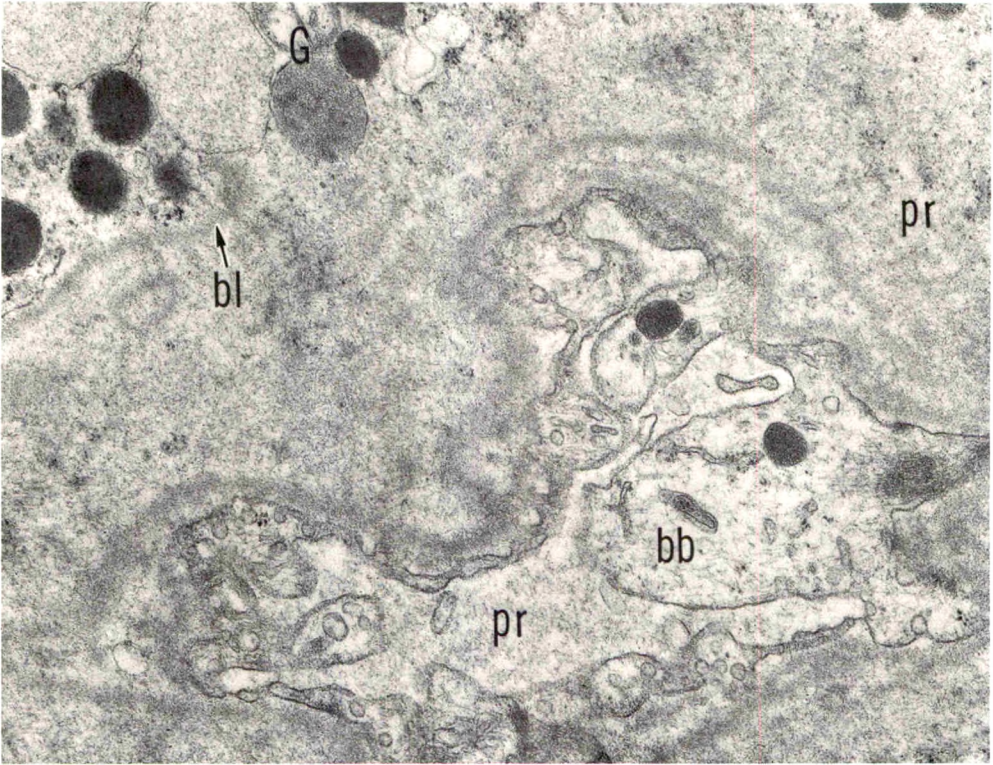


1

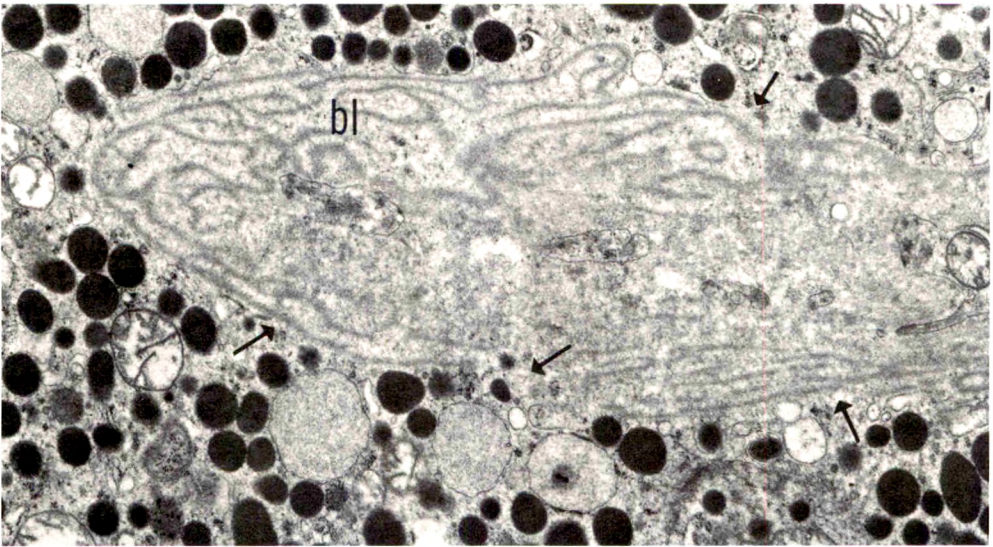


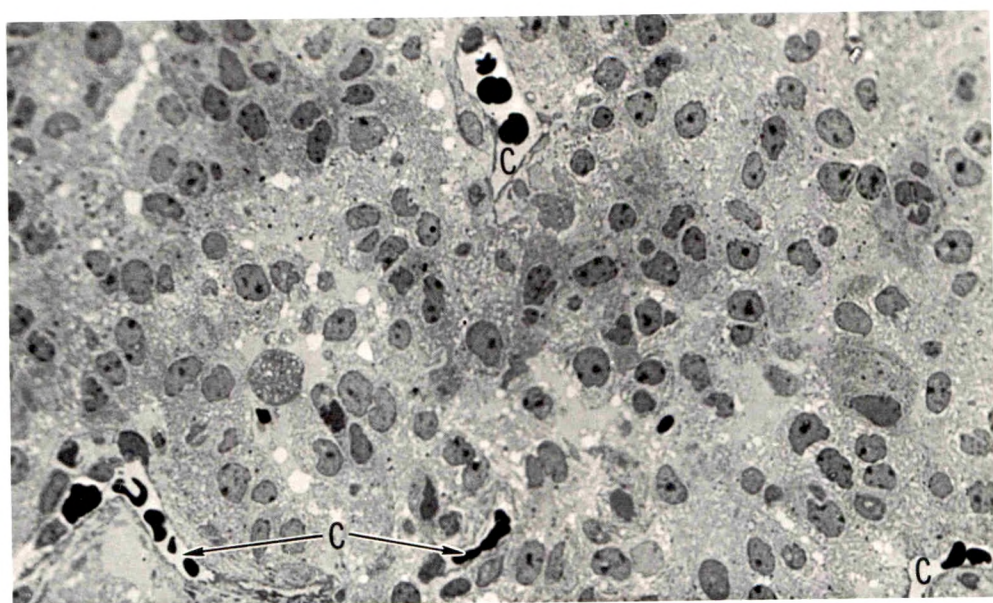
2

3

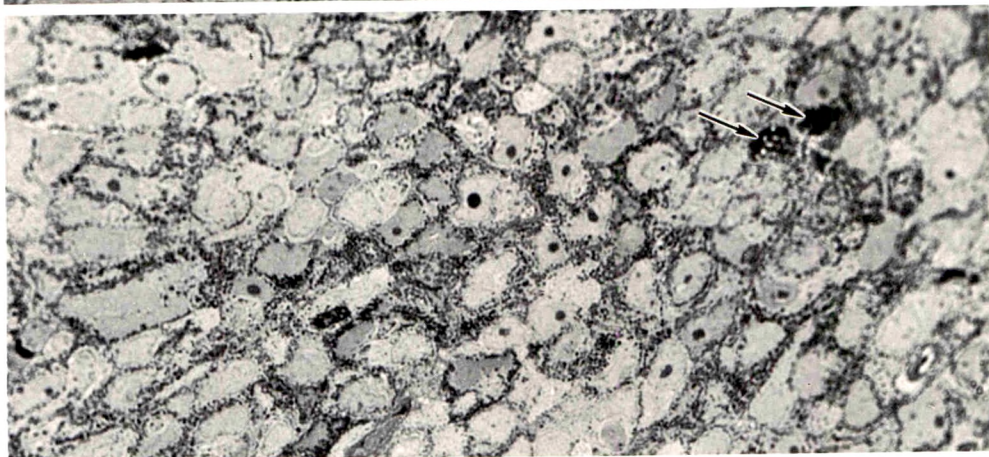


4

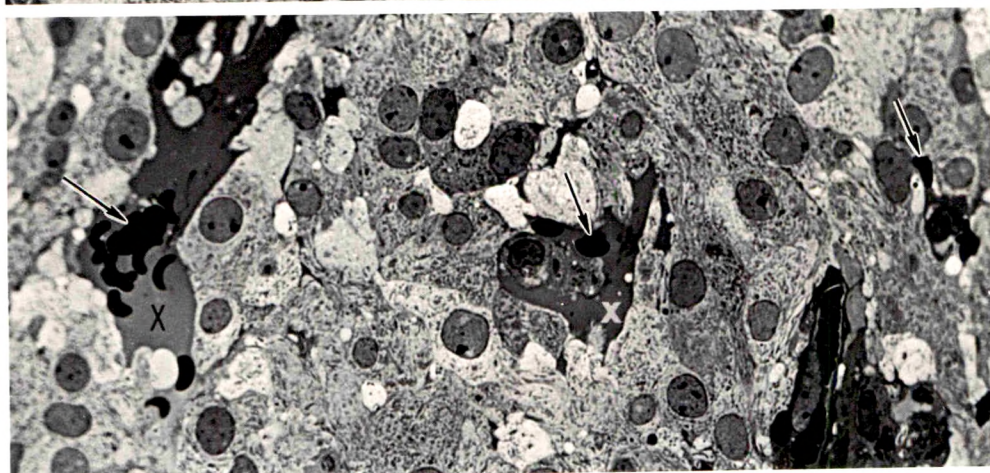




5

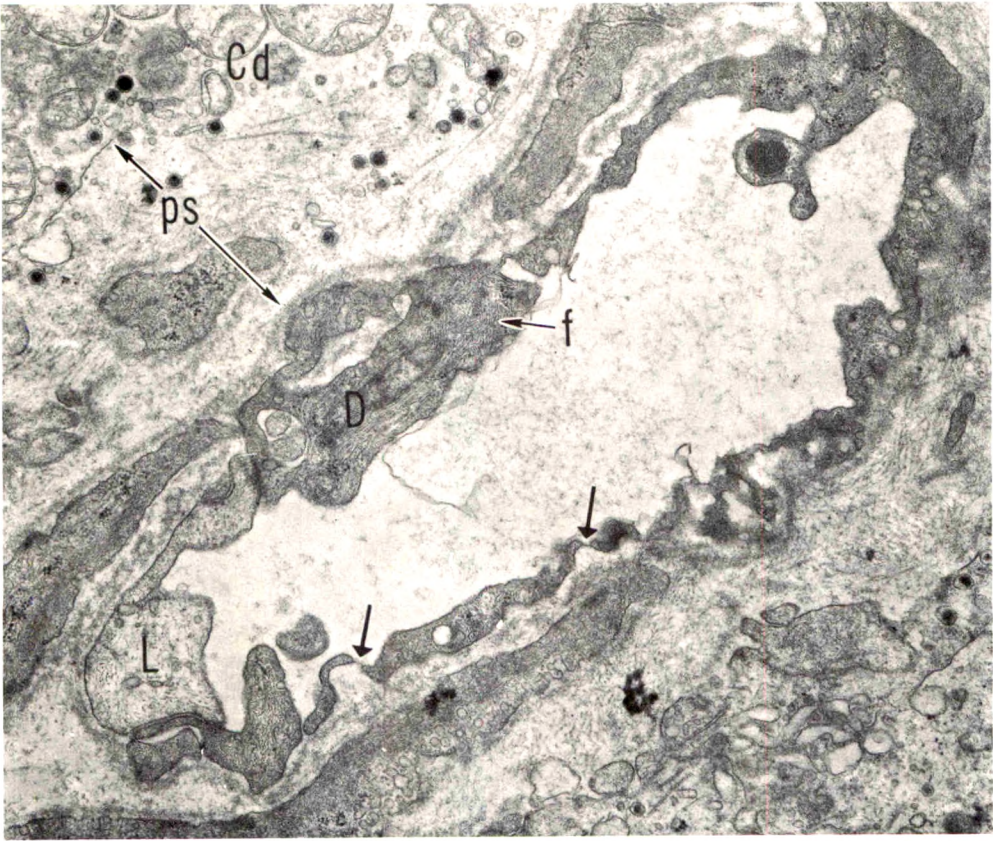


6

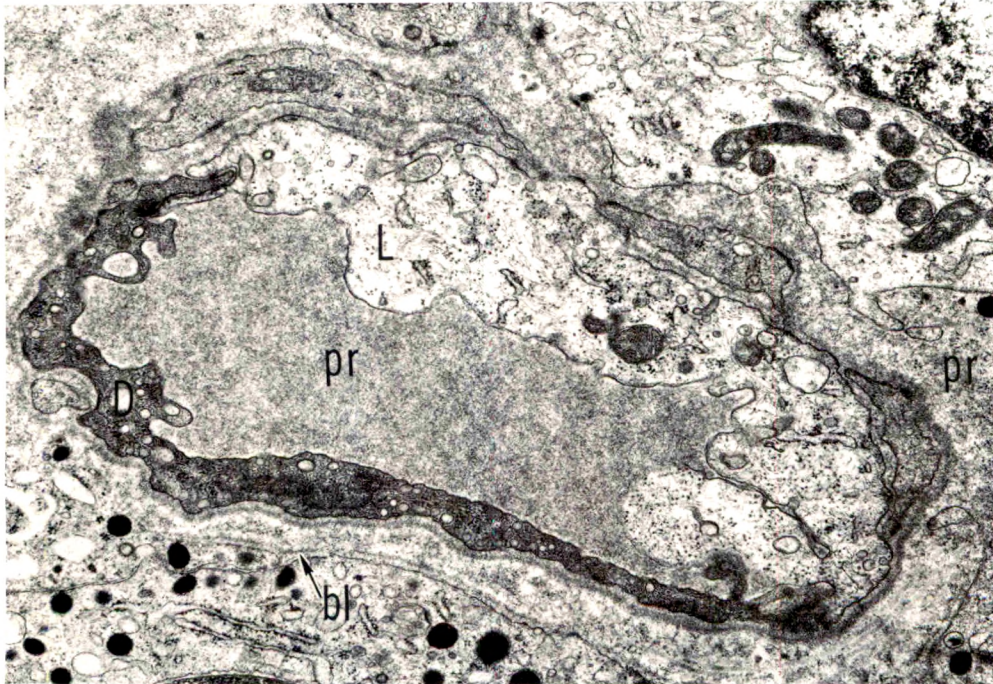


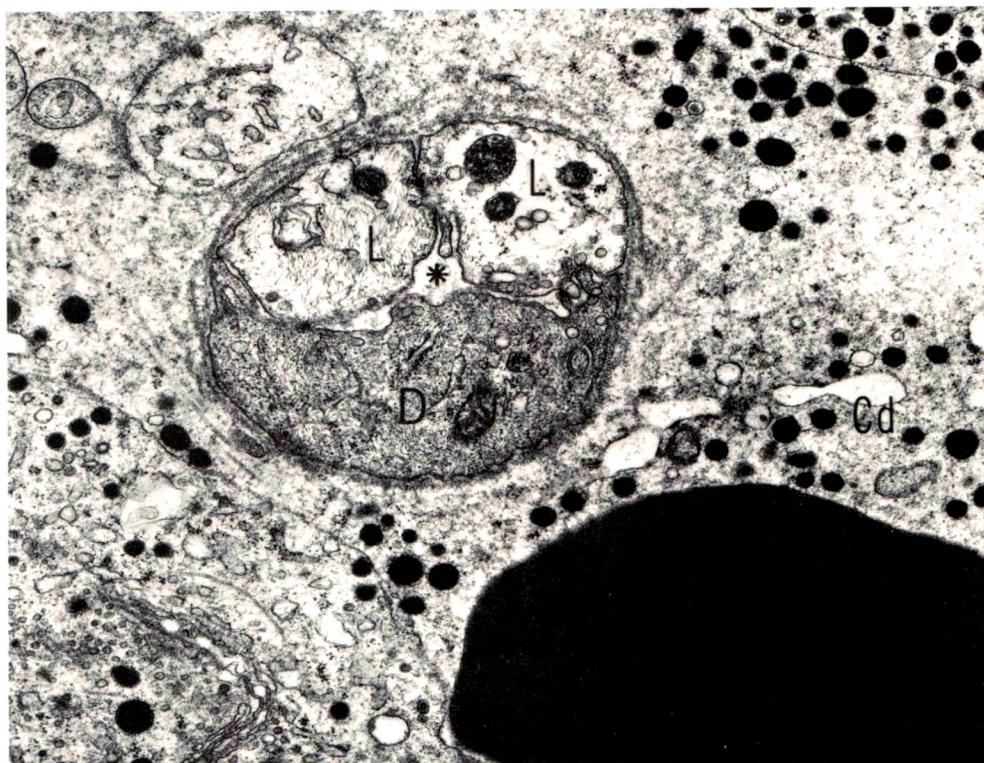
7

8

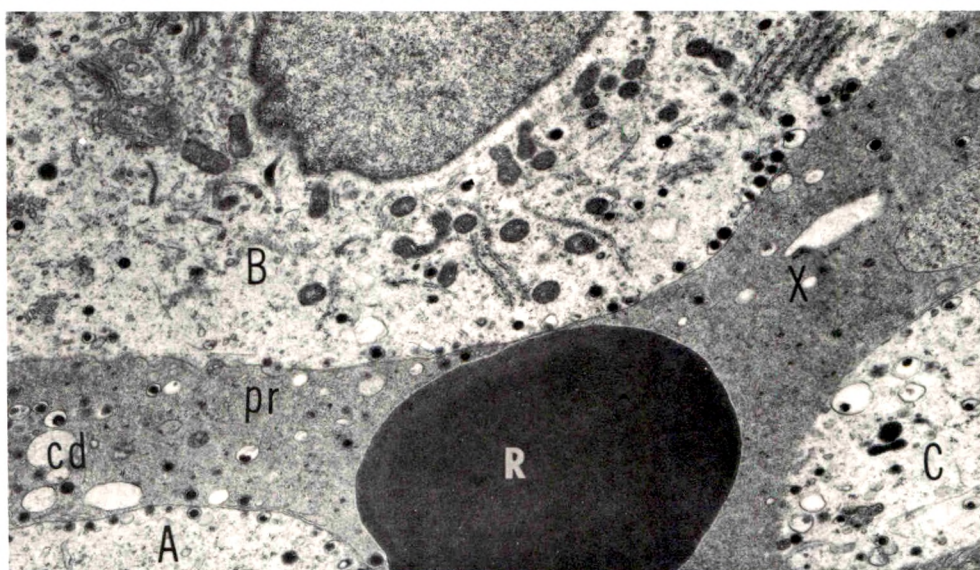


9



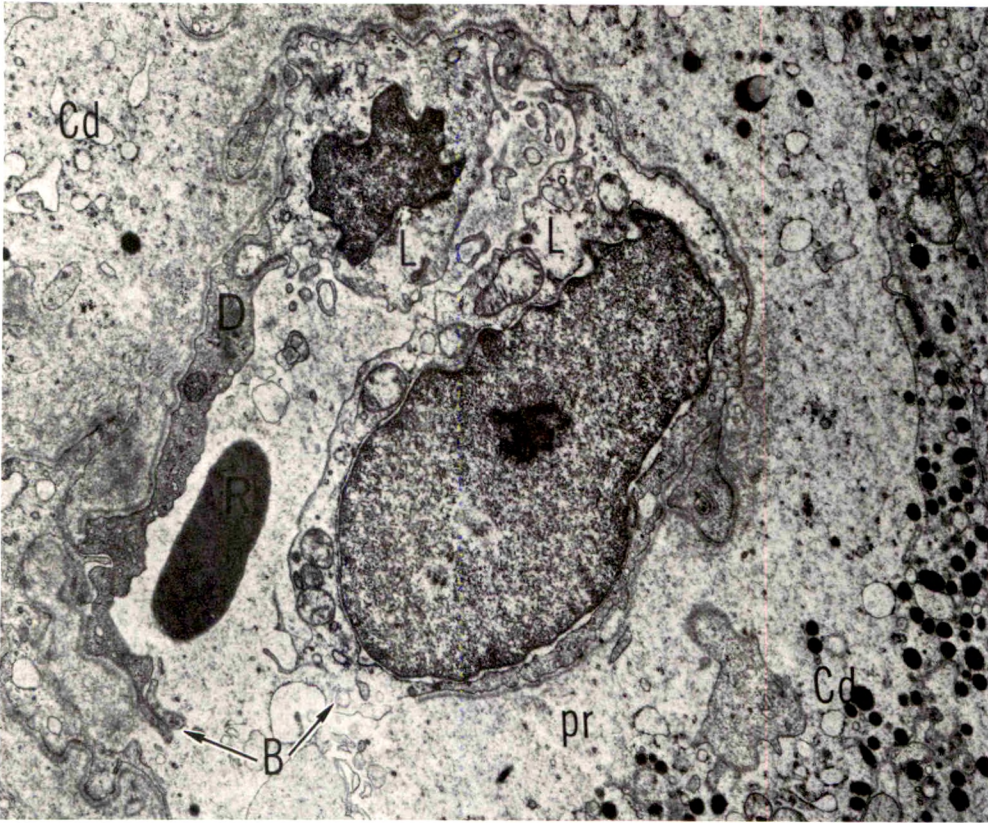


10

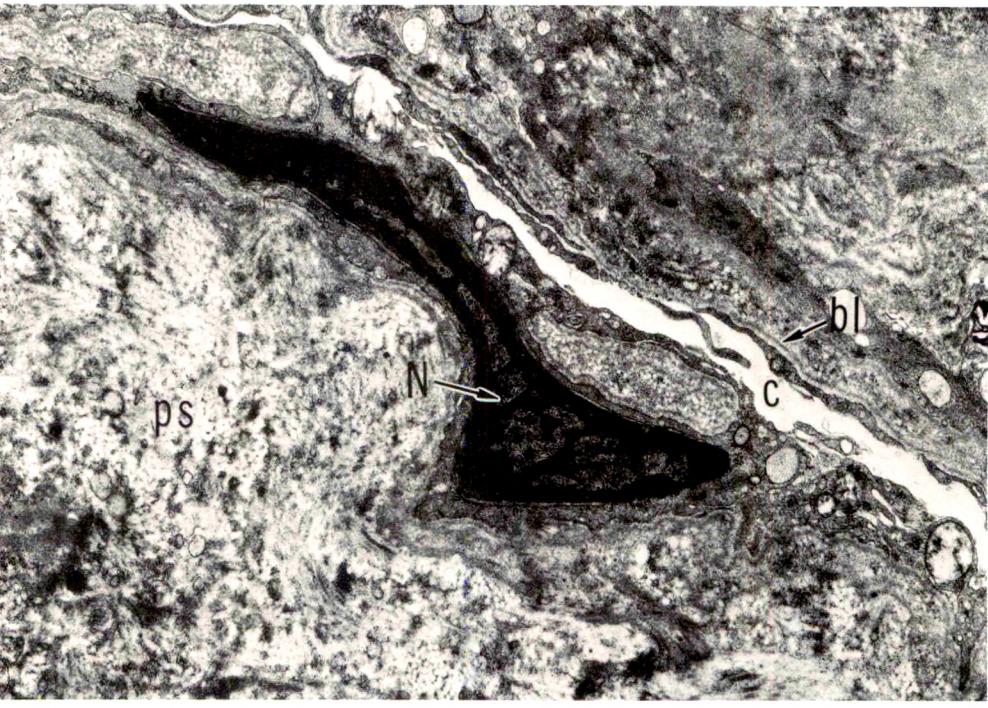


11

2



3



Myonecrosis Induced by Rattlesnake Venom

An Electron Microscopic Study

John M. Stringer MD, Robert A. Kainer DVM, MS and Anthony T. Tu PhD

The myonecrotic effect of rattlesnake (*Crotalus viridis viridis*) venom on mouse skeletal muscle was studied. The biceps femoris muscle was examined with the electron microscope after one-fourth the LD₅₀ of the crude venom was injected into the gracilis and semimembranosus muscles. Focal areas of myonecrosis were abundant. Injured fibers contained dilated sarcoplasmic reticulum, disoriented, coagulated myofilamentous components and condensed, rounded and enlarged mitochondria. The external lamina and sarcolemma remained intact in many fibers. Hemorrhage was apparent in the endomysial connective tissue, and hemolysis was discernible. In areas where the erythrocytes were tightly packed between the muscle fibers, there was disruption of the external lamina and sarcolemma. Degeneration of the fibers in these areas was pronounced. These findings correlate well with the breakdown of muscle fibers by various methods described in the literature. Myonecrosis induced by snake venom may serve as a useful model for studying muscle necrosis because of its rapid onset and relative ease of induction. (Am J Pathol 67:127-140, 1972)

SNAKEBITE IS NOT UNCOMMON throughout most of the world, predominantly in the tropical areas. Deaths due to snakebite have been estimated to be between 30,000 and 40,000 annually.¹ In the United States, it has been estimated that, of the 6000 individuals bitten each year, 15 cases are fatal.² No accurate statistics are available for snakebite, because no one can accurately assemble all the cases. However, a good record was kept by the Venomous Snakebite Committee of the Florida State Board of Health. The committee reported 382 verified and completed records of snakebite.³ Of this number, 168 were inflicted by pigmy rattlesnake (*Sistrurus miliarius*) and 71 by larger rattlesnakes (*Crotalus*). Cottonmouth moccasins (*Agkistrodon piscavorus*) accounted for 69 bites, copperheads (*Agkistrodon contortrix*) for 4, coral snakes (*Micrurus*) for 14 and unidentified venomous snakes for 56. Some snakebite victims survive, but sustain permanent tissue damage that may extend into the muscle, tendons and cartilage.^{4,5} The destruction of tissue, with possible disfunction or complete loss

From the Department of Anatomy and Department of Biochemistry, Colorado State University, Fort Collins, Colo.

Supported by grant 5R01 GM-15591 and 5R01 FD-00014 from the US Public Health Service and Career Development Award 5K04 GM-41786 from the National Institutes of Health (to A. T. Tu).

Accepted for publication October 7, 1971.

Address reprint requests to Dr. Anthony T. Tu, Department of Biochemistry, Colorado State University, Fort Collins, Colo 80521.

of a body part, is an important factor in snakebite cases, since, in many cases, the use of antivenin does not prevent histolysis unless it is injected minutes after the bite.^{6,7}

Most crotaline venoms produce hemorrhage and myonecrosis simultaneously upon envenomation.⁸ Many cases of myonecrosis after envenomation by snake venom have been reported.^{6,9,10}

A variety of toxins produce myonecrosis. The objective of this study was to determine if the myonecrosis produced by *Crotalus viridis viridis* (prairie rattlesnake) venom was similar to that reported to occur by other mechanisms—*ie*, ischemia due to cold, the drug plasmocid, cobra venom, *Clostridium perfringens* toxin and coxsackie virus.

Materials and Methods

Twenty-four Swiss white mice served as experimental subjects. Eight animals were used in three separate experiments. Six mice were injected intramuscularly in the medial aspect of the left thigh (gracilis and semimembranosus muscles) with 20 µg of crude *C. viridis viridis* venom (Ross Allen's Reptile Institute, Silver Springs, Fla) dissolved in 0.1 ml physiologic saline (PSS). Two control animals were injected similarly with 0.1 ml PSS. All animals were killed by cervical dislocation 3 hours after injection. The tissue was removed from the lateral aspect of the injected thigh (biceps femoris muscle) to avoid areas that might have been damaged by the needle. The excised tissue was fixed in 5% glutaraldehyde in Millonig's phosphate buffer, pH 7.2, for 5 hours at 10 C; then it was fixed secondarily for 1 hour in 2% osmium tetroxide in Millonig's phosphate buffer, pH 7.2. After dehydration in a graded series of ethanol, the tissue was embedded in Epon 812.¹¹ One-micron sections stained with toluidine blue O¹² were used for light microscopic observations of necrotic foci. Thin sections were cut on a Sorvall MT-2 ultramicrotome. The sections were picked up on uncoated 200-mesh copper grids and stained with uranyl acetate and lead citrate.¹³ Observations were made with a Zeiss EM 9A or RCA EMU 3F electron microscope.

Results

Control Muscle

Gross examination of the killed control animals revealed no lesions except for an occasional hemorrhagic area at the penetration site of the needle. Tissue from the control animals had all the fine structural aspects of skeletal muscle as described in the literature.^{14,17} There were thin actin filaments on either side of the thick myosin filaments with cross bridges between the two filament types. The Z lines were in register with one another. The A band, H band, I band and M lines were present in longitudinal sections of the skeletal muscle. The triad was located at the Z-line complex and the sarcotubular system was comprised of flattened cisternae. Moderate numbers of mitochondria were tightly packed at various locations between the myofibrils and

near the nuclei. Glycogen granules were scattered throughout the muscle fibers in moderate amounts, with the highest concentration near the triads and nuclei. The external lamina closely paralleled the uninterrupted plasma membrane as it encircled the muscle fiber. The elongated, hypolemmal nuclei were characteristic of glutaraldehyde-fixed nuclei. The sarcoplasm was relatively scant as the organelles were in close apposition to one another with no large areas devoid of organelles (Fig 1).

Experimental Muscle

The experimental animals had extensive ventral hemorrhage and edema extending from the gracilis muscle to the pectoralis muscles on either side of the midline.

Upon examination with the light microscope, hemorrhage was apparent between fibers, and focal areas of myonecrosis were observed.

Electron microscopic observations disclosed various levels of degeneration among muscle fibers. Relatively intact fibers were intermixed with fibers undergoing degeneration.

The first indication of degeneration was the obvious dilatation of the longitudinal sarcotubular cisternae. The characteristic, flattened vacuoles swelled and became more prominent as degeneration progressed. Vacuoles lying deep to the plasma membrane became swollen and many possessed myeloid figures (Fig 2). During the early dilatation of the sarcoplasmic reticulum, it retained some organization (Fig 3) but became more randomly scattered as the swelling increased until, in some instances, the cell was nearly 30% vacuoles (Fig 4). As the degeneration progressed, the vacuoles became smaller and fewer until they were mostly obliterated by the fibrils (Fig 5 and 9).

The T system remained intact throughout most of the degenerative process (Fig 2, 3, and 9). In the later stages, transverse tubules could not be readily identified but they might have been present as small, randomly scattered vesicles (Fig 7 and 9).

With the increase in vacuole size and distribution, the myofibrils appeared to atrophy (Fig 4 and 6). The first breakdown in the striated appearance occurred with the disappearance of the H band and its M line (Fig 3 and 11). The Z line retained the integrity and orientation of the myofibril. After the Z line broke down, the actin filaments became less apparent. The myosin filaments appeared thicker and less discrete (Fig 6). As degeneration progressed, myofibrillar organization was lost until the protein became long strands containing many fine filaments and lacking their complete linear

alignment (Fig 7). Degeneration of myofibrils appeared to be complete when they became an amorphous coagulation of light and dark masses (Fig 9).

Degeneration of the mitochondria seemed somewhat slower than that of other organelles. The mitochondrial size and/or the number of cristae increased, probably due to the metabolic activity (Fig 3 and 5). Extreme mitochondrial degeneration was not apparent before the fibrillar components broke down (Fig 2). As the mitochondrial degeneration progressed, the cristae ruptured and the mitochondrial fragment became surrounded by small vacuoles (Fig 7). Some ruptured mitochondria contained a flocculant material (Fig 10).

In early stages of degeneration, the nuclei became pyknotic with a dilatation of the double nuclear membrane. As the degeneration progressed, the chromatin became densely clumped around the periphery of the nucleus and made up the greatest portion of the nucleus (Fig 11).

The external lamina remained intact throughout most of the degenerative process; only in the latter stages was it destroyed (Fig 8 and 11). Destruction of the plasma membrane closely paralleled that of the external lamina. Some breaks in the plasma membrane were seen in degenerating cells (Fig 4, 7 and 11).

Glycogen levels appeared to be at nearly normal levels in early stages of degeneration, but as the dilatation of the sarcoplasmic reticulum increased, the amount of glycogen was diminished.

In areas of extreme hemorrhage (Fig 12) where the erythrocytes were closely packed in the endomysial space, various changes were seen. The sarcolemma was broken, and myofibrillar degeneration was apparent. The mitochondria were swollen and tightly packed under the sarcolemma (Fig 12). There were many areas where the erythrocytes lay closely apposed to myofilaments and mitochondria (Fig 13). Hemolysis also occurred in these areas (Fig 8 and 13). A diagrammatic summary of these events is presented in Fig 14.

Discussion

Myonecrosis of striated muscle has been studied by means of the light microscope for some time. The types of injuries that develop as a result of various noxious agents vary from minimal cloudy swelling of the sarcoplasm to total necrosis of the muscle fiber. Ischemia or injection of chemical agents into muscle results in necrosis with preservation of a well-marked refractile Z line forming discs or short segments. Heat, cold or other physical trauma usually result in fragmentation or shredding of the muscle fibers.^{18,19}

Stenger *et al* observed ischemic skeletal muscle after intervals of 6½, 24 and 48 hours. Myofibrillar integrity was maintained as late as 24 hours after ischemia. However, after a 48-hour interval, degeneration of the I band and Z line was noted with striking preservation of the A band, H band and M line. Glycogen diminished in the skeletal muscle fibers in the first 24 hours.²⁰

The most marked alterations in the ultrastructure of diaphragm muscle after hemorrhagic shock were seen in the mitochondria. They swelled and ruptured prior to the swelling of the other intracellular organelles.²¹

After congestive cardiomyopathy,²² alterations in the Z line were the primary defect. The most severe lesion was a complete disruption of myofibrils adjacent to an irregular Z line. This consisted of an unstructured mass containing irregularly arranged intercalated discs.

In necrosis induced by cold, Price *et al* observed the disappearance of the striations at the I and H bands.²³ The mitochondria were swollen and their cristae disintegrated. The plasma membrane was broken in places, but the external lamina remained to constitute the sarcolemmal tube. The nuclear chromatin was clumped at the periphery, and the outer nuclear membranes contained blebs. The myofibrils became a uniform mass of thin filaments and eventually changed into finely granular debris.

In necrosis induced by plasmocid, a drug related to the antimalarial drugs primaquine and pamaquine, an early focal dissolution of the I-band filaments and the Z line, with eventual disappearance of both these structures, was described; yet the A band was remarkably stable.²⁴ The sarcoplasmic reticulum was observed to be dilated while the T system was not changed. D'Agostino used larger doses of plasmocid and detected focal loss of the myofilaments including the A band.²⁵ Aggregates of vesicles under the sarcolemma were also observed.

Strunk *et al* described the myonecrotic effect of *Clostridium perfringens* toxin.²⁶ The initial lesion was the disruption of the plasma membrane. They believe the degeneration of the myofilaments, mitochondria, sarcoplasmic reticulum and nucleus to be secondary manifestations of lesions of the plasma membrane.

Muscle degeneration due to infection of muscles in suckling mice with coxsackie A4 virus was reported by Harrison *et al*.²⁷ They noted myofibrillar degeneration with swollen and distorted mitochondria. The nuclei were crenated and pyknotic, with margination and condensation of chromatin. The nuclear membranes had wide separations.

Myocardial damage induced by scorpion venom varied with means

of injection. Swollen mitochondria, focal destruction of myofibrils and sarcoplasmic reticulum resulted, but the cell membrane remained intact.²⁸

Trevino reported loss of myofibrillar organization and clumping of material after *Crotalus atrox* envenomation of porcine muscle.²⁹ He postulated that this material may be precipitated protein globules. He reported irregularly shaped erythrocytes with a dark, granular substance adhering to the plasma membrane and thought this material might be a conjugation of venom with phospholipids.

Myonecrosis induced by cobra venom³⁰ produced complete degeneration of muscle fibers. The sarcoplasmic reticulum was dilated and myofibrils were disoriented, resulting in an amorphous electron-dense mass. Complete lysis of the cell was observed within 1 hour after the venom was injected.

In many of the aforementioned experimental lesions,²³⁻²⁶ there was minimal damage to the plasma membrane and consequently to the T system. In the case of *Clostridium perfringens* toxin, there was measurable damage to the plasma membrane, but no reference was made to the T system. We have demonstrated that although the sarcoplasmic reticulum was very disorganized and swollen in muscle fibers damaged by venom from *C. viridis viridis*, a well-organized and cohesive T system was still maintained (Fig 4, 5 and 10).

It is quite evident that the sarcoplasmic reticulum is more susceptible to the effects of injurious substances than is the T system.^{19,31}

Augustyn *et al*³² correlated swollen mitochondria having broken limiting membranes and cristae with respiratory inhibition that occurred when isolated mitochondria from rat liver were subjected to either crude venom from water moccasins or purified phospholipase A obtained from the venom.

If this correlation is true, we might assume that the mitochondria are metabolically active throughout most of the myofibrillar degenerative process (Fig 4, 5 and 9). The mitochondria are swollen and condensed but still maintain structural integrity, indicating that respiration may still be in progress.

Retention of the Z-line structure may be indicative of its different protein complement (tropomyosin) or the very tight interwoven meshwork of its construction³² that prohibits early penetration by the toxins.

Cytochemical and biochemical studies need to be performed before many of these observations can be fully understood. However, snake venom-induced myonecrosis may conceivably provide an excellent model for studying the mechanisms of muscle degeneration.

References

1. Swaroop S, Grab B: The snakebite mortality problem in the world, *Venoms*. Edited by EE Buckley, N Porges. Washington DC, American Association for the Advancement of Science, 1956
2. Parrish HM, Silberg SL, Grolldner JC: Snakebite: a pediatric problem. *Clin Pediatr* 4:237-241, 1965
3. Andrews CE, Dees JE, Edwards RO: Venomous snakebite in Florida. *J Fla Med Assoc* 55:308-316, 1968
4. Emery JA, Russell FE: Lethal and hemorrhagic properties of some North American snake venoms, *Venomous and Poisonous Animals and Noxious Plants of the Pacific Region*. Edited by HL Keegan, WJ MacFarlane. New York, Pergamon Press, 1963, pp 409-414
5. McCollough ND, Gennaro JF: Evaluation of venomous snakebite in the southern United States from parallel clinical and laboratory investigations: development of treatment. *J Fla Med Assoc* 40:959-967, 1963
6. Stahnke HL: *The Treatment of Venomous Bites and Stings*. Tempe, Ariz, Bureau Publications of Arizona State University, 1966
7. McCollough ND, Gennaro JF: Treatment of venomous snakebite in the United States. *Clin Toxicol* 3:483-500, 1970
8. Tu AT: The mechanism of snake venom actions: rattlesnakes and other crotalids. *The Pathophysiological Actions of Several Biological Poisons*. Edited by L Simpson. New York, Plenum Press, 1971, pp 87-109
9. Tenery JH, Koefoot RR: Snakebite. *Plast Reconstr Surg* 15:483-488, 1955
10. Abalos JW, Pirotsky I: Venomous Argentine serpents ophidism and snake antivenin,⁴ pp 363-371
11. Luft JH: Improvements in epoxy resin embedding methods. *J Biophys Biochem Cytol* 9:409-414, 1961
12. Lynn JA: Rapid toluidine blue staining of Epon-embedded and mounted "adjacent" sections. *Am J Clin Pathol* 44:57-58, 1965
13. Fahmy A: An extemporaneous lead citrate stain for electron microscopy, *Proceedings of Electron Microscopy Society of America*. Baton Rouge, La, Claitor's Book Store, 1969, pp 148-149
14. Huxley HE: The contraction of muscle. *Sci Am* 199:67-82, 1958
15. *Idem*: The mechanism of muscular contraction. *Sci Am* 213:18-27, 1965
16. Bennett HS: The structure of striated muscle as seen in the electron microscope, *The Structure and Function of Muscle*. Vol 1. Edited by GH Bourne. New York, Academic Press Inc, 1960, pp 136-182
17. Porter KR, Palade GE: Studies on the endoplasmic reticulum. III. Its form and distribution in striated muscle cells. *J Biophys Biochem Cytol* 3:269-300
18. Adams RD, Denny-Brown D, Pearson CM: *Diseases of Muscle: A Study in Pathology*. Second edition. New York, Harper & Row, 1962
19. Pellegrino C, Franzini-Armstrong C: Recent contributions of electron microscopy to the study of normal and pathological muscle, *Int Rev Exp Pathol* 7:139-226, 1969
20. Stenger RJ, Spiro D, Scully RE, Shannon JM: Ultrastructural and physiologic alterations in ischemic skeletal muscle. *Am J Pathol* 40:1-20, 1962
21. Holden WD, DePalma RG, Drucker WR, McKalen A: Ultrastructural

- changes in hemorrhagic shock; electron microscopic study of liver, kidney and striated muscle cells in rats. *Ann Surg* 162:517-536, 1965
22. Rodin HE, Harris LC, Nghiem QX: Idiopathic, nonobstrusive cardiomyopathy. *Arch Pathol* 91:62-69, 1971
 23. Price HM, Pease DC, Blumberg JM: Ultrastructural alterations in skeletal muscle fibers injured by cold: the acute degenerative changes. *Lab Invest* 13:1265-1278, 1964
 24. Price HM, Pease DC, Pearson CM: Selective actin filament and Z band degeneration induced by plasmocid: an electron microscopic study. *Lab Invest* 11:549-562, 1962
 25. D'Agostino AN: An electron microscopic study of skeletal and cardiac muscle of the rat poisoned by plasmocid. *Lab Invest* 12:1060-1071, 1963
 26. Strunk SW, Smith CW, Blumberg JM: Ultrastructural studies on the lesion produced in skeletal muscle fibers by crude type A *Clostridium perfringens* toxin and its purified alpha fractions. *Am J Pathol* 50:89-108, 1967
 27. Harrison AK, Murphy FA, Gary GW Jr: Ultrastructural pathology of coxsackie A4 virus infection of mouse striated muscle. *Exp Mol Pathol* 14:30-42, 1971
 28. Yarom R, Braun K: Electron microscopic studies of the myocardial changes produced by scorpion venom injections in dogs. *Lab Invest* 24:21-30, 1971
 29. Trevino GS: Pathologic effects of the venoms of *Crotalus atrox* and *Naja naja* in pigs. PhD thesis. East Lansing, Michigan State University, 1968
 30. Stringer JM, Kainer RA, Tu AT: Ultrastructural studies of myonecrosis induced by cobra venom in mice. *Toxicol Appl Pharmacol* 18:442-450, 1971
 31. Fahimi HD, Cotran RS: Permeability studies in heat induced injury of skeletal muscle using lanthanum as fine structural tracer. *Am J Pathol* 62:143-157, 1971
 32. Augustyn JM, Parsa B, Elliott WB: Structural and respiratory effects of *Agkistrodon piscivorus* phospholipase A on rat liver mitochondria. *Biochim Biophys Acta* 197:185-196, 1970
 33. MacDonald RD, Engel AG: Observations on organization of Z-disk components and on rod bodies of Z-disk origin. *J Cell Biol* 48:431-437, 1971

The authors wish to thank Mr. Dennis Giddings for the drawings and the Electron Microscopy Training Laboratory for the facilities to do this study.

[Illustrations follow]

Legends for Figures

Fig 1—Electron micrograph of a portion of a skeletal muscle fiber from a control animal. Z indicates Z line; A, A band; I, I band; H, H band; M, M line; sr, sarcoplasmic reticulum; mi, mitochondria; black arrows, transverse tubules or T system ($\times 9000$).

Fig 2—The degenerate fiber at lower left contains many large vacuoles under the plasma membrane, some of which contain myeloid figures (*long arrows*). The separation and atrophy of the myofibrils is apparent in this fiber when compared to the fiber in Fig 1. *Short arrows* indicate transverse tubules; Em, endomysial space; F, myofilaments ($\times 9000$).

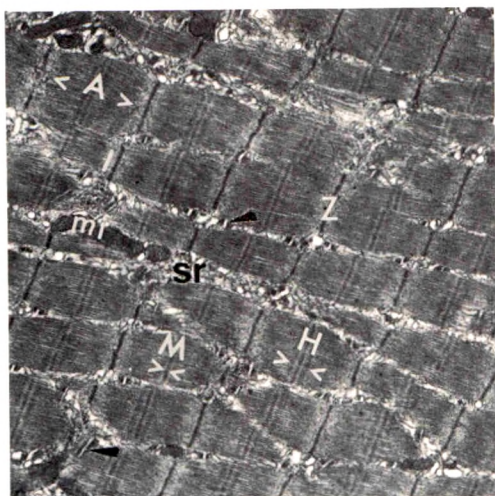
Fig 3—Electron micrograph of venom-injected skeletal muscle. The proliferated sarcoplasmic reticulum can be seen as many small vesicles between the myofibrils (Fb). The myofibrils are smaller and the H band and M line are less dense than in the control muscle. The mitochondria (mi) are enlarged and irregularly shaped. The transverse tubules still appear intact. Z indicates Z line ($\times 9000$).

Fig 4—Portion of a degenerated skeletal muscle fiber with extreme dilation of the sarcoplasmic reticulum (sr). The myofibrils are smaller and the interfibrillar space is more abundant than in the control muscle. Myofilaments (F) can be resolved at this stage of degeneration. The plasma membrane (PL) is broken at irregular intervals and the external lamina appears granular. The nucleus (N) is pyknotic and lacks a distinct double membrane. E indicates erythrocyte; mi, mitochondria ($\times 9000$).

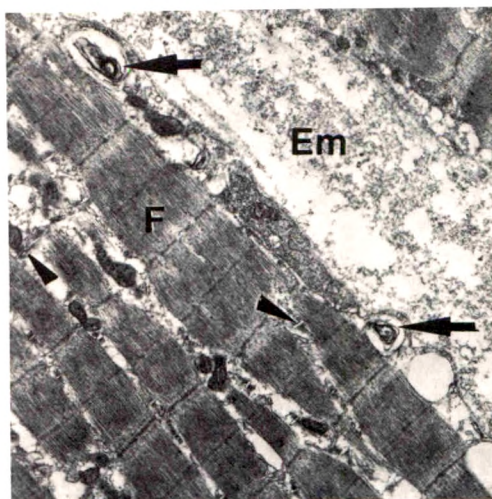
Fig 5—In this electron micrograph of venom-injected skeletal muscle, the mitochondria (mi) are greatly enlarged and their cristae are abnormally arranged. The myofibrils are closely packed together and lack their cross-striated appearance. Individual myofilaments (F) can be resolved. The vesicles of the sarcoplasmic reticulum (*arrows*) appear fewer and smaller than those in Fig 6. The transverse tubules are difficult to identify positively. E indicates erythrocytes ($\times 9000$).

Fig 6—This degenerate muscle fiber lacks the characteristic cross striations. The thick myosin filaments (*arrows*) are present but disoriented. The thin actin filaments are not discernible. The sarcoplasmic reticulum (sr) is dilated ($\times 28,500$).

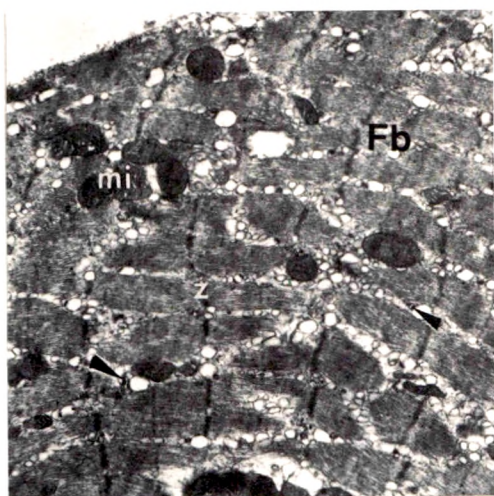
1



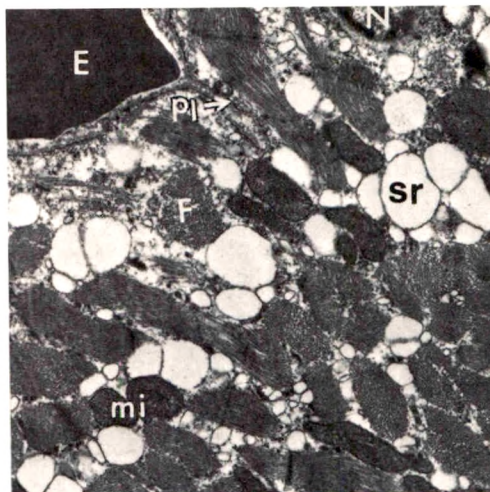
2



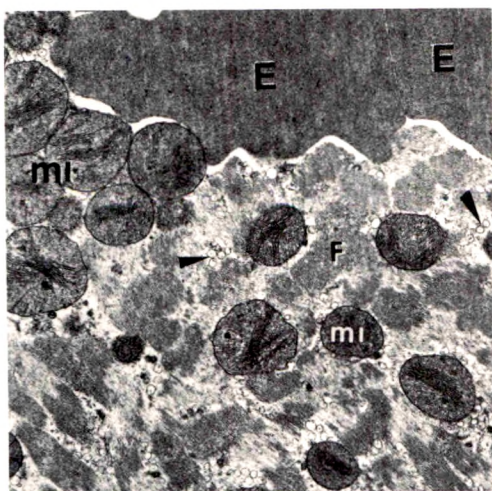
3



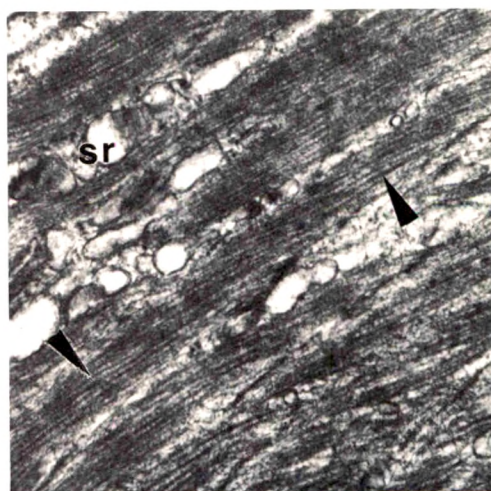
4



5



6



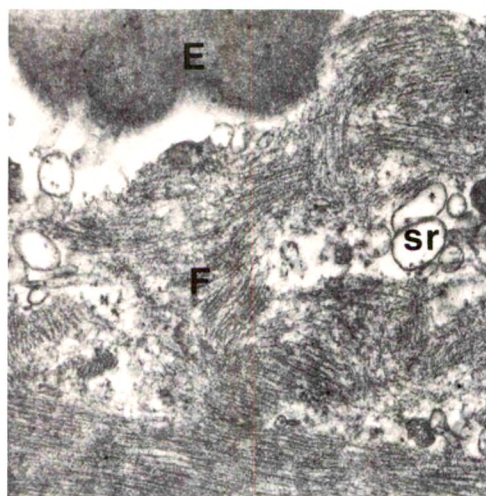
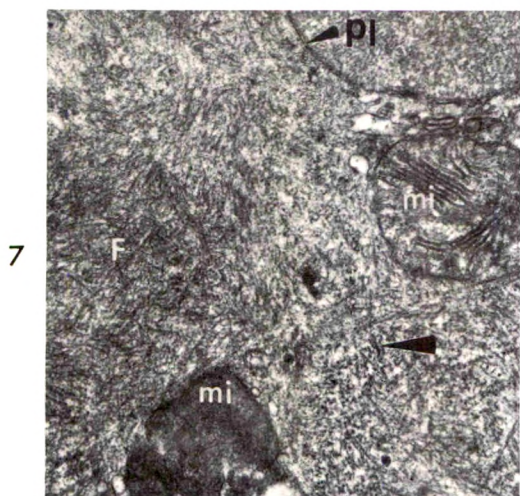


Fig 7—Portion of a venom-injected skeletal muscle fiber. The degenerate mitochondria (*Mi*) and disoriented meshwork of myofilaments (*F*) can be seen. Some of the small vesicles (*arrows*) may be remnants of the transverse tubules. *PL* indicates plasma membrane ($\times 21,600$). **Fig 8**—High-magnification electron micrograph of venom-injected skeletal muscle with no plasma membrane or external lamina between the fiber and the erythrocyte (*E*). The myofilaments (*F*) and sarcoplasmic reticulum (*sr*) are in irregular array. The erythrocyte is hemolyzed ($\times 28,500$).

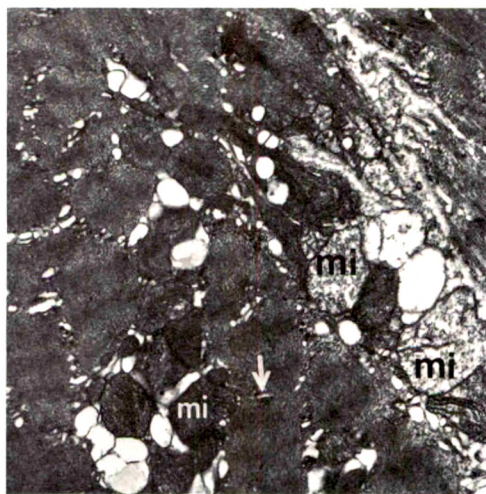
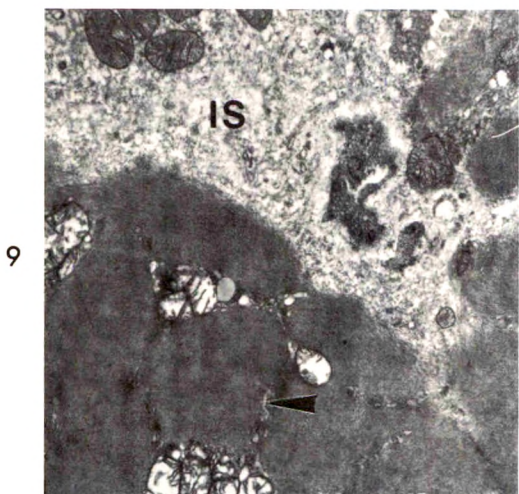
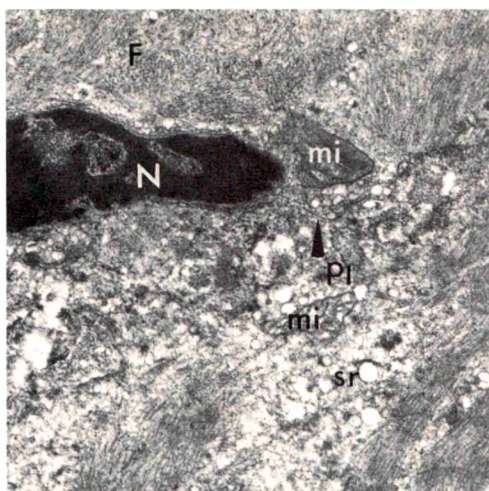


Fig 9—In this damaged muscle fiber, the myofilaments have precipitated into an amorphous mass. The filamentous structure is no longer evident, and the mitochondria within it are swollen with fewer, shorter cristae. The intrafibrillar space (*IS*) is greatly increased, the mitochondria in this area are more intact. *Arrows* indicate transverse tubules ($\times 7950$). **Fig 10**—This experimental muscle fiber contains many degenerate mitochondria (*mi*). The mitochondria at the right center of the micrograph contain a flocculant material. Glycogen granules can be seen as black dots in the areas near the mitochondria. *Arrows* indicate transverse tubules ($\times 9000$).

11



1

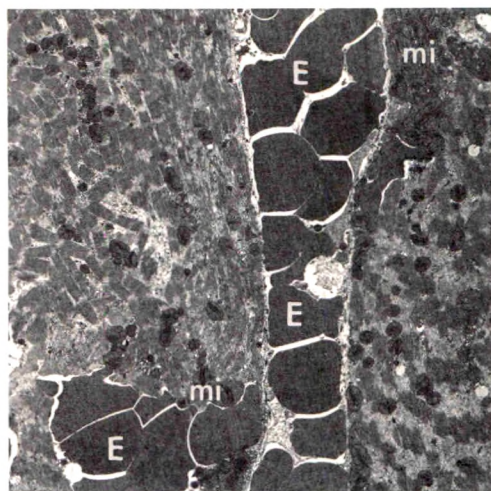


Fig 11—Electron micrograph of necrotic skeletal muscle. The upper fiber contains a pyknotic nucleus (*N*) and disoriented myofilaments (*F*). The lower cell contains disrupted sarcoplasmic reticulum (*sr*) and degenerate mitochondrion (*mi*). The myofibrillar striations are faintly visible in the fibrils in the lower right portion of this fiber. The plasma membrane (*PL*) and external lamina are interrupted at various intervals ($\times 11,600$). **Fig 12**—Low-magnification electron micrograph of venom-injected skeletal muscle. Interfibrillar hemorrhage is prominent along with swollen mitochondria (*mi*) and disruption of the integrity of the myofibrils. *E* indicates erythrocytes ($\times 2600$).

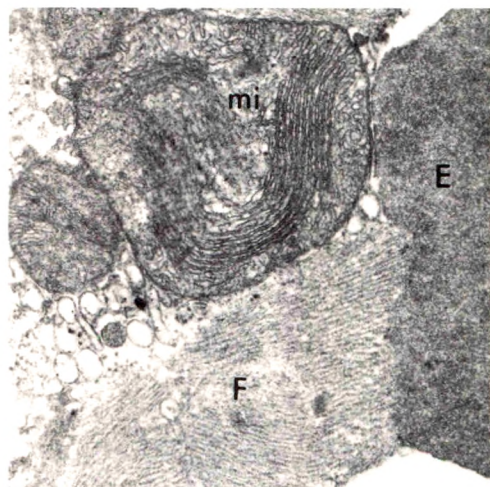


Fig 13—Electron micrograph showing the relationship between the damaged fibers and the erythrocytes. In areas of extreme hemorrhage (Fig 12), the erythrocytes were in close apposition to the muscle fibers with no plasma membrane or external lamina separating them. The myofilaments (*F*) seemed to fuse directly with the hemolyzed erythrocyte (*E*). Mitochondria indicated by *mi* ($\times 28,500$).

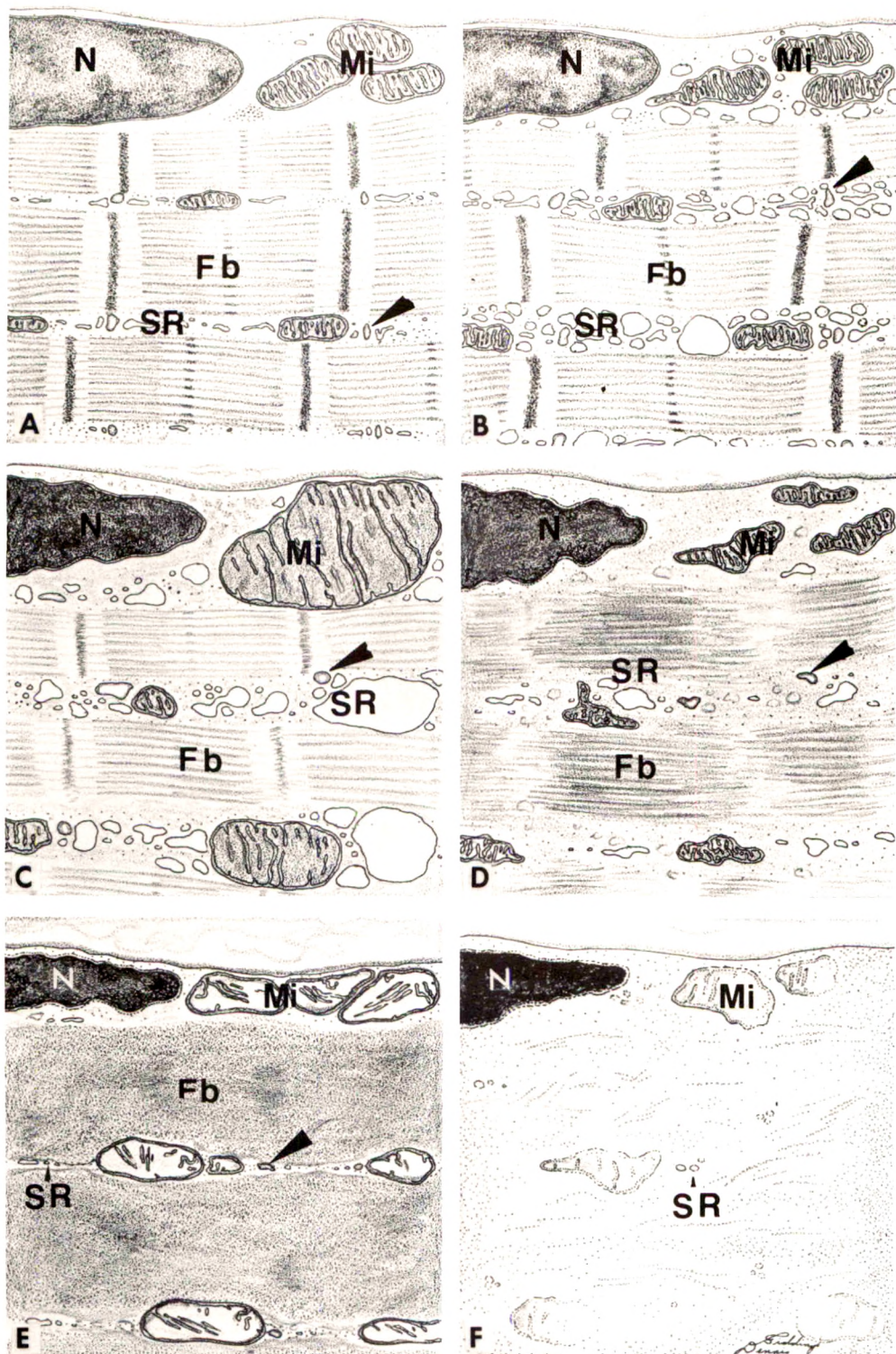


Fig 14—Diagrammatic representation of myonecrosis after rattlesnake envenomation. A depicts a normal fiber and F is that same fiber 3 hours after venom injection. All the sequences shown above can be seen in the electron micrographs presented in the text. *N* indicates nucleus; *mi*, mitochondria; *sr*, sarcoplasmic reticulum; *Fb*, myofibrils; arrows, transverse tubules.

Light and Electron Microscopic Studies of Rat Kidney After Administration of Inhibitors of the Citric Acid Cycle In Vivo

II. *Effects of Sodium Malonate on Proximal Convoluted Tubule*

Elizabeth M. McDowell, PhD

The morphologic changes that occurred in the proximal convoluted tubule of the rat after sodium malonate at 888 mg and 1776 mg/kg of body weight was injected have been studied by light and electron microscopy. Mitochondrial matrix swelling and loss of matrix granules and an increase in the smooth-surfaced endoplasmic reticulum were early changes. Varying degrees of cytoplasmic rarefaction occurred during the first 3 hours. Marked cytoplasmic swelling occurred only in female rats. Intracistal dilatation accompanied cytoplasmic rarefaction but there was no evidence that the mitochondrial matrix was condensed as judged by its electron density. During the early stages, dilatation of the rough endoplasmic reticulum was not necessarily associated with cytoplasmic rarefaction but varying degrees of dilatation occurred at later time intervals in the swollen cells. The changes appeared for the most part to be reversible. Focal areas of tubular necrosis occurred in a few rats. (Am J Pathol 67:141-158, 1972)

THE MORPHOLOGIC CHANGES that occur in the proximal convoluted tubules of the rat after administration of three agents that inhibit the citric acid cycle have been studied.¹ The effects of sodium fluoroacetate poisoning have been described in a previous paper.² The present paper describes those changes occurring in the tubules after a single subcutaneous dose of sodium malonate ($\text{CH}_2(\text{COONa})_2$).

After studies on the *in vivo* accumulation of citrate in the tissues of fluoroacetate-poisoned rats,³ it was found that injection of sodium malonate, either before or simultaneous with fluoroacetate, reduced the amount of citrate that accumulated.⁴ This was called *sequential blocking*.⁴ After dosing with sodium malonate, tissue succinate levels were raised and were greatest at 1 hour, at a time when tissue malonate levels were highest,⁵ providing evidence that malonate had inhibited the citric acid cycle at the level of succinic dehydrogenase.

From the Department of Pathology, University of Cambridge, Cambridge, England. Supported by a food safety training scholarship from the Nuffield Foundation.

Accepted for publication November 1, 1971.

The present address of Dr. McDowell is the Department of Pathology, University of Maryland, Baltimore, Md 21201.

hours before dehydration in graded alcohols. The tissue was embedded in Araldite. Thick (0.5 to 1.0 μ) and thin sections were cut with glass knives on a Huxley ultramicrotome (Cambridge Instrument Co, United Kingdom). Thick sections for light microscopy were stained with alkaline toluidine blue solution.⁹ Thin sections were mounted on uncoated copper grids and stained with lead citrate,¹⁰ before examination in a Siemens Elmiskop Ib microscope.

For light microscopy, the remainder of one kidney and the opposite one were put into formol saline and embedded in paraffin. Five-micron-thick sections were stained with hematoxylin and eosin (H&E) and by the periodic acid-Schiff method (PAS). Before PAS staining, sections were brought to water and soaked in aqueous Dimedone (British Drug Houses Ltd, Dorset, United Kingdom) for 24 hours to block the free aldehyde groups produced by glutaraldehyde fixation.

Results

Control

Urine Tests

Blood, protein, glucose and ketone bodies were absent. Between 30 minutes and 3 hours, urine was very dilute from those rats that had received hypertonic sodium chloride solution.

Light Microscopy

The proximal convoluted tubules of rats that had received hypertonic sodium chloride solution showed no obvious abnormalities and the morphology of the first and second segments, S₁ and S₂, appeared as previously described.^{1,2}

Electron Microscopy

The ultrastructure of the tubules of rats that had received hypertonic solutions of sodium chloride was similar to that already described in rats given physiologic saline.² The typical appearance of an S₁ tubule 2 hours after dosing with 888 mg/kg sodium chloride is shown in Fig 1. The mitochondrial matrices had considerable electron density and contained dense matrix granules, the intracrystal spaces were not dilated. Small chains of rough-surfaced endoplasmic reticulum (RER) and polysome groups were scattered in the cytoplasm. Aggregates of smooth-surfaced endoplasmic reticulum (SER) were not seen in control cells and the SER was seen only as cuffs around microbodies and as profiles running parallel to the lateral cell membranes as the paramembranous tubular or cisternal system, (pcs).¹¹⁻¹³ The cytoplasm was relatively electron-dense.

Malonate Poisoning

General Condition of Poisoned Rats

None of the rats died before the scheduled time of killing after re-

ceiving 1776 mg/kg subcutaneously. Anesthetic was given to the rats at the time of dosing to alleviate any discomfort that the rats might have suffered from receiving a large volume of hypertonic solution subcutaneously. The anesthetic effects wore off within 1–2 hours and male rats showed no obvious toxic symptoms but after the higher dose some female rats were very quiet and sat with their backs arched.

Urine Tests

Hematuria did not occur and pH values were within the control range. Between 30 minutes and 3 hours, urine was very dilute. After both dose levels, a proteinuria (100–300 mg/100 ml) was recorded between 2 and 6 hours with Hema-Combistix strips but the sulfosalicylic acid test did not confirm this. Ketone bodies were detected between 30 minutes and 6 hours. Glycosuria did not occur after 888 mg/kg but a “light” positive was recorded from 2 female rats at 2 and 3 hours, respectively, after 1776 mg/kg.

Light Microscopy

Paraffin Sections. Abnormalities were not apparent in some rats while in others, varying degrees of increased eosinophilia, granularity and swelling of the cytoplasm occurred during the first 3 hours after 1776 mg/kg; the most severe changes occurred in female rats. Abnormalities were not seen after 4 hours except for necrotic foci in the proximal tubules and eosinophilic PAS-positive casts in distal tubules and collecting ducts of 2 female rats at 12 hours. Medullary casts were seen in 1 female at 48 hours.

Araldite Sections Stained with Alkaline Toluidine Blue Solution. The mitochondria stained less densely and some cytoplasmic and nuclear pallor occurred in tubules of both sexes during the first hour after 888 mg/kg. During the first 3 hours, similar changes occurred in male rats after 1776 mg/kg. More severe changes were seen in 4 female rats; the cytoplasm was swollen and pale and the mitochondria were densely stained in contrast. No segmental distribution occurred. From 6–48 hours, abnormalities were not apparent at the light microscopic level with the exception of females showing focal necrotic changes.

Electron Microscopy

At 30 Minutes After 1776 mg/kg. The numbers of apical vacuoles had increased in some cells, the mitochondrial matrices were pale and swollen and matrix granules were absent (Fig 2). Cytoplasmic pallor was seen in some cells of the female rats and polysome groups were

dispersed (Fig 5). Aggregates of SER were seen in both sexes; they appeared to be most common in S_2 tubules and were associated with the pcs and SER cuffs around microbodies. Microtubules were sometimes seen near to the aggregates (Fig 5).

At 1 to 4 Hours; Mild Changes After 888 and 1776 mg/kg. In less severely affected rats, changes were similar at both dose levels. The mitochondrial matrix density was increased compared with that seen after 30 minutes, although it remained less than that of the controls. Moderate pallor of the cytoplasm occurred in some cells and was at times more marked at the cell base; widening of the intracristal space occurred in some mitochondria simultaneous with this change (Fig 3). The RER was not dilated.

At 1 to 3 Hours; Severe Changes After 1776 mg/kg. Severe changes occurred in 4 of the 6 female rats studied. Cytoplasmic swelling was marked and the mitochondria were swollen due to dilatation of their intracristal spaces; however, the matrix density was comparable with that of control mitochondria (compare Fig 1 and 4). Some mitochondria assumed bizarre shapes (Fig 4). The brush border was lost only from very swollen cells (Fig 9) and some apical dense tubules were retained (Fig 4 and 9). Normal dense cytosomes persisted but, in addition, numerous small single-membrane-bound dense bodies, 100–500 m μ in diameter, were seen in all regions of some cells (Fig 4); images suggestive of budding were observed (Fig 4, inset). The ribosomes were reduced in number and were dispersed (Fig 4 and 6) and in many cells the identity of the RER was lost. Aggregates of SER persisted and retained their association with microbody cuffs (Fig 6) and the pcs. Extensive dilatation of the ER occurred in some cells at 2 and 3 hours and dilated profiles were seen partially trapped within cupped mitochondria (Fig 9) so that in favorable planes, profiles of dilated ER appeared to be trapped within them (Fig 8). The Golgi apparatus was recognizable and the cisternae were not dilated (Fig 7). Smooth-membrane ring forms were seen spatially related to the Golgi apparatus and also in the apical cell regions (Fig 8). Necrosis was not observed at these times.

At 6 hours. The effects of malonate at 888 mg/kg were not studied after 4 hours (Table 1). After the higher dose, the mitochondria of the tubules of the female rats were a little swollen, the matrix density was reduced and matrix granules were absent. The cytoplasm appeared normal, SER aggregates were not observed, nor was autophagy increased. No abnormality was seen in the male rat.

At 12 hours. Abnormalities were not seen in the male rat and many

tubules appeared normal in the females. In the latter, however, focal groups of necrotic cells were seen intercalated between viable cells. In some cells, cytoplasmic volume was reduced, the mitochondria were tight-packed and the nuclei were pyknotic (Fig 10). Interdigitating with these "dehydrated" cells were necrotic cells characterized by grossly swollen, pale mitochondria; flocculent densities were seen in their matrices (Fig 10). Bare basement membrane was not seen and where cells had sloughed, processes from adjacent viable cells had spread to cover it.

At 24 and 48 hours. The tubules appeared normal at both time intervals.

Discussion

Biochemical Lesion

During this study, biochemical parameters were not investigated but the doses used were comparable with those used in some previous studies of the biochemical and functional consequences of poisoning. These will be discussed and where relevant a tentative interpretation of the morphologic changes will be made.

Succinate accumulation was highest in the kidneys and greatest at 1 hour after subcutaneous injection of 1.0 M sodium malonate at 1.2 ml/100 g body weight; at 2 hours succinate levels had fallen.⁵ The same dose was used in the present study. The ability of the rat kidney to accumulate *p*-aminohippurate was depressed during the first hour but rose steadily thereafter after 1 g/kg body weight.¹⁴ These findings indicate that the maximum inhibition of succinic dehydrogenase activity is during the early stages of poisoning and it may be that the changes seen in the kidneys after the first hour in the present study were not a direct expression of succinic dehydrogenase inhibition. Mudge¹⁵ claimed that oxidation of fatty acids in kidney slices was inhibited by concentrations of malonate lower than that required for complete inhibition of succinate oxidation and that inhibition of electrolyte transport in kidney slices induced by malonate was not mediated by inhibition of a specific enzyme.

Dose Response and Site of Action

Advanced cellular swelling and necrosis occurred in only a proportion of female rats after the higher dose of malonate. The distribution was not segmental, as occurred during fluorocitrate poisoning.¹ The sex difference may not be significant as small numbers of rats were used and

sex variations were not apparent in histochemical studies made on another series of rats.¹

Mitochondrial Changes

Swelling of Mitochondrial Matrix

Succinic dehydrogenase is an integral part of the inner mitochondrial membrane¹⁶ and succinate will accumulate, presumably within the matrix, upon inhibition of the enzyme. Swelling of the matrix, accompanied by pallor and loss of matrix granules, was one of the earliest changes seen. Expansion of the matrix is associated with water uptake,¹⁷ which would be expected in order to equilibrate osmotic pressures between the mitochondrial matrix and the cytoplasm. The significance of the loss of the matrix granules is not understood. The dense granules are thought to be binding sites for cations; Mg^{++} may be the major cation.¹⁸ Malonate is a chelating agent⁶ and loss of granules may be related to this.

Mitochondrial "spheroids," with swollen matrices of low density, fragmentation of cristae and floccular dense matrix deposits, are typical of necrotic change and have been described during necrosis induced by many noxious agents.¹⁹ This change is irreversible and is associated with loss of selective permeability of the cell membrane.²⁰ Necrotic mitochondria were seen only in 12-hour female rats, and the cellular and mitochondrial changes immediately preceding the necrotic state could not be followed in detail.

Mitochondrial Morphology in Relation to Cell Swelling

The study of mitochondrial metabolically linked structural organization is in its infancy and in the absence of metabolic data any interpretation of the present observations can only be speculative.

Failure to maintain cell volume may be due to an impaired sodium pump, resulting either from insufficient energy production or from a failure to utilize energy. Adenosine triphosphate (ATP)²¹ and a Na^+ , K^+ -activated adenosine triphosphatase (ATPase)^{22,23} are thought to be involved in extrusion of Na^+ from the cells. Protein anions are the only nonpermeable intracellular ions and the internal concentration of cations is held constant by active transport and extrusion of Na^+ , in effect rendering the cell impermeable to them. Failure to maintain the pump produces imbalance in the internal osmotic pressure and the cells will swell until they rupture or become permeable to protein.²⁴ Depression of metabolic activity is associated with an isosmotic increase in cellular hydration.²⁵

Condensation of the mitochondrial matrix judged upon an increased electron density did not occur at anytime and dilatation of the intracristal space occurred secondary to rarefaction of the cell sap, indicative of a continuous phase between the cytoplasm and the outer mitochondrial compartment.²⁶ Mitochondrial morphology in the swollen cells superficially resembled that seen in swollen cells during fluorocitrate poisoning but, in the latter, condensation of the mitochondrial matrices preceded and heralded cellular hydration, indicating that the condensed mitochondrial form was linked with the inability to maintain cellular volume.¹ During malonate poisoning, cytoplasmic swelling occurred at times when succinic dehydrogenase activity was probably partially restored (*vide supra*) and the change may be attributed to chelation of cations, which are essential for maintenance of normal intra- and extracellular cation levels. Malonate at 10 mM will reduce Mg^{++} by 49% and Ca^{++} by 23% in Krebs Ringer solution.⁶ In the absence of Ca^{++} , the passive leak of Na^+ into kidney cells is increased.²⁷

Necrosis was not seen when the hydropic change was widespread at 2 and 3 hours and the change appeared for the most part to be reversible but it progressed in some cells to necrosis, apparently preceded by an intermediate stage when the cytoplasmic volume was reduced.

Comments on Other Organelles

Apical Structures

Primary changes in the brush border and related structures were not observed during malonate poisoning.

Endoplasmic Reticulum and Ribosomes

Augmentation of the SER occurred early. The SER was sparse in control cells and this must represent synthesis *de novo*. It did not occur during fluoroacetate² or fluorocitrate poisoning.¹ The significance of the change in renal cells is unknown²⁸ but inhibition of succinic dehydrogenase may be an associated factor. An increase in SER was described during CCl_4 poisoning, when quantitative analysis showed a decrease in enzyme activity in the kidney.²⁹ The SER was also increased early during mercuric chloride poisoning.^{30,31} In the present study, aggregates of SER were not seen after 3 hours and their fate was obscure. The aggregates were stable when the cytoplasm was swollen and at times when dilatation of the RER was marked.

Dilatation of the RER has been reported in many types of cellular injury.¹⁹ In the present study, mitochondrial change always preceded

dilatation and undilated cisternae were seen in some cells where the cytoplasm was rarefied. The sequence of differential expansion of sub-cellular compartments during cell injury has been discussed³² and this finding is at variance with the pattern described. Obvious fragmentation of the RER did not occur in the proximal tubule.

Dissociation of polysome groups occurred in the swollen cells. The factors responsible for the maintenance of polysome groups are poorly understood. Polysome groups consist of several ribosomes bound by a strand of mRNA; Mg^{++} is involved in the binding.³³ Chelation of Mg^{++} by malonate may be one factor involved in polysomal disaggregation.

The Golgi Apparatus, Related Structures and Cytosomes

The Golgi cisternae were recognizable in swollen cells and were not dilated at times when the RER cisternae were. Maintenance of the Golgi apparatus may be an important factor governing the potential reversibility of cellular damage.

The significance of the smooth-membrane ring forms is unknown. Similar forms were seen during fluoroacetate^{1,2} and fluorocitrate poisoning.¹

Autophagy did not occur above control level and the fate of the SER aggregates was obscure, which is similar to the situation reported in phenobarbital-induced SER hypertrophy in the liver.³⁴

Budding from what appeared to be dense cytosomes occurred only in swollen cells. The change appeared to be reversible and cytosomes were unchanged in cells where cytoplasmic density was normal. The cause of the change is unknown.

References

1. McDowell EM: An Ultrastructural and Histochemical Study of the Rat Kidney after *in vivo* Administration of Inhibitors of Krebs' Cycle. PhD Thesis. University of Cambridge, 1971
2. *Idem*: Light and electron microscopic studies of the rat kidney after administration of inhibitors of the citric acid cycle, *In Vivo*. I. Effects of sodium fluoroacetate on the proximal convoluted tubule. *Am J Pathol* 66:513-542, 1971
3. Potter VR, Busch H, Bothwell J: Method for the study of tissue metabolism *in vivo* using fluoroacetate. *Proc Soc Exp Biol Med* 76:38-41, 1951
4. Potter VR: Sequential blocking of metabolic pathways *in vivo*. *Proc Soc Exp Biol Med* 76:41-46, 1951
5. Busch H, Potter VR: Succinate accumulation *in vivo* following injection of malonate. *J Biol Chem* 198:71-77, 1952
6. Leyden Webb J: Malonate, Enzyme and Metabolic Inhibitors. Vol 11. New York, Academic Press Inc, 1966, pp 1-244

7. Harvey DG: On the routine chemical analysis of small volumes of urine. *Br Vet J* 113:52-64, 1957
8. Farquhar MG, Palade GE: Cell junctions in amphibian skin. *J Cell Biol* 26:263-291, 1965
9. Pease DC: Staining. *Histological Techniques for Electron Microscopy*. Second edition. New York, Academic Press Inc, 1964, p 260
10. Reynolds ES: The use of lead citrate at high pH as an electron-opaque stain in electron microscopy. *J Cell Biol* 17:208-212, 1963
11. Ericsson JLE: Absorption and decomposition of homologous hemoglobin in renal proximal tubular cells: an experimental light and electron microscopic study. *Acta Path Microbiol Scand: Suppl* 168:1-106, 1964
12. Trump BF, Ericsson JLE: The effect of the fixative solution on the ultrastructure of cells and tissues: a comparative analysis with particular attention to the proximal convoluted tubule of the rat kidney. *Lab Invest* 14:1245-1323, 1965
13. Ericsson JLE, Trump BF: Electron microscopic studies of the epithelium of the proximal tubule of the rat kidney. III. Microbodies, multivesicular bodies and the Golgi apparatus. *Lab Invest* 15:1610-1633, 1966
14. Dominguez AM, Shideman FE: Effect of malonate and antimycin A on renal tubular transport of *p*-aminohippurate. *Proc Soc Exp Biol Med* 90:329-332, 1955
15. Mudge GH: Electrolyte and water metabolism of rabbit kidney slices: effect of metabolic inhibitors. *Am J Physiol* 167:206-223, 1951
16. Greville GD: Intracellular compartmentation in the citric acid cycle, *Citric Acid Cycle*. Edited by JM Lowenstein. New York, Marcel Dekker, 1969, pp 1-119
17. Lehninger AL: Water uptake and extrusion by mitochondria in relation to oxidative phosphorylation. *Physiol Rev* 42:467-517, 1962
18. Pasquali-Ronchetti I, Greenawalt JW, Carafoli E: On the nature of the dense matrix granules of normal mitochondria. *J Cell Biol* 40:565-567, 1969
19. Trump BF, Ericsson JLE: Some ultrastructural and biochemical consequences of cell injury, *The Inflammatory Process*. Edited by BW Zweifach, L Grant, RT McCluskey. New York, Academic Press Inc, 1965, pp 35-120
20. Trump BF, Ginn FL: The pathogenesis of subcellular reaction to lethal injury, *Methods and Achievements in Experimental Pathology*. Vol 4. Edited by E Bajusz, G Jasmin. Basel Karger, 1969, pp 1-29
21. Whitembury G: Sodium and water transport in kidney proximal tubular cells. *J Gen Physiol* 51:303s-314s, 1968
22. Dunham ET, Glynn IM: Adenosine triphosphatase activity and the active movements of alkali metal ions. *J Physiol (Lond)* 156:274-293, 1961
23. Wheeler KP, Whittam R: Structural and enzymic aspects of the hydrolysis of adenosine triphosphate by membranes of kidney cortex and erythrocytes. *Biochem J* 93:349-363, 1964
24. Dick DAT: Relation between water and solutes, *Cell Water: Butterworths Molecular Biology Series*. Butterworth and Company Publishers, Ltd, London, 1966, pp 15-43
25. Leaf A: On the mechanism of fluid exchange of tissues *in vitro*. *Biochem J* 62:241-248, 1956
26. Parsons DF: Recent advances correlating structure and function in mitochondria. *Int Rev Exp Pathol* 4:1-54, 1965

27. Kleinzeller A, Knotková A, Nedvidková J: The effect of calcium ions on the steady state ionic distribution in kidney cortex cells. *J Gen Physiol* 51:326s-334s, 1968
28. Ericsson JLE, Mostofi FK: Experimental hemoglobinuric nephropathy. 11. Electron microscopic studies. *Virchows Arch [Zellpathol]* 3:201-218, 1969
29. Striker G, Smuckler EA, Kohnen PW, Nagle RB: Structural and functional changes in rat kidney during CCl_4 intoxication. *Am J Pathol* 53:769-789, 1968
30. Gritzka TL, Trump BF: Renal tubular lesions caused by mercuric chloride: electron microscopic observations. Degeneration of the pars recta. *Am J Pathol* 52:1225-1277, 1968
31. Holgersen Ø, Gloor F, Rohr HP, Torhorst J: Frühveränderungen an der proximalen Tubuluszelle der Rattenniere nach Sublimatvergiftung: degenerative und adaptive Phänomene in den proximalen Tubuluszellen. *Virchows Arch [Zellpathol]* 3:324-338, 1969
32. Ginn FL, Shelburne JP, Trump BF: Disorders of cell volume regulation. I. Effects of inhibition of plasma membrane adenosine triphosphatase with ouabain. *Am J Pathol* 53:1041-1071, 1968
33. Peterman ML: The Physical and Chemical Properties of Ribosomes. Amsterdam, New York, Elsevier Publishing Co, 1964, pp 204-206
34. Orrenius S, Ericsson JLE: Enzyme-membrane relationship in phenobarbital induction of synthesis of drug-metabolizing enzyme systems and proliferation of endoplasmic membranes. *J Cell Biol* 28:181-198, 1966

Legends for All Figures

Figures 1–10 are electron micrographs. All tissue was stained en bloc with uranyl acetate followed by lead citrate stain on the grids.

Fig 1—Control, 2 hours after 888 mg/kg NaCl. Typical appearance of cells of S₁ after dosing with hypertonic sodium chloride solution. Tubular invaginations are seen at the bases of the microvilli (arrows) and the apical cytoplasm is filled with tubular images and apical vesicles; larger apical vacuoles (AV) lie below their level. Cytoplasmic interdigitation is well developed and long mitochondria lie perpendicular to the basement membrane (BM). The mitochondrial matrices have considerable electron density, matrix granules are present and the intracristal space is not dilated. Small chains of rough-surfaced endoplasmic reticulum and polysomes are scattered in the cytoplasm ($\times 16,000$).

Fig 2—30 minutes after 1776 mg/kg malonate, male rat. Normal apical structures are retained but the numbers of apical vacuoles (AV) are increased. The mitochondrial matrices are swollen and electron density is low; matrix granules are absent. Normal cytoplasmic density is retained ($\times 16,000$).

Fig 3—1 hour after 1776 mg/kg malonate, male rat. Apical structures appear normal. The mitochondrial matrix density is lower than in control cells (Fig 1) but is greater than at 30 minutes (Fig 2); matrix granules are absent. (The dark spots in the central mitochondrion result from blemishes in the photographic plate.) The cytoplasmic density is largely retained in the apical regions but is lost in the basal areas (large arrows). Some intracristal spaces are dilated in those mitochondria lying in the rarefied cytoplasm (small arrows). The ribosomes remain in polysome groups ($\times 16,000$).

Fig 4—2 hours after 1776 mg/kg malonate, female rat. The cytoplasm is hydropic and the cells are swollen but microvilli (mv) and some apical tubules are retained (top right). The ribosomes are ill-defined and scattered; the rough-surfaced endoplasmic reticulum has lost its identity but some smooth-membrane profiles persist and the paramembranous cisternal system is recognizable (small arrows). The Golgi apparatus (G) retains its identity. The mitochondria are swollen due to dilatation of the intracristal space but the matrix density is not above that of control cells (Fig 1). The mitochondria assume bizarre shapes; M1 and M2 probably represent cup-shaped mitochondria cut in different plane of section. In addition to normal dense cytosomes, small dense cytoplasmic bodies are numerous at all cell levels. A "light" glycosuria was associated with this degree of cellular damage ($\times 16,000$). **Inset**—Apparent budding of a dense cytoplasmic body. The dense contents have segregated into three distinct zones inside the limiting membrane ($\times 33,000$).

Fig 5—30 minutes after 1776 mg/kg malonate, female rat. Cytoplasmic rarefaction occurred early in some tubules, the ribosomes are scattered. The mitochondrial matrix retains electron density and the intracristal space is not dilated. An aggregate of smooth-surfaced endoplasmic reticulum is closely associated with the cuff around a microbody (Mb). A microtubule (T) traverses the cytoplasm ($\times 23,000$).

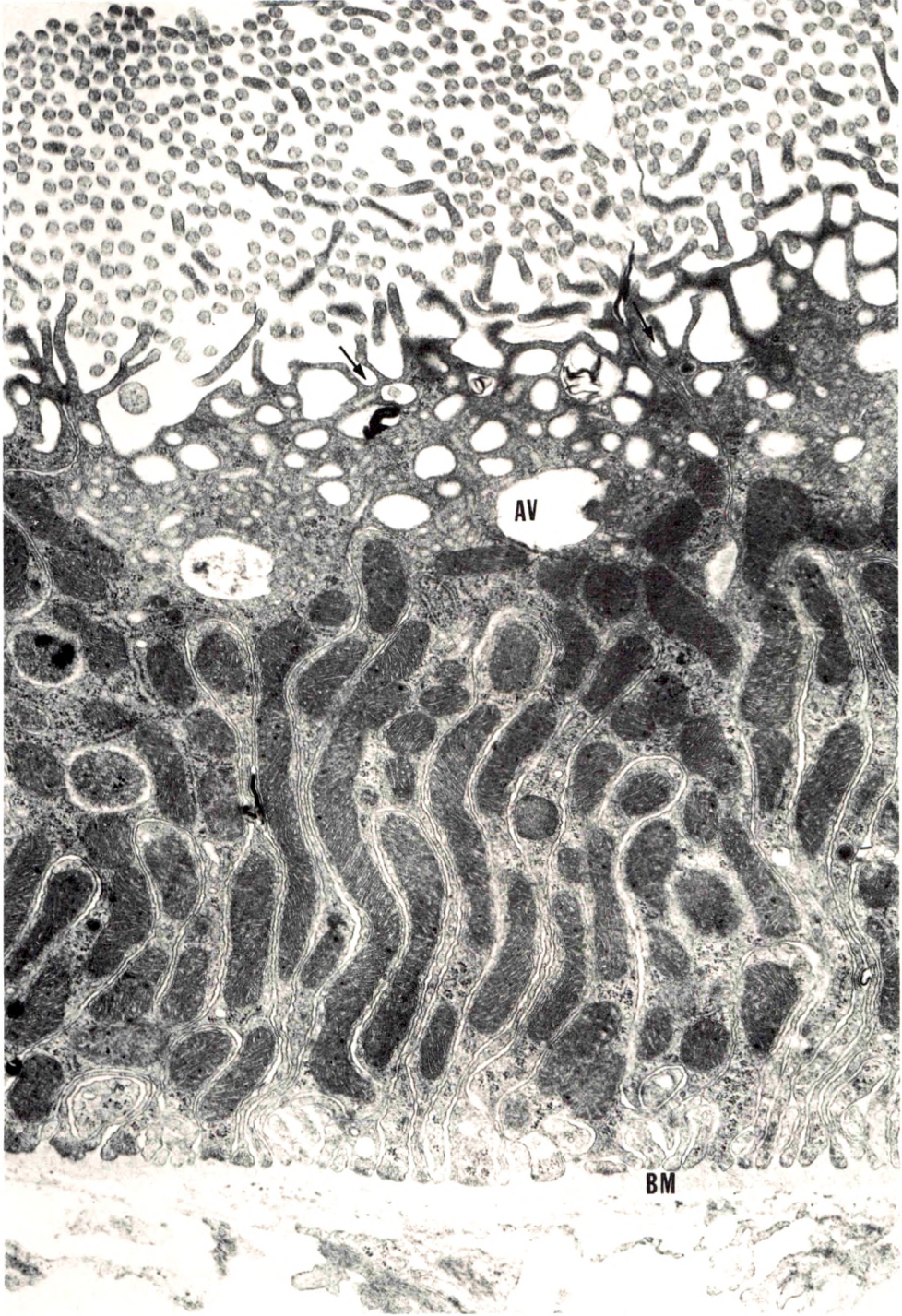
Fig 6—1 hour after 1776 mg/kg malonate, female rat. Aggregates of smooth-surfaced endoplasmic reticulum persist in hydropic cells and their relationship with microbody cuffs is maintained. The paramembranous cisternal system (arrow) is stable. The microbody matrix (Mb) is floccular. The intracristal space is dilated ($\times 19,000$).

Fig 7—1 hour after 1777 mg/kg malonate, female rat. The Golgi apparatus (G) retains its identity in the hydropic cell; the electron density of the cisternal content is not increased. The intracristal space is dilated but the mitochondrial matrix density is not increased ($\times 37,000$).

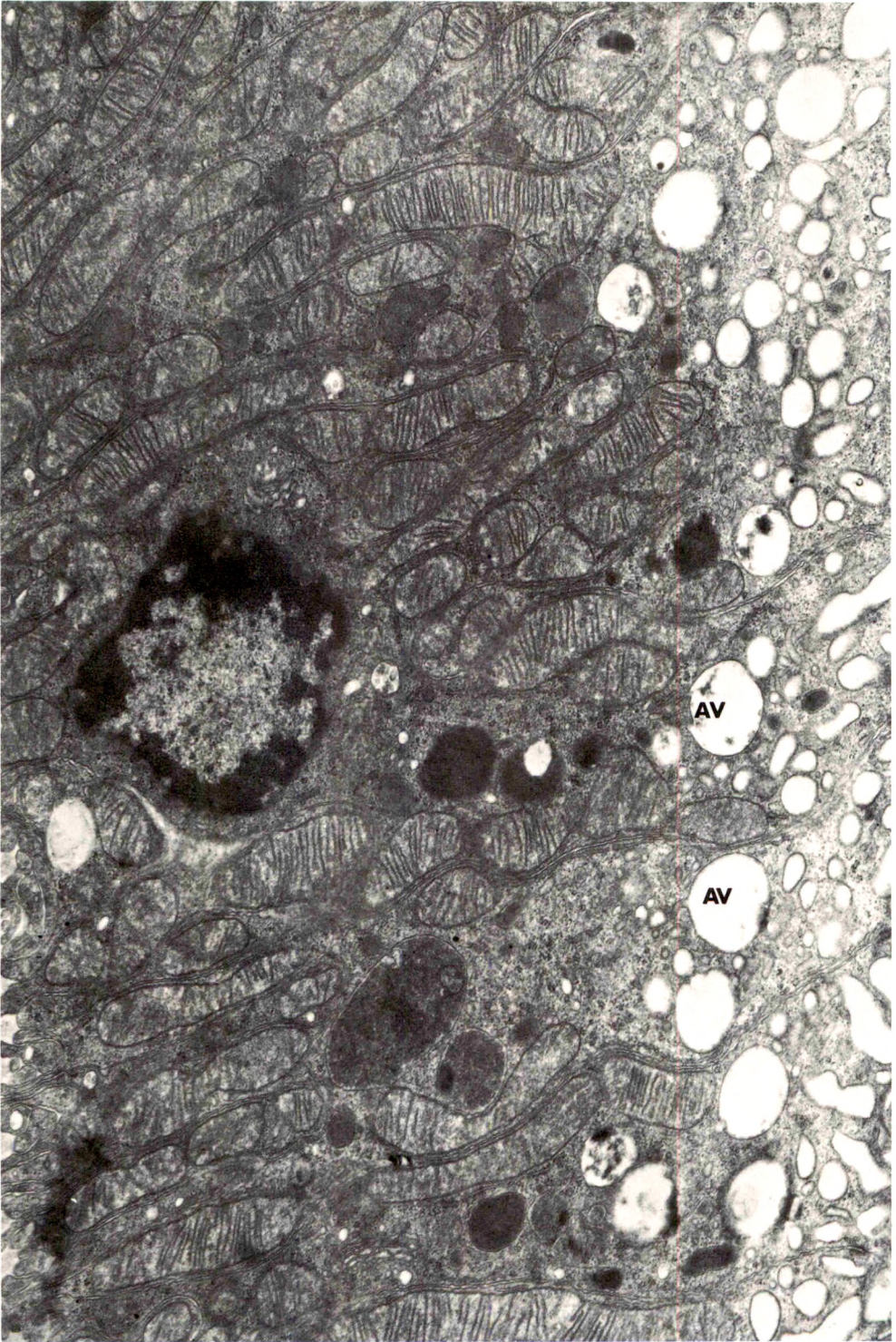
Fig 8—3 hours after 1776 mg/kg malonate, female rat. A ring form (rf) is present in the apical cytoplasm of a hydrated cell. The central area within the mitochondrion is thought to be a dilatation of the endoplasmic reticulum (see Fig 9) ($\times 27,000$).

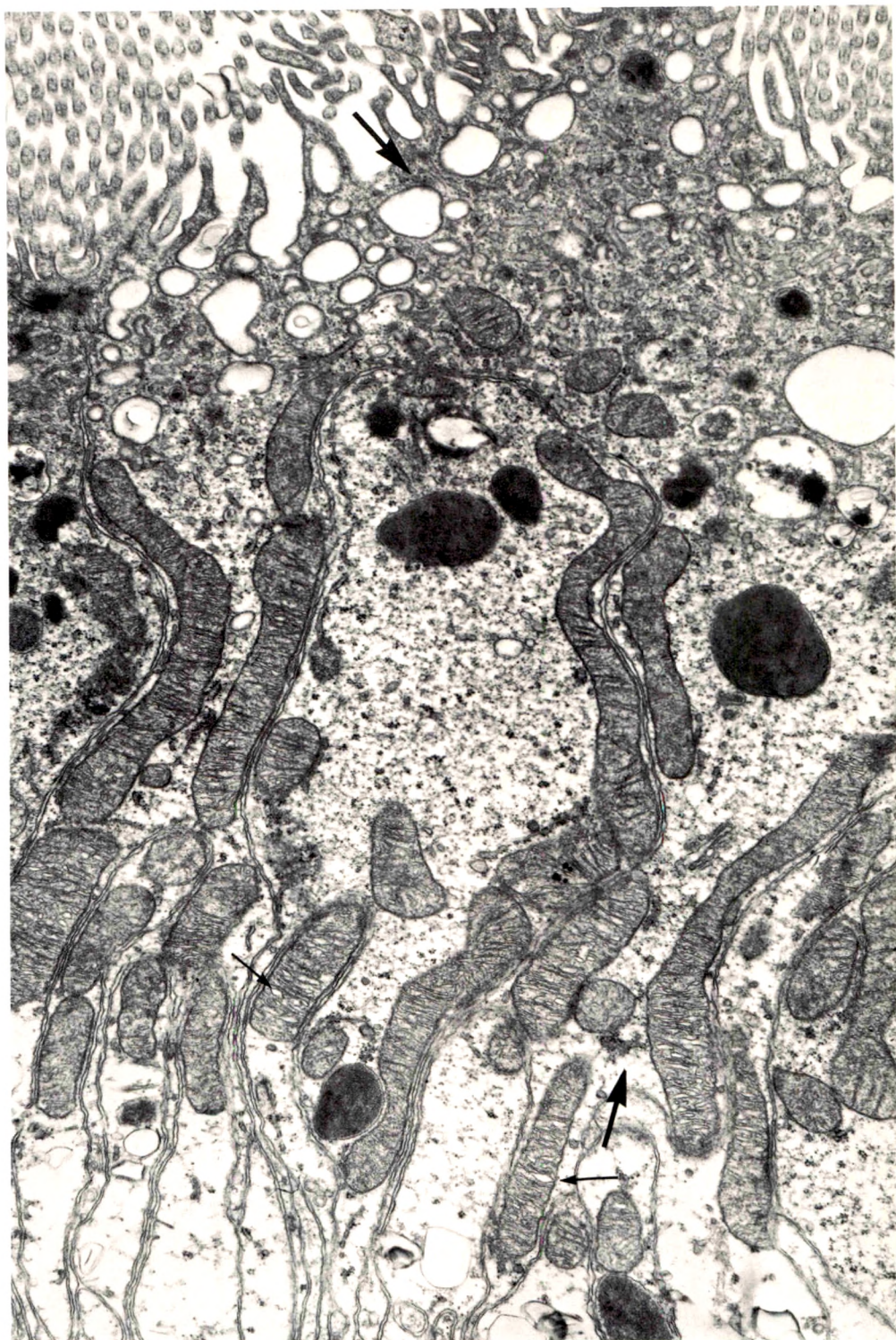
Fig 9—3 hours after 1776 mg/kg malonate, female rat. The brush border is retained in the cell on the left but is lost from the domed cell apex of the cell at the right. Normal apical structures persist despite cytoplasmic rarefaction (small arrows). Dense cytosomes appear normal (base). The clear vacuoles at the base are dilated profiles of endoplasmic reticulum. A mitochondrion is cupped around one of them (large arrow) ($\times 8200$).

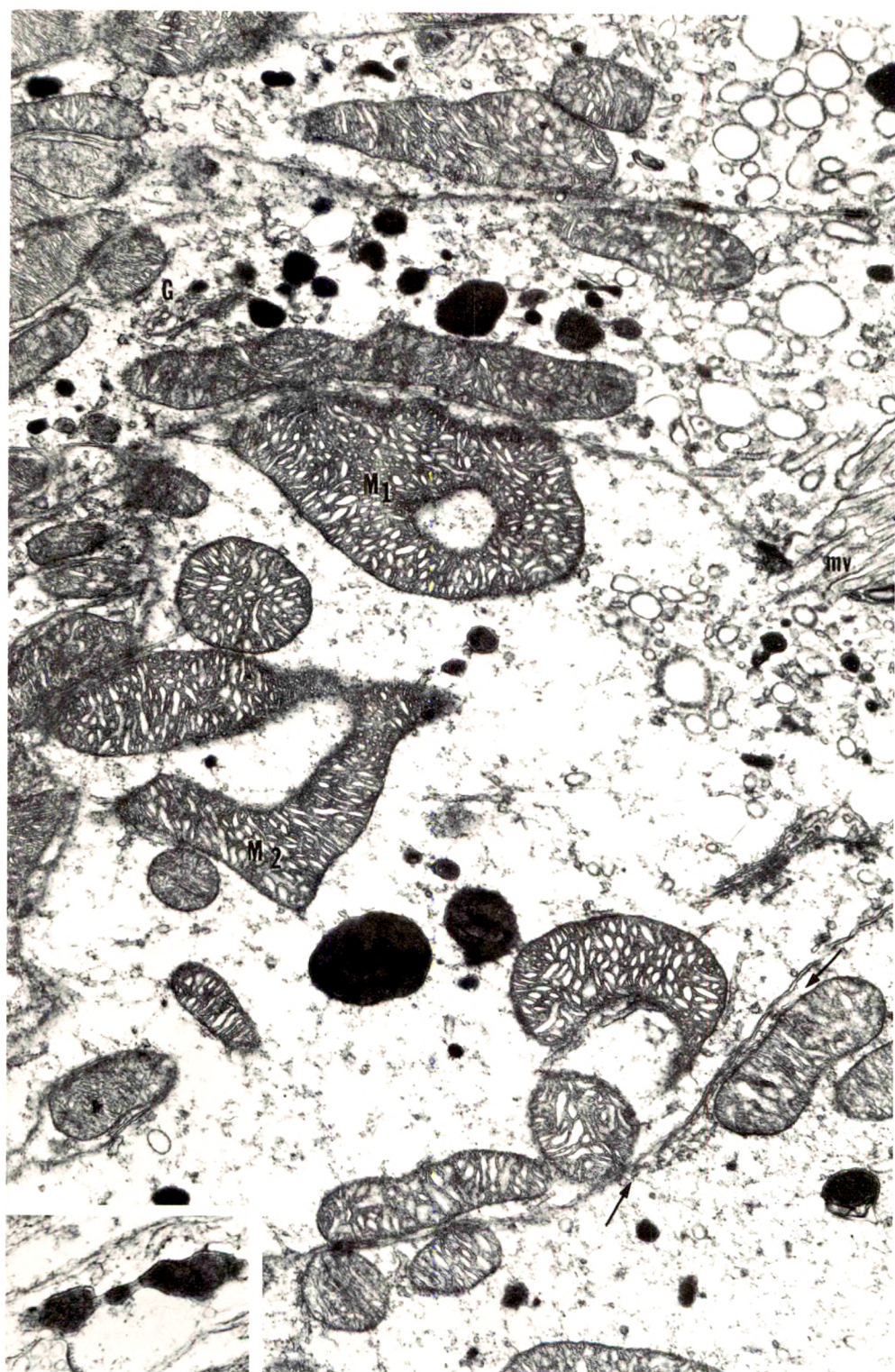
Fig 10—12 hours after 1776 mg/kg malonate, female rat. Cytoplasmic volume is much reduced in the central cells and they consist of tightly packed mitochondria; some appear dark and some light. Matrix densities are not seen. The nucleus (N, top) is pyknotic. Typical necrotic change has occurred in adjacent and interdigitating cells and the mitochondria are palely staining spheroids; the cristae have fragmented and dense matrix deposits are seen (arrows) ($\times 8500$).



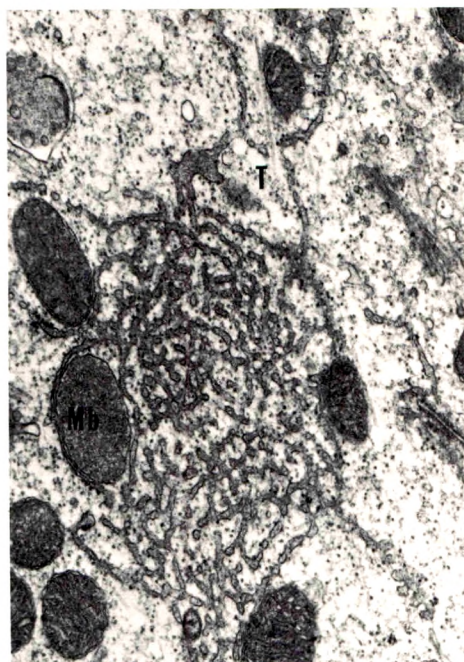
2



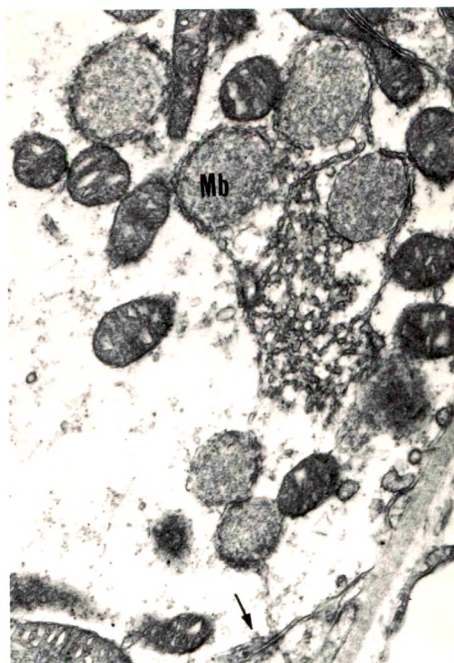




5



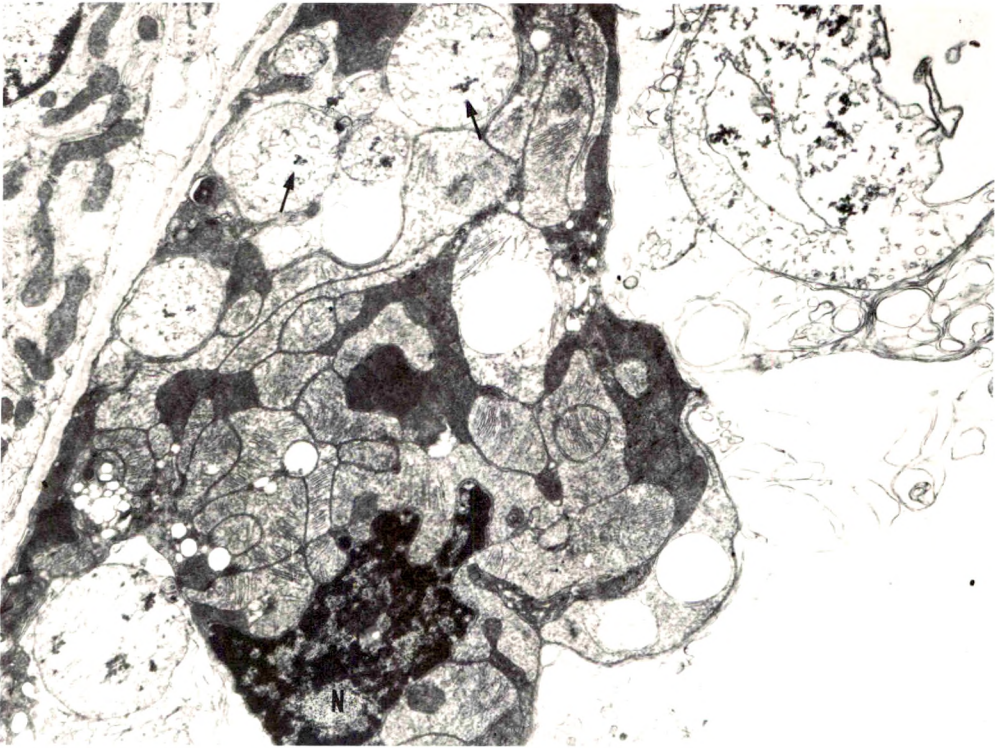
6



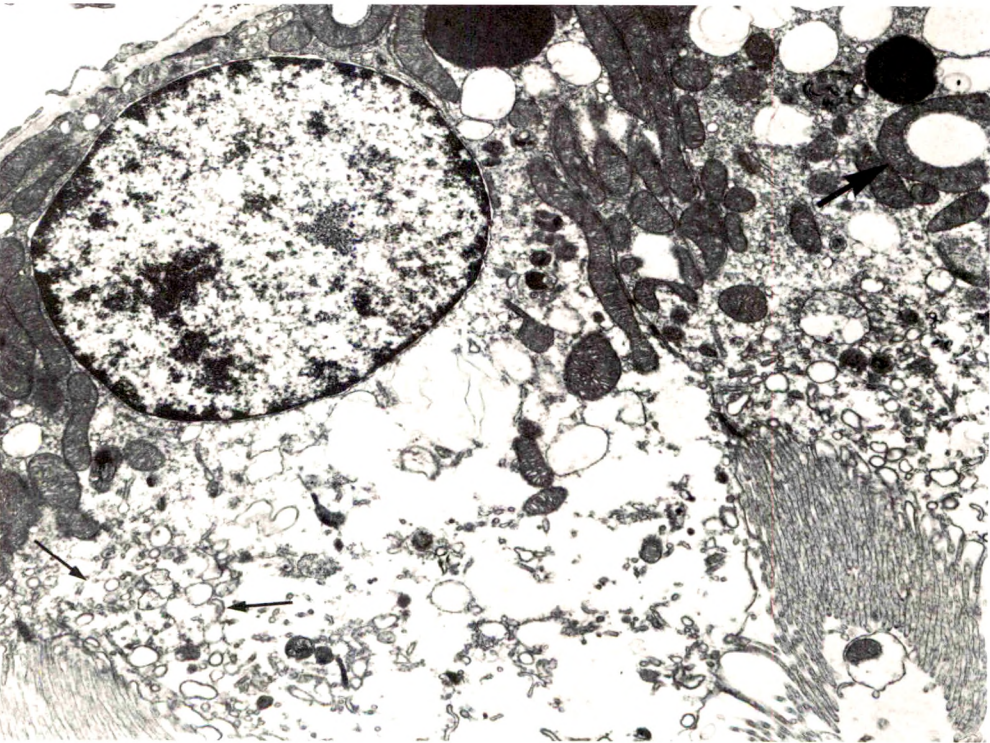
7



9



10



Macrophage Accumulation, Division, Maturation, and Digestive and Microbicidal Capacities in Tuberculous Lesions

I. Studies Involving their Incorporation of Tritiated Thymidine and their Content of Lysosomal Enzymes and Bacilli

Kiyoshi Shima, MD, Arthur M. Dannenberg, Jr, MD, Masayuki Ando, MD, Saroj Chandrasekhar, PhD, Judith A. Seluzicki and Jacob I. Fabrikant, MD

Dermal and pulmonary tuberculous lesions were produced in rabbits with BCG, biopsied, incubated *in vitro* with tritiated thymidine (^3HT) under hyperbaric oxygen, quickly frozen, sectioned in a cryostat, stained for the lysosomal enzyme β -galactosidase, autoradiographed, stained for acid-fast bacilli and counterstained with hematoxylin. As macrophages developed into epithelioid cells, they could still divide—*ie*, incorporate ^3HT . However, once they became fully mature epithelioid cells that were 4-plus in β -galactosidase, they could not do so. Tubercle bacilli did not stimulate macrophage division. On the contrary, macrophages containing bacilli did not divide, except when the lesions began. During the development of tuberculous lesions, macrophages (including those rich in enzymes and those containing bacilli) died, forming caseous centers. Therefore, local cell division did not seem to be the main mechanism by which macrophages reduced their bacillary load. Such division seemed mainly to occur in young macrophages that had recently immigrated into the lesions from the bloodstream and had not yet ingested bacilli.

THE ABILITY OF MACROPHAGES^{*} to destroy or inhibit the growth of tubercle bacilli within their cytoplasm determines both

From the Department of Radiological Science, School of Hygiene and Public Health, and the Department of Pathology, School of Medicine, Johns Hopkins University, Baltimore, Md.

Supported by Grant AI 08876 from the United States–Japan Cooperative Medical Science Program of the National Institute of Allergy and Infectious Diseases, US Public Health Service; Grant HE 14153 from the National Heart and Lung Institute, US Public Health Service, for the Johns Hopkins Specialized Research Center on Lung; and by contracts with Fort Detrick and with the Defense Atomic Support Agency (administered by the Army Medical Research and Development Command).

Accepted for publication November 1, 1971.

Address reprint requests to Dr. Arthur M. Dannenberg, Jr, Johns Hopkins School of Hygiene and Public Health, 615 North Wolfe Street, Baltimore, Md 21205.

^{*} Macrophages are the main cell responsible for the destruction of tubercle bacilli in the host. Mononuclear cells (MN) refer to a macrophage population in which lymphocytes may be present since it is not always possible to distinguish between these two cell types in tissue sections. All MN containing bacilli or showing high β -galactosidase activity are macrophages, not lymphocytes.

the native and acquired resistance of the host to tuberculosis.¹⁻³ A large part of the effectiveness of these cells in controlling this disease is due to their ability to manufacture new lysosomes containing bactericidins and digestive enzymes³⁻⁶ and then to discharge the contents of these lysosomes into vacuoles containing the bacilli.⁷ An additional way in which macrophages might control the intracellular growth of bacteria involves the divide-and-rule principle. Every time the phagocyte undergoes mitosis, it halves its bacterial load. Alternatively, the death of macrophages containing bacilli and the uptake of these bacilli by many new macrophages produce the same result. Light loads of intracellular bacilli should be more easily eliminated by the phagocytes than heavy loads.

This first report on macrophage accumulation, division, maturation and digestive and microbicidal capacities in tuberculous lesions describes the relation of macrophage division to their content of lysosomal enzymes and tubercle bacilli. A second report⁸ describes their rate of entry and how long they continue to divide in the lesions. A third report⁹ describes macrophage turnover and its relation to acquired cellular immunity.

Materials and Methods

Animals

Randomly bred New Zealand white 2-3 kg rabbits of both sexes were employed. Tuberculous lesions produced in rabbits closely resemble those of man in the growth and destruction of tubercle bacilli within macrophages and in the amount of caseation and liquefaction present.¹ Necropsies were performed on all animals to assure the absence of other grossly evident diseases.

Bacilli

The Phipps strain of BCG, maintained in our laboratory on Lowenstein-Jensen's egg medium, was prepared for intradermal or intravenous injection, according to the procedure previously described.^{10,11}

Since isolated bacilli would be easily destroyed and hard to find in the lungs, the BCG suspension injected intravenously was not centrifuged to remove the bacillary clumps. Such clumps gave rise to 1-day pulmonary lesions that were readily visible under the microscope.

The virulent human strain of tubercle bacillus (H₃₇Rv) and the virulent bovine strain (Ravenel) were obtained from Trudeau Institute, Inc, Medical Research Laboratories, Saranac Lake, NY 12983. They were aerosolized by Dr. William G. Roessler at Fort Detrick in a modified Henderson apparatus to expose the rabbits (see Dannenberg *et al*¹²). Tuberculin reactions were produced by the intradermal injection of a 1:10 dilution of old tuberculin (Eli Lilly and Co, Indianapolis, Ind 46206) and measured 2 days later with calipers.¹⁰

Preparation of Biopsies of Dermal BCG Lesions: *In Vitro* Incubation with ^3HT ; Staining for β -Galactosidase and Acid-Fast Bacilli; Autoradiography and Methods of Counting ^3H -Labeled MN

These lesions were measured with calipers and biopsied according to the methods described by Kambara *et al.*¹⁰

The biopsies were cut into pieces 1 and 2 mm thick and incubated while shaking at 37 C for 1 hour under 100% oxygen at 3 atmospheres of pressure¹³ in the presence of tritiated thymidine (^3HT) (1.0 $\mu\text{Ci/ml}$ Medium 199 with 20% fetal calf serum added).^{*,†} The specimens were then quickly frozen in isopentane that was brought to its freezing point in liquid nitrogen. They were then placed on a dry-ice block and the isopentane allowed to evaporate. Subsequently, they were sealed in Parafilm (Marathon Products Div, American Can Co, Neenah, Wisc) and stored at -23 C for a varying number of weeks. For sectioning at 8 μ in an International cryostat, they were mounted, without thawing, on brass microtome mounts resting on dry ice with the aid of an embedding matrix for frozen sectioning (M1 embedding matrix, Lipshaw Manufacturing Co, Detroit, Mich 48210).

The frozen sections were placed on glass slides (kept at room temperature) and then dehydrated *in vacuo* over silica gel usually for $\frac{1}{2}$ to 20 hrs.[‡] The sections were fixed for 4 minutes in cold buffered 1.25% glutaraldehyde,¹⁴ rinsed in saline and incubated overnight in Pearson's indolyl substrate¹⁵ for β -galactosidase (5-bromo-4-chloro-3-indolyl- β -D-galactoside, Cyclo Chemical Division of Travenol Laboratories, Inc, Los Angeles, Calif 90001, prepared according to methods previously described by our laboratory).^{4,14} They were then rinsed in distilled water, fixed for 4 minutes in 20:2:1 fixative (20 parts 70% ethanol, 2 parts 10% neutral formalin, 1 part glacial acetic acid—mixed within 1 week of use) and air-dried. Within 2 weeks, they were dipped in nuclear emulsion (Nuclear Emulsion K-5, Ilford Ltd, Ilford, Essex, England, or Kodak Nuclear Emulsion, Type NTB2, Eastman Kodak Co, Rochester, NY), dried, and stored at 4 C in a light-tight box, usually for 7 weeks. The autoradiographs were then developed in Kodak D19 solution, fixed in Kodak acid fixer, washed with tap water, stained with carbofuchsin, followed by acid-alcohol, counterstained with hematoxylin, dehydrated in alcohols of ascending concentration, and mounted with Permount (No. SO-P-15, Fischer Scientific Co, Fair Lawn, NJ) under coverslip. Only mononuclear cells (MN) with nuclear ^3HT labeling were counted, although occasionally cytoplasmic labeling was seen. The latter could arise from the ingestion of labeled dead cells by these phagocytes.

Established dermal lesions usually had necrotic centers surrounded by tuber-

* Thymidine-methyl- ^3H with specific activity at 16.6 to 20.2 Ci/mmol: New England Nuclear Corporation, Boston, Mass 02118 (catalog No. NET-027X); or thymidine-methyl- ^3H with specific activity of 13.4 Ci/mmol: Schwartz BioResearch, Inc, Orangeburg, NY 10962 (catalog No. 2632-97). Medium 199, Earle base, pH 7.0 \pm 0.2 (catalog No. 71-026S), and fetal calf serum, pooled, no preservative (catalog No. 50509): Baltimore Biological Laboratories, Cockeysville, Md 21030.

† This procedure is not an organ culture or a true cell culture. It is merely a short-term supportive measure in which cells in S phase of their mitotic cycle (which lasts about 8 hours) continue DNA synthesis under adequate nutritional conditions. Increasing the oxygen tension increases the amount of tissue that is fully oxygenated. Cells at the end of the G₁ phase may enter the S phase and also become labeled during the 1-hour incubation period.

‡ This method of preparation, developed by Dr. Robert G. Wyllie of our pathology department, excellently preserves various tissue enzymes.

culous granulation tissue containing β -galactosidase-positive MN (see Fig 1). This proximal granulation tissue was in turn surrounded by granulation tissue of more recent origin usually containing β -galactosidase-negative MN. We counted *only* the MN in areas containing β -galactosidase-positive cells—*ie*, most of the non-necrotic area depicted in Fig 1. In other words, the MN in the peripheral granulation tissue were not included in our evaluation of either MN activation (β -galactosidase content) or MN division (^3HT incorporation). Since ^3HT did not penetrate deeply into the tissue specimen, only MN in the outer portions of the biopsies were counted.

Preparation of Specimens of Pulmonary Tuberculous Lesions

Pieces of pulmonary tissue (3–4 mm in diameter) were obtained immediately after the rabbit was killed by air embolism. They were incubated as above in ^3HT under hyperbaric oxygen for 1 hour. Specimens containing virulent bacilli were then fixed in the 20:2:1 fixative, embedded in paraffin, cut at 8 μ and prepared for autoradiography and subsequent staining as just described. Specimens containing BCG were frozen, placed on brass microtome mounts, cut at 8 μ and processed as the dermal biopsies.

Lung specimens consisted of three regions (Fig 2): (a) a central necrotic core, (b) a perifocal area of MN and (c) a surrounding alveolar area. The MN in area b and those in area c were usually evaluated separately (see Table 3). Because of poor penetration of ^3HT , only lesions near the outer surface of the lung specimen were counted.

Administration of Intravenous Tritiated Thymidine (^3HT)

To rabbits bearing dermal and pulmonary BCG lesions, ^3HT was given as a single intravenous pulse (0.5 $\mu\text{Ci/g}$ of body weight) 30 or 60 minutes before sacrifice. The purpose and details of these experiments are described below.

Experimental Data and Results

Comparison of the *In Vitro* and *In Vivo* Methods of ^3HT Labeling of MN in Tuberculous Lesions

The following experiment was performed for this purpose. Eight rabbits were injected intravenously with 2.8×10^8 viable BCG (opacity, 1.100)* to produce pulmonary lesions, and also intradermally with 1.0×10^6 viable BCG (opacity, 0.400) in each of eight sites to produce skin lesions. Ten days later when their tuberculin reactions were moderate (about 200 cu mm), 4 rabbits were injected intravenously with ^3HT (0.5 $\mu\text{Ci/g}$) and 4 were injected intravenously with saline. They were sacrificed 30 or 60 minutes later. Biopsies of skin and pulmonary lesions from the ^3HT -injected rabbits were frozen in semisolid isopentane, sectioned, stained for β -galactosidase and bacilli, and autoradiographed. Biopsies of skin and pulmonary lesions from the saline-

* The opacity of the bacillary suspension is the optical density reading at 540 nm made in a 1.25-cm test tube in a Bausch and Lomb Spectronic 20 spectrophotometer. It is an index of the total number of (live plus dead) bacilli injected.

injected rabbits were first incubated for 1 hour with ^3HT ($1.0 \mu\text{Ci/ml}$) *in vitro* under hyperbaric oxygen and then similarly prepared.

The results, presented in Table 1, showed that the *in vitro* method of labeling with ^3HT was less effective than the *in vivo* method, in spite of the fact that only MN in the outer portions of the *in vitro* incubated biopsies were counted. In both skin and lung lesions, the *in vitro* method labeled about half as many mononuclear cells. This result may be due to mild cell injury (possibly from anoxia or trauma) during the biopsy procedure. *In vitro* results were more comparable to those *in vivo* with MN in the alveolar spaces surrounding the pulmonary lesions. Possibly the sponge-like nature of this region reduced the amount of anoxia.

Rabbits sacrificed 30 minutes after the intravenous (iv) injection of ^3HT showed the same percentage of labeled MN in their lesions as rabbits sacrificed 60 minutes after iv ^3HT . This result was not unexpected because the duration of ^3HT incorporation into DNA (*ie*, the duration of the S phase of the mitotic cycle) is usually 8 or more hours. This result also indicated that few additional ^3HT -

Table 1—Comparison of **In Vitro** and **In Vivo** Methods of ^3HT -Labeling of MN in Tuberculous Lesions*

Percentage of ^3HT -labeled MN in lesions from individual rabbits						
Skin lesions		Pulmonary lesions				
In vitro †	In vivo	Perifocal area		Surrounding alveolar area		
		In vitro	In vivo	In vitro	In vivo	
1.3	2.6‡					
1.4	3.0§	3.6	7.9‡	3.0	3.6‡	
1.4	3.8§	3.9	9.7§	3.3	3.7§	
1.7	4.1‡	4.4	10.0‡	3.4	4.4§	
1.9		4.7	12.6§	3.9	4.9‡	
2.0						
Mean \pm SE	1.6 \pm 0.1	3.4 \pm 0.3	4.1 \pm 0.2	10.1 \pm 1.0	3.4 \pm 0.2	4.1 \pm 0.3
	P < 0.001		P = 0.001		P = 0.046	

* Biopsies of three skin lesions and four lung areas were taken from each rabbit, and two or three sections made from each biopsy. The figures in the table were obtained by counting about 1000 MN for the **in vivo** ^3HT experiments and about 400 MN for the **in vitro** ^3HT experiments. Although MN were mostly macrophages, they included some lymphocytes.

† Two of these rabbits came from the **in vivo** injected group. Their skin biopsies were taken before the ^3HT was injected intravenously.

‡ Animals sacrificed 30 minutes after intravenous ^3HT .

§ Animals sacrificed 60 minutes after intravenous ^3HT .

positive MN enter BCG lesions from the bloodstream during the 30-minute period after the ^3HT injection. In other words, the higher percentage of ^3HT -positive MN found in BCG lesions labeled *in vivo* compared with those labeled *in vitro* cannot be attributed to the entry of new ^3HT -positive cells from the bloodstream.

With rabbits, the *in vitro* method is much less costly, because relatively little ^3HT is used. In addition, the animal does not become radioactive, and other skin biopsies can be taken at a later time. Therefore, even though the *in vitro* method labels cells less efficiently, it has distinct advantages over the *in vivo* method.

Local Incorporation of ^3HT by MN in Tuberculous Lesions

Dermal BCG Lesions of Rabbits; *In Vitro* Incubation with ^3HT

Dermal BCG lesions were biopsied as they developed and regressed over a 5-week period. A different lesion was used for each biopsy, which was incubated for 1 hour in ^3HT under hyperbaric oxygen, sectioned in a cryostat and autoradiographed.

The percentage of MN incorporating ^3HT changed little during the period studied (Table 2). However, in the 2-week lesions of Experiment III, the percentage of ^3HT -positive MN was elevated. At this time, hypersensitivity to tuberculin was developing and many new MN were infiltrating. These lesions were produced by relatively small numbers of bacilli, so the environment may have been less toxic than in the other experiments and therefore more conducive to cell division.

Pulmonary Tuberculous Lesions of Rabbits; *In Vitro* Incubation with ^3HT

Pulmonary tuberculous lesions were produced by the intravenous injection of BCG or by the inhalation of virulent tubercle bacilli (Table 3). At various times thereafter, the animals were sacrificed, and lung biopsies were incubated *in vitro* with ^3HT and processed as above.

The lungs of normal uninfected rabbits were first evaluated among three separate experiments. The percentage of MN that incorporated ^3HT varied widely (Table 3). The reason for this variation is unknown.

In another experiment, the rabbits were sacrificed 1, 2 and 3 days after a high intravenous dose of BCG. Few MN had accumulated around the bacilli at 1 day, but at 2 and 3 days distinct granulomata were present (see below). Such granulomata contained a rather high percentage (averaging 12%) of ^3HT -positive MN (Table 3), evidently because they were composed of newly arriving MN.

In the remaining experiments, lesions 10–19 days old were evaluated.

Table 2—Percentage of ^3HT -Labeled MN* in Dermal BCG Lesions

	Time after id injection of BCG			
	7 days	12-14 days	18-21 days	33-35 days
Exp I—0.1 Million BCG in Each of 8 id Sites; Opacity = 0.400†				
Percent of ^3HT -labeled MN‡	2.2 ± 0.5	5.0 ± 0.8	2.8 ± 0.2	2.1 ± 0.2
Size of lesion (cu mm)	6 ± 1	16 ± 4	37 ± 7	13 ± 3
Tuberculin reaction§	0	+	2+	2+
Exp II—9 Million BCG in Each of 10 id Sites; Opacity = 3.050				
Percent of ^3HT -labeled MN‡	1.8 ± 0.3	2.1 ± 0.6	0.9 ± 0.2	1.1 ± 0.2
Size of lesion (cu mm)	117 ± 22	167 ± 20	118 ± 14	42 ± 7
Tuberculin reaction§	+	3+	3+	3+
Exp III—60 Million BCG in Each of 6 id Sites; Opacity = 1.080				
Percent of ^3HT -labeled MN‡	—	3.6 ± 1.7	4.2 ± 1.6	3.6 ± 0.7
Size of lesion (cu mm)	112 ± 39	239 ± 72	257 ± 94	91 ± 30
Tuberculin reaction§	=	3+	4+	3+
Exp IV—15 Million BCG in Each of 8 id Sites; Opacity = 0.690				
Percent of ^3HT -labeled MN‡	0.6 ± 0.2	1.3 ± 0.3	1.2 ± 0.2	1.5 ± 0.2
Size of lesion (cu mm)	39 ± 5	61 ± 9	117 ± 20	47 ± 7
Tuberculin reaction§	0	2+	4+	4+

* MNs signifies mononuclear cells. Although they were mostly macrophages, they included some lymphocytes. They were labeled by incubating biopsies of the lesions in ^3HT (1.0 $\mu\text{Ci}/\text{ml}$) for 1 hour under hyperbaric oxygen.

† The opacity of the bacillary suspension is an index of the total number of (live plus dead) bacilli injected (see asterisk footnote on page 162), id signifies intradermal. The average number of rabbits in each experiment was 6.

‡ The size of the dermal BCG lesion is listed as a volume in cu mm (see Kambara *et al*¹⁰). The means and their standard errors are given.

§ Tuberculin reactions of 10-50 cu mm were +; 50-250 cu mm were 2+; 250-500 cu mm were 3+; 500-900 cu mm were 4+.

These lesions contained only 1-4% ^3HT -positive MN (Table 3). The virulence of the bacilli did not apparently affect this percentage.

In general there was a parallelism between the percentage of MN dividing in (a) the perifocal granulation tissue within the lesions, (b) the adjacent alveolar areas and (c) the lung parenchyma between the lesions (Table 3).

Macrophage Activation, Multiplication and Content of Tubercle Bacilli

Macrophage activation (*ie*, maturation) was determined histochemically by staining these cells for the lysosomal enzyme β -galactosidase,⁴ macrophage multiplication was determined with ^3HT and autoradiography, and their content of bacilli was determined after acid-fast staining. These three procedures were performed in sequence on the same

Table 3—³HT-Labeled MNs* in Pulmonary Tuberculous Lesions

		Percent of labeled MNs* in biopsies incubated with ³ HT for 1 hr <i>in vitro</i>		
No. of rabbits	Time after infection that animals were sacrificed (days)	Perifocal area†	Surrounding alveolar area†	Lung parenchyma between lesions
Normal Uninfected Lung				
4	—		1.1 ± 0.1	
4	—		3.2 ± 0.8	
4	—		11.5 ± 0.8	
67 × 10 ⁶ BCG iv; Opacity = 2.000‡				
2	1	0.4 (0-0.8)	1.4 (0-2.8)	4.0 (3.9-4.0)
2	2	7.2 (4.4-9.7)	12.1 (12.0-12.1)	8.1 (7.1-8.1)
2	3	11.6 (7.8-15.4)	15.6 (13.7-17.5)	11.4 (11.2-11.6)
4 × 10 ⁹ BCG iv; Opacity = 1.500§				
5	10	3.1 ± 1.8	1.3 ± 0.4	
2.8 × 10 ⁹ BCG iv; Opacity = 1.100				
4	10	4.2 ± 0.2	3.4 ± 0.2	1.8 ± 0.7
0.6 × 10 ⁹ BCG iv; Opacity = 1.300§				
6	12	2.5 ± 0.7	1.8 ± 0.7	
5.6 × 10 ⁶ Virulent Bovine-type Tubercle Bacilli (Ravenel) by Inhalation				
5	13		3.6 ± 0.9	
42 × 10 ⁶ Virulent Human-type Tubercle Bacilli (H ₃₇ Rv) by Inhalation				
5	19		2.8 ± 0.7	

* MNs are mononuclear cells (mostly macrophages, but some lymphocytes).

† The "perifocal area" contains MN entering the lesion from the bloodstream. The "surrounding alveolar area" contains alveolar macrophages (AM) that came from the adjacent alveolar spaces, as well as MN emigrating from the blood. About 1000 MNs were counted to obtain the percent of labeled MN in each area for each rabbit. The means and their standard errors are given (except in the second experiment).

‡ The opacity of the bacillary suspension is an index of the total number of (live plus dead) bacilli injected (see asterisked footnote on page 162); iv indicates intravenously.

§ Tuberculin tests, performed 2 days before death, were negative in the case of 4 × 10⁹ BCG, and slightly positive in the case of 0.6 × 10⁹ BCG. No such tests were done in the other experiments.

frozen section of biopsies of dermal and pulmonary BCG lesions (see Materials and Methods).

MN Incorporation of ^3HT and β -Galactosidase Activity

The percentage of activated macrophages in the granulation tissue near the necrotic centers of *dermal BCG lesions* increased for 3 weeks and then slowly decreased (Text-Fig 1). (The more pronounced decrease in the second of the experiments illustrated in Text-fig 1 was a rarity.)

During the first 2 weeks, there were more immature (β -galactosidase-negative) MN incorporating ^3HT than mature (β -galactosidase-positive) MN. After about 3 weeks (when tuberculin sensitivity had developed), both immature and mature MN incorporated ^3HT to about the same extent (Text-fig 1, *cf* Fig 3). These findings support those in paper III of this series,⁹ namely that the young MN (*ie*, those incorporating ^3HT) developed cellular immunity (*ie*, rich β -galactosidase activity) faster after delayed hypersensitivity was present.

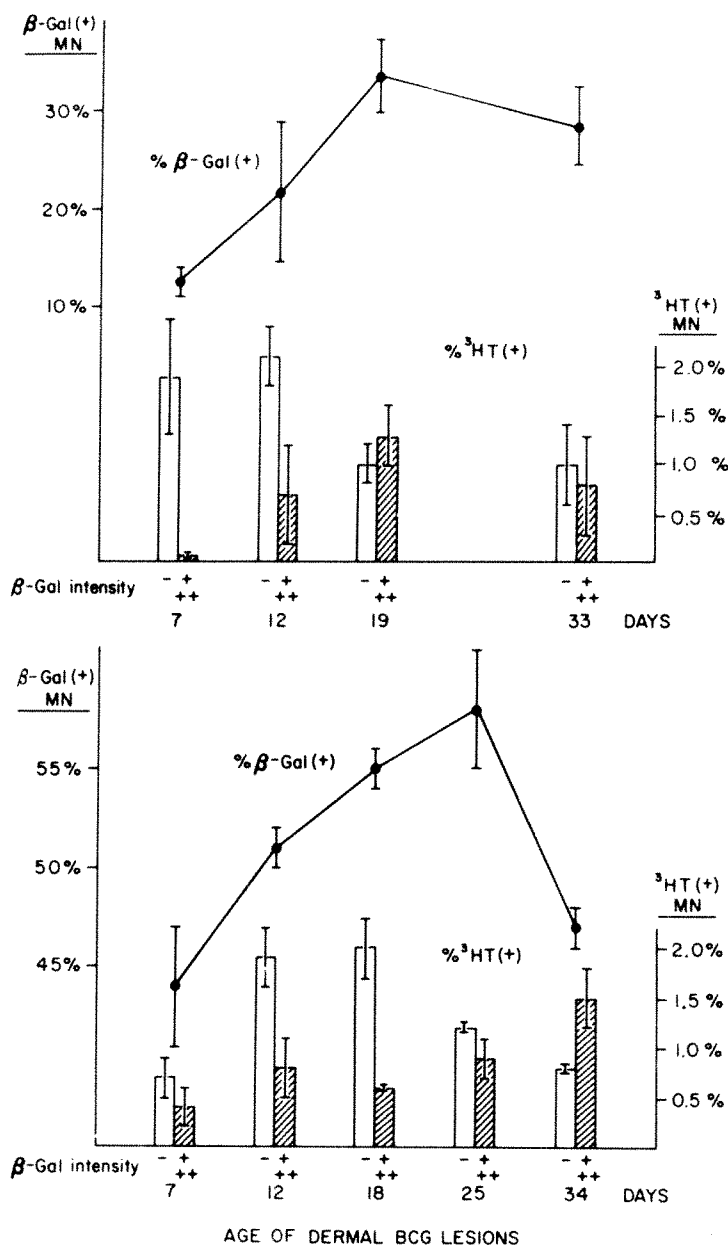
In dermal BCG lesions, there was no ^3HT incorporation by fully mature epithelioid cells staining 3+ and 4+ for β -galactosidase. These cells had evidently specialized completely for digestion and no longer divided.

With 10-and 12-day *pulmonary lesions*, produced by injecting BCG intravenously, the patterns of MN activation and division (Fig 3 and Table 3) resembled those found in dermal lesions. ^3HT incorporation was found in young MN in the granulation tissue surrounding the necrotizing centers of the lesions (Fig 2).

The pulmonary alveolar macrophages (AM) were, however, different from the ordinary macrophages that immigrated into the lesions directly from the bloodstream. In both normal and BCG-infected lungs, AM could become highly activated (+ and 4+ β -galactosidase-positive) and still incorporate ^3HT (Fig 2 and Table 3). Alveolar macrophages, therefore, seemed to be a major exception to the principle that macrophages extremely rich in enzymes do not divide.

Effect of Tubercle Bacilli on MN Division

In pulmonary BCG lesions 2 and 3 days old, all of the MN were recent arrivals and many incorporated ^3HT (Table 3). ^3HT -positive MN containing bacilli could sometimes be found (Fig 5). In pulmonary lesions 6 or more days old, such doubly marked MN were rare, because most of the bacilli had disappeared.



AGE OF DERMAL BCG LESIONS

TEXT-FIG 1—Percentage of ^3HT -positive MN (bar graphs and right ordinates) and β -galactosidase-positive MN (line graphs and left ordinates) in the granulation tissue near the necrotic centers of rabbit dermal BCG lesions biopsied at various times after infection. The minus symbols and the 1+ and 2+ symbols under the abscissae refer respectively to the unshaded and shaded bar graphs immediately above them. The results of experiment IV (see Table 2) are shown above; those of experiment VI are shown below. No ^3HT -labeled MN were found that stained 3+ and 4+ for β -galactosidase. The biopsies were incubated *in vitro* for 1 hour in ^3HT (1.0 $\mu\text{Ci}/\text{ml}$) under oxygen at 3 atm, sectioned and then incubated for 18 hours in the 5-bromo-4-chloro-3-indolyl- β -D-galactoside substrate solution. Standard errors of the means are shown by I-bars.

Table 4—Effect of Intracellular Tubercle Bacilli on MN Division in Dermal BCG Lesions*

Age of lesion when biopsied (days)	A	B	C	Total No. of MN with both ³ HT label and intracellular tubercle bacilli	
	Total No. of MN counted	Percent of ³ HT-positive MN†	Percent of MN containing tubercle bacilli†	Expected‡	Observed
Experiment I§					
7	14,100	2.0±0.02	3.5±0.8	8.1	0
12	13,800	4.0±1.3	2.7±0.8	7.5	5
19	31,500	2.3±0.6	0.4±0.2	5.7	0
Experiment II§					
7	17,900	1.0±0.3	3.4±0.7	4.9	0
12	8,300	1.6±0.3	4.4±0.5	4.3	0
19	22,400	0.8±0.2	0.8±0.4	2.4	0
Experiment III§					
7	27,500	1.6±0.3	4.6±1.2	16.7	5
14	29,600	2.6±0.5	3.5±1.1	24.0	7

* MN were mostly macrophages, but included some lymphocytes.

† Means and their standard errors are listed.

‡ Expected numbers of "doubly marked" MN could have been obtained by multiplying the values in columns A, B and C. More representative numbers were obtained, however, by adding the similar product from individual rabbits.

§ These experiments were the same as those listed in Table 2. MN were labeled by incubating biopsies of the lesions in ³HT (1.0 μCi/ml) for 1 hour under hyperbaric oxygen.

In dermal BCG lesions, bacilli were more plentiful, and a few ³HT-positive MN containing bacilli could occasionally be found in lesions 1 and 2 weeks old. From the total number of ³HT-positive MN and the total number of MN containing bacilli found in the lesions, the expected number of ³HT-positive MN containing bacilli was calculated. The number of such doubly marked MNs was found to be somewhat less than expected (Table 4 and Fig 4).

These results indicate that in lesions one or more weeks old MN division was not stimulated by the presence of intracellular tubercle bacilli. The results also offer additional support for the contention that only recent MN immigrants divided in the tuberculous lesion.¹¹ By the time these new immigrants reached the bacilli, which were more centrally located, many would have become older cells.

MN Enzyme Activity and ³HT Incorporation as Pulmonary Lesions Form and Caseation Develops

Macrophage function during the formation of pulmonary tuberculous lesions produced by inhalation is difficult to evaluate, because early

lesions are so small that they are hard to find. A much larger dose of bacilli can be given intravenously than by the respiratory route, thereby increasing the probability of finding 1-day lesions. Although such lesions do not exactly mimic those produced by inhalation, they do arise from relatively few bacilli in one location and therefore enable the genesis of this disease to be studied. In addition, the macrophages entering such small lesions frequently ingest isolated bacilli that have spread from the initial site of lodgment. Such macrophages would closely resemble those that ingest bacilli delivered by the respiratory route.

One-, 2- and 3-Day Pulmonary Lesions: Genesis of Tuberculous Foci

An uncentrifuged suspension of viable BCG was injected intravenously into rabbits (Table 3). It contained many bacilli in units of 1-4 as well as in clumps of 5-30. The latter acted as emboli and were found microscopically 1 day later lodged in the capillaries and the smaller arterioles of the lung (Fig 6). The clump protected the BCG against initial destruction and a small lesion was established.

In 1-day lesions, MN accumulated around the central bacillary core (Fig 6). At this stage, young MN present in many of the lesions showed 1+ and 2+ β -galactosidase activity. The clumps of bacilli seemed to have some inherent toxicity, as the MN and capillary endothelial cells were frequently necrotic. Nearby MN did not incorporate ^3HT (Table 3), apparently because of the toxic local environment. Even perifocally, little ^3HT incorporation was present, because few cells had accumulated there.

In 2- and 3-day lesions, this picture had changed. Macrophages ingesting the bacilli and necrotic cell debris became activated (*ie*, richer in β -galactosidase). Some of these MN died (Fig 7); some of them divided (Fig 5). Perifocally, many new MN accumulated, and these cells frequently divided (Table 3 and Fig 7). At this point, typical tuberculous lesions became established. They contained a central core of dead and dying cells and a perifocal region of accumulating and proliferating cells.

Six-, 10- and 12-Day Pulmonary Lesions: Enzymes in Caseating Epithelioid Cells

At 6 days, the β -galactosidase in the necrotic cells in the center of the tuberculous lesion had diffused away. Cytochrome oxidase, however, still remained (Fig 8), apparently because it was a mitochondrial enzyme. (The mitochondria may not have completely disintegrated at this time.) At 10 and 12 days, neither type of enzyme was active in the caseous centers of the lesions.

Role of Pulmonary Alveolar Macrophages

The microbicidal capacities of alveolar macrophages (AM) (the dust phagocytes) undoubtedly determine whether an inhaled tubercle bacillus will be immediately destroyed in the alveolar spaces or whether it will grow intracellularly and eventually produce a lesion. AM therefore play a critical role in resistance to attack by this bacillus.¹⁶ After the lesion is established, the role of AM in the pathogenesis of tuberculosis is less certain, as most of the macrophages in the tubercle come from the bloodstream.

The presence of high levels of β -galactosidase in many alveolar macrophages enabled us to identify these cells when they were in the peripheral parts of the lesion, where none of the blood-borne macrophages had as yet attained this level of activation. More AM were frequently present near the lesions than in the uninvolved alveolar spaces (Fig 2). Perhaps chemotactic factors were released from the lesion, and the AM traveled there along the surface of nearby alveoli and through the interalveolar pores of Kohn.¹⁷ Since these pulmonary alveolar macrophages are rich in enzymes and probably bactericidins, they should reduce the spread of the disease from the local site.

Discussion

Lurie¹⁸ described an intense accumulation and proliferation of mononuclear cells (MN) around a core of young epithelioid cells 1 week after BCG was injected intravenously into rabbits. Many mitotic figures were seen by him in these perifocal MN. He called this the stage of symbiosis.¹ The bacilli had multiplied to 30 or 40 times their original number, and MN had both emigrated from the bloodstream into the tubercle and multiplied locally, so that many defense cells were present.

Such tubercle formation was further analyzed in our study employing tritiated thymidine (³HT) and autoradiography. The original macrophages did *not* continue to multiply and provide clones of local MN: No ³HT incorporation was found in more centrally located macrophages (frequently containing bacilli) which had evidently resided in the lesion more than a few days. Local division of MN did occur, but apparently was confined to the newly arrived immigrants.

The destruction of tubercle bacilli was accomplished by the development of high levels of cellular immunity in a relatively small, but critical, proportion of the macrophages in the lesion.^{3,4} These MN could be found in healthy perifocal granulation tissue, not too far

from the caseous center (Fig 1), and only in areas where the bacilli were present.⁴ Such macrophages had the morphology of epithelioid cells and developed a very high content of lysosomes and their enzymes, mitochondria and their enzymes, and undoubtedly bactericidins.¹⁹⁻²⁴ Their content of these factors was many times that of surrounding MN in the same lesion.⁴ In other words, only a relatively few defense cells in strategic areas of the lesion accomplished the task of destroying the tubercle bacillus.

In the present report, the formation, multiplication and destruction of these highly activated, mature macrophages were studied by *in vitro* labeling with ³HT. Maturing epithelioid cells, staining 2+ for β -galactosidase, incorporated ³HT as readily as unstained MN (Fig 4 and Table 3). Since MN can increase their enzyme content in 24 hrs,²⁵ these 2+, ³HT-positive MN may be young cells that recently immigrated into the lesion.

No fully mature macrophages (*ie*, no fully activated epithelioid cells staining 4+ for β -galactosidase) incorporated ³HT in dermal BCG lesions. In other words, these cells no longer divided, but appeared to be end cells specialized for digestive and probably microbicidal functions. According to Lurie,^{1,18} they had destroyed the bacilli they once contained, and only rarely can one find a bacillus in such cells.⁴

Little information is available on the longevity of these mature macrophages. Epithelioid cells in the centers of 10- and 12-day pulmonary BCG lesions were apparently dead (Fig 2). They had lost their high content of enzymes and had indistinct cytoplasmic boundaries and even pyknotic or absent nuclei. In active tuberculosis lesions, it is quite possible that epithelioid cells frequently die when they destroy tubercle bacilli. This process would release tuberculin-like products that are directly or indirectly toxic for these cells.³

Further evidence for a high turnover of MN in tuberculous lesions will be presented in subsequent papers of this series^{8,9} in which *in vivo* ³HT labeling was employed in contrast to the *in vitro* studies of the present report. Multiple dermal BCG lesions, begun in rabbits 1 day after an intravenous pulse of ³HT, were biopsied periodically as they developed and regressed. The appearance and disappearance of labeled MN and ³HT grain count analyses gave quantitative support to the results in the present paper: Newly arrived MN could have divided once or twice. They functioned awhile and then died; they were not long-lived cells.

Thus, whether a tubercle progressed or regressed would depend on whether the macrophages killed all of the bacilli within them before

they died, or whether they died first, releasing viable bacilli to be ingested by other macrophages. Virulent bacilli, which are not readily destroyed, would pass through a series of macrophages. In each successive macrophage the speed of developing microbicidins and enzymes would be enhanced by the developing immune process (involving lymphocytes²⁶⁻³⁰), and the last few macrophages of the series would develop immunity so rapidly that all of the intracellular bacilli present would be inhibited or killed. The elimination of bacillary foci within the lesion by this process seems to be the mechanism by which the host overcomes the infection (see also references 8 and 9).

Summary

Dermal and pulmonary tuberculous lesions were produced in rabbits with BCG (and in two experiments with virulent tubercle bacilli). Biopsies of these lesions were made and incubated for 1 hour *in vitro* with tritiated thymidine (³HT). Tissue sections prepared from these biopsies were (a) stained for the lysosomal enzyme, β -galactosidase, (b) autoradiographed to detect ³HT incorporation, (c) stained for acid-fast bacilli and (d) counterstained with hematoxylin.

In established dermal lesions (1-5 weeks of age), *in vitro* incubation with ³HT usually labeled 1-4% of the mononuclear cells (MN), a mixture of lymphocytes and macrophages. (*In vivo* ³HT, given as a single intravenous pulse within an hour of sacrifice, labeled about twice as many MNs.) The labeling index remained more or less constant throughout the growth and regression of the BCG lesions.

In the local area of the tuberculous lesion that contained bacilli, many macrophages developed into epithelioid cells rich in mitochondrial and lysosomal enzymes. Such cells can effectively destroy the tubercle bacillus. As the macrophages became mature epithelioid cells, they continued to divide (*ie*, incorporate ³HT). However, once they reached full maturity (*ie*, 4+ in β -galactosidase) they rarely divided. Apparently they had become completely differentiated for digestive functions.

Pulmonary alveolar macrophages (AM) were an exception to this tent: AM were frequently found with 4+ β -galactosidase activity and nuclear labeling from a pulse of ³HT. Such highly activated (immune) pulmonary macrophages—*ie*, dust phagocytes (rich in β -galactosidase) from neighboring alveoli, frequently migrated to the periphery of young pulmonary lesions where they could limit the local spread of this disease.

The genesis of pulmonary tuberculous lesions (produced by injecting

large numbers of bacilli intravenously) was evaluated. Local activation of macrophages, shown by an increase in their β -galactosidase content, occurred within 24 hours. By 6 days, however, these activated macrophages had died, lost their enzyme activity, and formed the necrotic center of the developing tubercle. Only recently arrived MN (*ie*, those in 2- and 3-day lesions and those in the peripheral areas of older lesions) seemed to incorporate ^3HT locally. Apparently, older MN were on the road to death and no longer divided.

The relation of MN division to their content of virulent or avirulent tubercle bacilli was also investigated. In pulmonary BCG lesions 2 and 3 days old and in dermal BCG lesions 1 and 2 weeks old, occasional ^3HT -positive MN containing bacilli could be found. The observed number of such "doubly marked" cells found in the dermal lesions was less than the expected number calculated from the observed percentages of ^3HT -positive MN and bacilli-containing MN. We therefore concluded that MN division was not stimulated by the presence of intracellular bacilli, and that division was not the mechanism by which these cells reduced their bacillary load. The same purpose is apparently accomplished by cell death and the reingestion of the bacillary load by several adjacent phagocytes. In this manner, the divide-and-rule principle could play a role in the control of tuberculous infections.

References

1. Lurie MB: Resistance to Tuberculosis: Experimental Studies in Native and Acquired Defense Mechanisms. Cambridge, Harvard University Press, 1964
2. Lurie MB, Dannenberg AM Jr: Macrophage function in infectious disease with inbred rabbits. *Bacteriol Rev* 29:466-476, 1965
3. Dannenberg AM Jr: Cellular hypersensitivity and cellular immunity in the pathogenesis of tuberculosis: specificity, systemic and local nature, and associated macrophage enzymes. *Bacteriol Rev* 32:85-102, 1968
4. Dannenberg AM Jr, Meyer OT, Esterly JR, Kambara T: The local nature of immunity in tuberculosis, illustrated histochemically in dermal BCG lesions. *J Immunol* 100:931-941, 1968
5. Mackaness GB: Editorial: The immunology of anti-tuberculous immunity. *Am Rev Resp Dis* 97:337-344, 1968
6. Mackaness GB: Resistance to intracellular infection. *J Infect Dis* 123:439-445, 1971
7. Cohn ZA, Wiener E: The particulate hydrolases of macrophages. II. Biochemical and morphological response to particle ingestion. *J Exp Med* 118:1009-1020, 1963
8. Ando M, Dannenberg AM Jr, Shima K: Macrophage accumulation, division, maturation, and digestive and microbicidal capacities in tuberculous lesions. II. Rate at which mononuclear cells enter and divide in primary BCG lesions and those of reinfection. Unpublished data

9. Dannenberg AM Jr, Ando M, Shima K: Macrophage accumulation, division, maturation, and digestive and microbicidal capacities in tuberculous lesions. III. Macrophage turnover and its relation to cellular immunity in primary BCG lesions and those of reinfection. Unpublished data
10. Kambara T, Chandrasekhar S, Dannenberg AM Jr, Meyer OT: Radiation, infection, and macrophage function. I. Effects of whole body radiation on dermal tuberculous lesions in rabbits: development, histology, and histochemistry. *J Reticuloendothel Soc* 7:53-78, 1970
11. Chandrasekhar S, Shima K, Dannenberg AM Jr, Kambara T, Fabrikant JI, Roessler WG: Radiation, infection and macrophage function. IV. The effect of radiation on the proliferative abilities of mononuclear phagocytes in tuberculous lesions of rabbits. *Infection Immunity* 3:254-259, 1971
12. Dannenberg AM Jr, Roessler WG, Meyer OT, Chandrasekhar S, Kambara T: Radiation, infection, and macrophage function. III. Recovery from the effects of radiation illustrated by dermal BCG lesions; resistance of pulmonary alveolar macrophages to radiation illustrated by tuberculosis produced by the airborne route. *J Reticuloendothel Soc* 7:91-108, 1970
13. Fabrikant JI, Wisseman CL III, Vitak MJ: The kinetics of cellular proliferation in normal and malignant tissues. II. An *in vitro* method for incorporation of tritiated thymidine in human tissues. *Radiology* 92:1309-1320, 1969
14. Yarborough DJ, Meyer OT, Dannenberg AM Jr, Pearson B: Histochemistry of macrophage hydrolases. III. Studies on β -galactosidase, β -glucuronidase and aminopeptidase with indolyl and naphthyl substrates. *J Reticuloendothel Soc* 4:390-408, 1967
15. Pearson B, Wolf PL, Vazquez J: A comparative study of a series of new indolyl compounds to localize β -galactosidase in tissues. *Lab Invest* 12:1249-1259, 1963
16. Lurie MB, Dannenberg AM Jr: Macrophage function in infectious disease in inbred rabbits. *Bacteriol Rev* 29:466-476, 1965
17. Wang NS, Thurlbeck WM: Scanning electron microscopy of the lung. *Hum Pathol* 1:227-231, 1970
18. Lurie MB: The correlation between the histological changes and the fate of living tubercle bacilli in the organs of tuberculous rabbits. *J. Exp Med* 55:31-54, 1932
19. Kanai K, Kondo E: Separation and properties of the mycobactericidal principle from lysosomal components of tuberculous mice. *Japan J Med Sci Biol* 22:309-317, 1969
20. Mackaness GB: The monocyte in cellular immunity. *Sem Hematol* 7:172-184, 1970
21. Evans DG, Myrvik QN: Increased phagocytic and bactericidal activities of alveolar macrophages after vaccination with killed BCG. *J Reticuloendothel Soc* 4:428-429, 1967
22. Miller TE: Metabolic event involved in the bactericidal activity of normal mouse macrophages. *Infection Immunity* 3:390-397, 1971
23. Thalinger KK, Mandell GL: Bactericidal activity of macrophages in an anaerobic environment. *J Reticuloendothel Soc* 9:393-396, 1971
24. Simon HB, Sheagren JN: Cellular immunity *in vitro*. I. Immunologically mediated enhancement of macrophage bactericidal capacity. *J Exp Med* 133:1377-1389, 1971

25. Cohn ZA, Benson B: The *in vitro* differentiation of mononuclear phagocytes. III. The reversibility of granule and hydrolytic enzyme formation and the turnover of granule constituents. *J Exp Med* 122:455-466, 1965
26. Dumonde DC, Wolstencroft RA, Panayi GS, Matthew M, Morley J, Howson WT: Lymphokines: non-antibody mediators of cellular immunity generated by lymphocyte activation. *Nature* 224:38-42, 1969
27. Mediators of Cellular Immunity. Edited by HS Lawrence, M Landy. New York, Academic Press Inc, 1969
28. Mooney JJ, Waksman BH: Activation of normal rabbit macrophage monolayers by supernatants of antigen-stimulated lymphocytes. *J Immunol* 105:1138-1145, 1970
29. Adams DO, Biesecker JL, Koss LG: The differentiation of mononuclear phagocytes in vitro: the effect of lymphokines. *J Reticuloendothel Soc* 9:595, 1971
30. Nathan CF, Karnovsky ML, David JR: Alterations of macrophage functions by mediators from lymphocytes. *J Exp Med* 133:1356-1376, 1971

We appreciate the assistance of Miss Mary Jo Vitak, Mrs. Lita P. Fay, Mrs. Barbara Y. Morrison and Mrs. Joan E. Desmond in parts of this work.

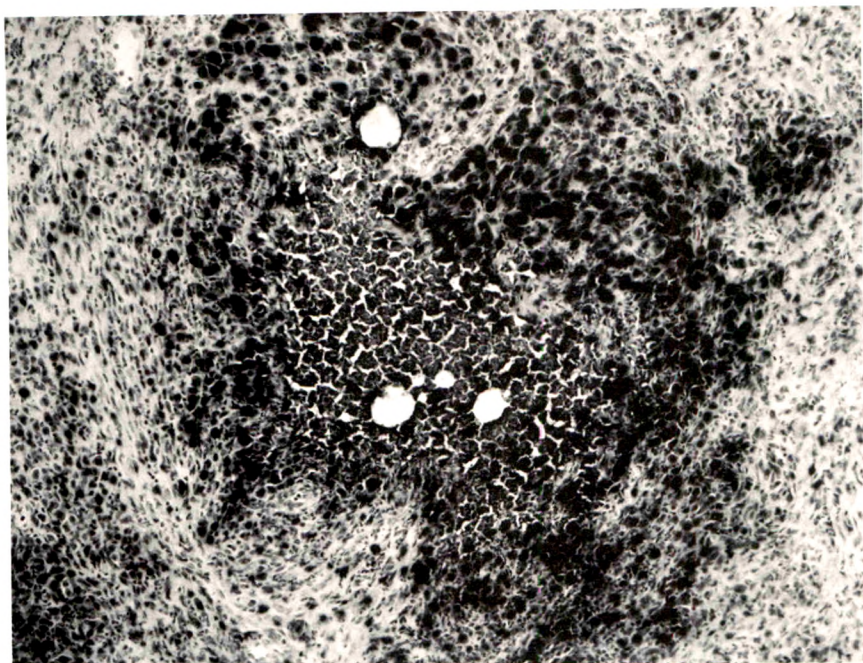
In conducting the research reported herein, the investigators adhered to the *Guide for Laboratory Animal Facilities and Care*, established by the *ad hoc* committee of the Institute of Laboratory Animal Resources, National Academy of Sciences-National Research Council.

Dr. Shima and Dr. Ando are on leave of absence from the First Department of Internal Medicine, Kumamoto University School of Medicine, Kumamoto, Japan. Dr. Chandrasekhar was on leave of absence from Vallabhbbhai Patel Chest Institute, University of Delhi, Delhi-7, India. Dr. Fabrikant's present address is Department of Radiology, University of Connecticut School of Medicine, Hartford, Conn 06112.

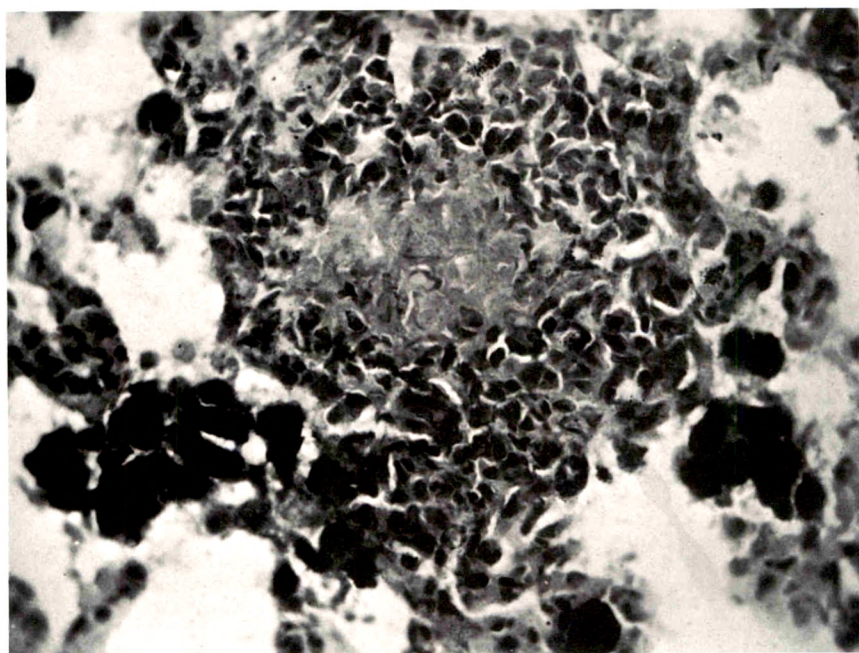
Legends for Figures

Fig 1—A 12-day dermal BCG lesion. Surrounding the caseous center are many epithelioid cells that stain 3+ and 4+ for β -galactosidase. Surrounding these cells, near the periphery of the photograph, are many immature macrophages with weak or absent β -galactosidase activity. This figure suggests that dead tissue and bacilli and their tuberculin-like products, directly or indirectly, cause macrophages to become epithelioid cells rich in enzyme activity (5-bromo-4-chloro-3-indolyl- β -D-galactoside and hematoxylin, $\times 100$).

Fig 2—A 10-day pulmonary BCG lesion. In the center are disintegrating β -galactosidase-negative epithelioid cells, containing more than 10 faintly staining tubercle bacilli. Around the center are viable, young β -galactosidase-negative MN, several of which show ^3HT incorporation. Alveolar macrophages (AM), staining 3+ and 4+ for β -galactosidase, have accumulated in the surrounding alveolar area below the lesion. These AM contained no acid-fast bacilli, but several had incorporated ^3HT (not clearly shown in the photograph) (*in vitro* ^3HT , 5-bromo-4-chloro-3-indolyl- β -D-galactoside, carbolfuchsin and hematoxylin, $\times 400$).



1



2

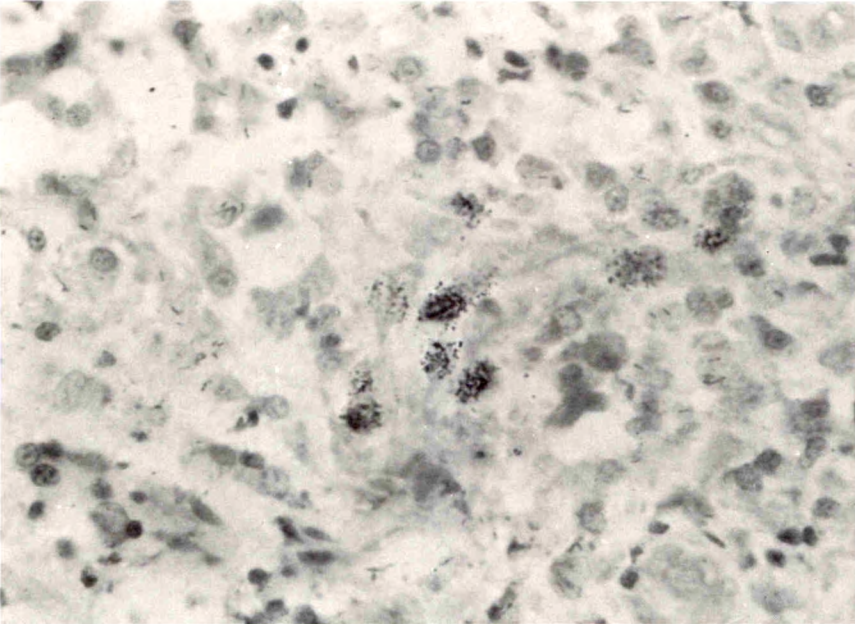
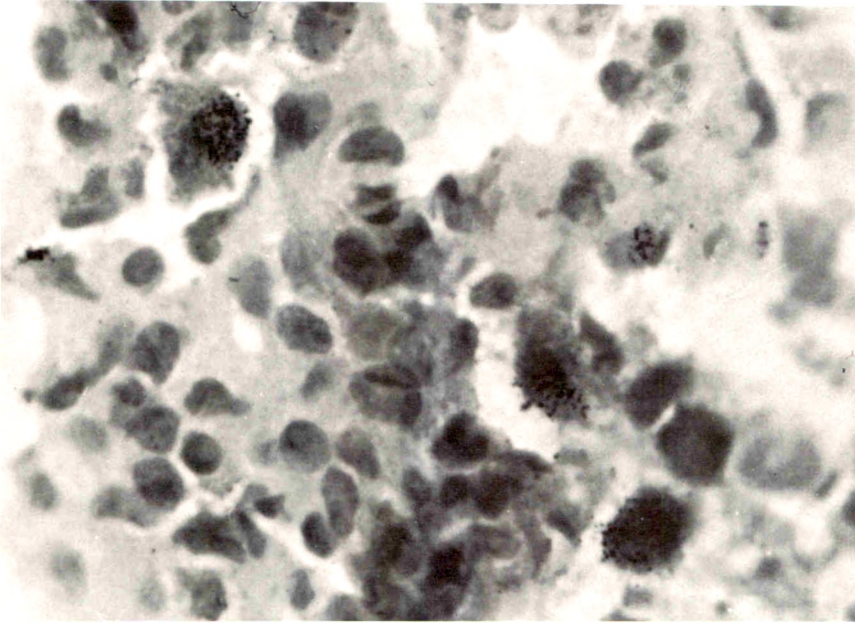
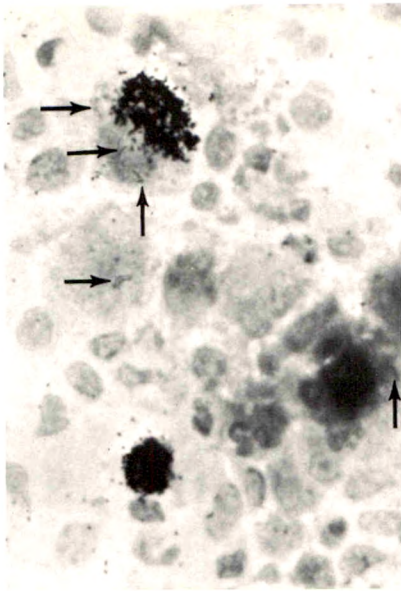
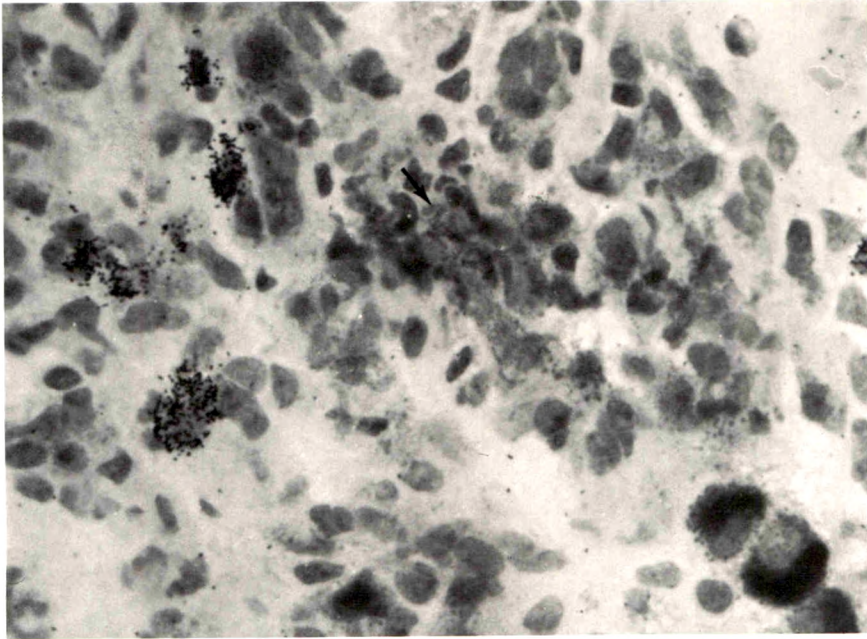
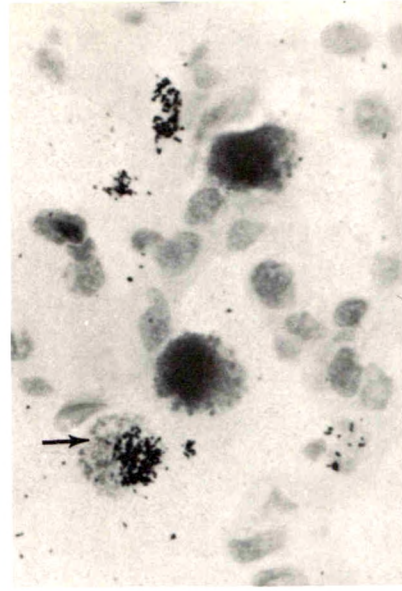


Fig 3—A 10-day *pulmonary* BCG lesion. Three large macrophages are depicted with ^3HT -labeled nuclei and 2+ cytoplasmic staining for β -galactosidase. Their striking blue color is not well demonstrated in black-and-white photographs (*in vitro* ^3HT , 5-bromo-4-chloro-3-indolyl- β -D-galactoside, carbolfuchsin and hematoxylin $\times 1000$). Fig 4—A 7-day *dermal* BCG lesion in Experiment IV (see Table 2). In this representative photograph, MN incorporating ^3HT show no bacilli in their cytoplasm, and MN containing bacilli do not show ^3HT incorporation. No MN are present that are doubly marked with both ^3HT and bacilli (*in vitro* ^3HT , carbolfuchsin and hematoxylin; $\times 600$).

5A



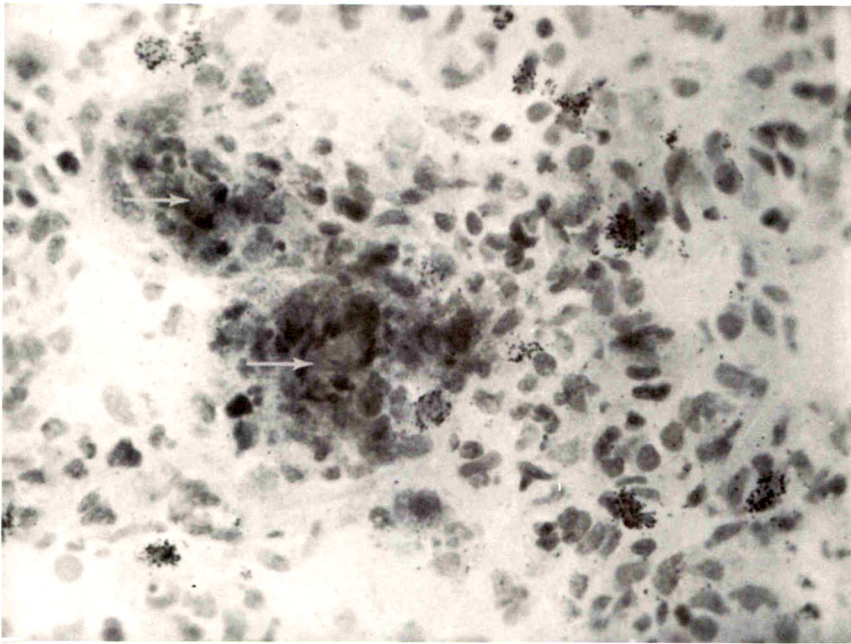
5B



6

Fig 5—Macrophages in 3-day *pulmonary* lesions produced by injecting BCG intravenously. **A**—An ^3HT -positive, 2+ β -galactosidase-positive macrophage contains over 10 bacilli (three arrows). Next to this cell is an ^3HT -negative, 1+ β -galactosidase-positive macrophage containing four bacilli (horizontal arrow). A 3+ β -galactosidase-positive MN with two bacilli (vertical arrow) and an ^3HT -positive, β -galactosidase-negative MN (possibly a lymphocyte) are also present. **B** is similar. An ^3HT -positive, 1+ β -galactosidase-positive macrophage containing two bacilli is marked with an arrow. Two 3+ β -galactosidase-positive (^3HT -negative) MN are also present. (^3HT -positive MN containing bacilli were rare, and could be found with assurance only in early pulmonary lesions.) (*in vitro* ^3HT , 5-bromo-4-chloro-3-indolyl- β -D-galactoside, carbolfuchsin and hematoxylin; $\times 720$). **Fig 6**—A 1-day *pulmonary* lesion produced by intravenously injected BCG. A small blood vessel (part of which is cut tangentially) is depicted with an embolus of tubercle bacilli in its center (arrow). The macrophages in this lesion stain 2+ for β -galactosidase. In the surrounding alveolar spaces, six or seven ^3HT -positive MN can be seen. In the lower right corner are three alveolar macrophages staining 3+ for β -galactosidase (*in vitro* ^3HT , 5-bromo-4-chloro-3-indolyl- β -D-galactoside, carbolfuchsin and hematoxylin; $\times 760$).

7



8

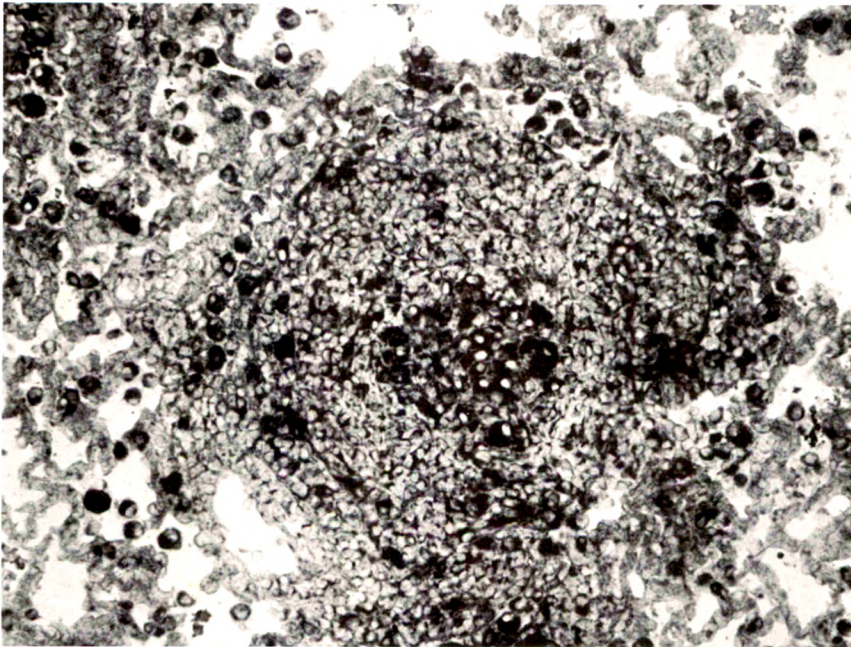


Fig 7—Two-day pulmonary lesions produced by intravenously injected BCG. Acid-fast tubercle bacilli (arrows) can be seen in the small necrotic centers. Cells of the blood vessel wall have a concentric arrangement around these centers. The rest of the lesions are composed of bright-blue, $2+$ β -galactosidase-positive MN, some of which also seem to be necrotic. In the surrounding alveolar areas, about a dozen young macrophages show ^3HT incorporation (*in vitro* ^3HT , 5-bromo-4-chloro-3-indolyl- β -D-galactoside, carbolfuchsin and hematoxylin; $\times 500$).

Fig 8—A pulmonary BCG lesion stained for cytochrome oxidase (CO) 6 days after 4×10^6 viable bacilli (opacity, 0.950) were injected intravenously. In the center are epithelioid cells rich in CO. Surrounding them are young infiltrating macrophages most of which are still poor in CO. At the periphery are numerous alveolar macrophages rich in CO, that were apparently attracted to the site by chemotactic agents released from the lesion. Some of the epithelioid cells in the center are already necrotic, but at this early stage their CO activity still remains (1,2,3,4-tetrahydroquinoline and *p*-aminodiphenylamine; no counterstain [see Dannenberg *et al*¹⁴] $\times 180$).

Participation of Components of the Blood Coagulation System in the Inflammatory Response

Donald G. McKay, MD

THE INFLAMMATORY RESPONSE and blood coagulation mechanism, as separate fields of study, have been analyzed continuously for many years. A great deal of information on both phenomena has been acquired through numerous investigations, and yet, no definitive explanation of the mechanisms of these basic biologic reactions has, as yet, been achieved.

In the recent past, several experiments provided evidence indicating that components of the blood coagulation mechanism play a role in certain types of inflammation—the Arthus reaction, arthritis produced by sodium urate crystals and the local Shwartzman reaction—each of which represents a special type of inflammation, although they obviously share mechanisms in common.

It is the purpose of this review to present known points of interdigitation between the blood coagulation mechanism and the inflammatory response and to question the extent to which they can be applied, as generalizations, to all inflammatory reactions. It is conceivable that from the backlog of information in each field, mechanisms now considered to apply exclusively to the clotting system may be found applicable to the inflammatory process and vice versa.

Fibrinogen—Fibrin

Fibrin deposition plays a major role in some inflammatory reactions, whether it is deposited within or outside of blood vessels supplying inflamed tissue. The deposition of fibrin in any location carries with it certain implications. Fibrin formation is the end stage of the blood coagulation mechanism. Thus far two pathways for initiating coagulation have been elucidated: a) the intrinsic system, initiated by surface contact with activation of Hageman Factor and Factor XI and b) the extrinsic system, initiated by tissue thromboplastin which requires Factor VII as an intermediary substance. These two systems converge

From the Department of Pathology, University of California School of Medicine, San Francisco General Hospital, 1001 Potrero Avenue, San Francisco, California 94110.

Supported by Grant HE-12033 from the National Institutes of Health United States Public Health Service.

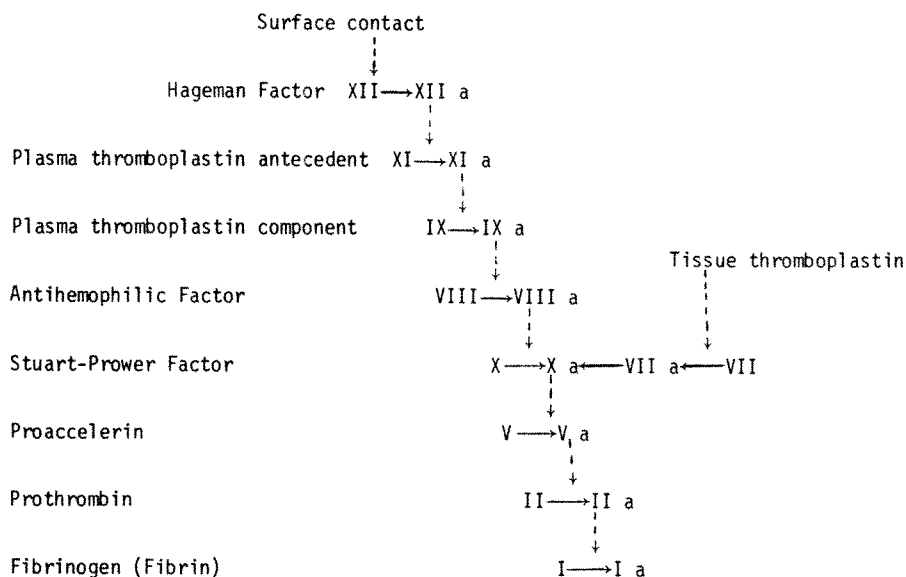
at the point in which Factor X is activated and from thereon the reaction is the same for both (Text-fig 1).

Fibrin deposition in any location implies that certain precursors were present. Factor X (Stuart-Prower), Factor V (proaccelerin), phospholipid (platelet factor 3), Factor II (prothrombin), thrombin and calcium are required in addition to an activator of the intrinsic or extrinsic system. The inactive precursor substances are all present in circulating blood and are readily available for intravascular fibrin deposition. Most often the presence of fibrin outside blood vessels probably is due to blood that has leaked from the vessel into the surrounding tissues.

Inflammation of Connective Tissue

Experimental (intravascular and extravascular fibrin). Two different types of experimentally induced inflammation illustrate the role of fibrin in the inflammatory response.

ACUTE INFLAMMATION PRODUCED BY BACTERIAL ENDOTOXIN: Small doses of lipopolysaccharide (bacterial endotoxin), injected subcutaneously, induce an inflammatory response characterized by: a) increased permeability of the microcirculation and b) leukocyte adherence to the endothelium and migration into connective tissue. As early as 4 hours



TEXT-FIG 1—The essentials of the coagulation cascade based on the concept of Davie and Ratnoff¹ and MacFarlane.²

after 0.1 mg of endotoxin (Difco Bacto-Lipopolysaccharide) is injected into rabbit skin, electron microscopy revealed small deposits of fibrin adherent to the capillary endothelium (Figure 2). A few capillaries contain small aggregates of platelets, and small amounts of fibrin can be seen in connective tissue.

Seventeen hours later, the intravascular deposits have become so large that focal thrombi occlude the lumens of capillaries (Figure 3) and the amount of extravascular fibrin is greatly increased. Exposure to bacterial endotoxin represents a nonspecific (nonimmune) inflammatory reaction clearly associated with fibrin deposition within the microcirculation (thrombosis) and outside the vessels (plasma leakage).

The manner in which the intrinsic and/or extrinsic activator systems are involved in this process has not been determined. Although bacterial endotoxin is known to activate Hageman Factor directly,³ there is reason to suspect that *in vivo* it induces the appearance of an endogenous Hageman Factor activator. Collagen is capable of activating Hageman Factor *in vitro*,⁴ but whether it acts on plasma that has leaked from the vessels *in vivo* remains to be determined. Extrinsic prothrombin activator may play a role, since potentially tissue thromboplastin is available from any cell damaged by the inflammatory agent.

THE DIRECT ACTIVE ARTHUS REACTION: A second type of inflammatory response, illustrating immunogenic inflammation, is the direct active Arthus reaction. This reaction takes place when precipitating antibody from the bloodstream and antigen from surrounding connective tissue unite, together with complement, in the vessel walls.^{5,6} The early response is an intense polymorphonuclear leukocyte infiltrate and increased vascular permeability followed, at 5 to 6 hours, by grossly visible hemorrhagic necrosis of the region injected with antigen. The hemorrhagic necrosis is caused by thrombosis of the microcirculation. The fact that pretreatment with heparin prevents the thrombosis and hemorrhagic necrosis,⁷ indicates that fibrin and the conversion of prothrombin to thrombin are essential to this phase of the reaction.

Although antigen-antibody complex is known to activate Hageman Factor, the same questions that were raised for endotoxin can be raised for antigen-antibody complex with respect to the precise manner in which extrinsic and/or intrinsic prothrombin activators are themselves activated.

For these two categories of inflammation, it is clear that: a) fibrin deposition is part of the inflammatory reaction, b) fibrin deposition occurs *late* in the reaction (4 to 8 hours), c) intravascular fibrin is responsible for ischemic tissue damage, d) extravascular fibrin deposi-

tion occurs in both types of inflammation and is indicative of leakage of blood from the vessels, e) since fibrin formation requires fibrinogen, thrombin, prothrombin, proaccelerin, Stuart-Prower Factor, calcium and either activation of the contact system or tissue thromboplastin, these components of the blood coagulation mechanism participate in the later phase of the inflammatory response.

Clinical-Ischemic Peripheral Corneal Disease. Knowledge that thrombosis or fibrin deposition is part of the inflammatory response is of more than theoretic significance; it has been put to practical use by Aronson *et al.*⁸ Twenty-two patients with inflammatory reactions of the cornea, characterized by a progressive wasting away of the peripheral cornea, sometimes leading to perforation, were treated with heparin. The patients were classified as having: a) primary ischemic corneal disease (idiopathic) (including Terriens' senile marginal degeneration and Mooreus' ulcers) and; b) secondary ischemic corneal disease (including infections by *Pseudomonas aeruginosa*, paracolon bacillus and Herpes simplex; chemical inflammation produced by acid and alkali burns; postoperative necrosis and necrosis of corneal grafts). Patients with idiopathic necrosis were treated with heparin alone, while those with a known pathogenetic mechanism (secondary) were treated with adrenal corticoids and antibiotics as well as heparin. Ninety-six percent of the eyes involved improved and 71% improved dramatically; often, vision was restored completely.

Glomerulonephritis (Intravascular and Extravascular Fibrin)

In certain types of inflammation, extravascular fibrin deposition may play a demonstrably significant role in the inflammatory process. In some specific types of glomerulonephritis, both experimental and clinical, the deposition of fibrin appears to be the lethal factor.

Experimental (Nephrotoxic Nephritis)

The experimental model that best demonstrates the possible lethal effects of extravascular fibrin deposition is nephrotoxic nephritis. Anti-kidney antibody injected into the bloodstream of the animal species from which the kidney antigen was obtained results in glomerulonephritis characterized by: a) swelling of endothelial cells, b) fusion of foot processes of glomerular epithelium, c) glomerular capillary thrombosis, d) extravasation of plasma with fibrin deposition in capsular spaces (Figure 4) and e) eventual crescent formation in the capsular space (Figure 5). Fifty to ninety percent of the animals die of renal insufficiency.

Silfverskiöld,⁹ Kleinerman¹⁰ and Halpern¹¹ demonstrated that heparin, administered systemically, reduced proteinuria, hematuria and the mortality rate from 50 to 10%. That this effect was due to the antithrombotic (anticoagulant) activity of heparin and not to an "anticomplementary" effect was shown by Vassalli and McCluskey,¹² who successfully reduced the mortality rate by administering the anticoagulant warfarin.

Light and electron microscope studies revealed a significant diminution in glomerular thrombi and in the formation of crescents in these animals (Figure 6). The formation of thrombi, with rupture of capillary vessels, leakage of plasma with fibrin deposition in the capsular space and the subsequent formation of fibrous crescents appear to be the lethal factor in this disease process. The precise mechanism by which fibrin deposition results in crescent formation remains to be elucidated. One possibility is that leakage of plasma into the capsular space, with extravascular fibrin deposition, results in fibroblast proliferation so that fibrin is replaced by connective tissue, in essence, the chain of events in ordinary wound healing.

Clinical (chronic progressive glomerulonephritis)

The beneficial effects of anticoagulants on experimental nephritis led Kincaid-Smith¹³ to use anticoagulant therapy in certain forms of human glomerulonephritis. In addition to heparin and phenindione, Kincaid-Smith used an anti platelet-aggregating agent, dipyridamole, in these patients. This agent produced beneficial effects on several severe and/or previously fatal renal disorders, but the disorder most germane to this discussion was chronic progressive glomerulonephritis. In 1 patient, clinical laboratory evidence of renal damage cleared completely after a year's treatment, and histologic examination revealed a return to essentially normal glomeruli. This effect was observed in a disease which, for all practical purposes, is irreversible with the usual modalities of therapy. Also, it demonstrates the important role of platelets and fibrin in this form of glomerular inflammation.

These experimental and clinical observations indicate that platelet damage and fibrin deposition are not only a part of the inflammatory process but, in certain specific diseases, they are the major factor, whether the end-point is local tissue necrosis or mortality.

Hageman Factor

Several recent studies of activated Hageman Factor indicate that it not only plays a role in fibrin deposition, but it also participates, as an integral part, in the early stages of the acute inflammatory response.

Inflammatory Response to Purified Activated Hageman Factor

Perhaps the keystone experiment in implicating Hageman Factor in the inflammatory response was that of Ratnoff and Miles¹⁴ who, in earlier studies,¹⁵ had obtained a highly purified Hageman Factor. Using this material, concentrated 5000 times and activated by ellagic acid, Ratnoff and Miles injected guinea pigs intracutaneously and observed increased vascular permeability to circulating Pontamine Sky Blue at the site of injection. The reaction was inhibited by soybean trypsin inhibitor.

Subsequently, the influence of activated Hageman Factor on leukocyte sticking and migration was demonstrated by Graham *et al.*¹⁶ Purified activated Hageman Factor (human), injected into the rabbit ear chamber, produced a delayed and prolonged inflammatory response characterized by prominent sticking and emigration of leukocytes. (In its inactive form Hageman Factor had insignificant inflammatory effects). These experiments indicate that activated, purified Hageman Factor is capable of inducing two major components of the local acute inflammatory response—increased vascular permeability and leukocyte migration.

Hageman Factor and Experimental Gouty Arthritis

The fact that activated purified Hageman Factor is capable of producing an inflammatory response experimentally does not necessarily mean that it participates in the inflammatory response caused by various agents. Therefore, Kellermeyer's studies provided an important extension of the theory, since he demonstrated that a known inflammatory agent (monosodium urate crystals) produced gouty arthritis by activating Hageman Factor.

Urate crystals play a primary role in the clinical syndrome of acute gouty arthritis.¹⁷ Crystals of monosodium urate are found in the synovial space of affected joints and acute arthritis is produced by injecting urate crystals intra-articularly.¹⁸

Kellermeyer and Breckenridge¹⁹ demonstrated that monosodium urate crystals activate Hageman Factor in normal blood plasma; amorphous urates failed to activate Hageman Factor, whereas other crystalline substances, including sodium orotate, hypoxanthine and calcium pyrophosphate, did. All of these substances migrated toward the anode in an electrophoretic field, indicating that the crystals carried a negative charge. The negative charge on the surface of glass is thought to be a major factor in the activation of Hageman Factor.²⁰

Subsequently Kellermeyer and Breckenridge²¹ showed that Hage-

man Factor (as well as plasma thromboplastin antecedent (Factor XI), predominantly in inactive form (99%), is present in normal synovial fluid.

In a later series of experiments, Kellermeyer²² demonstrated that: a) urate crystals induce permeability enhancing activity in synovial fluid, b) an antibody to purified Hageman Factor inhibited the permeability factor, c) ellagic acid could be substituted for urate crystals with the same results, and d) enhanced permeability could be produced in normal plasma but not in Hageman-deficient plasma.

He concluded that the high negative charge on the surface of urate crystals activated Hageman Factor which, in turn, activated the kallikrein system, causing local increased vascular permeability and, thus, gouty arthritis. What remained somewhat equivocal at this point was whether or not the kallikrein system was responsible for the cellular exudate. Kellermeyer suggested that leukocyte chemotaxis might possibly be due to the activation of complement.

Hageman Factor and the Kinin System

The kinin system has long been thought to play a role in the inflammatory response. As Lewis²³ pointed out, this hypothesis is based on the fact that even in small quantities, kinins increase blood flow as well as vascular permeability and induce pain and, possibly, leukocyte emigration. Concentrations of kinins are increased at sites of tissue damage and induce an inflammatory response when injected into the joint space. Kinins are released from kininogen by cellular elements of acute inflammatory reactions and their release is inhibited by anti-inflammatory compounds, such as cortisol and colchicine. Lymph draining a limb damaged by trauma, heat or ischemia contains increased concentrations of kinins.

Although there is little doubt that kinins and some of the precursor enzymes—*ie*, PF-dil, kallikrein—increase vascular permeability, the precise role of the kallikrein system in spontaneous acute inflammation is somewhat problematic. Also, there appears to be some question about the ability of kinin to cause leukocyte sticking and emigration.

Webster²⁴ pointed out that kinins are liberated into the plasma in one form of acute inflammation of circulating blood—anaphylaxis. Plasma kininogen levels fall²⁵ when circulating blood is exposed to bacterial endotoxin, another agent causing acute inflammation of circulating blood. Plasma kinin levels are elevated during the first hours after blood is exposed to bacterial endotoxin.²⁶ This finding constitutes

strong evidence for a role of the kallikrein system in spontaneous acute inflammation.

The first evidence of a relationship between the kallikrein²⁷ and clotting systems came from Margolis' studies demonstrating the appearance of a factor that increases vascular permeability when human plasma is exposed to a glass surface. This reaction did not take place in Hageman Factor deficient "noncontact" or plasma heated to 60C for 20 minutes. Margolis stated: "although the permeability factor and plasma kinin are not the same, they seem to represent different products of the same chain of reactions."

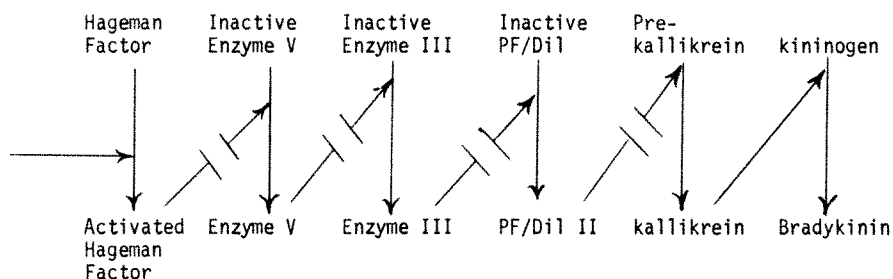
Webster²⁴ presented the current (1970) working hypothesis of the plasma kallikrein system (Text-fig 2).

Although she cautioned that this concept is subject to revision when further purification and characterization of these enzymes allow a more definitive sequence, there is little question that activated Hageman Factor is capable of activating the kallikrein system.

Activation of Complement by Hageman Factor

The complement system is composed of a chain of nine enzymes which act, in sequence, upon each other and are triggered by the activation of C1 esterase.^{28,29} These enzymes can be derived from the α -, β - and γ - globulins of blood plasma and their molecular weights range from 79,000 to 400,000. When the complement system is activated, small molecular fragments are derived. These fragments have been shown to play an important role in certain types of inflammation.

Fragments C3a (MW 7,000) and C5a (MW 10,000 to 15,000) act as *anaphylotoxins* capable of releasing histamine from mast cells, causing smooth muscle contraction, changes in capillary permeability and hypotension. Another major action of these fragments is their ability to cause directed migration of leukocytes into areas of antigen-antibody



TEXT-FIG 2—Current Working Hypothesis of Plasma Kallikrein System.

reactions—*ie*, chemotaxis; C6 and C7 also appear to have chemotactic properties.

The role of complement as a permeability and chemotactic factor was first established for immune inflammatory reactions. Ward and Cochrane⁶ prevented the reverse passive Arthus reaction by lowering complement levels in circulating blood. Similar results were observed in experimental glomerulonephritis and serum sickness.³⁰

That complement may play a role in nonspecific (nonimmune) inflammation is indicated by the studies of Willoughby *et al.*³¹ These investigators lowered complement levels in circulating blood to varying degrees by intravenously injecting heat-aggregated γ -globulin, antigen-antibody complex, antilymphocyte serum, carageenin, antipolymorphonuclear leukocyte serum and anticomplement serum. Using rats and guinea pigs, they induced a skin inflammatory response and quantitated inflammation by measuring the water content of skin 4 hours after injury. A direct relationship existed between the degree of blood complement depletion and the amount of increase in the water content of skin. They concluded that complement plays a significant role in non-allergic as well as allergic acute inflammation.

A connection between the complement system and Hageman Factor was first established by Donaldson.³² She demonstrated that plasma from patients with hereditary angioneurotic edema lacked an inhibitor of C1 esterase. This lack seems to be the essential defect in these individuals. During clinical attacks of edema, evidence of spontaneous activation of C1 esterase is found in patient plasma.³³ In a later study, Donaldson used ALTEE (N-acetyl-L-tyrosine ethyl ester monohydrate) esterase activity, in the test system. This substance was identified with C1 esterase because it was associated with the development of a property which inactivated C4 and because its activity was reduced by a purified C1 esterase inhibitor.

In this study, purified activated Hageman Factor enhanced the generation of C1 esterase activity in plasma from patients with hereditary angioneurotic edema. Fractionation (purification) of plasma from patients with Hageman Factor-deficiency yielded a protein which failed to activate C1 esterase in hereditary angioneurotic edema plasma, and failed to activate the coagulation system.

The fact that Hageman Factor did not activate C1 esterase in normal plasma was thought to be due to the presence of normal inhibitor.

Two other substances, heparin and soybean trypsin inhibitor do not inhibit C1 esterase, but do have an inhibitory effect on the release of C1 esterase from the plasma of patients with hereditary angioneurotic

edema, when the plasma is exposed to activated Hageman Factor. These substances do not act directly to inhibit Hageman Factor itself. Ratnoff³⁴ demonstrated that heparin can block the interaction of PTA (Factor XI) and PTC (Factor IX), initiated by activated Hageman Factor. Breckenridge and Ratnoff³⁵ showed that soybean trypsin inhibitor interferes with activation of Factor V (proaccelerin) by Factor X (Stuart-Prower Factor); soybean trypsin inhibitor and heparin interfere with the release of kinin when plasma is exposed to glass. Thus, these two agents inhibited both the release of kinin and C1 activation under similar conditions. Donaldson concluded that soybean trypsin inhibitor and heparin inhibited some intermediate step in the chain of enzymes in the coagulation sequence.

Polymorphonuclear Leukocytes and Hageman Factor

The migration of polymorphonuclear leukocytes through vessel walls into connective tissue and their subsequent disintegration in the extravascular location is a long established feature of acute inflammation. That this process may be cyclic is suggested by the studies of Hurley³⁶ who showed that saline extracts of polymorphonuclear leukocytes were capable of inducing leukocyte migration *in vivo*. Concentrations of 50 million cells/ml or higher were required to induce leukocyte migration when the cells were incubated in saline, whereas concentrations as low as 6 million/ml were effective when the cells were incubated with serum. Similar results were obtained using the *in vitro* system—*ie*, leukocyte migration through the millipore filter of the Boyden chamber. Thus, leukocytes can generate leukocyte chemotaxis.

The relationship of polymorphonuclear leukocytes to the kinin system and Hageman Factor has been shown by Melmon and Cline,³⁷ who demonstrated that normal human granulocytes and eosinophils have both kinin generating and kininase activities *in vitro*. At physiologic pH, these activities were found predominantly in the soluble cell fraction. At pH 5.5, leukocyte granules exhibited a similar property. In these experiments, kinins were generated *in vitro* in normal plasma but not in plasma deficient in Hageman Factor. These findings may have an implication for the *in vivo* inflammatory response and not only suggest that plasma kallikrein is required for leukocyte-mediated release of kinin but that Hageman Factor is also necessary. Although a direct relationship between Hageman Factor and leukocyte migration has not been shown in a similar system, the demonstration by Graham *et al*¹⁶ that activated Hageman Factor produces leukocyte migration *in vivo* is suggestive. It is possible that the perpetuating influence of extra-

vasated polymorphonuclear leukocytes on inflammation may be mediated by their action on Hageman Factor.

Plasmin

Whether or not the plasminogen-plasmin system plays a role in inflammation is problematic. Wherever fibrin is deposited, plasminogen is deposited. The active enzyme, plasmin, is capable of degrading fibrin and has been shown to clear unwanted fibrin from the vascular system. Plasminogen requires an activator, and endogenous activator has been demonstrated by Todd³⁸ in the vascular endothelium, predominantly in veins and venules. Thus, from the standpoint of anatomy, the pro-enzyme and activator are potentially available in blood and tissue for the inflammatory response.

Two studies suggest a link between plasmin and the inflammatory response. Ratnoff³⁹ demonstrated that plasmin was capable of producing increased capillary permeability in the guinea pig skin. Lepow, Ratnoff and Levy⁴⁰ showed the effects of plasmin on the early reacting components of the complement system (C1, C4, C2 and C3). Generation of the chemotactic activity was blocked by EACA.

Taylor⁴¹ and Ward⁴² have shown that polymorphonuclear leukocyte chemotactic activity can be generated in rabbit serum by plasminogen streptokinase mixtures. In addition, they found that plasmin destroys the biologic activity of the trimolecular complex.

These observations, linking increased capillary permeability, complement activation and cell migration to plasmin, are of great interest, but the precise role of plasmin in inflammation is not clear. Studies of the effects of plasmin inhibitors on the inflammatory response *in vivo* have yielded conflicting results. Weimer⁴³ found that crystalline soybean trypsin inhibitor, applied to the cornea of rabbits up to 6 hours after injury, prevented not only exudation but most of the subsequent inflammatory response. This is difficult to reconcile with our own observation that soybean trypsin inhibitor not only failed to prevent the inflammatory response in the skin of rabbits injected locally with kaolin or bacterial endotoxin, but that the soybean trypsin inhibitor, by itself, produced an intense exudation of cells and fluid into connective tissue. It is also at odds with the observation by Allison *et al*⁴⁴ that soybean trypsin inhibitor, given intravenously, did not modify the reactions to thermal (burn) injury, as seen in the ear chamber of rabbits. They also reported that EACA, another plasmin inhibitor, failed to modify the thermal inflammatory response.

It may be that plasmin plays a role in the inflammatory response, but that it is obscured by more potent agents.

Platelets

Because of their exclusively intravascular existence and important role in blood coagulation, platelets are seldom considered participants in the inflammatory process. Yet, obviously, wherever fibrin is deposited within vessels in any inflammatory response where the intrinsic prothrombin activator system is the trigger mechanism, platelets participate through their required contribution of phospholipid (platelet factor 3).

In a much less obvious manner, platelets participate in at least one type of local inflammation—*ie*, the direct active Arthus reaction. Margaretten⁴⁵ has shown that the platelet is absolutely essential for the reaction. He sensitized rabbits with crystalline bovine serum albumin (BSA) and Freund's adjuvant and 6 weeks later challenged them with an intradermal injection of BSA. The animals were killed 8 hours after the challenging injection and the skin sites examined by light microscopy. An antibody to rabbit platelets, prepared in goats, was injected into the test rabbits 30 minutes before and 3½ hours after the challenging intradermal injection of BSA. A virtually complete thrombocytopenia, in the presence of an unchanged leukocyte count, was maintained for the 8-hour period of examination.

Removing the platelets from circulating blood not only prevented thrombosis and hemorrhagic necrosis characteristic of the late phase of the direct active Arthus reaction, but prevented endothelial sticking and the emigration of leukocytes into perivascular connective tissue. Since Ward and Cochrane⁶ had shown that the reverse passive Arthus reaction was prevented by removing complement from the circulation and, since platelet antigen-antibody complex in circulating blood could be expected to activate (bind) complement, it was necessary to determine whether or not complement depletion prevented the direct active Arthus reaction. Measurements of C3 revealed that this component of the system was not depleted and, by using the Boyden chamber, it was shown that enough complement remained in rabbit serum to cause migration of leukocytes *in vitro*.

Subsequent studies by Margaretten,⁴⁶ using pharmacologic agents to prevent the aggregation and release of platelets confirmed the conclusion that the direct active Arthus reaction was prevented by removing circulating platelets. The intravenous infusion of prostaglandin E and dipyridamole, both of which prevent platelet aggregation, and neither of which is known to affect the complement system, prevented the reaction.

To understand the mechanism of action of platelets in the Arthus reaction, it must be realized that to produce local inflammation, antigen-antibody and complement must be present in perivascular connective tissue. Complement (C5 is probably the major component) is the proximate chemotactic agent for leukocytes, but in this reaction, antigen-antibody complex is required for activation. Since antigen had been injected into the connective tissue, in the thrombocytopenic animals either antibody or complement or both failed to cross the vascular barriers into the connective tissue. Fluorescein labeled γ -globulin was present in perivascular connective tissue in the Arthus reaction but was absent from the injection site in thrombocytopenic animals. This suggests that platelets are necessary for the exudation of γ -globulin from the blood vessel in this reaction. According to Humphrey,⁴⁷ thrombocytopenia does not prevent the reverse passive Arthus, indicating that platelets are not necessary for the diffusion of antigen from the blood vessel. The explanation may lie in differences in the molecular size of antigen (approximately 40,000 BSA) and antibody (γ -globulin 160,000) and/or the nature of the action of platelet permeability factor.

Since platelets seemed to be necessary for the diffusion of γ -globulin, they were first thought to act by releasing histamine and/or serotonin. Kniker and Cochrane⁴⁸ and Henson and Cochrane⁴⁹ showed that in serum sickness, platelets, histamine and serotonin influence the localization of antigen-antibody complexes. However, when histamine and/or serotonin were injected locally or systemically into thrombocytopenic animals they failed to restore the direct active Arthus reaction. However, the systemic infusion of platelets did restore the reaction and it seemed likely that platelets contained some other permeability factor. Mustard⁵⁰ demonstrated such a factor. This factor (or factors) which increases vessel permeability passes through a dialysis sac and is heat stable. Fractionation through Diaflo filters indicated permeability activity in substances of molecular weight 10,000 to 20,000, 1000 to 10,000 and in molecules smaller than 1000. Some of the activity in the low molecular-weight fraction may have been due to histamine. The exact nature of platelet permeability factor remains to be determined. It, or something like it, seems to be required for the exudation of γ -globulin in the direct active Arthus reaction.

It may be that platelets have this function only in the special case of the direct active Arthus reaction. The intradermal injection of heat-aggregated γ -globulin in thrombocytopenic animals resulted in a typical acute inflammatory response histologically,⁴⁵ indicating that platelets are not essential in this nonspecific inflammatory response. Nevertheless,

to what extent platelets participate in the inflammatory response in a general and nonimmune sense, remains to be determined.

Systemic Activation of the Coagulation Mechanism and Local Acute Inflammation

Depending on when it occurs, an episode of disseminated intravascular coagulation may produce more or less opposite effects on local inflammation. If it develops after local inflammation is established, the inflammatory site may be converted into an area of gangrenous necrosis. If it precedes the local injection of an inflammatory agent, it may completely prevent inflammation.

Hemorrhagic Necrosis—the Local Shwartzman Reaction

The injection of small amounts of bacterial endotoxin into the skin results in a typical nonspecific acute inflammatory response. This reaction will subside within a few days, leaving little or no evidence of its existence. However, if at some time between 6 and 72 hours after the skin injection a second injection is given intravenously, the area of local inflammation is converted into a hemorrhagic necrotic slough.⁵¹ The hemorrhage and necrosis are due to the development of occlusive thrombi in the microcirculation (venules and capillaries) of the local area. This reaction was originally thought to be a "hypersensitivity" phenomenon. However, that it is predominantly a phenomenon related to the blood coagulation system and is not specific for the development or presence of specific antibodies, is indicated by the fact that the intravenous injection of endotoxin can be substituted for by such immunologically inert substances as kaolin, starch, glycogen, carageenin and India ink.⁵² All of these substances act by virtue of their ability to agglutinate platelets, activate Hageman Factor and activate α -adren-ergic receptor sites.

The conversion of a rather innocuous, transient, acute inflammatory process into a problem of gangrenous ischemic necrosis is a rather striking event. Clearly, it is mediated by a sudden increase in the local thrombotic phenomena initiated by the local injection of endotoxin, but the precise and proximate mechanism of this increase has not yet been elucidated.

The local Shwartzman reaction is only illustrative of this type of response which occurs in a variety of other clinical and experimental circumstances agents other than bacterial endotoxin.

Prevention of the Local Inflammatory Response Associated with Disseminated Intravascular Coagulation

The studies of Jancso⁵³ provide evidence that changes associated with the prior triggering of the blood coagulation mechanism sys-

temically, will prevent manifestations of a local inflammatory response.

Jancso's end points of observation of the inflammatory response were twofold: a) histologic observation of the deposition of intravenously administered colloidal silver on the endothelium of the microcirculation and in perivascular macrophages at the inflammatory site and; b) edema fluid was quantitated in the rat by measuring the increase in weight of the injected hindpaw. Unfortunately, the emigration of polymorphonuclear leukocytes was not studied. Jancso used a variety of inflammatory agents, including 5-hydroxytryptamine, compound 48/80, Wittes' peptone, dextran, kallikrein, human saliva, staphylococcus culture filtrate, bee venom and a variety of snake venoms.

Jancso believed that some kind of clotting process was involved in the mechanism of inflammation. Specifically, he evolved the theory that the fibrin which formed on the vascular endothelium at the site of inflammation, trapped colloidal silver and increased capillary permeability to fluid. He systemically administered "anticoagulants" and "defibrination" of blood to verify this theory. Although our own interpretation differs from the author's, the observations remain and seem to be of major interest in the light of newer knowledge of the action of the complement system and the blood coagulation system.

Jancso's first observation was that heparin, administered systemically, did not influence the inflammatory reaction. This finding has been confirmed by Allison and Lancaster⁵⁴ and constitutes strong evidence against the concept of fibrin deposition as the mechanism involved.

His next experiments involved the systemic administration of agents he classified as "anticoagulants." These agents included Liquoid (sodium polyanetholesulphonate) and the inorganic salts of the rare earths lanthanum, cerium, neodymium, praseodymium and samarium as well as the organic compounds Helodym 88 (didymium salt of β -acetyl propionic acid) and Thrombodym (neodymium salt of sulfo-isonicotinic acid). We now know that these substances, administered intravenously, are not "anticoagulant" but are procoagulant. In large concentrations they produce disseminated intravascular coagulation by activating Hageman Factor and platelet agglutination.

When high doses of these substances were given intravenously before the inflammatory agents were injected locally, evidence of inflammation did not appear. Our interpretation of these observations is that some change associated with disseminated intravascular coagulation prevented the inflammatory response to a wide variety of inflammatory agents.

Jancso's next experiment supports this concept. He induced disseminated intravascular coagulation to the point of "afibrinogenemia"

by infusing thrombin intravenously, which prevented the inflammatory response. With respect to animal experiments, the infusion of thrombin is the most direct and proximate means of producing disseminated intravascular coagulation.

In these experiments, a relationship between the systemic blood coagulation mechanism and the acute local inflammatory response is clearly established. What remains to be determined is the precise mechanism of this relationship and the points of interdigitation. The possibility that the points of overlap lie in activation of Hageman Factor and/or complement, raise a variety of intriguing questions.

As an addendum, Jancso produced local inflammation by injecting a variety of components of the coagulation mechanism, including thrombin, tissue thromboplastin and cephalin as well as Russell's viper venom. At first, this finding might seem to represent additional evidence of a relationship between the clotting mechanism and acute nonspecific inflammation. However, with the exception of thromboplastin, which was obtained from rat brain, all of these substances were heterospecific to the rate—*ie*, the source of thrombin was bovine; cephalin was obtained from pig brain; and the venom from the snake. The inflammation produced may have been an immune type related to heterospecific antibodies. Hence, the inflammation observed cannot be considered conclusive until the same result is obtained with species specific substances. Despite this, tissue thromboplastin can be accepted as a local acute inflammatory agent.

With a different purpose in mind and with a different ultimate interpretation, Willoughby³¹ recently repeated the fundamental observations of Jancso. The two studies are mutually confirmative and, taken together, provide additional insight into each other.

With the knowledge that de complementation of circulating blood prevents the immune inflammation of the indirect passive Arthus reaction, Willoughby raised the question of whether or not complement participated in nonspecific (nonimmune) acute inflammation.

His experimental procedure mainly involved heat as the inflammatory stimulus, but occasionally also turpentine. The end point in his study was the amount of edema at the inflammatory site based on wet weight/dry weight ratios. Complement levels in the circulating blood were reduced by a variety of means including antigen-antibody complexes (*ie*, antibodies to polymorphonuclear leukocytes, lymphocytes), heat-aggregated gamma globulin, antibody to complement and particulate matter (carrageenan).

There was a proportional relationship of the amount of edema and

the percent decrease in complement. His conclusion was that complement is as essential to the evolution of the nonspecific acute inflammatory response as to immune inflammation.

This was a major contribution to an understanding of the mechanism of inflammation. However, the materials and methods used contain other implicit interpretations which relate to Jancso's experiments. The main point is that the agents used to reduce (activate) complement in the circulating blood also produce disseminated intravascular coagulation by activating Hageman Factor and aggregating platelets. It is noteworthy that the greatest reduction in local edema was produced by the particulate matter carrageenan which also caused the greatest reduction in circulating complement. Carrageenan has long been known to activate the coagulation mechanism. Parenthetically, crystals of uric acid represent another particulate substance which has been demonstrated to activate both Hageman Factor and complement.

Complement depletion appears to be the proximate mechanism of preventing the local inflammatory response in Willoughby's and Jancso's experiments. But, since the coagulation mechanism was also triggered in both studies, the role of Hageman Factor or some other enzyme in the coagulation cascade is again questioned. It is possible that introducing these substances into the circulating blood activated complement directly and Hageman Factor simultaneously. It is equally possible that Hageman Factor was the primary target, triggering the complement system.

Basic Biologic Properties Common to Certain Inflammatory Agents

In addition to the specific experiments cited above, the inflammatory response and blood coagulation mechanism are brought close together by certain shared basic biologic properties of inflammatory agents.

Four inflammatory agents—bacterial endotoxin (lipopolysaccharide), antigen-antibody complex (protein + γ -globulin), heat-aggregated γ -globulin and particulate matter (carrageenan, sodium urate crystals)—commonly share the following biologic properties:

1. Produce local acute inflammation^{5,19,55,56}
 - a) Fluid exudation
 - b) Sticking of leukocytes to endothelium and leukocyte emigration (chemotaxis)
2. Activate complement^{6,31,57,58}
3. Activate Hageman Factor^{3,19,59}
4. Aggregate platelets and release platelet constituents⁶⁰⁻⁶⁴

These lists are only partial and, undoubtedly, there will be additions in the future.

At least two ideas are implicit in the above experimental observations:

1. Agents capable of activating the blood coagulation system as well as the inflammatory response provide evidence that the two systems share mechanisms and components in common and;

2. Inflammatory agents, thus far studied, are of such widely divergent chemical composition that their shared biologic activities are not mediated by their chemical components but rather by a property which the surface of the molecules, aggregates and particulate substances have in common. Most likely this is a physical property of their surfaces and provides an interesting example of the interface between a physical force and a chain of biochemical reactions.

Melmon and Cline²⁶ pointed out other interesting analogies on the subject. They noted that "plasma kinin, complement and intrinsic blood coagulation systems are similar in several ways and share certain key intermediates. Each is a complex system of serum proteins whose activities are latent until activated. Activation of both the intrinsic clotting system and the kinin system is initiated by activation of Hageman Factor. . . . the clotting process proceeds through a complex series of steps in which each clotting factor is sequentially activated and, in turn, acts on the next factor. This series of activities has been called a *waterfall* or *cascade*. The process of complement activation probably occurs by a similar cascade mechanism. The release of kinin appears to follow a similar, if somewhat more restricted, pattern of sequential activation of components. In each of the three systems some of the components are inactivated or depleted after they have fulfilled their function. In each system, a naturally occurring serum inhibitor of activation exists—*ie*, C1 esterase inhibitor, kallikrein inhibitor and . . . [an inhibitor of Hageman Factor]."

It may be that the activation of Hageman Factor is the center of both the blood coagulation system and the inflammatory reaction and that the activation of kinin, complement and coagulation systems are all secondary. The studies of Kellermeyer on sodium urate crystal arthritis provide the best experimental support for the theory, but whether or not this mechanism is operative for inflammation induced by other agents remains to be demonstrated.

Summary

1. Components of the blood clotting mechanism play a major role in certain types of inflammation. Fibrinogen (fibrin) and platelets in

vascular thrombi in the late stages of inflammation result in necrosis, which can be arrested experimentally and clinically by administering anticoagulants and antiplatelet aggregates.

2. Activated Hageman Factor, injected intradermally, produces an inflammatory response.

3. Monosodium urate crystals activate Hageman Factor in joint fluid and produce an acute arthritis which can be prevented by an antibody to Hageman Factor.

4. Hageman Factor activates the kallikrein system.

5. Hageman Factor is capable of activating complement in the plasma of patients with hereditary angioneurotic edema.

6. Platelets are required for the leakage of γ -globulin from the circulation and for the inflammatory response of the direct active Arthus reaction.

7. Plasmin is capable of eliciting increased vascular permeability and of activating a component of the complement system.

Disseminated intravascular coagulation may play a role in acute inflammation in two diametrically opposed ways: a) If it is induced after an acute local inflammation is established, it may increase the damage by increasing thrombotic vascular occlusion at the local site, leading to hemorrhagic necrosis. b) If it is induced before the local inflammatory stimulus is applied, even the early phases of inflammation may be prevented. Nonspecific (nonimmune) decompensation of the blood may be the responsible mechanism.

Such chemically diverse inflammatory agents as bacterial lipopolysaccharides, antigen-antibody complexes, heat-aggregated γ -globulin and a variety of particulate substances share four basic biologic properties—*ie*, production of acute inflammation, activation of complement, activation of Hageman Factor and aggregation of platelets with release of their constituents. These shared biologic properties imply a basic mechanism common for blood coagulation and acute inflammation.

These observations are fragmentary. They often deal with special cases or types of inflammation. Although overlapping is suggestive and proven in special cases, the extent to which they represent generalizations for other types, or for all inflammatory reactions, will require considerably more study.

References

1. Davie EW, Ratnoff OD: Waterfall sequence for intrinsic blood clotting. *Science* 145:1310-1311, 1964
2. MacFarlane RG: An enzyme cascade in the blood clotting mechanism, and its function as a biochemical amplifier. *Nature* 202:498-499, 1964

3. Ratnoff OD: Personal communication
4. Wilner GD, Nossel HL, Leroy EC: Activation of Hageman Factor by collagen. *J Clin Invest* 47:2608-2615, 1968
5. Cochrane CG: The Arthus reaction, The Inflammatory Process. Edited by BW Zweifach, L Grant, RT McCluskey. New York, Academic Press, Inc, 1965, pp 613-648
6. Ward PA, Cochrane CG: Bound complement and immunologic injury of blood vessels. *J Exp Med* 121:215-234, 1965
7. Benacerraf B, Biozzi G: Aspects quantitatifs des reactions anaphylactiques et du phenomene d'Arthus. International Congress of Microbiology Sixth Congress, Rome 1953. Inst Super de Sanita, Rome, Italy. Sections VI-VII, pp. 85-92
8. Aronson SB, Elliott JH, Moore TE, O'Day DM: Pathogenetic approach to therapy of peripheral corneal inflammatory disease. *Am J Ophthalmol* 70:65-90, 1970
9. Silfverskiold BP: Heparin und experimentelle glomerulonephritis. *Skand Arch Physiol* 83:175-180, 1940
10. Kleinerman J: Effects of heparin on experimental nephritis in rabbits. *Lab Invest* 3:495-508, 1954
11. Halpern B, Milliez P, Lagrue G, Fray A, Morard JC: Protective action of heparin on experimental immune nephritis. *Nature (Lond)* 205:257-259, 1965
12. Vassalli P, McCluskey RT: Coagulation process and glomerular disease. *Am J Med* 39:179-183, 1965
13. Kincaid-Smith P, Laver MC, Fairley KF, Mathews DC: Dipyridamole and anticoagulants in renal disease due to glomerular and vascular lesions—A new approach to therapy. *Med J Austral* 1:145-151, 1970
14. Ratnoff OD, Miles AA: The induction of permeability-increasing activity in human plasma by activated Hageman Factor. *Br J Exp Pathol* 45:328-345, 1964
15. Ratnoff OD, Davie EW: The purification of activated Hageman Factor (activated Factor XII). *Biochem J* 96:967-974, 1962
16. Graham RC, Ebert RH, Ratnoff OD, Moses J: Pathogenesis of inflammation. II. *In vivo* observations of the inflammatory effects of activated Hageman factor and bradykinin. *J Exp Med* 121:807-820, 1965
17. Seegmiller JE, Howell RR, Malawista SE: The inflammatory reaction to sodium urate. Its possible relationship to the genesis of acute gouty arthritis. *JAMA* 180:469-475, 1962
18. Faires JS, McCarty DJ Jr: Acute arthritis in man and dog after intrasynovial injection of sodium urate crystals. *Lancet* 2:682-684, 1962
19. Kellermeyer RW, Breckenridge RT: The inflammatory process in acute gouty arthritis. I. Activation of Hageman Factor by sodium urate crystals. *J Lab Clin Med* 65:307-315, 1965
20. Margolis J: Some physical aspects of plasma surface reactions. Proceedings of the Thirteenth International Congress of Hematology 1960, p 1820
21. Kellermeyer RW, Breckenridge RT: The inflammatory process in acute gouty arthritis. II. The presence of Hageman Factor and plasma thromboplastin antecedent in synovial fluid. *J Lab Clin Med* 67:455-460, 1966

22. Kellermeyer RW: Inflammatory process in acute gouty arthritis. III. Vascular permeability enhancing activity in normal human synovial fluid; induction by Hageman Factor activators; and inhibition by Hageman Factor antiserum. *J Lab Clin Med* 70:372-383, 1967
23. Lewis GP: Plasma kinin and other vasoactive compounds in acute inflammation. *Ann NY Acad Sci* 116:847-854, 1964
24. Webster ME: The kinin system—a review. *Cellular and Humoral Mechanisms in Anaphylaxis and Allergy*. Basel and New York, Karger, 1969, pp 207-214
25. Diniz CR, Carvalho IF: A micromethod for determination of bradykininogen under several conditions. *Ann NY Acad Sci* 104:77-89, 1963
26. Melmon KL, Cline MJ: Kinins. *Am J Med* 43:153-160, 1967
27. Margolis J: Hageman Factor and capillary permeability. *Aust J Exp Biol* 37:239-244, 1959
28. Müller-Eberhard HJ: Complement. *Adv Immunol* 8:1-80, 1968
29. Müller-Eberhard HJ: Complement. *Ann Rev Biochem* 38:389-414, 1969
30. Cochrane CG, Unanue ER, Dixon FJ: A role of polymorphonuclear leukocytes and complement in nephrotoxic nephritis. *J Exp Med* 122:99-116, 1965
31. Willoughby DA, Coote E, Turk JL: Complement in acute inflammation. *J Pathol Bacteriol* 97:295-305, 1969
32. Donaldson VH: Mechanisms of activation of C'1 esterase in hereditary angioneurotic edema plasma *in vitro*. The role of Hageman Factor, a clot promoting agent. *J Exp Med* 128:411-429, 1968
33. Donaldson VH, Evans RR: A biochemical abnormality in hereditary angioneurotic edema: Absence of serum inhibitor of C'1 esterase. *Am J Med* 35:37-44, 1963
34. Ratnoff OD, Davie EW: The activation of Christmas factor (Factor IX) by activated plasma thromboplastin antecedent (activated Factor XI). *Biochemistry* 1:672-685, 1962
35. Breckenridge RT, Ratnoff OD: The role of proaccelerin in human blood coagulation. Evidence that proaccelerin is converted to a prothrombin converting principle by activated Stuart Factor: with notes on the anticoagulant action of soybean trypsin inhibitor, protamine sulfate and hexadimethrine bromide. *J Clin Invest* 44:302-314, 1965
36. Hurley JV: Substances promoting leukocyte emigration. *Ann NY Acad Sci* 116:918-935, 1964
37. Melmon KL, Cline MJ: The interaction of leukocytes and the kinin system. *Biochem Pharm (Suppl)* 271-281, 1968
38. Todd AS: The histological localization of fibrinolysin activator. *J Pathol Bacteriol* 78:281-283, 1959
39. Ratnoff OD: Increased vascular permeability induced by human plasmin. *J Exp Med* 122:905-921, 1965
40. Lepow IH, Ratnoff OD, Levy LR: Studies on the activation of a pro-esterase associated with partially purified first component of human complement. *J Exp Med* 107:451-474, 1958
41. Taylor FB, Ward PA: Generation of chemotactic activity in rabbit serum by plasminogen-streptokinase mixtures. *J Exp Med* 126:149-158, 1967

42. Ward PA: A plasmin-split fragment of C'3 as a new chemotactic factor. *J Exp Med* 126:189-206, 1967
43. Weimer V: Polymorphonuclear invasion of wounded corneas. Inhibition by topically applied sodium salicylate and soybean trypsin inhibitor. *J Exp Med* 105:141-152, 1967
44. Allison F Jr, Lancaster MG, Crosthwaite JL: Studies on the pathogenesis of acute inflammation. V. An assessment of factors that influence *in vitro* the phagocytic and adhesive properties of leukocytes obtained from rabbit peritoneal exudate. *Am J Pathol* 43:775-795, 1963
45. Margaretten W, McKay DG: The requirement of platelets in the active Arthus reaction. *Am J Pathol* (In press)
46. Margaretten W, McKay DG: Unpublished observations
47. Humphrey JH: The mechanism of Arthus reactions. II. The role of polymorphonuclear leukocytes and platelets in reversed passive reactions in the guinea pig. *Br J Exp Pathol* 36:283-289, 1955
48. Kniker WT, Cochrane CG: The localization of circulating immune complexes in experimental serum sickness. The role of vasoactive amines and hydrodynamic forces. *J Exp Med* 127:119-136, 1968
49. Henson PM, Cochrane CG: Antigen-antibody complexes, platelets and increased vascular permeability. In: *Cellular and Humoral Mechanisms in Anaphylaxis and Allergy*. Basel and New York, Karger, 1969, pp. 129-143
50. Mustard JF, Evans G, Packham MA, Nishizawa EE: The platelet in intravascular immunological reactions. In: *Cellular and Humoral Mechanisms in Anaphylaxis and Allergy*. Basel and New York, Karger, 1969, pp 151-163
51. Shwartzman G: *The Phenomenon of Local Tissue Reactivity*. Harper (Hoeber), New York, 1937
52. McKay DG: *Disseminated Intravascular Coagulation. An Intermediary Mechanism of Disease*. New York, Paul B. Hoeber, 1965
53. Jancso N: Inflammation and the inflammatory mechanisms. *J Pharm Pharmacol* 13:577-594, 1961
54. Allison F Jr, Lancaster MG: Studies on the pathogenesis of acute inflammation. III. The failure of anticoagulants to prevent the leukocytic sticking reaction and the formation of small thrombi in rabbit ear chambers damaged by heat. *J Exp Med* 114:535-553, 1961
55. Stetson CA: Studies on the mechanism of the Shwartzman phenomena: Certain factors involved in production of the local hemorrhagic necrosis. *J Exp Med* 93:489-504, 1951
56. Christian CL: Studies of aggregated gamma-globulin. II. Effect *in vivo*. *J Immunol* 84:117-121, 1960
57. Snyderman R, Shin HS, Phillips JK, Gewurz H, Mergenhagen SE: A neutrophil chemotactic factor derived from C'5 upon interaction of guinea pig serum with endotoxin. *J Immunol* 103:413-422, 1969
58. Naff BG, Byers PH: Possible implication of complement in acute gout. *J Clin Invest* 1967, abstr
59. Robbins J, Stetson CA: Mechanisms of antigen-antibody reactions upon blood coagulation. *Fed Proc* 18:594, 1959, abstr 2333
60. Des Prez RM, Bryant RE: Effects of bacterial endotoxin on rabbit platelets. IV. The divalent ion requirements of endotoxin-induced and immunologically induced platelet injury. *J Exp Med* 124:971-982, 1966

61. McKay DG, Shapiro SS: Alterations in the blood coagulation system induced by bacterial endotoxin. I. *In vivo* (generalized Shwartzman reaction). J Exp Med 107:353-367, 1958
62. McKay DG, Shapiro SS, Shanberge JN: Alterations in the blood coagulation system induced by bacterial endotoxins. II. *In vitro*. J Exp Med 107:369-376, 1958
63. Evans G, Mustard JF: Platelet surface reaction and thrombosis. Surgery 64:273-280, 1968
64. Bloom G, Gustavson KH, Swensson A: On the reaction of the thrombocytes to submicroscopic particles *in vitro*. Acta Haematol 13:57-63, 1955

[*Illustrations follow*]

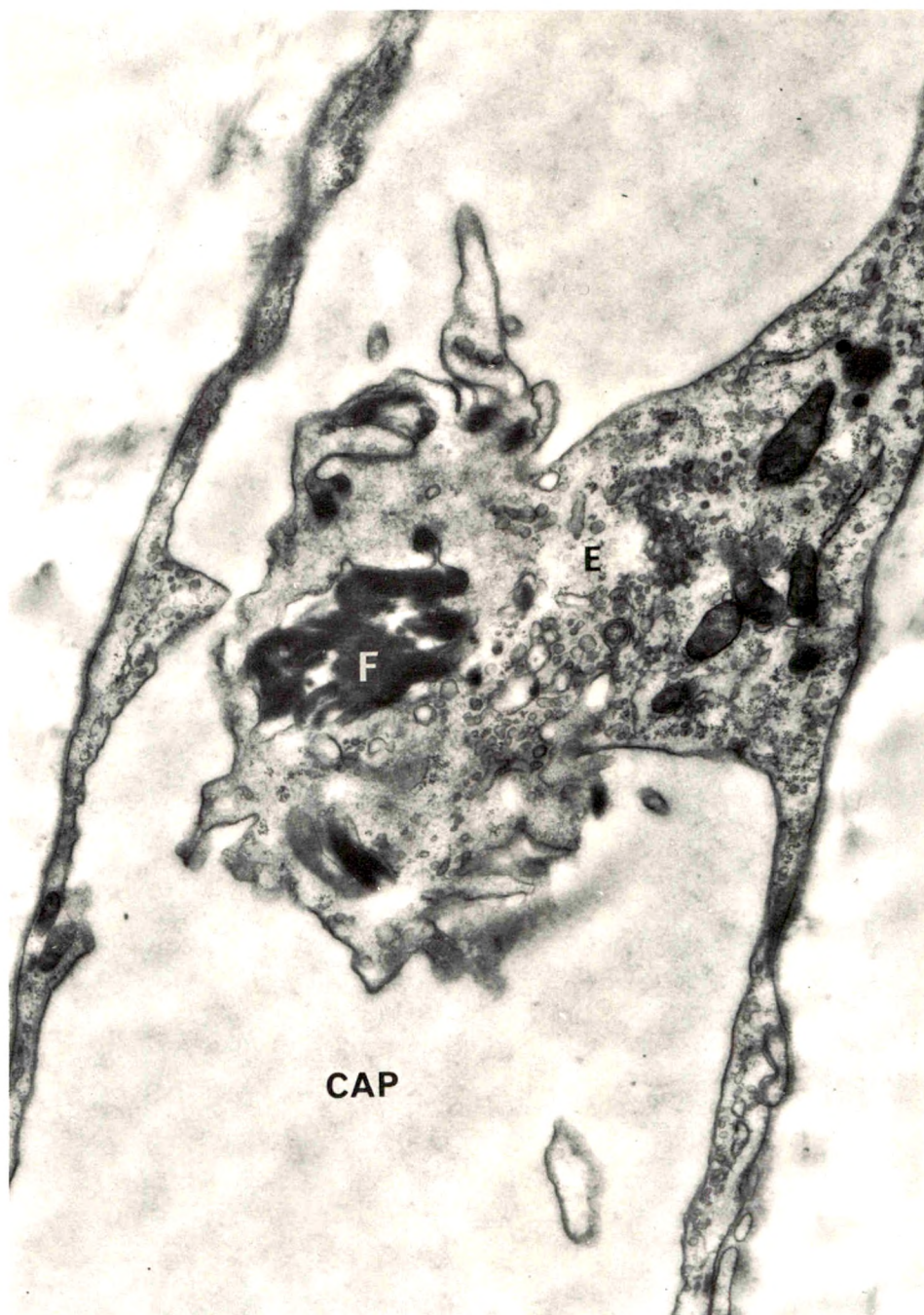


Fig 1—Local site of inflammation 4 hours after intradermal injection of bacterial endotoxin. The endothelial cell of the capillary has formed a pocket by extension of its cytoplasm and has trapped a small amount of fibrin ($\times 11,200$). CAP = Capillary lumen; E = Endothelial cell; F = Fibrin.

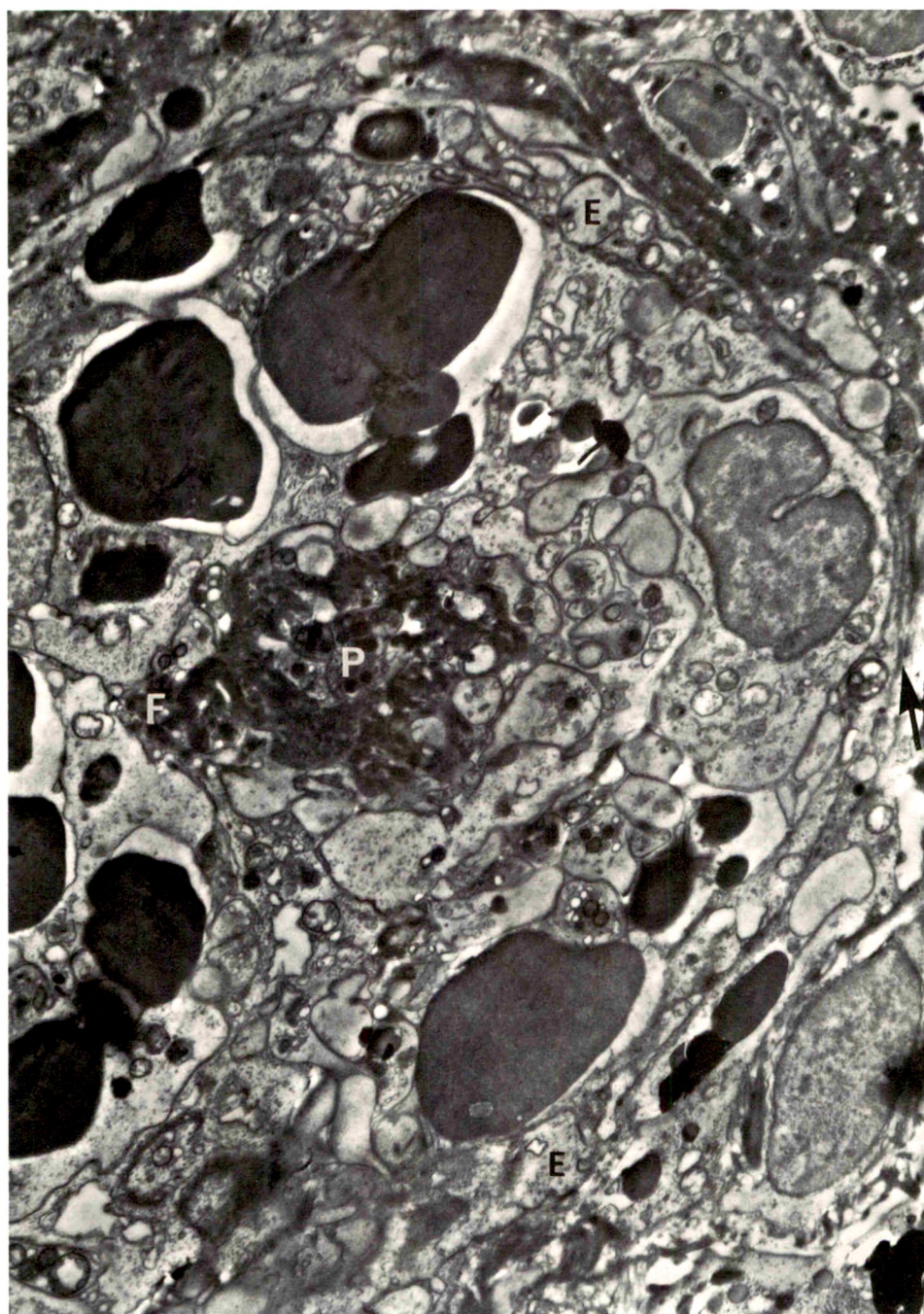


Fig 2—Local site of inflammation 21 hours after intradermal injection of bacterial endotoxin. This capillary is occluded by a thrombus composed of a central nidus of fibrin surrounded by platelets in various stages of degeneration. Red cells are trapped in the thrombus and the endothelium shows evidence of degeneration ($\times 6000$). *E* = Endothelial cells; *F* = Fibrin; *P* = Platelets.

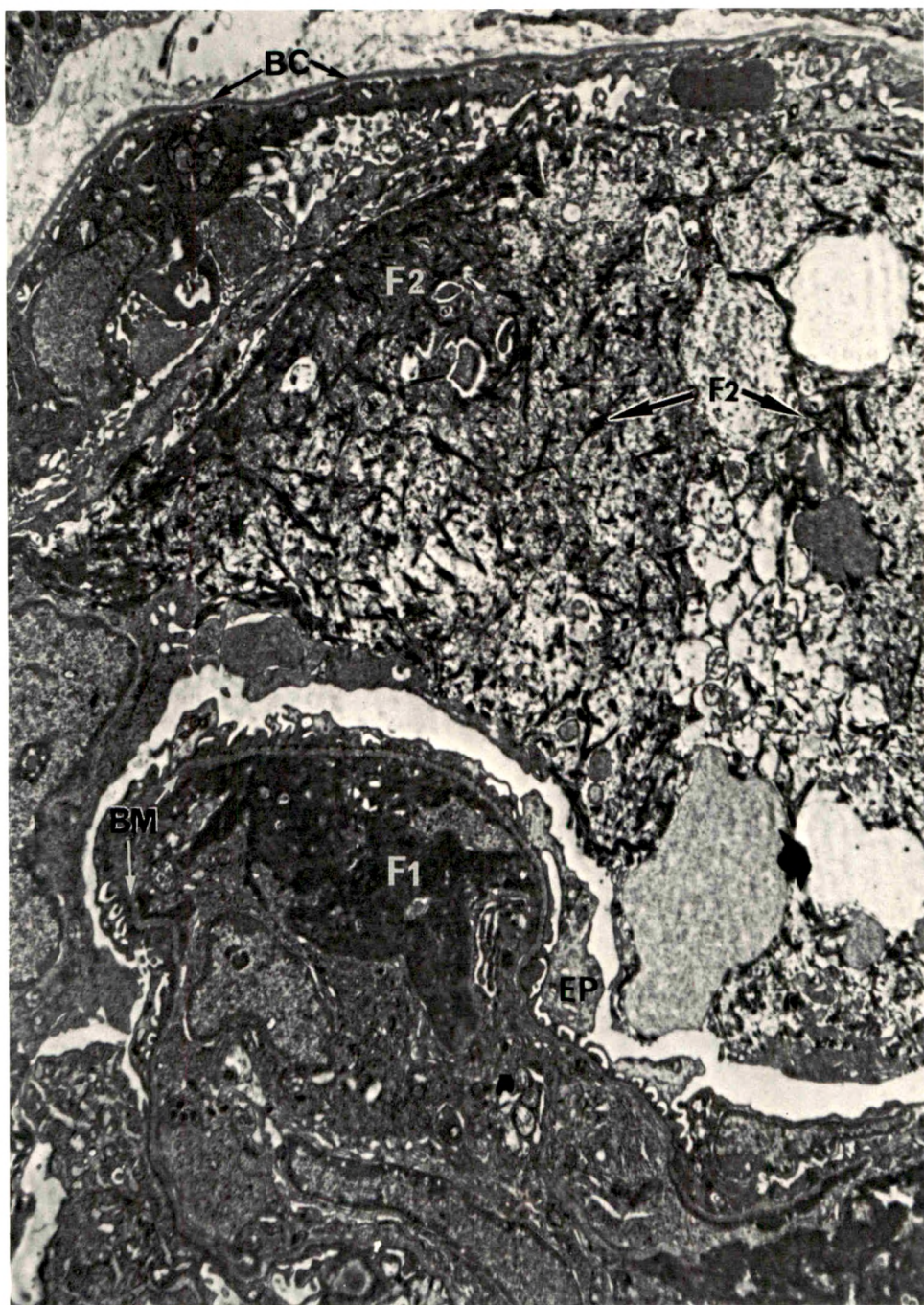


Fig 3—Nephrotic nephritis. Glomerulus 8 days after injecting anti-kidney antibody. The capsular space is filled with a loose meshwork of generally fine strands of fibrin ($\times 4000$). F_1 = Fibrin in capillary lumen; F_2 = Fibrin in capsular space; BC = Basement membrane of Bowman's capsule; EP = Epithelium (visceral); BM = Basement membrane (capillary).

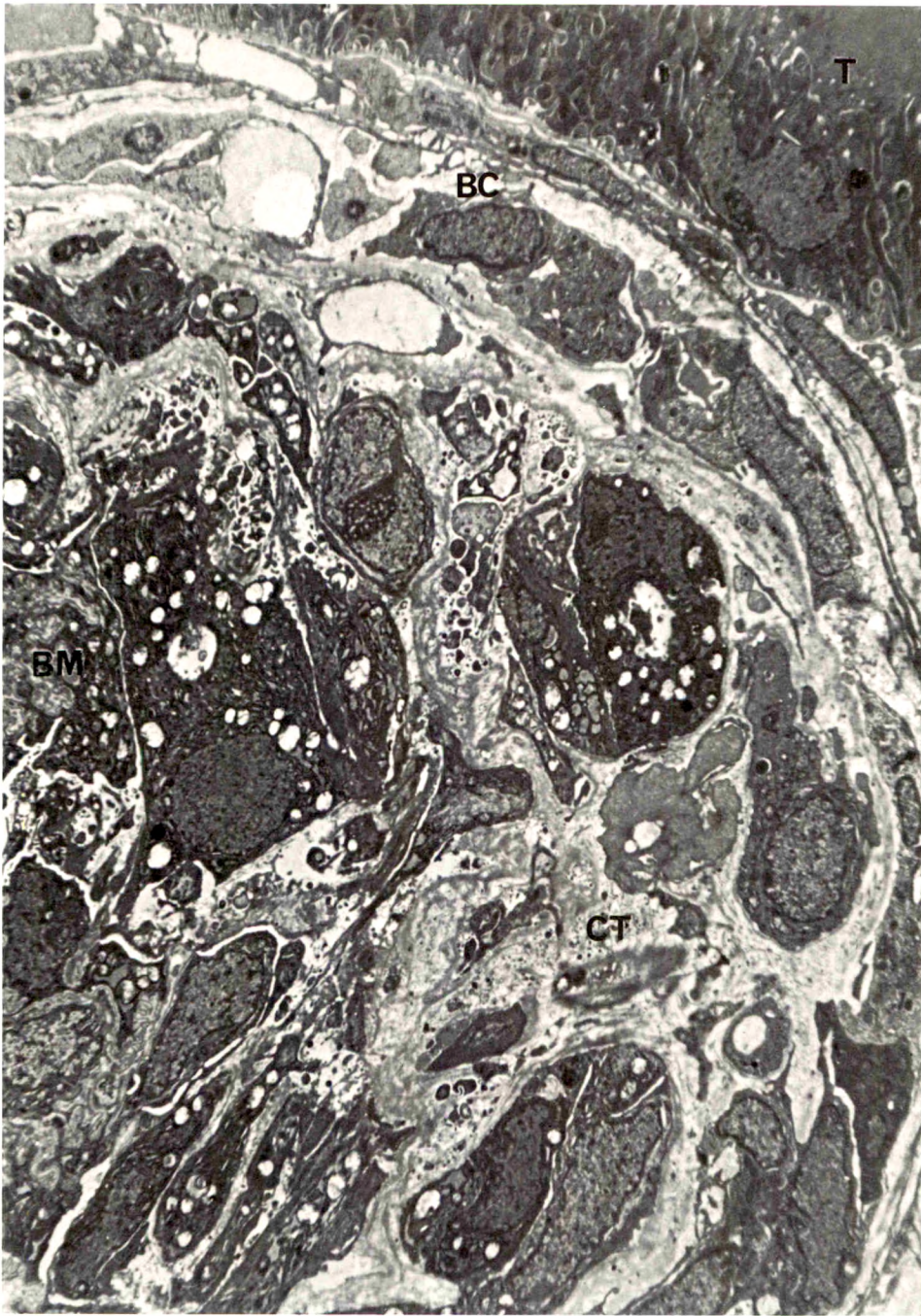


Fig 4—Nephrotoxic nephritis. Glomerulus 18 days after injecting anti-kidney antibody. The capsular space is filled with inflammatory cells, fibroblasts and epithelial cells with strands of collagen and fibrin interspersed (A crescent, $\times 2800$). *T* = Tubular cell; *BC* = Bowman's capsule; *CT* = Connective Tissue; *BM* = Wrinkled collapsed capillary basement membrane.

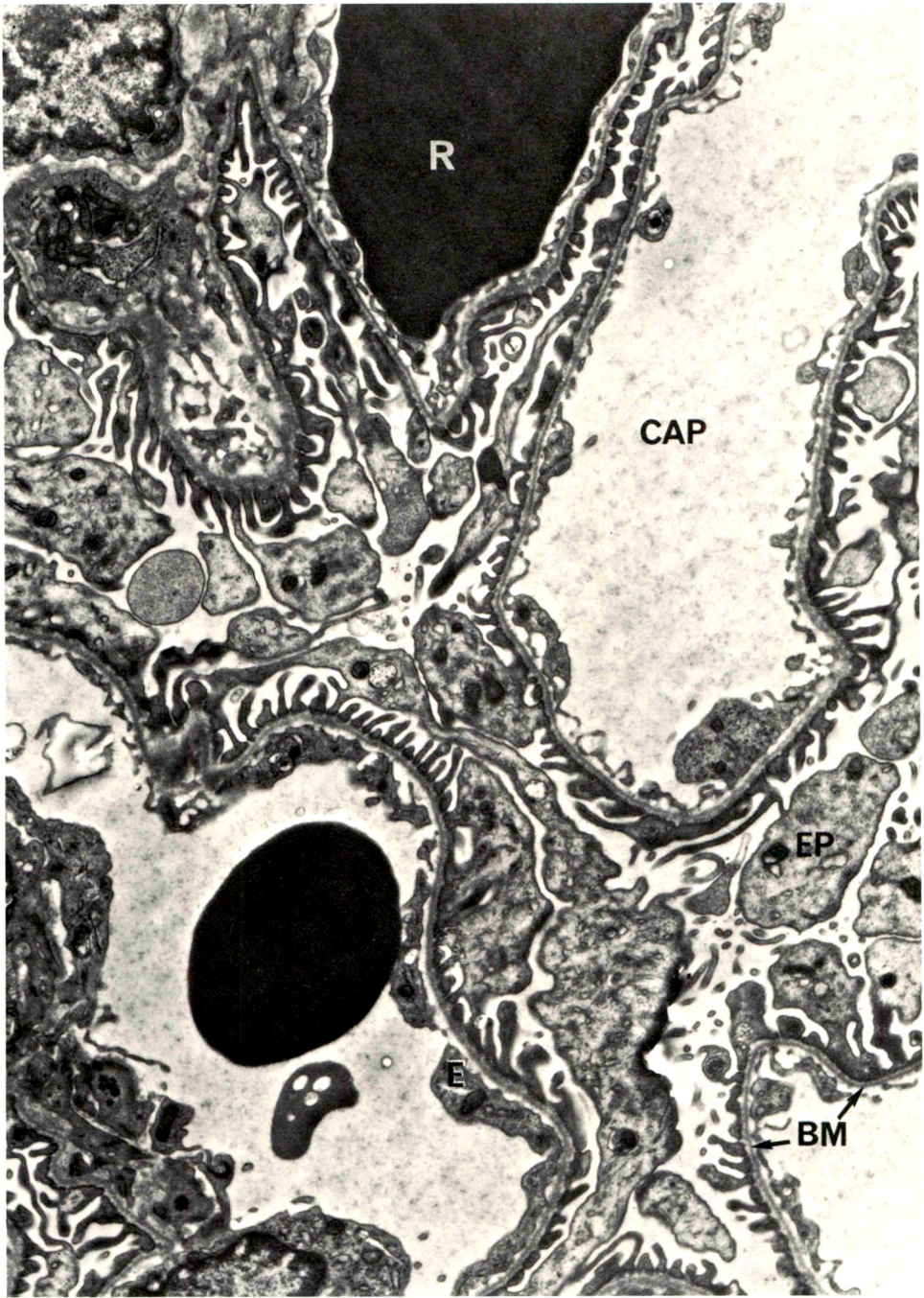


Fig 5—Nephrotic nephritis treated with heparin. Glomerulus 8 days after injection of anti-kidney antibody. This is essentially a normal capillary tuft ($\times 8000$). CAP = Capillary lumen; R = Red blood cell; EP = Epithelial cell; BM = Capillary basement membrane.

[End of Article]

**ANIMAL MODEL
FOR
HUMAN DISEASE**

Hydranencephaly, Porencephaly,
Cerebral Cysts, Retinal Dysplasia,
CNS Malformations

Animal Model: Bluetongue-vaccine-virus
Infection in Fetal Lambs

Contributed by: B.I. Osburn, DVM, PhD, Department of Pathology, School of Veterinary Medicine, University of California, Davis, Calif, and A.M. Silverstein, PhD, Wilmer Institute, Johns Hopkins University School of Medicine, Baltimore, Md.

Biologic Features

Cerebral malformations, including hydranencephaly and porencephaly have been reported in lambs and calves whose dams received a live attenuated bluetongue virus vaccine or contacted bluetongue infection during pregnancy.¹⁻⁴ Experimental studies, utilizing intrafetal inoculation at different stages of the 150 days gestation, indicated that the type of congenital anomaly found depended on the age of the fetal lamb at the time of inoculation.⁵

Lambs infected with bluetongue-vaccine-virus at 50 to 55 days of gestation developed a severe necrotizing encephalopathy and retinopathy which at 150 days of gestation, the time of birth, manifest as hydranencephaly and retinal dysplasia.⁵⁻⁷ Inoculation of lambs at 75 days resulted in a multifocal encephalitis and selective vacuolation of white matter which manifest as porencephalic cysts in the newborn. Ocular lesions were not observed in these newborn lambs. Lesions in brains of lambs inoculated after 100 days of gestation was confined to a mild focal meningoencephalitis.

The virus selectively parasitized and destroyed immature cells in the nervous system.⁸ Most of the lesions leading to the anomalies occur prior to the fetal age at which serum neutralizing antibodies to this virus are produced.⁸ These observations suggest that virus localization and growth in the developing nervous system and the late onset of the serum neutralizing antibody response to the virus may be of considerable importance in the pathogenesis of the viral infection leading to these anomalies.

Publication sponsored by the Registry of Comparative Pathology of the Armed Forces Institute of Pathology and supported by Public Health Service Grant RR00301 from the Division of Research Resources, US Department of Health, Education and Welfare, under the auspices of Universities Associated for Research and Education in Pathology, Inc.

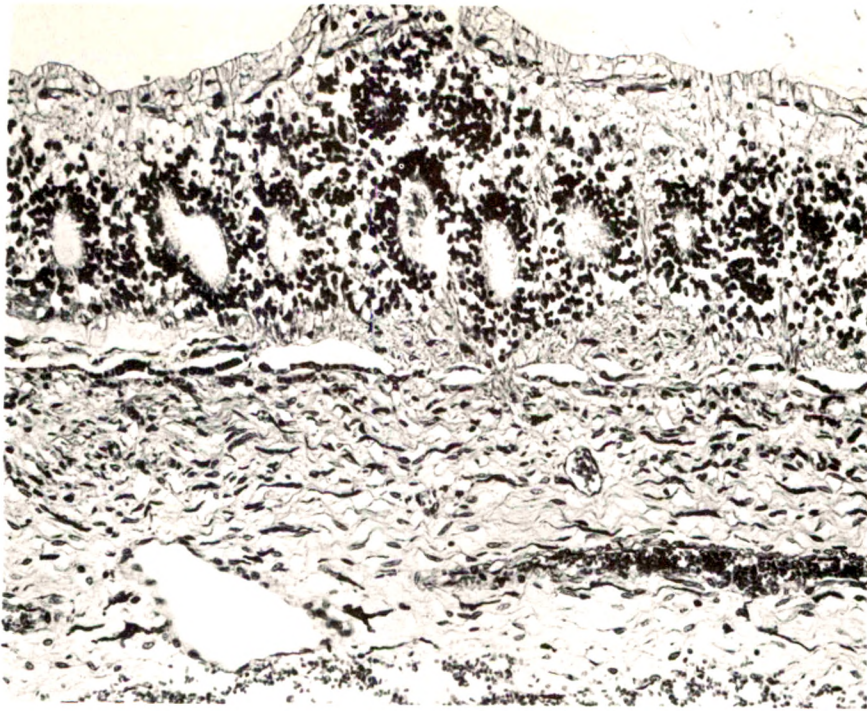


Fig 1 (top)—Oval rosettes typical of dysplastic retina in a newborn lamb inoculated with bluetongue-vaccine-virus at 50 days of gestation or 105 days prior to birth (Masson, $\times 140$).

Fig 2 (bottom)—Hydranencephaly. There are only modest remnants of neural tissue in the cranial cavity of this newborn lamb (150 days gestation) infected with bluetongue-vaccine-virus at 52 days of gestation.

Intrafetal inoculation with bluetongue vaccine virus (Blucine-Cutter Labs, Berkeley, Calif) of time-dated pregnant sheep provides the only known readily reproducible model for studying congenital hydranencephaly and porencephaly.

Comparison with Human Disease

The morphologic features of hydranencephaly, porencephaly and retinal dysplasia in fetal lambs are very similar if not identical to that in man. In man, the etiology and pathogenesis of these anomalies are largely unknown. Defects in embryogenesis, vascular related destructive lesions and infectious processes have been postulated in some cases; however the possibility of a viral etiology has not received serious consideration.

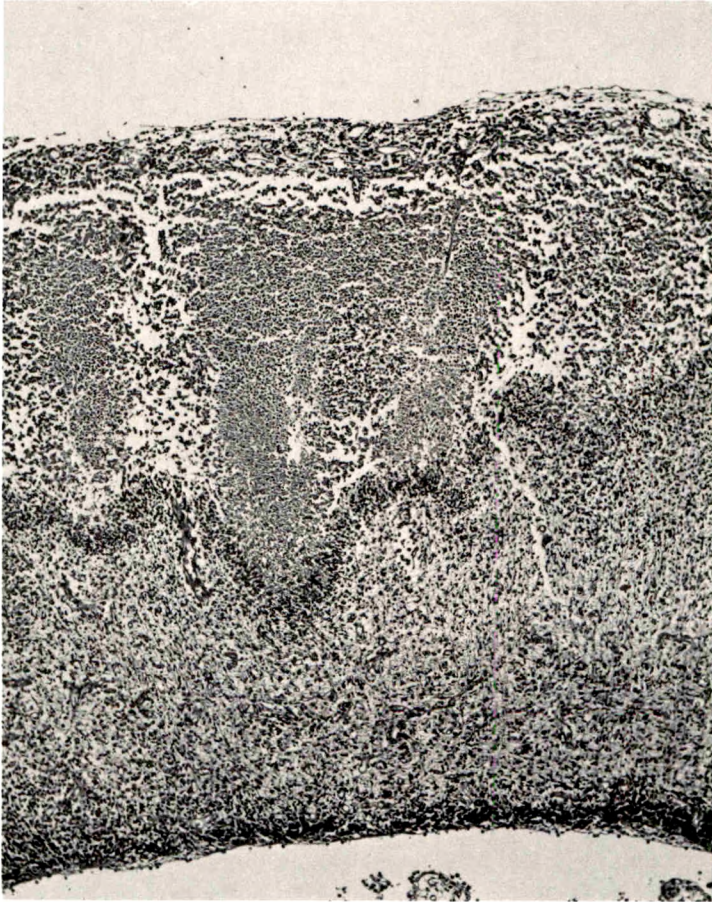


Fig 3—Focal necrosis in subventricular zone of a 62 day fetal lamb 9 days after inoculation of bluetongue-vaccine-virus (H&E, $\times 200$).



Fig 4—Extensive necrosis of the marginal and cortical zones of a 65 day fetal lamb 12 days after inoculation of bluetongue-vaccine-virus (H&E, $\times 380$).

Important problems remaining to be solved are the biochemical or physiologic characteristics of the developing nervous system conducive to virus localization and proliferation, and the modifying effects of the hosts immune and/or interferon responses on viral activity in the developing fetus.

References

1. Shultz G, Delay PD: Losses in newborn lambs associated with bluetongue vaccination of pregnant ewes. *J Am Vet Med Ass* 127:224, 1955
2. Cordy DR, Shultz G: Congenital subcortical encephalopathies in lambs. *J Neuropathol Exp Neurol* 20:554, 1961
3. Richards WPC, Crenshaw GL, Bushnell RB: Hydranencephaly of calves associated with natural bluetongue virus infection. *Cornell Vet* (In Press)
4. Griner LA, McCrory BR, Foster NM, Meyer H: Bluetongue associated with abnormalities in newborn lambs. *J Am Vet Med Ass* 145:1013, 1964
5. Osburn BI, Silverstein AM, Prendergast RA, Johnson RT, Parshall CJ Jr: Experimental viral-induced congenital encephalopathies: I. Pathology of hydranencephaly and porencephaly caused by bluetongue vaccine-virus. *Lab Invest* (In press)
6. Richard WPC, Cordy DR: Bluetongue virus infection: Pathologic responses of Nervous systems in sheep and mice. *Science* 156:530, 1967
7. Silverstein AM, Parshall CJ Jr, Osburn BI, Prendergast RA: An experimental, virus-induced retinal dysplasia in the fetal lamb. *Am J Ophthalmol* 72:22, 1971
8. Osburn BI, Johnson RT, Silverstein AM, Prendergast RA, Jochim MM, Levy SE: Experimental viral-induced congenital encephalopathies: II. The pathogenesis of bluetongue vaccine virus infection in fetal lambs. *Lab Invest* (In press)

The American Journal of PATHOLOGY

is published by the Medical Department of Harper & Row, Publishers, under the auspices of The American Association of Pathologists and Bacteriologists and The American Society for Experimental Pathology, and is edited by a Board appointed by the Councils of the two Societies. It is devoted to the prompt publication of original observations and investigations in the field of pathology and microbiology and is published monthly in four volumes per year.

Information for Authors

ORIGINAL PAPERS will be considered for publication on condition that they are contributed solely to THE AMERICAN JOURNAL OF PATHOLOGY. Address manuscripts to the Editor-in-Chief: THOMAS D. KINNEY, MD, Department of Pathology, Duke University Medical Center, Durham, NC 27706.

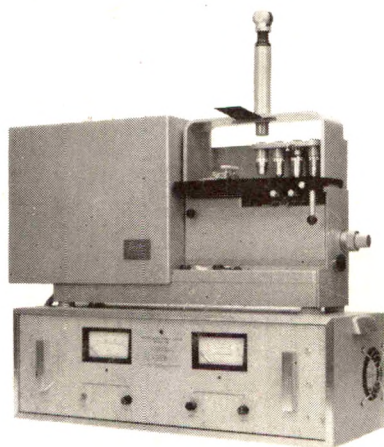
MANUSCRIPTS must be typed **double-spaced** (including tables, references, and legends for figures), and all material should be submitted in duplicate. The literature should be summarized as concisely as is consistent with establishing the necessary basis for new material, and original observations should be presented in a clear, well-organized manner. Papers should rarely exceed 20 printed pages. Tables should be planned to suit the page size of THE JOURNAL. Excess tabular matter must be paid for by the contributor.

REFERENCES to the literature should be numbered in the order of citation in the text and should conform to the following style: names of all authors, complete title of article (including subtitle), abbreviated name of periodical (use *Index Medicus* style abbreviations), volume in Arabic numerals, inclusive pagination, and year (eg, 14:111–120, 1938). Titles are to be in the original language when they can be reproduced in the English alphabet. Translated titles should be enclosed in square brackets.

ILLUSTRATIONS must be planned to suit the page size of THE JOURNAL (**maximum plate size is 5½ × 8 inches**) and should be submitted **unmounted**, with figure number, top, and author's name marked lightly on the back in soft pencil. Oversize illustrations should be avoided because handling of these delays publication. To be accepted, illustrations must reach a certain standard of excellence technically, present an attractive appearance, and add significantly to the value of the presentation. Marking lines and letters, if essential, must be kept at least ¼ inch inside all margins. If two or more illustrations are to appear on a page, they should be so trimmed that the edges may be butted and the outer margins squared. The legends for photomicrographs should state the staining method and the degree of magnification. Black and white illustrations will be furnished in moderate numbers. Excess illustrations, when accepted, and the cost of illustrations in color, must be paid for by the contributor.

REPRINTS: An order blank for reprints is sent with the proof.

Leitz® Microprojector XIC



The bright one at the rear of the class

Crisp bright images projected to any size audience from your slide specimens. Incomparable optics that only Leitz® can offer provide corner to corner sharpness.

Whether you switch to low magnification or the remarkable 160X oil apochromat, alignment is quick and focusing is easy ...without fuss, without bother. Your lecture is never disturbed because of complicated or unstable controls.

The brilliance of the color-balanced light source is without equal. Neutral density

filters control the light intensity to suit every projection requirement. A special interference filter system reduces heat radiation.

Write for our brochure describing the Microprojector that has become practically indispensable in every teaching situation.

Leitz
Leica

E. Leitz, Inc., Rockleigh, N. J. 07647 123371

VOLUME 67 • NUMBER 2 / WHOLE NUMBER 360

The American Journal of PATHOLOGY

MAY 1972

OFFICIAL PUBLICATION OF

THE AMERICAN ASSOCIATION OF
PATHOLOGISTS AND BACTERIOLOGISTS

THE AMERICAN SOCIETY FOR
EXPERIMENTAL PATHOLOGY

BOARD OF EDITORS

Thomas D. Kinney, *Editor-in-Chief*

Donald B. Hackel, *Associate Editor*

Orville T. Bailey	Robert H. Heptinstall
Frederick F. Becker	Morris J. Karnovsky
Baruj Benacerraf	Paul Kotin
Kurt Benirschke	Averill A. Liebow
Kenneth M. Brinkhous	Guido Majno
Joel G. Brunson	Donald G. McKay
John R. Carter	Henry D. Moon
Charles G. Cochrane	Councilman Morgan
John M. Craig	Hans J. Müller-Eberhard
Frank J. Dixon, Jr	Goetz W. Richter
John T. Ellis	David T. Rowlands, Jr
Frank W. Fitch	Philippe Shubik
Patrick J. Fitzgerald	Edward A. Smuckler
David G. Freiman	Leon Sokoloff
Jack C. Geer	Benjamin H. Spargo
Gabriel Godman	Jacinto J. Vazquez
John B. Hazard	F. Stephen Vogel


Editorial Assistant: Virginia Hotelling

MEDICAL DEPARTMENT

HARPER & ROW, PUBLISHERS



got a minute?



Sorry...
It's you know!

Now...T₃/T₄ Tests that don't mind interruptions.

(You won't have to control the temperature either.)



In vitro thyroid assays usually involve sampling a reaction **before** equilibrium is reached. Other T₃ and T₄ tests are of the "rate" reaction type and, therefore, control of both temperature and time is necessary, but with **THYOPACTM-3**, T₃ uptake kit and **THYOPAC-4**, T₄ assay kit, the reactions rapidly reach equilibrium. Since **THYOPAC-3** and **THYOPAC-4** are performed **at equilibrium**, exact control of time and temperature variables are not required.

Consider these advantages:

THYOPAC-4, T₄ assay kit

- Independent of time
- Independent of temperature
- Small serum sample required (0.5 ml)
- No extraction efficiency corrections
- Speed (only 30 minutes mixing time)
- Evaporation not required
- No washing required

THYOPAC-3, T₃ uptake kit

- Independent of time
- Independent of temperature
- Small serum sample required (0.1 ml)
- Speed (only 10 minutes mixing time)
- No washing required

Because **THYOPAC-3** and **THYOPAC-4** are performed at equilibrium, you can expect precise separation of normal/abnormal T₃/T₄ levels.

The combination of **THYOPAC-3** and **THYOPAC-4** into the Free **THYOPAC** Index helps eliminate complicating factors such as raised or lowered TBG levels.

our specific activity is service



Amersham/Searle

AMERSHAM / SEARLE CORPORATION:
An Activity of G. D. Searle & Co. and the Radiochemical Centre

2636 S. Clearbrook Drive
Arlington Heights, Illinois 60005
Telephone: 312-593-6300—Telex: 28-2452

Do the Reichert Zetopan Microscope and Automatic Camera come as a set? Or can I buy and use them independently?

Yes.

Bought separately or together, this one-tuosome offers unique capability and outstanding performance.

The Zetopan is an advanced research microscope that can be extended to cover fluorescence, polarization, microphotometry and phase techniques, and can be used with transmitted, incident, epi or Nomarski interference.

The Automatic Camera is adaptable to any microscope in your lab, and is the only camera with direct exposure readout. Built-in factor keys allow you to compensate the measured exposed time for film reciprocity failure. Light measurement may be detailed to one small spot or over the entire frame. Interchangeable 35 mm film magazines.

For a convincing demonstration of the microscope and/or camera write: American Optical Corporation, Reichert Products, Buffalo, New York 14215.



**AMERICAN OPTICAL
CORPORATION**

SCIENTIFIC INSTRUMENT DIVISION • BUFFALO, N.Y. 14215

The American Journal of PATHOLOGY



MAY 1972 • Volume 67, Number 2

CONTENTS

- 215 Separation of Beating Cardiac Myocytes from Suspensions of Heart Cells
Thomas G. Pretlow II, Melvin R. Glick and William J. Reddy
- 227 Defective Function of Renal Lysosomes in Mice with the Chediak-Higashi Syndrome
David J. Prieur, William C. Davis and George A. Padgett
- 241 Morphologic and Functional Characteristics of Long-Term Cultures of Murine Myeloma Cells
George D. Sorenson and Olive S. Pettengill
- 265 The Number and Dimensions of Small Airways in Emphysematous Lungs
Kenichi Matsuba and William M. Thurlbeck
- 277 High-Resolution Autoradiography of Malarial Parasites Treated with ^3H -Chloroquine
Masamichi Aikawa
- 285 Experimental Papillary Necrosis of the Kidney. I. Morphologic and Functional Data
G. Murray, R. G. Wyllie, G. S. Hill, P. W. Ramsden and R. H. Heptinstall
- 303 Cytochemical Localization of Peroxidase Activity in the Developing Erythrocyte
Ann M. Dvorak, Harold F. Dvorak and Morris J. Karnovsky
- 327 Chronic Actinic Keratopathy—A Condition Associated with Conjunctival Elastosis (Pingueculae) and Typified by Characteristic Extracellular Concretions
Gordon K. Klintworth
- 349 Inhibition of Macrophage Response to Brain Injury: A New Effect of Pertussis Vaccine Possibly Related to Histamine-Sensitizing Factor
Seymour Levine and Richard Sowinski
- 361 Ultrastructural Characteristics of the "Hairy Cells" of Leukemic Reticuloendotheliosis
I. Katayama, C. Y. Li and L. T. Yam
- 371 The Significance of Bronchial Atrophy
John C. Maisel, G. Wayne Silvers, Marlyce S. George, Gladys A. Dart, Thomas L. Petty and Roger S. Mitchell
- 387 Experimental Cerebral Atherosclerosis in the Dog. I. A Morphologic Study
Minoru Suzuki
- 403 Division of Protoplasmic Astrocytes in Acute Experimental Hepatic Encephalopathy: An Electron Microscopic Study
Michael D. Norenberg, Lowell W. Lapham, Mark W. Eastland and Allyn G. May
- 413 **Animal Model for Human Disease:** Down's Syndrome (Mongolism, Trisomy 21)
Harold M. McClure

© 1972 by The American Association of Pathologists and Bacteriologists

The seal commemorates The Year of Pathology, being celebrated from October 1971 to October 1972 by the major national pathology societies. Special educational events will emphasize the expanding role of pathology and the medical laboratory in modern health care.

Medical Department

•

HARPER & ROW, PUBLISHERS

The American Journal of PATHOLOGY

GENERAL INFORMATION

Editorial Communications: All correspondence concerning editorial matters should be addressed to the Editor-in-Chief, DR. THOMAS D. KINNEY, Department of Pathology, Duke University Medical Center, Durham, N.C. 27706.

Business Communications: All subscriptions and advertising inquiries should be addressed to: MEDICAL DEPARTMENT, HARPER & ROW, PUBLISHERS, 2350 Virginia Ave., Hagerstown, Md. 21740.

Rates: THE AMERICAN JOURNAL OF PATHOLOGY is issued monthly, four volumes per year. Regular (individual) subscriptions: \$27.50 per year in the U.S. and Possessions; \$30.00 per year in Canada and countries of the Pan-American Postal Union; and \$31.00 elsewhere. Special rate for Interns and Residents: \$16.00 per year (\$1.50 extra postage in Canada and countries of the Pan-American Postal Union; \$2.50 extra postage elsewhere). Regular (individual) subscriptions and Resident and Intern subscriptions must be in the names of, and billed to, individuals. Institutional subscriptions, available to all libraries, schools, clinics, and hospitals, to all government agencies, local or national, and to all private or public institutions and organizations: \$35.00 per year in the U.S. and Possessions; \$37.50 per year in Canada and countries of the Pan-American Postal Union; \$38.50 per year elsewhere. All subscriptions are payable in advance. Single copies, when available, \$4.00.

Back Issues: Single issues and complete volumes of THE JOURNAL published prior to 1961 may be purchased from Walter J. Johnson, Inc., 111 Fifth Ave., New York, N.Y. 10003.

INDEX TO ADVERTISERS

American Optical Company	2
Amersham/Searle Corporation	2nd Cover, 1
Dow Chemical Company	10, 11
Harco Scientific	6, 7
Harper & Row, Publishers	12
Ortho Diagnostics	9, 16
Shandon Southern Instruments, Inc. ...	13
Sigma Chemical Company	8
Sorvall, Inc., Ivan	5
Zeiss, Inc., Carl	15, 4th Cover

MOVING?

To avoid interruption in your receipt of this Journal, we need to know your new address—six weeks in advance.

When writing us, be sure to type or print clearly your name and your new address—complete with zip code. It is *essential* that you also list your old address.

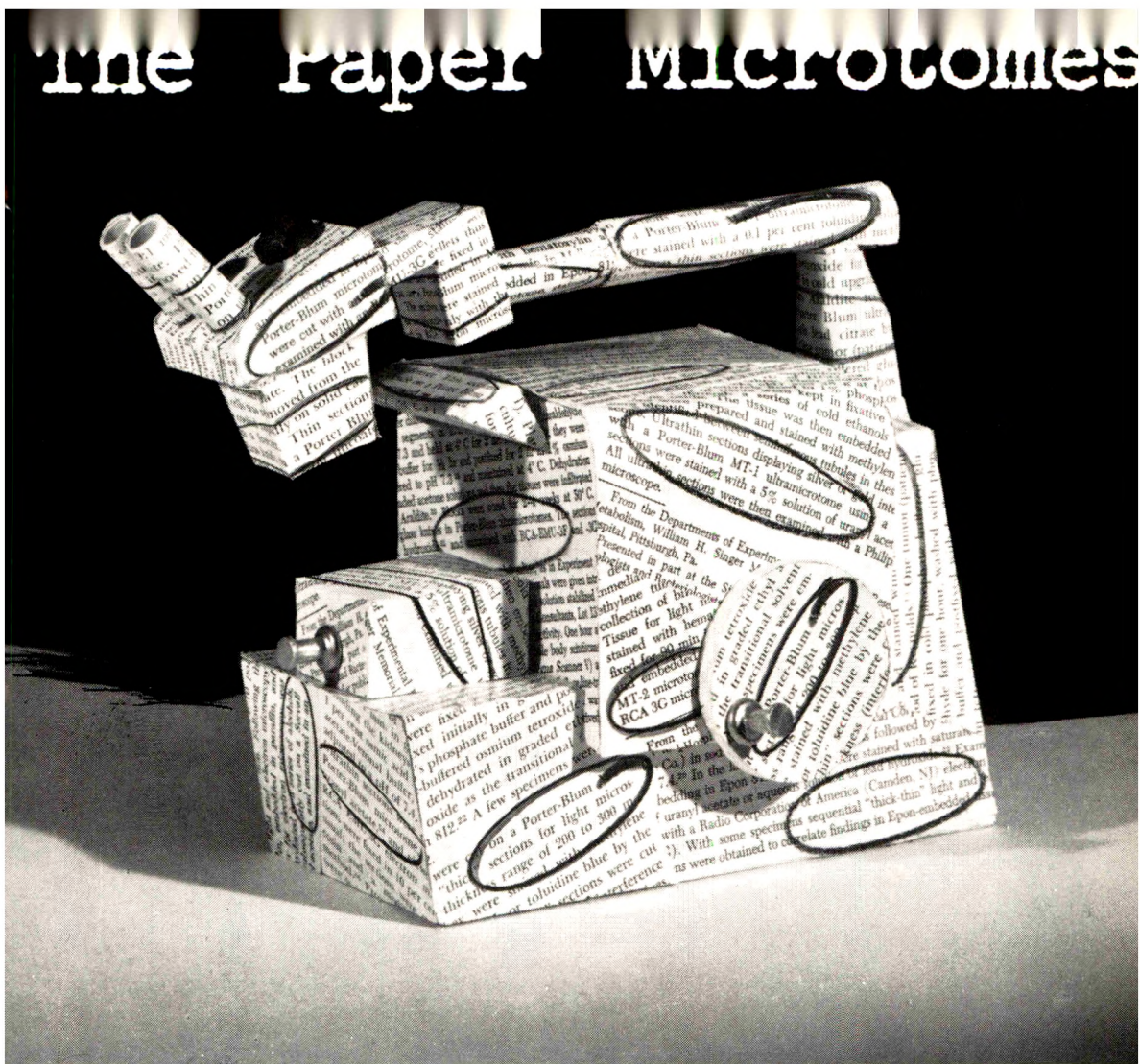
IMPORTANT: We publish a number of medical and scientific periodicals. Therefore, please be sure to give the name of THIS Journal when you write us.

Thank you for cooperating!

MEDICAL DEPARTMENT
Harper & Row, Publishers, Inc.

2350 Virginia Ave.
Hagerstown, Md. 21740.

(see page 14)

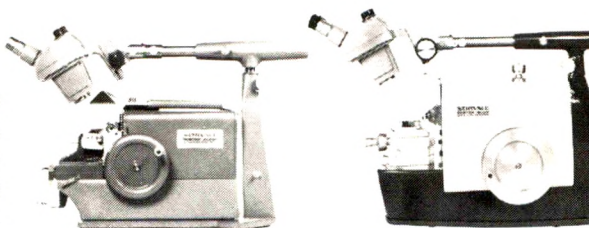


The "PORTER-BLUMS" are the "Paper" Microtomes

In scholarly paper after scholarly paper, where the "Materials & Methods" abstract discusses microtomy, you will find a "Porter-Blum" mentioned. The SORVALL "Porter-Blums" have earned a well-deserved reputation for reliability and accuracy that is unsurpassed by any other instrument in this field.

Also, ask for details on the "Smith & Farquhar" Tissue Sectioner for preparing fixed — and certain non-fixed — tissue; the FTS MT2-B (and older MT-2) Cryo-Sectioning Attachment; and the new JB-4 Microtome for clinical and research applications. Ivan SORVALL, Inc. Norwalk, Connecticut 06856.

SORVALL®



"PORTER-BLUM" MT-1, 25 m μ to 1/2 μ , is the ideal ultra-microtome for teaching and all routine sectioning — and many of them have been in the forefront of important research advances over many years.

"PORTER-BLUM" MT2-B, 10 Å to 4 μ , offers the highest precision sectioning in three operating modes — automatic / semi-automatic / manual. The MT2-B is the most advanced instrument in ultra-microtomy available today.

5 ways you can convince your boss to make life easier for you.

(With automatic watering.)



First, memorize the "5 ways."

Then, after rehearsing your lines to perfection, march into the boss's office and impress him with your cool logic. Failing that, try threats. (He has relatives in the old country, perhaps?)

1. Your people spend a lot of time washing, filling, and changing water bottles. A three-handed caretaker you haven't discovered yet. Tell the boss that Hardco Automatic watering can free people to do more important work. And you can re-deploy your staff to meet the demands of expansion without increasing cost.
2. Water bottles breed contamination and cause accidental dehydration. Sometimes people tend to forget that when a rat works his stopper loose or jams something up the sipper tube, he doesn't only get a wet cage. He also gets no more water. But you have to put up with this kind of frustration all the time. So tell your leader that a Hardco Automatic Watering System guarantees every animal a constant source of clean, fresh water. (Which can't hurt your image when the U.S.D.A. or S.P.C.A. comes around.)
3. Bottles break, and you not only have to clean up the mess, but replace the bottles—something that's getting harder to do all the time. Deliveries are slower, and prices are higher. Pretty soon getting new bottles will be like trying to find a new front grill for a '58 Edsel. Also, bottles require all kinds of back up equipment like carts and racks and washers. You can tell your boss that Hardco eliminates all those problems. And boosts the morale of his employees who just happen to know that the other lab in town has already installed automatic watering.
4. About this morale thing. Nothing can get a man down like having to work with bottles. (Unless it's having to work in a pig room with a broken air conditioner.) Your boss already knows it's hard to get good people to do this work. And even harder to keep them. Tell him Hardco will make everybody happy.
5. You have made recommendations to the brass of your company before and have always come up against the same problem: money. Well, here's one time when they won't be able to fight you. Tell your money man Hardco Automatic Watering will save him 30% to 40% of his total labor costs. Tell him the cost of maintaining bottles for an average 5,000 cage facility runs about \$20,000 a year. Every year. And then tell him that he will completely recover the cost of Hardco in about 17 months—and from then on it's all gravy.

It all adds up to this: your life is easier, your lab is more efficient, your animals are happier and healthier, and your boss is saving money.

If none of this works, Hardco has some very persuasive literature—not to mention some persuasive salesmen. For help, contact Hardco Scientific, 1705 Omni Drive, Cincinnati, Ohio 45245. Phone 513/752-0880.

hardco scientific
division of fieldstone corporation



Sigma is pleased to offer

Stat CPK

Creatine Phosphokinase

A carefully standardized
SINGLE or MULTI
DETERMINATION VIAL

in serum or other fluids, at 340m μ
per Sigma Technical Bulletin No. 45-UV

Remarkably simple, convenient and fast!

1. Add water and 0.1 ml serum; "equilibrate".
2. Take Initial Reading.
3. Take Second Reading 5 minutes later.

THAT IS ALL!

Request Sigma Technical Bulletin No. 45-UV, or order:

Stock No. 45-1 Single Assay Vials 10 vials 10 Assays \$11.50

Stock No. 45-5 5 Assay Vials 10 vials 50 Assays 42.50

Includes Air Mail postage to any Destination in the World.

SIGMA CPK PROCEDURES

SIGMA has probably done more developmental work on CPK than any other firm. These studies, plus SIGMA'S unique position as the world's largest producer of Research Biochemicals, has resulted in several extremely dependable methods for almost any instrument. We offer:

No. 661 — Colorimetric procedure. Uses 0.6 ml serum.

ATP + Creatine \rightarrow ADP + Phosphocreatine + Inorganic Phosphate. Measure the Inorganic Phosphate per Fiske and Subbarow.

With Fiske & Subbarow Reagents
Kit No. 661-PA 25 Assays \$13.00
Kit No. 661-PB 100 Assays 32.25

Without Fiske & Subbarow Reagents (Use your own)
Kit No. 661-A 25 Assays \$ 6.00
Kit No. 661-B 100 Assays 19.00

No. 520 — Colorimetric procedure. Uses only 0.01 ml Serum.

ADP + Phosphocreatine \rightarrow ATP + Creatine. Measure the Creatine released by reaction with Diacetyl and Naphthol. Very sensitive.

Kit No. 520 25 Assays \$18.75

Kit No. 520-C 100 Assays \$44.75

No. 80-F — Fluorometric procedure. Uses only 0.01 ml serum.

ADP + Phosphocreatine \rightarrow ATP + Creatine. Measure the fluorescence of the Creatine plus Ninhydrin.

Kit No. 80-F 20 Assays \$17.75

Kit No. 80F-C 100 Assays \$49.50

No. 40-UV — Kinetic Ultraviolet procedure at 340 m μ . Uses 0.2 ml serum.

ATP + Creatine \rightarrow ADP + Phosphocreatine. Couple this with Pyruvate Kinase, LDH and DPNH, and measure the rate of oxidation of the DPNH by the decrease in OD₃₄₀.

Kit No. 40-A 15 Assays \$25.00

Kit No. 40-B 45 Assays \$70.00

Kit No. 40-C 90 Assays \$138.50

No. 45-UV — Stat Ultraviolet procedure at 340m μ .

All reagents pre-standardized into one Single or Multi-Assay vial. Simply add water and 0.1 ml serum; equilibrate. Take initial reading. Read OD (or %T) after only 5 minutes. Remarkably simple, convenient and fast.

Stock No. 45-1 Single Assay Vials 10 vials 10 Assays \$11.50
Stock No. 45-5 5 Assay Vials 10 vials 50 Assays 42.50

No. 910 — Automated Colorimetric procedure.

An automated version of our No. 520 procedure. Although this is probably the most accurate automatic procedure available to date, we are now field-testing our improved No. 911 procedure which eliminates the α -Naphthol reagent and substitutes the much more stable Orcinol. Prices are the same as the No. 910. Inquiries or orders are invited. Satisfaction is guaranteed, of course.

Kit No. 910-A 300 Assays \$104.00

Kit No. 910-B 1500 Assays \$381.50

Also available: **CPK Enzyme Reference**. A carefully assayed preparation, which may be used as control or reference for various CPK procedures offered by Sigma. Available in two sizes for your convenience. Activity: 30-50 Sigma units per ml when reconstituted with water.

CPK-1 1 ml size vial 10 vials \$8.75

CPK-2 2 ml size vial 10 vials \$12.50

We pay all normal shipping charges on these reagents — anywhere in the World.

Free Sigma Technical Bulletins for the above methods are available to eligible Laboratories.

It's a pleasure doing business with Sigma

ORDER DIRECT — TELEPHONE COLLECT from ANYWHERE in the WORLD

Day, Station to Station, 314-771-5750 (Including Saturday and Sunday until 1 P.M.)

Night, Person to Person, Dan Broida, 314-993-6418

TWX [Teletype] Day or Night: COLLECT 910-761-0593

TELEGRAM: SIGMACHEM, Saint Louis, Missouri

SIGMA  **CHEMICAL COMPANY**

The Research Laboratories of

P.O. BOX 14508 • SAINT LOUIS, MISSOURI 63178 U.S.A.

MANUFACTURERS OF THE FINEST BIOCHEMICALS AVAILABLE

Distributed through:

SIGMA LONDON Chem. Co. Ltd. • 12, Lettice St., London, S.W.6., England • Telephone: 01-736-5823 (Reverse Charges)
SIGMA ISRAEL Chem. Co. Ltd. • 28 Kal-Gimel St., Givataim, Israel • Telephone: 03 760654 (Reverse Charges)

extensive quality through intensive research



ORTHO DIAGNOSTICS

Raritan, New Jersey 08869

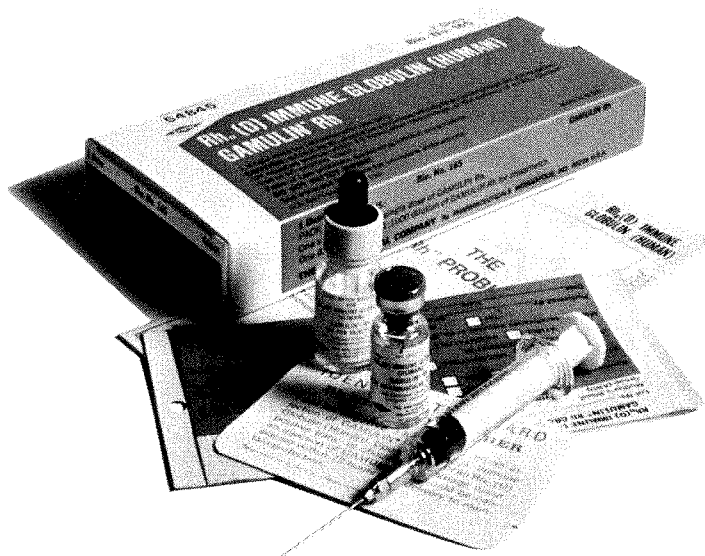
© O.D. 1968

To protect her next baby...



Gamulin® Rh Rh_o(D) immune globulin (human)

...complete with a disposable syringe
in a compact, space-saving package.



As a major producer of blood fractions, Dow now brings you a new source for Rh_o(D) immune globulin to protect the Rh negative mother's next baby from probability of hemolytic disease.

Studies to demonstrate its safety and effectiveness show that Gamulin Rh is effective in suppressing the production of Rh_o(D) antibodies.

And it comes in a space-saving, compact package that includes a vial, disposable syringe, lay literature, patient laboratory form, ID card, package insert and a crossmatch vial.

DESCRIPTION: GAMULIN Rh, Rh_o(D) Immune Globulin (Human), is a sterile concentrated solution of gamma globulin derived from blood of human donors known to have antibodies to Rh_o(D). It is standardized to contain 10.0 to 18.0 percent globulins with a level of antibody to Rh_o(D) equal to or greater than that of the NIH Reference Rh_o(D) Immune Globulin (Human). The final product contains 0.2 to 0.3 molar glycine as a stabilizer and 1:10,000 thimerosal as a preservative.

INDICATIONS: GAMULIN Rh suppresses the immune response of nonsensitized Rh_o(D) negative mothers following Rh incompatible pregnancies. The criteria for an Rh incompatible pregnancy are: That the mother shall be Rh_o(D) negative, D^u negative; and the infant shall be Rh_o(D) positive or D^u positive.

CONTRAINDICATIONS: Gamulin Rh must not be given to the infant. Gamulin Rh also should not be administered to an Rh_o(D) positive or D^u positive individual, to a recipient of an Rh_o(D) positive blood transfusion, or to an Rh_o(D) negative mother previously sensitized by an Rh incompatible pregnancy. Do not give intravenously.

PRECAUTIONS AND REACTIONS: It is essential that certain diagnostic and laboratory criteria be met before administering this product. (See package literature.) An occasional patient has shown a systemic reaction manifested by a low grade fever. Allergic reactions, although not expected, could occur.

ADMINISTRATION: Consult package insert for detailed instructions.

This product must be administered within 72 hours postpartum.

Gamulin® Rh

Rh_o(D) immune globulin (human)



THE DOW CHEMICAL COMPANY
Rx Pharmaceuticals
Indianapolis

A new panoramic presentation . . .

Freedman

Clinical Immunology

By **Samuel O. Freedman, M.D.**, *Professor of Medicine, McGill University; Director, Division of Clinical Immunology and Allergy, The Montreal General Hospital.* With Chapters by **Phil Gold, M.D., Ph.D.**, **David Hawkins, M.D.**, and **Joseph Shuster, M.D., Ph.D.**

Clinical immunology is a relatively new and rapidly developing specialty in medicine. Consequently, as with any new field, there is an urgent need to provide both the information and the practical understanding of what this new field offers. This new book satisfies that need.

Written by a well-known authority and several contributors from his own department, **CLINICAL IMMUNOLOGY** offers the knowledgeable range of a multi-authored text without repeating the material or presenting conflicting opinions so often associated with multi-authored books.

Throughout the book, the clinical significance of the latest developments in research is emphasized. The clinical manifestations, diagnosis, and treatment of common immunologic disorders are related to current concepts of etiology and pathogenesis. In addition, the application of immunologic principles to the prevention of disease is stressed.

Following a comprehensive introduction to the fundamentals of modern immunology (*The Biology of the Immune Response*), the clinical chapters present a broad viewpoint of immunologic diseases. *This panoramic presentation* includes immune deficiency states, diseases associated with hypergammaglobulinemia, organ transplantation, cancer immunology, collagen-vascular diseases, atopic diseases, allergic drug reactions, common immunization procedures, hypersensitivity to infectious agents, and the immunologic aspects of rheumatology, dermatology, nephrology, and hematology.

There is no question that this book will benefit all who must understand and consider on a practical level the immunologic factors involved in patient care or clinical research.

704 Pages. 50 Illustrations. \$20.00

HARPER & ROW, Publishers, Inc. *Medical Department*

Mail Order Dept. 2350 Virginia Avenue Hagerstown, Maryland 21740

Please send me on approval:

☐ Freedman: **CLINICAL IMMUNOLOGY**\$20.00

☐ Bill me. ☐ Check enclosed. (SAVE! We pay postage.)

Name

Address

City State Zip

AJP5

CYTOLOGISTS: now prepare more slides in less time, with less fluid



The Shandon Cyto-Centrifuge employs a unique cell concentrating and distributing technique permitting you to prepare a large quantity of microscope slides using a smaller amount of human blood plasma, synovial fluid, peritoneal exudates, seminal or other body fluids. Centrifugation and slide preparation are performed simultaneously, which eliminates prior centrifugation and saves you time. Improved head design ensures safety when working with pathogenic organisms.

The Shandon Cyto-Centrifuge produces a monolayer of cells and does not damage individual cell structure. Also, processed slides can be rapidly scanned using a preset high power objective without adjustment between slides. Get the full story on the Cyto-Centrifuge and other quality scientific tools . . . write Shandon Southern Instruments, Inc., 515 Broad Street, Sewickley, Pa. 15143 (Pittsburgh District).



P I T T S B U R G H • L O N D O N • F R A N K F U R T

Use this check list for other Shandon Catalogs and Monographs

- ☐ Paper Electrophoresis
- ☐ Acrylamide Gel Electrophoresis
- ☐ Immuno Electrophoresis
- ☐ Thin Layer Electrophoresis
- ☐ High Voltage Electrophoresis
- ☐ Paper Chromatography
- ☐ Thin Layer Chromatography
- ☐ Preparative Layer Chromatography
- ☐ Automatic Slide Staining Machine
- ☐ Tissue Processing Apparatus
- ☐ Cyto-Centrifuge

Please send your request for the above literature to Shandon Southern Instruments, Inc., 515 Broad Street, Sewickley, Pa. 15143.

Professional Opportunities

INTERNSHIPS/RESIDENCIES

BERKSHIRE MEDICAL CENTER—PATHOLOGY residency; a 425 bed acute care teaching hospital affiliated with Albany Medical College; fully approved for American Boards in pathologic anatomy and clinical pathology; year round vacation area, skiing, sailing, tennis, etc; close to Tanglewood (Boston Symphony Orchestra) and other music festivals; 2½ hours to Boston, 3 hours to New York, 4½ hours to Montreal; salary, internship \$9000; residency \$9600-\$13,000; rooms are available for single house staff to rent at \$40 per month; hospital-owned apartments for married house officers are available for rental; opportunities for additional income; large well equipped highly automated air-conditioned laboratories with computer being installed; approved School of Cytotechnology with 2 students; approved School of Medical Technology with 16 students; five Board certified pathologists and a Ph.D. chemist; each principal section of the laboratory, i.e., anatomic pathology, microbiology, clinical chemistry, hematology and blood bank is in the charge of a pathologist with special interest, experience and qualifications in these fields who devotes 95% of his time to the work of his section; ECFMG certificate required. Apply Dr. W. Beautyman, Pathologist, Berkshire Medical Center, 725 North Street, Pittsfield, Mass. 01201.

PATHOLOGIST. CERTIFIED AP AND CP, Ph.D IN BIOCHEMISTRY, 6 years experience. Desires academic position. Reply: Box 58 c/o AJP.

CLASSIFIED ADVERTISING INFORMATION

RATES:

	1 Time	3 Times	6 Times or more
Non Display:			
20 words or less	\$19.00	\$16.00	\$14.00
Each additional word	.50	.50	.50
Box Service—\$2.00—First insertion only			

	1 Time	3 Times	6 Times or more
Classified Display:			
	\$35.00	\$30.00	\$25.00
	per inch	per inch	per inch

Minimum Space—One (1) column inch

SEND ALL COPY,
AND BOX NUMBER INQUIRIES TO:

**THE AMERICAN JOURNAL
OF PATHOLOGY**

Classified Dept.
131 Mineola Blvd.
Mineola, N. Y. 11501
(516) PI 6-0092

CHANGING YOUR ADDRESS?

In order to receive your journal without interruption, please complete this Change of Address notice and forward to the Publisher, 60 days in advance, if possible.

Old Address: (PLEASE PRINT)

NAME _____

STREET _____

CITY _____

STATE (or Country) _____

ZIP CODE _____

New Address: (PLEASE PRINT)

NAME _____

STREET _____

CITY _____

STATE (or Country) _____

ZIP CODE _____

Date New Address Effective: _____

Name of Journal: _____

NEW ADDRESS—MEDICAL DEPARTMENT

Harper & Row, Publishers, Inc.

Medical Department
2350 Virginia Avenue
Hagerstown, Maryland 21740

Now, Automatic Quantitative Microscopic Image Analysis—from Zeiss!

We've added a unique precision scanning stage to our great optics, and the result is the most sophisticated system ever made for microphotometry. It's the Zeiss Scanning Microscope Photometer 05 for **all** types of photometric measurements in transmittance, absorbance, reflectance and fluorescence...and either on-line or off-line computer analysis. Cancer cytologists have already found it an invaluable tool...and other applications are developing daily in both the life sciences and industry.

Here's what this unusual system consists of:

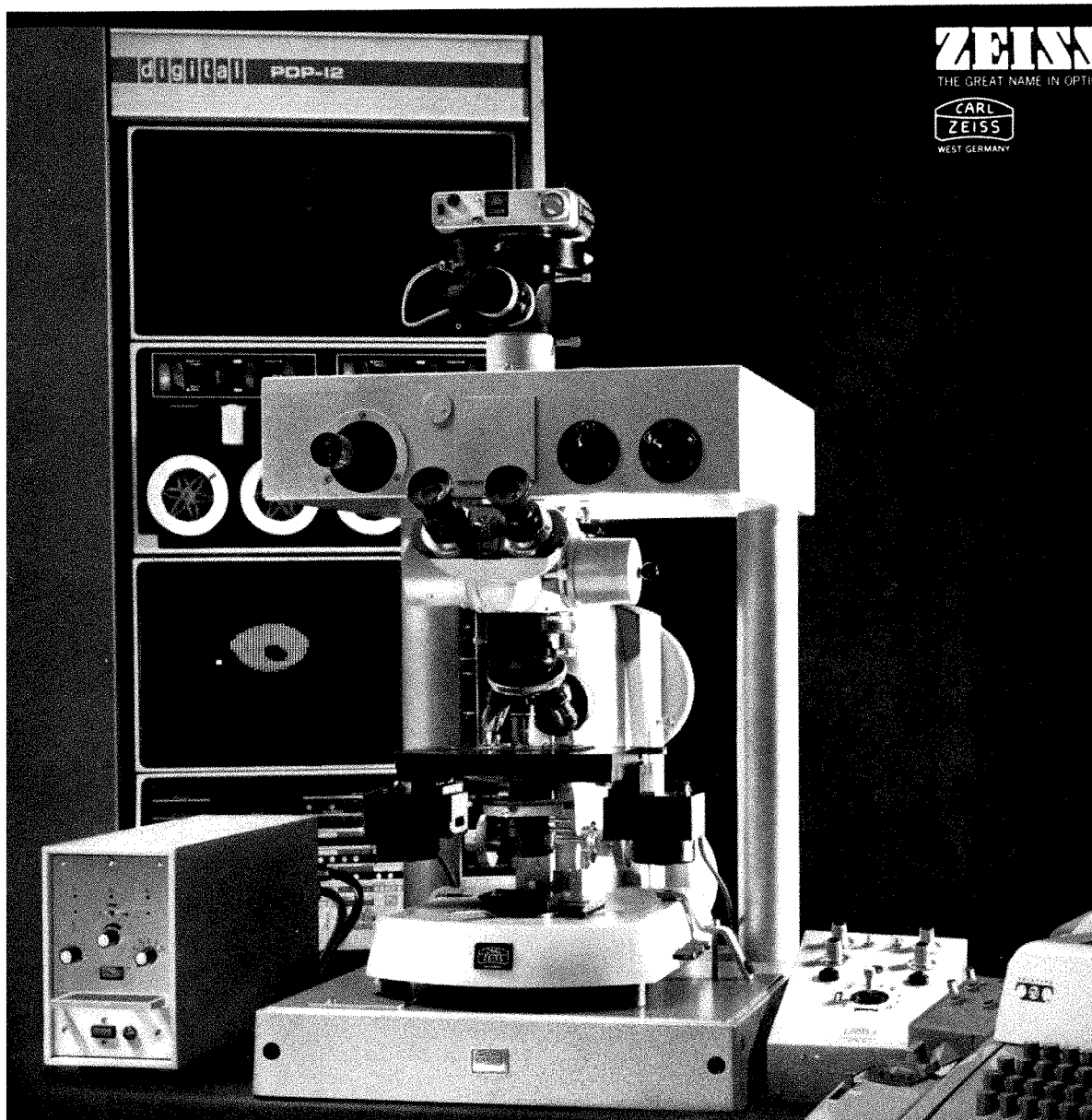
A Zeiss Universal or Photomicroscope. Any analytical system that utilizes a microscope, no matter how sophisticated the electronics, cannot be any better than its optics allow. Information that's lost in the optical channels will not be retrieved in the electronic channels. That's why it's important to start with world-famous Zeiss optics.

A unique Zeiss precision scanning stage. The two available scanning stages allow, respectively, minimum increment of 0.5 and 10 microns, perform up to 200 steps per second and travel 75mm and 25mm in the X and Y directions in several different scanning patterns, including meander, comb or line.

Much more. A modular electronic system that permits you to select components as you need them and as your budget permits. All the famous Zeiss accessories and photographic and analytical attachments—everything you might ever need for qualitative and quantitative microscopy—are, of course, available. We can even supply a PDP-12 computer with a number of programs prepared by well-known scientists. For the full story write Carl Zeiss, Inc., 444 5th Ave., New York, N.Y. 10018. Call phone (212) 736-6070.

Nationwide Service.

ATLANTA, BOSTON, CHICAGO, COLUMBUS, DALLAS, DENVER, FORT LAUDERDALE, HOUSTON, KANSAS CITY, LOS ANGELES, PHILADELPHIA, PHOENIX, SAN FRANCISCO, SEATTLE, WASHINGTON, D.C.



**speed...simplicity...certainty
...on the spot**

GRAVINDEX
TRADEMARK
slide test for pregnancy



ORTHO DIAGNOSTICS

Raritan, New Jersey 08869

© U. D. 1988

Separation of Beating Cardiac Myocytes from Suspensions of Heart Cells

Thomas G. Pretlow II, MD, Melvin R. Glick, MS and
William J. Reddy, PhD

Heart cells were obtained in suspension after incubation with collagenase and hyaluronidase in Saline A. Cardiac myocytes were separated by isopycnic centrifugation in 88.6 to 92.4% purity from other heart cells with different densities, and by velocity or rate-zonal sedimentation, in 92.8 to 97.4% purity from heart cells with different diameters. A previously described computer integration of the differential sedimentation equation was used to determine the centrifugal force, duration of centrifugation and gradient design, which would permit the separation of cardiac myocytes from other heart cells by velocity sedimentation. The myocytes continued to contract rhythmically after being recovered from the density gradients. Velocity sedimentation was superior to isopycnic sedimentation for the separation of cardiac myocytes from heart cell suspensions because it gave the most highly purified myocytes, resulted in recovery of the largest proportion of myocytes in purified fractions from the gradient and required lower centrifugal forces for shorter periods of time. The potential significance of the availability of pure cardiac myocytes is discussed (Am J Pathol 67:215-226, 1972).

BOTH AVIAN AND MAMMALIAN cardiac myocytes can be obtained from minced heart muscle following incubation of the heart muscle with a variety of proteolytic enzymes and chelating agents.¹⁻⁴ Numerous investigators have reported that these myocytes contract

From the Departments of Pathology, Engineering Biophysics and Medicine, The School of Medicine and Dentistry, University of Alabama in Birmingham, Birmingham, Alabama.

Supported in part by NIH Grants CA12870 and HE14301 from the US Public Health Services. Melvin R. Glick: Predoctoral student supported by NSF Institutional Grant NSFCW3203.

Accepted for publication Nov 1, 1971.

Address reprint requests to Dr. Thomas G. Pretlow, Department of Pathology, University of Alabama in Birmingham, The Medical Center, 1919 Seventh Avenue South, Birmingham, Ala 35233.

with an intrinsic rhythmicity when suspended in appropriate physiologic salines, and beat synchronously during extended periods of cultivation *in vitro*.⁵⁻⁷ DeHaan⁸ recently employed beating avian cardiac myocytes as an exquisitely sensitive assay for toxic substances in tissue culture medium. The rhythmicity of myocytes *in vitro* would appear to be a generally useful parameter for the study of the nutritional adequacy of tissue culture medium, response to hormones *in vitro*, etc. While many investigators have not specifically mentioned the composition of these heart cell suspensions, DeHaan⁹ noted cells which are similar to fibroblasts in addition to the myocytes; and Harary and Farley¹⁰ described their suspensions as containing blood cells, "stellar cells", myoblasts, and epithelial cells. This model system could be made more specific for the study of myocytes if pure myocytes could be cultivated *in vitro* in the absence of other heart cells. Similarly, the metabolism of the cardiac myocyte could be more specifically studied if pure cells could be obtained. We now report a method for obtaining highly purified beating cardiac myocytes by separating the myocytes from the fibroblasts, endothelial cells, and blood cells which are found together with myocytes in myocardium.

Materials and Methods

Suspension of Heart Cells

Heart cells were obtained in suspension using a modification of the method of Berry, Friend and Scheuer.⁴ The heart ventricles were excised from two 150-200 g, male, Sprague-Dawley rats, minced to fragments of approximately 2 mm in greatest dimension, washed and placed in 1.5 ml of Saline A¹ containing 0.1% collagenase and 0.05% hyaluronidase (Sigma Chemical Company, St Louis, Mo 63178). The cardiac muscle fragments were then gently agitated in this disaggregation medium at 100 cycles/min for 15 minutes on a Dubnoff Metabolic Shaker with the water bath at 37 C. The supernatant from this first 15-minute incubation, containing predominantly red blood cells, was discarded. The supernatants from three subsequent incubations under identical conditions were washed to remove the collagenase and hyaluronidase, combined, resuspended and diluted to contain $15-25 \times 10^6$ heart cells in 7 ml of Saline A and gently layered over the density gradients.

Gradient Centrifugation

Previous reports have presented detailed accounts of the theory of gradient centrifugation as applied to mammalian cells,¹¹⁻¹⁵ detailed descriptions of the technic which we employ¹⁴ for the separation of viable mammalian cells in gradients of Ficoll (polysucrose, average molecular weight 400,000; Pharmacia Fine Chemicals, Piscataway, NJ) in tissue culture medium and the results of specific separations which have been carried out in our laboratory;¹⁶⁻²⁰ therefore, we shall omit a detailed presentation of technic and theory from this report.

The gradients for isopycnic centrifugation varied linearly from 4.1% (w/w) Ficoll at the sample-gradient interface, 14.9 cm from the center of revolution, to 43.0% (w/w) Ficoll at the gradient-cushion interface, 26 cm from the center of revolution. Isopycnic centrifugation was carried out using a centrifugal force of 950 *g* at 4.0 C for 90 minutes. After isopycnic centrifugation, the gradients were collected in 3-ml fractions. Refractive indices were measured on all gradient fractions in order to confirm the linearity of all density gradients. Cell counts were performed on all gradient fractions using hemocytometer chambers. Slides for microscopic examination were prepared using the Cytocentrifuge (Shandon Scientific Company, Sewickley, Pa) and stained with Wright stain (Chroma-Gesellschaft Schmid and Company, Stuttgart-Unterturkheim, Germany). Differential cell counts were performed, counting 500 cells from each gradient fraction.

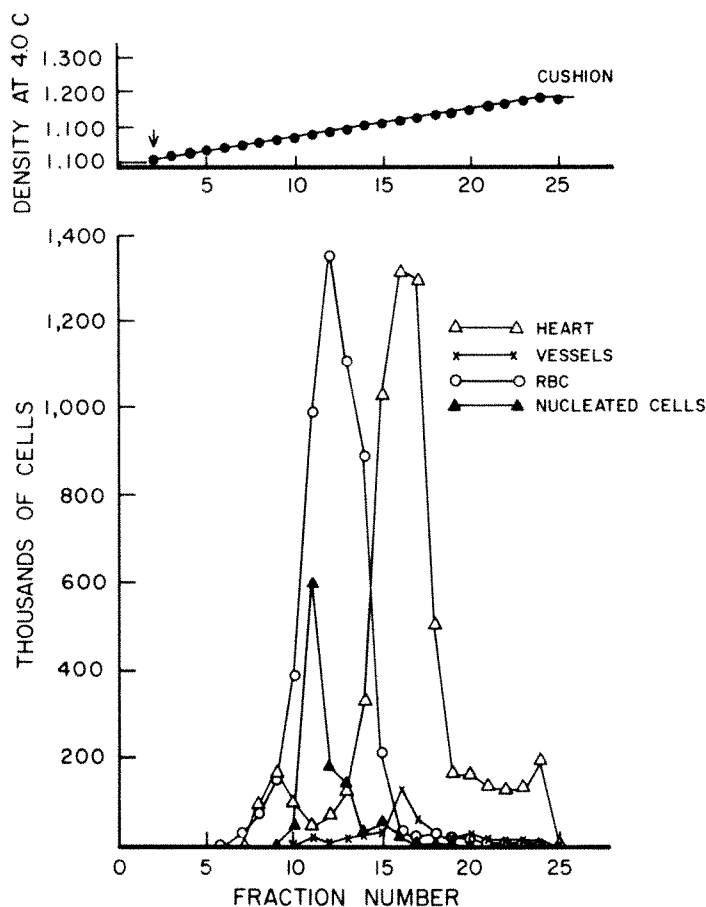
Gradients for the separation of cells by velocity sedimentation were constructed such that the Ficoll concentration varied linearly from 2.4% (w/w) Ficoll at the sample-gradient interface, 13.7 cm from the center of revolution, to 18.5% (w/w) Ficoll at the gradient-cushion interface 26.0 cm from the center of revolution. Preliminary velocity sedimentation was carried out at 18.7 *g* (measured at the sample-gradient interface 13.7 cm from the center of revolution) for short periods of time. Each respective type of cell was located on the gradient. The location of each type of cell, after the described velocity sedimentation, and the density of each type of cell, as determined experimentally using isopycnic sedimentation, were substituted in the computer integration of the differential sedimentation equation in order to calculate effective diameters for each of the modal populations of cells as described previously.¹⁴ The calculated effective diameters and the experimentally determined densities were then used in the computer integration of the differential sedimentation equation in order to ascertain: a) whether or not the described gradient would permit the purification of cardiac myocytes and b) a satisfactory speed and duration of centrifugation for the separation of myocytes from the other heart cells which were present in the cell suspension. Simulated experiments carried out in this fashion indicated that centrifugation at 24 *g* (measured at the sample-gradient interface 13.7 cm from the center of revolution) for 30 minutes would result in separation of the myocytes from the other heart cells; laboratory experiments were carried out using these conditions. After velocity sedimentation, 4-ml fractions were collected from the gradients; refractive indices were measured, cell counts were performed, and slides for microscopic examination were prepared as described above.

Results

Sample Composition

Suspensions of cells, which were obtained using the described procedure modified after Berry *et al*⁴ for the digestion of myocardium, contained consistently less than 23% cardiac myocytes. Preliminary purification of these heart cells could be accomplished by centrifuging them to form a pellet at 65 *g* for 3 minutes and selectively discarding the top portion of the pellet which was found to be rich in red blood cells. This preliminary step resulted in a maximum myocyte purity of 46%. Even after this preliminary purification step was repeated several times, the cardiac myocytes usually constituted considerably less than 46% of the

heart cells in this suspension. In some experiments, the hearts from heparinized rats (100 units intraperitoneally 20 minutes before sacrifice) were perfused with saline A before being minced and digested with the described enzymes. While this perfusion step removed many of the red blood cells, some red blood cells always remained and the myocytes were never obtained in greater than 46% purity. Berry *et al*⁴ described two-thirds of the myocytes examined with the electron microscope as being "morphologically intact." Using only light microscopy,



TEXT-FIG 1—Separation of rat heart cells by isopycnic sedimentation. In this experiment, 22.8×10^6 cells were separated on a linear, 11.1 cm, 4.1–43.0% w/w Ficoll gradient. Centrifugation was carried out at 950 *g* (measured at the sample-gradient interface) at 4.0 C for 90 minutes. In isopycnic sedimentation, cells are separated according to differences in density. It can be observed that there is an appreciable overlap between the densities of the various kinds of cells. An arrow marks the sample-gradient interface on the density plot.

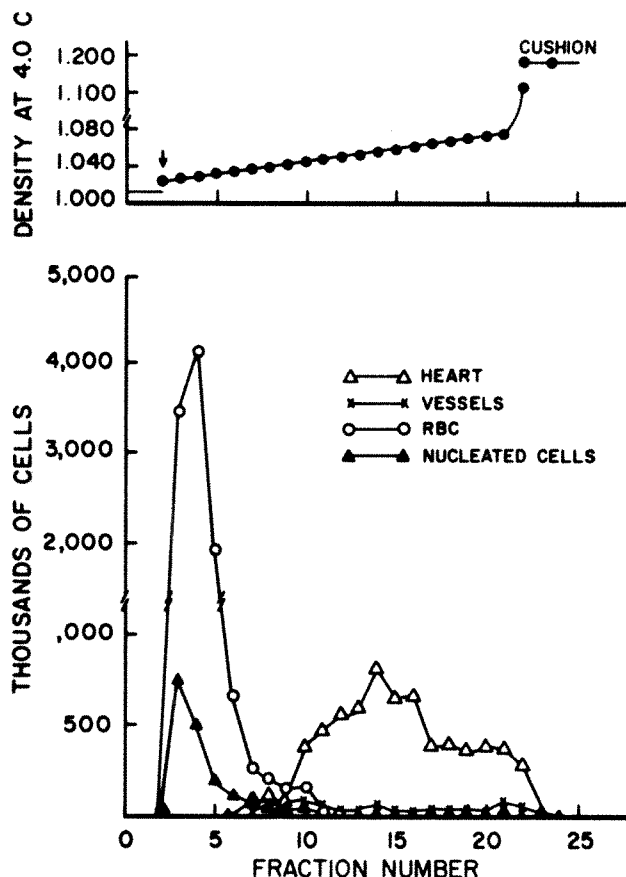
a very small proportion of the cells in our experiments appeared to be damaged.

Isopycnic Centrifugation

Isopycnic centrifugation resulted in an incomplete separation of the modal population of myocytes from the modal population of red blood cells (Text-figure 1). In repeated experiments, 76.4 to 79.8% of myocytes were recovered in five 3-ml fractions (Fractions 14 through 18) from the 72-ml gradient. These myocytes varied in density from 1.12 to 1.14 g/ml. Cardiac myocytes were obtained in a maximum purity of 88.6 to 92.4% myocytes in Fraction 18 after isopycnic centrifugation (Text-figure 1). Five adjacent 3-ml fractions from the gradient (Fractions 10 through 14) contained 90.4 to 92.5% of the erythrocytes recovered from the gradient. These erythrocytes varied in density from 1.10 to 1.12 g/ml. Erythrocytes were obtained in 76.2 to 83.0% purity in Fraction 12 (Text-figure 1). There are two well-defined modes of myocytes which are quite different from each other in density. As noted above, the overwhelming majority of myocytes is found in the mode having a density of 1.12 to 1.14 g/ml; these myocytes appear to be intact when examined microscopically. The less dense modal population of myocytes, which is present at a density of 1.07 through 1.1 g/ml, are fragmented and considered to have been severely damaged by mincing and enzyme digestion steps used for disaggregation.

Velocity Sedimentation

After velocity sedimentation at 24 g (measured at the sample-gradient interface 13.7 cm from the center of revolution) for 30 minutes, the cardiac myocytes were almost completely separated from other heart cells (Text-figure 2). As noted previously, the starting sample suspension of heart cells never contained more than 46% myocytes. In repeated experiments, 82.8 to 86.2% of the separated cardiac myocytes were recovered in Fractions 12 through 22, varying in purity between 92.8 and 97.4% myocytes. Both the maximum purity (Figure 1) and the largest number of myocytes were found in Fraction 15 (± 1 gradient fraction). Since our purpose was to prepare pure myocytes, no effort was made to separate red blood cells from nucleated cells. This separation has been demonstrated previously¹⁹ and requires a gradient having a lesser slope (g/ml/cm), such as the isokinetic¹⁵ gradient. Myocytes were not present in the fraction that contained erythrocytes and nucleated cell peak (Figure 2). When gradients were made of Ficoll and Joklik's modification of minimum essential medium, cardiac myocytes failed to



TEXT-FIG 2—Separation of rat heart cells by rate-zonal or velocity sedimentation. In this experiment, 24.7×10^6 cells were separated on a linear, 12.3 cm, 2.4–18.5% w/w Ficoll gradient. Centrifugation was carried out at 24 g (measured at the sample-gradient interface) at 4.0 C for 30 minutes. Rate-zonal sedimentation results in the separation of cells primarily because of differences in diameter. Cardiac myocytes are both more highly purified and more widely separated from the other heart cells than was observed after isopycnic centrifugation.

beat after their entry into the gradients; this cessation of myocyte contraction in media containing magnesium or calcium has caused most investigators to use media such as Saline A¹ which are free of calcium and magnesium. When gradients were made of Ficoll in Saline A, cardiac myocytes continued to contract rhythmically after they were separated by density gradient centrifugation.

Velocity sedimentation offers several advantages over isopycnic sedimentation for the separation of cardiac myocytes since: a) the modal population of myocytes is more widely separated from the other kinds of cells, b) the myocytes are obtained in higher purity, c) the cells are

subjected to much lower centrifugal forces and d) the cells are available more rapidly for subsequent experiments.

Recovery of Cells

After isopycnic centrifugation, 61.2 to 74.6% of the heart cells layered over the gradient were recovered in fractions from the gradient. After velocity or rate-zonal sedimentation, 64.4 to 75.2% of the cells in the starting sample suspension were recovered from the gradient. As noted above, the relative proportions of red blood cells and myocytes in the starting sample suspension varied as a function of the technic used for disaggregating the myocardium and according to the number of preliminary centrifugations carried out before gradient centrifugation. The peak heights and the areas under the peaks for each respective cell type varied as a function of the composition of the starting cell suspension. There did not appear to be a disproportionate loss of either red blood cells or cardiac myocytes. The numbers of neutrophils, vessel fragments and other nucleated cells in the starting sample suspension were too small to permit a rigorous evaluation of the recovery of each of these kinds of cells. The 24.8 to 38.8% of heart cells, which were present in the starting sample suspension and not recovered in the fractions from the gradient, represent a larger loss of cells than can be accounted for by experimental counting error. Much of this cell loss could have resulted from the wall effect artifact observed in all centrifugations carried out in cylindrical tubes. The wall effect artifact has been discussed in previous reports.^{12,14}

Discussion

The described technic for the purification of cardiac myocytes would appear to have considerable significance in several areas of investigation. Pure cultures of cardiac myocytes have not been obtained by the currently available technics for dissociating and culturing heart cells. Mark *et al*²¹ emphasize the changing proportions of endothelioid and muscle cells observed during the growth of heart cells in culture, and warn about interpreting enzyme or respiratory metabolic changes when such heterogeneous and changing cell populations are cultured together. The method reported here not only permits the inoculation of purified myocytes in culture, but allows immediate separation of millions of adult, differentiated heart muscle cells for metabolic and physiologic studies. One of our laboratories (Wm R and MG) has recently found that certain enzyme activities formerly attributed to heart muscle are, in fact, present in previously studied myocardium primarily because

the cardiac myocytes were adulterated with incompletely removed red blood cells.

Clark²² measured glucose utilization in dissociated heart cells under various experimental conditions. Schreiber *et al*²³ reported specific alterations in protein synthesis in the "overloaded" heart. Both the metabolism of cardiac myocytes under normal circumstances and the response of the cardiac myocyte to pathogenic stimulation could be more specifically elucidated using preparations free of other kinds of cells. Purified cardiac myocytes should prove particularly useful in the study of nutritional requirements of the heart cell. Gerchenson, Harary and Mead²⁴ reported that cultured heart cells require an exogenous supply of linoleic and palmitic acids for optimal growth and mitochondrial integrity. While, by definition, whole animals must be able to synthesize all nonessential amino acids, certain adult cells are not able to synthesize all of the required nonessential amino acids; for example, normal human bone marrow is not capable of synthesizing adequate amounts of serine and asparagine.²⁵ The availability of pure cardiac myocytes permits the investigator to study the nutritional requirements of this single cell type *in vitro* while excluding the possibility that other kinds of cells in the culture are altering the experimental conditions by exporting nutrients for use by the cardiac myocytes. Halle and Wollenberger²⁶ recently described a defined medium without macromolecules for the culture of avian myocytes. Cultures of pure, mammalian cardiac myocytes would be particularly suited to the development of a defined medium for mammalian cells. The intrinsic rhythmicity of the cardiac myocyte provides a very sensitive assay of the cell's milieu which is not available in work with other kinds of cells.

DeHaan⁸ recently detected a toxic substance readily eluted from disposable intravenous administration sets, that had been used to perfuse cultured chick heart cells. The toxicity of the medium delivered through these sets was detected before cell death occurred by a decrease in the fraction of cells actually beating. Other investigators^{27,28} studied the response of heart cells to drugs and other toxic substances. The information derived from this kind of study could be much more specific if the studies were carried out using only cardiac myocytes.

References

1. Vahouny GV, Wei R, Starkweather R, Davis C: Preparation of beating heart cells from adult rats. *Science* 167:1616-1618, 1970
2. Bloom S: Spontaneous rhythmic contraction of separated heart muscle cells. *Science* 167:1727-1729, 1970

3. Hilfer SR, Brown JM: Collagenase. *Exptl Cell Res* 65:246-249, 1971
4. Berry MN, Friend DS, Scheuer J: Morphology and metabolism of intact muscle cells isolated from adult rat heart. *Circ Res* 26:679-687, 1970
5. Halbert SP, Bruderer R, Lin TM: In vitro organization of dissociated rat cardiac cells into beating three-dimensional structures. *J Exp Med* 133:677-695, 1971
6. Wildenthal K: Long-term maintenance of spontaneously beating mouse hearts in organ culture. *J Applied Physiol* 30:153-157, 1971
7. Cavanaugh MW: Pulsation, migration and division in dissociated chick embryo heart cells *in vitro*. *J Exptl Zool* 128:573-589, 1955
8. DeHaan RL: Toxicity of tissue culture media exposed to polyvinyl chloride plastic. *Nature* 231:85-86, 1971
9. DeHaan RL: Regulation of spontaneous activity and growth of embryonic chick heart cells in tissue culture. *Develop Biol* 16:216-249, 1967
10. Harary I, Farley B: In vitro studies on single beating rat heart cells. I. Growth and organization. *Exptl Cell Res* 29:451-465, 1963
11. Pretlow TG, Boone CW: Centrifugation of mammalian cells on gradients: a new rotor. *Science* 161:911-913, 1968
12. Boone CW, Harell GS, Bond HE: The resolution of mixtures of viable mammalian cells into homogeneous fractions by zonal centrifugation. *J Cell Biol* 36:369-378, 1968
13. Pretlow TG, Boone CW, Shrager RI, Weiss GH: Rate-zonal centrifugation in a Ficoll gradient. *Anal Biochem* 29:230-237, 1969
14. Pretlow TG, Boone CW: Separation of mammalian cells using programmed gradient sedimentation. *Exp Molec Path* 11:139-152, 1969
15. Pretlow TG: Estimation of experimental conditions that permit cell separations by velocity sedimentation on isokinetic gradients of Ficoll in tissue culture medium. *Anal Biochem* 41:248-255, 1971
16. Abeloff MD, Mangi RJ, Pretlow TG, Mardiney MR: Isolation of human leukemic blasts from peripheral blood by density gradient centrifugation. *J Lab Clin Med* 75:703-710, 1970
17. Pretlow TG, Boone CW: Separation of malignant cells from transplantable rodent tumors. *Exp Molec Pathol* 12:249-256, 1970
18. Pretlow TG, Cassady IM: Separation of mast cells in successive stages of differentiation using programmed gradient sedimentation. *Am J Pathol* 61:323-340, 1970
19. Pretlow TG, Pushparaj N: A new method for separating peritoneal lymphocytes from macrophages. *Immunology* 22:87-91, 1972
20. Pretlow, TG, Pichichero ME, Hyams L: Separation of lymphocytes and macrophages from suspensions of guinea pig peritonitis exudate cells using programmed gradient sedimentation. *Am J Pathol* 63:255-272, 1971
21. Mark GE, Hackney JD, Strasser FF: Morphology and contractile behavior of cultured heart cells and their response to various oxygen concentrations, Factors Influencing Myocardial Contractility. Edited by RD Tranz, F Kavalier, J Roberts. New York, Academic Press, Inc, 1967, pp 301-315

22. Clark CM, Jr: Carbohydrate metabolism in the isolated fetal rat heart. *Am J Physiol* 220:583-588, 1971
23. Schreiber SS, Murray O, Evans CD, Gueyikian I, Rothschild MA: Myosin, myoglobin, and collagen synthesis in acute cardiac overload. *Am J Physiol* 219:481-486, 1970
24. Gerschenson LE, Harary I, Mead JF: Studies in vitro on single beating rat-heart cells. X. The effect of linoleic and palmitic acids on beating and mitochondrial phosphorylation. *Biochim Biophys Acta* 131:50-58, 1967
25. Regan JD: Serine requirement in leukemic and normal blood cells. *Science* 163:1452-1453, 1969
26. Halle W, Wollenberger K.: Differentiation and behavior of isolated embryonic and neonatal heart cells in chemically defined medium. *Am J Cardiol* 25:292-299, 1970
27. McCarl RL, Margossian SS: Restoration of beating and enzymatic response of cultured rat heart cells to cortisol acetate. *Arch Biochem Biophys* 130:321-325, 1969
28. Seraydarian MW, Sato E, Harary I: *In vitro* studies of beating heart cells in culture. XIII. The effect of 1-fluoro-2,4-dinitrobenzene. *Arch. Biochem Biophys* 138:233-238, 1970

Acknowledgments

We wish to thank Mrs. Linda Hamilton and Miss Rebecca McDaniel for their expert technical assistance.

[*Illustrations follow*]



Fig 1—Fraction 15 from the rate-zonal separation of rat heart cells. This fraction contains purified cardiac myocytes (Wright stain, $\times 100$).

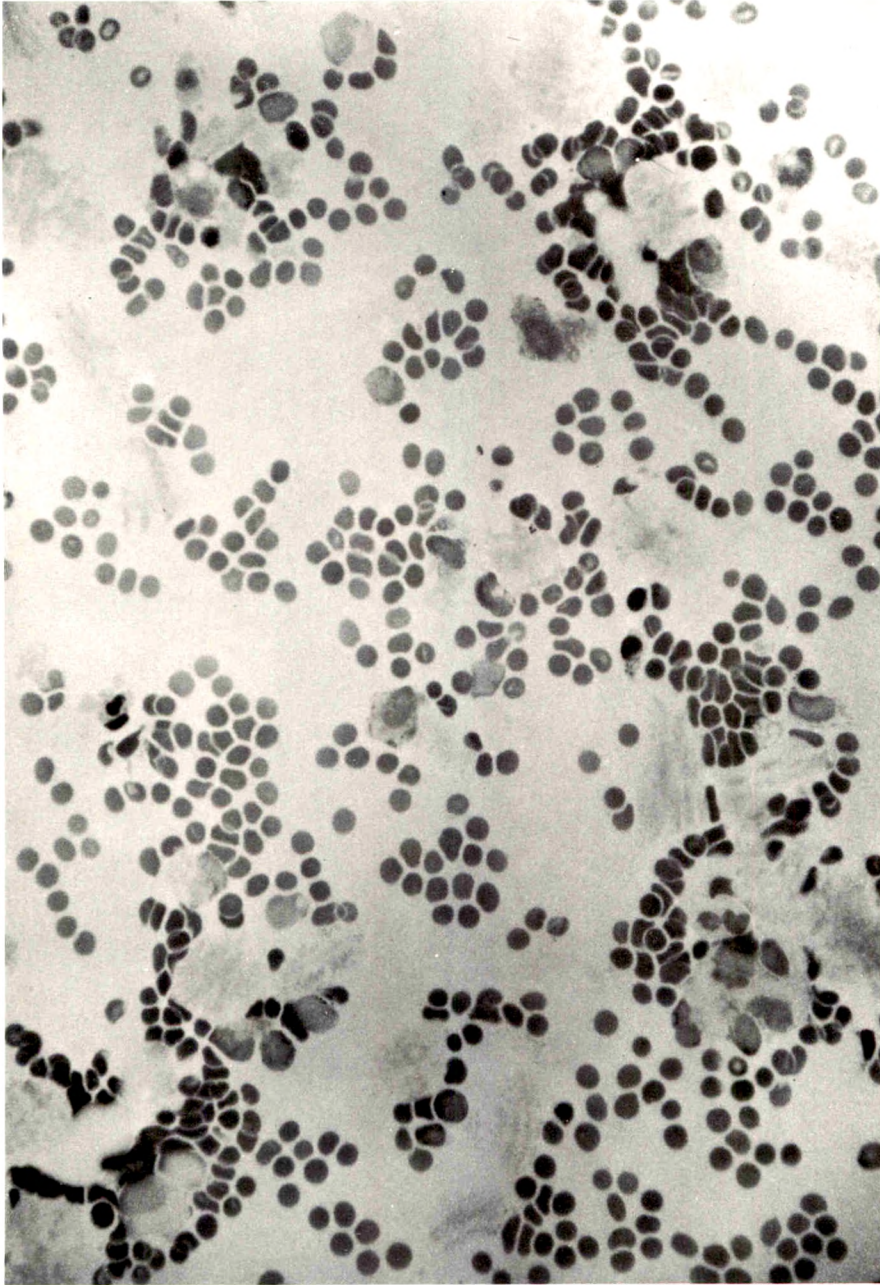


Fig 2—Fraction 4 from the rate-zonal separation of heart cells. This fraction contains the modal population of erythrocytes as well as nucleated cells and damaged cells. Red blood cells were not resolved from nucleated cells because of the very steep (g/ml/cm) gradient which was found to be optimal for the separation of cardiac myocytes from other cells (Wright stain, $\times 100$).

Defective Function of Renal Lysosomes in Mice with the Chediak-Higashi Syndrome

David J. Prieur, DVM, PhD, William C. Davis, PhD and
George A. Padgett, DVM

Morphologically abnormal lysosomes demonstrated in individuals with the Chediak-Higashi syndrome (CHS) suggested a defect in the function of these abnormal lysosomes. To gain direct experimental evidence of such a defect, horseradish peroxidase (HRP) was injected intravenously into CHS and control mice, the mice killed at varying intervals and the kidneys studied by ultrastructural cytochemistry. No morphologic difference was observed in the absorption and uptake of HRP by proximal convoluted tubules in the two groups of mice. In CHS mice, however, some of the HRP fused with enlarged lysosomes. By 48 hours after injection, the lysosomes of normal mice had digested all but trace amounts of HRP, whereas large amounts were still present in CHS mice at this time. In CHS mice, moderate amounts were still present at 72 hours and trace amounts 96 hours post injection. This slowed rate of digestion of HRP by lysosomes of the proximal convoluted tubule cells of CHS mice suggests a similar defect in all cells in CHS individuals in which there is a lysosomal degradation of protein or other matter obtained by endocytosis. Such a defect may explain some manifestations of impaired host defense observed in CHS (*Am J Pathol* 67:227-240, 1972).

THE CHEDIAK-HIGASHI SYNDROME (CHS) is an autosomal recessive disease which has been reported to occur in four species: man,¹ mink,² cattle³ and mice.⁴ The homology of the disease in the four species is well established,^{5,6} but the basic biochemical defect has not been identified. Chediak-Higashi syndrome is manifested by partial albinism, an increased susceptibility to infectious disease and enlarged anomalous granules in many cell types. The enlarged granules in leukocytes have been shown to be lysosomes,⁷ whereas others, such as melanin granules, have not been classified as lysosomes. The manner in which the abnormal granules form in some cell types has been demonstrated. In both leukocytes^{8,9} and melanocytes¹⁰ the abnormally enlarged granules are caused by an unregulated fusion of granules.

Although the function of cells with abnormal granules has been

From the Department of Veterinary Pathology, College of Veterinary Medicine, Washington State University, Pullman, Washington.

Supported in part by US Public Health Service, NIH Grants 5TI-GM-414-08, FR-05465 and AI-06591.

Accepted for publication Nov 22, 1971.

Address reprint requests to Dr. David J. Prieur, Room 5B21, Building 37, NCI, National Institutes of Health, Bethesda, Maryland 20014.

shown to be defective in some respects, such as chemotaxis,¹¹ killing of bacteria^{12,13} and degranulation,^{14,15} experimental evidence of a defect in lysosomal function has not been demonstrated directly. In a preliminary report on the catabolism of egg albumin in renal epithelial cells of mice and mink with CHS, evidence was obtained suggesting such a defect.¹⁶ In the present study, horseradish peroxidase was used to study further the functional capacity of morphologically abnormal lysosomes in the renal tubule cells of mice with CHS.

Materials and Methods

Animals

Mice with CHS and the background genes of C57BL/6J mice were obtained from Jackson Laboratories (Bar Harbor, Maine) as brother-sister pairs of b^gb^g (homozygous for the beige or CHS trait) and +b^g (heterozygous for the beige trait). They were maintained by brother-sister matings of b^gb^g to +b^g for five generations and then were mated at random. The CHS mice used in this study were obtained from these random matings. The control mice were offspring of C57BL/6J mice derived from matings of +b^g mice and shown, by test matings, to be free of the beige gene.

Technics

Beige and C57BL/6J young mature female mice were injected in the tail vein with 0.1 ml of saline containing horseradish peroxidase (Sigma Type II, Sigma Chemical Company), 12 mg/100 g body weight. These mice, along with saline-injected beige and C57BL/6J controls, were killed by cervical dislocation at scheduled times from 90 seconds to 96 hours after injection. After the renal veins were incised, the kidneys were perfused with physiologic saline (37 C) injected slowly into the left ventricle of the heart, and the kidneys were subsequently perfused with either 4% glutaraldehyde diluted with physiologic saline or with 1.5% glutaraldehyde in 0.1 M K₂PO₄ buffer to which 1% sucrose (KP-S buffer) pH 7.4 was added. The kidneys were placed in 1.5% glutaraldehyde-KP-S buffer for 2 to 6 hours, washed three times in KP-S buffer and stored at 4 C until sectioned. Kidney cortex was sectioned at 50 μ on a TC-2 Smith Farquhar tissue chopper (Ivan Sorvall, Inc). Cross-sections of cortex were collected, rinsed in KP-S buffer and stained for peroxidase.¹⁷ A saturated solution of 3,3'-diaminobenzidine was prepared by adding 6 mg of 3,3'-diaminobenzidine to 9 ml of 0.05 M Tris-HCl buffer, pH 7.4, and shaking the solution for 30 minutes at room temperature. One milliliter of a 1% solution of hydrogen peroxide was then added, the solution was shaken thoroughly and filtered. Sections of kidney were incubated in 2 to 3 ml of this solution for 10 minutes, washed three times in distilled water, post-fixed for 45 minutes in a 1% solution of osmium tetroxide on ice¹⁸ and *en-block* stained for 2 hours with a 1% aqueous solution of uranyl acetate. The tissues were washed twice with distilled water, dehydrated in graded solutions of ethanol and embedded in Epon-Araldite.¹⁹ Thick and thin sections were cut with glass and diamond knives, respectively, on a Porter-Blum MT-2 ultramicrotome. The thin sections were viewed, either unstained or stained with lead citrate and uranyl acetate, in a Philips 200 electron microscope.

Results

Horseradish peroxidase (HRP) is endocytized by cells of the renal tubules and when incubated with diaminobenzidine and hydrogen peroxide electron-dense deposits are produced which can serve as ultrastructural markers. None of this cytochemical reaction product was observed in saline-injected control mice of either the CHS or normal group.

Although post-staining with lead citrate and uranyl acetate helped visualize structures in the electron microscope, it was not essential, and electron micrographs were taken of the unstained sections.

In both CHS and black (control) mice killed 90 seconds after the injection of HRP, the reaction product of HRP was present just beneath the brush border in apical portions of the proximal convoluted tubule cells. Little HRP could be demonstrated attached to microvilli of brush borders in either group of mice killed at this or subsequent times. At this early stage of absorption of HRP, there was no demonstrable difference in the distribution or the amount of HRP in the two groups of mice. At 5 minutes after injection, there was no difference in the appearance of HRP in the apical vacuoles of the cells of the two groups (compare Figures 1 and 2), but by this time, some of the HRP had entered deeper parts of the cells and, in the CHS, had fused with enlarged granules in cells of animals with CHS (Figure 2). With mice killed at increasing time intervals after injection, there was an increasing amount of the HRP in phagolysosomes in deeper parts of the cell. In groups of mice killed beyond several hours after injection, there was a concomitant decrease in the amount of HRP present in apical portions of tubule cells in apical vacuoles. By 18 hours after injection, very little HRP was present in apical vacuoles (Figures 3 and 4). At this time, no difference in the amount of HRP in cells of the two groups of mice could be discerned. In individual phagolysosomes, however, because CHS cells had larger but fewer phagolysosomes, there was more HRP in the phagolysosomes of the CHS cells.

There was a gradual decrease in the amount of HRP present in phagolysosomes of both groups of mice killed after 18 hours postinjection. In the control group, however, the rate at which HRP disappeared from the phagolysosomes was more rapid. In the control mice killed 48 hours after injection, only trace amounts of HRP were present (Figure 5). In CHS mice killed at this time a considerable amount of HRP was present (Figure 6), but substantially less than was present in CHS mice killed 18 hours after injection (Figure 4). The amount of HRP in phagolysosomes of CHS mice continued to decrease and, in the group killed at 72 hours, there was a moderate amount of HRP present

(Figure 7), the quantity of which was only slightly less than that present in CHS mice killed at 48 hours (Figure 6). At 72 hours after injection, HRP was present in both enlarged phagolysosomes and in more normal appearing phagolysosomes (Figure 7). At 96 hours after injection, only trace amounts of HRP were present in CHS mice, the amount being roughly comparable to that observed in control mice at 48 hours after injection.

No HRP was evident in the proximal convoluted tubule cells of control mice killed at 72 and 96 hours. Because 96 hours was the longest time interval after injection that mice were killed, it was not ascertained how much longer the trace amounts of HRP persisted in the CHS mice. Because there was a more marked decrease in the amount of demonstrable HRP in the CHS mice between 72 and 96 hours than between 48 and 72 hours, it is assumed that the HRP persisted a relatively short time beyond 96 hours.

Homogeneous electron-lucent bodies were observed in the phagolysosomes of both CHS and control mice. Many of these bodies had a spherical shape, and some appeared to be membrane limited; HRP was not observed in them. In CHS mice, some of these bodies were much larger than those in control mice, but most were approximately the same size (compare Figures 3 and 4). These bodies may represent virgin lysosomes which have fused with the preexisting phagolysosome. On the other hand, they may be simply lipid bodies.

The basic structure of the phagolysosomes of CHS and control mice was similar. The CHS phagolysosomes were larger, however, and were often more irregular in shape (compare Figures 3 and 4). Although there was often a close association between lysosomes and other cellular organelles, especially mitochondria, the inclusion of these organelles in the lysosomes was not observed in either CHS or normal mice.

Discussion

Although enlarged granules have been observed in many cell types in CHS, evidence from several sources has suggested that it is not a classical storage disease. Cytochemical studies have demonstrated that the enlarged granules in CHS vary from one cell type to another but that the cytochemical reactions are similar to those of the normal granules in a particular cell type. Secondly, it has been demonstrated in leukocytes and melanocytes that the enlarged granules in these cell types arise by fusion of preexisting granules which arise by normal pathways.^{8,10} Finally, it has been demonstrated that CHS fibroblasts grown in cultures with fibroblasts from several inherited storage dis-

eases, corrected the cellular accumulation of metachromatic granules in fibroblasts from individuals with those diseases but were not in turn corrected by the fibroblasts of any of the inherited storage diseases.²⁰

Most of the studies on CHS involved neutrophils. Although differences have been demonstrated between neutrophils from normal and CHS individuals, attempts to demonstrate a functional defect in the digestive capacity of lysosomes of neutrophils was not obtained. Some of the difficulties associated with the demonstration of such a defect in neutrophils are directly related to the peculiarities of this cell type. Neutrophils produce their lysosomal granules in the bone marrow in a specific stage of maturation. After maturation, the neutrophil is released from the bone marrow and subsequently, either in the blood stream or in the tissues, it phagocytizes material such as bacteria. Upon phagocytosis, the lysosomes fuse with the phagocytized material, digest it and the cell dies.

In contrast to neutrophils, most cells of the body are long-lived, continually producing lysosomes and continually endocytizing and digesting material. To measure the digestive capacity of lysosomes it would be advantageous to use a long-lived cell that is stationary, has a definite orientation and has a primary function in the digestion of non-replicating material.

The use of the exogenous marker protein horseradish peroxidase (HRP), for functional studies of lysosomes of the renal proximal convoluted tubule cells is well established.^{21,22} Proteins with molecular weights of less than 70,000 pass through the glomeruli, with the permeability of glomeruli to smaller protein molecules increasing with decreasing molecular weights.²³ Horseradish peroxidase has a molecular weight of approximately 40,000 and is rapidly cleared by glomeruli.^{17,23} It has been shown that this protein accumulates at the base of the brush border of proximal convoluted tubule cells and enters the cells in apical tubular invaginations. The apical vacuoles containing the HRP appear to enlarge either through transport of additional HRP through apical tubules or by fusion with each other.²⁴ It has been shown that apical vacuoles fuse with the lysosomes and that the endocytized HRP is digested in the resulting phagolysosome.²⁵ Because there is no endogenous peroxidase in the kidney, the HRP can be positively identified in the aforementioned structures by cytochemical methods with no interference. It was with these advantages in mind that functional studies on lysosomes of proximal convoluted tubule cells of CHS mice and mink were performed using large doses of egg albumin.¹⁶ Although suggestions of a slowed rate of digestion were ob-

tained, good techniques were not available to directly identify egg albumin and its exact cellular location.

Thus, in this study, the HRP technic was used not only to identify the endocytized material, but also to reveal rough quantitative differences in the processing of the enzyme. It was concluded that the lysosomes of CHS mice digested the HRP at a slower rate than did normal mice. The present study did not reveal gross differences in the endocytosis of the enzyme, but an abnormality in the uptake of material in CHS has not been suggested by previous studies in the literature.

Although the large granules in the renal tubule cells of the CHS species do resemble nonfunctional residual bodies, the results of this study indicate that they are functional albeit they perform their function of digesting endocytized material more slowly than do phagolysosomes of normal animals.

Whether the slowed rate of digestion is due to a deficiency of a lysosomal enzyme or enzymes is not known. Although one group of investigators has demonstrated a reduced amount of lysosomal enzymes in CHS granulocytes,²⁶ most investigations have failed to demonstrate such a reduction. In fact, the current opinion is that the defect in CHS involves the membrane of the various granules rather than the content.^{14,27} In light of this, it might be speculated that the slowed rate of digestion in lysosomes in CHS is not due to any inherent lysosomal enzyme deficiency but is due, instead, to the steric relationships in enlarged lysosomes. It may take longer for all HRP to come in contact with digestive enzymes within the enlarged lysosomes, compared to the smaller lysosomes of normal cells.

Regardless of the exact reason for the slowed rate of digestion by lysosomes, the demonstration of this defect has implications in some manifestations of CHS related to impaired host defense. Because of the homology of CHS in the four species, findings in one species can be extrapolated to the other three. It has been shown that mink with CHS have a depressed immune response, especially the anamnestic response, to at least two antigens.^{28,29} It had been shown previously that macrophages, lymphocytes and plasma cells contain abnormal granules in CHS; and it is thought that these cells participate in some manner in the processing of antigen and the production of antibody. Although the exact role of each of these cells in the immune response is not resolved, there is evidence that the macrophage is necessary for an immune response with some antigens.³⁰ Although it is hazardous to extrapolate findings between species and cell types, slowed catabolism of HRP in the renal tubule cells in CHS mice may support the hypothe-

sis suggested previously²⁹ of a slower rate of metabolism of antigen in CHS mink. The application of technics used to study the digestion of peptides by lysosomes of normal macrophages³¹ may yield data that will resolve this point if applied to the study of CHS.

Mink with Chediak-Higashi syndrome also have been shown to die more rapidly after infection with Aleutian disease virus than did non-CHS mink.³² The cause of death in both CHS and non-CHS mink is apparently an immune complex glomerulonephritis.³³ Although no differences have been demonstrated in lesions or in the level of virus in the two groups of mink, the rate at which antigen-antibody complexes accumulate in the glomeruli of CHS mink appears to be increased.³⁴ Recognizing the role of the glomerular mesangial cell in the digestion of glomerular residues,²³ one may extrapolate findings of the present study to support the suggestion³⁴ that the increased rate at which immune complexes accumulate may be due to a slowed rate of removal.

References

1. Beguez-Cesar A: Neutropenia cronica maligna familiar con granulaciones atipicas de los leucocitos. Boletin de la Sociedad Cubana de Pediatria 15:900-922, 1943
2. Leader RW, Padgett GA, Gorham JR: Studies of abnormal leukocyte bodies in the mink. Blood 22:477-484, 1963
3. Padgett GA, Leader RW, Gorham JR, O'Mary CC: The familial occurrence of the Chediak-Higashi syndrome in mink and cattle. Genetics 49:505-512, 1964
4. Lutzner MA, Lowrie CT, Jordan HW: Giant granules in leukocytes of the beige mouse. J Hered 58:299-300, 1967
5. Padgett GA, Holland JM, Prieur DJ, Davis WC, Gorham JR: The Chediak-Higashi syndrome: a review of the disease in man, mink, cattle, and mice. Animal Models for Biomedical Research III:1-12, 1970
6. Davis WC, Padgett GA, Spicer SS: Aberrant formation of neutrophil primary (azurophil) granules in the three animal homologues of the Chediak-Higashi syndrome of man. J Cell Biol 47:469, 1970
7. White JG: The Chediak-Higashi syndrome: a possible lysosomal disease. Blood 28:143-156, 1966
8. Davis WC, Spicer SS, Greene WB, Padgett GA: Ultrastructure of bone marrow granulocytes in normal mink and mink with the homolog of the Chediak-Higashi trait of humans. I. Origin of the abnormal granules present in the neutrophils of mink with the C-HS trait. Lab Invest 24:303-317, 1971
9. Davis WC, Spicer SS, Greene WB, Padgett GA: Ultrastructure of cells in bone marrow and peripheral blood of normal mink and mink with the homolog of the Chediak-Higashi trait of humans. II. Cytoplasmic granules in eosinophils, basophils, mononuclear cells and platelets. Am J Pathol 63:411-431, 1971
10. Lutzner M.: Ultrastructure of giant melanin granules in the beige mouse

- during ontogeny. Abstract of paper presented at Seventh International Pigment Cell Conference, 1969
11. Clark R, Kimball H, Padgett G: Granulocyte chemotaxis (CTX) in the Chediak-Higashi syndrome (CHS) of mink. *Fed Proc* 30:342, 1971
 12. Davis WC: Leukocyte dysfunction in an animal homologue of the Chediak-Higashi syndrome of man. *Fed Proc* 29:1379, 1970
 13. Root RK: Defective bactericidal functions of Chediak-Higashi syndrome leukocytes. *Clin Res* 19:466, 1971
 14. Padgett GA: Neutrophilic function in animals with the Chediak-Higashi syndrome. *Blood* 29:906-915, 1967
 15. Root RK, Blume RS, Wolff SM: Abnormal leukocyte function in the Chediak-Higashi syndrome. *Clin Res* 16:335, 1968
 16. Prieur DJ, Padgett GA: Defective catabolism of egg albumin by the renal proximal convoluted tubule cells in the Chediak-Higashi syndrome. *Fed Proc* 29:783, 1970
 17. Graham RC, Karnovsky MJ: The early stages of absorption of injected horseradish peroxidase in the proximal tubules of the mouse kidney: ultrastructural cytochemistry by a new technique. *J Histochem Cytochem* 14:291-302, 1966
 18. Millonig G: The advantages of phosphate buffer for OsO_4 solutions in fixation. *J Appl Physics* 32:1637, 1961
 19. Mollenhauer HH: Plastic embedding mixtures for use in electron microscopy. *Stain Technol* 39:111-114, 1964
 20. Danes BS, Beam AG: Correction of cellular metachromasia in cultured fibroblasts in several inherited mucopolysaccharidoses. *Proc Nat Acad Sci (USA)* 67:357-364, 1970
 21. Straus W: Occurrence of phagosomes and phago-lysosomes in different segments of the nephron in relation to the reabsorption, transport, digestion and extrusion of intravenously injected horseradish peroxidase. *J Cell Biol* 21:295-304, 1964
 22. Straus W: Use of horseradish peroxidase as a marker protein for studies of phagolysosomes, permeability and immunology. *Meth Achievm Exp Path* 4:54-91, 1969
 23. Graham RC, Karnovsky MJ: Glomerular permeability. Ultrastructural cytochemical studies using peroxidase as protein tracers. *J Exp Med* 124:1123-1133, 1966
 24. Straus W: Changes in the intracellular location of small phagosomes (micropinocytic vesicles) in kidney and liver cells in relation to time after injection and dose of horseradish peroxidase. *J Histochem Cytochem* 15:381-393, 1967
 25. Straus W: Cytochemical observations on the relationship between lysosomes and phagosomes in kidney and liver by combined staining for acid phosphatase and intravenously injected horseradish peroxidase. *J Cell Biol* 20:497-507, 1964
 26. Kimball HR, Ford GH: Granulocyte lysosomal enzymes in the Chediak-Higashi syndrome (CHS). Abstract of paper present at American Federation for Clinical Research, April 27, 1970
 27. Windhorst DB, Zelikson AS, Good RA: Chediak-Higashi syndrome: hereditary gigantism of cytoplasmic organelles. *Science* 151:81-83, 1966

28. Lodmell DL, Hadlow WJ, Munoz JJ, Whitford HW: Hemagglutinin antibody response of normal and Aleutian disease-affected mink to keyhole limpet hemocyanin. *J Immunol* 104:878-887, 1970
29. Lodmell DL, Bergman RK, Hadlow WJ, Munoz JJ: Cellular and humoral antibody responses of normal pastel and sapphire mink to goat erythrocytes. *Infection and Immunity* 3:221-227, 1971
30. Shortman K, Diener E, Russell P, Armstrong WD: The role of nonlymphoid accessory cells in the immune response to different antigens. *J Exp Med* 131: 461-482, 1970
31. Ehrenreich BA, Cohn ZA: The fate of peptides pinocytosed by macrophages in vitro. *J Exp Med* 129:227-245, 1969
32. Padgett GA, Reiquam CW, Henson JB, Gorham JR: Comparative studies of susceptibility to infection in the Chediak-Higashi syndrome. *J Pathol Bacteriol* 95:509-522, 1968
33. Henson JB, Gorham JR, Padgett GA, Davis WC: Pathogenesis of the glomerular lesions in Aleutian disease of mink. *Arch Pathol* 87:21-28, 1969
34. Henson JB, Gorham JR, Tanaka Y, Padgett GA: The sequential development of ultrastructural lesions in the glomeruli of mink with experimental Aleutian disease. *Lab Invest* 19:153-162, 1968

Acknowledgments

We thank Miss Luann Hohenadel and Mrs. Phyllis Hoffman for technical assistance and Mr. Harold Conner for photographic work. We also acknowledge the Veterinary Sciences Research Division of the US Department of Agriculture at Pullman, Washington and its director, Dr. John R. Gorham, for furnishing the electron microscope.

[Illustrations follow]

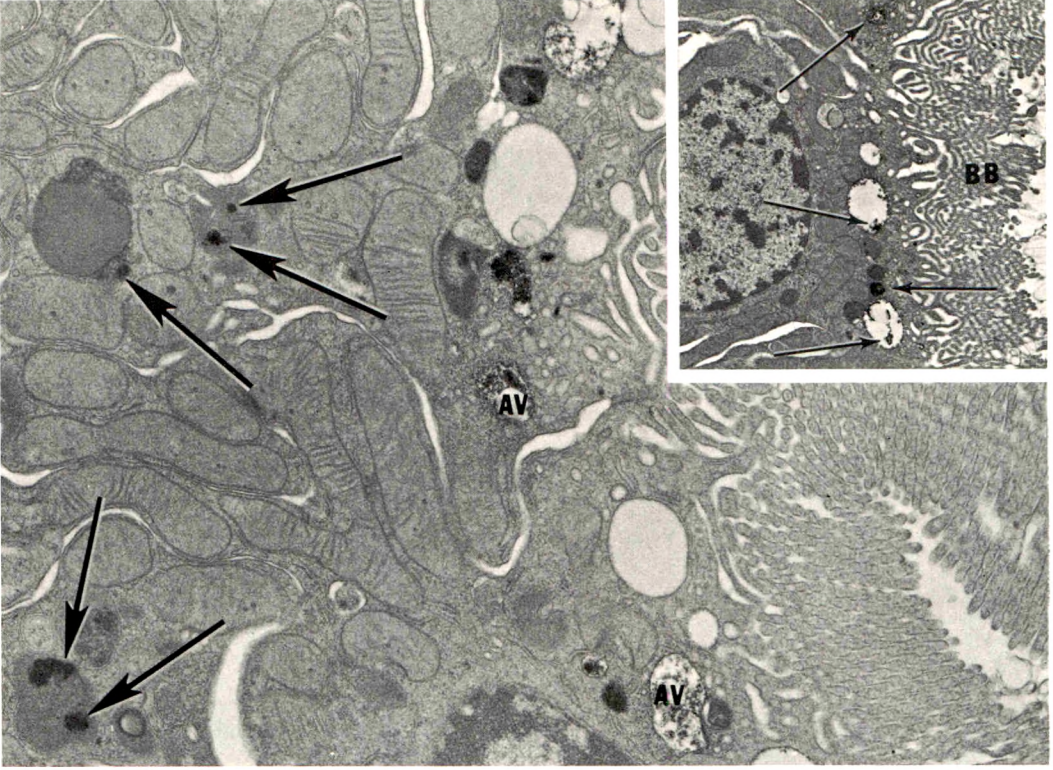
Legends for Figures

All figures are electron micrographs of horseradish peroxidase (HRP) preparations of mouse renal tubule cells. See text for details.

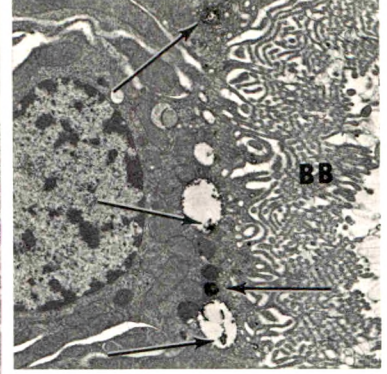
Fig 1—Control mouse kidney 5 minutes after HRP injection. **A**—HRP is present in the apical portion of the cell (*arrows*) beneath the base of the brush border (*BB*). **B**—In addition to HRP in the apical vacuoles (*AV*), some has penetrated deeper into the cells and has fused with lysosomes (*arrows*) ($A \times 4000$; $B \times 14,000$).

Fig 2—CHS mouse kidney 5 minutes after HRP injection. **A**—The HRP accumulated in apical vacuoles (*AV*) beneath the brush border (*BB*) in a manner similar to that of the control mouse kidney in Fig 1. **B**—A lower-power view illustrating a similar area. **C**—Particles of HRP (*arrows*) have fused with a lysosome in the deeper part of the cell. ($A \times 23,000$; $B \times 3500$; $C \times 23,000$).

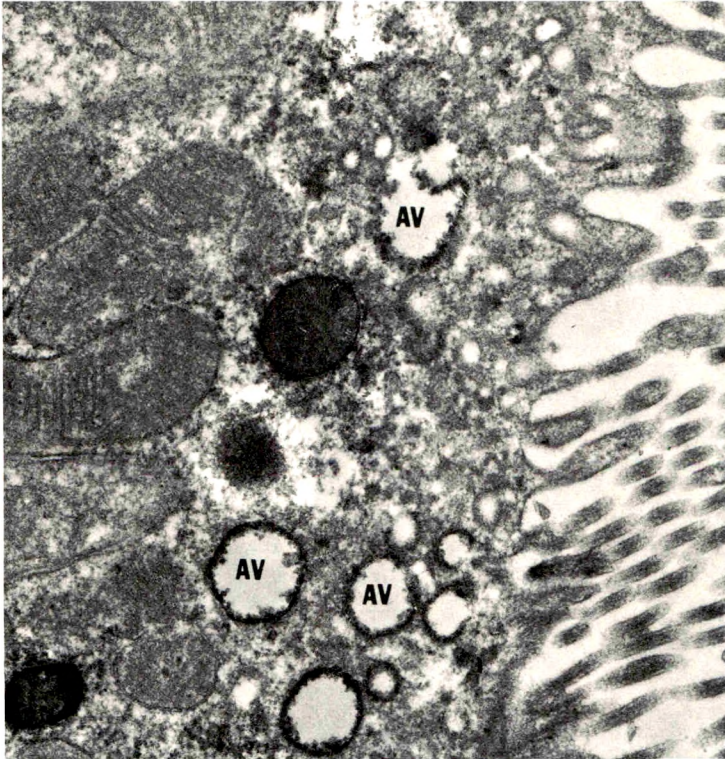
1A



1B



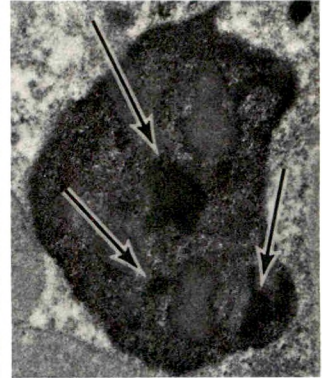
2A



2B



2C



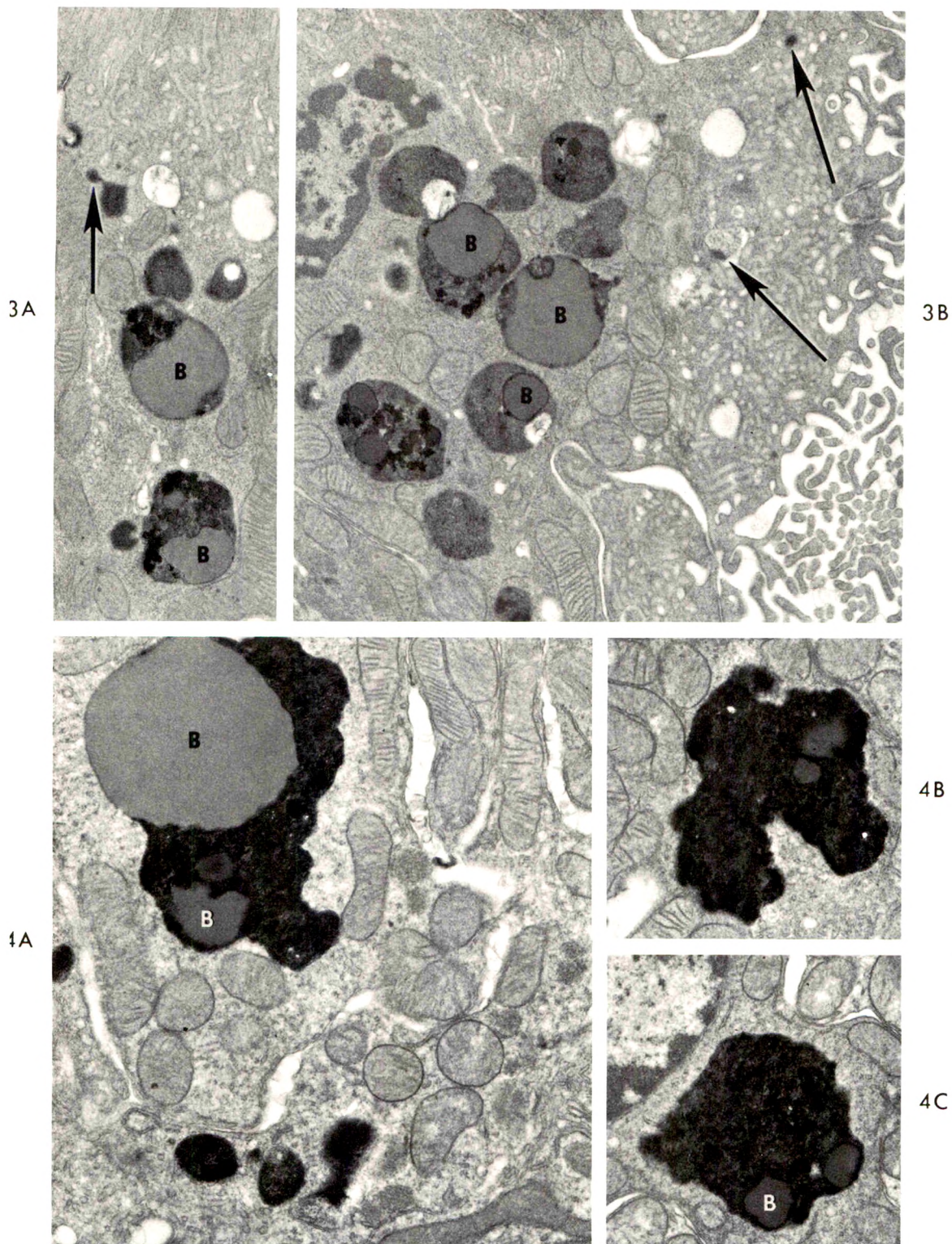
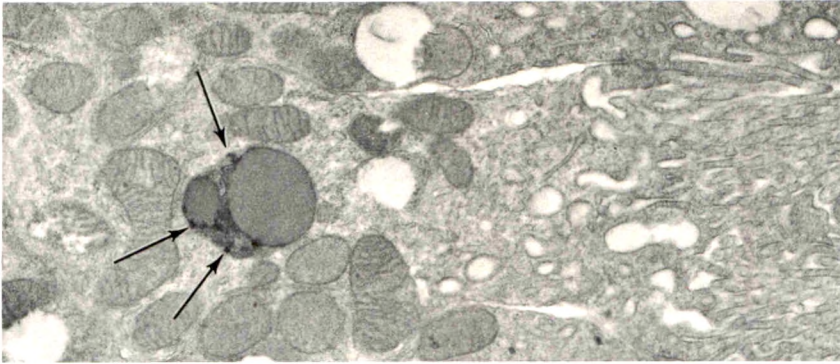
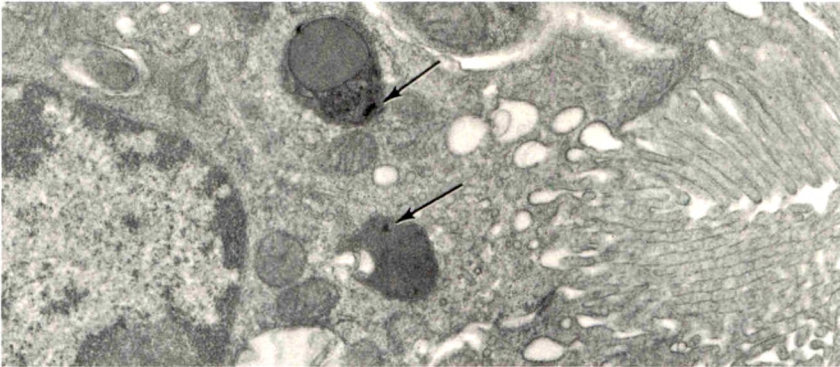


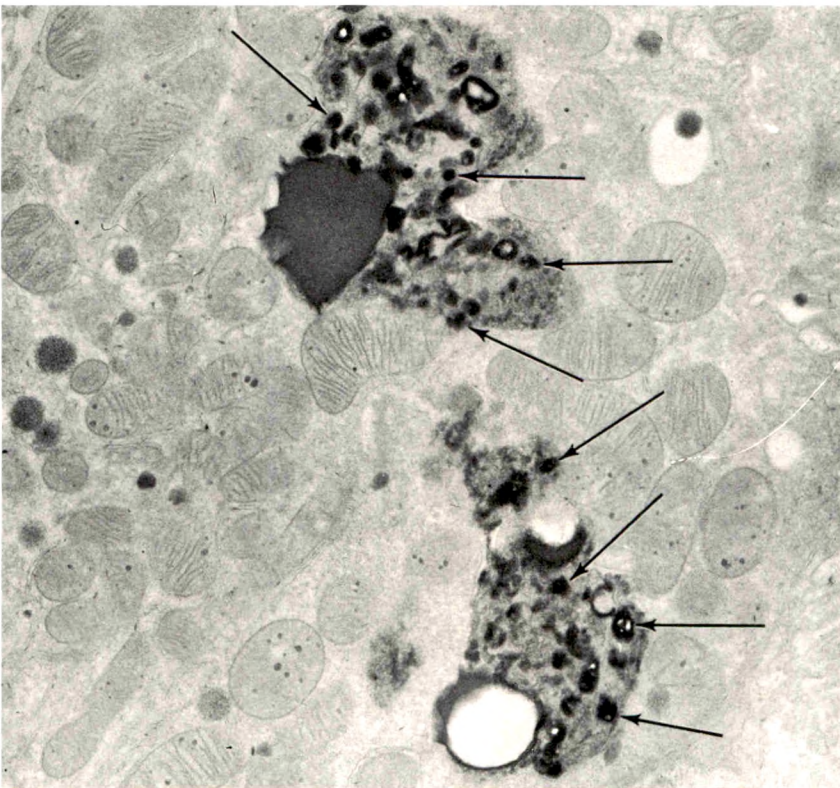
Fig 3—Control mouse kidney 18 hours after HRP injection. Most of the HRP is present in phagolysosomes in the deeper parts of the tubule cells. A little, however, is still present in apical vacuoles (arrows). Homogeneous bodies (B) appearing to be sometimes membrane limited, are present in most of the phagolysosomes and do not contain HRP (A and B, $\times 14,000$). **Fig 4**—CHS mouse kidney 18 hours after HRP injection. The HRP is present in phagolysosomes as was that of the control mice in Fig 3. The phagolysosomes in this figure are larger, which is characteristic of CHS, but in addition some of the homogeneous bodies (B) in the phagolysosomes are much larger than those of the control mice (compare with Fig 3) (A, B and C, $\times 14,000$).



5A



5B



6

Fig 5—Control mouse kidney 48 hours after HRP injection. Only trace amounts of HRP are present (arrows). The HRP that is present is located entirely within phagolysosomes (A and B, $\times 14,000$). **Fig 6**—CHS mouse kidney 48 hours after HRP injection. Relatively large amounts of HRP (compared to the control in Fig 5) are present in the phagolysosomes (arrows) ($\times 14,000$).

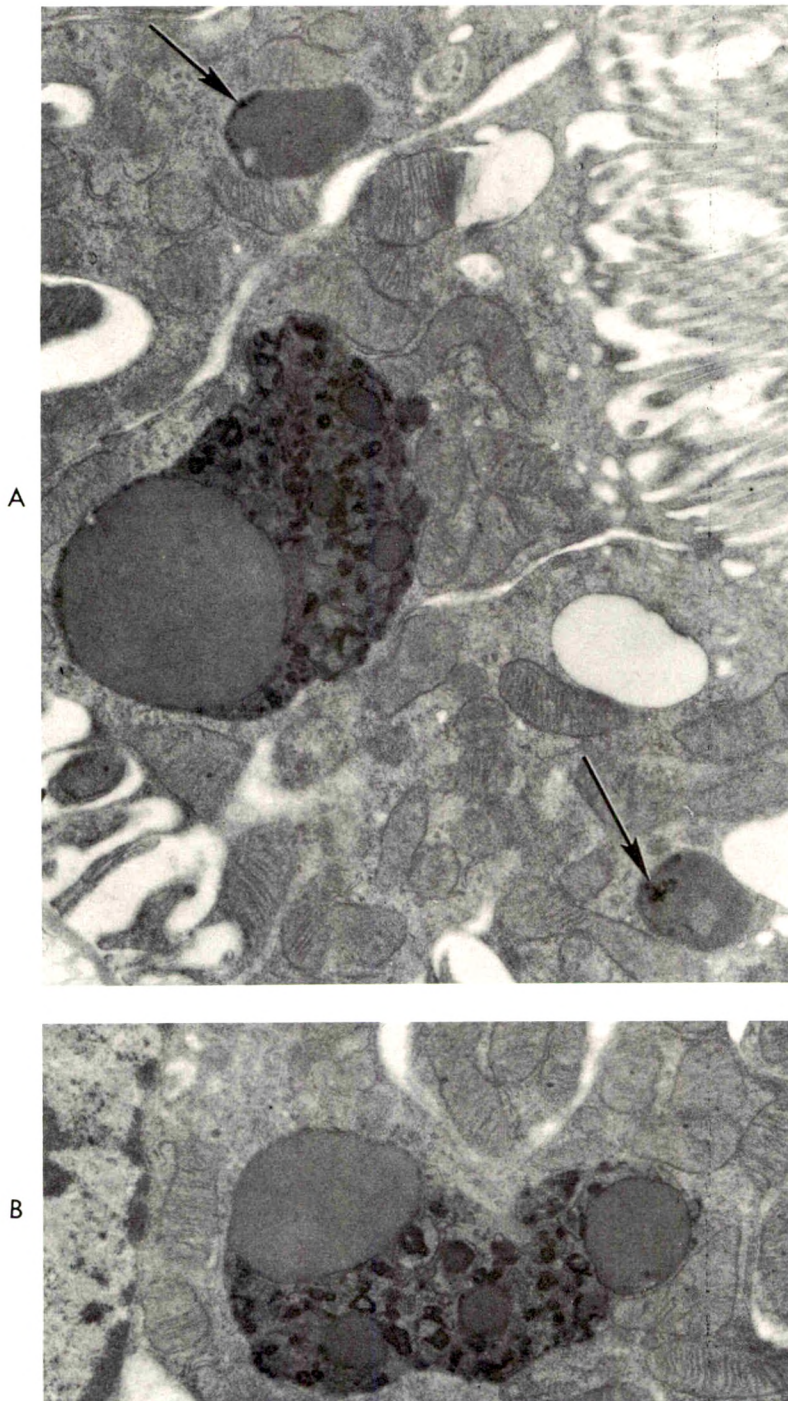


Fig 7—CHS mouse kidney 72 hours after HRP injection. Moderate amounts of HRP are present in the large phagolysosomes and some HRP is present (arrows) in what may be a normal-sized phagolysosome or possibly the sectioned end of a large phagolysosome (A and B, $\times 14,000$).

Morphologic and Functional Characteristics of Long-Term Cultures of Murine Myeloma Cells

George D. Sorenson, MD and Olive S. Pettengill, PhD

Murine myeloma cells proliferate well in cell culture even after up to 5 years *in vitro* and the globulin synthesized, as well as the ultrastructure, continues to be comparable to that of original tumor cells. Globulin synthesis by cultured cells from the C3H mouse tumor ($\times 5563$) ranged from 6 to 12.2 mg/g/48 hr and by cultured cells from Balb/c mouse plasmacytomas MOPC 21, 31C and 315 up to 40 mg/g/48 hr. This production is greater and occurs over a more prolonged period than those reported in other known published observations on globulin synthesis by normal or neoplastic cells from mice or other sources. However, both rate and quantity of globulin synthesis tend to decrease with time *in vitro* and this is inversely related to growth rate, which tends to increase with time *in vitro*. No evidence was found for increased globulin breakdown either intra- or extracellularly in these cultures (Am J Pathol 67:241-264, 1972).

THE DEVELOPMENT and ready availability of transplantable murine plasmacytomas has provided the opportunity for a wide variety of studies upon neoplastic plasma cells in recent years. Investigations have been made of tumor induction^{1,2} and development,^{3,4} ultrastructural features^{5,6} serum alterations^{7,8} and immunoglobulin characteristics,⁹⁻¹⁴ as well as numerous studies of immunoglobulin biosynthesis and assembly. Many of these investigations have been considered in recent reviews.^{15,16}

The development of methods for prolonged cell culture of murine myelomas has provided the opportunity to study these cells for extended periods under stabilized environmental conditions in which factors affecting growth as well as differentiated function may be examined.¹⁷⁻¹⁹ The established cell lines continued to synthesize and secrete the same immunoglobulin as is produced by tumors of origin *in vivo*. These cell cultures were studied to learn more about factors that affect the production of export proteins in general and, more specifically, factors that affect the production of globulin by cells that, although neoplastic, have many characteristics of normal plasma cells. Thus, information derived

From the Department of Pathology, St. Louis University School of Medicine, St. Louis, Missouri 63104.

Supported in part by National Institutes of Health Grants CA 11303, CA 11792 and GM 08574.

Accepted for publication Nov 5, 1971.

Address reprint requests to Dr. George Sorenson, Department of Pathology, Dartmouth Medical School, Hanover, NH 03755.

from these cell cultures *in vitro* may provide added insight into certain aspects of immunologic reactions *in vivo*. Some investigations of cell characteristics and protein synthesis by these cells, in this laboratory, have been presented in brief form previously.²⁰ The results of a long-term continuation and expansion of these studies are included in this report.

Materials and Methods

A cell line (WU-29) derived from murine myeloma $\times 5563^8$ was used initially for these studies. Methods for the suspension culture of these cells *in vitro* have been described previously.¹⁷ More recently, myeloma cells from Balb/c tumors MOPC 21 and MOPC 31C have been established *in vitro*, using similar methods, and MOPC 315 was established in culture by alternate passage through mouse and cell culture.^{21,22} The cell lines are termed SLU-5, SLU-K1 and SLU-J27, respectively. Analogous studies were made with these additional cell cultures.

WU-29 cultures were originally established by mechanically dissociating the tumor, and cells were grown in plastic flasks in Leibovitz L-15 medium containing 20% fetal calf serum, 50 units each of penicillin and streptomycin/ml and 1 mM glutamine. Batches of fetal calf serum were selected on the basis of ability to support growth and maintain viability of myeloma cell lines in this laboratory. Adapted cell cultures were established at concentrations of 4×10^5 cells/ml and incubated in 5% CO₂ in air at 36 C. The cells were centrifuged and the medium renewed 2 to 3 times weekly. After several years of continuous culture, it was necessary to replace the medium every 2 days to maintain viability. Cell counts were made in a hemocytometer or with a Coulter counter and viability was estimated by trypan-blue exclusion. The studies of protein synthesis were made with both freshly isolated tumor cells and, at intervals, with cells which had been grown *in vitro* for as long as 5 years. The latter will be referred to as adapted cells. SLU-5, SLU-K1 and SLU-J27 were grown in Dulbecco's modification of Eagle's medium with 20% fetal calf serum under the same conditions.

Antibody

Goat antimurine serum and antimurine globulin were obtained from Hyland Laboratories; rabbit antisera to egg albumin, crystallized four times, murine serum and purified mouse γ -globulin (Pentex) were prepared in our laboratory.

Electrophoresis

Serum and culture specimens were evaluated by starch gel electrophoresis²³ and by cellulose acetate electrophoresis, utilizing barbital buffer (pH 8.6, ionic strength 0.075) and the Beckman Microzone Electrophoresis Cell. In some instances, cells and medium were concentrated approximately ten times by vacuum dialysis before electrophoresis.

Immunoelectrophoresis

Serum and concentrated culture medium were analyzed by microimmunoelectrophoresis²⁴ in agar with veronal buffer at pH 8.6. Goat or rabbit antimurine serum was allowed to diffuse for 24 to 48 hours to develop immunoelectrophoretic patterns.

Autoradiography

Cells were cultured for 48 hours with 1 μCi ^{14}C -labeled amino acids (reconstituted protein hydrolysate, Schwarz Bioresarch) per milliliter. The contents of single flasks were dialyzed, concentrated and evaluated by micro immunoelectrophoresis, as previously described. Autoradiography was performed at room temperature with sheet film (Kodak RS Pan, ASA 650). The exposure time was 3 to 14 days. The globulin synthesized *in vitro* was detected and identified by comparing the autoradiographic image with the stained immunoelectrophoretic pattern. As a control for nonspecific attachment of radioactive label to previously synthesized protein, serum from tumor bearing mice was incubated for the same length of time with the complete cell culture medium and the same amount of radioactively labeled amino acids. This was then similarly concentrated and evaluated by immunoelectrophoresis and autoradiography.

Radial Diffusion

Quantitation of globulin within cultures was obtained using an immunologic method of single radial diffusion²⁵ and by micromodification of this technic.^{26,27} For the former, cells and medium from individual flasks were concentrated approximately 15-fold and then diluted to a uniform volume of 0.3 to 0.5 ml. Aliquots of 50 λ were added to center wells. Petri dishes were prepared with a layer of 1% agar containing goat antimurine globulin or rabbit antimurine γ globulin and sodium azide (0.1%).

More recently, a modified micro method of radial diffusion has been utilized similar to that described by Fahey *et al.*²⁷ and Mancini *et al.*²⁶ Agar wells were filled with unconcentrated cells and medium. Slides were stored in a humid chamber for 72 hours. Similar amounts of known concentrations of murine globulin were evaluated each time as standards. The slides were rinsed in two changes of 1% NaCl overnight and once in water before drying. The zone of precipitate on the dried, stained slide was measured.

Double Diffusion

Micro double diffusion (Ouchterlony) studies were prepared in 1% agar upon glass slides and evaluated after 24 hours.

Purification of $\times 5563$ Globulin

Using the method described by Askonas,²⁸ $\times 5563$ tumor-bearing mouse serum was dialyzed overnight against three changes of 0.01 M K_2HPO_4 - KH_2PO_4 buffer, pH 6.5. Separation was made on a DEAE-cellulose 1 g) column. Serum was added in dialyzing buffer, and eluted with a gradient produced by the addition of 0.2 M K_2HPO_4 - KH_2PO_4 buffer (pH 6.5) through a mixing vessel.

Iodination of Globulin

This was performed by a modified method of McConahey and Dixon²⁹ in which 2 mCi ^{125}I (NaI , New England Nuclear) was added to 2 mg purified mouse γ -globulin (Pentex), in 4 ml of 0.05 M phosphate buffer, pH 7.0, 100 μg chloramine-T was added and the mixture stirred for 5 minutes. Then 0.1 ml of a 1 mg/ml solution of sodium metabisulfite was added. After 10 minutes, the mixture was dialyzed for 48 hours with four changes of buffer. Labeled globulin was sterilized by Millipore filtration. Preparations were counted as washed TCA precipitates on a Millipore filter, wrapped in aluminum foil in tubes in a Nuclear-Chicago gamma counter equipped with a well-type crystal scintillation detector.

Preparation of DNP-antigen

2, 4-Dinitrophenyl-bovine serum albumin conjugate was prepared as described by Little and Eisen.³⁰

Radioimmunoassay

To evaluate changes in rate of synthesis of globulin at specific times, radioimmunoassay was used. Cell cultures were labeled for 2 hours with 10 or 20 μCi L-(C₁₁, UL) leucine or 50 to 75 μCi L-(³H,4,5)-leucine/5 ml. Aliquots of cells and medium were quick-frozen and sonicated at the time of assay. All samples were corrected to the same amount of globulin (on the basis of radial diffusion quantitation of globulin) by addition of normal mouse serum. For non-specific precipitations, equivalent amounts of egg albumin and anti-egg albumin were added and removed by centrifugation two times. The third specific precipitate was made with rabbit anti-mouse globulin slightly on the side of antibody excess. This precipitate was collected, centrifuged, washed and dissolved in 0.3 ml of 0.1 N NaOH. Aliquots of 50 λ were neutralized with 3.5% acetic acid and counted in a Beckman Scintillation Counter in 10 ml of 10% Bio-Solv Solubilizer 3 (Beckman) in F'uoralloy-toluene (Beckman) to within an error of ± 10 to 15%.

Electron Microscopy

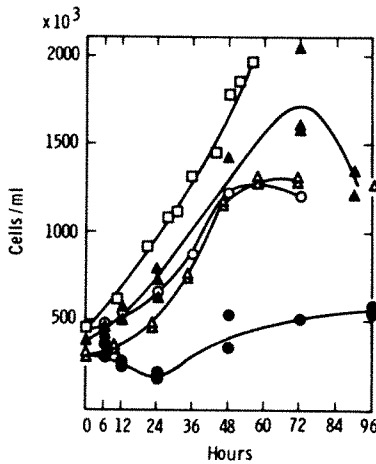
Cultured cells were fixed in 6.5% glutaraldehyde in cacodylate or phosphate buffer (pH 7.3), centrifuged, rinsed with buffer and post-fixed in 1% osmium tetroxide in phosphate buffer. Cell pellets were embedded in a mixture of Epon-Araldite,³¹ sectioned and examined in either an RCA 3F or Siemens electron microscope. Sections 1 to 2 μ in thickness were stained with methylene blue and examined by light microscopy to determine cell sizes.

Results**Cell Proliferation**

The myeloma cells proliferate extremely well under the described conditions of culture, and representative growth curves are presented in Text-figure 1. In the newly established line, there is a short lag phase of growth lasting 6 to 9 hours followed by cell proliferation over the next 72 hours until a plateau is reached. The lag period has tended to diminish as the cultures are maintained *in vitro* for a longer time. Maximum proliferation was between 24 and 48 hours, but recent cultures grow at a uniform rate from 0 to 48 hours. The average doubling time during the first 48 hours after subculturing was approximately 24 hours for cells newly adapted to continuous culture. After 4 years, this was reduced to 20 hours.

Morphology of Tumors and Cultured Cells

The solid tumor consists of a uniform population of large cells with big nuclei and prominent nucleoli. The cytoplasm of these cells pos-



TEXT-FIG 1—Growth curves of WU-29 cells at different times. Each point represents the average of duplicate Coulter counts from one flask. As the cells became better adapted to culture conditions, the growth rate increased, the lag period disappeared and cells were subcultured more frequently. Freshly isolated tumor cells ($\times 5563$), 1966 (solid circles); WU-29 cells, 1966 (solid triangles); WU-29 cells, 1967 (open circles); WU-29 cells, 1968 (open triangles) and WU-29 cells, 1970 (open squares).

sesses abundant rough endoplasmic reticulum as well as many free ribosomes (Figure 1). The Golgi area is prominent. Vital particles are observed in three locations in these cells. These are a) intracisternal double shelled particles which appear to form from the rough endoplasmic reticulum, b) double shelled particles free in the cytoplasm which are frequently in or near the Golgi area, and c) double shelled particles which appeared to bud from the plasma membrane or to be incorporated into the end of cell processes. The intracytoplasmic and peripheral forms have been proposed as stages of mammary tumor virus (MTV) by ultrastructural and transmission studies.³² The freshly dissociated neoplastic cells are rounded and appear unharmed by this manipulation. The ultrastructure is essentially the same as that of cells in the solid tumor (Figure 2).

Light and electron microscopic examination indicate that the murine myeloma ($\times 5563$) cells have retained a relatively stable morphology *in vitro* for 5 years, although the number of cytoplasmic viral particles identified as mouse mammary tumor virus appears to be decreasing in WU-29. Otherwise, the cells appear essentially the same as the freshly isolated cells from the solid tumor (Figure 3). The cells remain suspended as individual round cells which do not attach to the wall of the culture vessel. The Epon-Araldite embedded cells vary in size from approximately 10 to 20 μ in diameter. All cells possess abundant free ribosomes and also much rough endoplasmic reticulum. Viral particles persist which are identical to those present in the original $\times 5563$ murine tumor.

The ultrastructure of SLU-5 cells differs from WU-29 in that the

former show a greater number of membranous structures (myelin figures) in the cytoplasm (Figure 4), the significance of which is unknown, and do not contain viral particles comparable to MTV. These features are characteristic of the original tumors. Likewise, cell lines established from MOPC 31C and MOPC 315 have retained the ultrastructure of the tumors from which they were derived.

Characteristics of Globulin

The $\times 5563$ tumor produces an IgG type of myeloma globulin *in vivo*.⁸ Evaluation of cultured cells and medium by immunoelectrophoresis reveals the presence of protein in cells and medium which is comparable to the myeloma globulin. When the patterns are developed with anti-murine serum, there is a single arc in the globulin region which is analogous to the arc formed by the myeloma protein in the serum of tumor-bearing mice (Figure 5). The globulin in the culture fluid also exhibits the same electrophoretic migration as serum myeloma protein, with both starch gel and cellulose acetate electrophoresis.

The globulin produced *in vitro* is closely related antigenically to the myeloma globulin in the serum. Micro-Ouchterlony double diffusion agar plates were used to compare myeloma globulin produced *in vitro* with that in serum from tumor-bearing mice. Fusion of the precipitation bands formed by two adjacent globulins produced a reaction of identity indicating the proteins shared antigenic determinants (Figure 6). Globulin produced in eight cell lines derived from $\times 5563$ at various times has been compared utilizing the double diffusion method (Figure 7). These studies reveal a reaction of identity which indicates a close antigenic relationship among globulins produced by cell culture lines isolated at different times, except for WU 43. This culture produces a globulin that is antigenically slightly different from the others. With time in culture, no changes have been observed.

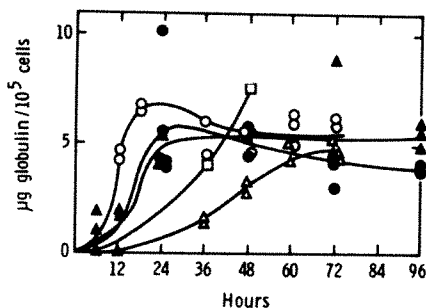
The $\times 5563$ myeloma globulin is similar to normal murine IgG and reacts strongly with antisera prepared against normal gamma globulin.⁹ Ouchterlony double diffusion experiments with culture fluid and purified mouse myeloma globulin in adjacent wells against anti-murine globulin indicate the immunologic similarity between normal mouse globulin and mouse myeloma globulin (Figure 6). The result is a reaction of partial identity which indicates that the myeloma globulin reacts with antibody to normal murine globulin although the latter has additional antigenic determinants beyond those present in myeloma globulin. On this basis, normal mouse globulin has been used as a standard of reference in these experiments utilizing radial diffusion technics.

Quantitation of Globulin

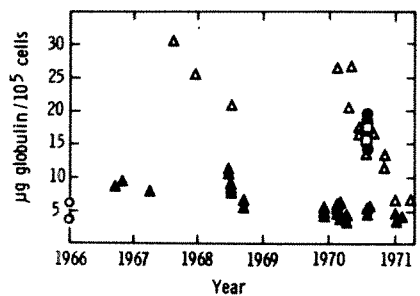
Globulin production has been studied during the 2 to 4 day period between feeding (Text-figure 2) in WU-29 cells, at intervals during 5 years. In early adapted cultures, where there is an initial longer lag after feeding and before cell division begins to occur, more globulin is present at an earlier time. As the lag phase of growth disappears, a period also associated with increased viability (greater than 90%) and slightly increased growth rate, less globulin is synthesized during the first 24 hours. In different experiments, the rate of increase in globulin concentration per 10^5 cells varies somewhat, and this may be related to varying degrees of synchrony of the cell cycle within the culture related to suspension of the cells in new medium. It has been demonstrated that globulin synthesis occurs during G_1 and early S of the cell cycle.^{33,34}

The quantity of globulin produced in cultures from 0 to 48 hours has been measured as a standard procedure for comparing different cell lines. Data collected on WU-29 cells for 5 years has been compared to more recent values of globulin production by cell lines isolated from other mouse plasmacytomas (Text-figure 3) WU-29 globulin production decreased approximately 50% rather abruptly, after 2½ years of continuous culture. The lower rate of synthesis has been maintained since then. When the globulin produced in 48 hours by 10^5 cells is plotted as its reciprocal versus the ratio of final cell count to initial cell count (proliferation index) measured for each flask, it is evident that more rapid growth rate is associated with decreased globulin synthesis (Text-figure 4).

Radioimmuno-electrophoresis was used to demonstrate the incorporation of labeled amino acids into the myeloma globulin during the period of culture. The autoradiographs demonstrated a single dark line corresponding to the stained arc of the abnormal precipitated protein in

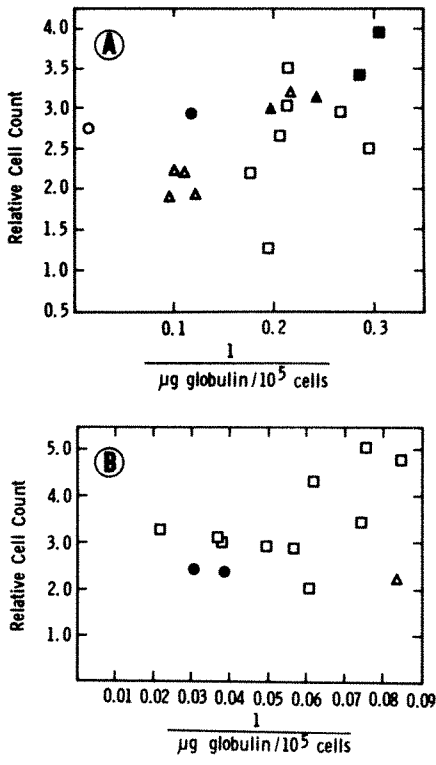


TEXT-FIG 2—Measurements of globulin by radial diffusion in cell cultures over 48, 72 or 96 hours at various times after adaptation to continuous culture. Freshly isolated tumor cells (closed circles); WU-29 (6 months *in vitro*) (closed triangles); WU-29 (18 months *in vitro*) (open circles); WU-29 (2 years *in vitro*) (open triangles) and WU-29 (5 years *in vitro*) (open squares). Initial cell count of 4×10^5 cells/ml. Globulin production has decreased in quantity with time and the increased adaptation of each cell line to conditions *in vitro*.



TEXT-FIG 3—Total globulin production over a 48-hour period by WU-29 cells evaluated at various times during years of continuous culture. For comparison, recent measurement of globulin production by 3 cell lines derived from other tumors are included. Freshly isolated ×5563 tumor cells (*open circles*); WU-29 cell line (*closed triangles*); SLU-K1 derived from MOPC 31 C murine plasmacytoma (*open squares*) and SLU-J27 derived from MOPC 315 murine plasmacytoma (*closed circles*). The quantity of globulin produced by cell lines of different origins and at different times in the same line, varies from two- to tenfold.

TEXT-FIG 4—Relationship between increasing growth of cell lines and globulin production during a 48-hour period. Data is identified by year. A—WU-29 cell line. B—SLU-5 cell line. 1966 (*open circles*); 1967 (*closed circles*); 1968 (*open triangles*); 1969 (*closed triangles*); 1970 (*open squares*) and 1971 (*closed squares*). The data demonstrates an inverse relationship between growth rate and globulin production.



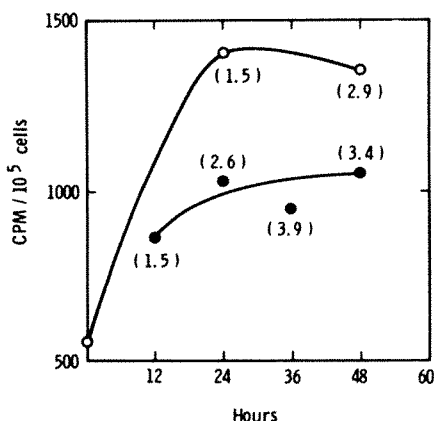
the immunoelectrophoretic pattern. The serum from tumor-bearing mice, which was incubated under the same conditions as a control for nonspecific attachment of radioactive label, produced a blank autoradiograph. Similar results, demonstrating the *in vitro* synthesis of myeloma globulin, were obtained with both newly isolated cells and with cells which have been *in vitro* continuously.

More recently, a radioimmunoassay (RIA) has been used to measure the rate of globulin synthesis directly (Text-figure 5). The relative slope of leucine incorporation into globulin is similar in two experiments; the rate of synthesis increases markedly between 0 and 24 hours and then remains approximately the same through 48 hours.

Relationship of Globulin Synthesis to Cell Growth

The figures in parentheses in Text-figure 5 are the relative growth rates (proliferation indices) of each culture flask used for radioimmunoassay. The rate of globulin synthesis was greater in the experiment in which the rate of cell growth was slower. This is analogous to data in Text-figure 4, where the quantity of globulin produced is shown to be inversely related to growth rate.

Globulin production by SLU-5 has been studied by similar methods to determine rate and quantity of globulin synthesized. Experiments were carried out over a 6-month period, during which time it was learned, from subsequent evaluation of other data obtained simultaneously, a major alteration was taking place in the cell population. This included a change in the generation time, which was reduced from 24 to 10.5 hours within this period of 6 months.³⁵ During this time, the quantity of globulin synthesized showed a sudden downward trend, al-



TEXT-FIG 5—Radio-immuno-assay; WU-29 cells. Data from two experiments. At each time point, cultures were pulsed 2 hours with 75 $\mu\text{Ci}^3\text{H-l-leucine}$. The rate of globulin synthesis per cell increased during the first 24 hours of culture and remains approximately the same from 24 to 48 hours of culture.

though this cell line still produces more globulin than WU-29 (Text-figure 3).

The studies of SLU-5 cells produced results which were similar to those obtained from WU-29 cells except that the rate of globulin synthesis per cell appeared to increase linearly with time (Text-figure 6). With an increase in growth rate there is a decrease in globulin synthesis (Text-figures 4, 6). Small differences in rate changes with respect to time, may be related to partially synchronized populations.

A limited number of determinations of globulin production by SLU-J27 and SLU-K1 are also included in Text-figure 3. SLU-J27 globulin exhibits anti-DNP activity which has been demonstrated by micro-Ouchterlony techniques.²²

Globulin Breakdown in Cell Cultures

With the development of cell cultures which produced less globulin, the possibility of globulin breakdown was considered. Two types of experiments were carried out. In one type, globulin synthesized during a 2-hour-period was labeled with radioactive leucine, unincorporated labeled leucine was removed and the cultures were continued for 48 hours. Evaluation by RIA indicated the same number of CPM/ml in globulin at 48 hours as was present initially. Thus, this labeled globulin was not degraded during this period (Table 1). The decrease in labeled globulin per cell over this period is a reflection of cell proliferation. In the second series of experiments, purified mouse γ -globulin (Pentex) was labeled with ¹²⁵I and added to the cell culture medium with and

TEXT-FIG 6—SLU-5 cells. Data collected in two experiments. A—Relative growth rate; ratio of final to original cell count for each culture. B—Globulin ($\mu\text{g}/10^5$ cells, measured by microradial diffusion. C—Rate of globulin synthesis measured by radioimmunoassay. SLU-5 cells synthesize more globulin than the WU-29 cells even when the growth rate of the two cell lines is comparable.

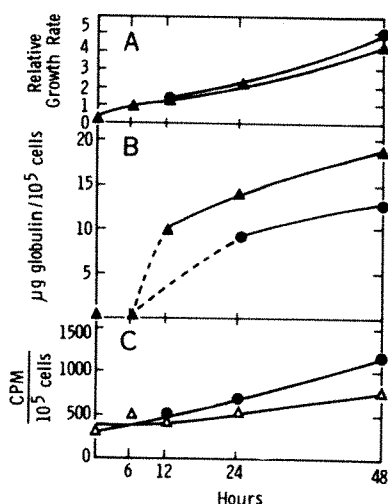


Table 1—Globulin Degradation in Cell Cultures

A. SLU-5 cells incubated with ^3H -leucine.

Hour	Radioimmunoassay	
	Counts/min/ml	Counts/min/ 10^6 cells
0	1639	371
48	1704	147

SLU-5 Cells incubated 2 hours with $15\ \mu\text{Ci}^3\text{H}$ -leucine/ml at 37°C . (SA 40 Ci/mM, NEN). Cells washed once in equal volume cold medium and resuspended at 4×10^6 cells/ml in fresh growth medium. Two aliquots were taken from each flask at 0 and 48 hours for radioimmunoassay and cell count. Values represent average counts from the 2 flasks.

B. Cell culture with normal mouse γ -globulin labeled with ^{125}I added.

Hours	Radioimmunoassay	
	Counts/min/ml	Cultures + $400\ \mu\text{gM}\gamma\text{G/ml}$
0	2761	2195
48	2567	2059

Normal mouse γ -globulin (Pentex) labeled with ^{125}I was added to the medium of cell cultures at 0 hour. Aliquots were immediately removed for assay in Nuclear-Chicago γ Spectrometer. After 48 hours, aliquots again removed for assay. Measurements were made with and without the addition of $400\ \mu\text{g}$ normal mouse IgG at 0 hour. Values represent average counts from 2 flasks.

without additional unlabeled $\text{M}\gamma\text{G}$. In neither group was there any loss of ^{125}I labeled globulin from the medium. It has been previously demonstrated that WU-29 cells will phagocytize colloidal gold (unpublished data), and entry into the cell was not considered to be a limitation in breakdown in this experiment.

Discussion

Immunoglobulin synthesis *in vitro* has been previously demonstrated utilizing normal lymphoid cells³⁶⁻³⁹ as well as myeloma cells from man⁴⁰⁻⁴² man and mice.^{12,28,43,44,45} Many of these have been short-term investigations, lasting only a few hours or a few days, which were limited by the lack of cell survival. An increasing number of long-term cell cultures have been reported as producing globulin, such as the cell lines derived from the Burkitt lymphoma or from normal or leukemic human leukocytes.⁴⁶⁻⁵² In these instances, the cells are relatively undifferentiated and the amount of globulin produced is limited. A recent report describes human myeloma cells which have been adapted to long-term culture and continue to produce measurable amounts of IgE globulin.⁵³ Another distinctive type appears to be a long-term culture of immature

myeloma cells which is producing light chains of immunoglobulin.⁴¹ A number of mouse myeloma cell lines have been described which synthesize globulin^{21,54-56} and most recently several producing globulin with antibody activity.²²

The establishment of murine myeloma cells *in vitro* for prolonged periods of time under tissue culture conditions has provided a readily available system for a wide variety of correlative biologic, biochemical and ultrastructural experiments. In the 5 years during which WU-29 cells have been observed, the cells *in vitro* have reduced by half their capacity for globulin synthesis and have acquired a more rapid growth rate. Horibata⁵⁴ described similar changes in growth rate with time. Generation time analysis of the WU-29 cell line is reported elsewhere.³⁵ By light microscopy, there is some variation in nuclear size and cell diameter among the cultured cells but the overall appearance is of a homogeneous population of cells which has not changed with time *in vitro*. The number of chromosomes per cell has been monitored at intervals and WU-29 has progressively lost acrocentric chromosomes and has accumulated a few metacentric markers.³⁵

The ultrastructure of the $\times 5563$ murine myeloma was first described in detail by Dalton⁵ in 1961. The electron microscopic appearance, 10 years and many passages later, is remarkably similar to this. Cells can be mechanically dissociated from the solid tumor to prepare cultures, and the ultrastructure is not disturbed. The cultured cells have been examined by electron microscopy periodically during the years of culture. Definite alterations have not been observed, although certain quantitative changes of slight degree cannot be excluded. The nuclei continue to appear unchanged. The cytoplasm contains large numbers of free and membrane-associated ribosomes. Viral particles persist in the same locations as seen in the solid tumor except for the decrease in quantity of the MTV cytoplasmic particles in WU-29. MTV particles have not been found in any tumors from Balb/c mice in our laboratory. The presence of abundant rough endoplasmic reticulum has been associated with the synthesis of secretory protein.⁵⁷ The continued presence of this cytoplasmic feature by these cells can be correlated with the persistence of their ability to synthesize and secrete globulin.

The cultured cells continue to synthesize the same type of myeloma globulin as is present within the serum of tumor-bearing mice. The immunoelectrophoretic pattern reveals a single arc in the same location as is observed from myeloma globulin in the serum. The migration of globulin produced by cultured cells is also comparable to serum globulin, by cellulose acetate and starch gel electrophoresis. The incorpora-

tion of isotopically labeled amino acids into globulin as revealed by autoradiography confirms the synthesis of the globulin by the cells during the period of culture. This is substantiated in a more sensitive and quantitative manner by the radioimmunoassay data.

Comparison of globulin production by freshly isolated cells and young adapted cells on a per cell basis demonstrates that both kinds of cells synthesize about the same amount of globulin per hour. However, freshly isolated cells divide one or two times and then gradually die during the 96 hours of the experiment. The sustained viability of adapted cells provides more reliable measurements on a per cell basis, and the globulin quantitated can be related to viable cells rather than to a mixture of living, injured and dead cells, as present in freshly isolated cell preparations.

The original level of globulin production per adapted cell has not been maintained by the continuous cell line WU-29. The decrease has coincided with an increase in growth rate and an increase in percentage of viable cells. Alterations can not be related to changes in laboratory conditions. Since it has been necessary to select lots of fetal calf serum on the basis of cell growth and viability, it is possible that faster growing variants have dominated the population in this way. However, serum has not been selected only for growth-promoting properties. The experiments described here have been carried out with the parent cell line, and not with clones isolated from it. Instead, efforts have been made to minimize selection and to maintain a stable population, by pooling cells during feeding operations, thus minimizing the possibility of selecting a part of the population for subculture.

Variants have been described by others in both the cultivation of mouse myeloma cells *in vitro*^{54,58,59} and in tumor transplantation in mice.^{60,61} Clones isolated from WU-29³⁵ have not exhibited marked changes from the parent culture in terms of globulin synthesis or ultrastructure. Variants such as nonproducers of globulin or cultured cells without viral particles have not been observed. SLU-5, which has undergone a fairly sudden change in growth rate with the coincident appearance of a large metacentric chromosome, appears to have been overgrown by a variant cell type and its capacity for globulin synthesis has decreased quantitatively.

Variation from one experiment to another with respect to rate of globulin production can reflect partial synchrony of the cell population. It has been established for lymphoid cell lines^{33,62} as well as a mouse myeloma cell line³⁴ that globulin synthesis occurs during the G₁ and early S period of the cell cycle. Fluorescent antibody studies carried

out on WU-29 cell lines and $\times 5563$ tumor¹⁹ have provided evidence in support of these data. Experiments reported here have been carried out on cell populations subcultured in a uniform manner in order to decrease differences which may be produced by partial synchrony. In comparing one cell line with another, the standard comparison is based on globulin production over a 48-hour-period, in order to minimize this variation. Both rate and quantity of globulin synthesis have been shown to be inversely related to cell growth rate. Experiments are in progress to determine if this is related to alterations in the length of G_1 and S of the cell cycle as would be expected.

Kimmel⁶³ has studied immunoglobulin synthesis in a cell line derived from the same mouse myeloma as SLU-5—*ie*, MOPC 21, but which has been grown under different culture conditions. His studies extended over a culture period of 7 days and indicated that globulin synthesis reached a maximum during the stationary phase of growth, which occurred at 4 days with a cell density of 8×10^5 cells/ml. If the cultures were diluted with new medium, proliferation increased and the higher rate of globulin synthesis persisted. SLU-5 cells have a faster doubling rate, and viable cell density reaches 1×10^6 /ml or greater in 48 hours. At this time, viability begins to drop, but the cells continue to proliferate to a concentration of 2 to 3×10^6 viable cells at 72 hours. The rate of globulin synthesis increases at a constant rate from 0 to 48 hours, and globulin accumulates in a linear fashion after 12 hours (Text-figure 6). Thus two cell lines, derived from the same tumor in different laboratories, vary in regard to doubling time and the cell density at which proliferation is limited. These differences may be largely related to differences in the growth medium.

The quantity of globulin produced by these cells compares favorably with other studies of rates of globulin synthesis by murine myeloma cells. WU-29 adapted cells have at times synthesized as much as 12.2 mg/g/48 hr, and never less than 6 mg/g/48 hr. Cell lines isolated from plasmacytomas of Balb/c mice have a greater globulin synthetic capacity, ranging from 20 to 40 mg/g/48 hr for the three lines described here. The calculations above were based on a value of 1.28×10^8 cells/g wet weight, measured with WU-29 cells. Freshly isolated $\times 5563$ cells synthesize 6.0 mg/g tumor tissue/48 hr, compared to a value of 1.5 to 2.0 mg obtained with tumor slices in 24 hours.²⁸ In another study, up to 14 mg of myeloma globulin was produced per gram wet weight of tumor per day.⁴⁴ In these instances, the estimates were based upon short-term *in vitro* studies or gross estimates of *in vivo* synthesis utilizing an evaluation of turnover in labeled protein.

If one compares the globulin produced by these cultured cells with studies of globulin synthesis in nonmurine cells, the difference in rate of synthesis is observed to be still greater. These reports have varied from 24 μg globulin/day/g of unstimulated monkey splenic cells³⁸ to 384 μg globulin/day/g of hyperstimulated rabbit lymphoid cells.³⁹ These evaluations were all based upon observations over a few hours. Quantitation of globulin production by established cell lines of human origin shows wide variation; 40 μg lambda chain/24 hr/ 10^8 human lymphoid cells,⁵² 1500 μg lambda chain/day/ 10^8 cells from peripheral blood of a patient with myelomatosis,⁴¹ and 2 to 7 μg IgE/ 10^6 cells/48 hr from cells from a myeloma patient.⁵³ It is apparent that the murine myeloma cells *in vitro* are producing many fold the amount of globulin produced by other cultured cells.

Degradation of myeloma globulins by myeloma cells has been studied in two other systems, with opposite conclusions. Schubert and Cohn^{64,65} demonstrated breakdown of heavy and light chains, while Laskov and Scharff were not able to demonstrate any degradation.²¹ On the basis of pulse-chase studies described here, intra- or extracellular degradation of intrinsically produced myeloma globulin does not appear to take place in SLU-5 cells. Similarly, the addition of ^{125}I labeled mouse γ -globulin to the medium and recovery of it 48 hours later indicates that even this exogenous normal globulin is not degraded. Increasing the concentration of exogenous globulin several fold did not alter these results.

References

1. Merwin RM, Redmon LW: Induction of plasma cell tumors and sarcomas in mice by diffusion chambers placed in peritoneal cavity. *J Nat Cancer Inst* 31:997-1017, 1963
2. Potter M, Boyce CR: Induction of plasma cell neoplasms in strain Balb/c mice with mineral oil and mineral oil adjuvants. *Nature* 193:1086-1087, 1962
3. Potter M, MacCardle RC: Histology of developing plasma cell neoplasia induced by mineral oil in Balb/c mice. *J Nat Cancer Inst* 33:497-515, 1964
4. Scholle RH, Foft JW: Virus-like particles in developing plasma cell tumors induced in Balb/c mice. *Exp Molec Pathol* 13:147-157, 1970
5. Dalton A J, Potter M, Merwin R M: Some ultrastructural characteristics of a series of primary and transplanted plasma cell tumors of the mouse. *J Nat Cancer Inst* 26:1221-1267, 1961
6. Parsons DF, Darden EB Jr, Lindsley DL, Pratt GT: Electron microscopy of plasma cell tumors of the mouse. I. MPC-I and $\times 5563$ tumors. *J Biophys Biochem Cytol* 9:353-368, 1961
7. Humphrey JH, Fahey JL: The metabolism of normal plasma proteins and gamma-myeloma proteins in mice bearing plasma cell tumors. *J Clin Invest* 40:1696-1705, 1961
8. Potter M, Fahey JL, Pilgrim HI: Abnormal serum protein and bone

- destruction in transmissible mouse plasma cell neoplasm. (Multiple myeloma) *Proc Soc Exp Biol Med* 94:327-333, 1957
9. Fahey JL: Immunochemical studies of twenty mouse myeloma proteins: Evidence for two groups of proteins similar to gamma and beta-2-A globulins in man. *J Exp Med* 114:385-398, 1961
 10. Fahey JL: Physiochemical characterization of mouse myeloma proteins: Demonstration of heterogeneity for each myeloma globulin. *J Exp Med* 114:399-413, 1961
 11. Potter M, Fahey JL: Studies on eight transplantable plasma cell neoplasms of mice. *J Nat Cancer Inst* 24:1153-1165, 1960
 12. Potter M, Kuff EL: Disorders in the differentiation of protein secretion in neoplastic plasma cells. *J Mol Biol* 9:537-544, 1964
 13. Potter M, Kuff EL: Myeloma globulins of plasma cell neoplasms in inbred mice: I. Immunoelectrophoresis of serum with rabbit antibodies prepared against microsomal fractions of neoplasms. *J Nat Cancer Inst* 26:1109-1138, 1961
 14. Potter M, Lieberman B, Dray S: Isoantibodies specific for myeloma γ G and γ H immunoglobulins of Balb/c mice. *J Mol Biol* 16:334-346, 1966
 15. Potter M: The plasma cell tumors and myeloma proteins of mice, *Methods in Cancer Research*. New York, Academic Press, 1967, pp 105-157
 16. Uhr JW: Intracellular events underlying synthesis and secretion of immunoglobulin. *Cellular Immunol* 1:228-244, 1970.
 17. Pettengill OS, Sorenson GD: Murine myeloma cells in suspension culture. *Exp Cell Res* 47:608-613, 1967.
 18. Hartmann BH, Pettengill OS, Sorenson GD: Chloramphenicol: Effects on mouse myeloma cells in tissue culture. *Science* 165:297-298, 1969
 19. Gandini-Attardi D, Fleischman JB, Pettengill OS, Sorenson, GD: The use of quantitative immunofluorescence to measure immunoglobulin levels in mouse myeloma cells during the cell cycle. *Cell Immunol* 2:101-113, 1971
 20. Sorenson GD, Pettengill OS: *In vitro* synthesis of globulin by cultured murine myeloma cells. *J. Cell Biol* 31:111-112A, 1966
 21. Laskov R, Scharff M: Synthesis, assembly and secretion of gamma globulin by mouse myeloma cells. I. Adaptation of Merwin plasma cell tumor-11 to culture, cloning and characterization of gamma globulin subunits. *J Exp Med* 131:515-541, 1970
 22. Periman P: Cell culture of three antibody producing murine plasmacytomas. *J Nat Cancer Inst* 46:403-410, 1971
 23. Smithies O: An improved procedure for starch-gel electrophoresis: Further variations in the serum proteins of normal individuals. *Biochem J* 71:585-587, 1959
 24. Scheidegger JJ: Une micro-methode de l'immunoelectrophorese. *Int Arch Allergy Appl Immunol* 7:103-110, 1955
 25. Mancini G, Vaerman JP, Carbonara AO, Heremans JF: A single radial-diffusion method for the immunological quantitation of proteins. *Colloquium on Protides of the Biological Fluids*. Edited by H Peeters. Amsterdam, Elsevier Publishing Co, 1963, pp 370-373
 26. Mancini G, Carbonara AO, Heremans JF: Immunochemical quantitation of antigens by single radial immunodiffusion. *Immunochemistry* 2:235-254, 1965

27. Fahey JL, McKelvey EM: Quantitative determination of serum immunoglobulins in antibody-agar plates. *J Immunol* 94:84-90, 1965
28. Askonas BA: A study of globulin formation by plasma cell neoplasm (5563) transplantable in mice. *Biochem J* 79:33-43, 1961
29. McConahey P, Dixon F: A method of trace iodination of proteins for immunologic studies. *Int Arch Allergy Appl Immunol* 29:185-189, 1966
30. Little JR, Eisen HN: Preparation of immunogenic 2,4-dinitrophenyl and 2,4,6-trinitrophenyl proteins. *Methods in Immunology and Immunochemistry*, New York, Academic Press, Inc, 1967, 1:128-133
31. Mollenhauer HH: Plastic embedding mixtures for use in electron microscopy. *Stain Technol* 39:111-114, 1964
32. Dalton AJ, Potter M: Electron microscopic study of the mammary tumor agent in plasma cell tumors. *J Nat Cancer Inst* 40:1375-85, 1968
33. Buell DN, Fahey JL: Limited periods of gene expression in immunoglobulin-synthesizing cells. *Science* 164:1524-25, 1969
34. Byars N, Kidson C: Programmed synthesis and export of immunoglobulin by synchronized myeloma cells. *Nature* 226:648-50, 1970
35. Pettengill OS, Sorenson GD: Growth characteristics of long term cultures of mouse myeloma cells. *Exp Cell Res* 70:65-72, 1972
36. Dutton RW: *In vitro* studies of immunological responses of lymphoid cells. *Advances in Immunology*, vol 6. New York, Academic Press, Inc, 1967, pp 253-336.
37. Forbes IJ, Turner KJ: Synthesis of protein by human lymphocytes *in vitro*. I. Clinical studies. *Aust Ann Med* 14:304-310, 1965
38. Van Furth RV, Schuit HRE, Hijmans W: The formation of immunoglobulins by human tissues *in vitro*. *Immunology* 11:1-40, 1966
39. Helmreich E, Kern M, Eisen HN: The secretion of antibody by isolated lymph node cells. *J Biol Chem* 236:464-473, 1961
40. Sorenson GD, Pettengill, OS: Human neoplastic plasma cells *in vitro*. Electron microscopy and protein synthesis. *Am J Pathol* 50:51A, 1967
41. Matsuoka Y, Moore GE, Yagi Y, Pressman D: Production of free light chains of immunoglobulin by a hematopoietic cell line derived from a patient with multiple myeloma. *Proc Soc Exp Biol Med* 125:1246-1250, 1967
42. Van Furth R, Schuit HRE, Hijmas W: The formation *in vitro* of paraproteins in multiple myeloma & Waldenstroms' macroglobulinemia. *Br J Haematol* 12:202-211, 1966
43. Kuff EL, Potter M, McIntire KR, Roberts NE: The *in vitro* synthesis of specific secretory protein by an ascites plasma cell tumor. *Biochemistry* 3:1707-1712, 1964
44. Nathans D, Fahey JL, Potter M: The formation of myeloma protein by a mouse plasma cell tumor. *J Exp Med* 108:121-130, 1958
45. Truax WE, Bray JP: Synthesis of M protein by mouse myeloma tumor: Correlation of *in vitro* and *in vivo* methods. *Blood* 18:176-181, 1961
46. Fahey JL, Finegold I, Rabson AS, Manaker RA: Immunoglobulin synthesis *in vitro* by established human cell lines. *Science* 152:1259-1261, 1966 124:107-111, 1967
47. Hinuma Y, Grace JT Jr: Cloning of immunoglobulin-producing human leukemic and lymphoma cells in long-term cultures. *Proc Soc Exp Biol Med*

48. Tanagaki N, Yagi Y, Moore GE, Pressman D: Immunoglobulin in human leukemia cell lines. *J Immunol* 97:643-646, 1966
49. Takahashi N, Tagaki N, Yagi Y, Moore GE, Pressman D: Immunoglobulin production in sublines of a human lymphocytoid cell line. *J Immunol* 102:1388-1393, 1969
50. Finegold I, Fahey JL, Granger H: Synthesis of immunoglobulins by human cell lines in tissue culture. *J Immunol* 99:839-848, 1967
51. Wakefield JD, Thorbecke GJ, Old LJ, Boyse EA: Production of immunoglobulins and their subunits by human tissue culture cell lines. *J Immunol* 99:308-319, 1967
52. Fahey JL, Finegold I: Synthesis of immunoglobulins in human lymphoid cell lines. *Symp Quant Biol* XXXII:283-290, 1967
53. Nilsson K, Bennich H, Johansson SGO, Ponten J: Established immunoglobulin producing myeloma (IgE) and lymphoblastoid (IgG) cell lines from an IgE myeloma patient. *Clin Exp Immunol* 7:477-89, 1970
54. Horibata K, Harris AW: Mouse myelomas and lymphomas in culture. *Exp Cell Res* 60:61-77, 1970
55. Cohn M: Natural history of the myeloma. *Symp Quant Biol* XXXII:211-222, 1967
56. Namba Y, Hanaoka M: Immunoglobulin synthesis by cultured mouse myeloma cells. *J Immunol* 102:1486-97, 1969
57. Porter KR: The ground substance: Observation from electron microscopy. *The Cell* Vol 2. Edited by J Brachet, AE Mirsky. New York, Academic Press, Inc, 1961, pp 621-675
58. Coffino P, Laskov R, Scharff MD: Immunoglobulin production: Method for quantitatively detecting variant cells. *Science* 167:186-188, 1970
59. Coffino P, Scharff MD: Rate of somatic mutation in immunoglobulin production by mouse myeloma cells. *Proc Nat Acad Sci* 68:219-23, 1971
60. Schubert D, Munro A, Ohno S: Immunoglobulin biosynthesis. I A myeloma variant secreting light chain only. *J Mol Biol* 38:253-62, 1968
61. Schubert D, Horibata K: Immunoglobulin biosynthesis: II Four independently isolated myeloma variants. *J Mol Biol* 38:263-71, 1968
62. Lerner RA, Hodge LD: Gene expression in synchronized lymphocytes: Studies on the control of synthesis of immunoglobulin polypeptides. *J Cell Physiol* 77:265-276, 1971
63. Kimmel CB: Immunoglobulin, protein and nucleic acid synthesis in cultured myeloma cells. *Exp Cell Res* 65:202-208, 1971
64. Schubert D, Cohn M: Immunoglobulin biosynthesis: III. Blocks in defective synthesis. *J Mol Biol* 38:273-88, 1968
65. Schubert D: Immunoglobulin assembly in a mouse myeloma. *Proc Nat Acad Sci* 60:683-690, 1968

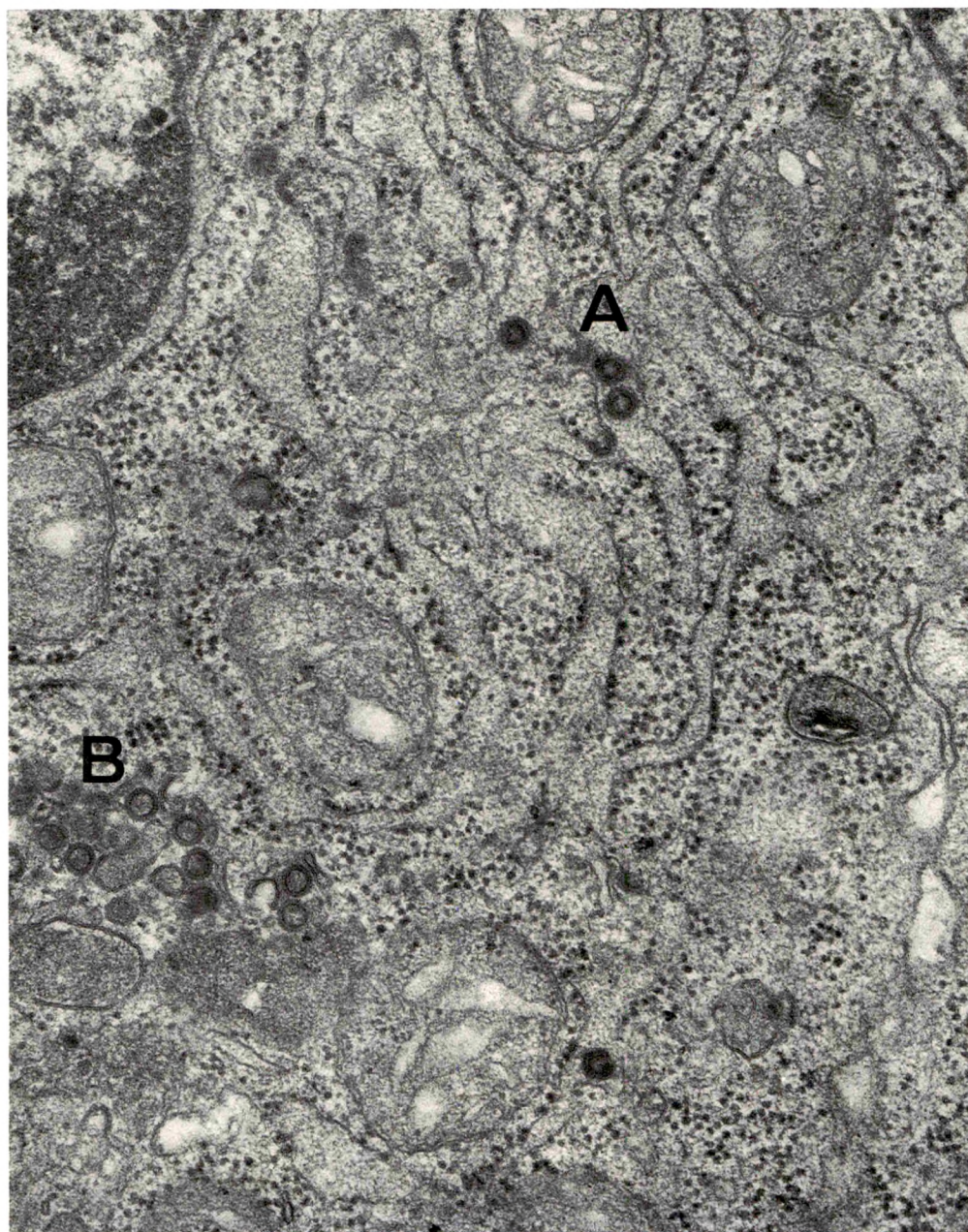


Fig 1—Electron micrograph of X5563 tumor. Viruses bud from and occur within the endoplasmic reticulum (A). In addition, there are intracytoplasmic viruses (B) which have been indicated to be a form of mouse mammary tumor virus (approximately $\times 40,000$).



Fig 2—Electron micrograph of a freshly dissociated X5563 tumor cell. The dissociation does not disturb the characteristic ultrastructure (approximately $\times 12,000$).



Fig 3—Electron micrograph of a cell from WU-29, which is an established cell line from X5563 tumor. After many passages *in vitro*, the cultured cells retain the ultrastructure typical of the original tumor (approximately $\times 15,000$).

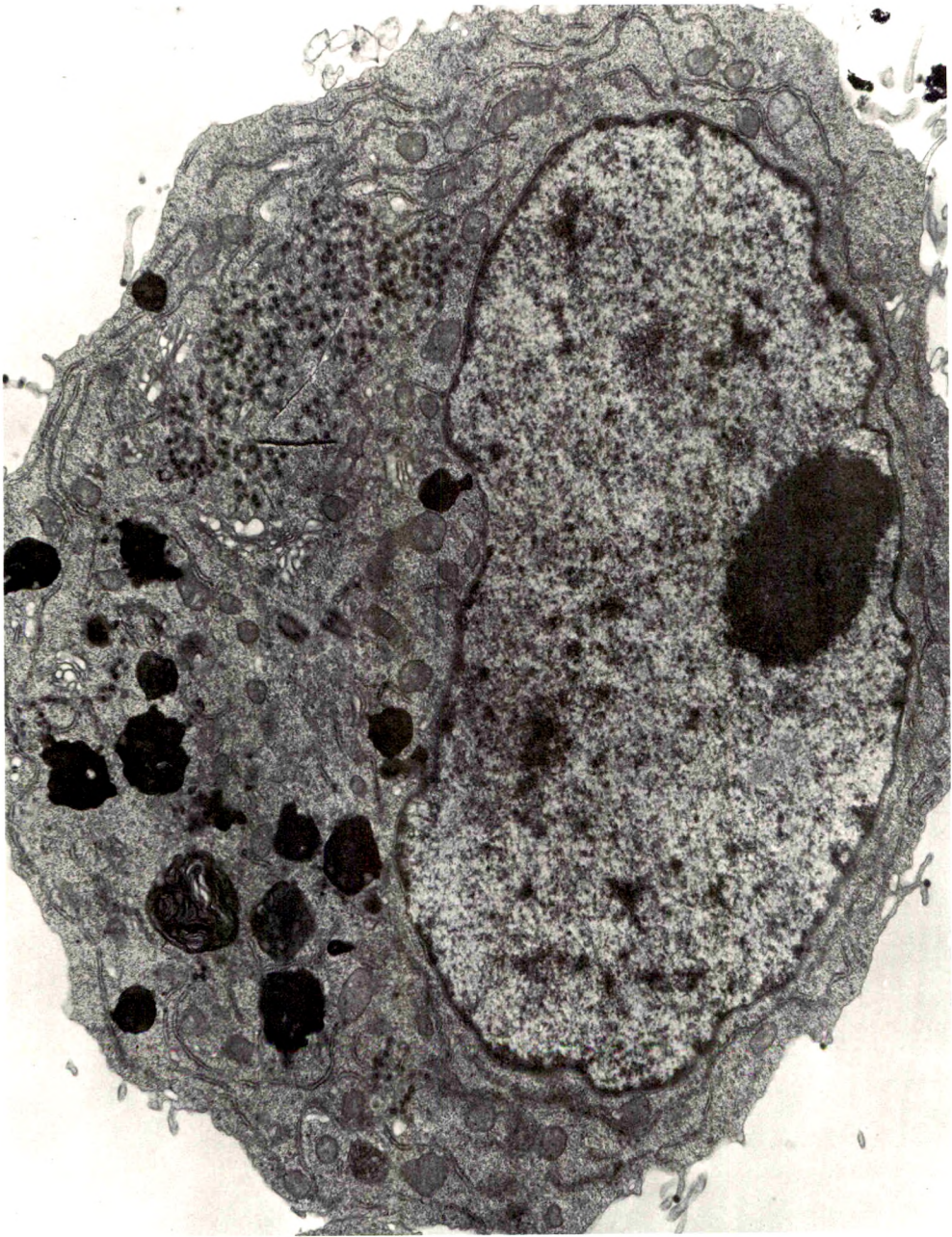


Fig 4—Electron micrograph of a cell from SLU-5, which is an established cell line from MOPC 21 tumor. Cells in this culture contain many intracytoplasmic membranous bodies (myelin figures) which are not observed in cultures derived from X5563 tumors (approximately $\times 11,000$).

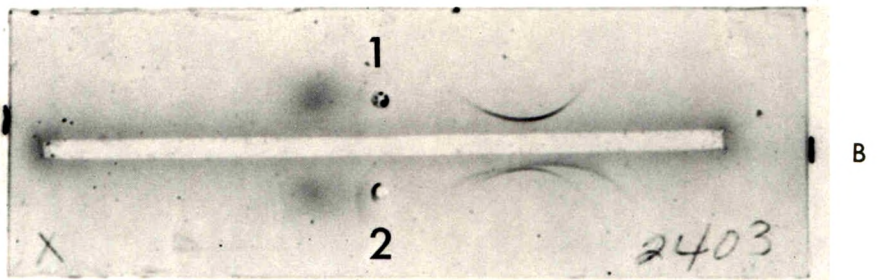
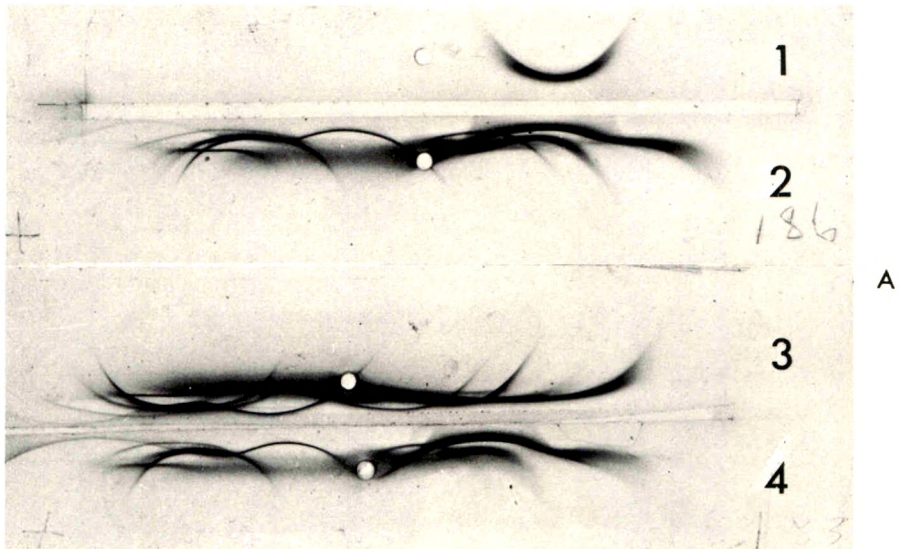


Fig 5—Immunoelectrophoresis, for comparison of globulins from different sources. **A**—Antigens in wells from top to bottom: (1) WU-29 medium, concentrated ten fold; (2) serum from mouse with X5563 tumor; (3) normal mouse serum and (4) same as 2. Antibody in both troughs was antimurine serum. Globulin present in cell culture medium is identical to the myeloma globulin in the tumor serum. **B**—Comparison of WU-29 medium (1) and a mixture of WU-29 and SLU-5 medium (2) against anti-mouse γ globulin. Globulin produced by SLU-5 is distinctive from that of WU-29 cells.

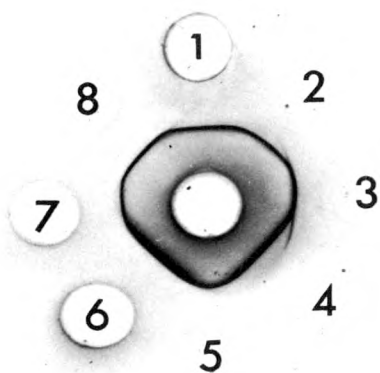


Fig 6—Micro-Ouchterlony plate. Reading clockwise from top (1), wells contained the following: (1) WU-29 concentrated medium; (2) Purified X5563 globulin; (3) Normal mouse globulin; (4) Tumor serum (X5563); (5) Same as 2; (6) Normal serum (C₃H mouse); (7) Same as 2; (8) Same as 3. Center well contained goat anti-mouse globulin.

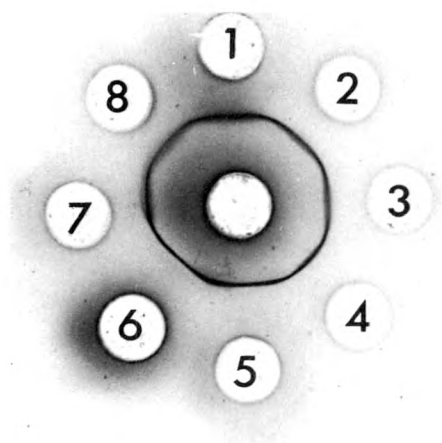


Fig 7—Micro-Ouchterlony plate. Concentrated medium from 8 cell lines derived from X5563 tumors at different times. Reading clockwise from top (1), wells contained the following: (1) WU-29; (2) WU-33; (3) WU-38; (4) WU-40; (5) WU-42; (6) WU-43; (7) WU-61 and (8) WU-83. Center well contained anti-X5563 globulin (DEAE-purified). All appear identical except WU-43 which shows slight spur formation.

The Number and Dimensions of Small Airways in Emphysematous Lungs

Kenichi Matsuba and William M. Thurlbeck

The number of conducting airways less than 2 mm in internal diameter was only slightly reduced in the lungs of 12 patients with pulmonary emphysema and diminished flow rates. There was a change in the distribution of the smallest remaining airways, with a deficit of airways 0.4 to 0.6 mm in diameter and an excess of airways smaller than this. The change in airway caliber and number was small in emphysematous lungs and increased airway resistance in emphysematous lungs is more likely related to loss of elastic recoil, central flow limitation and associated chronic bronchitis (Am J Pathol 67:265-276, 1972).

ALTHOUGH it is generally thought that pulmonary emphysema is associated with airways obstruction, the site and mechanism of obstruction are far from clear. Pathologic studies are conflicting, and the available information is shown in Table 1.¹⁻⁷ The majority of these reports are purely descriptive and nonquantitative. On the other hand, the site of flow resistance has been demonstrated physiologically by Hogg *et al*⁸ who partitioned airway resistance in excised postmortem lungs into a central (R_c) and a peripheral component (R_p) (in airways less than 2 mm in internal diameter). They showed that an increase in R_p was the common denominator in bronchitis, emphysema and bronchiectasis and that central resistance was inconstantly raised. We have, therefore, counted and measured airways less than 2 mm in internal diameter in the lungs of patients with emphysema to identify the nature of the lesions which might produce obstruction in these small airways.

Materials and Methods

Twenty-one emphysematous lungs from 12 patients, 11 of whom were male, were studied. The age range of the 12 patients was 51 to 74 years. All had had antemortem tests of pulmonary function and all had symptomatic obstructive lung disease which, in 10, was the cause, or the underlying cause, of death.

The number and dimensions of airways were determined as previously described for normal lungs.⁹ In brief, the lungs were inflated at a transpulmonary pressure of 25 cm of 10% formalin for 18 to 24 hours. The volume of the distended

From the Department of Pathology, McGill University, Montreal, Quebec, Canada.

Supported by a grant from the Medical Research Council of Canada.

Accepted for publication Nov. 19, 1971.

Address reprint requests to Dr. William M. Thurlbeck, Department of Pathology, McGill University, Montreal 110, Quebec, Canada.

Table 1—Obstruction or Narrowing of the Airway

Author(s)	Site	Nature
Spain, Kaufman ¹	Terminal bronchiole	Mural inflammation and fibrosis of bronchioles
Leopold, Gough ²	Between a terminal bronchiole and an emphysematous space	Inflammatory fibrosis with narrowing of 60% of bronchioles supplying centrilobular emphysematous spaces
McLean ³	Proximal order of respiratory bronchiole	Inflammation of airways and mucous plugging
Wright ⁴	First, second and third bronchi, distal to the segmental bronchi	Bronchial atrophy
Anderson, Foraker ⁵	Non-respiratory bronchiole	Collapse of bronchioles (reduced bronchoalveolar attachment)
Pratt et al ⁶	Bronchioles	Loss or distortion of the radial support of bronchioles
Bignon et al ⁷	Bronchioles	Inflammatory bronchiolar narrowing

lung (total lung volume or TLV) was then measured by water displacement. The lungs were cut into sagittal slices 1.0 to 1.5 cm thick. The proportion of the lung occupied by emphysema and nonparenchyma was calculated from a stratified random point count over the slices of lung, after impregnation with barium sulfate, floated under water. The mid-sagittal slices were submitted for the paper-mounted whole lung sections, and the amount of emphysema was estimated on these, both by using a standard set of grading pictures¹⁰ and the Ryder grid.¹¹ The former measurements were made by two observers who were unaware of the measurements of the small airways (Dr. George Massarella, Royal Post-Graduate School, London and Dr. M. W. Thurlbeck), and the mean score of the two observers was used. The latter measurements were made by Dr. Thurlbeck only.

Either five or six stratified random blocks were taken from the lateral slice of each lung for counting and for measuring small airways as well as alveolar surface area. Correction was made for shrinkage during processing, and all results are corrected to formalin-fixed tissue. Conducting (*ie*, nonalveolated) airways, less than 2 mm in internal diameter, were counted, their diameters measured as described previously,⁹ and the diameters used are those of all airways, rather than ideal airways. This was done because of the bias, in the latter method, toward smaller mean diameters.⁹ In addition, the proportion of points falling on airway lumen (Q_{SAT}) (the lumen of airways less than 2 mm, irrespective of whether the lumen contained air, mucus or exudate), compared to the total number of points falling over lung tissue or its contents, was calculated.

A method of correction was devised for possible overinflation of emphysematous lungs, making the usual assumption that all structures expand equally in all directions. We had anticipated that emphysematous lungs would be overinflated, and, therefore, the number of small airways per unit area or volume would appear decreased. From previously described data,⁹ it is possible to predict the ratio of TLV to the cube of body length at a given age. Thus, if body length is known, it is possible to predict TLV at age 20 (TLV_p). Volumetric change corrections would be directly related to the ratio of observed TLV (TLV_o) to TLV_p. Two dimen-

sional changes, such as the number of airways per unit area, would be corrected to the two third power of the ratio, and one dimensional change, such as diameter, to the one third power of the ratio. Where structures would be expected to increase due to overinflation (for example, diameters), the correction would thus be $d_c = d \times (TLV_p/TLV_o)^{1/3}$, where d_c is corrected diameter and d is observed diameter. Where results might be artificially decreased by overinflation, such as number of airways per unit area, the correction would be $n_c = n \times (TLV_o/TLV_p)^{2/3}$, where n_c is the corrected number of airways per unit area and n is the observed number of airways per unit area.

Correction for the proportion of small airways lumen (Q_{SAT}) is difficult. Clearly, if the lung is overinflated, then the amount of air is increased in small, large and alveolated airways as well as alveoli. Thus the proportion of air (lumen) to tissue in the lung increases with overinflation. However, the ratio of small airways lumen to lumen of other structures will remain approximately constant, since the basic assumption, in all corrections, is that structures expand equally. Using these assumptions, it can be shown that (see Appendix):

$$Q_{SATc} = Q_{SAT} \times \frac{(TLV_p - V_t)}{(TLV_o - V_t)} \times \frac{(TLV_o)}{(TLV_p)}$$

Where Q_{SATc} is the proportion of small airways lumen corrected to TLV_p , Q_{SAT} is the proportion of small airways lumen as measured and V_t is the volume of tissue. When V_t is zero, or when TLV_p and TLV_o are the same, then Q_{SATc} is equal to Q_{SAT} . The degree to which the ratio of $Q_{SATc}:Q_{SAT}$ varies from unity depends on the ratio of $TLV_o:TLV_p$ and V_t . The variation is small. For example, when TLV_o is 1.5 times TLV_p and V_t 10% of TLV_p , $Q_{SATc} = 0.9642 Q_{SAT}$. This represents the maximum change likely, since more than 50% overinflation is rarely found and V_t derived from the usually quoted density of the lung at total lung capacity (TLC)¹² and the density of air-free lung tissue¹³ is 9.93% of TLV_p . Thus, while we have corrected Q_{SAT} for overinflation, it is unlikely to be of major significance.

The assumption that air-containing structures expand equally must be examined critically. Although it used to be thought that alveolar volume did not expand with lung volume¹⁴ this is no longer thought to be true¹⁵⁻¹⁷ and alveolar volume increases directly with lung volume.^{16,17} The precise change in the dimensions of alveolar ducts with inflation is controversial,^{16,17} but the most recent view is that the alveolar duct-volume fraction of the lung is constant throughout inflation.¹⁷ By contrast, the dimensions of major bronchi¹⁸ change little above functional residual capacity. All the above results were obtained in healthy animals. Since alveoli and alveolar ducts form, by far, the greatest proportion of the lung, and since they change in parallel with lung volume, it is likely that our method of correcting (n) for overinflation is appropriate. The elastic tissue of the small airways is in direct continuity with the elastic framework of the alveoli, and alveolar ducts; thus they are more likely to behave as do the alveoli and alveolar ducts than as major bronchi. If this is true, then our corrections of diameter (d_c) and of Q_{SA} are adequate. If the small airways behave like bronchi, diameter as measured (d) is the best measurement. Also, if small airways expand like major bronchi, then V_{sap} is equal to V_{sao} in equation 2, and, thus, $Q_{sap} = Q_{sao} \times (TLV_o/TLV_p)$. The effect of this latter assumption on our results is discussed below.

Results

The complete data are shown in Table 2.

We have not illustrated the effect of sampling but, as in the normal

Table 2—Emphysematous Lungs

Case No.	Age (yr.)	Sex	Body length (cm)	Amount of emphysema		Total lung volume (liter)		No. of small airways/sq cm		Average diameter of small airways (mm)		Proportion of small airways lumen	
				Standard set ¹⁰	Ryder grid ¹¹	TLV _o	TLV _p	n	n _c	d	d _c	Q _{SAT}	Q _{SATc}
1	74	M	167	45	16	—	4.93	0.94	—	.62	—	.0111	—
2	62	M	183	70	25	4.00	6.48	0.58	0.42	.88	1.03	.0111	.0119
3	64	M	168	41	18	5.20	5.02	1.03	1.05	.63	0.62	.0083	.0083
4	62	M	178	59	18	—	5.97	0.57	—	.90	—	.0096	—
5	73	M	167	54	17	4.46	4.93	0.58	0.54	.79	0.82	.0091	.0092
6	56	M	165	60	18	3.86	4.75	0.86	0.75	.59	0.63	.0096	.0098
7	70	M	182	34	14	8.59	6.38	0.40	0.49	.86	0.78	.0086	.0084
8	57	F	165	38	13	5.68	4.75	0.49	0.55	.73	0.69	.0067	.0066
9	62	M	188	60	20	6.19	7.03	0.50	0.46	.87	0.91	.0073	.0074
10	66	M	167	81	26	5.79	4.93	0.65	0.72	.75	0.71	.0095	.0096
11	68	M	177	44	14	9.27	5.87	0.53	0.72	.41	0.35	.0014	.0013
12	51	M	180	43	14	4.69	6.17	0.52	0.43	.82	0.90	.0116	.0120
Mean			173.9	52.4	17.8	5.773	5.601	0.638	0.613	0.738	.744	.00866	.00845
SE			±2.4	±4.1	±1.2	±.581	±.232	±.057	±.062	±.043	±.060	±.00071	±.00089

TLV_o = observed total lung volume
TLV_p = predicted total lung volume
n = observed number of small airways/sq cm
n_c = number of small airways/sq cm corrected to TLV_p
d = observed average diameter of small airways
d_c = average diameter of small airways corrected to TLV_p
Q_{SAT} = observed proportion of small airways lumen
Q_{SATc} = proportion of small airways lumen corrected to TLV_p

lung,⁹ there was no significant difference between lungs or within lobes and five blocks of tissue provided reasonably precise data. Moderate to severe emphysema was present in all lungs.

Table 3 summarizes the findings in the 12 patients and contrasts these to the results in nonemphysematous lungs from 20 subjects.⁹ The number of small airways per unit area (n) and the number of small airways per unit area corrected to total lung volume at age 20 (n_c) are significantly diminished in emphysema ($t = 2.3853$, $P < 0.05$ and $t = 2.9056$, $P < 0.01$, respectively). However, this difference is largely due to the fact that patients with emphysema were taller than our subjects without emphysema. Text-figure 1 shows that the majority of patients were more than 160 cm tall (average body length 173.9 cm) and that there is a negative correlation between (n) and body length ($r = -0.5851$, $P < 0.05$) as we have previously found in nonemphysematous lungs.⁹ Text-figure 2 compares (n_c) observed in the emphysematous lungs to that predicted from body length in normal subjects.⁹ It is apparent that most have a lower value for observed (n_c) than predicted, but the difference does not reach conventional levels of significance ($0.1 > P > .05$).

Table 3 indicates that the mean diameter of airways less than 2 mm in diameter is similar in controls and in emphysema, whether corrected or not. Text-figure 3 compares the distribution of diameters of the small airways. This shows that in emphysema there is an excess of airways less than 0.2 mm in diameter, a small excess in airways 0.2–0.4 mm in diameter and a deficit in airways between 0.4 and 0.6 mm. The distribution of the remaining airways is essentially similar in emphysematous and nonemphysematous lungs.

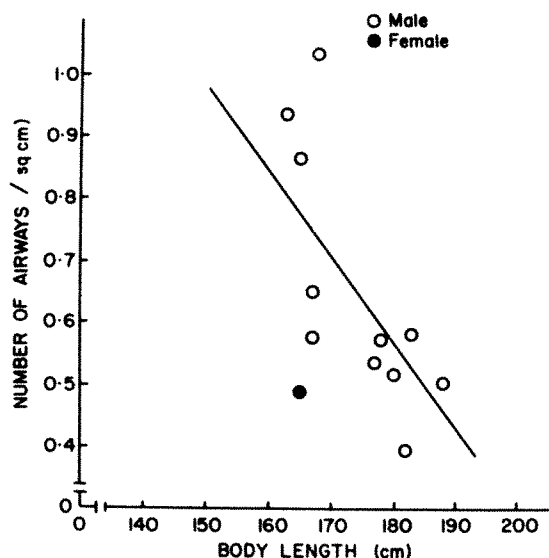
The proportion of small airways lumen (Q_{SAT}) is diminished in emphysema ($t = 3.9052$, $P < 0.001$). There were no significant correlations between any of the measurements of small airways and either measurements of flow rates or amounts of emphysema.

Discussion

Our results show that there are alterations in the number and dimensions of small airways in emphysema but that these changes are

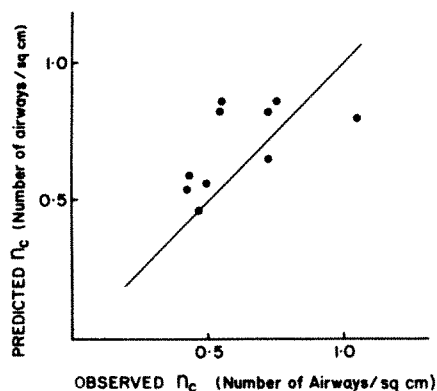
Table 3—Comparison of Nonemphysematous and Emphysematous Lungs

Lung	n	n_c	Q_{SAT}	d	d_c
Nonemphysema	0.840	0.931	0.0142	0.756	0.723
Emphysema	0.638	0.613	0.0087	0.738	0.744

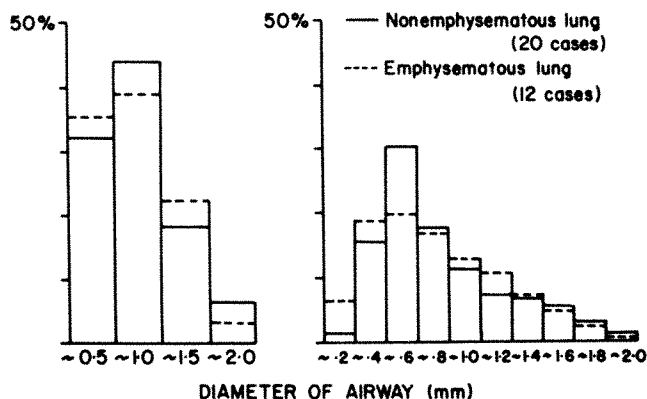


TEXT-FIG 1—The relationship between the number of small airways/sq cm and body length ($r = -0.5851$, $P < 0.05$).

relatively slight. There is also a paradox in our data. At first sight, it appears that there is a marked change in the number of airways per unit area and no change in diameter. The striking diminution in number of small airways per unit area (n) is due primarily to the fact that our patients with emphysema were taller than the nonemphysematous subjects used in a previous study.⁹ Since body length and (n) are negatively correlated, this would diminish (n) in emphysema, as opposed to the nonemphysematous subjects. The latter were shorter than the patients with emphysema since the controls were selected primarily because they did not have emphysema. Because emphysema is much less common in women, we have more female controls, hence the smaller



TEXT-FIG 2—In 7 cases, the observed n_c is less than that predicted from body length in normal subjects.



TEXT-FIG 3—In emphysematous lungs, there are more airways less than 0.5 mm in diameter. When the diameter of airways is examined at 0.2 mm intervals, it becomes apparent that there is an excess of airways of less than 0.4 mm in diameter and a deficit of airways between 0.4 and 0.6 mm diameter in emphysema.

average body height of the group without emphysema. When allowance is made for height, the change in our emphysematous subjects is small and does not reach conventional levels of significance. For reasons discussed below, a real loss of airways is likely.

Another feature of the paradox is that no change in average diameter was noted, yet there was a small shift in distribution of airway diameter with an excess number of very small airways in emphysema. A simple example will show how this apparent contradiction may arise. Let us imagine that a normal subject had nine airways per unit area and that these airways were 1, 2, 3, 4, 5, 6, 7, 8 and 9 mm in diameter, respectively. The average airway diameter would be 5 mm. If the two smallest airways (1 and 2 mm in diameter) were destroyed, then the average diameter would be increased to 6 mm. There could be considerable narrowing of the remaining airways, yet the average diameter would be unchanged if the smallest airways were lost. That this is not speculation is shown by the alteration of proportion of small airways lumen (Q_{SAT}). This represents the sum effect of airway number per unit area and airway volume, and it is an accurate and reproducible measurement. Since there is no reason to suspect that there is loss of airway length, diminution of Q_{SAT} indicates diminution of airway diameter and/or airway number. The reduction in Q_{SAT} is significantly larger than that of (n_c) and thus airway lumen must also be compromised. It follows that the airways which are lost must be the smallest ones, otherwise average diameter would have diminished. Reference to Text-figure 3 shows that the narrowing of airways also involves only the smallest ones (<0.6 mm in diameter) and thus the overall effect

on average diameter will be small. However the change in Q_{SAT} is not likely to have a major effect on airway resistance. Since normally airways less than 2 mm only contribute some 10% of resistance to air flow in the lung,⁸ the smallest airways, which are affected, contribute even less. Thus, the changes we recorded would make little difference to total resistance, even allowing for the fact that increase in resistance increases to the fourth power of the reduction in radius. Even in our patients with the most severe airway abnormalities, the change in total airway resistance would have been only doubled.

It follows that the changes we observed and which we would like to refer to as fixed airways disease, are insufficient to account for the high levels of airway resistance found in some patients with emphysema. There are several other mechanisms of increased resistance to flow which have been described. Since our measurements were made under isopressure conditions, there was no loss of force acting on the airways. We would anticipate that under isovolume conditions, diminished elastic recoil of emphysematous lungs would result in narrowed airways. Another mechanism is flow limitation of central airways which occurs in about half of patients with emphysema.¹⁹ However, the most important cause of increased resistance is likely to be due to associated chronic bronchitis. There is evidence that patients with the "bronchial type" of airways obstruction have higher levels of airways resistance, particularly on inspiration, than patients with emphysema and mild or no bronchitis.²⁰ It seems likely that this is due to mucous plugging in the small airways although it may, in part, be due to encroachment on the lumen by enlarged bronchial glands. Our methodology (intra-bronchial distension) was not appropriate to assess intrabronchiolar mucus and we are presently investigating the extent of mucous plugging in bronchitis, using fixation via the pulmonary artery. We would emphasize that our definition of bronchial lumen included mucus—*ie*, hits on the lumen were counted as hits, irrespective of the content.

We have considered, and dismissed, two possible reasons for the small difference between controls and emphysema. First, it is possible that some patients with emphysema have a diminished number and caliber of airways while others do not. One might anticipate that the latter patients would be relatively asymptomatic. Thus, if one studied random necropsies, it is possible that such a series might include patients with limited symptoms and normal airways. Our series is not random and all patients were symptomatic with demonstrable airways obstruction, as determined by FEV or MMFR. Second, our method of measuring only airways less than 2 mm in diameter, while it is the only practical

method, has inherent disadvantages, as discussed elsewhere.⁹ In particular, if airways that were normally greater than 2 mm in diameter were reduced to less than 2 mm in diameter in emphysema, then these airways would be included in our count and would tend to obscure a difference between emphysema and normals. This is unlikely to have a major effect. We have shown⁹ that about 5% of the airways less than 2 mm in diameter are in the size range, 1.5–2.0 mm, and it is likely that perhaps half of this number (*ie*, 2.5%) are in the range of 2.0–2.5 mm. Thus, even if all this class of airways were rearranged and then included in our counts, it would make no material difference.

Our methodology contains another potential error. If airways were dilated in emphysema, some airways normally less than 2 mm in diameter would be increased over our arbitrary limit and the number of airways less than 2 mm in diameter per unit area would be decreased. However, for the reasons listed previously, this effect is likely to be small, affecting less than 5% of the airways, and cannot account for the marked reduction in proportion of airways lumen. It should also be noted that if large airways were excluded then the average diameter would be reduced, which was not the case.

A point of minor technical interest is the fact that 5 of the 10 patients with emphysema had smaller measured lung volumes than those predicted from body length. Bignon *et al* have had similar experience.⁷ The likely reasons include the fact that terminal pulmonary infection is common in emphysematous lungs and this tends to make them stiff. The lack of anticipated lung overinflation made our attempts at correction largely unnecessary. Using the assumption of uniform inflation of all components of the lung, the mean values for observed and corrected (d), (Q) and (n) were essentially identical. If the alternative assumption is made that airway dimensions are not affected by overinflation, only Q_{SAT} is changed significantly, and the mean value in the emphysematous subjects becomes 0.00797 as opposed to 0.00866 uncorrected and 0.00845 when corrected to assumed uniform pulmonary overexpansion. In the section on methods, we have pointed out why we do not favor the assumption of fixed airway dimension. Even using this assumption, which maximizes the change in emphysema, changes in dimensions of airways are insufficient to account for observed alterations in airway resistance, strengthening the conclusions drawn earlier.

Appendix

Where TLV = total lung volume (volume of air plus tissue in lung)

V = volume, Q = proportion, t = tissue, a = air, o = observed, p = predicted and sa = small airways.

By definition:

$TLV_p = V_t + V_{ap}$, $V_{ap} = TLV_p - V_t$, $TLV_o = V_t + V_{ao}$, $V_{ao} = TLV_o - V_t$
thus:

$$\frac{V_{ap}}{V_{ao}} = \frac{TLV_p - V_t}{TLV_o - V_t} \quad (1)$$

since by definition:

$$Q_{sap} = \frac{V_{sap}}{TLV_p}$$

therefore:

$$V_{sap} = Q_{sap} \times TLV_p$$

similarly:

$$Q_{sao} = \frac{V_{sao}}{TLV_o}$$

therefore:

$$V_{sao} = Q_{sao} \times TLV_o$$

thus:

$$\frac{V_{sap}}{V_{sao}} = \frac{Q_{sap} \times TLV_p}{Q_{sao} \times TLV_o} \quad (2)$$

The assumption is made that volume changes are equally distributed throughout the lung. Thus:

$$\frac{V_{ap}}{V_{ao}} = \frac{V_{sap}}{V_{sao}} \quad (3)$$

Substituting (1) and (2) in (3) yields:

$$\frac{TLV_p - V_t}{TLV_o - V_t} = \frac{Q_{sap} \times TLV_p}{Q_{sao} \times TLV_o}$$

and:

$$Q_{sap} = Q_{sao} \times \left(\frac{TLV_p - V_t}{TLV_o - V_t} \right) \times \left(\frac{TLV_o}{TLV_p} \right)$$

References

1. Spain DM, Kaufman G: The basic lesion in chronic pulmonary emphysema. *Am Rev Tuberc* 68:24-30, 1953
2. Lepold JG, Gough J: The centrilobular form of hypertrophic emphysema and its relation to chronic bronchitis. *Thorax* 12:219-235, 1957
3. McLean KH: The pathogenesis of pulmonary emphysema. *Am J Med* 25: 62-74, 1958
4. Wright RR: Bronchial atrophy and collapse in chronic obstructive pulmonary emphysema. *Am J Pathol* 37:63-77, 1960

5. Anderson AE Jr, Foraker AG: Relative dimensions of bronchioles and parenchymal spaces in lungs from normal subjects and emphysematous patients. *Am J Med* 32:218-226, 1962
6. Pratt PC, Jutabha O, Klugh GA: Quantitative relationship between structural extent of centrilobular emphysema and postmortem volume and flow characteristics of lungs. *Med Thorac* 22:197-208, 1965
7. Bignon J, Khouri F, Even P, André J, Brouet G: Morphometric study in chronic obstructive bronchopulmonary disease: Pathologic, clinical and physiologic correlation. *Am Rev Resp Dis* 99:669-695, 1969
8. Hogg JC, Macklem PT, Thurlbeck WM: Site and nature of airway obstruction in chronic obstructive lung disease. *N Engl J Med* 278:1355-1360, 1968
9. Matsuba K, Thurlbeck WM: The number and dimensions of small airways in non-emphysematous lungs. *Am Rev Resp Dis* 104:516-524, 1972
10. Thurlbeck WM, Dunnill MS, Hartung W, Heard BE, Heppleston AG, Ryder RC: A comparison of three methods of measuring emphysema. *Human Pathol* 1:215-226, 1970
11. Ryder RC, Thurlbeck WM, Gough J: A study of inter-observer variation in the assessment of the amount of pulmonary emphysema in paper-mounted whole-lung sections. *Am Rev Resp Dis* 99:354-364, 1969
12. Fraser RG, Pare JAP: *Diagnosis of disease of the chest—an integrated study based on the abnormal roentgenogram*. Philadelphia, London, Toronto, WB Saunders Co, 1970, p 86
13. Hogg JC, Nepszy S: Regional lung volume and pleural pressure gradient estimated from lung density in dogs. *J Appl Physiol* 27:198-203, 1969
14. Macklin CC: Musculature of bronchi and lungs. *Physiol Rev* 9:1-60, 1929
15. Storey WF, Staub NC: Ventilation of terminal air units. *J Appl Physiol* 17:391-397, 1962
16. Dunnill MS: Effect of lung inflation on alveolar surface area in the dog. *Nature* 214:1013-4, 1967
17. Forrest JB: The effect of changes in lung volume on the size and shape of alveoli. *J Physiol* 210:533-547, 1970
18. Marshall R: Effect of lung inflation on bronchial dimensions in the dog. *J Appl Physiol* 17:596-600, 1962
19. Macklem PT, Fraser RG, Brown WG: Bronchial pressure measurements in emphysema and bronchitis. *J Clin Invest* 44:807-905, 1965
20. Burrows B, Saksena FB, Diener CF: Carbon dioxide tension and ventilatory mechanics in chronic obstructive lung disease. *Ann Intern Med* 65:685-700, 1966

[*End of Article*]

High-Resolution Autoradiography of Malarial Parasites Treated with ^3H -Chloroquine

Masamichi Aikawa, MD

Electron microscope autoradiography was performed on the erythrocytic stages of the rodent malarial parasite, *Plasmodium berghei*, after exposure to ^3H -chloroquine. ^3H -Chloroquine becomes selectively localized within the parasite food vacuoles 1 hour after it is administered, and remains in this structure for up to 24 hours. This study indicated that the food vacuoles were the primary site of chloroquine concentration within the parasite (Am J Pathol 67:277-284, 1972).

THE SYNTHETIC ANTIMALARIAL DRUG, chloroquine [7-chloro-4-(4'-diethylamino-1'-methylbutylamino) quinoline], is effective against the erythrocytic stages of most strains of malaria. It has been suggested that chloroquine becomes highly concentrated in the erythrocytes infected by malarial parasites and enters into the parasite as it ingests red cell cytoplasm.^{1,2} This suggestion was supported by electron microscopic studies which showed that the first morphologic changes occur in the parasite food vacuoles containing host cell cytoplasm after the administration of chloroquine.³⁻⁵ However, evidence to support this hypothesis has been lacking.

The present communication describes the results of electron microscope autoradiography on the erythrocytic stages of the rodent malarial parasite, *Plasmodium berghei*, after exposure to ^3H -chloroquine and confirms the primary site of chloroquine concentration as the food vacuoles within the parasite.

Materials and Methods

Twenty mice of the ICR strain, each weighing an average of 25 g, were inoculated intraperitoneally with the erythrocytic stages of *P. berghei* (NYU-2 strain). When the parasitemia reached about 50%, a single dose of chloroquine- ^3H (5.6×10^{-3} moles/liter) was injected intraperitoneally into each infected mouse.* The specific activity of chloroquine- ^3H used was 75.7 mCi/m mole (0.2366 mCi/mg) and its radiochemical purity was 95.4%, as determined by a radiometric thin-layer

From the Institute of Pathology, Case Western Reserve University, Cleveland, Ohio 44106.

Supported in part by a Research Grant (AI-08970) from the US Public Health Service and an US Army R & D Command Contract (DADA-17-70-C-0006). It is contribution No 974 from the Army Research Program on Malaria. Dr. Aikawa is a Research Career Development Awardee (AI-46237) from the US Public Health Service.

Accepted for publication Oct 7, 1971.

* The chloroquine- ^3H was generously supplied by the US Army Research and Development Command.

chromatographic technic using methanol on silica. Each mouse received 250 μCi of chloroquine-3- ^3H . One set of controls received the same dose of chloroquine without radioactivity; another set was not treated. At varying time intervals of up to 24 hours, the mice were sacrificed and blood samples were obtained from the heart. These samples were fixed in 2% glutaraldehyde, 4% sucrose in 0.05 M PO_4 . The fixed materials were then processed for electron microscopy.

For autoradiography, sections of 400 to 600 \AA thickness were placed on Formvar and carbon-coated copper grids and were stained with uranyl acetate and lead citrate.⁶ Thereafter, the grids were covered with a monolayer of emulsion (Ilford L4) by the wire loop method.⁷ The emulsion-covered grids were kept in the dark at 4°C for 6 to 10 weeks. After the emulsion was exposed to radioactive chloroquine, the grids were developed in Microdol X (Kodak) for 2 minutes and fixed in Kodak rapid fixer for 2 minutes. The grids were washed in 1N NaOH for 5 minutes and examined with a Siemens Elmiskop 101 electron microscope.

Results

The most noticeable morphologic changes after the erythrocytic stages of *P. berghei* were exposed to chloroquine occurred in the food vacuoles. During the first hour after the administration of chloroquine, the food vacuole, which contains erythrocyte cytoplasm and is limited by a unit membrane, becomes slightly larger than those in untreated parasites. It measures 500 $\text{m}\mu$ in diameter, whereas a food vacuole of the untreated parasite measures 400 $\text{m}\mu$ in diameter. However, at this stage, the matrix of the food vacuole is similar to that of the untreated parasite and contains crystalloid malarial pigment particles (Figures 1 and 2).

During 3 to 5 hours after the drug was administered, the affected food vacuoles become much larger and measure up to 0.8 to 1 μ in diameter (Figure 3). Unlike the food vacuole of the untreated and the 1-hour treated parasites, which contain only host cell cytoplasm and malarial pigment particles, the food vacuoles show various inclusions at this stage (Figure 3). The enlarged food vacuoles contain electron-dense granules and vesicles, of various sizes, in the matrix, and the food vacuoles without host cell cytoplasm possess more granules than those with host cell cytoplasm. The electron-dense granules measure ~ 60 $\text{m}\mu$ in length and the vesicles measure ~ 300 $\text{m}\mu$ in diameter, and the matrix is often electron-translucent. However, no malarial pigment particles are observed in these food vacuoles. The food vacuoles with various inclusions can be observed as long as 24 hours after chloroquine administration (Figure 4). In addition to changes in the food vacuoles, the parasite cytoplasm demonstrates dilated endoplasmic reticulum and vacuoles 5 to 24 hours after administration of the drug.

Electron microscope autoradiography on the parasites exposed to ^3H -chloroquine revealed silver grains in the overlying emulsion as

twisted, electron-dense filaments, the location of which indicates the presence of radioactive chloroquine. One hour after exposure to ^3H -chloroquine, exposed silver grains are noted directly over and in close proximity to some food vacuoles (Figure 5). The incidence with which silver grains are associated with food vacuoles increases as the exposure time to the drug increases. Twenty-four hours after the administration of radioactive chloroquine, about 50% of the food vacuoles are overlain with silver grains. All of the food vacuoles associated with silver grains show the changes described earlier (Figures 6-8).

In addition to the silver grains overlying the food vacuoles, a few clusters of silver grains are also observed over the cytoplasm of the parasitized erythrocytes.

Discussion

The erythrocytic stages of malarial parasites form food vacuoles by ingesting the erythrocyte cytoplasm through a cytosome.⁸ Digestion of the erythrocyte cytoplasm occurs within the food vacuoles leaving an undigested residue known as malarial pigment.⁸ It has been suggested that chloroquine acts on this digestion system of the parasite.³⁻⁵

In 1966, Macomber and his colleagues¹ reported that chloroquine becomes highly concentrated in erythrocytes infected by the malarial parasite, *P. berghei*, and suggested that the selective concentration of chloroquine in the parasitized erythrocyte is a necessary condition for its antimalarial activity. A similar observation on *P. falciparum* was also made by Fitch.² Although it is still not clear whether the binding of chloroquine to hemoglobin is of direct significance in the action of chloroquine, various investigators^{3-5,9,10} have suggested that such binding would facilitate entry into the parasite with ingestion of the host erythrocyte cytoplasm during the formation of the food vacuoles. This route of entry was supported by the electron microscope observation that the first morphological changes occur in the food vacuoles after the administration of chloroquine.³⁻⁵ The absence of typical malarial pigments in the food vacuoles of chloroquine-treated parasites was suggested as additional evidence for the impairment of the digestion process in the presence of chloroquine. On the other hand, merozoites do not show any noticeable changes after chloroquine treatment. This was thought due to the fact that this stage does not actively ingest host cell cytoplasm and, therefore, chloroquine does not gain entrance into the merozoite.⁴ All of these observations are compatible with the hypothesis that chloroquine impairs digestion of hemoglobin by the parasites, lead-

ing to starvation of the parasites. However, direct proof of this hypothesis has yet to be obtained.

The resolution of electron microscope autoradiography on thin sections by the present technic is of the order of 0.1μ .⁷ Since the size of the parasite food vacuole is in the range of 0.4 to 1μ , location of ^3H -chloroquine can be determined relative to this organelle. The much greater concentration of silver grains overlying the food vacuoles as compared with cytoplasm after exposure to ^3H -chloroquine demonstrates the selective concentration of radioactive chloroquine within the food vacuoles at early times. This accumulation of chloroquine occurs as early as one hour after drug administration.

Though the cytoplasm of the parasites shows morphologic alterations at the later stages of chloroquine treatment, few silver grains are observed within the cytoplasm at any time up to 24 hours. This observation may suggest that the morphologic changes in the cytoplasm are secondary to the altered digestive process in the food vacuoles.

References

1. Macomber PB, O'Brien RL, Hahn F: Chloroquine: Physiological basis of drug resistance in *Plasmodium berghei*. *Science* 152:1374-1375, 1966
2. Fitch CD: *Plasmodium falciparum* in owl monkeys: Drug resistance and chloroquine binding capacity. *Science* 169:289-290, 1970
3. Macomber PB, Sprinz H, Tousimis AJ: Morphological effects of chloroquine on *Plasmodium berghei* in mice. *Nature* 214:937-939, 1967
4. Aikawa M, Beaudoin RL: Effects of chloroquine on the morphology of the erythrocytic stages of *Plasmodium gallinaceum*. *Am J Trop Med Hyg* 18:166-181, 1969
5. Warhurst DC, Hockley DJ: Mode of action of chloroquine on *Plasmodium berghei* and *P. cynomolgi*. *Nature* 214:935-936, 1967
6. Aikawa M, Beaudoin RL: *Plasmodium fallax*: High-resolution autoradiography of exoerythrocytic stages treated with primaquine *in vitro*. *Exp Parasitol* 27:454-463, 1970
7. Caro LG: A common source of difficulty in high-resolution radioautography. *J Cell Biol* 41:918-919, 1969
8. Aikawa M, Hepler PK, Huff CG, Sprinz H: The feeding mechanism of avian malarial parasites. *J Cell Biol* 28:355-373, 1966
9. Peters W: *Chemotherapy and Drug Resistance in Malaria*. London and New York. Academic Press, Inc, 1970, pp 540-553
10. Howells RE, Peters W, Homewood CA, Warhurst DC: Theory for the mechanism of chloroquine resistance in rodent malaria. *Nature* 228:625-628, 1970

[Illustrations follow]

Fig 1—The erythrocytic trophozoite of *P. berghei* before exposure to chloroquine. A food vacuole (F) contains several electron-dense crystalloid malarial pigment particles (P) and is surrounded by a unit membrane (arrow). The matrix is electron opaque ($\times 43,000$).



Fig 2—A food vacuole (F) of *P. berghei* 1 hour after administration of nonradioactive chloroquine. The food vacuole is slightly enlarged and its matrix is less electron opaque than that of the untreated parasite, but still contains a malarial pigment particle (P) ($\times 25,000$).

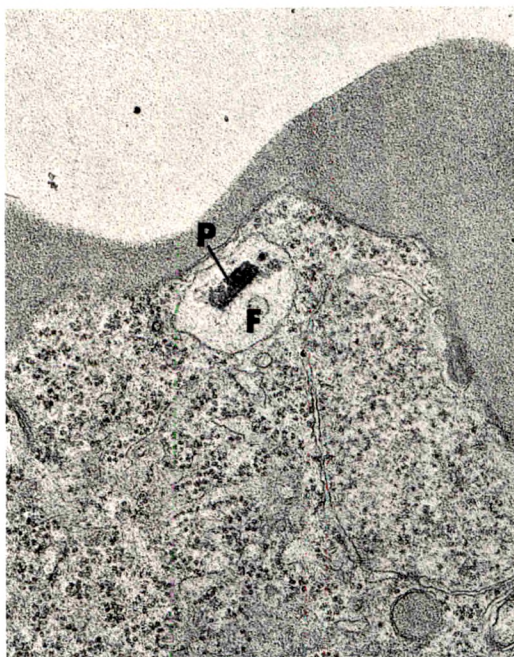
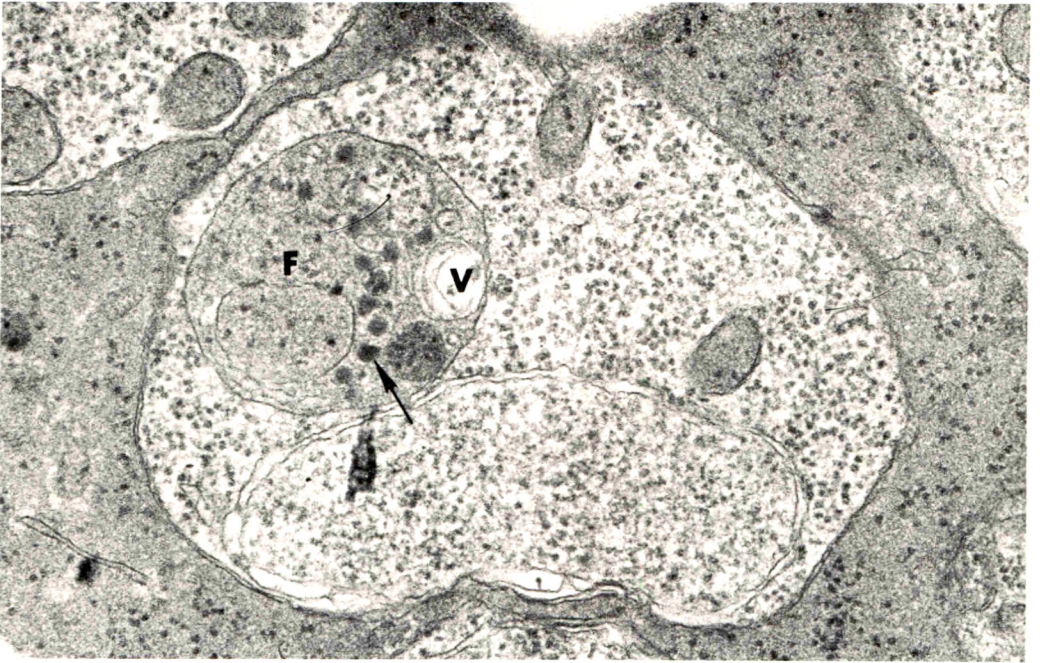


Fig 3—A food vacuole (*F*) of *P. berghei* 5 hours after exposure to nonradioactive chloroquine. The food vacuole is enlarged and contains several vesicles (*V*) and electron-dense particles (*arrow*). No typical malarial pigment particles are observed. However, the matrix of the food vacuole is still electron opaque ($\times 48,000$).

Fig 4—The erythrocytic trophozoite of *P. berghei* 24 hours after administration of non-radioactive chloroquine. The enlarged food vacuole (*F*) contains many vesicles (*V*) and electron-dense particles (*arrow*). Its matrix is electron translucent and no malarial pigment particles can be seen in this affected food vacuole ($\times 26,000$).



3



4

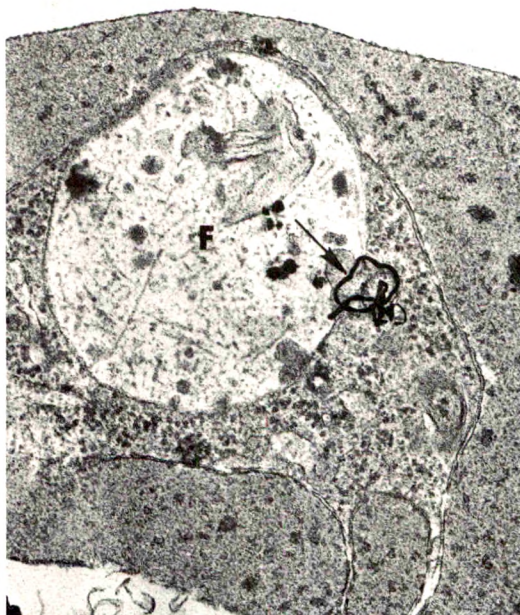
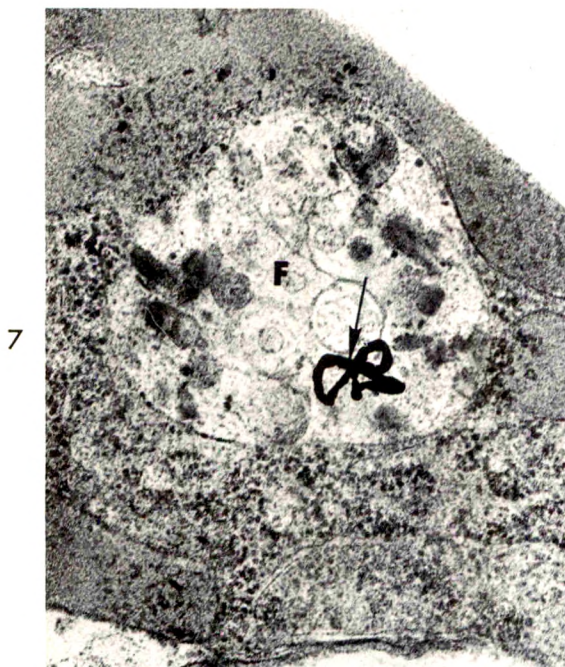


Fig 5—The erythrocytic stage of *P. berghei* 1 hour after administration of ^3H -chloroquine. Electron-dense filaments composed of silver grains (arrow) which indicate location of ^3H -chloroquine are present over the food vacuole (F) ($\times 34,000$).

Fig 6—The erythrocytic stage of *P. berghei* 5 hours after exposure to ^3H -chloroquine. A cluster of silver grains (arrow) is present over the enlarged food vacuole (F) ($\times 29,000$).

Fig 7—An enlarged food vacuole (F) of *P. berghei* 24 hours after administration of ^3H -chloroquine is closely associated with silver grains (arrow) ($\times 46,000$).

Fig 8—Another example of the affected food vacuole (F) of *P. berghei* 24 hours after exposure to ^3H -chloroquine. Silver grains are again observed over the altered food vacuole (arrow) ($\times 38,000$).

Experimental Papillary Necrosis of the Kidney

I. Morphologic and Functional Data

G. Murray, MD, R. G. Wyllie, MD, G. S. Hill, MD, P. W. Ramsden and R. H. Heptinstall, MD

Papillary necrosis was produced in rats by a single intravenous injection of bromoethylamine hydrobromide (BEA). The earliest changes as seen by light microscopy were necroses of the limbs of Henle and eosinophilic droplets in collecting ducts. Complete necrosis of the papilla took place between 4 and 7 days and the dead papilla was usually sequestered completely by 21 days. Cortical changes occurred secondary to papillary necrosis. Tubular atrophy and loss was greatest in the deeper parts of the central cortex, the more superficial nephrons frequently being spared. The perihilar cortex was the least involved. This distribution was considered to be related to the respective lengths of the limbs of Henle, nephrons with limbs extending into the papilla being those undergoing change. Increased urine output occurred during the first day and continued thereafter. There was a profound defect in concentrating ability (*Am J Pathol* 67:285-302, 1972).

PAPILLARY NECROSIS of the kidney is well known to be a complication of either diabetes mellitus or obstruction to the urinary tract. The incidence at autopsy in the United States during the 1940's was reported to be 0.16 and 0.26% in two series.^{1,2} In the 1950's, Spühler and Zollinger³ observed that papillary necrosis could be associated with, and presumably caused by, a high intake of analgesic mixtures. Data from Switzerland, Scandinavia and Australia indicated a great increase in the incidence of the condition, almost solely a result of analgesic abuse.⁴⁻¹⁰ Thus, percentage incidences of about 4¹¹ and 9%¹² in routine autopsies have been found in Australia.

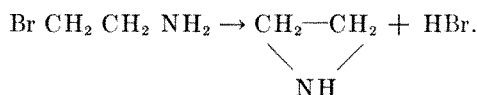
Little is known of the pathogenetic mechanisms at work in papillary necrosis, regardless of its etiology, and the present series of experiments were designed to obtain some information on one particular experimental model—the bromoethylamine hydrobromide (BEA) model in the rat. This compound was first used to produce experimental papillary

From the Department of Pathology, Johns Hopkins University School of Medicine and Hospital, Baltimore, Maryland.

* Supported by Grants HE-07835 and GH-00415 from the US Public Health Service. Accepted for publication Nov. 27, 1971.

Address reprint requests to Dr. R. H. Heptinstall, Department of Pathology, The Johns Hopkins Hospital, Baltimore, Maryland 21205.

necrosis in 1913 by Oka,¹³ and more recently by Fuwa and Waugh;¹⁴ with a suitable dose, the incidence of necrosis approaches 100%. It is a halogenated amine salt, $\text{Br} \cdot \text{CH}_2 \cdot \text{CH}_2 \cdot \text{NH}_2 \cdot \text{HBr}$ derived from ethylamine ($\text{CH}_3 \text{ CH}_2 \text{ NH}_2$) and readily soluble in water in which the strength of ionic bonds linking hydrobromide is so weakened that the salt is lost to solvent molecules. The rest of the molecule undergoes rapid solvolysis¹⁵ accompanied by ring closure.



This three-membered ring is stable in solution.¹⁶ When an aqueous solution of BEA is injected intravenously into the rat it produces a rise in blood pressure after a brief period of hypotension. This particular compound was chosen because the induced necrosis is reproducible and can be produced by a single injection. That the pathogenesis may be different from that after analgesic abuse, is, of course, appreciated.

In this first paper, the sequence of morphologic changes in the kidney after the injection of BEA is described. In particular, attention is paid to the manner in which certain areas of the cortex are selectively damaged after necrosis of the papilla. A brief account is also given of the concentration defect that occurs.

Materials and Methods

A single intravenous injection of 50 mg of bromoethylamine hydrobromide (BEA), prepared as a 10% aqueous solution, was given to 116 female Holtzman rats each weighing 200 to 220 g. They were fed Purina Chow and given unlimited quantities of water to drink. Rats were killed at various time intervals from 6 hours to 40 weeks. Blood was drawn for serum urea nitrogen (SUN) estimations before BEA was administered and immediately before the animals were killed. In long term survivors, blood was drawn at four weekly intervals. Serum urea nitrogen was determined on .2 ml samples, using a modified Berthelot reaction. The animals were killed by exsanguination from the heart after ether anesthesia. Tissue was taken for light microscopy and fixed in formol-saline. The tissues taken were coronal sections through the papilla in most cases; a few longitudinal sections were taken. Sections were stained with hematoxylin-eosin, by the periodic acid-Schiff method, and with Martius scarlet for fibrin. In certain animals, tissue was taken for electron microscopy, but no account of this will be given at the present time.

Urine output was measured for several weeks in the long-term survivors and tests for ability to concentrate urine were performed as follows: The animals were placed in metabolism cages several days before the test was performed so that they could adapt to their surroundings. On the day of the test, the rats were deprived of food and water for a 12-hour-period, at the end of which time, the animals' bladders were emptied and the urine discarded. Urine was collected over a further 12-hour-period, during which time the animals were deprived of food and water. The amount of urine was measured and osmolality determined on either 2 or 0.2 ml

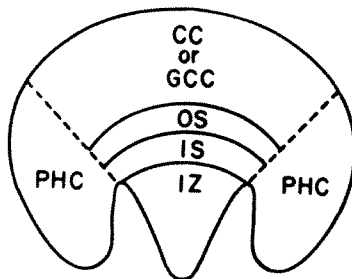
samples, using a model 31 LAS Advanced osmometer (Advanced Instruments Inc).

Anatomy of the Medulla

In this, and subsequent articles the nomenclature adopted by Peter¹⁷ is used (Text-figure 1). The cortex is defined as that part of the kidney containing glomeruli. Besides glomeruli, it contains the pars convoluta of the proximal tubular segment, thick ascending limbs, distal convoluted tubules, radicles of collecting ducts as well as arteries, veins and capillaries. Deep to this is the outer zone of the medulla, which is divided into an outer stripe and an inner stripe. The outer stripe is made up, for the main part of the pars recta of the proximal tubular segment, together with thick ascending limbs and collecting ducts. The inner stripe contains mainly thick ascending limbs and collecting ducts. The thin part of the descending limb begins at the junction between the outer and inner stripes. Deep to the inner stripe of the outer zone is the inner zone of the medulla, or papilla. This contains collecting ducts of varying orders which eventually give rise to the ducts of Bellini which open on to the tip of the papilla. The inner zone also contains the thin limbs of the loop of Henle and the interstitial cells. The thin ascending limb gives way to the thick ascending limb at the junction of the inner zone and inner stripe of the outer zone. The limbs of Henle are of variable length, some descending to the tip of the papilla, others not penetrating as far as the inner zone. More will be said of this in the discussion section.

The blood supply to the medulla has been well described by Moffat,¹⁸ Moffat and Fourman,¹⁹ and by Kriz and Lever.²⁰ It is derived from the efferent vessels of the juxtamedullary glomeruli which break up into a series of vasa recta which pass down to the papilla in the form of vascular bundles. This "arterial side" of the vasa recta breaks out from the vascular bundle at various points to form capillary plexuses. The "venous side" of the vasa recta originates in the various capillary plexuses and at intervals gains admission to the vascular bundles. These "venous" vasa recta ascend in the bundle and end by draining into either the arcuate or interlobular veins.

For the purpose of ease of description we have divided the cortex into two main areas, using a coronal section as the basis for this (Text-figure 1). That part of the cortex in a direct line with the papilla has been designated the central or greater curvature cortex. That part which lies to either side of the papilla (this would constitute the medial part of the anterior and posterior surfaces of the kidney) we have called the perihilar cortex.



TEXT-FIG 1—Coronal view of rat kidney to illustrate areas referred to in text. CC = central cortex. GCC = greater curve cortex. OS = outer stripe. IS = inner stripe. IZ = inner zone or papilla. PHC = perihilar cortex.

Results

Original Observations

With light microscopy there were no striking changes during the first 6 hours with the possible exception of an increased prominence of the vascular bundles in the inner stripe of the outer zone of the medulla. The bundles showed an increased eosinophilia and this change was more pronounced at 12 hours. At this time the vasa recta of the inner stripe contained many red blood cells. There was difficulty in accurately identifying the various components in the inner stripe, but certain structures contained eosinophilic coagula and it is probable that these were thin descending limbs. In the papilla at 12 hours there was an apparent mild dilatation of collecting ducts.

At 24 hours, definite changes were present in the papilla. The cytoplasm of collecting ducts contained rounded eosinophilic droplets which varied in size, some of them being larger than red blood cells, and others smaller (Figure 1). Some of these droplets had been extruded into the lumen but the lumina contained no casts or coagula. The droplets were strongly PAS-positive and stained red with the Martius scarlet method. The collecting ducts in the middle and distal parts of the papilla were maximally affected except for the ducts of Bellini which still demonstrated their usual pale uninteresting appearance. Similar droplets were seen in the epithelium covering the papilla, and particularly at the papillary tip, the epithelium was often lost. The thin limbs were the structures with the greatest changes and the lumina of these contained homogeneous eosinophilic material (Fig 2). The staining intensity of the luminal contents varied; in some instances it was strongly eosinophilic whereas in others it was very pale. The paler staining pattern predominated in the more distal part of the papilla. Some of the limbs—particularly nearer the papillary tip—had already lost their nuclei so that the limb was often represented by an eosinophilic mass. Red cells were usually present in vasa recta and capillaries, and polymorphonuclear leukocytes could be seen in the more distal capillaries. Homogeneous coagula were present in some of the vasa recta and capillaries and in an occasional animal some more granular appearing eosinophilic material was present. Interstitial cells revealed no remarkable changes with the stains employed. In the inner stripe of the outer zone eosinophilic casts were seen in thick ascending limbs. Similar casts could be found in a scattered way in the cortex.

At 2 days the papilla showed similar, although more advanced, changes. The collecting ducts were more severely affected by the drop-

let change and droplets could be seen in tubules opening on to the papillary tip. Mitotic figures were conspicuous in collecting ducts of certain rats. The limbs of Henle were now almost structureless and could be recognized—where they were cut transversely—only as rounded eosinophilic areas with no nuclei (Fig. 3). The vasa recta and capillaries were not conspicuous and an impression was gained that there had been a decrease in numbers. At this stage it was often difficult to differentiate between limbs and capillaries. The covering epithelium of the papilla had disappeared in places whereas in others it contained the droplets seen at 24 hours.

Over the next two days the picture of papillary necrosis became evident. In some animals necrosis was confined to the tip, but in others it was more extensive. From 7 days onwards, the whole of the papilla showed necrosis of all the constituent parts (Figure 4) with a definite line between dead and living tissue being apparent. This line in general corresponded to the junction between the papilla (inner zone) and the inner stripe of the outer zone. Elongated cells resembling fibroblasts, and polymorphonuclear leukocytes were present at the line of demarcation; in some animals there were large numbers of polymorphonuclear leukocytes in the dead or dying papilla. The dead papilla had no covering epithelium and the tubules in the papilla were recognizable only as empty shells. It is of interest that apparently intact collecting ducts persisted in certain animals, in an otherwise dead papilla. The outer zone of the medulla and the cortex showed a certain degree of dilatation of tubules of all types in certain animals, but in others there was no such change. The papilla at this stage was grossly white and opaque.

From this time on changes took place that led to separation of the papilla. The zone of polymorphonuclear leukocytes became less conspicuous but increased fibroblastic activity produced a denser type of tissue at the junction of dead and healthy tissue. The time at which the papilla separated was variable; in some animals this was achieved by 14 days but in others not until 21 days. Following separation there was a rapid ingrowth of epithelium to cover the raw stump (Figure 5), this epithelium on occasion being several layers thick. Collecting ducts at a later stage were seen discharging at this new surface. Considerable amounts of dense fibrous tissue developed in the stump, being much in evidence as early as 28 days after administration of BEA. It was invariably denser in the more central parts of the stump, the density increasing with time and being fully developed by 2 months.

There were certain points of interest in the behavior of the papilla up to the time of separation. In some animals between 2 and 21 days

there was persistence of epithelium on the surface of the dead papilla. This occurred in a patchy way and sometimes there were several underlying intact tubules. In certain animals there was a partial papillary necrosis and when this occurred it was usually in the central part, with intact tubules proximal, distal and lateral to it (Figure 6). One animal seen at 9 days had a remarkable heminecrosis of the papilla with a zone of polymorphonuclear leukocytes running down the middle of the papilla at the junction of necrotic and nonnecrotic tissue. When papillary necrosis occurred it was invariably bilateral and no example of a unilateral necrosis was seen.

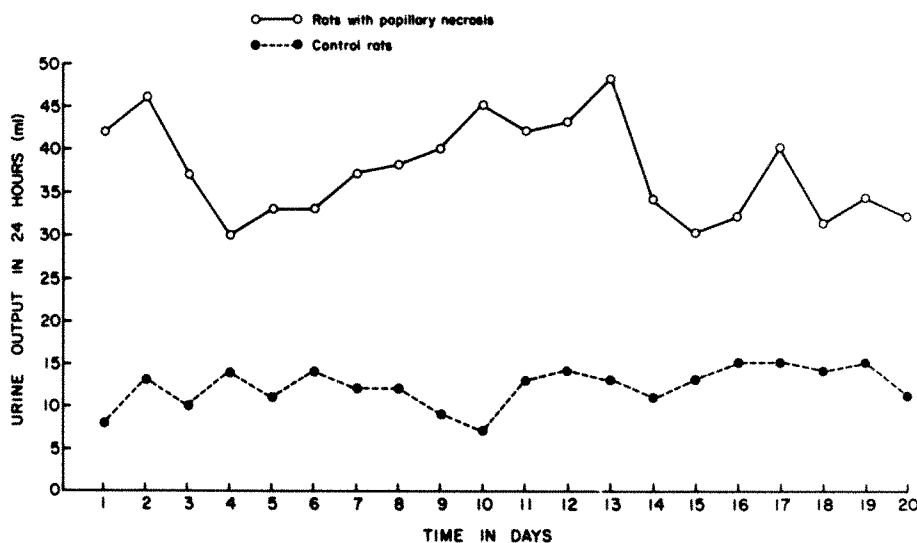
In animals killed at later periods, say after 2 months, it was frequent to find a yellow papilla lying free in the pelvis of the kidney. This papilla was frequently extensively calcified.

Changes in the cortex followed those in the papilla. As early as 12 hours there was in certain animals a mild dilatation of the collecting ducts, but it was never extreme. Eosinophilic coagula were often present in the ascending limbs and this change was noted as early as 24 hours after administration of BEA. Other changes present at this time were mild vacuolization and hyaline droplets in proximal segments, which very occasionally showed overt necrosis. These changes were usually worse in the deeper parts of the cortex. Mitotic figures in proximal segments were sometimes seen at 2 to 3 days, the significance not being fully understood. By 7 days there was a mild dilatation of other segments of the tubules and the pars recta of the proximal segment was particularly affected. By 9 days a basophilic tint was present in the proximal convoluted tubules. This was a focal change and occurred in particular in those nephrons whose glomeruli were situated in the deep part of the central cortex. The change was less conspicuous in those nephrons arising from the superficial part of the central cortex and in those in the perihilar cortex. At this time there was dilatation, again of a focal type, in all segments of the nephron, including the pars convoluta of the proximal segment. The basophilic change in the proximal convoluted tubule gradually progressed into atrophy and eventual disappearance in certain instances. Atrophy was clearly apparent by 28 days. The atrophic changes occurred predominantly in the deeper nephrons of the central part of the cortex (Figure 7) but similar atrophic changes, although less widespread, occurred in the more superficial nephrons. By 56 days enclaves of intact nephrons could be seen in this superficial part interspersed among atrophic areas. The perihilar cortex varied in its behavior. In some animals there was a virtual sparing of this area (Figure 8), but in others there was extensive patchy atrophy and

loss. The sparing of the perihilar cortex was often apparent even on gross inspection, the anterior and posterior surfaces at 2 months being smooth with depressed scarring over the greater curvature.

By 28 days pale blue casts could be found within tubules. These were sometimes large and blocked the lumen; they were PAS positive. As time went by, some of these pale blue structures became very large and did not always appear to be confined to tubules. In animals of 3 months, or greater duration, cysts were often seen in the cortex, protruding out from the subcapsular surface. These cysts were lined by cubical epithelium; it is not apparent which segment of the tubule was involved in cyst formation. The kidneys at this time were often grossly and uniformly scarred with large numbers of cysts being present.

By 90 days, scattered glomeruli—which hitherto had not been affected, apart from thickening of Bowman's capsule—showed areas of eosinophilia such as are seen in hypertension. This change was often extreme in animals of over 6 months' duration. In an occasional animal necrotizing arterial changes were found in both kidney and mesentery. These were almost certainly brought about by hypertension and blood pressure recordings in rats with a 6 month interval following BEA administration were frequently elevated. These pressures were measured after cannulation of the femoral artery immediately prior to death. There was almost invariably an elevation of serum urea nitrogen to levels of over 60 mg/100 ml in these old hypertensive animals.



TEXT-FIG 2—Comparison of 24-hour urine output in animals receiving BEA to produce papillary necrosis and in control group. Means of 10 rats in each group.

Urine output. The 24 hour urine output of 10 control rats on unrestricted food and water is shown in Text-fig. 2. There were slight fluctuations from day to day from animal to animal and some animals produced more urine than others. Only very occasionally did a rat in this group produce more than 20 ml in 24 hours. By contrast the same figure shows the 24 hour urine output for a comparable number of rats with papillary necrosis. The output was considerably greater although there was a wide range of output from animal to animal. Some animals produced over 60 ml of urine over a 24 hour period. The osmolality of the urine was invariably low when this was tested 48 hours following administration of BEA. It is of great interest that the urine output was considerably elevated during the first 12 hours of collection following the administration of BEA, and the output during the first 24 hours was comparable to the daily output which occurred over the ensuing several weeks. It is also of interest that we could detect no significant fluctuation in urinary output during the period over which sequestration of the papilla was taking place.

No detailed study of the amount of protein in the urine was made but there was a 2 to 4 plus recording in most animals with papillary necrosis.

Tests for concentration. Table 1 compares the concentrating ability of rats with papillary necrosis—using the regimen described in an earlier section—with a group of control rats. All rats with papillary necrosis had received BEA at least 21 days beforehand so that it is a reasonable assumption that sequestration of the papilla had occurred. There is a pronounced difference between the two groups, and in general the animals with papillary necrosis were unable to concentrate above 1000 milliosmoles per kg water. The table also demonstrates the significant

Table 1—Animals Deprived of Food and Water for 12 Hours; Bladder Emptied and Urine Discarded.
Urine collected over next 12 hour period during which time animals are deprived of food and water.

	Number	Mean Urine Volume with SD (ml)	Mean Osmolality of Urine with SD (mOsm/kg water)
Rats with papillary necrosis	21	8.6 (2.8)	781 (146)
Control rats	19	2.3 (0.7)	1908 (397)

Difference between two groups for means of urine volume and osmolality statistically significant ($P \gg .001$).

difference in urine output between the two groups on the fluid and food restricted regimen.

Nitrogen retention. The level of serum urea nitrogen (SUN) was determined at different stages in the evolution of the papillary necrosis. The level rose to a mean of 51.7 mg/100 ml (SD 21.5) after 2 months, from a pretreatment level of 19.8 mg/100 ml (SD 2.97). The level attained was proportional to the amount of damage in the kidney as a whole. Very high levels of over 100 mg/100 ml were found in several animals allowed to survive for over 6 months. These animals had often developed hypertension by this time.

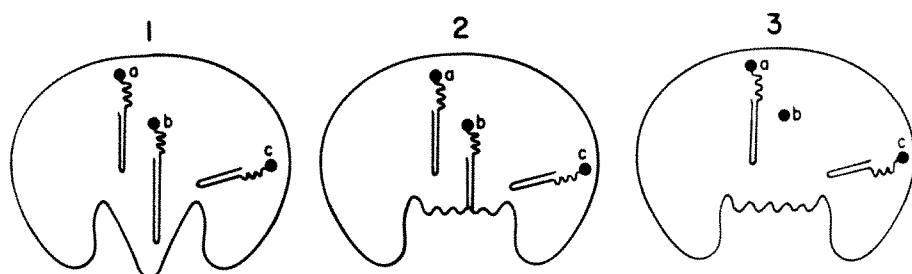
Discussion

The early changes, as revealed by light microscopy, are found in the thin limbs of Henle in the renal papilla. By 48 hours there is considerable dissolution of these structures. Changes in the collecting ducts are well developed at 24 hours, rounded eosinophilic "droplets" appearing in the cytoplasm at that time. Over the ensuing few days, overt necrosis of the entire papilla takes place, with a zone of polymorphonuclear leukocytes developing at the junction of dead and healthy tissue. With conventional light microscopy we have not been able to demonstrate with any regularity in the early stages an organic blockage of the vasa recta, and a similar absence of changes using the same model was described by Fuwa and Waugh.¹⁴ Electron microscopic studies are being performed to study the early phases. We are faced with several possible mechanisms to account for the death of the papilla; of these two seem most likely. In the first instance there could be a direct poisoning of the tubules by the bromoethylamine. In the second, bromoethylamine might interfere with the blood supply to the papilla in such a way that necrosis ensues. Studies were performed to determine which of these two alternatives was the more likely, and a detailed account and discussion of these are given in a later paper.

One of the features of papillary necrosis in man is the way in which the cortex may also show changes. So common are these that it was once considered that a chronic interstitial nephritis was the fundamental lesion in analgesic abuse.²¹ It is now felt that cortical changes occur secondarily to papillary necrosis. The current experiments show that the cortex becomes involved in virtually every animal with experimental papillary necrosis, and this takes place only after the papillary necrosis is established. The changes are in some way related to the obstruction of nephrons in a manner akin to those seen in the cortex following obstruction to the urinary tract. It is unlikely that the obstruc-

tion is in the collecting ducts; the reasons for believing this are as follows. First, if cortical changes were brought about by obstruction to the collecting ducts passing through the necrotic papilla, it would be anticipated that they would be diffuse, as all nephrons have a final common pathway through the ducts of Bellini that discharge on to the papillary tip. As described earlier, the changes are not diffuse. Second, the tremendous output of urine from the first day onwards would argue against any significant obstruction to the collecting ducts. Presumably in the early stages, before sloughing of the papilla takes place, urine can pass freely down dead conduits: in the later stages, after the papilla has become detached, urine is discharged into the renal pelvis from collecting ducts which end at the proximal papillary stump. We believe it is much more likely that the cortical changes are brought about by obstruction occurring in the thin limbs. In the first place there is good histologic evidence that the limbs become necrotic within the first few days of obstruction and after this time they may be impossible to identify. In the second place it is noticed that the nephrons showing maximal changes are those arising from glomeruli in the deeper part of the central cortex. In contrast less severe involvement is found in those nephrons arising from glomeruli in the superficial part of the cortex over the greater curvature, and even less severe involvement may be found in the perihilar cortex. In some rats with profound changes in the central cortex, the perihilar cortex may be virtually normal. From the work of Munkácsi and Palkovits,²² and of Wahl and Schnermann.²³ It is appreciated that the superficial glomeruli have loops which do not as a rule descend into the papilla. In contrast the deeper glomeruli have long thin limbs which descend into the papilla.²² Interference with the continuity of the long thin limbs which reach the papilla would produce changes in the tubules arising from the deeper glomeruli, whereas the tubules arising from the superficial areas would be relatively spared. This, in fact, was the finding in the experiment, although the degree of damage to tubules arising from superficial glomeruli was greater than anticipated. It should be noted that Lechène *et al.*²⁴ described that 19.8% of the superficial glomeruli had long loops of Henle. This would fit our data much better. There is insufficient information in the literature on the length of thin limbs of nephrons in the perihilar cortex, but because of the fewer changes in this area we would predict that the majority are short and do not descend into the papilla. The proposed sequence is shown in Text-fig. 3.

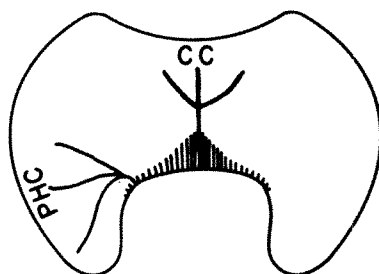
The less severe involvement of the perihilar cortex could alternatively be explained by obstruction to collecting ducts in the following way.



TEXT-FIG 3—Explanation of involvement of deeper glomeruli in central cortex. a, b, and c = those in perihilar cortex. 1, 2 and 3 are different stages in time.
limbs. a = those in outer part of central cortex, b = those in deeper part of central cortex, and c = those in perihilar cortex. 1, 2 and 3 are different stages in time.

If we accept for the moment that the cortical changes are secondary to blockage of collecting ducts (we have explained why we are reluctant to do this) then there must be some less severe involvement of the collecting ducts draining the perihilar cortex. It is conceivable that this could happen if a greater degree of fibrosis were produced in the central part of the remaining papillary stump compared with the more peripheral part where the collecting ducts from the perihilar cortex discharge their contents in the newly created situation. Fibrosis in the central part of the stump does indeed appear denser than that at the periphery in most animals (Text-fig. 4). However, the objections to this idea are, first, the way in which the superficial nephrons from the greater curvature or central cortex are frequently spared; these drain through the more fibrous part. Second, atrophy of proximal convoluted tubules begins to occur at a time before which there is any great degree of fibrosis in the stump.

It is of considerable interest to consider the distribution of cortical changes in man. As in the rat there is maximal damage in that part of the cortex directly overlying the damaged papilla. In contrast the col-



TEXT-FIG 4—Alternative explanation for greater involvement of central cortex. Collecting ducts from perihilar cortex (PHC) traverse less fibrotic area than those from central cortex (CC).

umns of Bertin are frequently spared, the columns of Bertin being the analogue in the multipapillary kidney of the perihilar cortex in the unipapillary kidney. This sparing of the columns of Bertin has been commented on by both Kincaid-Smith²⁵ and by Burry.¹⁰ They regard the cortical changes as resulting from obstruction by the necrotic papilla. Kincaid-Smith²⁵ points out the lateral disposition in the papilla of the collecting ducts from the columns of Bertin, and goes on to explain the sparing of the columns by a reestablishment of connection of their collecting ducts with the newly formed calyceal cavity following papillary necrosis. We have had insufficient experience of analgesic papillary necrosis in man to enable us to comment on this. A very large number of cases studied at different stages would be required to substantiate this thesis, but by analogy with the experimental model we would consider obstruction to thin limbs a more plausible concept. It is apparent that the main reason for differing explanations is the lack of information available on the distribution in the different part of the cortex of nephrons with thin limbs which descend into the papilla compared with those with short limbs.

The functional data are of interest in several respects. In the first instance the tremendously increased urine output occurs within a short time after administration of BEA, indicating that some defect in the concentrating mechanism has occurred very early and at a time before there are any anatomical changes detectable by light microscopy. Further evidence that a concentrating defect occurs within a few hours after administration of BEA will be presented in a later paper. The high output of urine continues over the next few days and, as commented earlier, the urine must be transmitted along dead collecting ducts until such time as sequestration occurs. From this time onward urine is discharged from shortened collecting ducts which open on to the reepithelialized stump of the papilla. In view of the fact that the papilla has by this time disappeared, it is probable that all the urine is being produced by nephrons which have short thin limbs, *ie*—those that do not descend into the papilla and which have therefore not had their continuity interrupted. This idea could be countered by supposing that thin limbs might discharge directly on to the surface of the papillary stump. We have seen no morphologic evidence for this and it seems unlikely that the delicate thin limbs could traverse the dense fibrous tissue present in the stump.

The defect in concentration is predictable because the structures necessary to effect the counter current mechanism have been eliminated; at the time the tests were performed the animals were without

their papillae. No concentration tests were performed in the early stages of papillary necrosis, but casual determinations of urine osmolality 48 hours following administration of BEA showed extremely low values. At this time the limbs of Henle were necrotic and the collecting ducts showed an accumulation of PAS-positive droplets. There is therefore at this time, and at 24 hours, morphologic evidence by light microscopy of damage to the structures concerned with the concentration mechanism.

References

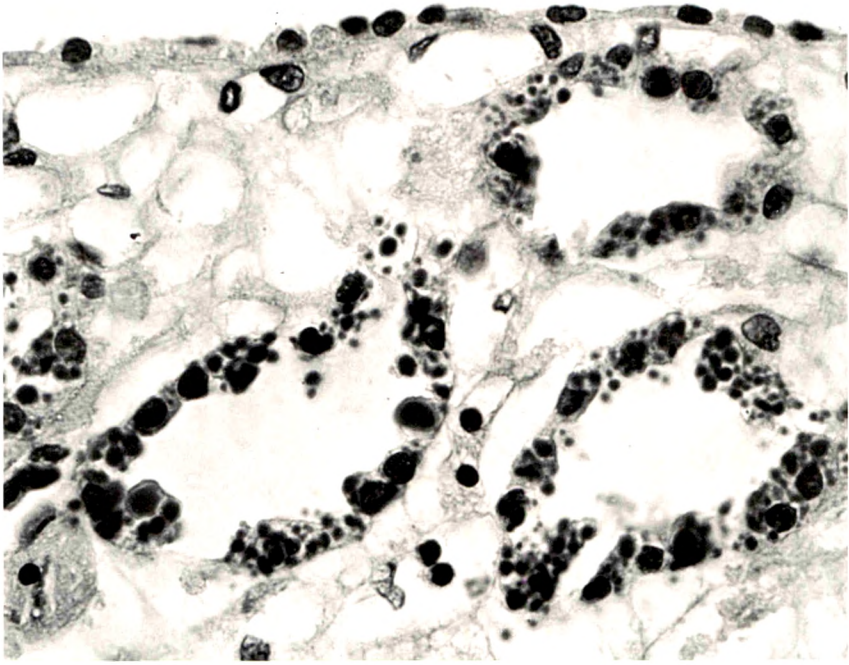
1. Edmondson HA, Martin HE and Evans N: Necrosis of renal papillae and acute pyelonephritis in diabetes mellitus. *Arch Intern Med* 79:148-175, 1947
2. Robbins SL, Mallory GK and Kinney TD: Necrotizing renal papillitis: A form of acute pyelonephritis. *N Eng J Med* 235:885-893, 1946
3. Spühler O, and Zollinger HU: Die chronisch-interstitielle Nephritis. *Z Klin Med* 151:1-50, 1953
4. Zollinger HU: Chronische interstitielle Nephritis bei Abusus von phenacetin-haltigen Analgetica (Saridon usw). *Schweiz Med Wochenschr* 85:746, 1955
5. Lindeneg O, Fischer S, Pedersen J, and Nissen NI: Necrosis of the renal papillae and prolonged abuse of phenacetin. *Acta Med Scand* 165:321-328, 1959
6. Gloor F: Über verschiedene Formen der Papillennekrosen der Nieren. *Pathol Microbiol (Basel)* 23:263-272, 1960
7. Hultengren N: Renal papillary necrosis: A clinical study of 103 cases. *Acta Chir Scand [Suppl]* 277:1-84, 1961
8. Bengtsson U: A comparative study of chronic non-obstructive pyelonephritis and renal papillary necrosis. *Acta Med Scand [Suppl]* 388:1-71, 1962
9. Harvald B: Renal papillary necrosis: a clinical survey of sixty-six cases. *Am J Med* 35:481-486, 1963.
10. Burry AF: The evolution of analgesic nephropathy. *Nephron* 5:185-201,
11. Jacobs LA and Morris JG: Renal papillary necrosis and the abuse of phenacetin. *Med J Aust* 2:531-538, 1962
12. Burry AF, de Jersey P and Weedon D: Phenacetin and renal papillary necrosis: results of a prospective autopsy investigation. *Med J Aust* 1:873-879, 1966
13. Oka A: Zur histologie der vinylaminnephritis. *Virchow Arch [Pathol Anat]* 214:149-160, 1913
14. Fuwa M and Waugh D: Experimental renal papillary necrosis. Effects of diuresis and antidiuresis. *Arch Pathol* 85:404-409, 1968
15. Chuchani G: Directing and activating effects. *The Chemistry of the Amino Group*. Edited by S Patai. Rexdale, Ontario, John Wiley and Sons Canada Ltd, Interscience Publishers, 1968 p 205
16. Salomon G: Kinetics of ring formation and polymerisation in solution. *Trans Farad Soc* 32:153-178, 1936
17. Peter K: Untersuchungen über Bau und Entwicklung der Niere. Jena, Gustav Fischer, 1927

18. Moffat DB: The fine structure of the blood vessels of the renal medulla with particular reference to the control of the medullary circulation. *J Ultrastruct Res* 19:532-545, 1967
19. Moffat DB and Fourman J: The vascular pattern of the rat kidney. *J Anat* 97:543-553, 1963
20. Kriz W and Lever AF: Renal countercurrent mechanisms: structure and function. *Am Heart J* 78:101-118, 1969
21. Zollinger HU and Spühler O: Die nicht-eitrige, chronische interstitielle Nephritis. *Schweiz Z Allg Pathol* 13:807-811, 1950
22. Munkácsi I and Palkovits M: Study on the renal pyramid, loops of Henle and percentage distribution of their thin segments in mammals living in desert, semi-desert and water-rich environment. *Acta Biol Acad Sci Hung* 17:89-104, 1966
23. Wahl M and Schnermann J: Microdissection study of the length of different tubular segments of rat superficial nephrons. *Z Anat Entwicklungsgesch* 129:128-134, 1969
24. Lechène C, Corby C and Morel F: Distribution des néphrons accessibles à la surface du rein en fonction de la longueur de leur anse de Henle chez le rat, le hamster, le mérion et le psammomys. *C R Acad Sci [D] (Paris)* 262:1126-1129, 1966
25. Kincaid-Smith P: Pathogenesis of the renal lesion associated with the abuse of analgesics. *Lancet* 1:859-862, 1967

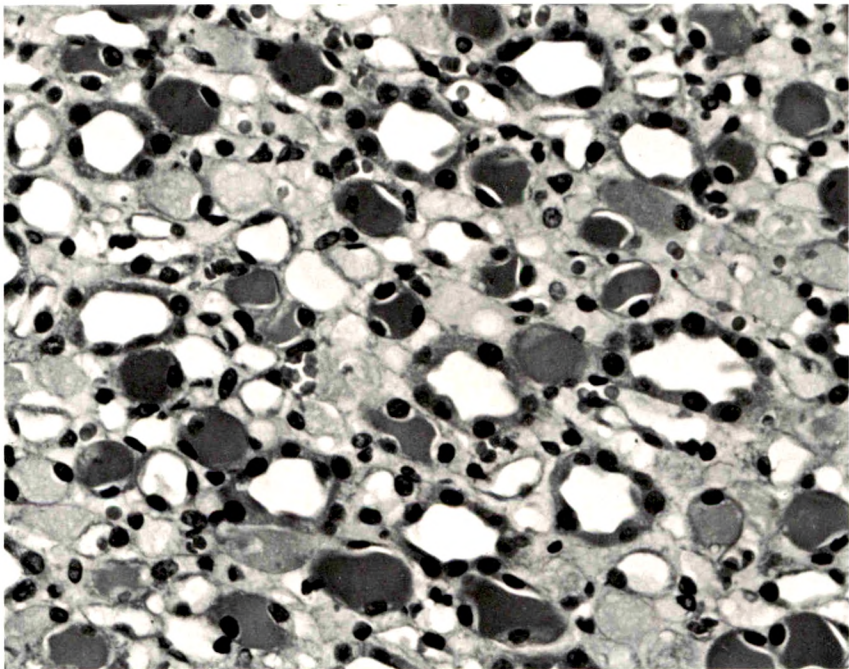
Acknowledgment

Dr. Murray is a Kellogg Fellow; his present address is Casilla 6539, Correo 4, Santiago, Chile.

[*Illustrations follow*]



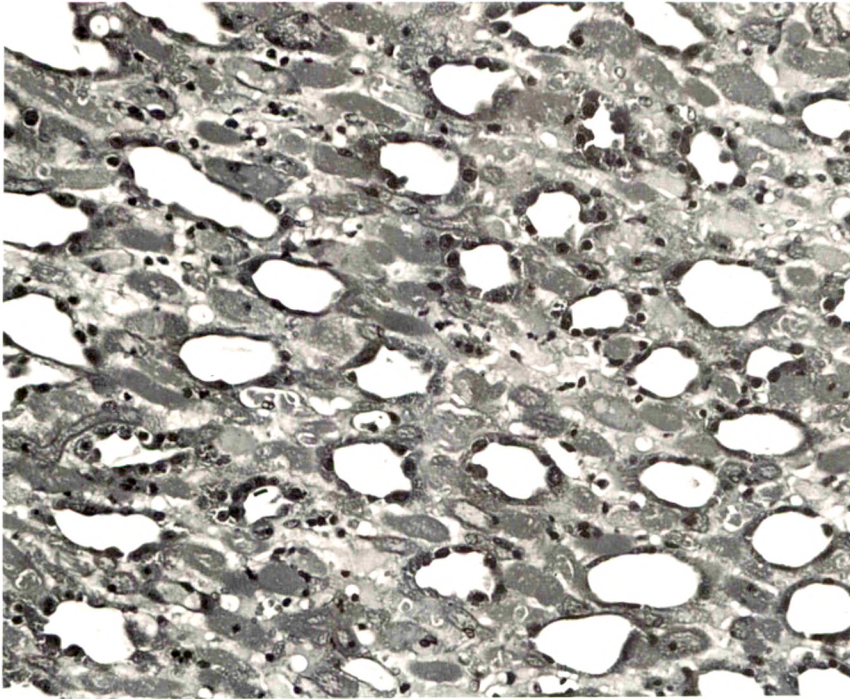
1



2

Fig 1—Section through papilla in proximal part of distal one-third. Collecting tubules contain granules of varying size (Martius scarlet, $\times 750$).
Fig 2—Section through midportion of papilla at 24 hours. Casts are seen in limbs of Henle. No appreciable change in collecting tubules at this level (H&E, $\times 400$).

3



4

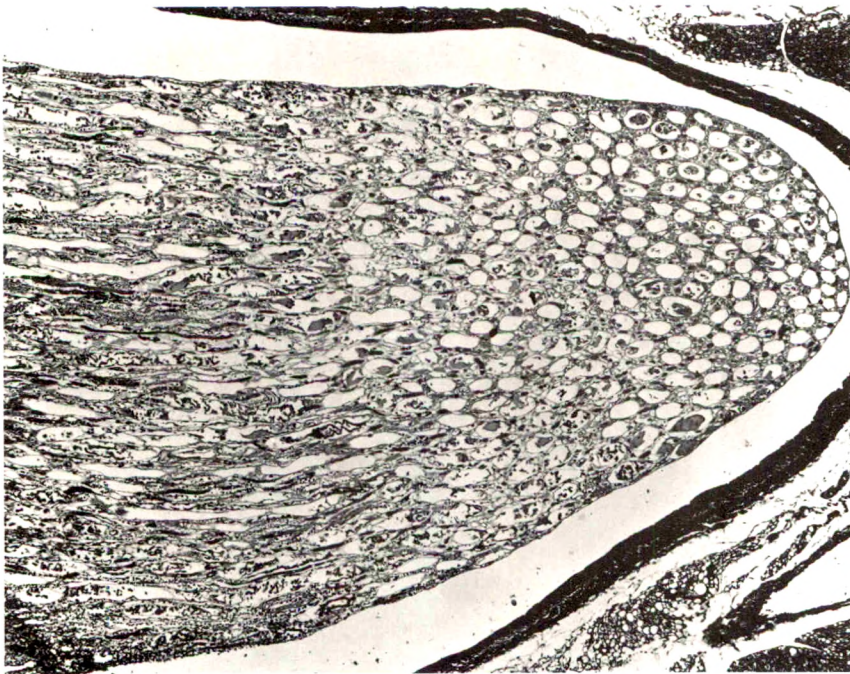
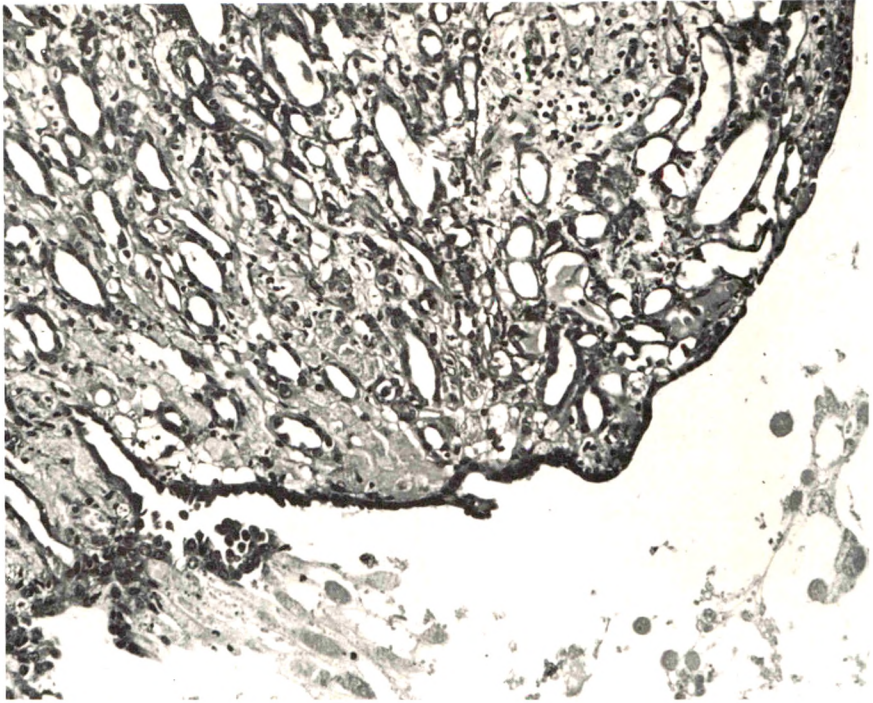
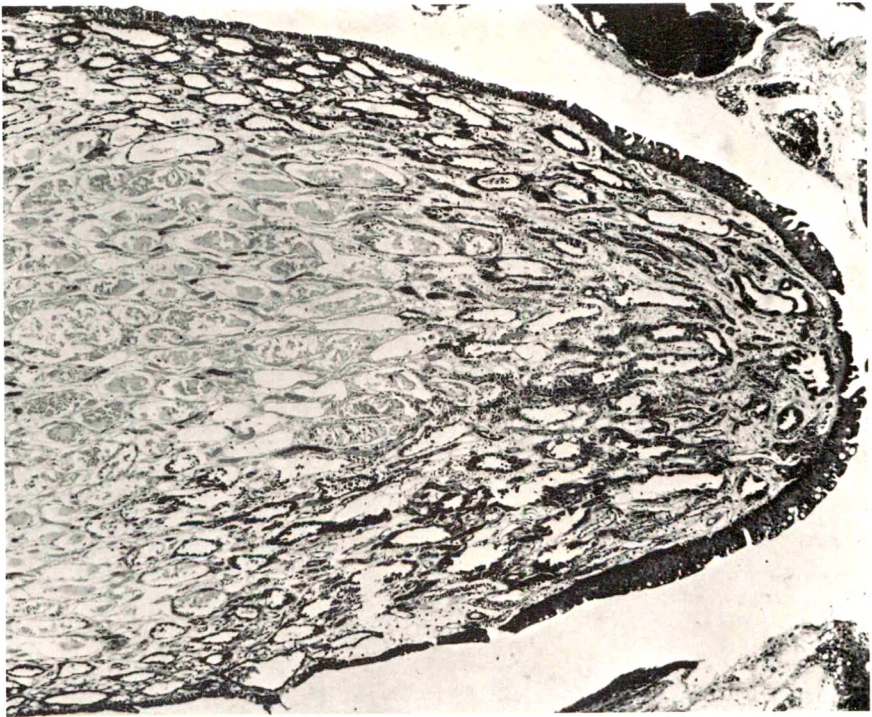


Fig 3—Section through midportion of papilla at 48 hours. Complete necrosis of limbs of Henle. Collecting tubules of this size, which are smaller than in Fig 1 contain barely discernible fine granules (H&E, $\times 200$).

Fig 4—Necrotic papilla at 7 days. The covering epithelium is lost and, in the distal part, empty shells of tubules can be seen. Necrosis is most apparent in the more proximal part. The zone of polymorphs at the junction of live and dead tissue can be partially seen in the bottom left corner (H&E, $\times 40$).



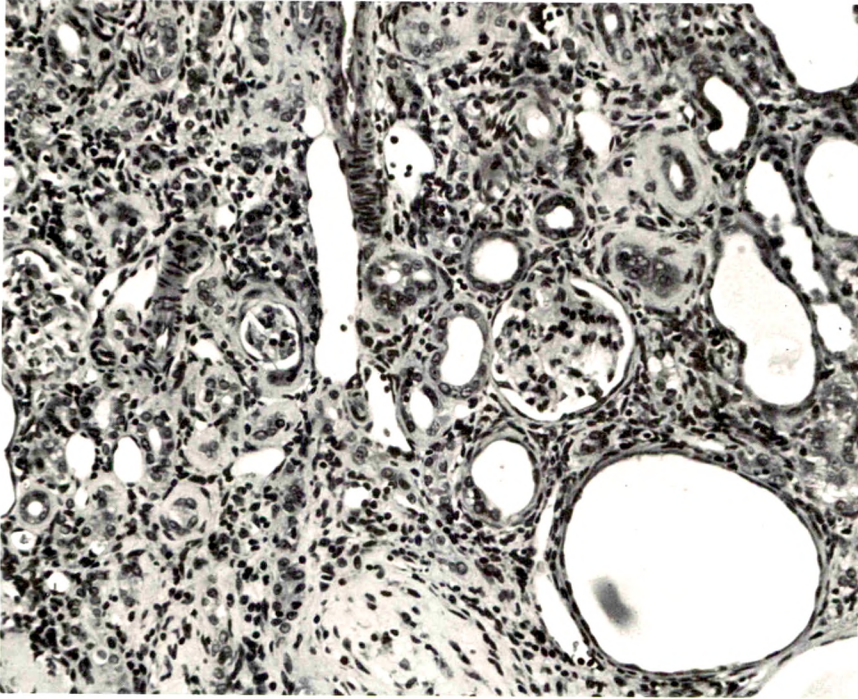
5



6

Fig 5—Stump of papilla at 56 days to show how the raw surface has been covered by epithelium. Some areas of dense interstitial tissue can be seen and there is mild tubular dilatation. The remains of the distal part of the papilla can still be seen, one small fragment being adherent to the stump (H&E, $\times 175$).
 Fig 6—Papilla at 18 days to show how occasionally the necrosis is confined to the central part, sparing the tip and peripheral part (H&E, $\times 50$).

7



8

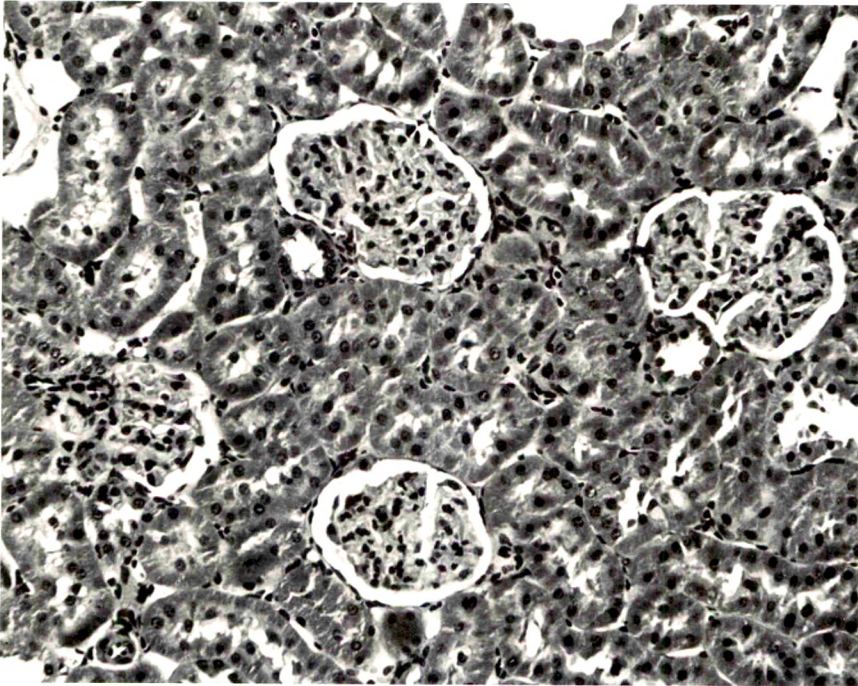


Fig 7—Section through deep part of central cortex at 2 months. There is considerable tubular loss and atrophy. Some tubules are much dilated (H&E, $\times 200$).
 Fig 8—Section through perihilar cortex at 2 months. Glomeruli and tubules are preserved (H&E, $\times 200$).

Cytochemical Localization of Peroxidase Activity in the Developing Erythrocyte

Ann M. Dvorak, MD, Harold F. Dvorak, MD and
Morris J. Karnovsky, MD

Peroxidase activity, demonstrated with diaminobenzidine as the electron donor according to the method of Graham and Karnovsky, was used as a cytochemical marker in a study of developing erythrocytes in guinea pig and rabbit bone marrow. Peroxidase activity was deposited diffusely in the cytoplasm and nuclear matrix of developing cells and was thought to represent hemoglobin, which others have shown by independent criteria to have a similar distribution. Diffuse localization was first observed in erythroblasts and at all subsequent stages of development. Another finding was the significant particulate localization of peroxidase activity apparently associated with cytoplasmic ribosomes and nuclear particles of immature erythrocytes. This activity differentiated the most primitive erythroid precursors from hemocytoblasts of other marrow cell lines, a distinction impossible by strictly morphologic criteria. Particulate peroxidase localization was identified in erythroid hemocytoblasts, erythroblasts, normoblasts and reticulocytes but not in mature erythrocytes. The nature of the particle-associated peroxidase activity was not determined with certainty. However, it could not be differentiated from the diffuse activity, thought to reflect hemoglobin, by several inhibitors and could not be attributed to erythrocyte catalase. The possibility is therefore raised that this activity represents hemoglobin, newly assembled either on or immediately adjacent to nuclear particles and cytoplasmic ribosomes (Am J Pathol 67:303-326, 1972).

A VARIETY OF ENDOGENOUS PEROXIDASE ACTIVITIES exists in plant and animal tissues and may be detected by both biochemical and histochemical methods.¹

Several of the enzymes responsible for this activity have been well characterized and all have been found to be heme proteins. These include the peroxidases of milk, white blood cells, thyroid microsomes and the horseradish plant.²

Mature erythrocytes of many species exhibit peroxidase activity. This activity has generally been attributed to the presence of the heme protein, hemoglobin, which catalyzes the oxidation of a variety of

From the Departments of Pathology, Harvard Medical School and the Massachusetts General Hospital, Boston, Mass.

Supported by National Institutes of Health Training Grant GM-01235, Research Grant HE-09125, and by US Public Health Service Grant AI-09529.

Dr. A. M. Dvorak was a Post Doctoral Trainee, NIH, US Public Health Service, and Dr. H. F. Dvorak is Career Development Awardee 1-K04-AI-46352, US Public Health Service.

Accepted for publication Nov 1, 1971

Address for reprint requests: Dr. Ann M. Dvorak, Department of Pathology, Tufts University School of Medicine, 136 Harrison Avenue, Boston, Massachusetts 02111.

substrates by hydrogen peroxide and which is often referred to as a "pseudoperoxidase."¹ Red blood cells also contain a catalase which might contribute activity under certain circumstances. The peroxidase activity of erythrocytes is stable during fixation and tissue processing, can produce an insoluble reaction product which is readily visualized in the electron microscope and might, therefore, be expected to afford a useful cytochemical marker in developing cells.

We have used peroxidase activity, as demonstrated with diaminobenzidine as the electron donor, to study the development of erythrocytes in guinea pig and rabbit bone marrow. We have been able to identify red blood cell precursors at earlier stages of differentiation than has been possible by morphologic criteria alone. An unexpected finding was the presence of significant peroxidase activity associated with ribosomes and nuclear particles of immature erythrocytes, an observation which may have relevance to biochemical theories of hemoglobin synthesis.

Materials and Methods

Observations were made on 14 normal adult English short hair guinea pigs and 2 adult New Zealand rabbits whose bone marrow had been stimulated by treatment with phenylhydrazine.³ Animals were sacrificed and small blocks of femoral bone marrow were immediately fixed by immersion for 2 hours at room temperature in a mixture⁴ containing 1% paraformaldehyde, 1.25% glutaraldehyde and 1.5×10^{-3} M CaCl_2 in 0.1M sodium cacodylate buffer, pH 7.4. Tissues were then washed overnight in 0.1M sodium cacodylate buffer, pH 7.4.

Normal Morphology

Tissue was postfixed in 1.5% collidine-buffered osmium tetroxide for 2 hours at 4°C before being dehydrated in a graded series of alcohols and embedded in Epon 812. For purely morphologic observation, sections were stained lightly with lead citrate.⁵ However, for comparison with tissues reacted for peroxidase activity, sections were routinely examined unstained, and only photographs of unstained sections are illustrated in this paper.

Cytochemistry

After the overnight wash in 0.1M sodium cacodylate buffer, 40 μ sections were cut with a Smith-Farquhar tissue chopper and incubated for 1 hour at room temperature in Graham and Karnovsky's medium⁶ containing 5 mg of 3-3' diaminobenzidine tetrachloride (DAB-Sigma Chemical Co, St Louis, Mo) and 0.01% hydrogen peroxide in 10 ml of 0.05M Tris-HCl buffer at pH 7.6 or pH 6.0. Sections were also incubated according to the method of Novikoff and Goldfischer.⁷ A variety of controls was employed. In some instances either DAB or H_2O_2 was omitted from the reaction mixture. To exclude nonspecific binding of reduced DAB to tissue components, the sections were incubated for 1 hour in 0.05M Tris-HCl buffer containing 5 mg of DAB, were washed three times in buffer and were then incubated for 15 minutes in 0.05M Tris-HCl buffer containing 10^{-3} M potassium ferricyanide.⁶ To exclude nonspecific binding of oxidized

DAB to tissue components, 5 mg of DAB in 0.05M Tris-HCl buffer was oxidized by reaction for 15 minutes with 10^{-3} M potassium ferricyanide. Bone marrow sections were then added to the mixture, incubated for 1 hour at room temperature and then washed three times in buffer.

Following appropriate incubation, the sections of bone marrow were washed overnight in 0.05M Tris-HCl buffer, pH 7.6, postfixed, dehydrated, and embedded as described above. Sections were cut with an LKB II ultratome and were studied in an RCA 3F or Philips 200 electron microscope. To avoid confusion of peroxidase reaction product with deposits of heavy metal stain, only unstained sections were examined.

Inhibitors. The inhibitory effects of several chemicals and heat on the cytochemical reaction were evaluated. Forty μ chopped sections were preincubated for 30 minutes at room temperature in 0.05M Tris-HCl buffer, pH 7.6 containing either 10^{-1} M or 10^{-2} M potassium cyanide, 10^{-1} M sodium azide, or 2×10^{-2} M 3-amino-1,2,4-triazole or were boiled for 10 minutes in buffer. After this treatment, sections were incubated for 1 hour in complete Graham and Karnovsky's medium supplemented with the same concentration of the appropriate inhibitor. After incubation, sections were processed as above and unstained sections were examined in the electron microscope.

Peroxidatic Activities of Hemoglobin and Hematin. The peroxidatic activities of hemoglobin (bovine, twice crystallized, Sigma Chemical Company, St Louis, Mo) and hematin were measured by following spectrophotometrically the change in absorbance due to the oxidation of O-dianisidine in the presence of H_2O_2 ^{8,9} and were compared to the values obtained using horseradish peroxidase (Type II, Sigma Chemical Co). According to the manufacturer, the preparation of the hemoglobin studied contained up to 75% by weight methemoglobin, the remainder being largely oxyhemoglobin. Bovine hemin (Mann Research Laboratories, NY, NY) was solubilized and quantitatively converted to hematin by dissolution in water with NaOH. The reaction mixture contained 0.003% H_2O_2 and 0.008% O-dianisidine in 0.01M phosphate buffer, pH 7.3. One-tenth milliliter aliquots of the various compounds tested were added to 3 ml of reaction mixture, and the change in absorbance at 460 m μ was measured at 15-second intervals at room temperature. Activity was expressed as the change in absorbancy per minute per micromole as measured in a Zeiss spectrophotometer.

Results

Normal Morphology of Developing Red Blood Cells

The fine structure of developing red blood cells has been described by several authors¹⁰⁻¹³ and our results agree with their findings. In brief, the most primitive marrow cell, the hemocytoblast, was a large cell with a large nucleus and prominent nucleoli. The pale interchromatinic substance (nuclear matrix) contained small particles many of which resembled ribosomes in size and shape. Some, however, were larger and more irregular than ribosomes. The cytoplasm contained many free ribosomes, often grouped as polysomes, varying numbers of mitochondria, and a Golgi area. Phenylhydrazine-treated rabbits had large numbers of hemocytoblasts, presumably of the erythroid series, in their marrow. Until differentiation took place (for example, granule

production in the myeloid series) one could not reliably determine the developmental potential of a given marrow hemocytoblast by morphologic criteria alone.

Differentiation in the erythroid series involved progressive reduction in nuclear and cytoplasmic size and condensation of nuclear chromatin into large dense angular masses. The nuclear interchromatinic space with its complement of particles also became markedly reduced in size. Prominent nuclear pores were seen, some of which were bridged by a thin septum.

The cytoplasm of the erythroblast contained numerous free ribosomes, often grouped as polysomes, a few mitochondria, and a small Golgi zone. Ferritin particles were adherent to the fuzzy surface coat at cup-shaped depressions of the cell membrane and were apparently taken into the cell as these membrane depressions invaginated to form vesicles. With further maturation, fewer ribosomes were visualized and the cytoplasm and nuclear matrix contained homogeneous, light staining material identified as hemoglobin.¹¹ The normoblast had a greatly condensed nucleus with little interchromatinic space. With nuclear extrusion, the normoblast became a reticulocyte, a cell retaining moderate numbers of ribosomes. Finally, the mature erythrocyte was a dense, anucleate cell, smaller than the reticulocyte, and lacking ribosomes.

Cytochemical Localization of Reaction Product in Differentiating Erythrocytes

The various stages of erythrocyte development in guinea pig and rabbit bone marrow, as illustrated in micrographs of sections incubated for peroxidase activity, appear in Figure 1, 2, 5-8, and 10-13. Figure 3, 4 and 9 represent micrographs of sections not reacted for peroxidase. None of the sections illustrated was exposed to heavy metal stains. The results obtained in the two species were similar and are considered together. Cytochemical incubation of guinea pig marrow at pH 7.6, 6.0 and 9.0 gave comparable results.

Hemocytoblasts. Primitive erythrocyte precursors, indistinguishable from other blast cells by morphologic criteria in routine sections, were readily identified by the presence of peroxidase reaction product on their cytoplasmic ribosomes (Figure 2 and 8). The interchromatinic area of the nucleus of these cells (nuclear matrix) also contained positively reacting particles some of which had the size and shape of ribosomes (Figure 2). Mitochondria, perinuclear cisternae, and small Golgi vesicles and saccules were uniformly negative. The density of the nucleolus of these cells was not increased after incubation in cytochemical reaction mixture and was therefore also considered negative. The ribo-

somes, positive for reaction product, were aggregated into polysomes generally containing 4–6 ribosomal units (Figure 10). The cytoplasm of erythrocyte hemocytoblasts lacked diffuse positive cytoplasmic material (Figure 10) corresponding to the hemoglobin of more mature cells.

The ribosomes of other hemocytoblasts in the bone marrow, presumably the precursors of nonerythrocyte cell lines, did not show peroxidase activity (Figure 1). Myeloblasts had numerous ribosomes, usually associated with endoplasmic reticulum, but these invariably lacked reaction product. Focal staining of eosinophil myelocyte ribosomes was noted occasionally but usually in an area adjacent to intense reaction product associated with the strong peroxidase reaction of the mature granule. It could not be decided whether this erratic staining represented diffusion of enzyme or reaction product or in fact reflected ribosomal synthesis of eosinophil peroxidase.

Erythroblasts. Erythroblasts were somewhat smaller cells with a smaller nucleus and less ample cytoplasm (Figure 1, 4, 5, 7 and 8). The nucleus contained larger aggregates of chromatin. The nuclear matrix, in contrast to that of nonerythroid cells, contained peroxidase-positive material (compare Figure 1, 5 and 8, peroxidase reacted, with Figure 4). Nuclear particulate staining was less obvious in older erythroblasts (Figure 7) which had fewer nuclear particles. The cytoplasmic ribosomes of erythroblasts, for the most part arranged as polysomes, were intensely positive (Figure 5 and 11). In addition, reaction product was sometimes deposited focally in the cytoplasm between ribosomes and unassociated with any cell organelles (Figure 11). In agreement with earlier studies¹¹ this localization was thought to represent newly synthesized hemoglobin.

Normoblasts. Normoblasts were smaller cells with a small nucleus containing dense aggregates of chromatin in osmium-collidine postfixed tissues. After incubation in peroxidase reaction medium, the interchromatinic areas of the nucleus of these cells contained peroxidase-positive material, not associated with particles, and thought to represent hemoglobin. Fewer ribosomes were present, although those remaining were intensely positive for reaction product and stained more densely than the diffuse deposits of cytoplasmic hemoglobin (Figure 6 and 12). Ferritin was also recognized within cytoplasmic vesicles of these cells and was attached to cup-shaped depressions of the surface membrane. Ferritin was readily distinguished from cytochemical reaction product at all stages of cell development.

Reticulocytes. Reticulocytes lacked nuclei and had relatively fewer ribosomes than normoblasts. Residual ribosomes stained more intensely

for peroxidase activity than did the surrounding cytoplasm which was intermediate in density between that of normoblasts and mature erythrocytes (Figure 7).

Mature red blood cells

Mature erythrocytes lacked ribosomes and the cytoplasm was diffusely and densely positive for reaction product (Figure 8).

Controls

No cytochemical reaction. Material postfixed in osmium-collidine and unstained with heavy metals was examined to determine the relative densities of structures in developing red cells in the absence of a cytochemical reaction. In this material, it was noted that ribosomes were slightly more dense than the surrounding cytoplasm, and the interchromatinic area of the nucleus had minimal density (Figure 3, 4 and 9). The relative densities of cellular structures were thus similar to those observed in unstained sections of nonerythroid bone marrow cell lines. Following incubation for peroxidase activity, however, the striking changes in density described above, cytoplasmic and nuclear, particulate and diffuse, became obvious (compare Figure 2 and 8, incubated, with Figure 3, nonincubated; likewise, compare Figure 1, 5, 7 and 8 with Figure 4; and Figure 11 with Figure 9). Similar dense particulate and diffuse reaction product did not develop in nonerythroid cells following incubation for peroxidase activity except for rare staining of ribosomes in eosinophils adjacent to strongly positive specific granules.

Absence of H_2O_2 or DAB from reaction media. Omitting either H_2O_2 or DAB resulted in a negative cytochemical reaction in developing and mature red blood cells, analogous to that observed in Figure 3, 4 and 9.

Control for nonspecific absorption of reduced DAB. When tissue was preincubated for 1 hour in the presence of DAB but without H_2O_2 and subsequently incubated for 15 minutes in 0.05M Tris-HCl containing 10^{-3} potassium ferricyanide, developing and mature red blood cells lacked densities of the type observed in cells incubated in complete medium. This is convincingly illustrated when Figure 9, a high magnification micrograph of an erythroblast studied for nonspecific absorption of DAB, is compared with Figure 11, a micrograph of a similar cell reacted for peroxidase and photographed at the same magnification.

Control for nonspecific absorption of oxidized DAB. When sections of bone marrow were incubated in DAB which had been oxidized with potassium ferricyanide, developing and mature erythrocytes were again

negative for reaction product, indicating that nonspecific binding of oxidized DAB to the tissue was not responsible for the results observed.

Inhibitors

The peroxidase activity observed on ribosomes and nuclear particles, as well as the diffuse nuclear and cytoplasmic activity of mature and developing erythrocytes, were completely inhibited by 10^{-1} M but not 10^{-2} M KCN. Sodium azide, 10^{-1} M, caused a moderate loss of activity in mature red cells and a greater loss of reactivity, both particle associated and diffuse, in immature erythrocytes. Aminotriazole, in a concentration of 2×10^{-2} M, produced no detectable inhibition of peroxidase activity in either the mature or developing red blood cell (Figure 8 and 13). Lack of inhibition of the peroxidatic activity of mature red blood cells with this concentration of aminotriazole has been previously described.^{14,15} Heating caused a patchy and irregular loss of peroxidase activity in red cells with sparing of activity in intervening areas.

The peroxidase activity of mature eosinophil granules was unaffected by 10^{-1} M KCN, 10^{-1} M sodium azide, and 2×10^{-2} M aminotriazole, confirming earlier work.^{16,17}

Peroxidatic activities of hemoglobin and hematin. Since the cytochemical peroxidase activity observed in erythrocytes could be attributed either to free hematin or to hemoglobin, it was of interest to measure the relative peroxidatic activities of these compounds biochemically with reference to the true peroxidase derived from the horseradish plant. The results of this comparison, using O-dianisidine as the electron acceptor are summarized in Table 1. The relative peroxidase activities of bovine hematin, bovine hemoglobin, and horseradish peroxidase, expressed in molar terms, were found to be 1, 11 and 7852 respectively. Comparable relative activities of hematin and hemoglobin were obtained by Bancroft and Elliott.¹⁸

Table 1—Peroxidatic Activities of Bovine Hematin and Hemoglobin Relative to Horseradish Peroxidase

	Molecular weight	Units*/ μ mole	Relative molar activities
Hematin	633	2.7	1
Hemoglobin	68,000	29.7	11
Horseradish peroxidase	40,000	21,200	7852

* Change in absorbancy at 460 m μ /min at room temperature and at pH 7.3

Discussion

We have used the well known peroxidase activity of erythrocytes as a cytochemical marker in studies of red blood cell differentiation in the bone marrows of guinea pigs and phenylhydrazine-treated rabbits. Mature erythrocytes, reticulocytes, normoblasts and late erythroblasts of both species contained diffuse deposits of peroxidase-positive material, unassociated with ribosomes, in their cytoplasm corresponding to the distribution of hemoglobin identified by others in strictly morphologic studies. Similar deposits were observed in the nuclei of erythroblasts and of older cells in the erythroid series. These cytochemical data, therefore, considered in the light of earlier studies of erythrocyte ultrastructure,^{11,13} absorption microspectroscopy¹⁹ and fluorescence microscopy,²⁰ suggest that the diffuse nuclear and cytoplasmic peroxidase activity observed may be attributed to hemoglobin. Although small amounts of free heme may be present in the mature erythrocyte, quantitative considerations make it likely that the great bulk of cytochemical activity reflects the presence of hemoglobin.²¹ Peroxidase staining was not observed in mitochondria, the site of heme synthesis, and in a biochemical assay system bovine hematin was found to possess only one-eleventh of the peroxidatic activity of hemoglobin.

Unexpected was the demonstration of peroxidase activity associated with ribosomes and nuclear particles of developing erythrocytes. Particle-associated peroxidase activity, both nuclear and cytoplasmic, appeared at an earlier stage of development than diffuse activity (presumably hemoglobin) and was well developed in erythroid hemocytoblasts and erythroblasts but was not seen in nonerythroid hemocytoblasts, myeloblasts or lymphoblasts. With differentiation, additional peroxidase activity appeared diffusely both in the nucleus and in the cytoplasm (Figure 6, 11 and 12), unassociated with cell organelles, as described above. As the nucleus condensed, the interchromatinic space with its particulate and diffuse peroxidase activities was reduced in size and little nuclear activity remained in the mature normoblasts. Ribosome associated activity persisted in the cytoplasm through the reticulocyte stage (Figure 7) but mature erythrocytes, lacking ribosomes, had only diffuse staining (Figure 8).

The particle associated reactivity observed in the cytoplasm was localized to ribosomes. Breton-Gorius,²² in a study of developing human bone marrow erythrocytes, also suggested the possibility of ribosomal peroxidase activity. However, her observations did not exclude the possibility of diffusion from the adjacent, hemoglobin-rich, cytoplasm. In our study the cytochemically reactive particles were commonly

arranged in configurations with the appearance and dimensions of polysomes (Figure 10-13), and in the youngest erythroid cells, lacking diffuse peroxidase activity, unstained ribosomes could not be visualized between peroxidase positive cytoplasmic particles. Finally, the particulate cytoplasmic reactivity and the number of cytoplasmic ribosomes declined in parallel as erythrocytes matured such that both were considerably reduced in reticulocytes and absent in mature erythrocytes.

The nuclear particles observed by us in erythrocyte precursors would seem to be analogous to those which have been previously noted in the nuclei of other cells.^{23,24} These particles have some morphologic similarities to ribosomes but have less tendency to form polysome-like structures. The finding that erythrocyte nuclear particles have peroxidase activity similar to that of cytoplasmic ribosomes is of interest since Hammell and Bessman have demonstrated hemoglobin synthesis in nuclear preparations of avian erythrocytes.²⁵ Similarly, Orlic²⁶ has demonstrated ⁵⁵Fe incorporation in the nuclei of mouse spleen erythroblasts using electron microscopic autoradiography. Some authors have felt that nuclear hemoglobin resulted from the flow of this material from the cytoplasm, where it was synthesized, to the nucleus by means of the nuclear pores.^{13,19} The most primitive erythroid cells we observed contained nuclear particles as well as cytoplasmic, polysome-associated peroxidase activity. Primitive cells containing only cytoplasmic or nuclear activity were not identified. We therefore have no morphologic evidence for a flow of particles or of hemoglobin between nucleus and cytoplasm. Indeed, the nuclear particles and hemoglobin observed could have resulted from the generalized mixing of nuclear and cytoplasmic elements at the time of cell division.

The nature of the particle associated peroxidase activity in developing erythrocytes was not established with certainty. Ribosome or microsome-bound peroxidases have been described in plant and animal tissues.^{27,28} Glutathione peroxidase does occur in erythrocytes but this enzyme has been shown to be devoid of activity at pH 6.0²⁹ and therefore probably did not contribute to our results. Neither particulate nor diffuse activity was inhibited by aminotriazole at any stage of erythrocyte development. Since this compound is a known inhibitor of the catalases isolated from several organs and species, including the human erythrocyte, it seems unlikely that either activity observed in our studies could be attributed to catalase.³⁰ A variety of other enzyme inhibitors were likewise unable to distinguish between diffuse and particle associated peroxidase activity, possibly suggesting that both reflect the activity of the same protein; namely, hemoglobin. However,

hemoglobin is not known to be bound to ribosomes in significant quantities.^{31,32} Current biochemical opinion³³ holds that the α chains of globin are released from polysomes as soon as they are synthesized and combine with newly completed β chains still attached to ribosomes. Subsequently, it is thought, $\alpha\beta$ subunits are freed into the cytoplasm and only then combine with heme which is synthesized independently by cytoplasmic and mitochondrial enzymes. Finally, the $\alpha\beta$ subunits with attached heme join to form the tetrad of $\alpha_2\beta_2$ hemoglobin. Only a small amount of ^{59}Fe becomes associated with rabbit reticulocyte polysomes *in vitro* and this is not released by puromycin whereas nascent chains of globin are completely released. Moreover, well washed rabbit reticulocyte ribosomes that have been passed through a sucrose density gradient do not possess peroxidase activity in our hands.³⁴ Therefore, whatever the nature of the particle associated peroxidase activity, it would seem to be loosely bound to ribosomes. Possibly this activity represents newly synthesized hemoglobin whose assembly was completed either on or immediately adjacent to nuclear particles and cytoplasmic ribosomes. Further work will be required to settle this question.

Endogenous peroxidase activity in ribosomes has also been reported in salivary gland acinar cells³⁵ and in epithelial cells of the large intestine.³⁶ In salivary gland cells which synthesize a peroxidase for secretion, Strum and Karnovsky noted that focal clusters of ribosomes were peroxidase positive. While this staining was thought to reflect newly synthesized enzyme, the possibility was also considered that enzyme was released from adjacent peroxidase-containing organelles and became nonspecifically bound to ribosomes. The irregular and focal ribosomal staining noted in eosinophils in our material is likewise subject to either interpretation. However, differentiating erythrocytes lack peroxidase containing organelles other than ribosomes and nuclear particles. Further, the particle staining in these cells probably cannot be attributed to diffusion from the sites of hemoglobin reaction in the nucleus or cytoplasm since particle reactivity appeared in young cells before diffuse nuclear or cytoplasmic enzyme activity could be identified (Figure 10 and 13). It remains possible that diffuse hemoglobin is present at activities below the sensitivity of our methods and during fixation and processing becomes bound to ribosomes in concentrations sufficient to be detected. This, however, seems unlikely due to the uniformity of ribosomal staining observed.

Peroxidase staining of ribosomes and nuclear particles was observed in guinea pig hemocytoblasts situated in islands of erythropoiesis, and

we conclude that these cells are committed to develop in the erythroid series—*ie*, that hemocytoblasts exhibiting particulate peroxidase activity are in fact erythroid hemocytoblasts. Support for this inference was obtained from study of phenylhydrazine-treated rabbits whose marrow showed striking erythroid hyperplasia with numerous immature forms. Here the great majority of hemocytoblasts present could safely be assumed to be erythroid precursors and were found in fact to possess peroxidase-positive particulate material both in their nuclei and cytoplasm. Thus, the presence of particulate peroxidase activity allowed identification of erythroid hemocytoblasts at a stage of development when they could not otherwise be distinguished from the hemocytoblast precursors of other marrow cell lines. This finding suggests that primitive cells, undifferentiated and indistinguishable morphologically from the blast cells of the marrow, spleen, or lymph nodes, may in fact already be committed to differentiate in a particular cell line. Independent evidence for this conclusion is found in the cytochemical work of Avrameas and Leduc³⁷ who localized antibody to horseradish peroxidase on the ribosomes of primitive lymphoid cells from lymph nodes, thereby demonstrating that another type of blast cell is already committed to the synthesis of a specific protein. Taken together, these data indicate that not all hemocytoblasts are totipotent but do not exclude the possibility that some are or that the blasts described by us and by Avrameas and Leduc arose from some unrecognized common totipotent precursor.

Acknowledgments

The authors wish to thank the Misses Blanche Simpson and Patricia Borys for technical assistance.

We also wish to thank Dr. C. Baglioni for helpful discussion and review of the manuscript.

References

1. Pearse AGE: Histochemistry. Boston, Little, Brown and Co, 1960
2. Hosoya T, Morrison M: A study of the hemoproteins of thyroid microsomes with emphasis on the thyroid peroxidase. *Biochemistry* 6:1021–1026, 1967
3. Borsook H, Deasy CL, Gaagen-Smit AS, Keighley G, Lowy PH: Incorporation in vitro of labeled amino acids into protein of rabbit reticulocytes. *J Biol Chem* 196:669–694, 1952
4. Karnovsky MJ: A formaldehyde-glutaraldehyde fixative of high osmolality for use in electron microscopy. *J Cell Biol* 27:137A, 1965
5. *Idem*: Simple method for staining with lead at high pH in electron microscopy. *J Biophys Biochem Cytol* 11:729, 1961

6. Graham RC, Karnovsky MJ: The early stages of absorption of injected horseradish peroxidase in the proximal tubule of the mouse kidney: Ultrastructural cytochemistry by a new technique. *J Histochem Cytochem* 14:291-302, 1966
7. Novikoff AB, Goldfischer S: Visualization of peroxisomes (microbodies) and mitochondria with diaminobenzidine. *J Histochem Cytochem* 17:675-677, 1969
8. Shannon LM, Kay E, Lew JY: Peroxidase isozymes from horseradish roots. I. Isolation and physical properties. *J Biol Chem* 241:2166-2172, 1966
9. Worthington Biochemical Corporation, Descriptive Manual No 11, Freehold, New Jersey, 1961
10. Bloom W, Fawcett DW: A Textbook of Histology. Philadelphia-London-Toronto, WB Saunders Co, 1968
11. Fawcett DW: The Cell. Philadelphia-London, WB Saunders Co, 1966
12. *Idem*: Surface specialization of absorbing cells. *J Histochem Cytochem* 13:75-91, 1965
13. Skutelsky E, Danon D: An electron microscopic study of nuclear elimination from the late erythroblast. *J Cell Biol* 33:625-635, 1967
14. Venkatachalam MA, Fahimi HD: The use of beef liver catalase as a protein tracer for electron microscopy. *J Cell Biol* 42:480-489, 1969
15. Strum JM, Karnovsky MJ: Cytochemical localization of endogenous peroxidase in thyroid follicular cells. *J Cell Biol* 44:655-666, 1970
16. Cotran RS, Litt M: The entry of granule-associated peroxidase into the phagocytic vacuoles of eosinophils. *J Exp Med* 129:1291-1306, 1969
17. Bainton DF, Farquhar MG: Segregation and packaging of granule enzymes in eosinophilic leukocytes. *J Cell Biol* 45:54-73, 1970
18. Bancroft G, Elliott KA: The distribution of peroxidase in animal tissues. *Biochem J* 28:1911-1919, 1934
19. Davies HG: Structure in nucleated erythrocytes. *J Biophys Biochem Cytol* 9:671-687, 1961
20. Granick S, Levere RD: Heme synthesis in erythroid cells. *Progr Hematol* 4:1-47, 1964
21. Allen DW: Hemoglobin metabolism within the red cell, *The Red Blood Cell*. Edited by C Bishop, DM Surgenor. New York, Academic Press, 1964
22. Breton-Gorius J: Utilisation de la diaminobenzidine pour la mise en évidence, au microscopie électronique, de l'hémoglobine intracellulaire. La reactivité des différents organelles des érythroblastes. *Nouv Rev Fran d'Hématol* 10:243-256, 1970
23. Hay ED: Structure and function of the nucleolus in developing cells. *The Nucleus*. Edited by AJ Dalton, F Haguenau. New York, Academic Press, 1968
24. Frenster JH, Allfrey VG, Mirsky AE: Metabolism and morphology of ribonucleoprotein particles from the cell nucleus of lymphocytes. *Proc Nat Acad Sciences (USA)* 46:432-444, 1960
25. Hammell CL, Bessman SP: Hemoglobin synthesis in avian erythrocytes. *J Biol Chem* 239:2228-2238, 1964
26. Orlic D: The use of ⁵⁵Fe in high-resolution radioautography of developing red cells. *J Cell Biol* 39:201-207, 1968
27. Lanzani GA, Galante E: Peroxidase activities from wheat embryo ribosomes. *Arch Biochem Biophys* 106:20-24, 1964

28. Shichi H, Kamiryo T, Funahashi S: Haemoproteins in heart microsomes. *Biochim Biophys Acta* 99:381-383, 1965
29. Mills GC: The purification and properties of glutathione peroxidase of erythrocytes. *J Biol Chem* 234:502-506, 1959
30. Margoliash E, Novogrodsky A: A study of the inhibition of catalase by 3 amino 1,2,4 triazole. *Biochem J* 68:468-475, 1958
31. Waxman HS, Freedman ML, Rabinovitz M: Studies with ⁵⁹Fe-labeled hemin on the control of polyribosome formation in rabbit reticulocytes. *Biochim Biophys Acta* 145:353-360, 1967
32. Felicetti L, Colombo B, Baglioni C: Assembly of hemoglobin. *Biochim Biophys Acta* 129:380-394, 1966
33. Harris JW, Kellermeyer RW: The Red Cell. Production, metabolism, destruction: Normal and abnormal. Cambridge, Harvard University Press, 1970
34. Dvorak AM, Baglioni C: Unpublished data
35. Strum JM, Karnovsky MJ: Ultrastructural localization of peroxidase in submaxillary acinar cells. *J Ultrastruct Res* 31:323-336, 1970
36. Venkatachalam MA, Saltani MH, Fahimi HD: The fine structural localization of peroxidase activity in the epithelium of large intestine of rat. *J Cell Biol* 46:168-173, 1970
37. Avrameas S, Leduc EH: Detection of simultaneous antibody synthesis in plasma cells and specialized lymphocytes in rabbit lymph nodes. *J Exp Med* 31:1137-1168, 1970

All figures represent electron photomicrographs of guinea pig and rabbit bone marrow sections which were not exposed to heavy metal stains.

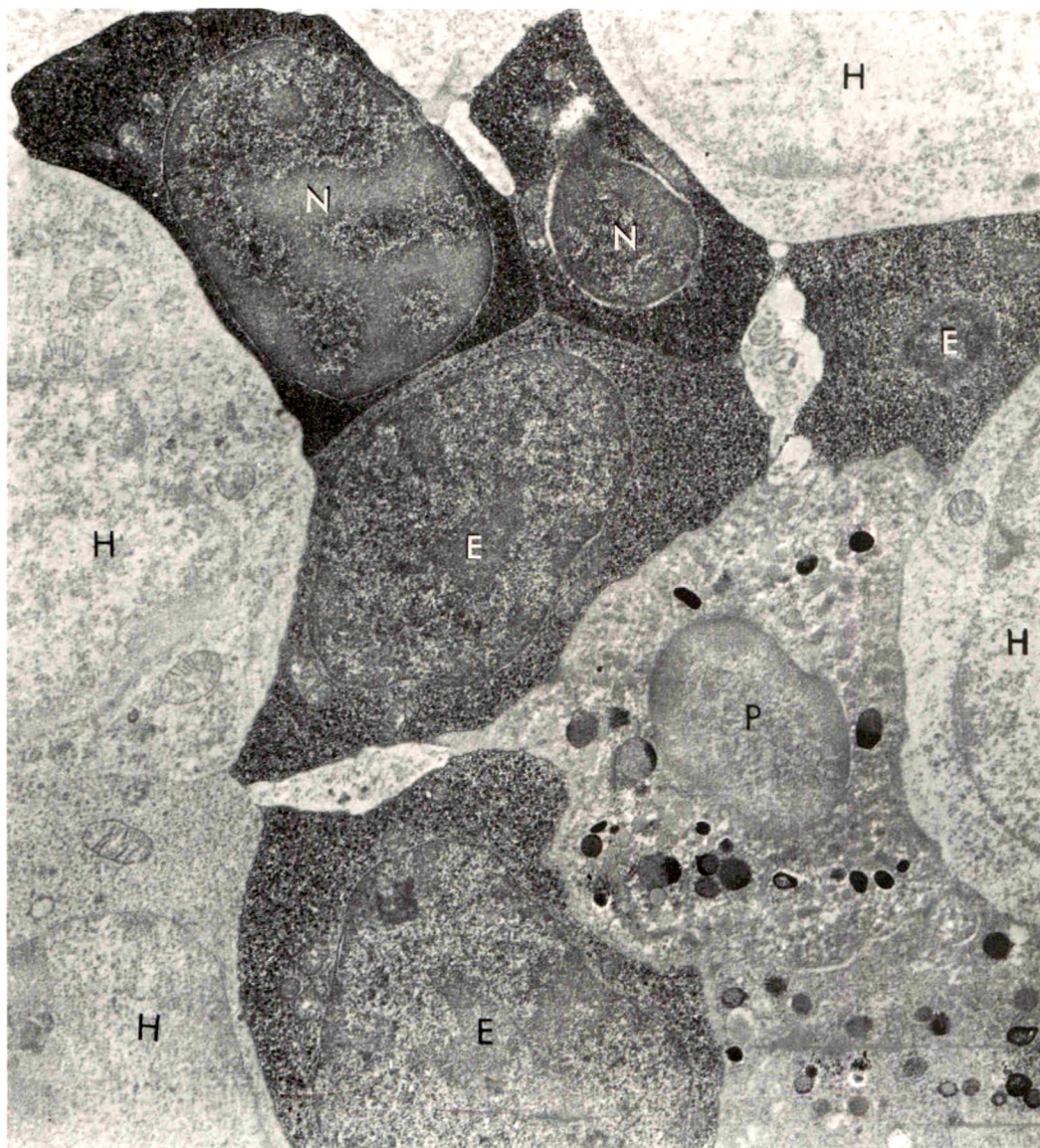


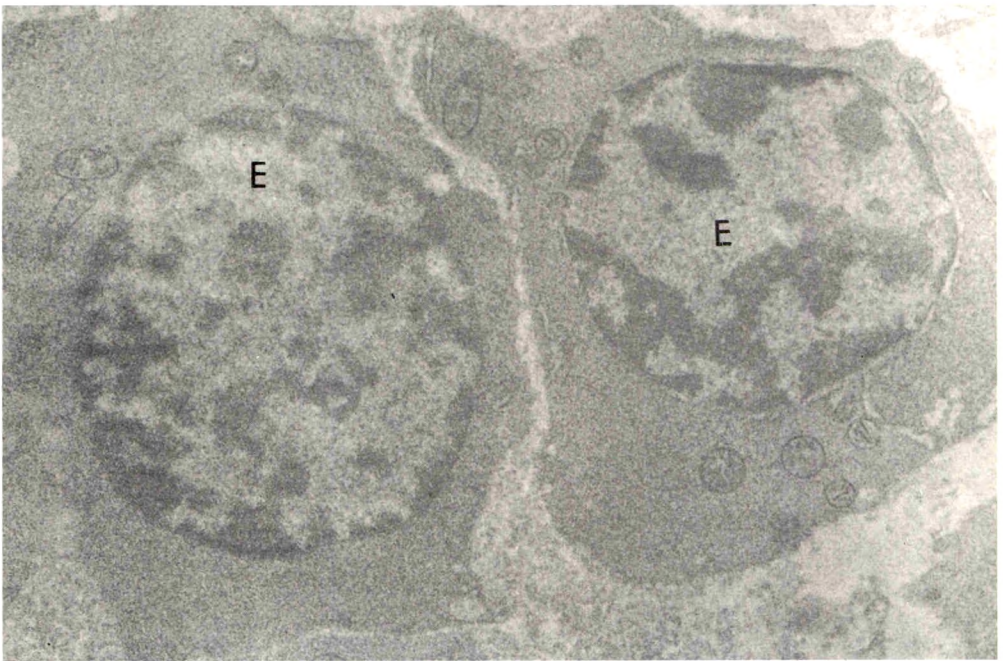
Fig 1—Specimen of guinea pig bone marrow incubated for peroxidase activity. This low magnification picture shows negative hemocytoblasts (*H*). These cells, presumably not of the erythroid series, show cytoplasmic ribosomes and nuclear interchromatinic particles that are negative for peroxidase activity. Also present are a polymorphonuclear leukocyte (*P*) with positive granules, three positive erythroblasts (*E*), and two positive normoblasts (*N*) ($\times 9000$).



Fig 2—Specimen of guinea pig bone marrow incubated for peroxidase activity. The large erythroid hemocytoblast (*H*) has peroxidase-positive polysomes throughout the cytoplasm. The nuclear matrix is filled with positive particles. The adjacent polymorphonuclear leukocyte (*P*) has several positive cytoplasmic granules. The basophilic leukocyte (*B*) has negative granules ($\times 16,000$).



3



4

Fig 3—Specimen of guinea pig bone marrow not incubated for peroxidase activity. The nuclear matrix of the hemocytoblast (*H*) has minimal density. In addition, the cytoplasmic ribosomes are visible but are of low density when compared with the ribosomes in erythroid hemocytoblasts incubated in the medium for peroxidase activity, as seen in Figure 2 ($\times 14,000$). **Fig 4**—Specimen of guinea pig bone marrow not incubated for peroxidase activity. The erythroblasts (*E*) are smaller than hemocytoblasts and have more densely condensed nuclear chromatin. Nuclear matrix is minimally dense. Ribosomes have low density compared with ribosomes in erythroblasts incubated in medium for peroxidase activity, as seen in Figure 5 ($\times 14,500$).



Fig 5—Specimen of guinea pig bone marrow incubated for peroxidase activity. In contrast to Figure 4, erythroblasts (E) have intensely positive particles filling nuclear matrix and positive ribosomes in cytoplasm. Polymorphonuclear leukocyte (P) with positive granules and several positive normoblasts (N) also present ($\times 9000$). Inset is a higher magnification of positive cytoplasmic ribosomes and polysomes in erythroblast cytoplasm ($\times 29,000$).

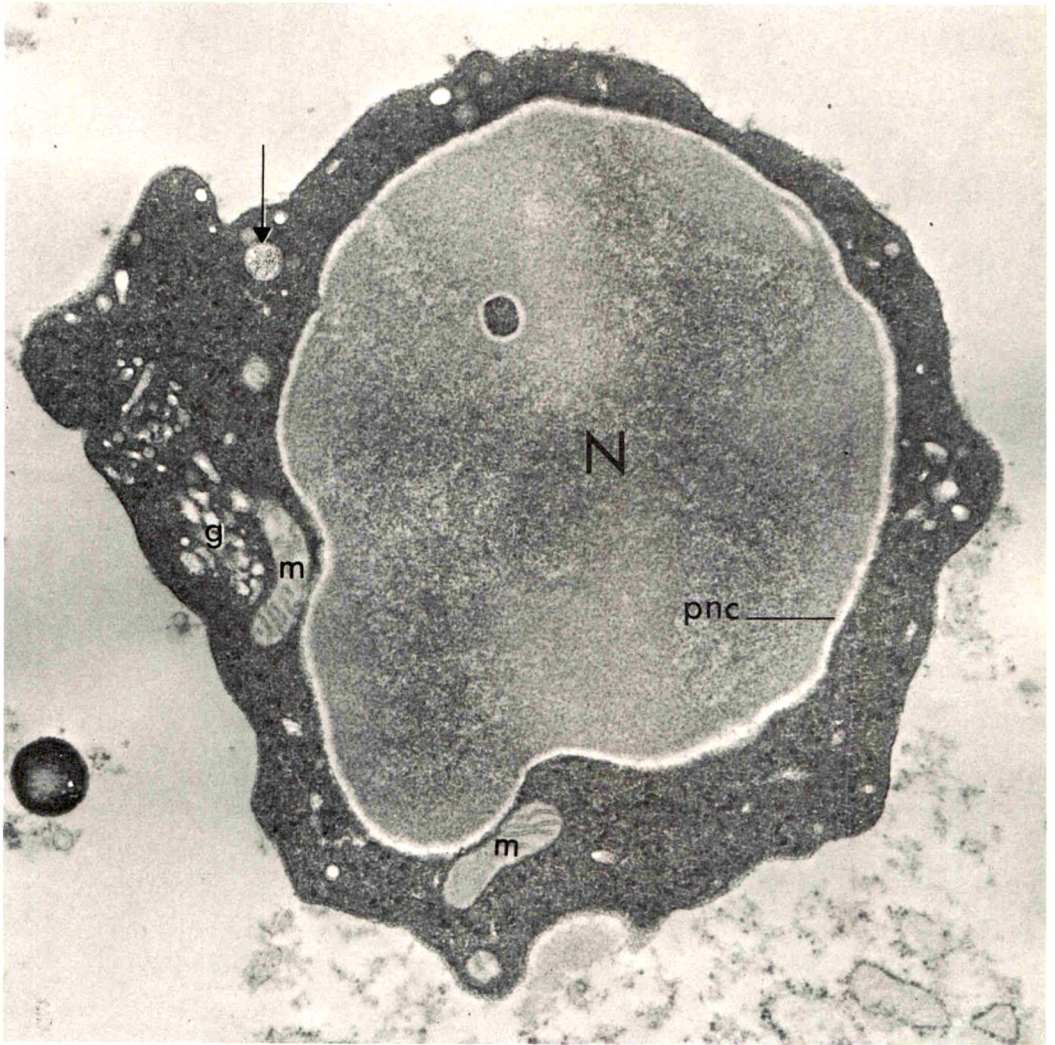


Fig 6—Specimen of guinea pig bone marrow incubated for peroxidase activity. This higher magnification of normoblast (*N*) demonstrates diffuse positive staining in the nuclear matrix and cytoplasm. Perinuclear cisternae (*PNC*), Golgi saccules (*G*) and mitochondria (*m*) are negative. Cytoplasmic vesicle filled with particles of ferritin also present (*arrow*) ($\times 22,000$).

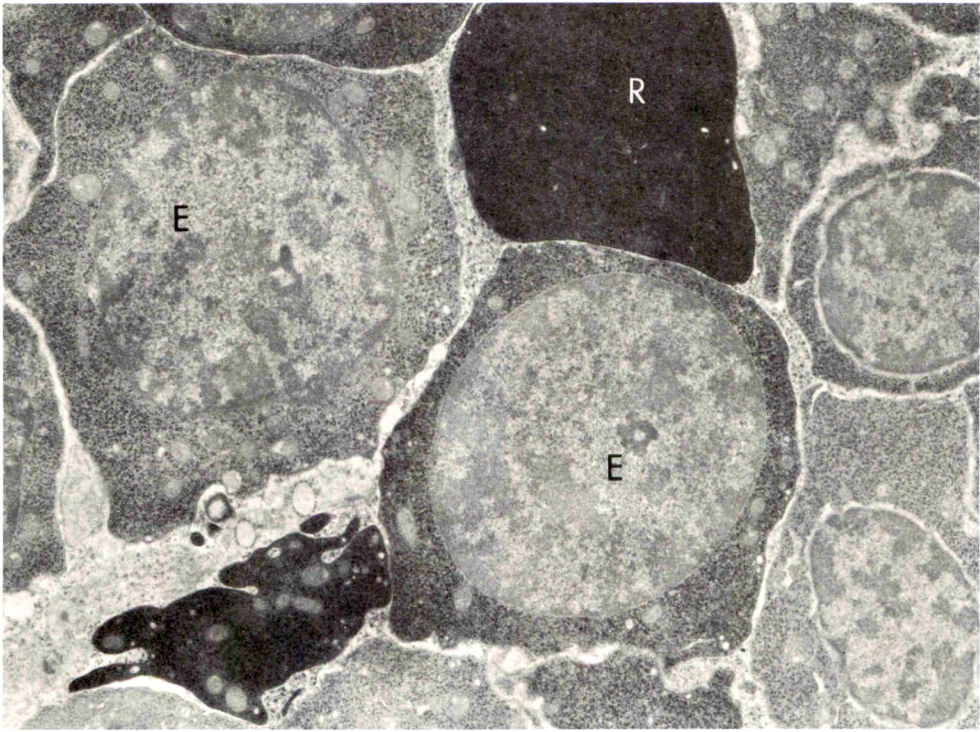
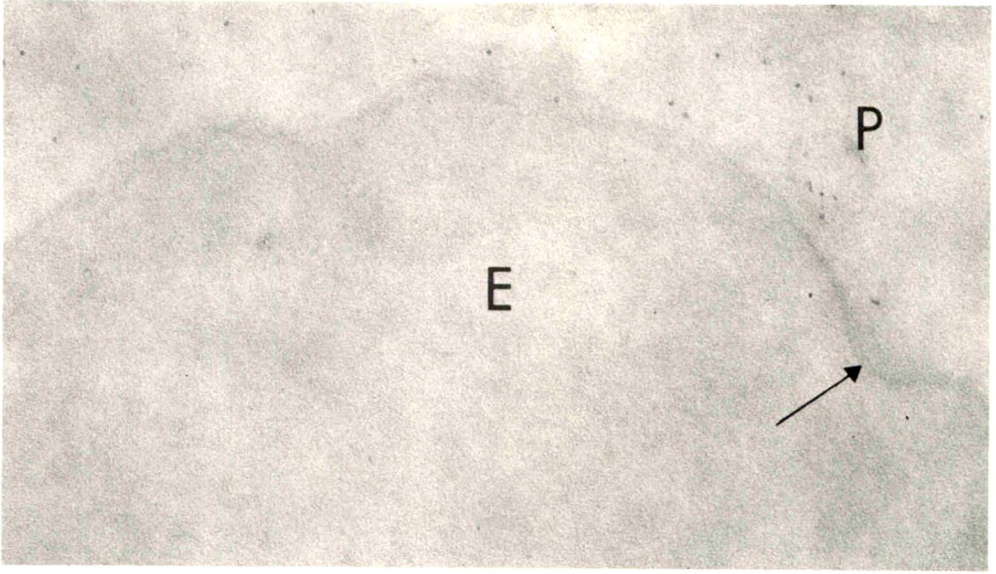


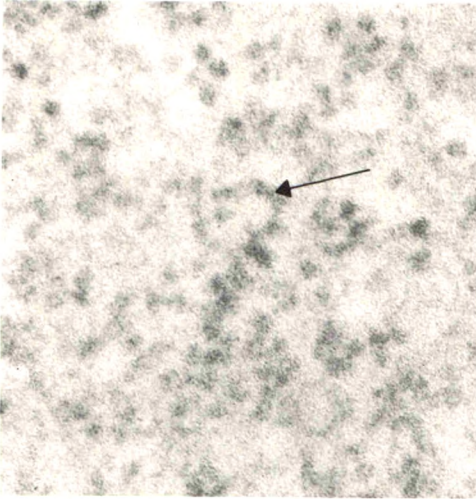
Fig 7—Specimen of phenylhydrazine-treated rabbit bone marrow incubated for peroxidase activity showing several positive erythroblasts (*E*), and one positive reticulocyte (*R*) ($\times 8000$).



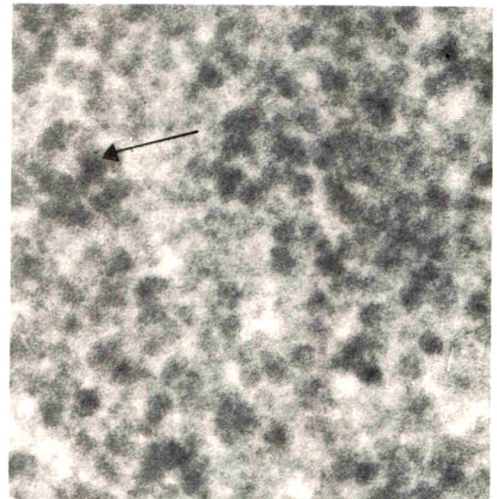
Fig 8—Specimen of phenylhydrazine-treated rabbit bone marrow, preincubated with aminotriazole followed by incubation in complete medium for peroxidase, also contained aminotriazole. Numerous positive erythroid hemocytoblasts (*H*) and erythroblasts (*E*) are seen. A mature red blood cell (*RBC*) also is positive. This lack of inhibition of reaction product formation indicates positive material is not red blood cell catalase ($\times 8000$).



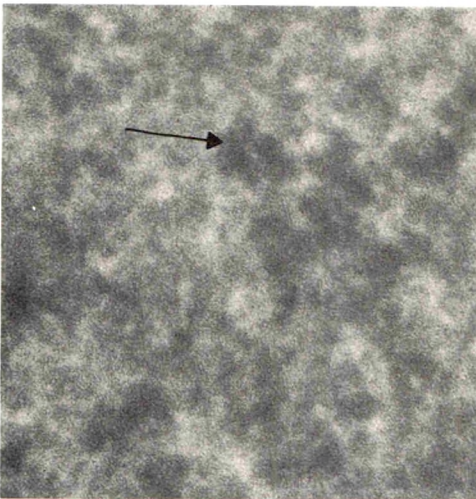
9



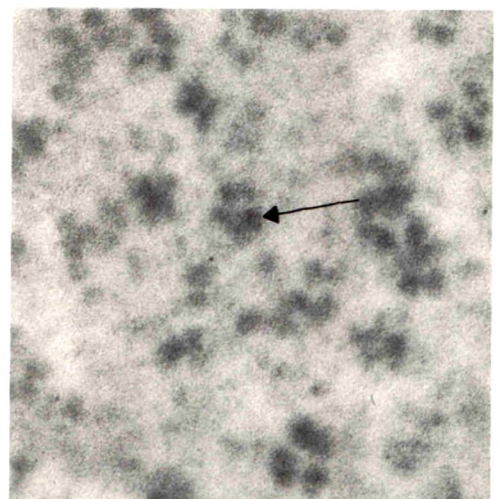
10



11



12



13

[*End of Article*]

Chronic Actinic Keratopathy—A Condition Associated with Conjunctival Elastosis (Pingueculae) and Typified by Characteristic Extracellular Concretions

Gordon K. Klintworth, MD, PhD

Morphologic observations on a peculiar type of corneal reaction with a predisposition for the superficial stroma of the interpalpebral portion of the cornea are reviewed. Histochemical evidence is provided which indicates that the corneal concretions, though not homogenous, are proteinaceous in nature and contain amino acids not normally detectable in the cornea. The corneal concretions were associated with conjunctival elastosis (pingueculae) in all 22 instances in which the eyes were sectioned in the horizontal plane. Identical concretions were identified within these associated pingueculae, as well as in a large percentage of other pingueculae and cutaneous lesions with actinic elastosis. The findings suggest that the abnormal material arises in the pericorneal conjunctival connective tissue from whence it diffuses into, and deposits in, the superficial corneal stroma. The data also raise the possibility that the concretions may be derived, at least in part, from altered elastic tissue. Morphologic and epidemiologic observations on the condition taken together strongly suggest that this unique reaction is a sequel to the cumulative effect of chronic actinic irradiation. Further observations on this keratopathy are needed to establish whether this unique response can be provoked by other noxious stimuli (*Am J Pathol* 67:327–348, 1972).

NUMEROUS CORNEAL DISEASES are recognized today, due largely to meticulous clinical observations that have accumulated since the birth of ophthalmology. Some are characterized by the occurrence of opacities with a predisposition for the horizontal meridian in the exposed interpalpebral portion of the superficial cornea. In the most

From the Departments of Pathology and Ophthalmology, Duke University Medical Center, Durham, North Carolina.

Supported in part by Research Grant 1 R01 EY 00146-01A2 from the US Public Health Service.

The author is a recipient of a Research Career Development Award 1 K04 EY44795-01 from the National Eye Institute.

Accepted for publication Nov 1, 1971.

Address for reprint requests: Dr. G. K. Klintworth, Department of Pathology, Duke University Medical Center, Durham, North Carolina 27710.

What may be the same phenomenon has been described in the literature under a variety of terms including hyaline degeneration of the cornea, *degeneratio hyaloidea granuliformis corneae*, Bietti's nodular dystrophy, nodular hyaline band-shaped degeneration, *degeneratio sphaerularis elaioides*, "the blindness of Dahalach," tropical corneal dystrophy, type II white limbus girdle of Vogt, keratinoid corneal degeneration or keratopathy, Labrador keratopathy, nodular band-shaped dystrophy of tropical countries of arid soil, and *degeneratio primaria oleoguttata centrale et superficiale*.¹⁻¹⁰

common variety, termed band keratopathy, the deposits are calcified granules, and the corneal lesions commonly accompany other ocular lesions, particularly uveitis, chronic glaucoma and phthisis bulbi. In another entity, bilateral, white, greyish or yellow noncalcific opacities accumulate in the same location. The latter condition is designated chronic actinic keratopathy in the present paper, for reasons which will become apparent later. Initially, the deposits concentrate in the peripheral cornea and form symmetric bilateral concentric arcs between the limbus and the cornea. With time the opacities often converge towards the center of the cornea, and form a nontransparent horizontal band across the entire cornea. The deposits accumulate with advancing age, often in the absence of other associated ocular disease, and as a rule without clinical features of inflammation. Though the latter condition has been observed in inhabitants of several countries, it is prevalent, particularly in its severe form, in certain geographic areas such as Labrador, Libya, Somali Republic and countries bordering the Red Sea.²⁻⁵

The present report reviews morphologic observations on the entity in patients that had spent all, or most, of their life in the south eastern United States. Evidence is provided which strongly suggests that this unique reaction may be a sequel to the accumulative effect of chronic actinic irradiation.

Materials and Methods

Corneal tissue from 35 patients with variable degrees of the keratopathy was studied. The material included 6 corneal buttons obtained from penetrating keratoplasty, 4 corneal biopsies, 13 surgically enucleated eyes and 12 eyes obtained at autopsy (Table 1). Representative corneal and other ocular tissue, from these cases was fixed in 10% buffered formaldehyde (pH 6.8) and embedded in paraffin for light microscopy. In one (Case 10), unfixed corneal tissue obtained at a superficial keratectomy was rapidly frozen to -20°C and sectioned with a cryostat. Control tissue included normal eyes procured at necropsy and enucleation for orbital neoplasms. All corneal tissue was sectioned at $7\text{ }\mu$ perpendicular to the epithelial surface and stained by numerous techniques including: hematoxylin and eosin; nuclear fast red; connective tissue stains [Masson's trichrome (standard method with both solution A and B, as well as with each solution separately), Weigert's resorcin-fuchsin, Verhoeff's elastic tissue stain, Wilder's reticulum, Taenzer-Unna acid orcein and phosphotungstic acid hematoxylin]; glycosaminoglycans [periodic acid-Schiff (PAS), Mowry's modification of Hale's colloidal iron reaction, alcian blue]; proteins [diazotisation-coupling, Danielli's coupled tetrazolium (with and without prior blocking with dinitro fluorobenzene, performic acid, and benzyol chloride), performic acid-alcian blue, *p*-dimethylaminobenzaldehyde (DMAB)-nitrite, dihydroxy-dinaphthyl disulphide (DDD), thioglycollate-DDD, diazo-reaction, post-coupled benzyldiene, Sakaguchi, ferric ferricyanide, ninhydrin-Schiff, Millon]; lipids [luxol fast blue, Oil red O, Sudan III, osmium tetroxide—naphthyl-

Table 1—Summary of Cases Studied

Case and tissue examined	Age	Sex	Race	Location	Severity	Associated pinguecula	Associated conditions
1. Corneal button	48	F	N	CC, PC	++++	?	Cataracts
2. Corneal button	54	M	C	CC, PC	++++	?	Postsympathetic ophthalmitis
3. Corneal button	61	F	N	CC, PC	+++	?	Neonatal keratitis
4. Corneal button	45	M	N	CC, PC	+++	?	Keratoconus
5. Corneal button	43	M	N	CC, PC	+++	?	Keratoconus
6. Corneal button	23	F	N	CC, PC	+++	?	Congenital corneal dystrophy
7. Corneal biopsy	30	F	N	CC, PC	++++	?	
8. Corneal biopsy	62	M	C	PC	++	+	
9. Corneal biopsy	51	M	C	PC	+	+	Basal cell carcinoma nose Carcinoma of conjunctiva
10. Corneal biopsy	47	M	N	CC, PC	++	?	Vascularized corneal leukoma
11. Globe	38	F	C	PC	+	+	
12. Globe	65	M	N	PC	+	+	
13. Globe*	32	M	N	CC	+++	?	Glaucoma
14. Globe	69	F	N	PC	+	+	Glaucoma, diabetic retinopathy
15. Globe	69	M	N	PC, SS	+	+	
16. Globe	52	M	N	PC	+	+	Acute leukemia
17. Globe	75	M	N	CC, PC	++++	+	Glaucoma (post-traumatic)
18. Globe*	56	M	N	CC	++++	?	Chronic buphthalmos
19. Globe	62	M	C	PC	+	+	Glaucoma (post-traumatic)
20. Globe	84	F	N	PC	+	+	
21. Globe	65	M	N	PC	+	+	
22. Globe*	46	M	C	CC	+++	?	
23. Globe	75	M	C	PC	+	+	
24. Globe	59	M	N	PC	+	+	
25. Globe	55	F	N	PC	+	+	Glaucoma, diabetic retinopathy
26. Globe	53	M	C	PC	+	+	Diabetic retinopathy
27. Globe	50	M	C	PC	+	+	Diabetic retinopathy
28. Globe	52	F	N	PC	+	+	
29. Globe	68	M	C	PC	+	+	Glaucoma
30. Globe	56	M	C	PC	+	+	
31. Globe	?	?	?	PC	+	+	
32. Globe	?	?	?	PC	+	+	

Table 1—(CONT.)

Case and tissue examined	Age	Sex	Race	Location	Severity	Associated pinguecula	Associated conditions
33. Globe	62	M	C	PC	++	+	Glaucoma (chronic open angle)
34. Globe	76	M	N	PC	+	+	
35. Globe	63	M	N	PC	+	+	

F = Female

M = Male

N = Negroid

C = Caucasoid

PC = Peripheral interpalpebral cornea

CC = Central interpalpebral cornea

SS = Superficial bulbar sclera

* = Eye sectioned vertically; calottes not examined

amine (OTAN)], nucleic acids [Feulgen, methyl green pyronin]; amyloid [Congo red, thioflavin T]; phosphates [Von Kossa]; calcium [alizarin red]; ferric ions [Perl's Prussian blue]; pre-keratin and keratin [hematoxylin-phloxine-alcian blue-orange G, hematoxylin-Shorr S3 stain, performic acid-Schiff].¹¹⁻¹⁵ Unstained sections were examined for birefringence under a polarized light, with and without a first order interference filter. Unstained tissue sections, as well as those stained with the fluorescent dye thioflavin T were mounted in a nonfluorescent mounting medium (glycerine or Harleco Fluorescence Mountant, Hartman-Leddon Company, Philadelphia, Pennsylvania) and studied by fluorescence microscopy. Observations were made with bright and dark field illumination using both an ultra-violet and a blue violet light source and appropriate barrier filters to eliminate the excitation radiation.

The cornea from Case 24 was excised from the globe immediately following enucleation. It was sectioned into small pieces and fixed in cold 1% sodium cacodylate-buffered osmium tetroxide (pH 7.4) for 1 hour, dehydrated in graded alcohols, infiltrated with propylene oxide and embedded in Epon 812 for electron microscopy. Corneal biopsies from two other cases with clinically observed yellow deposits (Cases 9 and 10) were processed in an identical manner. A portion of the lesion from another patient (Case 2) that had previously been embedded in paraffin was excised from the paraffin block, deparaffinized, fixed in cold 1% sodium cacodylate-buffered osmium tetroxide (pH 7.4), and processed for electron microscopy as well. Thick sections (2 μ m) were cut with the Sorvall Porter-Blum microtome, and stained with thionine-azure blue for orientation.¹⁶ Companion thin sections were cut and mounted on 200-mesh copper grids and stained for 6 minutes with 4% magnesium uranyl acetate in distilled water, rinsed with distilled water (2 changes) and then stained for 4 minutes with lead citrate (pH 12) at room temperature.¹⁷ Electron microscopic observations were made with a RCA EMU-3G microscope at 50 kV.

In view of evidence that basophilic degeneration of the cutis (solar elastosis, actinic elastosis), and pingueculae (focal conjunctival elastotic degeneration) are both causally related to chronic ultraviolet irradiation, tissue from 50 consecutive examples of cutaneous actinic elastosis and 50 pingueculae were examined for concretions with morphologic and tinctorial attributes similar to those of the keratopathy.

Observations

A. Cornea

Light microscopy. The superficial corneal stroma in all cases contained granules and concretions of variable size and shape in the horizontal meridian (Figures 1–6). In 22 instances in which the periphery of the interpalpebral portion of the cornea was available for examination, it was involved without exception, and in the mildest cases the deposits were limited to the marginal cornea. When the keratopathy was more extensive, the deposits were more numerous, as well as larger, and extended towards the central cornea sometimes forming a horizontal band across the entire cornea. In three instances the entire inferior half of the cornea was affected. Bowman's zone was frequently involved, but in some instances the abnormal material was extensively deep to it (Figure 7), and in corneas with a superficial subepithelial pannus, the deposits were often predominantly external to Bowman's zone.

In unstained preparations the smaller concretions (1 to 3 μ in diameter) were granular and generally of the same color as the surrounding cornea. The larger globules (10 to 60 μ in diameter), which were often restricted to the central cornea, frequently manifest a distinct yellow hue (Figure 3), and in at least three instances globules with this color were evident in the cornea with the slit lamp (Cases 7, 9, 10). When viewed by fluorescence microscopy the corneal deposits frequently manifest a pronounced autofluorescence in unstained tissue sections. The fluorescence was greenish-yellow (about 575 m μ) with blue violet exciting radiation, and blue (about 470 m μ) in ultraviolet light (Figure 4). Though the concretions varied in size, shape, and in certain staining characteristics there were sufficient morphologic gradations between them to suggest a common nature. The deposits consistently manifest a marked avidity for the red dyes in Masson's trichrome stain (acid fuchsin and Ponceau de xylinine). They also gave positive reactions with histochemical techniques that demonstrate protein, including those thought to demonstrate amino (ninhydrin—Schiff), guanidyl (Sakaguchi reaction), indole (*p*-dimethylaminobenzaldehyde (DMAB)—nitrite method), and sulfhydryl (Dihydroxy-dinaphthyl disulphide (DDD) reaction) groups (Table 2). The concretions, including the yellow ones, failed to stain in unfixed frozen tissue with a variety of methods used to demonstrate lipids. Several other staining attributes of the concretions varied from case to case, and sometimes even within the same cornea. In some cases the abnormal material was

Table 2—Characteristics of Corneal Deposits

Method	Present study	Other investigations
Unstained Preparations		
Color	Pale yellow or colorless	
Fluorescence microscopy	Most nonfluorescent, but often autofluorescent (especially large globules)	
Polarization microscopy	Not birefringent	
Tinctorial Reactions		
Proteins		
Reactive Groups		
Amino (eg, lysine, ornithine, peptide terminal)		
Ninhydrin-Schiff	Positive (except large globules)	
Guanidyl (eg, arginine)		
Sakaguchi reaction	Positive	Positive [6]
Danielli's coupled tetrazonium*	Positive	
Imidazole (eg, histidine)		
Diazo reaction	Negative	
Danielli's coupled tetrazonium*	Positive	
Phenyl (eg, tyrosine)		
Danielli's coupled tetrazonium*	Positive	Positive +++ [6]
Millon	Some positive, others negative	
Diazo reaction	Negative	
Diazotisation-coupling	Negative	Positive [6]
Indole (eg, tryptophan)		
Danielli's coupled tetrazonium*	Positive	
p-dimethylaminobenzaldehyde (DMAB)-nitrite	Positive	
postcoupled benzylidene	Positive (blue)	
Sulfhydryl (eg, cysteine)		
Dihydroxy-dinaphthyl disulfide (DDD)	Positive	Positive [6]
Danielli's coupled tetrazonium*	Positive	
Tetrazolium	Positive	
Ferric ferricyanide	Negative	
Disulfide (eg, cystine)		
Performic acid-Schiff	Negative	± or + [6]
Performic acid-alcian blue	Negative	Negative [6]
Thioglycollate-ferric ferricyanide	Negative	
Tetrazolium following reduction	Positive	
DDD following reduction (thioglycollate-DDD)	Positive	Positive [6]
Stains for Basophilic Compounds		
Phosphates		
Von Kossa	Negative	Negative [6]
Calcium		
Alizarin red	Negative	
Ferric Ions		
Perl's iron	Negative	

Table 2.—(CONT.)

Method	Present study	Other investigations
DNA		
Feulgen	Negative	Negative [6]
RNA		
Methyl green pyronin	Purple	Pink or Green/Pink [6]
Glycosaminoglycans		
Hale's colloidal iron-binding method	Few positive, most negative	
Periodic acid-Schiff	Usually negative	Negative [6]
Alcian blue (pH 2.5)	Negative	Negative [6]
Lipids		
Unsaturated Lipids		
Sudan black B	Negative	Negative [6]
Triglycerides		
Oil red O	Negative	Negative [6]
Sudan III	Negative	Positive [21], negative [8]
Phospholipids		
Luxol fast blue (copper phthalocyanine)	Usually negative, some globules positive	Negative [6]
Osmium tetroxide-naphthylamine (OTAN)		Positive (red-brown) [6]
Pre-keratin + Keratin		
Hematoxylin-phloxine-alcian blue-orange G	Positive (orange to red)	
Hematoxylin-Shorr S3	Positive	
Performic acid-Schiff	Negative	± or + [6]
Cationic Dyes		
Nuclear fast red	Positive	
Stains for Amyloid		
Congo red	Negative	Negative [6]
Thioflavin T	Negative	Negative [6]
Miscellaneous Stains		
Hematoxylin-eosin	Variable (hematoxyphilic, eosinophilic, or not stain)	Basophilic, eosinophilic or either [6]
Connective Tissue Stains		
Masson's trichrome	Red or purple	Purple, red/purple [6]
Solution A: Ponceau Masson	Red	
Solution B: Masson	Red	
(Mallory's) phosphotungstic acid hematoxylin	Purple	
Wilder's reticulum stain (Wilder silver method)	Black, olive or negative	Negative or fine particulate [6]
Elastic Fiber Stains		
Taenzer-Unna acid orcein	Negative	
Verhoeff Van Gieson (Verhoeff's elastica stain)	Usually negative, some olive or black	
Weigert's Resorcin-Fuchsin (Weigert's elastica stain)	Yellow	
Gomori's aldehyde-fuchsin	Negative	

* Reaction diminished but not completely blocked by prior treatment with dinitrofluorobenzene, performic acid or benzoyl chloride.

predominantly, or entirely intensely, hematoxophilic; in some it was eosinophilic; in other corneas individual granules stained variably. The small basophilic granules often suggested calcification, but this impression was not borne out by histochemical methods for calcium which were invariably negative. Inconsistent tinctorial reactions were also noted with several stains (including elastic fiber stains, Wilder's reticulum stain, luxol fast blue, alcian blue, and Hale's colloidal iron-binding method and some histochemical methods for protein). Though most concretions did not stain with methods used for elastic fibers or Wilder's reticulum method, some concretions were intensely argyrophilic with these techniques (Figure 5). As a rule the abnormal accumulates lacked the histochemical attributes of glycosaminoglycans. However, in several instances they either stained positively with alcian blue and Hale's colloidal iron method, or were intimately surrounded by material possessing this property. The larger, and presumably older, concretions frequently reacted poorly with stains that usually discolored those with smaller dimensions.

In the mildest cases the overlying epithelium was as a rule ostensibly unremarkable, though some cases manifest variations in nuclear size, atypical epithelial cells, and slight deviations in epithelial differentiation. Occasionally the concretions encroached upon the overlying epithelium, and sometimes basal epithelial cells surrounded several of them (Figure 6). Even when numerous concretions were present the epithelium like that of the normal cornea was not keratinized.

Of the 25 globes that were examined, 22 were sectioned horizontally. The subepithelial connective tissue of the bulbar conjunctiva in the interpalpebral fissure adjacent to the corneal limbus in all of these eyes, with corneal concretions, possessed the morphologic characteristics of pingueculae (Figure 8). The conjunctival lesions, though commonly not appearing to the naked eye as elevated yellow patches, were characterized by typical connective tissue alterations. These included variable sized large convoluted fibers that resembled hypertrophic collagen fibers, but which possessed an affinity for a variety of dyes known to stain elastic tissue. These tortuous tangles were insensitive to elastase, and though usually limited to the subepithelial connective tissue of the bulbar conjunctiva, they were occasionally also evident in the superficial subconjunctival sclera, but not in the cornea. The tortuous fibers frequently intermingled with granules and globules possessing the identical morphologic, and tinctorial attributes to those previously described in the contiguous cornea.

Electron microscopy. When viewed in the transmission electron

microscope the concretions were invariably extracellular and electron dense (Figures 9 and 10). The concretions were surrounded by intact collagen fibers of the usual uniform diameter and periodic cross-striational pattern. Most of the overlying corneal epithelium, and adjacent stromal cells, were conspicuously unremarkable (Figures 11-13). As a rule they did not manifest any of the fine structural attributes of cells actively engaged in phagocytosis, or in the synthesis of macromolecules. Their cytoplasm was devoid of material with the morphologic attributes of keratohyalin granules, the extracellular concretions, or possible precursors of them. Some of the closely related cells exhibited features of cellular degeneration, such as intracytoplasmic autophagic vacuoles.

Pingueculae

Random tissue sections of 34 of the 50 consecutive pingueculae studied contained concretions indistinguishable from those described in the keratopathy (Figure 14). In 3 others equivocally similar granules were identified. In 2 of 24 investigated globes with pingueculae, identical concretions were evident in the conjunctival lesions, but not in the cornea.

Cutaneous solar elastosis

The essential morphology and staining characteristics of the 50 consecutive examples of basophilic degeneration of the cutis studied was as described by others.¹⁸⁻²¹ In common with pingueculae, variable sized tortuous fibers were prominent in the altered dermis. These possessed an affinity for those dyes known to stain elastic fibers, but also manifest numerous additional tinctorial attributes that distinguished them from normal elastic or collagen fibers.¹⁸ The fibers were frequently surrounded by material with the cytochemical attributes of glycosaminoglycans. Amorphous homogenous masses that closely resembled the corneal concretions existed in the involved areas of cutaneous elastosis in 42 of the lesions investigated. (Figure 15)

Discussion

Though insufficient tissue for chemical analyses preclude a precise identification of the corneal concretions, their tinctorial and cytochemical attributes provide an indication about certain characteristics. As Garner⁶ recently pointed out in a study of what is probably the identical phenomenon, the cytochemical findings indicate that the abnormal material is probably predominantly proteinaceous with several reactive amino acid groups including tyrosine, tryptophan, arginine, and

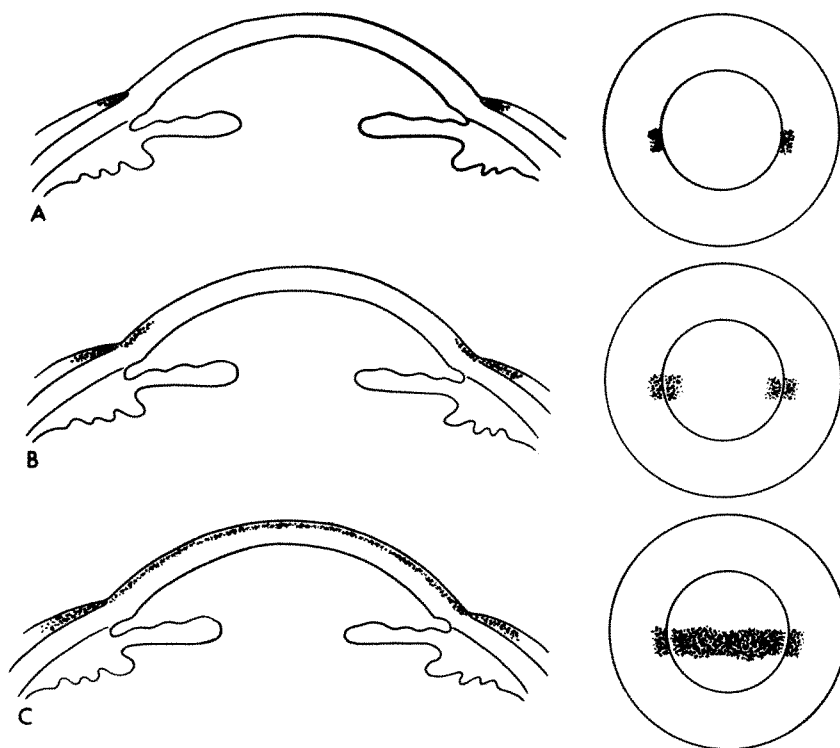
sulphur-containing amino acids. The resemblance of the larger yellow globules to oil droplets has led some clinical ophthalmologists to suspect that the corneal deposits are composed of lipid. This question has not been entirely resolved as the literature contains data on relatively few cases in which the material was analyzed for lipid. Using histochemistry conflicting views have been expressed about the lipid content. In one case unfixed material was reported to be sudanophilic,²² while in others there was no evidence of lipid.^{6,8} In the present investigation the concretions including the yellow ones were insoluble in organic solvents and did not possess an affinity for lipid stains, even when such techniques were performed on unfixed cryostat frozen tissue. Though the avidity of the material for osmic acid in preparation for electron microscopy may connote the presence of some lipid, lipid is clearly not a major component.

As Garner indicated the material is probably an insoluble protein composed in part of amino acids not normally detected in the corneal stroma. Proteins produced by epithelial cells and possessing many disulphide cross links, and a high content of basic amino acids have been designated keratin by some investigators.^{23,24} Viewing the corneal deposits in the light of this all-embracing definition of keratin, Garner⁶ was impressed not only by a composition suggestive of a keratin related protein, but by several observations that led him to suspect that the material might be a product of the corneal epithelium. In the corneal tissue which he studied by light microscopy, the deposits were in close proximity to the epithelium, and in some instances apparently within it. He also noted signs of epithelial disturbance in the form of excessive desquamative activity, individual cell keratinization, and epitheliolysis.

The present study confirms Garner's observation that the corneal concretions have many tinctorial attributes of keratin, but several additional observations cast doubt on his interpretation of the data. The concretions not only lack the birefringence characteristic of keratin, as produced in other locations in man, but were not associated with keratinizing cells. In most cases and particularly in the mildest, which are presumably also the earliest, the epithelium was ostensibly devoid of similar material. Corneal epithelial keratinization was not observed, even when the stromal deposits were abundant, and in some instances the deposits were a considerable distance from the overlying epithelium. Moreover, the cytoplasm of the overlying corneal epithelium of the cases studied by electron microscopy lacked keratohyalin granules, as well as material with the ultrastructural attributes of the extracellular concretions.

Certain observations raise the possibility that the concretions are not synthesized in the cornea, nor formed there by the degradation of formed components: morphologic evidence of concretion synthesis by either corneal epithelial or stromal cells was not detected; histochemical evidence indicates that the concretions contain a high content of amino acids not normally detectable in the cornea. It would seem more likely that the abnormal corneal deposits are derived from tissue other than the cornea. A likely site of their origin can be inferred from observations on eyes with variable quantities of them. In the mildest examples of the keratopathy, which presumably reflect an early stage in the genesis of the condition, the deposits are restricted to the superficial peripheral cornea in the interpalpebral fissure. This finding together with the observation of the co-existence of corneal lesions with conjunctival elastosis containing identical concretions, and the occasional detection of the concretions in pingueculae of eyes that do not have them in the adjacent cornea, strongly suggests that the abnormal material arises in the pericorneal conjunctival connective tissue. One is led to suspect that they progressively diffuse into the superficial cornea, and precipitate in it over a prolonged period of time, with the larger globules forming by the coalescence of minute granules (Text-figure 1). This perception is consistent with clinical observations on individuals with variable degrees of keratopathy. Frequently the earliest clinically detectable deposits involve only the medial and lateral portions of the cornea in the interpalpebral strip, with subsequent progression occurring by centripetal extension across the cornea. Parenthetically, it should be stressed that the peripheral cornea has not been examined microscopically in those few instances in which it appeared to be clear clinically, and one might suspect that the smaller deposits may be of insufficient dimension to be observed with the slit lamp.

Though relatively few corneal concretions stain positively with dyes that demonstrate elastic tissue, the co-existence of the corneal concretions with conjunctival elastosis poses the question of whether the concretions are derived from constituents of the elastotic material. The nature of the latter substance is not entirely settled, but it is thought to contain derivatives of both collagen and elastic tissue. It is of interest that these elastic fibers are not normally present in the cornea. Moreover, elastic fibers like the elastotic material, and some of the concretions exhibit a brilliant autofluorescence when viewed by fluorescence microscopy.^{25,26} Ultrastructural observations of elastic fibers have revealed two components—a microfibril (110 Å in diameter) and an amorphous component (elastin).²⁷⁻²⁹ Elastin is markedly insoluble, resistant to hydrolysis by mild acid and alkali, and demonstrates a selec-



TEXT-FIG 1—The inferred sequence of events in the genesis of the keratopathy is depicted schematically. It is postulated that the earliest concretions occur in the exposed interpalpebral portion of the pericorneal conjunctival connective tissue (A) and that these progressively diffuse into the adjacent cornea where they precipitate in the superficial cornea (B). In advanced cases they extend across the entire cornea (C).

tive susceptibility to elastase digestion, and consists of a unique combination of amino acids, including two special amino acids—desmosine and its isomer isodesmosine. Though it contains very little cystine, this amino acid is present in large quantities in the microfibrillary protein component.^{29,30}

At present the cause of this unique corneal reaction remains speculative. It is axiomatic that all tissues, including the cornea possess limited responses to noxious stimuli and one would anticipate that this reaction could be provoked by several factors. Unlike several other corneal diseases in which abnormal materials accumulate in the cornea, there is almost no evidence to suggest that the primary defect resides in the DNA molecule, and that the lesions are the culmination of a genetically controlled chain of biochemical events. Ultraviolet light possessing wave lengths of less than 295 m μ are known to be almost entirely absorbed by the cornea, and in short term experiments, single

or multiple exposures to ultraviolet light have a detrimental effect on the cornea, particularly its epithelium.³¹⁻³³ Though the keratopathy discussed in the present report is clearly different from that produced by acute ultraviolet irradiation, several epidemiologic and morphologic observations strongly suggest that actinic irradiation over a prolonged period of time may be an important cause of it. At least 22 of the 35 cases had morphologically confirmed evidence of other probable sun induced lesions such as pingueculae, and cutaneous basal cell carcinomas of the face.^{34,35} Five patients in the present series were exposed to abundant solar irradiation because of an outdoor occupation (Cases 7, 11, 12, 17, 19) and the remainder certainly had the opportunity to spend abundant leisure time outdoors in the sun-exposed southeastern United States. Though the geographic areas prone to the type of keratopathy discussed in the present article differ climatically, abundant sunshine is prevalent in them, and their inhabitants have in common the potentiality for excessive exposure to radiant energy from the sun. The male preponderance can be accounted for, at least in part, by outdoor occupations that expose individuals to excessive ultraviolet light, known to be reflected by sun, desert, and water. A causal relationship to the absorption of radiant energy from the sun would also account for the predisposition for the exposed portion of the eye in the interpalpebral fissure, and their usual bilaterality. Moreover, as the condition is not related to aging alone, its increased incidence with advancing years may reflect an increase in time of solar exposure.

Not only was the keratopathy associated with morphologic evidence of conjunctival elastosis (pingueculae) in the same eye, but concretions indistinguishable from those of the keratopathy existed in the associated pingueculae. Similar concretions were also identified in a high percentage of other pingueculae, and in the morphologically, and probably etiologically analogous actinic elastosis of the skin. In the absence of x-irradiation, there is abundant evidence that basophilic degeneration of the cutis (solar elastosis, actinic elastosis) is due to prolonged exposure to sunlight.^{36,37} It is limited to parts of the body customarily exposed to solar irradiation, the degree of change is greatest in sites that receive the most intense and prolonged exposure to sunlight, and it is less evident in heavily pigmented skin. In addition these changes have been produced experimentally with ultraviolet light.³⁸

As the corneal deposits are occasionally unilateral and may accompany other ocular diseases, it remains an open question whether this corneal reaction can be provoked by other stimuli. Nevertheless, almost all instances of the keratopathy included in the present study are con-

sistent with the hypothesis that they are secondary to exposure to ultraviolet light over a prolonged period of time. Associated lesions are variable and dissimilar, and many are probably coincidental. In some an impaired blink reflex protective mechanism may have exposed the eye to excessive ultraviolet light and dessication.

The possibility of the keratopathy being causally related to ultraviolet light poses the question of how actinic rays could produce the concretions. Does the irradiation result in an alteration of preexisting structural components of connective tissue, or on the other hand does it provoke a cellular synthesis of abnormal extracellular constituents? One of the primary effects of ultraviolet light on protein is the cleavage of disulfide bonds,³⁹ and one might wonder whether the apparent increase in histochemically detectable thiol groups might be due to an effect on non-corneal proteins such as those of elastic tissue.

References

1. Alamjo A: Su di una forma non comune di degenerazione corneale. *Rass Ital Ottalmol* 22:26-34, 1953
2. Bietti GB, Guerra P, Ferraris de Gaspare PF: La dystrophie cornéene nodulaire en ceinture des pays tropicaux à le sol aride. *Bull Soc Ophtalmol Fr* 68:101-129, 1955
3. Falcone G: La distrofia corneale dei tropici. *Rav Ital Tracoma* 6:3-17, 1954
4. Freedman A: Labrador keratopathy. *Arch Ophthalmol* 74:198-202, 1965
5. Gandolfi A: Osservazioni di distrofia corneale nodulare a bandellata dei paesi tropicali a suolo arido in Cirenaica (Libia). *Bull Oculist* 41:129-134, 1962
6. Garner A: Keratinoid corneal degeneration. *Br J Ophthalmol* 54:769-780, 1970
7. Kozłowski B: A peculiar form of hyaloid degeneration of the cornea. *Klin Oczna* 23:249-253, 1953
8. Lugli L: Degeneratio corneae sphaerularis elaioides. v Graefes *Arch Ophthalmol* 134:211-226, 1935
9. Puglisi-Duranti G: Sulla degenerazione sferulare elaioides della cornea. *Rass Ital Ottalmol* 4:752-766, 1935
10. Sugar HS, Kobernick S: The white limbus girdle of Vogt. *Am J Ophthalmol* 50:101-107, 1960
11. Barka T, Anderson PJ: *Histochemistry: Theory, Practice, and Bibliography*. New York, Evanston and London, Harper and Row, Publishers, Inc, Hoeber Medical Division, 1963
12. Dane ET, Herman DL: Hematoxylin-phloxine-alcian blue-orange G differential staining of pre-keratin, keratin, and mucin. *Stain Technol* 38:97-101, 1963
13. Lillie RD: *Histopathologic Technic and Practical Histochemistry*, Third edition. New York, Toronto, Sydney and London, McGraw-Hill Book Company, The Blakiston Division, 1965

14. Page WG, Green RG: An improved diagnostic stain for distemper inclusions. *Cornell Vet* 32:265-268, 1942
15. Pearse AGE: *Histochemistry: Theoretical and Applied*, Second edition. Boston, Little, Brown and Company, 1961
16. Tzitsikas H, Rdzok EJ, Vatter AE: Staining procedures for ultrathin sections of tissues embedded in polyester resin. *Stain Technol* 36:355-359, 1961
17. Reynolds ES: The use of lead citrate at high pH as an electron-opaque stain in electron microscopy. *J Cell Biol* 17:208-212, 1963
18. Gillman T, Penn J, Brooks D, Roux M: Abnormal elastic fibers—appearance in cutaneous carcinoma, irradiation injuries, and arterial and other degenerative connective tissue lesions in man. *Arch Pathol* 59:733-749, 1955
19. Percival GH, Hannay PW, and Duthie DA: Fibrous changes in the dermis, with special reference to senile elastosis. *Br J Dermatol* 61:269-276, 1949
20. Sams WM Jr, Smith JG Jr: The histochemistry of chronically sun-damaged skin: an investigation of mucopolysaccharides and basophilia in actinically damaged skin using Alcian Blue, Mowry's and Hicks-Matthaei stains, methylation, and saponification. *J Invest Dermatol* 37:447-453, 1961
21. Unna PG: *The Histopathology of the Diseases of the Skin*. Translated by N Walker. Edinburgh, William F. Clay, 1896
22. Volpi U, Serra A: Contributo alla conoscenza della degenerazione sferulare elaiioidea della cornea. *Ann Ottalmol* 93:1305-1310, 1967
23. Mercer EH: *Keratin and Keratinization. An Essay in Molecular Biology*. Oxford, Pergamon Press Ltd, 1961
24. Mercer EH, Munger BL, Rogers GE, Roth SI: A suggested nomenclature for fine-structural components of keratin and keratin-like products of cells. *Nature (Lond)* 201:367-368, 1964
25. Cohen AS, Hashimoto K: Electron microscopic observations on the lesion of elastosis perforans serpiginosa. *J Invest Dermatol* 35:15-20, 1960
26. Vassar PS, Culling CFA: Fluorescent stains with special reference to amyloid and connective tissues. *Arch Pathol* 68:487-498, 1959
27. Greenlee TK, Ross R, Hartman JL: The fine structure of elastic fibers. *J Cell Biol* 30:59-71, 1966
28. Ross R, Bornstein P: The elastic fiber. I. The separation and partial characterization of macromolecular components. *J Cell Biol* 40:333-381, 1969
29. Ross R, Bornstein P: Elastic fibers in the body. *Sci Am* 224:44-52, 1971
30. Thomas J, Elsdon DF, Partridge SM: Partial structure of two major degradation products from the cross linkages in elastin. *Nature (Lond)* 200:651-652, 1963
31. Buschke W, Friedenwald JS, and Moses SG: Effect of ultraviolet irradiation on corneal epithelium: mitosis, nuclear fragmentation, post-traumatic cell movements, loss of tissue cohesion. *J Cell Physiol* 26:147-164, 1945
32. Cogan DG, Kinsey VE: Action spectrum of keratitis produced by ultraviolet radiation. *Arch Ophthalmol* 35:670-677, 1946
33. Duke-Elder WS, Duke-Elder PM: A histological study on the action of short-waved light upon the eye, with a note on "inclusion bodies." *Br J Ophthalmol* 13:1-37, 1929
34. Hogan MJ, Alvarado J: Pterygium and pinguecula: electron microscopic study. *Arch Ophthalmol* 78:174-186, 1967

35. Gellin GA, Kopf AW, Garfinkel L: Basal cell epithelioma: a controlled study of associated factors. *Arch Dermatol* 91:38-45, 1965
36. Cockerell EG, Freeman RG, Knox JM: Changes after prolonged exposure to sunlight: a study of factors influencing actinic degeneration. *Arch Dermatol* 84:467-472, 1961
37. Lund HZ, Sommerville RL: Basophilic degeneration of the cutis: data substantiating its relation to prolonged solar exposure. *Am J Clin Pathol* 27:183-190, 1957
38. Sams WM Jr, Smith JG Jr, Burk PG: The experimental production of elastosis with ultraviolet light. *J Invest Dermatol* 43:467-471, 1964
39. Jagger J: *Introduction to Research in Ultraviolet Photobiology*. Englewood Cliffs, NJ, Prentice-Hall, Inc, pp 102-107, 1967

Acknowledgments

The author wishes to acknowledge the assistance of Mr. Bernard Lloyd and Mr. Leonard W. Noble (technical aid) and Mr. Carl Bishop (photography).

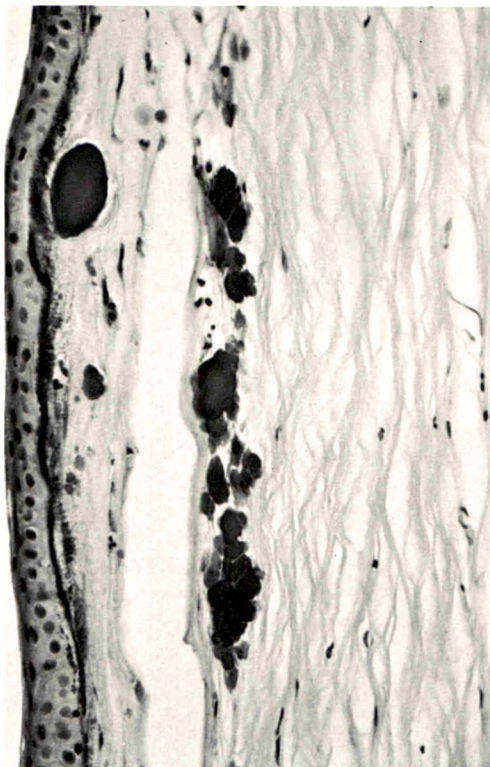
Legends for Figures

Fig 1—Numerous concretions of variable shape and size are shown in the superficial corneal stroma (H&E, $\times 228$).

Fig 2—A more extensive accumulation of the abnormal material is evident in the anterior portion of this cornea from a patient who had an opaque cornea for many years (Masson's trichrome stain, $\times 190$).

Fig 3—The larger deposits are sometimes evident in unstained sections of the cornea because of a distinct yellow hue (unstained preparations, $\times 112$).

Fig 4—Yellow and colorless concretions frequently manifest autofluorescence when viewed in ultraviolet or blue violet light (unstained preparation, $\times 102$).



1



2



3



4

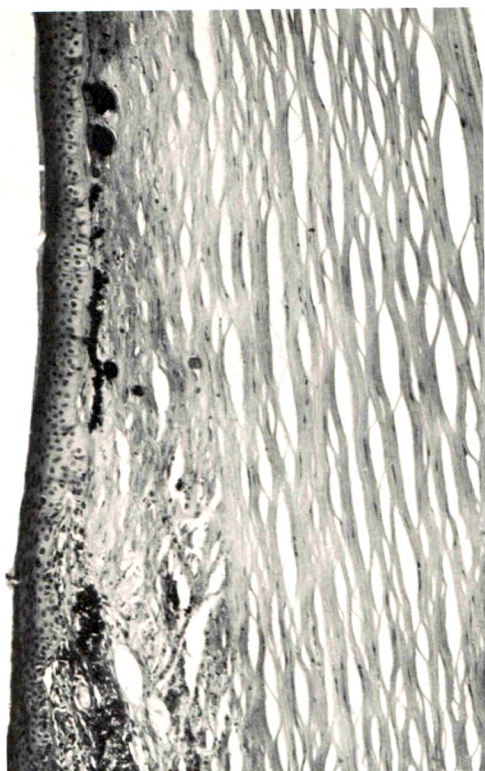
Fig 5—Though most of the corneal deposits lack an affinity for stains used to demonstrate elastic tissue, some do, such as these (Verhoeff–Van Gieson stain, $\times 100$).

Fig 6—The corneal deposits are frequently in close proximity to the corneal epithelium (Masson's trichrome stain, $\times 200$).

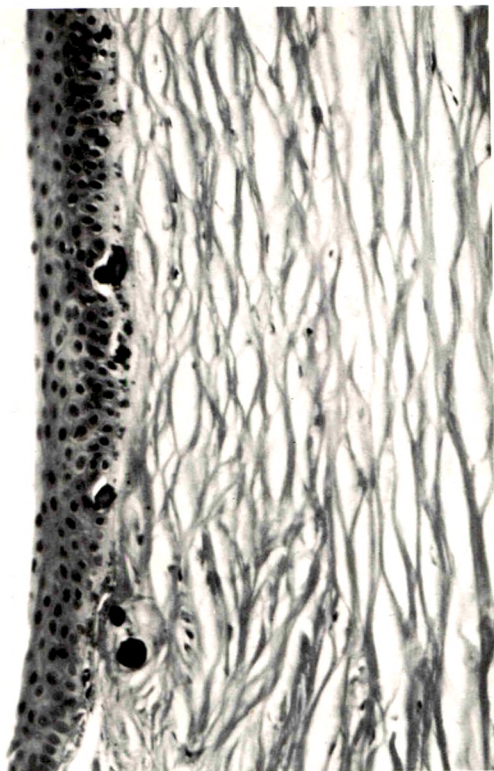
Fig 7—In some instances the corneal concretions, though in the superficial cornea, are distinctly separated from the overlying epithelium (Masson's trichrome stain, $\times 300$).

Fig 8—At the limbus corneae of eyes containing corneal concretions, tangles of argyrophilic fibers can be demonstrated in the horizontal plane using stains that demonstrate elastic fibers (Verhoeff–Van Gieson, $\times 152$).

5



6



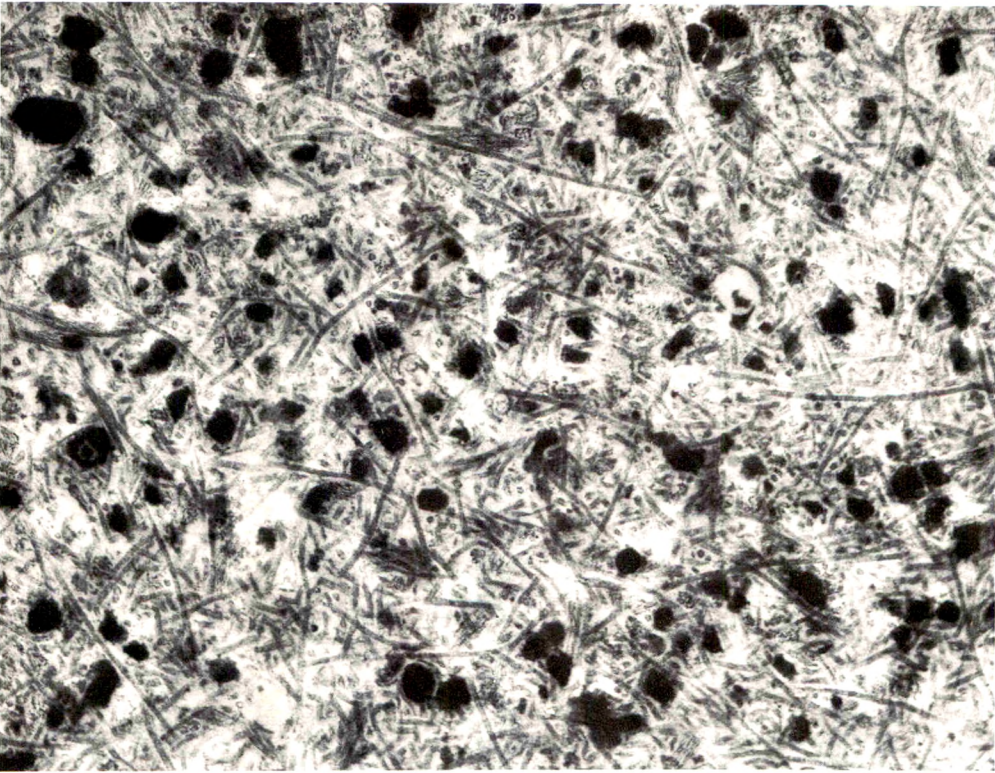
7



8



9



10

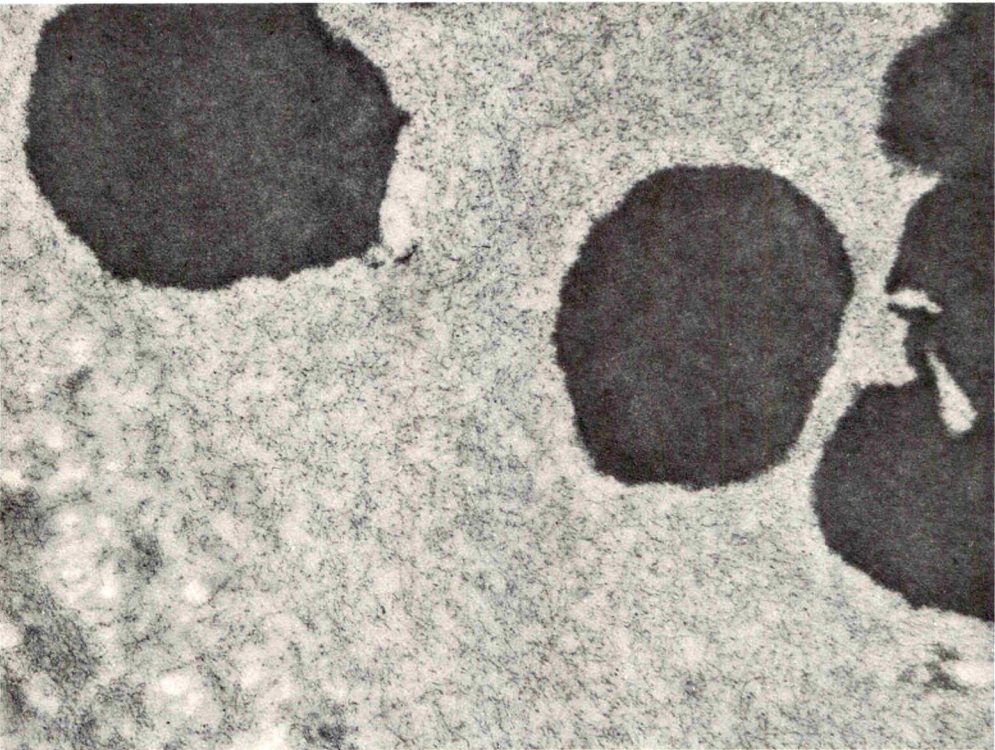
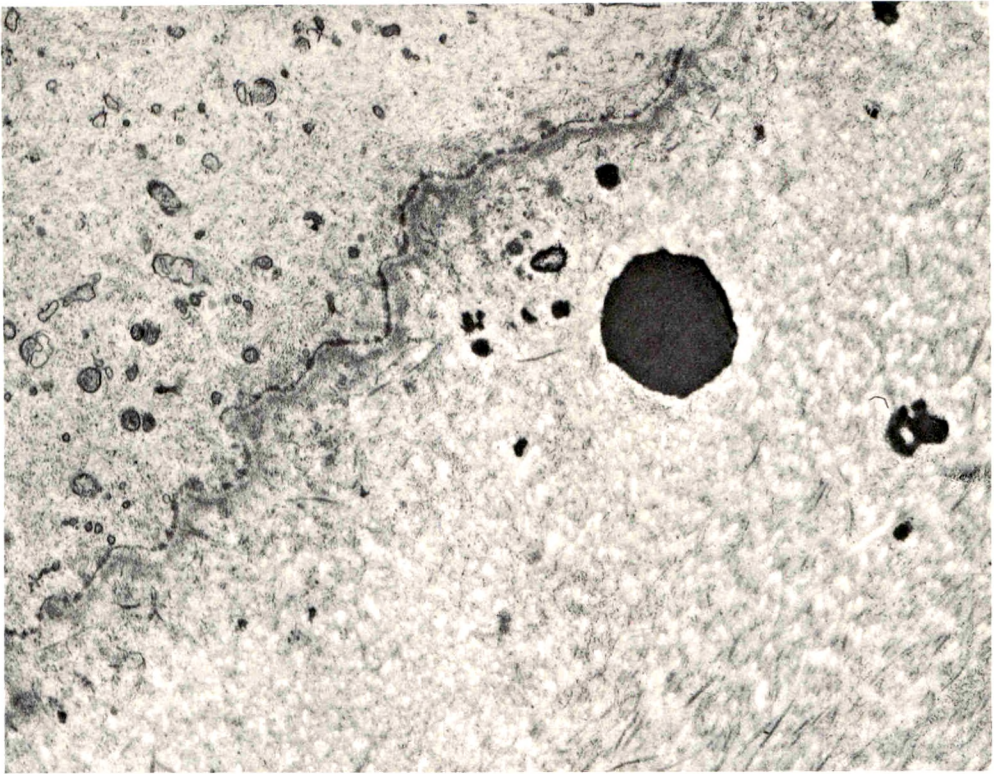
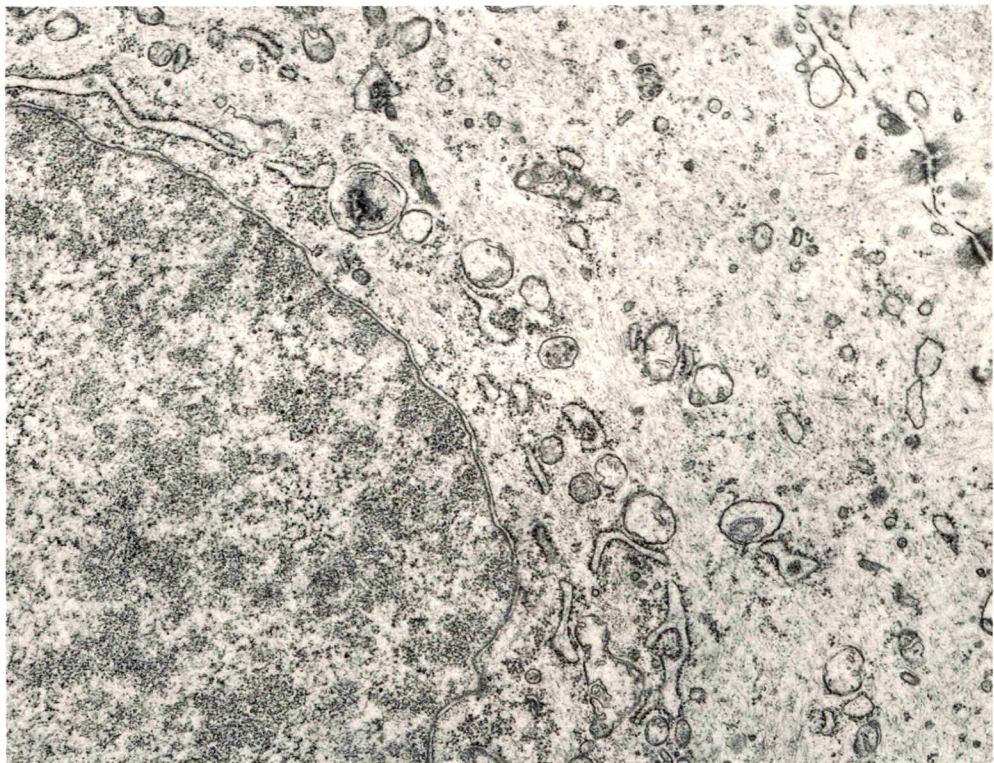


Fig 9—Numerous irregularly shaped electron-dense deposits are interspersed between the haphazardly arranged collagen fibers in Bowman's zone of this affected cornea ($\times 24,000$).
Fig 10—The extracellular deposits are markedly electron dense and are often surrounded by delicate microfibrils ($\times 44,500$).



11

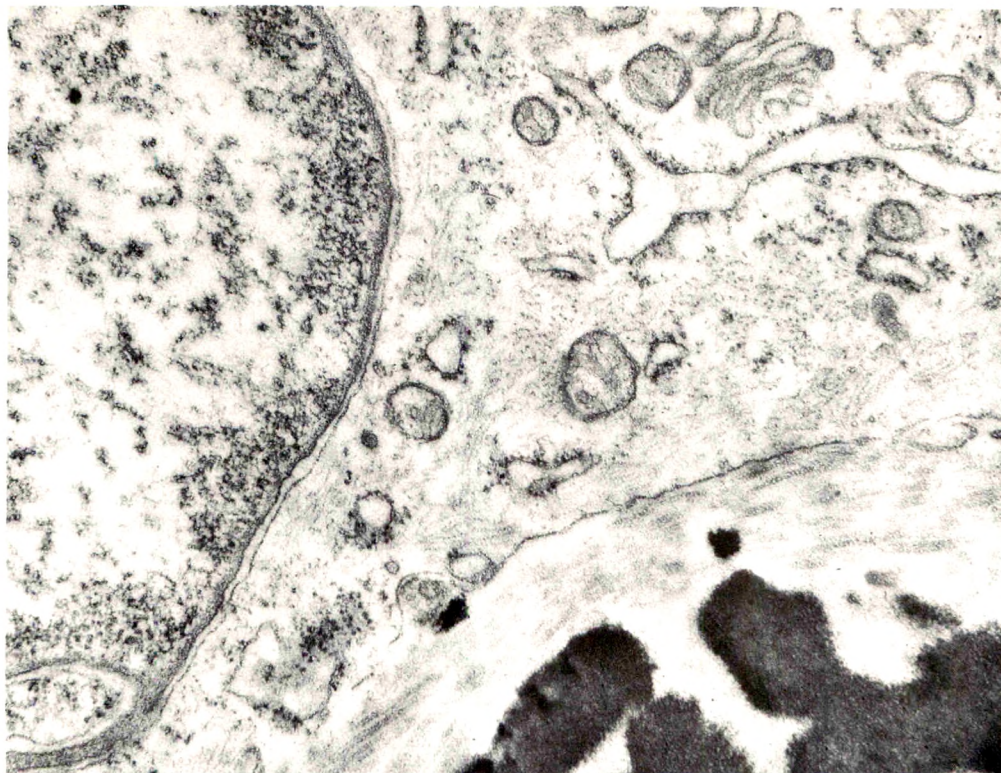


12

Fig 11—The corneal epithelium adjacent to the deposits lacks electron-dense material ($\times 17,000$).

Fig 12—The overlying corneal epithelium is usually unremarkable. Significant negative features include the lack of intracellular electron-dense material resembling the concretions and the absence of morphologic evidence of synthetic activity. ($\times 16,500$).

13



14



15

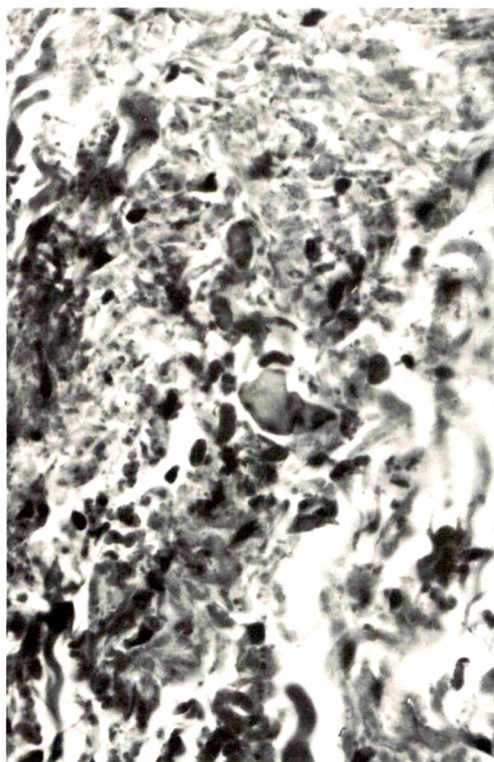


Fig 13—Like the corneal epithelium, shown in Fig 12, the corneal fibroblasts (keratocytes) usually show no significant abnormality, even when adjacent to extracellular concretions ($\times 43,000$). **Fig 14**—Concretions, such as these, which closely resemble those of the cornea in morphology and staining characteristics were observed in the conjunctival elastosis of eyes with the keratopathy and in numerous other pingueculae (Masson's trichrome, $\times 100$). **Fig 15**—Aside from the cornea and conjunctiva, similar concretions were identified in numerous examples of cutaneous actinic elastosis (Masson's trichrome, $\times 470$).

Inhibition of Macrophage Response to Brain Injury

A New Effect of Pertussis Vaccine Possibly Related to Histamine-Sensitizing Factor

Seymour Levine, MD and Richard Sowinski, BS

Intravenous injection of pertussis vaccine inhibited the outpouring of macrophages into a zone of thermal coagulation necrosis in the brain. The inhibition of this cellular reaction to injury was observed in rats and mice, and was especially notable in gerbils. It was not due to nonspecific stress or to endotoxin. A relationship of this new activity to pertussis vaccine's histamine-sensitizing factor was suggested by the use of partially purified extracts and heat-inactivated vaccines. There was a close parallel between the effects of pertussis vaccine on brain macrophages and on the spleen (Am J Pathol 67:349-360, 1972).

PERTUSSIS VACCINE has numerous and diverse effects on rats and mice. It causes leukocytosis and increased susceptibility to histamine and serotonin and to induction of autoimmune diseases.^{1,2} While studying the latter effects of pertussis vaccine, we noted impairment of the macrophage response to brain injury. Our data indicate that this new phenomenon is not caused by nonspecific stress or endotoxin, but may be related to histamine-sensitizing factor (HSF), a unique, biologically active constituent of *Bordetella pertussis* organisms.

Materials and Methods

Rats, 170 to 350 g in weight, were of Wistar (Hemlock Farms), Lewis, Fischer 344 or LxBN strains (Microbiological Associates). Mongolian gerbils, 60 to 70 g in weight were from Tumblebrook Farms, Brant Lake, NY. Swiss-Webster mice, 22 to 35 g weight, were from Hemlock Hollow Farms. All animals were male and were maintained on Purina Laboratory Chow and tap water *ad libitum*. Under ether anesthesia, a large thermal brain injury was produced through the intact skull after the skull was exposed by a midline scalp incision.³ A preheated 37½ watt pyramid-tip electric soldering iron was applied for 7 seconds with moderate pressure to the rat calvaria behind the bregma and to the right of the midline. A smaller, flat tip, 3/16 inch chisel type, was applied for 5 seconds to gerbils and 3 seconds to mice.

Pertussis vaccine was a formalin-killed merthiolate-preserved concentrate that contained about 2×10^{11} organisms/ml. It was injected into the dorsal penile vein, usually 0.05 ml/100g in rats, 0.05 ml per gerbil and 0.025 ml per mouse.

From the Pathology Department, New York Medical College Center for Chronic Disease, Bird S. Coler Hospital, Welfare Island, New York, New York.

Supported wholly by Grant 536C12 from the National Multiple Sclerosis Society.

Accepted for publication Nov 15, 1971.

Address reprint requests to Dr. Seymour Levine, Pathology Department, New York Medical College Center for Chronic Disease, Bird S. Coler Hospital, Welfare Island, New York, NY 10017.

The animals were killed 3 or occasionally 4 days after brain injury by exsanguination under ether anesthesia. The skull was unroofed, and the brain fixed *in situ* in Bouin's fluid in order to minimize artifactual displacement and loss of the softened necrotic area. Spleen and four coronal slices of brain, including the entire lesion, were embedded in paraffin, sectioned and stained with periodic acid-Schiff-hematoxylin. Slides were randomized and scored without knowledge of group of origin. Animals that died were not studied.

Adrenalectomy was done 2 or 3 days before thermal brain injury through incisions in the dorsal midline skin and lumbar muscles. Sole drinking fluid thereafter was 1% NaCl.

Results

As previously reported,³ the burn caused a large zone of coagulation necrosis in cerebral cortex and subjacent structures. Three days after the injury, rats had abundant macrophages and some capillaries in the necrotic zone (Figure 1). Macrophages had eccentric nuclei and abundant cytoplasm filled with vacuoles and periodic acid-Schiff-positive material. They were most numerous just beneath the pia mater at the edge of the lesion, but others were distributed irregularly along the remainder of the perimeter. Macrophages were more numerous at later times, but alterations in number were more easily detected at 3 days.

Intravenous injection of pertussis vaccine immediately after burning the brain of rats caused a notable decrease in the number of phagocytes detected 3 days later (Table 1). The inhibition was detected most readily where macrophages were most numerous, that is, at the junction of the pia and the perimeter of the lesion. In this area, there was a reduction to $\frac{1}{2}$, $\frac{1}{4}$ or less of the normal numbers (Figure 2). Cell counts were not attempted because of the large number of macrophages and because of their irregular distribution. Although evaluation was subjective, it was always possible to identify pertussis-treated rats by reading randomized slides "blind."

Subcutaneous injection of the same dose of pertussis vaccine had no inhibitory effect. Also, this route is known to be ineffective for the production of other pertussis effects.⁴

Intravenous pertussis vaccine is known to be stressful and to cause liberation of adrenal steroids,^{5,6} and steroids are known to interfere with macrophage accumulation.⁷ However, there was an undiminished inhibitory effect when pertussis vaccine was injected intravenously into adrenalectomized rats (Table 1). Because intravenous pertussis vaccine is often lethal to adrenalectomized animals, these rats were protected with one or two small doses of dexamethasone (5 γ /100g) intraperitoneally. Neither adrenalectomy nor the small amount of adrenocorticoid, of themselves, influenced the macrophage response to brain injury.

Table 1—Inhibition of Rat Brain Macrophages by Pertussis Vaccine is not Due to Stress or Endotoxin

Pretreatment	Inhibitor (IV)*	Inhibition of macrophages†
Adrenalectomy‡	Pertussis	8/8
	56°-pertussis	6/6
	80°-pertussis	0/6
	<i>E coli</i> endotoxin	0/3
	Saline	0/7
None	Pertussis	17/17
	56°-pertussis	2/2
	80°-pertussis	0/6
	<i>E coli</i> endotoxin	0/5
	Saline or none	0/14

* Composite of 6 experiments. All endotoxin and some pertussis injections given on day of thermal injury; all others 1 day earlier.

† Numerator, number with marked reduction of brain macrophages 3 days after thermal injury. Denominator, total number of rats.

‡ A small amount of dexamethasone (5γ/100g, intraperitoneally, on day before and/or day of thermal injury) was given to all adrenalectomized rats to reduce mortality. It did not affect brain macrophages.

|| Heated 30 minutes at 56°C (destroys heat-labile toxin but not HSF) or 80°C (destroys HSF but not endotoxin).

Therefore, the undiminished effect of pertussis vaccine in adrenalectomized dexamethasone-treated rats excluded the possibility of an adrenal-mediated mechanism.

Pertussis organisms are gram-negative bacilli and contain endotoxin. The possibility that the inhibitory phenomenon was caused by endotoxin was excluded in several ways (Table 1). Many endotoxin effects are transient and are dissipated in 1 day.⁸ Nevertheless, pertussis vaccine inhibited brain macrophages when given 1 day *before* thermal injury (Table 1) or even 4 days before (3 rats not included in Table 1). Furthermore, 0.2 mg purified endotoxin from *E coli* 026:B6 (Difco) injected intravenously on the day of thermal injury had no inhibitory effect. Most important, the inhibitory effect of pertussis vaccine was destroyed by heating the vaccine to 80° for 30 minutes, while endotoxin is known to be heat stable. Parenthetically, inhibition persisted despite heating the vaccine to 56°C for 30 minutes, which eliminates pertussis' heat-labile toxin as a factor in these experiments.

These thermal resistance data correspond to the well-known characteristics of HSF.^{1,2} Through the kindness of Dr. J. Munoz, we obtained specimens of partially purified HSF.⁹ Each proved to be capable of inhibiting brain macrophages after intravenous injection. Titration

of these materials (Table 2) did not show a very high specific activity compared to whole cell vaccines, a fact which may be due to their relatively insoluble nature.¹ The most potent product was fully effective at the lowest dose tested (25 γ /rat), but the supply was exhausted before this relatively high specific activity could be confirmed. It should be noted that these preparations are not likely to contain endotoxin¹ and, as an added precaution, they were injected 1 day before the thermal injury.

Inhibition in Other Rodents

It was of particular interest to compare the new inhibitory phenomenon in rats and mice because both species are responsive to other pertussis effects, but normal mice have less macrophage response to thermal injury than rats.³ In fact, the paucity of response in mice made it difficult to detect inhibition. Nevertheless, a reasonably consistent, albeit small, inhibition was observed in 3 different experiments and 3 different strains of mice. Only one "false positive" and four "false negative" readings were made among the 39 mice of Table 3. Therefore, the inhibition by pertussis was not restricted to the exuberant macrophage reaction of rats.

Gerbils have a macrophage response only slightly less than that of

Table 2—Partially Purified HSF Inhibits Rat Brain Macrophages

Inhibitor	Dose/rat*	Inhibition of macrophages
MgSO ₄ precipitated	0.4 mg	4/4
HSF	0.1	2/4
	0.025	0/4
1M NaCl extract of	0.4	3/3
MgSO ₄ precipitate	0.1	5/5
	0.025	0/5
	0.006	0/5
1M NaCl extract of	0.4	1/1
MgSO ₄ precipitate	0.1	1/1
	0.025	3/3
Vaccine concentrate 1	0.1 ml	4/4
	0.025	1/3
	0.006	0/3
Vaccine concentrate 2	0.1	5/5
	0.025	2/5
	0.006	0/5

* These doses were chosen because 0.1 ml of the vaccine concentrates contain approximately 0.4 mg dry weight of pertussis organisms. This permits a rough comparison between vaccine and HSF. All injections 1 day before thermal injury by IV route. Composite results of three experiments.

rats.³ The inhibition of gerbil macrophages by pertussis was particularly striking. This nearly total inhibition suggested that this species may be of great value for further investigation. Endotoxin was not responsible for the results in gerbils and mice because all injections were done 1 day before thermal injury, and because there was no inhibition from vaccine that had been heated to 80°C to destroy HSF (Table 3).

Attempted Reversal of Pertussis Effect

In an effort to overcome the inhibition of brain macrophages, 4 Lewis rats were given normal spleen cells within 3 hours after inflicting the thermal brain injury and 24 hours after intravenous injection of pertussis vaccine. The spleen cells were prepared by mincing and sieving 3 normal Lewis spleens for each recipient, and washing three times in saline. The recipient rats were killed 3 days later. However, their brain macrophage response was inhibited to the same degree as 3 control rats that were similarly treated except for saline in place of spleen cells.

This failure might be due to a residual effect of pertussis organisms on the transfused spleen cells. In an effort to provide a more continuous supply of macrophage progenitors, eight pairs of Lewis rats were united in parabiosis.¹⁰ Two weeks later, the *left* partners, as well as normal control animals, were given pertussis vaccine or saline intravenously. On the next day, thermal brain injuries were induced in both partners of all pairs and in controls. Before sacrifice 3 days later, the presence of a cross-circulation was proven by intravenous injection of 5ml 0.5% trypan blue into the right partner and observing coloration of the left partner. Histological examination revealed abundant brain macrophages in normal controls, in *both* partners of saline inoculated

Table 3—Pertussis Vaccine Inhibits Brain Macrophages in Mice and Gerbils

Animal	Inhibitor (IV)	Inhibition of macrophages*
BSVS mice	Pertussis	5/5
	None	1/6
BRVR mice	Pertussis	3/5
	None	0/6
Swiss-Webster mice	Pertussis	6/8
	80°C-pertussis*	0/3
	Saline	0/6
Gerbils	Pertussis	11/11
	80°C-pertussis	0/2
	Saline	0/7

* As in Table 1. All injections 1 day before thermal injury; composite results of three experiments

parabionts, and in the uninoculated *right* partner of pertussis injected parabionts. This last observation indicated that parabiotic cross-circulation did not carry sufficient pertussis organisms from the inoculated left partner to inhibit the macrophage response of the right partner. The pertussis-inoculated left partner exhibited the expected inhibition of macrophage response; however, the degree of inhibition was not as great as that observed in the normal controls. This could be interpreted as a partial reversal of the pertussis effect by macrophages or their progenitors derived from the right partner. However, it is possible that the attenuation of inhibition in the left partner was caused by loss of pertussis vaccine through the cross-circulation, even though the amount transferred was not sufficient to inhibit the macrophages of the right partner. Therefore, the parabiotic data only suggest but do not prove that the pertussis inhibition can be reversed by normal hematogenous cells.

Effects of Pertussis Vaccine on the Spleen

In rats, intravenous pertussis vaccine caused marked hyperplasia of the red pulp with blurring of the normally clear demarcation from the perifollicular sheath. Depletion of small lymphocytes in the Malpighian corpuscles was observed, and sometimes increased extramedullary hematopoiesis and neutrophils in the red pulp. It was of particular interest that these same splenic changes were observed after partially purified HSF was administered, and the degree of hyperplasia of red pulp was proportional to the dose of HSF. The spleen was altered in a similar manner after the whole vaccine had been injected unheated or heated to 56°C into intact or adrenalectomized rats. On the other hand, these changes were not detected after injection of vaccine heated to 80°C, in intact or in adrenalectomized rats, or after subcutaneous injection of unheated vaccine. In all respects, then, splenic changes paralleled the inhibition of brain macrophages.

Similar changes in the spleen were seen in mice and gerbils, but were less prominent and consistent in the former and much more extensive in the latter. These observations, also, were in close accord with inhibition of brain macrophages.

Changes in the spleen caused by pertussis vaccine have been recorded by others,^{4,11,12} but we have not found previous data in the literature that establishes the close relationship between splenic changes and HSF, their independence of the adrenal gland and the variable degree to which they occur in other rodents.

Discussion

The data clearly exclude endotoxin and adrenal-mediated nonspecific stress effects from the pathogenesis of the pertussis inhibition of brain macrophages. Nevertheless, there is no doubt that injections of adrenal steroid or transplants of an ACTH-secreting pituitary tumor can inhibit macrophage accumulation around brain wounds.^{7,13} In addition to steroids, cytotoxic and antimitotic drugs could be expected to inhibit the macrophage response. We tested cyclophosphamide (125mg/kg intraperitoneally) and triethylenemelamine (1 mg/kg intravenously) on the day of thermal injury or one day before. Both agents reduced the number of macrophages observed 3 days after injury, often to a greater degree than pertussis vaccine. However, the devastation of bone marrow and spleen by the cytotoxic drugs indicated an entirely different mechanism.

The fact that an inhibitory effect on brain macrophages can be achieved by steroids or cytotoxic drugs does not diminish the great interest in establishing the mechanism of the pertussis effect. There is no definite relation of this new phenomenon to the heterogeneous group of encephalopathies that follow pertussis infection or vaccination in children; however, one might speculate on potential harmful effects of a lack of brain macrophages or of macrophage products (interferon, complement components, lysosomal enzymes). Nor is there any obvious relation to pertussis effects on animals, most of which involve an increase or enhancement of one or another parameter: antibody titers, enzyme levels, white blood cell counts, anaphylaxis, autoimmune diseases, etc. Indeed, the *suppressive* effect described herein might seem paradoxical. However, inhibitory effects of pertussis or its fractions have been reported on occasion: antibody production in one instance¹⁴ and slight reduction of passive cutaneous anaphylaxis.¹⁵ Because brain macrophages are probably derived from the reticuloendothelial system, it is particularly pertinent to note a reduction in a detoxifying function of this system reported to be caused by pertussis vaccine.¹⁶ This functional deficiency might be related to the prominent effects of pertussis on the spleen described above, which paralleled so closely the inhibition of brain macrophages. Although our data on heat lability and on partially purified extracts suggest that HSF was the active component of pertussis vaccine, we are unable to make correlations with HSF effects that involve histamine, serotonin or beta-adrenergic receptors.^{1,2} However, Morse and Barron¹⁷ and Iwasa *et al*¹⁸ have shown that pertussis vaccine interferes with emigration of lymphocytes from the blood. The present results could be explained if a similar inhibition of migration

affects the progenitors of brain macrophages (presumably blood monocytes,¹⁹ but possibly a subclass of blood lymphocytes, as well²⁰).

References

1. Munoz J, Bergman RK: Histamine-sensitizing factors from microbial agents, with special reference to *Bordetella pertussis*. *Bacteriol Rev* 32:103-126, 1968
2. Munoz J: Protein toxins from *Bordetella pertussis*, *Microbial Toxins*. Vol 2A. *Bacterial Protein Toxins*. Edited by S Kadis, TC Montie, ST Ajl. New York, Academic Press, Inc, 1971, pp 271-300
3. Levine S: Repair of thermal brain injury in laboratory rodents. *Exp Neurol* 32:69-77, 1971
4. Morse SI: Studies on the lymphocytosis induced in mice by *Bordetella pertussis*. *J Exp Med* 121:49-68, 1965
5. Schayer RW, Ganley OH: Relationship of increased histidine decarboxylase activity to *Bordetella pertussis* vaccine sensitization of mice. *J Allergy* 32:204-213, 1962
6. Levine S, Wenk EJ: Hyperacute allergic encephalomyelitis: Lymphatic system as site of adjuvant effect of pertussis vaccine. *Am J Pathol* 50:465-483, 1967
7. Field EJ: Histogenesis of compound granular corpuscles in the mouse brain after trauma and a note on the influence of cortisone. *J Neuropath Exp Neurol* 16:48-56, 1957
8. Berthrong M, Cluff LE: Studies of the effect of bacterial endotoxins on rabbit leucocytes. I. Effect of intravenous injection of the substances with and without induction of the local Shwartzman reaction. *J Exp Med* 98:331-355, 1953
9. Munoz J, Smith RF, Cole RL: Some physical properties of histamine-sensitizing factor. *International Symposium on Pertussis, Bilthoven 1969; Symposium Series on Immunobiological Standardization*. 13:265-270, 1970
10. Bunster E, Meyer RK: An improved method of parabiosis. *Anat Rec* 57:339-343, 1933.
11. Beneke G, Finger H, Emmerling P: Einfluss von *Bordetella pertussis* auf das lymphatische Gewebe von Mäusen. II. Proliferierende Zellsysteme in der Milz nach Injektion von *Bordetella pertussis*. *Z med Mikrobiol Immunol* 154:178-195, 1968
12. Fruhman GJ: Hematopoietic changes in mice following *Bordetella pertussis* vaccine. *Proc Soc Exp Biol Med* 124:728-730, 1967
13. Levine S, Strebel R: Allergic encephalomyelitis: inhibition of cellular passive transfer by exogenous and endogenous steroids. *Experientia* 25:189-190, 1969
14. Asakawa S: Effects of the lymphocytosis-promoting factor of *Bordetella pertussis* on antibody production in mice. *Jap J Med Sci Biol* 22:23-42, 1969
15. Munoz J, Anacker RL: Anaphylaxis in *Bordetella pertussis*-treated mice. III. Passive cutaneous anaphylaxis. *J Immunol* 83:640-644, 1959
16. Rutenberg S, Michael JG: Endotoxin-detoxifying capacity of reticulo-endothelial system in normal and pertussis-treated mice. *Proc Soc Exp Biol Med* 117:301-302, 1964
17. Morse SI, Barron BA: Studies on the leukocytosis and lymphocytosis in-

- duced by *Bordetella pertussis*. III. The distribution of transfused lymphocytes in pertussis-treated and normal mice. J Exp Med 132:663-672, 1970
18. Iwasa S, Yoshikawa T, Fukumura K, Kurokawa M: Effects of the lymphocytosis-promoting factor from *Bordetella pertussis* on the function and potentiality of lymphocytes. I. Effect on the ability of lymphocytes to recirculate in the body. Jap J Med Sci Biol 23:47-60, 1970
 19. Konigsmark BW, Sidman RL: Origin of brain macrophages in the mouse. J Neuropath Exp Neurol 22:643-676, 1963
 20. Pearsall NN, Weiser RS: The Macrophage. Philadelphia, Lea and Febiger 1970, pp 27-30

Acknowledgments

We are greatly indebted to Dr. J. Munoz of National Institute of Allergy and Infectious Diseases, Rocky Mountain Laboratory, Hamilton, Montana, for supplies of partially purified HSF, to Dr. H. B. Devlin of Parke, Davis and Company, Detroit, Michigan, for pertussis vaccine, to Dr. V. Schwentker, Tumblebrook Farms, Brant Lake, NY, for the supply of gerbils, and to M. Moritz for the photomicrographs.

[Illustrations follow]

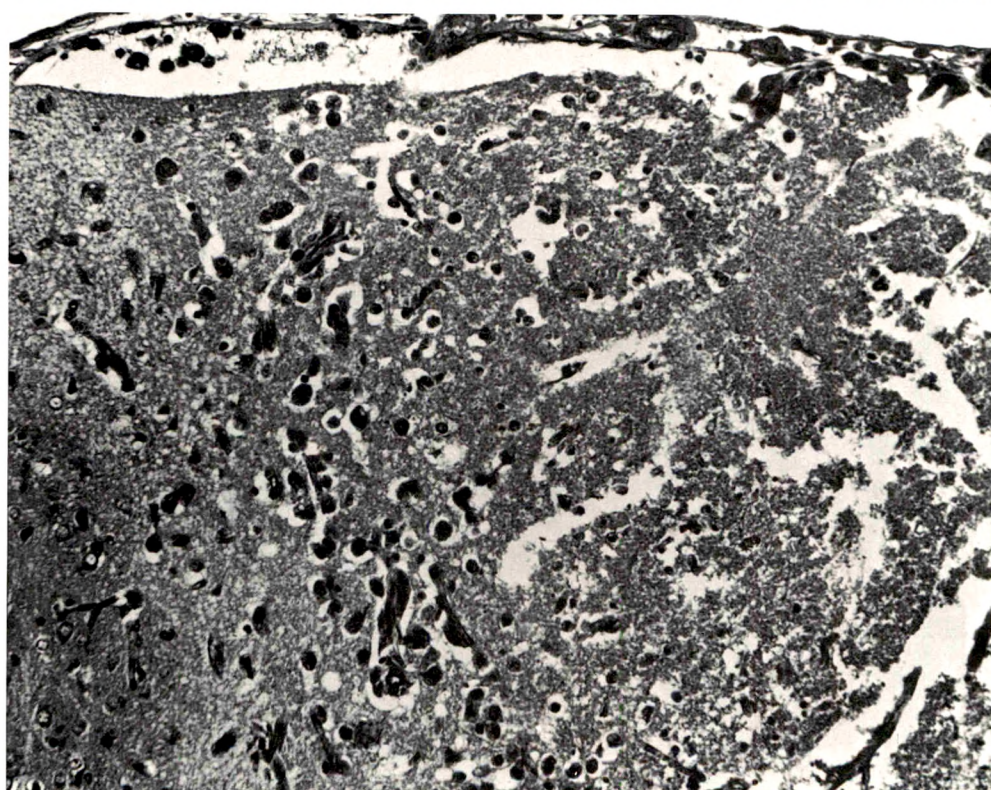
Figures 1 and 2 are photomicrographs of the dorsolateral margin of 3-day-old thermal injuries of rat brain. Pia mater on top, intact cerebral cortex with neurons and vessels on the extreme left; necrotic zone on the right (periodic acid–Schiff–hematoxylin, $\times 150$).

Fig 1—Control, treated with saline 1 day before thermal injury. There are numerous macrophages filling junctional zone between necrotic tissue and viable cortex. The same result was obtained after injection of pertussis vaccine provided it had been heated sufficiently to destroy HSF.

Fig 2—Inhibitory effect of injection of pertussis vaccine 1 day before thermal injury. Far fewer macrophages have accumulated in the junctional zone. The same result was obtained after injection of partially purified HSF.



1



2

[End of Article]

Ultrastructural Characteristics of the "Hairy Cells" of Leukemic Reticuloendotheliosis

I. Katayama, MD, C. Y. Li, MD and L. T. Yam, MD

The pathognomonic neoplastic reticulum cells, or "hairy cells" of leukemic reticuloendotheliosis from 6 patients were studied with the electron microscope. These cells demonstrated characteristic ultrastructural features which were distinctly different from those of lymphocytes, monocytes, or histiocytes. In 3 patients a distinctive ribosome-lamella complex was found. The biologic significance of this unusual cytoplasmic inclusion is still unknown. Its frequent presence in leukemic reticuloendotheliosis and its rarity in other neoplastic diseases suggest a substantial yet unexplained relationship between this complex and leukemic reticuloendotheliosis (*Am J. Pathol* 67:361-370, 1972).

LEUKEMIC reticuloendotheliosis (LRE) is a disease characterized by chronic course, anemia, frequent leukopenia, massive splenomegaly and the presence of neoplastic reticulum cells (hairy cells) in the peripheral blood and bone marrow. Its recognition as a hematologic and pathologic entity was advanced by the recent demonstration of tartrate resistant acid phosphatase isoenzyme in the neoplastic reticulum cells of this disease from blood smears¹ and frozen sections of the tumor tissues.² The pathognomonic cells have a distinctive appearance by the Wright-Giemsa stain (Figure 1, inset) or by phase contrast microscopy. Namely, they have a fine chromatin network, distinct nuclear membrane and serrated or "hairy" cytoplasmic border.^{3,4} This cytologic characteristic has not been clearly born out by previous electron microscopic studies.⁵⁻⁷ In the present study, the ultrastructure of the neoplastic reticulum cell was observed in both blood and tumor tissue. The cell thus recognized showed a characteristic assortment of organelles, hairy villi and frequent ribosome-lamella complex. This particular cytoplasmic inclusion so far had been described only in one case of human tumor.⁸

From the Department of Pathology, University Hospital and Boston University School of Medicine, Boston, Massachusetts (Dr. Katayama) and from the Blood Research Laboratory, New England Medical Center Hospital and Tufts University School of Medicine, Boston, Massachusetts (Drs. Li and Yam).

Supported by 1971 GRS 611, U. S. Public Health Service Grant AM 12444 and Atomic Energy Commission Contract Number AT (30-1) 3808.

Accepted for publication Nov 1, 1971.

Address for reprint requests: Dr. Isao Katayama, Department of Pathology, University Hospital, Boston, Massachusetts 02118.

Materials and Methods

Six patients with LRE were the subject of this electron microscopic investigation. The diagnosis in all cases had been established by hematologic, cytochemical and biochemical examination. Eight specimens, including five peripheral blood samples, two spleens and one marrow were studied. The neoplastic reticulum cells in these specimens ranged from 17 to 91% (Table 1). Blood from a patient with chronic lymphocytic leukemia and 5 healthy volunteers as well as a normal spleen removed at surgery were used as controls.

All specimens were fixed in 3% glutaraldehyde in 0.1M cacodylate buffer at pH 7.4 containing 1 drop of 1% CaCl_2 per 10 ml fixative, at 4C for 2 hours. Blood was processed as a solidified disc of the buffy coat.⁹ After fixation the specimens were washed and then stored at 4C in 0.2M sucrose solution in 0.1M cacodylate buffer (pH 7.4).

The specimens were post-fixed by 1.3% osmium tetroxide in 0.67M collidine buffer at pH 7.4 with 7.5% sucrose and 1 drop of 1% CaCl_2 per 10 ml fixative at 4C for 1 hour. This was followed by dehydration in graded ethanols, embedding in Epon 812 and sectioning on an LKB Ultratome III. Thick sections were stained with toluidine blue and examined by light microscopy. Thin sections were stained with uranyl acetate and lead citrate and examined with a Phillips 300 electron microscope.

Results

All blood specimens (cases 1, 2, 3, 5 and 6) and bone marrow aspirate (Case 1) showed a mononuclear cell type with distinct ultrastructural features (Figures 1-4). Most characteristic were long cytoplasmic villi measuring up to 4 μ in length. The cells contained numerous vesicles, multiple oval mitochondria, rough surfaced endoplasmic reticulum, free ribosomes, Golgi apparatus, frequent centrioles, and occasional fine fibrils. The incidence of cells with this electron microscopic characteristic was directly proportional to the percentage of hairy cells seen by light microscopy (Table 1). In addition, 5 to 25% of neoplastic reticulum cells from Cases 1, 2 and 3 showed a cyto-

Table 1—Some Hematologic Data and Resume of Electron Microscopic Findings in Study Subjects

Subject	Specimen	Light microscope		Electron microscope	
		Leukocyte	Hairy cell %	Hairy cell	Ribosome-lamella complex
MM	Blood	6.400	60	1+	1+
	Bone marrow	—	71	2+	1+
HN	Blood	26.900	89	2+	1+
JP	Blood	11.900	82	2+	2+
	Spleen (4.000g)	—	91 (imprint)	3+	3+
HA	Spleen (1.000g)	—	75 (imprint)	2+	0
JD	Blood	40.000	60	2+	0
HH	Blood	12.700	17	1+	0

plasmic ribosome-lamella complex, which was composed of a central hollow space communicating with the surrounding cytoplasm and an outer sheath consisting of multiple parallel lamellae and ribosomes (Figure 6 and Table 1).

Sections of the spleen from Cases 3 and 4 showed proliferation of the neoplastic reticulum cells which almost completely replaced the normal cellular elements of the spleen (Figure 5). Here the long cytoplasmic villi of these mononuclear cells tended to interdigitate. The villi also frequently encircled or engulfed platelets and erythrocytes. Occasionally a bundle of collagen fibrils was introduced deep into the cytoplasm with contiguous plasma membrane envelope around it, a phenomenon observed in murine reticulum cell sarcoma.¹⁰ The ribosome-lamella complex was seen frequently in tumor cells of Case 3, but none in Case 4. Definite evidence of erythrophagocytosis was seen only in one cell within a sinusoid after extended search of multiple thin sections. This cell contained one degenerate erythrocyte and multiple ribosome-lamella complexes, but it did not exhibit the characteristic long cytoplasmic villi (Figure 7).

In view of the large size of the ribosome-lamella complex, a light microscopic search for a corresponding structure was made. Granules and rods were observed on Wright-Giemsa stained smears and toluidine blue stained thick sections. The only cytoplasmic structure in the neoplastic reticulum cell that may simulate them was azurophilic granule. Their size, shape, location and incidence correlated well with those of the ribosome-lamella complex in all except Case 5. Case 5 showed granules and rods on light microscopy of thick sections, while electron microscopy of thin sections showed no unequivocal ribosome-lamella complex though there were frequent intracytoplasmic loci suggestive of distorted or altered ribosome-lamella complex. Control specimens showed neither hairy cell nor ribosome-lamella complex electron microscopically.

Discussion

The fine structure of the neoplastic reticulum cell had been studied by three groups of investigators previously. In a classic review on a series of 26 cases, Bouroncle et al⁵ illustrated an electron photomicrograph of a cell with irregular pseudopods similar to cell processes of monocyte.¹¹ Others⁶ considered the hairy cell to be a lymphocyte because of its ultrastructural similarity and its ability to synthesize immunoglobulin. In another study⁷ the hairy cell was observed to have endocytotic organelles similar to Langerhans cell granules and was con-

sidered a histiocyte. Two studies were based on the circulating blood cells of a single case;^{6,7} there was little elaboration on the electron microscopy in the review.⁵ None could correlate the ultrastructure with the light microscopic features of hairy cells as far as the long cytoplasmic projections were concerned. In the absence of such a specific marker, one could not be certain if a cell under the electron microscope did actually represent a hairy cell.

In the present study, the neoplastic reticulum cells were studied in the spleen and bone marrow as well as the blood of six patients with LRE, and the number of cells with the typical electron microscopic features was found to be proportional to the number of hairy cells as seen by light or phase microscopy (Table 1). These cells were characterized by long cytoplasmic villi and frequent ribosome-lamella complexes. There was no difference in the fine structure of the neoplastic reticulum cell whether it was seen circulating in the blood (Fig 1-4) or fixed in the spleen (Figure 5). The cell maintained the morphologic features described under the phase contrast microscope, for example, numerous mitochondria observed by Mitus *et al*³ and the cytoplasmic projection coined "hair" by Schrek *et al*.⁴

It was not feasible at this time to trace the origin of the neoplastic reticulum cell of LRE or classify it as lymphocyte, monocyte or histiocyte (reticulum cell). According to some criteria,¹¹ the neoplastic reticulum cell has too many large mitochondria and rough surfaced endoplasmic reticulum and too little phagocytic activity to be a histiocyte, while for it to be a monocyte there are too few electron dense granules (cytosomes). Moreover, as compared with the multiple long slender villi of neoplastic reticulum cell, the pseudopods of monocyte are fewer in number and have a broad base with tapering end. On the other hand, there is a rather striking resemblance between the neoplastic reticulum cell and intermediate type lymphocyte.¹² The neoplastic reticulum cell, however, has villi as long as 4μ , less clumping of ribosomes, frequent ribosome-lamella complex, and "resting" nuclear features; the intermediate lymphocyte in contrast has shorter villi ($0.1-0.3\mu$)⁶ frequent clumping of ribosomes, "active" nuclear morphology in form of prominent nucleolus and reduced heterochromatin to euchromatin ratio,¹² and no ribosome-lamella complex.

In adrenocortical adenoma cells of a patient with Cushing's syndrome. Hoshino⁸ found a cytoplasmic inclusion which he called polysome-lamellae complex. Other somewhat similar structures were reported in animals^{13,14} and vinblastine treated human leukocytes.^{13,15} All patients included in this study had not been treated with chemotherapy when

the specimens were obtained for study. The structure observed in our material appears identical with the polysome-lamellae complex of Hoshino. It is different from other cytoplasmic inclusions in being a centrally hollow cylindrical structure, and it has not been encountered in large series of lymphomas and leukemias.¹⁶⁻¹⁸ Auer bodies in leukemia are electron microscopically homogeneous or laminated crystalline structures¹⁹ from which the ribosome-lamella complex is readily distinguishable, although both structures may appear similar on the light microscopic level. So far as we know the adrenal adenoma reported by Hoshino and the cases of LRE reported here are the only instances of human neoplasms known to have this complex.

The biologic significance of the ribosome-lamella complex and other related structures is still unknown. Most observers^{8,14,15} propose a role in protein synthesis, and some²⁰ postulate a product of aberrant viral replication. In this series of eight specimens from 6 LRE patients, the complex was found in five specimens of 3 cases. Its high incidence in LRE and its rarity in other neoplasms appear to indicate a substantial yet unexplained relationship between the ribosome-lamella complex and leukemic reticuloendotheliosis, somewhat analogous to that between Auer bodies and myelogenous leukemia.

Addendum

After this manuscript was completed, an ultrastructural study on one patient with LRE was published by Sidney Trubowitz, MD, *et al* (*Blood* 38:288-298, 1971), who demonstrated long cytoplasmic villi in the neoplastic reticulum cells.

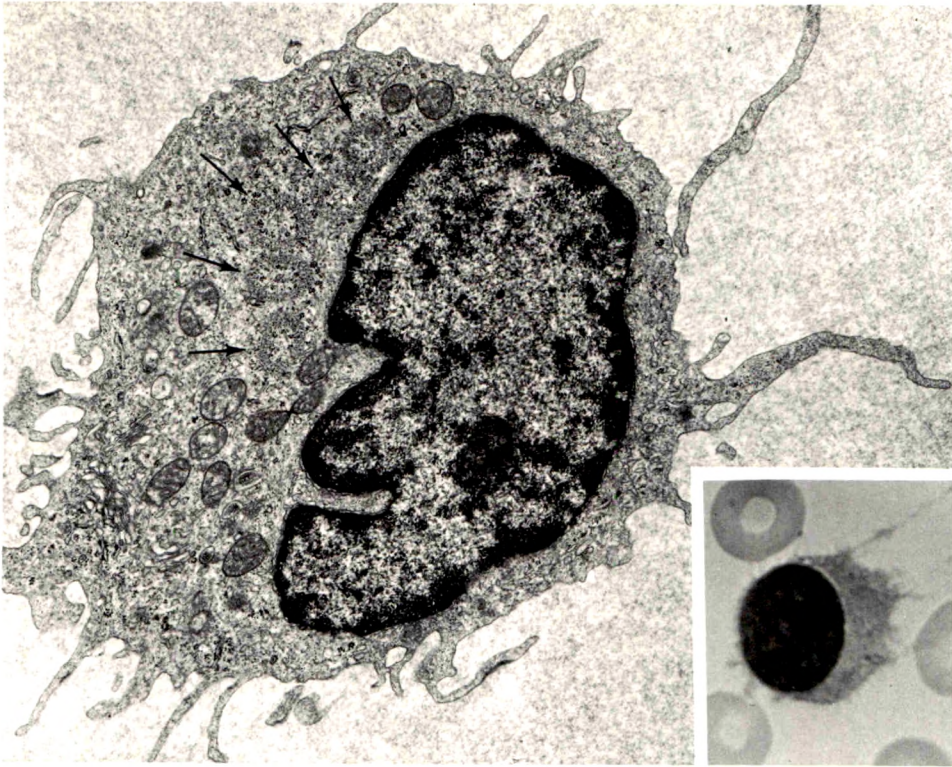
Acknowledgement

The authors are indebted to Dr. T. Shirahama for his helpful discussions during the process of this study, to Dr. R. Cotran for his critical review of the manuscript and to Dr. W. H. Crosby for his continuous interest and support.

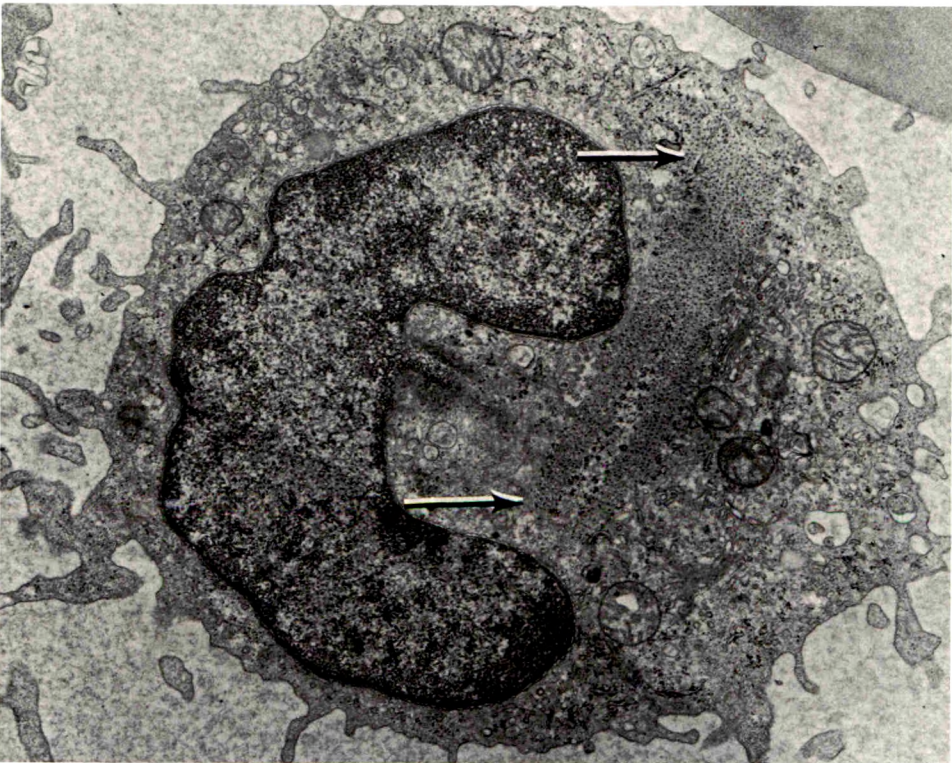
References

1. Yam LT, Li CY, Lam KW: Tartrate-resistant acid phosphatase isoenzyme in the reticulum cells of leukemic reticuloendotheliosis. *N Eng J Med* 284: 357-360, 1971
2. Katayama I, Li CY, Yam LT: Histochemical study of acid phosphatase isoenzyme in leukemic reticuloendotheliosis. *Cancer* 29:157-164, 1972
3. Mitus WJ, Mednicoff IB, Wittels B, Dameshek W: Neoplastic lymphoid reticulum cells in the peripheral blood: a histochemical study. *Blood* 17:206-215, 1961
4. Schrek R, Donnelly WJ: "Hairy" cells in blood in lymphoreticular neoplastic disease and "flagellated" cells of normal lymph nodes. *Blood* 27:199-211, 1966

5. Bouroncle BA, Wiseman BK, Doan CA: Leukemic reticuloendotheliosis. *Blood* 13:609-630, 1958
6. Rubin AD, Douglas SD, Chessin LN, Glade PR, Dameshek W: Chronic reticulolymphocytic leukemia. Reclassification of "Leukemic Reticuloendotheliosis" through functional characterization of the circulating mononuclear cells. *Am J. Med* 47:149-162, 1969
7. Beachey EH, Hashimoto K, Burkett LL: Histiocytic leukemia: Ultrastructure and phagocytic capacity of hairy cells. *Clin Res* 17:530, 1969, abstr
8. Hoshino M: "Polysome-Lamellae Complex" in the adenoma cells of the human adrenal cortex. *J Ultrastruct Res* 27:205-215, 1969
9. Anderson DR: Ultrastructure of normal and leukemic leukocytes in human peripheral blood. *J Ultrastruct Res Suppl* 9:1-42, 1966
10. Siegler R, Rich MA: Pathogenesis of reticulum cell sarcoma in mice. *J Nat Cancer Inst* 41:125-143, 1968
11. Huhn D, Stich W: *Fine Structure of Blood and Bone Marrow*. New York, Hafner Publ, 1969
12. Zucker-Franklin D: The ultrastructure of lymphocytes. *Seminars Hemat* 6:4-27, 1969
13. Bensch KG, Malawista SE: Microtubular crystals in mammalian cells. *J Cell Biol* 40:95-107, 1969
14. Bulger RE: Granule-lamella complex in monkey renal proximal tubular cells. *J Ultrastruct Res* 24:150-156, 1968
15. Krishan A: Ribosome-granular material complexes in human leukemic lymphoblasts exposed to vinblastine sulfate. *J Ultrastruct Res* 31:272-281, 1970
16. Dmochowski L, Yumoto T, Grey CE, Designer E, Hales RL, Langford PL, Taylor HG, Freireich EJ, Shullenberger CC, Shively JA, Howe CD: Electron microscopic studies of human leukemia and lymphoma. *Cancer* 20:760-777, 1967
17. DeHarven E, Clarkson B, Strife A: Electron microscopic study of human leukemic cells in tissue culture. *Cancer* 20:911-925, 1967
18. Seman G, Seman C: Electron-microscopic search for virus particles in patients with leukemia and lymphoma. *Cancer* 22:1033-1045, 1968
19. Amromin GD: *Pathology of Leukemia*. New York, Hoeber Medical Division, Harper & Row, 1968, pp 88-90
20. Campbell JG, Woode GN: Demonstration of a herpes-type virus in short-term cultured blood lymphocytes associated with Marek's disease. *J Med Microbiol* 3:463-473, 1970



1



2

Fig 1—Neoplastic reticulum cell in blood with long cytoplasmic projections. There are multiple ribosome-lamella complexes (arrows) in the cytoplasm ($\times 10,000$). **Inset**—Light photomicrograph of a hairy cell from a blood smear (Wright-Giemsa stain, $\times 1300$). **Fig 2**—Neoplastic reticulum cell in blood with a longitudinal profile of ribosome-lamella complex (arrows) ($\times 9400$).



Fig 3—Another neoplastic reticulum cell in blood with ribosome-lamella complex (arrows). In this section, the ratio of nucleus to cytoplasm is markedly increased ($\times 10,000$).



Fig 4—Neoplastic reticulum cell in blood with the characteristic assortment of organelles enabling its recognition as such, though there is no ribosome-lamella complex ($\times 9700$).

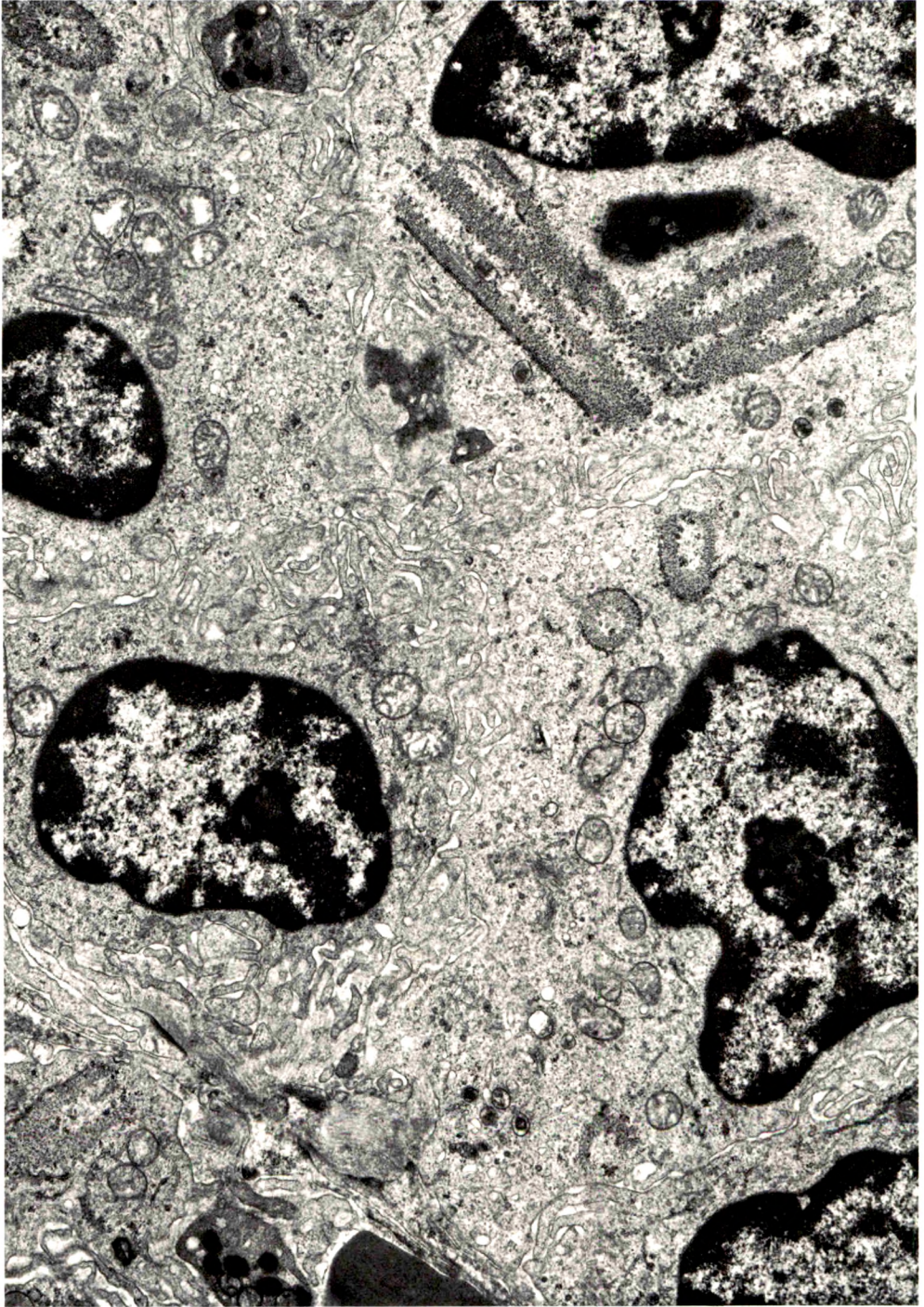
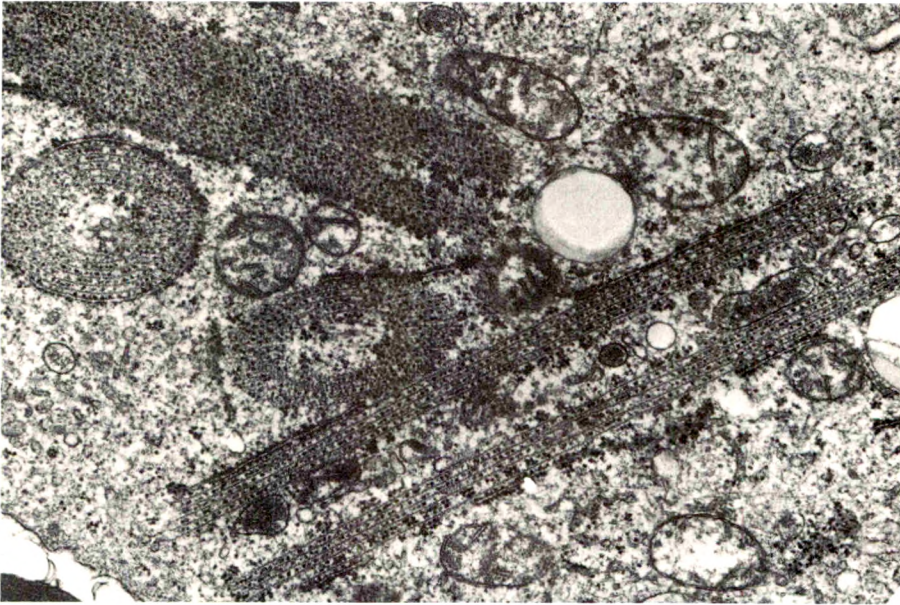


Fig 5—Spleen involved by LRE with proliferation of “hairy” tumor cells. Note multiple ribosome-lamella complexes, interdigitation of cytoplasmic villi and ensheathing of platelets and collagen fibers by the tumor cells ($\times 16,000$).

6



7

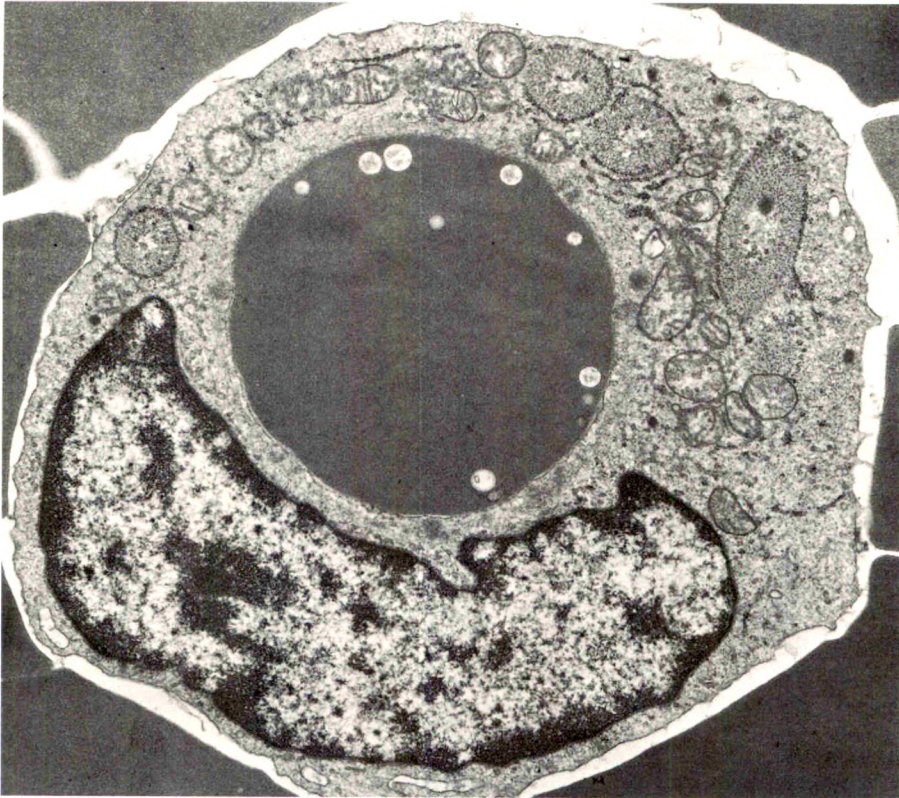


Fig 6—Ribosome-lamella complexes of neoplastic reticulum cell in the spleen. The complex is demonstrated in its cross, oblique and longitudinal sections ($\times 20,000$).
Fig 7—A cell with ribosome-lamella complexes but no long villi in a splenic sinusoid, in which a degenerative erythrocyte is being phagocytosed ($\times 10,000$).

The Significance of Bronchial Atrophy

John C. Maisel, MD, G. Wayne Silvers, BA, Marlyce S. George, HT (ASCP), Gladys A. Dart, BA, Thomas L. Petty, MD and Roger S. Mitchell, MD

In a 4-year period, 196 lungs from patients with and without chronic obstructive pulmonary disease were examined postmortem for the presence of atrophy in segmental and subsegmental bronchi. As a result of simultaneous postmortem spirometry, cinefluorobronchography and partitioning of airways resistance, plus later assessment of anatomic emphysema, bronchial atrophy emerges as only one of at least three factors usually cooperating in production of abnormal expiratory airway collapse. In selected cases, bronchial atrophy appears to be an important contributor to expiratory airways obstruction (Am J Pathol 67:371-386, 1972).

ATROPHY OF BRONCHIAL CARTILAGE and other wall components was first reported 15 years ago by Kiener *et al*¹ in 2 brothers with nonallergic expiratory wheezing. At bronchoscopy and during expiration, they were found to have excessive dynamic airways compression which later was attributed to the bronchial atrophy found at autopsy. Despite this dramatic introduction, however, the concept that atrophy of bronchial wall structures could lead to significant airways obstruction has lain dormant. A decade ago, Wright² noted at autopsy an association of atrophic airways and anatomic emphysema in the lungs of 20 patients with chronic airways obstruction. The ectatic and thin-walled medium-sized bronchi (in which cartilage, smooth muscle and fibrous connective tissue were notably deficient³) were predicted to undergo expiratory collapse *in situ*,² but no direct studies were made of the pulmonary mechanics. Likewise, excessive dynamic expiratory airways compression was noted on fluorobronchography in the airways of patients with chronic airways obstruction, and this expiratory collapse was interpreted by Macklem *et al*^{4,5} as a major obstruction to expiratory flow. A structural defect in the wall was postulated as the best explanation for these findings, but anatomic studies were not made.

From the Webb-Waring Lung Institute and the Departments of Pathology and Medicine, University of Colorado School of Medicine, Denver, Colorado.

Supported by US Public Health Service Research Grants HE-13419 and HE-01910 and by funds from El Paso County and Central Colorado Tuberculosis and Respiratory Disease Association and the Tuberculosis and Respiratory Disease Association of North Central Colorado.

Accepted for publication Nov 15, 1971.

Address for reprint requests: Dr. John C. Maisel, Webb-Waring Lung Institute, University of Colorado Medical Center, 4200 East 9th Avenue, Denver, Colorado 80220.

Petty *et al*⁶ at this time noted the association between dynamic expiratory airway collapse and the clinically assessed impairment in patients with chronic airways obstruction; reduction in the one-second forced expiratory volume and grade of anatomic emphysema were more severe in cases exhibiting early dynamic expiratory airway collapse. Maisel *et al*⁷ studied excised lungs, utilizing the dynamic structural-functional correlation intrinsic to postmortem cinefluorobronchography performed during spirometry, followed by dissection of marked airways. Their findings fulfilled the expectation that collapsing airways were atrophic, but with two reservations: excessive bronchial compression was found to occur only in lungs with atrophic first, second or third generation segmental bronchi, and the co-presence of anatomic emphysema was apparently needed for early collapse to occur. Atrophy and emphysema occurred independently of each other, however. The time in expiration at which collapse occurred appeared roughly related to both the degree of obstruction and the severity of emphysema. More recently, Silvers *et al*^{8,9} extended the model of airway collapse to include airway resistance.

We reevaluate here the significance of bronchial atrophy in chronic airways obstruction. The morphologic abnormalities found at the sites of excessive dynamic airways compression in subsegmental bronchi are interpreted in the light of the associated functional studies of postmortem lungs and of measurements of peripheral and central expiratory airway resistance in these excised lungs. Bronchial atrophy emerges as only one variable in the production of dynamic compression.

Materials and Methods

Our methods of general study have been detailed.⁶⁻¹³ Lungs were obtained from autopsies performed at the University of Colorado Medical Center, which serves the Colorado General, Denver Veterans Administration and National Jewish Hospitals. A specimen was chosen for these studies if the clinical diagnosis of chronic airways obstruction (chronic bronchitis and emphysema) (and lack of other evident respiratory disease) was made during life and confirmed by postmortem review of the clinical record.^{10,13} Static pressure-volume curves were constructed on stepwise deflation. For spirometry, the lungs were suspended in an artificial thorax, by the largest glass cannula which would fit into the mainstem bronchus, and ventilated at 15 cycles/sec and pressure settings reproducing the forced expiratory volume in one second (FEV₁) maneuver in life. The values obtained were compared with the predicted FEV₁ values, according to height and age. For bronchography, approximately 2 ml of dry Micropaque powder was blown into the mainstem bronchus, sufficient to visualize airways down to 2 mm in diameter. The fluorobronchogram was recorded at 60 frames/sec by a 35-mm cinefluorography camera, simultaneously with the oscilloscope image of the tracing of stem bronchial flow, lung volume and artificial thorax pressure.

Collapse is defined as the abnormalities of airway movements during expiration

of diseased lungs⁶⁻⁹ which may be distinguished from normal expiratory tapering. Collapsing airways narrow abruptly rather than gradually; they do so within the first 0.75 second rather than after 1 second, and this narrowing progresses to the point of complete closure centrally with lumens still patent peripherally, suggesting air trapping. Collapse occurs centrally, rather than peripherally, being found primarily in second and third generation segmental bronchi and occasionally in first order segmental or lobar bronchi. It varies in time of onset in different affected bronchi but in most cases, more than one airway is involved. The elapsed time of expiration at which abnormal dynamic expiratory bronchial collapse occurred was recorded as the frame number in the cinebronchogram. The earlier collapse occurred, the higher the grade of severity (see footnote to Table 1).

When the physiologic study was completed, all lungs were inflated through the mainstem bronchus to a pressure of +20 cm of water with 1.8% (iso-osmolar) neutral buffered gluteraldehyde. Fixation pressure was maintained for 1 week using a modified aquarium "bubble pump" to recycle liquid that leaked out of the lung. After this, the lungs were sliced in the sagittal plane and slices impregnated with barium sulfate.¹⁵ Severity and extent of emphysema was graded first in four categories and then by our adaptation of the rank-ordered method I of Thurlbeck *et al*,¹⁶ scoring life-sized photographs of the whole lung slices instead of paper-mounted Gough sections. We used a grading panel previously standardized against the panel published by Thurlbeck.¹⁷ Emphysema was typed as absent, trace, focal, irregular, mixed, mainly centriacinar, mainly panacinar or endstage. Transverse bronchial sections were taken from the mainstem, lobar, and origin of the segmental bronchi; these were stained with hematoxylin and eosin and assessment of chronic bronchitis was determined by the mucus gland/bronchial wall ratio (Reid Index)¹⁸ for mucus gland hyperplasia. A marker catheter was followed into the collapse zone and serial blocks taken of the abnormal airway, or, in other cases, all basal segmental bronchi were isolated for at least three branchings, and these were serially blocked and embedded. Transverse sections of segmental and sub-segmental airways were stained with the Verhoef-van Gieson method. Assessment that bronchial atrophy was "definitely" present was made subjectively, utilizing the relative loss of cartilage, smooth muscle, glands, connective tissue, fibrosis of blood vessels, and flattening of epithelium noted by Wright² and by Wright and Stuart.³ Cases in which 2 observers could not agree, or in which 1 observer could not reproduce his own reading, were scored as questionable. In addition, in one sub-set, atrophy was quantitated by planimetry of

Table 1—Association of Collapse and Postmortem FEV₁

Collapse grade†	FEV ₁ , Percent of predicted*						Total No. of cases
	0-25	26-50	51-75	75-100	101-125	126→	
0	1	10	18	15	10	7	61
1+	3	4	12	4	3	0	26
2+	19	18	18	1	0	0	56
3+	32	16	2	0	0	0	50
Total	55	48	50	20	13	7	193

* Postmortem measurement. Predictions according to age-height nomogram of Kory *et al* (Am J Med 30:243, 1961).

† 3+, collapse within 0-15 frames; 2+, 16-30 frames; 1+, 31-45 frames; 0, none in 120 frames (60 frames in cinefluorobronchogram = 1 second of expiration).

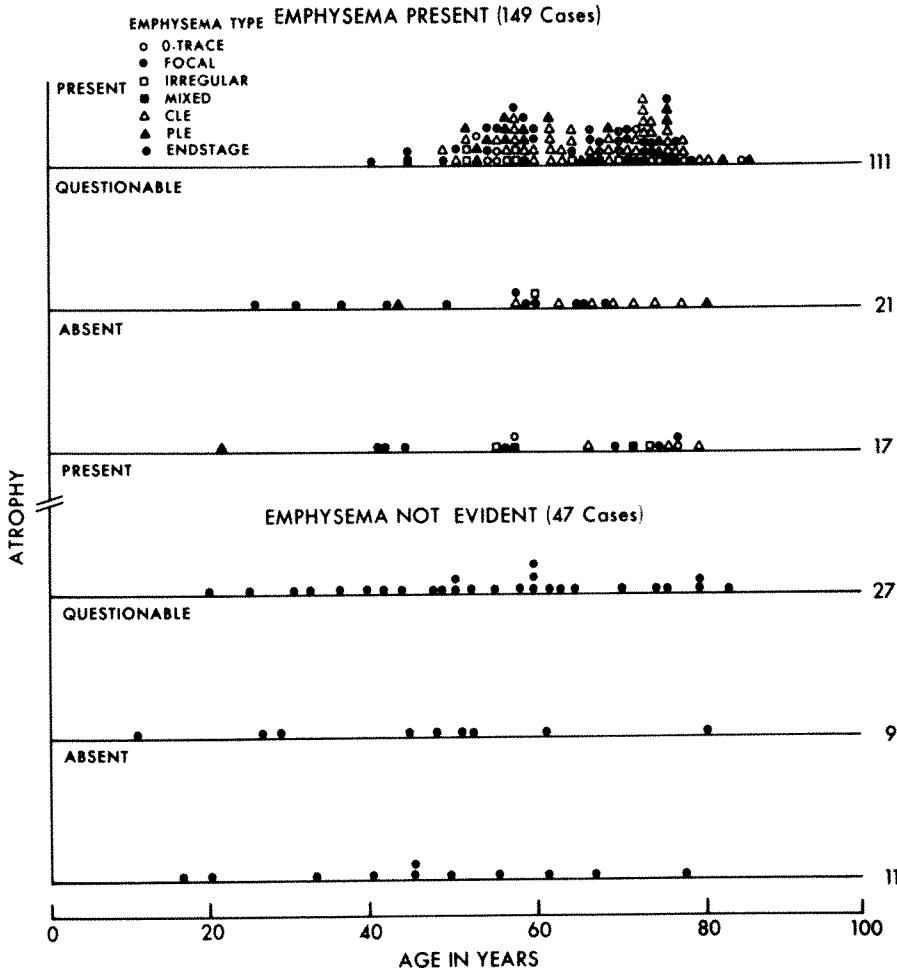
10X enlarged projected images, utilizing the ratio of wall area to total cross-sectional area. In a second sub-set of cases, a "point count" grid¹⁹ was used to determine percentages of the cross-sectional area occupied by each component.

Results

In the combined autopsy service of the University of Colorado Medical Center, 2687 autopsies were performed during the years 1967 through 1970. Of these, 262 were selected for special postmortem studies in the Webb-Waring Lung Institute, and were chosen for a history of chronic obstructive pulmonary disease or as "controls" within the same age group lacking COPD or other evident respiratory disease. Of those selected, 196 received a complete evaluation, that is, in addition to assessments of morphology, we were able to measure postmortem FEV₁ and perform cinefluorobronchograms. In these 196 cases, bronchial atrophy was unequivocally present in the sub-segmental branches of 138 cases, questionable in 30 and absent in 28. The range of values found by "point counting" for cartilage percent of the total wall area was within the range of values found by Dunnill *et al*²⁰ for segmental bronchi of "normal" persons. An illustration of bronchial atrophy is shown in Figure 1.

The cases studied were mostly men over age 40 and do not represent a random study of the autopsy population any more than the autopsy population is a random sample of our hospitals' population or the population at large. Within this limitation, we did not find an association of the questionable or definite presence of bronchial atrophy with the sex or smoking history (pack-years) of the patients. Neither the presence nor severity of bronchial atrophy showed a statistically significant association with the clinical assessment of obstructive disease, with low values of the postmortem FEV₁, or with the time in expiration at which bronchial collapse occurred.

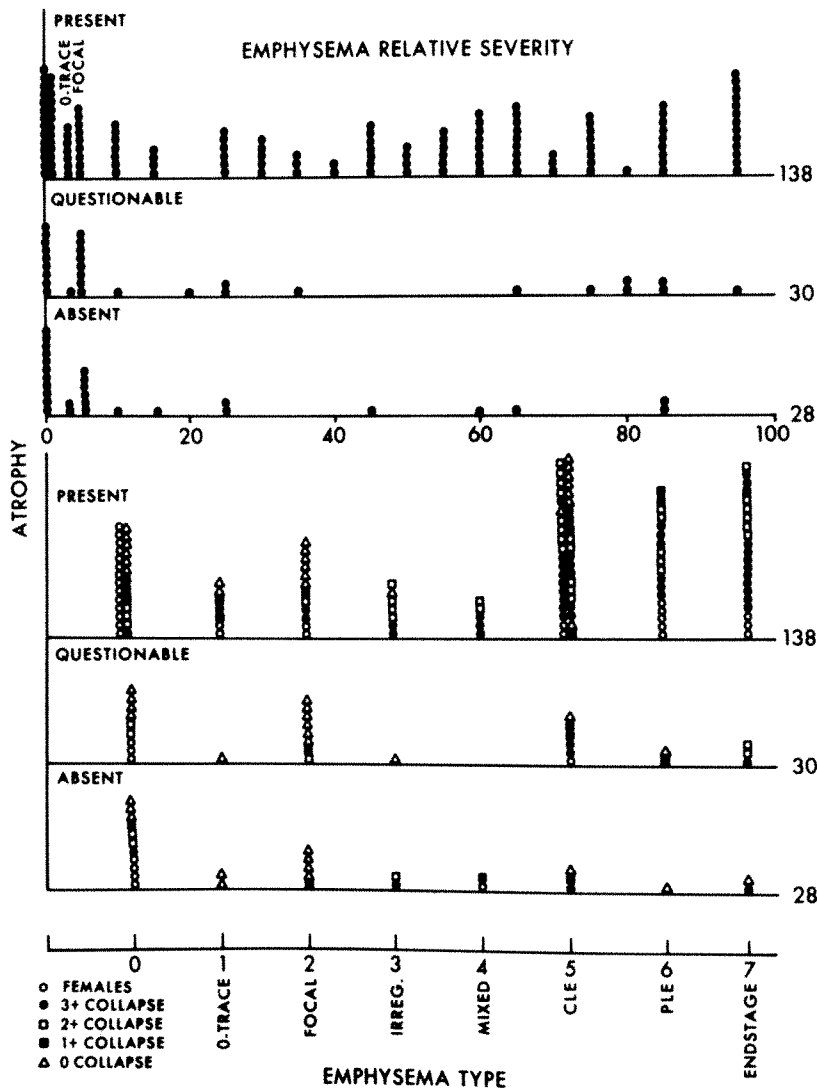
The relationship of *bronchial atrophy* to patients' ages is shown in Text-figure 1; cases are separated according to presence (upper half) or absence (lower half) of anatomic emphysema. The bias of our sample for older ages is apparent in the cases with emphysema. The larger portion of the cases with bronchial atrophy was observed among older persons, and in persons over age 50 there was a higher ratio of atrophy cases to total cases, although the difference is not statistically significant. It is unclear whether this difference is an effect of age *per se* or of emphysema bias. Text-figure 2 illustrates the lack of association between the presence of bronchial atrophy and anatomic emphysema whether by grade (upper half) or type (lower half); the two lesions coexisted no more often than expected by chance. In cases within the



TEXT-FIG 1—Relationship of bronchial atrophy and age of patients, shown separately for cases with emphysema present and coded for type (*upper half*), and without emphysema evident on gross examination (*lower half*). For explanation of emphysema type, see text and refs 12 and 16.

two sub-sets in which atrophy was quantitated, the severity of atrophy as assessed by planimetry or point counting was not related to emphysema grade. We did find that most cases with increased Reid Index also had emphysema; Text-figure 3 portrays this together with the lack of relationship between bronchial atrophy and Reid Index shown separately for cases with (*upper half*) and without (*lower half*) anatomic emphysema.

Expiratory collapse of medium-sized bronchi was the lesion directing our attention to atrophy (see *Methods* for description of collapse).

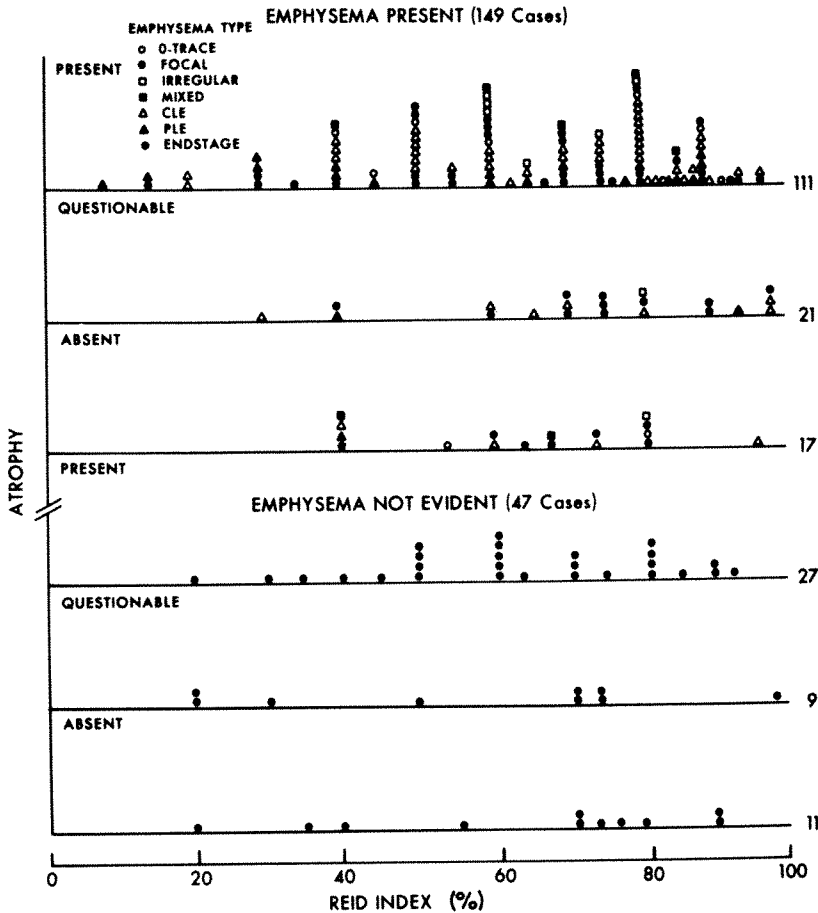


TEXT-FIG 2—Relationship of bronchial atrophy and emphysema, shown separately for emphysema severity (*upper half*), and emphysema type coded for collapse grade (*lower half*). For explanation of emphysema grade, see text and refs 12 and 16; for emphysema type, see legend to Fig 1; for collapse grade, see text, footnote to Table 1, and refs 7–9.

Collapse was found to be associated with the degree of loss of the expected FEV₁ postmortem, as indicated in Table 1. A similar association of collapse grade and emphysema severity is shown in Table 2. However, correlation coefficients were low (0.66 or less) when regression analysis was made between the time at which expiratory collapse occurred and the postmortem FEV₁ value, or expiratory collapse time and emphysema grade. A significant association of collapse grade and

clinical assessment of obstructive disease severity was found, as shown in Table 3; this confirms the experience of Mitchell *et al.*¹¹ The value of early dynamic expiratory bronchial collapse as an indicator of more severe obstructive impairment is thus supported in general but the specific or quantitative relationship is inexact, since early collapse does not correlate well with marked loss of FEV₁. Likewise, the lesion producing early collapse is not readily identified by these data; in particular, collapse timing is not a straightforward function of emphysema, nor is it significantly associated with bronchial pathology.

An interpretation of the role of bronchial atrophy in the airway



TEXT-FIG 3—Relationship of bronchial atrophy and bronchial mucus gland hyperplasia, shown separately for emphysema present coded for type (*upper half*) and emphysema not evident (*lower half*). Atrophy was scored in the lower lobe segmental bronchi and their branches; see text for explanation of categories. Mucus gland hyperplasia was scored in the mainstem, lobar and innominate bronchi as the gland/wall ratio (Reid index, ref 18); the maximum value is used here.

Table 2—Association of Collapse and Emphysema

Collapse grade†	Emphysema, Relative Severity*											Total No. of cases
	0	1-9	10-19	20-29	30-39	40-49	50-59	60-69	70-79	80-89	90-100	
0	23	20	7	3	2	1	1	3	0	1	0	61
1+	7	6	4	4	0	2	1	0	1	1	2	28
2+	14	4	2	3	6	4	13	8	3	3	7	57
3+	3	3	1	1	1	3	6	8	8	12	4	50
Total	47	33	14	11	9	10	11	19	12	17	13	196

* Cases rank-ordered at intervals of 10%—see refs 16, 17 and text for details.

† See Table 1.

collapse phenomenon may be made by considering this paradox: atrophy is usually present when collapse occurs, but is as frequently present without collapse, and when atrophy is present the extent as scored by planimetry or point counting does not correlate with collapse severity. Such data suggest that other factors must contribute to the collapse phenomenon. For example, an atrophic segmental bronchus might not collapse if sufficiently guyed, as by intact parenchyma. A first attempt to construct a multiplex variable model of collapse is shown in Table 4. This analysis, first made for the two variables and 38 cases in 1968,⁷ is confirmed now for 196 cases, and additional observations are made. As before, the cases lacking collapse tend to be those with no lesion or a single anatomic lesion, whereas cases with early collapse tend to be cases in which both anatomic emphysema and bronchial atrophy are definitely co-present. However, in contrast to the earlier experience, we now have many cases with both emphysema and atrophy present, but lacking collapse, and many cases in which moderate or severe

Table 3—Association of Collapse and Clinical Evaluation

Collapse grade†	Clinical assessment*				Total No. of cases
	0	1+	2+	3+	
0	54	3	2	2	61
1+	18	4	3	3	28
2+	17	10	12	18	57
3+	4	4	4	38	50
Total	93	21	21	61	196

* 0, no signs or symptoms; 1+, signs and/or symptoms, no disability; 2+, disability but died of other causes; 3+, disability and died of chronic airways obstruction (see ref 13 for related causes of death).

† See Table 1.

Table 4—Association of Collapse and Morphologic Findings

Anatomic diagnosis	Collapse Grade†				Total No. of cases
	0	1+	2+	3+	
Neither emphysema nor bronchial atrophy evident	7	1	3	0	11
Emphysema alone, 3% or more	9	4	1	3	17
Questionable atrophy alone	5	0	3	1	9
Definite atrophy alone	11	6	8	2	27
Questionable atrophy plus emphysema, 3% or more	10	4	4	3	21
Definite atrophy plus emphysema, 3% or more	19	13	38	41	111
Total	61	28	57	50	196

† See Table 1.

collapse occurs in cases exhibiting either emphysema without atrophy, atrophy without emphysema, or even no lesion. In those cases with atrophy present, moreover, we could not show that the severity of collapse correlated with emphysema severity. This strongly suggests that still more factors, not assessed morphologically, must operate in the production of collapse.

Discussion

It should surprise no one that the dynamic consequences of structural change would contribute to expiratory airway obstruction, even if we cannot quantitatively relate these changes in static morphology to dynamic measurement. In particular, compliance of lung parenchyma might increase before gross or histologic observations detected changes, and radial traction²¹ support of intraparenchymal bronchi might decrease.

Elsewhere^{8,9} we have presented an analysis of the mechanisms of collapse based on partitioning of airways resistance,¹⁴ and have implicated a moderate increase in peripheral airways resistance as a third component interacting in most cases with both bronchial atrophy and anatomic emphysema. Yet we have several cases with normal peripheral resistance in which collapse seems dependent on both bronchial atrophy and anatomic emphysema. On the other hand, in one case markedly elevated peripheral resistance seemed solely responsible for the production of dynamic expiratory compression of medium-sized bronchi which were histologically normal and surrounded by parenchyma judged to be structurally normal in gross and microscopic examination.

The occurrence of bronchial atrophy in our patients is seemingly independent of the other parameters definable, whether demographic or anatomic. We interpret our data as showing a lack of clear relationship between bronchial atrophy and emphysema; this opinion requires explanation, in view of the literature. First Restrepo and Heard,²² Dunnill *et al*,²⁰ Greenberg *et al*,²³ and Takizawa and Thurlbeck²⁴ found no relationship between emphysema presence or severity, and measurements of cartilage in segmental or larger bronchi. In contrast, Wright,² Wright and Stuart,³ Maisel *et al*,⁷ and Tandon and Campbell²⁵ all found atrophy of cartilage in the sub-segmental bronchi (or higher-ordered branches of segmental bronchi) in lungs with emphysema present. Branching order of the bronchi examined evidently determines whether one finds atrophy of cartilage. (One must also not overinterpret the lesser amounts of bronchial cartilage found in the fifth or higher branching orders, as Hayward and Reid²⁶ pointed out the rather abrupt transition of cartilage amount and distribution found at this level in normal lungs.) We noted (in Figures 2 and 3) the clear bias among our patient sample both for older ages and presence of more than trivial emphysema. The apparent association with emphysema (Figure 2) is not borne out quantitatively (Figure 3) and may be as much one with age in these patients although the effect of age is not apparent in cases with atrophy but lacking emphysema. The presence of emphysema may represent, in part, accelerated aging. Our sample of cases lacks an adequate number of older persons without emphysema; we cannot settle the issue.

The only known observations on causes of atrophy of bronchial cartilage are those of the Silberbergs,²⁷ who related it to the early and predominant regressions seen in articular cartilage and associated with age, race and hormonal effects; the cellular and matrix changes were described. We have no knowledge of the role of racial or hormonal factors in our patients. All we can offer on the cause of this atrophy is to suggest that it could result at least in part from the "wear and tear" of an increased transmural pressure at a critical point in the bronchial tree. Why the subsegmental bronchi seem critical to collapse deserves comment. Whereas bronchial atrophy seems to begin more peripherally and progress centrally both in our cases and in those of Wright,² the segmental bronchi are the last order, moving centrally, to be tightly invested by pulmonary parenchyma.²⁶ This feature is double-edged: radial traction support is supplied in the normal lung²¹ but alveolar pressure is also brought to bear. In the diseased lung, alveolar pressure remains even if the parenchyma no longer provides adequate

radial traction. Alveolar pressure must be considered in the effective transmural pressure across the bronchial wall during expiration.^{28,29} Collapse occurs when transmural pressure exceeds the bronchial wall strength. Since the more central or downstream the airway, the greater the transmural pressure during expiration,²⁹ the segmental level is where collapse would first appear (in the absence of parenchymal support) whenever bronchial atrophy sets in. A second cause of atrophy could be degeneration following the inflammatory aftermath of mucus plugging; this could explain some of the sharp localizations we have observed with airways proximal and distal to the collapse segment appearing grossly and histologically normal.⁷

Summary and Conclusions

The significance of bronchial atrophy in chronic airways obstruction is not apparent until one studies the sub-segmental or medium-sized bronchial branches identified by bronchography and also takes into account the coexistence of anatomic emphysema; although the two lesions appear to occur together in our patients no more frequently than expected by chance, when they do coexist, the dynamic expiratory collapse phenomenon is more likely to be present and to occur earlier during expiration; likewise the limitation of expiratory flow is apt to be more severe, accounting for the significant association of the collapse phenomenon with the clinical assessment of airways obstruction severity. Our mechanistic analysis^{8,9} has demonstrated the multifactorial nature of the collapse phenomenon. Bronchial atrophy may be thought of as a permissive phenomenon, and emphysema, operating as loss of radial traction²¹ (or other disturbances), may be likened to a regulator. Peripheral resistance usually interacts with these as a third variable but may contribute independently of atrophy or emphysema to collapse of medium airways. It is significant that collapse is associated in time and place with a significant increase in the central component of airways resistance.^{8,9} Central resistance remains high for the remainder of expiration after collapse; it is against this increased central resistance that the bulk of the expirable volume must be expelled, however small that volume may be in the obstructed patient. Thus, although we have little understanding of why atrophy occurs in medium-sized bronchi, it is clear that in many cases it contributes significantly to expiratory airway collapse. In particular, the number of these cases in our experience is sufficient for us to suggest that segmental bronchial atrophy may account for some of those cases in which the severity of obstruction is disproportional to the severity of parenchymal destruction (anatomic

emphysema) or chronic bronchitis (mucous gland hyperplasia). In general, atrophy emerges as another variable in the increasingly complex equation of chronic airways obstruction.

References

1. Kiener M, Koblet H, Wyss F: Zur Pathologie des stenosierenden Bronchialkollapses mit Lungenemphysem. *Schweiz Med Wschr* 87:660-663, 1957
2. Wright RR: Bronchial atrophy and collapse in chronic obstructive pulmonary emphysema. *Am J Path* 37:63-77, 1960
3. Wright RR, Stuart CM: Chronic bronchitis with emphysema: a pathologic study of bronchi. *Med Thorac* 22:210-218, 1965
4. Macklem PT, Fraser RG, Bates DV: Bronchial pressures and dimensions in health and obstructive airway disease. *J Appl Physiol* 18:699-706, 1963
5. Macklem PT, Fraser RG, Brown NG: Bronchial pressure measurements in emphysema and bronchitis. *J Clin Invest* 44:897-904, 1965
6. Petty TL, Miercort R, Ryan SF, Vincent TN, Filley GF, Mitchell RS: The functional and bronchographic evaluation of postmortem human lungs. *Am Rev Resp Dis* 92:450-458, 1965
7. Maisel JC, Silvers GW, Mitchell RS, Petty TL: Bronchial atrophy and dynamic expiratory collapse. *Am Rev Resp Dis* 98:988-997, 1968
8. Silvers GW, Maisel JC, Filley GF, Petty TL, Mitchell RS: An evaluation of airway resistance in excised artificially ventilated lungs. *Chest* 59:39S, 1971
9. Silvers GW, Maisel JC, Petty TL, Filley GF, Mitchell RS: Central airway resistance in excised emphysema lungs. *Chest* 1972, Unpublished data
10. Mitchell RS, Silvers GW, Dart GA, Petty TL, Vincent TN, Ryan SF, Filley GF: Clinical and morphologic correlations in chronic airway obstruction. *Am Rev Resp Dis* 97:54-61, 1968
11. Mitchell RS, Petty TL, Filley GF, Dart GA, Silvers GW, Maisel JC: Clinical, physiologic, and morphologic correlations in chronic airways obstruction. *Bronchitis III Proceedings of the Third International Symposium on Bronchitis*, Groningen, The Netherlands, September 1969, Royal Van Gorcum, Assen, The Netherlands, 1970, pp 164-174
12. Mitchell RS, Silvers GW, Goodman N, Dart GA, Maisel JC: Are centrilobular emphysema and panlobular emphysema two different diseases? *Human Pathol* 1:433-441, 1970
13. Mitchell RS, Walker SH, Silvers GW, Dart G, Maisel JC: The causes of death in chronic airway obstruction: I. The unreliability of death certificates and routine autopsies; II. Myocardial infarction. *Am Rev Resp Dis* 98:601-612, 1968
14. Macklem PT, Mead J: Resistance of central and peripheral airways measured by retrograde catheter. *J Appl Physiol* 22:395-401, 1967
15. Heard BE: A pathological study of emphysema of the lungs with chronic bronchitis. *Thorax* 13:136-149, 1958
16. Thurlbeck WM, Horowitz J, Siemiatycki J, Dunnill MS, Maisel JC, Pratt, Ryder R: Intra- and inter-observer variations in the assessment of emphysema. *Arch Environ Health* 18:646-659, 1969
17. Thurlbeck WM: Grading emphysema: Panels 1, 2, and 3. Philadelphia, WB Saunders Company, 1970

18. Reid L: Measurement of the bronchial mucous gland layer: a diagnostic yardstick in chronic bronchitis. *Thorax* 15:132-141, 1960
19. Dunnill MS: Quantitative methods in the study of pulmonary pathology. *Thorax* 17:320-328, 1962
20. Dunnill MS, Massarella GR, Anderson JA: A comparison of the quantitative anatomy of the bronchi in normal subjects in *status asthmaticus*, in chronic bronchitis, and in emphysema. *Thorax* 24:176-179, 1969
21. Pratt PC: Intrapulmonary radial traction: measurement, magnitude, and mechanics. *Current Research in Respiratory Disease*. United States Public Health Service Publication No 1879, Washington, DC, Government Printing Office, 1969, pp 159-181
22. Restrepo GL and Heard BE: Air trapping in chronic bronchitis and emphysema: measurements of bronchial cartilage. *Am Rev Resp Dis* 90:395-400, 1964
23. Greenberg SD, Boushy SF, Jenkins DE: Chronic bronchitis and emphysema: correlation of pathologic findings. *Am Rev Resp Dis* 96:918-928, 1967
24. Takizawa T and Thurlbeck WM: A comparative study of four methods of assessing the morphologic changes in chronic bronchitis. *Am Rev Resp Dis* 103:774-783, 1971
25. Tandon MK, Campbell AH: Bronchial cartilage in chronic bronchitis. *Thorax* 24:608-612, 1969
26. Hayward J, Reid L: The cartilage of the intrapulmonary bronchi in normal lungs, in bronchiectasis, and in massive collapse. *Thorax* 7:98-110, 1952
27. Silberberg M, Silberberg R: Aging changes in cartilage and bone. *Structural Aspects of Aging*. Edited by GG Bourne. New York, Hofner Publishing Co, 1961, p 1952
28. Pride NB, Permutt S, Riley RL, Bromberger-Barnea B: Determinants of maximal expiratory flow from the lungs. *J Appl Physiol* 23:646-662, 1967
29. Mead J, Turner JM, Macklem PT, Little JB: Significance of the relationship between lung recoil and maximum expiratory flow. *J Appl Physiol* 22:95-108, 1967

Acknowledgments

The authors wish to express their indebtedness to Dr. Hollis Boren for providing the gluteraldehyde formulation for fixation of lungs, to Dr. Charles Carrington for the "bubble pump" design for maintaining inflation, and to C. Ahrens and B. B. Higgins for their technical assistance. Margaret Braun prepared the manuscript. Special thanks go to Assistants in Pathology, Drs. David Mulkey, Edward Farkas, Galyn Stahl, Ray Stanford and Thomas Stocker.

Presented in part at the Sixty-eighth Annual Meeting of the American Association of Pathologists and Bacteriologists, Montreal, Canada, March 7, 1971.

[Illustrations follow]

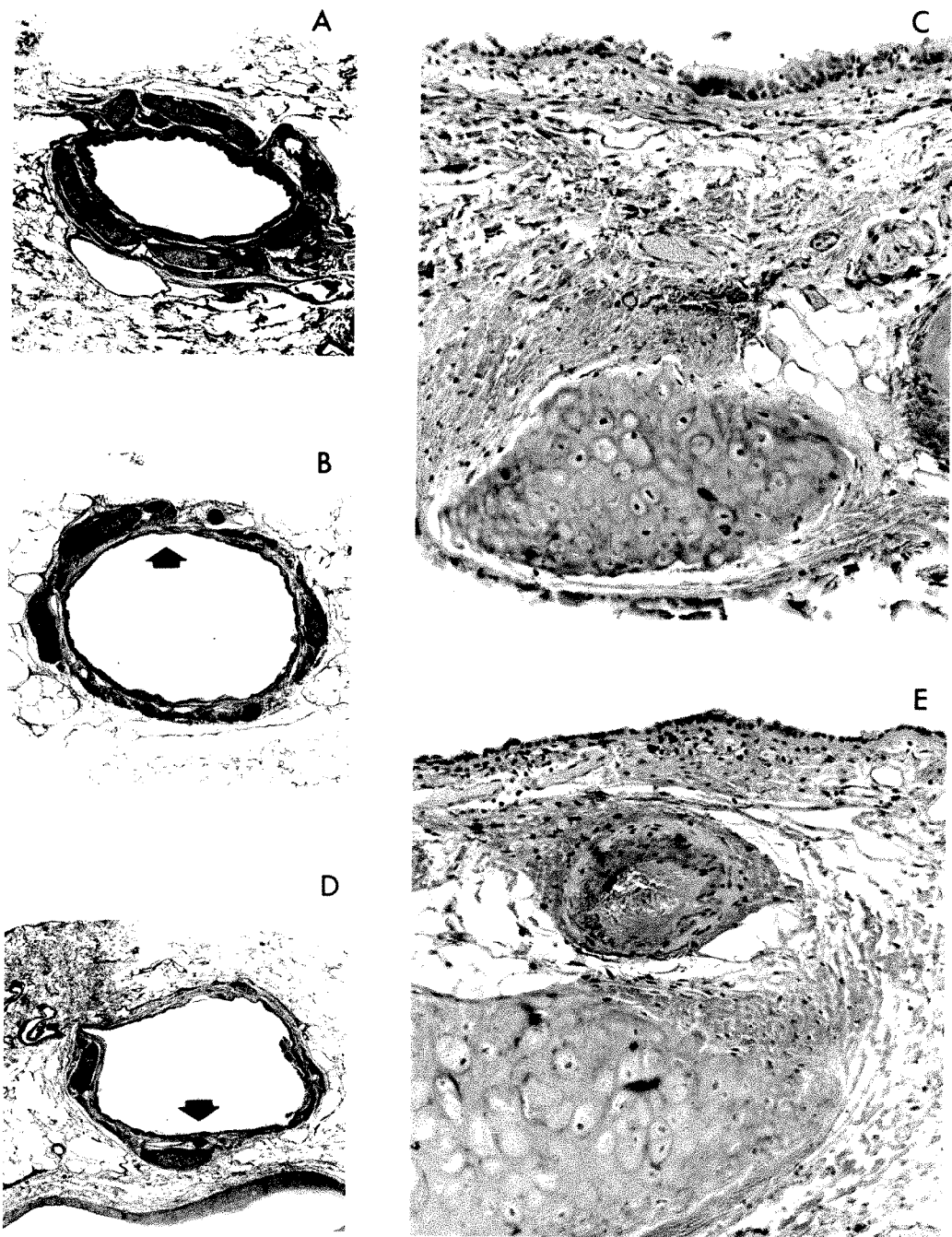


Fig 1—Sections stained with Verhoeff-van Gieson stained sections. **A**—Second generation bronchus, antero-medial basal segment, 2 mm internal diameter, exhibiting preserved bronchial wall elements (original $\times 10$). Man, age 58, clinically not obstructed; postmortem FEV₁ 104% of predicted; no collapse in cinebronchogram; anatomic diagnoses: trace emphysema, Reid index 55%. **B**—Second generation bronchus, lateral basal segment, 3 mm internal diameter, exhibiting definite atrophy of cartilage, smooth muscle and collagen (original $\times 10$). **C**—Detail of B (original $\times 120$). **D**—Second generation bronchus, posterior basal segment, 3 mm internal diameter, also exhibiting definite atrophy (original $\times 10$). **E**—Detail of D (original $\times 120$). Man, age 80; clinically not obstructed; post-mortem FEV₁, 137% of predicted, 1+ collapse in cinebronchogram; anatomic diagnoses: focal emphysema, but large bronchi normal.

[*End of Article*]

Experimental Cerebral Atherosclerosis in the Dog

I. A Morphologic Study

Minoru Suzuki, MD, DSc

Prolonged feeding with an atherogenic diet can induce occlusive disease of the intracranial arteries and cerebral infarction in dogs. The morphologic findings suggest that separation of the internal elastic lamina from the endothelial basement membrane is a consistent change and probably an initiating mechanism in the pathogenesis of atherosclerosis of the cerebral arteries (*Am J Pathol* 67:387-402, 1972).

ALTHOUGH ATHEROSCLEROSIS can be produced readily in the extracranial major arteries by dietary means in various mammals, arteries of the central nervous system are resistant to the induction of lesions.¹⁻³ There have been experimental studies dealing with occlusive atherosclerotic lesions of the cerebral arteries.^{4,5} The purpose of this report is to present morphologic lesions of the intracranial arteries produced by diet in dogs as a model of cerebral atherosclerosis.

Materials and Methods

Three mongrel dogs, weighing 10 to 15 kg, approximately 1 year old, were housed in air-conditioned animal quarters and fed an equal mixture of commercial canned horse meat and semisynthetic test diet. Each animal was given 250 g of the mixed ration per day, Monday through Saturday. The test diet contained saturated animal fat (butter), cholesterol, cholic acid and propylthiouracil as atherogenic ingredients, supplemented with sucrose, casein, minerals and vitamins (Table 1). The addition of horsemeat equal to the quantity of the test diet was necessary to maintain general physical condition of the animals in this chronic experiment. Two dogs were killed at 48 and 1 at 55 months of feeding, respectively, by intravenous injection of sodium pentobarbital. The brain was removed quickly and immersed in neutral 10% formalin after small blocks from the middle cerebral arteries had been obtained and fixed in buffered 5% glutaraldehyde for electron microscopy. In addition to the examination of the brain, a complete autopsy was performed on each dog. The formalin-fixed brains were cut coronally, and sections of the internal carotid, anterior, middle and posterior cerebral, basilar and cerebellar arteries were obtained for histologic examination. The histologic sections of the intracranial arteries were cut 6 μ thick and stained with hematoxylin-eosin, aldehyde

From the Department of Pathology, Baylor College of Medicine, Houston, Texas.

Supported by Research Grant HE-05435 from the National Heart and Lung Institute, US Public Health Service.

Presented in part at the Sixty-Seventh annual meeting of the American Association of Pathologists and Bacteriologists, March 8, 1970.

Accepted for publication Nov. 22, 1971.

Address reprint requests to Dr. Minoru Suzuki, Department of Pathology, Baylor College of Medicine, Houston, Texas 77025.

Table 1—Test Diet*

Ingredients	Percent (weight)
Butter	40.0
Cholesterol	5.0
Sodium cholate	2.0
Propylthiouracil	0.3
Sucrose	20.5
Casein	20.0
Salt mix	4.0
Vitamin mix	2.0
Choline chloride	0.2
Nonnutritional bulk	6.0
Total	100.0

* One hundred twenty-five grams of the test diet was mixed with 125 g of canned horse meat (Hill's) to make 1-day ration for each dog.

fuchsin van Gieson, Masson's trichrome, periodic acid Schiff, colloidal iron and Alcian blue stains. The petrous and cavernous segments of the internal carotid arteries were removed with the temporal bones, fixed in Heidenhain's susa fluid, decalcified by 5% trichloroacetic acid solution, embedded in paraffin, sectioned 20 μ thick, and stained with hematoxylin-eosin. The specimens for electron microscopy were postfixed in buffered 1% osmium tetroxide, dehydrated with a graded series of ethanol and propylene oxide and embedded in epoxy resin. Sections 1 μ thick, from the resin-embedded blocks, were stained with 0.2% basic fuchsin ethanol solution, after oxidation in 2% periodic acid solution, and counterstained in methylene blue. Thin sections for electron microscopy were doubly stained with uranyl acetate and lead citrate.

Three mongrel dogs of approximately the same age and size were fed 1800 g per day of a commercial dog chow (Purina) Monday through Friday, and 900 g per day on Saturdays and Sundays. The chow contained (by weight) 27% crude protein and 9% crude fat. These control dogs were maintained for the same period and killed at the same time as the test dogs. Their cerebral arteries were examined in the manner described above.

Blood specimens obtained at autopsy were analyzed for serum levels of major lipid fractions by the following methods: Total and esterified cholesterol was extracted with 1:1 ethanol-ethyl acetate treated with $\text{Al}(\text{OH})_3$ to remove interfering bilirubin and the color reaction developed by ferric chloride-sulfuric acid solution.⁶ Phospholipids were extracted 2:1 chloroform-methanol, the dry residue digested with perchloric acid and the color developed by ammonium molybdate.⁷ Triglycerides were extracted with chloroform, treated with doulcil to remove phospholipids, hydrolyzed by alcoholic KOH and the color developed by chromotropic acid.⁸

Results

Intracranial Arteries

Gross Findings. The brains of the 3 test dogs revealed moderate to severe degrees of atherosclerosis. The arteries were characterized by

tortuosity and thickening of the walls, and arteriosclerotic changes involved the internal carotid-anterior and middle cerebral and the vertebral-basilar arteries (Figures 1 and 2). Although vascular lesions were extensive, segmental portions in each artery were spared. The severity of the lesions among the test dogs was variable. The caudate nucleus of 1 test animal revealed a cystic lesion, 3 mm in diameter. The intracranial arteries of control dogs were not remarkable grossly.

Histologic Findings. Cross sections of intracranial arteries of test dogs showed marked destruction and thickening of the arterial wall, frequently causing eccentric narrowing of the lumen (Figure 3). Arterial lesions contained lipid-laden macrophages, cholesterol crystal clefts and myointimal cells, appearing as fibroblasts and smooth muscle cells (Figure 4). The disruption of internal elastic lamina was common. One-micron-thick sections prepared from the glutaraldehyde- and osmium-fixed and the epoxy resin-embedded blocks of middle cerebral arteries, stained with basic fuchsin after oxidation in periodic acid, showed a distinct but weakly stained basement membrane under the endothelium and a strongly fuchsinophilic internal elastic lamina separate from the endothelial basement membrane. Thickening of the intima was largely attributed to the accumulation of smooth muscle cells and thin, strongly fuchsinophilic, apparently newly formed elastic laminae between the endothelial basement membrane and the internal elastic lamina (Figure 5). In contrast with the staining reaction on resin-embedded tissue, arterial sections prepared from formalin-fixed and paraffin-embedded blocks and stained by the periodic acid Schiff (PAS) method showed a strongly positive endothelial basement membrane and a negatively stained internal elastic lamina. Between the endothelial basement membrane and the internal elastic lamina was a PAS-positive substance (Figure 6). Apparently associated with the formation of immature elastic tissue, colloidal iron- and Alcian blue-stained sections showed acid mucopolysaccharide accumulation in the intima (Figure 7). Lipid-laden leukocytes were frequently found in the arterial lumen. The above histologic lesions were noted in all major cerebral arteries of test dogs but in different degrees of severity. Small arteries and arterioles of the brains were normal. The intraosseous segments of the internal carotid arteries frequently revealed severe occlusive lesions; an aneurysmal dilatation due to destruction of the media was noted in 1 test animal (Figure 8). The cystic lesion described grossly in the caudate nucleus of 1 dog consisted of plump phagocytes (gitter cells) and gliosis similar to those seen in human cerebral infarct (Figure 9).

The cerebral arteries of control dogs revealed a strongly PAS-positive

layer of basement membrane between the endothelium and the internal elastic lamina, and there was no evidence of separation of the internal elastic lamina from the endothelial basement membrane (Figure 10).

Electron Microscopic Findings. The middle cerebral arteries of the test dogs revealed a distinct basement membrane under the endothelium, separation of the internal elastic lamina from the basement membrane and the accumulation of smooth muscle and lipid-laden cells as well as collagen in the thickened intima (Figures 11 and 12). Leukocytes containing lipids in the cytoplasm were found occasionally within the arterial lumen, and some of them appeared to cling to the intimal endothelial cells (Figure 13). Between the endothelial basement membrane and the internal elastic lamina were electron-dense amorphous layers corresponding to the thin, fuchsinophilic laminae of the 1- μ thick sections (Figures 5 and 14). These electron-dense layers were frequently contiguous with both the endothelial basement membrane and the internal elastic lamina, and they partitioned smooth muscle cells in the widened intima. Extracellular vacuoles consistent with lipid were also noted in the intima. Intracytoplasmic laminated structure similar to that described in atherosclerotic lesion of human aorta⁹ was found in some smooth muscle cells (Figure 15).

The middle cerebral arteries of the control dogs revealed a distinct basement membrane under the endothelium that was similar to that seen in the test dogs but contiguous with the internal elastic lamina, with electron-dense substance between the two layers; there was no evidence of separation of the internal elastic lamina from the basement membrane. This electron-dense substance was in a granular, rather than laminar, form and appeared to incorporate closely with both the endothelial basement membrane and the internal elastic lamina of the normal arteries (Figures 16 and 17).

Extracranial Arteries

The intraosseous segments of the internal carotid arteries of all 3 test dogs revealed severe occlusive atherosclerotic changes, as described above. Likewise, the aortas and the coronary, mesenteric, celiac, renal, caudal and iliac arteries had moderate to severe degrees of occlusive atherosclerotic lesions. Electron microscopy of the coronary arteries, to compare with the cerebral arteries, showed a recognizable basement membrane under the endothelium which was not as thick and distinct as that seen in the cerebral arteries. However, as in the cerebral arteries, detachment of the internal elastic lamina from the endothelial basement membrane, accumulation of extracellular and intracellular vacuoles

consistent with lipid, electron-dense laminar substance and smooth muscle cell proliferation were commonly noted (Figure 18).

Serum Lipids

Results of chemical analyses on serum lipids of test and control dogs are summarized in Table 2. Differences in serum levels of cholesterol, phospholipids and triglycerides between test and control groups were highly significant. Total cholesterol levels of test dogs averaged more than four times the values of the controls, but the percent of cholesterol as ester remained within a normal range of 70 to 80%. Between test and control groups, levels of phospholipids and triglycerides showed lesser degrees of differences than did cholesterol levels.

Discussion

In general, intracranial arteries of mammals are resistant to dietary induction of atherosclerosis.^{1,2,10} In a study using the cebus monkey fed cholesterol, cerebral arteries were spared despite extensive atherosclerosis in the aorta and the coronary and carotid arteries.³ In the present experiment, animals also developed severe atherosclerosis of extracranial arteries, such as the aorta and the coronary, carotid and other major arteries. A study on cerebral arteries of pigs fed a high fat diet with cholesterol revealed light and electron microscopic evidence of atheromatous changes, but occlusive intimal lesions were not produced.¹¹ In a study reported by Belza *et al* using dogs that were administered cholesterol and thiouracil, various degrees of gross and histologic lesions of atherosclerosis were observed in major intracranial arteries, and cerebral infarcts similar to the lesion of the present study were found.⁴ However, atherosclerotic occlusive lesions of the extracranial internal carotid and vertebral arteries should be taken into consideration in the pathogenesis of cerebral infarction, because atherosclerotic occlusive disease in the high cervical and intraosseous segments of the internal carotid arteries (such as the lesions in the present

Table 2—Levels of Serum Lipid Fractions (Mean \pm SD, mg/100 ml)

Group	No. of dogs	Total cholesterol	Esterified cholesterol	Phospholipids*	Triglycerides
Test	3	1015 \pm 58	698 \pm 74	702 \pm 88	129 \pm 17
Control	3	239 \pm 48	170 \pm 44	327 \pm 47	55 \pm 10
P (t-test)		<0.001	<0.001	<0.001	<0.001

* Expressed as lecithin by multiplying the values of phospholipid phosphorus by 25.

experiment) is known to be a potential source of thromboemboli causing cerebral infarction in man.^{12,13}

Spontaneous atherosclerosis of the intracranial arteries occurs in aged dogs, pigs and primates.^{14,15} Andrus *et al* reported that spontaneous atherosclerotic lesions were commonly found in the cerebral arteries of control chimpanzees, so that the effects of high-fat diets with and without cholesterol could not be correlated.⁵ However, in the present experiment the possibility of spontaneous atherosclerosis in the intracranial arteries of the test dogs was excluded, and the development of cerebral arterial lesions was the result of the atherogenic diet, because similar vascular changes did not occur in control animals maintained on a commercial dog chow in an otherwise identical condition. All dogs of the present experiment were 5 to 6 years old when they were killed. Induced intracranial atherosclerosis of the test dogs was present only in major and medium-sized vessels, and small arteries and arterioles of the brains were normal.

A thick basement membrane under the endothelium, noted by light and electron microscopy in both test and control dogs, appeared to be a hallmark of cerebral arteries. The endothelial basement membrane of coronary arteries and aortas was recognizable in the present and previous experiments,¹⁶ but it did not appear as distinct as that seen in the cerebral arteries. Electron-dense laminar substance was frequently noted between the endothelial basement membrane and the internal elastic lamina. The distribution of this substance in relation to the elastic lamina and its staining reaction on PAS suggest that it is a newly formed elastin. In man, increased quantities of the basement membrane and ground substance between the endothelium and the internal elastic lamina were described in atherosclerotic cerebral arteries.¹⁷ In the present study, one consistent ultrastructural finding in atherosclerotic cerebral arteries was the separation of the internal elastic lamina from the endothelial basement membrane. As far as the author is aware, no studies dealing with the ultrastructure of experimental cerebral atherosclerosis in the dog have been reported previously.

Summary

Moderate to severe atherosclerosis was produced in the cerebral arteries of 3 mongrel dogs fed an atherogenic diet. Gross atherosclerotic changes were noted in all major intracranial arteries and, histologically, the arteries revealed destruction of the intima and media, deposition of cholesterol clefts and lipid, proliferation of fibroblasts, smooth muscle cells and collagen and accumulation of elastin and acid mucopolysac-

charide. A 3-mm cystic infarct occurred in the caudate nucleus of 1 animal. Electron microscopy revealed a distinct endothelial basement membrane, frequently separated from the internal elastic lamina. Extracranial systemic arteries of all 3 test dogs revealed moderate to severe atherosclerosis. In 3 control dogs, the intracranial arteries were normal. There was no evidence that the internal elastic lamina had separated from the endothelial basement membrane. Serum levels of cholesterol, phospholipids and triglycerides of test dogs averaged 2 to 4 times the levels of controls.

References

1. Duff GL: Experimental cholesterol arteriosclerosis and its relationship to human arteriosclerosis. *Arch Pathol* 20:81-123, 259-304, 1935
2. Pollak OJ: Attempts to produce cerebral atherosclerosis. *Arch Pathol* 39:16-21, 1945
3. Bullock BC, Clarkson TB, Lehner NDM, Lofland HB Jr, St Clair RW: Atherosclerosis in *Cebus albifrons* monkeys. III. Clinical and pathologic studies. *Exp Mol Pathol* 10:39-62, 1969.
4. Belza J, Rubinstein L, Maier N, Haimovici H: Experimental cerebral atherosclerosis in dogs. *Ann NY Acad Sci* 149:895-906, 1968
5. Andrus SB, Portman OW, Riopelle AJ: Comparative studies of spontaneous and experimental atherosclerosis in primates. II Lesions in chimpanzees including myocardial infarction and cerebral aneurysms. *Progr Biochem Pharmacol* 4:393-419, 1968
6. Babson AL, Shapiro PO, Phillips GG: A new assay for cholesterol and cholesterol esters in serum which is not affected by bilirubin. *Clin Chim Acta* 7:800-804, 1962
7. Zilversmit DB, Davis AK: Microdetermination of plasma phospholipids by trichloroacetic acid precipitation. *J Lab Clin Med* 35:155-160, 1950.
8. Van Handel E, Zilversmit DB: Micromethod for direct determination of serum triglycerides. *J Lab Clin Med* 50:152-157, 1957
9. Geer JC, McGill HC, Strong JP: The fine structure of human atherosclerotic lesions. *Am J Pathol* 38:263-287, 1961
10. Altschul R: Experimental arteriosclerosis in the nervous system. *J Neuropath Exp Neurol* 5:333-341, 1946
11. Imai H, Thomas WA: Cerebral atherosclerosis in swine: Role of necrosis in progression of diet-induced lesions from proliferative to atheromatous stage. *Exp Mol Pathol* 8:330-357, 1968
12. Yates PO, Hutchinson EC: Cerebral infarction; the role of stenosis of the extracranial arteries. Medical Research Council Special Report No. 300, London, Her Majesty Stationery Office, 1961, pp 1-95
13. Suzuki M: Pathologic anatomy of atherosclerotic occlusive lesions of extracranial arteries and cerebrovascular disease. *Cardiovas Res Cent Bull* 7:158-166, 1969
14. Luginbühl H, Detweiler DK: Animal models for the study of cerebrovascular disease, National Academy of Sciences monograph, Animal Models for

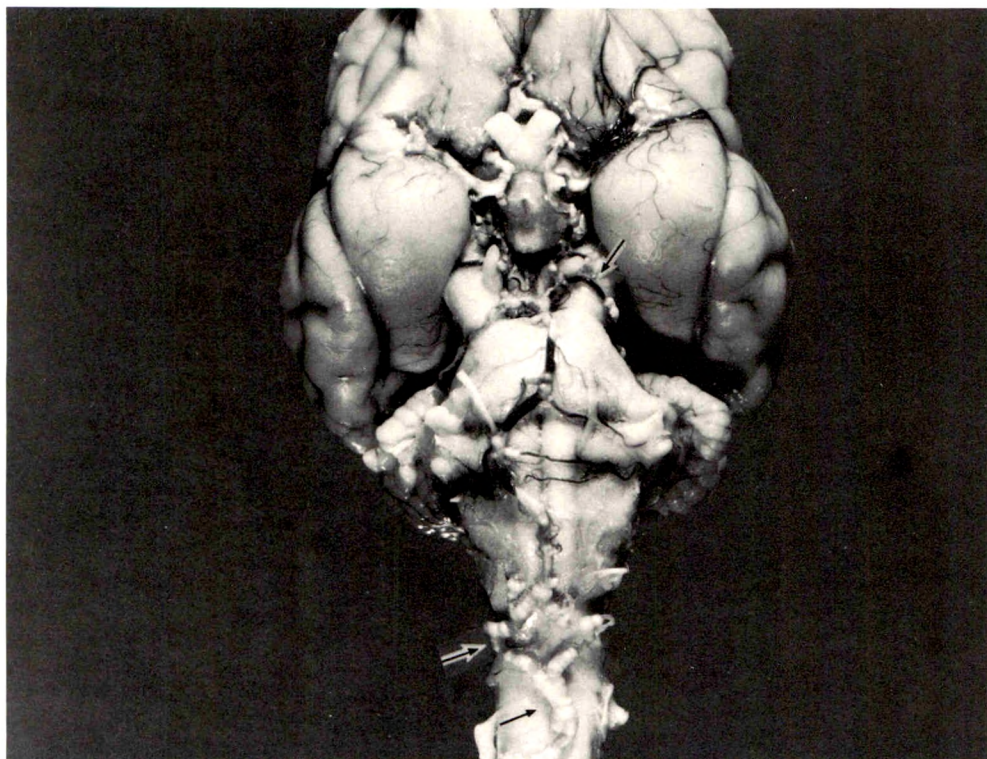
- Biomedical Research, Proceeding of a Symposium. Sponsored by the Institute of Laboratory Animal Medicine. Washington, DC, 1968, pp 35-41
15. Stout C, Lemmon WB: Predominant coronary and cerebral atherosclerosis in captive nonhuman primates. *Exp Mol Pathol* 10:312-322, 1969
 16. Suzuki M, Greenberg SD, Adams JG, O'Neal RM: Experimental atherosclerosis in the dog: A morphologic study. *Exp Mol Pathol* 3:455-467, 1964
 17. Flora G, Dahl E, Nelson E: Electron microscopic observations on human intracranial arteries: Changes seen with aging and atherosclerosis. *Arch Neurol* 17:162-173, 1967

Acknowledgment

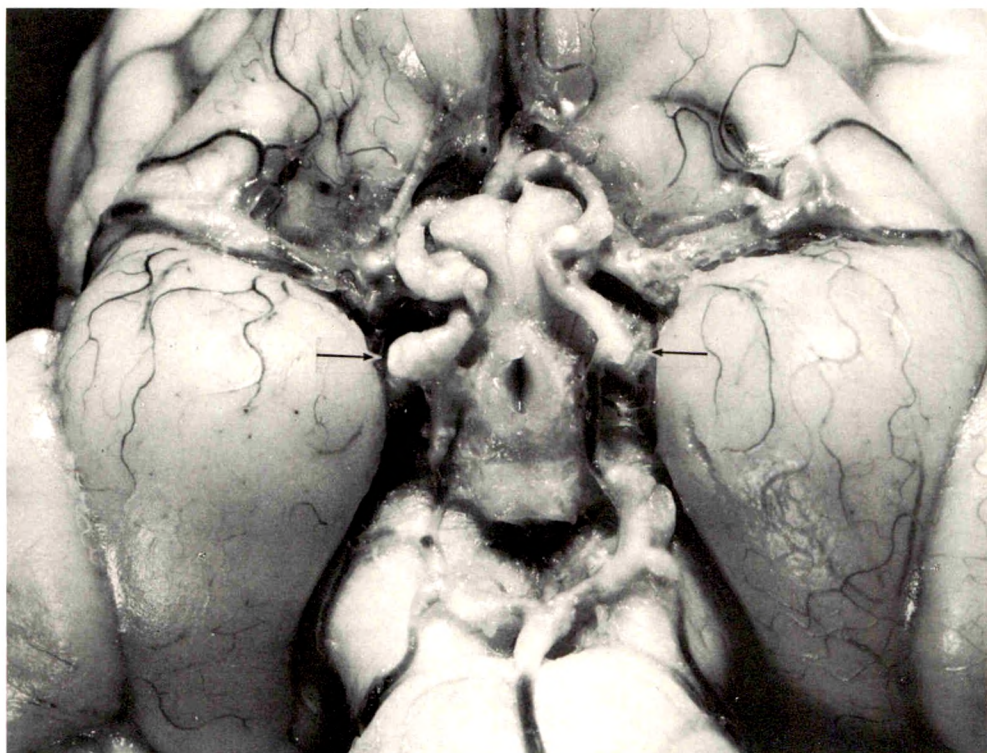
The author is indebted to Mrs. Elsa Ramos for her technical assistance in this study.

Fig 1—The ventral surface of the brain of a test dog. Atheromatous lesions are opaque and distinct from relatively uninvolved segments of the arteries (*top arrow*). The ventral spinal artery and the cerebrospinal artery (a branch of the vertebral) are thickened and tortuous (*bottom two arrows*).

Fig 2—The arterial circle of the brain (circle of Willis) of another test dog. All major cerebral arteries have severe atheromatous lesions, but small vessels visible through the leptomeninges appear grossly uninvolved. Both arrows point to the cross sections of the internal carotid arteries. The pituitary stalk, distal portions of the optic nerves, and the oculomotor nerves have been dissected.



1



2



Fig 3—The posterior cerebral artery showing eccentric narrowing of the lumen. Atheroma destroyed almost the entire thickness of the artery (H&E, $\times 75$).

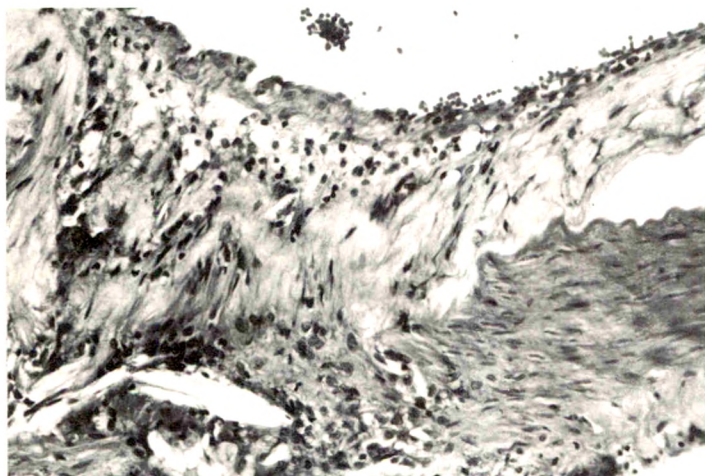


Fig 4—The anterior cerebral artery with disruption of the internal elastic lamina. The arterial lesions are composed mainly of formation of foam cells, proliferation of myointimal cells and deposition of cholesterol clefts (H&E, $\times 192$).

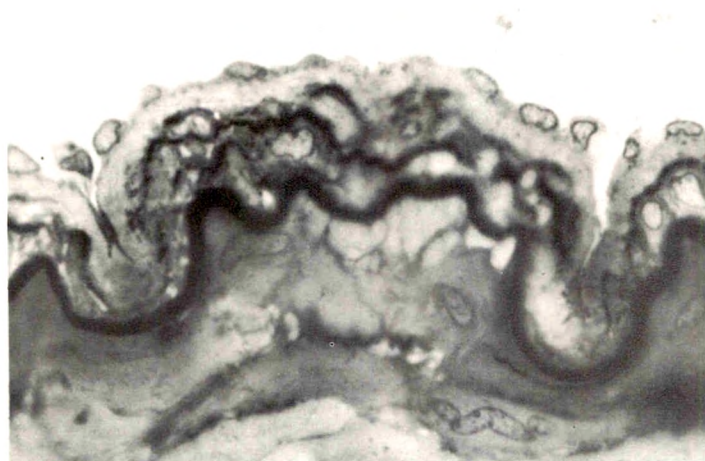


Fig 5—One-micron-thick section from epoxy resin-embedded block of the middle cerebral artery, stained with basic fuchsin after oxidation in periodic acid. A pale zone of basement membrane under the endothelium is discernible and separate from a strongly fuchsinophilic internal elastic lamina. Between the endothelial basement membrane and the internal elastic lamina are several thin layers of fuchsinophilic tissue, probably newly formed elastin, separating myointimal cells which were proved to be smooth muscle cells by electron microscopy ($\times 1200$).

Fig 6—The anterior cerebral artery stained by the periodic acid-Schiff (PAS) method. The endothelial basement membrane is strongly PAS-positive. The PAS negative internal elastic lamina is separate from the endothelial basement membrane, thus widening subendothelial space ($\times 1200$).

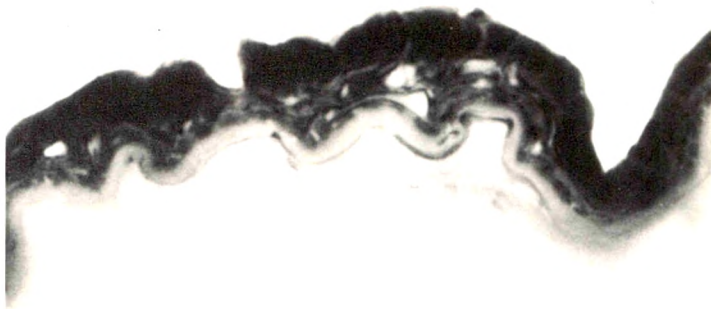


Fig 7—The middle cerebral artery stained with colloidal iron showing accumulation of acid mucopolysaccharide. The strongly positive substance is entirely in the thickened intima and not recognizable in the media. Cholesterol crystal clefts are also abundant ($\times 400$).

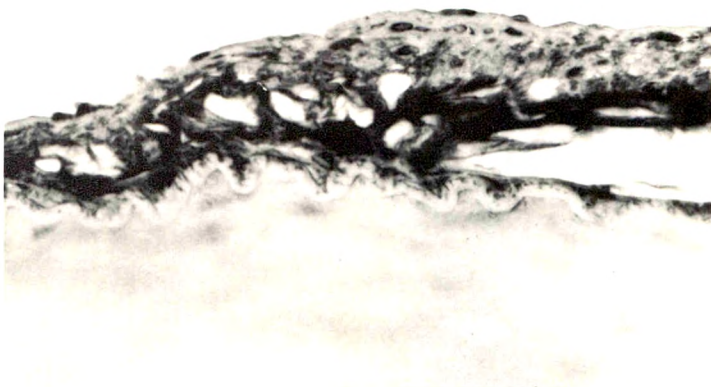
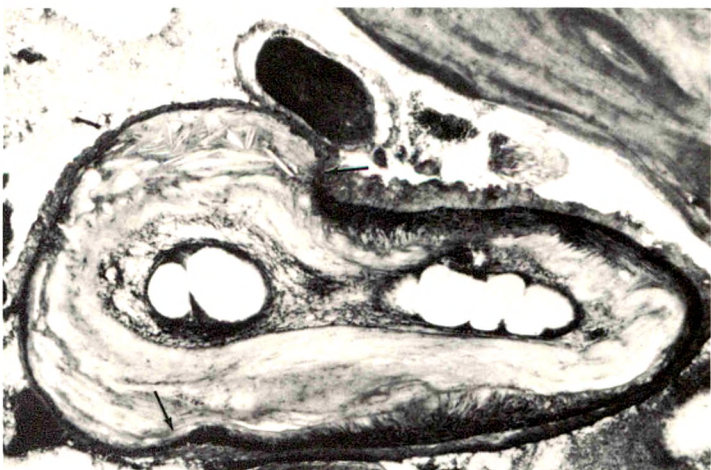


Fig 8—The petrous segment of the internal carotid artery. The lumen is markedly narrowed by atheromatous changes which destroyed the media, causing aneurysmal dilatation of the arterial wall (arrows). Decalcified and sectioned at $20\ \mu$ (H&E, $\times 48$).



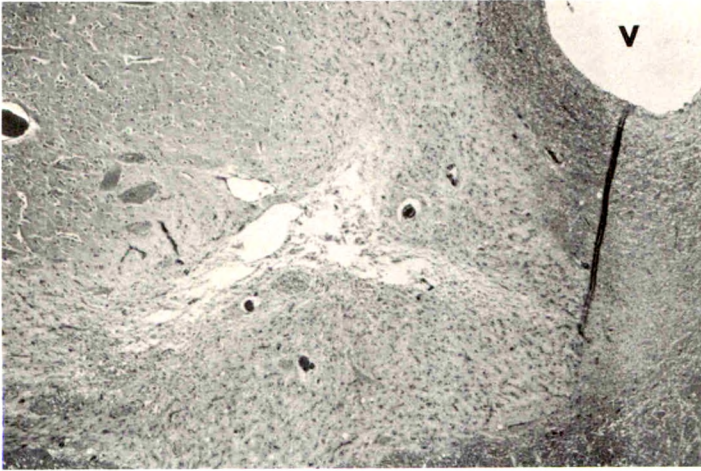


Fig 9—The caudate nucleus with a cystic infarct. The lateral ventricle (V) is in the right upper corner (H&E, $\times 30$).

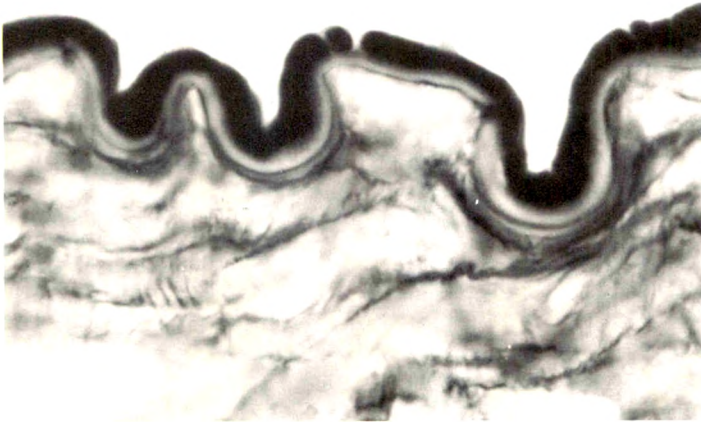
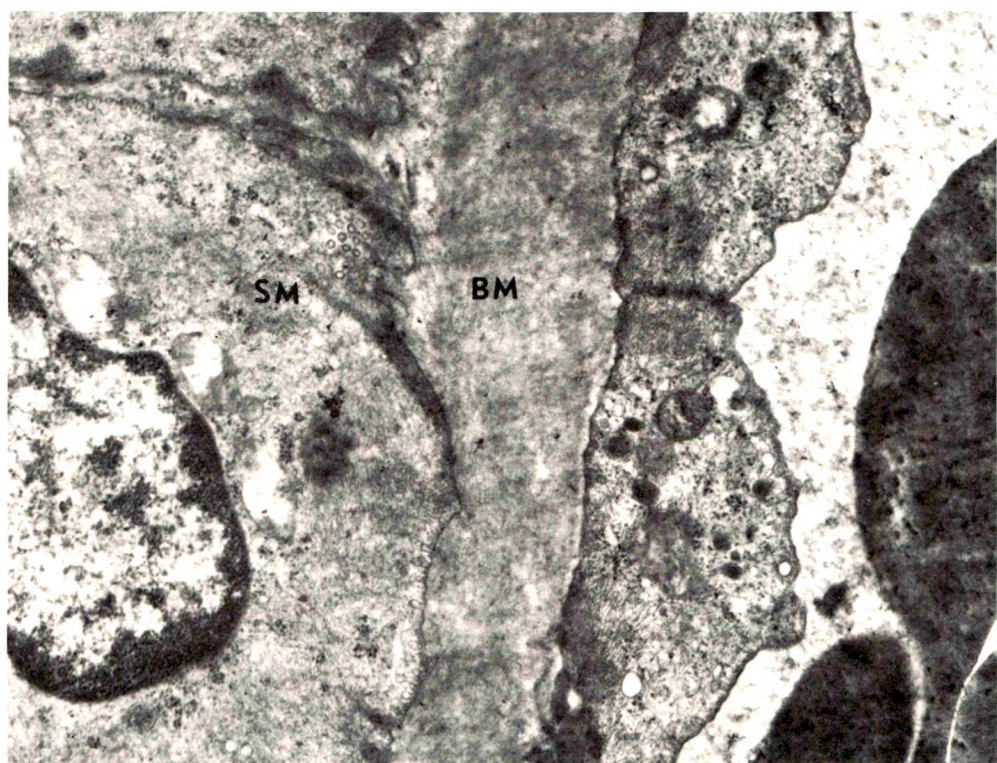


Fig 10—The middle cerebral artery of a control dog stained with PAS. There is no evidence of separation of the internal elastic lamina (PAS-negative) from the endothelial basement membrane (PAS-positive) ($\times 1200$).

Fig 11 and 12—The middle cerebral arteries of test dogs. The basement membrane (BM) partitions the endothelium from subendothelial structure which contains abundant collagen and smooth muscle cells (SM) (11, $\times 9930$; 12, $\times 16,500$).

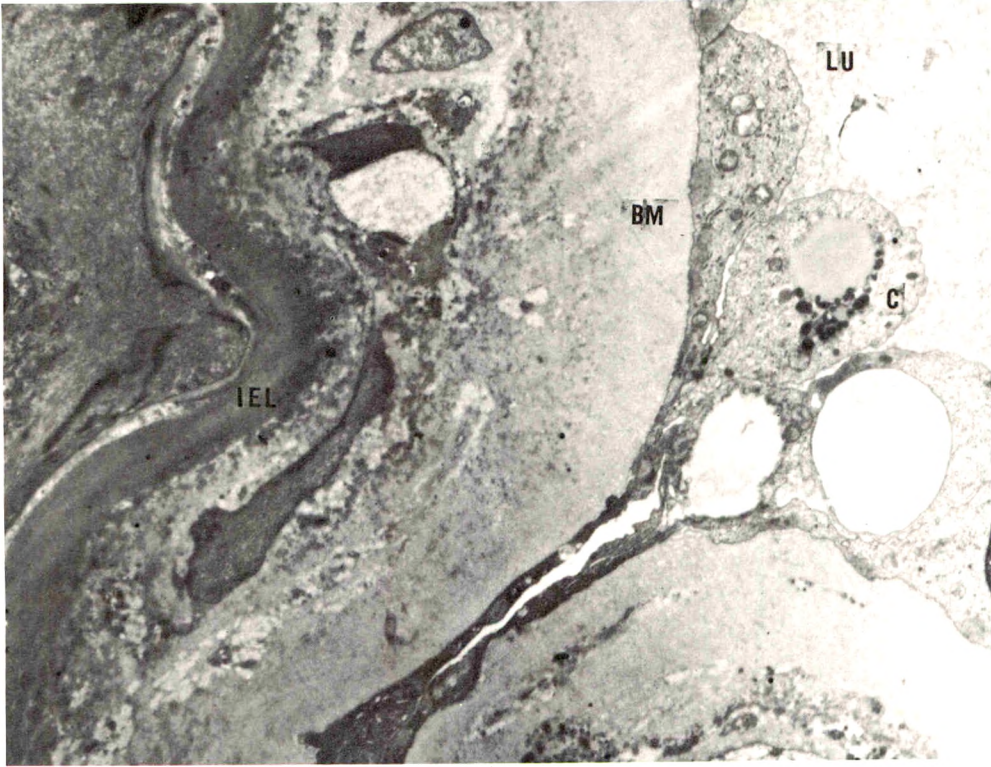


11



12

13



14

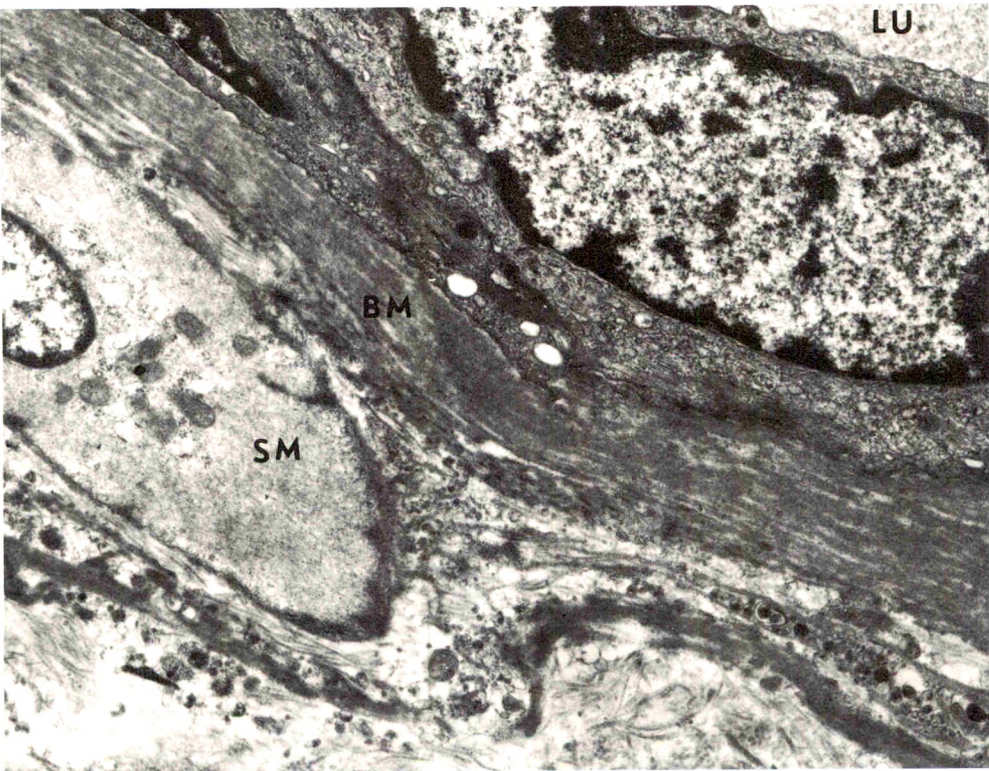
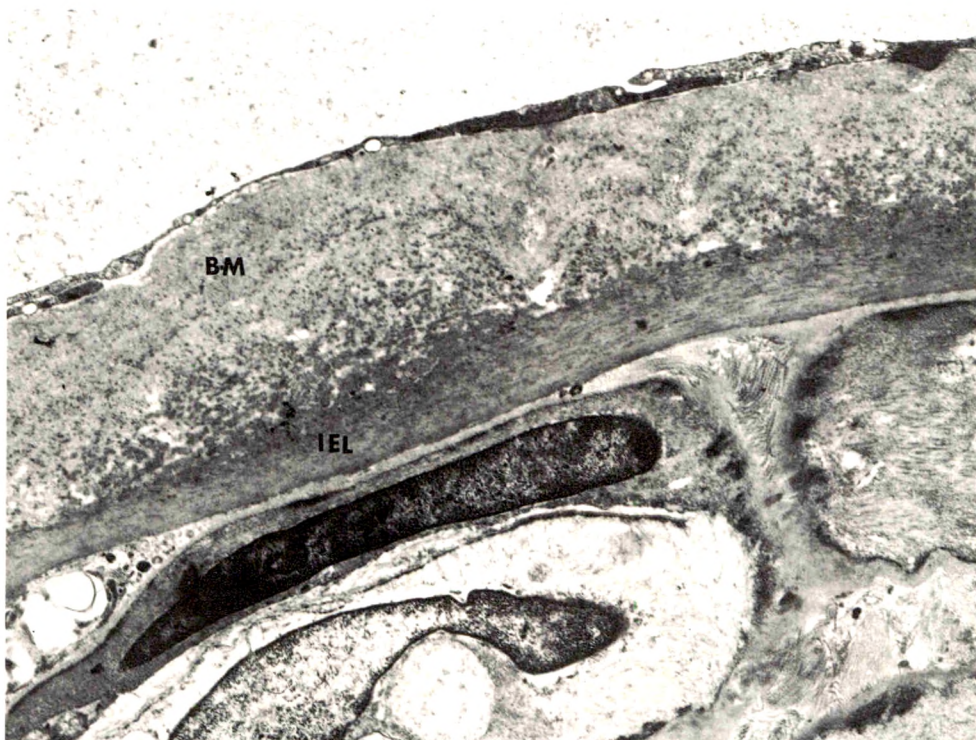


Fig 13—The middle cerebral artery of test dog. Between the endothelial basement membrane and the internal elastic lamina (*IEL*) are smooth muscle cells. A cell (*C*) in the arterial lumen (*LU*), probably a blood leukocyte containing cytoplasmic vacuoles, clings to the endothelial surface ($\times 6880$). **Fig 14**—The middle cerebral artery of test dog. Under the endothelial basement membrane, the intima contains layers of electron-dense amorphous substance which extend between smooth muscle cells ($\times 10,820$).



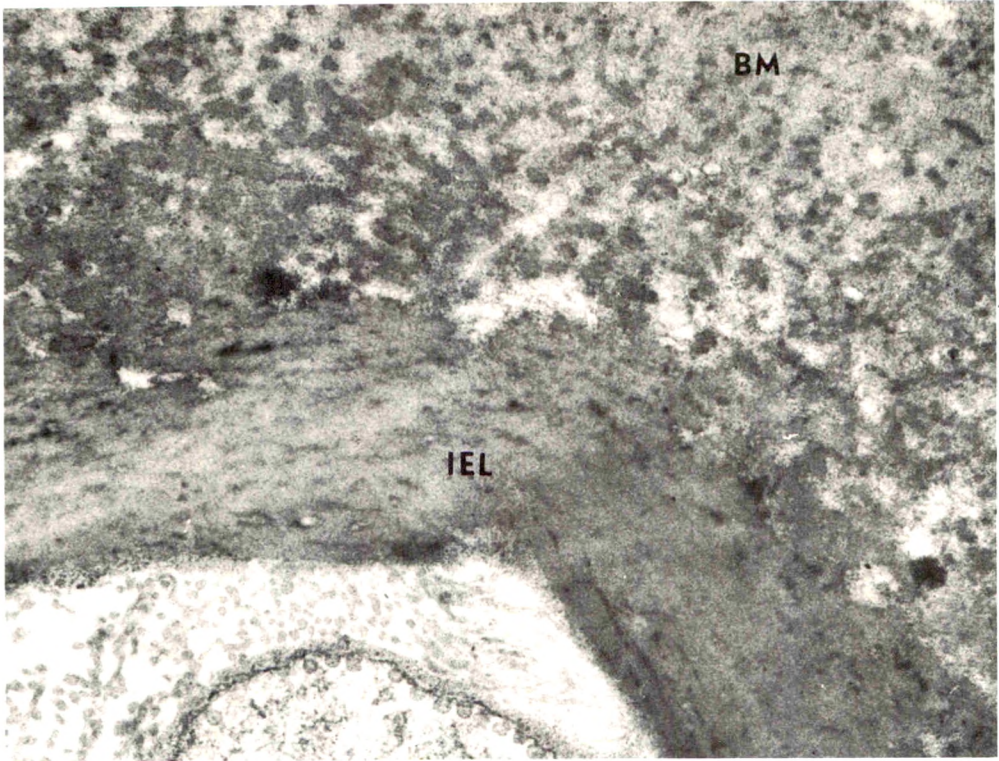
15



16

Fig 15—The middle cerebral artery of test dog. Under the endothelium is an extended layer of basement membrane. One smooth muscle cell contains intracytoplasmic laminated bodies (arrow) ($\times 4585$). **Fig 16**—The middle cerebral artery of control dog. There is no evidence of separation of the internal elastic lamina from the endothelial basement membrane ($\times 6010$).

17



18

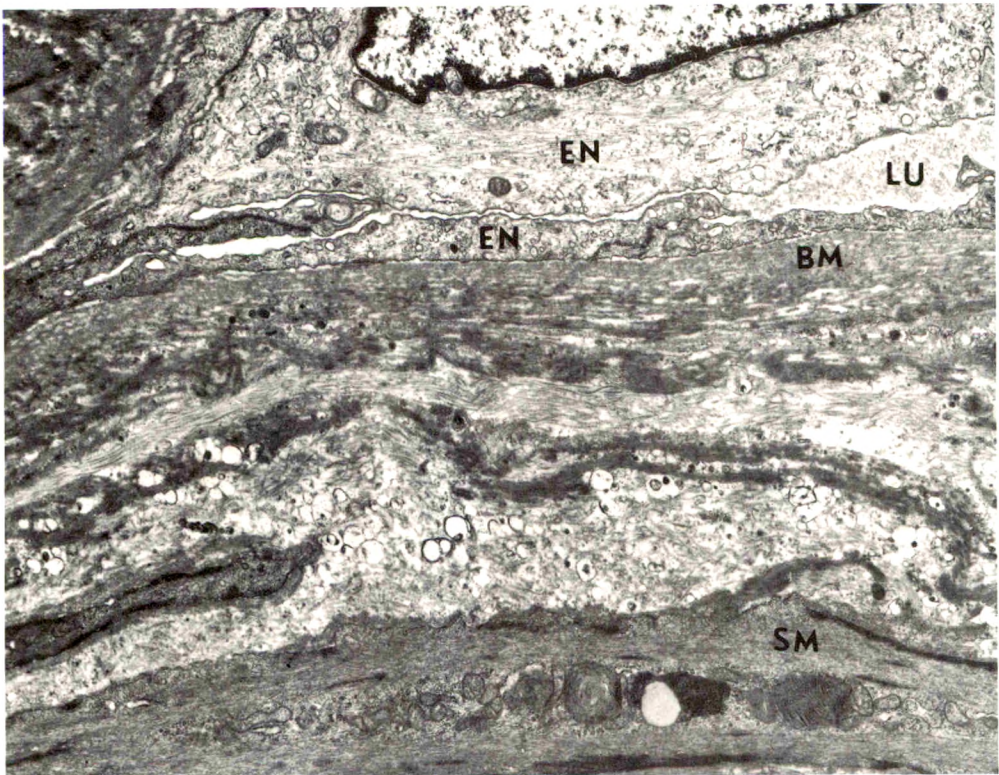


Fig 17—Higher magnification of the middle cerebral artery of control dog. Electron-dense granular substance, probably elastic fibrils, is closely incorporated with the endothelial basement membrane ($\times 31,110$). **Fig 18**—The coronary artery of test dog. The basement membrane under endothelial cells (*EN*) is recognizable but not as thick as that of the cerebral arteries. The internal elastic lamina has been detached and not seen here. A few layers of amorphous dark substance are present in the widened subendothelial space, which contains smooth muscle cells, extracellular lipid vacuoles and collagen. One smooth muscle cell contains intracytoplasmic laminated bodies similar to those seen in Fig 15 ($\times 9025$).

Division of Protoplasmic Astrocytes in Acute Experimental Hepatic Encephalopathy

An Electron Microscopic Study

Michael D. Norenberg, MD, Lowell W. Lapham, MD, Mark W. Eastland, MD and Allyn G. May, MD

The ultrastructural features of dividing protoplasmic astrocytes, induced by the production of hepatic encephalopathy, are described. True cellular hyperplasia, as manifested by cytokinesis at the site of paired nuclei, was demonstrated. The cytoplasm contained structural elements suggesting that cell division occurs by a highly organized process. Some of the observations were similar to those found in mitotic division in other types of cells, raising the possibility that cell division in protoplasmic astrocytosis might occur by mitosis rather than by amitosis, as widely held (*Am J Pathol* 67:403-412, 1972).

A BASIC REACTIVE CHANGE to injury of the central nervous system is proliferation of astrocytes. This phenomenon has been extensively studied following destructive lesions which result in fibrous astrocytosis and the formation of a glial scar. A less well understood process is that of protoplasmic astrocytosis (or hyperplasia of protoplasmic astrocytes). This type of astrocytic response is the most striking change in some of the metabolic encephalopathies and is best exemplified in hepatic encephalopathy. It is characterized by an increase in the number of astrocytic nuclei, nuclear swelling and pallor and enlargement of nucleoli, leading to the Type II Alzheimer astrocyte. A common feature is the presence of paired astrocytic nuclei. In contrast to fibrous astrocytosis, glial fiber production is conspicuously absent.

Although nuclear proliferation in protoplasmic astrocytosis is undisputed,¹ an important unanswered question from previous studies is whether the process involves only multinucleation, or leads to true cellular hyperplasia. A closely related issue is the mechanism of division. Mitotic figures have not been described in disorders of man in which

From the Department of Pathology (Neuropathology), and Department of Surgery, University of Rochester Medical Center, Rochester, New York.

Supported in part by Grant GM-00133-15 from the National Institutes of Health.

Presented in part before the Forty-Seventh Annual Meeting of the American Association of Neuropathologists, June, 1971, in San Juan, Puerto Rico.

Accepted for publication Nov 15, 1971.

Address for reprint requests: Dr. Lowell W. Lapham, Department of Pathology, University of Rochester Medical Center, Rochester, New York 14642.

protoplasmic astrocytosis is found,^{1,2} although they are sometimes observed in fibrous astrocytosis (see Discussion). In the few reported experimental studies concerning protoplasmic astrocytes, mitotic figures have also not been mentioned.³⁻⁷ The possibility has been raised that in protoplasmic astrocytosis division might occur by amitosis.^{1,2} By whatever method, it is reasonable to postulate that division is a well-organized process in protoplasmic astrocytosis, inasmuch as each daughter nucleus contains a diploid amount of DNA.²

It is the purpose of this report to describe some of the ultrastructural features of division in protoplasmic astrocytes. There is currently little basic information about the biologic properties of protoplasmic astrocytes and their behavior in pathologic states. Emphasis here is placed upon those morphologic aspects relevant to the question of multinucleation, as compared with true cellular hyperplasia, and the problem of the mode of division. We have chosen experimentally produced hepatic encephalopathy as a means of inducing protoplasmic astrocytosis. Although the course is acute in the model we have used, protoplasmic astrocytosis is the most prominent neuropathologic change by light microscopy, simulating closely the early stages of this response in hepatic encephalopathy in man.

Materials and Methods

Hepatic encephalopathy was produced in 4 mongrel dogs. Briefly, a modification of Rappaport's⁸ two-stage ischemic hepatic injury was performed.⁹ The first stage was accomplished by constructing a portacaval shunt. At the same time, a snare was loosely applied around the hepatic artery and the end brought out into the subcutaneous tissue. The second stage was performed on the following day, by which time the animal was fully recovered from anesthesia and behavior was normal. At this time, the snare was exposed under local anesthesia and tightened, completely occluding the hepatic artery. This procedure enabled us to follow the development of coma from the conscious state. Throughout this post-ligation period, the animals were maintained on hourly glucose infusions (0.5 g/kg body weight). Blood chemistries, including blood glucose, serum electrolytes and arterial blood gases, were monitored every 6 hours. During the period of deep coma, occurring, on the average, 29 hours after hepatic artery ligation, the brain was fixed by perfusion using a mixture of paraformaldehyde (2%) and glutaraldehyde (2.5%) in 0.1 M phosphate buffer adjusted to pH 7.4. Blocks of frontal lobe were subsequently post-fixed in 1% osmium tetroxide and embedded in Durcupan (Fluka). Thin sections were obtained with an LKB Ultratome III, stained with uranyl acetate and lead citrate and examined with an RCA EMU-3F electron microscope. Eight normal and 2 sham-operated dogs formed the control material for this study.

Results

The course following post-hepatic artery ligation consisted initially of lethargy and emesis. The dogs then gradually developed ataxia, rigid-

ity, bizzare posturing and eventually coma. In preliminary studies, we observed that the natural course of the illness led to death within 48 hours after ligation. The time interval between hepatic artery ligation and coma ranged between 21 and 35 hours. As expected, serum tests reflected hepatocellular necrosis. Blood glucose and serum electrolytes, however, remained normal; arterial blood gases also remained normal except for a slight respiratory alkalosis terminally.

By light microscopy, the nuclei of astrocytes in the frontal cortex were markedly increased in number as compared to normal dogs (from a comparison of astrocytic nuclei counts, P was < 0.001).¹⁰ Paired nuclear forms were frequently noted.⁹ At the ultrastructural level, the paired nuclei were separated by a set of apposing cytoplasmic membranes, one belonging to each daughter cell (Figure 1A). This feature characterized all paired astrocytic nuclei (over 50 pairs were examined). Even when nuclei were in close proximity and appeared to abut on each other, there was evidence of complete cytokinesis (Figure 1B and C). Binucleate or multinucleate astrocytes were not observed.

Mitotic figures were not found nor were stages of division identified. Pertinent to the issue of division, however, was the finding of centrioles in approximately 1 of 4 astrocytes studied, whereas in our control material, centrioles were found in less than 1 of 10 astrocytes. Furthermore, when encountered in normal astrocytes, centrioles were usually embedded in an amorphous osmiophilic matrix. In contrast, centrioles were often associated with complex structures in our experimental model. Procentrioles were occasionally identified adjacent to parent centrioles (Figure 2A). Other pericentriolar findings included fibrogranular aggregates, and groups of microtubules (Figure 2B and C). In some instances, striated rootlets (Figure 2A and C) and apparent production of microtubules from centrioles were identified (Figure 2A). Apart from pericentriolar structures, there was often an increase in scattered microtubules throughout the cytoplasm (Figure 3). Production of glial filaments was not observed in any of the astrocytes examined.

Discussion

Although it generally has been assumed that proliferation of astrocytic nuclei indicated cellular hyperplasia, this has not previously been proven. Furthermore, the close proximity of paired nuclei has made it impossible to exclude multinucleation. We have established, in our experimental model of hepatic encephalopathy, that true cellular hyperplasia takes place in protoplasmic astrocytosis, not merely nuclear division. Despite little knowledge regarding the function of protoplasmic

astrocytes, cellular proliferation may occur as part of their basic reaction in certain pathologic conditions.

The mechanism of astrocytic division, however, remains an enigma. With regard to division of astrocytes in general, it has traditionally been held that all forms of astrocytes divide by amitosis, since the introduction of this concept by Del Rio Hortega and Penfield.¹¹ This view is still expressed in current texts of neuropathology.^{12,13} Amitotic division in other cell systems has been thought to result principally in multinucleation and is regarded by some investigators as a reactive change by means of which an increase in cell function can take place in response to various types of stress, especially to metabolic derangements.^{14,15} This process would, therefore, favor cell economy, avoiding the disruption of other cellular activities that mitotic division and subsequent cytokinesis might incur. Not all investigators, however, have accepted the concept that amitosis occurs in mammalian cells,¹⁶ or, more pertinently, in the nervous system.¹⁷ Since protoplasmic astrocytosis, in our experimental material, led to cell division and never to multinucleation, as far as we could ascertain, doubt is cast upon amitosis as the mechanism of division.

Insofar as fibrous astrocytosis with formation of a glial scar is concerned, mitotic figures have been noted in studies of human neuropathologic disorders.¹⁷⁻¹⁹ These observations are strengthened in a report by Cavanagh who showed in experimental studies that fibrous astrocytes are, in fact, capable of mitotic division.²⁰ He emphasized that adequacy and speed of tissue fixation were important in being able to demonstrate mitosis.

Despite fixation by perfusion in our study, mitotic figures were never observed. A number of observations from our material, however, bear on the problem of division. Centrioles may play an important role, as illustrated by their increased numbers and by the presence of pro-centrioles. Procentrioles are seen in the early phase of centriolar replication in other cell systems as part of mitosis.²¹ Of particular interest were two additional findings which support the possibility that division of protoplasmic astrocytes may occur by mitosis. These were pericentriolar microtubular aggregates and increased numbers of scattered cytoplasmic microtubules. When microtubules are increased throughout the cytoplasm at the time of cell replication, they are generally concerned with formation of a spindle, whereas microtubular aggregates in a pericentriolar location may represent ultrastructural elements of an aster.²² The role of fibrogranular aggregates and striated rootlets in protoplasmic astrocytosis is more puzzling, as they have been described

primarily as structural components of cilia or in ciliogenesis.²³ Although cilia have been described in astrocytes,²⁴ they were not found in our experimental material.

We recognize that definitive conclusions regarding the mode of division cannot be drawn from this study. The finding of complete cytokinesis in protoplasmic astrocytosis, however, along with many centrioles, complex pericentriolar structures and increased numbers of microtubules, favor the view that mitosis, rather than amitosis, was responsible for cellular division. These observations certainly suggest that protoplasmic astrocytes divide by a complex mechanism and, in our opinion, justify reexamination of the method whereby they replicate.

References

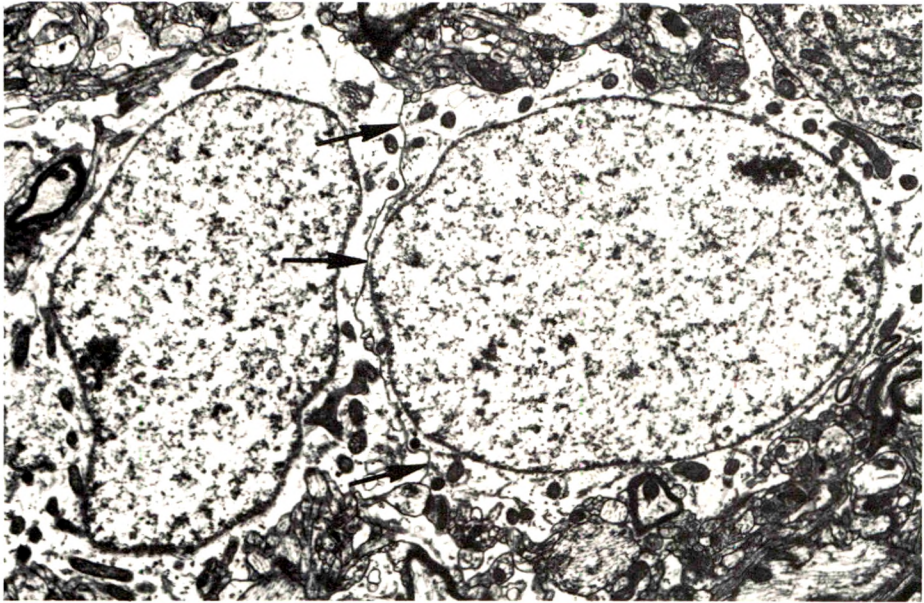
1. Adams RD, Foley JM: The neurological disorder associated with liver disease, metabolic and toxic diseases of the nervous system. *Proceedings of the Association for Research in Nervous and Mental Disease*. Vol 32. Edited by HH Merritt, CC Hare. Baltimore, Williams and Wilkins Co, 1953, p. 214
2. Lapham LW: Cytologic and cytochemical studies of neuroglia: I. A study of the problem of amitosis in reactive protoplasmic astrocytes. *Am J Pathol* 41:1-21, 1962
3. Cavanagh JB, Kyu MH: Type II Alzheimer change experimentally produced in astrocytes in the rat. *J Neurol Sci* 12:63-75, 1971
4. Cole M, Rutherford RB, Smith FO: Experimental ammonia encephalopathy in the primate. *Arch Neurol* 26:130-136, 1972
5. Hasson J, Leech RW: Experimental hepatocerebral disease: Astrocytic changes in the globus pallidus of rats with carbon tetrachloride induced cirrhosis. *Arch Pathol* 84:286-289, 1967
6. Kline DG, Crook JN, Nance FC: Eck fistula encephalopathy: Long-term studies in primates. *Ann Surg* 173:97-103, 1971
7. Kline DG, Doberneck RC, Chun BK, Rutherford RB: Encephalopathy in graded portacaval shunts. *Ann Surg* 164:1003-1012, 1966
8. Rappaport AM, MacDonald MH, Borowy ZJ: Hepatic coma following ischemia of the liver. *Surg Gynecol Obstet* 97:748-762, 1953
9. Benson RW, May AG, Norenberg MD, Lapham LW: Protoplasmic astrocytosis of the brain in experimental hepatic coma. *Surg Forum* 21:357-359, 1970
10. Benson RW, May AG, Norenberg MD, Lapham LW: An experimental model for the study of acute hepatic encephalopathy. Unpublished data
11. Del Rio-Hortega P, Penfield W: Cerebral cicatrix: The reaction of neuroglia and microglia to brain wounds. *Bull Johns Hopkins Hosp* 41:278-303, 1927
12. Adams RD, Sidman RL: *Introduction to Neuropathology*. New York, McGraw-Hill, 1968, p 34
13. Blackwood W, McMenemey WH, Meyer A, Norman RM, Russell DS: *Greenfield's Neuropathology*. Second edition. Baltimore, Williams and Wilkins Co, 1963, p 50

14. Bucher O: Die Amitose der tierschen und menschlichen Zelle, Protoplasmatologia Handbuch der Protoplasmaforschung. Vol 6. Edited by LV Heilbrunn, F Weber. Berlin, Springer-Verlag, 1959
15. Grundmann E: General Cytology: An Introduction to Functional Morphology of the Cell. Baltimore, Williams and Wilkins Co, 1966, pp 228-240
16. Lash JW, Holtzer H, Swift H: Regeneration of mature skeletal muscle. Anat Rec 127:678-697, 1957
17. Luse S: Neuroglia, Pathology of the Nervous System. Vol 1. Edited by J Minckler. New York, McGraw-Hill, 1968, p 541
18. Cancilla PA, Andrews JM, Rose AS: Subacute demyelinating disease in an adult (diffuse-disseminated sclerosis). Neurology 21:825-832, 1971
19. Lapham LW, Norenberg MD: Unpublished observations
20. Cavanagh JB: The proliferation of astrocytes around a needle wound in the rat brain. J Anat 106:471-487, 1970
21. Stubblefield E, Brinkley BR: Architecture and function of the mammalian centriole, Formation and Fate of Cell Organelles. Vol 6. Symposia of the International Society for Cell Biology. Edited by KB Warren. New York, Academic Press, 1967, p 195
22. Threadgold LT: The Ultrastructure of the Animal Cell. Oxford, Pergamon Press, 1967, pp 271-295
23. Sorokin SP: Reconstruction of centriole formation and ciliogenesis in mammalian lungs. J Cell Sci 3:207-230, 1968
24. Peters A, Palay SL, Webster H deF: The Fine Structure of the Nervous System. New York, Harper and Row, 1970, p 108

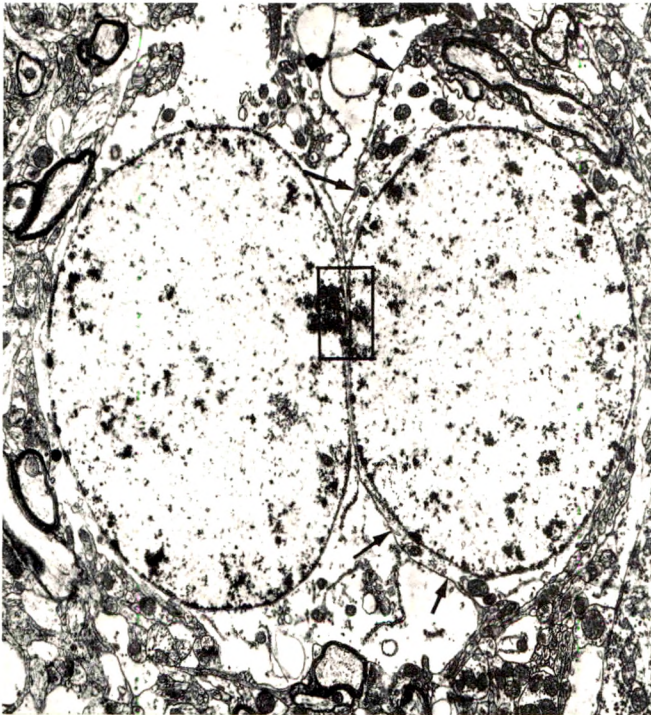
Acknowledgment

We wish to acknowledge the helpful advice of Drs. James Coleman and Manuel del Cerro, and the technical assistance of Theresa Colwell.

[*Illustrations follow*]



A



B



C

Fig 1A—A pair of protoplasmic astrocytes. Two distinct daughter cells are separated by a set of apposing plasma membranes (*arrows*). **B**—Another pair of astrocytic nuclei that appears at this magnification to present a binucleate cell. The nuclei, however, belong to separate daughter cells, as established by the set of plasma membranes between the two nuclei (*arrows*). The plasma membranes are seen to better advantage in **C** (*arrows*) which is a higher magnification of the blocked region in **B**. *N* indicates nucleus (A and B $\times 7000$; C $\times 55,000$).

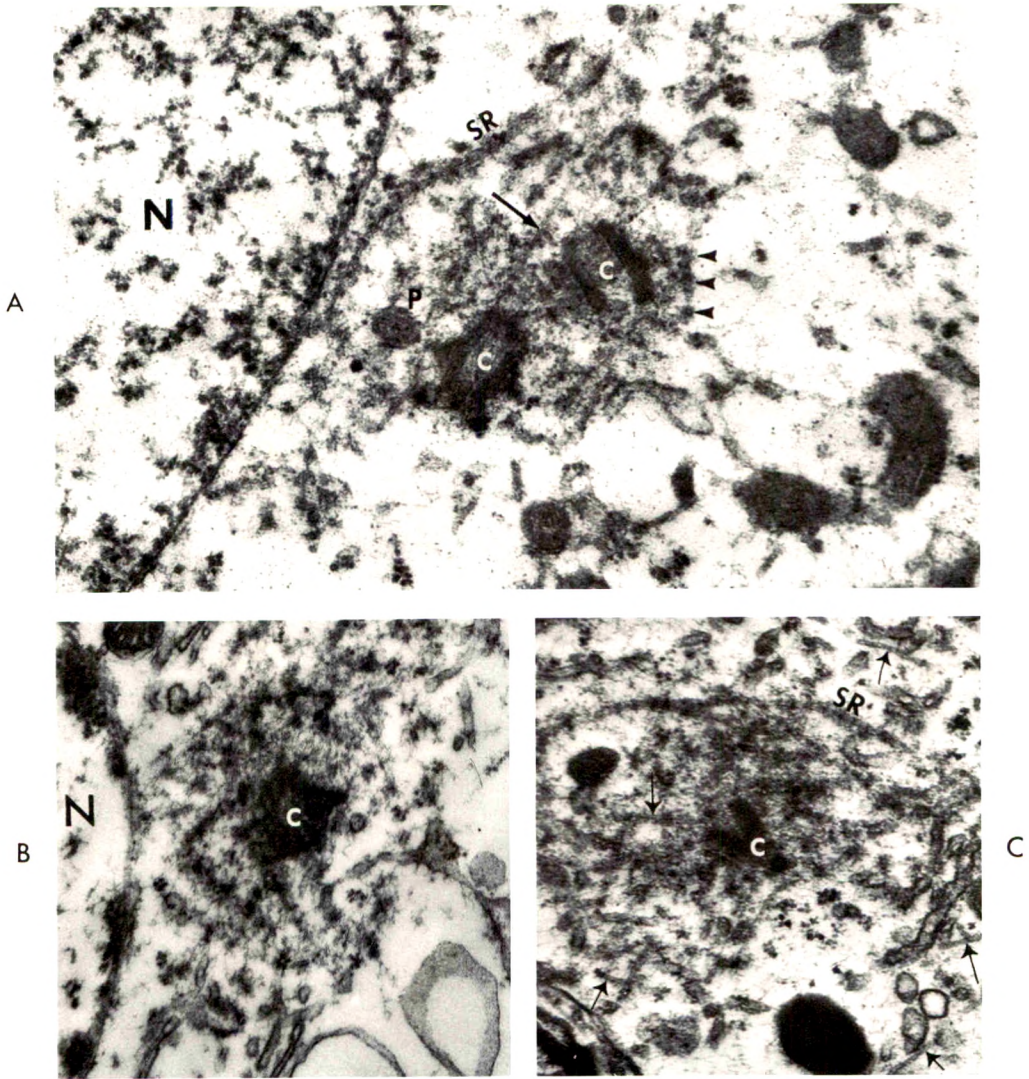


Fig 2A—A pair of centrioles (c) adjacent to nucleus (N). A pro-centriole (P) lies in close proximity to the parent centriole on the left. A microtubule projects from the same centriole (arrow). Circumferentially positioned about the centrioles are fibrogranular aggregates (arrow heads), microtubules and a single striated rootlet (SR). **B**—Many fibrogranular aggregates are situated around this centriole. **C**—Aggregates of microtubules (arrow) and other tubular profiles are associated with a centriole. A striated rootlet (SR) lies along the periphery of the pericentriolar complex. N indicates nucleus (A $\times 31,000$; B and C $\times 26,000$).



Fig 3—There are increased numbers of scattered microtubules in the cytoplasm of this astrocyte (*arrows*). *A* indicates axon; *D*, dendrite; *N*, nucleus ($\times 30,000$).

[End of Article]

ANIMAL MODEL
FOR
HUMAN DISEASE

Down's Syndrome (Mongolism, Trisomy 21)

Animal Model: Trisomy in a Chimpanzee

Contributed by: Harold M. McClure, DVM, Department of Veterinary Pathology, Yerkes Regional Primate Research Center, Emory University, Atlanta, Ga 30322.

Features of Down's-Like Syndrome in a Chimpanzee

The subject of this report, a female chimpanzee (*Pan troglodytes*) named Jama, was born after an apparently normal uncomplicated pregnancy. Her mother, a 15-year-old chimpanzee, had 1 previous pregnancy which was terminated by the delivery of a premature stillbirth. No other relevant medical history had been recorded for either of the parents. The father was 22 years old at the time of Jama's birth.

Jama was of low-normal birth weight and had a markedly decreased rate of growth as compared to other laboratory-reared chimpanzees. She also had bilateral partial syndactyly of the toes with clinodactyly, prominent epicanthal folds, hyperflexibility of the joints, muscle hypotonia and a short neck with excess skin folds. Radiographic studies conducted at birth revealed an abnormality of the left thoracic cavity that appeared to be adjacent to or associated with the heart.

Cytogenetic studies conducted on peripheral blood cell cultures revealed a modal chromosome number of 49, as opposed to the normal diploid number of 48 for the chimpanzee. Karyotypes prepared from the aneuploid cells showed an additional small acrocentric chromosome. This autosomal trisomy was confirmed in bone marrow preparations and in fibroblast cultures obtained from skin biopsy. Cytogenetic studies on both parents revealed normal chromosome complements.

Behavioral observations indicated that Jama's postural development was markedly retarded when compared with other Yerkes nursery animals and the critical age norms reported for chimpanzees. When individual items of postural maturation were examined, Jama exceeded the critical age norms in 31 of 34 measures. She was slower in all 34 tasks when compared with 2 nursery animals tested at the same time.

Publication sponsored by the Registry of Comparative Pathology, under the auspices of the Universities Associated for Research and Education in Pathology, Inc., and supported by Grant RR00301 from the US Public Health Service, Division of Research Resources, and Grant RR00165 from the National Institutes of Health.



Fig 1—Photograph illustrating facial features of Jama. Note tongue protrusion and prominent epicanthal folds.

Jama had frequent clinical episodes of anoxia, as manifested by cyanosis of the lips and cold extremities, and continued to show poor clinical progress throughout her 17 months of life. Her clinical condition was characterized by retarded growth, delayed neurologic and postural development and general inactivity. She died at the age of 17 months while anesthetized for diagnostic cardiac catheterization procedures.

Major findings at necropsy included: a patent ductus arteriosus, an atrial septal defect, and a ventricular septal defect. The left side of the diaphragm was projecting into the left thoracic cavity and contained a lobe of the liver. The right ventricle showed marked hypertrophy; a generalized moderate lymphadenopathy was noted. Other postmortem findings which were felt to be associated with terminal events included petechial and diffuse hemorrhage of the cerebrum and ecchymotic hemorrhage of the myocardium.

Features of Down's Syndrome in Man

This condition was first described as a clinical entity in 1867, but it was not until 1959 that the syndrome was shown to be associated with a specific chromosomal abnormality—trisomy of one of the small acrocentrics. The condition is reported to occur in the human population with a frequency of approximately 1 in 600 births, with increasing frequency associated with advancing maternal age.



Fig 2—Photograph of Jama illustrating the degree of muscle hypotonia still present at 40 weeks of age.

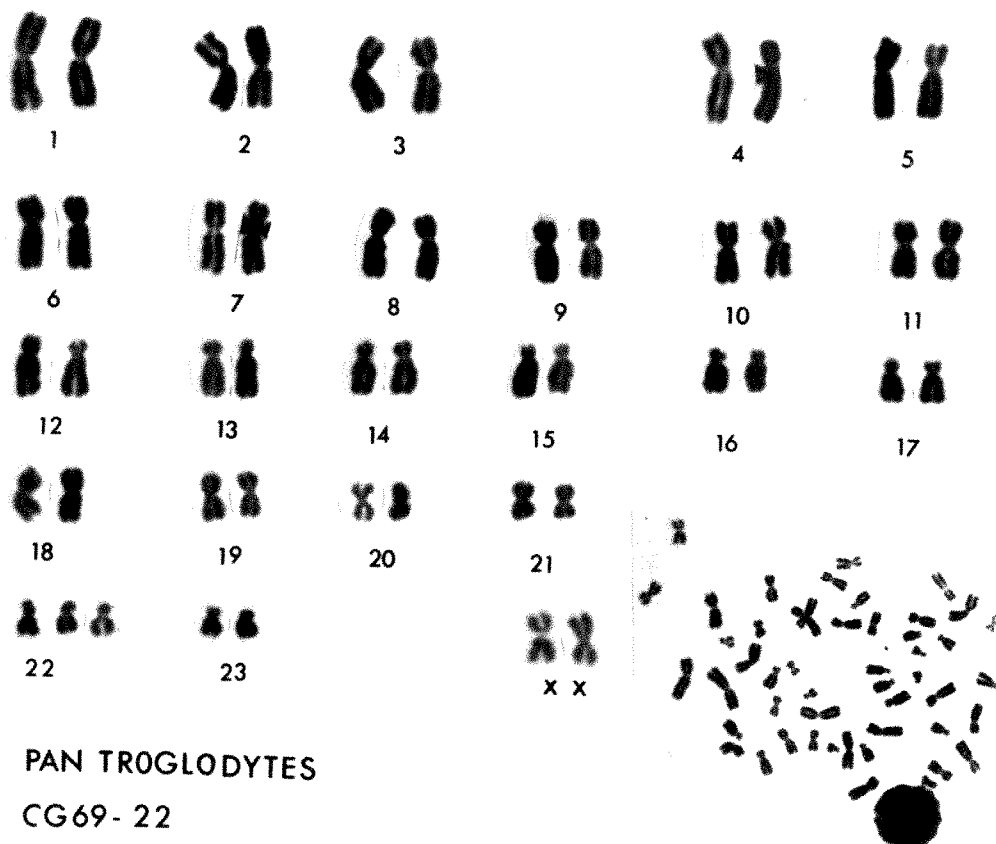


Fig 3—Karyotype prepared from a peripheral blood cell culture of Jama. Trisomy of the small acrocentric has been arbitrarily designated chromosome No. 22.

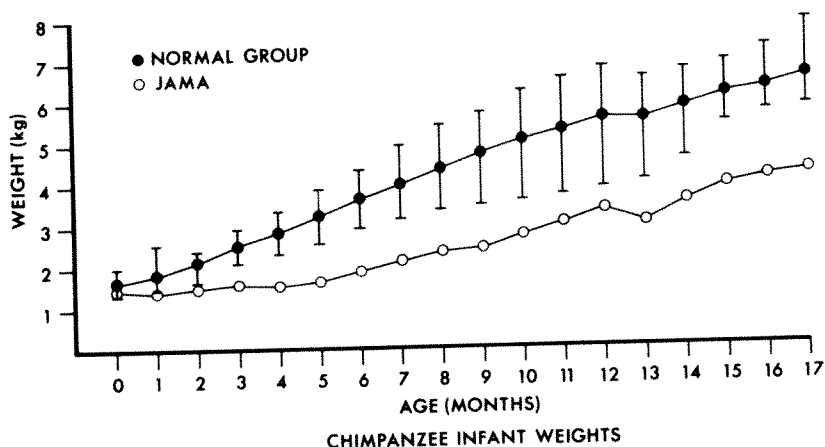


Fig 4—Graph showing the markedly decreased rate of growth of Jama as compared to other laboratory-reared chimpanzees.

The characteristic cytogenetic abnormality of mongolism is accompanied by prominent anomalies of physical and mental development. These include: oblique palpebral fissures with epicanthal folds; a short broad neck; cardiac anomalies; muscle hypotonia and hyperflexibility of the joints; dysplastic ears; short broad hands; dysplastic middle phalanx of the fifth finger; and mental retardation. Syndactyly of the toes is reported to occur with a frequency of 2 to 11%.

Summary

The clinical, behavioral, cytogenetic and pathologic features of this case demonstrate its similarity to Down's Syndrome of man. Although it was not possible to maintain this animal to maturity for expanded studies on this relatively common human disease, it is encouraging to know that such a condition does occur in nonhuman primates. Its occurrence indicates that these animals may be used in investigations pertaining to the etiology of this condition. Continued cytogenetic studies in nonhuman primate populations may reveal additional cases of this type, as well as other chromosomal anomalies.

References

1. Penrose LS, Smith GF: Down's Anomaly. Boston, Little, Brown and Company, 1966
2. Lejeune J, Gautier M, Turpin, R: Etude des chromosomes somatiques de neuf enfants Mongoliens. C R Acad Sci 248: 1721-1722, 1959
3. McClure HM, Belden KH, Pieper WA, Jacobson CB: Autosomal trisomy in a chimpanzee: resemblance to Down's syndrome. Science 165: 1010-1012, 1969
4. Riesen AH, Kinder EF: Postural Development of Infant Chimpanzees. New Haven, Yale University Press, 1952
5. Chiarelli, B: Comparative morphometric analysis of primate chromosomes. I. The chromosomes of anthropoid apes and of man. Caryologia 15: 99-121, 1962
6. Lilienfeld AM, Benesch CH: Epidemiology of Mongolism. Baltimore, The Johns Hopkins Press, 1969

The American Journal of PATHOLOGY

is published by the Medical Department of Harper & Row, Publishers, under the auspices of The American Association of Pathologists and Bacteriologists and The American Society for Experimental Pathology, and is edited by a Board appointed by the Councils of the two Societies. It is devoted to the prompt publication of original observations and investigations in the field of pathology and microbiology and is published monthly in four volumes per year.

Information for Authors

ORIGINAL PAPERS will be considered for publication on condition that they are contributed solely to THE AMERICAN JOURNAL OF PATHOLOGY. Address manuscripts to the Editor-in-Chief: THOMAS D. KINNEY, MD, Department of Pathology, Duke University Medical Center, Durham, NC 27706.

MANUSCRIPTS must be typed **double-spaced** (including tables, references, and legends for figures), and all material should be submitted in duplicate. The literature should be summarized as concisely as is consistent with establishing the necessary basis for new material, and original observations should be presented in a clear, well-organized manner. Papers should rarely exceed 20 printed pages. Tables should be planned to suit the page size of THE JOURNAL. Excess tabular matter must be paid for by the contributor.

REFERENCES to the literature should be numbered in the order of citation in the text and should conform to the following style: names of all authors, complete title of article (including subtitle), abbreviated name of periodical (use *Index Medicus* style abbreviations), volume in Arabic numerals, inclusive pagination, and year (eg, 14:111-120, 1938). Titles are to be in the original language when they can be reproduced in the English alphabet. Translated titles should be enclosed in square brackets.

ILLUSTRATIONS must be planned to suit the page size of THE JOURNAL (**maximum plate size is 5½ × 8 inches**) and should be submitted **unmounted**, with figure number, top, and author's name marked lightly on the back in soft pencil. Oversize illustrations should be avoided because handling of these delays publication. To be accepted, illustrations must reach a certain standard of excellence technically, present an attractive appearance, and add significantly to the value of the presentation. Marking lines and letters, if essential, must be kept at least ¼ inch inside all margins. If two or more illustrations are to appear on a page, they should be so trimmed that the edges may be butted and the outer margins squared. The legends for photomicrographs should state the staining method and the degree of magnification. Black and white illustrations will be furnished in moderate numbers. Excess illustrations, when accepted, and the cost of illustrations in color, must be paid for by the contributor.

REPRINTS: An order blank for reprints is sent with the proof.

Rudolf Partsch wanted to repeal Murphy's Law. Thus, the world's easiest-to-operate Electron Microscope.

"What I want," said Rudolf Partsch of Carl Zeiss, Inc. to the designers in Oberkochen, West Germany, "is a totally reliable, extremely easy-to-operate, compact electron microscope with good resolution (7\AA) in the 0-60,000x range. And I want it at a low price." He wanted an electron microscope for researchers and teachers interested in electron microscopic studies, not electron microscopes—an instrument designed for everyday use.

The Zeiss EM9S-2 with fully automatic camera system, foolproof airlock, and fingertip controls is what he got. And it looks as though Mr. Partsch really had a keen insight into the needs of a large section of the American scientific community . . . judging both by the reception this instrument has had, and by the numerous attempts to copy it. The copies never catch up, because Partsch keeps in regular contact with users, to find out what kind of modifications can be made to

keep abreast of research's ever-changing requirements. When he finds one, he gets it incorporated *post haste* into the design. And, what's more, makes it available for incorporation into previously sold instruments. Because ease-of-modification is a feature inherent in the original uncomplicated design, a Zeiss Electron Microscope never gets old.

For the whole story, contact Partsch. He'll send you complete specifications and the illustrated brochure "How to Operate the World's Easiest-to-Operate Electron Microscope."

You can reach him by phone at: (212) 736-6070.
Or write Carl Zeiss, Inc., 444 5th Ave., New York, N.Y. 10018.
Canada: 45 Valleybrook Drive, Don Mills 405, Ontario.

Ask for leasing and time payment terms.

Nationwide service.

ATLANTA, BOSTON, CHICAGO, COLUMBUS, DALLAS, DENVER, FORT LAUDERDALE, HOUSTON, KANSAS CITY, LOS ANGELES, PHILADELPHIA, PHOENIX, SAN FRANCISCO, SEATTLE, WASHINGTON, D.C.



ZEISS
THE GREAT NAME IN OPTICS



The American Journal of PATHOLOGY

OCTOBER 1972

OFFICIAL PUBLICATION OF

THE AMERICAN ASSOCIATION OF
PATHOLOGISTS AND BACTERIOLOGISTS

THE AMERICAN SOCIETY FOR
EXPERIMENTAL PATHOLOGY

BOARD OF EDITORS

Thomas D. Kinney, *Editor-in-Chief*

Donald B. Hackel, *Associate Editor*

Orville T. Bailey

Frederick F. Becker

Baruj Benacerraf

Kurt Benirschke

Kenneth M. Brinkhous

Joel G. Brunson

John R. Carter

Charles G. Cochrane

John M. Craig

Frank J. Dixon, Jr

John T. Ellis

Frank W. Fitch

Patrick J. Fitzgerald

David G. Freiman

Jack C. Geer

Gabriel Godman

John B. Hazard

Robert H. Heptinstall

Paul Kotin

Averill A. Liebow

Guido Majno

Donald G. McKay

Henry D. Moon

Councilman Morgan

Goetz W. Richter

David T. Rowlands, Jr

Edward A. Smuckler

Leon Sokoloff

Benjamin H. Spargo

Lewis Thomas

Jacinto J. Vazquez

F. Stephen Vogel

Editorial Assistant: Virginia Hotelling

To protect her next baby...



Gamulin[®] Rh Rh_o(D) immune globulin (human)

...complete with a disposable syringe
in a compact, space-saving package.



As a major producer of blood fractions, Dow now brings you a new source for Rh_o(D) immune globulin to protect the Rh negative mother's next baby from probability of hemolytic disease.

Studies to demonstrate its safety and effectiveness show that Gamulin Rh is effective in suppressing the production of Rh_o(D) antibodies.

And it comes in a space-saving, compact package that includes a vial, disposable syringe, lay literature, patient laboratory form, ID card, package insert and a crossmatch vial.

DESCRIPTION: GAMULIN Rh, Rh_o(D) Immune Globulin (Human), is a sterile concentrated solution of gamma globulin derived from blood of human donors known to have antibodies to Rh_o(D). It is standardized to contain 10.0 to 18.0 percent globulins with a level of antibody to Rh_o(D) equal to or greater than that of the NIH Reference Rh_o(D) Immune Globulin (Human). The final product contains 0.2 to 0.3 molar glycine as a stabilizer and 1:10,000 thimerosal as a preservative.

INDICATIONS: GAMULIN Rh suppresses the immune response of nonsensitized Rh_o(D) negative mothers following Rh incompatible pregnancies. The criteria for an Rh incompatible pregnancy are: That the mother shall be Rh_o(D) negative, D^u negative; and the infant shall be Rh_o(D) positive or D^u positive.

CONTRAINDICATIONS: Gamulin Rh must not be given to the infant. Gamulin Rh also should not be administered to an Rh_o(D) positive or D^u positive individual, to a recipient of an Rh_o(D) positive blood transfusion, or to an Rh_o(D) negative mother previously sensitized by an Rh incompatible pregnancy. Do not give intravenously.

PRECAUTIONS AND REACTIONS: It is essential that certain diagnostic and laboratory criteria be met before administering this product. (See package literature.) An occasional patient has shown a systemic reaction manifested by a low grade fever. Allergic reactions, although not expected, could occur.

ADMINISTRATION: Consult package insert for detailed instructions.

This product must be administered within 72 hours post-partum.

Gamulin[®] Rh

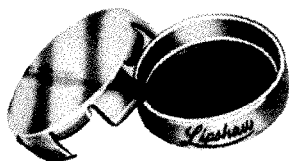
Rh_o(D) immune globulin (human)



DOW PHARMACEUTICALS

The Dow Chemical Company
Indianapolis, Indiana

VERSATILE . . .

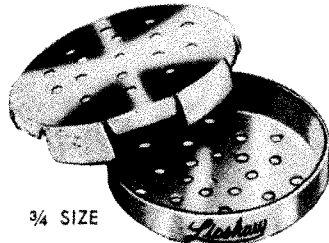


NO. 350 ¾ SIZE

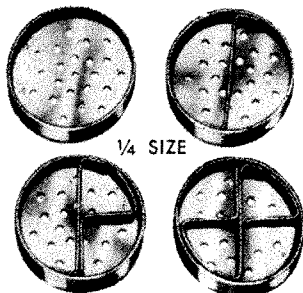
General purpose capsule for routine or micro specimen. Very precise enclosure. 25 mm in diameter by 6 mm deep. Extra fine (50 x 50) bottom mesh.

\$1.75 each \$19.00 dozen

. . . FOR ROUTINE HISTOLOGY



¾ SIZE



¼ SIZE

NO. 330

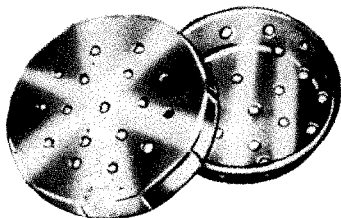
Allows partitioning up to four sections. Five sturdy lugs grasp the base securely. Inside measurements 37 mm x 6 mm deep.

\$1.60 each \$17.60 dozen

NO. 330-S

Separators for same.

.20 set \$2.20 doz. sets



NO. 339

½ SIZE

Has expansion feature. Closed dimensions are 40 mm by 7 mm deep and may be expanded to 11 mm deep.

\$1.50 each \$16.50 dozen

SOLID STAINLESS STEEL
**TISSUE CAPSULES and
AUTOPSY BASKETS**

Lipshaw of the finest quality by
MANUFACTURING CO.

7446 CENTRAL AVENUE • DETROIT 10, MICHIGAN

Immediate Delivery

COMPLETE LITERATURE
AND CATALOG AVAILABLE

. . . FOR MICRO SPECIMEN



NO. 331 ACTUAL SIZE

Positive clip-on cover for micro specimen. 20 mm in diameter by 5 mm deep. Fine mesh (20 x 20).

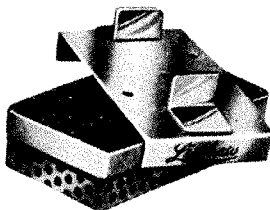
\$1.50 ea. \$16.50 doz.

NO. 331-X

With extra fine mesh (50 x 50).

\$1.60 ea. \$17.60 doz.

LARGE CAPACITY



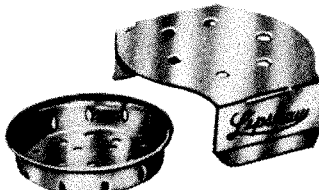
NO. 349

½ SIZE

Flexible snap cover easily attached and removed. 50 mm long, 25 mm wide, 12 mm deep.

\$5.00 each \$55.00 dozen

UNIQUE DESIGN . . .

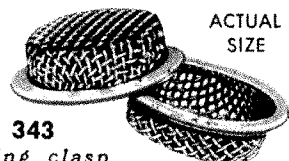


NO. 338

½ SIZE

Clip-on cover provides a tight and positive enclosure. Inside dimensions are 33 mm by 7 mm deep.

\$1.50 ea. \$16.50 dozen



ACTUAL
SIZE

NO. 343

Spring clasp provides a secure enclosure.

Inside dimensions 19 x 12 mm. Fine mesh (20 x 20).

\$1.75 each

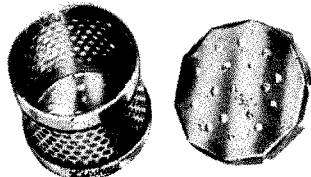
\$19.00 dozen

NO. 343-X

With extra fine mesh (50 x 50).

\$1.90 ea. \$20.90 doz.

. . . FOR AUTOPSY

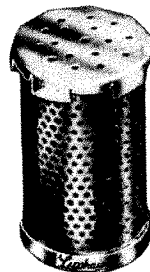


NO. 342

½ SIZE

Perforated throughout for free movement of fluids. Snap cap provides positive enclosure. 35 mm in diameter by 30 mm deep.

\$3.00 each \$33.00 dozen



NO. 332

½ SIZE

Same construction as No. 342 (above). Dimensions are 35 mm in diameter by 70 mm deep.

\$3.50 each \$38.00 dozen

The American Journal of PATHOLOGY

OCTOBER 1972 • Volume 69, Number 1

CONTENTS

- 1 Presentation of The Gold Headed Cane to Sidney Farber
Benjamin Landing
- 7 Peroxidase Arthritis. II. Lymphoid Cell-Endothelial Interactions During a Developing Immunologic Inflammatory Response
Richard C. Graham Jr and Sarajayne Limpert Shannon
- 25 Morphologic Variants of Alcoholic Hyalin
Hidejiro Yokoo, Odell T. Minick, Fawzia Batti and Geoffrey Kent
- 41 Exocytosis of Secretory Organelles from Blood Platelets Incubated with Cationic Polypeptides
James G. White
- 55 Experimental Visceral Aspergillosis
Herschel Sidransky, Sheldon M. Epstein, Ethel Verney and Claire Horowitz
- 71 Morphologic Study of the Participation of the Complement System in Hyperacute Rejection of Renal Xenotransplants
Jaime E. Mejía-Laguna, Adolfo Martínez-Palomo, Carlos E. Biro, Bibiana Chávez, Fernando López-Soriano and Marcelo García-Cornejo
- 79 A Comparative Immunohistochemical Study of Splenic Arterial Hyalinosis in Health and Disease
Raj K. Gupta, R. Schuster and W. D. Christian
- 89 Developing Elastic Tissue: An Electron Microscopic Study
Ernest N. Albert
- 103 Cytolysis Induced by Human Lymphotoxin: Cinemicrographic and Electron Microscopic Observations
Stephen W. Russell, Werner Rosenau and John C. Lee
- 119 Thermal Noise in Cells: A Cause of Spontaneous Loss of Cell Function
Horton A. Johnson and Mildred Pavelec
- 131 Induction of the Generalized Schwartzman Reaction in Pregnant and Nonpregnant Rats by Colchicine
Gert Müller-Berghaus and Rolf Obst
- 139 Ultrastructural and Histochemical Studies of Murine Megacolon
Robert P. Bolande and William F. Towler
- 163 The Morphologic Effects of Dieldrin and Methyl Mercuric Chloride on Pars Recta Segments of Rat Kidney Proximal Tubules
Bruce A. Fowler
- 179 Irreversibility of Methylandrostenediol-Induced Hypertension in the Rat After Suspension of the Androgen Treatment
Agostino Molteni, Alexander C. Brownie, Peter A. Nickerson and Floyd R. Skelton
- 195 Immune Reactions in Mucous Membranes. IV. Histochemistry of Intestinal Mast Cells During Helminth Expulsion in the Rat
H. R. P. Müller and R. Walshaw
- 212 **Animal Model of Human Disease: Kuru, Creutzfeldt-Jakob Disease (Slow Virus Infections)**
R. F. Marsh

© 1972 by The American Association of Pathologists and Bacteriologists

Medical Department

• HARPER & ROW, PUBLISHERS

The American Journal of PATHOLOGY

GENERAL INFORMATION

Editorial Communications: All correspondence concerning editorial matters should be addressed to the Editor-in-Chief, DR. THOMAS D. KINNEY, Department of Pathology, Duke University Medical Center, Durham, N.C. 27706.

Business Communications: All subscriptions and advertising inquiries should be addressed to: MEDICAL DEPARTMENT, HARPER & ROW, PUBLISHERS, 2350 Virginia Ave, Hagerstown, Md. 21740.

Rates: THE AMERICAN JOURNAL OF PATHOLOGY is issued monthly, four volumes per year. Regular (individual) subscriptions: \$27.50 per year in the U.S. and Possessions; \$30.00 per year in Canada and countries of the Pan-American Postal Union; and \$31.00 elsewhere. Special rate for Interns and Residents: \$16.00 per year (\$1.50 extra postage in Canada and countries of the Pan-American Postal Union; \$2.50 extra postage elsewhere). Regular (individual) subscriptions and Resident and Intern subscriptions must be in the names of, and billed to, individuals. Institutional subscriptions, available to all libraries, schools, clinics, and hospitals, to all government agencies, local or national, and to all private or public institutions and organizations: \$35.00 per year in the U.S. and Possessions; \$37.50 per year in Canada and countries of the Pan-American Postal Union; \$38.50 per year elsewhere. All subscriptions are payable in advance. Single copies, when available, \$4.00.

Back Issues: Single issues and complete volumes of THE JOURNAL published prior to 1961 may be purchased from Walter J. Johnson, Inc., 111 Fifth Ave., New York, N.Y. 10003.

INDEX TO ADVERTISERS

Dow Chemical Company, The	Cover 2, 1
Erie Scientific	11
Harper & Row, Publishers	8, 10, 12, 14, 15
Leitz, Inc., E.	5
Lipshaw Manufacturing Corporation	2
Ortho Diagnostics	16
Oxford University Press	13
Shandon Southern Instruments	7
Sigma Chemical Company	9
Worthington Biochemical Corporation	6
Zeiss, Inc., Carl	Cover 4

MOVING?

To avoid interruption in your receipt of this Journal, we need to know your new address—six weeks in advance.

When writing us, be sure to type or print clearly your name and your new address—complete with zip code. It is *essential* that you also list your old address.

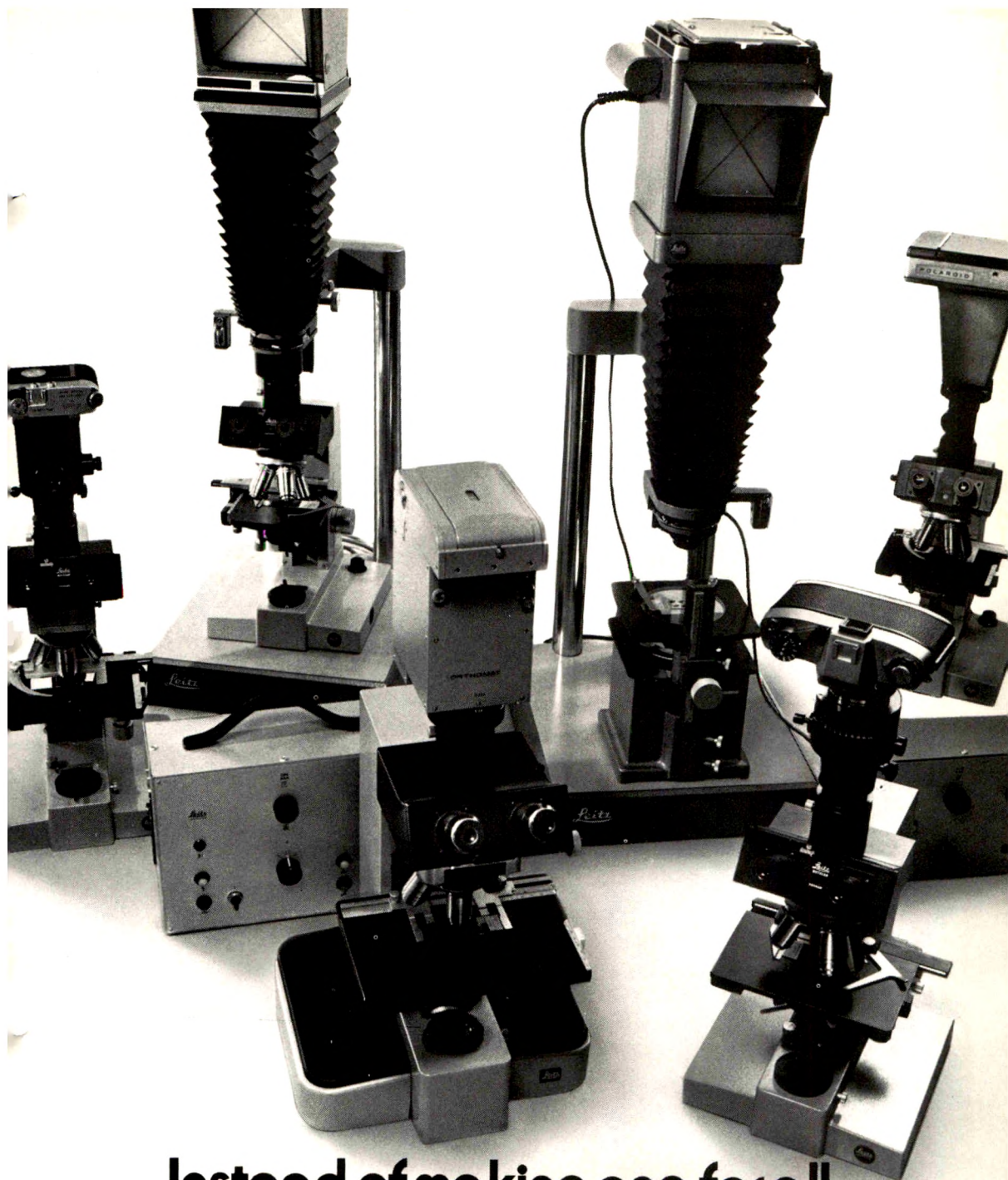
IMPORTANT: We publish a number of medical and scientific periodicals. Therefore, please be sure to give the name of THIS Journal when you write us.

Thank you for cooperating!

MEDICAL DEPARTMENT
Harper & Row, Publishers, Inc.

2350 Virginia Ave,
Hagerstown, Md. 21740.

(see page 13)



Instead of making one for all, we let you choose one from all.

As certainly as no single microscope can serve all disciplines, no single photomicrographic camera can meet all needs. Your preference may be a large format, small format, Polaroid®, automatic, manual, without camera back, with camera back, single frame, multiple frame, or time-lapse.

Leitz lets you choose. And whether it's your budget or your specific need that dictates

preference, you get the same common denominator . . . optical performance second to none, precision and dependability.

To help you make a decision, let us send you our brochure. There is *one* that's just right for you.

Leitz® E. Leitz, Inc., Rockleigh, N.J. 07647
Leica®

126272

Worthington STATZYMES — reagents for precise measurements of LDH, CPK, GOT, and GPT — are fully red and freeze dried. One pipetting of distilled instantly transforms the STATZYME wafer into an working analytical system.

All reagents for single or multiple testing are in a single vial.

With a single reconstitution, you have at your tips 24 years of Worthington work in biochemical and enzyme testing. Our methods are the cal UV procedures which we meticulously simplified. Multiple testing? A single reconstitution is still all ed. Besides the single test, Worthington ZYMES also are packaged in 5 and 25-test vials. cover the range for "stats," profiles, series, utomated and automated enzyme measurements. hese packages eliminate waste of reagent;

single pipetting eliminates measurement error and effort; precise measurement eliminates repeats and wasted time.

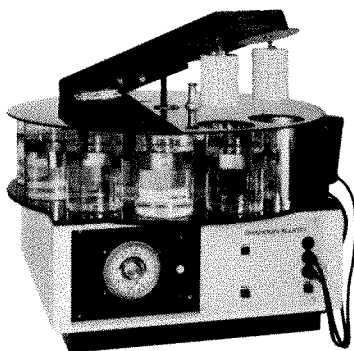
With these advantages, you'll see why Worthing STATZYMES are easily the most convenient and economical reagents you can use. Evaluate them in your own laboratory. Contact our local distributor for product literature and request a demonstration.



Worthington Biochemical Corporation | Freehold, New Jersey 07728 U.S.A.



NOW...UP TO 72 TISSUES PROCESSED AT ONE TIME



The Shandon-Elliott Duplex Automatic Tissue Processor cycles two baskets, each holding up to 36 tissues, through a series of equal immersion-time routines requiring up to 12 processing stations. Equal-time routines involving less than 12 stations can be started at any point. Or the machine can process up to 36 tissues for special routines. Other features include 24-hour timer, delayed action, automatic agitation, and a third hot wax bath unit.

Send for literature and prices to Shandon Southern Instruments, Inc., 515 Broad Street, Sewickley, Pa. 15143 (Pittsburgh District).



P I T T S B U R G H • L O N D O N • F R A N K F U R T

**Use this
check list for
other Shandon
Catalogs and
Monographs**

- ☐ Paper Electrophoresis
- ☐ Acrylamide Gel Electrophoresis
- ☐ Immuno Electrophoresis
- ☐ Thin Layer Electrophoresis
- ☐ High Voltage Electrophoresis
- ☐ Paper Chromatography
- ☐ Thin Layer Chromatography
- ☐ Preparative Layer Chromatography
- ☐ Automatic Slide Staining Machine
- ☐ Tissue Processing Apparatus
- ☐ Cyto-Centrifuge

Please send your request for the above literature to Shandon Southern Instruments, Inc., 515 Broad St., Sewickley, Pa. 15143.

Two major new works from Harper & Row:

INFECTIOUS DISEASES

A Guide to the Understanding and Management of Infectious Processes

With 89 Contributors. Edited by **Paul D. Hoeprich, M.D.**, Professor of Medicine and Pathology, and Chief, Section of Infectious and Immunologic Diseases, School of Medicine, University of California, Davis, California. About 1,300 Pages. 180 Illustrations, 53 in full color. **\$42.50**

INFECTIOUS DISEASES has been painstakingly prepared to serve as a definitive reference book for all physicians concerned with infectious diseases. Comprehensive in scope, the book covers diseases caused by viruses, chlamydia, rickettsia, mycoplasmas, bacteria, spirochetes, protozoa, helminths, and ectoparasites. Each disease is thoroughly examined according to etiology, epidemiology, pathogenesis and pathology, manifestations, diagnosis, prognosis, therapy, and prevention. Considerable emphasis is placed on epidemiology and pathogenesis as the keys to understanding host-parasite interactions.

Although comprehensive, this book is not just an encyclopedic assemblage of data. *In fact, the real hallmark of INFECTIOUS DISEASES is the organ-system presentation of the subject matter.* Specific infectious disease are approached according to the system involved. This practical approach is consistent with the facts of clinical life. Moreover, the organ-system arrangement facilitates quick reference for the busy practitioner.

Comprehensive, well organized, generously illustrated, and fully indexed, this important new work fills a real need for students and practicing physicians alike.

BRONCHOPULMONARY DISEASES AND RELATED DISORDERS

With 54 Contributors. Edited by **Cranston W. Holman, M. D.**, Clinical Professor of Surgery, Cornell University Medical College; and **Carl Muschenheim, M.D.**, Clinical Professor of Medicine, Cornell University Medical College, New York. 2 Volumes. About 1,035 Pages. 477 Illustrations. **\$60.00**

The field of bronchopulmonary diseases has recently undergone an unique evolution of medical and surgical collaboration. BRONCHOPULMONARY DISEASES AND RELATED DISORDERS is a new profusely illustrated two volume work which assembles the vast amount of accumulated medical and surgical knowledge in a logical, consistent sequence. Up-to-date information from fifty-four distinguished contributors has been organized to form a comprehensive presentation of current theory and practice concerning pulmonary and thoracic diseases.

Pertinent physiologic principles, medical knowledge, and surgical interests are thoroughly examined. Topics of particular importance include: pulmonary function tests and their physiologic significance; surgical principles and technics, amplified by detailed anatomical illustrations; developmental anomalies and pulmonary disorders of infancy and early childhood; pathology and patho-physiology of various disorders; principles for the management of respiratory failure; medical and surgical intensive care.

HARPER & ROW, Publishers, Inc.		Medical Department
Mail Order Dept.	2350 Virginia Ave.	Hagerstown, Md. 21740
Please send me, on approval:		
<input type="checkbox"/> Hoeprich: INFECTIOUS DISEASES	\$42.50
<input type="checkbox"/> Holman & Muschenheim: BRONCHOPULMONARY DISEASES AND RELATED DISORDERS	\$60.00
<input type="checkbox"/> Bill me	<input type="checkbox"/> Check enclosed (Save! We pay postage)	AJP-10
NAME		
ADDRESS		
CITY	STATE	ZIP



Call SIGMA for

SINGLE and TWO-REAGENT SYSTEMS

For the Ultraviolet Determination of

SGOT/SGPT

(Glutamic-Oxalacetic + Glutamic-Pyruvic Transaminase)

in serum or other fluids at 340 mμ

"Stat", Manual, or Automated Kinetic Procedures

SINGLE REAGENT SYSTEM — Per Sigma Technical Bulletin No. 55-UV.

A rapid, convenient procedure for routine or "stat" determinations — Manual or single reagent automated systems such as GEMSAEC, Centrifichem, Rotochem, etc. All you do is add water and serum — then read your O.D. One, five or ten assay vials - to fit your need.

Ask for free Sigma Technical Bulletin No. 55-UV or order:

Stock No.	For SGOT		Max. Assays*	Price	Stock No.	For SGPT		Max. Assays*	Price
55-1	Single Assay Vial	10 vials	10	\$5.00	55-1P	Single Assay Vial	10 vials	10	\$5.00
55-5	5 Assay Vial	5 vials	5 x 5	7.50	55-5P	5 Assay Vial	5 vials	5 x 5	8.00
		10 vials	10 x 5	14.85			10 vials	10 x 5	15.50
55-10	10 Assay Vial	5 vials	5 x 10	12.50	55-10P	10 Assay Vial	5 vials	5 x 10	14.00
		10 vials	10 x 10	24.85			10 vials	10 x 10	27.00

*Although vials for the above procedures are designed for a 3 ml Reaction Volume, many instruments can use much less. If so, the number of assays per vial can be increased proportionately and cost per test greatly reduced.

TWO REAGENT SYSTEMS — Per Sigma Technical Bulletin No. 155-UV.

For Automated analyzers designed for two-reagent systems such as the LKB Reaction Rate Analyzer and the Beckman DSA-560 and 564-B.

Can also be used in single reagent automated analyzers and for manual procedures.

Ask for free Sigma Technical Bulletin No. 155-UV or order:

Kit No.	For	Max. Assays*	Price
155-A	SGOT	100	\$22.50
155-B	SGPT	100	24.50

See above comment re: number of assays

Of course we still offer the **Original** Colorimetric Procedure — proven the world over — imitated everywhere, but still unequalled.

No. 505 — Sigma-Frankel Colorimetric
at 490-530 mμ.

Kit No.	For	Assays	Price
505	SGOT	100	\$10.00
505-M	SGOT	25	5.50
505-P	SGPT	100	10.00
505-PM	SGPT	25	5.50
505-OP	SGOT/SGPT Combination	100	15.00

Also available:

No. 410-UV — Ultraviolet at 340 mμ.

Kit No.	For	Assays	Price
410-50	SGOT	50	\$11.55
410-100	SGOT	100	22.45
410-50P	SGPT	50	14.75
410-OP	SGOT/SGPT Combination	50 each	26.30

Free Sigma Technical Bulletins for the above methods are available upon request.

All prices **include** normal postage to you anywhere in the world.

It's a pleasure doing business with Sigma

ORDER DIRECT — TELEPHONE COLLECT from ANYWHERE in the WORLD

Day, Station to Station, 314-771-5750

Night, Person to Person, Dan Broida, 314-993-6418

TWX [Teletype] Day or Night: COLLECT 910-761-0593

TELEGRAM: SIGMACHEM, Saint Louis, Missouri

 **The Research Laboratories of**
SIGMA CHEMICAL COMPANY
P.O. BOX 14508 • SAINT LOUIS, MISSOURI 63178 U.S.A.
MANUFACTURERS OF THE FINEST BIOCHEMICALS AVAILABLE

Distributed through:

SIGMA LONDON Chem. Co. Ltd. • 12, Lettice St., London, S.W.6., England • Telephone: 01-736-5823 (Reverse Charges)
SIGMA ISRAEL Chem. Co. Ltd. • 28 Kef-Gimel St., Givataim, Israel • Telephone: 03 760654 (Reverse Charges)

Professional Opportunities

POSITION WANTED

PATHOLOGIST, D.V.M., Ph.D. 5 YRS. EXPERIENCE IN gross and microscopic path. of animal and human tissues. Organizing and teaching path. to med. students. 11000 Wabash, Kansas City, Mo. 64131 Tel: (816) 942-8121.

PHYSICIAN WANTED

WANTED—PATHOLOGIST QUALIFIED TO ASSUME full and sole responsibility in clinical and anatomic pathology for a small but enlarging department. Early partnership. Substantial fringe benefits with excellent non-contributory retirement program. Write or call Sam Packer, M.D., Medical Director, 11717 Euclid Avenue, Cleveland, Ohio 44106. Area Code 216, 795-4400.

PATHOLOGIST BEING SOUGHT BY CHILDRENS HOS-pital of Newark, affiliated with New Jersey Medical School. Experience and interest in anatomic pathology of infants and children desirable. Apply to: Richard H. Rapkin, M.D., Director of Pediatrics, 15 South Ninth Street, Newark, New Jersey 07107.

CLASSIFIED ADVERTISING INFORMATION

RATES:

Non Display:	1 Time	3 Times	6 Times or more
20 words or less	\$19.00	\$16.00	\$14.00
Each additional word	.50	.50	.50
Box Service—\$2.00—First insertion only			

Classified Display:	1 Time	3 Times	6 Times or more
	\$35.00	\$30.00	\$25.00
	per inch	per inch	per inch

Minimum Space—One (1) column inch

SEND ALL COPY,
AND BOX NUMBER INQUIRIES TO:

THE AMERICAN JOURNAL OF PATHOLOGY

Classified Dept.
P.O. Box 1510
617-A Cleveland Street
Clearwater, Florida 33517
Tele: 813-443-3047

A book for every physician

THE DIAGNOSTIC INTERVIEW

by Ian Stevenson, M.D.

Formerly titled **MEDICAL HISTORY-TAKING**, this new edition describes in a systematic manner what is known about the *do's* and *don'ts* of medical history-taking. Part I discusses the important factors affecting the doctor-patient relationship and how this relationship influences the outcome of medical interviews. It also considers other general principles of importance for the interview. Part II describes what information is to be obtained during the interview. In Part III, the author considers the techniques to be employed. Numerous examples of actual interviews are given including examples of common errors that should be avoided. Throughout the book, the author emphasizes the importance of observing the patient's non-verbal communications as well as his verbal statements.

In the new second edition, more emphasis has been given to the influence of the interviewer-patient relationship in shaping the information given by the patient. Greater emphasis is also given to the current situation of the patient as an influence on how he sees and describes his earlier life.

The references have been completely updated. This book is written for the practitioners of all branches of medicine, at all levels, who wish to improve their skills in interviewing while avoiding specialized psychiatric jargon.

By **IAN STEVENSON, M.D.**, *Alumni Professor of Psychiatry, Department of Psychiatry, University of Virginia School of Medicine, Charlottesville.* 320 pp., 12 illus., \$6.00.

HARPER & ROW, Publishers

Medical Department
Mail Order Department
2350 Virginia Avenue, Hagerstown, Md. 21740

Please send me on approval.

☐ Stevenson:

THE DIAGNOSTIC INTERVIEW .. \$6.00

☐ Bill me ☐ Check enclosed (SAVE!)

We pay postage and handling)

Name

Address

City State Zip

AJP-10

*A perfect balance of quality
and convenience*



Esco

microscope slides

GUARANTEED* PRE-CLEANED

*Satisfaction guaranteed or merchandise replaced.

- ☐ Made in U. S. A. from finest L•O•F glass
- ☐ Individually selected for uniform cleanliness
- ☐ Precision-ground edges on all four sides
- ☐ Annealed to minimize chipping and breakage
- ☐ Thin, flat, highly resistant to corrosion or fogging
- ☐ Dispensing package allows easy removal of slides

Esco

micro cover glasses

SUPERIOR QUALITY—MAXIMUM CLARITY

- ☐ Individually selected
- ☐ Superior resistance to corrosion and fogging
- ☐ Free from striae, oily film, fingerprints
- ☐ Precision uniformity in thickness, flatness and size
- ☐ Free from ragged edges
- ☐ Clear-vue crush-resistant plastic box



ERIE SCIENTIFIC
SYBRON CORPORATION

WRITE FOR BROCHURE NO. 9

BUFFALO, NEW YORK 14210

DERMAL PATHOLOGY

This new work presents current concepts of dermal pathology including related embryology, anatomy, histology, electron microscopy and histochemistry. The highly illustrated text is divided into five sections, with the first section providing basic information and defining the special language of dermal pathology. The other four sections consist of: inflammatory dermatoses; granulomatous dermatoses; nevi and neoplasms; and reticuloendothelial and alternative dermatoses.

The diseases are arranged according to histopathologic features, with disorders presenting similar histopathologic changes grouped together. This approach stresses the differential diagnosis and emphasizes the differentiating features between diseases. The discussion of each disease includes a brief description of gross pathology or clinical morphology, histopathologic characteristics, pertinent histochemistry, the differential diagnosis, and a short clinical description. This book should enable the reader to improve his ability to diagnose skin lesions and to understand the pathogenesis of the diseases discussed.

With 17 Contributors. Edited by **James H. Graham, M.D.**, Professor of Medicine (Dermatology), Department of Medicine; Chairman, Division of Dermatology; Professor of Pathology, Department of Pathology; and Director, Section of Dermal Pathology, University of California, Irvin; **Wayne C. Johnson, M.D.**, Professor of Dermatology, Department of Dermatology; Associate Professor of Pathology, Department of Pathology, Temple University School of Medicine; Director of Laboratories, the Skin and Cancer Hospital of Philadelphia, Philadelphia; and **Elson B. Helwig, MD.**, Chief, Department of Pathology and Branch of Dermal Pathology, Armed Forces Institute of Pathology, Washington, D.C.

1,155 Illustrations, 77 in full color

Available in October. Advance orders now accepted.

HARPER & ROW, PUBLISHERS

Medical Department

Mail Order Department, 2350 Virginia Avenue, Hagerstown, Maryland 21740

When published, please send me on approval:

AJP-10

GRAHAM, JOHNSON & HELWIG: Dermal Pathology \$45.00

NAME _____

ADDRESS _____

CITY _____ STATE _____ ZIP _____

CHANGING YOUR ADDRESS?

In order to receive your journal without interruption, please complete this Change of Address notice and forward to the Publisher, 60 days in advance, if possible.

Old Address: (PLEASE PRINT)

NAME _____

STREET _____

CITY _____

STATE (or Country) _____

ZIP CODE _____

New Address: (PLEASE PRINT)

NAME _____

STREET _____

CITY _____

STATE (or Country) _____

ZIP CODE _____

Date New Address Effective: _____

Name of Journal: _____

NEW ADDRESS—MEDICAL DEPARTMENT

Harper & Row, Publishers, Inc.
Medical Department
2350 Virginia Avenue
Hagerstown, Maryland 21740

Oxford



Color Atlas of Histopathology

Second Edition

By R. C. CURRAN, M.D., *The University of Birmingham Medical School*. Designed to complement textbooks of pathology, the Atlas features a superb selection of 765 color reproductions of photomicrographs displaying sections of diseased cellular tissue. The lesions illustrated are with few exceptions common conditions likely to be encountered in any large hospital, and this volume enables the pathologist to study carefully a greater diversity of histopathological specimens than many laboratories can readily supply. Lengthy explanatory captions to the illustrations furnish the information essential to the study of the sections depicted, and a full index covers all the different regions and systems of the body.

1972 94 pp. 765 illus. \$15.50

The Early Diagnosis of the Acute Abdomen

Fourteenth Edition

By SIR ZACHARY COPE, *St. Mary's Hospital, London*. For the fourteenth edition this classic monograph has been revised and enlarged by the inclusion of a short chapter on abdominal lesions arising in the left hypochondrium, and a new section on a form of intestinal obstruction due to malrotation of the mid-gut. Dr. Cope has rewritten the chapter on cholecystitis, including a new diagnostic sign which he first described. As in previous editions, the author stresses the importance of a sound clinical history, an intensive clinical examination, and early diagnosis.

1972 224 pp. 59 illus.
cloth \$6.95 paper \$4.50

OXFORD UNIVERSITY PRESS
200 Madison Avenue, New York, N.Y. 10016

Laboratory

it's brand new now...

and

for years to come,

it will stay that way...

Medicine

Editor: George J. Race, M.D., M.S.P.H., Ph.D., Pathologist-in-Chief and Director of Laboratories, Baylor University Medical Center, Dallas, Texas.

Associate Editors: Clinical Pathology—Samih Y. Alami, M.D., Ph.D. Hematology—Eugene P. Frenkel, M.D. Chemistry—Robert J. Speer, Ph.D., Harold H. Varon, M.D., and Joel E. Young, Ph.D. Microbiology—Ralph Tompsett, M.D. With 100 Contributors.

In Four Volumes. Here is a new exhaustive coverage presented for the first time as a loose-leaf reference. The dynamic loose-leaf concept means that your three volumes will always be new and updated through the ANNUAL SERVICE. *Volume 1* is entirely devoted to Clinical Chemistry, including the most modern automated techniques in use. *Volume 2* concerns Hematology, Blood Banking, Medical Microbiology, Virology, Serology, and Immunology. *Volume 3* covers Special Techniques (with modern methods and approaches to forensic pathology). *Volume 4* includes Body Fluids including Urine, Cytology and Cytogenetics, and Laboratory Management and Function. A separate annually revised index is included. *For all the future information coming out in the various fields covered in these volumes, it is a worthwhile investment for knowledge and practice.*

ANNUAL SERVICE includes:

"New pages for old." Partially or completely rewritten monographs, addenda and chapters on new subjects supplied annually along with a completely revised index.

HARPER & ROW, Publishers, Inc.

2350 Virginia Avenue

Medical Department

Hagerstown, Maryland 21740

☐ Please send more information on LABORATORY MEDICINE

LABORATORY MEDICINE (4 volumes, index volume & 1st yr. Annual Service): About \$175.00.

About \$27.50 a year thereafter for Annual Service. (Terms Available)

☐ Bill me @ full price.

☐ Bill me @ \$_____ a month
(minimum \$10.00 a month)

Name

Address

City State Zip AJP-10



ORTHO coagulation reagents

reflect the standard of excellence in laboratory medicine

ACTIVATED THROMBOFAX* REAGENT
(Partial Thromboplastin with Activator)

THROMBOFAX* REAGENT
(Partial Thromboplastin)

ORTHO* BRAIN THROMBOPLASTIN

ORTHO* PLASMA COAGULATION CONTROL
(Human Plasma)

FIBRINDEX* Thrombin (Human)



ORTHO DIAGNOSTICS

Raritan, New Jersey 08869

GOLD
HEADED
CANE
AWARD



SIDNEY FARBER, MD

and Robbins the Nobel Prize was done in the Department of Laboratories and Research of the Childrens Medical Center, and it is not irrelevant that Drs. Weller and Robbins began their careers as interns in Pathology under Dr. Farber. Both ends of the medical career received support from Dr. Farber, and our discipline was enriched thereby—his Department helped Drs. S. B. Wolbach, J. L. Bremer, J. L. Conel, Alwin Pappenheimer and others to continue their work and teaching after they had retired from other duties, so as to give their wisdom to many younger pathologists.

Thus we salute an illustrious career, but we are honoring more than a life of honest hard work, we are recognizing a role and an influence. We all know much of the role, because we have the same ones—service or diagnostic pathology, teaching, research, administration, in varying mix—and they are no small thing. But Dr. Farber's recognition rests even more on a theme he taught and spread through all facets of his career—an unswerving dedication to quality. All those who were privileged to work with or learn from him have felt this influence and have passed it on to what is now, in some lines of descent, third and fourth generations. He did not teach there was only one way to do an autopsy, but that there are good ways and there are poor ways, and there was no excuse for a poor way because the patient deserved one's best. It was the same with teaching—when we would complain that teaching duties interfered with the smooth running of things, he upheld quality, insisted that students were not some lower form of life but our colleagues, and that the greatest mistake we could make was to talk down to them. He insisted that it was an error, not only in terms of the product desired—which was a good physician—but also a spiritual and philosophic one, because the implied elitism was the kiss of death. He practiced, and expected from others, recognition of the worth of every other person, because every other person knows something one does not. In research his standards were also unfailingly high—his pained look when he thought a colleague was stepping beyond the data could be devastating. Dr. Farber has taught us all many things—not least, the importance of a goal and a vision. The present stature of pediatric pathology as a discipline comes very largely from Dr. Farber, who has maintained his position on this matter for over 30 years. The Childrens Medical Center in Boston, the Childrens Cancer Research Foundation, the chemotherapy of cancer in general, owe much to him. It has not been grim determination, because Dr. Farber is incapable of being grim, but he has been unswerving toward good and worthy goals. Columbus got across the ocean with similar vision and determination, and Paul Ehrlich

tried 605 other chemicals before he hit on Salvarsan. Dr. Farber has seen things with similar vision for many years.

He has received many other awards over the years, but we hope this award—the Gold Headed Cane of the Association—has special meaning. It does to us, because it comes from his peers on the firing lines—of doing one's best to give correct diagnoses, of doing one's best to teach the truth and find more and newer truths, of trying with finite bodies and finite minds and finite resources to keep things going, and get things done, and do more and better tomorrow, because we owe it to patients. Dr. Farber has shown us what can be done.

So it is for all these reasons that we present our highest award to Dr. Sidney Farber—physician, pathologist, pediatric pathologist, scientist and student of disease, teacher, visionary, accomplisher, guide and friend to all of us.

BENJAMIN LANDING

[*End of Article*]

Peroxidase Arthritis

II. Lymphoid Cell-Endothelial Interactions During a Developing Immunologic Inflammatory Response

Richard C. Graham Jr, MD and Sarajayne Limpert Shannon

The interaction of lymphoid cells with vascular endothelium was studied during the development of immunologic synovitis in response to repeated intraarticular injections of a heterologous protein antigen. Lymphoid cells emigrated in venules and small veins, both by penetrating the endothelial cytoplasm and by traversing intercellular junctions. Frequent endothelial mitoses were coincident with lymphoid cell emigration. Endothelial cells in the involved vessels increased in number and bulged prominently into the vascular lumen. Endothelial nuclei contained dispersed chromatin and prominent nucleoli; the cytoplasm contained many vacuoles and abundant polyribosomes and rough-surfaced endoplasmic reticulum. Intercellular junctions were numerous and complex. These phenomena were prominent in rabbits studied after 12 to 16 daily injections; they then receded, despite continued antigenic stimulation. In animals studied after 35 or 37 daily injections, the venules appeared relatively normal, and lymphoid cell emigration was observed infrequently. Growth of new vessels was prominent at this stage. The present data do not establish whether the endothelial changes were the cause or the result of lymphoid cell emigration, although the latter seems more likely. Further studies are needed to elucidate the exact nature of these interactions (Am J Pathol 69:7-24, 1972).

EMIGRATION OF LYMPHOID CELLS across the vascular endothelium is important to the development of a variety of immunologically mediated inflammatory responses. Electron microscopic studies of processes which depend largely on cellular immune mechanisms, such as tuberculin reactions^{1,2} and experimental allergic neuritis,³ have indicated that lymphocytes leave the circulation by passing through the cytoplasm of endothelial cells. In those studies, the majority of involved endothelial cells were little altered by this interaction. In homograft rejection, striking endothelial changes, including occasional mitosis, have been reported.⁴⁻⁷ These changes are thought to be a consequence of immunologic attack by host lymphocytes on donor endothelium.⁷

The inflammatory reaction of rheumatoid arthritis appears to be

From the Department of Medicine, Case Western Reserve University, University Hospitals of Cleveland, Cleveland, Ohio.

Supported by Research Grant AM 11308 from the National Institute of Arthritis and Metabolic Diseases.

Accepted for publication June 9, 1972.

Address reprint requests to Dr. Richard C. Graham, Jr, Department of Medicine, University Hospitals of Cleveland, University Circle, Cleveland, Ohio 44106.

mediated, at least in part, by immunologic mechanisms. Lymphocytes and plasma cells are prominent in the inflammatory infiltrate,⁸ and local immunoglobulin synthesis has been demonstrated in the lesions.⁹ The stimulus for these immunologic phenomena is unknown; it has been suggested that they may represent a response to a persistent foreign antigen, perhaps in the form of an infectious agent.¹⁰ The nature of lymphoid cell-endothelial interactions during the development of this type of immunologic inflammatory response is unknown.

This report describes the interactions between lymphoid cells and endothelium which occur during the development of peroxidase arthritis, a model of the immune inflammatory response to a persistent local antigen (horseradish peroxidase).¹¹ In this inflammatory response, which histologically resembles that of rheumatoid arthritis, local specific antibody synthesis is demonstrable by ultrastructural cytochemistry. As the reaction develops, lymphoid cells emigrate by penetrating the endothelial cytoplasm and by passing through intercellular junctions. Coincident with lymphoid cell emigration, endothelial cell proliferation occurs.

Materials and Methods

The experimental procedures used in the production of peroxidase arthritis are described in detail in the previous report.¹¹ The results reported here were observed in the rabbits described in that report, plus an additional 16 rabbits injected daily for from 3 to 9 days. Briefly, the shaved knee joints of New Zealand white rabbits were injected aseptically with 2 mg horseradish peroxidase (HRPO) (type VI, Sigma Chemical Co) in 0.5 ml 0.15 M NaCl. The injections were repeated daily for 3 to 37 days. Twenty-four hours after the last injection, the rabbits were killed with an overdose of sodium thiamylal and the knee joints were fixed for 4 hours in 2% formaldehyde and 2.5% glutaraldehyde¹² in 0.05 M phosphate buffer, pH 7.4, and washed overnight in the same buffer. The synovial membrane and subsynovial tissue, medial and lateral to the patella, was dissected free with a razor blade and cut into 1- to 3-mm thick strips. A portion of the tissue was reacted for cytochemical demonstration of peroxidase activity by the method of Graham and Karnovsky.¹³ The remaining tissue was preincubated with HRPO before reaction for peroxidase activity, so that antibody to HRPO could be revealed as described by Leduc and her associates.¹⁴ All tissues were then washed three times in distilled water, fixed for 1 hour in 1% OsO₄ in 0.05 M phosphate buffer, pH 7.4, dehydrated in ethanol and embedded in Araldite. Thick (0.5 μ) sections were cut on Sorvall MT-1 or MT-2 microtomes and stained with toluidine blue for light microscopy. Thin sections were cut on the same microtomes, stained with uranyl acetate and lead citrate, and examined in an AEI EM-6B electron microscope.

Sera were obtained from rabbits at the beginning and completion of each experiment and at intervals during the course of injections. Serial dilutions of sera were assayed for antibody to HRPO by double diffusion in agar, and by passive hemagglutination, using sheep erythrocytes coupled to HRPO with glutaraldehyde, as described by Avrameas *et al.*¹⁵

Results

Controls

The fine structure of the microvasculature in joints repeatedly injected with diluted autologous serum was indistinguishable from that of normal synovial tissue,¹⁶⁻¹⁸ and will not be described in detail. In general, the *superficial* vessels (*ie*, those immediately beneath the synovial lining cells) were predominantly capillaries. The attenuated endothelial cytoplasm of many of these vessels was partially fenestrated, with the fenestrations enclosed by thin diaphragms. Among the deep vessels, arterioles and venules of various sizes were observed. The venules, which had a continuous endothelium, differed in structure from those observed in tissues such as skeletal muscle. In subsynovial venules, the endothelium often was thicker and contained more abundant cytoplasmic organelles—notably, rough-surfaced endoplasmic reticulum and vacuoles.

Peroxidase Arthritis

As lymphoid cell emigration occurred and the subsynovial infiltrate developed, striking changes were observed in the small blood vessels. Superficial capillaries with fenestrated endothelium were rarely seen in the more prolonged reactions (those occurring after 35 or 37 daily injections). Emigration of lymphoid cells occurred in venules and small veins; the endothelial cells of these venules and small veins underwent striking proliferative and morphologic changes (described in detail below). Emigration and the coincident vascular changes were markedly focal; extensively involved venules frequently were observed near normal venules of similar size. On occasion, extensive emigration and endothelial proliferation occurred along one wall of a small vein and the remainder of the vein was uninvolved (Figure 1).

After 4 daily injections of HRPO, the structure of most venules was not remarkable. Occasional endothelial cells bulged prominently into the vascular lumen. Such cells had dispersed nuclear chromatin and prominent nucleoli, and their cytoplasm contained abundant rough-surfaced endoplasmic reticulum.

Occasional lymphoid cells were observed at this stage. Some of these cells had the structural characteristics of *activated* lymphocytes—*ie*, cytoplasm containing many free polyribosomes and moderately condensed nuclear chromatin. Others were similar in appearance except that only monoribosomes could be identified within the cytoplasm. Such cells were seen most frequently within venular lumens. Some of

these had multiple pseudopods which interdigitated with pseudopods from an adjacent endothelial cell (Figure 2). Small numbers of similar lymphoid cells were observed in extravascular tissues. Lymphoid cells in the process of emigration were seen infrequently at this stage.

Synovial tissue from rabbits given 6 to 9 daily HRPO injections contained venules and small veins with increasingly prominent endothelial changes. Endothelial cells frequently were observed in mitosis, both by light (Figure 3A, 3B) and electron (Figure 4) microscopy. In some vessels, the number of endothelial cells appeared to be increased. In these vessels, the endothelial cells, which had the active appearance described above, often projected prominently into the vascular lumen.

Perivascular accumulations of lymphoid cells were observed near the affected vessels, suggesting that they were preferential sites of lymphoid cell emigration. The actual process of emigration was still seen rather infrequently at this stage. The emigrating lymphoid cells, which were observed, appeared to pass through the endothelial cytoplasm rather than through intercellular junctions.

The peak of endothelial activity and lymphoid cell-endothelial interaction was observed in synovial tissues from rabbits given 12 to 16 daily HRPO injections. Involved venules and small veins, when compared with normal vessels of similar diameter, contained an increased number of endothelial cells. The endothelial cells had a rounded contour; many of them projected prominently into the lumen, giving the endothelium a pseudocolumnar appearance (Figures 5 and 6). Endothelial nuclei had dispersed chromatin and prominent nucleoli. The cytoplasm contained many vesicles and vacuoles and abundant rough-surfaced endoplasmic reticulum and free polyribosomes. Adjacent cells were extensively interdigitated, as reflected by the observation of numerous and complex intercellular junctions. Junctional complexes were prominent (Figures 5 and 6). Pericytes also were increased in number and displayed numerous thin cell processes which projected into the surrounding tissue for considerable distances, often in close association with numerous perivascular lymphoid cells.

Emigration of lymphoid cells was very prominent in the involved venules and small veins. These cells emigrated in several ways. Frequently, lymphocytes appeared to emigrate by traversing the endothelial cytoplasm. In early stages of the process a portion of the lymphocyte, frequently containing its rounded nucleus, was seen to deeply indent an endothelial cell (Figure 7). At this stage, an expanded *tail* of cytoplasm remained within the lumen. Lymphoid cells entirely within the endothelial cell (Figure 8) appeared to represent a sub-

sequent stage in this process. The lymphocytes then appeared to emerge from the endothelial cytoplasm by penetrating the plasma membrane of the outer surface of the cell (Figure 9). Other lymphocytes seemed to emigrate in a similar manner, except that their course of emigration traversed an intercellular junction (Figure 10). It is possible that such junctional involvement was actually quite common, since extensive study of serial sections would be required to exclude it in sites such as those shown in Figures 7-9.

In altered vessels in which interendothelial junctions were particularly numerous and complex, the usual path of emigration of lymphoid cells was through junctions. Frequently, activated lymphocytes penetrated junctions in a manner resembling that by which they penetrated the endothelial cytoplasm in other sites. In this process, a portion of the cell containing the rounded nucleus penetrated and widely separated the junction, while a tail of cytoplasm continued to protrude into the vascular lumen (Figure 11). Occasionally, however, cells emigrating through junctions presented a somewhat different appearance (Figure 12). In such instances the junctions were less widely separated, and the emigrating cells were elongated with a marked constriction in that portion of the cell within the junction. Although many of the emigrating cells contained the numerous polyribosomes characteristic of activated lymphocytes, others had a predominance of monoribosomes in the cytoplasm. No correlation between these differences and the mode of emigration could be determined.

Immunoblasts were observed to emigrate through intercellular junctions, usually in areas of marked endothelial alteration (Figure 13).

Polymorphonuclear leukocytes and monocytes emigrated through intercellular junctions, often in the same altered venules which were the site of extensive emigration of lymphoid cells. In the altered vessels, cells within the lumen extended long pseudopods into the narrow space between the protruding cell bodies of adjacent endothelial cells. This phenomenon was not necessarily associated with evidence of adherence of the leukocyte to the endothelial surface. Otherwise, emigration of polymorphonuclear leukocytes and monocytes occurred in a manner similar to that first described by Marchesi and Florey in the acute inflammatory response.¹⁹

In rabbits killed after 35 or 37 daily HRPO injections, endothelial alterations were much less prominent. Lymphoid cell emigration was infrequently observed, despite the fact that the extravascular cellular infiltrate was much more extensive than that present after 16 daily HRPO injections. Evidence of new vessel formation was frequently

noted in the form of endothelial sprouts and incompletely canalized vessels.

Discussion

The developmental stages of peroxidase arthritis are characterized by a very complex series of cellular changes and cell-to-cell interactions. For convenience, we will discuss certain of these phenomena separately before speculating on their interrelationships.

The striking changes in small veins and venules which occur in peroxidase arthritis have no exact counterpart in those types of immune inflammation previously studied by electron microscopy. Vascular changes reported during homograft rejection⁴⁻⁷ bear a superficial resemblance to alterations which occur during the development of peroxidase arthritis. In both, the endothelial nuclei become large and rounded, with prominent nucleoli. Also common to both is an increase in the amount of free polyribosomes and rough-surfaced endoplasmic reticulum within the endothelial cytoplasm. Endothelial mitosis has been described in rejecting ovine renal homografts,⁷ but the striking degree of endothelial proliferation observed in the present studies has not been described. The endothelial changes observed in rejecting homografts are generally considered the result of immunologic attack by host lymphoid cells upon donor endothelium.⁴⁻⁷ The ultimate result is endothelial degeneration. In contrast, in peroxidase arthritis the endothelium is autologous with respect to the emigrating lymphocytes, and endothelial degeneration is inconspicuous even when the reaction is prolonged. Thus, it seems likely that the endothelial changes of peroxidase arthritis differ in their pathogenesis and significance.

Small blood vessels have been studied by electron microscopy in several other models of inflammation, the pathogenesis of which, for the most part, appears to depend upon cellular immunity. Vascular alterations, in general, have not been striking. Wiener and his associates,^{1,2} in studies of the tuberculin reaction, described no vascular structural changes other than the formation of endothelial processes, in venules and small veins, associated with emigration of lymphocytes through these vessels. Willms-Kretschmer *et al* studied hapten-specific delayed hypersensitivity and contact dermatitis and found no vascular alterations.²⁰ In experimental allergic neuritis, Åström and his colleagues³ found that most of the endothelial cells appeared normal. In a few of the cells, free ribosomes and rough-surfaced endoplasmic reticulum were increased and nucleoli were prominent. None of these reports mention endothelial proliferation.

The reason that endothelial changes, comparable to those observed in the present study, were not seen in the types of immune inflammation cited above is uncertain. Perhaps it is relevant that the pathogenesis of each depends primarily on cellular immune mechanisms, and that, for the most part, the lesions studied were quite early ones.

Ultrastructural studies of a reaction comparable to peroxidase arthritis are limited to a report by Movat and Fernando.²¹ These investigators observed that proliferation of venular pericytes occurred after repeated injections of foreign protein into rabbit knee joints. These *stimulated* pericytes, which had prominent nucleoli and abundant rough-surfaced endoplasmic reticulum, were thought to detach themselves from the vascular wall and to become ameboid. Unfortunately, details such as number of injections and nature of the foreign protein were not given, and the endothelial cells were not described.

Emigration of lymphoid cells during immunologic reactions has been described by a number of investigators. In homograft rejection, lymphoid cells and blasts within the vascular lumen are seen with their membranes in close apposition to the membranes of endothelial cells.⁴⁻⁷ Interdigitation of cell processes is common, and apparent points of cytoplasmic continuity have been observed.^{4,5} Although blasts have been observed to emigrate through intercellular junctions during homograft rejection,²² the mode of emigration of other lymphoid cells is unclear. In some instances they appear to pass through discontinuities created by endothelial degeneration.

In other types of cell-mediated immune inflammation, lymphocytes have been observed to emigrate directly through endothelial cytoplasm.^{2,3,23} Whether this process involves an active role for the endothelium^{2,23} or the lymphoid cell³ has been in dispute. The former possibility was suggested by observations, in the tuberculin reaction² and in experimental allergic encephalomyelitis,²³ that rounded, non-motile-appearing lymphoid cells were enveloped by long, slender endothelial cell processes which subsequently fused, incorporating the lymphoid cell into the endothelial cytoplasm. In contrast, observations made on experimental allergic neuritis³ suggested that the lymphoid cell was an active participant in the process of emigration. Initially, intraluminal lymphoid cells often displayed a large process, the end of which interdigitated with the endothelial cell membrane. Subsequently, the lymphoid cells flattened out along the endothelial surface, with lymphoid cell processes invaginating the endothelium at multiple sites. Emigration of lymphocytes through intercellular junctions was not observed in these studies.

Emigration of lymphocytes in peroxidase arthritis differed from that described above in a number of respects. First, cells that were clearly lymphocytic in nature emigrated through both endothelial cytoplasm and intercellular junctions. Lymphocytic emigration by the latter route has not, to our knowledge, been reported previously. In part, junctional involvement in emigration may have been related to the increased number and complexity of junctions in the altered venules of peroxidase arthritis. In some areas, junctions were so numerous that it is difficult to imagine a route of emigration that would not involve contact with a junction at some point in its course. Indeed, some emigrating lymphoid cells resembled those fully encased in endothelial cytoplasm, except that a junction intersected the vacuole at some point. It is possible that study of serial sections would reveal that most or all of the apparently intraendothelial lymphoid cells would have shown contact with junctions in some plane of section. In contrast to the above lymphoid cells, which maintained a generally rounded contour during emigration, others emigrated through junctions in a manner similar to that of polymorphonuclear leukocytes and monocytes. These cells became elongated and showed marked constriction in their intrajunctional portions. Lymphoid cells emigrating by any of the routes observed in peroxidase arthritis appeared actively motile, supporting the observation of Åström and his colleagues³ that the lymphocyte is an active participant in the process of emigration.

The striking vascular phenomena of peroxidase arthritis seem to be limited to the earlier stages of the developing immune inflammatory response. With time they become much less prominent, despite continued antigenic stimulation. Despite a marked decline in observable lymphoid cell emigration, the number of these cells in the extravascular infiltrate continued to increase, presumably because of mitotic activity among the cells composing the infiltrate. Endothelial mitotic activity continues in the more prolonged reactions, but appears to be chiefly directed toward the formation of new blood vessels. Although the explanation of these sequential changes is unknown, the changes are of interest in view of the controversy over the existence of vascular alterations in lesions of rheumatoid arthritis.^{24,25} Whether or not such changes are found might depend on the stage and activity of the disease.

The relationship of the striking endothelial changes of peroxidase arthritis to cellular emigration cannot be established with certainty on the basis of the presently available data. Endothelial changes in peroxidase arthritis could be primary and in some manner facilitate lym-

phoid cell emigration, or they could occur as a result of the interaction of endothelium with lymphoid cells. In support of the latter possibility, we have not observed unequivocal endothelial changes in advance of emigration of lymphoid cells. Normal recirculation of lymphocytes involves lymphocytic emigration through lymph node postcapillary venules, which have a peculiar pseudocolumnar endothelium²⁶ which in some respects resembles the altered endothelium observed in evolving peroxidase arthritis. Observations of lymph node postcapillary venules by light microscopy²⁷ suggest that the peculiar structure of these vessels may indeed be the *result* of lymphocytic emigration. In rats subjected to neonatal thymectomy, or depleted of lymphocytes by thoracic duct drainage, the postcapillary venular endothelial cells were *smaller* than normal and lacked the usual pyroninophilia. These changes were reversible when the lymphocyte-depleted animals were given lymphocytes from normal syngeneic donors. This evidence suggests that interaction with autologous lymphoid cells may result in *stimulation* and subsequent mitosis of endothelial cells. Such an effect could result either from physical interaction of the two cell types, or from a soluble mediator released by the lymphoid cells. The latter hypothesis seems plausible, since lymphocytes are known to elaborate a variety of other active substances upon stimulation. In this regard, it is of interest that tumor cells have been shown to contain a substance which is mitogenic to endothelium.²⁹ Further studies, including the use of *in vitro* systems, will be required to elucidate the mechanism of the lymphoid cell-endothelial interactions described in the present report.

References

1. Wiener J, Zunker HO: A cellular study of tuberculin sensitivity. *Am J Pathol* 47:723-763, 1965
2. Wiener J, Lattes RG, Spiro D: An electron microscopic study of leukocyte emigration and vascular permeability in tuberculin sensitivity. *Am J Pathol* 50:485-521, 1967
3. Åström KE, Webster H de F, Arnason BG: The initial lesion in experimental allergic neuritis: a phase and electron microscopic study. *J Exp Med* 128: 469-495, 1968
4. Williams PL, Williams MA, Kountz SL, Dempster WJ: Ultrastructural and haemodynamic studies in canine renal transplants. *J Anat* 98:545-569, 1964
5. Porter KA, Joseph NH, Rendall JM, Stolinski C, Hoehn RJ, Calne RY: The role of lymphocytes in the rejection of canine renal homotransplants. *Lab Invest* 13:1080-1098, 1964
6. Feldman JD, Lee S: Renal homotransplantation in rats. I. Allogeneic recipients. *J Exp Med* 126:783-794, 1967
7. Pedersen NC, Morris B: The role of the lymphatic system in the rejection

- of homografts: a study of the lymph from renal transplants. *J Exp Med* 131:936-969, 1970
8. Parker F, Keefer CS: Gross and histologic changes in the knee joint in rheumatoid arthritis. *Arch Pathol* 20:507-522, 1935
 9. Fish AJ, Michael AF, Gewurz H, Good RA: Immunopathologic changes in rheumatoid arthritis synovium. *Arthritis Rheum* 9:267-280, 1966
 10. Christian CL: Rheumatoid arthritis: etiologic considerations. *Arthritis Rheum* 7:455-466, 1964
 11. Graham RC, Shannon SL: Peroxidase arthritis. I. A model of immunologically mediated inflammation with ultrastructural cytochemical localization of antigen and antibody. *Am J Pathol* 67:69-94, 1972
 12. Karnovsky MJ: A formaldehyde-glutaraldehyde fixative of high osmolality for use in electron microscopy. *J Cell Biol* 27:137A, 1965 (Abstr)
 13. Graham RC, Karnovsky MJ: The early stages of absorption of injected horseradish peroxidase in the proximal tubules of mouse kidney. Ultrastructural cytochemistry by a new technique. *J Histochem Cytochem* 14:291-302, 1966
 14. Leduc EH, Avrameas S, Bouteille M: Ultrastructural localization of antibody in differentiating plasma cells. *J Exp Med* 127:109-118, 1968
 15. Avrameas S, Tandow B, Chivilon S: Glutaraldehyde, cyanuric chloride and tetraazotized *o*-dianisidine as coupling reagents in the passive hemagglutination test. *Immunochemistry* 6:67-76, 1969
 16. Suter ER, Majno G: Ultrastructure of the joint capsule in the rat: presence of two kinds of capillaries. *Nature (Lond)* 202:920-921, 1964
 17. Schumacher HR: The microvasculature of the synovial membrane of the monkey: ultrastructural studies. *Arthritis Rheum* 12:387-404, 1969
 18. Shannon SL, Graham RC: Protein uptake in synovial cells. I. An ultrastructural cytochemical study of the fate of intra-articularly injected peroxidases. *J Histochem Cytochem* 19:29-42, 1971
 19. Marchesi VT, Florey HW: Electron micrographic observations on the emigration of leukocytes. *Q J Exp Physiol* 45:343-348, 1960
 20. Willms-Kretschmer K, Flax MH, Cotran RS: The fine structure of the vascular response in hapten-specific delayed hypersensitivity and contact dermatitis. *Lab Invest* 17:334-349, 1967
 21. Movat HZ, Fernando NVP: The fine structure of the terminal vascular bed. IV. The venules and their perivascular cells (pericytes, adventitial cells). *Exp Mol Pathol* 3:98-114, 1964
 22. Wiener J, Lattes RG, Peare JS: Vascular permeability and leukocyte emigration in allograft rejection. *Am J Pathol* 55:295-327, 1969
 23. Bubis JJ, Luse SA: An electron microscopic study of experimental allergic encephalomyelitis in the rat. *Am J Pathol* 44:299-317, 1964
 24. Kulka JP: The pathogenesis of rheumatoid arthritis. *J Chronic Dis* 10:388-402, 1959
 25. Branemark PI, Ekholm PI, Goldie I: To the question of angiopathy in rheumatoid arthritis: an electron microscopic study. *Acta Orthop Scand* 40:153-175, 1969
 26. Marchesi VT, Gowans JL: The migration of lymphocytes through the endothelium of venules in lymph nodes: an electron microscopic study. *Proc R Soc Lond [Series B]* 159:283-290, 1964

27. Goldschneider I, McGregor DD: Migration of lymphocytes and thymocytes in the rat. I. The route of migration from blood to spleen and lymph nodes. *J Exp Med* 127:155-168, 1968
28. Folkman J, Merler E, Abernathy C, Williams G: Isolation of a tumor factor responsible for angiogenesis. *J Exp Med* 133:275-288, 1971

Acknowledgments

Dr. Graham is the recipient of Research Career Development Award AM 42,397 from the National Institute of Arthritis and Metabolic Diseases.

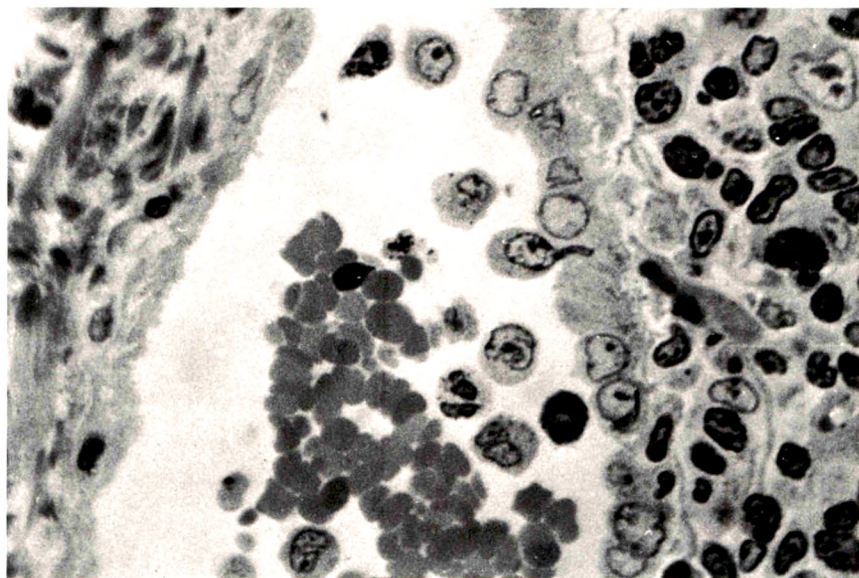
[Illustrations follow]

Legends for Figures

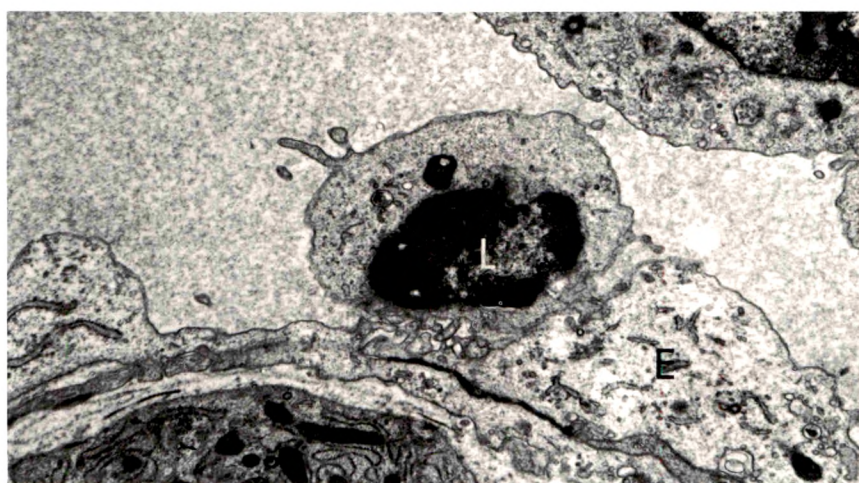
Fig 1—Small vein from synovial tissue taken after 16 daily HRPO injections, illustrating the focal nature of endothelial alteration and lymphoid cell emigration. To the left, the endothelium is flattened, nuclei are inconspicuous, and few cells are present in the perivascular connective tissue. To the right, the endothelial cells are rounded, and numerous large, clear nuclei are evident. Polymorphonuclear leukocytes, monocytes and immunoblasts are evident in the lumen. One cell, probably an immunoblast, has inserted a pseudopod into the altered, pseudocolumnar endothelium. Beneath the altered endothelium is an extensive cellular infiltrate (Light micrograph, $\times 650$).

Fig 2—Portion of venule from synovial tissue taken after 4 daily HRPO injections. A lymphocyte (L) in the lumen has multiple small pseudopods which interdigitate with similar processes from an endothelial cell (E) (Electron micrograph, $\times 7200$).

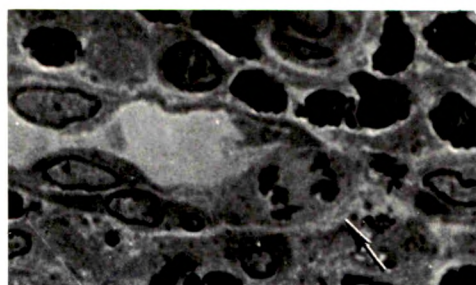
Fig 3A—Subsynovial venule from a rabbit killed after 6 daily injections of HRPO. A mitotic figure is present in one of the endothelial cells (arrow). The remaining endothelium appears normal. Polymorphonuclear leukocytes are prominent in the surrounding inflammatory infiltrate (Light micrograph, $\times 800$). **3B**—Subsynovial venule from a rabbit sacrificed after 6 daily injections. Multiple mitotic figures (arrows) are evident in the endothelium. A lymphocyte is present between two endothelial cells with mitotic figures (Light micrograph, $\times 700$).



1



2



3A



3B

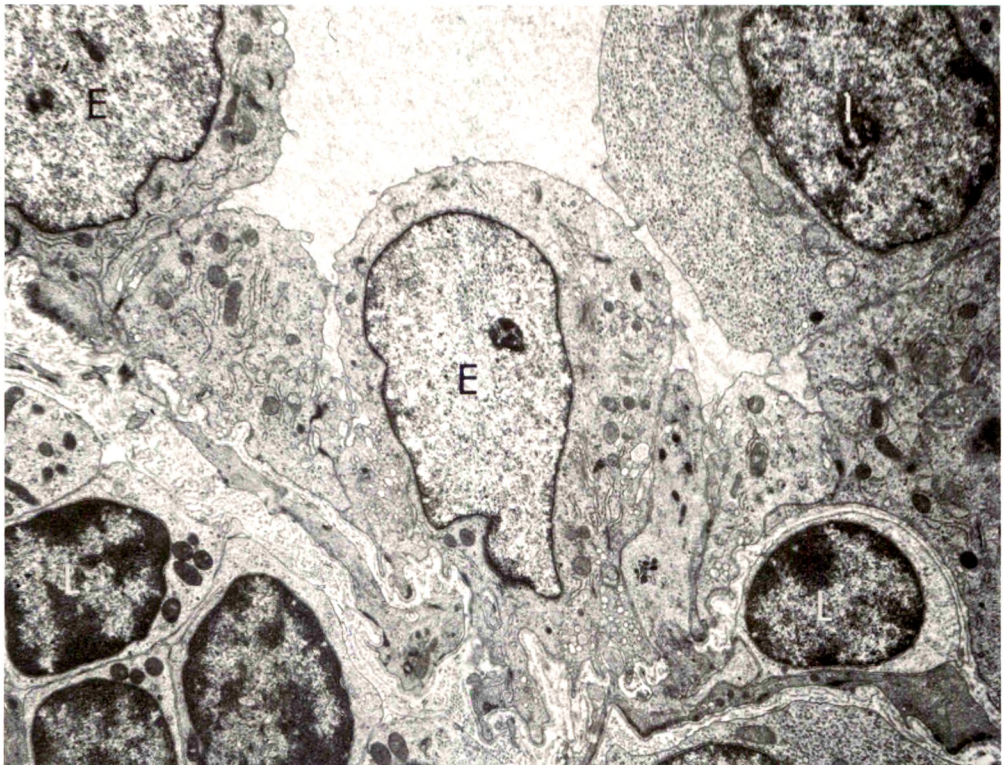
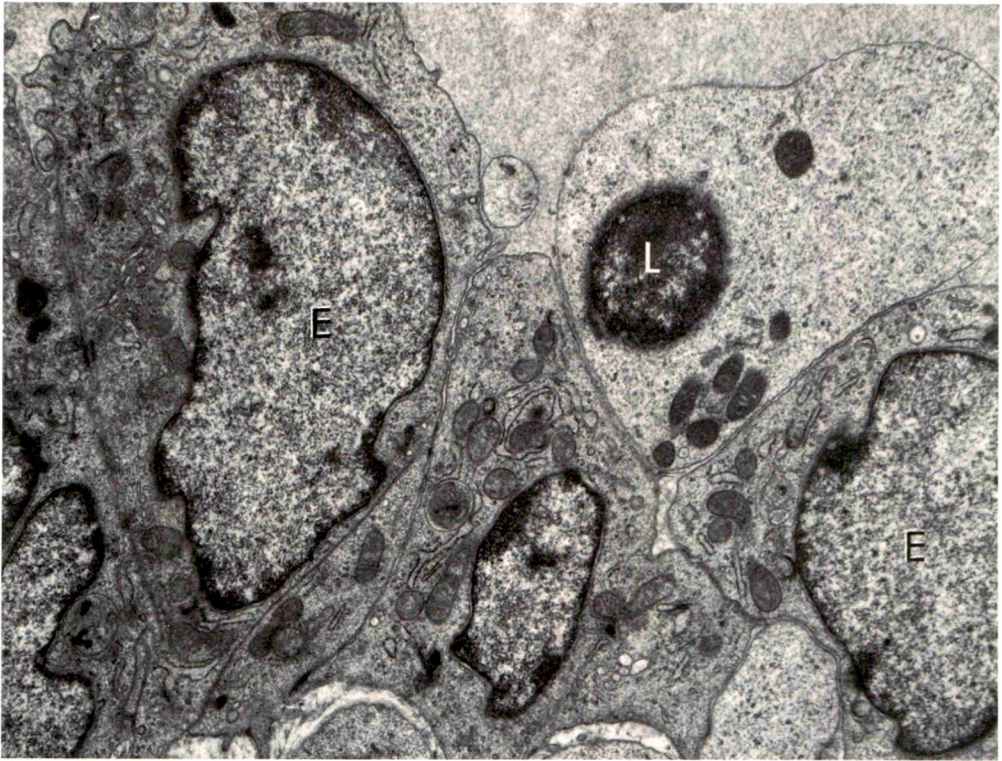
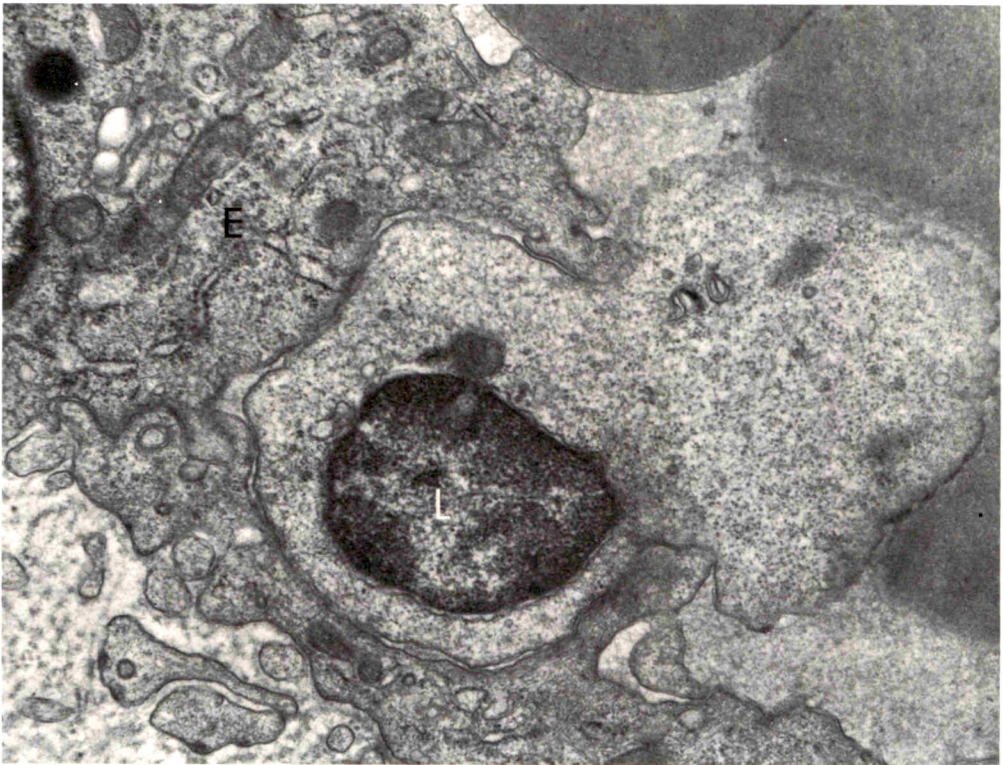


Fig 4—Mitotic figure in venular endothelial cell from subsynovial tissue obtained after 4 daily HRPO injections. Aggregation of chromatin and discontinuity of nuclear membrane are apparent. Intercellular junctions between adjacent endothelial cells are intact (arrows). Collagen fibers (*cf*) are present in the perivascular space; *L*=lumen (Electron micrograph, $\times 8200$). **Fig 5**—Venule from synovial tissue taken after 16 daily HRPO injections. Endothelial cells (*E*) are numerous and project prominently into the lumen. The endothelial nuclei have dispersed chromatin and prominent nucleoli; the cytoplasm contains abundant rough-surfaced endoplasmic reticulum and frequent vacuoles. Intercellular junctions are numerous. An immunoblast (*I*) lies within the lumen, and several lymphoid cells (*L*) are seen beneath the endothelium (Electron micrograph, $\times 4500$).



6



7

Fig 6—Wall of subsynovial venule from rabbit killed after 16 daily injections of HRPO. The pseudocolumnar-appearing endothelial cells (*E*) display abundant cytoplasmic organelles and numerous intercellular junctions. An activated lymphocyte (*L*) is closely apposed to two endothelial cells in the region of an intercellular junction (Electron micrograph, $\times 11,000$). **Fig 7**—Portion of subsynovial venule from a rabbit sacrificed after 16 daily HRPO injections. Part of a lymphocyte (*L*) containing the rounded nucleus deeply indents an endothelial cell (*E*) (Electron micrograph, $\times 14,800$).

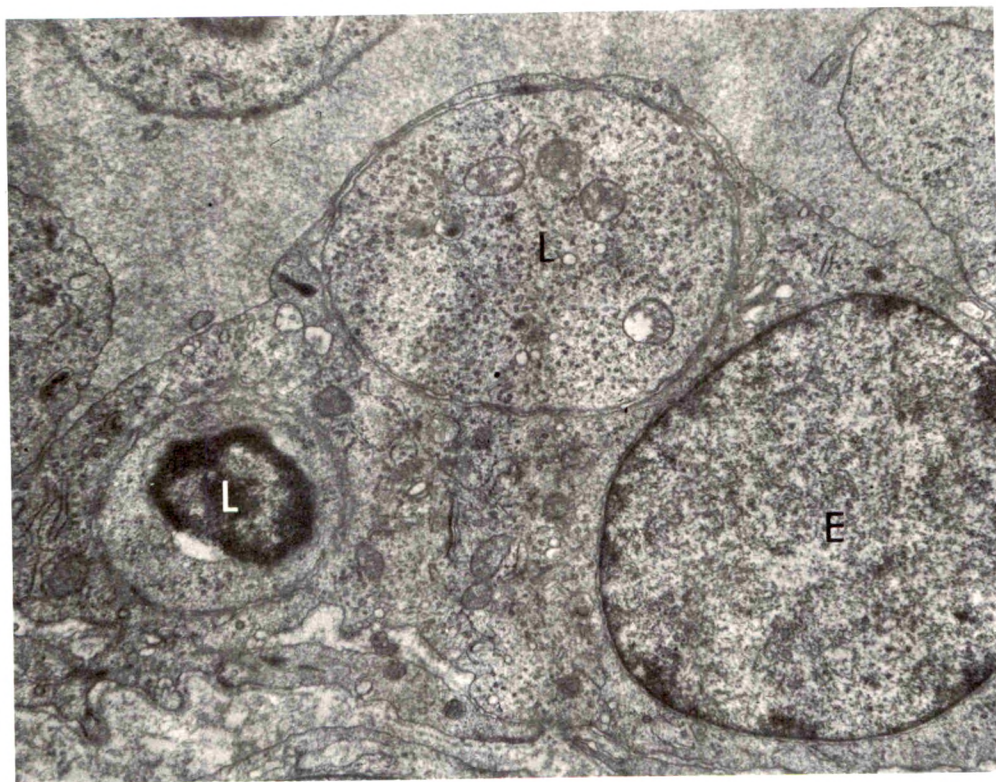
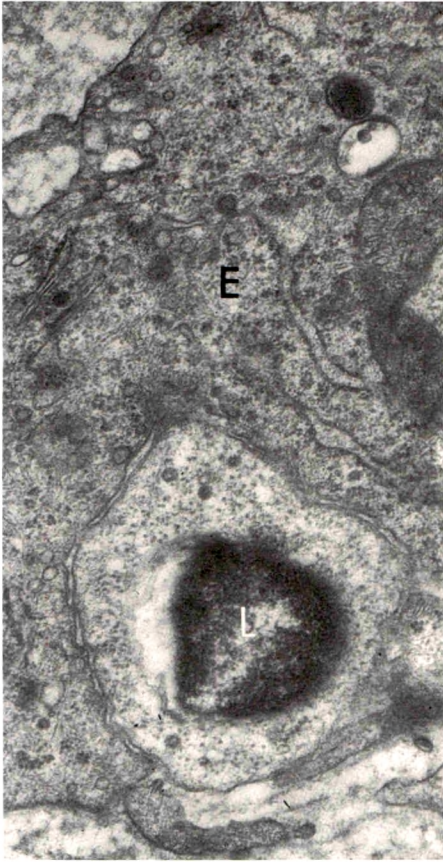


Fig 8—Portion of subsynovial venule from rabbit killed after 16 daily HRPO injections. Two activated lymphocytes (L) appear to be encased within the cytoplasm of an endothelial cell (E). The vascular lumen is at the top (Electron micrograph, $\times 7200$).

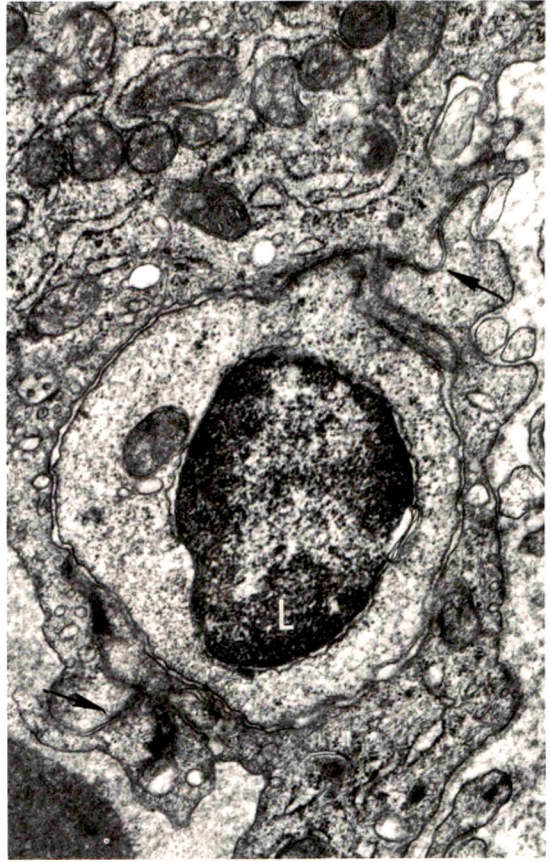
Fig 9—Portion of subsynovial venule from tissue taken after 16 daily HRPO injections. A lymphocyte (L) appears to be emerging from the abluminal surface of the endothelial cell (E). The lumen is at the upper left (Electron micrograph, $\times 15,000$).

Fig 10—Wall of venule from subsynovial tissue obtained after 16 daily HRPO injections. A lymphocyte (L) is encased within the venular wall. In this case, the vacuole surrounding the lymphocyte is continuous with intercellular junctions (arrows). The lumen is at the lower left (Electron micrograph, $\times 15,000$).

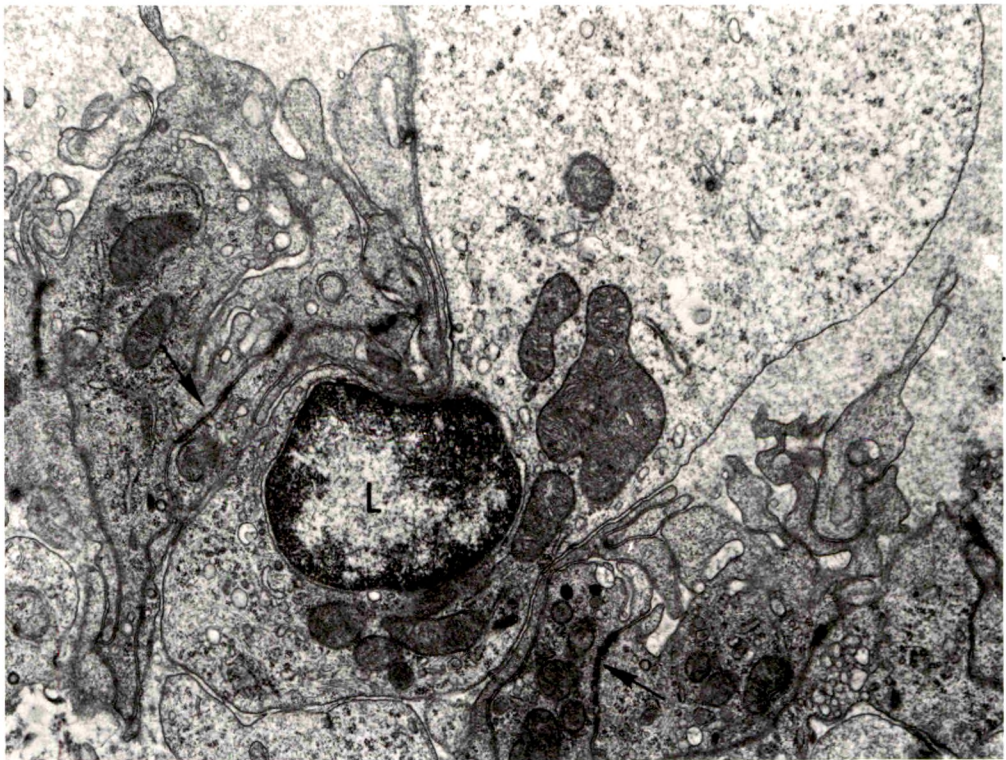
Fig 11—Portion of subsynovial venule from tissue taken after 16 daily HRPO injections. Numerous complex intercellular junctions (arrows) are present in the endothelium. An activated lymphocyte (L) has penetrated one of the junctions. The portion of the lymphocyte already within the junction contains the rounded nucleus. A large tail of rather electron-lucent cytoplasm remains within the lumen (Electron micrograph, $\times 11,000$).



9

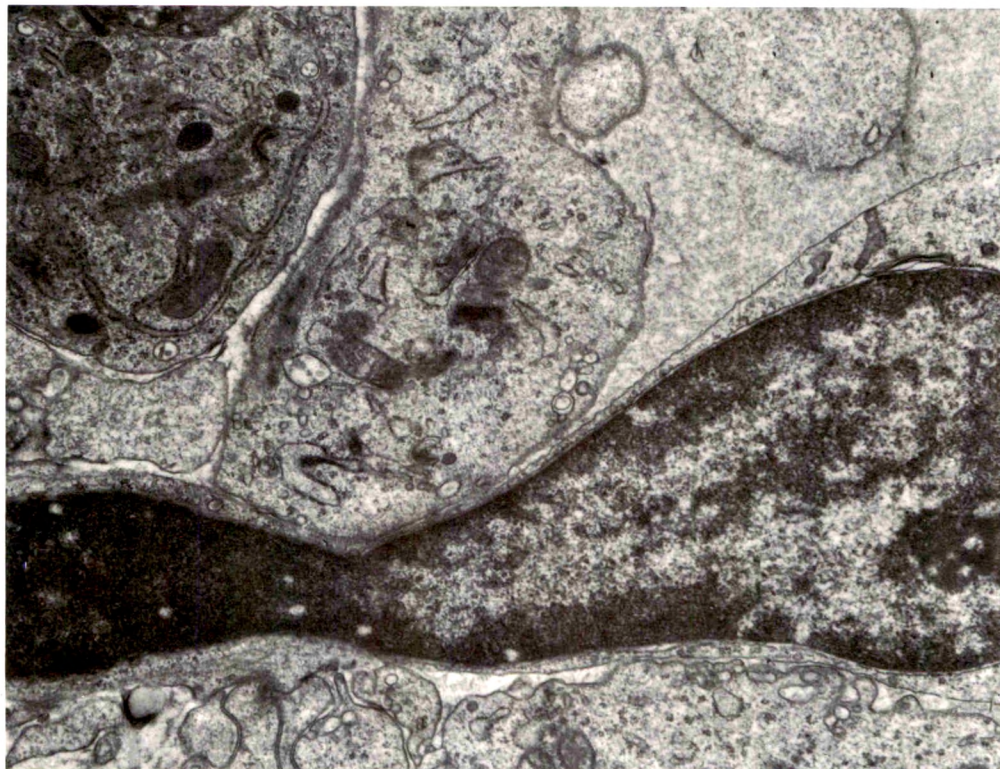


10



11

12



13

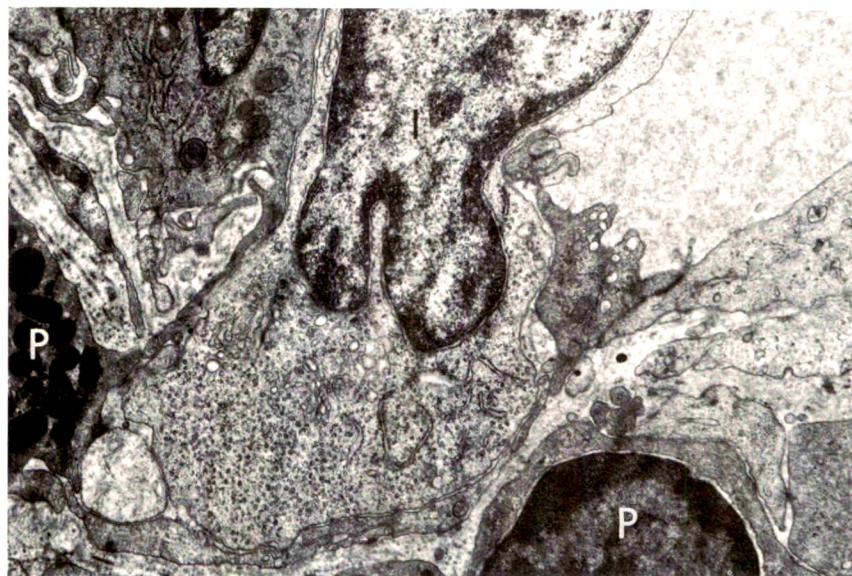


Fig 12—Subsynovial venule from rabbit killed after 16 daily HRPO injections. An activated lymphocyte is seen within a portion of a complex intercellular junction. The portion of the lymphocyte within the junction is markedly constricted (Electron micrograph, $\times 11,000$). **Fig 13**—Portion of subsynovial venule from rabbit killed after 16 daily injections of HRPO. An immunoblast (*I*) is passing through an intercellular junction. Portions of two polymorphonuclear leukocytes (*P*) are seen in the perivascular space (Electron micrograph, $\times 7500$).

Morphologic Variants of Alcoholic Hyalin

Hidejiro Yokoo, MD, Odell T. Minick, Fawzia Batti, MD and
Geoffrey Kent, MD

Liver biopsies obtained from 24 patients with alcoholic liver disease were studied by light and electron microscopy. Comparisons of the same cells in adjacent sections revealed that alcoholic hyalin is a fibrillar deposit without limiting membranes and is readily distinguished from giant mitochondria. This characteristic fibrillar structure was encountered in hepatocytes, ductular cells and in benign and malignant hepatomas. Three distinct morphologic forms of alcoholic hyalin were observed: a) bundles of filaments in parallel arrays, b) clusters of randomly oriented fibrils and c) a granular or amorphous substance containing only scattered remains of fibrils. Closely associated with alcoholic hyalin and often found along its entire circumference, were bundles of fine filaments in parallel arrangement of much smaller size. These occasionally displayed variations in orientation and merged with the filaments in the alcoholic hyalin body. Similar fine filaments were observed, in considerable excess, in cells which did not contain alcoholic hyalin. According to our findings, the fine filaments and the significantly larger filaments in alcoholic hyalin could be parts of a contractile system elaborated by host cells during the course of hepatic injury (Am J Pathol 69:25-40, 1972).

ALCOHOLIC HYALIN, first described by Mallory in 1911,¹ is an eosinophilic hyalin intracytoplasmic inclusion found chiefly in patients with alcoholic liver disease. Its distinctive morphologic features, especially its shape and tinctorial properties, have long been an important aid in the diagnosis of this disease. The inclusions occur in a number of other conditions²⁻⁷ and probably are not pathognomonic of alcohol abuse. Nevertheless, they represent a unique reaction of the liver cell to injury, and their nature and origin are of considerable interest.

Electron microscopic studies of Biava,⁸ Flax and Tisdale⁹ and others^{10,11} have demonstrated the fibrillar character of alcoholic hyalin, and there have been suggestions that this material is derived from degenerating organelles.^{8,9} Others^{10,12} have considered this possibility unlikely. The present study provides further information on the fine structure of alcoholic hyalin and focuses on the fine cytoplasmic filaments which were observed along with these inclusions, which in some way seem to be related.

From the Departments of Pathology, Northwestern University Medical School, Veterans Administration Research Hospital and Chicago Wesley Memorial Hospital, Chicago, Ill.

Accepted for publication Nov 16, 1971.

Address reprint requests to Dr. Geoffrey Kent, Department of Pathology, Chicago Wesley Memorial Hospital, 250 E Superior St, Chicago, Ill 60611.

Material and Methods

Twenty-two liver biopsies and one autopsy specimen from 23 patients were studied. All of the patients had liver disease and a history of chronic alcoholism. On light microscopic examination, all showed alcoholic hyalin and varying degrees of fatty metamorphosis, fibrosis or cirrhosis. In 3 patients, alcoholic liver disease was complicated by malignant hepatoma and in 1 by adenoma or hepatocytic hamartoma (autopsy specimen).

For electron microscopy, three minute portions of liver tissue were fixed in Millonig's fixative¹³ for 1 to 2 hours, dehydrated and embedded in Epon.^{14,15} In some cases, an additional portion of liver tissue was fixed in 2.5% glutaraldehyde buffered to pH 7.4 with 0.1 M sodium cacodylate, postosmicated, dehydrated and embedded in Epon. The remaining liver tissue was fixed in formalin for paraffin embedding. The paraffin-embedded tissues were sectioned and stained with hematoxylin and eosin, periodic-acid-Schiff reagent before and after digestion with diastase, and with Masson's trichrome stain.

Thin sections were stained with uranyl acetate and lead citrate¹⁶ and examined with a Philips EM-300 electron microscope. After thin sections were prepared for electron microscopy adjacent, 1- μ -thick Epon sections were cut. These were stained with toluidine blue¹⁷ and hematoxylin and eosin, and cells containing alcoholic hyalin were correlated with those in electron micrographs.

Results

Light microscopy of paraffin-embedded material revealed alcoholic hyalin as an irregularly outlined cytoplasmic inclusion, typically located around the nucleus. The nucleus stained brightly eosinophilic with hematoxylin and eosin and bluish gray with Masson's trichrome stain; occasionally the trichrome stain revealed a central red core and a peripheral blue zone. This reaction was seen more often in biopsies taken several weeks after admission and may reflect an altered form of alcoholic hyalin, the fine structural features of which will be described.

Cells containing alcoholic hyalin often had large and hyperchromatic nuclei with prominent nucleoli; double nuclei were common. The large majority of cells containing alcoholic hyalin were swollen and pale, and averaged approximately 30 μ in diameter. They corresponded to cells often described as *hydropic*.^{18,19} In patients without cirrhosis, alcoholic hyalin was found chiefly in centrolobular areas, particularly around central veins. In more advanced liver disease, alcoholic hyalin was seen mostly about septums. Glycogen was depleted in most patients; however, in approximately 10%, glycogen was abundant and also conspicuous within hydropic cells containing alcoholic hyalin.

Fine Structural Counterpart of Alcoholic Hyalin

Examination of the same cells in adjacent sections by light and electron microscopy revealed that alcoholic hyalin corresponded to non-membrane-enclosed arrays of fibrillar material (Figure 1). This tech-

nic failed to reveal any correlation between alcoholic hyalin and giant mitochondria; in 1- μ sections stained with hematoxylin and eosin, the latter were readily recognized as sharply defined, pink-staining bodies.

Morphologic Variants of Alcoholic Hyalin

Three morphologic variants of alcoholic hyalin were discerned (Table 1). The first of these (Type 1) occurred with moderate frequency and consisted of bundles of fibrils aligned in parallel arrays and which often displayed concentric whorled formations (Figures 2 and 3). Individual fibrils sometimes exhibited bead-like densities (Figure 2), but showed no definite periodicity. The fibrils measured 90 to 210 Å in diameter and their mean diameter was 141 Å (Table 1). In all instances, the sizes of fibrils, as compiled in Table 1, were measured in at least 15 different bodies by two observers working independently.

The second variant (Type 2) was the most common as well as the most characteristic form of alcoholic hyalin and often made up the entire bulk of the material. It consisted of a network of nonmembrane-bounded, closely packed, randomly oriented fibrils measuring 115 to 200 Å in width. Their mean diameter was 152 Å (Figure 4). The fibrils were more electron-dense than those in parallel arrangement (Type 1). The two variants of alcoholic hyalin often were found in the same body. Their borders usually were well demarcated, but occasionally were indistinct. Sometimes small irregular islands of randomly oriented (Type 2) fibrils appeared within bundles of Type 1 filaments (Figure 3), suggesting that these filaments may lose their orientation and become Type 2 filaments.

The third variant (Type 3) was characterized by a further increase in electron density and partial (Figure 5), or almost complete, loss of fibrillar structure (Figures 6, 7). It was observed most often in speci-

Table 1—Morphologic Characteristics of Alcoholic Hyalin and Associated Filaments

Types of structure	Arrangement of fibrils	Electron density	Size of fibrils (Å)	
			Mean \pm 1 SD	Range
Alcoholic hyalin				
Type 1	Parallel orientation, whorled formation	++	141 \pm 42	90-210
Type 2	Random orientation	+++	152 \pm 33	115-200
Type 3	Loss of fibrillar structure	++++	—	—
Fine filaments	Parallel orientation, rarely random	+	74 \pm 21	40-100

mens obtained several weeks after the patient's admission and is considered to be an altered form of alcoholic hyalin. The material was granular or homogeneous; however, careful examination revealed filamentous structures around the edges or within the mass itself. These filaments were often broad in the center and had tapered ends. Type 3 forms were also closely associated with Type 1 filaments (Figure 5), but in other instances, randomly oriented filaments lay between the bundles of Type 1 filaments and the smudgy material.

Fine Filaments Associated with Alcoholic Hyalin

Not infrequently, the alcoholic hyalin body was closely associated with bundles of fibrils in parallel arrangement of much smaller diameter (Figures 8–11). These fibrils were located about the periphery of the body and often surrounded the bulk of alcoholic hyalin material in a rim-like fashion (Figures 8 and 9). The fibrils had a mean diameter of 74 Å, ranging from 40 to 100 Å. Some bundles resembled tonofilaments normally present in small numbers in hepatocytes. The fibrils were most often arranged in parallel, but in some instances they ran in different directions (Figure 9). Occasionally the fine filaments seemed to merge with the larger, randomly oriented fibrils of the alcoholic hyalin body (Figure 8).

Bundles of fine filaments similar in size and arrangement to those in the periphery of the bodies were sometimes conspicuous in liver cells and ductular cells which did not seem to contain alcoholic hyalin (Figures 12–14).

Types of Cells Containing Alcoholic Hyalin

Bodies with the ultrastructural characteristics of alcoholic hyalin were observed not only in hepatocytes but also in bile ductular cells (Figures 15 and 16). Alcoholic hyalin was also found within cells of an adenoma (Figure 17) and of malignant hepatomas (Figure 18).

Fine Structural Counterparts of Hydropic Cells

When comparing adjacent sections by light and electron microscopy, it became apparent that the enlargement and the pallor of cells which contained alcoholic hyalin was caused predominantly by an accumulation of fat droplets and dilatation of the endoplasmic reticulum (Figures 1, 19 and 20). The contributions of these changes, however, varied considerably in different cells. Another factor contributing to the pale-staining properties of the alcoholic hyalin-containing cells was the occasional abundance of glycogen, as stated earlier.

Transitions between endoplasmic reticulum and fibrils of alcoholic

hyalin were not observed. A frequent finding, however, was the presence of a flocculent, electron-dense material within cisternae of the endoplasmic reticulum.

Discussion

The present study of patients with alcoholic liver disease provides further information on the fine structure of alcoholic hyalin and calls attention to its frequent association with bundles of filaments of significantly smaller diameter. There has been some doubt regarding the identity of alcoholic hyalin and, although most investigators have held it to be a fibrillar deposit,⁸⁻¹⁰ the possibility has been considered that the material represented enlarged mitochondria.^{20,21} Comparisons of the same cells by light and electron microscopy in adjacent sections leave little doubt that alcoholic hyalin is a fibrillar deposit without a limiting membrane and is readily distinguished from giant mitochondria. The same conclusion was reached by Iseri and Gottlieb¹¹ in their study. Material with the ultrastructural characteristics of alcoholic hyalin was observed in hepatocytes, ductular cells and benign and malignant hepatomas, indicating that the elaboration of alcoholic hyalin does not depend upon processes peculiar to hepatocytes.

The enlargement and pallor so prominent in histologic material in many of the cells containing alcoholic hyalin was chiefly caused by an accumulation of fat droplets and dilatation of the endoplasmic reticulum. Rarely, an excess of glycogen contributed to the pale appearance. In light of these changes, the term *hydropic*, which is frequently used to describe such cells,^{18,19} does not seem appropriate.

Alcoholic hyalin occurred in three morphologically distinct forms. These forms displayed increasing degrees of electron density and consisted of: a) bundles of fibrils in parallel arrays, b) a meshwork of randomly oriented fibrils and c) a granular or amorphous substance containing only scattered remains of fibrils. The latter was interpreted as a more advanced or altered form of alcoholic hyalin. Type 1 and 2 fibrils differed chiefly in fibril orientation and density and were approximately the same width. Our measurements for Type 2 fibrils agree with those reported by Smuckler,¹⁰ but they differ significantly from the much smaller dimensions given by Biava.⁸ Because of the relatively large size of the fibrils, their derivation from membranes of the endoplasmic reticulum is questionable. The intertwining of the three morphologic variants of alcoholic hyalin and the transition forms occasionally observed suggest that they are closely related and that fibrils may undergo changes in orientation from parallel to random and/or lose their fibril-

lar character. No evidence was found, in this study, that products of cellular degeneration were the source of the fibrillar deposit. The close association of parallel and reticular arrays, the range and average size of fibril diameters, and the absence of limiting membranes are further evidence against this notion and suggest instead that the material is synthesized *de novo*.

The most significant structures immediately peripheral to the alcoholic hyalin body appeared to be bundles of filaments in parallel arrangement of much smaller size. These filaments were often conspicuous along the entire circumference of the alcoholic hyalin body. Occasionally, they ran in different directions or merged with filaments in the alcoholic hyalin body. Similar filaments were found, in excess, in hepatocytes and ductular cells not containing alcoholic hyalin. Fine cytoplasmic filaments, free or in bundles, considered to have a cytoskeletal function were observed in a variety of cells.²² Such filaments are found in small numbers in hepatocytes and ductular cells around nuclei^{23,24} and have been reported in increased numbers in cholestasis.²³ Prominent filamentous structures, in straight bundles or in whorls, with a similar range of diameter have also been described in Yoshida ascites hepatoma²⁵ and in liver cells propagated *in vitro*.²⁶ The filaments were assumed to have contractile and stabilizing properties and their synthesis was thought to be triggered by changes in cellular environment.²⁶

The association of thick filaments within the alcoholic hyalin body with a population of fine filaments is of considerable interest. A wide range in the thickness of filaments presumed to play a role in contractile activities has been observed in muscle and other cell types, including renal parenchymal and interstitial cells.²⁷⁻³⁰ Analysis of reported measurements indicates that the filaments fall into two main groups, those well above 90 Å and those generally ranging from 40 to 80 Å;²⁸ however, whether or not they represent a single population of filaments or two chemically distinct classes in most instances is debatable. Two types of filaments, 50 to 70 Å and 160 Å, were found in *Amoeba proteus*.²⁷ These filaments were considered to be chemically distinct and both seemed to be required to produce movement.²⁷ The 160 Å filaments were arranged in parallel arrays or in randomly oriented clusters and resembled the fibrillar deposit in alcoholic hyalin bodies. In motile extracts, furthermore, thin filaments radiated from clusters of thick filaments, suggesting that the two types of filaments interacted to produce the movement observed. Whether or not the large filaments were myosin was not established.

In light of present knowledge, alcoholic hyalin would seem to fit into the category of cytoplasmic filaments and, in this respect, could be the thick component of a two-filament system or part of a single population of filaments with widely varying diameters. The chemical nature of the material, its functional significance and mechanism of formation still need to be established.

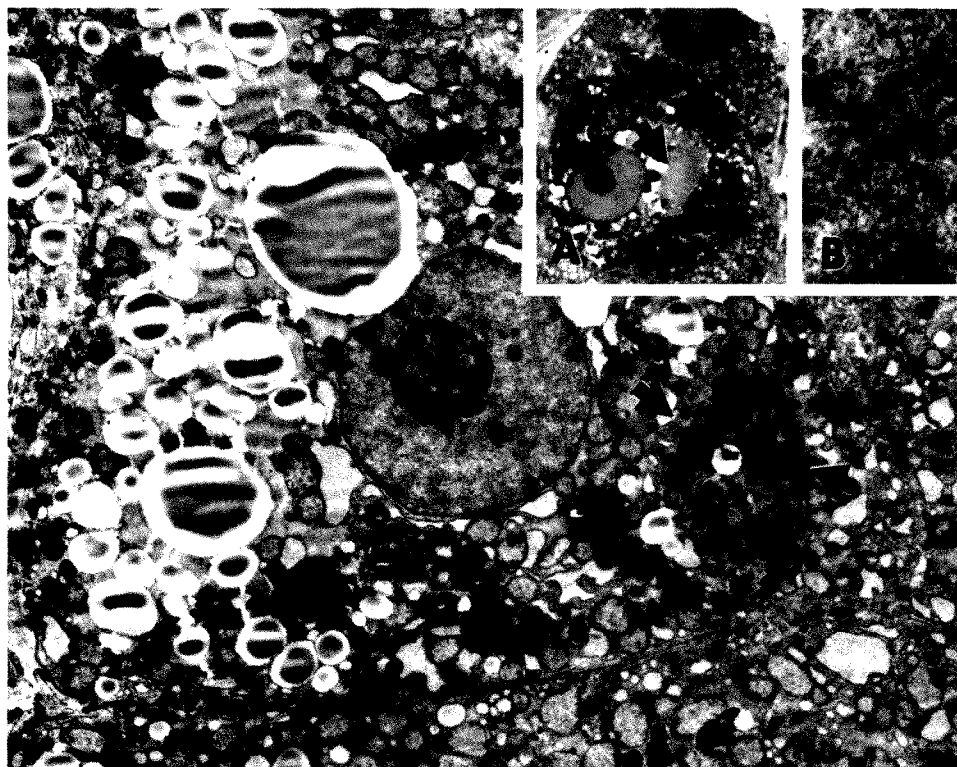
References

1. Mallory FB: Cirrhosis of the liver. Five different types of lesions from which it may arise. *Bull Johns Hopkins Hosp* 22:69-75, 1911
2. Smetana HF, Hadley GG, Sirat SM: Infantile cirrhosis: an analytical review of the literature and a report of 50 cases. *Pediatrics* 28:107-127, 1961
3. Nayak NC, Sagreiya K, Ramalingaswami V: Indian childhood cirrhosis: the nature and significance of cytoplasmic hyaline of hepatocytes. *Arch Pathol* 88:631-637, 1969
4. Edmondson HA: Tumors of the liver and intrahepatic bile ducts. Armed Forces Institute of Pathology, Section 7, Part 25, 1958, p 49
5. Norkin SA, Campagna-Pinto D: Cytoplasmic hyaline inclusions in hepatoma. *Arch Pathol* 86:25-32, 1968
6. Popper H: Comments, Wilson's disease, Birth Defects, Original Article Series. Vol 4, No 2. Edited by D Bergsma. New York, The National Foundation, 1968, p 103
7. Scheuer PJ: Liver Biopsy Interpretation. Baltimore, The Williams and Wilkins Co, 1968, p 39
8. Biava C: Mallory alcoholic hyalin: A heretofore unique lesion of hepatocellular ergastoplasm. *Lab Invest* 13:301-320, 1964
9. Flax MH, Tisdale WA: An electron microscopic study of alcoholic hyalin. *Am J Pathol* 44:441-454, 1964
10. Smuckler EA: The ultrastructure of human alcoholic hyalin. *Am J Clin Pathol* 49:790-797, 1968
11. Iseri OA, Gottlieb LS: Alcoholic hyalin and megamitochondria as separate and distinct entities in liver disease associated with alcoholism. *Gastroenterology* 60:1027-1035, 1971
12. Schaffner F, Popper H: Electron microscopy of liver, Diseases of the Liver. Edited by L Schiff. Philadelphia, JB Lippincott Co, p 66
13. Millonig G: Advantages of a phosphate buffer for OsO_4 solutions in fixation. *J Appl Physics* 3:1637, 1961 (abstr)
14. Luft JH: Improvements in epoxy resin embedding methods. *J Biophys Biochem Cytol* 9:409-414, 1961
15. Minick OT: Low temperature storage of epoxy embedding resins. *Stain Technol* 38:131-133, 1963
16. Reynolds ES: The use of lead citrate at high pH as an electron opaque stain in electron microscopy. *J Cell Biol* 17:208-212, 1963
17. Trump BF, Smuckler EA, Benditt EP: A method for staining epoxy sections for light microscopy. *J Ultrastruct Res* 5:343-348, 1961
18. Edmondson HA, Peters RL, Reynolds TB, Kuzma OT: Sclerosing hyaline

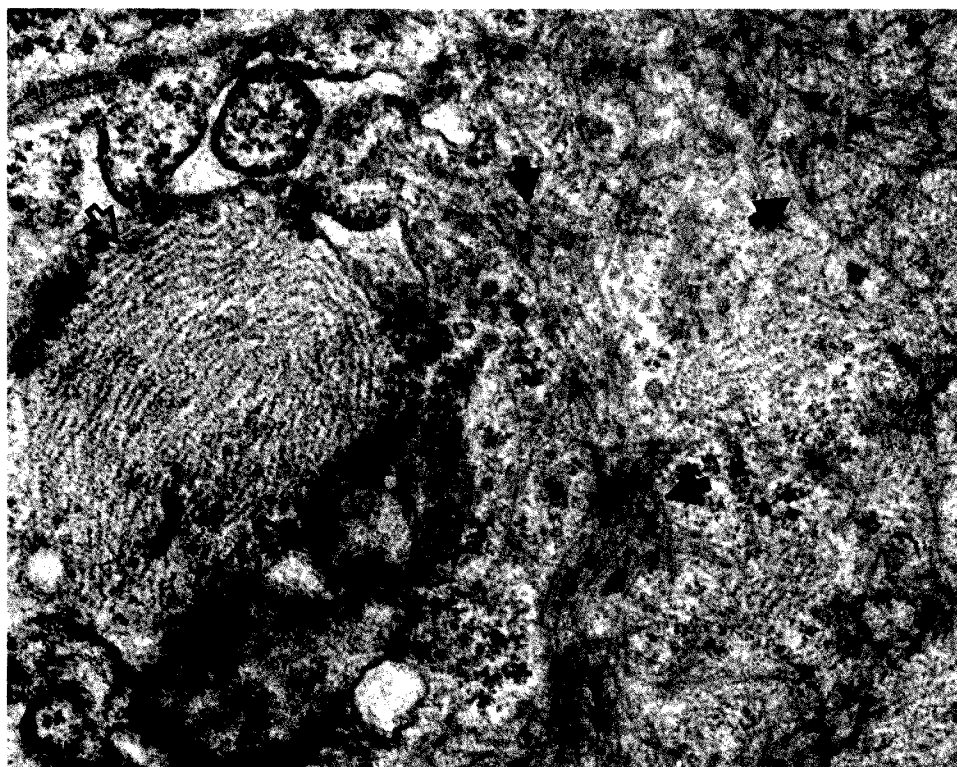
- necrosis of the liver in the chronic alcoholic. *Ann Intern Med* 59:646-673, 1963
19. Thaler H: Leberbiopsie. Berlin, Springer-Verlag, 1969, p 178
 20. Porta EA, Bergman BJ, Stein AA: Acute alcoholic hepatitis. *Am J Pathol* 46:657-688, 1965
 21. Steiner JW, Jezequel AM, Phillips MK, Arakawa JK: Some aspects of the ultrastructural pathology of the liver, *Progress in Liver Disease*. Edited by H Popper, F Schaffner. New York, Grune and Stratton, Inc, 1965, p 303.
 22. Ishikawa H, Bishoff R, Holtzer R: Formation of arrowhead complexes with heavy meromyosin in a variety of cell types. *J Cell Biol* 43:312-323, 1969
 23. Biava CG: Studies on cholestasis—A re-evaluation of the fine structure of normal human bile canaliculi. *Lab Invest* 13:840-864, 1964
 24. Sternlieb I: Perinuclear filaments and microtubules in human hepatocytes and biliary epithelial cells. *J Microscopie* 4:551-558, 1965
 25. Bairati A: Submicroscopic structure of Yoshida ascites hepatoma. *Cancer Res* 21:989-992, 1961
 26. Biberfeld P, Ericsson LE, Perlmann P, Raftell M: Increased occurrence of cytoplasmic filaments in *in vitro* propagated rat liver epithelial cells. *Exp Cell Res* 39:301-305, 1965
 27. Pollard TD, Susumu I: Cytoplasmic filaments of *Amoeba proteus*. I. The role of filaments in consistency changes and movement. *J Cell Biol* 46:267-289, 1970
 28. Newstead JD: Filaments in renal parenchymal and interstitial cells. *J Ultrastruct Res* 34:316-328, 1971
 29. Pease DC: Structural features of unfixed mammalian smooth and striated muscle prepared by glycol dehydration. *J Ultrastruct Res* 23:280-303, 1968
 30. Schaefer-Danneel S: Structurelle und funktionelle, Voranssetzungen fuer die Bewegung von *Ameba proteus*. *Z Zellforsch Mikrosk Anat* 78:441-450, 1967

Fig 1—Electron micrograph of an hepatocyte containing alcoholic hyalin. The inclusion, indicated by arrows, corresponds to the body observed by light microscopy in **Insert A** (arrow). The inclusion is shown in higher magnification in **Insert B** and reveals the characteristic structure of alcoholic hyalin ($\times 4000$; **Insert A**, $\times 1000$; **Insert B**, $\times 11,000$).

Fig 2—Type 1 alcoholic hyalin (clear arrows) showing bundle of fibrils in parallel arrangement and displaying whorled formation and bead-like densities in some of the fibrils. The black arrows point to randomly oriented fibrils (Type 2 alcoholic hyalin) ($\times 35,000$).



1



2

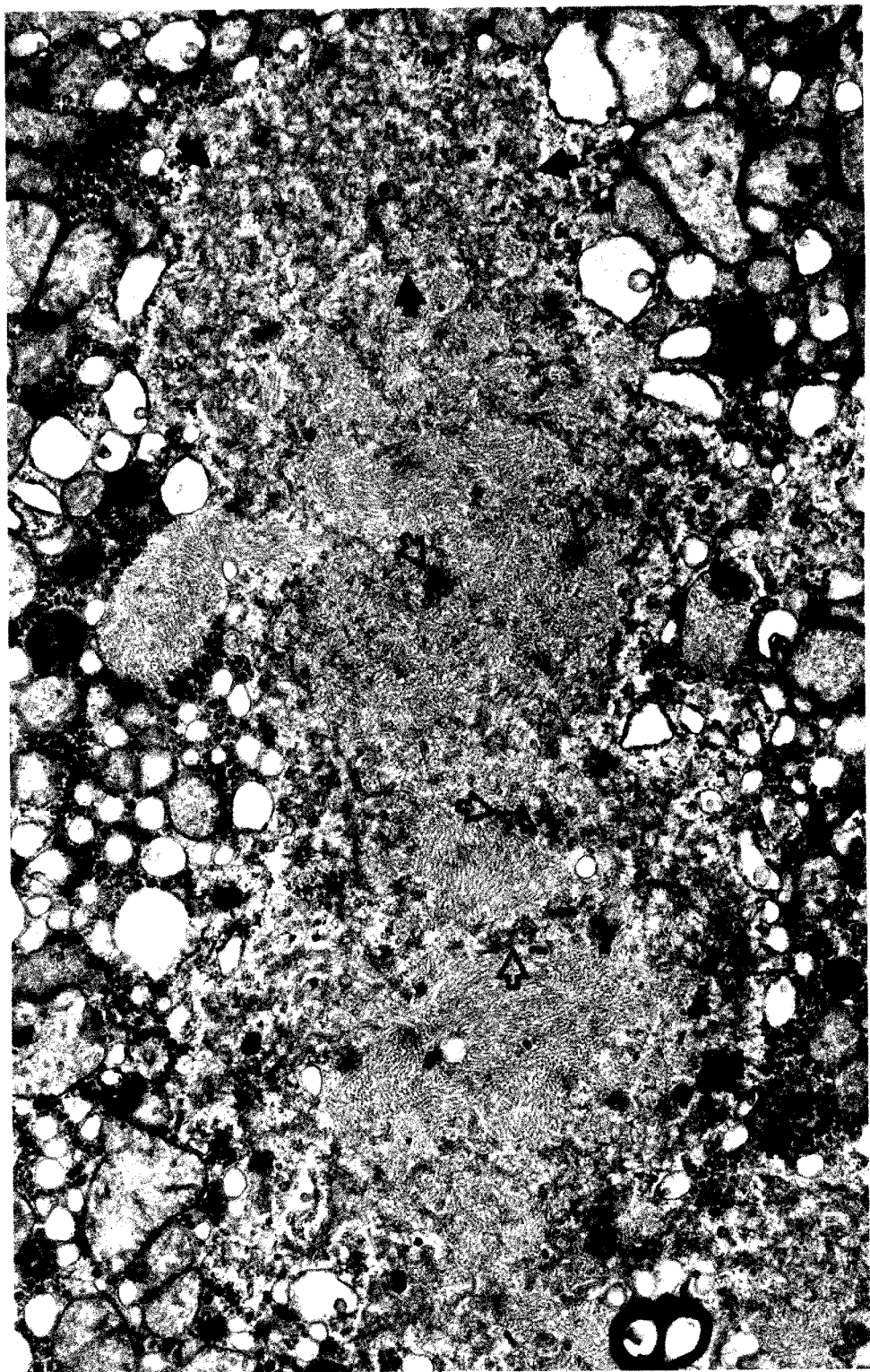
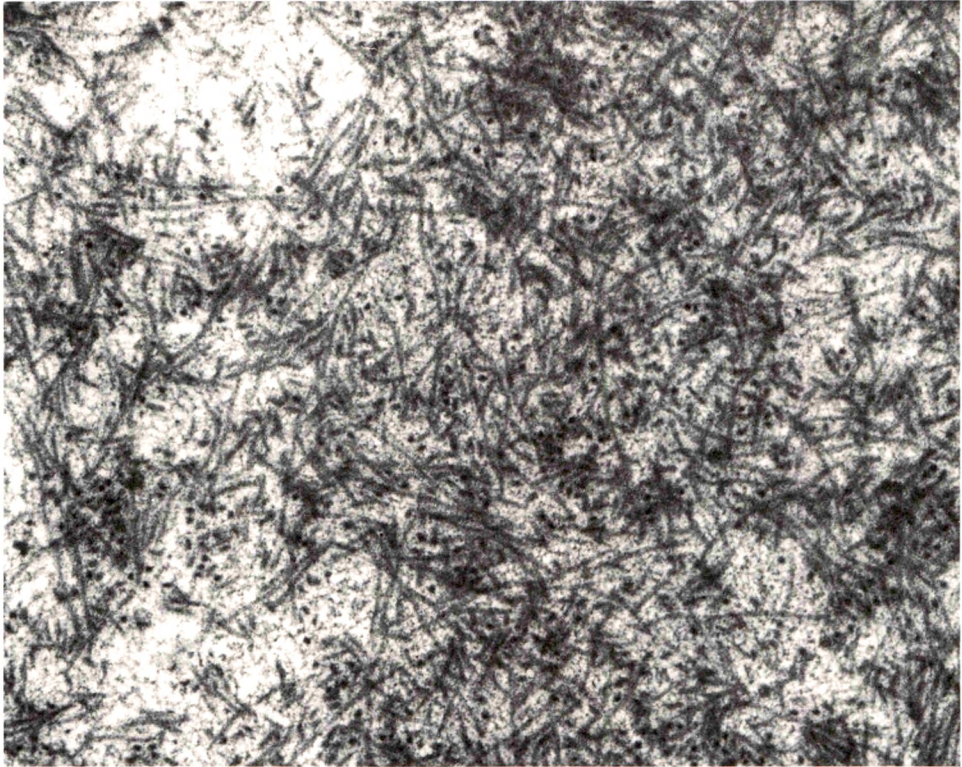
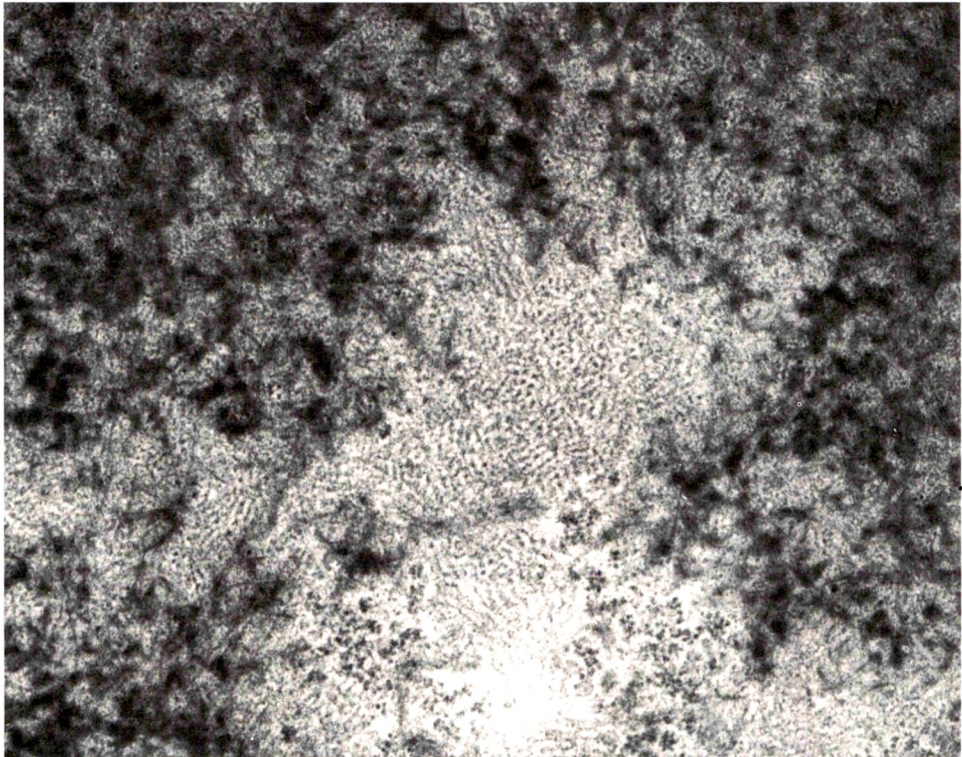


Fig 3—Alcoholic hyalin body (Type 1) composed mainly of fibrils in parrallel arrangement and containing small islands of randomly oriented fibrils (*clear arrows*). *Black arrows* indicate an adjacent small mass of randomly oriented fibrils ($\times 18,000$).



4

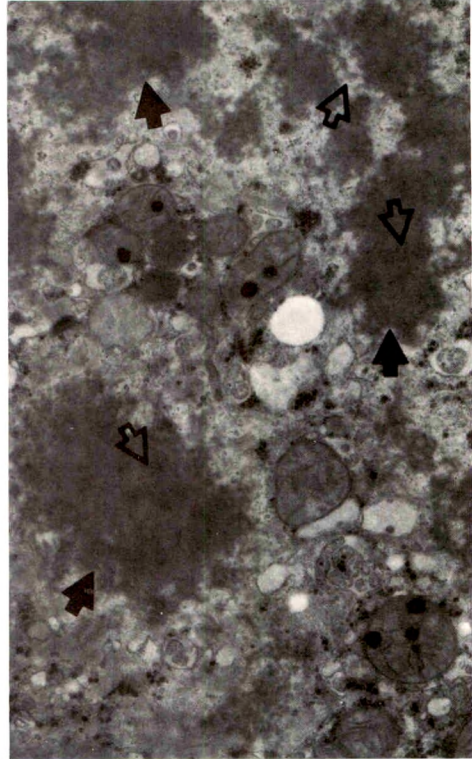


5

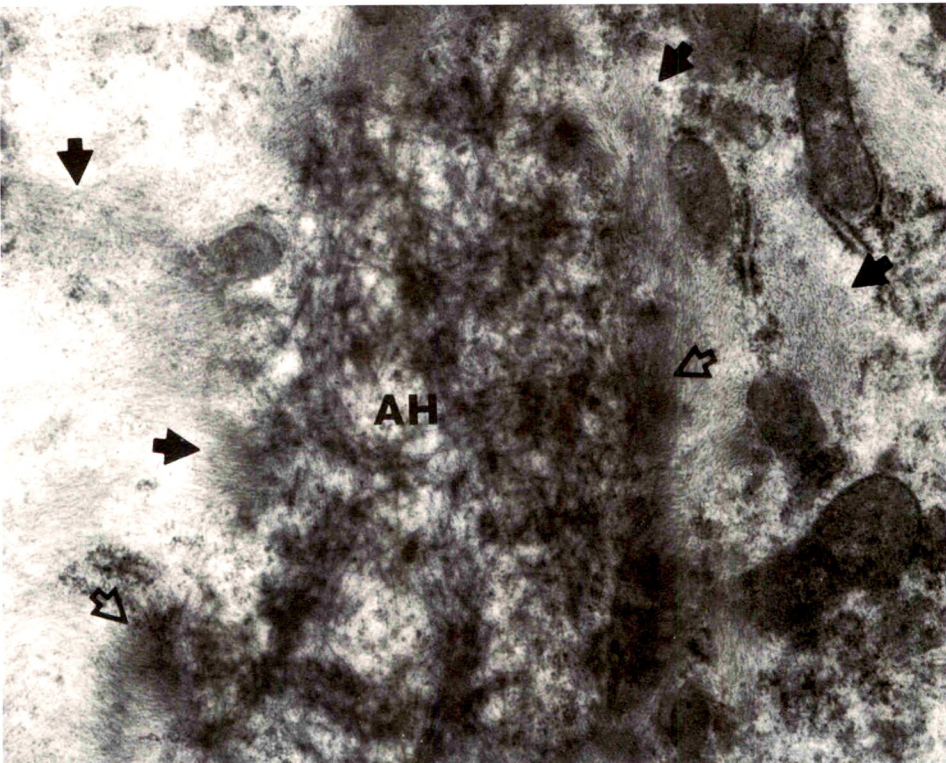
Fig 4—Type 2 alcoholic hyalin, the most common form, showing network of fibrils in random orientation ($\times 41,000$). **Fig 5**—Type 1, 2 and 3 alcoholic hyalin. Fibrils in parallel arrays (*light central area*) surrounded by fibrils in random orientation. In many of these the fibrillar pattern is no longer distinct. Note also marked increase in electron density ($\times 31,000$).



6

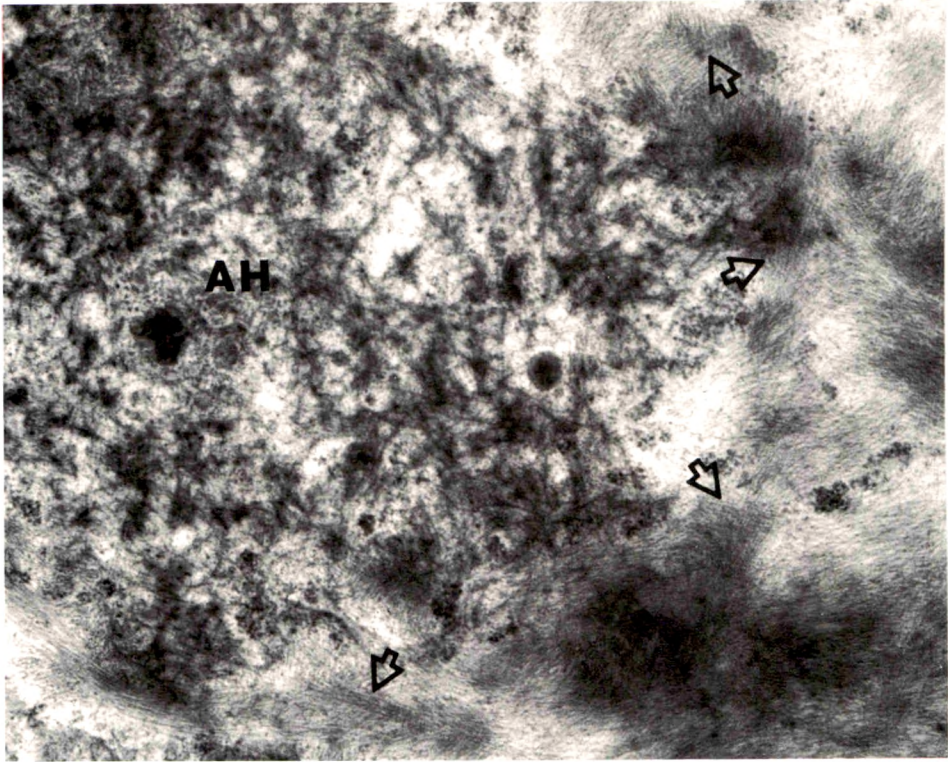


7

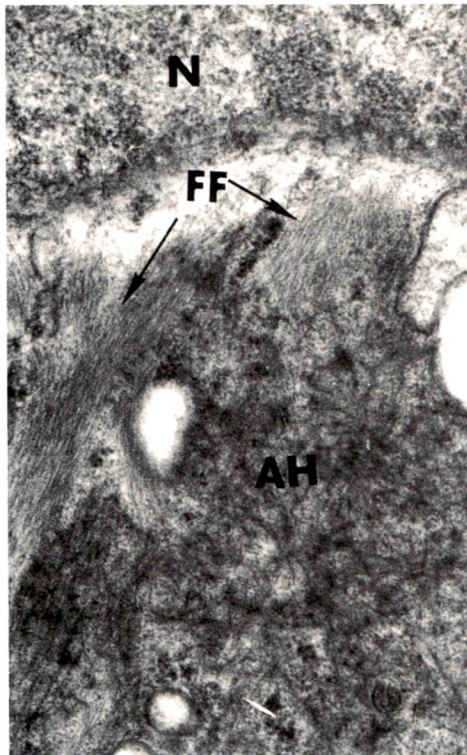


8

Fig 6—More advanced form of Type 3 alcoholic hyalin (*black arrows*). Irregularly outlined electron-dense body. Remnants of fibrils are seen in the periphery of the body and within the mass (*clear arrows*) ($\times 9000$). **Fig 7**—Type 3 alcoholic hyalin (*black arrows*) showing an almost homogeneous structure. *Clear arrows* indicate remnants of fibrils ($\times 9000$). **Fig 8**—Alcoholic hyalin body surrounded by bundles of fine filaments (*black arrows*). In some areas the fine filaments seem to merge with the larger fibrils of the body (*clear arrows*) ($\times 22,000$).



9



10



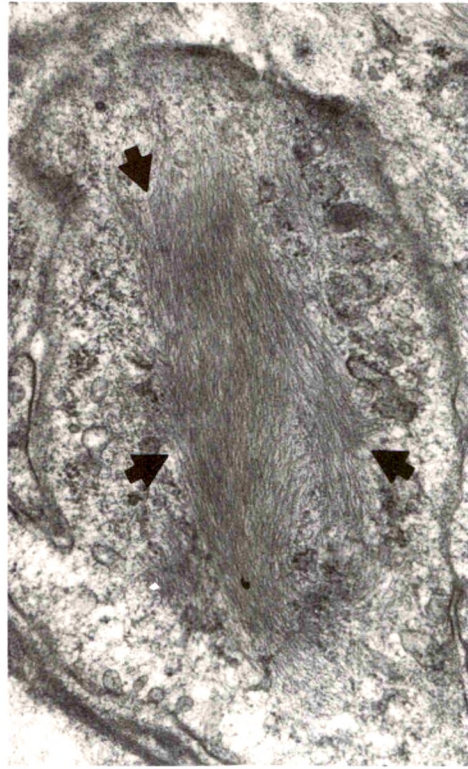
11

Fig 9—Alcoholic hyalin surrounded by masses of fine filaments. *Clear arrows* indicate bundles of fine filaments going in different directions ($\times 29,000$). **Fig 10**—Bundles of fine filaments (*FF*) in perinuclear location closely associated with Type 2 alcoholic hyalin showing larger fibrils in random orientation. *N*=nucleus ($\times 31,000$). **Fig 11**—Similar to Figure 10. Fine filaments (*FF*) are seen in proximity of Type 2 alcoholic hyalin ($\times 29,000$).

12



13



14

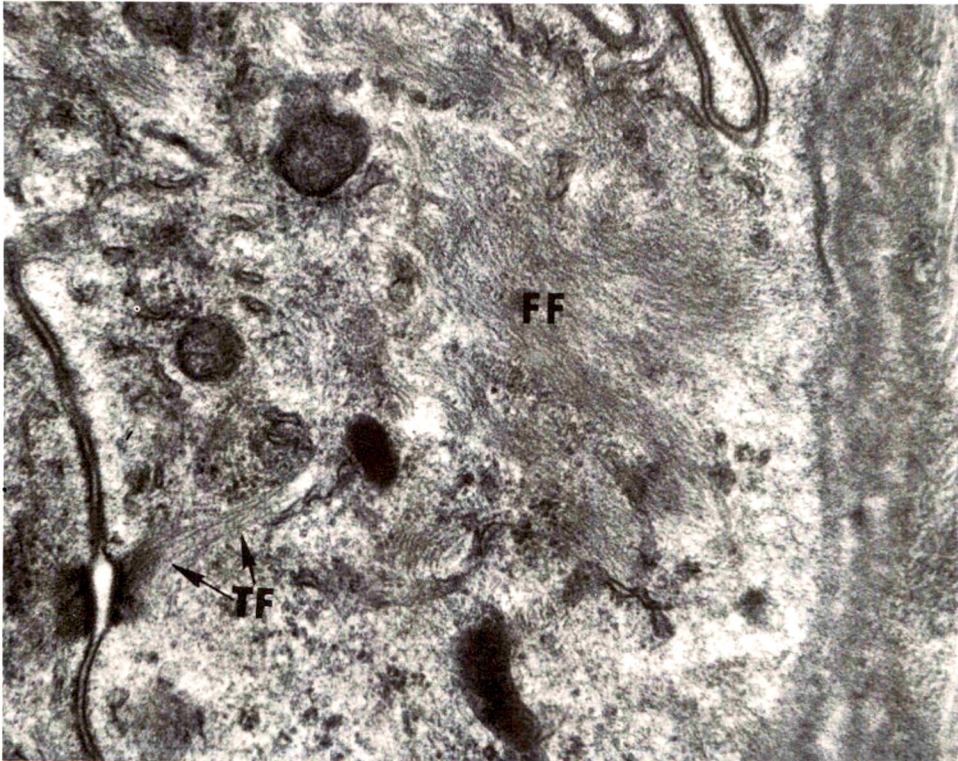
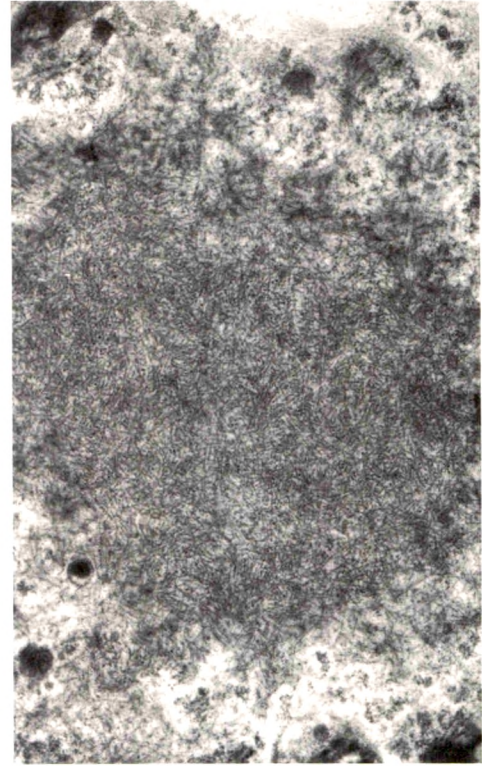


Fig 12—Fine filaments (arrows) in hepatocyte not containing alcoholic hyalin ($\times 22,000$).
 Fig 13—Fine filaments in ductular cell not containing alcoholic hyalin ($\times 27,000$). Fig
 14—Abundant fine filaments (FF) in ductular cell not containing alcoholic hyalin body.
 Note resemblance to tonofilaments (TF) attached to desmosome ($\times 35,000$).



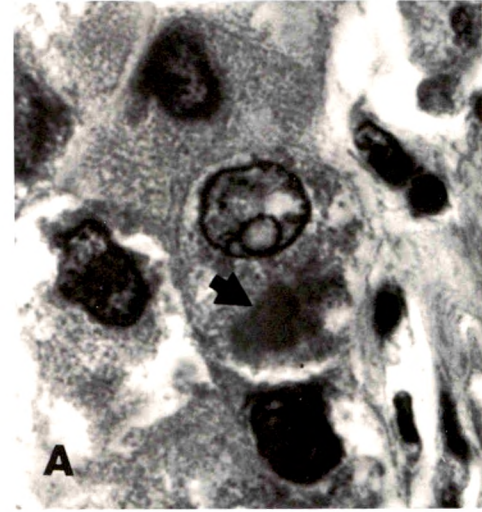
15



16



17



18

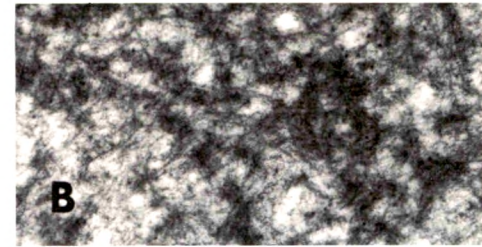
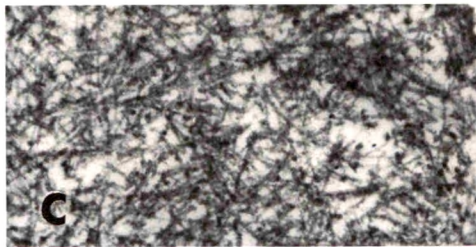
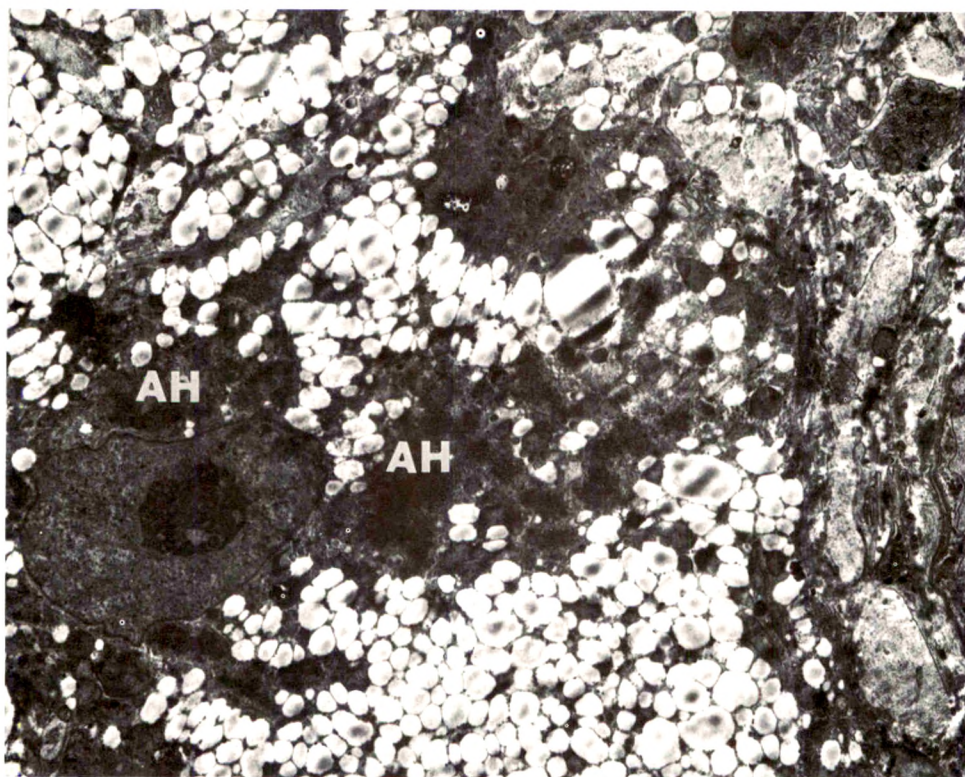


Fig 15—Alcoholic hyalin in ductular cell ($\times 2000$). **Fig 16**—Higher power of alcoholic hyalin in Figure 15 showing characteristic fibrillar structure ($\times 15,000$). **Fig 17A**—A liver which contains an adenoma (arrow). **B**—Light microscopy of alcoholic hyalin body (clear arrow). **C**—Electron micrograph of the body (**A** $\times 0.5$; **B** $\times 1100$; **C** $\times 28,000$). **Fig 18A**—Light microscopy of alcoholic hyalin in hepatoma. **B**—Electron micrograph showing Type 2 alcoholic hyalin (**A** $\times 1100$; **B** $\times 22,000$).

19



20

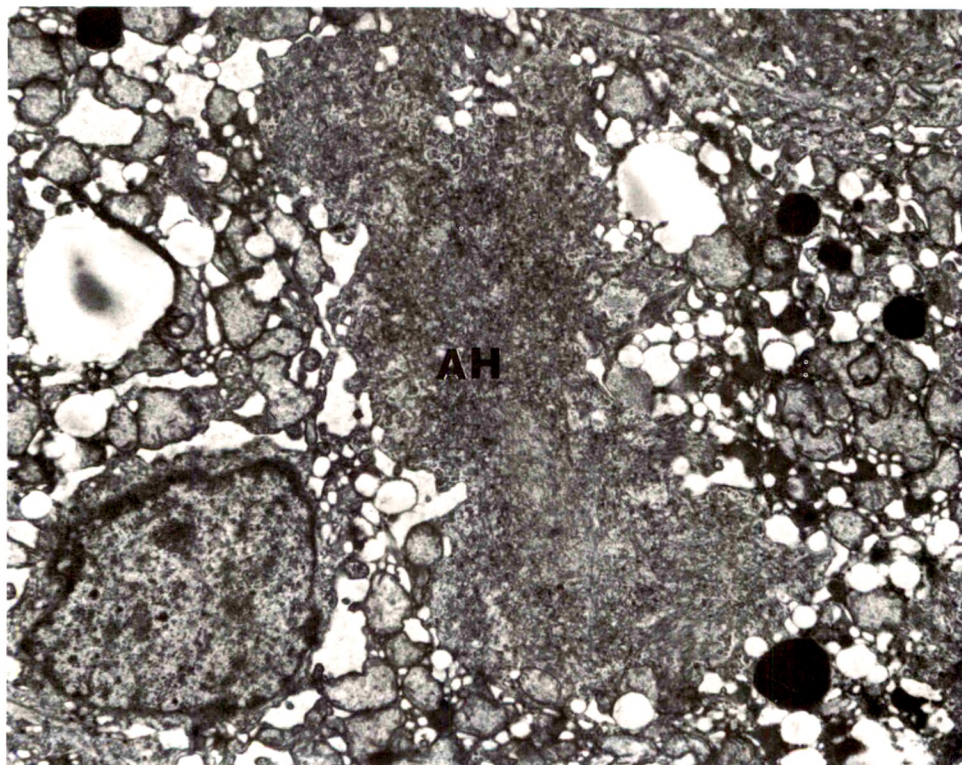


Fig 19—A hepatocyte which contains alcoholic hyalin. Note large number of fat droplets ($\times 4000$). Fig 20—A hepatocyte which contains alcoholic hyalin. Note dilatation of endoplasmic reticulum ($\times 7000$).

Exocytosis of Secretory Organelles from Blood Platelets Incubated with Cationic Polypeptides

James G. White, MD

The blood platelet release reaction involves the secretion, in parallel, of specific chemical constituents stored in intracellular organelles to the plasma without loss of substances suggestive of cell damage. The present investigation has employed an unusual effect of cationic polypeptides to follow the platelet secretory process. When platelets were incubated with polybrene and polylysine, the agents were taken up and deposited in cytoplasmic organelles. The matrix of granules developed a lattice-like substructure not produced by other chemical agents, and dark zones of granules and dense bodies became more electron opaque. Subsequently, the platelets exposed to cationic polypeptides underwent the shape change and internal transformation similar to that produced by potent aggregating agents. Granules and dense bodies appeared in the open canalicular system and were extruded in a relatively intact state from the altered platelets. No differences were observed in the response of normal, afibrinogenemic or thrombasthenic platelets to incubation with polybrene and polylysine. The results indicate that cationic polypeptides can stimulate the extrusion of secretory organelles, and support the previous reports suggesting that channels of the open canalicular system serve as conduits for discharging the products of the release reaction (*Am J Pathol* 69:41-54, 1972).

IN THE COURSE of maximal response to aggregating agents, blood platelets extrude several specific chemical constituents without losing components which might suggest cell damage or destruction.¹⁻³ The physiologic process of secretion, or release as Grette termed it,¹ involves the transfer of chemical products confined to granules and dense bodies inside the platelet to the surrounding plasma. Attempts to define the sequence of extrusion have indicated that randomly dispersed organelles are drawn together prior to and during release, and ultimately fuse into granular masses after secretion has occurred.^{4,5} During this process some granules and dense bodies, or their contents, appear to be extruded into a serpentine system of channels which is continuous with the platelet surface.^{6,7} The actual transfer of secretory products into the open canalicular system, however, has rarely been

From the Department of Pediatrics, University of Minnesota Medical Center, Minneapolis, Minn.

Supported by Grants HE-11880, AI-05153, CA-08832 from the US Public Health Service and the Cardiovascular Clinical Research Program Project.

Accepted for publication Feb 21, 1972.

Address reprint requests to Dr. James G. White, Department of Pediatrics, University of Minnesota School of Medicine, Box 284 Mayo Memorial Bldg, Minneapolis, Minn 55455.

observed because the substances secreted apparently dissolve on contact with plasma in the channels.

The present investigation has utilized a peculiar effect of cationic polypeptides to shed further light on this problem. Normal and abnormal platelets incubated with polylysine and polybrene adsorbed the agents and transferred them to intracellular organelles. Uptake of the cationic polypeptides caused loss of granules and dense bodies. Polylysine and polybrene apparently stabilize the organelles so that they are expelled in a relatively intact form from the altered platelets through the open canalicular system.

Materials and Methods

The technics used for obtaining blood in 3.8% trisodium citrate anticoagulant, separating platelet-rich plasma (C-PRP) by centrifugation at $200 \times g$ for 20 minutes at room temperature, examining the effects of chemical agents on platelet function, and preparing samples for study in the electron microscope were described in previous publications.^{4,8,9} Blood was obtained from normal donors, from a patient with afibrinogenemia and three children with thrombasthenia. The clinical and laboratory studies in the patients have been described in previous reports.¹⁰⁻¹² Polybrene and polylysine were dissolved in Tris-buffered saline in various amounts so that 0.1 ml added to 0.9 ml of C-PRP would yield a specific final concentration. Platelet samples from normal donors and the patients with afibrinogenemia and thrombasthenia were combined with either polylysine or polybrene at a concentration of 0.1, 0.5 or 1.0 mg/ml of C-PRP. The small amount of buffered saline containing cationic polypeptide was layered carefully on the surface of the C-PRP, and the sample was not disturbed during a 15-, 30-, or 60-minute incubation at 37 C. Control samples of normal and patient platelets were incubated with the same volume of buffered saline for similar periods of time. On completion of the period of incubation, all samples were fixed in glutaraldehyde and osmic acid in the manner described in earlier reports.^{4,8,9} Thin sections of the plastic-embedded platelets were usually stained with uranyl acetate and lead citrate to enhance contrast. Observations were made in a Philips 200 electron microscope.

The method used to localize endogenous peroxidase activity in platelets¹³ is similar to the variation of the Graham-Karnovsky¹⁴ procedure utilized by Novikoff and Goldfischer¹⁵ to demonstrate catalase in various cells and tissues. Platelets fixed in a mixture of glutaraldehyde and paraformaldehyde were washed and incubated in a solution containing hydrogen peroxide, diaminobenzidine, and dimethylsulfoxide at 37 C for 60 minutes at pH 6. The incubated samples were washed in buffer, refixed in osmic acid and prepared for study in the electron microscope.

Results

General effects

The addition of polylysine or polybrene to samples of citrate platelet-rich plasma (C-PRP) at final concentrations of 0.1, 0.5 and 1.0 mg/ml for 15, 30 or 60 minutes did not result in gross aggregation or precipi-

tation of the sample. The alterations observed in the platelets were dependent on the concentration of cationic polypeptides and the duration of exposure. Both agents produced essentially identical effects. A concentration of 0.1 mg/ml of C-PRP did not induce morphologic changes until incubation for 60 minutes. An amount of 1 mg/ml of C-PRP produced alterations at 15 minutes, and many platelets were damaged or destroyed by 60 minutes. Thus, the low concentrations and brief incubation caused changes compatible with those stimulated by physiologic aggregating agents triggering platelet release,⁵ while the larger amounts and longer exposure to cationic polypeptides caused destructive effects in many platelets similar to those observed in cells exposed to hypotonic stress, cocaine, detergents or antihistamines.^{16,17}

Specific effects

Initial morphologic changes produced in platelets after incubation with polylysine or polybrene were evident in the granules (Figure 1A-D). Cells retained the discoid shape and internal organization characteristic of unaltered platelets, but some of the granules were swollen and developed an unusual lattice-like appearance in their matrix (Figure 1A-C). As more platelets and platelet granules became involved in the interaction with cationic polypeptides, the cells lost their discoid form and became irregular with multiple pseudopods (Figures 1D, 2A). More of the granules were affected in these cells and manifested the unusual changes in matrix substructure. Dense zones of the membrane bound organelles appeared more electron opaque as did the serotonin-rich dense bodies derived from granules (Figure 1C, D). Channels of the open canalicular system were frequently dilated in the irregular cells and often contained dense and light particles identical in consistency to granules and dense bodies (Figures 1D, 2C, D).

Many of the platelets in samples exposed to 0.1 mg of cationic polypeptide for 60 minutes, to 0.5 mg for 30 or 60 minutes and to 1 mg for 15 to 30 minutes manifested alterations similar to those induced by potent aggregating agents (Figure 2A). The platelets were irregular in form and most of the organelles were concentrated in the cell centers. In many cells the granules and contractile gel were fused in a central mass (Figures 2F, 3A-F).

The alterations described above were accompanied by a phenomenon of particular interest. Particles of dense bodies and granules appearing in the open canalicular system during the physical changes induced by cationic polypeptides remained intact (Figures 1D, 2B-F). As the platelet alterations progressed, the granule and dense body

fragments were observed in various stages of extrusion from channels of the canalicular system (Figures 2B-F, 3A-F). The fragments of intraplatelet organelles were frequently accompanied by matrix elements revealing the peculiar lattice structure caused by uptake of cationic polypeptides.

Cationic polypeptides are known to cause the gelling of fibrinogen;¹⁸ it was important to determine if the absence of fibrinogen would affect the results of this study in normal cells. Incubation of platelets from a patient with congenital afibrinogenemia with polylysine and polybrene under the same conditions as normal cells produced identical results (Figures 1C, 3A).

Polybrene and polylysine fail to stimulate immediate irreversible aggregation of thrombasthenic platelets.^{19,20} Therefore, platelets from 3 patients with thrombasthenia were incubated with cationic polypeptides at the same concentrations and durations of exposure as normal cells. The changes in form, internal transformation and extrusion of organelles were indistinguishable from alterations in normal control platelets (Figures 1A, 2C, F, 3B).

The possibility that all of the findings were due to cell damage was also considered. Cationic polypeptides have been shown to stimulate the physiologic platelet release reaction by one group, and to cause leakage of chemical constituents suggestive of cell damage by another. In the present study, platelets were examined for peroxidase activity after exposure to polylysine at a final concentration of 1 mg/ml of C-PRP for 30 minutes. Endogenous peroxidase was easily defined in the platelets after exposure to polylysine (Figure 1E). The electron-dense reaction product of peroxidase activity was confined specifically to channels of the dense tubular system as it is in normal platelets.

Discussion

Several years ago Lalezari and Spaet recognized the capacity of cationic polyelectrolytes to agglutinate blood platelets,²¹ and subsequently several groups of workers have studied the effects of positively charged polymers on platelet aggregation.²²⁻²⁴ However, the influence of cationic polypeptides on platelet structure after incubation with the agents for various intervals of time has apparently not been evaluated previously. Our interest was stimulated by the observation that the cationic polypeptides, polylysine and polybrene, failed to cause immediate irreversible aggregation in stirred samples of platelets from patients with thrombasthenia, but did produce the shape change and internal transformation induced in the abnormal cells by collagen and

other potent aggregating agents.²⁰ This finding indicated that cationic polypeptides must have an influence on platelets beyond their capacity to initiate immediate aggregation.

The results of the present investigation support this hypothesis. Polylysine and polybrene produced physical changes in normal and abnormal platelets in a time and concentration dependent manner. Larger amounts and long incubation produced damaged platelets, while low concentrations and relatively short incubations caused changes similar to those induced in the cells by potent aggregating agents. Polylysine and polybrene were taken up by platelets and deposited in the granules and dense bodies. Granules became swollen, and their matrices developed a lattice-like substructure not present in the organelles of normal platelets,²⁵ or cells exposed to other drugs. Dense bodies and dark zones in granules developed a more electron-opaque appearance following incubation with polybrene and polylysine.

The interaction of the cationic polypeptides with platelet organelles had a striking effect on their stability, particularly during secretion. Fragments of granules and dense bodies were observed in channels of the open canalicular system and in the process of extrusion from platelets incubated with polylysine and polybrene. The expelled organelles were not enclosed by membranes but were frequently accompanied out of the cell by the lattice-like matrix material observed in intact granules. Intact dense bodies and masses of granular substance were evident at the periphery of the cells or detached from the platelets in the surrounding plasma. Substances from dense bodies and granules have occasionally been identified in open channels during the phase of platelet release in previous investigations,⁷ but this is the first time that significant numbers of secretory organelles have been identified in the process of extrusion in a relatively intact form without their enclosing membranes.

The possibility that cationic polypeptide interaction with fibrinogen produced the alterations in platelets required consideration, since the agents are known to produce non-thrombin-dependent conversion of fibrinogen to fibrin gel.¹⁸ When afibrinogenemic platelets were incubated with either polylysine or polybrene the cells developed the same sequence of alterations produced in normal platelets after exposure to these agents. It is doubtful, therefore, that fibrinogen is the substrate for the action of cationic polypeptides on platelets, or the substance responsible for the stability of the secretory organelles during their extrusion from the cells. Thrombasthenic platelets also responded

in a manner identical to normal and afibrinogenemic platelets during incubation with polybrene and polylysine; the significance of this finding, in view of the failure of cationic polypeptides to induce immediate aggregation in stirred samples of thrombasthenic platelets, has been discussed in a previous report.²⁰

Cationic polypeptides are known to stimulate surface membrane activities of various kinds in many different types of cells.²⁶⁻³⁰ The most frequent effect is to cause an increase in cell stickiness resulting in subsequent agglutination. Positively charged polypeptides probably adhere to negatively charged cell walls, reduce the net negative surface charge and appear to form macromolecular bridges linking cells together in aggregates. Polylysine, polybrene and other cationic polyelectrolytes also stimulate the processes of pinocytosis, channel formation and phagocytosis, and alter membrane permeability. These effects have been related to a bridging of areas of the surface membrane by macromolecular complexes formed between cationic polypeptides and components of the exterior coat on cell walls, but may also reflect a response of the cell to irritation or injury. Membrane phenomena activated by cationic polypeptides do not require energy from the cell and are not blocked by metabolic inhibitors.

The effects of polylysine and polybrene on blood platelets observed in this investigation are unusual. Cationic polypeptides do not appear to be taken up and deposited in neutrophil or eosinophil cytoplasmic organelles, and do not cause fusion or discharge of granules from these cells. However, the response of platelets is not unique. Padawer has shown that polylysine produces analogous effects in mast cells from the rat.³¹ When polylysine was incubated with mast cells at a concentration of 1 mg/ml or injected intraperitoneally, the agent was taken up and transferred to intracellular granules. Mast cell granules were stabilized by polylysine and remained intact despite subsequent partial fusion and discharge from the cell. The degranulation caused by polylysine did not appear lethal to the mast cell, for multiple stages in recovery were observed in material obtained after intraperitoneal injection of the agent.

Jenkins *et al*²⁴ have demonstrated that polylysine causes immediate irreversible aggregation, in stirred samples of blood platelets, which is independent of ADP, calcium, energy metabolism or platelet shape change. Polylysine did not trigger the parallel release of serotonin, ATP or ADP from platelet granules, but did induce the leakage of adenine nucleotides and other substances suggestive of cell injury from the platelet cytoplasm. Electron micrographs of polylysine-induced

aggregates revealed a tight mosaic of platelets with electron-dense material between adjacent cell membranes. Platelets in the aggregates retained their complement of granules and dense bodies, even though other cytoplasmic constituents appeared to be lost in some cells. Massini and Luscher³² have also studied the effects of polylysine on blood platelets. They concluded that close cell contact alone was sufficient to stimulate platelet secretion, and that products characteristic of the release reaction were made available from platelets aggregated by polylysine.

The experiments described in this report have examined the effects of cationic polypeptides on platelets during incubation in unstirred systems in order to avoid aggregation. Under these conditions platelets exposed to high concentrations of polybrene and polylysine developed changes indicative of irreversible damage, while cells exposed to smaller amounts for brief periods revealed alterations similar to those produced in platelets by aggregating agents capable of inducing the platelet release reaction.⁵ During evolution of the apparent physiologic transformation resulting in extrusion of secretory organelles, the mitochondria and the other cytoplasmic structures remained relatively unaltered, and peroxidase activity demonstrated by a cytochemical method¹³ retained its specific localization in undilated channels of the dense tubular system. These findings suggest that cationic polypeptides can stimulate the extrusion of secretory organelles from morphologically and cytochemically intact platelets, while, at the same time, it is clear that the agents can also cause irreversible cell injury under more drastic conditions. The unusual propensity of cationic polypeptides to stabilize secretory organelles during extrusion from platelets may interfere with chemical determinations for products of the release reaction made after immediate aggregation in stirred systems.²⁴ Aggregation induced by cationic polypeptides occurs so rapidly that secretory organelles may be trapped within the interstices of the tightly packed mosaic of clumped platelets. Since the organelles remain intact despite extrusion into the channel system, their products would remain with the pellet of aggregated cells and not appear in the supernate after centrifugation. Chemical analysis of secretory products under these conditions could be misleading.

In conclusion, the present investigation has shown that polypeptides stimulate physical alterations in platelets during incubation in unstirred systems which resemble closely the changes induced by aggregating agents. One striking difference is the tendency of polybrene and polylysine to deposit in cytoplasmic organelles, alter their struc-

tural appearance and stabilize the granules and dense bodies in a relatively intact state during extrusion from the transformed platelets. The findings support previous investigations^{5,7} which indicated that products secreted during the platelet release reaction leave the cell through channels of the open canalicular system.

References

1. Grette K: Studies on the mechanism of the thrombin-catalyzed hemostatic reactions in blood platelets. *Acta Physiol Scand* 56 (Suppl 195):1-93, 1962
2. Holmsen H, Day HJ, Stormorken H: The blood platelet release reaction. *Scand J Haematol* 1 (Suppl 8):1-33, 1969
3. Day HJ, Holmsen H: Concepts of the blood platelet release reaction. *Scand J Haematol* 4:3-27, 1971
4. White JG: Fine structural alterations induced in platelets by adenosine diphosphate. *Blood* 31:604-622, 1968
5. White JG: Platelet morphology. *The Circulating Platelet*. Edited by SA Johnson. New York, Academic Press, Inc, 1971, pp 45-121
6. Behnke O: Electron microscopic observations on the membrane systems of the rat blood platelet. *Anat Rec* 158:121-137, 1967
7. White JG: A search for the platelet secretory pathway using electron dense tracers. *Am J Pathol* 58:31-49, 1970
8. White JG: The transfer of thorium particles from plasma to platelets and platelet granules. *Am J Pathol* 53:567-575, 1968
9. White JG: The dense bodies of human platelets: Origin of serotonin storage particles from platelet granules. *Am J Pathol* 53:791-808, 1968
10. White JG, Yunis E, Colliander M, Krivit W: The correction of prolonged bleeding times in two brothers by platelet transfusion despite normal *in vitro* platelet tests. *Pediatrics* 33:579-587, 1964
11. White JG, Krivit W: Platelet viscous metamorphosis in a child with total afibrinogenemia. *Thromb Diath Haemorrh* 13:4, 1964
12. Owen CH, Thompson JH: Prothrombin utilization in congenital coagulation deficiency states. *Thromb Diath Haemorrh* 25:297-311, 1971
13. White JG: Interaction of membrane systems in blood platelets. *Am J Pathol* 66:295-312, 1972
14. Graham RC, Karnovsky MJ: The early stages of absorption injected horse-radish peroxidase in the proximal tubules of mouse kidney. Ultrastructural cytochemistry by a new technique. *J Histochem Cytochem* 14:291-302, 1966
15. Novikoff AB, Goldfischer S: Visualization of peroxisomes (microbodies) and mitochondria with diaminobenzidine. *J. Histochem Cytochem* 17:675-680, 1969
16. Behnke O: Microtubules in disk-shaped blood cells. *Int Rev Exp Pathol* 9:1-92, 1970
17. White JG: Ultrastructural physiology and cytochemistry of blood platelets. *The Platelet* Edited by KM Brinkhous, RW Shermer, FK Mostofi. Baltimore, The Williams and Wilkins Co, 1971, pp 83-115
18. Biezunski N, Shafrir E, de Vries A, Kotchalski E: The action of polylysine

- on the conversion of fibrinogen into fibrin by coagulase thrombin. *Biochem J* 59:55-64, 1955
19. Zucker MB, Pert JH, Hilgartner MW: Platelet, function in a patient with thrombasthenia. *Blood* 28:524-534, 1966
 20. White JG: Effects of cationic polypeptides on thrombasthenic and afibrinogenemic blood platelets. *Am J Pathol* 68:447-460, 1972
 21. Lalezari P, Spaet TH: Antiheparin and hemagglutinating activities of polybrene. *J Lab Clin Med* 57:868-873, 1961
 22. Schneider W, Kubler W, Gross R: Induction of blood platelet aggregation by cationic polypeptides. *Thromb Diath Haemorrh* 19:307, 1968
 23. Grottum KA: Platelet surface and aggregation: Effects of polyelectrolytes. *Thromb Diath Haemorrh* 21:450-462, 1969
 24. Jenkins CSP, Packham MA, Kinlough-Rathbone RL, Mustard JF: Interactions of polylysine with platelets. *Blood* 37:395-412, 1971
 25. White JG, Davis RB: Alterations in platelet ultrastructure in patients with carcinoid syndrome. *Am J Pathol* 56:519-531, 1969
 26. Kotchalsky A, Danon D, Nevo A, de Vries A: Interactions of basic polyelectrolytes with the red cell. II. Agglutination of red cells by polymeric bases. *Biochim Biophys Acta* 33:120-138, 1959
 27. Kotchalsky A: Polyelectrolytes and their biological interactions. *Biophys J* 4 (Suppl): 9-14, 1964
 28. Mamelak M, Wissig SL, Bogaroch R, Edelman IS: Physiological and morphological effects of poly-L-lysine on the toad bladder. *J Membrane Biol* 1:144-157, 1969
 29. Ryser HJP, Hancock R: Histones and basic polyaminoacids stimulate the uptake of albumin by tumor cells in culture. *Science* 150:501-503, 1965
 30. Sanders EJ, Bell LGE: Some physiological and morphological effects of polylysine on amoeba proteus. *J Cell Sci* 7:739-753, 1970
 31. Padawer J: The reaction of rat mast cells to polylysine. *J Cell Biol* 47:352-372, 1970
 32. Massini P, Luscher EF: On the importance of close cell contact for initiation of the release reaction of blood platelets. Second International Congress on Thrombosis and Hemostasis, Oslo, 1971, p 234 (abstr)

Legends for Figures

Fig 1A and 1B—Early stages in the uptake of cationic polypeptides by blood platelets. The cell in Figure 1A is from a sample of thrombasthenic citrate platelet-rich plasma (C-PRP) fixed 15 minutes after exposure to polybrene (PB) at a concentration of 1 mg/ml. Microtubules (MT) retain their usual location at the poles of the discoid platelet. Elements of the open canalicular system (OCS) are slightly dilated. Granules (G) and other cytoplasmic structures are randomly dispersed as in normal platelets. The granule indicated (arrow) has developed a mottled appearance characteristic of the early uptake of cationic polypeptide. The platelet in 1B is from a sample of normal C-PRP incubated with polylysine (PL) at a concentration of 0.5 mg/ml for 30 minutes. The circumferential band of microtubules (MT) is sectioned in the equatorial plane close to the cell surface. Several of the granules (G) and the outside surface of the cell appear relatively more electron dense than the cytoplasmic matrix due to uptake of PL. The granule indicated (arrow) has the same mottled matrix as the organelle in 1A, but the organization is obscured by the electron opacity (1A, $\times 35,600$; 1B, $\times 24,900$).

Fig 1C—Platelet from a sample of afibrinogenemic C-PRP incubated with PB (0.1 mg/ml) for 60 minutes. The cell contains a dense body (DB). Two granules (arrow) exhibit swelling and the lattice-like alteration of substructure characteristically produced by uptake of cationic polypeptide ($\times 29,000$).

Fig 1D—Platelet from sample of normal C-PRP incubated with PL (0.5 mg/ml) for 30 minutes. Dense bodies (arrow) and fragments of dense bodies appear to occupy dilated membranous channels or vacuoles. The channel occupied by one dense body fragment (starred arrow) is in continuity with the cell surface ($\times 25,200$).

Fig 1E—Platelet from sample of normal C-PRP fixed after 30 minutes incubation with PL (1.0 mg/ml) and subsequently stained for endogenous peroxidase activity. Lattice-like alterations in the matrix of granules (G) can readily be identified. Dense reaction product at sites of peroxidase activity is localized specifically to channels of the dense tubular system (DTS) ($\times 28,700$).

Fig 2A and 2B—The platelet in 2A is from a sample of normal C-PRP incubated for thirty minutes with PB (0.5 mg/ml). Discoid form has been lost and the surface contour is irregular. Organelles are concentrated in the cell center and enveloped by a close fitting band of microtubules (MT). Mitochondria (M) appear well preserved. A fragment resembling a dense body is present on the outside surface of the cell at the base of the illustration. The platelets in 2B are normal cells incubated for 30 minutes with PL (0.5 mg/ml). Several stages in the exocytosis of dense bodies are apparent, and two are indicated (arrows) (2A, $\times 24,900$; 2B, $\times 23,800$).

Fig 2C and 2D—The thrombasthenic platelet in 2C was exposed to PB (0.5 mg/ml) for 30 minutes. Dark zones of swollen granules and dense bodies are relatively more electron opaque. Fragments of a granule or a dense body are in the process of extrusion from a channel of the open canalicular system (arrow). The normal platelet in 2D combined with PL (0.5 mg/ml) for 30 minutes is almost identical to the cell in 2C. Fragments of granules or dense bodies embedded in lattice-like matrix material are in the process of exocytosis (arrow) (2C, $\times 24,900$; 2D, $\times 25,200$).

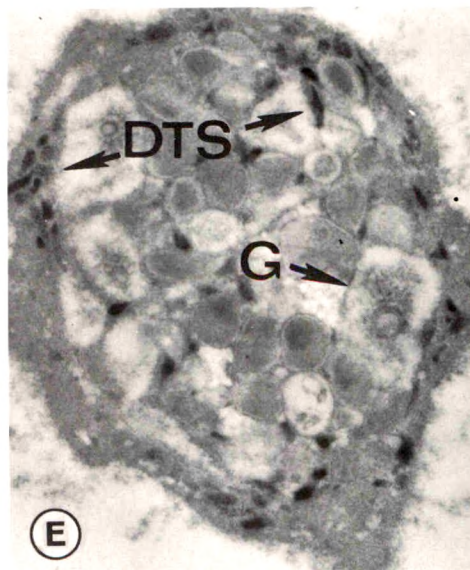
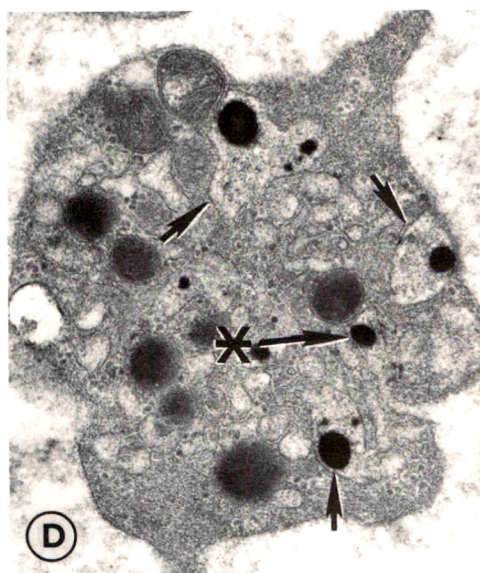
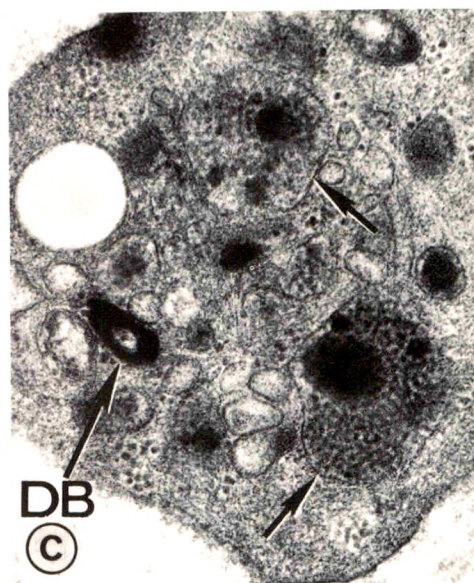
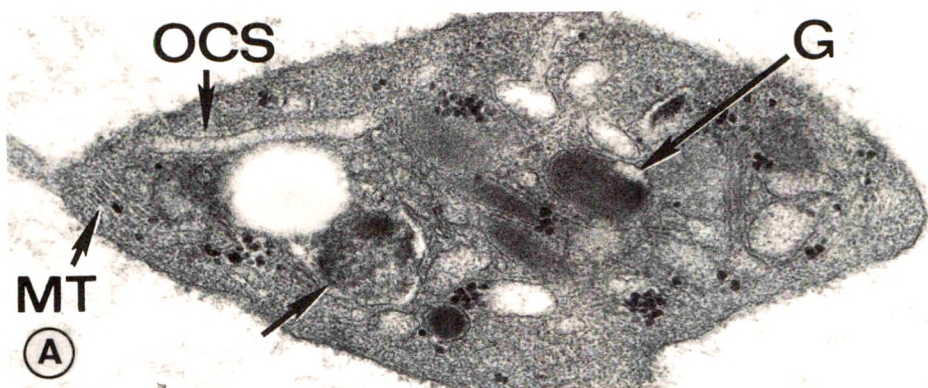
Fig 2E—An afibrinogenemic platelet fixed 60 minutes after incubation with polybrene (0.1 mg/ml). Two masses of electron-opaque material resembling dense bodies are in the process of exocytosis from this cell (arrow). Other structural components of the platelet appear well preserved.

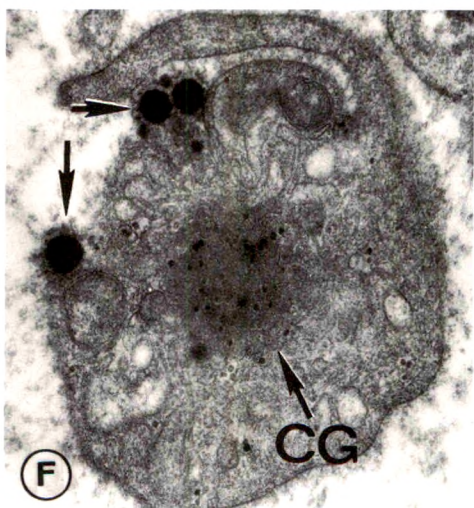
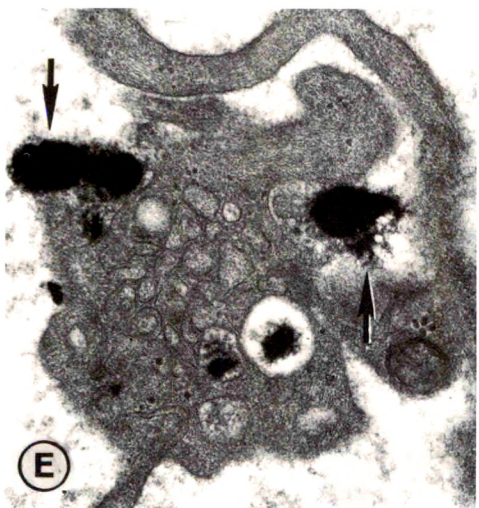
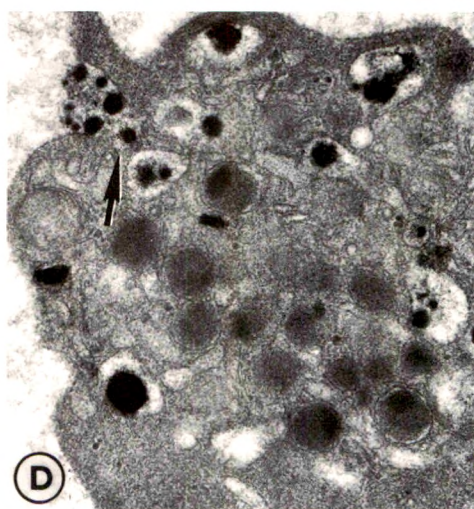
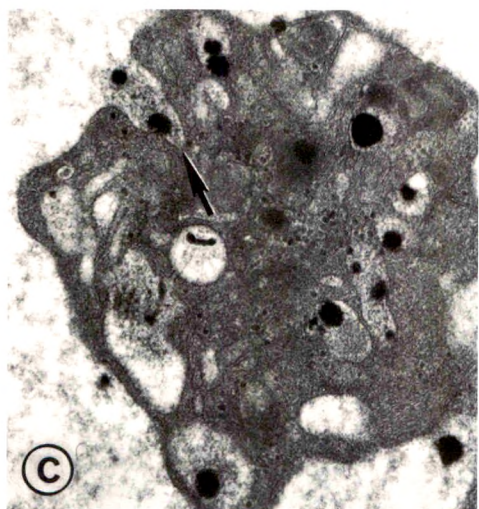
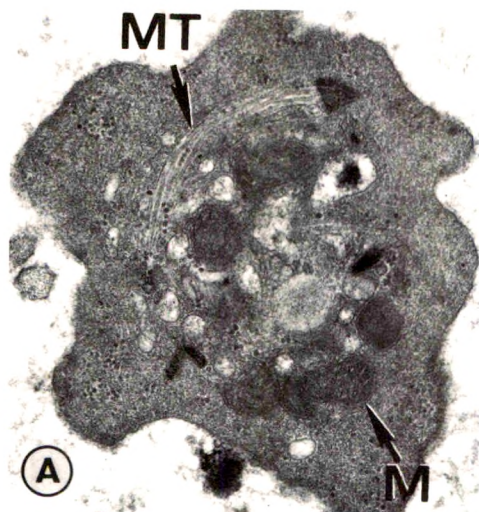
Fig 2F—Platelet from sample of thrombasthenic C-PRP incubated with PL (0.5 mg/ml) for 1 hour. Dense zones of granules in the process of exocytosis are surrounded by lattice-like matrix material (arrow). Internal transformation is complete in this cell, and residual organelles are fused in a mass of filamentous elements formed by the contractile gel (CG) ($\times 24,300$).

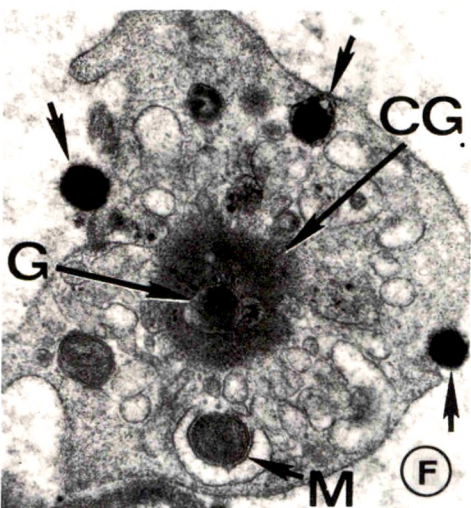
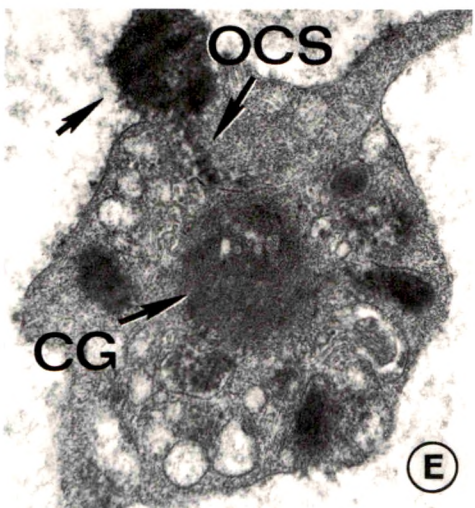
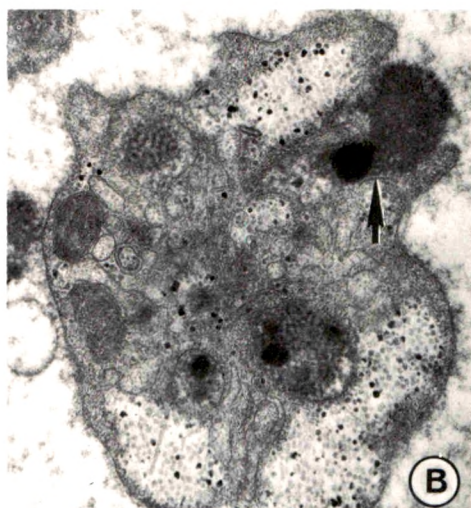
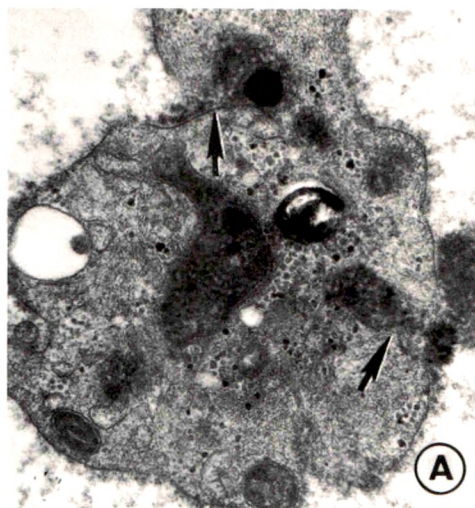
Fig 3A and 3B—Platelets in 3A and 3B are from samples of afibrinogenemic and thrombasthenic C-PRP, respectively, fixed after incubation with PB (0.5 mg/ml) for 60 minutes. The alteration in granule substructure produced by uptake of cationic polypeptide, and the exocytosis of granules and matrix material (arrow) are evident in the two examples (3A, $\times 25,600$; 3B, $\times 24,700$).

Fig 3C and 3D—Normal platelets from samples of C-PRP incubated for 1 hour with PL (0.5 mg/ml). The loss of discoid shape and internal transformation are advanced in these cells, and the contractile gel (CG) is concentrated in the cell centers (3C, $\times 27,400$; 3D, $\times 26,200$).

Fig 3E and 3F—The normal platelet in 3E was exposed to PB (0.5 mg/ml) for 1 hour, and the normal cell in 3F to PL (1 mg/ml) for 30 minutes. A mass of granular material (arrow) is in the process of exocytosis from a channel of the open canalicular system (OCS) in 3E. The contractile gel (CG) is concentrated in the center of this cell and in the platelet in 3F. Dense bodies (arrows) appear to be the principal structures being extruded from the cell in 3F. Residual mitochondria (M) in this platelet appear well preserved (3E, $\times 24,900$; 3F, $\times 25,600$).







[End of Article]

Experimental Visceral Aspergillosis

Herschel Sidransky, MD, Sheldon M. Epstein, MD, Ethel Verney, MS
and Claire Horowitz, BS

Studies conducted to gain insight into the pathogenesis of experimental aspergillosis indicated that mice pretreated with cortisone acetate and then injected intraperitoneally with nongerminating spores of *Aspergillus flavus* developed a high incidence of lethal visceral hyphal aspergillosis. A similar, high incidence of fatal infections was observed in cortisone-treated animals in which the number of peritoneal macrophages had been increased by prior injection of thioglycollate. To determine whether germination of spores within the host was important to the subsequent development of disseminated hyphal aspergillosis, germinating spores of *A. flavus* were injected intraperitoneally into normal animals. While a similar dose of nongerminating spores, administered intraperitoneally into normal mice, induced a low incidence of lethal infection, germinating spores induced a high incidence of fatal disease associated with widely disseminated visceral hyphal aspergillosis. Our studies indicate that phagocytic cells in the peritoneal cavity of normal mice are able to ingest nonperminating spores of *A. flavus* and kill them, preventing germination. However, the phagocytic cells are unable to cope with early germinating spores, which then continue to proliferate, leading to extensive hyphal invasion of visceral organs and death (Am J Pathol 69:55-70, 1972).

THE INCREASING INCIDENCE, in recent years, of secondary infections due to opportunistic fungi, such as *Aspergillus*, *Mucor* and *Candida*, has been well documented.¹⁻⁹ It is apparent that these infections usually occur in chronically debilitated patients treated with potent therapeutic agents. In aspergillosis, infections develop in a variety of organs, including the lung, gastrointestinal tract, brain, liver and kidney.²

To gain insight into the pathogenesis of human infections due to opportunistic fungi, a number of studies have been conducted, using experimental models of such disease in animals.¹⁰⁻¹⁸ In our laboratory we previously have been concerned with *Aspergillus flavus* infections of the lung¹⁹⁻²⁴ and brain²⁵ of mice. In studies with pulmonary aspergillo-

From the Department of Pathology, University of Pittsburgh School of Medicine, Pittsburgh, Pa and the Department of Experimental Biology, Weizmann Institute of Science, Rehovoth, Israel.

Supported in part by US Public Health Service Research Grant AI-05519 from the National Institute of Allergy and Infectious Diseases, US Public Health Service Special Fellowship of the National Cancer Institute and a grant of the American Cancer Society, awarded by the International Union Against Cancer.

Accepted for publication June 9, 1972.

Address reprint requests to Dr. Herschel Sidransky, Department of Pathology, University of South Florida, College of Medicine, Tampa, Fla 33620.

sis, we found that normal mice that inhaled viable spores of *A flavus* are resistant to lethal infection, while mice pretreated with corticosteroids and exposed to spores develop a high incidence of fatal hyphal bronchopneumonia.¹⁹ Based upon our earlier studies,²²⁻²⁵ we concluded that alveolar macrophages play an important role early in the host response to inhaled spores. By acting to stabilize biologic membranes, as suggested by others,²⁶⁻²⁸ corticosteroid treatment may interfere with the interaction of lysosomes with phagocytized spores, thus interfering with the intracellular destruction of spores, thereby allowing them to germinate. In considering the possible importance of early germination of spores within alveolar macrophages of steroid-treated mice in the pathogenesis of lethal pulmonary aspergillosis, we decided to conduct further studies designed to evaluate this observation. After unsuccessful attempts at administering germinating spores of *A flavus* into the lungs of mice, we were forced to utilize a different route and site of administration. Suspensions of nongerminating (resting) as well as germinating spores of *A flavus* were injected into the peritoneal cavities of normal mice. Morphologic and biologic studies were conducted and responses to the administration of the same organism under two different stages of growth and development were compared. Whether cortisone would alter the susceptibility of mice to lethal infection after the intraperitoneal administration of nongerminating spores of *A flavus* was also investigated.

Material and Methods

White female mice (Swiss strain from the Weizmann Institute and CF₁ strain from Carworth Farms) were used in the experiments. Treated mice received 5 or 10 mg cortisone acetate, subcutaneously, 2 days before the spores were injected. Untreated control mice were injected with spores at the same times as the cortisone-treated mice.

Spores of *Aspergillus flavus* were of the same strain used in earlier studies.¹⁹⁻²⁵ Nongerminating (resting) spores were diluted in sterile saline, counted in a hemacytometer and injected intraperitoneally. Mice received 1.25 to 5×10^6 spores which were collected by vacuum suction from dried cultures of *A flavus* grown on Sabouraud's dextrose agar plates, as described previously.¹⁹

To stimulate the induction of peritoneal macrophages, mice received 3 ml Difco Fluid Thioglycollate Medium (3%), intraperitoneally, 4 days before they received the spores. In earlier studies,²⁹ it was shown that this medium induced a marked increase in the number of peritoneal macrophages.

To obtain germinating spores, resting spores were inoculated into Difco Czapek broth, which was then incubated in an water bath, with shaking, at 30 C for the intervals given in Tables 3 and 4. Mice were injected intraperitoneally with resting spores in broth (taken before incubation), germinating spores after different intervals of incubation or with the broth alone.

Animals were necropsied shortly after death or after they were killed at selected intervals. For routine histologic study, visceral organs were fixed in 10% formalin

and paraffin sections stained with hematoxylin and eosin and with Gridley stain.³⁰ Cells obtained from peritoneal washings were centrifuged and the pelleted cells stained with hematoxylin and eosin.

Results

In the first series of experiments, the effect of cortisone on the development of fatal visceral aspergillosis was investigated in mice that received varying numbers of nongerminating spores of *A flavus* intraperitoneally. Table 1 summarizes the results of experiments in which control and cortisone-treated animals received 1.25×10^6 to 5×10^6 spores intraperitoneally. The results indicate that pretreatment with cortisone caused a high incidence of deaths from visceral aspergillosis, especially at higher concentrations of spores.

To determine whether peritoneal macrophages of cortisone-treated mice react to the injected spores differently than do cells of control mice (as was observed earlier with alveolar macrophages²²); in one experiment, control and cortisone-treated mice (10 mg cortisone acetate 2 days before) were injected intraperitoneally with nongerminating spores¹⁹ of *A flavus* and killed 17 hours later. After sterile isotonic saline was injected intraperitoneally, peritoneal cells were aspirated from animals of each group. Pooled specimens from each group were centrifuged and the pellets stained. Intracellular spores were seen in the pellets of both groups. In cells from cortisone-treated animals, occasional germinating spores were seen intracellularly. In cells from control ani-

Table 1—Effect of Cortisone Acetate on Fatal Visceral Aspergillosis in Mice Receiving Nongerminating *A flavus* Spores Intraperitoneally

No. of mice	Cortisone acetate* (mg)	No. of spores	Death with intraabdominal aspergillosis†
7	5	1.25×10^6	2 (29%)
7	0	1.25×10^6	0
8	5	2.5×10^6	6 (75%)
6	0	2.5×10^6	0
19	5	5×10^6	12 (63%)
20	0	5×10^6	0
18	10	5×10^6	17 (94%)
18	0	5×10^6	0

* Cortisone acetate was administered subcutaneously 1 or 2 days before exposure to spores.

† Deaths occurred between 3 and 10 days after exposure to nongerminating spores; diagnoses were made after histologic examination

mals, spores frequently were surrounded by pale areas, giving the interior of phagocytic cells a *moth eaten* appearance.

Another series of experiments was conducted to determine whether pretreatment with thioglycollate, intraperitoneally, to stimulate increased numbers of peritoneal macrophages, would influence the development of lethal visceral (abdominal) aspergillosis in control or cortisone-treated mice subsequently injected, intraperitoneally, with nongerminating spores of *A flavus*. Since it has been demonstrated that cortisone decreases circulating leukocytes as well as tissue monocytes,^{22,31} it became of interest to investigate whether animals containing increased numbers of peritoneal macrophages, despite cortisone treatment, would behave the same or differently after the spores were injected intraperitoneally. The results of these experiments are summarized in Table 2. Even though thioglycollate stimulated the number of intraperitoneal macrophages, subsequent treatment with cortisone before nongerminating spores were injected intraperitoneally led to an incidence of lethal infections essentially as high as that in animals not pretreated with thioglycollate (Table 2).

In experiments designed to determine whether germinating spores of *A flavus* would cause visceral hyphal aspergillosis, nongerminating

Table 2—Effect of Cortisone Acetate on Fatal Visceral Aspergillosis in Mice in Which Increased Numbers of Peritoneal Macrophages were Stimulated by Thioglycollate and then Treated with Nongerminating *A flavus* Spores Intraperitoneally

No. of Mice	Thioglycollate medium* (3 ml)	Cortisone acetate† (mg)	No. of spores	Deaths with intraabdominal aspergillosis‡	
				No.	%
13	+	5	5×10^6	10	77
13	+	0	5×10^6	2	15
9	0	5	5×10^6	7	78
10	0	0	5×10^6	0	0
28	+	10	$5-7 \times 10^6$	26	93
21	+	0	$5-7 \times 10^6$	0	0
8	0	10	$5-7 \times 10^6$	8	100
8	0	0	$5-7 \times 10^6$	0	0

* Mice received 3 ml Difco Fluid Thioglycollate Medium (3%), intraperitoneally, 4 days before receiving spores

† Cortisone acetate was administered subcutaneously 1 day before exposure to spores

‡ Deaths occurred between 3 and 10 days after exposure to nongerminating spores; diagnoses were made after histologic examination

and germinating spores, obtained by incubation in a liquid medium for varying intervals, were injected intraperitoneally into mice. The results of two experiments are summarized in Table 3. It is apparent that when equal concentrations of spores (nongerminating and germinating, incubated for 4.2 to 10 hours in liquid media) were administered intraperitoneally, germinating spores caused the highest incidence of lethal infections. Moreover, the incidence of lethal visceral aspergillosis increased the longer the spores were incubated *in vitro*. Histologic studies revealed inflammatory infiltrations along with hyphal invasion, particularly in the perisplenic region and also in the perirenal regions in animals that died from lethal infections after they received germinating spores.

In subsequent experiments, nongerminating spores were incubated in a liquid medium for 7 hours to obtain germinating spores. The results of two experiments, in which two concentrations of nongerminating and germinating spores were administered to mice, are summarized in Table 4. It is apparent that a higher incidence of lethal visceral hyphal aspergillosis infection developed in mice treated with germinating spores than in those treated with similar concentrations of nongerminating spores. Although some control animals died after the broth alone was administered, histologic examination revealed that in only one instance was death caused by fungal invasion. On the other hand, visceral hyphal invasion, as summarized in Table 4, was seen in mice that received spores.

Morphologic Alterations Associated With Fatal Visceral Aspergillosis

Gross Findings

At necropsy, in all groups a number of gross alterations commonly were noted in animals that died with visceral hyphal aspergillosis. The parietal and serosal peritoneum appeared moist, dull grey to grey-black and were focally mottled with small-to-large areas of friable, fibrinous exudate. Nodular green-grey to yellow-tan granulomas or abscesses were found throughout the abdominal cavities of animals that died within 7 days after they had received spores intraperitoneally. In addition, extensive intraabdominal fibrosis, with frequent adhesions between visceral organs were found in animals that died after a week. Abscesses involving the livers, kidneys and perisplenic areas were often noted in both preceding groups. The largest lesions were found in the perihilar region of the spleen and in the perirenal areas. Also, infarcts of the kidneys were also observed; some were wedge-shaped with the base to the periphery and others were localized in the medullary areas and grossly

Table 3—Influence of Type of Spores (Nongerminating and Germinating) of *A flavus* Administered Intraperitoneally on Incidence of Fatal Visceral Aspergillosis in Mice

Treatment	No. of mice	No. of deaths (weeks after treatment)				Intraabdominal hyphal aspergillosis	
		1	2	Total		No.	%
				No.	%		
Nongerminating spores	10	1	1	2	20	1	10
4.2-hour Germinating spores	10	2	3	5	50	2	20
7-hour Germinating spores	10	5	2	7	70	7	70
8.5-hour Germinating spores	10	4	3	7	70	7	70
Nongerminating spores	6	1	1	2	33	2	33
10-hour Germinating spores	10	6	0	6	60	6	60

resembled renal papillary necrosis. In many animals, the pancreases were hyperemic, swollen, focally necrotic and the peripancreatic fat was mottled with numerous small, white-to-yellow, chalky deposits. In some animals that died 2 to 4 weeks after receiving spores and in others killed at the end of the experiment (after 29 days), the kidneys were multicystic; when these kidneys were sectioned, the medullary areas were dilated and the cortical areas were compressed.

Table 4—Influence of Different Doses of Spores (Nongerminating and Germinating) of *A flavus* Administered Intraperitoneally on Incidence of Fatal Visceral Aspergillosis in Mice

Treatment and No. of organisms administered*		No. of mice	No. of deaths (weeks after treatment)				Intraabdominal hyphal aspergillosis	
			1	2	Total		No.	%
					No.	%		
Nongerminating spores	(10×10^6)	10	1	4	5	50	1	10
Germinating spores	(10×10^6)	10	3	3	6	60	2	20
Nongerminating spores	(10×10^7)	10	1	2	3	30	1	10
Germinating spores	(10×10^7)	10	7	2	9	90	7	70
Broth alone	—	10	2	1	3	30	1	10
Nongerminating spores	(10×10^6)	10	3	1	4	40	3	30
Germinating spores	(10×10^6)	10	1	3	4	40	4	40
Nongerminating spores	(10×10^7)	10	3	1	4	40	4	40
Germinating spores	(10×10^7)	10	9	0	9	90	9	90
Broth alone	—	10	2	2	4	10	0	0

* Germinating spores were incubated in a liquid medium for 7 hours

Histopathologic Findings

Microscopic examination revealed alterations in the perietal and serosal peritoneum, interabdominal fat, spleen and its perihilar area, kidneys, adrenals, pancreas, liver and lungs. The frequency of organ involvement is summarized in Table 5. Hyphal invasion of numerous organs was observed readily. Hyphae penetrated fibro-fatty tissue, the spleen (Figure 1), kidneys (Figure 2), adrenals (Figure 3), pancreas (Figure 4) and stomach (Figures 5, 6). Vascular permeation by hyphae and numerous thrombi in both arteries and veins frequently were found. This was accompanied by infarction of the parenchyma supplied by the involved vessels. All tissues or organs with hyphal invasion showed a sparse-to-dense degree of acute inflammatory reaction with frequent foci of necrosis and infarction. Fibrous tissue permeated with acute and chronic inflammatory cells and hyphae (Figures 5 and 6) frequently caused the serosa of the stomach to adhere to the splenic capsule. Extensive hyphal invasion was seen in the spleen. The perihilar region of the spleen generally contained the most numerous aggregates of germinating or nongerminating spores. Acute and chronic lesions were seen in the kidneys. The acute renal lesions consisted of pyelonephritis and/or infarction. Hyphal invasion, along with an acute inflammatory reaction, was most marked at the peripheral portions of the kidneys in animals that died early; extensive hyphal infiltration was observed in animals that died after a week or more. Renal infarction involved all portions of the kidneys. The chronic renal lesions were observed in animals that

Table 5—Organ Involvement of Mice Dying with Visceral Hyphal Aspergillosis After Intra-peritoneal Administration of Nongerminating or Germinating Spores of *A flavus*

Organ	No. of lesions in mice dying after spores injected			
	Nongerminating spores (6 deaths)		Germinating spores (36 deaths)	
	No.	%	No.	%
Liver	1	17	8	22
Kidney	5	83	24	66
Spleen	—	—	7	19
Pancreas	—	—	7	19
Adrenal	—	—	5	14
Intestinal tract	—	—	5	14
Lung	—	—	1	3
Heart	—	—	1	3
Uterus	—	—	1	3
Ovary	—	—	1	3
Oviduct	—	—	1	3

died or were killed after 3 or more weeks. The lesions consisted of marked dilation of the medullary portions of the kidneys, with cystic spaces lined by stratified squamous or transitional epithelium surrounded by fibrotic parenchyma containing lymphocytes. The renal cortical areas were compressed and fibrotic. The adrenals were invaded peripherally by hyphae that extended from the periadrenal fat, which contained many hyphae and acute and chronic inflammatory cells (Figure 3). Inflammation and necrosis (Figure 4) were found in the pancreas. Focal subcapsular as well as deep parenchymal abscesses and/or granulomas containing hyphae and hyphal invasion of vessels with areas of hepatic infarction were observed in the liver. The lungs were normal usually, except for a few instances in which thromboemboli containing hyphae were noted in arteries and veins but were usually unassociated with pulmonary infarction (Figure 7). Occasionally, hyphae invaded the heart and genital organs.

Selected Morphologic Differences Under Various Experimental Conditions

In general, the preceding gross and microscopic findings were observed in most of the mice that died with visceral hyphal aspergillosis. However, certain differences were observed, depending upon experimental conditions, and these will be cited.

Control mice injected intraperitoneally with nongerminating spores and sacrificed after different intervals (beyond the first day—*ie*, days 3 and 5) contained numerous granulomatous foci, with central necrosis, in the perihilar areas of the spleens. These granulomas contained nongerminating spores surrounded by acute and chronic inflammatory cells with many mononuclear macrophages (Fig. 8). In mice killed 3 or more days after they received nongerminating spores, the granulomas were circumscribed by fibrous tissue. Other organs did not appear to be involved, and no spore germination, hyphal infiltration or parenchymal damage were observed. In comparison, control mice that received germinating spores, and also cortisone-treated mice that received nongerminating or germinating spores, had more advanced lesions in the perisplenic areas as well as lesions in the spleen and in other organs (Figures 1–7). The lesions were diffuse and contained hyphae, which showed extensive invasion. Many animals died from hyphal aspergillosis with organ involvement, as described previously.

In general, as an overall appraisal of the lesions in animals under different experimental conditions, it appeared that the earliest and most extensive lesions occurred in cortisone-treated mice that received germinating spores intraperitoneally. In cortisone-treated mice that received

nongerminating spores intraperitoneally, visceral lesions were as extensive as in the previous group, but deaths occurred somewhat later. In control mice that received germinating spores intraperitoneally, lesions appeared to develop somewhat more slowly and were less extensive than in the previous two groups.

Sequential Histopathologic Changes After Nongerminating and Germinating Spores

To study the sequence of pathologic changes after the intraperitoneal injection of spores (nongerminating or germinating), mice in one experiment were treated with nongerminating spores, germinating spores or broth, and then 5 animals from each group were killed after 1, 3 or 5 days. The animals inoculated with spores received 24×10^6 nongerminating or germinating spores in 1 ml of broth. The histologic findings in the three groups, after the different intervals, were as follows:

Animals Receiving Broth Alone. On day 1 there was an inflammatory cell infiltrate, consisting predominantly of lymphocytes, with only a few polymorphonuclear cells and monocytes, in perisplenic, perihepatic and/or perirenal regions in all 5 mice of this group. By day 5, the inflammatory response had decreased in intensity.

Animals Receiving Nongerminating Spores. On day 1, many spores were present, along with predominantly lymphocytic infiltrate, in the perisplenic, perihepatic and/or perirenal areas in 5 mice. On day 3, two animals had perisplenic granulation tissue and a few germinating spores were found in only one animal. On day 5, one animal had germinating spores perirenally, with short hyphae penetrating into a kidney; a second animal had a walled-off area of germinating spores retroperitoneally.

Animals Receiving Germinating Spores. On day 1, four animals had mild perihepatitis, 2 had pancreatitis and 2 had perisplenic granulation tissue. On day 3, in addition to the lesions described at day 1, one animal had pyelonephritis. On day 5, perisplenic lesions were prominent with some hepatic abscesses in 2 mice and all of these lesions were infiltrated and invaded with hyphae.

Discussion

The results of this study indicate that mice pretreated with corticosteroids and then injected intraperitoneally with nongerminating spores of *Aspergillus flavus* develop a high incidence of lethal visceral hyphal aspergillosis. This occurs even after the number of peritoneal macrophages has been increased by prior injection of thioglycollate. Histologically, it appears that shortly after the spores are ingested by

peritoneal phagocytes (*ie*, after a moderate number of spores are inoculated intraperitoneally), those in the cells of cortisone-treated animals germinate intracellularly, while those in the cells of control animals are arrested and do not germinate. The intraperitoneal injection of germinating spores of *A flavus* into normal animals leads to a high incidence (significantly higher than with nongerminating spores) of lethal visceral aspergillosis.

Our present results are consistent with the previous impression, based on studies with cortisone-treated mice exposed to the inhalation of aerosols of nongerminating spores of *A flavus*,²² that germination of spores may play an important role in the early pathogenesis of the disseminated disease which leads to lethal infection. This stresses the importance, under normal conditions, of the host's ability to mobilize its phagocytic cells to destroy the ingested organism. Furthermore, it is vital that the digestive system within the phagocytic cell, centering around the lysosomes and their enzymes, functions effectively. If not, spores of *A flavus* germinate intracellularly, and the host's response to germinating spores is much more limited than its response to resting spores.

The results of this study, which reveal that the administration of cortisone enhances the susceptibility of mice to lethal infection after nongerminating spores of *A flavus* are injected intraperitoneally, are consistent with an earlier report by Mankowski and Littleton.¹⁰ Mankowski¹¹ also demonstrated that intraperitoneal administration of mucin, along with resting spores of an *Aspergillus* species, enhanced the susceptibility of mice to lethal infection. Although the mechanism by which mucin acts has not yet been clarified, it has been shown to play a role in enhancing the infectious process of bacteria and of other fungi.³²

To our knowledge, this report is the first demonstration that germinating spores of *A flavus*, administered intraperitoneally to normal mice, are capable of inducing a high incidence of lethal infection. This evidence is in accord with and further supports earlier observations in studies with experimental pulmonary aspergillosis,²² which suggested that the germination of spores within alveolar macrophages of cortisone-treated mice was important in the pathogenesis of lethal infection. Likewise, studies by Sheldon and Bauer,¹⁷ using alloxan-diabetic rabbits exposed subcutaneously to spores of *Rhizopus*, indicated that delayed degranulation of tissue mast cells appeared to be associated with the ability of spores to germinate and proliferate and thus infect the experimental animals. Thus, it appears that once organisms are allowed to germinate and proliferate within the cells and tissue of the visceral cav-

ity, lungs or subcutaneous tissue, the response of the host is much more limited, and severe infection may then ensue.

Based on earlier histologic studies with experimental pulmonary and cerebral aspergillosis,¹⁹⁻²⁵ we were impressed by the ability of the hyphae to penetrate and breach anatomic barriers and often to extend indiscriminately through structures, such as bronchial cartilage and arterial walls. Similar hyphal invasion and penetration into visceral organs was observed in this study. This invasion, occasionally without any detectable tissue response, suggests that the invading organisms may be liberating digestive or proteolytic enzymes which enable them to penetrate rapidly. It is recognized that hyphae of many strains of *Aspergilli* produce numerous enzymes when grown in various media.³³ It is interesting to speculate that one or many of the enzymes elaborated by germinating spores and hyphae, but not by nongerminating spores of *A. flavus*, contribute to the organism's invasiveness, as well as to the host's decreased responsiveness to the organism, when it gains entrance into the body. Experimental studies are needed to clarify whether these speculations do occur during the pathogenesis of experimental *Aspergillus* infection.

References

1. Heffernan AGA, Asper SP Jr: Insidious fungal disease: A clinicopathological study of secondary aspergillosis. *Bull Johns Hopkins Hosp* 118:10-26, 1966
2. Young RC, Bennett JE, Vogel CL, Carbone PP, DeVita VT: Aspergillosis. The spectrum of the disease in 98 patients. *Medicine* 49:147-173, 1970
3. Zimmerman RA, Miller WT: Pulmonary aspergillosis. *Am J Roentgenol* 109:505-515, 1970
4. Seelig MS: The role of antibiotics in the pathogenesis of *Candida* infections. *Am J Med* 40:887-917, 1966
5. Straatsma BR, Zimmerman LE, Gass JDM: Phycomycosis: A clinicopathologic study of fifty-one cases. *Lab Invest* 11: 963-985, 1962
6. Bodey GP, Powell RD Jr, Hersh EM, Yeterian A, Freireich EJ: Pulmonary complications of acute leukemia. *Cancer* 19:781-793, 1966
7. Rifkind D, Marchioro TL, Schneck SA, Hill RB Jr: Systemic fungal infections complicating renal transplantation and immunosuppressive therapy. *Am J Med* 43:28-38, 1967
8. Hart PD, Russell E Jr, Remington JS: The compromised host and infection. II. Deep fungal infection. *J Infect Dis* 120:169-191, 1969
9. Lurie HL, Duma RJ: Opportunistic infections of the lungs. *Human Pathol* 1:233-257, 1970
10. Mankowski ZT, Littleton BJ: Action of cortisone and ACTH on experimental fungus infections. *Antibiot Chemother* 4:253-258, 1954
11. Mankowski ZT, The influence of various sex hormones on experimental fungus infections. *Antibiot Chemother* 4:1100-1104, 1954

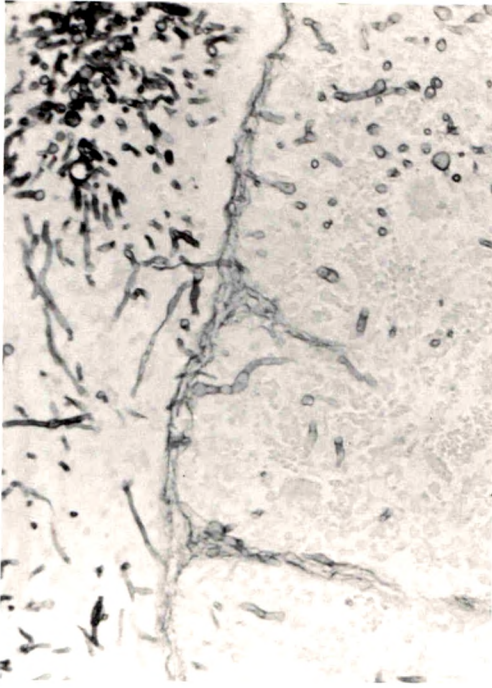
12. Bauer H, Flanagan JF, Sheldon WH: Experimental cerebral mucormycosis in rabbits with alloxan diabetes. *Yale J Biol Med* 28:29-36, 1955
13. Elder TD, Baker RD: Pulmonary mucormycosis in rabbits with alloxan diabetes: increased invasiveness of fungus during acute toxic phase of diabetes. *Arch Pathol* 61:159-168, 1956
14. Schofield RA, Baker RD: Experimental mucormycosis (*Rhizopus* infection) in mice: the failure of chronic alloxan diabetes to modify host susceptibility. *Arch Pathol* 61:407-415, 1956.
15. Roth FJ Jr, Friedman J, Syverton JT: Effects of roentgen radiation and cortisone on susceptibility of mice to *Candida albicans*. *J Immunol* 78:122-127, 1957
16. Louria DB, Fallon N, Browne HG: The influence of cortisone on experimental fungus infections in mice. *J Clin Invest* 39:1435-1449, 1960
17. Sheldon WH, Bauer H: The role of predisposing factors in experimental fungus infections. *Lab Invest* 11:1184-1191, 1962
18. Ford S, Friedman L: Experimental study of the pathogenicity of *Aspergilli* for mice. *J Bacteriol* 94:928-933, 1967
19. Sidransky H, Friedman L: The effect of cortisone and antibiotic agents on experimental pulmonary aspergillosis. *Am J Pathol* 35:169-184, 1959
20. Sidransky H, Verney E: Experimental aspergillosis. *Lab Invest* 11:1172-1183, 1962
21. Sidransky H, Verney E, Beede H: Experimental pulmonary aspergillosis. *Arch Pathol* 70:299-309, 1965
22. Epstein SM, Verney E, Miale TD, Sidransky H: Studies on the pathogenesis of experimental pulmonary aspergillosis. *Am J Pathol* 51:769-788, 1967
23. Merkow L, Pardo M, Epstein SM, Verney E, Sidransky H: Lysosomal stability during phagocytosis of *Aspergillus flavus* spores by alveolar macrophages of cortisone-treated mice. *Science* 160:79-81, 1968
24. Merkow LP, Epstein SM, Sidransky H, Verney E, Pardo M: The pathogenesis of experimental pulmonary aspergillosis: An ultrastructural study of alveolar macrophages after phagocytosis of *A. flavus* spores *in vivo*. *Am J Pathol* 62:57-73, 1971
25. Epstein SM, Miale TD, Moossy J, Verney E, Sidransky H: Experimental intracranial aspergillosis. *J Neuropathol Exp Neurol* 27:473-482, 1968
26. Weissmann G, Thomas L: Studies on lysosomes. I. The effects of endotoxin, endotoxin tolerance, and cortisone on the release of acid hydrolases from a granular fraction of rabbit liver. *J Exp Med* 116:433-450, 1962
27. Weissmann G: Studies on lysosomes. VI. The effect of neutral steroids and bile acids on lysosomes *in vitro*. *Biochem Pharmacol* 14:525-535, 1965
28. DeDuve C, Wattiaux R, Wibo M: Effects of fat-soluble compounds on lysosomes *in vitro*. *Biochem Pharmacol* 9:97-116, 1962
29. Gallily R, Warwick A, Bang FB: Effect of cortisone on genetic resistance to mouse hepatitis virus *in vivo* and *in vitro*. *Proc Natl Acad Sci* 51:1158-1164, 1964
30. Gridley MF: A stain for fungi in tissue sections. *Am J Clin Pathol* 23:303-307, 1953
31. Dougherty TF, White A: Influence of hormones on lymphoid tissue structure and function. The role of the pituitary adrenotrophic hormone in the regula-

- tion of the lymphocytes and other cellular elements of the blood. *Endocrinology* 35:1-14, 1944
32. Scherr GH: The role of mucin in enhancing the infectious process. *Ann NY Acad Sci* 106:680-682, 1963
 33. Raper KB, Fennell DL: *The Genus Aspergillus*. Baltimore, The Williams and Wilkins Co, 1965

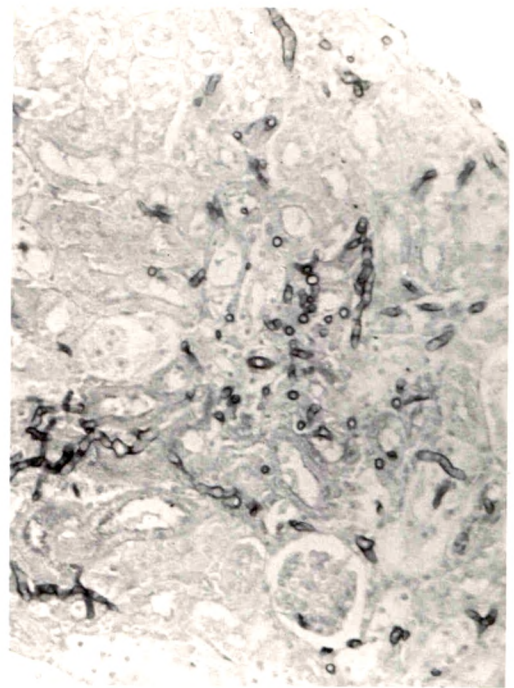
Acknowledgments

Dr. Epstein is a recipient of a Cancer Research Development Award KO3CA-15245 from the National Cancer Institute.

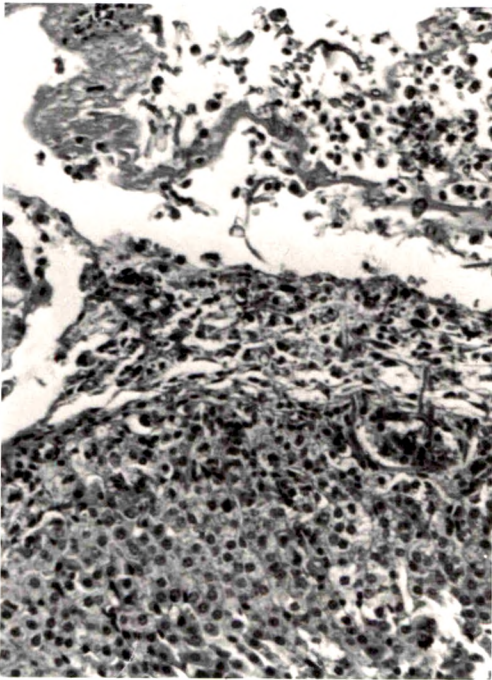
[*Illustrations follow*]



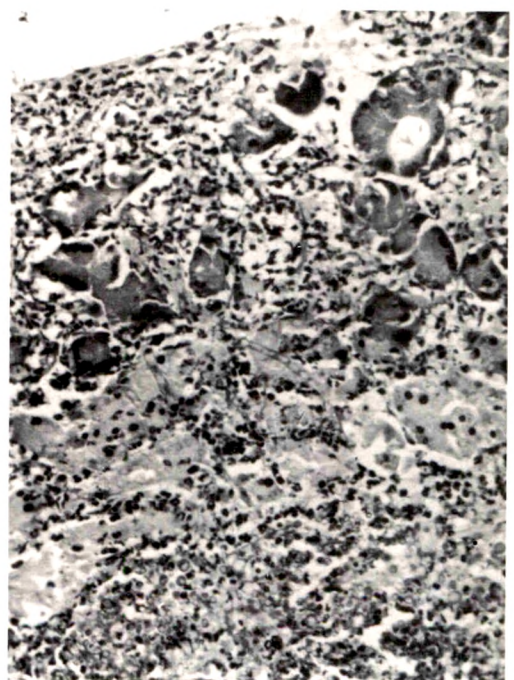
1



2



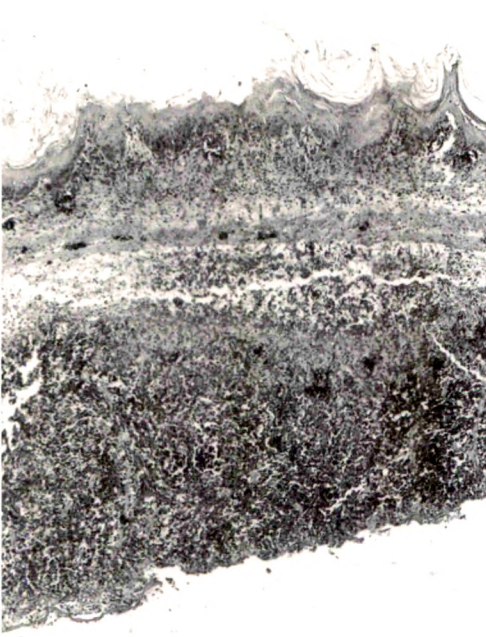
3



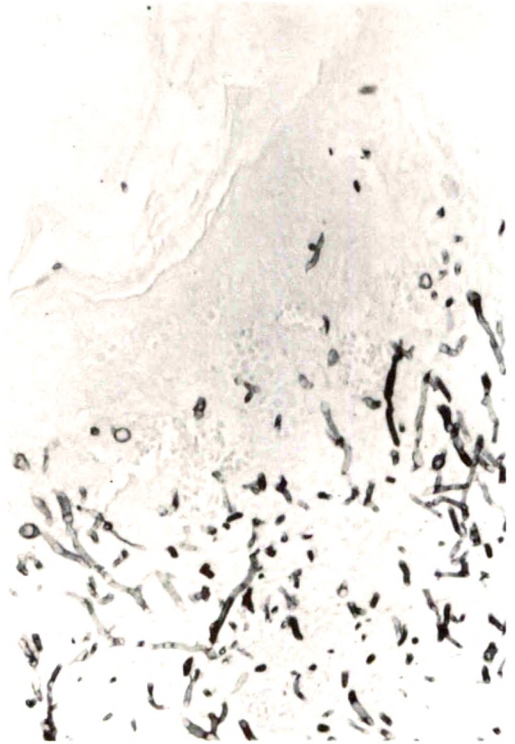
4

Fig 1—Spleen from cortisone-treated mouse that received germinating spores of *A. flavus* intraperitoneally 4 days before death. Note hyphal involvement of perisplenic tissue with invasion of spleen (Gridley stain, $\times 230$). **Fig 2**—Kidney from normal mouse that received germinating spores of *A. flavus* intraperitoneally 4 days before death. Hyphae are proliferating throughout cortex of kidney (Gridley stain, $\times 230$). **Fig 3**—Adrenal from cortisone-treated mouse that received germinating spores of *A. flavus* intraperitoneally 4 days before death. Note inflammatory cell infiltration of periadrenal tissue with hyphae, some of which are invading into adrenal. One capsular vessel shows hyphal invasion (H&E, $\times 230$). **Fig 4**—Pancreas of normal mouse that received germinating spores of *A. flavus* intraperitoneally one day before being killed. Note dense acute inflammatory cell infiltration with invading hyphae and necrosis of acini (H&E, $\times 230$).

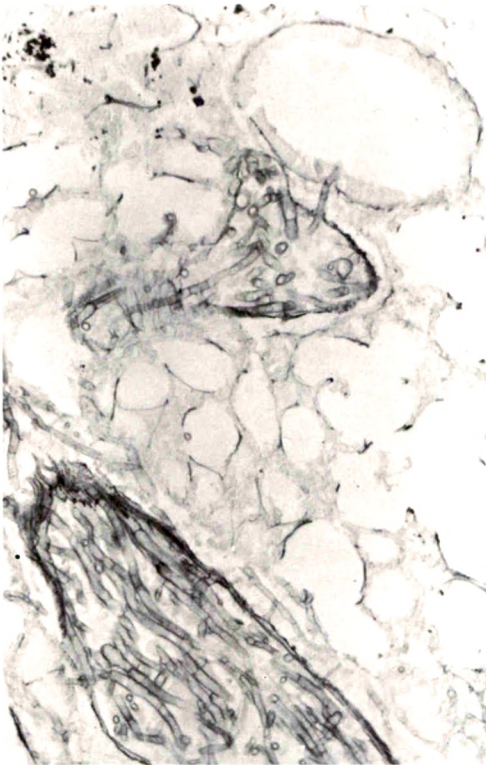
5



6



7



8



Fig 5—Stomach and spleen of cortisone-treated mouse that received germinating spores of *A. flavus* intraperitoneally 4 days before death. Stomach (stratified squamous portion) is adherent to spleen by inflammatory cell reaction containing hyphae (H&E, $\times 45$). **Fig 6**—Stomach from mouse described in Figure 5. Note extensive hyphal invasion of gastric wall (Gridley stain, $\times 230$). **Fig 7**—Lung of cortisone-treated mouse that received germinating spores of *A. flavus* intraperitoneally 6 days before death. Hyphae are present within vessels and some are invading adjacent lung parenchyma (Gridley stain, $\times 230$). **Fig 8**—Spleen of normal mouse that received non-germinating (resting) spores of *A. flavus* intraperitoneally 3 days before being killed. Note granuloma in perisplenic tissue (H&E, $\times 45$).

Morphologic Study of the Participation of the Complement System in Hyperacute Rejection of Renal Xenotransplants

Jaime E. Mejía-Laguna, MD, Adolfo Martínez-Palomo, MD, Carlos E. Biro, MD, Bibiana Chávez, BS, Fernando López-Soriano, MD and Marcelo García-Cornejo, MD

The role of polymorphonuclear leukocyte (PMN) and platelet infiltration in the hyperacute rejection of renal xenotransplants was studied. In a first group, a dog kidney was grafted to rabbit recipients with intact immune adherence and chemotaxis. A second group included recipients depleted of PMN's with nitrogen mustard, and in a third group, immune adherence and chemotaxis were modified by depleting the third component of complement by means of cobra venom factor. Serial kidney biopsies were studied with light and electron microscopic technics. A semiquantitative evaluation of PMN and platelet glomerular infiltration indicated that a reduction in the number of PMN's or platelets is associated with an increased survival time of the transplanted kidney (*Am J Pathol* 69:71-78, 1972).

IN RECENT YEARS an increasing number of studies have dealt with the morphologic changes that appear during the hyperacute rejection of renal xenotransplants. Interest in this type of rejection derives chiefly from the similarity with the acute phases of human kidney allotransplant rejection.¹⁻³

The presence of polymorphonuclear leukocytes (PMN's) in the glomerular capillaries of kidney xenografts represents one of the early morphologic manifestations of acute rejection.^{4,5} Glomerular infiltration with PMN's is accompanied by an important reduction in circulating PMN's.⁶ Infiltration of renal cortical tissue with leukocytes has also been found during the acute phases of renal allograft rejection, both in experimental animals^{7,8} and in human allotransplants.^{1-3,9} In addition to PMN's, platelet glomerular thrombi are present in the kidney of sensitized allograft recipients.^{1,2} In xenografts, the number of platelets in the efferent circulation has been found to be lower than that in the afferent renal circulation.¹⁰

From the Departments of Immunology, Electron Microscopy and Experimental Surgery, Instituto Nacional de Cardiología, México City, Mexico.

Accepted for publication June 7, 1972.

Address reprint requests to Dr. Adolfo Martínez-Palomo, Centro de Investigación y de Estudios Avanzados del Instituto Politécnico Nacional, Apartado Postal 14-740, México 14, DF, Mexico.

Taking these results into account, it was deemed important to study the relationship among graft survival time, PMN, and platelet infiltration. A first group of xenografts included recipients with intact immune adherence and chemotaxis mechanisms. In a second group, circulating PMN's were depleted in the recipient by means of nitrogen mustard. In a third group, studies were done on kidney biopsies of recipients treated with cobra venom factor to modify immune adherence and chemotaxis through depletion of complement system. The results demonstrate that the survival time of the kidney xenograft is related to the presence of PMN and platelet glomerular infiltration.

Material and Methods

Normal young Beagle dogs were used as kidney donors, and adult rabbits of either sex were used as recipients. Surgical procedures involved in transplanting the dog kidney to the rabbit have been described in detail in a previous publication.⁵ Dogs with abnormal urinary findings were not used as donors. A total of 14 xenotransplants were carried out in three different groups: a) kidney transplants from a normal dog to a normal untreated rabbit; b) kidney transplants from a normal dog to a rabbit rendered leukopenic by means of nitrogen mustard (1.73 mg/kg, 72 hours prior to the graft) and c) kidney transplants from a normal dog to a rabbit treated with cobra venom factor (1.6 mg total protein, 12 to 24 hours before transplantation) to deplete C₃ and thus modify immune adherence and chemotaxis.¹¹

After surgical manipulations, zero time of kidney transplant was established as the time when the arterial clamps were released. Kidney biopsies were subsequently taken at 10, 20 and 30 minutes. A fourth biopsy was taken 15 minutes after urinary flow ceased; in some cases, biopsies were also taken 2 minutes after reestablishment of blood flow into the transplanted organ. Control biopsies were obtained from the contralateral kidney of the donor immediately after laparotomy. The criteria used to evaluate kidney rejection included: the presence of brownish discoloration of the kidney surface, collapse of surface vessels, edema, cyanosis and cessation of urinary flow. Wedge-shaped biopsy specimens approximately $5 \times 2 \times 3$ mm were obtained and immediately fixed in 2.5% glutaraldehyde in 0.1 M phosphate or cacodylate buffer, pH 7.3, for 15 minutes. Smaller fragments were cut and fixation in glutaraldehyde was continued for 1 hour. After postfixation in 1% osmium tetroxide for 1 hour at room temperature, specimens were dehydrated in alcohol and embedded in Epon. All blocks were sectioned for light microscopy; 9 to 63 kidney corpuscles (average 14.4) were studied in each biopsy specimen. Semithin sections were stained with toluidine blue and studied for the presence of PMN's and platelets in glomerular loops, and for modifications of mesangial cells and mesangial matrix. A total of 76 biopsies were studied; the total number of glomeruli examined with the light microscope was 1110 (286 from controls, 824 from grafts). Selected glomeruli were sectioned for electron microscopy, stained with uranyl acetate and lead citrate and examined with a Zeiss EM 9-S electron microscope.

Results

The morphologic findings in biopsy specimens of the three groups of renal xenotransplants are presented in Table 1. In each group the

Table 1—Morphologic Changes

Treatment of recipient	No. of glomeruli		Total PMN's		PMN/Glomeruli		Platelets		Survival time (min)
	Control	Graft	Control	Graft	Control	Graft	Control	Graft	
None	130	266	43 ↓ $P \cong 0.25$	152 ↓ $P = >0.01$	0.3307 ↓ ($P > 0.01$)	0.5714	0	++	17.6
Nitrogen mustard	55	298	25 ↓ $P = >0.01$	31 ↓ $P = >0.01$	0.4545 ↓ ($P > 0.01$)	0.1040	0	++	76.2
Cobra venom factor	101	260	13 ↑	57 ↑	0.1287 ↑ ($P = 0.01$)	0.2192	0	0	74.8

number of glomeruli examined, the number of intracapsular PMN's, the index of PMN's to glomeruli and the presence of intraglomerular platelets are presented, comparing the data found in control specimens with that observed in the grafted kidneys.

The average survival time for each group was considerably extended, both for the nitrogen mustard-treated group and for the cobra venom factor-treated group. In the first group, which included recipients with intact immune adherence and chemotactic mechanisms, the average survival time (taken as the time until urinary flow ceased) was 17.6 minutes (15 to 25 minutes). When recipients were depleted of leukocytes with nitrogen mustard, the average survival time of the graft increased to 76.2 minutes (23 to 110 minutes); in the cobra venom-treated group, the survival time was prolonged to 74.8 minutes (50 to 126 minutes).

The degree of PMN infiltration in the glomeruli of the transplanted kidney (Figure 1) was compared with the ratio PMN's to the number of glomeruli found in controls for each group. In the normal recipient group, the index was 0.3307 in controls and 0.5714 in the grafts. This difference is statistically significant ($P > 0.01$).

In the nitrogen mustard-treated group, the index of PMN's to glomeruli was found to be significantly lower ($P > 0.01$) in the transplanted kidneys, whereas in the cobra venom-treated group, a slight increase in this index was observed. The latter is not statistically significant ($P = 0.1$).

The presence of intraglomerular platelets (Figures 2, 3) was evaluated semiquantitatively (+ to ++++). No platelet thrombi were found in 286 control glomeruli from the three different groups. Intraglomerular platelet thrombi were found in the normal recipient group and the nitrogen mustard-treated group. Platelets were not found in 260 glomeruli of the cobra venom-treated group.

In addition to the PMN's and platelet infiltration observed with light and electron microscopy, an important increase in the amount of mesangial matrix was found in most grafted kidneys. However, a similar change was observed in control kidneys subjected to surgical manipulations, which included variable periods of anoxia, as well as perfusion of heparinized saline solution at 4 C.

Discussion

In a previous report, our demonstration of a significant delay in the rejection of renal xenotransplants in leukopenic recipients suggested that PMN's play an important role in the hyperacute rejection of kidney

xenografts.¹² Present morphologic findings tend to strengthen this view, since the number of intraglomerular PMN's increased after transplantation in untreated recipients. In addition, the increased survival time observed in leukopenic recipients was related to a diminution of the PMN to glomeruli ratio.

These results are in agreement with the observations of Linn *et al*⁶ and Mejía-Laguna *et al*^{5,12} concerning xenograft rejection and those of Lindquist *et al*,^{8,9} Kincaid-Smith,¹ Porter *et al*² and Weymouth *et al*³ pertaining to acute allograft rejection. They are, in fact, a concrete example of the more general phenomenon of PMN infiltration in complement-mediated inflammatory processes such as the Arthus phenomenon^{11,13} and the marked decrease of this infiltration upon depletion of C₃ during treatment with cobra venom factor.¹¹

The survival of kidney xenografts in these experiments was equally prolonged in rabbits treated with cobra venom factor and in those treated with nitrogen mustard. This, in conjunction with the fact that glomerular platelet thrombi were present in the latter group and not in the former, would seem to indicate that PMN infiltration, not platelet thrombi, was chiefly responsible for the delay in onset of rejection. The presence of platelet infiltration may be related to the AgAbC phagocytic property of platelets.¹⁶

Since rabbit platelets have immune adherence receptor sites on their surface,¹⁷ and in view of the fact that no glomerular platelet thrombi were found in C₃-depleted rabbits, it seems likely that immune adherence was the cause of platelet aggregation. If so, the platelet thrombi found in human allograft rejection may have been attracted by a different mechanism, since human platelets do not participate in immune adherence.¹⁷

Taking these results into account, the semiquantitative estimation of PMN and platelet infiltration in biopsy specimens of the transplanted kidneys can be a useful method for evaluating the evolution of the rejection process in human allografts.

References

1. Kincaid-Smith P: Histological diagnosis of rejection of renal homografts in man. *Lancet* 2:849-852, 1967
2. Porter KA, Dossetor JB, Marchioro TL, Peart WS, Rendal JM, Starzl TE, Terasaki PI: Human renal transplants. I. Glomerular changes. *Lab Invest* 16:153-181, 1967
3. Weymouth RJ, Seibel HR, Lee HM, Hume DM, Williams GM: The glomerulus in man one hour after transplantation. An electron microscopic study. *Am J Pathol* 58:85-104, 1970

4. Gewurz H, Clark DS, Finstad J, Kelly WD, Varco RL, Good RA, Gabrielsen AE: Role of the complement system in graft rejection in experimental animals and man. *Ann NY Acad Sci* 129:673-713, 1966
5. Mejía-Laguna JE, García-Cornejo M, López-Soriano F, Biro CE: The role of the sixth component of complement in the rejection of kidney xenografts. *Immunology* 19:767-769, 1970
6. Linn BS, Jensen JA, Portal P, Snyder GB: Renal xenograft prolongation by suppression of natural antibody. *J Surg Res* 8:211-213, 1968
7. Foker JE, Clark DS, Pickering RJ, Good RA, Varco RL: Mechanisms of leucocyte infiltration of allografts. I. The separation and early appearance of two components. *Surgery* 66:42-50, 1969
8. Lindquist RR, Guttman RD, Merrill JP: Renal transplantation in the inbred rat. II. An immuno-histochemical study of acute allograft rejection. *Am J Pathol* 52:531-545, 1968
9. Lindquist RR, Guttman RD, Merrill JP, Dammin GJ: Human renal allografts: interpretation of morphologic and immunohistochemical observations. *Am J Pathol* 53:851-881, 1968
10. Rattazzi L, Haimov MN, Glabman S, Papatestas A, Galen IM, Burrows L: Role of the platelet in the obliterative vascular transplant rejection phenomenon. *Surg Forum* 21:241-242, 1970
11. Cochrane CG, Müller-Eberhard HJ, Aikin BS: Depletion of plasma complement *in vivo* by a protein of cobra venom: its effect on various immunologic reactions. *J Immunol* 105:55-69, 1970
12. Mejía-Laguna JE, Martínez-Palomo A, López-Soriano F, García-Cornejo M, Biro CE: Prolonged survival of kidney xenografts in leukopenic rabbits. *Immunology* 21:879-882, 1971
13. Biro CE: The role of the sixth component of complement in some types of hypersensitivity. *Immunology* 10:563-565, 1966
14. Lowenhaupt R, Nathan P: Platelet accumulation observed by electron microscopy in the early phase of renal allotransplant rejection. *Nature* 220:822-825, 1968
15. Lowenhaupt R, Nathan P: The participation of platelets in the rejection of dog kidney allotransplants: hematologic and electron microscopic studies. *Transplantation Proc* 1:305-310, 1969
16. Movat HZ, Mustard JF, Taichman NS, Uriuhara T: Platelet aggregation and release of ADP, serotonin and histamine associated with phagocytosis of antigen-antibody complexes. *Proc Soc Exp Biol Med* 120:232-237, 1965
17. Nelson DS, Nelson RA Jr: On the mechanisms of immune adherence. *Yale J Biol Med* 31:185-212, 1959

Acknowledgments

We wish to thank Dr. Charles G. Cochrane for his valuable suggestions concerning the role of immune adherence in the hyperacute rejection of kidney grafts. We also wish to thank Dr. Luis Alvarez Balbás for performing the statistical evaluation.

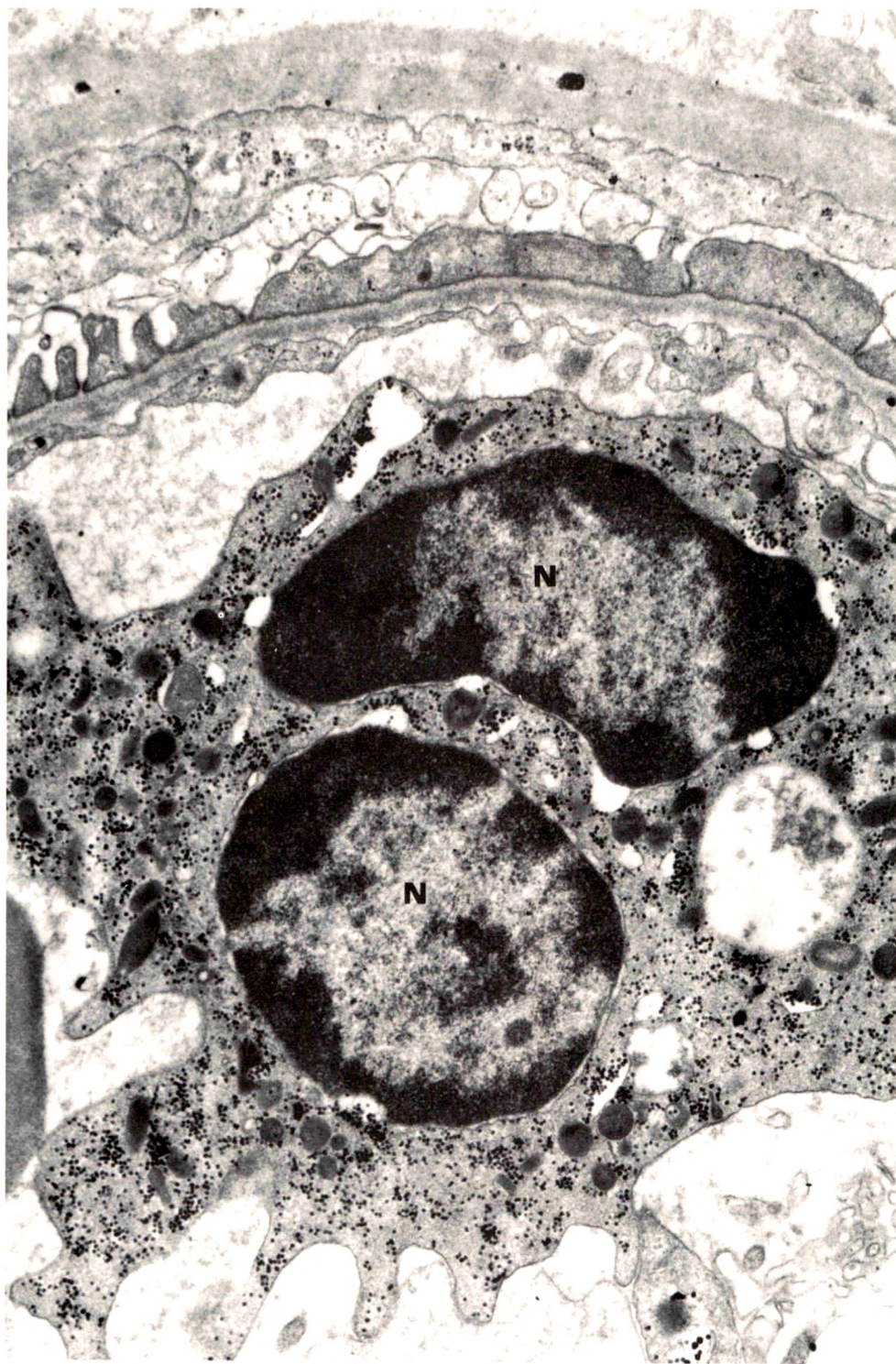
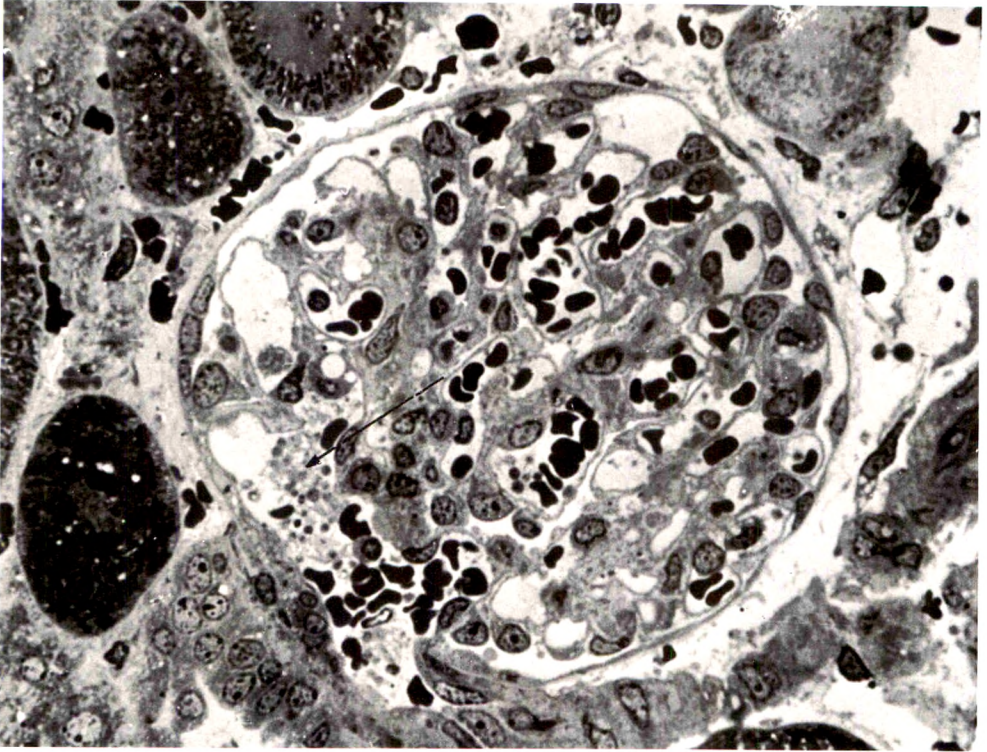


Fig 1—All figures represent sections from biopsy specimens of dog kidneys transplanted to untreated normal rabbits. Peripheral portion from a renal corpuscle showing the presence of a typical PMN within a glomerular loop. Notice the abundant glycogen deposition and the numerous dense cytoplasmic granules. Two nuclear segments are present (N) (uranyl and lead, $\times 21,000$).

2



3

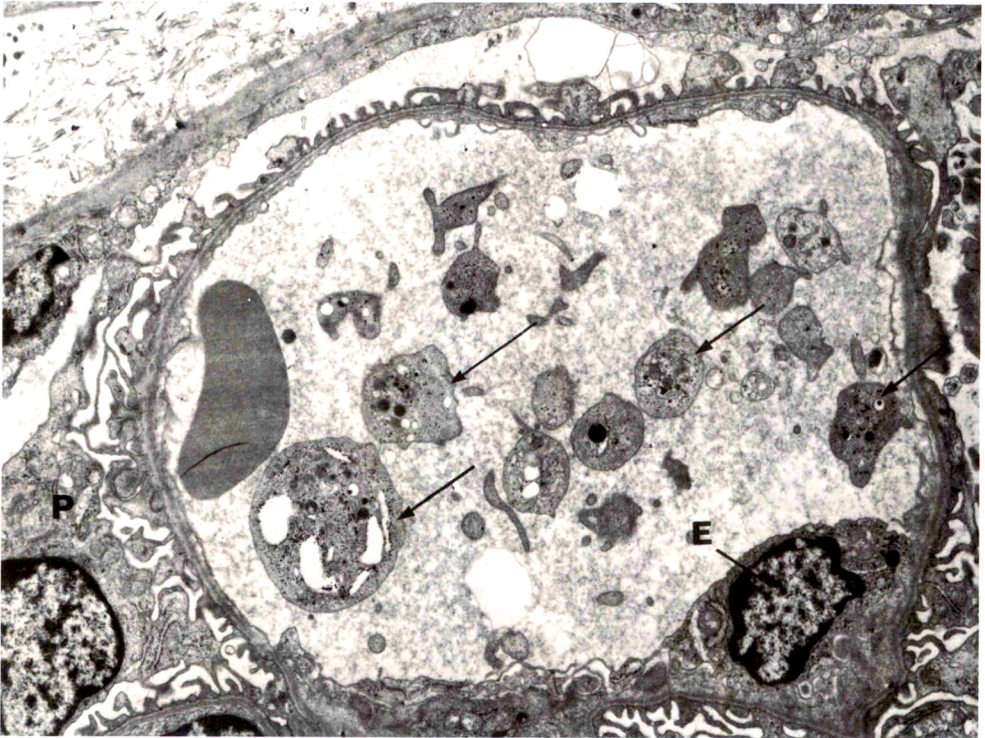


Fig 2—Renal corpuscle from a biopsy specimen taken 30 minutes after the graft was completed. Abundant platelets (arrow) are found within a peripheral glomerular loop (toluidine blue, $\times 1200$). Fig 3—Same material as for Figure 2. The presence of intraglomerular platelets (arrows) is confirmed with the electron microscope. E=endothelial cell; P=podocyte (uranyl acetate and lead, $\times 5000$).

A Comparative Immunohistochemical Study of Splenic Arterial Hyalinosis in Health and Disease

Raj K. Gupta, MD, FCAP, R. Schuster, BS and W. D. Christian, FIMLT

Hyaline deposits in arterioles and arteries of spleen were studied immunohistochemically. Hyaline lesions in arteriosclerotic heart disease were characterized by significant deposits of IgG, IgM, β 1C- β 1A-globulins and β -lipoproteins. These corresponded to histochemically stained deposits of acid mucopolysaccharides and microscopic areas of musculoelastic tissue damage in the hyaline masses. While, in young adults and a few other cases of other diseases, an occasional granular to linear deposit of IgG, IgM, β 1C- β 1A-globulin and β -lipoprotein was noted, no localization of IgA, rabbit antihuman fibrin and rabbit antihuman fibrinogen was seen. A variety of other histochemical staining reactions were found to be negative. These findings suggest that: a) hyaline deposits in splenic arterioles and arteries occur with greater severity in patients with hypertensive and arteriosclerotic heart disease; b) a possible abnormality related to filtration defects in arteries and arterioles, resulting in the trapping of plasma proteins, appears likely; c) increased localization of acid mucopolysaccharides and destruction of musculoelastic tissue is not an uncommon feature in hyaline masses; d) fibrin is not a component of these deposits and e) further study of other organs is necessary to observe the composition of hyaline in arterioles and arteries (Am J Pathol 69:79-88, 1972).

SIMPLE HYALINOSIS primarily affects the arterioles and arteries and may be defined as a degenerative lesion characterized by granular to homogeneous eosinophilic deposits in relation to the intima impinging on the smooth muscle of the media, without inflammation or necrosis of the vessel wall. For many years, the composition of these deposits has been the subject of many studies,¹⁻⁷ yet the exact nature of the hyaline material has not been defined conclusively. This may be attributed, in part, to a lack of organized structural component in this material. Recent studies using electron microscopy have compared these deposits to basement membranes,^{4,5,7} while others have suggested that plasma constituents (plasma proteins) leaking from circulating blood may be responsible for the formation of the deposits.^{1-3,6} Based on immunofluorescent studies and histochemical observations, it has been postulated that the hyaline material is composed of fibrin and γ -globulins.^{2,3,6}

From the Departments of Pathology, The St. Catherines General Hospital, St. Catharines, Ontario, Canada and The State University of New York at Buffalo, School of Medicine, Buffalo, NY.

Accepted for publication May 24, 1972.

Address reprint requests to Dr. Raj K. Gupta, Department of Pathology, The St. Catherines General Hospital, St. Catharines, Ontario, Canada.

Considering that the morphogenesis of arteriolar hyalinosis, despite many studies, remains somewhat controversial, a comparative study in spleens from patients with a variety of common diseases and from healthy subjects was designed with the following objectives in mind: a) study the deposits histochemically, to determine whether they contain significant amounts of amyloid, fibrin, lipids, carbohydrates, proteins and common minerals; b) note whether fluorescein conjugates of rabbit antihuman fibrinogen, immunoglobulins IgG, IgM and IgA, β -lipoproteins and β 1C- β 1A-globulin (complement) were localized in hyaline deposits, and whether these corresponded to histologic or maximal histochemically stainable areas of affinity in vessel walls; c) compare significant differences in the appearances of hyaline material, if any, in healthy subjects and in patients with common disease conditions and d) elucidate if the above findings suggest a possible etio-pathogenetic mechanism to explain the composition of hyaline deposits.

Materials and Methods

Fifty spleens from a selected group of subjects, ranging from 5 hours to 90 years of age, were studied. The spleen was selected because the incidence of hyalinosis in the organ is known to be high. The tissue was collected from autopsies within 4 to 6 hours after death or after an operation. Twenty samples of tissue from the spleens of subjects from birth to 30 years of age (nondiseased group) were included. The cause of death in all these subjects was accidental; there was no anatomic evidence of a disease process. The remaining 30 subjects (diseased group) died during the course of common clinicopathologic illnesses; these included: malignancies in 5; arteriosclerotic heart disease in 5; liver cirrhosis in 4; pneumonias in 5; polycystic disease of the kidneys in 1; obstructive respiratory disease in 5 and cerebrovascular accidents (hypertensive) in 5. Two or three random samples of spleen were collected from each subject.

The tissues were fixed in 10% buffered normal saline for 2 days and processed by a standard technic through an autotechnicon. After the tissues were embedded in paraffin, 5- μ sections were cut and stained with hematoxylin and eosin. For histochemical procedures, each section was studied utilizing procedures described by Gurr⁹ and by Lillie¹⁰ (Table 1).

The immunofluorescent staining procedure was carried out according to the method of Coon and Kaplan⁸ in all 50 spleens selected for study. Fresh samples of splenic tissue were trimmed, then quick-frozen in CO₂ and stored at a temperature between -40 to -60 C. Sections were cut at 5 μ in a Lab Tek cryostat and were air-dried at room temperature for 1 hour after they were mounted on clean glass slides. These were rinsed for 5 to 10 minutes in several changes of phosphate-buffered saline at pH 7.2. Immunofluorescence reagents, labeled with fluorescein isothiocyanate, included antibodies reactive with human IgG, IgA, IgM, β 1C- β 1A-globulin, β -lipoprotein, rabbit antihuman fibrin and rabbit antihuman fibrinogen. These were purchased from Hyland or Hoechst Laboratories and were pretested for monospecific reactivity by immunoelectrophoresis before conjugation with fluorochrome. Tissue sections were covered with a few drops of directly

Table 1—Summary of Histochemical Procedures

Lipids (frozen sections of fresh, unfixed tissue)
Saturated oil red O in isopropanol (neutral lipids)
Sudan black B saturated in 90% ethanol (acid lipids)
Nile blue sulfate (acid and neutral lipids)
Luxol fast blue in 95% ethanol
Carbohydrates (paraffin-embedded sections)
Periodic acid-Schiff (PAS) reaction with and without digestion (diastase, sialadase and hyaluronidase)
Alcian blue (AB) at pH 2.5
Hale's colloidal iron
Proteins (frozen sections of fresh, unfixed tissue)
Tyrosine (Millon reaction)
Dihydrodinaphthylidissulfide method (Barnett-Seligmann reaction)
Miscellaneous (paraffin-embedded sections)
Elastic tissue stain (Weigert and Verhoff's methods)
Phosphotungstic-acid-hematoxylin stain (Bohacek and Gupta's modification) ¹¹
Masson's trichrome stain
Congo red, toluidine blue method (using cross polarization technic) ¹² and thioflavin T stain (amyloid)
Alizarin S stain
Perl's iron stain
Picro Mallory's stain (fibrin)

applied, fluorescent-labeled antibodies, incubated in a moisture chamber for 45 to 60 minutes at room temperature, washed 3 to 4 times in phosphate-buffered saline (10 minutes each) and, after brief drying, were coverslipped with buffered glycerol. Immunofluorescence in tissue sections was immediately studied and photographed using a Leitz microscope equipped with a Leicaflex camera, and HBO Osram mercury vapor light source, a 2 mm BG12 exciter filter and a 510 μ barrier filter.

Ten control sections of spleen were stained and: a) reacted with fluorescein-labeled antisera from which γ -globulin had been precipitated; b) reacted with conjugated serum of unrelated specificity; c) treated with labeled antibodies absorbed with specific antigens or treated with unlabeled antiserum first and then with respective labeled antibodies, to demonstrate specific inhibition.

Results

Light Microscopy

In this study, uniform homogeneous deposits of hyaline material were noted in the wall and subendothelial spaces in 90% of the arteries and arterioles of the 10 subjects with arteriosclerotic heart disease and cerebrovascular accidents with hypertension, using hematoxylin and eosin (Figure 1). Twelve of the total 20 subjects with malignancies, portal cirrhosis, pneumonias, polycystic disease of the kidneys and chronic obstructive respiratory diseases (including emphysema) had coexistent arteriosclerotic heart disease. In these 12 subjects, the hy-

aline appeared to be comparable to that seen in the 10 subjects with arteriosclerotic heart disease and cerebrovascular accidents with hypertension, using the hematoxylin and eosin staining technic. In the remaining 8 subjects, no evidence of appreciable arteriosclerotic heart disease was found; only focal, hematoxylin and eosin-stained, interrupted deposits, suggestive of hyaline-like material, were noted in the wall and subendothelial spaces of approximately 20% of the arterioles and arteries of the spleens. Similar, granular, hyaline-like material was seen in an occasional vessel in the 20 subjects of the nondiseased group. Using periodic acid-Schiff, Alcian blue (pH 2.5) and Hale's colloidal iron stains, the hematoxylin and eosin-stained material from the 20 subjects with arteriosclerotic heart disease and hypertension (of the 30 in the diseased group) had a selective, uniform-staining affinity for acid mucopolysaccharides in the walls and subendothelial space, corresponding to the hematoxylin and eosin-stained deposits. In these 20 subjects, digestion with hyaluronidase failed to abolish the selective, periodic acid-Schiff-staining reactivity in the hyaline masses, indicating that hyaluronic acid was not a component of the acid mucopolysaccharides in the hyaline masses. In these subjects, digestion with diastase and sialadase had no effect on the hyaline material, suggesting an absence of other substances, such as sialomucins, in the hyaline deposits. Abnormal histochemical staining reactions to the above technics were not observed in the remaining 30 of the 50 subjects.

Use of elastic tissue stains showed that elastic tissue was fragmented and the appearance of microscopic areas of hyaline deposits was distorted in all 22 subjects with arteriosclerotic heart disease and hypertension (of the 30 in the diseased group). Plain muscle in Masson's trichrome-stained splenic tissue samples from these same subjects appeared smudged, and preserved muscle components in the walls of vessels in areas of hyaline deposits were lost. This finding, therefore, might be considered an indication of musculoelastic tissue destruction in areas of abnormal hyaline deposits. In the remaining 8 subjects from the above group, and in 20 subjects from the nondiseased group, use of elastic tissue stain and Masson's trichrome revealed no significant alteration in the musculoelastic components. Stains for proteins, fibrins, amyloid, fat and other miscellaneous histochemical reactions, listed in Table 1, were consistently negative in all 50 subjects of this study.

Immunofluorescence

The conjugates of IgG, IgM, β 1C- β 1A-globulin (complement) and β -lipoprotein were distinctly localized as lumpy, diffuse to somewhat

interrupted deposits in the walls and subendothelial space of arteries and arterioles in all 22 subjects with arteriosclerotic heart disease and hypertension, with or without other diseases. These deposits correspond to those areas in which histochemical evidence suggested that the hyaline material was somewhat like acid mucopolysaccharides (Figures 2-5). In all these deposits, IgA, rabbit antihuman fibrin and rabbit antihuman fibrinogen were absent (Figures 6 and 7). Conjugates of IgG, IgM, complement and β -lipoprotein were localized as nonspecific, linear to somewhat streak-like deposits in the wall and subendothelial spaces in 4 of the 8 subjects in the diseased group without arteriosclerotic heart disease (Figure 8), while IgA, rabbit antihuman fibrin and rabbit antihuman fibrinogen were not localized. No conjugates were localized in 10 of the 20 spleens from subjects in the nondiseased group that were from newborn to 15 years of age. In the remaining 10 subjects of the nondiseased group that were from 16 to 30 years of age, no IgA, rabbit antihuman fibrin or rabbit antihuman fibrinogen was found, although an occasional nonspecific, finely granular to linear pattern of IgG, IgM complement and β -lipoprotein was noted in the wall and subendothelial space. In all 50 subjects, autofluorescence was constantly seen at the endothelial lining and at the adventitia (comparable to that of unstained frozen sections of spleen). However, no true fluorescence was noted in these components. Control sections of spleens in all cases were negative for specific fluorescence.

Discussion

In this study, the presence of conjugates of IgG, IgM, β 1C- β 1A-globulins and β -lipoprotein suggests that the hyaline deposits in arteriosclerotic heart disease and hypertensive disease may be composed of plasma proteins. To some extent, it also seems to support previous studies,^{1,7} although the hypothesis that plasma components are the only source of this material, which possibly filters abnormally through the walls of arteries and arterioles, is not proven. It seems likely that these filtered plasma proteins are trapped in increasing amounts in the hyaline masses and become visible by immunofluorescence as demonstrable immunoglobulins and β -lipoprotein. However, it is of interest to note that in these hyaline deposits there was no histochemical evidence of proteins or lipids to suggest that these deposits contained tyrosine, SS and SH groups or any form of acidic, neutral or complex lipids. IgA, rabbit antihuman fibrin and rabbit antihuman fibrinogen were absent, and histochemical staining for fibrin was negative. This miti-

gated the fibrin composition theory of hyaline masses advanced by other workers.^{3,4}

Using elastic tissue stains and Masson's trichrome stain, the appearance of these components in the hyaline masses was altered in all cases of arteriosclerotic heart disease and hypertensive disease. The elastic tissue appeared fragmented, while the muscle appeared to show a smudging effect in the hyaline areas. The hyaline deposits stained intensely for acid mucopolysaccharides, suggesting that hyaluronic acid may be one of the components. The conjugates of IgG, IgM, β 1C- β 1A-globulin and β -lipoprotein were preferentially localized in these deposits and corresponded to histochemical areas of acid mucopolysaccharide affinity in all cases of arteriosclerotic heart disease and hypertensive disease. The remaining spleens from subjects in the diseased group without arteriosclerotic heart disease or hypertensive disease and from the nondiseased group showed no abnormal immunofluorescent or histochemical changes in the vessels. These results, therefore, seem to differ from those of previous workers, who showed γ -globulins and fibrin as the main constituents of hyaline deposits.^{3,4} Our results also suggest that the hyaline deposits occur with greater severity in arteriosclerotic heart disease and hypertensive disease; it is in these cases that immunofluorescence and histochemistry show demonstrable alterations. It may, therefore, seem likely that the composition of hyaline deposits in these cases can be based on an abnormality related to filtered and trapped plasma proteins in the wall and subendothelial spaces of vessels. These hyaline masses may originate from filtered and trapped plasma constituents, or from some other mechanism, but it seems likely that the altered musculoelastic tissue and its destruction in areas of hyaline, combined with an altered physicochemical status of acid mucopolysaccharides, may also have some role, through an unknown stimulus, resulting in abnormal accumulations of hyaline material, especially in arteriosclerotic heart disease and hypertensive disease. A further study of arteries and arterioles of other organs, for example, in arteriosclerotic heart disease and hypertension, may give some of these answers if similar changes can be demonstrated.

The exact reason for the presence of hematoxylin and eosin-stained, linear to interrupted hyaline-like deposits in some of our subjects from the diseased and nondiseased groups is not clear. Immunofluorescent and histochemical study in these subjects did not show specific staining of the hyaline-like substance comparable to that seen in subjects with arteriosclerotic heart disease. It may, therefore, appear that the composition of the hematoxylin and eosin-stained hyaline-like material, in

some of these specimens, probably may be different or the composition of the vessel wall may be different in different pathologic states and in health, as compared to arteriosclerotic heart disease and hypertensive disease. This observation, in our opinion, needs to be evaluated comparatively in the arteries and arterioles of other organs.

References

1. Biava SG, Dydra I, Genest J, Bencosme A: Renal hyaline arteriosclerosis: an electron microscopic study. *Am J Pathol* 44:349-363, 1964
2. Crawford T, Woolf N: Hyaline arteriosclerosis of spleen: an immunohistochemical study. *J Pathol Bacteriol* 79:221-225, 1960
3. Kuhns JC, Puchtler H, Sweat F: Histochemical evidence of plasma proteins in arteriosclerosis. *Anat Rec* 142:250, 1962
4. McGee WG, Ashworth CT: Fine structure in chronic hypertensive arteriopathy in the human kidney. *Am J Pathol* 43:273-291, 1957
5. Montgomery PO, Muirhead EE: A differentiation of certain types of fibrinoid and hyaline. *Am J Pathol* 43:273-299, 1963
6. Montgomery PO, Muirhead EE: A characterization of hyaline arteriolar sclerosis by histochemical procedures. *Am J Pathol* 30:521-531, 1954
7. Weiner J, Spiro D, Lattes RJ: The cellular pathology of experimental hypertension. II. Arteriolar hyalinosis and fibrinoid change. *Am J Pathol* 47:457-458, 1965
8. Coons AH, Kaplan MH: Localization of antigen in tissue cells: a method for detection of antigen by fluorescent antibody. *J Exp Med* 91:1-13, 1960
9. Gurr GT: *Biological Staining Methods*, Seventh edition. London, George T. Gurr, Ltd, 1963
10. Lillie RD: *Histopathologic Technique and Practical Histochemistry*. New York, McGraw Hill Book Company, Blakiston Division, 1954
11. Bohacek L, Gupta RK: A simplified Mallory's phosphotungstic acid-hematoxylin stain. *Can J Med Tech* Aug 1967, pp 135-137
12. Wolman M: Amyloid: its nature and molecular structure. Comparison of a new toluidine blue polarized light method with traditional procedures. *Lab Invest* 25:104, 1971
13. Burkholder PM: Malignant nephrosclerosis. *Arch Pathol* 80:583-589, 1965

Acknowledgments

The authors gratefully acknowledge the help of Drs. Stanley Cohen and Lorne Whitaker for their critical review of the manuscript. The typing and secretarial assistance of Miss Nadia Besruky is also acknowledged.

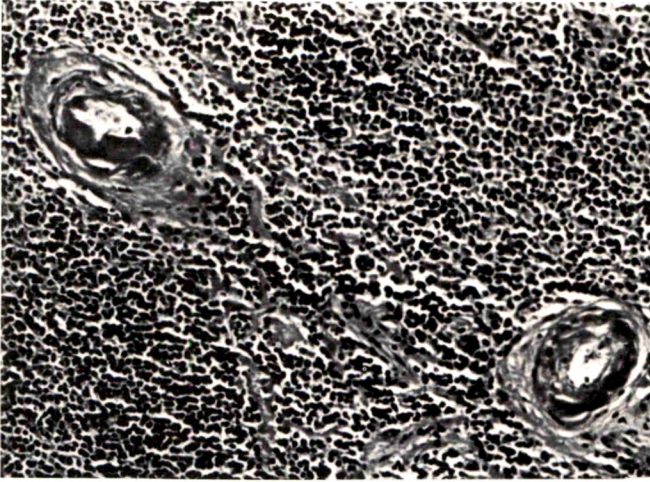
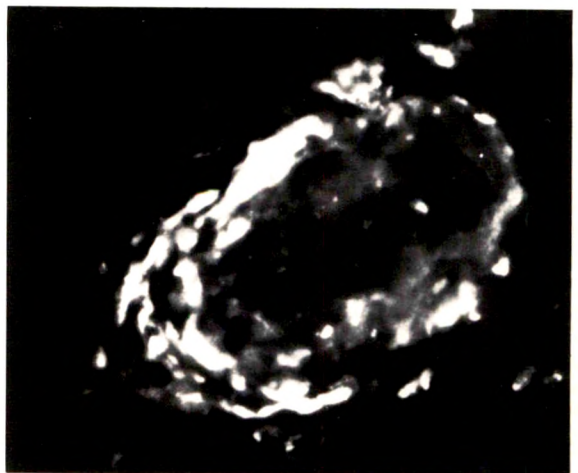
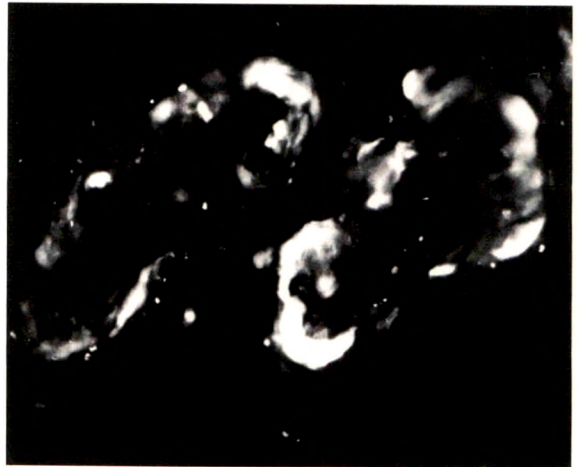
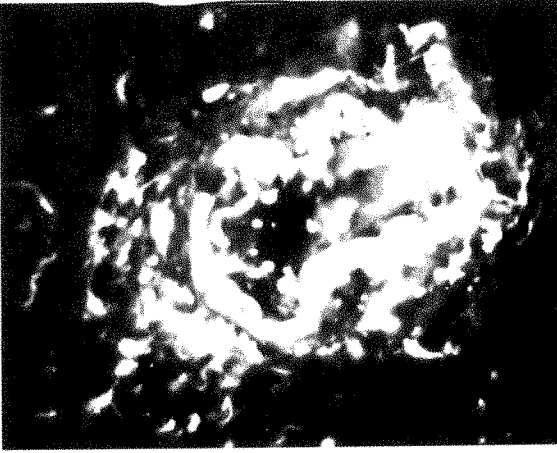


Fig 1—Section of spleen from a 58-year-old male with arteriosclerotic heart disease, showing hyaline deposits in follicular arteries of the spleen (H&E, $\times 250$). Fig 2—Frozen section of spleen from an 80-year-old male with arteriosclerotic heart disease, showing diffuse deposits of IgG in a follicular artery of the spleen ($\times 250$). Fig 3—Spleen from a 65-year-old male with arteriosclerotic heart disease and hypertension, showing interrupted to lumpy deposits of the conjugate of IgM in a splenic artery ($\times 400$). Fig 4—The distribution of immunofluorescent deposits of $\beta 1C$ - $\beta 1A$ -globulin deposits were similar to those seen in Figure 3 ($\times 400$).



5



6



7

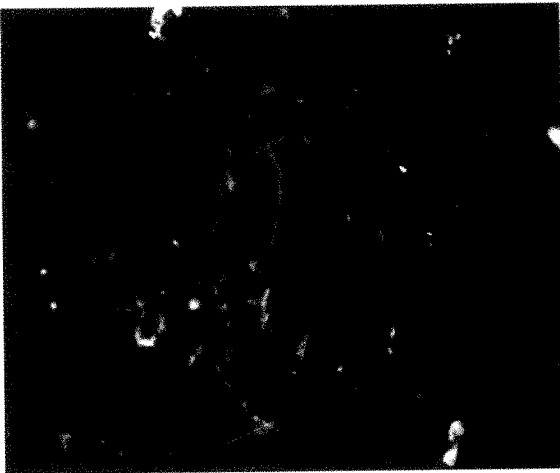


Fig 5—Section of spleen from a 90-year-old female with arteriosclerotic heart disease, showing diffuse immunofluorescent deposits of β -lipoprotein in a splenic artery ($\times 450$). **Fig 6**—Spleen from a 55-year-old male with arteriosclerotic heart disease and hypertension, showing the absence of the conjugate of IgA in a follicular artery ($\times 250$). **Fig 7**—Another section of spleen from a female subject with arteriosclerotic heart disease, showing the absence of rabbit antihuman fibrin ($\times 400$). **Fig 8**—Section of spleen from a 72-year-old male with malignancy but without arteriosclerotic heart disease or hypertension, showing immunofluorescent trace deposits and linear streaks of IgG in a splenic artery ($\times 450$).



Developing Elastic Tissue

An Electron Microscopic Study

Ernest N. Albert, PhD

Electron microscopic identification of elastic tissue in normal and disease states has been uncertain due to the lack of a specific electron-dense stain. Recently we introduced a silver porphyrin electron microscopic stain (silver tetraphenylporphine sulfonate) for the identification of adult elastic tissue. This stain has now been employed to study the development of elastic tissue with the aim that new and old elastica can be differentiated at the electron microscopic level. Present observations showed that developing elastica consisted of two distinct morphologic components. Each portion exhibited different staining properties with the silver porphyrin and lead citrate. One component was fibrous and the other amorphous. The fibrous component stained with lead citrate while the amorphous stained with the silver porphyrin. The fibrous component was the first to appear; the amorphous portion appeared later in development and was formed within the fibrous matrix. Mature elastic tissue was devoid of the fibrous component. Based upon the morphologic appearance and staining properties, one can now differentiate between newly formed elastic tissue and the existing one in various disease states (Am J Pathol 69:89-102, 1972).

ELASTIC TISSUE is an important functional component of the cardiovascular system. Damage to the intimal vascular connective tissue is often associated with formation of new *fibroelastic* tissue. Similar problems of elastic proliferation, condensation and hyalinization exist in conditions of hypertension, lupus erythematosus, generalized scleroderma, atherosclerosis and pregnancy. Reviews on the involvement of elastic tissue in these diseases are treated in detail by Page.^{1,2}

In order to understand ultrastructural changes in elastic tissue during various diseases, it is essential that the normal ultrastructural morphology of adult and developing elastic tissue be known. Several investigators³⁻⁵ have pointed out that isolated elastica has a fibrillar and an amorphous component. Similar fibrillar components of elastica have been observed *in vivo* in blood vessels,⁶⁻⁹ in skin,¹⁰ in lung¹¹⁻¹³ and an ligamentum nuchae.^{14,15} However, Cox and Little¹⁶ report that no fibrillar com-

From the Department of Anatomy, The George Washington University, School of Medicine, Washington, DC.

Supported by Grant HL 12557 from the National Institutes of Health and the Washington Heart Association.

Accepted for publication June 13, 1972.

Address reprint requests to Dr. Ernest N. Albert, Department of Anatomy, The George Washington University, School of Medicine, Washington, DC 20005.

ponents of elastica were observed in any of the above tissues. The specific identification of elastic tissue has been further complicated because of the lack of satisfactory electron microscopic stains.

Phosphotungstic acid and osmium tetroxide are the most frequently used stains for elastica; however, neither imparts a consistent density to elastica. Haust¹⁷ states that elastic tissue elements have variable and inconsistent staining qualities, even in the same block of tissue. This author and several other investigators have had similar experiences with elastic tissue staining. This inconsistency makes the identification of newly formed elastica from degenerating or old elastic tissue difficult and at times impossible.

Since the morphologic criteria for elastic tissue are not completely established and no satisfactory electron microscopic stains for its identification were available, we decided to develop a specific marker for electron microscopic observation of elastic tissue. Subsequently, a metallic porphyrin, silver tetraphenylporphine sulfonate was synthesized in our laboratory and used as a specific electron-dense stain for elastic tissue.^{18,19} Nonmetallic tetraphenylporphine sulfonate imparts specific red fluorescence to elastic tissue. The silver porphyrin was employed in this investigation to study the sequence of elastogenesis in fetal rat aorta.

It is the purpose of this report to: a) establish the specific morphology of developing and adult elastic tissue using silver tetraphenylporphine sulfonate in conjunction with uranyl acetate and lead citrate, and b) gain some understanding about the staining properties of newly forming and mature elastic tissue. Information thus obtained will also allow investigators to distinguish between old and newly formed elastica during repair.

Materials and Methods

Pregnant rats were anesthetized and the fetuses were removed from the uterus between the fourth and eighteenth day of gestation. The fetuses were decapitated and the thoracic cavity opened. Four percent ice cold glutaraldehyde in .2 M phosphate buffer was gently placed in the thoracic cavity with a Pasteur pipette to initially fix the aortic tissue. After 5 minutes the fetal aortas were dissected out and further fixed in fresh 4% glutaraldehyde in phosphate buffer for 2 hours. The tissues were then washed in the phosphate buffer and postfixed in 4% osmium tetroxide for an additional 2 hours. The aortae were again washed with phosphate buffer and dehydrated in an ascending series of ethanol. They were then flat-embedded in Epon 812. This embedding procedure was desirable, since one could easily orient the blocks for obtaining cross or longitudinal sections of the aortae. The thoracic aorta of the pregnant mother was also fixed and removed in the same manner as the fetal portion. Sections were cut and divided in three groups for staining: Group I—stained with uranyl acetate and/or lead citrate; Group II—stained with 10 percent silver tetraphenylporphine sulfonate for forty-five minutes;¹⁹ and Group III—grids

were first stained with 10% silver tetraphenylporphine sulfonate as in Group II and then counterstained with uranyl acetate and lead citrate. The silver tetraphenylporphine sulfonate was synthesized in our laboratory. The details of the synthetic process have been published previously.¹⁹

Results

Staining with Uranyl Acetate and Lead Citrate

It appeared that the formation of elastic lamellae in aorta generally occurred in three stages. However, this was a continual process and there was considerable overlap in the various stages of development.

First Stage. This stage lasted from the fourth to the ninth day of gestation. Initially, a filamentous material appeared in the extracellular spaces around cells of the aortic wall. This filamentous material was clearly visible in 6-day-old fetal aortae (Figure 1) and stained positively with uranyl acetate. They appeared more dense when stained with lead citrate, however; a much stronger reaction occurred when both uranyl and lead stains were employed together.

During the latter part of this stage one could usually discern small amorphous areas (*loci*) scattered amongst the filaments. These homogeneous areas were first recognized in the aorta of 6-day-old fetuses. By the ninth day, several small amorphous *loci* could be seen. These *loci* were often difficult to identify with certainty at lower magnifications but were easily discernible at higher magnifications (Figure 2). However, these amorphous areas were easily identifiable, even at very low magnifications, when the porphyrin stain was used (Figure 8).

Second Stage. This stage was most prominent between the tenth and fourteenth days of gestation. During this stage there was a general increase in the number and size of the pale-staining areas. These pale homogeneous *loci* appeared to be surrounded by filaments (Figure 3). Higher magnification showed that the homogeneous *loci* and the filaments were intimately associated with each other and thus appeared as one continuous structure (Figure 4). Henceforth, the amorphous *loci* and the peripheral filamentous structures will be referred to as the *elastic units*. The central amorphous area of the elastic unit demonstrated no affinity for uranyl and/or lead stains, but the peripheral fibrous structure stained with uranyl and lead (Figures 3, 4).

Third Stage. During the fourteenth through the eighteenth day of gestation the elastic units continued to increase in size and number. They coalesced with adjacent dense units to form larger masses of elastic tissue and lamellae (Figure 5). As the elastic units increased in size and formed bands and lamellae, there was a concomitant decrease in the filamentous structures. Some of the filaments appeared to be

incorporated in the homogeneous matrix (Figure 5). A thin layer of filaments usually remained at the periphery of the elastic bands.

Staining with Tetraphenylporphine Sulfonate Only

When various stages of developing aorta were stained with silver tetraphenylporphine sulfonate only, the central amorphous areas of elastic units exhibited a strong positive reaction (Figure 6). The peripheral fibrillar structures did not demonstrate any specific affinity for this stain. During the early stages of development, small electron-dense homogeneous loci were scattered throughout the extracellular spaces of the aortic wall. As the gestational age increased, more and more of the dark staining loci could be recognized. Some of the loci were seen to coalesce with adjoining electron-dense centers and began to form bands of elastic tissue (Figure 7). During maturation, no filamentous structures stained with the metallic porphyrin.

Staining with Silver Tetraphenylporphine Sulfonate, Uranyl Acetate and Lead Citrate

When the various developmental stages of elastic tissue described above were first stained with the metallic porphyrin and then with uranyl and lead, electron-dense homogeneous loci were clearly visible along with the peripheral filamentous structures (Figure 8). These electron-dense areas always appeared in intimate contact with the grey filamentous microfibrils. The dark-staining central loci were interpreted as the structures that appeared unstained with uranyl and lead (compare Figure 8 with Figure 2).

During the early stages of development, few elastic units were observed in the extracellular spaces (Figures 6, 8). In the later gestational stages, greater numbers of electron-dense loci could be seen individually, while others appeared to coalesce with adjacent units (Figures 7, 9). Eventually, most of the elastic units coalesced to form elastic bands (Figure 10). The electron-dense homogeneous areas became larger and the fibrillar components decreased in amount and appeared to be either absent or restricted to the periphery of elastic lamellae as a thin layer (Figure 10).

Very few collagenous fibers were identifiable during the early stages of elastogenesis. However, greater numbers became apparent with increased gestational age. It also appeared that collagenous fibers were closely related to the microfibrils that were associated with elastic units.

Discussion

The observations have established some basic morphologic and staining criteria for the identification of newly formed elastic tissue.

It is reasonable to suggest that the earliest form of recognizable elastin or its precursor is a fibrillar structure. Later in development, the conventional morphology of elastic tissue begins to manifest itself in the form of amorphous loci embedded within the fibrillar mass. As maturation of elastic tissue progresses, the amount of amorphous material increases and the fibrillar material decreases. Thus, one could speculate and suggest that mature elastic tissue is formed from a recognizable fibrillar precursor. This fibrillar precursor probably plays the following role in the formation of adult elastin: a) The fibrils become cross-linked and, as a result, lose their fibrous structure and appear as homogeneous masses which continue to enlarge in size until most or all of the fibrils are cross-linked. b) Some other amorphous substance begins to accumulate in the fibrillar matrix and masks the fibrous structure. This could be a protein-polysaccharide complex.

Others have also reported that the microfibrils were the first structures to appear in elastogenesis.^{15,20} This study has clearly shown that fibrillar components are only one part of the developing elastic tissue; the major portion of mature elastica is the amorphous component. However, some authors have expressed the view that only the fibrillar component constitutes the elastic tissue.²¹

The staining properties of the two components were entirely different. The peripheral microfibrils exhibited the greatest contrast when stained with both uranyl acetate and lead citrate. The central amorphous component of elastic units showed no affinity for either the uranyl acetate or lead citrate stains, or both stains employed together.

When developing elastica was stained with silver tetraphenylporphyrine sulfonate only, the central amorphous component of the elastic units showed a positive reaction. Further, the application of all three stains together resulted in a combined staining reaction of the metallic porphyrin, uranyl and lead—*ie*, both the peripheral fibrils and the central amorphous portion were stained. It may, therefore, be concluded that the fibrillar structures stain with the uranyl and lead, while the amorphous portion stains with the metallic porphyrin. Based upon the staining properties of the fibrillar and amorphous components, it can be assumed that the two morphologic components are chemically different.

It can also be stated that the newly formed elastic tissue consists of two readily distinguishable, distinct components (amorphous and fibrous). On the other hand, mature elastic tissue is almost exclusively formed of the amorphous component. It is proposed that the staining of elastic tissue with the porphyrin and uranyl and lead stains will en-

able qualitative and quantitative differentiation between newly formed and old elastin during disease and repair processes.

References

1. Page IH (Editor). Symposium on Atherosclerosis. National Academy of Science-National Research Council Publications 338:3, 1954
2. Page IH: Connective Tissue, Thrombosis and Atherosclerosis. New York, Academic Press, Inc, 1959
3. Partridge SM: Elastin. *Adv Protein Chem* 17:227, 1962
4. Gotte L, Serafini-Fracassini A, Moret V: The chemical composition of the NaCl soluble fraction from autoclaved elastin. *J Atheroscler Res* 3:244, 1963
5. Hall DA, Keech MK, Reed R, Saxl H, Tunbridge RE, Wood MJ: Collagen and elastin in connective tissue. *J Gerontol* 10:388, 1955
6. Haust MD, More RH, Bencosme SA, Balis JV: Elastogenesis in human aorta: an electron microscopic study. *Exp Mol Pathol* 4:508, 1965
7. Jensen JG: An electron microscopic study on the morphology of the elastin in foetal, human aorta. *Acta Pathol Microbiol Scand* 56:388, 1962
8. Karrer HE: Electron microscope study of developing chick embryo aorta. *J Ultrastruct Res* 4:420, 1960
9. Parker F: An electron microscope study of coronary arteries. *Am J Anat* 103:247, 1958
10. Banfield WG, Brindley DC: Preliminary observations on senile elastosis using the electron microscope. *J Invest Derm* 41:9, 1963
11. Karrer HE: The fine structure of connective tissue in the tunica propria of bronchioles. *J Ultrastruct Res* 2:96, 1958
12. Low FN: Microfibrils: fine filamentous components of the tissue space. *Anat Rec* 142:131, 1962
13. Rhodin J, Dalhamn T: Electron microscopy of collagen and elastin in lamina propria of the tracheal mucosa of rat. *Exp Cell Res* 9:371, 1955
14. Usuku G: Electron microscopical studies on the ultrastructure of the elastic fiber. I. Electron microscopical observation of bovine ligamentum nucae in ultrathin sections after potassium permanganate fixation. *Kumamoto Med J* 11:84, 1958
15. Greenlee TK, Ross R, Hartman JC: The fine structure of elastic fibers. *J Cell Biol* 30:59, 1966
16. Cox RC, Little K: An electron microscope study of elastic tissue. *Proc R Soc Lond (Series B)* 155:232, 1961
17. Haust MD, More RH: Electron microscopy of connective tissue and elastogenesis, *The Connective Tissue*. Edited by D Smith. Wagner, B. Baltimore, The Williams and Wilkins Co, 1967, p 352
18. Albert EN: A new electron dense stain for elastin. *Proceedings of the Twenty-seventh Annual Meeting of The Electron Microscopy Society of America*, 1969, p. 414
19. Albert EN, Fleischer E: A new electron dense stain for elastic tissue. *J Histochem Cytochem* 18:697, 1970
20. Fahrenbach WH, Sanberg LB, Cleary EG: Ultrastructural studies on early elastogenesis. *Anat Rec* 155:563, 1966
21. Bierring F, Kobayasi T: Electron microscopy of the normal rabbit aorta. *Acta Pathol Microbiol Scand* 57:154, 1963

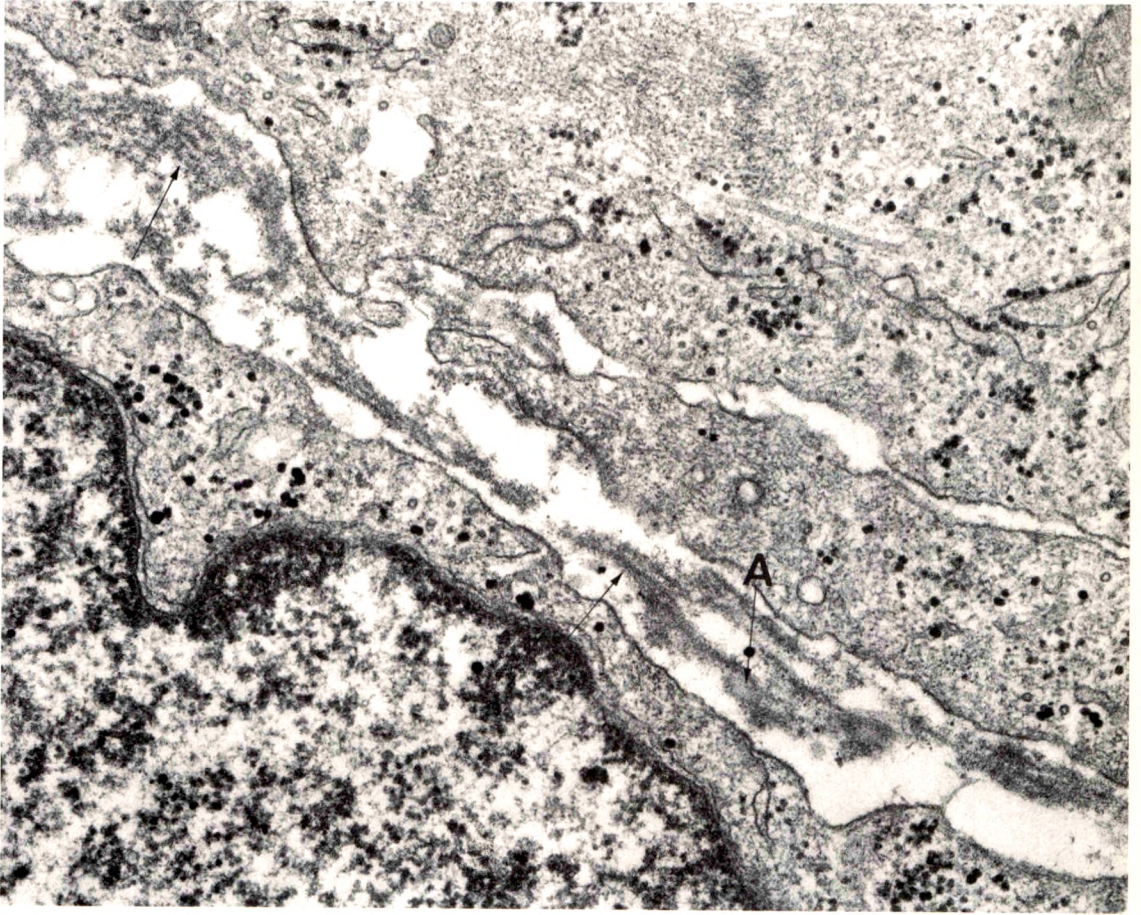


Fig 1—Shows portions of two maturing smooth muscle cells from 6-day fetal aorta. The first recognizable structures in the extracellular space are filamentous bundles (*arrows*). A few amorphous loci (*A*) can be recognized amongst the filamentous material.

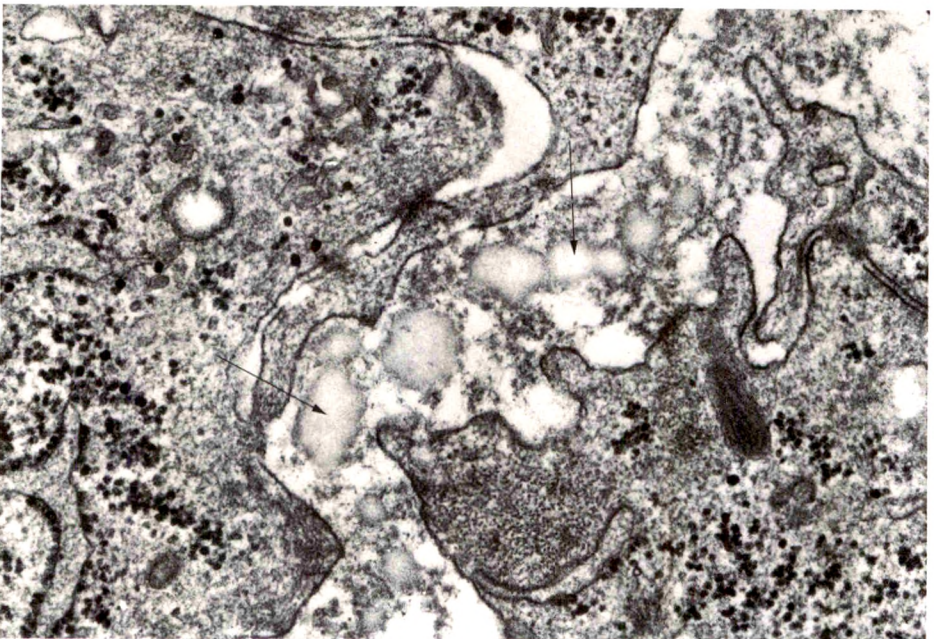


Fig 2—Micrograph from a 9-day fetal aorta. Several small and larger amorphous loci (arrows) can be recognized in the extracellular space (uranyl and lead).

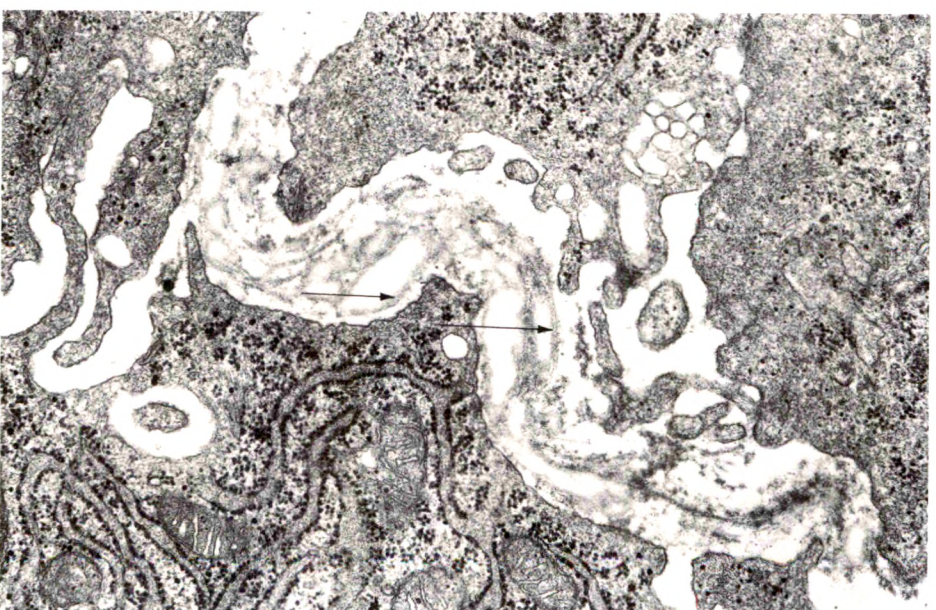
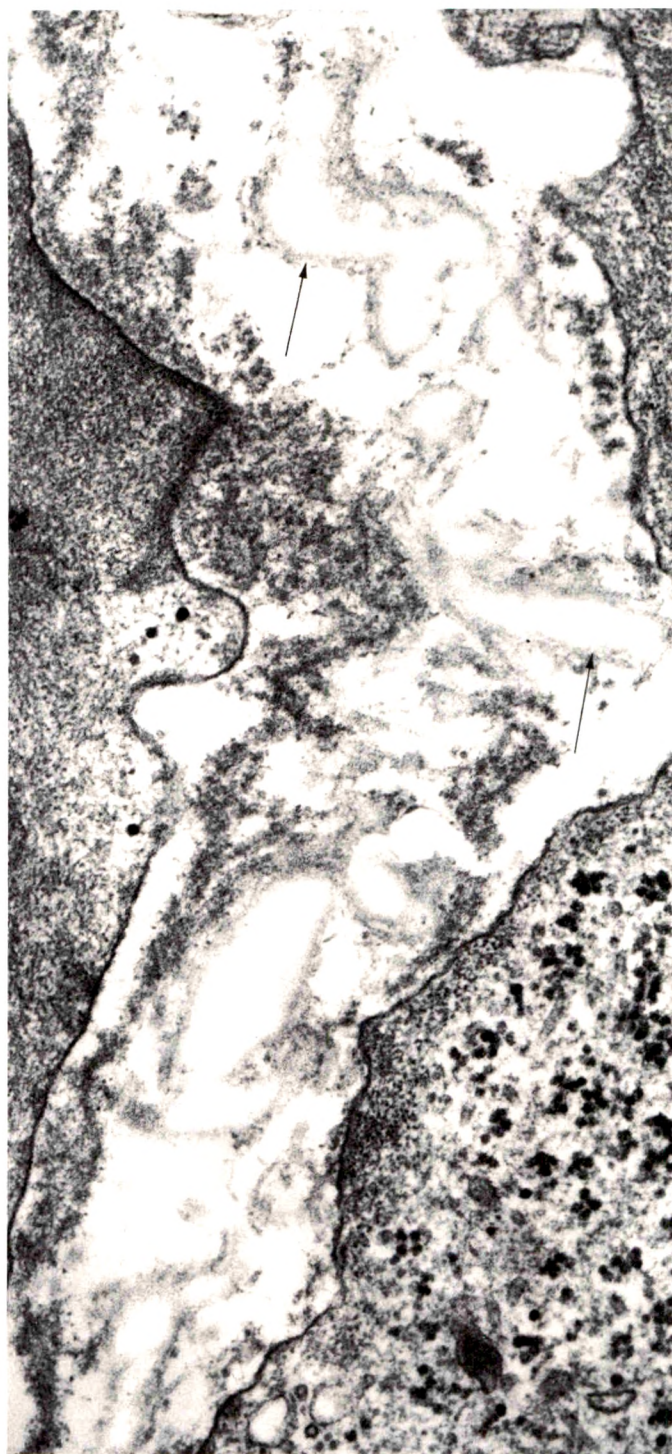


Fig 3—Portion of 11-day fetal aorta. Notice the fibrillar mantle around the amorphous loci (arrows) (uranyl and lead).

Fig 4 — Higher magnification demonstrating that there is no distinct separation between the filamentous and the amorphous portions of the elastic unit (*arrows*). The two areas blend in with each other (uranyl and lead).



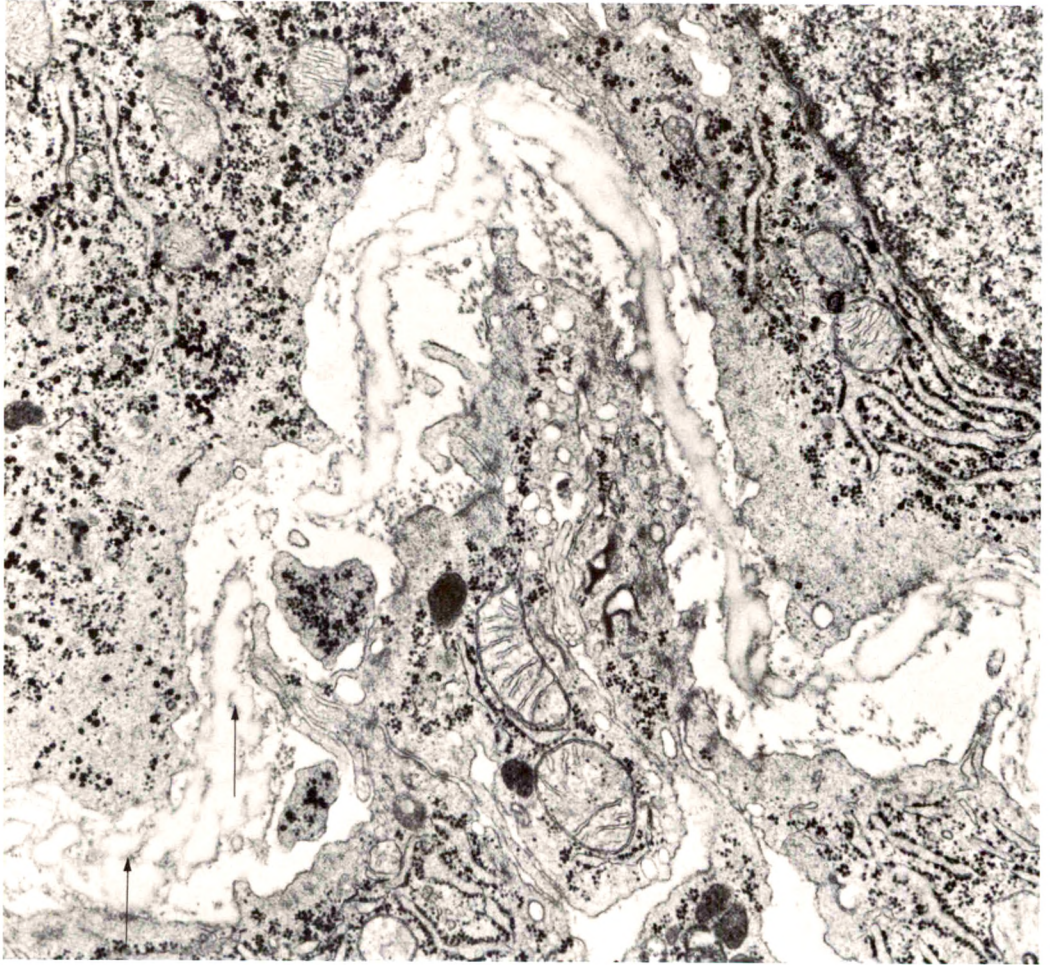


Fig 5—Portion of an 18-day fetal aorta. Notice that elastic lamellae are partially formed. Evidence of smaller elastic units coalescing to form larger bands. Some filaments appear to be trapped in the larger elastic masses (arrows) (uranyl and lead).

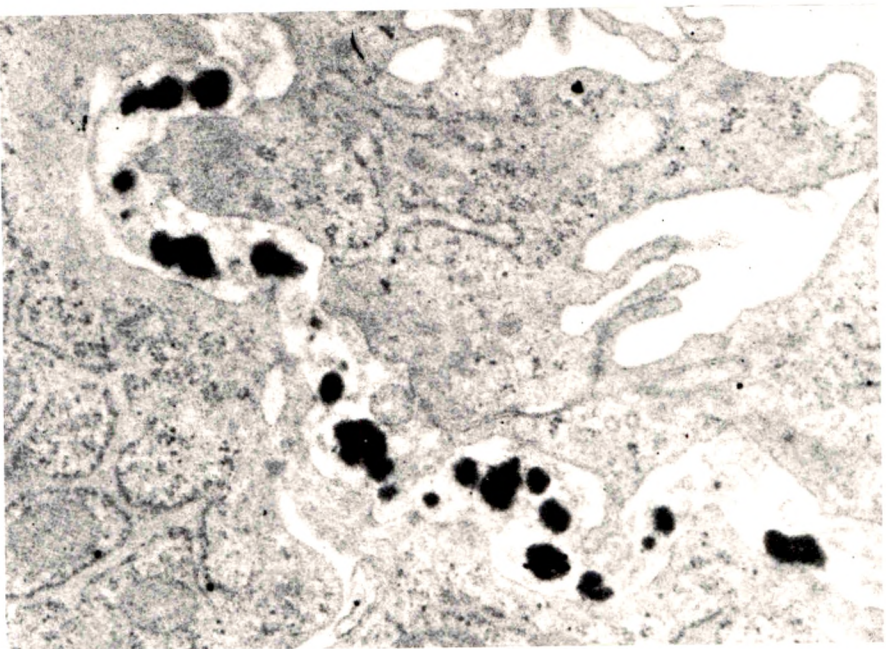


Fig 6—Notice the specific dense staining of amorphous structures in the extracellular space. There is a general background stain also (MetPPS only).

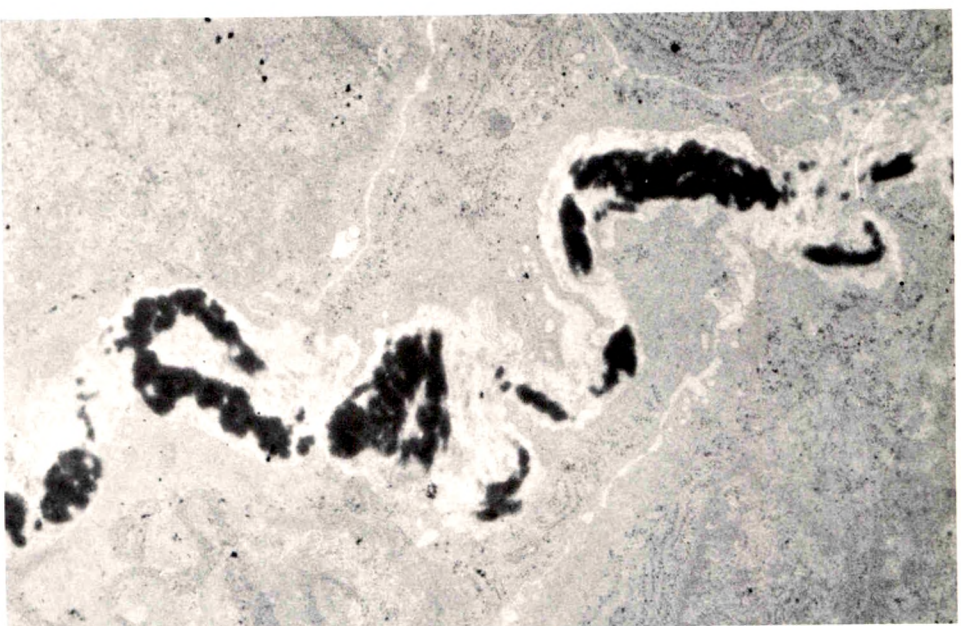
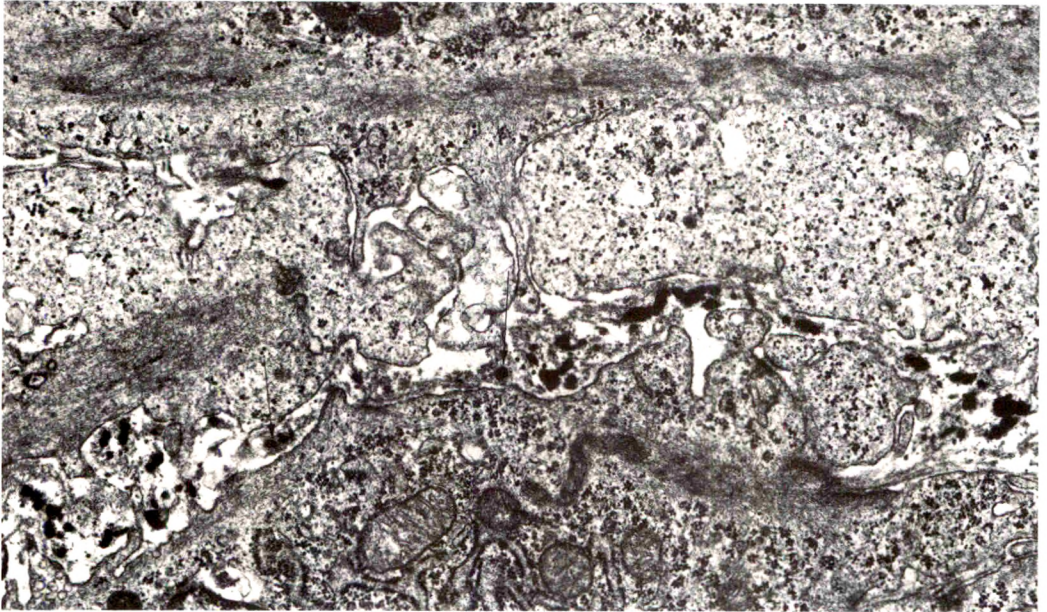


Fig 7—Note that the small dark staining homogeneous loci have coalesced and are apparently going to form elastic lamellae (MetPPS only).

8



9

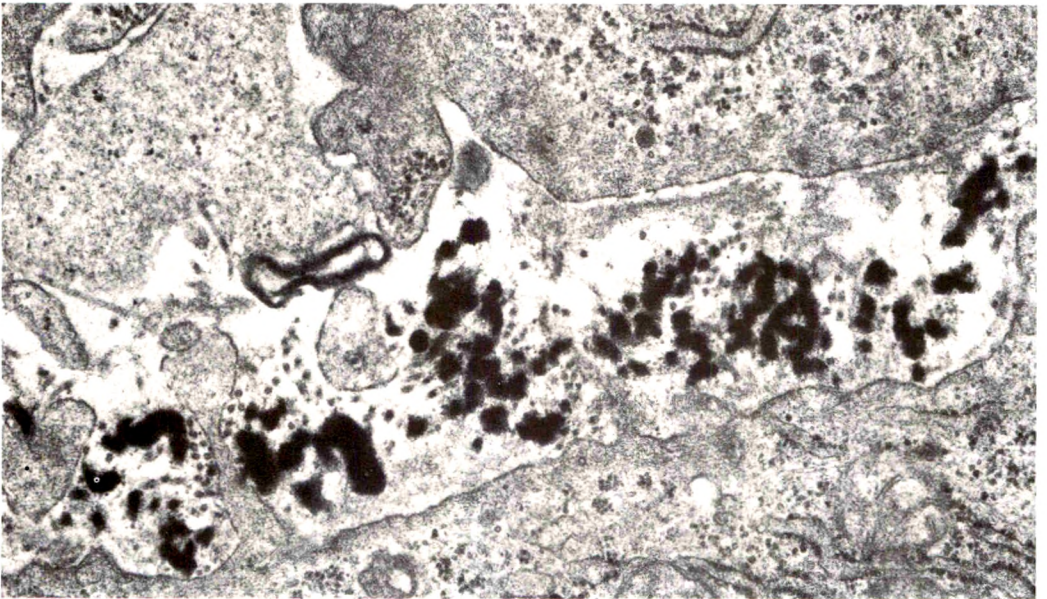


Fig 8—Portion of aorta from a 10-day fetus. Notice that the dense staining areas are surrounded by grey filamentous material (MeTPPS, uranyl and lead). **Fig 9**—Taken from a 12-day fetal aorta. Notice that there are many small elastic units. Some of them are merging with adjoining units (MeTPPS, uranyl and lead).

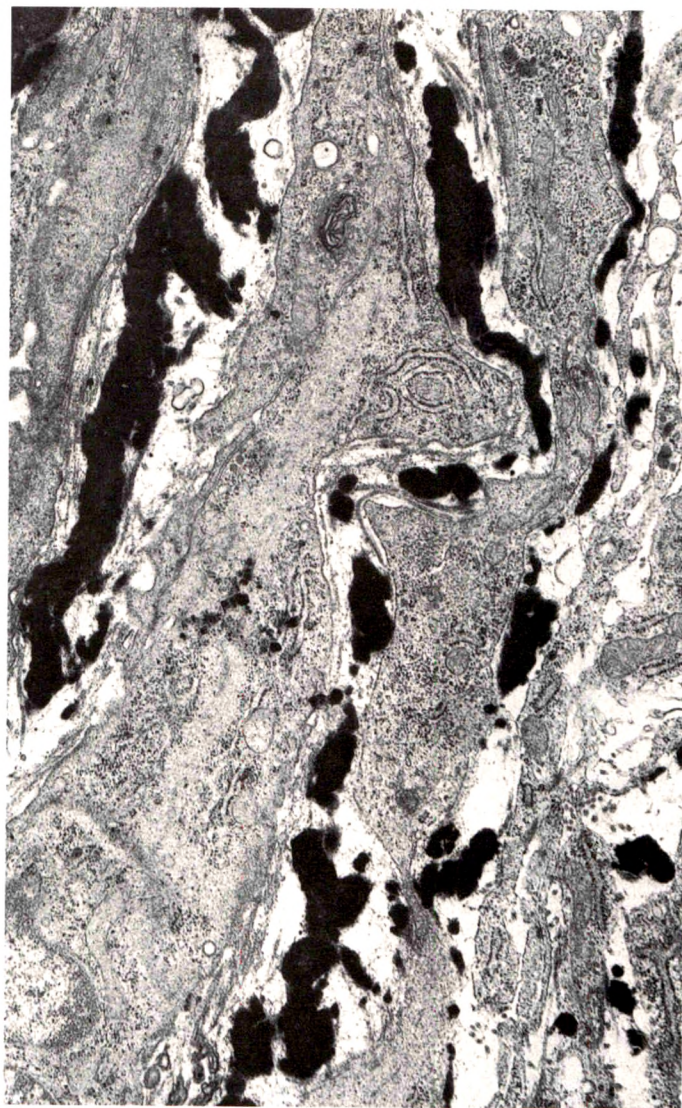


Fig 10—From 20-day fetal aorta. Notice the formation of some elastic lamellae (MeTPPS, uranyl and lead).

ALBERT
DEVELOPING ELASTIC TISSUE

American Journal
of Pathology

[*End of Article*]

Cytolysis Induced by Human Lymphotoxin

Cinematic and Electron Microscopic Observations

Stephen W. Russell, DVM, PhD, Werner Rosenau, MD and
John C. Lee, MD

By phase-contrast cinemicroscopy, highly purified human lymphotoxin induced two forms of cytolysis—one characterized by slow (1 to 2 hours) swelling (*ballooning-type*) and the other by sudden (3 to 5 minutes) shrinkage of the cell body and violent agitation of residual debris (*popcorn-type*). Specifically sensitized lymphocytes likewise caused both forms of lysis, morphologically indistinguishable from lymphotoxin-induced cytolysis. Lymphotoxin also inhibited cell division; mitoses diminished and virtually ceased before the onset of cytolysis. Many of the ultrastructural features preceding early lysis were similar to those associated with failure of osmoregulatory mechanisms—*ie*, condensation of mitochondria, dilation of rough-surfaced endoplasmic reticulum, separation of polyosomes into individual units and expansion of the cell sap. After exposure to lymphotoxin for 12 hours or more, most remaining cells exhibited these same ultrastructural changes but lacked striking mitochondrial lesions (*Am J Pathol* 69:103–118, 1972).

LYMPHOCYTES are an integral part of the mononuclear inflammatory infiltrate characteristic of cell-mediated immune reactions. The ability of lymphocytes to destroy other cells *in vitro* (target cell destruction) and to mediate tissue injury *in vivo* (allograft rejection, graft *vs* host reactions) suggests that these cells may cause at least a portion of cell-mediated immune injury. If this premise is correct, it is probable that the effector of injury is a cytotoxin(s) released from stimulated lymphocytes.

Rich and Lewis¹ noted that cytolysis followed the addition of tuberculo-protein to splenic explant or buffy coat cultures prepared from tuberculous guinea pigs. Ruddle and Waksman² extended and refined this observation, later attributing cell death to a toxic mediator liberated from immune lymphocytes in response to specific antigen.³ Granger and Kolb^{4,5} demonstrated that nonimmune lymphocytes, if stimulated by mitogenic agents such as phytohemagglutinin (PHA), also produced a soluble cytotoxin, which they later named *lymphotoxin*. From

From the Departments of Pathology, Schools of Veterinary Medicine and Medicine, and the Cancer Research Institute, University of California, Davis and San Francisco, Calif.

Supported in part by Grant CA-07191-09 from the US Public Health Service.

Accepted for publication June 22, 1972.

Address reprint requests to Dr. Werner Rosenau, Department of Pathology, University of California School of Medicine, San Francisco, Calif 94122.

studies performed with crude lymphocyte culture supernates,⁶ it was concluded that lymphotoxin effects cytolysis by "acting on the cell membranes" of susceptible tissue culture cells, causing "disintegration" of the plasmalemma.

The primary objective of this *in vitro* study was to document the sequence of changes which occur in mouse fibroblasts after exposing them to lymphotoxin. The use of highly purified test material minimized the possibility that the results were due to lymphocyte products other than lymphotoxin. Our findings demonstrate that, at the light microscopic level, lymphotoxin causes two morphologically distinct types of cytolysis, and that many of the ultrastructural lesions preceding cytolysis are those associated with impaired osmoregulation.

Materials and Methods

The preparation and purification of human lymphotoxin have been described.⁷ Briefly, adenoidal cells consisting of 95% or more lymphocytes were cultured at 37 C in RPMI 1640 tissue culture medium (Associated Biomedic Systems, Buffalo, NY) containing 10% fetal bovine serum (FBS), antibiotics and 5 to 7 $\mu\text{g}/\text{ml}$ phytohemagglutinin (PHA-P, Difco Laboratories, Detroit, Mich). After 24 hours, the cells were collected by centrifugation and resuspended in serum-free RPMI containing a reduced amount of PHA (usually 3 $\mu\text{g}/\text{ml}$). After an additional 4 to 6 days' incubation at 37 C, cell-free supernates were harvested by centrifugation. Control material was prepared similarly, except that PHA was added at the time of harvest, after all cells had been removed.

Supernates from lymphocyte cultures were concentrated and sequentially fractionated by column chromatography (Sephadex G-150 followed by DEAE-cellulose) and preparatory slab acrylamide gel electrophoresis. The final product was purified greater than 2000-fold. Identically fractionated control material lacked cytotoxicity. Briefly, a cytotoxic unit (cu) was defined as sufficient lymphotoxin activity to reduce the number of cells in experimental tubes by 1000, compared with control cultures. The details of cytotoxic unit calculation have been described previously.⁷

Electron Microscopy

Stock cultures of logarithmically growing mouse fibroblasts (L-cell strain 929) were treated with 0.25% trypsin in Hanks' balanced salt solution for 5 minutes at room temperature. The freed cells were washed once with RPMI and resuspended in RPMI + 5% FBS at a concentration of $1.4 \times 10^5/\text{ml}$. Disposable sterile Petri dishes (60 \times 15 mm), containing pieces of 300-gauge Melinex O polyester sheeting⁸ (Transilwrap West Corp, San Francisco), each received 4 ml of the L-cell suspension and were subsequently incubated for 24 hours at 37 C in an atmosphere of 95% air and 5% CO₂. The supernatant medium was then replaced with RPMI + 5% FBS, containing either purified lymphotoxin (1200 cu/ml) or an equivalent amount of control material; incubation was continued under the same conditions. This larger dose of lymphotoxin insured that there were enough affected cells to permit representative sampling. At subsequent intervals of 6, 12, 24 and 48 hours, cells were fixed with distilled, ice-cold 1.5% glutaraldehyde containing 2% (w/v) sucrose. This was accomplished by adding an

appropriate amount of 15% stock glutaraldehyde (containing 20% sucrose) directly to the medium in tissue cultures. Fixation was continued at 4 C for at least 12 hours (up to 72 hours) before cells were postfixated for 30 minutes with 1% osmium tetroxide. After dehydration in a graded series of ethanol and in propylene dioxide (10 minutes each step), the Melinex O coverslips with attached cells were inverted on embedding capsules filled with Araldite. After polymerization, the coverslips detached easily from the plastic, leaving the fibroblasts embedded in the face of the block. Ultrathin sections were cut, stained with lead citrate and uranyl acetate and examined in a Siemens 1A electron microscope equipped with a 35- μ objective aperture.

Phase-Contrast Cinemicrographic Studies

Rose chambers were inoculated with a cell suspension prepared by the procedures described above. After incubation for 24 hours at 37 C, when the fibroblasts were firmly attached to the glass, the supernatant medium was withdrawn and the chamber was refilled with RPMI + 5% FBS containing either purified lymphotoxin (400 cu/ml) or an equivalent amount of control material. Cells were photographed with an inverted phase-contrast microscope, using a 16-mm motion picture camera and Plus-X (Kodak) black-and-white reversal film. A frame interval of 30 seconds was employed in low-magnification (22 \times) studies, while a 5-second interval was used at higher (90 \times) magnification. We analyzed films with a variable-speed projector and, frame-by-frame, with a 16-mm film-editing machine, which additionally magnified the image seven times. The cells pictured in the initial frame of each film were identified by number and, together with any progeny, were followed thereafter.

Results

Control Cultures

It was observed by phase-contrast microscopy, 24 hours after seeding, at the time control material was added, that the individual cells were uniformly distributed and formed a complete monolayer within the subsequent 25 to 30 hours. Thereafter the frequency of mitosis diminished but did not stop entirely.

Mitosis was heralded by a sudden cessation of cell movement and the retraction of cytoplasmic processes. At the magnification employed, a dividing cell became increasingly refractile as it rounded into a small sphere; a cleavage furrow appeared; and the cell separated into two smaller, refractile spheres. The two daughter cells then flattened on the glass, losing their refractility, meanwhile pulling apart. Cytokinesis was frequently incomplete and, in these instances, a cytoplasmic bridge could be detected joining the two daughter cells for up to 2 or more hours.

During interphase, cells in all control cultures varied only slightly in their morphologic appearance and behavior. They were polygonal, flattened on the glass, and they frequently extended cytoplasmic processes with wavy or ruffled leading margins. Cellular movement often

followed the extension of such a process. Activity diminished, however, as the cultures became more populous. The cytoplasm of L-cells was finely granular, except for the presence of round to rod-like mitochondria and occasional pinocytic vacuoles. Nuclear rotation was occasionally seen.

Ultrastructurally (Figure 1), the chromatin of normal L-cells was dispersed, except for occasional aggregates and a thin layer along the nuclear membrane. Nucleoli were prominent and often multiple. Mitochondria were large, oval-to-elongated and myriad polyribosomes were a conspicuous cytoplasmic feature. Microtubules, microfilaments, various types of membrane-bound inclusions and narrow profiles of rough-surfaced endoplasmic reticulum (RER) were also frequently observed. In older cells, digestive vacuoles and lipid droplets were common. Golgi complexes were an infrequent finding; rarely, a structure morphologically akin to a virus particle was detected budding from a membranous structure. The plasma membrane characteristically formed numerous microvillous projections.

Lymphotoxin Treated Cells

Initially, by phase-contrast cinemicroscopy, 400 cytotoxic units of lymphotoxin per milliliter had no observable effect. Fibroblasts continued their movement and division without apparent change. By 12 hours, however, diminished movement and fewer mitoses were evident, and occasional cells had begun to lyse. Thereafter, the L-cells became increasingly granular and, by 18 to 24 hours, cytolysis had become a widespread phenomenon. Two morphologically distinct types of cytolysis were observed.

Popcorn-type Cytolysis. This name was given to the most common form of cytolysis because the residual cellular mass often resembled a kernel of popped corn (Figure 2). This lytic event, sudden in onset, progressed to completion within 3 to 5 minutes and was characterized by sudden shrinkage and violent *bubbling* of the cell body. Attenuated cytoplasmic processes formed during shrinkage (Figure 2B and C) quickly withdrew and rounded into small refractile spheres which clustered around the central granular mass of cellular debris (Figure 2D). Nuclear architecture and detail were lost. Remaining debris detached from the glass and either stuck to an adjacent cell or floated freely in the medium.

Ballooning-type Cytolysis. This form of cytolysis lacked the dramatic immediacy and violent bubbling characteristic of the popcorn-type (Figure 3). Quite simply, it consisted of slow swelling and

rounding-up of the cell (Figure 3B and C), until a large cytoplasmic bleb abruptly appeared (Figure 3D). The process frequently required 60 or more minutes (occasionally longer than 2 hours) and always involved both the nucleus and the cytoplasm. Residual debris detached from the glass as an amorphous granular mass.

Electron microscopic examination of L-cells exposed to lymphotoxin (1200 cytotoxic units/ml) for 6 hours revealed extensive ultrastructural lesions in some; many, however, appeared unaffected. The least severe alterations detected (Figure 4) were dilation of RER, separation of polyribosomes into individual units and condensation of mitochondria. Chromatin was clumped along the nuclear membrane. At this stage, microvillous processes still protruded from the cell surface. More extensively affected cells (Figure 5) exhibited marked dilation of RER and other membrane-bound structures. The matrix of some mitochondria appeared homogeneous and had become intensely black, with transverse lines of lesser osmiophilia. There was extensive clumping of chromatin, principally along the nuclear membrane, and the angularity of cells and their microvillous processes had been lost.

At 12 hours, fewer cells were present within the cultures. Those which remained on the cover slips exhibited many of the changes (including dilated RER, disintegration of polysomes and expansion of the cell sap) described at 6 hours; however, the majority of the cells now lacked striking mitochondrial changes (Figure 6). Structures resembling virus particles were seen with increasing frequency as degenerative changes in L-cells became more severe. Small discontinuities in the plasma membrane could occasionally be detected.

After 24 hours, very few cells remained attached to the cover slips. Those present (Figure 7) consisted of little more than degenerating nuclei surrounded by cytoplasmic debris. Mitochondria, when present, were swollen, usually spherical and exhibited dilated intracristal spaces. Extensive breaks were found in the plasma membranes of these cells.

By 48 hours, no cells adhered to coverslips in lymphotoxin-treated cultures.

In addition to causing cytolysis, lymphotoxin (400 cytotoxic units/ml) inhibited mitosis (Table 1). In control cultures photographed for 28 hours or more, every cell initially present divided at some time during the course of the film, with the rare exception of those which developed into giant cells. In striking contrast, after exposure to lymphotoxin, many cells present in the initial microscopic field failed to divide,

Table 1—Effect of Purified Human LT (400 cytotoxic units/ml) on L-cell Strain 929 Target Cells (Representative Films)

No. of cells initially in field	Control		Lymphotoxin	
	No.	%	No.	%
Divide	50	98	18	31.6
Lyse	0	0	22	38.6
Neither divide nor lyse	1*	2	17	29.8
No. of daughter cells observed	100		36	
	No.	%	No.	%
Divide	33	33	0	0
Lyse	3	3	7	19.4
Neither divide nor lyse	59	59	28	77.8
Lost to view	5	5	1	2.8
Total number of mitoses	83		18	

* Developed into giant cell

Film durations were 28 hours for control cells and 32 hours for cells exposed to lymphotoxin. Control medium consisted of identically purified supernate from unstimulated lymphocyte cultures, diluted similarly (1:150) to the lymphotoxin-containing medium.

Daughter cells are the progeny of **cells initially in the field**.

These data show that, in addition to causing cytolysis, lymphotoxin also inhibits the proliferation of L-cell 929 fibroblasts. Lysis which occurred in control cultures was observed late in the incubation period. Nonspecific cytolysis is a well-documented phenomenon in aged L-cell cultures.⁹

and after 18 to 24 hours, when cytolysis had begun in earnest, mitoses were extremely rare.

Discussion

By phase-contrast cinemicroscopy, there were two morphologically distinct forms of lymphotoxin-induced cytolysis, one characterized by cell swelling (which we termed ballooning-type) and the other by sudden shrinkage of the cell body followed by violent agitation of the residuum (popcorn-type). These were indistinguishable from the two kinds of cytolysis previously observed when L-cell 929 fibroblasts were exposed to specifically sensitized lymphocytes.¹⁰

The cardinal feature of ballooning-type cytolysis—early cell swelling—suggests that lymphotoxin may impair target cell osmoregulatory mechanisms. Many of the ultrastructural changes we found are consistent with this hypothesis in that they closely resembled the alterations observed by Trump and his colleagues.^{11,12} In cells which had lost the capacity to regulate their volume, these investigators described swelling as the principal light microscopic feature, while the earliest

ultrastructural changes reported were dilation of the endoplasmic reticulum and nuclear envelope. Subcellular alterations of moderate severity included contraction and condensation of the inner mitochondrial compartment, with relative expansion of intracristal spaces and enlargement of the cell sap. Advanced stages of injury were heralded by severe swelling of mitochondria, loss of polysomes, karyolysis and interruptions in the plasma membrane. In spite of the marked similarities between our observations and those of Trump *et al*, we stress that the finding of morphologic alterations compatible with osmoregulatory failure does not indicate a primary site of action for lymphotoxin. Numerous agents, acting at different levels within the cell, are capable of interfering directly or indirectly with the maintenance of cell volume.¹²

Since cell swelling was not associated with popcorn-type lysis, we expected to find a second group of ultrastructural changes which would correlate with this form of cytolysis. We were unable to do so, in spite of examining hundreds of lymphotoxin-treated cells by electron microscopy. Among a number of plausible explanations for this apparent discrepancy, two seem most likely. First, the mechanism of injury was the same in both types of cytolysis and caused similar ultrastructural changes in all affected cells. However, because of differences in our target cell population (these cells had not been cloned for many years), the morphologic expression of injury varied at the light microscopic level. Alternately, we were simply unable to detect the ultrastructural changes associated with popcorn-type lysis because of inherent sampling difficulties. By light microscopy, this event was unheralded and occurred rapidly (3 to 5 minutes). Individual cells were affected at different times after exposure, and the residuum usually quickly detached from the glass. To clarify these points, further studies are planned, employing cloned and synchronized cells.

At the ultrastructural level, severe mitochondrial vacuolation has been described as the earliest discernible lesion caused in L-cell strain 929 fibroblasts by specifically sensitized lymphocytes.¹³ Mitochondrial vacuolation was also observed in our target cells, but this change was detected in both control and experimental material, and the incidence increased greatly when fixative was placed directly onto the cells rather than into the tissue culture medium. We therefore believe that this mitochondrial alteration was an artifact of fixation rather than a lesion induced by lymphotoxin.

The inhibition of mitosis we observed probably reflects cellular injury caused by lymphotoxin. This is supported by our finding that the frequency of mitosis gradually diminished and virtually ceased just

before the onset of cytolysis. Proliferation inhibitory factor (PIF), an agent released from PHA-stimulated human lymphocytes, also interferes with cellular division.¹⁴ The relationship of our highly purified lymphotoxin to this agent is unknown; however, PIF was described as having no effect on L-cell 929, the strain of fibroblast employed in our investigation.

Thus, highly purified human lymphotoxin causes both cytolysis and inhibition of mitosis, and many of the subcellular alterations it produces may reflect failure of osmoregulatory mechanisms. We are currently extending these morphologic studies with biochemical investigations designed to elucidate specifically how lymphotoxin mediates such changes.

References

1. Rich AR, Lewis MR: The nature of allergy in tuberculosis as revealed by tissue culture studies. *Bull Johns Hopkins Hosp* 50:115-131, 1932
2. Ruddle NH, Waksman BH: Cytotoxic effect of lymphocyte-antigen interaction in delayed hypersensitivity. *Science* 157:1060-1062, 1967
3. Ruddle NH, Waksman BH: Cytotoxicity mediated by soluble antigen and lymphocytes in delayed hypersensitivity. III. Analysis of mechanism. *J Exp Med* 128:1267-1279, 1968
4. Granger GA, Kolb WP: Lymphocyte *in vitro* cytotoxicity: Mechanisms of immune and non-immune small lymphocyte mediated target L cell destruction. *J Immunol* 101:111-120, 1968
5. Kolb WP, Granger GA: Lymphocyte *in vitro* cytotoxicity: Characterization of human lymphotoxin. *Proc Natl Acad Sci USA* 61:1250-1255, 1968
6. Williams TW, Granger GA: Lymphocyte *in vitro* cytotoxicity: Mechanism of lymphotoxin-induced target cell destruction. *J Immunol* 102:911-918, 1969
7. Russell SW, Rosenau W, Goldberg ML, Kunitomi GM: Purification of human lymphotoxin. *J Immunol* (In press)
8. Firket H: Polyester sheeting (Melinex O), a tissue-culture support easily separable from epoxy resins after flat-face embedding. *Stain Technol* 41:189-191, 1966
9. McQuilkin WT, Earle WR: Cinemicrographic analysis of cell populations *in vitro*. *J Natl Cancer Inst* 28:763-799, 1962
10. Russell SW: Purification and some properties of human lymphotoxin. PhD Dissertation, University of California, Davis, March 1972, pp 94-112
11. Ginn FL, Shelburne JD, Trump BF: Disorders of cell volume regulation. I. Effects of inhibition of plasma membrane adenosine triphosphatase with ouabain. *Am J Pathol* 53:1041-1071, 1968
12. Trump BF, Bulger RE: Experimental modification of lateral and basilar plasma membranes and extracellular compartments in the flounder nephron. *Fed Proc* 30:22-41, 1971
13. Weiss L: Interactions of sensitized lymphoid cells and homologous target cells in tissue culture and in grafts: an electron microscopic and immunofluorescence study. *J Immunol* 101:1346-1362, 1968

14. Green JA, Cooperband SR, Rutstein JA, Kibrick A: Inhibition of target cell proliferation by supernatants from cultures of human peripheral lymphocytes. *J Immunol* 105:48-54, 1970

Acknowledgments

We were privileged to have had the technical assistance of Mr. John Barbano and Miss Linda Dybas (electron microscopy), as well as Mr. Richard Beindorf and Mr. Jonathan Flaccus (cinemicroscopy). We are also grateful for the editorial advice given by Rosamond Bettencourt.

Dr. Russell was supported by training grant T01-GM-00537 from the National Institutes of Health and US Public Health Service Special Fellowship 1-F03-AM-49756-01. His current address is Department of Experimental Pathology, Scripps Clinic and Research Foundation, 476 Prospect St, La Jolla, Calif 92037.

[*Illustrations follow*]

•

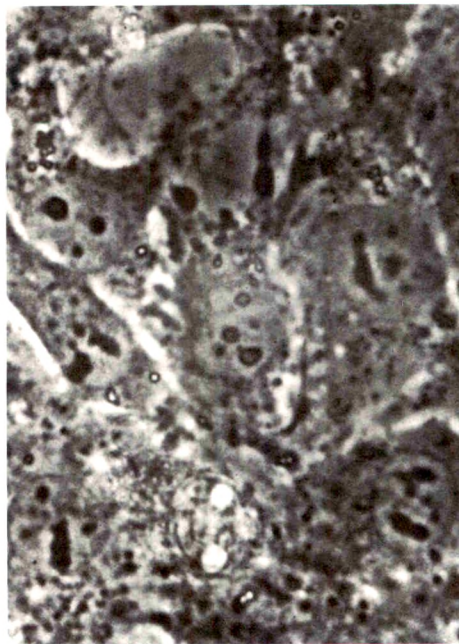


Fig 1—Normal fibroblasts of L-cell strain 929. Numerous polyribosomes are a characteristic cytoplasmic feature of these cells. Incomplete cytokinesis is a common, though transient, finding. The two cells depicted have recently divided, but remain joined by a tangentially sectioned cytoplasmic bridge. A midbody (MB) and attached spindle fibers are seen in the bridge. M = mitochondrion, RER = rough-surfaced endoplasmic reticulum, DV = digestive vacuole, N = nucleus (X 21,000).

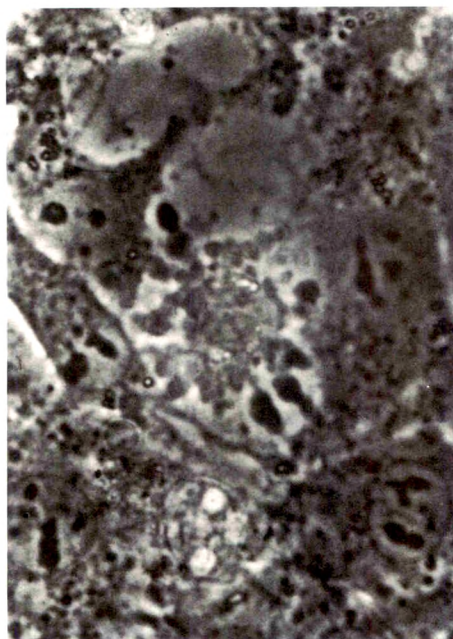
A



B



C



D



Fig 2—Popcorn-type lysis of L-cell strain 929 fibroblast exposed to 400 cytotoxic units of purified human lymphotoxin/ml. The events depicted here occur within 3 to 5 minutes (phase-contrast, $\times 1150$). **Fig 2A**—Fibroblast (*center*) 30 seconds prior to initiation of the lytic process. There are no specifically discernible degenerative changes which suggest impending cytolysis. Previously lysed cell (*arrow*). **Fig 2B**—The initial event is sudden retraction of the cell body, leaving attenuated cytoplasmic processes still attached to the glass. Early distortion of the nucleus is evident. **Fig 2C**—The cell body has fully shrunk and there is severe distortion of the nucleus. The peripheral cytoplasmic processes are retracting and becoming globular. **Fig 2D**—The fully retracted cytoplasmic processes have become refractile spheres peripherally arranged around the main mass of granular debris. Violent *bubbling* of the entire debris mass and detachment from the glass follow.

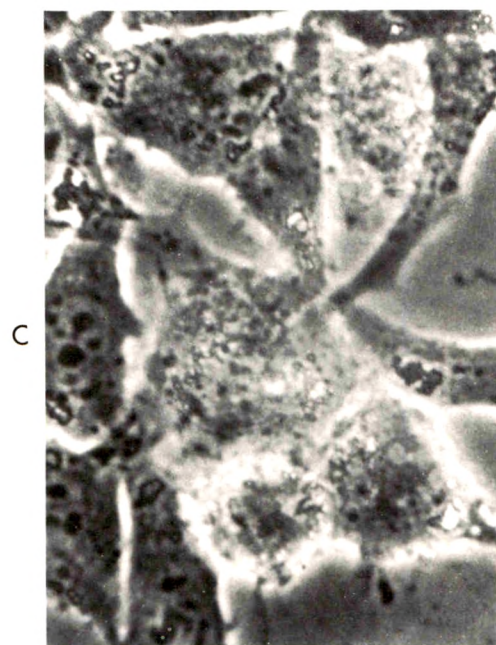
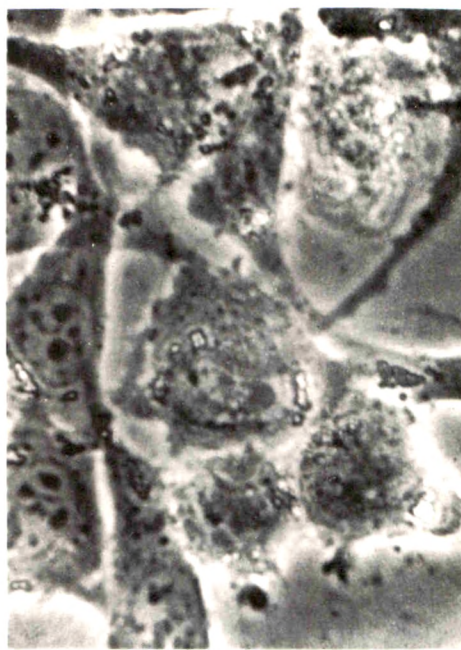
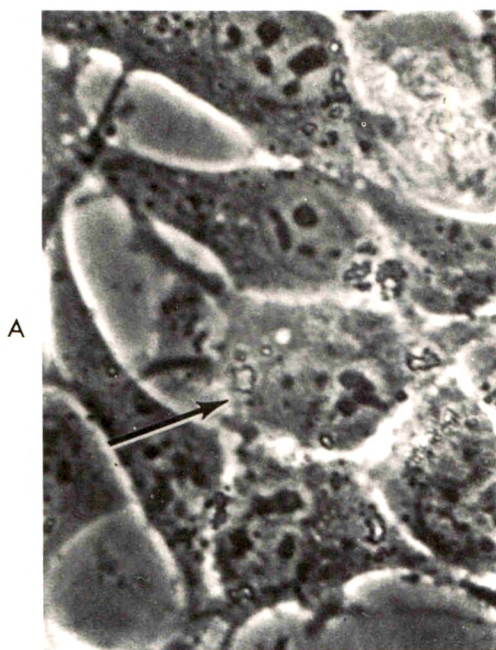


Fig 3—*Ballooning*-type lysis of L-cell strain 929 fibroblast exposed to 400 cytotoxic units of purified human lymphotoxin/ml. In contrast to popcorn-type cytolysis, the events depicted here often require more than 60 minutes and sometimes as long as 2 hours (phase-contrast, $\times 1150$). **Fig 3A**—Fibroblast (arrow) approximately 30 minutes before earliest detection of changes associated with ballooning cytolysis. The two cells below the subject fibroblast are similarly degenerating. **Fig 3B**—The earliest detectable changes are slight swelling and rounding-up of the affected cell. **Fig 3C**—Fifty minutes after earliest detectable changes, the affected cell is much more spherical than normal and its cytoplasm has become quite granular. Nuclear architecture has been lost. **Fig 3D**—Termination of the lytic process (100 minutes from earliest detectable changes) is heralded by the sudden appearance of a cytoplasmic bleb (arrows). Thereafter, the residual mass increases in granularity, shrinks, and usually detaches from the glass to float freely in the medium.

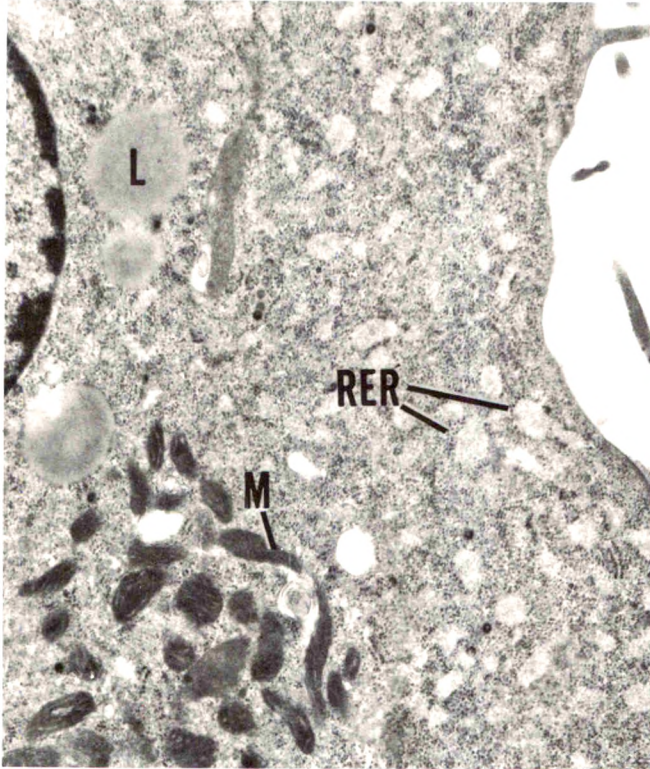


Fig 4—Early stage of lymphotoxin-induced cell injury. Rough-surfaced endoplasmic reticulum (RER) is dilated, mitochondria (M) appear *condensed* due to increased osmiophilia of their matrix, and polyribosomes have disintegrated into individual units. Microvillous processes, a characteristic feature of normal L-cells, still protrude at the cell surface. There is clumping of chromatin along the nuclear membrane. L=lipid droplet. Six-hour exposure to 1200 cytotoxic units lymphotoxin/ml ($\times 15,000$).



Fig 5—Intermediate stage of lymphotoxin-induced cell injury, also after 6-hour exposure to 1200 cytotoxic units LT/ml. The time-course of injury varied, due to apparent differences in individual cell susceptibility to lymphotoxin. In addition to the type of mitochondrion illustrated in Figure 4, there are some that appear black (arrow), with transverse lines of decreased osmiophilia. Dilated endoplasmic reticulum and multiple membrane-bound spaces are also characteristic of this stage of injury. Microvillous processes have been lost as a result of cytoplasmic volume increase ($\times 28,000$).

Fig 6—After 12 hours of exposure to lymphotoxin, many of the cells remaining on cover slips exhibit extensive dilation of their endoplasmic reticulum, fragmentation of poly-somes and expansion of their cell sap, but lack condensed mitochondria. Structures morphologically consistent with virus particles (arrow) are seen with increasing frequency in degenerating cells. N=nucleus ($\times 30,000$).

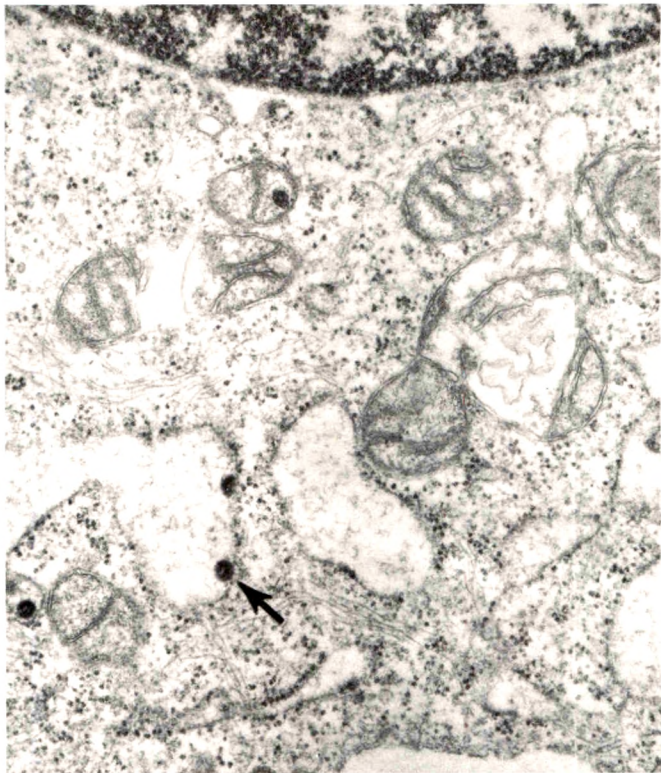
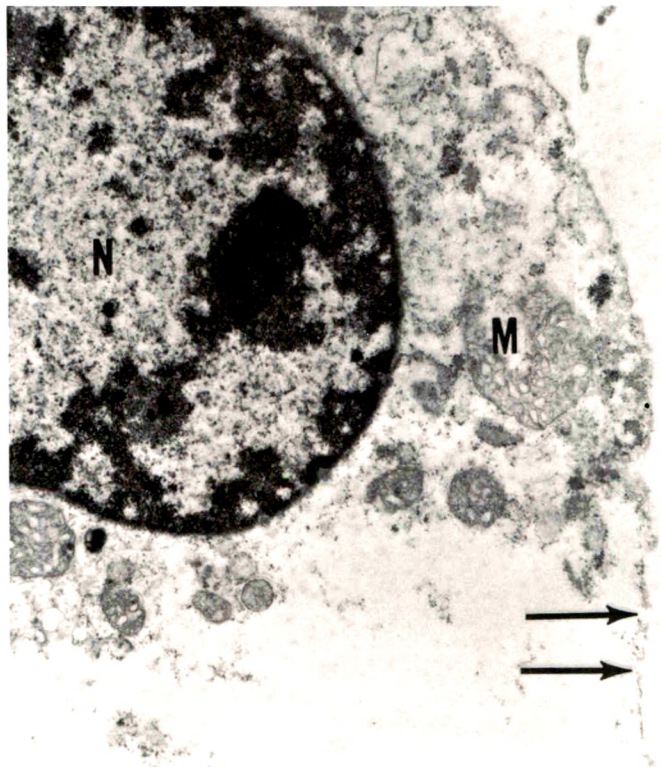


Fig 7—Terminal stage of lymphotoxin-induced cell injury (24-hour exposure to 1200 cytotoxic units lymphotoxin/ml). The plasmalemma of such cells is extensively disrupted (arrows) and very few cytoplasmic organelles remain. Mitochondria (M), when observed, are swollen and exhibit dilated intracristal spaces. N=nucleus ($\times 13,000$).



[*End of Article*]

Thermal Noise in Cells

A Cause of Spontaneous Loss of Cell Function

Horton A. Johnson, MD, and Mildred Pavelec, MS

Background noise due to random thermal perturbations of molecules has a disruptive effect on all information handling systems, including cells and organisms. This thermal noise appears to be largely responsible for the spontaneous loss of proliferative cells in cell cultures. The rates at which proliferative cells are lost as a result of heat injury, in cultured hamster cells, have been measured at high temperatures and extrapolated down to 37 C. This gives an expected 0.2% loss per hour due to thermal injury at physiologic temperature. That such a loss does in fact occur can be shown by comparing cell generation time with population doubling time, when these cells are growing at physiologic temperatures. Apparently, internal thermal noise presents a primary hazard to the reliable functioning of the cell quite apart from the insults it receives from its external environment (Am J Pathol 69:119-130, 1972).

THERMAL NOISE LIMITS THE PERFORMANCE of all information handling devices. In the past there has been little interest in this problem outside of the field of electronics engineering, where it is a matter of fundamental and practical importance.¹ And yet, since in all living things successful function depends upon the reliable storage and processing of information, it seems that the disruptive effects of internal noise might be a concern important to the biologist as well as the communications engineer.

In this report we will show that the unexplained *spontaneous* death of cells *in vitro* can be largely accounted for by the effects of background noise within these cells.

The Nature of Thermal Noise

There are random energy fluctuations in the particles which make up all matter, living and nonliving, except at the inaccessible temperature of absolute zero.

These random fluctuations are manifested in a number of ways. The randomly fluctuating kinetic energy of molecules is experienced as heat. Other particles in thermal equilibrium with molecules are also subject to thermal agitation. Brownian motion is the thermal

From the Medical Department, Brookhaven National Laboratory, Upton, NY, and the Department of Pathology, Indiana University School of Medicine, Indianapolis, Ind. Supported by the US Atomic Energy Commission.

Accepted for publication June 20, 1972.

Address reprint requests to Horton A. Johnson, MD, Department of Pathology, Indiana University School of Medicine, Indianapolis, Ind. 46202.

agitation of visible particles that collide repeatedly with randomly moving molecules. Electrical noise results from thermal agitation of electrons in a conductor.

In the living cell there are also manifestations of thermal noise: thermal motion of solutes causes random fluctuations in local concentrations, and, in large information-laden molecules, thermal vibrations of adjacent atoms may by chance rupture the chemical bond between them. In this way the molecular order, essential to the survival of the cell, is in constant jeopardy due to thermal perturbations.

The mean energy of these perturbations is proportional to absolute temperature, so that the mean energy in any one degree of freedom is

$$\bar{E} = \frac{1}{2} kT \quad (1)$$

where the constant of proportionality is k , or Boltzmann's constant, and T is the Kelvin temperature. At biologic temperatures, thermal noise reaches a significant level; the mean energy at 37 C is approximately 0.014 eV. Because of the probabilistic nature of these perturbations, some will be many times greater than the mean, often sufficient to rupture hydrogen bonds with energies of 0.05 to 0.1 eV, and occasionally violent enough to break covalent bonds with energies of 0.5 to 1.0 eV.

The random corpuscular motion of matter interferes unavoidably with the storage and flow of information in matter. Thermal agitation of oriented magnetic molecules can garble information stored in a computer, and thermal agitation of electrons can disrupt the flow of information along a transmission line. In the cell, thermal rupture of chemical bonds may garble information flow through transcription and translation, and thermal motion of electrons may cause spurious excitation of membranes.² In electrical devices and cells the modes of information storage and flow are very different, but, in principle, thermal noise jeopardizes the reliable handling of information in both cases. There is no doubt that internal noise interferes, to some degree, with the functioning of all cells, but the important question is whether this is of practical or merely academic importance. In this study we have asked whether in some cases intracellular noise may present a significant and measurable obstacle to cell function under physiologic conditions.

Experimental Design

By comparing the anticipated loss of proliferative cells due to thermal injury at physiologic temperature with the actual spontaneous loss,

one can see how significant a role thermal noise plays in the spontaneous inactivation of these cells and to what extent thermal noise may determine the natural rate of cell turnover.

The naturally occurring or spontaneous loss of proliferating cells at physiologic temperatures can be measured by measuring the discrepancy between the mean cell generation time and the population doubling time. That is to say, if cells are being lost from a growing population, the population will fail to double in one mean generation time, and the generation time will be less than the doubling time.

The effects of thermal noise may be very subtle at body temperature, but, according to Equation 1, the mean energy of thermal perturbations can be amplified by increasing the temperature. If thermal noise is amplified at elevated temperature to the extent that it becomes an overriding factor in cell survival, then its effects can be identified and quantified. These measurements can then be extrapolated down to 37 C to estimate the magnitude of thermal injury at physiologic temperatures. Since the temperature of mammalian cells can only be manipulated accurately *in vitro*, we have used the rate of loss of clone-forming cells *in vitro* as a measure of the rate of thermal injury.

Materials and Methods

All of these experiments were carried out on a subline of the V strain of Chinese hamster cells originally isolated from lung tissue by Ford and Yerganian.³ Cells were grown in Eagles medium⁴ enriched with 15% fetal calf serum.

Thermal Injury

Details of the method used in measuring the rates of thermal injury have been presented previously.⁵ Briefly, the procedure was as follows. Known numbers of cells were plated in culture flasks and allowed to attach to the glass for 3.5 hr at 37 C. Flasks were then placed in incubators at elevated temperatures for various periods of time. After heat treatment the flasks were returned to the 37 C incubator for 1 week, after which time cells were fixed and stained so that clones could be counted. The number of clones per cells plated in the experimental flask was divided by the number of clones per cells plated in control flasks to obtain the fraction of surviving clones. Cell survival was calculated from clone survival.⁵

Population Doubling Time

For each measurement of doubling time, 10^5 cells were placed in each of 6 flasks and allowed to grow at a fixed temperature. At various times on each of the following 2 days, cells were trypsinized and counted in a Coulter counter. Each count was done during the logarithmic growth phase. At temperatures other than 37 C, attempts were made to measure the effects of temperature adaptation on the rate of cell population growth. Population growth rates were measured in colonies which had been seeded from stock cultures which had been temperature adapted for 1 to 14 days. The length of adaptation had no measureable effect on the population growth rates.

Mean Cell Generation Time

The mean cell generation time can be measured by the method of percent labeled mitoses.⁶ This is done by flash-labeling a cohort of cells with tritiated thymidine and following this cohort autoradiographically as it proceeds through two successive mitoses. Cultures were grown at 37 C for 48 hr on cover slips in Leighton tubes. The medium was then aspirated and replaced by medium containing 0.05 μ Ci of tritiated thymidine/ml (specific activity 1.9 Ci/mM). After 15 min the radioactive medium was removed. The cultures were rinsed immediately with Puck saline A (PSA), and fresh medium containing nonradioactive thymidine, 1 μ g/ml, was added. Cultures were then incubated at 34, 37, or 39 C. At various intervals after ³H labeling, cultures were removed from the incubator, washed with PSA, and fixed in absolute methanol. Cover slips were cemented to glass slides with the cells exposed. The slides were dipped in Kodak NTB2 liquid emulsion and processed for autoradiography.

Results

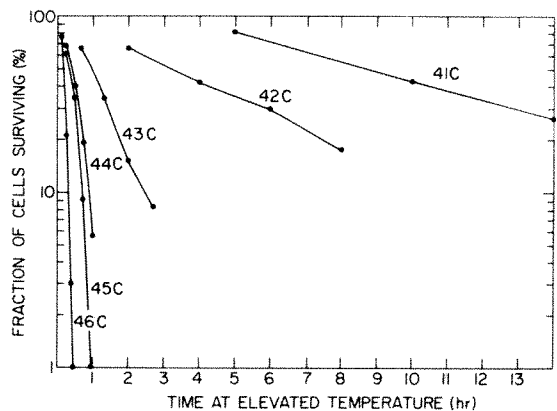
It must be emphasized at the outset that, in these experiments, cell survival implies survival of a cell's clone-forming ability—its capacity to give rise to some eight or more successful mitotic divisions resulting in a clone of over 300 cells. Nonsurvivors are cells which are unable to give rise to a grossly visible clone in 7 days. These cells, having lost their proliferative capacity, are unable to contribute to the growth of a cell population and will be referred to as dead cells. It must be remembered, however, that although such cells are reproductively dead we have no way of knowing from these data just what fraction of them may be metabolically dead.

Thermal Death Rate

The progressive destruction of cell proliferative capability at various elevated temperatures is shown by the survival curves in Text-figure 1. The decrease in survivors of thermal injury is more rapid at higher temperatures, as would be expected. The survival curves are exponential, so that the slopes give the rate constants (k_d) for each temperature. Least squares regressions were calculated in each case, and the slopes of these were taken as rate constants, which were then plotted on Arrhenius coordinates as shown in Text-figure 2. The least squares regression line for these points (solid line) has been extrapolated down to 37 C, indicating a thermal death rate (k_d) of 0.002/hr at normal body temperature. This agrees with an earlier series of experiments,⁵ the results of which are indicated by the dashed line of Text-figure 2.

This means that if the relationship between temperature and cell death rate which operates from 46 through 41 C also extends to 37 C, then 0.2% of cells must become reproductively dead each hour, due to

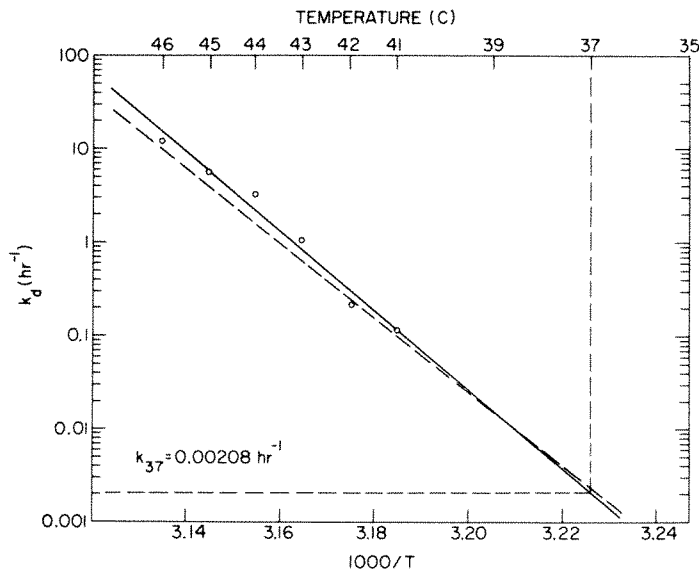
TEXT-FIG 1—Survival curves for clone-forming cells at various temperatures.



heat injury at physiologic temperature. The fibroblasts used in these experiments have a mean generation time of about 10 hr, so that the thermal death rate at 37 C is about 2% generation.

Rate of Spontaneous Cell Death

The rate at which cells are lost from a proliferating population can be measured by the discrepancy between the mean cell generation time (t_g) and the population doubling time (t_p). If all cells in a popu-



TEXT-FIG 2—Cell death rate (k_d) plotted against temperature on Arrhenius coordinates. The continuous line is the regression line for the data points (*open circles*). The dashed regression line is for data points of a previous experiment.⁵ The extrapolation to 37 C is indicated.

lation continue to proliferate, the size of the population should double in one mean generation time. If cells are steadily lost from the proliferative pool, the population will fall short of doubling in one mean generation time. Here again, the observed effect is the failure of a cell to take part in the exponential growth of the population; this will be referred to as reproductive death, although the affected cell may or may not be metabolically dead.

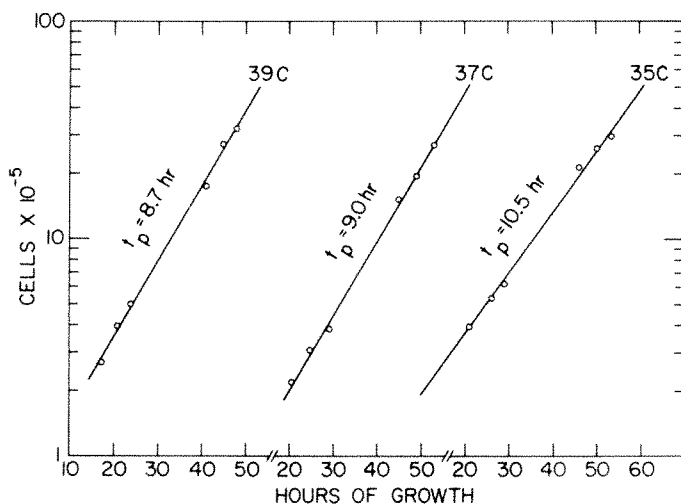
The rate of population growth is equal to the rate of cell proliferation minus the rate of cell death. In terms of rate constants,

$$k_p = k_g - k_d \quad (2)$$

where k_p is the rate constant for population growth, k_g is the rate constant for the generation of new cells, and k_d is the rate constant for cell death.

The growth curves of cell populations at 35, 37 and 39 C are shown in Text-figure 3, and the corresponding doubling times (t_p) are given. The population doubling time shows only a weak temperature dependence.

The curves of percent labeled mitoses at 34, 37 and 39 C are shown in Text-figure 4, and the mean generation times are indicated. The length of the mitotic cycle is more sensitive to temperature variation than is the population growth rate.



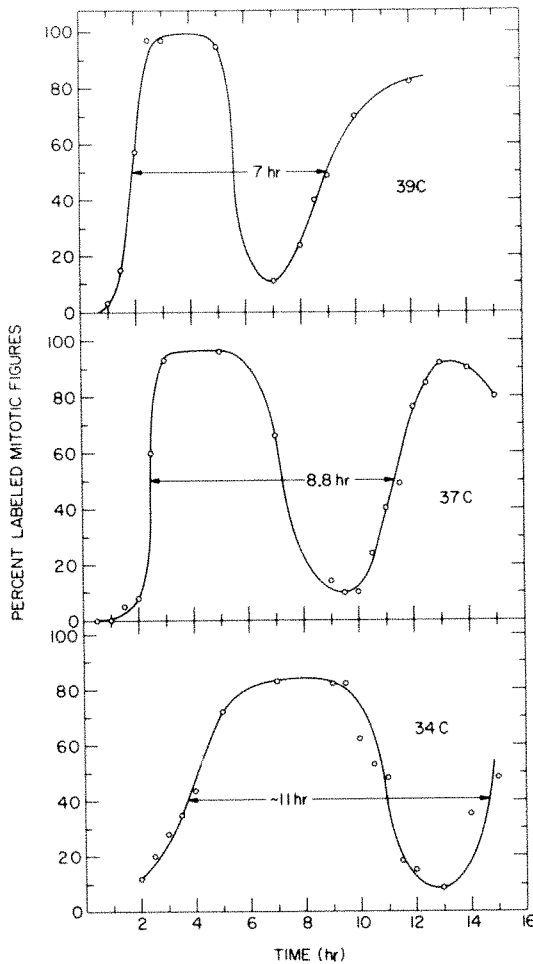
TEXT-FIG 3—Population growth curves at 3 different temperatures. Population doubling times (t_p) are indicated.

The time constants (t_p and t_g) can be converted to rate constants, since

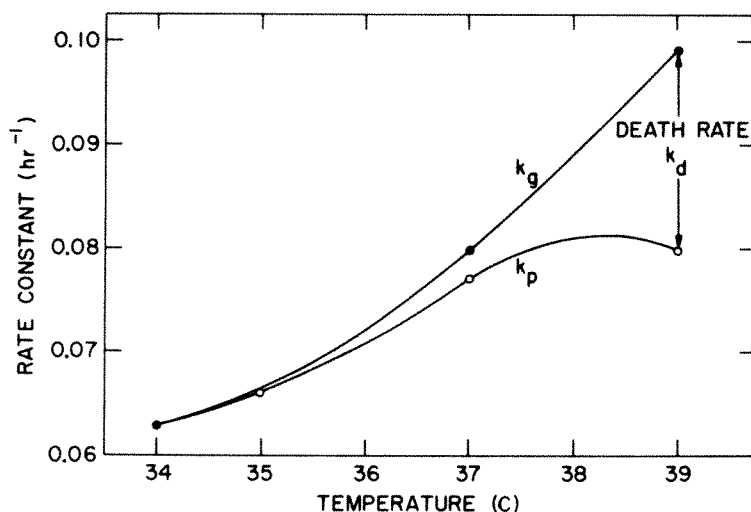
$$k_p = \frac{\ln 2}{t_p} \text{ and } k_g = \frac{\ln 2}{t_g}$$

These rate constants are plotted against temperature in Text-figure 5. The difference between the rate constants can be interpreted as the rate of cell death (k_d) as in Equation 2. The rate of spontaneous cell death is strongly temperature dependent; it is scarcely perceptible below 37 C and increases sharply above 37 C.

Spontaneous death rates are compared with thermal death rates in Text-figure 6. Spontaneous death rates at 37 and 39 C are nearly identical to the expected thermal death rates at those temperatures. This



TEXT-FIG 4—Percent of mitotic figures labeled after flash-labeling with tritiated thymidine. Mean generation time (duration of mitotic cycle) is given for each temperature.



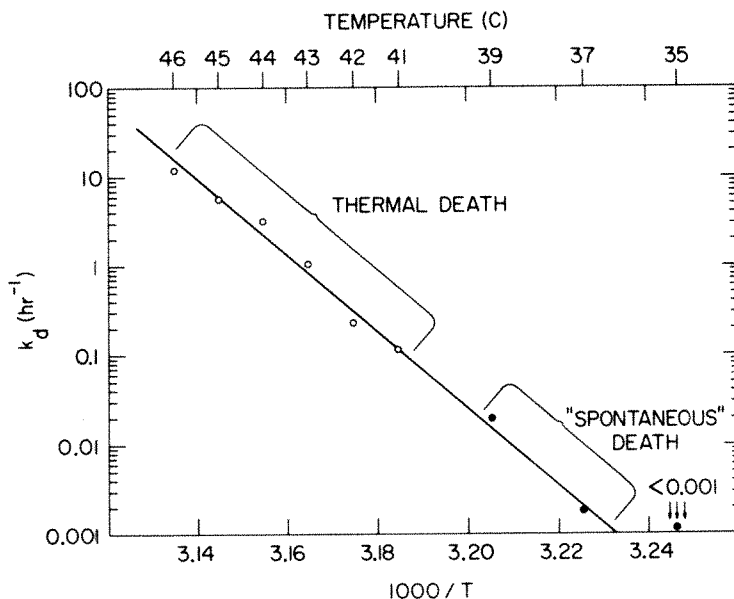
TEXT-FIG 5—Cell generation constants (*solid circles*), and population growth constants (*open circles*) versus temperature. The difference between these values is the death rate constant, k_d , which increases sharply with increasing temperature.

means that the spontaneous loss of cells observed at physiologic temperatures can be almost completely accounted for by the same kind of thermal injury which is responsible for cell inactivation at high temperatures.

Discussion

All cell populations, *in vitro* and *in vivo*, apparently suffer a continual loss of cells, even under ideal conditions. This is a prominent feature of cell renewal populations such as hemopoietic tissue and intestinal epithelium. Under normal physiologic conditions there is also a steady basal level of cell turnover in such stable cell populations as hepatic⁷ and renal⁸ parenchyma. Even the nonproliferative neuron population undergoes a continuous attrition throughout life: by the time the mouse reaches advanced old age it has lost about two-thirds of its original neuron population.⁹

Continuous cell loss is also characteristic of cell populations *in vitro*, as evidenced by the failure of populations to double with each generation. If this failure simply represented an initial growth fraction of less than one, the discrepancy between generation time and population doubling time would disappear as the population continued to grow. The discrepancy remains constant, however, signifying a constant rate of cell loss from the proliferating population, either by reproductive or metabolic death.¹⁰ A constant death rate is characteristic of established



TEXT-FIG 6—Actual spontaneous death rates at physiologic temperatures (solid circles) coincide with the extrapolation of thermal death rates at elevated temperatures (open circles).

cell lines, in which k_d remains small relative to k_g , and the population growth constant (k_p) remains positive so that the population continues to grow at a constant rate after any number of passages. Primary cell lines such as human diploid cells are fundamentally different in this respect; the death rate increases with time, so that k_d eventually approaches k_g and, using Equation 2, the population growth constant (k_p) approaches zero, so that the population can no longer be sub-cultured.¹¹ Interestingly enough, mouse neurons *in vivo*, like diploid cells *in vitro*, also have an accelerating death rate constant.⁹

Our experiments show that the basal death rates of cells *in vitro*, and perhaps *in vivo*, are largely a result of thermal perturbations, or thermal noise. One wonders about the chemical nature of this thermal injury. Our data allow us to draw several inferences. The slope of the Arrhenius plot indicates that this process has a heat of activation of 185,000 cal/mole and an entropy of activation of approximately 500 entropy units.⁵ These large values mean that the critical chemical reaction is preceded by a denaturation equilibrium involving the rupture of many hydrogen bonds. This implies the loss of tertiary structure in a macromolecule. The chemical injury is one which cannot be repaired in 7 days, suggesting an irreversible change in DNA rather than in a

protein or RNA molecule which could be replaced. Because of the high activation energy, denaturation of DNA is more likely than chemical degradation such as depurination, which has an activation energy of only 28,000 cal/mole.¹² But these inferences are highly speculative. All one can really say for certain from our data is that the same thermal injury which disables cells rapidly at 46 C also disables cells slowly at 37 C.

All ordered things drift inevitably toward chaos. Since living things must maintain a certain level of order for survival, life is largely a struggle against this tendency.¹³ The continuous random motion at the molecular level which we call thermal noise is a manifestation of nature's tendency toward disorder. The disruptive effect of thermal noise limits the efficiency of information handling organs such as the kidney¹⁴ and the brain.¹⁵ From the experiments presented here, it now appears that thermal noise also limits, to a significant degree, the storage of information in macromolecules and thus limits the lifespans of cells. When we consider the broad implications of this, it seems likely that we may suffer more from the hazards of our internal thermal noise than from the insults of our external environment.

References

1. King R: Electrical Noise. London, Chapman and Hall, Ltd., 1966
2. Fatt P, Katz B: Spontaneous subthreshold activity at motor nerve endings. *J Physiol* 117:109-128, 1952
3. Ford DK, Yerganian G: Observations on the chromosomes of Chinese hamster cells in tissue culture. *J Natl Cancer Inst* 21:393-425, 1958
4. Eagle H: Amino acid metabolism in mammalian cell cultures. *Science* 130:432-437, 1959
5. Johnson HA, Pavelec M: Thermal injury due to normal body temperature. *Am J Pathol* 66:557-564, 1972
6. Johnson HA: Some problems associated with the histological study of cell proliferation kinetics. *Cytologia* 26:32-41, 1961
7. Johnson HA: Liver regeneration and the "critical mass" hypothesis. *Am J Pathol* 57:1-16, 1969
8. Johnson HA, Vera Roman JM: Compensatory renal enlargement: hypertrophy versus hyperplasia. *Am J Pathol* 49:1-13, 1966
9. Johnson HA, Erner S: Neuron survival in the aging mouse. *Exp Gerontol* 7:111-117, 1972
10. Schindler R, Ramseier L, Schaer JC, Grieder A: Studies on the division cycle of mammalian cells. III. Preparation of synchronously dividing cell populations by isotonic sucrose gradient centrifugation. *Exp Cell Res* 59:90-96, 1970
11. Merz GS Jr, Ross JD: Viability of human diploid cells as a function of *in vitro* age. *J Cell Physiol* 74:219-222, 1969

12. Greer S, Zamenhof S: Studies on depurination of DNA by heat. *J Mol Biol* 4:123-141, 1962
13. Johnson HA: Information theory in biology after 18 years. *Science* 168: 1545-1550, 1970
14. Johnson HA, Knudsen KD: Renal efficiency and information theory. *Nature* 206:930-931, 1965
15. Johnson HA: Limitations imposed by thermal noise in biocontrol systems. *Proceedings of the Symposium on Biomedical Engineering, Vol I. Milwaukee, Marquette University Press, 1966, pp 345-348*

[End of Article]

Induction of the Generalized Schwartzman Reaction in Pregnant and Nonpregnant Rats by Colchicine

Gert Müller-Berghaus, MD and Rolf Obst, MD

The intravenous injection of colchicine (2 mg/kg body weight) into pregnant rats on the last 4 to 5 days of gestation induced disseminated intravascular coagulation, occluding glomerular capillaries with fibrin thrombi, typical of the generalized Schwartzman reaction. Thrombi did not form earlier than 9 hours after the injection of colchicine, whereas in the endotoxin-induced generalized Schwartzman reaction, thrombi were already observed 2½ hours after the injection of endotoxin. The colchicine-induced generalized Schwartzman reaction could also be produced in hysterectomized "pregnant" rats. A single injection of colchicine into nonpregnant rats did not induce disseminated intravascular coagulation. If, however, fibrinolysis was inhibited with ε-aminocaproic acid, the colchicine-induced generalized Schwartzman reaction could also be elicited in nonpregnant rats. In this regard fibrinolysis inhibition represents one mechanism by which pregnancy prepares for the generalized Schwartzman reaction (*Am J Pathol* 69:131-138, 1972).

THE GENERALIZED SCHWARTZMAN REACTION can be produced in rabbits with two appropriately spaced intravenous injections of endotoxin.¹ In the pregnant rabbit or rat it can be elicited by a single injection of bacterial endotoxin.^{2,3} The reaction is characterized by the appearance of glomerular capillary thrombi, leading to bilateral cortical necroses of the kidneys.⁴ Glomerular capillary thrombosis is mediated by disseminated intravascular coagulation.^{5,6}

Similar pathoanatomic changes are observed in pregnant golden hamsters in response to a single intraperitoneal injection of colchicine.^{7,8} The importance of pregnancy is of particular interest, since, until now, the generalized Schwartzman reaction could not be induced by colchicine in a nonpregnant animal. This drug blocks mitosis, leading to cell death. It has been proposed that the injection of colchicine causes fetal death and damages the placenta.⁵ Consequently, thrombo-plastic material released from the pregnant uterus would initiate intravascular coagulation. This theory implies that the pregnant uterus, placentae and fetuses are required to induce the generalized Schwartzman reaction.

From the Department of Medicine, Justus Liebig-Universität, Giessen, Germany. Supported by the Deutsche Forschungsgemeinschaft.

Accepted for publication June 20, 1972.

Address reprint requests to Dr. G. Müller-Berghaus, Department of Medicine, Justus Liebig-Universität, Klinikstrasse 32b, 63 Giessen, Germany.

The aim of this study was to transfer the model of colchicine-induced Shwartzman reaction to another species and evaluate the importance of pregnancy. The results demonstrate that the generalized Shwartzman reaction could be initiated by a single injection of colchicine into the pregnant rat. Furthermore, the generalized Shwartzman reaction could be evoked in nonpregnant rats, if activation of the fibrinolytic system was inhibited by ϵ -aminocaproic acid.

Materials and Methods

Animals

Female albino Sprague-Dawley rats weighing 200 to 300 g were used throughout this study. All of the animals were fed Altromin K laboratory chow and given tap water *ad libitum*.

Hysterectomy

Hysterectomy was performed on animals in their twentieth day of pregnancy. Ether was used as an anesthetic. The uterus with its various horns was removed after applying one ligature around the cervix and two ligatures between the right and left ovaries and the uterus, thus leaving the ovaries *in situ*. Subsequently, the abdomen was sutured. In sham-operated animals, the uterus was pulled out of the abdominal cavity, repositioned and the abdominal walls sutured. The entire procedure lasted about 10 to 15 minutes.

Colchicine

Colchicine (Merck, Darmstadt, Germany) was dissolved in sterile, pyrogen-free physiologic saline solution to obtain a concentration of 1 mg/ml. The rats were injected intravenously with 2 mg of colchicine/kg body weight.

Endotoxin

Escherichia coli endotoxin, O55:B5, lipopolysaccharide B (Difco Laboratories, Detroit, Mich.) was used. The endotoxin was freshly dissolved in sterile pyrogen-free isotonic saline before every experiment, so that 400 μ g were contained in 1 ml of saline. The rats were anesthetized with ether and the endotoxin administered through the lateral tail vein.

ϵ -Aminocaproic Acid

In rats that received an inhibitor of the fibrinolytic system, 200 mg of ϵ -aminocaproic acid (EACA) were injected intraperitoneally 8, 9 and 10 hours after the administration of colchicine, in 3 doses, for a total dose of 600 mg. Control animals received the same volume of saline instead of EACA.

Histology

Necropsies were performed immediately after death. Organs were fixed in 5% neutral formalin and histologic sections stained with hematoxylin and eosin. Fibrin was detected by the dimethylaminobenzaldehyde-nitrite reaction for the histochemical demonstration of tryptophane, according to the method described by Adams.⁹

Results

Group 1. Induction of the Generalized Shwartzman Reaction in the Pregnant Rat

Sixteen nonpregnant rats were injected with colchicine (2 mg/kg); 62 pregnant rats were given the same dose of colchicine on different days of gestation (Table 1). All animals survived for at least 10 hours after the injection of colchicine. Those surviving longer were sacrificed 12 to 48 hours postinjection.

At necropsy, nonpregnant rats injected with colchicine did not show any hemorrhages. The gross appearance of the lungs, spleen and adrenal glands were within normal limits, livers of most animals were fatty and their kidneys were sometimes hyperemic. Colchicine-treated pregnant rats differed from nonpregnant animals; their kidneys were enlarged and hyperemic and sometimes petechial hemorrhages were seen on their surfaces. The lobular pattern of the liver was mostly accentuated, and livers were fatty; spleen, adrenal glands and lungs were within normal limits.

The most striking differences were those seen histologically. Colchicine triggered the formation of glomerular capillary thrombi in all 32 rats on days 19, 20 and 21 of gestation at the time of the injection (Table 1). The incidence of glomerular capillary thrombi was reduced in rats with shorter gestational periods. Fibrin thrombi in the kidneys were first observed on day 16 of gestation. None of 16 nonpregnant rats showed renal fibrin thrombi.

The incidence of microthrombi in other organs is summarized in Table 1. Fibrin thrombi were never seen in the lungs or adrenal glands, regardless of whether animals were pregnant or nonpregnant. Most interestingly, fibrin thrombi were detected microscopically in the liver and spleen of pregnant as well as nonpregnant rats. The frequency with which fibrin was found in the liver and spleen did not seem to be related to pregnancy, since the percentage incidence did not increase with the duration of pregnancy.

Group 2. Time Dependence of the Occurrence of Microthrombosis after Colchicine and Endotoxin Injections

Thirty-three pregnant rats were injected with colchicine on day 20 of gestation and sacrificed at different intervals after the administration of colchicine. Forty-two pregnant rats were injected with endotoxin on day 20 of gestation and surviving animals were sacrificed 24 hours later. When the colchicine-treated animals were sacrificed 9 or 10 hours after the injection, the kidneys were pale and patchy, whereas at 12 hours postinjection the kidneys were enlarged and hyperemic.

Table 1—Incidence of Microthrombosis in Kidneys, Lungs, Liver, Spleen and Adrenal Glands and Incidence of Focal Liver Necrosis after Intravenous Injection of Colchicine into Pregnant and Nonpregnant Rats*

Length of gestation (days)	Incidence of glomerular capillary thrombosis	Incidence of pulmonal micro-thrombosis	Incidence of hepatic focal necrosis and/or micro-thrombosis	Incidence of splenic micro-thrombosis	Incidence of adrenal micro-thrombosis
—	0/16	0/16	5/16	2/16	0/16
10	0/3	0/3	0/3	0/3	0/3
14	0/5	0/5	4/5	1/5	0/5
16	1/7	0/7	2/7	1/7	0/7
17	3/7	0/7	3/7	0/7	0/7
18	6/8	0/8	4/8	4/8	0/8
19	9/9	0/9	3/9	3/9	0/9
20	13/13	0/13	4/13	7/13	0/13
21	10/10	2/10	2/10	3/10	0/10

* Values given as the ratio of number of animals affected to number of animals tested

Glomerular capillary thrombi were first observed 9 hours after the injection of colchicine, whereas, in the endotoxin-induced generalized Schwartzman reaction, fibrin was already detected 2½ hours after the administration of endotoxin (Table 2). Fibrin was found in the glomerular capillaries of all colchicine-treated animals 12 hours after the injection. Renal cortical necrosis was observed only in animals sacrificed 12 hours after postinjection, whereas, in the endotoxin-induced generalized Schwartzman reaction, renal cortical necrosis was already seen 9 hours after endotoxin was administered. The presence of fibrin thrombi in liver and spleen parallels the appearance of renal thrombi (Table 2).

Group 3. Induction of the Generalized Schwartzman Reaction by Colchicine in Hysterectomized "Pregnant" Rats

The importance of the conceptus was studied in 12 rats hysterectomized on day 20 of gestation. Colchicine was injected immediately after the operation. Fibrin thrombi were found in the glomerular capillaries of all hysterectomized as well as the 5 sham-operated animals after the injection of colchicine (Table 3).

Group 4. Production of the Generalized Schwartzman Reaction by Colchicine in Nonpregnant Rats Treated with ϵ -Aminocaproic Acid

The observation that pregnancy is associated with the retention of glomerular capillary thrombi by fibrinolysis inhibition^{4,10,11} made it

Table 2—Incidence of Renal Cortical Necrosis and Microthrombosis in Renal Glomerular Capillaries, Liver and Spleen at Different Times after Intravenous Injection of Endotoxin or Colchicine into Pregnant Rats*

Time after injection of endotoxin or colchicine (hours)	Treatment	No. of Rats	Incidence of glomerular capillary thrombosis	Incidence of renal cortical necrosis	Incidence of hepatic focal necrosis and/or micro-thrombosis	Incidence of splenic micro-thrombosis
2½	Endotoxin	2d	2/2	0/2	—	—
3	Endotoxin	14d	11/14	0/14	—	—
4	Endotoxin	8d	6/8	0/8	—	—
9-10	Endotoxin	4d	4/4	3/4	—	—
12-24	Endotoxin	14d, s	6/14	6/14	—	—
6	Colchicine	4s	0/4	0/4	0/4	0/4
8	Colchicine	5s	0/5	0/5	0/5	0/5
9	Colchicine	7s	2/7	0/7	4/7	3/7
10	Colchicine	9s	5/9	0/9	2/9	0/9
12	Colchicine	8s	8/8	4/8	4/8	3/8

* Values given as the ratio of number of animals affected to number of animals tested
d = animals died; s = animals sacrificed

reasonable to substitute the exogenous inhibition of the fibrinolytic system for pregnancy. Fifteen nonpregnant rats were injected with colchicine. Ten of these were injected intraperitoneally three times with 200 mg of EACA 8, 9 and 10 hours after the administration of colchicine, whereas 5 rats (controls) received saline instead of EACA. The animals were sacrificed 11 hours after the injection of colchicine. In 9 of 10 animals injected with colchicine and EACA, fibrin thrombi were found in the glomerular capillaries, whereas thrombi were not detected in the controls. The degree of thrombosis in glomerular capillaries seemed less in nonpregnant rats treated with EACA than in pregnant rats.

Table 3—Incidence of Renal Glomerular Capillary Thrombosis after Intravenous Injection of Colchicine into Hysterectomized or Sham-Operated Pregnant Rats*

Treatment	No. of Rats	Incidence of glomerular capillary thrombosis
Hysterectomy	12	12/12
Sham operation	5	5/5

* Values given as the ratio of number of animals affected to number of animals tested

Table 4—Incidence of Renal Glomerular Capillary Thrombosis after Intravenous Injection of Colchicine into Nonpregnant Rats Treated with ϵ -Aminocaproic Acid (EACA) or Isotonic Saline*

Treatment	No. of Rats	Incidence of glomerular capillary thrombosis
EACA	10	9/10
Saline	5	0/5

* Values given as the ratio of number of animals affected to number of animals tested

Discussion

The injection of colchicine into pregnant rats caused disseminated intravascular coagulation with fibrin thrombi in the renal glomerular capillaries characteristic of the generalized Schwartzman reaction. Bilateral renal cortical necroses as well as hemorrhages and necroses in various organs were observed. Glomerular capillary thrombi were found in 100% of the rats on day 19 to 21 of gestation who lived at least 12 hours after the injection of colchicine. Renal cortical necrosis occurred secondary to the occlusion of glomerular capillaries, since necrosis was not seen before the generation of microthrombi. The results demonstrate that colchicine may induce the generalized Schwartzman reaction in other species besides the golden hamster. Interestingly enough, endotoxin, the most studied procoagulant substance, does not induce the generalized Schwartzman reaction in either the nonpregnant or pregnant golden hamster.⁸ If endotoxin is injected into a pregnant rat, fibrin strands can be seen in the glomerular capillaries as early as 2½ hours after the injection of endotoxin. If, however, colchicine is used to induce the generalized Schwartzman reaction, the first fibrin thrombi were seen 9 hours postinjection, indicating a quite different mechanism for triggering the coagulation system. Since colchicine does not act directly on the coagulation system, several indirect pathways have been postulated to explain the induction of disseminated intravascular coagulation. Initially it was thought that endotoxin was released from the gastrointestinal tract into the circulatory system after colchicine injection.⁷ This explanation for the effect of colchicine in the golden hamster had to be abandoned, since endotoxin did not initiate disseminated intravascular coagulation and sterilization of the gastrointestinal tract failed to reduce the incidence of colchicine-induced generalized Schwartzman reaction.⁸

The observation that all fetuses were macerated at the time of autopsy suggested the theory that procoagulant material might have been

released by macerated fetuses or placentas. We examined this theory by trying to induce the generalized Schwartzman with colchicine in hysterectomized pregnant rats. The importance of uterus, fetus and placenta was excluded, since all hysterectomized rats developed the generalized Schwartzman reaction after colchicine injection. However, in the golden hamster, hysterectomy prevented the reaction.⁸ It cannot be decided whether species differences, different timing or anesthetics are responsible for these contrasting results.⁸ It is known that agents such as anesthetics which influence vasomotor activity have modifying effects on the induction of the generalized Schwartzman reaction.¹² That the uterus, fetus and placenta do not play an important role in the generalized Schwartzman reaction is stressed by the observation that, in hysterectomized pregnant rats, this reaction can still be induced by a single injection of endotoxin.¹³

Since the uterus, fetuses and placentas are not essential for the induction of the generalized Schwartzman reaction in the pregnant rat by colchicine injection, it seemed conceivable that it could be produced in the nonpregnant rat. However, a single injection of colchicine did not induce the reaction in these animals until the fibrinolytic system was inhibited. These findings again demonstrate that the uterus, fetus and placenta are not necessary for the induction of colchicine-induced generalized Schwartzman reaction in the rat. Obviously, fibrinolysis inhibition is at least one mechanism by which pregnancy prepares for the colchicine-induced generalized Schwartzman reaction. This observation is in accordance with experiments by Margaretten *et al*,⁴ who established the importance of fibrinolysis inhibition in the thrombin-induced generalized Schwartzman reaction in the rat.

The present study demonstrates that only the third trimester of pregnancy prepares for the generalized Schwartzman reaction. This is true whether the reaction is induced by colchicine or by endotoxin. Most likely, inhibition of the fibrinolytic system, which increases during the course of pregnancy and is most pronounced at the time of parturition,¹⁴⁻¹⁶ is responsible for this phenomenon.

References

1. Thomas L, Good RA: Studies on the generalized Schwartzman reaction. I. General observations concerning the phenomenon. *J Exp Med* 96:605-623, 1952
2. Apitz K: Die Wirkung bakterieller Kulturfiltrate nach Umstimmung des gesamten Endothels beim Kaninchen. *Virchows Arch [Pathol Anat]* 293:1-33, 1934
3. Wong T-C: A study on the generalized Schwartzman reaction in pregnant rats induced by bacterial endotoxin. *Am J Obstet Gynecol* 84:786-797, 1962

4. Margaretten W, Zunker HO, McKay DG: Production of the generalized Schwartzman reaction in pregnant rats by intravenous infusion of thrombin. *Lab Invest* 13:552-559, 1964
5. McKay DG: Disseminated Intravascular Coagulation. An Intermediary Mechanism of Disease. New York, Harper and Row Publishers, Inc, Hoeber Medical Division 1964
6. Kleinmaier H, Georgen K, Lasch HG, Krecke H-J, Bohle A: Untersuchungen zur Frage der Gerinnungsstörung beim Sanarelli-Schwartzman-Phänomen (Sog. generalisierten Schwartzman-Phänomen) des Kaninchens. *Z Gesamte Exp Med* 132:275-294, 1959
7. Galton M: Studies of the generalized Schwartzman reaction in the pregnant golden hamster. *Am J Pathol* 44:613-627, 1964
8. Galton M: Thrombosis in the pregnant syrian hamster. *Trans NY Acad Sci* 28:423-438, 1966
9. Adams CWM: A *p*-dimethylaminobenzaldehyde-nitrite method for the histochemical demonstration of tryptophane and related compounds. *J Clin Pathol* 10:56-62, 1957
10. Epstein MD, Beller FK, Douglas GW: Kidney tissue activator of fibrinolysis in relation to pregnancy. *Obstet Gynecol* 32:494-504, 1968
11. Beller FK, Graeff H, Gorstein F: Disseminated intravascular coagulation during the continuous infusion of endotoxin in rabbits. *Am J Obstet Gynecol* 103:544-554, 1969
12. Müller-Berghaus G, McKay DG: Prevention of the generalized Schwartzman reaction in pregnant rats by α -adrenergic blocking agents. *Lab Invest* 17:276-280, 1967
13. Müller-Berghaus G, Schmidt-Ehry B: The role of pregnancy for the induction of consumption coagulopathy. (In press)
14. Shaper AG, Macintosh DM, Evans CM, Kyobe J: Fibrinolysis and plasminogen levels in pregnancy and the puerperium. *Lancet* II: 706-708, 1965
15. Beller FK, Douglas GW, Morris RH, Johnson AJ: The fibrinolytic enzyme system in pregnancy. A comparison between ovarian and antecubital blood. *Am J Obstet Gynecol* 101:587-592, 1968
16. Kleiner, GJ, Merskey C, Johnson AJ, Markus WB: Defibrination in normal and abnormal parturition. *Br J Haematol* 19:159-178, 1970

Ultrastructural and Histochemical Studies of Murine Megacolon

Robert P. Bolande, MD and William F. Towler

The myenteric plexus of the colon was studied ultrastructurally in a colony of an Ls/Ls strain of mice manifesting a piebald coat color mutation associated with a high incidence of genetically determined aganglionic megacolon. Ultrastructural studies were histochemically supplemented by the Maillet technic and stains for acetylcholinesterase and catecholamines. The development of megacolon did not appear to require total aganglionosis, since ostensibly aganglionic areas contained rare ganglion cells. In the distal narrowed segment, both cholinergic and adrenergic fibers in the muscularis, submucosa and mucosa were somewhat reduced. In the mouse, the dilated portion showed an abrupt increase in adrenergic fibers. These findings are related to the pathophysiology of the disorder. The increasing degenerative changes seen in myenteric plexus structures from the fetus to adult suggest that aganglionic megacolon may be an *abiotrophy*, wherein the congenitally deficient myenteric plexus may be unusually predisposed to postnatal injury and degeneration (Am J Pathol 69:139-162, 1972).

IT HAS BEEN APPRECIATED for some time that the profound constipation and megacolon characterizing Hirschsprung's disease is associated with a deficiency of ganglion cells in the myenteric plexus of the distal colon.¹⁻⁴ A sizable body of information has accumulated concerning the details of the gross and microscopic anatomy of this disease from which a rational surgical treatment and cure have been developed.⁵ Nevertheless, considerable uncertainty and confusion about many aspects of its pathophysiology and pathogenesis still exist.

The degree of neural deficiency needed to produce the clinical and pathologic features of Hirschsprung's disease is uncertain. Complete aganglionosis is required by many pathologists for a histologic diagnosis of Hirschsprung's disease. Yet fairly severe megacolon has been observed in which ganglion cells are reduced in number rather than completely absent; this has been referred to as *hypoganglionosis*.⁵⁻⁹ Conversely, the degree to which the myenteric plexus structure can

From the Departments of Pathology, The Children's Hospital of Akron, Akron, Ohio, and Case Western Reserve University, Cleveland, Ohio.

Presented in part at the Pediatric Pathology Club section of the American Association of Pathologists and Bacteriologists at the annual meeting in Montreal, Quebec, Canada, 1971.

Accepted for publication July 11, 1972.

Address reprint requests to Dr. Robert P. Bolande, Director of Laboratories, The Children's Hospital of Akron, Buchtel Ave at Bowery, Akron, Ohio 44308.

be reduced and the bowel still maintain its relatively normal function is unknown.

The deficiency of ganglion cells and the abnormality of myenteric plexus structure is generally assumed to result from a defective migration of parasympathetic ganglion cell precursors of the neural crest into the embryonic hindgut.¹⁰⁻¹³ The validity of this concept has not been firmly established. Similarly, the role played by genetic, teratogenic or other postnatal influences in the evolution of megacolon has not been fully delineated.⁵

The distal narrowed segment is generally thought to result from the spastic, contracted state of the muscularis. Parasympathetic stimulation ordinarily results in spastic contraction of the intestine, while sympathetic stimulation results in relaxation and dilatation. A parasympathetic deficiency of the bowel wall would seem to be inconsistent with a spastic state of the narrowed segment. Thus, some have maintained that the narrowed segment is, in reality, flaccid and incapable of transmitting peristalsis. It is a well-known physiologic fact that denervated smooth muscle is abnormally sensitive to stimuli and tends to contract permanently (Cannon's Law). According to Ehrenpreis,⁵ Cannon's law offers "a simple and perfectly good explanation of the pathophysiology in Hirschsprung's disease, covering all the observations made by different methods of approach."

Recent physiologic studies have shown that in Hirschsprung's disease there is an abnormal anorectal reflex.¹⁴⁻¹⁶ In normal individuals, distension of the rectum causes reflex relaxation of the internal anal sphincter, permitting evacuation. This reflex does not occur in individuals with Hirschsprung's disease. Indeed, high muscular tone of the entire distal colon seems to be maintained and the colon appears to be incapable of relaxation, even after sympathetic stimulation.^{17,18}

Histochemical techniques capable of specifically demonstrating the presence of catecholamines and acetylcholinesterase in nervous tissue have been developed. These methods have proved useful in attempts to study the interplay of adrenergic and cholinergic effects on the terminal autonomic nervous system in normal intestine and in Hirschsprung's disease.¹⁹⁻²⁹ These studies have been aimed at reconciling some of the peculiar features of the disease and have suggested explanations of its pathophysiology through variations in the terminal autonomic nervous innervation of the colon. The use of some of these techniques in the diagnosis of Hirschsprung's disease has been proposed.²⁷⁻²⁹

Elucidation of the ultrastructural morphology of the terminal au-

tonomic nervous system³⁰⁻³² has made it possible to distinguish cholinergic and adrenergic nerve fibers by the structural nature of their neurosecretory contents. Nerve fibers were found to contain both small, clear vesicles (200 to 500 Å in diameter), as well as dense-core granules (500 to 1100 Å in diameter). The former probably represent acetylcholine, while the latter are thought to represent norepinephrine or related biogenic amines. In addition, the fine features of the presynaptic axon and its axosomatic and axodendritic junctions with ganglion cells, as well as terminations of the postganglionic fibers at the neuroeffector site have been described (Figures 1 and 2).

The innervation of the intestinal tract has been specifically studied by a number of investigators, and the knowledge derived has helped to form a basis for the ultrastructural study of aganglionic megacolon.³³⁻⁴¹

The purpose of this study was to apply a combination of ultrastructural and histochemical technics to study of the terminal autonomic nervous system relationships in a genetic form of megacolon in the lethal spotted (Ls) mutant strain of mice. Through such an approach it was hoped that answers to some of the questions, cited above, concerning the nature and pathogenesis of megacolon in both mouse and man, might be suggested.

Materials and Methods

A colony of the Jackson Laboratory lethal spotting strain of C57BL-a+ mice was established for study.⁴²⁻⁴⁴ This mouse strain, characterized by a black-and-white, spotted or piebald mutation in coat color, manifests a high incidence of aganglionic megacolon (Figure 3). It is derived from an Agouti-colored parent strain which is heterozygous for the genetic defects described. By cross-breeding black and white homozygotes (Ls/Ls), it was possible to produce litters in which all sibs had aganglionosis.⁴⁴ Cross-breeding must be carried out prior to 3 months of age since, after this time, the homozygotes tend to sicken and die from megacolon.

A total of 45 mice from 16-day-old fetuses to 3 months of age were studied; all showed clear-cut histologic evidence of aganglionosis and/or megacolon. Particular emphasis was placed on the 16 animals which had severe gross megacolon. Gross megacolon is manifested as a markedly distended colon filled with either soft, gelatinous fecal material or a condensed, impacted mass of fecal pellets extending into the proximal rectum. A short, narrow segment from distal rectum to anus which is devoid of feculent material is always present (Figure 4). This contrasts markedly with the narrow caliber and beaded configuration caused by small fecal pellets, seen in normal mice. The experimental animals were compared with a series of normal Agouti control mice of comparable age. The experimental series is recorded in Table 1.

The animals were sacrificed by cervical dislocation; the abdominal contents were immediately immersed in 6.25% buffered gluteraldehyde, in which dissection and final sectioning of the colon were carried out. Tiny sections of the colon, which were oriented cephalocaudally to include samples of the distal narrowed segment, dilated

Table 1—Study Series of Ls/Ls Mice

Age	Aganglionic	Gross Megacolon
Fetuses (16 to 19 days' gestation)	10	0
Newborns (day 1)	7	0
Day 7-8	12	1
2 to 3 Weeks	8	8
4 to 6 Weeks	4	3
Adults (7 Weeks-3 Months)	4	4
Total	45	16

segment and proximal normal colon, were fixed for 1 hour in glutaraldehyde. These tissues were washed in buffered sucrose and postfixed in 1% OsO₄ in acetate-veronal buffer, then dehydrated in graded alcohols and embedded in Araldite. Ultrathin sections (0.1 μ) were prepared on a Porter-Blum microtome and stained with toluidine blue (0.5%). These sections were evaluated, histologically and optimal blocks were selected from them for electron microscopy. From these blocks, carbon-coated Formvar grids, doubly-stained with aqueous uranyl acetate and lead citrate, were prepared. The grids were examined on an RCA-EMU-3H electron microscope.

In 4 Ls/Ls mice (age 3 weeks) which showed severe gross megacolon, frozen sections were prepared from different levels of fresh colon. These sections were dried rapidly and stained according to the method of El-Badawi and Schenk⁴⁵ so as to demonstrate catecholamines and acetylcholinesterase simultaneously. The prepared slides were examined by ultraviolet, dark-field⁴⁶ and conventional light microscopy. Colonic tissue from 4 age-matched Agouti control mice was processed in the same manner.

Fresh colonic tissue from two adult and two 3-week old Ls/Ls mice with gross megacolon was prepared and stained according to the method of Maillet.⁴⁷ Comparable control colons from 2 adult Agouti mice were handled in an identical manner. Tiny tissue fragments, which were cephalocaudally oriented, were immersed immediately in a reagent of 2% OsO₄ and 3% ZnI₂ (1:4) for 15 hours at room temperature. Tissue aliquots were dehydrated and embedded in both paraffin and Araldite. Sections were prepared for light microscopy from the paraffin blocks in a conventional manner. Ultrathin sections and Formvar grids were prepared from the Araldite blocks, as described above. Sections were then studied by light and electron microscopy. The Maillet stain appears to have a remarkable selectivity for neural tissue, particularly nonmyelinated nerve fibers, nerve terminals and synaptic vesicles.⁴⁵ The stain does not affect adrenergic fibers or their dense-core granules; thus it may have some selective affinity for cholinergic fibers.^{48,49}

Results

Despite the seeming barrenness of the zone between the longitudinal and circular muscle layers in aganglionic colon, neural structure was regularly encountered ultrastructurally. Fairly large axon bundles enveloped in Schwann cell cytoplasm were seen. In some areas, the nerve fibers tended to be swollen and tortuous and often

had lost their distinct neurotubulation (Figure 5). Dense-core granules were rare in these fibers, in contrast with the abundance of such granules in normal areas.

In normal areas, clusters of ganglion cells were present; numerous axon bundles enclosed in Schwann cell cytoplasm were seen around these clusters. Some of these fibers, which were devoid of Schwann cell investment, were closely apposed to ganglion cell cytoplasm or its dendritic extensions. These formed preganglionic synapses (axosomatic and axodendritic), which were characterized by a bulbous enlargement of the fiber which could indent the neuronal cytoplasm and which contained numerous dense-core granules.

In overt megacolon, ganglion cells were often found in histologically aganglionic areas. Generally, the cells occurred singly, but occasional clusters of 2 to 3 cells could be identified. The cells were small, ovoid and relatively devoid of dendritic extensions. Presynaptic axons and nerve trunks were only focally related to their surfaces, and synaptic areas were rare. Fibers with dense-core granules are unusual in these areas (Figure 10). Large nerve bundles which were completely or partially tunicated by Schwann cells were present throughout the zone between longitudinal and circular muscle masses (Figure 6). In the distal narrowed segment, these nerve fibers were unusually swollen and tortuous; they showed evidence of neurotubular and neurofibrillary disintegration and dense body formation (Figure 7). This change seemed characteristic of this area and was associated with a marked paucity of both types of neurosecretory granules within fibers.

In the intermuscular spaces of the circular and longitudinal muscle layers, the aganglionic colon showed the presence of rare axon bundles. These were not as prominent or numerous as in normal colons; clearly there was no increase. Deeper in the muscular layers, the fibers tended to become smaller and lose their Schwann cell investment and approached the smooth muscle surface without distinct synaptic junctions. At this level, fibers with dense-core granules were definitely seen but were rare and irregularly distributed. Fibers with no definite neurosecretory structures or small, clear vesicles were preponderant. Occasionally, fibers contained both small, clear vesicles and dense-core granules.

Particular emphasis was placed on the analysis of intermuscular fibers within the circular and longitudinal muscles of the distal narrowed segments; there was clearly no increase in the number and size of fibers; generally, the trend was toward a decrease. Analysis of

the mucosal and submucosal fibers suggested a marginal degree of increase in the narrowed segments, as compared to the dilated or normal portions of colon.

Proceeding proximally into the dilated segment and then into the normal areas, there was a gradual increase in numbers of ganglion cells, greater evidence of axosomatic and axodendritic synapses, less evidence of degenerative alterations and, particularly, a striking increase in the number of dense-core granules in nerve fibers. Differences between the various levels were chiefly quantitative, with the exception of the narrowed segment, where swelling and degenerative changes in nerve fibers, indicated above, seemed to be distinct and pronounced.

When the series was viewed chronologically, it was apparent (Table 1) that the development of gross megacolon increases with age in aganglionic mice. This seemed to be accompanied by increasing evidence of degenerative changes in myenteric plexus constituents. There was increasing formation of dense bodies and vacuolar degeneration of cells, so that significant disruption of cell structure took place after 4 weeks of age.

Analysis of the series of late-gestation fetuses showed that normal myenteric plexus structure was at first composed of a mosaic of closely-packed, round ganglion cells with little intervening Schwann cell substance or nerve fibers (Figure 8). Shortly after birth, the number of Schwann cells and nerve fibers surrounding the nerve cells increased remarkably. In aganglionic (Ls/Ls) mice, the fetuses and newborns did not differ significantly. There was a distinct reduction of ganglion cells in these animals but ganglion cells were clearly present. Degenerative changes affecting nerve cells and nerve fibers were present to a slight extent in the fetus and newborn as well. These changes were characterized by focal swelling of nerve fibers, retraction of ganglion cell-cytoplasm and diminution or loss of cytoplasmic organelles (Figures 9 and 10). These degenerative changes were not as extensive as those found in animals after 4 weeks of age. Furthermore, intact ganglion cells were more frequent and thus easier to identify than in older animals.

Colonic tissue from control Agouti mice stained by the El-Badawi-Schenk method revealed, on light microscopy, the intense orange-brown staining of the neurons and nerve fibers within the myenteric plexus and submucosal plexus, indicating the presence of acetylcholinesterase activity. Fine fiber staining was identified between

muscle fibers in both the circular and longitudinal muscle layers; fine fiber ramifications were stained in the submucosa which terminated near mucosal glands. Staining appeared to be limited to neural tissue (Figure 11). Examination of this material under dark-field microscopy revealed illumination of the same sites of staining.⁴⁶ Further examination of these same slides under ultraviolet light showed the presence of adrenergic fibers by their yellowish-green fluorescence, which was produced by the condensation of catecholamines with hot formaldehyde vapor to form an intensely fluorescent isoquinolone.²³ Fluorescence was chiefly concentrated around the cell bodies of the myenteric plexus. Intermuscular fiber staining was also present, but to a much lesser extent. Fibers which contained catecholamine were not prominent in the mucosa and submucosa.

By comparison Ls/Ls mice with megacolon showed a marked reduction of both acetylcholinesterase- and catecholamine-staining fibers in all layers of aganglionic colon. The extent of reduction was comparable in the narrowed segment and the dilated portion. Rare nodular and linear aggregates of dense acetylcholinesterase staining were present in the zone between the longitudinal and circular muscle layer, suggesting the presence of nerve fibers or rare ganglion cells (Figure 12). There was clearly no evidence of increased numbers of either acetylcholinesterase- or catecholamine-containing fibers between muscle fibers of either the circular or longitudinal muscle layers.

The distribution of nerve fibers indicated by all the methods used was paralleled and emphasized by both light and electron microscopic studies of Maillet-stained material. The selective intensity of the staining reaction in nerve fibers allows for more precise quantitation, particularly on the electron microscope. With the Maillet staining technic, the diminution of small intermuscular fibers within the circular and longitudinal muscle layers of the distal narrowed segment, as well as the slight or marginal increase of mucosal and submucosal fibers was reaffirmed (Figures 13-15).

Discussion

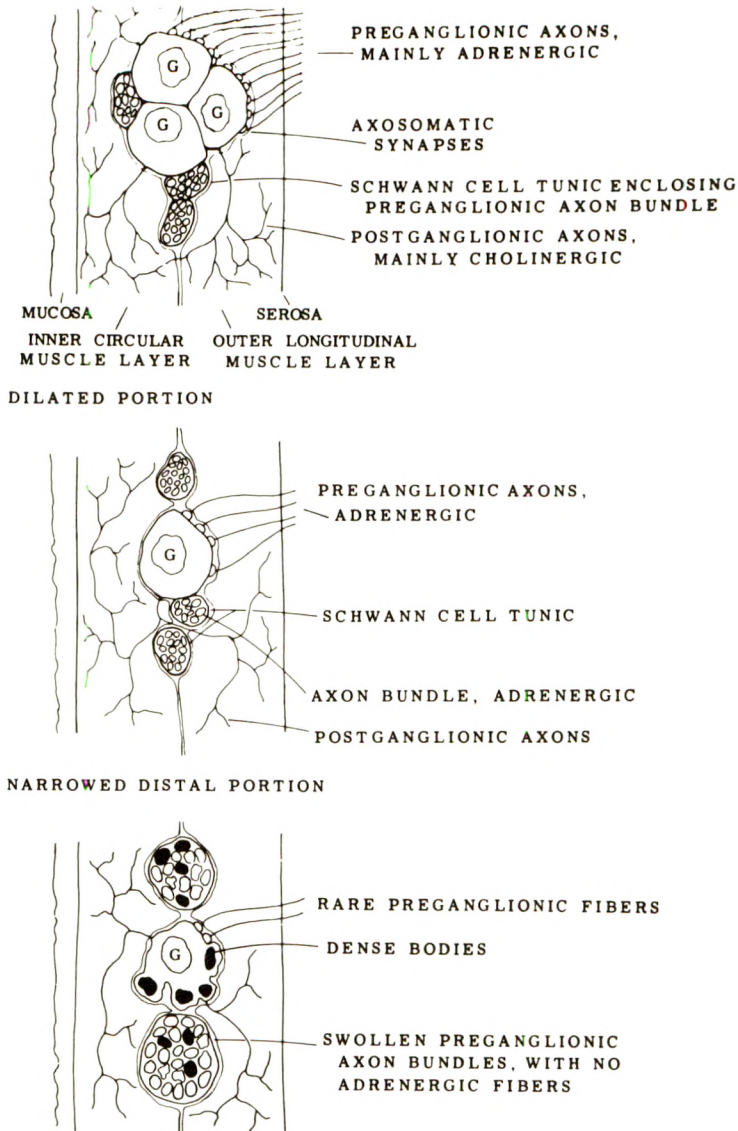
The major thrust of this study was based on electron microscopic observations. With this method, assessment of quantitative differences in nerve cell and fiber constituency was difficult because of the limitations of sample size. Also, the appraisal of adrenergic and cholinergic relationships from neurosecretory granule content was subject to similar practical and other theoretical criticisms. The histochemical studies on a series of mice gave a better quantitative perspective.

In our hands, the acetylcholinesterase staining methods proved extremely reliable, while the catecholamine fluorescence technic was difficult to control. Furthermore, the unequivocal identification of a cholinergic fiber by acetylcholinesterase staining alone is not acceptable, since it appears clear that adrenergic fibers contain acetylcholinesterase and acetylcholine, as well as norepinephrine.^{50,51} The presence of both dense-core granules and small clear vesicles in the same fiber, observed by us and others on the electron microscope, goes along with this concept.^{31,33,37}

Despite the cited weaknesses in methodology, certain semiquantitative and even qualitative differences seem apparent when ultrastructure, acetylcholinesterase staining and the Maillet technic are all used to compare aganglionic and normal colon. Ultrastructurally, aganglionic colon has a surprisingly complex and prominent neural structure. Large tunicated nerve bundles are present in the zone between the circular and longitudinal muscle layers. Extending between muscle fibers in both the circular and longitudinal layers are delicate, tiny nerve bundles, some of which are probably postganglionic fibers. These seem somewhat reduced in number in the aganglionic colon.

The development of severe megacolon in the mouse does not appear to require complete aganglionosis, since rare, and often bizarre, degenerate ganglion cells are usually demonstrable in histologically aganglionic areas. These tend to be more prominent in the dilated portion but may also be found in the distal narrowed segment, particularly in the mouse. The term *hypoganglionosis* would thus seem to be more descriptive.

The distal narrowed segment is characterized by a marked deficiency of dense-core granules within nerve fibers. At the same time, there is a marked swelling and tortuosity of existing nerve fibers within the plexus. Proximally there is increasing evidence of dense-core granules, particularly in the dilated portion of the colon. We could not demonstrate an increase in intermuscular acetylcholinesterase-containing fibers, either histochemically or ultrastructurally. Distinct acetylcholinesterase activity, although considerably reduced, was present in mouse colon at all levels, but was chiefly limited to nerve fibers and rare ganglion cells in the zone between the circular and longitudinal muscle layers. Yet a marked diminution of catecholamine fluorescence could be detected in aganglionic colon, so that the fluorescent nerve fiber networks ramifying about the ganglion cells in normal colon were not identifiable. Also, fine fluorescent fibers ramifying between muscle cells could not be identified. Our findings are schematically summarized in Text-figure 1.



TEXT-FIG 1—Schematic representation of pathologic changes in murine megacolon. Normal is represented at the top, with changes then shown in the dilated and finally the distal, narrowed segments. G = ganglion cells.

These findings suggest that the narrowed segment of aganglionic mouse colon is indeed spastic, as a result of a deficiency of the adrenergic inhibition of cholinergic nervous activity, despite the fact that cholinergic nerves are also deficient. The small numbers of the latter may still be sufficient to induce spastic contraction in the absence of adrenergic innervation. Proximally, increasing adrenergic

innervation might cause greater relaxation and dilatation of the bowel, but under these conditions the persisting cholinergic deficiency is insufficient for adequate propulsion. A similar interpretation is possible in the human material, except that the abrupt increase of adrenergic fibers in the dilated portion is not as striking.

It was hoped that the addition of electron microscopic evidence might resolve some of the conflicting data derived from previous histochemical studies of aganglionic bowel. Both our ultrastructural and histochemical findings in the mouse and man are corroborative of the fluorescent studies of catecholamine distribution in Hirschsprung's disease by Ehrenpreis *et al.*²⁴ In our ultrastructural material there was a greater degree of adrenergic fiber distribution to normal colonic musculature than indicated by their studies. We were unable to demonstrate, by any method, an increase in cholinergic nerve fibers distributed to the aganglionic bowel musculature analogous to that as reported by other investigators in human Hirschsprung's disease.^{22,23,28,29} Instead, there seemed to be diminution of small fibers, demonstrable by electron microscopy, and acetylcholinesterase- and Maillet-staining of the distal narrowed segment and dilated portions as well. It is possible that the mouse might significantly deviate from the human in this regard. Yet no increase in intermuscular fibers of the circular and longitudinal muscle layers of aganglionic distal colon was apparent to us on ultrastructural examination of material from 6 patients with Hirschsprung's disease.⁵² Similarly, we were unable to demonstrate an increase of adrenergic fibers to aganglionic musculature in the mouse, analogous to that reported by other workers in humans.^{25,26} Our ultrastructural findings clearly deviate from the few published reports in this area.^{26,28} These conflicting data emphasize the difficulty and complexity of morphologically studying the terminal autonomic nervous system, by currently available techniques.

In the murine disease, progressive degenerative changes in myenteric plexus structure has important implications. These changes may well begin in fetal life and increase in intensity in postnatal life, possibly resulting in a progressive diminution of ganglion cells and their adnexal structures. This is further suggested by an increasing incidence of gross megacolon with advancing age in aganglionic mice. It is thus conceivable that aganglionic megacolon is an *abiotrophy*, wherein congenitally inadequate innervation of the colon predisposes to ongoing degeneration of the myenteric plexus in postnatal life. The mechanisms accounting for this degeneration are unknown. It is clear, in the mouse at least, that some ganglion cells have migrated

from the embryonic neural crest, but in insufficient quantities. This deficiency is genetically determined, but the postnatal degenerative changes may be environmentally or metabolically influenced.

These studies may have some relevance for the clinical approach to patients with Hirschsprung's disease. The pathologist should not require total aganglionosis in order to suggest the presence of a functionally abnormal bowel. Conversely, the presence of isolated ganglion cells in the presence of other clinical and pathologic features of Hirschsprung's disease in no way assures normal bowel function. Secondly, it is conceivable that the congenital deficiencies of neural structure present in the bowel might render the myenteric plexus unduly sensitive to injury by adverse metabolic conditions often encountered in the perinatal period—*e.g.*, anoxia, hypoglycemia, acidosis and electrolyte imbalance. Similarly, these defective structures may be unusually prone to injury by other neurotoxic agents in later life. It is clear that, in the mouse strain studied, hypoganglionosis is the result of a genetic defect which affects neural crest development and coat color; the entire syndrome can be explained as arising from an abnormality in primitive neuroectoderm. The extent to which genetic and environmental factors might interact in producing the congenital neural deficiency in the human is unknown.

References

1. Zuelzer WW, Wilson JL: Functional intestinal obstruction on a congenital neurogenic basis in infancy. *Am J Dis Child* 75:40-64, 1948
2. Swenson O, Bill AH Jr: Resection of rectum and rectosigmoid with preservation of sphincter for benign spastic lesions producing megacolon: an experimental study. *Surgery* 24:212-220, 1948
3. Whitehouse FR, Kernohan JW: Myenteric plexus in congenital megacolon. *Arch Intern Med* 82:75-111, 1948
4. Bodian M, Stephens FD, Ward BCH: Hirschsprung's disease and idiopathic megacolon. *Lancet* i:6-11, 1949
5. Ehrenpreis T: *Hirschsprung's Disease*. Chicago, Year Book Publishers, 1970
6. Roviralta E: Nouvelles orientations chirurgicales dans le traitement du megacolon congenital. *Ann Chir Infant* 3:155-158, 1962
7. Bentley JFR, Nixon HH, Ehrenpreis T, Spencer B, Lister J, Duhamel B, Paget R, Katz A: Seminar on Pseudo-Hirschsprung's disease and related disorders. *Arch Dis Child* 41:143-154, 1966
8. Madsen CM: *Hirschsprung's Disease*. Copenhagen, Munksgaard, 1964
9. Weinberg AG: The ano-rectal myenteric plexus: its relation to hypoganglionosis of the colon. *Am J Clin Pathol* 54:637-642, 1970
10. Yntema CL, Hammond WS: The origin of intrinsic ganglia of trunk viscera from vagal neural crest in the chick embryo. *J Comp Neurol* 101:515-541, 1954

11. Yntema CL, Hammond WS: Experiments in the presacral parasympathetic nerves and ganglia of the chick embryo. *Anat Rec* 115:382, 1953
12. Bodian M, Carter CO: A family study of Hirschsprung's disease. *Ann Hum Genet* 26:261-277, 1963
13. Okamoto E, Ueda T: Embryogenesis of intramural ganglia of the gut and its relation to Hirschsprung's disease. *J Pediatr Surg* 2:437-443, 1967
14. Lawson JON, Nixon HH: Anal canal pressures in the diagnosis of Hirschsprung's disease. *J Pediatr Surg* 2:544-552, 1967
15. Schnauffer L, Talbert JL, Haller JA, Reid NC, RW, Tobon F, Schuster MM: Differential sphincteric studies in the diagnosis of ano-rectal disorders of childhood. *J Pediatr Surg* 2:538-543, 1967
16. Tobon F, Reid NCRW, Talbert JL, Schuster NM: Nonsurgical test for the diagnosis of Hirschsprung's disease. *New Engl J Med* 278:188-194, 1968
17. Shepherd JJ, Wright PG: The application of studies *in vitro* to the management of Hirschsprung's disease and of megacolon in adults. *Am J Dig Dis* 13:434-441, 1968
18. Suster G, Kim IC, Barbero GJ: Rectal motility patterns in infants and children with aganglionic megacolon. *Am J Dis Child* 119:494-497, 1970
19. Kamijo K, Hiatt RB, Koelle GB: Congenital megacolon. A comparison of the spastic and hypertrophied segments with respect to cholinesterase activities and sensitivities to acetylcholine, DFB, and the barium ion. *Gastroenterology* 24:173, 1953
20. Niemi M, Kouvalainen K, Hjelt L: Cholinesterase and monoamine oxidase in congenital megacolon. *J Pathol Bact* 82:363-366, 1961
21. Norberg KA: Adrenergic innervations of the intestinal wall studied by fluorescence microscopy. *Neuropharmacology* 3:379-382, 1964
22. Emery JL, Finch E, Lister J: Use of circumferential tangential cryostat sections of the intestine in the diagnosis of Hirschsprung's disease. *J Clin Pathol* 20:263-266, 1967
23. Meier-Ruge W, Morger R: Neue Gesichtspunkte ur Pathogenese und Klinik des Morbus Hirschsprung. *Schweiz Med Wochenschr* 98:209-214, 1968
24. Ehrenpreis T, Norberg KS, Wirsén C: Sympathetic innervation of the colon in Hirschsprung's disease: a histochemical study. *J Pediatr Surg* 3:43-49, 1968
25. Garrett JR, Howard ER, Nixon HH: Autonomic nerves in rectum and colon in Hirschsprung's disease. *Arch Dis Child* 44:406-417, 1969
26. Cannon BJ, Noblett HR, Burnstock G: Adrenergic innervation of bowel in Hirschsprung's disease. *Br Med J* 3:338-340, 1969
27. Cannon BJ, Burnstock G, Noblett HR, Campbell PE: Histochemical diagnosis of Hirschsprung's disease. *Lancet* i:894-895, 1969
28. Howard ER, Garrett JR: Histochemistry and electron microscopy of rectum and colon in Hirschsprung's disease. *Proc R Soc Med* 63:1264-1266, 1970
29. Meier-Ruge W, Lutterbeck PM, Herzog B, Morger R, Moser R, Scharli A: Acetylcholinesterase activity in suction biopsies small of the rectum in the diagnosis of Hirschsprung's disease. *J Pediatr Surg* 7:11-17, 1972
30. Taxi J: Morphological and cytochemical studies of synapses in the autonomic nervous system. *Progr Brain Res* 31:5-20, 1969
31. Pick J: The Autonomic Nervous System. Morphologic, Comparative, Clinical and Surgical Aspect. Philadelphia, J. B. Lippincott Co, 1970

32. van der Zypen E: Elektronen mikroskopische Befunde an der Endausbreitung des vegetativen Nervensystems und ihre Deutung. *Acta Anat (Basel)* 67:481-515, 1967
33. Richardson KC: Electron microscopic observations on Auerbach's plexus in the rabbit with special reference to the problem of smooth muscle innervation. *Am J Anat* 103:99-135, 1958
34. Yamamoto T: Electron microscope investigation on the relationship between the smooth muscle cell of the *Proc. vermiformis* and the autonomic peripheral nerve. *Acta Neuroveget* 21:406-425, 1960
36. Thaemert JC: Ultrastructural relationship of nerve processes and smooth muscle cells in three dimensions. *J Cell Biol* 28:37-49, 1966
37. Pick J: Fine structure of nerve terminals in the human gut. *Anat Rec* 159:131-138, 1967
38. Couturier-Turpin MH: Données Recentes sur l'ultrastructure et l'innervation du muscle lisse gastrointestinal. *Presse Med* 76:319-321, 1968
39. Bennett MP, Rogers DC: A study of the innervation of the Taenia Coli. *J Cell Biol* 33:573-596, 1967
40. Ono M: Electron microscopic observations on the ganglia of Auerbach's plexus and nerve endings in muscularis externa of the mouse small intestine. *Sapporo Med J* 32:56-64, 1967
41. Baumgarten HG: Auerbach's plexus of mammals and man: electron microscopic identification of three different types of neuronal processes in myenteric ganglia of the large intestine from Rhesus monkeys, Guinea pigs, and man. *Z Zellforsch Mikrosk Anat* 106:376-397, 1970
42. Lane PW: Association of megacolon with two recessive spotting genes in the mouse. *J Hered* 57:29-31, 1966
43. Green EL: *Biology of the Laboratory Mouse*, Second edition. New York, McGraw-Hill Book Co, 1966
44. Lane PW: Personal communication
45. El-Badawi A, Schenk EA: Histochemical methods for separate consecutive and simultaneous demonstration of acetylcholinesterase and norepinephrine in cryostat sections. *J Histochem Cytochem* 15:580-588, 1967
46. Norvell JE, Harris TM, Weitsen HA: The use of dark-field microscopy for the visualization of acetylcholinesterase in cholinergic neurons. *Stain Technol* 46:19-21, 1971
47. Maillet M: Le reactif au tetraoxyde d'osmium-iodure-du zinc. *Z Mikrosk Anat Forsch* 70:397-425, 1963
48. Taxi J: Contribution a l'etude des connexions des neurones moteurs de systeme nerveux autonome. *Ann Sci Natl Zool* 7:413-674, 1965
49. Akert K, Sandri C: An electron microscopic study of zinc-iodide-osmium impregnation of neurons. I. Staining of synaptic vesicles at cholinergic junctions. *Brain Res* 7:286-295, 1968
50. Burn JH, Rand MJ: Acetylcholine in adrenergic transmission. *Ann Rev Pharmacol* 5:163-182, 1965
51. Eränkö O, Reckardt L, Eränkö L, Cunningham A: Light and electron microscopic histochemical observations on cholinesterase-containing sympathetic nerve fibers in the pineal body of the rat. *Histochem J* 2:479-489, 1970
52. Bolande RP, Towler WF, Weinberg AG: An ultrastructural study of human and murine megacolon. *Am J Pathol* 62:22a, 1971

Acknowledgments

The authors wish to express their gratitude to Mr. T. Campbell for his artistic and photographic help and to Miss Clara Pappas for the manuscript preparation and typing. Dr. Arthur Weinberg of the Dallas Children's Hospital was a vital intellectual stimulus for this study.

[*Illustrations follow*]

Legends for Figures

Fig 1—Myenteric plexus of a normal adult mouse. The nucleus (N) and cytoplasm of a ganglion cell of the myenteric plexus is shown. The cytoplasm contains numerous irregular dense bodies and mitochondria. The free ribosome granules are Nissl substance. Closely apposed to the periphery of the cell are tortuous axons containing dense-core granules. Indenting the cytoplasm is a pear-shaped synapse containing both small clear vesicles and dense-core granules (Sy). This is an axosomatic synapse. The vesicles probably represent acetylcholine, and the dense-core granules norepinephrine ($\times 13,900$).

Fig 2—Myenteric plexus of a normal human. Small axon bundles extend between the muscle cells of the circular and longitudinal muscle layers. A single axon (arrow) is shown leaving the axon bundle to approach the surface of a smooth muscle cell (m) after having shed its Schwann-cell tunic. It contains both clear vesicles and dense core granules ($\times 27,000$).

Fig 3—Ls/Ls mouse and Agouti parent strain. The typical black and white coat color of the Ls/Ls strain is shown at the left and contrasted with the speckled brown coat of the parent Agouti strain. Although these animals are of the same age, note the growth retardation in the Ls/Ls mouse due to aganglionic megacolon.

Fig 4—Mouse megacolon. The enormous dilatation of the colon is apparent in this Ls/Ls mouse. Note the distal, narrowed segment devoid of feces (arrow).

Fig 5—Ls/Ls mouse with megacolon, age 5 days. This illustrates the surface of a rare ganglion cell (G) found in the ostensibly aganglionic distal colon of a very young Ls/Ls mouse with gross megacolon. The ganglion cell is structurally intact, but swollen axons are in synaptic apposition at only one pole. Occasional dense core granules are present in one synapse (Sy). Dense bodies are present in ganglion cell cytoplasm and in a swollen axon (A) ($\times 13,900$).

Fig 6—Ls/Ls mouse with megacolon, age 3 weeks. Large axon bundles are present in the zone between the circular and longitudinal muscle layers. Nucleated cells are Schwann cells (S) whose cytoplasm extends to enclose nerve fibers. Schwann cell cytoplasm is characteristically contained by a double membrane. Fibroblast cytoplasmic processes are present at the bottom and tend to circumscribe the entire complex ($\times 7100$).

Fig 7—Ls/Ls mouse with megacolon. This shows the marked swelling, tortuosity and loss of neurotubulation characteristically found in axon bundles of the distal, narrowed segment of aganglionic mice. Neurosecretory granules and vesicles are not apparent. ($\times 9100$).

Fig 8—Myenteric plexus of normal mouse fetus at term. The colonic myenteric plexus is a mosaic of densely packed ganglion cells with few synaptic forms, or preganglionic axons intervening. Accordingly, the cells surfaces are smooth and simple. Cytoplasmic organelles characteristic of ganglion cells seems fairly well-developed ($\times 9100$).

Fig 9—Newborn aganglionic (Ls/Ls) mouse colon. This shows two degenerate myenteric plexus ganglion cells in apposition. The cells are small, their surfaces irregular and devoid of axons on synaptic forms. Cytoplasmic constituents are indistinct ($\times 9100$).

Fig 10—Fetal aganglionic (Ls/Ls) mouse colon. A markedly degenerate cell form adjacent to degenerating, but still identifiable fetal ganglion cells ($\times 9100$).

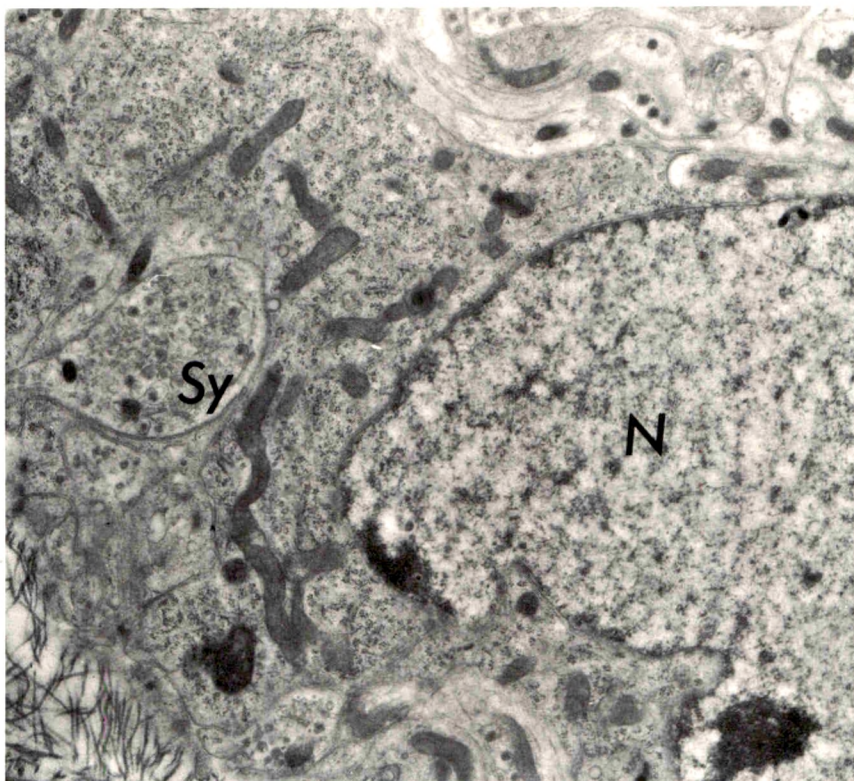
Fig 11—AChE staining of normal mouse colon. The serosa is at the top and mucosa at the bottom. Note the dense staining of ganglion cells and nerve fibers in the plexus. Note the extent of fine fiber staining in the circular and longitudinal muscle layers and in the submucosa (El-Badawi-Schenk method), ($\times 100$).

Fig 12—AChE staining of aganglionic mouse colon. This shows the area of the myenteric plexus. The serosa is at the top. Staining is much reduced from normal and limited to a few nerve bundles in the plexus area. Staining of fibers within the circular and longitudinal muscle layers is markedly reduced (El-Badawi-Schenk method, $\times 75$).

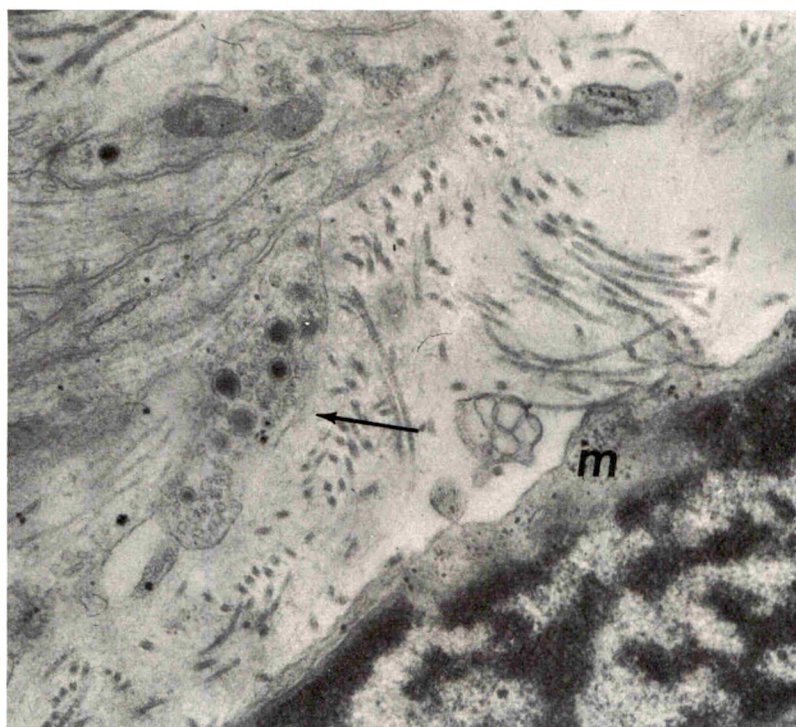
Fig 13—Normal mouse colon. The serosa (s) is above and mucosa (mu) below. The dark staining material can be shown ultrastructurally to be limited to neural structures. The ganglion cells and periganglionic nerve bundles are heavily impregnated. Nerve fibers are stained mainly in the inner muscle layer and submucosa. Note their size and distribution. im = inner muscular layer, om = outer muscular layer (Maillet technic, $\times 170$).

Fig 14—Aganglionic mouse colon. There is a marked reduction of staining in the plexus. Nerve fibers in the inner muscle layer (im) appear thicker, but are irregularly distributed and wider apart. Significant increase in the muscularis, mucosa or submucosa is not apparent (Maillet technic, $\times 170$).

Fig 15—Aganglionic colon Ls/Ls mouse. This shows the selectivity of the Maillet stain for neural tissue. In the myenteric plexus an isolated ganglion cell (g) is surrounded by densely-staining nerve fibers and trunks. An intermuscular fiber is shown below (arrow) (Maillet technic, $\times 4500$).



1



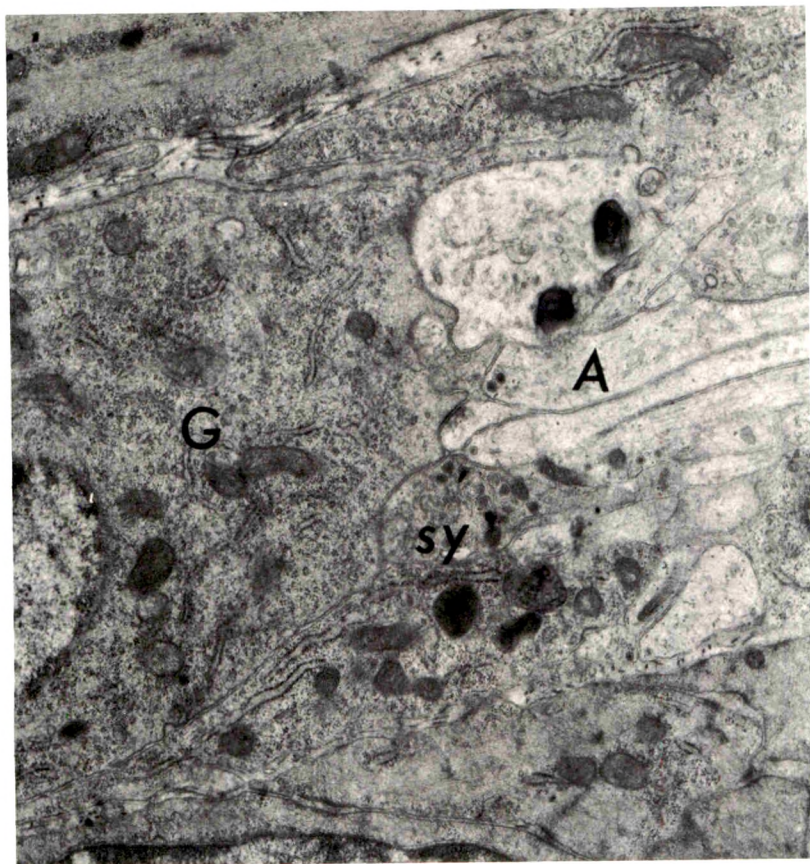
2

3

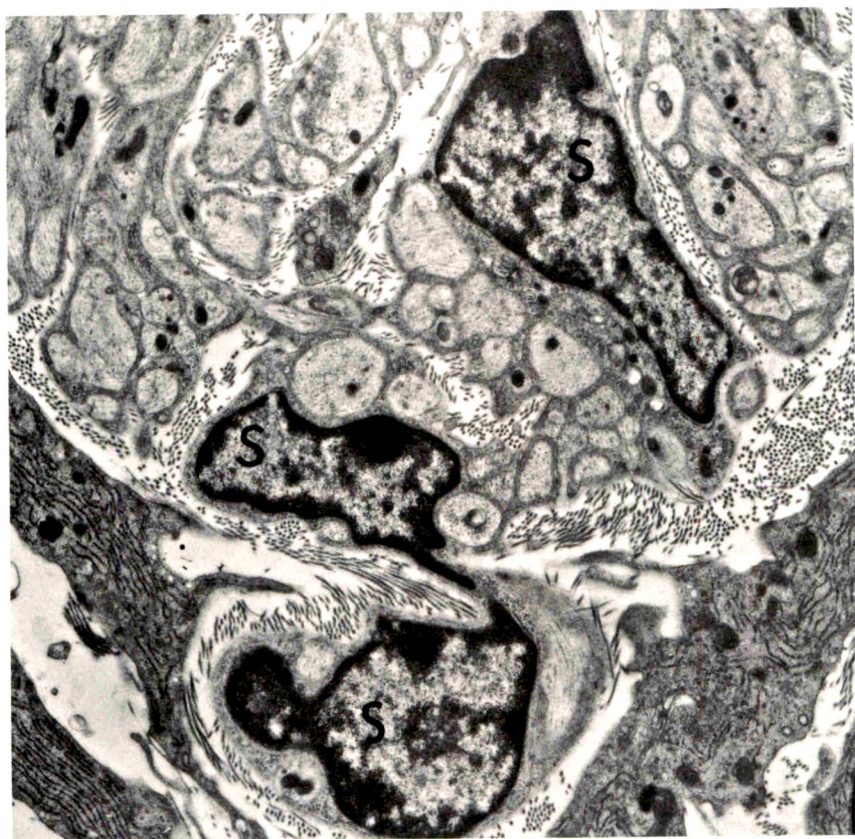


4



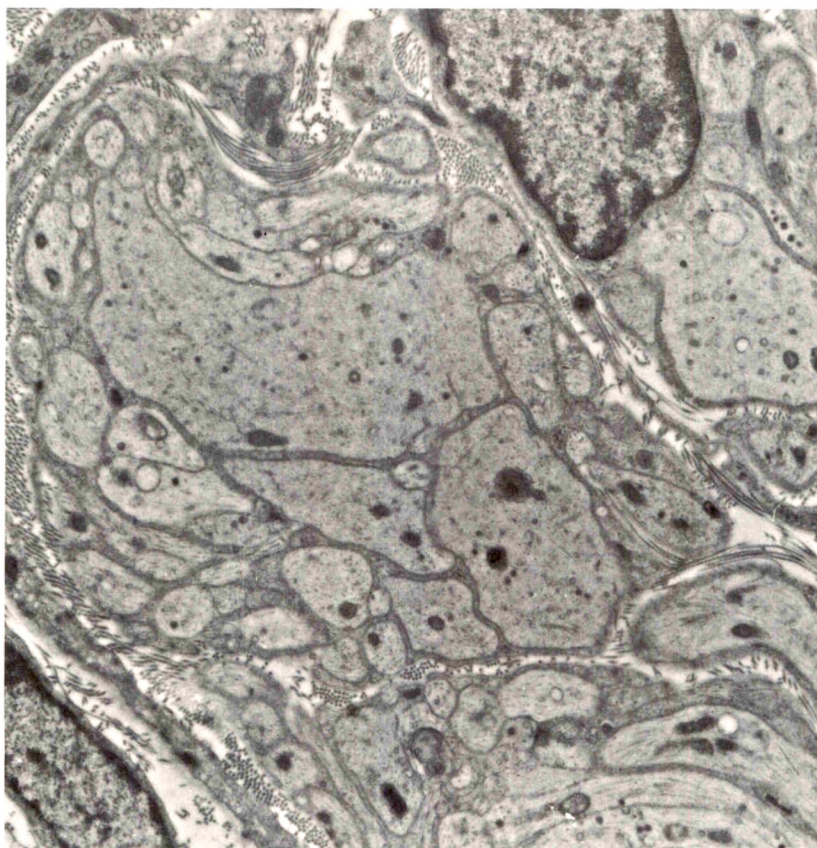


5

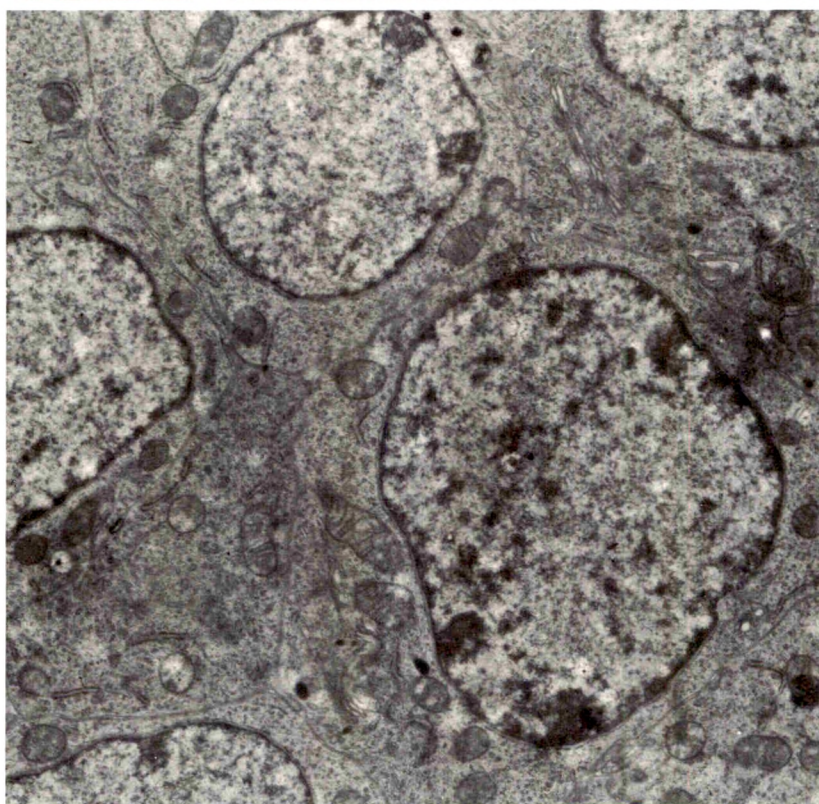


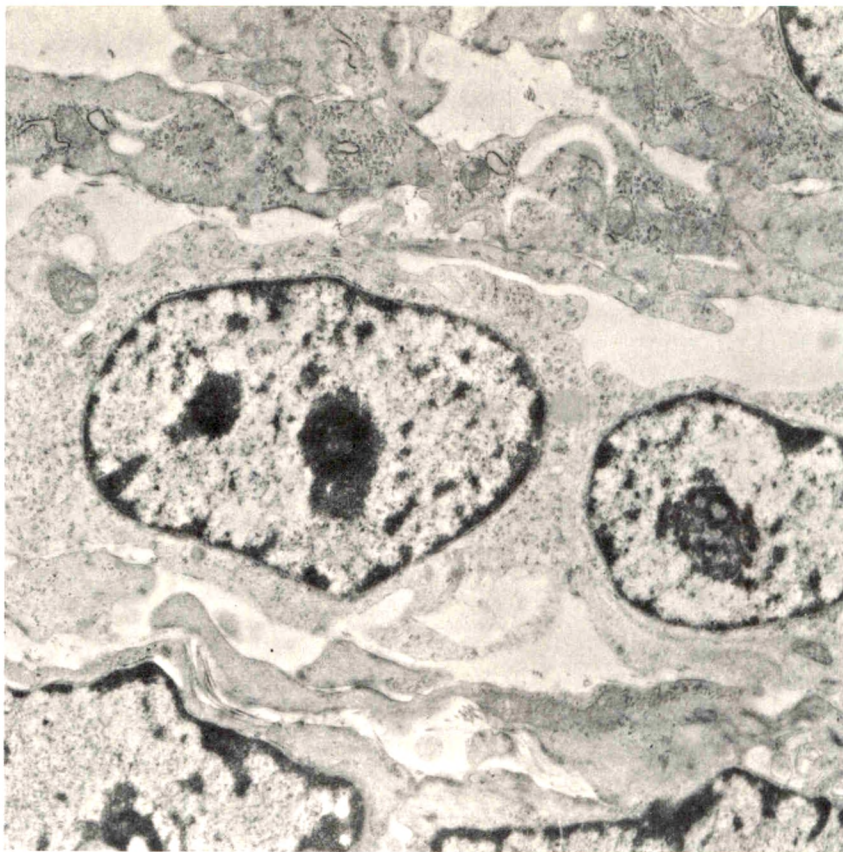
6

7



8





9

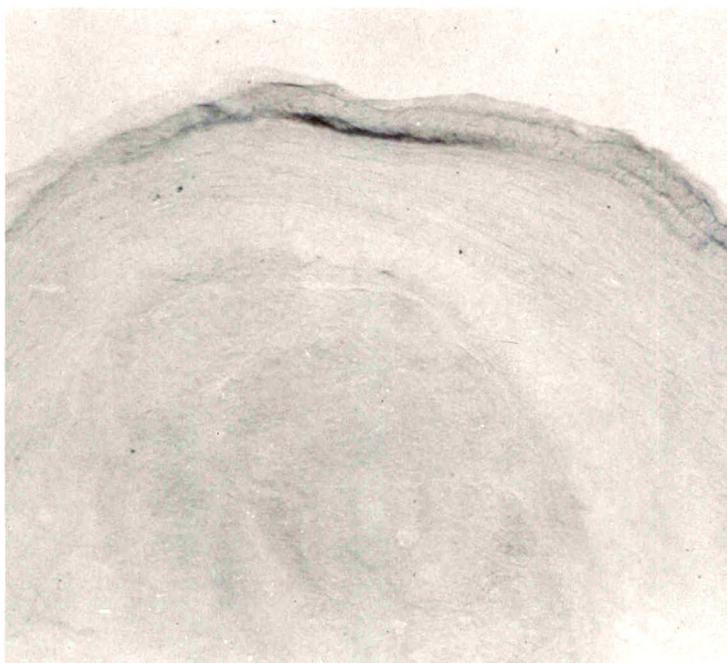


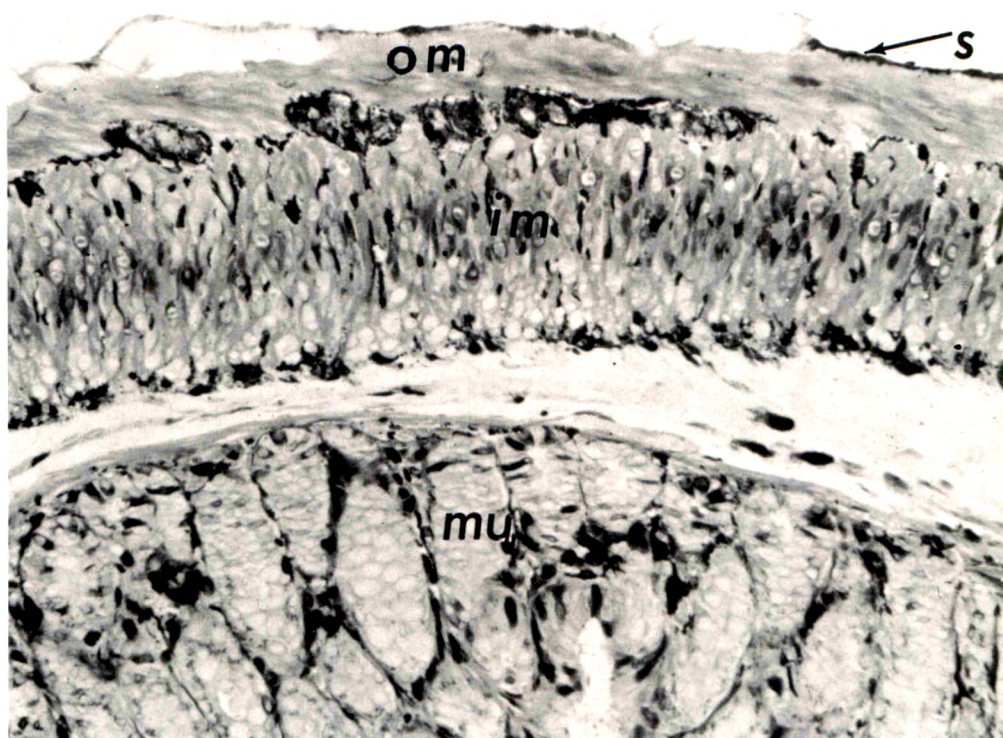
10

11



12





13



14

15



The Morphologic Effects of Dieldrin and Methyl Mercuric Chloride on Pars Recta Segments of Rat Kidney Proximal Tubules

Bruce A. Fowler, PhD

This investigation was undertaken to evaluate the morphologic effects in rat kidney resulting from chronic exposure to low doses of the pesticide dieldrin, methyl mercuric chloride (CH_3HgCl) and the combination of dieldrin plus CH_3HgCl . Histologic and ultrastructural changes were confined to the proximal tubules. Alterations in these tubules were consistent and reproducible for each regimen and did not become more severe with duration of exposure. The straight segment of the proximal tubule (pars recta) was more severely affected by dieldrin and CH_3HgCl than the convoluted portion. Female rats were more markedly affected than males. Pars recta tubule cells of male and female rats exposed to dieldrin showed an increase of smooth endoplasmic reticulum (SER). Male rats displayed a greater increase in SER than females. Pars recta tubule cells of animals given CH_3HgCl also exhibited increased amounts of SER, degenerating mitochondria and cell death. Pars recta tubules of females were dilated and contained within the lumen many spherical, hematoxylin-positive staining, cytoplasmic masses, which were visible by light microscopy. These masses were characterized ultrastructurally by the presence of an SER aggregate in an area of material similar to cell matrix. In addition, cells of the pars recta of female animals contained electron-dense membranous cytosomes not present in control animals. Pars recta cells of males showed an increase in SER, but the dense membranous cytosomes observed in the pars recta cells of female rats were not seen. Rats exposed to dieldrin plus CH_3HgCl showed less morphologic alteration of the pars recta tubules than animals given methyl mercuric chloride; however, increased amounts of SER and more degeneration in tubule cells were observed in these animals when compared to control animals. The findings are discussed in relation to the conversion of CH_3HgCl to inorganic mercury *in vivo* and the known toxicity of inorganic mercury to the pars recta. Decreased tubular alteration in males and dieldrin-treated animals may be explained by sexual differences in renal enzyme levels or activities and the induction of microsomal enzyme systems by dieldrin (Am J Pathol 69:163-178, 1972).

CHLORINATED HYDROCARBON PESTICIDES and organomercury compounds are examples of environmental contaminants that can be concentrated in biologic systems and which are potentially toxic to man. Dieldrin is an extensively used chlorinated hydrocarbon pesti-

From the Department of Pathology, University of Oregon Medical School, Portland, Oregon and the Environmental Health Sciences Center, Oregon State University, Corvallis, Oregon.

Supported in part by Grants RR-05412, CA-05191 and ES-00040 from the US Public Health Service.

Accepted for publication July 11, 1972.

Address reprint requests to Dr. Bruce A. Fowler, National Institute of Environmental Health Sciences, Pathologic Physiology Branch, Box 12233, Research Triangle Park, NC 27709.

cide. Methyl mercury is the most common organomercurial found in the environment.

Most investigations concerning the effects of chlorinated hydrocarbons on mammalian systems have centered on the liver. A variety of such agents are known to cause a proliferation of smooth endoplasmic reticulum (SER) in hepatic cells.¹⁻⁵ Hutterer *et al*^{2,3} observed an induction by dieldrin of aniline hydroxylase and cytochrome P450. In addition, these authors noted a decrease in oxidative phosphorylation from continued exposure to this agent.

Although the kidney has not been of primary concern in most investigations, several authors have reported high levels of chlorinated hydrocarbon pesticides in this organ.^{6,7} Boyd *et al*⁸⁻¹¹ described congestion and fatty degeneration of renal tubules in rats fed with these pesticides. Treon *et al*¹² reported necrosis of the convoluted tubules in a variety of laboratory animals poisoned with endrin, another chlorinated hydrocarbon pesticide.

Studies on the toxicity of organomercury compounds in humans have been concerned with damage to the central nervous system. Individuals poisoned by the ingestion of fish containing high levels of organic mercury showed severe neurologic disorders resulting from destruction of the granule cell layer in the cerebellum.¹³⁻¹⁵ Several other clinical investigations^{16,17} have described a significant increase in proteinuria in persons occupationally exposed to organomercury compounds.

Long-term experimental laboratory studies¹⁸⁻²⁰ have shown that both organic and inorganic mercury derived from exogenous organomercury compounds is concentrated in the kidneys. Other investigators²¹⁻²³ have reported that this inorganic mercury is an *in vivo* metabolic product. Inorganic mercury is known to be highly toxic to the proximal tubules.^{24,25}

The present study was undertaken to evaluate the morphologic effects of long-term exposure to dieldrin and methyl mercuric chloride on the kidney, since this organ accumulates these two environmental toxicants and their effects on renal ultrastructure have not been reported. Because living organisms are simultaneously exposed to numerous environmental toxicants, and since one toxicant may influence the toxicity of another, the combined effects of dieldrin and methyl mercuric chloride were also investigated.

Materials and Methods

A total of 84 inbred Oregon State University-Wistar rats (39 males and 45 females) were housed in sterile chambers²⁶ throughout the experiment. Dieldrin,

methyl mercuric chloride (CH_3HgCl) and the combination of dieldrin plus CH_3HgCl were added to the daily diet. All experimental and control animals received a stock laboratory ration described by Harr *et al.*²⁷ The average food intake for both control and experimental male rats was 19 g/rat/day. Both control and experimental female rats consumed an average of 15 g/food/rat/day.²⁸ The groups of animals were studied for the time periods indicated in Table 1.

The animals were anesthetized with ether and their right kidneys excised. For light microscopy, samples from the kidneys of all animals were fixed overnight at room temperature in 10% formalin. These were embedded in paraffin and sectioned at 5 μ . Sections of tissue from each animal were stained with hematoxylin and eosin. In addition, sections from both mercury-treated female rats and control female rats killed at 84 days were stained with the periodic acid-Schiff procedure.

For electron microscopy, tissue blocks approximately 1 cu mm in volume were cut from samples of both inner and outer cortex of all kidneys. These blocks were immersed for 3 hours in a fixative containing glutaraldehyde, 2.5%, formaldehyde, 2.0%, CaCl_2 , 250 mg/liter and 0.085 M cacodylate buffer (pH 7.4).

In addition, in a duplicate series of experiments, the right kidneys of 4 mercury-treated female rats and 4 control female rats that had been treated for 84 days with methyl mercuric chloride were perfused via cardiac puncture with a Ringer's-procaine solution²⁹ followed by the above fixative containing sucrose. The kidneys were removed and small pieces were subsequently fixed by immersion for 3 hours at room temperature.

All tissues were postfixed in a solution of 1.5% osmium tetroxide in 0.1 M Sørensen's phosphate buffer (pH 7.4) for 2 hours at room temperature,³⁰ then dehydrated in a 50 to 100% graded series of alcohols, passed into propylene oxide and embedded in Araldite according to the method of Luft.³¹ Thin sections were cut on an LKB ultratome and mounted on 300 mesh uncoated copper grids. The sections were double stained first with lead citrate³² and then with 3% uranyl acetate and examined with either an RCA EMU 3-G or Philips EM 200 electron microscope.

Results

The histiologic and ultrastructural morphology of the normal rat kidney has been extensively described.^{33,34} In this study the segmentation of the proximal tubule was determined using the criteria estab-

Table 1—Dose Level, Numbers, Duration of Exposure and Age at Death of Experimental and Control Rats

Regimen (level in diet)	No. of Rats		Days of diet	Age at death (days)
	Male	Female		
Dieldrin (5.0 ppm)	8	8	84	112
	7	6	142	170
CH_3HgCl^* (2.0 ppm)	3	6	84	112
	3	4	142	170
Dieldrin (5.0 ppm) plus CH_3HgCl (2.0 ppm)	2	2	84	112
	3	4	142	170
Control	7	11	84	112
	6	4	142	170

* 2 ppm Hg as CH_3HgCl

lished by Maunsbach.³⁴ The histology and ultrastructure of kidneys from control rats in this study did not vary from these descriptions. In experimental animals, morphologic alterations were most marked in the pars recta segment of the proximal tubule. These changes are summarized in Table 2.

Animals Exposed to 5.0 ppm Dieldrin in the Diet

Light microscopic histology of tissue from animals of both sexes was indistinguishable from controls.

The ultrastructural changes produced by dieldrin in the pars recta of the proximal tubule were similar in both sexes. Increased amounts of SER characterized pars recta cells of dieldrin treated animals. Pars recta tubule cells from male rats showed a greater relative increase in SER aggregates than was observed in females (Figures 1 and 2).

Animals Exposed to 2.0 ppm CH₃HgCl in the Diet

Morphologic alterations of pars recta tubule cells from female rats were different from those observed in males.

Female rats

Histologic sections of kidneys from female animals displayed dilatation of the pars recta segments as a result of flattening of the pars recta epithelium and the presence of many large, hematoxylin-positive, PAS-negative spherical cytoplasmic masses in tubule lumens (Figure 3). The masses did not arise from the collapse of tubules during fixation, since they were observed in the patent lumens of pars recta segments from perfusion-fixed tubules. These cytoplasmic mas-

Table 2—The Ultrastructural Effects of Dieldrin and CH₃HgCl on the Pars Recta in Comparison to Control Animals

Changes in pars recta tubule cells	Male	Female
Dieldrin		
Dense membranous cytosomes	—	—
Increased SER	++	+
SER-containing cytoplasmic masses	—	—
CH ₃ HgCl		
Dense membranous cytosomes	—	+++
Increased SER	+	+++
SER-containing cytoplasmic masses	—	+++
Dieldrin plus CH ₃ HgCl		
Dense membranous cytosomes	—	+
Increased SER	+	±
SER-containing cytoplasmic masses	—	±

+ indicates increase; — indicates no change

ses were characterized ultrastructurally by the presence of an SER bundle and an occasional microbody (Figure 4). Rough endoplasmic reticulum profiles were sometimes observed in these masses, usually around the periphery of the SER aggregated. Other organelles were rarely observed in these masses.

Pars recta cells of treated females contained large aggregates of SER and dense membranous cytosomes (Figures 5 and 6).

Male Rats

Paraffin-embedded sections of kidneys from males given 2.0 ppm CH_3HgCl in the diet could not be distinguished from controls. In contrast to females, dilatation of the pars recta segments and the presence of cytoplasmic masses were not observed. By electron microscopy, these pars recta cells displayed more SER per thin section of tissue than controls, but less than the females. No dense membranous cytosomes were observed (Figure 7).

Animals Exposed to 5.0 ppm Dieldrin plus 2.0 ppm CH_3HgCl in the Diet

Morphologic alterations observed in kidneys of animals exposed to dieldrin plus CH_3HgCl were less extensive than those in animals given CH_3HgCl alone.

Female rats

Light microscopy of kidney sections from female rats showed moderate dilatation of the pars recta tubules, but fewer cytoplasmic masses within tubule lumens than in animals exposed only to CH_3HgCl (Figure 8; compare with Figure 3).

Cells of the pars recta, by electron microscopy, showed little if any increase in SER and fewer dense membranous cytosomes than females given CH_3HgCl alone. Their ultrastructure was similar in appearance to those of males on this regimen.

Male rats

Histologic sections of kidney from male rats fed dieldrin plus mercury in the diet showed normal morphology. Ultrastructural morphology of cells of the pars recta showed slightly more SER in comparison to controls but less than males given dieldrin or CH_3HgCl alone (Figure 9).

Discussion

Low doses of dieldrin and CH_3HgCl produced different effects in kidneys of rats exposed to either substance for long periods of time.

The severity of ultrastructural changes in cells of the pars recta was more dependent upon the sex of animals than on the duration of exposure. Administration of both compounds together did not produce an additive response but appeared to result in less cellular change than when either compound was given alone.

Increased amounts of SER were noted in animals given dieldrin. Several investigators^{2,3} have associated proliferation of SER with induction of microsomal detoxification enzyme systems. Furthermore, biochemical studies³⁵⁻³⁸ have shown dieldrin to be a potent inducer of microsomal detoxification enzymes. Therefore, the proliferation of SER in pars recta tubule cells seen in this experiment probably represents a cellular attempt to detoxify dieldrin.

The more marked effect of dieldrin on the pars recta of female rats may be explained by sexual differences in detoxification enzyme activities. Numerous investigators^{36,38,39} have reported that the activity level of liver microsomal enzymes is higher in the adult male rat than in the adult female. Sexual differences have also been reported³⁹⁻⁴² for a number of renal enzymes. Koerner and Hellman³⁹ found that the activity of the microsomal enzyme 11β -hydroxysteroid dehydrogenase in kidneys of male Wistar rats was twice that of kidneys from female Wistar rats. In the present study, pars recta cells from dieldrin-treated male rats showed a greater relative increase in SER than those of dieldrin-treated females. This may suggest a greater intrinsic responsiveness by males to dieldrin, via an inducible enzyme system.

The kidneys of CH_3HgCl -treated female rats were more severely affected than those of male rats. Organomercury compounds are known to be converted to inorganic mercury in the kidney^{21-23,43} where they are concentrated to high levels.^{18-20,44-47} Fitzhugh *et al*⁴⁸ found the kidneys of female rats to be more sensitive to low doses of phenyl mercury and inorganic mercury. Inorganic mercury (*eg*, HgCl_2) is known to damage selectively the pars recta of the proximal tubule.^{24,25} Swollen mitochondria and proliferation of SER and cellular necrosis characterize acute inorganic mercury poisoning.^{24,25}

Mercury derived from methyl mercury has been reported to concentrate in the microsomal fraction of rat kidney and liver.^{49,50} The SER is a logical site for the conversion of methyl mercury to inorganic mercury because detoxification enzyme activities including oxidative demethylation⁵¹⁻⁵³ are present in microsomes. It is not known whether the conversion of methyl mercury to inorganic mercury is an enzymatic or nonenzymatic process, but it seems likely that cleavage of the carbon-mercury bond by either mechanism could release inorganic mercury

which might then react with microsomal enzymes as a noncompetitive inhibitor. The mechanism by which the mercurials cause enzyme inhibition is through combination of mercury with sulfhydryl (SH) groups present at the active sites of many enzymes, including those found in microsomes.^{54,55} The inhibition of microsomal enzymes in pars recta cells could render SER aggregates nonfunctional. This could then account for their selective extrusion in cytoplasmic masses⁵⁶ through a process of potocytosis.^{33,57,58}

It has been previously suggested⁵⁶ that the loss of these masses from pars recta cells into the urine could produce a proteinuria similar to that observed in persons occupationally exposed to organomercurials.^{16,17}

The more marked effect of CH_3HgCl on the pars recta cells of female rats, in comparison to males, is again probably due to sex differences in the levels or activities of renal enzymes.³⁹⁻⁴² The enzymes, alkaline phosphatase, acid phosphatase, β -hydroxybutyrate dehydrogenase, glucose-6-phosphatase and nonspecific esterase, all show sex differences exclusively in the pars recta segments.⁴⁰⁻⁴² Microsomal enzymes containing SH groups which interact with mercury may be less able to metabolize mercury or excrete it conjugated with cysteine,⁵⁹ allowing it to inhibit mitochondrial and other enzyme systems.

The dense membranous cytosomes found in pars recta cells of mercury-treated females may represent a means for sequestering mercury. It has been demonstrated by others⁶⁰⁻⁶² that cytosomes (lysosomes) from renal tubule cells concentrate cations and drugs *in vivo*. Mercury derived from methyl mercury also accumulates in the lysosomal fractions of rat kidney and liver.^{49,50} Cytosomes in other female rats given the same level of methyl mercury in the diet have been shown to contain acid phosphatase activity,⁶³ thus identifying them as lysosomes. Unstained thin sections of tissue from these animals, fixed in glutaraldehyde but not OsO_4 , contained dense particulate inclusion bodies in pars recta cells.⁶⁴ These observations suggest that mercury concentrated in kidney lysosomes of these animals.

The membranous appearance of the cytosomes observed in this investigation suggest a lipidic character. A number of investigators⁶⁰⁻⁶² have isolated an acidic lipoprotein component of lysosomes, which is thought to be responsible for the binding of cationic compounds. Large membranous cytosomes have been observed⁶⁵ in proximal convoluted tubule cells of mice given the cationic herbicide paraquat, and it was suggested that proliferation of acidic lipoprotein in response to paraquat resulted in their membranous appearance. An

analogous situation could exist in the pars recta cells of mercury-treated female rats if these cells were unable to detoxify completely or excrete the mercury present. The cationic mercury might stimulate production of an acidic lipoprotein component of lysosomes, thus giving rise to their membranous appearance.

Animals exposed to both dieldrin and CH_3HgCl exhibited similar but less extensive cytologic changes than animals given either compound alone. This protective effect was more easily appreciated in female rat kidneys. One possible explanation is that dieldrin may stimulate microsomal enzyme systems and increase the metabolic activity of SER aggregates also metabolizing CH_3HgCl . Chlorinated hydrocarbon pesticides are known to stimulate the microsomal metabolism and decrease tissue storage of numerous compounds.³⁶ Street *et al*^{66,67} have reported that the administration of DDT to animals receiving dieldrin reduced tissue storage and enhanced excretion of dieldrin. A synergistic effect of one toxicant on the metabolism of another is indicated. Dieldrin induction of microsomal enzymes in the female rat kidney could enhance the metabolism of CH_3HgCl or increase the available number of SH groups so that the inhibitory effect of mercury would be reduced.

This study shows that chronic long-term exposure to low doses of these environmental toxicants produced definite morphologic alterations in kidney tubules which are detectable by electron microscopy. The extent of these changes in the pars recta cells is largely dependent on the sex of the animal and may reflect sex-based enzymic differences. The lack of increased pathologic changes in animals given dieldrin and/or CH_3HgCl for even longer periods suggests that the detoxification enzyme systems of the proximal tubule cells reach a *steady state* condition in the presence of low-level doses of these chemicals.

Biochemical studies concerning the effects of dieldrin, CH_3HgCl and dieldrin plus CH_3HgCl on microsomal, mixed-function oxidases in renal cortical parenchyma are presently underway. These investigations should elucidate the manner in which CH_3HgCl interacts with microsomal enzymes and the extent to which dieldrin influences this interaction.

References

1. Chedid A, Nair V: Diurnal rhythm in endoplasmic reticulum of rat liver. Electron microscopic study. *Science* 175:176-179, 1972
2. Hutterer F, Schaffner F, Klion FM, Popper H: Hypertrophic, hypoactive

- smooth endoplasmic reticulum: a sensitive indicator of hepatotoxicity exemplified by dieldrin. *Science* 161:1017-1019, 1968
3. Hutterer F, Klion FM, Wengraf A, Schaffner F, Popper H: Hepatocellular adaption and injury. Structural and biochemical changes following dieldrin and methyl butter yellow. *Lab Invest* 20:455-464, 1969
 4. Ortega P: Light and electronmicroscopy of dichlorodiphenyltrichlorethane (DDT) poisoning in the rat liver. *Lab Invest* 15:657-679, 1966
 5. Ortega P: Partial hepatectomy in rats fed dichlorodiphenyltrichloroethane (DDT). *Am J Pathol* 56:229-250, 1969
 6. Fiserova-Bergerova V, Radomski JL, Davies JE, Davis JH: Levels of chlorinated hydrocarbon pesticides in human tissues. *Ind Med Surg* 36:65-70, 1967
 7. Morgan DP, Roan CC: Chlorinated hydrocarbon pesticide residue in human tissues. *Arch Environ Health* 20:452-457, 1970
 8. Boyd EM: Dietary protein and pesticide toxicity in male weanling rats. *Bull WHO* 40:801-805, 1969
 9. Boyd EM, Chen CP: Lindane toxicity and protein-deficient diet. *Arch Environ Health* 17:156-163, 1968
 10. Boyd EM, DeCastro ES: Protein-deficient diet and DDT toxicity. *Bull WHO* 38:141-150, 1968
 11. Boyd EM, Taylor FI: The acute oral toxicity of chlordane in albino rats fed for 28 days from weaning on a protein-deficient diet. *Ind Med Surg* 38:434-441, 1969
 12. Treon JF, Cleveland FP, Cappel J: Toxicity of endrin for laboratory animals. *J Agric Food Chem* 3:842-848, 1955
 13. Ackefors H, Löfroth G, Roßen CG: A survey of the mercury pollution problem in Sweden with special reference to fish. *Oceanogr Marine Biol Ann Rev* 8:203-224, 1970
 14. Eyl TB, Wilcox KR, Reizen MS: Mercury, fish and human health. *Mich Med* 69:880, 1970
 15. Löfroth G: Methylmercury: A Review of Health Hazards and Side Effects Associated With Emission of Mercury Compounds Into Natural Systems, Bulletin 4, Ecological Research Committee, Second Edition. Stockholm, Swedish National Research Council, 1969
 16. Joselow MM, Goldwater LJ: Absorption and excretion of mercury in man. XII. Relationship between urinary mercury and proteinuria. *Arch Environ Health* 15:155-159, 1967
 17. Taylor W, Guirgis HA, Stewart WK: Investigation of a population exposed to organomercurial seed dressings. *Arch Environ Health* 19:505-509, 1969
 18. Aberg B, Ekman L, Falk R, Greitz U, Persson G, Snihs JO: Metabolism of methyl mercury (^{203}Hg) compounds in man. Excretion and distribution. *Arch Environ Health* 19:478-484, 1969
 19. Swensson A, Ulfvarson U: Distribution and excretion of mercury compounds in rats over a long period after a single injection. *Acta Pharmacol Toxicol* 26:273-283, 1968
 20. Ulfvarson U: The absorption and distribution of mercury in rats fed organs from rats injected with various mercury compounds. *Toxicol Appl Pharmacol* 15:525-531, 1969
 21. Clarkson TW: Isotope exchange methods in studies of the biotransformation of organomercurial compounds in experimental animals, Chemical Fallout:

- Current Research on Persistent Pesticides. Edited by MW Miller, GG Berg. Springfield, Charles C. Thomas, Publisher, 1969, pp 274-196
22. Norseth T, Clarkson TW: Studies on the biotransformation of ^{203}Hg -labeled methyl mercury chlorides in rats. *Arch Environ Health* 21:717-727, 1970
 23. Takeda Y, Ukita T: Metabolism of ethylmercuric chloride ^{203}Hg in rats. *Toxicol Appl Pharmacol* 17:181-188, 1970
 24. Gritzka TL, Trump BF: Renal tubular lesions caused by mercuric chloride: electron microscopic observations: degeneration of the pars recta. *Am J Pathol* 52:1225-1278, 1968
 25. Rodin AE, Crowson CN: Mercury nephrotoxicity in the rat. I. Factors influencing the localization of tubular lesions. *Am J Pathol* 41:297-314, 1962
 26. Harr JR, Tinsley IJ, Weswig PH: Haemophilus isolated from a rat respiratory epizootic. *J Am Vet Med Assoc* 155:1126-1130, 1969
 27. Harr JR, Claeys RR, Benedict W: Dieldrin toxicosis in rats: long-term study of brain and vascular effects. *Am J Vet Res* 31:1853-1862, 1970
 28. Harr JR: Personal communication
 29. Fowler BA: Ruthenium red staining of rat glomerulus: perfusion of ruthenium red into normal and nephrotic rat kidney. *Histochemie* 22:155-162, 1970
 30. Millonig G: Further observations on a phosphate buffer for osmium solutions in fixation. *Fifth International Congress of Electron Microscopy* 2: p 8, 1962
 31. Luft JH: Improvements in epoxy resin embedding methods. *J Biophys Biochem Cytol* 9:409-414, 1961
 32. Reynolds ES: The use of lead citrate at high pH as an electron-opaque stain in electron microscopy. *J Cell Biol* 17:208-212, 1963
 33. Ericsson JLE, Trump BF: Electron microscopy of the uriniferous tubules, *The Kidney*, Vol I. Edited by C Rouiller, AF Muller, New York, Academic Press, Inc 1969, pp 351-447
 34. Maunsbach AB: Observations on the segmentation of the proximal tubule in the rat kidney. Comparison of results from phase contrast, fluorescence, and electron microscopy. *J Ultrastruct Res* 16:239-258, 1966
 35. Brooks GT: The metabolism of diene-organo-chlorine (cyclodiene) insecticides. *Residue Rev* 27:81-138, 1969
 36. Durham WF: The interaction of pesticides with other factors, *Residue Rev* 18:21-103, 1967
 37. Gillett JW, Chan TM: Cyclodiene insecticides as inducers, substrates, and inhibitors of microsomal epoxidation. *J Agric Food Chem* 16:590-593, 1968
 38. Kuntzman R, Welch R, Conney AH: Factors influencing steroid hydroxylases in liver microsomes. *Adv Enzyme Regul* 4:149-160, 1966
 39. Koerner DR, Hellman L: Effect of thyroxine administration on the 11β -hydroxysteroid dehydrogenases in rat liver and kidney. *Endocrinology* 75: 592-601, 1964
 40. Schiebler TH, Mühlenfeld E: Über die geschlechtsspezifische Chemodifferenzierung der Rattenneire. *Naturwissenschaften* 53:311, 1966
 41. Von Deimling O, Baumann G, Noltenius H: Hormonabhängige Enzymverteilung in Geweben. V. Wirkung von Kastration und Sexualhormon auf fünf Enzyme der Mauseiere. *Histochemie* 5:1-10, 1965
 42. Von Deimling O, Wessels CH, Otterman U, Noltenius H: Hormonabhängige Enzymverteilung in Geweben. VII. Die quantitative Verteilung der alkalischen

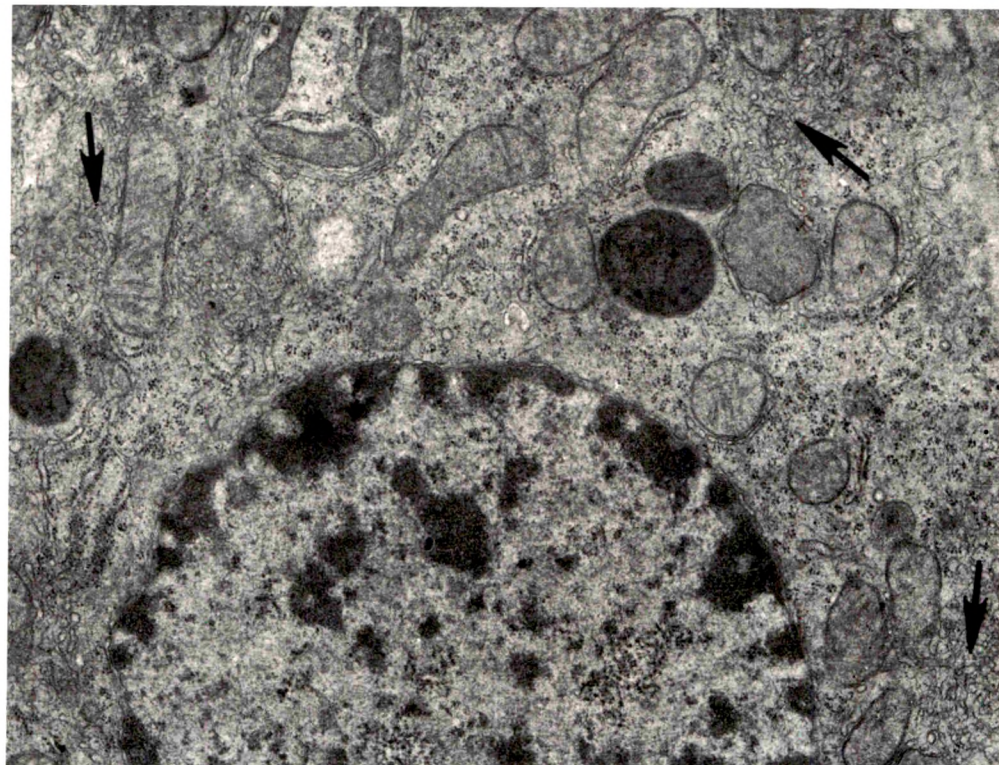
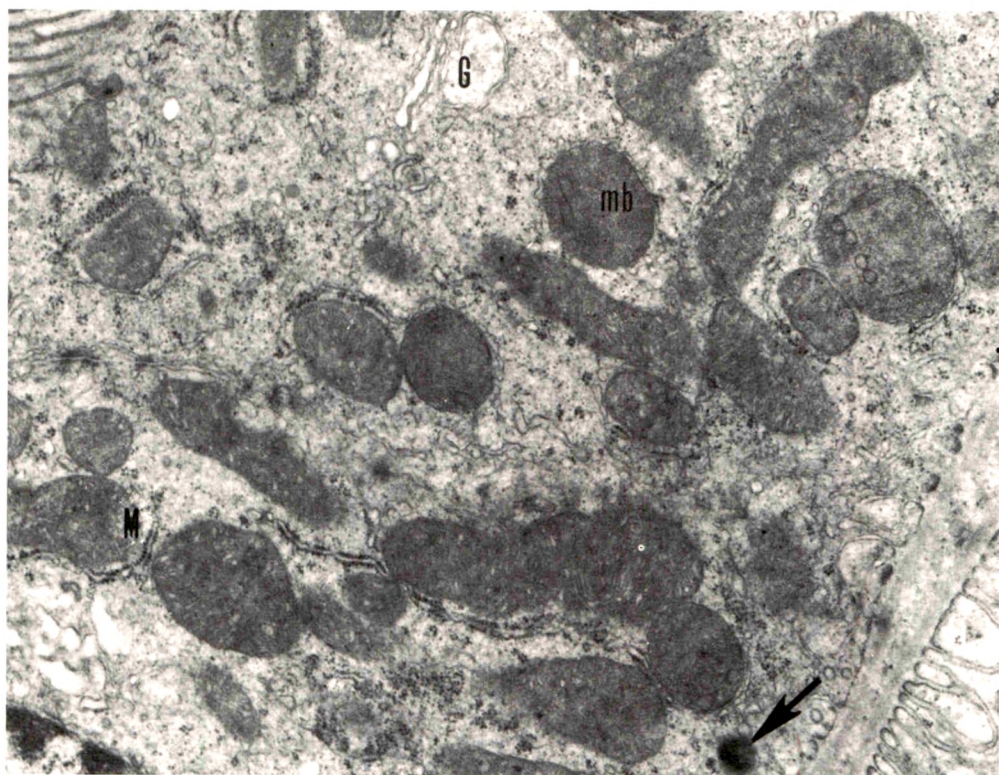
- Nierenphosphatase bei normalen Ratten beiderlie Geschlechts. *Histochemie* 8:200-215, 1967
43. Webb JL: *Enzyme and Metabolic Inhibitors*, Vol. II. New York, Academic Press, Inc, 1966, p 961
 44. Berglund F, Berlin M: Risk of methyl-mercury cumulation in man and mammals, and the relation between body burden of methyl mercury and toxic effects.²¹ pp 258-269
 45. Berlin M, Renal uptake, excretion, and retention of mercury. II. A study in the rabbit during infusion of methyl and phenylmercuric compounds. *Arch Environ Health* 6:626-633, 1963
 46. Berlin M, Ullberg S: Accumulation and retention of mercury in the mouse. II. An autoradiographic comparison of phenylmercuric acetate with inorganic mercury. *Arch Environ Health* 6:602-609, 1963
 47. Berlin M, Ullberg S: Accumulation and retention of mercury in the mouse. III. An autoradiographic comparison of methylmercuric dicyandiamide with inorganic mercury. *Arch Environ Health* 6:610-616, 1963
 48. Fitzhugh OG, Nelson AA, Laug EP, Kunze FM: Chronic oral toxicities of mercuri-phenyl and mercuric salts. *Arch Ind Hyg Occup Med* 2:433-442, 1950
 49. Norseth T: The intracellular distribution of mercury in rat liver after methoxyethyl mercury intoxication. *Biochem Pharmacol* 16:1645-1654, 1967
 50. Norseth T: Studies of intracellular distribution of mercury.²¹ pp 408-419
 51. Orrenius S: On the mechanism of drug hydroxylation in rat liver microsomes. *J Cell Biol* 26:713-724, 1965
 52. Orrenius S: Further studies on the induction of the drug-hydroxylating enzyme system of liver microsomes. *J Cell Biol* 26:725-734, 1965
 53. Orrenius S, Ericsson JLE, Ernster L: Phenobarbital-induced synthesis of the microsomal drug-metabolizing enzyme system and its relationship to the proliferation of endoplasmic membranes. *J Cell Biol* 25:627-640, 1965
 54. Webb JL: *Enzyme and Metabolic Inhibitors*, Vol. II. New York, Academic Press, Inc 1966, pp 768-790
 55. Webb JL: *Enzyme and Metabolic Inhibitors*, Vol II.⁵⁴ p 886
 56. Fowler BA: Ultrastructural evidence for nephropathy induced by long-term exposure to small amounts of methyl mercury. *Science* 175:780-781, 1972
 57. Chatelanat F, Simon GT: Ultrastructural pathology of the tubules and interstitial tissue.³³ pp 495-498
 58. Zollinger HU: Cytologic studies with the phase microscope. I. The formation of "blisters" on cells in suspension (potocytosis), with observations on the nature of the cellular membrane. *Am J Pathol* 24:545-568, 1948
 59. Weiner IM, Levy RI, Mudge GH: Studies on mercurial diuresis: renal excretion, acid stability and structure-activity relationships of organic mercurials. *J Pharmacol Exp Ther* 138:96-112, 1962
 60. Dingle JT, Barret AJ: The uptake of biologically active substances by lysosomes. *Biochem J* 109:198, 1968
 61. Goldstone A, Koenig H: Lysosomal lipoproteins and enzymes: Characteristics and biosynthesis, *J Cell Biol* 43:44a, 1969
 62. Goldstone, A, Szabo E, Koenig H: Isolation and characterization of acidic lipoprotein in renal and hepatic lysosomes. *Life Sciences* 9:607-616, 1970
 63. Fowler BA, Beard ME: Unpublished data

64. Fowler BA: Unpublished data
65. Fowler BA, Brooks RE: Effects of the herbicide paraquat on the ultrastructure of mouse kidney. *Am J Pathol* 63:505-520, 1971
66. Street JC: DDT antagonism to dieldrin storage in adipose tissue of rats. *Science* 146:1580-1581, 1964
67. Street JC, Chadwick RW: Stimulation of dieldrin metabolism by DDT. *Toxicol Appl Pharmacol* 11:68-71, 1967

Legends for Figures

Fig 1—Pars recta cell from a normal male (control) rat showing the low profile of this cell-type, cytosome (*arrow*), Golgi (G), mitochondria (M), microbodies (*mb*). Similar cells in control females contained slightly more SER ($\times 15,960$).

Fig 2—Pars recta cell from a male rat fed dieldrin for 142 days showing numerous SER aggregates (*arrows*). Compare presence of SER with Figure 1 ($\times 15,960$).



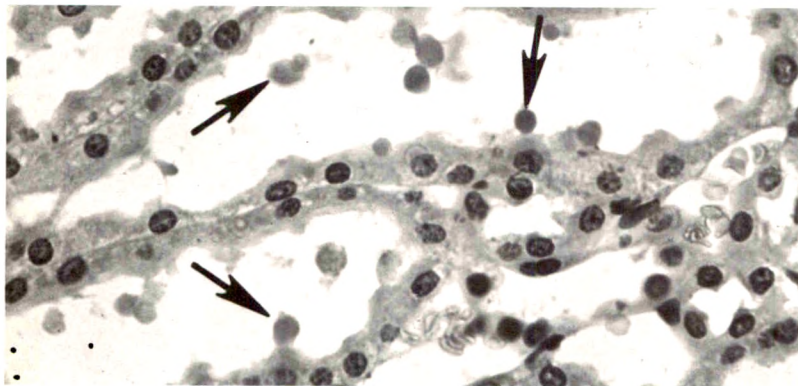
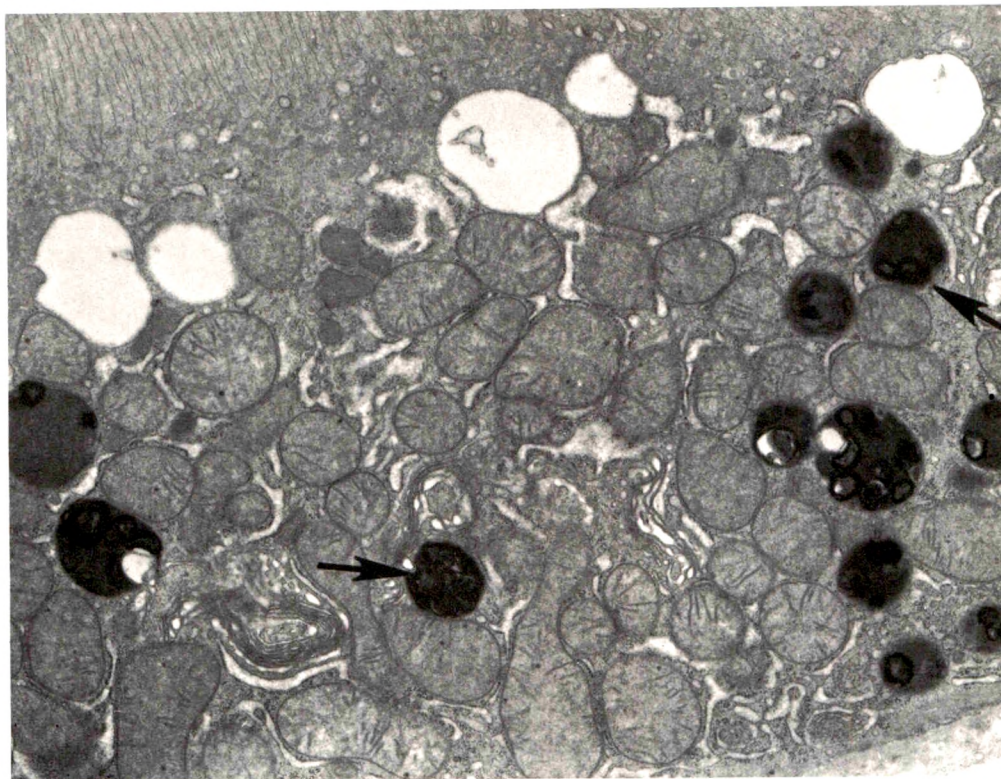


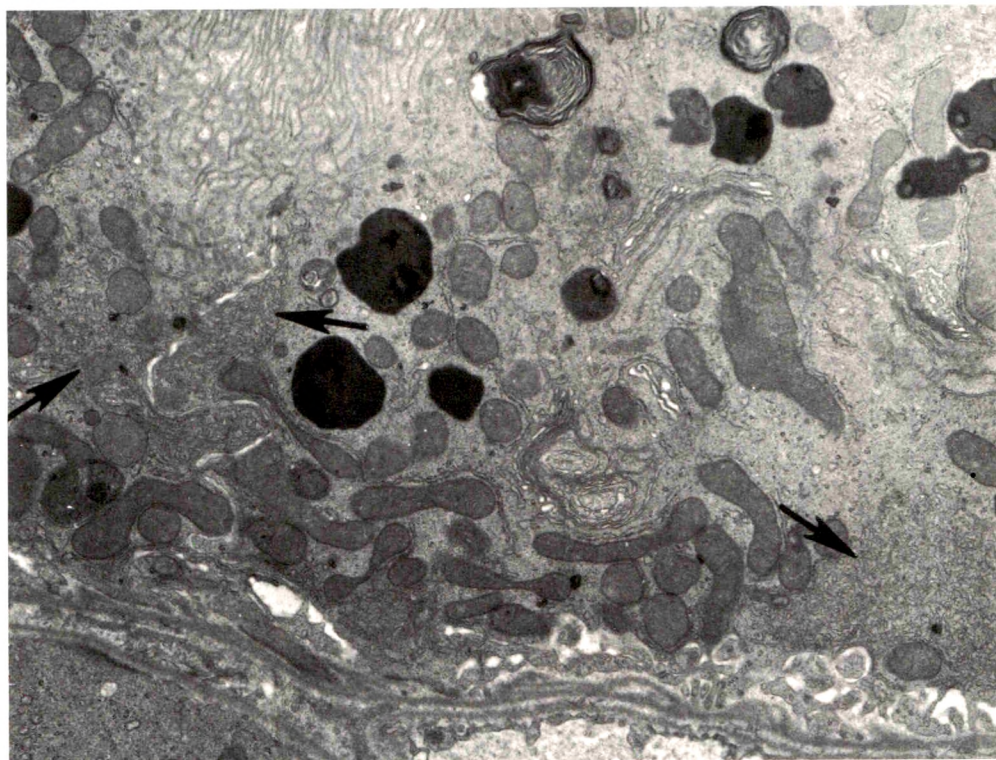
Fig 3—Light micrograph of pars recta segment from a female rat given CH_3HgCl for 84 days. Note that flattened epithelial cells line a dilated tubule lumen. Spherical cytoplasmic masses (arrows) are present in tubule lumen ($\times 610$).



Fig 4—Tissue of the pars recta from the kidney of a female rat receiving CH_3HgCl for 84 days is shown. A spherical cytoplasmic mass (arrow) containing SER and a microbody is present in the patent tubule lumen. In the adjacent pars recta cell, SER, a dilated Golgi, and dilated rough endoplasmic reticulum are seen ($\times 10,875$).

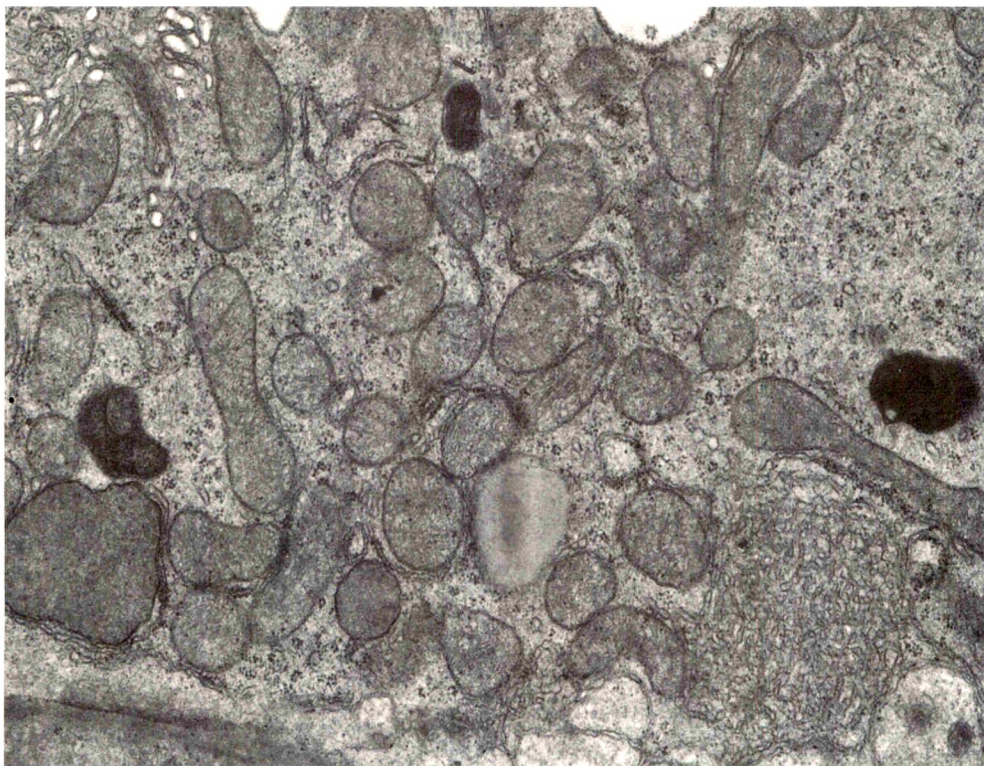


5

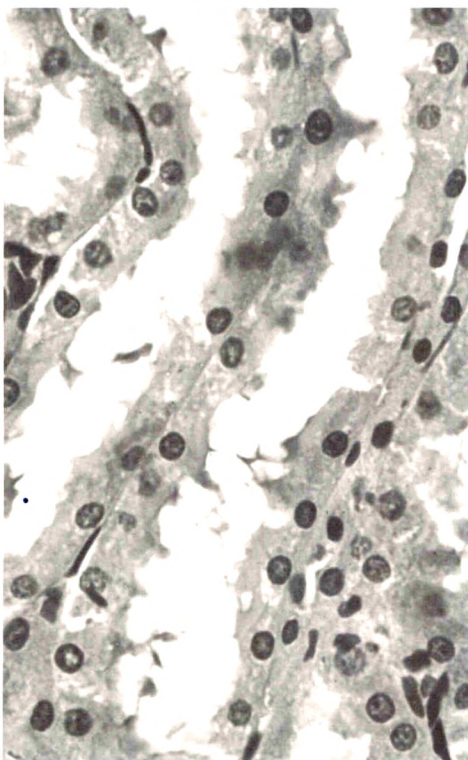


6

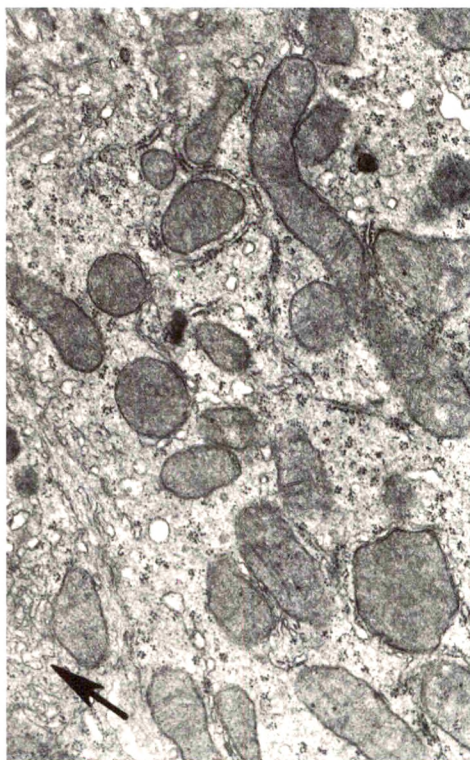
Fig 5—Dense membranous cytosomes (arrows) and somewhat swollen mitochondria in pars recta cell of a female rat exposed to CH_3HgCl for 84 days ($\times 13,750$). Fig 6—Pars recta segment of a female rat given CH_3HgCl for 142 days illustrating membranous dense cytosomes and myelin-like residual bodies. SER aggregates are prominent (arrows) ($\times 11,310$).



7



8



9

Fig 7—Pars recta cell from a male animal exposed to CH_3HgCl for 142 days showing large aggregate of SER but few cytosomes in comparison to females. Compare with Figures 5 and 6 ($\times 13,750$). **Fig 8**—Light micrograph of pars recta segments from a female rat exposed to dieldrin plus CH_3HgCl for 142 days. Note moderate dilatation of tubules but absence of spherical cytoplasmic masses free in the lumen ($\times 610$). **Fig 9**—Pars recta cell of a male rat receiving dieldrin plus CH_3HgCl for 142 days exhibiting small amounts of SER (arrow) ($\times 15,170$).

Irreversibility of Methylandrostenediol-Induced Hypertension in the Rat After Suspension of the Androgen Treatment

Agostino Molteni, MD, PhD, Alexander C. Brownie, PhD,
Peter A. Nickerson, PhD and Floyd R. Skelton, MD, PhD

Administration of 10 mg of methylandrostenediol for 10 weeks to uninephrectomized, salt drinking, female Sprague Dawley rats caused severe hypertension with extensive renal and cardiovascular damage. The hypertension was accompanied by increased consumption of sodium, high sodium levels in peripheral plasma, decreased weight of the pituitary, thymus, adrenals and ovaries and decreased content of renal renin. Methylandrostenediol treatment also produced impairment of normal adrenal steroidogenesis, reflected in elevated production *in vitro* of 11-deoxycorticosterone during incubation of adrenal gland homogenates with ¹⁴C-progesterone. Such increased production of deoxycorticosterone is probably responsible for the development of the hypertensive disease. If the methylandrostenediol-treated animals were kept alive for 12 additional weeks after suspension of the treatment with the androgen, the hypertension, as well as the high sodium consumption, high plasma sodium concentrations and low levels of renal renin, persisted to the end of the experiment. The cardiovascular and renal lesions in these animals, killed 12 weeks after suspension of the androgen administration, were similar to those seen in the rats receiving methylandrostenediol but killed at the tenth week of the treatment. Suspension of methylandrostenediol administration, however, resulted in a return to normal weight of the pituitary, thymus, adrenals and ovaries within 12 weeks. Normal amounts of deoxycorticosterone were formed *in vitro* by the adrenal glands of these rats and the return to normal structure was also confirmed by an electron microscopic study. Thus, contrary to a previous experiment where methylandrostenediol was given for a shorter period of time and the hypertension was reversible, it was shown in this study that metacorticoid hypertension is induced by methylandrostenediol administration, as it is with treatment with deoxycorticosterone. Since adrenal steroidogenesis returned to normal, some other mechanisms must be involved in maintaining the hypertension. It is very likely that these factors are consequent to the extensive and irreversible renal and cardiovascular damage (Am J Pathol 69:179-194, 1972).

SEVERAL INVESTIGATORS have shown that hypertension and panarteritis induced by deoxycorticosterone acetate in rats and dogs subsides after the steroid is discontinued, as long as it was admin-

From the Departments of Pathology and Biochemistry, State University of New York at Buffalo, Buffalo, NY 14214.

Supported by Research Grant HE 06975 from the National Heart and Lung Institute and by Training Grant GM 01500 from the National Institute of General Medical Sciences.

Accepted for publication July 5, 1972.

Address reprint requests to Dr. A. Molteni, Department of Pathology, State University of New York at Buffalo, Bell Plant Facilities, 180 Race St, Buffalo, NY 14214.

We regretfully announce the death of Dr. Floyd R. Skelton, October 22, 1969.

istered for a short period of time.¹⁻⁴ However, with prolonged treatment the hypertensive syndrome persists after the administration of deoxycorticosterone acetate is stopped.⁵

Skelton⁶ and, later, Salgado and Selye⁷ showed that severe hypertensive vascular disease, indistinguishable from that induced by deoxycorticosterone acetate, occurred in rats after the administration of an androgenic steroid, 17 α -methyl-5-androstene-3 β , 17 β -diol (methylandrostenediol). Salgado and Selye⁸ further showed that methylandrostenediol-induced hypertension did not occur in adrenalectomized rats. Recent *in vitro* investigations have demonstrated that the adrenals of rats made hypertensive by methylandrostenediol treatment synthesize greatly increased amounts of deoxycorticosterone,^{9,10} and that high levels of this corticosteroid were present in blood from the adrenal vein of such animals.¹¹ These findings have suggested that the hypertensive effect of methylandrostenediol is mediated through the hypersecretion of deoxycorticosterone, a mechanism which would explain the similarities between deoxycorticosterone acetate- and methylandrostenediol-induced hypertension.

Administration of methylandrostenediol for a short period of time (4 weeks) moderately increased systolic blood pressure but values returned to normal within 4 weeks after the androgen was withdrawn.¹² The normal structure of the adrenal glands of animals treated with methylandrostenediol for 4 weeks was also seen once treatment with the androgen was suspended.¹³

The present study was performed to ascertain whether the hypertensive effect of methylandrostenediol was still reversible when treatment with the androgen was prolonged beyond 4 weeks and if the hypertension persisted once it was discontinued.

Materials and Methods

Forty-two-day old, female Sprague Dawley rats weighing approximately 120 g were supplied by Charles River Laboratories, Inc, Wilmington, Mass. All rats were uninephrectomized, fed a diet containing 0.5% NaCl, given free access to a 1% NaCl drinking solution and maintained in a room kept at 22.5 C with 12-hour light and dark cycles.

The rats were randomly divided into two groups. One group of 40 rats was injected subcutaneously each day for 10 weeks with 0.2 ml of corn oil containing 10 mg of methylandrostenediol. About 30% of the rats in this group were killed at the end of the treatment. A further 30% were killed 6 weeks after and 40% 12 weeks after treatment with the androgen was withdrawn. The second group consisted of 20 control rats which were injected subcutaneously with 0.2 ml of corn oil each day for 10 weeks. Some rats were killed at this time and others 6 and 12 weeks later.

Systolic blood pressure was measured weekly in the tail of rats, under light ether anesthesia, with a Physiograph Four (E & M Instruments, Houston, Texas)

according to a procedure already reported in detail.¹⁴ Total sodium consumption was determined from the combined intake of food and drinking solution. Blood was collected, centrifuged immediately and the plasma obtained. Plasma concentrations of sodium and potassium were determined using a Beckman B Flame Photometer, as described by Rapp.¹⁵

All organs that were to be studied histologically were placed in 10% buffered formalin, trimmed after fixation of adherent tissue and weighed. Representative blocks were embedded in paraffin, cut at 5 μ and stained by the periodic acid-Schiff procedure. The kidneys were trimmed of fat, weighed fresh and bisected. One-half was used to determine the juxtaglomerular index and the other half to measure renin content, according to methods described previously.¹⁴

Adrenals from 4 methylandrostenediol-treated and 3 control animals were removed for electron microscopic observation at the 10-, 16- and 22-week time periods. The adrenals were trimmed of adherent fat, and slices 1-mm thick were cut and fixed in 3% glutaraldehyde buffered to pH 7.3 with 0.1 M phosphate. After an overnight wash in 0.1 M phosphate buffer (pH 7.3), slices of the adrenocortical zones were isolated as described previously,¹⁶ postfixed in 1% osmium tetroxide, dehydrated in ethanol and embedded in Epon 812 and Araldite. One-micron thick sections were cut from the tissue blocks to verify the identification of each of the three cortical zones. Thick sections were cut on a Porter-Blum Mt-1 ultramicrotome with glass knives. Sections were double stained in methanolic uranyl acetate followed by lead citrate before examination with a Siemens 101 electron microscope.

In the remaining animals, one of the adrenal glands from each rat was fixed in formalin for histologic studies and the other, after being weighed fresh, was pooled and used for the study of *in vitro* steroid biosynthesis, as described by Brownie and Skelton.⁸

All numerical data were analyzed according to Student's *t* test for small sample size; throughout the remainder of this report the differences between means having a *P* value <0.05 are considered significant and *P* values of <0.01 are considered highly significant.

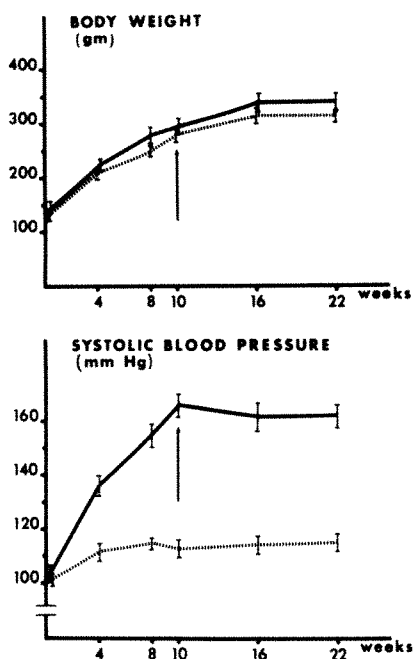
Results

Body Weight

Injections of methylandrostenediol were very well tolerated. One control and 3 methylandrostenediol-treated rats died during the first 4 weeks of the experiment from bronchopneumonia; 7 other methylandrostenediol-treated rats, which were severely hypertensive during the previous weeks, died after the eighth week. Data collected on all of these rats were discarded. The mean body weight of all rats increased regularly until the sixteenth week of the experiment and then remained constant (Text-figure 1, top). The mean weight for methylandrostenediol-treated rats was higher than that of controls and remained high even after androgen administration was discontinued.

Systolic Blood Pressure

In contrast to the stable blood pressure values of controls, methylandrostenediol-treated rats showed a progressive increase in blood



TEXT-FIG 1—Body weights (*top*) and systolic blood pressures (*bottom*) of control and methylandrostenediol-treated rats. The arrows indicate when the administration of methylandrostenediol was suspended. The vertical bars represent one standard error of the mean. Controls (*dotted line*); methylandrostenediol-treated rats (*solid line*).

pressure such that, at the tenth week, mean blood pressure for the group was approximately 160 mm Hg (Text-figure 1, bottom). After androgen administration was withdrawn, blood pressure remained in a range of 150 to 160 mm Hg until the end of the experiment (12 additional weeks).

Sodium Consumption

Sodium consumption in methylandrostenediol-treated animals was significantly higher than that of controls from the fourth week onward and remained elevated even after treatment with the androgen was withdrawn. (Text-figure 2, top).

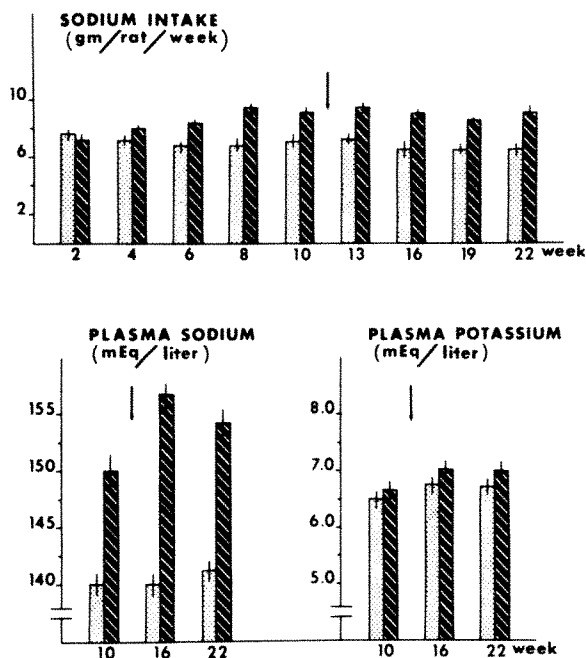
Plasma, Sodium and Potassium

Plasma levels of sodium were significantly increased above those of untreated controls after 10 weeks of androgen treatment and remained elevated in the same animals killed 6 and 12 weeks later (Text-figure 2, bottom). No significant changes were seen in plasma levels of potassium.

Renal Renin and Juxtaglomerular Indices

It is shown in Table 1 that the renal concentration of renin as well as

TEXT-FIG 2—Sodium intake (*top*) and plasma levels of sodium and potassium (*bottom*) of control and methylandrostenediol-treated rats. The arrows indicate the time at which administration of methylandrostenediol was suspended. The vertical bars represent one standard error of the mean. Controls (*dotted columns*); methylandrostenediol-treated rats (*hatched columns*).



the granulation indices of juxtaglomerular cells were greatly depressed in methylandrostenediol-treated rats killed after 10 weeks of androgen treatment. Animals of the same group killed 6 or 12 weeks later, when treatment with methylandrostenediol was suspended, also had a low renal renin content and low granularity.

Organ Weights

The mean renal weight of untreated control rats was similar at each interval (Table 2). Administered for 10 weeks, methylandrostenediol produced a definite increase in renal weight which persisted in rats of the same group killed 6 or 12 weeks after treatment with the antigen was stopped. An identical trend was evident in the weight of the heart. Thymic and ovarian weights, although depressed after 10 weeks of androgen treatment, recovered somewhat in animals killed 6 or 12 weeks after methylandrostenediol was withdrawn. Administration of the androgen for 10 weeks also produced a significant reduction in the weight of the adrenal glands and the pituitary. Suspension of treatment, however, allowed a partial recovery of the weight of these organs by 12 weeks. No significant changes were recorded in the weights of the spleen, liver and thyroid.

Table 1—Renal Content of Renin and Granulation Indices of Juxtaglomerular Cells of Control and Methylandrostenediol-Treated Rats

Groups	Weeks on MAD	Weeks off MAD	Renal renin (ng angiotensin II/mg renal cortical tissue)	Granulation indices
10-week				
Control	—	—	24.0 ± 8.0	15 ± 3
MAD	10	0	1.5 ± 0.5*	6 ± 1†
16-week				
Control	—	—	26.0 ± 8.0	18 ± 3
MAD	10	6	2.0 ± 0.3*	4 ± 1†
22-week				
Control	—	—	34.0 ± 9.0	16 ± 3
MAD	10	12	6.0 ± 2.0*	4 ± 1†

* $P < 0.001$ † $P < 0.05$

Values given as mean ± SE; MAD = methylandrostenediol

Morphologic Observations**Kidneys**

The kidneys of methylandrostenediol-treated rats were enlarged, pale and soft, with numerous hemorrhagic spots scattered over the capsular surface. Microscopic examination revealed that lesions produced by the steroid consisted of hyaline degeneration of the small arterioles, glomerular enlargement and hyalinization, tubular dilation with cloudy swelling of the epithelial cells and hyaline casts in the tubular lumen. Cessation of treatment with the androgen did not lead to a more normal appearance of the lesioned organs, even in animals killed 12 weeks after treatment with methylandrostenediol was discontinued.

Hearts

Methylandrostenediol treatment produced cardiac hypertrophy with scars visible on the epicardial surface. Microscopic lesions consisted of focal areas of myocardial necrosis and hyaline degeneration on the intima and media of small arteries often accompanied by adventitial infiltration of chronic inflammatory cells and fibroblasts. Such gross and microscopic lesions were seen in all animals whether they were killed after 10 weeks of methylandrostenediol treatment or 6 or 12 weeks after the androgen was stopped.

Adrenals

The adrenal glands of methylandrostenediol-treated rats after 10 weeks of treatment were reduced in size, and the color changed from

Table 2—Organ Weights of Control and Methylandrostenediol-Treated Rats

Groups	No. of animals	Weeks on MAD	Weeks off MAD	Organs weights (mean \pm SE)					
				Kidneys (mg)	Heart (mg)	Thymus (mg)	Pituitary (mg)	Adrenals (mg)	Ovaries (mg)
10-week									
Control	6	—	—	1753 \pm 100	1012 \pm 57	394 \pm 45	16.1 \pm 1.0	74 \pm 2	75 \pm 9
MAD	10	10	—	2817 \pm 141*	1252 \pm 43*	147 \pm 17†	10.7 \pm 0.5*	50 \pm 2*	25 \pm 2†
16-week									
Control	6	—	—	1609 \pm 80	930 \pm 60	289 \pm 17	15.8 \pm 1.3	66 \pm 6	61 \pm 8
MAD	11	10	6	2646 \pm 120*	1454 \pm 70*	192 \pm 30*	12.8 \pm 0.6	58 \pm 3	55 \pm 8
22-week									
Control	7	—	—	1623 \pm 53	1015 \pm 46	277 \pm 57	18.1 \pm 1.0	68 \pm 5	82 \pm 4
MAD	9	10	12	2532 \pm 100†	1280 \pm 50*	229 \pm 18	14.9 \pm 0.8	59 \pm 4	77 \pm 6

* $P < 0.05$

† $P < 0.001$

MAD = methylandrostenediol

yellow-pink to red. Microscopically, the thickness of the cortex was decreased; this reduction was particularly evident in the zona glomerulosa and reticularis. The cells of the zona fasciculata contained vacuoles and PAS-positive droplets scattered throughout the cytoplasm. A moderate recovery in size and a definite change in color from reddish to yellow-pink was seen in the glands of animals killed 12 weeks after treatment with methylandrostenediol was stopped. Microscopic examination of glands of these animals revealed that the structure and thickness of all three zones returned to normal.

Fine Structure of the Adrenal Gland

Severe morphologic alterations were localized to the zona fasciculata and to reticularis cells after 10 weeks of treatment with methylandrostenediol. The mitochondrial cristae were reduced in number (Figure 1), as compared to those of controls. Many of the cristae were localized peripherally and appeared as projections of the inner mitochondrial membrane. This was seldom seen in mitochondria of control animals. The smooth endoplasmic reticulum was hypertrophic (Figure 1) and often arranged in whorl-like configurations. Bundles of microfilaments traversed the cytoplasm, seemingly at random.

Six weeks after methylandrostenediol treatment ceased, alterations in the fine structure of adrenocortical cells were no longer present. Mitochondria possessed an increased complement of cristae (Figure 2) and could not be distinguished from those in controls. The cristae were tubulovesicular and virtually filled the entire matrix. Smooth endoplasmic reticulum was no longer hypertrophic at this time and was localized to several cisternae of flattened tubules interspersed and often adherent to the cytoplasmic organelles (Figure 2). Microfilaments were not observed in the cytoplasm, although an occasional microtubule was seen. The picture at 12 weeks of recovery was virtually identical to that at the 6-week period.

Corticosteroidogenesis in Adrenal Homogenates

That normal adrenal steroidogenesis was impaired was evident in methylandrostenediol-treated rats killed after 10 weeks of androgen administration. Deoxycorticosterone was formed in elevated amounts in homogenates of adrenal glands from these animals incubated with progesterone *in vitro* (Table 3). Withdrawal of methylandrostenediol, however, caused normal steroidogenesis to return so that the conversion of progesterone to corticosterone was high and deoxycorticosterone levels in incubations were low.

Table 3—Adrenal Steroidogenesis in Control and Methylandrostenediol-treated Rats

Groups	Weeks on MAD	Weeks off MAD	Percent conversion of progesterone-4- ¹⁴ C to		
			DOC	B	18-OH-DOC
10-week					
Control	—	—	11	46	36
MAD	10	—	81	12	4
16-week					
Control	—	—	10	57	22
MAD	10	6	14	55	24
22-week					
Control	—	—	15	62	22
MAD	10	12	16	59	18

DOC = 11-deoxycorticosterone; B = corticosterone; 18-OH-DOC = 18-hydroxy-11-deoxycorticosterone

Discussion

The hypertensive effect of methylandrostenediol is fully reversible after injections of this androgen are discontinued, provided that the treatment is of 4 weeks duration.¹² However, the present studies indicate that when treatment is more prolonged (10 weeks), the hypertension persists despite the fact that the androgen is discontinued. Some of the factors which initiate methylandrostenediol-induced hypertension and associated lesions have been fairly well characterized. Previous studies in methylandrostenediol-treated hypertensive rats have shown that steroidogenesis in the adrenal cortex of these animals is impaired and that homogenates of these adrenal glands are unable to convert progesterone to corticosterone, thereby resulting in the accumulation of deoxycorticosterone in the incubation medium.¹⁷ Above normal levels of deoxycorticosterone have been found in adrenal venous blood of methylandrostenediol-treated hypertensive animals.¹¹ An increased consumption of sodium was also observed in methylandrostenediol-treated animals, both in the present study and in previous investigations from our laboratory.¹⁰ In the attempt to define the pathogenesis of androgen-induced hypertension, it is interesting to note that the increased sodium retention and the cardiovascular and renal lesions are similar to those produced by injections of deoxycorticosterone.^{2,5-18} For all of these reasons, it was suggested that deoxycorticosterone overproduction and the consequent increase in sodium consumption are the factors responsible for the onset of androgen-induced hypertensive cardiovascular disease;¹⁰ indeed, elevated peripheral plasma levels of deoxycorticosterone have been found in testosterone-induced hypertension.¹⁹

Short-term administration of methylandrostenediol, followed by suspension of treatment, leads to full recovery of normal adrenal structure and function.¹³ In addition, sodium consumption, plasma levels of sodium and potassium, systolic blood pressure and renal renin content return to within normal limits.¹² Renal and cardiac weights of these animals also returned to normal after the androgen was withdrawn. These results are in agreement with the observation that deoxycorticosterone-induced hypertension is reversible when the steroid is given for a short period of time.^{2,3} However, when methylandrostenediol treatment as well as deoxycorticosterone treatment are more prolonged, the cardiovascular disease and hypertension are irreversible and persist even after the steroid treatment is withdrawn. Selye and Horava²⁰ coined the term *metacortical hypertension* for the sustained forms of hypertension which occur after the hypertensive agent is discontinued, and such a term can apparently be extended to the hypertensive disease which persists after treatment with methylandrostenediol is discontinued.

The factors which sustain the elevated blood pressure in methylandrostenediol-induced metacortical hypertension are not fully clear. It seems unlikely that the disease is sustained by continuous secretion of deoxycorticosterone from the adrenal glands. Although steroid biosynthesis was markedly impaired at 10 weeks of methylandrostenediol-treatment, the conversion of progesterone to corticosterone was similar to that of controls at 6 and 12 weeks after the injections of androgen ceased. Normal corticosteroid biosynthesis is reflected by the recovery of adrenal weight, histology and ultrastructure. The recovery of the ultrastructure of the adrenal zona fasciculata is supported by the observation that mitochondrial cristae of rats previously treated with androgen were similar to those of the controls 6 and 12 weeks after the treatment ceased. Mitochondrial cristae contain the 11 β -hydroxylating enzyme,²¹ which is involved in the conversion of deoxycorticosterone to corticosterone in the rat adrenal.²² Previous studies from our laboratory have shown that it is this step in steroid biosynthesis that is abnormal and that this adrenal cortical dysfunction is involved in the production of several forms of hypertensive vascular disease in the rat.^{9,10,14,17} Mitochondrial cristae are reduced in numbers in these forms of hypertensive disease,^{23,24,16} as they were in the present study after 10 weeks of androgen treatment. However, the recovery seen 6 or 12 weeks after suspension of methylandrostenediol treatment suggests that the 11 β -hydroxylase activity is restored; the results of *in vitro* incubation of adrenal glands support this view.

It does not seem likely that metacorticoid hypertension is sustained by the secretion of renin from the renal juxtaglomerular apparatus. The renin content in methylandrostenediol-treated rats was greatly decreased and did not return to normal values, even 12 weeks after methylandrostenediol was withdrawn. It is known that renal renin content decreases in rats consuming high amounts of sodium;²⁵ this has been observed in deoxycorticosterone-induced hypertension,^{26,27} as well as in other experimental forms of the same disease.¹⁴

The role of sodium in the induction of sustaining metacorticoid hypertension is also controversial. The androgen-treated rats continued to consume more sodium than did the controls, even after the injections of methylandrostenediol were discontinued. Was this sodium adequate to maintain high blood pressure and to continue damaging the renal and cardiovascular apparatus of the rats? It is well known that severe hypertension and cardiovascular and renal damage may be induced in the rat by adding high amounts of sodium chloride to the diet.²⁸⁻³⁰ However, larger amounts of salt and a more protracted treatment than that given in our experiment were required. On the other hand, deoxycorticosterone or methylandrostenediol treatment in the rat may raise blood pressure and induce mild vascular lesions even in animals maintained on a sodium restricted diet.^{31,32} Furthermore, sodium restriction does not reduce the already established postdeoxycorticosterone hypertension.⁵ These findings, taken together, suggest that sodium may be an important, although not essential cofactor in the development of the disease.

The renal and cardiovascular damage were irreversible even though the rats were allowed to recover for 12 weeks after methylandrostenediol was withdrawn. It seems likely, therefore, that the extensive damage to these systems sustains the elevated blood pressure, a phenomenon reminiscent of what is sometimes seen in humans when hypertension follows extensive renal damage.

References

1. Davis WB, Segalof A, Jacobs W: The effect of deoxycorticosterone acetate and propylene glycol in experimental renal hypertension. *J Lab Clin Med* 33:1483, 1948
2. Knowlton AI, Loeb EN, Seegal BC, Stoerk HC: Deoxycorticosterone acetate: studies on the reversibility of its effect on blood pressure and renal damage in rat. *Endocrinology* 45:435, 1949
3. Friedman SM, Friedman CL: Self-sustained hypertension in the albino rat: a hypothesis to explain it. *Can Med Assoc J* 61:596 1949
4. Prado JL: Estudos sobre hipertensao hormonal experimental. Tese a' apresentada a Escola Paulista de Medicina, Sao Paulo, Brazil, 1950

5. Green DM, Saunders FJ, Wahlgren N, Craig RL: Self-sustaining post-desoxycorticosterone acetate hypertensive cardiovascular disease. *Am J Physiol* 170:94, 1952
6. Skelton FR: The production of hypertension nephrosclerosis and cardiac lesions by methylandrostenediol treatment in the rat. *Endocrinology* 53:492, 1953
7. Salgado E, Selye H: The production of hypertension, nephrosclerosis and cardiac lesions by methylandrostenediol treatment in the rat. *Endocrinology* 55:550, 1954
8. Salgado E, Selye H: The role of the adrenals in the production of cardiovascular and renal changes by methylandrostenediol. *Arch Int Physiol Biochim* 57:352, 1954
9. Brownie AC, Skelton FR: The metabolism of progesterone-4-¹⁴C by adrenal homogenates from rats with adrenal-regeneration hypertension. *Steroids* 6:47, 1965
10. Skelton FR, Brownie AC, Nickerson PA, Molteni A, Gallant S, Colby HD: Adrenal cortical dysfunction as a basis for experimental hypertensive disease. *Circ Res* 24: Suppl. 1:35-57, 1969
11. Hyde PM, Daigneault EA: Adrenal plasma levels of corticosterone and deoxycorticosterone in methylandrostenediol-salt induced hypertension. *Steroids* 11:721, 1968
12. Molteni A, Brownie AC, Skelton FR: Reversibility of methylandrostenediol hypertension after cessation of the androgen treatment. Fifty-third Annual Meeting of the Federation of the American Society for Experimental Biology, Atlantic City, April 1969. *Fed Pro* 28:367, 1969 (abstr)
13. Nickerson PA, Molteni A: Recovery of adrenal ultrastructure after cessation of androgen treatment. *Am J Pathol* 64:31-44, 1971
14. Molteni A, Brownie AC, Skelton FR: Production of hypertensive vascular disease in the rat by methyltestosterone. *Lab Invest* 21:129, 1970
15. Rapp JR: Electrolyte and juxtaglomerular changes in adrenal regeneration hypertension. *Am J Physiol* 206:93, 1964
16. Nickerson PA, Brownie AC, Skelton FR: An electron microscopic study of the regenerating adrenal gland during the development of adrenal-regeneration hypertension. *Am J Pathol* 57:335-364, 1969
17. Brownie AC, Skelton FR: Adrenocortical function and structure in adrenal-regeneration and methylandrostenediol hypertension, *Function of the Adrenal Cortex*. Edited by KW McKerns. New York, Appleton-Century-Crofts, 1968, p 691
18. Selye H, Hall CE, Rowley EM: Malignant hypertension produced by treatment with deoxycorticosterone acetate and sodium chloride. *Can Med. Assoc J* 49:88, 1943
19. Colby HD, Skelton FR, Brownie AC: Testosterone induced hypertension in the rat. *Endocrinology* 86:1093, 1970
20. Selye H, Horava A: Second Annual Report on Stress. Montreal, Acta Inc, 1952, pp 21-22
21. Dodge AH, Christensen AK, Clayton RB: Localization of a steroid 11- β -hydroxylase in the inner membrane subfraction of rat adrenal mitochondria. *Endocrinology* 87:254, 1970
22. Brownie AC, Grant JK: In vitro enzymic hydroxylation of steroid hormones.

- I. Factors influencing the enzymic 11- β -hydroxylation of 11-deoxycorticosterone. *Biochem J* 57:255, 1954
23. Levine AJ, Skelton FR: A light and electron microscopic study of hyaline droplet and vacuole formation in the adrenal glands of rats treated with methylandrostenediol. *Am J Pathol* 51:831, 1967
 24. Skelton FR, Brownie AC: Studies on the pathogenesis of adrenal-regeneration and methylandrostenediol hypertension. *Endocrine Aspects of Disease Process*. Edited by G Jasmin. St. Louis, Warren H Green, Inc. 1968, pp 271-301
 25. Cockett AT, Moore RS, Kazmin M, Roberts AP: Extraction and bioassay of renin from kidneys of sodium depleted and sodium-loaded rats. *J Urol* 97: 168, 1967
 26. De Jong W: Release of renin by rat kidney slices; relation to plasma renin after deoxycorticosterone and renal hypertension. *Proc Soc Exp Biol Med* 130:85 1969
 27. Robb CA, Davis JO, Johnston CI, Hartroft PM: Effects of deoxycorticosterone on plasma renin activity in conscious dogs. *Am J Physiol* 216:884 1969
 28. Sapirstein LA, Brandt WL, Drury DR: Production of hypertension in the rat by substituting hypertonic sodium chloride solutions for drinking water. *Proc Soc Exp Biol Med* 73:82, 1950
 29. Meneely GR, Tucker RG, Darby WJ, Auerbach SH: Chronic sodium chloride toxicity in the albino rat. II. Occurrence of hypertension and of a syndrome of edema and renal failure. *J Exp Med* 98:71, 1953
 30. Koletsky S: Hypertensive vascular disease produced by salt. *Lab Invest* 7:377, 1958
 31. De Champlain J, Krakoff LR, Axelrod J: Relationship between sodium intake and norepinephrine storage during the development of experimental hypertension. *Circ Res* 23:479 1968
 32. Hall CE, Hall O: Methylandrostenediol hypertension induced without salt excess. Observations on organ changes and serum composition. *Am J Pathol* 54:489-506, 1969

Acknowledgments

The authors are grateful to Mr. Luther B. Joseph, Mrs. Geneva Joseph, Mrs. Dorothy Ide, Mrs. Yam Qun Pun, Mr. Robert Linsmair, Mrs. Elizabeth Lawson, Miss Christine Szymanski and Mrs. Neonila Fylypiw for skilled technical assistance, and to Mrs. Irene Hartwig and Mrs. Berta Cole for typing of the manuscript.

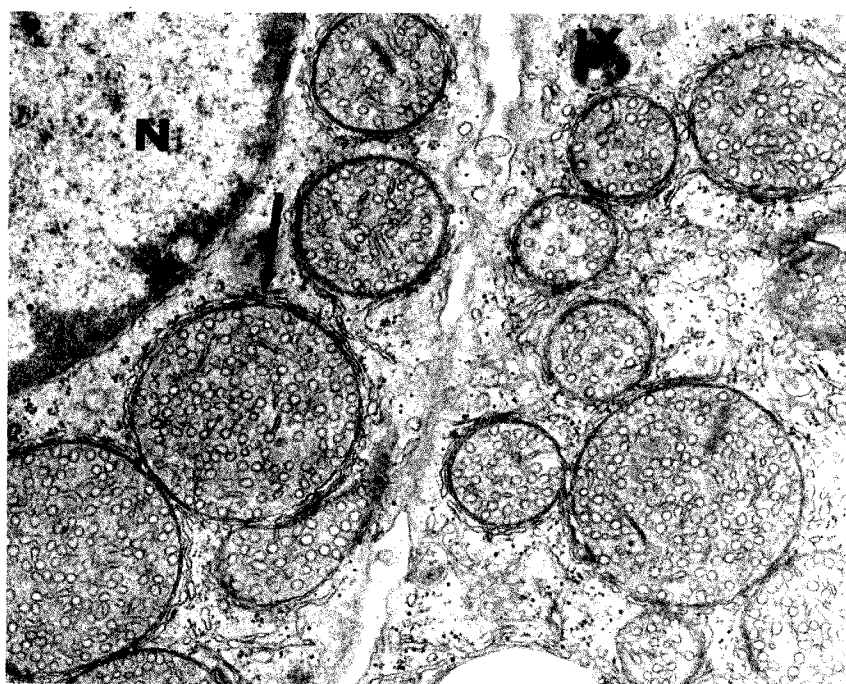
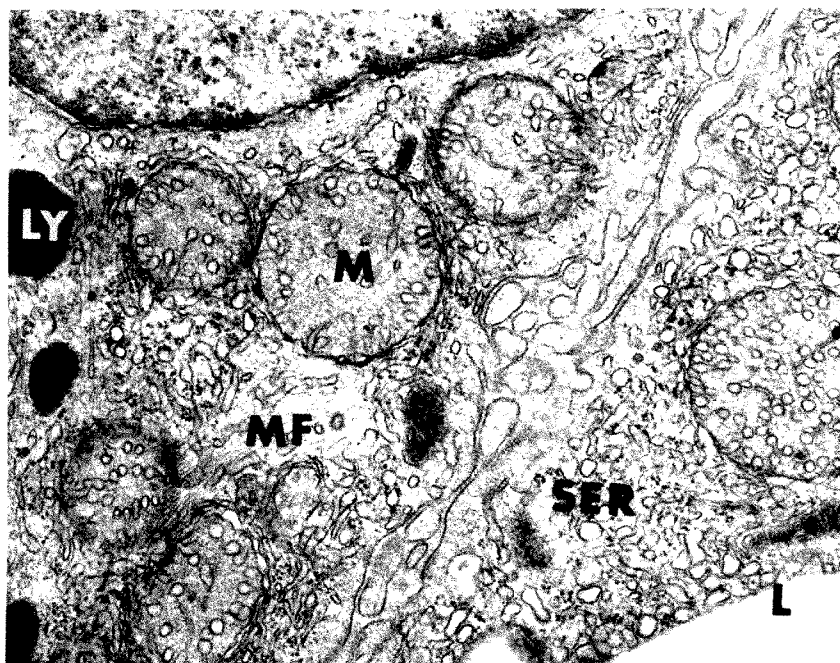


Fig 1—Portions of two zona fasciculata cells after 10 weeks of methylandrostenediol injections. Some mitochondria (*M*) show reduced numbers of cristae. The cytoplasm contains numerous microfilaments (*MF*) which traverse the cytoplasm, seemingly at random. Smooth endoplasmic reticulum (*SER*) is hyperplastic in these cells. A portion of a large lipid vacuole (*L*) is seen in the cytoplasm of one of the cells. Numerous lysosomes (*LY*) are observed in another cell ($\times 23,200$).

Fig 2—Portions of two zona fasciculata cells from an animal treated with methylandrostenediol for 10 weeks and allowed to recover for 6 weeks. Mitochondria contain numerous tubulo-vesicular cristae which virtually fill the entire mitochondrial matrix. Tubules of smooth endoplasmic reticulum are scattered throughout the cytoplasm and are sometimes closely associated with mitochondria (*arrow*). Other structures include the nucleus (*N*) and lysosomes (*LY*) ($\times 23,200$).

[*End of Article*]

Immune Reactions in Mucous Membranes

IV. Histochemistry of Intestinal Mast Cells During Helminth Expulsion in the Rat

H. R. P. Miller, BVMS, PhD and R. Walshaw

The histochemistry of intestinal (IMC) and connective tissue mast cells (CTMC) in the normal rat is compared. Acid mucopolysaccharide appears to be less strongly sulfated and the granule content of monoamines is lower in IMC. After infection with the intestinal helminth, *Nippostrongylus brasiliensis*, the mucosal content of IMC is altered. During the early phase of immunologic expulsion of this parasite (self-cure) the IMC proliferate and differentiate; the histochemical properties of the granules appear to reflect this process. Very large numbers of mature IMC are found in the mucosa during the later, rapid phase of worm expulsion. Both acid mucopolysaccharide and monoamines are depleted from the granules of these cells; this is consistent with previous studies suggesting that IMC discharge occurs at this stage. These findings lend further support to the hypothesis that the biogenic products of IMC discharge are responsible for the increase in mucosal permeability which occurs during self-cure and which may facilitate the rapid translocation of antiworm antibody into the intestinal lumen (Am J Pathol 69:195-208, 1972).

IF RATS ARE INFECTED with the intestinal helminth *Nippostrongylus brasiliensis*, the numbers and distribution of mast cells in the intestinal mucosa (IMC) fluctuate.¹⁻³ During immunologic expulsion of the parasite from the intestine (self-cure), a new population of IMC differentiates and proliferates in the mucosa,^{2,4,5} and many of the cells migrate into the epithelium and discharge to become globule leukocytes (GL).^{2,6,7} A clear-cut temporal relationship exists between the increase in IMC numbers, IMC discharge and worm expulsion.^{1-3,8}

The IMC in the normal rat differs not only morphologically but in its fixation and cytochemical properties from the connective tissue mast cell (CTMC).⁹⁻¹¹ Moreover, during self-cure, IMC discharge involves the lysis of cells without extrusion of their granules,⁸ a process which may be mediated by reaginic antibody and allergen.^{12,13} It was of interest, therefore, to further characterize the histochemical properties of IMC and to compare the results with histochemical changes among proliferating and discharging IMC at the time of self-cure. Three as-

From the Department of Veterinary Pathology, Veterinary School, University of Glasgow, Glasgow, Scotland.

Supported by grants from the Agricultural Research Council, Glaxo-Hanbury Limited and the Wellcome Trust.

Accepted for publication July 11, 1972.

Address reprint requests to Dr. H. R. P. Miller, Unité de l'Immunocytochimie, Département de Biologie Moléculaire, Institut Pasteur, Paris 15e, France.

pects were studied: a) the nature and fate of the acid mucopolysaccharide in the IMC granules; b) the presence or absence of basic protein in IMC and c) the granule content and fate of the biogenic amines, 5-hydroxytryptamine and histamine.

Materials and Methods

Fifty-five of 70 female hooded Lister rats, weighing 170 to 220 g, were infected subcutaneously in the region of the groin with 3000 *N. brasiliensis* larvae; the remaining 15 were kept as controls. Groups of 4 to 5 rats were anesthetised on days 10, 11, 12, 14, 16, 19 and 35, and several segments of jejunum were taken from an area 12 to 15 cm behind the pylorus;² the rats were then killed by cervical dislocation. The tongues and an equivalent region of jejunum were taken from control rats. In addition, 2 rats from each group, on days 10 to 12, 14 and 19, one rat on day 35 and 5 controls, were given 3 intraperitoneal injections of 40 mg/kg L-Dopa (L- β -3, 4-dihydroxyphenylalanine, Koch-Light Laboratories Limited, England) at hourly intervals and were killed 1 hour after the third dose.^{2,11}

Fixation and Tissue Preparation

The intestinal mucosa was orientated as described previously² and the tissues were fixed in either Carnoy's fluid or 4% phosphate-buffered formaldehyde, prepared from paraformaldehyde, for 24 to 48 hours, then dehydrated and cleared in an alcohol-amyl acetate-chloroform series and embedded in paraffin wax. Sections were cut at 6 μ .

To demonstrate monoamines,^{14,15} small pieces of tissue were quenched in isopentane cooled in liquid nitrogen, transferred directly to a freeze-drying apparatus maintained at -40°C and dried *in vacuo* with a phosphorus pentoxide water vapor trap for 24 hours. Some of the tissue was treated with paraformaldehyde for 1 hour at 80°C and was embedded either in degassed molten paraffin wax at 57 to 60°C or in an Epon-Araldite mixture, using a Pearse-Edwardes resin-embedding accessory. The rest of the unfixed tissue was embedded immediately in paraffin wax.

Staining Procedures

Demonstration of Acid Mucopolysaccharides

Toluidine blue was used in a 0.5% aqueous solution at pH 4 (McIlvaine's citric acid-disodium phosphate buffer); staining time was 45 seconds.^{6,7,10} A 0.1% aqueous solution of toluidine blue was made by diluting the dye in 0.7 N HCl. Sections were stained for 10 minutes after which they were rinsed in 0.7 N HCl for 10 minutes.^{6,7,10}

Astrablue (G. T. Gurr Ltd, London) was used in a 0.5% aqueous solution at pH 0.3;^{6,7,10} staining time was 30 minutes. Sections were also stained with 0.5% Alcian blue 8GX (E. Gurr Ltd, London and I.C.I. Ltd, Manchester), following the same procedure used for Astrablue.¹⁰ Some sections stained with either Astra or Alcian blue were counterstained with 0.5% Safranin O (Hopkin and Williams Ltd) in 0.125 N HCl (approximately pH 1) for 30 seconds.^{7,10}

Alcian blue 8GX was also used for the critical electrolyte concentration technic.¹⁶ Serial deparaffinized sections were immersed in upright Coplin jars filled with 0.04% dye solution (buffered with calcium acetate at pH 5.8) containing increasing concentrations of electrolyte (0.1 M increments of MgCl_2). Molarities ranged from 0.0 to 1.4. After rinsing in distilled water, the sections were dehydrated, cleared and mounted.

Demonstration of Basic Proteins

Biebrich scarlet was used as a 0.04% solution in glycine buffer at pH 8, 9 and 10; staining time was 30 to 90 minutes.¹⁷ Some sections were transferred directly to 95% alcohol, dehydrated and cleared; others were rinsed in distilled water prior to dehydration.

Demonstration of Monoamines

Catecholamines and 5-hydroxytryptamine fluorescence were detected in both paraffin and 1- μ plastic sections of freeze-dried paraformaldehyde-treated tissues. Sections of tissues which had not been treated with paraformaldehyde were used as controls. In addition, 1- μ plastic sections were examined for fluorescence, and the adjacent sections, stained by the method of Richardson *et al*,¹⁸ were examined in the light microscope.

Intracellular histamine was detected by staining sections of freeze-dried tissues with *o*-phthalaldehyde in ethyl benzene, using the method of Shelly, Ohman and Parnes.¹⁵ Similar results were obtained with tissues fixed briefly in Carnoy's fluid and rapidly dehydrated.¹⁹ Control sections were treated with ethyl benzene to which no *o*-phthalaldehyde was added.

Sections were examined in a Leitz Ortholux fluorescence microscope using a mercury vapor lamp (Wotan HBO220W) as a light source and, for catecholamines, a BG12 3-mm exciting filter with a Leitz K530 barrier filter. For histamine, UG1 and BG12 exciting filters and K410 and K530 barrier filters were used.

Results

Acid Mucopolysaccharide

Normal Rats

The histochemical properties of the acid mucopolysaccharides of the IMC and tongue CTMC fixed by different methods are shown in Table 1. Formaldehyde-fixed IMC were only demonstrable with the critical electrolyte concentration (CEC) technic at molarities between

Table 1—Histochemistry of the Acid Mucopolysaccharides in IMC and CTMC in Normal Rats

Fixative	Alcian or Astra blue/safranin		Toluidine blue (pH 0.3)		Toluidine blue (pH 4)		CEC*	
	IMC	CTMC	IMC	CTMC	IMC	CTMC	IMC	CTMC
Carnoy	B+++	R+++ (B+) [†]	B++	P+++	RP+	P+++	1.2	‡
Formaldehyde	—	R+++ (B+) [†]	—	P+++	—	P+++	0.9	‡

* Molarity of $MgCl_2$ at which Alcian blue staining is extinguished.

† A few cells stained blue and others had red and blue granules.

‡ Still staining in 1.4 M $MgCl_2$.

B = blue; R = red; P = purple. Staining intensity: — = none; + = weak; ++ = moderate; +++ = strong

0.4 to 0.9 M. Apart from the IMC, no other cell type in the intestinal mucosa was stained by any of the technics used.

Parasitized Rats

The elimination of the worm burden from female hooded Lister rats follows a recognizable pattern.^{3,20} Ten to twelve days after infestation, there is a period during which the worms are expelled at a slow rate;³ IMC differentiation and proliferation take place during this time.^{2,4} During the second phase, 12 to 16 days after infection, the worms are expelled very rapidly,³ and at this stage there is evidence of massive IMC discharge.^{2,8}

The results shown in Table 2 summarize the histochemistry of the acid mucopolysaccharides in Carnoy-fixed IMC during the different phases of worm expulsion. The toluidine blue metachromasia of acid mucopolysaccharide in infected rats and its affinity for thiazine and copper phthalocyanine dyes at low pH are indistinguishable from those of the normal rat. However, application of the CEC technic shows that the maturing IMC and GL, 11 days after infection, have a slightly reduced alcianophilia (Table 3). In addition the majority of GL on days 14 and 16, as well as many IMC, are cut out at low CEC when compared with IMC in normal rats (Table 3, Figures 1 and 2).

Basic Protein

Normal Rats

The CTMC did not stain with Biebrich scarlet with either of the fixatives employed. When fixed in Carnoy's fluid, the IMC stained

Table 2—Histochemistry of IMC and GL during the Immunologic Expulsion of *Nippostrongylus brasiliensis*

	Normal Rats	Infected Rats					
		Day 11		Days 14 and 16		Day 19	
		IMC	GL	IMC	GL	IMC	GL
Toluidine blue (pH 0.3)	B++	B++	B++	B++	B++	B++	B++
(pH 4.0)	RP+	RP+	RP+	RP+	RP+	RP+	RP+
Astra or Alcian blue/safranin	B+++	B+++	B+++	B+++	B+++	B+++	B+++
Biebrich Scarlet (pH 10.0)	++	+	+	++	+(+)	++	++

B = blue; R = red; P = purple. Staining intensity: + = weak, ++ = moderate; +++ = strong

Table 3—The Critical Electrolyte Concentrations for the Staining of IMC and GL with Alcian Blue 8GX During Expulsion of *N brasiliensis*

Molarity of $MgCl_2$	Normal Rat	Infected Rats					
	IMC	Day 11		Days 14 and 16		Day 19	
		IMC	GL	IMC	GL	IMC	GL
0.4	+++	+++	+++	+++	+++	+++	+++
0.5	+++	+++	+++	+++	+++	+++	+++
0.6	+++	+++	+++	+++	+++	+++	+++
0.7	+++	+++	+++	+++*	+++*	+++	+++*
0.8	+++	+++*	+++*	+++*	+++†	+++*	+++†
0.9	++	++*	++†	++†	++†	++*	++†
1.0	++*	++†	++†	++†	++†	++*	++†
1.1	++†	++†	++†	++†	++†	++†	++†
1.2	++†	++†	++†	++†	++†	++†	++†
1.4	—	—	—	—	—	—	—

* Staining of a few cells cut out.

† Staining of many cells cut out.

Staining intensity: — = none; + = weak; ++ = moderate; +++ = strong

strongly and, if the sections were dehydrated without prior rinsing, their nuclear morphology distinguished the IMC from other granule-containing cells, such as eosinophils and polymorphonuclear leukocytes, whose granules did not stain.

Parasitized Rats

Basic protein was present in the granules of both IMC and GL, although the staining intensity was reduced in both on days 10 to 12, and was slightly reduced in GL on days 14 and 16 (Table 2). A cell type resembling the basophil was also present in the mucosa during the period 10 to 14 days.⁵ Its granules were slightly smaller and stained less strongly than those in the IMC; it was distinguished from the IMC by its polymorphous nucleus.

Monoamines

Normal Rats

CATECHOLAMINES AND 5 HYDROXYTRYPTAMINE. The IMC in the villi and upper crypt regions fluoresced a weak, dull green. Those in the basal mucosa had a yellow fluorescence characteristic of 5-hydroxytryptamine, but were smaller and fluoresced less intensely than the CTMC in the tongue. Intestinal mast cells were distinguished from enterochromaffin cells by their different morphology, the larger

size of their granules and their location in the lamina propria (Figure 3). Nonspecific fluorescence was recognized because it did not diminish with prolonged exposure to ultraviolet light and was present in freeze-dried tissues not pretreated with paraformaldehyde.

In rats treated with L-Dopa the IMC fluoresced a bright green, except the IMC in the basal mucosa, which remained yellow. Connective tissue mast cells and enterochromaffin cells continued to fluoresce yellow. Intestinal mast cells in 1 to 1.5- μ plastic sections had a bright green fluorescence after treatment with L-Dopa and were identified in the adjacent section stained with Azure II—methylene blue (Figures 5 and 6).

Parasitized Rats

Days 10 to 12. The IMC and GL contained relatively few granules which, in the IMC, had a moderately bright but dirty yellow fluorescence; small numbers of GL had a similar bright fluorescence (Figure 3) and the remainder fluoresced dull green. After treatment with L-Dopa, both IMC and GL fluoresced a bright apple green (Figure 3, inset).

Days 14 and 16. IMC and GL were more fully granulated than on days 10 to 12, but the intensity of their fluorescence varied. In some areas there were IMC which fluoresced a moderately bright dirty yellow, but the majority either were not fluorescent or were a dull green. Globule leukocytes, although as numerous as IMC,² mostly did not fluoresce and the few that were detected were a faint, dull green. Some IMC, including occasional fragmented cells (Figure 4), fluoresced bright green in L-Dopa-treated rats; in contrast, very few GL were detected and they contained fewer, more weakly fluorescent granules than the IMC (Figure 4).

Days 19 and 35. As in the normal rat, the IMC in the basal mucosa fluoresced yellow and those in the villi were a faint dull green. Globule leukocytes exhibited little or no fluorescence.

In the rats given L-Dopa the IMC of the villi and upper crypt region were bright green, well granulated and compact (Figure 5). In contrast, many GL failed to fluoresce (compare Figures 5 and 6) and others showed, at best, a weak green fluorescence.

Histamine

Normal Rat

Mast cells in both freeze-dried and Carnoy-fixed tissues were demonstrable with *o*-phthaldialdehyde. The CTMC fluoresced bright yellow,

indicating the presence of histamine. Intestinal mast cells also had a yellow fluorescence but of lower intensity than the CTMC.

Parasitized Rats

Days 10–12. The numbers and morphology of the IMC and GL treated with *o*-phthaldialdehyde were similar to those seen in intestine treated with paraformaldehyde. Their granules also fluoresced yellow.

Days 14 and 16. Although IMC and GL were numerous at this time,² only a small proportion of IMC and an occasional GL fluoresced yellow. Fluorescent cells were more fully granulated than on days 10 to 12.

Day 19. Yellow, fluorescent, fully granulated IMC were detected at all levels in the lamina propria. Their numbers were only slightly increased above the normal levels although, at this time, four times as many IMC were present in the mucosa.² Fluorescent GL were rare and contained fewer granules than IMC.

Discussion

Normal Rat

In the normal rat, the IMC is considered atypical because cells are smaller, more irregular in size and contain fewer granules than CTMC.⁹ The histochemical properties of the granules are different from those of the CTMC because, in the mature CTMC, the majority of granules stain red in the Alcian blue/safranin sequence,²¹ whereas IMC granules stain blue.¹⁰ The present results confirmed these observations and, in addition, showed that the alcianophilia of IMC granules was extinguished at lower CEC than that of the CTMC granules. This would suggest that the acid mucopolysaccharides of IMC granules is less strongly sulfated than that in the CTMC.

A further striking difference was that formaldehyde-fixed IMC were not demonstrable with thiazine or copper phthalocyanin dyes at low pH. It has been suggested that this may be due to dissolution of the granules⁹ but, using the CEC method, the IMC stained at molarities between 0.4 to 0.9. This would suggest that the polyanions are blocked by cationic proteins, a phenomenon known to be reversed by staining with Alcian blue in salt solutions.²² The fact that neither acid mucopolysaccharides nor basic protein⁵ were demonstrable after formaldehyde fixation, whereas both were detected after Carnoy fixation lends further support to the possibility that basic protein blocks the basophilia of the acid mucopolysaccharides.

The IMC contains relatively small amounts of catecholamines and 5HT^{11,23} which, because of the low intensity of the fluorescence in the majority of cells, could be dopamine or low concentrations of 5-hydroxytryptamine.²³ The IMC in the basal mucosa of the hooded Lister rat did have relatively high concentrations of 5-hydroxytryptamine; these cells, unlike the IMC in the villi, did not appear to take up L-Dopa. After treatment with *o*-phthalaldehyde, the fluorescent intensity of the IMC was always lower than that of the CTMC, suggesting that the IMC had a smaller histamine content.

These results provide a basis for studies of the IMC changes during infection with *Nippostrongylus brasiliensis*. Previous work has shown that two phenomena are associated with worm expulsion: a) IMC proliferation and differentiation,^{2,4} and b) discharge of the granule contents of IMC at the same time they migrate into the epithelium to become GL.^{2,6-8}

Parasitized Rats

Proliferation of IMC

New IMC arise from blast cells, probably of lymphoid origin, approximately 10 days after infection.⁴ The granules are elaborated from the Golgi complexes,⁴ and the cells proliferate and differentiate^{2,4} so that, by day 14, very large numbers of mature cells are found in the mucosa.² On days 10 to 11, the IMC are immature and contain few granules;^{2,4} this study shows that these immature cells contain acid mucopolysaccharide, basic protein and monoamines.

There were several histochemical differences between maturing IMC in infected rats and mature IMC in normal rats. The acid mucopolysaccharide in the maturing cell had reduced alcianophilia and the staining intensity of the basic protein was also lower than in the mature IMC. This would be consistent with the accumulation and/or sulfation of the acid mucopolysaccharide and the addition of basic protein to the maturing granules because, on days 10 to 11, there is little evidence of granule discharge.⁸ An analogous situation exists in the maturing CTMC, although, in this cell, the sulfation of the heparin precursors is accompanied by a shift from alcianophilia to an affinity for safranin.²¹ The granules of the maturing IMC also contained monoamines and were able to take up L-Dopa.

Ultrastructurally, the maturation of IMC differs from that of CTMC because, in the latter, marked changes in granule structure accompany the shift in staining properties attributed to N-sulfation of heparin precursors.²⁴ No equivalent change in granule morphology is seen

in the maturing IMC,⁴ although histochemical comparison with the normal mature IMC suggests that the acid mucopolysaccharide of the IMC does become more fully sulfated during maturation. There are, therefore, clear cut differences, not only with regard to the morphology and histochemistry of IMC and CTMC, but also in the maturation of these two cells. This would suggest that the IMC and CTMC are different cell-types, rather than the same cell modified by different environments.

• Discharge of IMC

Mature GL are IMC which have migrated intraepithelially and discharged their granule contents^{6,7} so the proportion of mature GL present is a useful measure of the extent of IMC discharge.² During the rapid phase of worm expulsion 14 and 16 days after infection, 50% of the IMC population are GL² and, ultrastructurally, many IMC in the lamina propria also appear to be partially discharged at this time.⁸

Intestinal mast cell discharge could not be demonstrated by standard histochemical technics because the altered granules retained their affinity for basic dyes even at very low pH. However, application of the CEC method showed that the majority of GL and many IMC had a markedly reduced alcianophilia and were cut out at much lower electrolyte concentrations than in the normal rat. It would seem, therefore, that there is a degree of acid mucopolysaccharide depletion from these cells; this would account for the reduced basophilia of their granules in 1- μ plastic-embedded sections.⁸

Basic proteins were consistently present in both IMC and GL, although their staining intensity was slightly reduced in GL. Different technics would be necessary to determine any changes in the nature or amount of the basic protein. In the electron microscope, paracrystalline structures were found in the granules of discharged cells, and these were probably remnants of basic protein.^{7,8}

Although monoamines were present in maturing IMC and GL between days 10 to 12, the mature cells on days 14 and 16 contained little or no detectable monoamines. A further striking difference was that maturing GL and IMC both took up L-Dopa, whereas GL, on day 14 and subsequently, were unable to do so. Since, ultrastructurally, the majority of granules in the maturing IMC and GL were intact, whereas those in the mature cells, on days 14 and 16, were disrupted,^{4,8} it is likely that the decreased ability of the latter to store and to take up monoamines was due to the loss of integrity of the perigranular membranes.

These results clearly demonstrate that, during the rapid phase of worm expulsion, the GL and many IMC are unable to store and have also released monoamines. In addition, there appears to be a reduction of their content of acid mucopolysaccharide and, possibly, of basic protein. This is consistent with kinetic and ultrastructural studies which point to extensive mast cell discharge during self-cure.^{2,8}

It is known that, during this rapid phase of expulsion, mucosal permeability increases^{3,12} and is associated with extensive mucosal damage.⁵ Furthermore, experiments with antagonists^{25,26} and depletors²⁷ of monoamines suggest that both histamine and 5-hydroxytryptamine are involved in worm expulsion. The present findings thus provide further support for the hypothesis that biogenic products released from the mast cell granules could be partly responsible for increased mucosal permeability.^{3,5,8,12} This latter event is thought to enhance the passage of antiworm antibodies into the intestinal lumen^{3,7,12,28} and effect the rapid expulsion of the parasites.

References

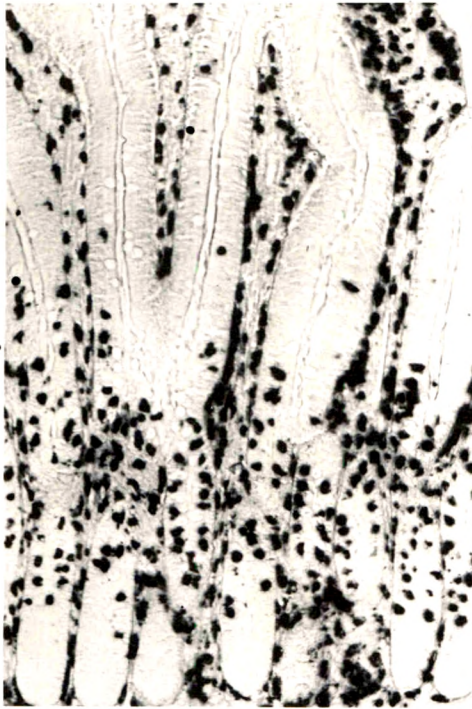
1. Jarrett WFH, Jarrett EEE, Miller HRP, Urquhart GM: Quantitative studies on the mechanism of self-cure in *Nippostrongylus brasiliensis* infections. Proceedings of the Third International Congress of the World Association for the Advancement of Veterinary Parasitology, Lyon. Marburg/Lahn, Germany. 1967, pp 191-198
2. Miller HRP, Jarrett WFH: Immune reactions in mucous membranes. I. Intestinal mast cell response during helminth expulsion in the rat. *Immunology* 20:277-288, 1971
3. Murray M, Jarrett WFH, Jennings FW: Mast cells and macromolecular leak in intestinal immunological reactions: the influence of sex of rats infected with *Nippostrongylus brasiliensis*. *Immunology* 21:17-31, 1971
4. Miller HRP: Immune reactions in mucous membranes. II. The differentiation of intestinal mast cells during helminth expulsion in the rat. *Lab Invest* 24:339-347, 1971
5. Miller HRP: The intestinal mast cell in normal and parasitized rats. PhD thesis, University of Glasgow, Glasgow, Scotland, 1969
6. Miller HRP, Murray M, Jarrett WFH: Globule leukocytes and mast cells.¹ pp 198-210
7. Murray M, Miller HRP, Jarrett WFH: The globule leukocyte and its derivation from the subepithelial mast cell. *Lab Invest* 19:222-234, 1968
8. Miller HRP: Immune reactions in mucous membranes. III. The discharge of intestinal mast cells during helminth expulsion in the rat. *Lab Invest* 24:348-354, 1971
9. Enerbäck L: Mast cells in rat gastrointestinal mucosa. I. Effects of fixation. *Acta Pathol Microbiol Scand* 66:289-302, 1966
10. Enerbäck L: Mast cells in rat gastrointestinal mucosa. II. Dyebinding and metachromatic properties. *Acta Pathol Microbiol Scand* 66:303-312, 1966

11. Enerbäck L: Mast cells in rat gastrointestinal mucosa. IV. Monoamine storing capacity. *Acta Pathol Microbiol Scand* 67:365-379, 1966
12. Jarrett WFH, Miller HRP, Murray M: Immunological mechanisms in mucous membranes. *Resistance to Infectious Disease*. Edited by RH Dunlop, HW Moon. Saskatoon, Saskatchewan, Saskatoon Modern Press, 1970, pp 287-304
13. Wilson RIM, Bloch KJ: Homocytotropic antibody response in the rat infected with the nematode *Nippostrongylus brasiliensis*. II. Characteristics of the immune response. *J Immunol* 100:622-628, 1968
14. Falck B, Hillarp N-Å, Thieme G, Torp A: Fluorescence of catecholamines and related compounds condensed with formaldehyde. *J Histochem Cytochem* 10:348-354, 1962
15. Shelley WB, Ohman S, Parnes HM: Mast cell stain for histamine in freeze-dried embedded tissue. *J Histochem Cytochem* 16:433-439, 1968
16. Scott JE, Dorling J: Differential staining of acid glycosamino-glycans (Mucopolysaccharides) by Alcian blue in salt solutions. *Histochemie* 5:221-233, 1965
17. Spicer SS, Lillie RD: Histochemical identification of basic proteins with Biebrich scarlet at alkaline pH. *Stain Technol* 36:365-371, 1961
18. Richardson KC, Jarrett L, Finke EH: Embedding in epoxy resins for ultrathin sectioning in electron microscopy. *Stain Technol* 35:313-320, 1960
19. Enerbäck L: Detection of histamine in mast cells by *o*-phthalaldehyde reaction after liquid fixation. *J Histochem Cytochem* 17:757-759, 1969
20. Jarrett EEE, Jarrett WFH, Urquhart GM: Quantitative studies on the kinetics of establishment and expulsion of intestinal nematode populations in susceptible and immune hosts. *Nippostrongylus brasiliensis* in the rat. *Parasitology* 58:625-639, 1968
21. Combs JW, Lagunoff D, Benditt EP: Differentiation and proliferation of embryonic mast cells of the rat. *J Cell Biol* 25:577-592, 1965
22. Scott JE, Dorling J, Stockwell RA: Reversal of protein blocking of basophilia in salt solutions: implications in the localisation of polyanions using Alcian blue. *J Histochem Cytochem* 16:383-386, 1968
23. Enerbäck L, Häggendal J: Uptake and storage of catecholamines in mucosal mast cells of the rat. *J Histochem cytochem* 18:803-811, 1970
24. Combs JW: Maturation of rat mast cells. An electron microscope study. *J Cell Biol* 31:563-575, 1966
25. Murray M, Smith WD, Waddell AH, Jarrett WFH: *Nippostrongylus brasiliensis*: histamine and 5-hydroxytryptamine and worm expulsion. *Exp Parasitol* 30:58-63, 1971
26. Urquhart GM, Mulligan W, Eadie RM, Jennings FW: Immunological studies on *Nippostrongylus brasiliensis* infection in the rat. The role of local anaphylaxis. *Exp Parasitol* 17:210-217, 1965
27. Sharp NCC, Jarrett WFH: Inhibition of immunological expulsion of helminths by reserpine. *Nature* 218:1161-1162, 1968
28. Barth EEE, Jarrett WFH, Urquhart GM: Studies on the mechanism of the self-cure reaction in rats infected with *Nippostrongylus brasiliensis*. *Immunology* 10:459-464, 1966

Acknowledgments

We thank Miss Morag Falconer for excellent technical assistance, Mr. A. Finnie for preparing the photomicrographs and Mrs. E. Paterson for typing the manuscript. Mr. Walshaw was in receipt of a Wellcome Trust Vacational Scholarship.

[Illustrations follow]



Figs 1 and 2—Intestinal mast cells and GL in the mucosa 16 days after infection with *N. brasiliensis* and stained with Alcian Blue 8GX in electrolyte. Note the reduced staining and disappearance of cells in 0.8 M $MgCl_2$ (1, 0.4 M $MgCl_2$; 2, 0.8 M $MgCl_2$, $\times 150$). **Fig 3**—IMC and GL (arrows) are poorly granulated but are brightly fluorescent in the jejunal mucosa 12 days after infection. Enterochromaffin cell (arrowhead) ($\times 350$). **Inset**—GL in an L-Dopa treated rat 12 days after infection ($\times 1500$).

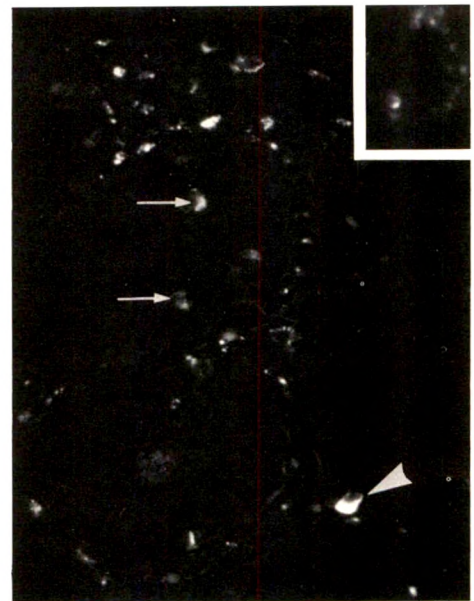
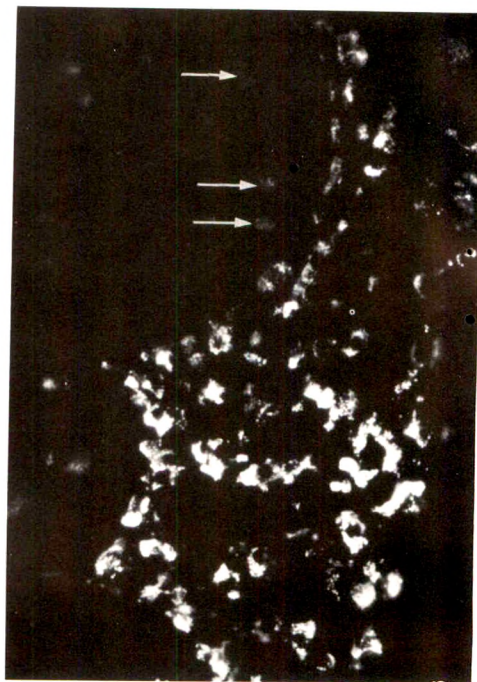
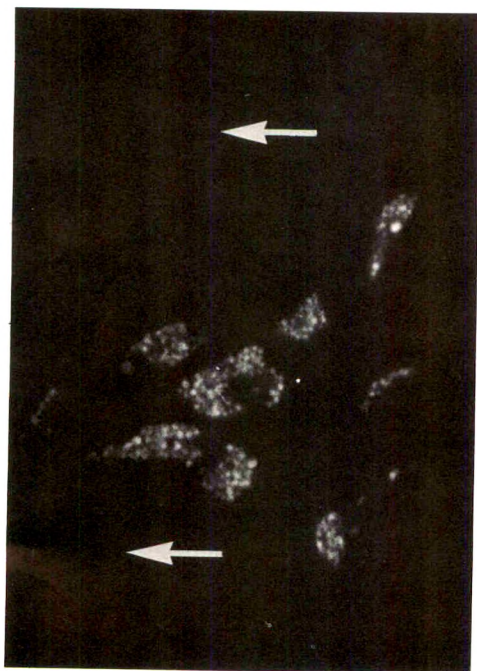


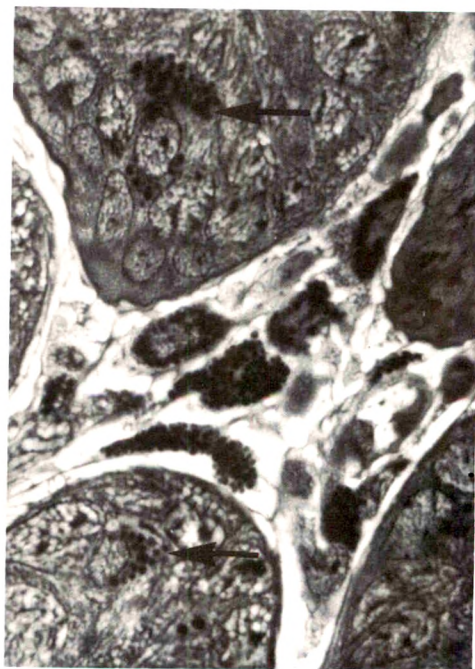
Fig 4—Intestinal mast cells and fragmented IMC, fluoresce a bright green in the lamina propria of a L-Dopa treated rat 14 days after infection. In contrast, GL (arrows) have a weak fluorescence ($\times 350$). **Fig 5**—One micron Epon-Araldite section from L-Dopa treated rat 19 days after infection. The intestinal mast cells are compact and have bright green fluorescence. The location of GL (arrows) is confirmed in Figure 6 ($\times 1300$). **Fig 6**—One-micron section adjacent to that in Figure 5 and stained with Azure 2-Methylene Blue illustrates the distribution of intestinal mast cells and GL (arrows) present in Figure 5 ($\times 1300$).



4



5



6

ANIMAL MODEL
OF
HUMAN DISEASE

Kuru, Creutzfeldt-Jakob Disease
(Slow Virus Infections)

Animal Model: Transmissible Mink
Encephalopathy, Scrapie-Like Disease
of Mink

Contributed by: R. F. Marsh, DVM, Department of Veterinary Science, University of Wisconsin, Madison, Wisc.

Biologic Features

Transmissible mink encephalopathy (TME) is a naturally occurring disease of commercially raised mink (*Mustela vison*) which was first described in the United States in 1947. The natural disease is characterized by an incubation period of 8 to 12 months followed by a clinical course of progressive nervous deterioration ending in complete debilitation and death. The only detectable lesion in TME has been limited to the central nervous system and is microscopic in nature. Principal alterations, as seen by the light microscope, have been microvacuolation of the gray matter (Figure 1), reactive astrocytosis (Figure 2) and neuronal degeneration. These changes have been found to precede clinical disease by approximately 6 weeks, and are themselves preceded several weeks by ultrastructural changes. Electron microscopic studies from the laboratory of Dr. G. M. Zu Rhein, Department of Pathology, University of Wisconsin Medical School have shown the evolution of lesions in experimentally induced TME to be similar in mink, monkeys and hamsters. Early examination of affected brain revealed in the pre- and postsynaptic nerve endings and larger dendritic segments, swelling, dissipation or reduction of normal components, presence of variously shaped vesicles of differing sizes, and more frequent tubulovesicular profiles than seen in normal brain. As the lesions mature, vacuolated tissues contain distended neuronal processes with areas of rarefaction, membrane-bound vacuoles, large collections of vesicles and morphologically altered surface membranes.

Publication sponsored by the Registry of Comparative Pathology of the Armed Forces Institute of Pathology and supported by Public Health Service Grant RR 00301 from the Division of Research Resources, US Department of Health, Education and Welfare, under the auspices of Universities Associated for Research and Education in Pathology, Inc.

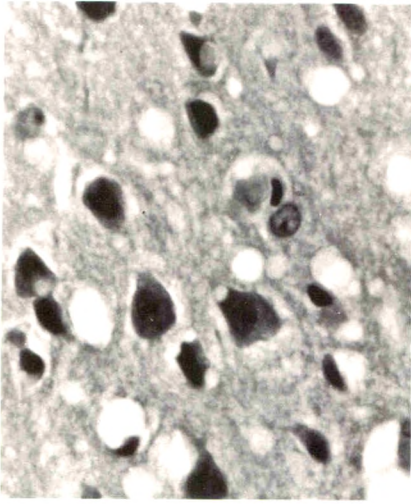


Fig 1—Vacuolar degeneration in the cerebral cortex of a rhesus monkey with transmissible mink encephalopathy (H&E, $\times 500$).

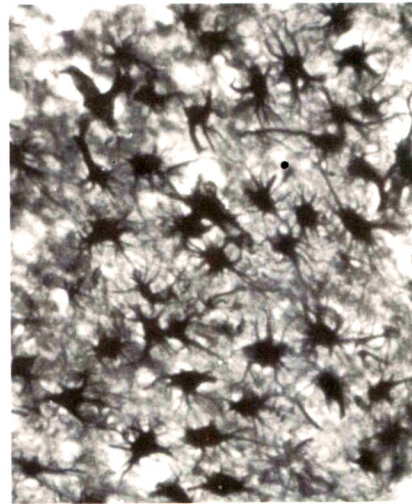


Fig 2—Reactive astrocytosis in the cerebral cortex of a mink with transmissible mink encephalopathy (Cajal's gold sublimate, $\times 240$).

Most of the large vacuoles have complex confinements and contain many curved, curled or circular profiles (Figure 3).

Studies on the physiochemical properties of the TME agent indicate that it is less than 50 nm in diameter, sensitive to ether, relatively resistant to 10% formalin and resistant to ultraviolet irradiation. Attempts to demonstrate a specific antibody response to the TME agent in infected mink have been unsuccessful. The disease has been experimentally transmitted to seven other species including the hamster, goat, striped skunk, raccoon, rhesus monkey, squirrel monkey and stump-tailed macaque.

Comparison with Other Transmissible Spongiform Polioencephalopathies

Transmissible mink encephalopathy is very similar to scrapie disease of sheep on the basis of clinicopathologic features and the properties of the transmissible agents. Intracerebral inoculation of mink with brain or spleen tissue from scrapie-affected Suffolk sheep has been found to produce a disease indistinguishable from TME. It may be that TME represents a carnivore-passaged strain(s) of scrapie. If this assumption is valid, it would appear that mink passage of *scrapie* has produced a modification in the agent(s) effecting host range. Transmissible mink

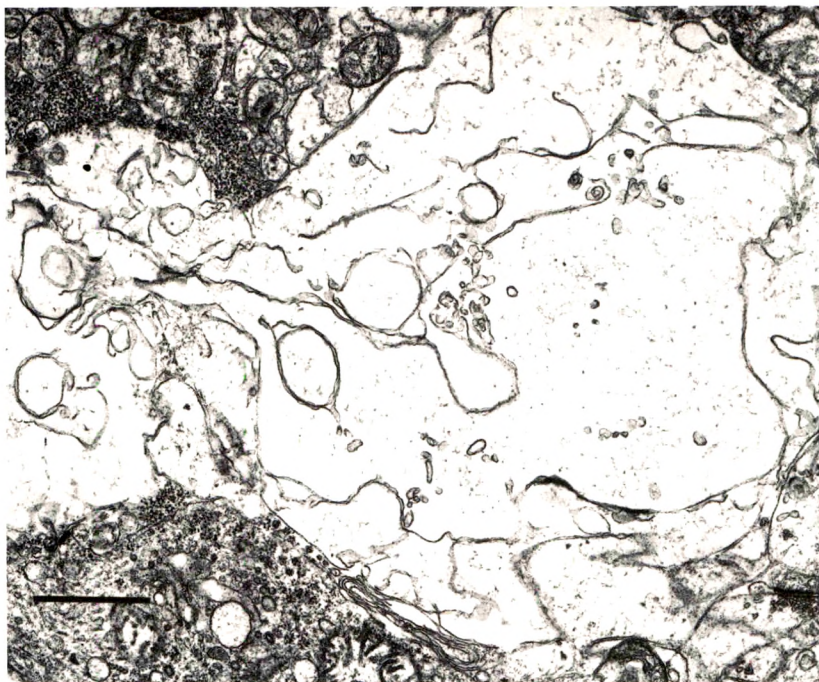


Fig. 3—Electron micrograph of lesion corresponding to a large vacuole in the neuropil by light microscopy. Mark = 1μ (Uranyl acetate and lead citrate, $\times 15,000$; courtesy of Dr. G. M. Zu Rhein).

encephalopathy has not as yet been transmitted directly from mink to Swiss white mice; scrapie is usually infectious for mice but appears to have a limited pathogenicity for primates. In this aspect, TME would seem to be more closely related to the human encephalopathies, kuru and Creutzfeldt-Jakob disease, which are also nonpathogenic for Swiss mice but are transmissible to subhuman primates.

Potential usefulness of model

The study of TME provides an opportunity to examine the pathogenesis and mode of action of a highly unorthodox group of neuropathic agents. The study of this disease may also uncover evidence for the etiologic and epidemiologic interrelationships between the animal and human spongiform encephalopathies. Finally, the mink itself may prove to be an extremely valuable animal in studying other neurologic diseases of unknown etiology.

Availability

Only a few laboratories are working on TME at the present time. Because of the close relationship between TME and scrapie, it is suggested that individuals requesting the agent first contact the Animal Health Division, Agriculture Research Service, Department of Agriculture. Brain tissue from TME-affected mink is on file at the Armed Forces Institute of Pathology (AFIP Acc. No. 1232805).

References

1. Burger D, Hartsough GR: Encephalopathy of mink. 2. Experimental and natural transmission. *J Infect Dis* 115: 393-399, 1965
2. Eckroade RJ, ZuRhein GM, Marsh RF, Hanson RP: Transmissible mink encephalopathy: Transmission to the squirrel monkey. *Science* 169: 1088-1090, 1970
3. Hanson RP, Eckroade RJ, Marsh RF, ZuRhein GM, Kanitz CL, Gustafson DP: Susceptibility of mink to sheep scrapie. *Science* 172: 859-861, 1971
4. Hartsough GR, Burger D: Encephalopathy of mink. 1: Epizootologic and clinical observations. *J Infect Dis* 115: 387-392, 1965
5. Marsh RF, Burger D, Eckroade RJ, ZuRhein GM, Hanson RP: A preliminary report on the experimental host range of the transmissible mink encephalopathy agent. *J Infect Dis* 120: 713-719, 1969
6. Marsh RF, Hanson RP: Physical and chemical properties of the transmissible mink encephalopathy agent. *J Virol* 3: 176-180, 1969
7. ZuRhein GM, Eckroade RJ: Experimental transmissible mink encephalopathy (TME). An ultrastructural study. *Proceedings of the Sixth International Congress of Neuropathology*. Paris, Masson et Cie, 1970, pp 939-940

The American Journal of PATHOLOGY

is published by the Medical Department of Harper & Row, Publishers, under the auspices of The American Association of Pathologists and Bacteriologists and The American Society for Experimental Pathology, and is edited by a Board appointed by the Councils of the two Societies. It is devoted to the prompt publication of original observations and investigations in the field of pathology and microbiology and is published monthly in four volumes per year.

Information for Authors

- ORIGINAL PAPERS will be considered for publication on condition that they are contributed solely to THE AMERICAN JOURNAL OF PATHOLOGY. Address manuscripts to the Editor-in-Chief: THOMAS D. KINNEY, MD, Department of Pathology, Duke University Medical Center, Durham, NC 27706.

MANUSCRIPTS must be typed **double-spaced** (including tables, references, and legends for figures), and all material should be submitted in duplicate. The literature should be summarized as concisely as is consistent with establishing the necessary basis for new material, and original observations should be presented in a clear, well-organized manner. Papers should rarely exceed 20 printed pages. Tables should be planned to suit the page size of THE JOURNAL. Excess tabular matter must be paid for by the contributor.

REFERENCES to the literature should be numbered in the order of citation in the text and should conform to the following style: names of all authors, complete title of article (including subtitle), abbreviated name of periodical (use *Index Medicus* style abbreviations), volume in Arabic numerals, inclusive pagination, and year (eg, 14:111-120, 1938). Titles are to be in the original language when they can be reproduced in the English alphabet. Translated titles should be enclosed in square brackets.

ILLUSTRATIONS must be planned to suit the page size of THE JOURNAL (**maximum plate size is 5½ × 8 inches**) and should be submitted **unmounted**, with figure number, top, and author's name marked lightly on the back in soft pencil. Oversize illustrations should be avoided because handling of these delays publication. To be accepted, illustrations must reach a certain standard of excellence technically, present an attractive appearance, and add significantly to the value of the presentation. Marking lines and letters, if essential, must be kept at least ¼ inch inside all margins. If two or more illustrations are to appear on a page, they should be so trimmed that the edges may be butted and the outer margins squared. The legends for photomicrographs should state the staining method and the degree of magnification. Black and white illustrations will be furnished in moderate numbers. Excess illustrations, when accepted, and the cost of illustrations in color, must be paid for by the contributor.

REPRINTS: An order blank for reprints is sent with the proof.

Rudolf Partsch wanted to repeal Murphy's Law. Thus, the world's easiest-to-operate Electron Microscope.

"What I want," said Rudolf Partsch of Carl Zeiss, Inc. to the designers in Oberkochen, West Germany, "is a totally reliable, extremely easy-to-operate, compact electron microscope with good resolution (7\AA) in the 0-60,000x range. And I want it at a low price." He wanted an electron microscope for researchers and teachers interested in electron microscopic studies, not electron microscopes—an instrument designed for everyday use.

The Zeiss M9S-2 with fully automatic camera system, foolproof airlock, and fingertip controls is what he got. And it looks as though Mr. Partsch really had a keen insight into the needs of a large section of the American scientific community . . . judging both by the reception this instrument has had, and by the numerous attempts to copy it. The copies never catch up, because Partsch keeps in regular contact with users, to find out what kind of modifications can be made to

keep abreast of research's ever-changing requirements. When he finds one, he gets it incorporated *post haste* into the design. And, what's more, makes it available for incorporation into previously sold instruments. Because ease-of-modification is a feature inherent in the original uncomplicated design, a Zeiss Electron Microscope never gets old.

For the whole story, contact Partsch. He'll send you complete specifications and the illustrated brochure "How to Operate the World's Easiest-to-Operate Electron Microscope."

You can reach him by phone at: (212) 736-6070. Or write Carl Zeiss, Inc., 444 5th Ave., New York, N.Y. 10018. Canada: 45 Valleybrook Drive, Don Mills 405, Ontario.

Ask for leasing and time payment terms. •

Nationwide service.

ATLANTA, BOSTON, CHICAGO, COLUMBUS, DALLAS, DENVER, FORT LAUDERDALE, HOUSTON, KANSAS CITY, LOS ANGELES, PHILADELPHIA, PHOENIX, SAN FRANCISCO, SEATTLE, WASHINGTON, D.C.



ZEISS
THE GREAT NAME IN OPTICS

CARL
ZEISS
WEST GERMANY